Talanta

The International Journal of Pure and Applied Analytical Chemistry

Comparative electrooxidation of sulphite by self-assembled monolayers (SAMs) of Co(II), Fe(II), Ni(II) and Mn(III) tetrakis benzylmercapto and dodecylmercapto metallophthalocyanines complexes on gold electrodes

Bolade Agboola, Tebello Nyokong [*]

Chemistry Department, Rhodes University, Grahamstown 6140, South Africa

Abstract

This work reports on the use of Co(II), Fe(II), Mn(III) and Ni(II) tetrakis benzylmercapto and dodecylmercapto phthalocyanine complexes for gold electrode modification for electrooxidation of sulphite ions. The complexes were successfully used to modify gold electrodes by self-assembled monolayer (SAM) technique. The self-assembled films are stable and showed blocking characteristics towards the following Faradaic processes; gold surface oxidation, underpotential deposition (UPD) of copper and solution redox chemistry of $[Fe(H_2O)_6^{3+}]/[Fe(H_2O)_6^{2+}]$. All the modified electrodes showed improved catalytic activities than the unmodified gold electrode towards sulphite ion electrooxidation with all the modified electrodes exhibiting high resistance to electrode surface passivation. Better catalytic performance were obtained for the CoPcs, FePcs and MnPcs which have metal based redox processes within the range of the sulphite electrooxidation peak, while the NiPcs which did not show metal based redox reaction performed less. The catalytic current was found to be linear with sulphite ion concentration in the concentration range employed in this work (0.1–1 mM) and sensitivities ranging from 1.68 to 2.96 μA/mM were observed for all the modified electrodes. Mechanisms of the catalytic oxidation of sulphite ions are proposed.
© 2006 Elsevier B.V. All rights reserved.

Keywords: Metallophthalocyanines complexes; Cyclic voltammetry; Self-assembled monolayers; Electrocatalysis; Sulphite oxidation

1. Introduction

Sulphur dioxide is a major atmospheric pollutant. It dissolves in water to give hydrated SO_2 species. In basic media, hydrogen sulphite and sulphite ions are formed from SO_2. Thus, measurement of sulphite in alkaline media can be used for the indirect determination of sulphur dioxide (SO_2). Atmospheric SO_2 can be absorbed as sulphite by plant [1,2] and this can lead to increase in toxic reactive oxygen species (ROS) [3–5].

Methods for SO_2 (or sulphite) determination include absorption spectroscopy [6], titrimetric [7], ion chromatography [8] and electrochemical methods [9,10]. Electrochemical methods provide a simple, cost effective and quick way of analysing SO_2 (or sulphite). The modification of electrodes improves their sensitivity and selectivity. Methods for electrode modification include electropolymerisation [11–15], dip-dry method [16], drop dry method [17], vapour deposition [18–20], spin coat-

ing [21], Langmuir–Blodgett [22] and recently self-assembled monolayer (SAM) technique. The SAM technique is simple and reproducible, and the molecules are chemically bound to the electrodes. Also the technique enables high order and stability of the molecules on electrodes [23–25]. First row transition metal phthalocyanine complexes are well known for their electrocatalytic properties and there have been reports on the interaction of metallophthacyanine complexes such as cobalt tetrasulphophthalocyanine (CoTSPc) with SO_2 [26] in which SO_2 coordinated to CoTSPc accompanied by the oxidation of Co(II) to Co(III).

In this work we report on the use of SAM electrodes of benzylmercapto and dodecylmercapto phthalocyanine complexes of Co(II), Fe(II), Mn(III) and Ni(II) for the oxidation of sulphite. The role of the central metal ion on the catalytic efficiency is explored.

2. Experimental

We have recently reported [27–29] on the syntheses of complexes **1**–**4** (Fig. 1). Sodium sulphite (SAARCHEM) was used

[*] Corresponding author. Tel.: +27 46 6038260; fax: +27 46 6225109.
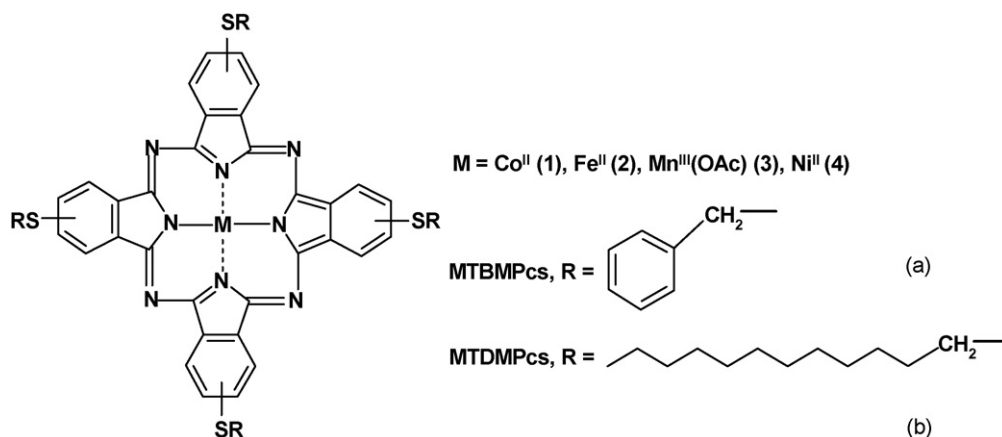*E-mail address:* t.nyokong@ru.ac.za (T. Nyokong).

Fig. 1. General representation of the molecular structures of the metallophthalocyanine complexes. Tetrabenzyl mercapto phthalocyanine (MTBMPc) and tetradodecyl mercapto phthalocyanine (MTDMPc) complexes with M = Co(II) (**1**), Fe(II) (**2**), Mn(III) (**3**), Ni(II) (**4**).

without further purification. Dichloromethane (DCM) was distilled before use. Solutions for electrochemical studies were deaerated by bubbling nitrogen prior to the experiments and the electrochemical cell was kept under nitrogen atmosphere throughout the experiments. Phosphate buffers were employed where needed.

SAM studies were carried out with the use of Autolab potentiostat PGSTAT 30 (Eco Chemie, Utretch, The Netherlands) driven by the General Purpose Electrochemical Systems data processing software (GPES, software version 4.9, Eco Chemie). We employed a three-electrode set-up consisting of either bare gold ($r = 0.8$ mm from Bioanalytical systems, BAS) or MPc-SAM modified gold electrodes, and a Ag|AgCl wire pseudo reference and platinum wire counter electrodes.

The gold electrode was polished with slurries of $1.0\,\mu$m alumina on a SiC-emery paper (type 2400 grit) and then subjected to ultrasonic vibration in ethanol to remove residual alumina particles at the surface. The gold electrode was then treated with 'Piranha' solution $\{1{:}3$ (v/v) 30% H_2O_2 and concentrated $H_2SO_4\}$ for about 1 min, this step is necessary in order to remove organic contaminants and was followed by thorough rinsing with distilled water. The electrodes were then rinsed with ethanol and finally with dichloromethane (DCM). Following this pretreatment, the electrodes were then placed in nitrogen-saturated 1 mM solutions of the MPcs in DCM. After allowing the SAMs to form for 18 h, the modified electrodes were then thoroughly rinsed with DCM and dried gently in a weak flowing nitrogen gas. The modified electrodes were stored in nitrogen-saturated phosphate buffer pH 4.0 at room temperature.

3. Results and discussion

3.1. Self-assembled monolayer (SAM) characterisation

The self-assembled films of the complexes on gold electrodes were characterised using the following well established Faradaic processes [30,31]; gold surface oxidation, solution redox chemistry of $[Fe(H_2O)_6{}^{3+}]/[Fe(H_2O)_6{}^{2+}]$ and underpotential deposition (UPD) of copper, Fig. 2a–c, respectively, shows typical cyclic voltammograms of (a) 10 mM aqueous

KOH, (b) 1 mM $Fe(NH_4)(SO_4)_2$ in 1 mM $HClO_4$ electrolyte and (c) 1 mM $CuSO_4$ in 0.5 M H_2SO_4 electrolyte at (i) bare gold electrode and (ii) complex **1a** (as an example) modified gold electrode at a scan rate of 100 mV s^{-1}. In all cases, the modified electrodes inhibited the Faradaic processes showing that the SAM formed on the gold electrodes are stable, well packed and defect free, as evidenced by inhibition of the gold oxidation and decrease in the corresponding reduction peak after SAM formation, Fig. 2a. In Fig. 2b, the Fe(III)/Fe(II) redox peak lost its shape and intensity on SAM electrodes. And finally the copper deposition was inhibited by the SAMs in Fig. 2c. In order to estimate the surface concentration of the complexes on gold electrodes, the real surface areas of the gold electrodes were first determined using the conventional method [32]. Using Randles–Sevcik equation (1):

$$I_{pa} = (2.69 \times 10^5)n^{3/2}D^{1/2}v^{1/2}AC \tag{1}$$

n is the number of electron transferred ($n = 1$), D the diffusion coefficient of $[Fe(CN)_6]^{3-}$ (7.6×10^{-6} cm^2/s [32]), v the scan rate (0.05 V/s), A the geometric surface area (0.0201 cm^2), and C is the bulk concentration of $[Fe(CN)_6]^{3-}$ (1 mM). The real gold surface area is expected to be larger than the geometric area due to surface roughness. The surface roughness of the electrode used in this work was found to be 1.32 (ratio of $I_{pa\,experimental}/I_{pa\,theoretical}$) corresponding to a real surface area of 0.0279 cm^2 (roughness factor X theoretical surface area). For a monolayer on gold electrode, the surface concentration of phthalocyanine complexes with flat orientation is approximately 1×10^{-10} Å [33,34]. The surface concentration was estimated using the charge difference between the bare gold (Q_{Bare}) and the MPc-SAMs (Q_{SAM}) (Fig. 2a) which is proportional to the fraction of the gold sites covered by the MPc-SAMs.

This fraction is divided by three to get the charge proportion of gold sites covered with MPc-SAM, according to Eq. (2) [35]:

$$Au \cdot H_2O + 2H_2O \rightleftharpoons Au(OH)_3 + 3H^+ + 3e^- \tag{2}$$

The amount of gold sites covered by the MPc-SAM is then divided by four (each MPc molecule is assumed to consume four gold sites since the complexes are tetra-substituted

day constant (96485 C mol^{-1}). The surface concentration in number of molecules per area (in cm^2) can be obtained by simply multiplying the Γ_{MPc} (mol/cm^2) by the Avogadro's constant (N_A). The surface concentration ranges from 0.87 to 1.25×10^{-10} mol cm^{-2} (Table 1) indicating monolayer formation with molecules having flat orientation. It is possible that not all of the four substituents are attached, hence the Γ_{MPc} values are a rough estimate. Thus, a second method for determining Γ_{MPc} value was employed using Eq. (3):

$$\Gamma_{MPc} = \frac{Q}{nFA} \tag{3}$$

where Q is the background corrected electric charge the anodic peaks in Fig. 3, A the real electrode surface area, and the other symbols have their usual meaning. The surface concentrations were not too different from those shown in Table 1. The Γ_{MPc} values were found to range from 0.83 to 1.04×10^{-10} mol cm^{-2} confirming monolayer formation.

Fig. 3a–d, respectively, shows the typical CVs of the MPc-SAMs of CoPcs, FePcs, MnPcs and NiPcs in phosphate buffer pH 7.4, broad peaks were observed. The peak assigned to Co(III)/Co(II) redox was observed near 0.4 V in solution [27], thus we assign the peaks between 0 and 0.4 V for complexes **1a** and **1b** to Co(III)Pc/Co(II)Pc processes. The subsequent peak between 0.6 and 0.8 for these complexes are assigned to ring oxidation processes. For complexes **2a** and **2b**, the Fe(III)/Fe(II) redox processes are also observed between 0 and 0.4 V, and the ring processes at ∼0.6 V. The Mn(IV)/Mn(III) processes are observed between 0 and 0.2 V for complexes **3a** and **3b**. Only ring based processes are observed for the NiPc complexes **4a** and **4b**. The plots of peak currents, I_p (for Co(III)/Co(II), Fe(III)/Fe(II), Mn(IV)/Mn(III) and NiPc(−1)/NiPc(−2) processes) versus the scan rates (Fig. 3 insets) were linear showing that the complexes are surface confined onto the gold electrodes [36]. The peaks are generally broad characteristic of the redox peaks of species confined to the surface, this can be attributed to the fact that the redox reactions may be kinetically hindered [32]. Cycling the CVs shown in Fig. 3 at a fixed scan rate resulted in an insignificant decrease in current on cycling, confirming stability of the electrode.

3.2. Electrocatalytic oxidation of sulphite

Fig. 4a and b show the cyclic voltamogramms of 1 mM sulphite in phosphate buffer (pH 7.4) at an unmodified gold electrode, and gold electrodes modified by SAMs of complexes **1a**, **1b**, **2a**, **2b**, **3a**, **3b**, **4a** and **4b**. All the SAM electrodes showed better catalysis than the unmodified gold electrode judging by the significant increase in the peak currents. The oxidation peak for sulphite at unmodified gold electrode was a slow redox reaction (as judged by a broad peak) with a potential peak (E_p) at around 0.59 V. With the exception of the NiPcs-SAM, the E_p was significantly lowered by the SAMs of all the complexes indicating catalysis. The increase in catalytic activity as judged by the shift of peak potential to less positive values, is as follows: **2b** > **2a** > **1a** ∼ **3a** ∼ **3b** > **1b** > **4b** > **4a** (Table 1). The trend shows that the worst activity is shown by NiPc complexes, this is

Fig. 2. Typical cyclic voltammograms of (a) 10 mM aqueous KOH, (b) 1 mM Fe(NH$_4$)(SO$_4$)$_2$ in 1 mM HClO$_4$ electrolyte and (c) 1 mM CuSO$_4$ in 0.5 M H$_2$SO$_4$ electrolyte at (i) bare gold electrode, (ii) complex **1a** modified gold electrode. Scan rate = 100 mV s^{-1}.

with thiol groups) and then divided by 0.0201 cm^2 which is the geometric area of the gold electrode surface to get the charge density proportional to each MPc molecule. These values can then be converted to the corresponding surface concentration (Γ_{MPc}, mol/cm^2) by dividing them with the Fara-

Table 1
Catalytic peaks for the detection of sulphite on the MPc modified electrodes and slope (sensitivity) of the plot of I_p vs. $[SO_3^{2-}]$

Modified electrodes	E_p (V)/I_p (μM) (SO_3^{2-}) vs. Ag/AgCl	Slope (sensitivity) of plot of I_p vs. concentration (μA/mM)/R^2 values	Surface concentration ($\times 10^{10}$ mol cm^{-2})
CoTBMPc SAM-Au, **1a**	0.54/3.09	2.96/0.9478	0.94
CoTDMPc SAM-Au, **1b**	0.55/3.8	2.82/0.9665	1.24
FeTBMPc SAM-Au, **2a**	0.53/3.3	1.94/0.9334	0.89
FeTDMPc SAM-Au, **2b**	0.52/2.93	3.05/0.9870	0.93
MnTBMPc SAM-Au, **3a**	0.54/2.73	2.51/0.9774	0.87
MnTDMPc SAM-Au, **3b**	0.54/2.41	2.72/0.9764	1.12
NiTBMPc SAM-Au, **4a**	0.63/3.21	1.68/0.9714	1.17
NiTDMPc SAM-Au, **4b**	0.62/3.06	2.10/0.9620	1.25

due to the fact that these species do not show metal based redox processes. The best activity is exhibited by the FePc species.

The catalytic activity of the SAM modified electrodes were also studied in a lower concentration range (1 μM sulphite), Fig. 5. The unmodified gold electrode hardly showed any activity while for the SAM modified electrodes, there were significant increases in peak currents; this observation shows that these modified electrodes are potential sensors for real samples applications, where low (∼ μM) concentrations of sulphite are required.

Fig. 6 shows near linear (R^2 values shown in Table 1) relationships between catalytic currents and the sulphite concentrations

for the concentration range chosen for the catalytic studies in this work (i.e., 1.0×10^{-4} to 1.0×10^{-3} mol dm^{-3}), resulting in slopes (sensitivities) ranging from 1.68 to 3.05 μA/mM for the various electrodes (Table 1). The peaks increased with increase in scan number as shown in Fig. 7, without passivation of the electrode, hence showing stability. Also there were no significant differences between the various electrodes, all the modified electrodes showed high resistance to passivation as shown in Fig. 7, which shows only a small decrease in current with scan number mainly observed between the first and second scan.

Fig. 8A shows the cyclic voltammogramms of electrooxidation of 1 mM sulphite at different scan rates catalysed by **1b**-SAM
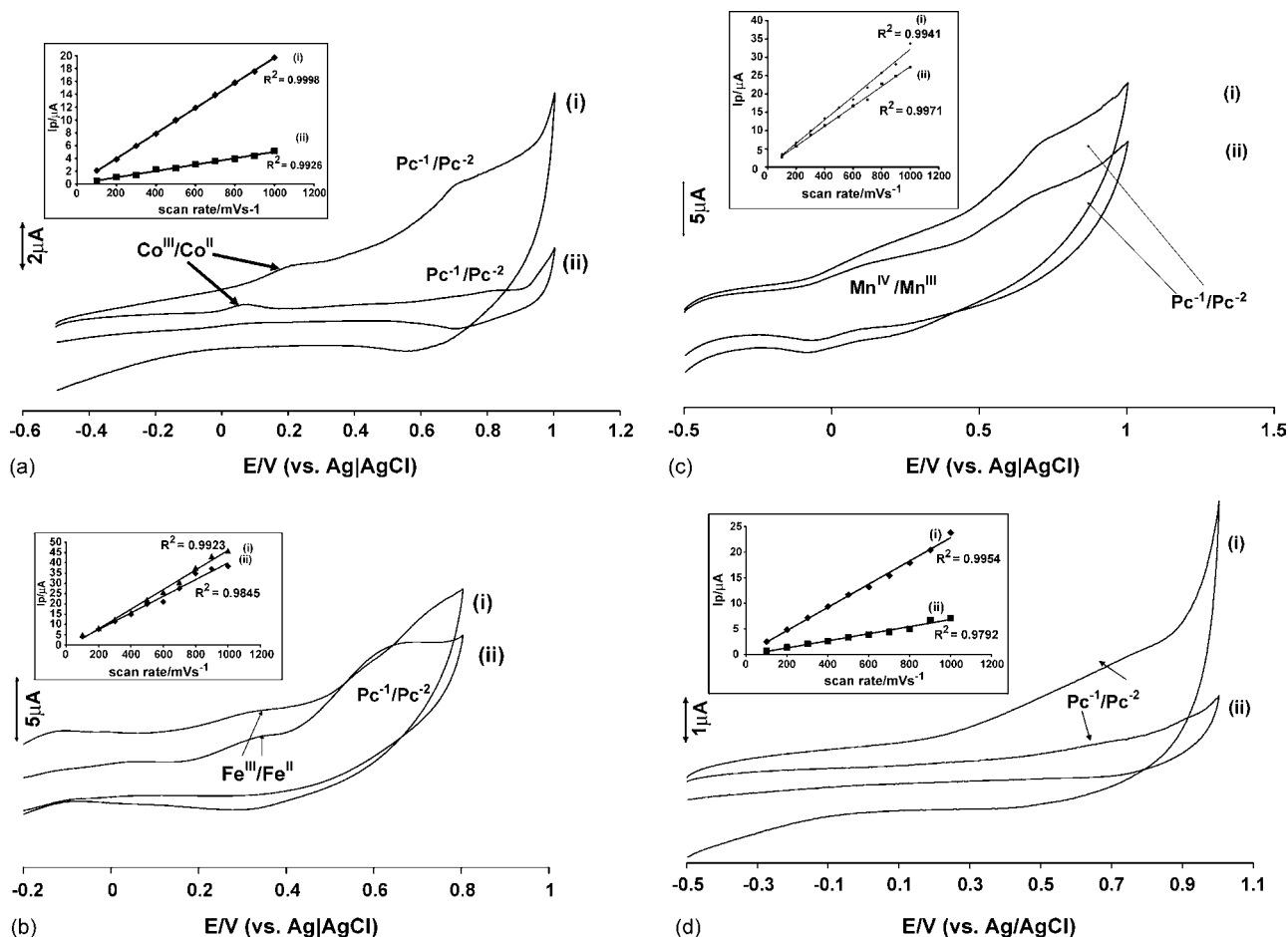
Fig. 3. Cyclic voltammogrames of the complexes in phosphate buffer pH 7.4: (a) CoPcs (**1**), (b) FePcs (**2**), (c) MnPcs (**3**) and (d) NiPcs (**4**). Curve (i) MTBMPc (**a**) and (ii) MTDMPc (**b**). Scan rate = 100 mV s^{-1}.
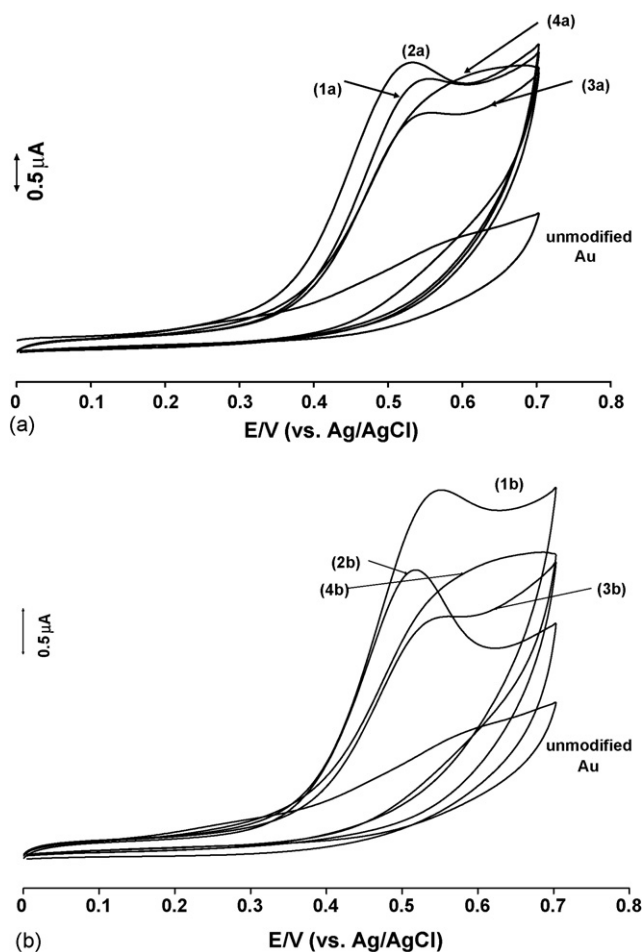
Fig. 4. Cyclic voltamogramms for 1 mM sulphite oxidation in phosphate buffer pH 7.4 solution at unmodified gold electrode and at SAMs of (a) **1a**, **2a**, **3a** and **4a**; (b) **1b**, **2b**, **3b** and **4b**. Scan rate 100 mV s^{-1}.

Fig. 6. Plots of I_p vs. [SO_3^{2-}] on SAMs of complexes **1a**, **2a**, **3a**, **4a**, **1b**, **2b**, **3b** and **4b**. Scan rate = 100 mV s^{-1}.

electrode. It is clear that there was a slight shift of peak potential to more positive values with increase in scan rate. For all SAMs, the plots of peak potentials versus log of scan rate were nearly linear (R^2 values ranged from 0.960 to 0.977), for sulphite oxidation, Fig. 8B, this indicates that the electrocatalytic oxidation of sulphite is irreversible [37], in agreement with the

cyclic voltammetry for sulphite oxidation (Fig. 4) which did not show any cathodic return peak. The slight variation in linearity is probably due to the involvement of chemical reactions coupled with electrochemical process [17]. Fig. 8C also shows a near linear (R^2 ranging from 0.977 to 0.993) relationship between the peak current and square root of the scan rate, indicating that the sulphite electrocatalytic oxidation is diffusion controlled. However, the slight deviations from total linearity

Fig. 5. Cyclic voltamogramms for 1 μM sulphite oxidation in phosphate buffer pH 7.4 solution on unmodified gold electrode, and on complexes **1a**, **2a**, **3a** and **4a**.
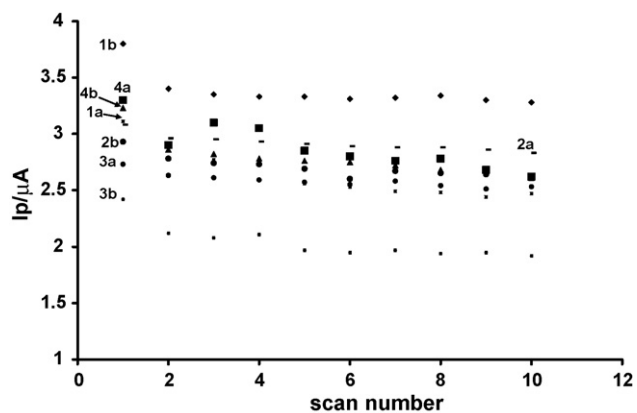
Fig. 7. Plots of I_p vs. number of scans for repetitive cycling of 1 mM sulphite at complexes **1a**, **1b**, **2a**, **2b**, **3a**, **3b**, **4a** and **4b**. Scan rate = 100 mV s^{-1}.
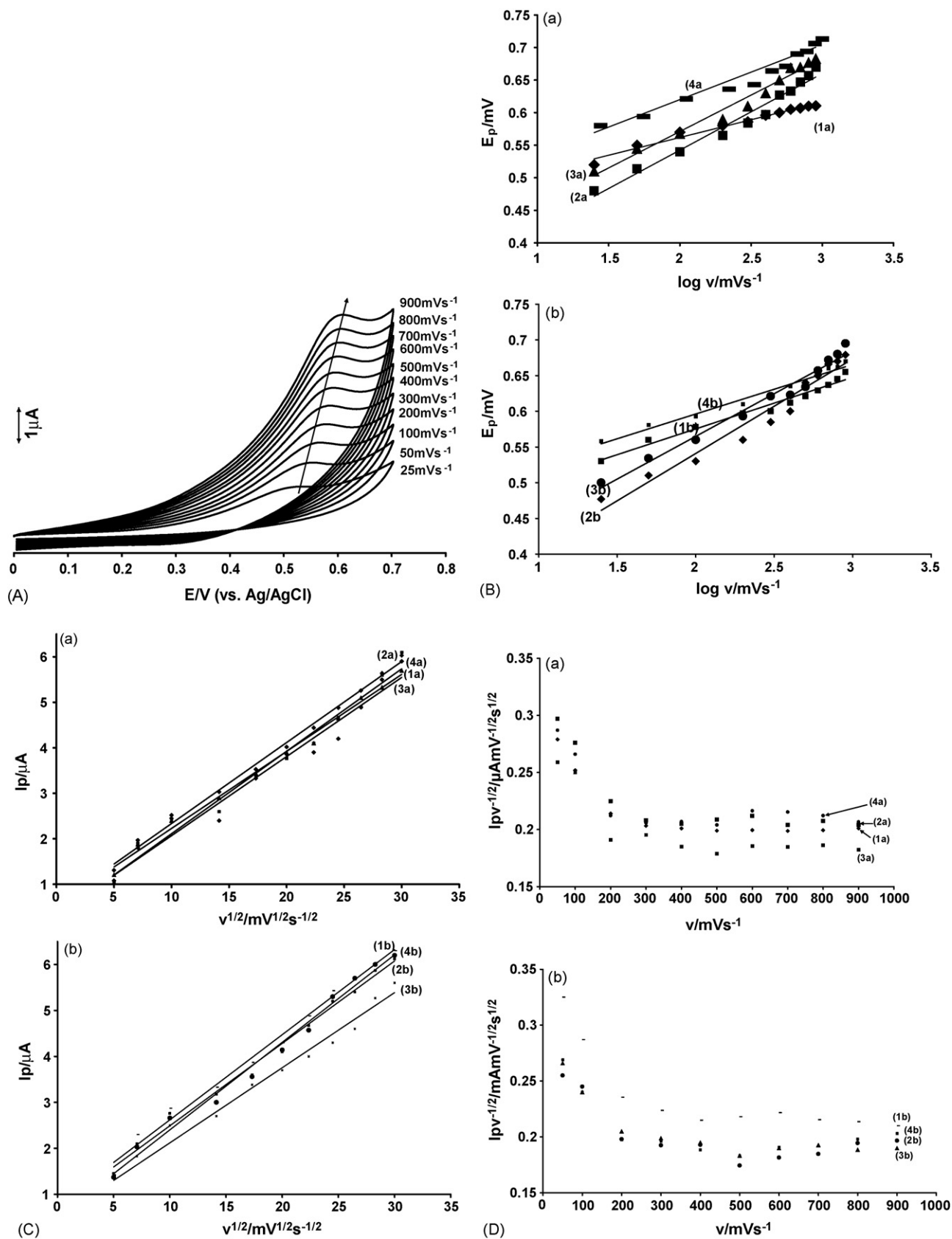
Fig. 8. (A) Cyclic voltamogramms of electrooxidation of 1 mM sulphite at different scan rates catalysed by complex **1b**-SAM electrode. (B) Plot of E_p vs. log v for electrooxidation of 1 mM sulphite solution in phosphate buffer pH 7.4 on the (a) complexes **1a–4a** and (b) complexes **1b–4b**. (C) Plot of I_p vs. $v^{1/2}$ for electrooxidation of 1 mM sulphite solution in phosphate buffer pH 7.4 on (a) complexes **1a–4a** and (b) complexes **1b–4b**. (D) Plot of $I_p v^{-1/2}$ vs. v for electrooxidation of 1 mM sulphite on (a) complexes **1a–4a** and (b) complexes **1b–4d**.

may be due to the involvement of both mass-transport and kinetic effects.

Fig. 8D further confirms that the electrooxidation of sulphite by the SAM modified gold electrodes is a catalytic process judging by the pattern of curves obtained which is typical of catalytic processes [17].

The mechanism of reactions for the catalysis of sulphite oxidation can be represented by Eqs. (4)–(7) below

$$2M(II)Pc \rightarrow 2[M(III)Pc]^+ + 2e^- \tag{4}$$

$$2[M(III)Pc]^+ + SO_3{}^{2-} + H_2O$$
$$\rightarrow 2M(II)Pc + SO_4{}^{2-} + 2H^+ \tag{5}$$

where M is Co, Fe.

$$2Mn(III)Pc \rightarrow 2[Mn(IV)Pc]^+ + 2e^- \tag{6}$$

$$2[Mn(IV)]Pc^+ + SO_3{}^{2-} + H_2O$$
$$\rightarrow 2Mn(III)Pc + SO_4{}^{2-} + 2H^+ \tag{7}$$
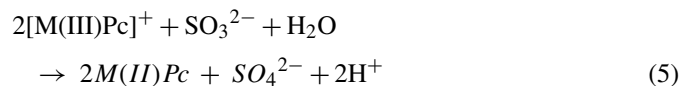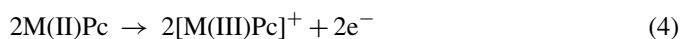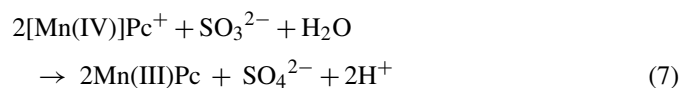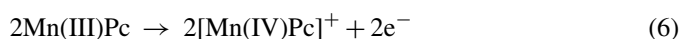
Eqs. (4) and (6) are proposed since from Fig. 4a, the foot of the oxidation wave for sulphite oxidation occurred at around 0.3 V. The metal based oxidation (between 0.0 and 0.4 V, Fig. 3a–c) occurs near this potential for the CoPc, FePc and MnPc complexes. Eqs. (5) and (7) are a result of the chemical reaction between the highly oxidising M(III)Pc species for the CoPc and FePc complexes (Mn(IV)Pc species for MnPc complexes) with sulphite ions which are highly reducing. The participation of water molecules from phosphate buffer pH 7.4 results in Eqs. (5) and (7). Similar mechanisms have been proposed before [38–40]. In the case of NiPcs, as shown in Fig. 3d, metal based oxidation was not observed, the observed catalytic activity towards the oxidation of sulphite is attributed to ring based processes as follows

$$2Ni(II)Pc(-2) \rightarrow 2Ni(II)Pc(-1) + 2e^- \tag{8}$$

$$2Ni(II)Pc(-1) + SO_3{}^{2-} + H_2O$$
$$\rightarrow 2Ni(II)Pc(-2) + SO_4{}^{2-} + 2H^+ \tag{8}$$
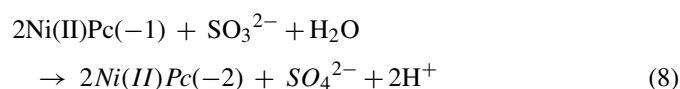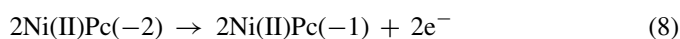
Ring based catalytic processes are known in MPc complexes [41].

4. Conclusion

It has been shown in this work that Au electrodes modified by SAM technique with Co(II), Fe(II), Ni(II) and Mn(III) tetrakis benzylmercapto and dodecylmercapto phthalocyanine complexes exhibited electrocatalytic activity towards the oxidation of sulphite. The involvement of metal based redox processes of the CoPcs, FePcs and MnPcs improved the catalytic activities towards sulphite electrooxidation while the NiPcs which did not

show metal based redox reaction, showed less catalytic activities in terms of shifting the potentials for sulphite oxidation to less positive values. A linear relationship with a high sensitivity between the peak current (I_p) and sulphite concentration was observed for all the modified complexes. In addition, high stability exhibited by these modified electrodes even after repeated use make the modified electrodes as potential electrodes for the development of suitable electrocatalysts for sulphite oxidation as well as in the fabrication of sulphite electrochemical catalysts and sensors.

References

[1] H. Pfanz, E. Martinoia, O.L. Lange, U. Heber, Plant Physiol. 85 (1987) 928.
[2] Z. Miszalski, H. Ziegler, Z. Naturforsch. 44c (1989) 509.
[3] G.D. Peise, S.F. Yang, Biochemical and physiological effects of SO$_2$ on non-photosynthetic process in plants, in: W.E. Winner, H.A. Mooney, R.A. Goldstein (Eds.), Sulphur Dioxide and Vegetation, Stanford University Press, 1985, p. 148.
[4] Ch. Bowler, M. Van Montagu, D. Inze, Annu. Rev. Plant Physiol. Plant Mol. Biol. 43 (1992) 83.
[5] R.G. Alscher, J.L. Donahue, C.L. Cramer, Physiol. Plant. (1997) 224.
[6] A. Safavi, B. Haghighi, Talanta 44 (1997) 1009.
[7] S. Williams, Official Methods of the AOAC, 14th ed., Method 20, Association of Official Chemists Incorporation, Arlington, VA, 1984, p. 123.
[8] C. Anderson, C.R. Warners, D.H. Daniel, K.L. Padgett, J. Assoc. Offic. Anal. Chem. 69 (1986) 14.
[9] J. Sadecke, J. Polonski, J. Chromatogr. A 834 (1999) 401.
[10] V.C. Trenerry, Food Chem. 55 (1996) 299.
[11] B. Agboola, K.I. Ozoemena, T. Nyokong, Electrochim. Acta 51 (2006) 6470.
[12] S. Griveau, F. Bedioui, Electroanalysis 13 (2001) 253.
[13] J. Obirai, T. Nyokong, Electrochim. Acta 49 (2004) 1417.
[14] F. Bedioui, Y. Bouhier, C. Sorel, J. Devynck, L. Coche-Guerente, A. Deronzier, J.C. Montet, Electrochim. Acta 38 (1993) 2485.
[15] A.J. Downard, Electroanalysis 12 (2000) 1085.
[16] I. Zilbermann, J. Hayon, T. Katchalski, R. Ydgar, J. Rishpon, A.I. Shames, E. Korin, A. Bettlelheim, Inorg. Chim. Acta 305 (2000) 53.
[17] C.A. Caro, F. Bedioui, J.H. Zagal, Electrochim. Acta 47 (2002) 1489.
[18] P.S. Vukusic, J.R. Sambles, Thin Solid Films 221 (1992) 311.
[19] M.J. Cook, J. Mater. Chem. 6 (1996) 677.
[20] M.J. Cook, D.A. Mayes, R.H. Poynter, J. Mater. Chem. 5 (1995) 2233.
[21] B.M. Hassan, H. Li, N.B. Mckeown, J. Mater. Chem. 10 (2000) 39.
[22] M.J. Cook, Pure Appl. Chem. 71 (1999) 2145.
[23] Z. Li, M. Liberman, in: J.P. Blitz, C.B. Little (Eds.), Fundamental and Applied Aspects of Chemically Modified Surfaces, Royal Society of Chemistry, 1999, pp. 24–35.
[24] Z. Li, M. Lieberman, W. Hill, Langmuir 17 (2001) 4887.
[25] K. Ozoemena, P. Westbroek, T. Nyokong, Electrochem. Commun. 3 (2001) 529.
[26] M. Thamae, T. Nyokong, Polyhedron 21 (2002) 133.
[27] B. Agboola, K.I. Ozoemena, T. Nyokong, Electrochim. Acta 51 (2006) 4379.
[28] B.O. Agboola, K.I. Ozoemena, T. Nyokong, Electrochim. Acta 51 (2006) 6470.
[29] B.O. Agboola, K.I. Ozoemena, Philippe Westbroek, T. Nyokong, Electrochim. Acta, in press.

[30] D. Losic, J.G. Shapter, J.J. Gooding, Langmuir 17 (2001) 3307.

[31] E. Sabatani, I. Rubinstein, J. Phys. Chem. A 91 (1987) 6663.

[32] H.O. Finklea, in: A.J. Bard, I. Rubinstein (Eds.), Electroanalytical Chemistry, 19, Marcel Dekker, New York, 1996, p. 109.

[33] M.P. Somashekarappa, J. Keshavayya, S. Sampath, Pure Appl. Chem. 74 (2002) 1609.

[34] D.J. Revell, I. Chambrier, M.J. Cook, D.A. Russell, J. Mater. Chem. 10 (2000) 31.

[35] K. Juodkazis, J. Juodkazyte, B. Sebeka, A. Lukinskas, Electrochem. Commun. 1 (2001) 315.

[36] D. Mimica, F. Bedioui, J.H. Zagal, Electrochim. Acta 48 (2002) 323.

[37] T. Malinsky, Z. Taha, Nature 358 (1992) 676.

[38] D.R. Shankaran, S.S. Narayanan, Sens. Actuators B 55 (1999) 191–194.

[39] I. Mayer, M.N. Eberlin, D.A. Tomazela, H.E. Toma, K. Araki, J. Braz. Chem. Soc. 16 (2005) 418.

[40] S.M. Chen, J. Electroanal. Chem. 407 (1996) 123.

[41] T. Nyokong, in: J.H. Zagal, F. Bedioui, J.-P. Dodelet (Eds.), N_4-Macrocyclic Metal Complexes: Electrocatalysis, Electrophotochemistry, and Biomimetic Electrocatalysis, Springer, New York, 2006 (Chapter 7).

High performance liquid chromatographic studies on lanthanides, uranium and thorium on amide modified reversed phase supports

M. Akhila Maheswari [a], D. Prabhakaran [a], M.S. Subramanian [a],*,
N. Sivaraman [b], T.G. Srinivasan [b], P.R. Vasudeva Rao [b]

[a] *Department of Chemistry, Indian Institute of Technology, Chennai 600036, India*
[b] *Chemistry Group, Indira Gandhi Centre for Atomic Research, Kalpakkam 603102, India*

Abstract

The retention behavior of uranium, thorium and lanthanides has been investigated with amide modified reversed phase C_{18} supports using α-hydroxy isobutyric acid (α-HIBA) as the mobile phase. Four structurally different amide moieties namely, 4-hydroxy-*N*,*N*-dihexyl butyramide (4HHBA), 4-hydroxy-*N*,*N*-di-2-ethylhexylhexanamide (4HEHHA), bis(*N*,*N*,*N*′,*N*′-2-ethylhexyl)malonamide (B2EHM) and *N*-methyl-tris(dihexylcarbamoyl-3-methoxy)pivolamide (MTDCMPA) have been synthesized and studied. Among the various amide coated columns, the supports modified with 4HHBA, B2EHM and MTDCMPA exhibit an interesting retention for uranium and thorium, which is different from 4HEHHA modified support. The retention time for uranium and thorium increases with increasing amide concentration for 4HHBA, B2EHM and MTDCMPA supports, while the same decreases with increasing 4HEHHA content. However, the separation factor for uranium and thorium is greater on a 4HEHHA support, compared to an unmodified C_{18} column, reflecting the amide's preferential complexation of uranium over thorium.

Columns modified with 4HHBA, B2EHM and MTDCMPA exhibit relatively higher retentions for lanthanides. However, MTDCMPA modified support shows a different elution profile for lanthanides compared to 4HHBA, and B2EHM modified columns. Individual separations of heavier lanthanides, i.e., from gadolinium to lutetium also have been achieved using 4HHBA and B2EHM modified supports.

The influence of modifier content, mobile phase concentration and its pH on the retention of metal ions has also been studied. Based on these investigations, an efficient high performance liquid chromatographic method (HPLC) has been developed for the rapid separation of uranium from thorium as well as for the individual separation of heavier lanthanides.
© 2006 Elsevier B.V. All rights reserved.

Keywords: Amides; Lanthanides; Uranium; Thorium; Modified reversed phase column; HPLC

1. Introduction

Over the past few decades, HPLC as a powerful separation and analytical technique has revolutionized the field of separation science. Rapid and accurate determination of lanthanides and actinides has received much attention, as industrial demands have expanded significantly, especially in the field of nuclear sciences like, the burn-up measurements of nuclear fuels [1] and also in the various fields of geochemistry [2]. The separation of individual trivalent lanthanides and actinides from respective mixtures is of great significance in view of the challenge posed by the close similarity in their chemical behavior, especially the lanthanides.

With the rapid advancements in HPLC methodology and the applications of superior metal ion complexing agents, significant enhancement in the potential applications of HPLC methods for inorganic analysis has been achieved. A variety of organic compounds such as dithiocarbamates [3], 4-(5-nitro-2-pyridylazo)-resorcinol [4], 2-(2-thiazolylazo)-5-dimethylaminophenol [5], porphyrin derivatives [6], 8-hydroxyquinoline [7], 2-(5-bromo-2-pyridylazo)-5-diethylaminophenol [8], etc., are being employed for the separation of various metal ions. However, only limited endeavors have been made for the separation of lanthanides, uranium and thorium using RP-HPLC methods, in which the supports are modified with organic extractants such as sulphonic acids [9,10], dialkyl phosphoric acid [11],

---

* Corresponding author. Tel.: +91 44 2257 4211; fax: +91 44 2257 4202.
E-mail address: mssu@rediffmail.com (M.S. Subramanian).

dialkylamides [12], etc. The developments and advances in the field of lanthanide separations have been reviewed [13]. In the methods involving the use of neutral metal complexing reagents as stationary phase modifiers, C_8 or C_{18} based columns were generally employed. In RP-HPLC, the stationary phase is modified either by "permanent" coating or by "dynamic" coating with various modifiers. An ion-pairing chromatographic technique was developed using water soluble modifiers such as octane sulphonate [14,15] on the reverse phase supports for the rapid separation of lanthanides and other metal ions. The water insoluble modifiers such as, di-(2-ethylhexyl) phosphoric acid [11] and $C_{20}H_{42}SO_4$ [9] were "permanently" coated on to a reverse phase support for the separation of individual lanthanides. The separation factor for metal ions on a reversed phase column depends on their relative distributions between the coated modifier (in the stationary phase) and the mobile phase, generally consisting of a complexing agent such as, α-HIBA, mandelic acid, lactic acid, citric acid, tartaric acid and EDTA [16–22]. The concentration of lanthanides and actinides is generally determined using post-column derivatization technique.

In the recent years, *N,N*-dialkyl amides and *N,N,N′,N′*-tetraalkyl diamides are found to be promising candidates for actinide recovery [23,24]. Since their solubility in aqueous phase is very low, they are expected to be attractive candidates for actinide separations by extraction chromatographic technique. In addition, they are extremely selective in complexing actinides over other metal ions. However, only limited studies have been reported on employing amide based supports in an extraction chromatographic mode, for studying the separation behavior of lanthanides and actinides. Considering the attractive features of amides, the present study was taken up to study the retention behavior of uranium, thorium and the separation of individual lanthanides on a reverse phase C_{18} support.

One of the most attractive features of these amide derivatives are that their extraction properties for lanthanides and actinides can be tuned by simply modifying the substituents on the *N*-side as well as on the carbonyl side. Therefore, a study was carried out using "permanently" coated columns using various amide derivatives as modifiers on a C_{18} support. In our earlier studies, amide derivatives such as 4-hydroxy-*N,N*-di-2-ethyl-hexyl hexanamide (4HEHHA) [25], 4-hydroxy-*N,N*-dihexyl butyramide (4HHBA) [26] and *bis(N,N,N′,N′*-2-ethylhexyl)-malonamide (B2EHM) [27] were chemically anchored on polymeric resins, which proved to be successful for the efficient extraction for uranium, thorium and certain lanthanides. Based on this study, the above amides were employed in the present work in RP-HPLC as column modifiers. Additionally, *N*-methyl-tris(dihexylcarbamoyl-3-methoxy)pivolamide (MTDCMPA)—a chelating tetramide derivative, was synthesized for the first time and investigated for the retention behavior of uranium, thorium and lanthanides. The amide modified supports were also investigated on the retention behavior of lanthanides to evolve out a procedure for their individual separation.

The influence of the structural aspects of amide derivatives such as the effect of branching, number of carbonyl centers per amide molecule, on the retention of actinides and lanthanides was also investigated. Finally, experiments were carried out to optimize the conditions for separation of U from Th and also for the individual separation of lanthanides. Based on these studies, a HPLC method has been developed for the rapid and accurate analysis of cerium in uranium matrix of pyrochemical reprocessing samples.

2. Experimental

2.1. Instrumentation

The liquid chromatographic system consists of a solvent delivery pump (Jasco PU-1580), a sampling valve (Rheodyne 7725, 20 μL loop), UV–VIS Spectrophotometric detector (Jasco UV-1570), reverse phase C_{18} column (Hypersil, 25 cm × 0.46 cm, 5 μm) and a post-column delivery system (Jasco PU-1580). Typically, a mobile phase flow rate of about 2 mL/min was employed. The post-column reagent, arsenazo(III) was delivered at the rate of 1.5 mL/min. The effluent from HPLC column was mixed with the post-column reagent using a T-connector before it reached the detector. The arsenazo(III) complexes of lanthanides or actinides were monitored at 655 nm. The signal response from the detector was processed by Borwin software.

The amides were characterized using NMR (Bruker-Avance 400 model), FT-IR (Perkin-Elmer Spectrum One model) and also with CHN analyzer (Elementar Vario EL model).

2.2. Reagents and procedures

The metal ion stock solutions and eluents were prepared using deionized water. Appropriate amount of α-HIBA (Across) was dissolved in deionized water and its pH was adjusted using dilute ammonia. In some studies, mandelic acid (Lancaster) was also employed as the mobile phase. Arsenazo(III) (Tokyo Kasei) of 1.5×10^{-4} M concentration was prepared in deionized water and used as such as post-column reagent (PCR).

Thorium and uranium stock solutions were prepared from thorium(IV) nitrate and uranyl nitrate, respectively, in 1 M HNO_3. The stock solutions of Th and U were standardized by complexometric titration with diethylenetriamine pentaacetic acid and gravimetry (as U_3O_8), respectively. The stock solutions of lanthanides were prepared by heating their respective oxides to 600 °C for an hour followed by their dissolution in concentrated HNO_3. Subsequently, the solutions were diluted with 0.1 M HNO_3 and standardized with EDTA. The reagents, chemicals and solvents used were of high purity HPLC grade.

All the coating solutions, mobile phases and post-column reagent solutions were degassed and filtered through 0.5 μm filter prior to usage.

2.3. Synthesis of amide derivatives

2.3.1. Hydroxy-amides and bis(N,N,N′,N′-2-ethylhexyl) malonamide (B2EHM)

The hydroxy amides, 4HHBA and 4HEHHA were synthesized by reacting their corresponding lactones with the respective secondary amines, in the presence of $AlCl_3$-Et_3N couple as catalysts, at 20–25 °C in 'dry' dichloroethane (DCE)

[25,26]. The crude reaction mixture was washed with 1:1 HCl solution and the organic phase was extracted with DCE. The organic layer was subsequently washed with water and then purified using column chromatography (column: silica gel, eluant: 40:60, v/v, ethylacetate:*n*-hexane). The resulting solution was further subjected to vacuum distillation, to remove all the impurities leaving behind a red-orange colored liquid of 4HEHHA and an orange-yellow colored liquid in the case of 4HHBA.

The diamide derivative (B2EHM) was synthesized by reacting 2-ethylhexylamine with malonyl chloride in presence of triethyl amine (2:1:2, mole ratios) in dry ether medium at −5 to 0 °C for 6 h [27]. The crude reaction mixture was subjected to alkali and acid treatments and later purified by vacuum distillation.

2.3.2. Tetramide derivative (MTDCMPA)

A new chelating tetramide derivative was synthesized via a two-step process. The Tris–buffer (5 g, 0.04 mol) was dissolved in 150 mL of dry diethyl ether in the presence of 1.1 equivalents of Et_3N (4.4 mL). To this solution, 1 equivalent of pivaloyl chloride (4.9 mL, 0.02 mol) was added slowly in a moisture free atmosphere at 0 °C, with constant stirring. The resultant bright yellow colored liquid, i.e., primary pivolamide was isolated and purified.

The pivolamide derivative (6.3 mL) was subsequently treated with 3 equivalents of sodium hydride (2.16 g) in presence of dry *N*,*N*-dimethyl formamide as solvent at 0 °C, followed by the addition of 30 mL of pre-synthesized 2-chloro-*N*,*N*-dihexylacetamide [28]. Further, the reaction mixture was heated to 80 °C for 48 h and the solvent was removed by vacuum distillation, resulting in a solid substance, which was subjected to work-up procedures similar to hydroxy amide derivatives. The product was obtained as a bright orange-yellow colored highly viscous liquid. The structures of the various amide modifiers are depicted in Fig. 1. All the synthesized amides and their intermediate compounds were characterized by ^{13}C, ^{1}H NMR, and FT-IR techniques. The amides were also characterized by CHN elemental analysis for their purity; CHN analysis results: theoretical values given in bracket; 4HHBA: C 70.7 (70.8), H 12.0 (12.1) and N 5.2 (5.0); 4HEHHA: C 74.5 (74.4), H 12.7 (12.7), N 4.0 (3.9); B2EHM: C 76.1 (76.3), H 13.0 (12.8), N 5.3 (5.1); MTDCMPA: C 68.7 (69.4) H 11.8 (11.3), N 6.2 (6.5).

2.4. Preparation of modified columns

The solutions of 4HEHHA (1.05×10^{-3}, 5.07×10^{-3} and 1.09×10^{-2} M), 4HHBA (2.14×10^{-3} and 4.29×10^{-3} M) and MTDCMPA (3.32×10^{-4}, 6.58×10^{-4} and 1.28×10^{-3} M) were prepared by dissolving appropriate amounts of respective amides in methanol–water mixture (60:40, v/v). However, 4HHBA (2.06×10^{-2} M), MTDCMPA (2.53×10^{-3} and 5.0×10^{-3} M) and B2EHM (0.54×10^{-3}, and 0.95×10^{-3} M) solutions were prepared using 70% (v/v) methanol, to ensure complete dissolution of amides. The preparation of 1.43×10^{-3} M B2EHM solution required the use of 80% (v/v) methanol for complete dissolution. But, the actual amount of amide sorbed on to the column was found to be lower for 1.43×10^{-3} M amide solution compared to that of 0.95×10^{-3} M solution, due to the presence of higher methanol content in the coating solution.

The C_{18} column was modified by passing amide solutions (500 mL) at a flow rate of 0.5 mL/min. After modification, it was washed with water and pre-equilibrated with about 60 mL of mobile phase. The same column was employed for preparing various amide modified supports in the present study. After studying the column with a particular amide, the sorbed compound was removed from the column using methanol, and was recoated with another amide and so on.

2.5. Determination of amide content coated in C_{18} column

The actual amount of amide coated on to the C_{18} column was determined as follows. The effluent solutions during coating process were collected and evaporated to near dryness and the sample was extracted into *n*-hexane. Subsequently, *n*-hexane was evaporated and the weight of uncoated amide was measured. The sorbed amide content in the column was also estimated after the experiments by its removal with about 60 mL of methanol followed by evaporation of the volatile solvent and weighing. The concentration of coating solution employed and the corresponding amounts actually sorbed are given in Table 1.

3. Results and discussion

3.1. Retention behavior of U and Th

3.1.1. 4HEHHA modified supports

The retention profiles obtained for U and Th with different amounts of 4HEHHA coatings are shown in Fig. 2. The retention times of both U and Th were found to decrease with an increase in 4HEHHA concentration. For example, the elution and separation of Th and U were performed within 8, 5 and 3 min, respectively, for 0.25, 0.45, 0.68 mmol of 4HEHHA coated supports. The retention behavior under similar conditions on an uncoated (bare) C_{18} column is also shown and the separation time was found to be about 14 min. A similar
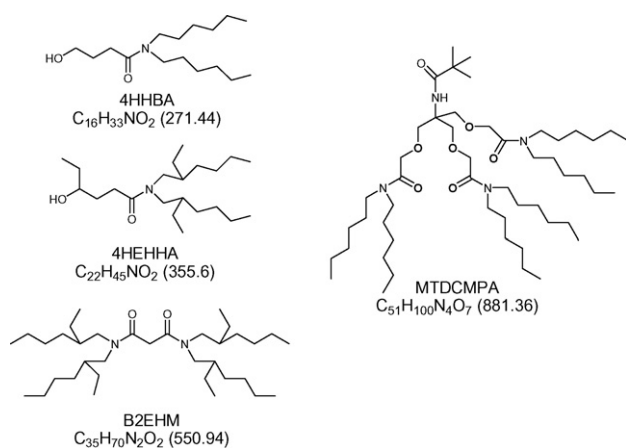
Fig. 1. Structure of amide modifiers.

Table 1
Amide coating solutions and sorbed amounts

Modifier	Methanol:water volume ratio	Concentration of coating solution (M)	Actually coated (sorbed) amount (mmol)
4HEHHA		1.05×10^{-3}	0.25
	60:40	5.07×10^{-3}	0.45
		1.09×10^{-2}	0.68
4HHBA		2.14×10^{-3}	0.17
	60:40	4.29×10^{-3}	0.25
	70:30	2.06×10^{-2}	0.54
MTDCMPA		3.32×10^{-4}	0.11
	60:40	6.58×10^{-4}	0.15
		1.28×10^{-3}	0.17
	70:30	2.53×10^{-3}	0.20
		5.00×10^{-3}	0.26
B2EHM		0.54×10^{-3}	0.16
	70:30	0.95×10^{-3}	0.29
	80:20	1.43×10^{-3}	0.26

500 mL of amide solutions passed through C_{18} (Hypersil, 250 mm × 4.6 mm; 5 μm), coating rate: 0.5 mL/min.

behavior was also observed in our earlier studies with modified C_{18} supports using extractants such as, *N,N*-dihexylhexanamide and trihexylphosphate [12]. This behavior is attributed to the predominant role played by the bare C_{18} support, which extracts the hydroxyisobutyrate complexes of both uranium and thorium
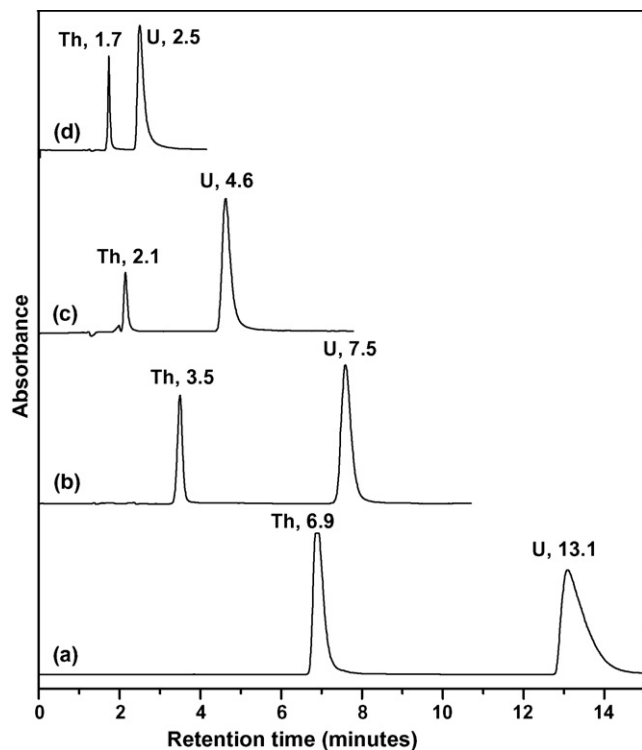
by a hydrophobic interaction. Therefore, it is concluded that the increased masking of hydrophobic surface of the bare C_{18} column by the increased amount of amide coating on the same leads to the shorter retentions, for both U and Th.

Despite the above reverse phase behavior, the 4HEHHA-modified supports contribute to a better separation of U from Th. For example, U and Th were rapidly separated from each other from a 0.25 mmol coated 4HEHHA support with α-HIBA solution at a pH 2.5, whereas the bare C_{18} support is unsuccessful to resolve them under similar conditions. Hence, the method paves a way for rapid separation and assay of U from Th in their mixture.

3.1.2. 4HHBA modified supports

The elution behavior for U and Th on a modified 4HHBA support is shown in Fig. 3. It corresponds to a lowest concentration of 4HHBA coated support (0.17 mmol) that was employed for the present work. Uranium did not elute from a 0.54 mmol of 4HHBA coated column with α-HIBA (0.1 M, pH 2.5) even after about 100 min. Under these experimental conditions, Th could be eluted in 15 min. Thus, 4HHBA modified support exhibits higher affinity for U over Th. These studies confirm a strong role played by the amide moiety for the selective complexation of uranium-hydroxyisobutyrate complexes over thorium complexes. The strongly retained uranium could be subsequently eluted with 0.01 M HNO_3. Elution under this condition maintained the unionized HIBA species, leading to the elution of uranium.

3.1.3. MTDCMPA modified supports

The MTDCMPA modified supports also exhibited high affinity for U over Th (Fig. 4). The retentions of both U and Th were found to increase with increase in amide concentration. It was also observed that both U and Th exhibit strong peak tailing particularly at higher MTDCMPA coatings. The increase in amide

Fig. 2. Retention profiles of Th and U as a function of 4HEHHA concentration. (a) C_{18} bare column; (b) 0.25 mmol 4HEHHA sorbed on C_{18}; (c) 0.45 mmol 4HEHHA sorbed on C_{18}; (d) 0.68 mmol 4HEHHA sorbed on C_{18}; mobile phase: α-HIBA (0.1 M, pH 3.0), flow rate: 2 mL/min; sample: Th (50 μg/mL) and U (75 μg/mL), injected amount: 20 μL; PCR: arsenazo(III), flow rate: 1.5 mL/min, detection: 655 nm.
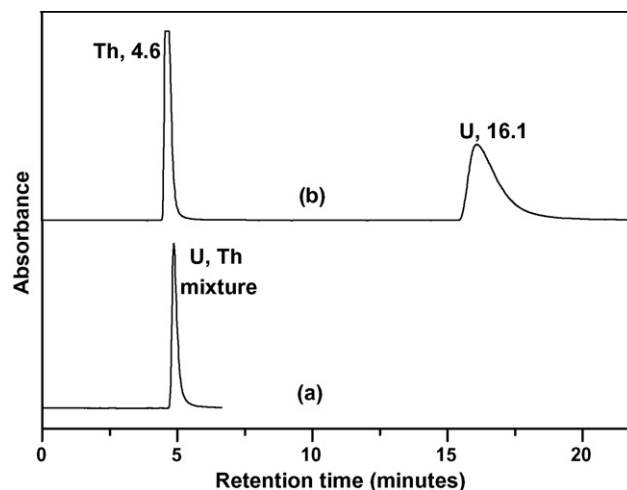
Fig. 3. Comparison of Th and U retentions on 4HHBA modified and unmodified supports. (a) C_{18} bare and (b) C_{18} modified with 4HHBA (0.17 mmol sorbed); mobile phase: α-HIBA (0.1 M, pH 2.5), flow rate: 2 mL/min; sample: Th (50 μg/mL) and U(75 μg/mL), injected amount: 20 μL; PCR: arsenazo(III), flow rate: 1.5 mL/min, detection: 655 nm.
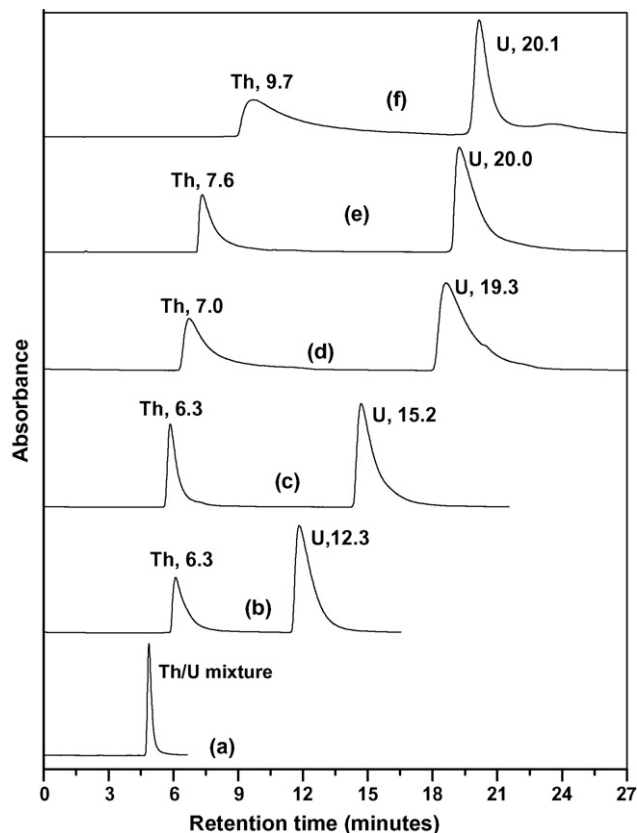
Fig. 4. Effect of MTDCMPA concentration on U/Th retentions. (a) C_{18} bare; (b) C_{18} modified with 0.11 mmol MTDCMPA; (c) 0.15 mmol MTDCMPA; (d) 0.17 mmol MTDCMPA; (e) 0.20 mmol MTDCMPA and (f) 0.26 mmol MTD-CMPA; mobile phase: 0.1 M α-HIBA (pH 2.5), flow rate: 2 mL/min; sample: Th (50 μg/mL) and U (100 μg/mL), injected amount: 20 μL; PCR: arsenazo(III), flow rate: 1.5 mL/min, detection: 655 nm.

concentration enhances the layer thickness on the modified support, leading to band broadening.

3.1.4. B2EHM coated column

The retention behavior of uranium and thorium was examined on a column coated using B2EHM solutions of various concentrations, i.e., 0.54×10^{-3}, 0.95×10^{-3} and 1.43×10^{-3} M, with α-HIBA (0.1 M, pH 2.5–3.5) as the mobile phase. The modified supports showed very higher retentions for both thorium and uranium with preferential sorption of uranium. Severe peak tailing was observed especially during the elution of uranium.

3.1.5. Separation factor of U to Th: influence of amides

The separation factors of U-Th from bare C_{18} and amide modified supports of 4HEHHA, 4HHBA, MTDCMPA and B2EHM are compared in Fig. 5. The separation factor generally increases with mobile phase pH. The values observed with 4HHBA were higher than that obtained with other amide modified supports and bare C_{18} column. In the case of MTDCMPA modified support, the actual amount of amide coated was marginally lower compared to 4HHBA as well as B2EHM supports.

The amide modified supports of 4HHBA, MTDCMPA and B2EHM exhibited higher separation factors compared to 4HEHHA, despite lower quantities of amide coated. How-
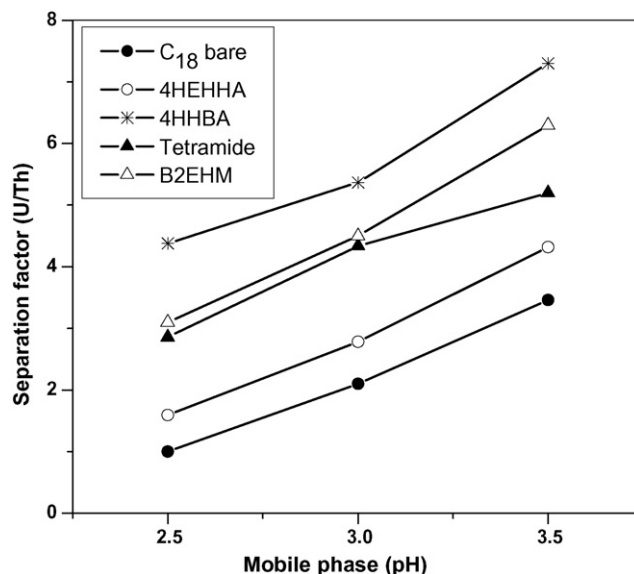
Fig. 5. Comparison of U–Th separation factors for various amide modified supports. C_{18} modified with 0.17 mmol 4HHBA, 0.25 mmol 4HEHHA, 0.15 mmol MTDCMPA and 0.16 mmol B2EHM; mobile phase: 0.1 M α-HIBA, flow rate: 2 mL/min.

ever, the 4HEHHA modified support, which showed separation behavior similar to reverse phase still exhibited a separation factor higher than that observed with bare C_{18} support. These studies indicate the strong influence of the amide moiety on the retention of uranium, i.e., the preferential extraction of uranium over thorium, which corroborates well with our earlier studies using amide grafted polymeric resins [26–28].

3.1.6. Structural influence of amides on U and Th retention

On comparing the retention behavior of U and Th on various amide modified supports, it is evident that the structure of amide influences the chromatographic retention behavior of these ions. C_{18} support retains both U and Th as their respective isobutyrate complexes by hydrophobic interaction. However in addition to hydrophobic interaction, amides also retain U and Th complexes through the carbonyl group coordination and hence higher retention on modified supports compared to bare column.

Among the four supports examined in the present study, 4HEHHA exhibited different separation behaviour. For example, the retention time for both U and Th on 4HEHHA supports decreases with increase in amide concentration whereas it increases for the other three amides. The separation factors observed with 4HEHHA supports are the lowest compared to the one observed with other three amides. The separation factors with 4HEHHA are only marginally higher than the one observed with bare C_{18} support. These studies clearly indicate the influence of branching in amide moiety on the retention and separation behaviour. Branching in amide structure is mainly responsible for lowering the separation factors. Thus, the separation factors decrease as one goes from 4HHBA to 4HEHHA. Based on this observation, one would expect the separation factors of U–Th to decrease further for B2EHM and MTDCMPA supports, as these compounds have more branched structures. However, the presence of two coordinating C=O moieties in

B2EHM and multiple C=O moieties in MTDCMPA would work towards increasing the retention for uranium and thorium, notably uranium. Thus, the separation factors for U-Th observed with B2EHM and MTDCMPA supports are higher compared to 4HEHHA system.

3.1.6.1. U and Th complexes. The various complexes of α-HIBA with U and Th are:

$$UO_2^{2+} + HIBA \rightarrow [UO_2(IBA)]^+, [UO_2(IBA)_2]$$

$$\text{and } [UO_2(IBA)_3]^-$$

$$Th^{4+} + HIBA \rightarrow [Th(IBA)]^{3+}, [Th(IBA)_2]^{2+}, [Th(IBA)_3]^+$$
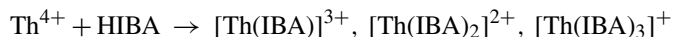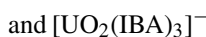
$$\text{and } [Th(IBA)_4]$$

The interaction of α-HIBA with uranyl ions results in the formation of species like $UO_2(IBA)^+$, $UO_2(IBA)_2$ and $UO_2(IBA)_3^-$ and with thorium, it forms $Th(IBA)_4$, $[Th(IBA)]^{3+}$, $[Th(IBA)_2]^{2+}$, $[Th(IBA)_3]^+$ and $[Th(OH)(IBA)_4]^-$ species [16]. However, with increasing pH, i.e., pH ≥ 3, it was reported that $[UO_2(IBA)_3]^- H^+$ (or NH_4^+) and $[Th(OH)(IBA)_4]^-$ and $Th(IBA)_4$ are the predominant species.

As amides are neutral extractants, they preferentially extract neutral species from a mixture of $[UO_2(IBA)_3]^-$ and $UO_2(IBA)_2$. The more abundant species, i.e., $NH_4^+[UO_2-(IBA)_3]^-$ is expected to be extracted into the amide moiety, which can also extract the $UO_2(IBA)_2$ species, from a mixture. In the case of thorium, which elutes prior to uranium indicates the extraction of $[Th(OH)(IBA)_4]^-$ species into the amide moiety, from the aqueous solutions.

3.1.7. Effect of mobile phase pH and concentration

The influence of the pH of α-HIBA (2.5–4.0) on the retention behavior of uranium and thorium was investigated. It was observed that the retention times for both Th and U were found to increase with the increase in mobile phase pH. However, the variation of α-HIBA concentration in the range of 0.05–0.15 M (pH 3.0) did not significantly affect the retention behavior of U and Th.

3.2. Retention and separation of lanthanides

3.2.1. 4HHBA and 4HEHHA modified supports

The retention profiles of lanthanides were initially investigated on a 4HEHHA modified supports with α-HIBA as the mobile phase. Individual lanthanides were not resolved from its mixture as in the case of bare C_{18} support.

However, supports modified with 4HHBA offered good resolution and peak profiles for individual heavier lanthanides, i.e., Gd–Lu, using 0.1 M α-HIBA (pH 2.8), as the mobile phase (Fig. 6).

The retention for heavier lanthanides was found to increase with increase in 4HHBA concentration, establishing the contribution of the amide moieties for better resolution. Moreover, the modified support offered rapid separations for lanthanides, which were eluted within 8 minutes. Individual calibration plots
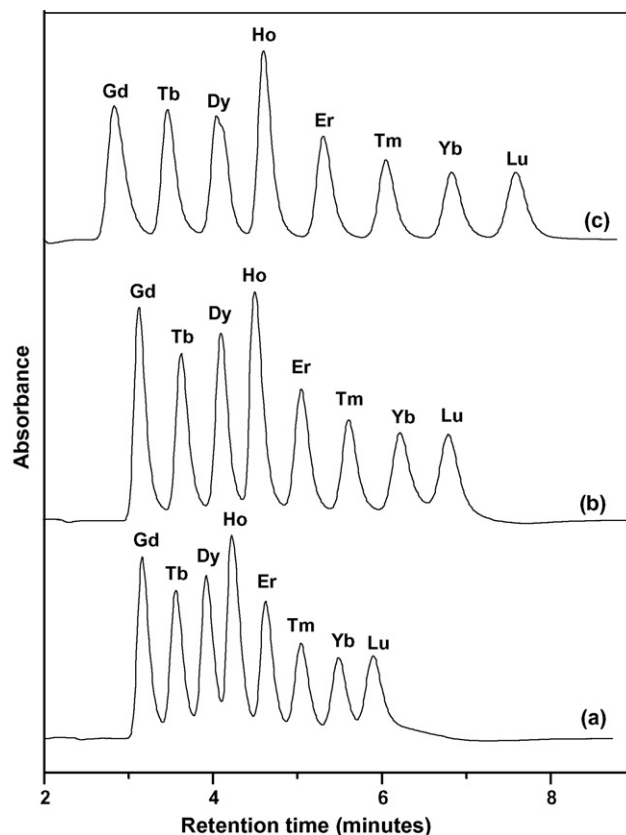
Fig. 6. Retention profiles of heavier lanthanides as a function of 4HHBA coated amounts. (a) C_{18} sorbed with 0.17 mmol 4HHBA; (b) 0.25 mmol 4HHBA; (c) 0.54 mmol 4HHBA; mobile phase: α-HIBA (0.1 M, pH 2.80), flow rate: 1 mL/min; sample: lanthanides (10 μg/mL), injected amount: 20 μL; PCR: arsenazo(III), flow rate: 1.5 mL/min, detection: 655 nm.

($r^2 \sim 0.998$) were obtained for heavier lanthanides using a 4HHBA (0.54 mmol) modified support. However, the lighter lanthanides, i.e., La–Eu were not completely resolved from each other and La, Ce, Pr and Nd were eluted together.

The separation factors (ratio of capacity factors) between adjacent lanthanides from a 4HHBA modified columns are given in Table 2. The separation factor increases marginally with increasing amide content. For example, in the case of Gd–Tb, it increased from 1.27 to 1.36, when the sorbed amide content was raised from 0.17 to 0.54 mmol. However, there

Table 2
Separation factor for lanthanides on 4HHBA supports

Lanthanide pair	Separation factor		
	0.17[a]	0.25[a]	0.54[a]
Gd–Tb	1.27	1.32	1.36
Tb–Dy	1.19	1.21	1.23
Dy–Ho	1.13	1.15	1.17
Ho–Er	1.16	1.17	1.18
Er–Tm	1.14	1.16	1.19
Tm–Yb	1.14	1.14	1.15
Yb–Lu	1.11	1.12	1.13

Mobile phase: 0.1 M α-HIBA (pH 2.8), flow rate: 1 mL/min.
[a] 4HHBA amount sorbed onto C_{18} column (mmol).

were no significant changes in separation factor for all other heavier lanthanide pairs.

The elution sequence of lanthanides was in the order of increasing atomic number, i.e., from La–Lu, the reverse of the order generally observed for cation exchange systems, i.e., Lu–La. In the present study, two complexing reagents, i.e., 4HHBA (stationary phase) and α-HIBA (mobile phase) compete for complexing the lanthanides. The stability constants (log K) of Ln(IBA)$_3$ complex increases from La to Lu, i.e., from 5.53 to 8.82 [18]. Similarly, the stability constant of the complex formed between Ln(IBA)$_3$ and the corresponding amide carbonyl group also increases in the same order, i.e., La to Lu; thus the amide moiety preferentially extracts the Lu(IBA)$_3$ over La(IBA)$_3$ complex.

The influence of mobile phase pH on the retention of lanthanides was studied and the corresponding chromatograms are given in Fig. 7. The capacity factor for lanthanides increases with an increase of pH of the mobile phase. However, there was no significant change in the resolution when raising the mobile phase pH from 2.8 to 3.0. However, the resolution between adjacent lanthanide pairs becomes poor from pH 3.5 and above.

3.2.2. Retention behavior with mandelic acid as mobile phase

Since the mandelate complexes of lanthanides would be expected to be more hydrophobic compared to hydroxyisobu-
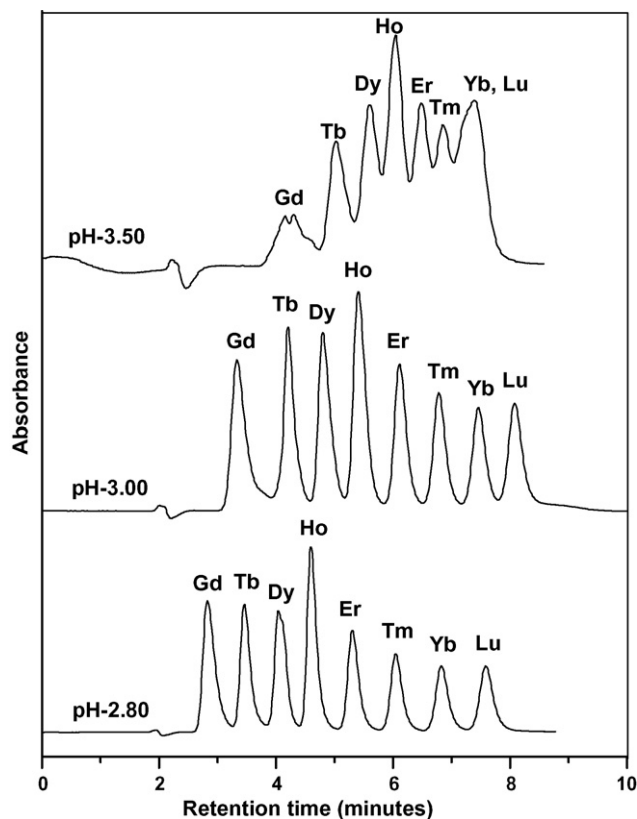
Fig. 7. Influence of α-HIBA pH on the retentions of lanthanides on a 4HHBA modified support. Column: C$_{18}$ sorbed with 0.54 mmol 4HHBA; mobile phase: α-HIBA (0.1 M), flow rate: 1 mL/min; sample: lanthanides (10 μg/mL), injected amount: 20 μL; PCR: arsenazo(III), flow rate: 1.5 mL/min, detection: 655 nm.
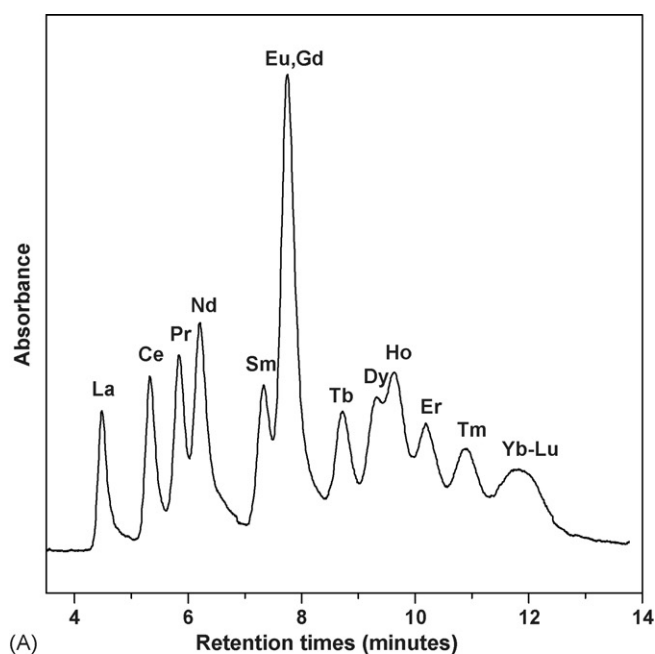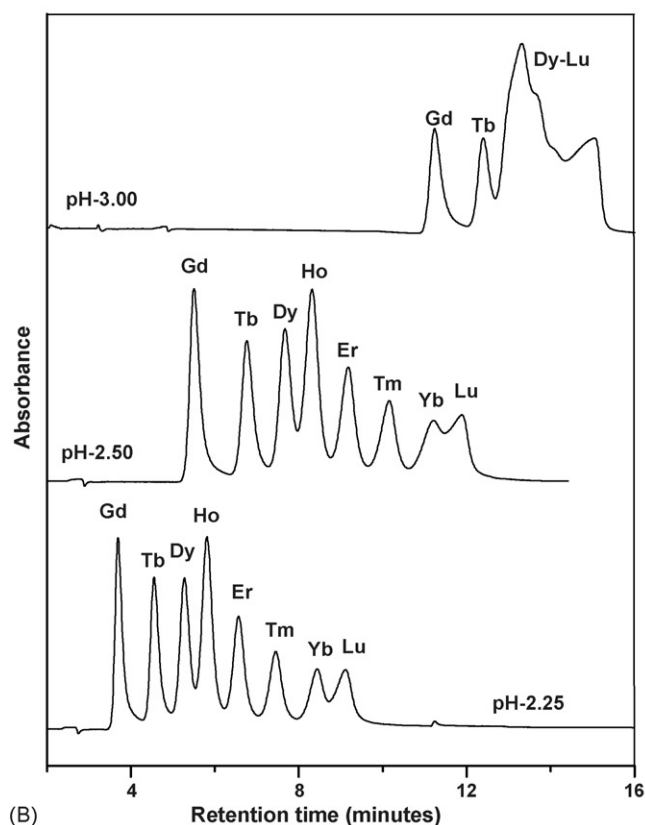
Fig. 8. (A) Retention of lanthanides using mandelic acid as eluent. Column: C$_{18}$ sorbed with 0.17 mmol 4HHBA; mobile phase: 0.1 M mandelic acid (pH 2.5), flow rate: 2 mL/min; sample: lanthanides (10 μg/mL); injected amount: 20 μL; PCR: arsenazo(III); flow rate: 1.5 mL/min; detection: 655 nm. (B) Elution profiles of heavier lanthanides as a function of mandelic acid pH on 4HHBA support. Column: C$_{18}$ sorbed with 0.54 mmol amide; mobile phase: 0.1 M mandelic acid, flow rate: 2 mL/min; sample: lanthanides (10 μg/mL), injected amount: 20 μL; PCR: arsenazo(III), flow rate: 1.5 mL/min, detection: 655 nm.

tyrate complexes, the retention behaviour of lanthanides was also investigated with mandelic acid as an eluent to improve the resolution between lighter lanthanides. The retention profiles of lanthanides were studied with 4HHBA support (0.17 mmol) using 0.1 M mandelic acid (pH 2.5) as the mobile phase (Fig. 8A). The lighter lanthanide pairs such as La–Ce, Pr–Nd and Nd–Sm were resolved and are better than with α-HIBA. However, there is a loss in resolution among the heavier ones such as, Dy–Ho and Yb–Lu. These heavier lanthanides, i.e., Dy–Ho and Yb–Lu, however were well separated with α-HIBA. The higher retention for lanthanides on 4HHBA support with mandelic acid can be attributed to the higher hydrophobicity of mandelate–lanthanide complexes compared to the hydroxyisobutyrate–lanthanide complexes.

The retention of lanthanides increases with the pH of the mobile phase (Fig. 8B). The resolution between individual heavier lanthanides was found to be better with mandelic acid at pH 2.25. This is due to predominant existence of Ln(MA)$_3$ complexes and its greater interaction with the amide moiety thereby, increasing their retention. However, the resolution becomes poorer with increasing pH and completely lost at pH 3.0.

3.2.3. MTDCMPA modified supports

The retention profiles of lanthanides from a 0.20, 0.15 and 0.11 mmol MTDCMPA coated supports are shown in Fig. 9A and B. Good resolution for certain lanthanide pairs such as Nd–Sm, Sm–Eu, Eu–Gd and Gd–Tb were observed. The separation factors of adjacent lanthanides from MTDCMPA support (0.15 mmol sorbed MTDCMPA support with 0.1 M α-HIBA, pH 4 as mobile phase) are found to be as follows: Nd–Sm (2), Sm–Eu (1.48), Eu–Gd (1.46) and Gd–Tb (1.48). The retention for lanthanides was found to increase with amide concentration (Fig. 10). The studies on the retention profile of lanthanides with variation in mobile phase pH indicated that unlike other amides, the MTDCMPA extractant offered better resolution with increase in mobile phase pH. For example, some lanthanide pairs are better resolved at a mobile phase pH 4 than at 3.5.

From Fig. 10, it is also evident that the MTDCMPA support showed a different elution order, i.e., higher affinity for lighter lanthanides and poor retention for heavier lanthanides. Also, it could be inferred that the elution order was not in sequence from Lu–La but La and Nd mixture followed by Ce and Pr mixture. The elution order observed was similar to the sequence observed
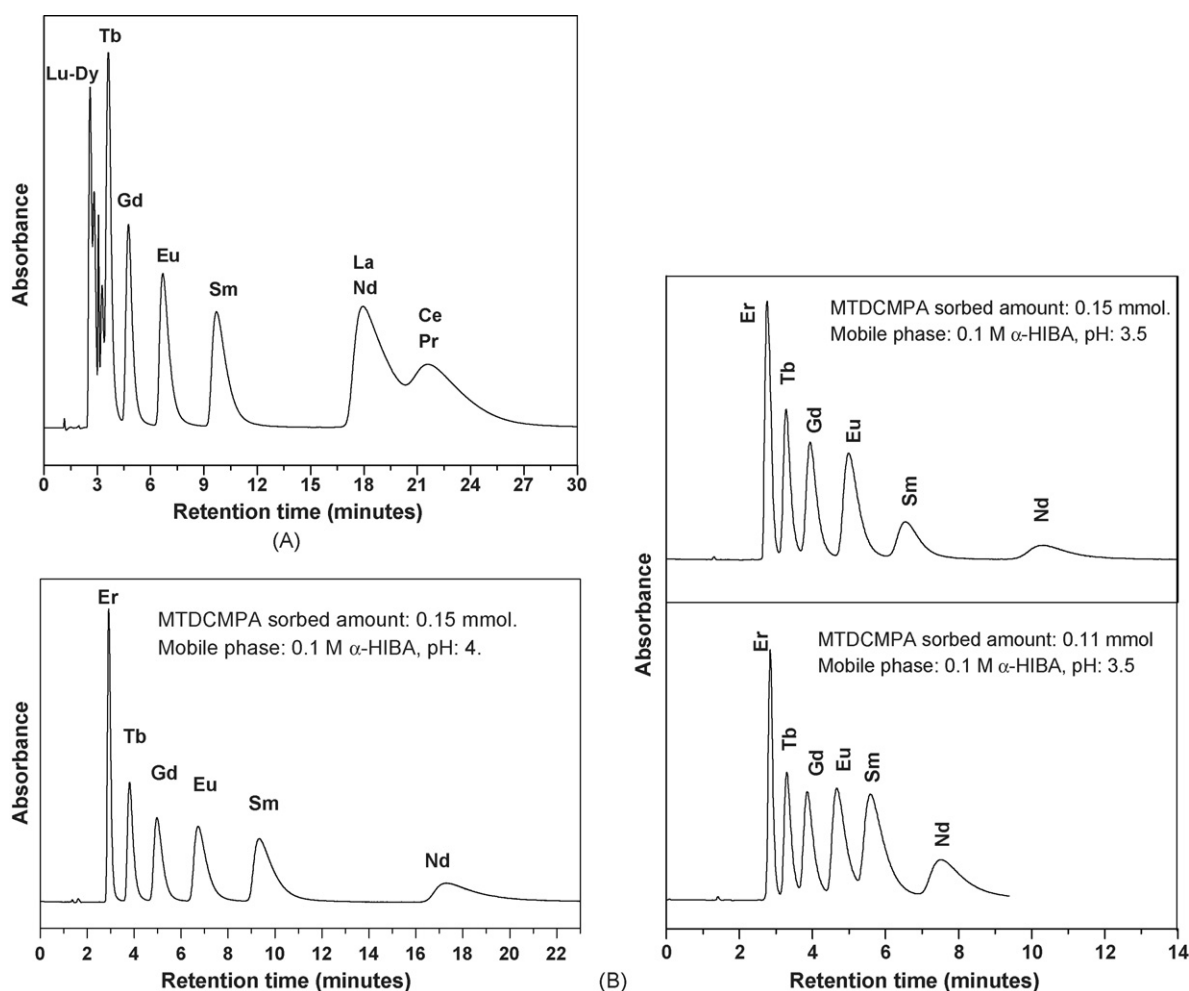
Fig. 9. (A) Peak profiles of lanthanides from a MTDCMPA coated column. Column: C$_{18}$ sorbed with 0.20 mmol amide; mobile phase: 0.1 M α-HIBA (pH 3.5), flow rate: 2 mL/min, sample: lanthanides (10 μg/mL), injected amount: 20 μL; PCR: arsenazo(III), flow rate: 1.5 mL/min, detection: 655 nm. (B) Separation of lanthanides on a MTDCMPA support. Mobile phase: 0.1 M α-HIBA, flow rate: 2 mL/min; sample: lanthanides (10 μg/mL), injected amount: 20 μL; PCR: arsenazo(III), flow rate: 1.5 mL/min, detection: 655 nm.
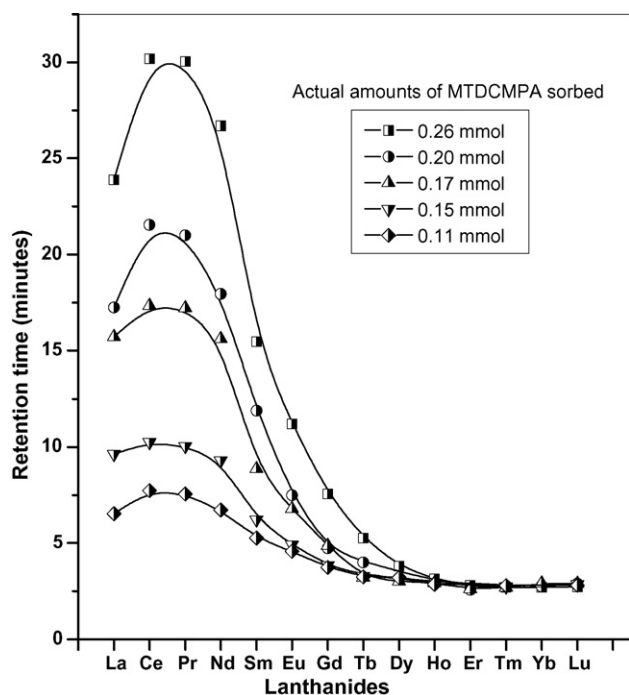
Fig. 10. Retention of lanthanides on MTDCMPA supports as a function of amide concentration: mobile phase: 0.1 M α-HIBA (pH 3.5), flow rate: 2 mL/min.
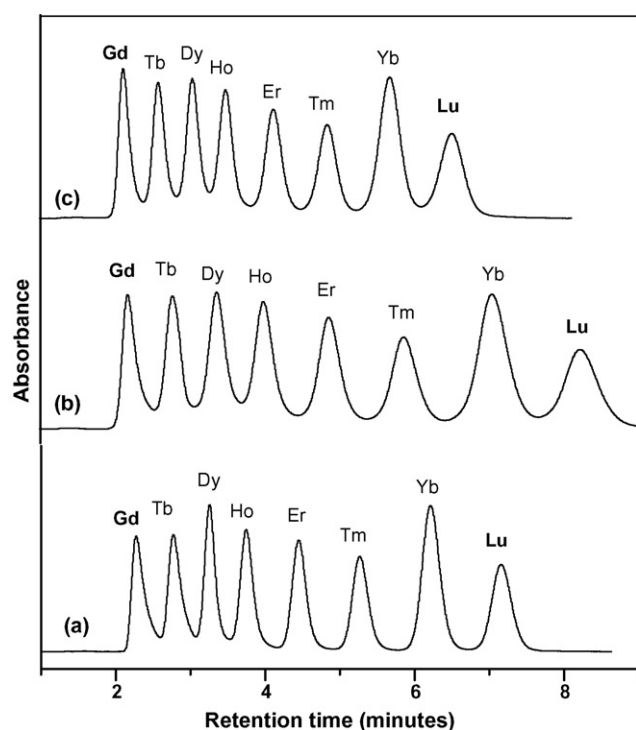
Fig. 11. Influence of B2EHM concentration on the retention of heavier lanthanides. Coated amounts (a) 0.26 mmol (b) 0.29 mmol (c) 0.16 mmol; mobile phase: 0.1 M α-HIBA, pH 2.5, flow rate of 1 mL/min; sample: lanthanides (10 μg/mL), injected amount: 20 μL; PCR: arsenazo(III), flow rate: 1.5 mL/min, detection: 655 nm.

with conventional ion-exchange separations though there are no ion-exchange sites in the MTDCMPA moiety, i.e., elution from Lu to La, and La showed an abnormal retention behavior. It is also observed that MTDCMPA modified support exhibits higher affinity for the lighter lanthanides compared to 4HHBA modified support.

3.2.4. B2EHM modified supports

The retention behavior of heavier lanthanides was investigated with B2EHM solutions of various concentrations and the results are shown in Fig. 11. The elution sequence for lanthanides was in the order of increasing atomic number. Good resolution with excellent peak profiles was achieved for individual heavier lanthanides. Lighter lanthanides, were however, not well resolved. It was also observed that, increase in amide content on the modified supports resulted in the enhanced affinity for lanthanides towards stationary phase. The retention time for lanthanides with 0.26 mmol modified support was lower than that observed with 0.29 mmol coated support, indicating the influence of amide concentration on the resolution. The separation factor for adjacent lanthanide pairs as a function of amide concentration is shown in Table 3. The separation factor marginally increases, especially for Gd–Tb pair; however, there was no significant change for other heavier lanthanide pairs.

The variation in the concentration of α-HIBA did not significantly affect the retention times of lanthanides. The retention time was found to increase, when the mobile phase pH was raised from 2.6 to 3 (Fig. 12). However, resolution started declining from pH 3.5 and was lost completely at pH 4.0.

Among the four amide supports examined in the present study, lanthanides did not resolve from each other with 4HEHHA modified support. Heavier lanthanides were resolved from each other with 4HHBA and B2EHM modified supports and lanthanides elute from lanthanum to lutetium. Lanthanides were however eluted in the reverse order (lutetium to lanthanum) from MTDCMPA support. However, separation of only some lanthanides could be demonstrated with this support. The presence of more than one C=O coordinating moiety in B2EHM and MTDCMPA would be responsible for exhibiting enhanced retention compared to branched 4HEHHA system. These experimental observations suggest that branching in some ways hinders the coordination at the coordinating sites, probably through steric interaction.

Table 3
Separation factor for lanthanides on B2EHM supports

Lanthanide pair	Separation factor		
	0.16[a]	0.26[a]	0.29[a]
Gd–Tb	1.52	1.56	1.62
Tb–Dy	1.33	1.33	1.37
Dy–Ho	1.24	1.25	1.29
Ho–Er	1.28	1.28	1.31
Er–Tm	1.25	1.25	1.27
Tm–Yb	1.23	1.23	1.26
Yb–Lu	1.19	1.19	1.20

Mobile phase: 0.1 M α-HIBA, pH 2.5, flow rate: 1 mL/min.
[a] Actual amount of amide sorbed (mmol).
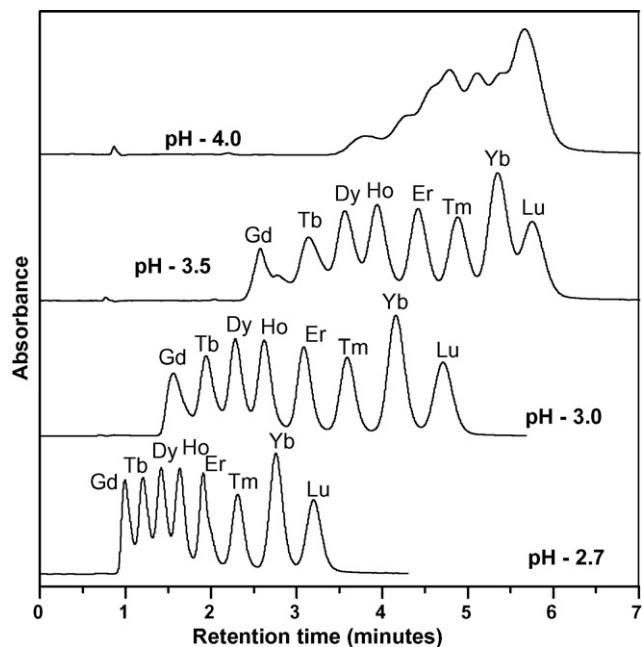
Fig. 12. Influence of mobile phase pH on retention behavior of lanthanides. B2EHM coated amount: 0.26 mmol; mobile phase: 0.05 M α-HIBA, flow rate: 2 mL/min; sample: lanthanides (10 μg/mL), injected amount: 20 μL; PCR: arsenazo(III), flow rate: 1.5 mL/min, detection: 655 nm.

3.3. Reproducibility of the modified columns

As a part of establishing the reproducible retention behavior, 4HEHHA, 4HHBA, MTDCMPA and B2EHM modified supports were investigated by studying the elution profiles of lanthanides, uranium and thorium. The capacity factors for both thorium and uranium did not vary even after passing several liters of mobile phase for all the supports under study. The reproducible coating behavior was also confirmed by washing the amide completely from the modified column with methanol and recoating the surface with the same concentration. Reproducible capacity factors were obtained for thorium, uranium and lanthanides.

3.4. Determination of cerium in uranium matrix: Analysis of pyrochemical reprocessing samples

The efficiency of the pyrochemical process [29] will be evaluated by the analysis of the cathode deposit and this requires analysis of lanthanides such as, cerium in trace levels in uranium matrix. Based on the encouraging results obtained with 4HEHHA support, a method has been developed for the rapid and accurate analysis of cerium in uranium matrix in a typical ratio of 1:10,000.

Several samples obtained from pyrochemical process were analyzed (Table 4) for their cerium contents in uranium matrix on a C_{18} column modified with 1×10^{-3} M 4HEHHA, using 0.1 M α-HIBA, as the mobile phase (pH 3), similar to experimental conditions shown in Fig. 2. Uranium contents of these samples were also determined. The results of these investigations were also compared with standard analytical methods. The cerium

Table 4
Estimation of cerium in uranium matrix of pyrochemical samples by HPLC

Sample (cathode deposit)	Uranium content (mg)	Cerium content (ppm)
1	17.8	4.8
2	13.2	4.6
3	20.1	2.1
4	16.5	2.1
5	19.4	4.5

Experimental conditions: C_{18} column modified with 1×10^{-3} M 4HEHHA; mobile phase: α-HIBA (0.1 M, pH 3). Concentrations of Ce (ICP-OES) and U (Davies and Gray method) were found to be in good agreement (within ±2%) with the HPLC technique.

concentrations were measured using ICP-OES (emission λ_{Ce}, 357.75 nm) after removing uranium matrix by solvent extraction and compared with the results obtained with the HPLC method. The concentration of uranium was also measured by Davies and Gray method and compared with HPLC. The cerium as well as uranium values were found to be in good agreement (within ±2%). These studies established that the HPLC method is fast, reliable and provides accuracy required for a typical routine analysis.

4. Conclusion

The retention behavior of uranium, thorium and lanthanides were investigated on various amide modified reversed phase supports. 4HHBA support showed higher separation factors for U–Th than bare C_{18}, 4HEHHA, MTDCMPA, and B2EHM supports. The 4HEHHA modified support was employed for the separation and assay of cerium in uranium matrix and it also offered rapid separation of U from Th in about 3 min. Hence this technique can be implemented for routine analysis.

A rapid and high-resolution separation technique for individual heavier lanthanides (Gd–Lu) has been developed using 4HHBA and B2EHM as column modifiers, and α-HIBA as mobile phase. With mandelic acid as the mobile phase, lighter lanthanides were also resolved from each other from a 4HHBA support. MTDCMPA modified columns also offered good resolution for certain lanthanides such as Eu, Sm and Nd and hence the method can be adopted for burn-up measurements using Nd as the fission monitor and in geochronology for age determination of rock samples.

The unusual elution order of lanthanides from a MTDCMPA support is to be further investigated. Modifications in diamide structural features may result in the development of a separation method for the isolation of entire lanthanide series. Studies on these aspects hold further excitement in the area of research.

References

[1] C.H. Knight, R.M. Cassidy, B.M. Recoskie, L.W. Green, Anal. Chem. 56 (1984) 474.
[2] K.N. Nicholson, S. Wood, J. Solution Chem. 31 (2002) 703.
[3] A. Munder, K. Ballschmiter, Z. Fresenius, Anal Chem. 327 (1987) 48.
[4] H.S. Zhang, W.Y. Mou, J.K. Cheng, Talanta 41 (1994) 1459.
[5] L.L. Ying, G. Ming-De, Z. Ya-Qiu, Talanta 42 (1995) 89.
[6] Z. Shi, C. Fu, Talanta 44 (1997) 593.
[7] J.M. Sanchez, O. Obrezkov, V. Salvado, J. Chromatogr. A 871 (2000) 217.

[8] L. Dongling, H. Xiaoyan, W. Haizhou, Anal. Chim. Acta 449 (2001) 237.

[9] C.A. Lucy, L. Gureli, S. Elchuk, Anal. Chem. 65 (1993) 3320.

[10] N. Sivaraman, S. Subramaniam, T.G. Srinivasan, P.R. Vasudeva Rao, J. Radioanal. Nucl. Chem. 253 (2002) 35.

[11] N. Sivaraman, R. Kumar, S. Subramaniam, P.R. Vasudeva Rao, J. Radioanal. Nucl. Chem. 252 (2002) 491.

[12] V. Vidyalakshmi, M.S. Subramanian, N. Sivaraman, T.G. Srinivasan, P.R. Vasudeva Rao, J. Liq. Chromatogr. Rel. Tech. 27 (2004) 2269.

[13] K. Robards, S. Clarke, E. Patsalides, Analyst 113 (1988) 1757.

[14] R.M. Cassidy, S. Elchuk, N.L. Elliot, L.W. Green, C.H. Knight, B.M. Recoskie, Anal. Chem. 58 (1986) 1181.

[15] R.M. Cassidy, S. Elchuk, Anal. Chem. 54 (1982) 1558.

[16] Hao Fuping, P.R. Haddad, P.E. Jackson, J. Carnevale, J. Chromatogr. 640 (1993) 187.

[17] Hao Fuping, B. Paull, P.R. Haddad, J. Chromatogr. A 739 (1996) 151.

[18] N.M. Raut, P.G. Jaison, S.K. Aggarwal, J. Chromatogr A 959 (2002) 163.

[19] S. Elchuk, K.I. Burns, R.M. Cassidy, C.A. Lucy, J. Chromatogr. 558 (1991) 197.

[20] W.N. Wang, Y.J. Chen, M.T. Wu, Analyst 109 (1984) 281.

[21] K. Yoshida, H. Haraguchi, Anal. Chem. 56 (1984) 2580.

[22] J.E. Girard, Anal. Chem. 51 (1979) 836.

[23] G. Thiollet, C. Musikas, Solvent Extr. Ion Exch. 7 (1989) 813.

[24] E.A. Mowafy, H.F. Aly, J. Radioanal. Chem. 250 (2001) 199.

[25] M. Akhila Maheswari, M.S. Subramanian, Sep. Sci. Tech. 39 (2004) 3629.

[26] M. Akhila Maheswari, M.S. Subramanian, Talanta 65 (2005) 735.

[27] D. Prabhakaran, M.S. Subramanian, Talanta 65 (2005) 179.

[28] M. Akhila Maheswari, M.S. Subramanian, Talanta 64 (2004) 202.

[29] S. Vavilov, T. Kobayashi, M. Myochin, J. Nucl. Sci. Tech. 41 (2004) 1018.

Short communication

Capillary electrophoresis for the determination of norfloxacin and tinidazole in pharmaceuticals with multi-response optimization

Ahmed Alnajjar, Hamed H. AbuSeada, Abubakr M. Idris *

Department of Chemistry, College of Science, King Faisal University, Al-Ahssa 31982, Saudi Arabia

Abstract

Capillary electrophoresis (CE) with UV photo-diode array detection technique was utilized to adopt new method for the analysis of norfloxacin and tinidazole in pharmaceuticals. Many CE aspects including separation, rapidity, sensitivity, ruggedness as well as the repeatability of qualitative and quantitative analyses were considered simultaneously for the purpose of optimization. Experimental design approach including factorial design and response surface methods were applied to optimize electrolyte concentration and the pH while injection time, voltage and column temperature were optimized using the univariate method. Successful results were obtained using 32.5 mmol l^{-1} phosphate electrolyte at pH 2.5, injection time 8.0 s, voltage 25 kV and column temperature 25 °C with detection at wavelength 301 nm. The analytical characteristics including recovery, intermediate precision, linear dynamic ranges, linearity and selectivity as well as limits of detection and quantification were demonstrated and the applicability to pharmaceuticals was studied. The newly provided method enjoys the advantages of CE over HPLC with respect to rapidity, ruggedness, simplicity in reagents and sample preparation as well as saving in reagents and samples.
© 2006 Elsevier B.V. All rights reserved.

Keywords: Capillary electrophoresis (CE); Experimental design; Pharmaceutical analysis; Norfloxacin; Tinidazole

1. Introduction

Norfloxacin (NFX) is a member of fluoroquinolones and it is chemically named as 1-ethyl-6-fluoro-1,4-dihydro-4-oxo-7-(piperazin-1-yl)quinoline-3-carboxylic acid (Fig. 1a). It is the first choice drug for the treatment of diseases caused by *Campylobacter*, *E. coli*, *Salmonella*, *Shigella* and *V. colera*. It is used for the treatment of gonorrhoea as well as eye and urinary tract infection [1].

Tinidazole (TNZ) is chemically named as (1-[2-(ethylsulphonyl)ethyl]-2-methyl-5-nitro-1H-imidazole (Fig. 1b). It is a 5-nitroimidazole derivative used for the treatment of giardiasis and susceptible protozoal infections. It has also been used in regimens for the eradication of Helicobacter pylori in peptic ulcer disease [2,3].

Previously, fluoroquinolones and 5-nitroimidazole were given individually to treat chronic nonspecific inflammatory conditions of the gastrointestinal tract [2]. Recently, NFX and TNZ were prepared in a combination. Therefore, analytical methods for their separation and simultaneous quantification are required for quality control purpose. A survey of literature reveals that no capillary electrophoresis (CE) method for simultaneous determination of these two antibiotics is available in the literature while other techniques were utilized including high performance liquid chromatography (HPLC) [3,4], high performance thin layer chromatography [5] and spectrophotometry [6–12].

The United States and British pharmacopoeias [13,14] proposed liquid chromatographic (LC) and potentiometric methods for the individual assay of NFX and TNZ in the generic form and pharmaceutical formulations. In addition, other methods including HPLC [15,16], packed column super critical LC [17], spectrophotometry [18–22], fluorescence [23] and chemiluminescence [24–27] as well as voltammetry [28,29] and polarography [30] were also provided for individual assay of NFX and TNZ in pharmaceuticals.

Traditionally, pharmaceutical analysis relies heavily on LC. CE has many advantages over LC that are including greater separation efficiency, small sample and reagents volume, fast
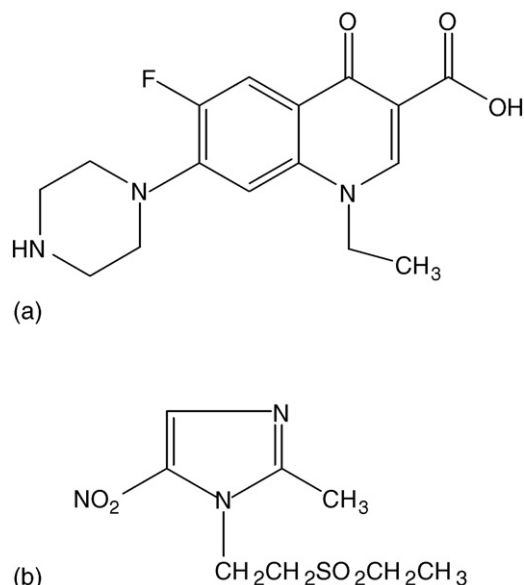
Fig. 1. Chemical structure of (a) NFX and (b) TNZ.

separation [31] and better ruggedness. Not least but more, unlike LC, reduction in sample preparation, simplicity in operating instrument and possibility of applying a single set of operating conditions to a wide variety of analytes all are available in CE analysis. These advantages empower CE with great utility to be successfully applied for routine pharmaceutical analysis.

Usually, experimental conditions affect the efficiency of chemical analysis and optimization of these conditions is always desirable. The univariate method is useful only for the optimization of irrelevant conditions. The experimental design, as multivariate methods, including factorial design and response surface are used to: (a) examine the main and interaction effects of conditions on the efficiency of analysis, (b) optimize simultaneously conditions regarding their interaction with minimum number of experiments and (c) reduce large amount of data that could be easily interpreted.

Analysis by CE generates large amount of data expressing selectivity, sensitivity, analysis time as well as precision; and many CE conditions potentially influence theses responses. This requires optimizing experimental conditions with considering CE responses simultaneously that can be performed using the multivariate methods. Unfortunately, the majority of the reported CE methods did not utilize the multivariate methods. This could be attributed to the fact that most of the CE practitioners have not yet discovered the inherent potential of the two scientific disciplines, i.e. CE analysis with multivariate optimization, working hand in hand.

The present work describes the development of a CE method for the analysis of NFX and TNZ in pharmaceutical formulations. Our attention was focused on the development of the major analytical aspects of the CE methods that are separation, rapidity, ruggedness and sensitivity as well as the repeatability of qualitative and quantitative analyses by optimizing the electrophoretic factors potentially controlling the analysis. Factorial design and response surface methods were utilized to optimize the relevant electrophoretic factors while other irrelevant electrophoretic factors were optimized using the univariate method.

2. Experimental

2.1. Chemicals and samples

All chemicals and reagents used in this study were of analytical grade. Cellulose, magnesium stearate, NFX, TNZ, starch and talc were supplied from Sigma–Aldrich (St. Louis, MO, USA). Phosphoric acid, sodium hydroxide and sodium phosphate were supplied from Merk (Darmstadt, Germany). Acetic acid, boric acid, sodium acetate and sodium tetraborate decahydrate were supplied from Sigma–Aldrich (Taufkirchen, Germany).

Conaz® tablets (400 mg NFX and 600 mg TNZ) was prepared by Pharaonia Pharmaceuticals (Cairo, Egypt).

2.2. Instrumentation and software

A P/ACE MDQ CE system coupled with a photo-diode array detector (PAD) supplied from Beckman (Fullerton, CA, USA) was used throughout the experiments. Separation was carried out in 31.2 cm long × 50 μm i.d. fused-silica capillary housed in a cartridge with a detector window 100 μm × 800 μm (10 cm to the detector, short way).

At each sequence experiment, the capillary was washed by 0.1 mol l^{-1} sodium hydroxide for 0.5 min and the separation electrolyte for 1.5 min. For sample loading, hydrodynamic injection mode was applied at the detector end of the capillary.

32 Karat Version 7.0 supplied from Beckman (Fullerton, CA, USA) was used for controlling the CE system as well as data acquisition and processing.

SigmaPlot® for Windows Version 8.0 supplied from Systat Software, Inc. (Point Richmond, CA, USA) was used for data interpolation and constructing response surface plots.

2.3. Preparation of standard solutions

Mixed primary standard solution was prepared by dissolving 100 mg NFX and 150 mg TNZ in about 80 ml of distilled deionized water with stirring in 100 ml volumetric flask. The volume was completed to the mark and stored protected from light at 4 °C, at this condition the solution is stable for at least 2 weeks. Working standard solutions were prepared from the primary standard solution by dilution in the appropriate way.

2.4. Preparation of samples

Twenty Conaz® tablets were powdered and amounts equivalent to 10 mg NFX and 15 mg TNZ were weighed and dissolved by stirring in about 80 ml of distilled deionized water. The solution was filtered in a 100 ml volumetric flask and filled to the mark. Other pharmaceutical samples were synthesized in our laboratories including NFX and TNZ in different concentrations with excipients (including cellulose, magnesium stearate, starch and talc) usually found in tablets formulation. In addi-

tion, placebo samples were also prepared including the same excipients.

3. Results and discussion

3.1. Preliminary investigation

Principally, solutes in CE analysis should be at least partially ionized. NFX has two relevant ionizable functional groups that mean their acid–base chemistry involves two equilibria, the dissociation of the carboxylic group and the deprotonation of the nitrogen of the piperazine ring (Fig. 1a) [32]. TNZ has a heterocyclic structure consisting of imidazole-based nucleus with nitro group. The nucleus contains two tertiary amine groups (Fig. 1b), which could be also protonated [33]. Therefore, separation of NFX and TNZ by CE is available.

The PAD at the wavelength range of 190–400 nm individually performed spectrum scan for NFX and TNZ. At 301 nm, higher absorbance by each drug was obtained and hence it was set for further measurements.

Acetate/acetic acid, borate/boric acid and phosphate/phosphoric acid in different concentrations with different pH values were examined. With respect to separation, peak shape and noise, better but not sufficient results were obtained by phosphate electrolyte and hence it was used for further method development.

3.2. Method optimization

Unless otherwise described, the term "responses" refers here to the aspects that would be developed in this study involving separation, rapidity, sensitivity, ruggedness as well as the repeatability of qualitative and quantitative analyses. The criteria that evaluated the separation is the resolution, which was calculated using Eq. (1) [34].

$$R = \frac{2(t_{m1} - t_{m2})}{(w_1 + w_2)} \qquad (1)$$

where R is the resolution, t_m is the migration time and w is peak width.

On the other hand, the sensitivity and rapidity were evaluated throughout the peak area and migration time, respectively. The relative standard deviation (R.S.D., $n = 10$) of the peak area and migration time were used to evaluate the repeatability of qualitative and quantitative analyses, respectively.

3.3. The univariate method

The most common range of the voltage used in CE is 5–30 kV [35], which was examined in this study. Higher voltage reduced analysis time and some loss in separation was occurred. Twenty-five kilovolt obtained suitable analysis time and better separation and thus it was adopted for further optimization.

One to twenty seconds, as the suitable range of the injection time [35], was examined at pressure 0.5 p.s.i. Injection time improves signal and causes some loss in resolution and peak

symmetry [35]. Eight seconds obtained acceptable result, which was used as the optimum.

The practicable range of column temperature that is, i.e. 15–30 °C [35], was applied. The temperature seemed to have no significant effect on the responses and therefore the normal temperature that is 25 °C was set for further analysis.

3.4. The factorial design and response surface methods

Factorial design and response surface are powerful tools when used as a part of optimization; in this concern, detailed information is available elsewhere [36]. When applying these methods, it is advisable to keep the number of variables as low as possible in order to avoid complex response models and large variability. Therefore, the relevant electrophoretic factors those are electrolyte concentration and pH were adopted to be optimized using these methods.

In this study, the 2^2 full factorial design was applied. The 10 and 55 mmol l^{-1} levels were examined as phosphate electrolyte concentration. Higher concentration is not generally possible because of internal heating problems within the capillary although it could improve the peak shape [35]. Lower concentration means lower conductivity, which increases analysis time but some loss in separation might be occurred. For the pH levels, 2.5 and 9.5 were examined. Lower pH increases the ionization of base solutes while higher pH increases the electro-osmotic flow (EOF).

Four experiments, as the result of the adopted factorial design, were conducted under other CE conditions optimized by the univariate method. The main and interaction effect factors (E_f) (electrolyte concentration and pH) on the response were calculated using Eq. (2) [36].

$$E_f = \frac{\sum y(+1)}{n} - \frac{\sum y(-1)}{n} \qquad (2)$$

where $y(+1)$ and $y(-1)$ are the response values at the maximum and the minimum levels of the examined factor, respectively; n is the number of variables at the same level (in this design, $n = 2$). The results obtained are introduced in Table 1.

In general, the pH effect on the response is the most dominant factor. This could be attributed to the fact that pH potentially effects on both electrophoretic mobility of solutes and the ionization of the acidic silanols of the capillary wall [35]. The electrolyte concentration is in the second order of effect. The ionic strength of the electrolyte that is related to its concentration has significant effect on the mobility of the solutes and hence on the separation [35]. The negative effect of the pH on the resolution, migration time and sensitivity indicates NFX and TNZ have more tendency to be ionized in lower pH, i.e. ionization increases the charge-to-size ratio and the mobility. The repeatability of the qualitative analysis was found to be co-related with the repeatability of the quantitative analysis, which agreed with a study reported elsewhere [37].

The coded levels of the adopted factorial design with their respective responses were interpolated and the response surface plots were constructed as a function of the electrolyte concentration and the pH. The surface plots of the resolution and the

Table 1
The main and interaction effect factors of electrolyte concentration and pH on the responses

Type of effect	Effect factor								
	R^a	$t_m{}^b$		R.S.D.^{c}, t_m		PA^d		R.S.D., PA	
		NFX	TNZ	NFX	TNZ	NFX	TNZ	NFX	TNZ
EC^e	1.50	−0.24	1.02	0.62	−0.13	6952	20710	−1.62	0.60
pH	−2.27	−0.66	−2.49	0.91	−2.78	−32683	−29774	1.71	−2.02
BC × pH^f	−1.02	0.07	−0.90	2.11	0.91	4501	−7353	1.19	−1.33

[a] Resolution.
[b] Migration time.
[c] Relative standard deviation ($n = 10$).
[d] Peak area.
[e] Electrolyte concentration.
[f] Interaction of electrolyte concentration and pH.

peak area of the both drugs appeared similar trend that is the separation and sensitivity increased toward higher electrolyte concentration and lower pH (Fig. 2 as an example). The analysis time of both drugs could be reduced at lower pH while the effect of electrolyte concentration on this response was negligible. Good ruggedness with respect to the repeatability of quantitative analysis for NFX was recorded in another surface plot, while the same migration time could be obtained at all levels of electrolyte concentration and pH with the exception of their high levels. Relatively, less ruggedness with respect to the repeatability of migration time of TNZ was recorded, where the same migration time could be obtained at many levels of electrolyte concentration and pH except high levels of the electrolyte concentration and low levels of the pH. Although adverse trends of the repeatability of peak area for both drugs were recorded, acceptable repeatability (R.S.D. less than 2.5%) could be obtained at wide ranges of both electrolyte concentration and pH.

The findings of the factorial design and response surface methods are that lower pH obtained better responses while other pH levels obtained different trends of the response. Hence, the pH 2.5 was adopted as the optimum. For the electrolyte con-

Fig. 2. Response surface plot of the resolution of NFX and TNZ as a function of electrolyte concentration and pH.

centration, no similar trend of the responses was recorded and therefore fitting the responses with each other is required. At the medium level of the electrolyte concentration, sufficient separation and suitable analysis time could be obtained, resolution above 1.5 with migration time 1.30 and 1.66 min for NFX and TNZ, respectively. In addition, at the same level of the electrolyte concentration, acceptable repeatability, R.S.D. less than 2.5%, of both qualitative quantitative analyses for NFX and TNZ, could be obtained. Thus, 32.5 mmol l^{-1} phosphate electrolyte was adopted as the optimum.

3.5. Method validation

A long series of mixed standard solutions including NFX and TNZ with different concentrations were examined under the optimized conditions. The method was found to be linear in the ranges of 10–50 and 15–75 mg l^{-1} with weighed regression described in Eqs. (3) and (4) for NFX and TNZ, respectively.

$$PA = 0.8304C + 0.8694, \quad r = 0.9996 \tag{3}$$

$$PA = 0.7716C - 2.8777, \quad r = 0.9998 \tag{4}$$

where PA is the peak area, C the concentration in mg l^{-1} and r is the correlation coefficient.

The limits of detection (LOD) and quantification (LOQ) were calculated. LOD was obtained as the concentration of solute resulting in a peak height three times the baseline noise level. LOQ was calculated as 10 times the baseline noise level. LOD for NFX and TNZ were 0.1 and 1.0 mg l^{-1}; LOQ were 0.33 and 3.33 mg l^{-1}, respectively.

The placebo samples were examined and no peak was recorded indicating the method is selective in the presence of excipients usually found in tablets formulation. In addition, the method was applied to the synthetic pharmaceutical samples. The recovery obtained was in the range of 89.3–101.4% indicating the reliability of the results obtained from the proposed method. The method was also applied to the tablets formulation and the typical electropherogram was depicted in Fig. 3. Figure shows successful separation and acceptable peaks shape.

To examine the intra-day precision, 10 runs were conducted in 10 consequent days for different concentrations of NFX and TNZ in tablets formulation. The R.S.D. of the migration time
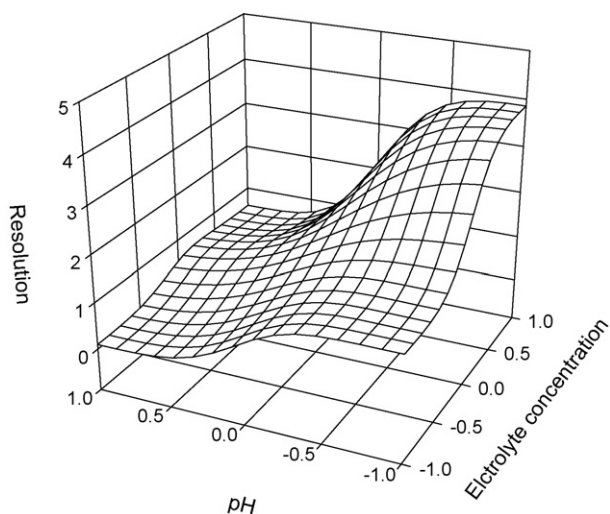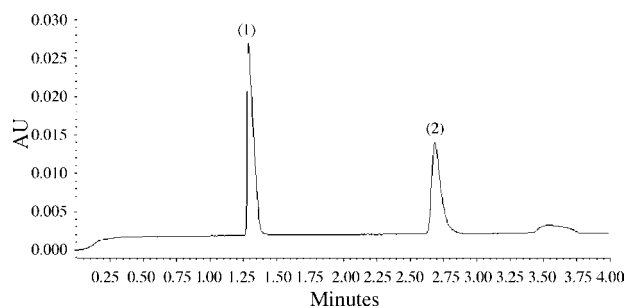
Fig. 3. Electropherogram of (1) NFX and (2) TNZ in tablets formulation under the optimized conditions: 8.0 s injection time, 25 kV voltage, 25 °C, 32.5 mmol l^{-1} phosphate electrolyte concentration, pH 2.5.

did not exceed 1.30% while the R.S.D. of the peak area was bellow 1.80%.

4. Conclusion

In this study, a simple, direct, rapid, rugged CE method was developed for simultaneous quantification of NFX and TNZ in pharmaceuticals. Multi-response of the CE method was developed by optimizing the relevant factors by applying the experimental design methods with minimum number of experiments. The univariate methods were successfully applied to optimize other irrelevant factors. NFX and TNZ were separated in 1.30 and 1.66 min, respectively. The method was linear in the range of 10–50 and 15–75 mg l^{-1} for NFX and TNZ, respectively, with correlation coefficients more than 0.9995. The LOD for NFX and TNZ were 0.1 and 1.0 while the LOQ were 0.33 and 3.33 mg l^{-1}, respectively. The repeatability and the intermediate precision of the quantitative and qualitative analyses for both drugs did not exceed 1.8%.

References

[1] A.R. Martin, in: J.N. Delgado, W.A. Remers (Eds.), Textbook of Organic Medicinal and Pharmaceutical Chemistry, Lippincott, Philadelphia, PA, 1991, p. 155.

[2] B.G. Katzung, Basic and Clinical Pharmacology, Lange Publications, Berlin, 1982, p. 593.
[3] S.K. Ghosh, M. Banerjee, Indian Drugs 33 (1996) 127.
[4] A.P. Argekar, S.U. Kapadia, S.V. Raj, J. Planar. Chromatogr. Mod. TLC 9 (1996) 208.
[5] A.P. Argekar, S.U. Kapadia, S. Raj, Anal. Lett. 29 (1996) 1539.
[6] P.P. Dahibhate, O.D. Chandwani, S.S. Kadam, S.R. Dhaneshwar, Indian Drugs 34 (1997) 48.
[7] G.K.S. Reddy, M.S. Bhatia, D.K. Jain, P. Trivedi, Indian Drugs 34 (1997) 190.
[8] C.V.N. Prasad, C. Parihar, K. Sunil, P. Parimoo, Pharm. Sci. 3 (1997) 337.
[9] H.N. More, K.R. Mahadik, S.S. Kadam, Indian Drugs 36 (1999) 144.
[10] G.K.S. Reddy, D.K. Jain, P. Trivedi, Indian J. Pharm. Sci. 61 (1999) 16.
[11] R. Gupta, A.K. Singhai, R.K. Agrawal, Indian Drugs 37 (2002) 348.
[12] R.K. Maheshwari, R.B. Maheshwari, P. Bhatt, Asian J. Chem. 18 (2006) 1481.
[13] United States Pharmacopoeia, E-copy on CD, Ver. 26 NF-21, 2003.
[14] British Pharmacopoeia, E-copy on CD, Ver. 6.0, 2002.
[15] L.A. Shervington, M. Abba, B. Hussain, J. Donnelly, J. Pharm. Biomed. Anal. 39 (2005) 769.
[16] Y.R. Ku, M.J. Tsai, K.C. Wen, J. Food Drug Anal. 4 (1996) 146.
[17] I.C. Bhoir, B. Raman, M. Sundaresan, A.M. Bhagwat, Anal. Chim. Acta 354 (1997) 123.
[18] A.M. El-Brashy, M.E. Metwally, F.A. El-Sepai, Farmaco 59 (2004) 809.
[19] M.V. Bombale, S.S. Kadam, S.R. Dhaneshwar, Indian J. Pharm. Sci. 59 (1997) 265.
[20] L. López-Martínez, F.J.L. Vazquez, P.L. Lopez-De-Alba, Anal. Chim. Acta 430 (1997) 241.
[21] P. Nagaraja, K.R. Sunitha, R.A. Vasantha, H.S. Yathirajan, J. Pharm. Biomed. Anal. 28 (2002) 527.
[22] A.B. Prasad, N.R. Reddy, Y.V.B. Reddy, I.E. Chakravarthy, Asian J. Chem. 16 (2004) 1905.
[23] L.M. Du, H.Y. Yao, M. Fu, Spectrochim. Acta Part A 61 (2005) 281.
[24] Y. Han, X. Wu, J. Yang, S. Sun, J. Pharm. Biomed. Anal. 38 (2006) 528.
[25] Z. Xie, S. Liao, G. Chen, Luminescence 20 (2005) 220.
[26] H. Ma, X. Zheng, Z. Zhang, Luminescence 20 (2005) 303.
[27] S.L. Chen, Y. Liu, H.C. Zhao, L.P. Jin, Z.L. Zhang, Y.Z. Zheng, Luminescence 21 (2006) 20.
[28] S.A. Ozkan, Analusis 25 (1997) 130.
[29] C. Yang, Anal. Sci. 20 (2004) 821.
[30] D.M. Joshi, A.P. Joshi, Indian Drugs 33 (1996) 338.
[31] G. Currell, Analytical Instrumentation, Performance Characteristics and Quality. Analytical Techniques in the Sciences, Wiley, 2000, p. 172.
[32] H. Lu, X. Wu, Z. Xie, X. Lin, L. Guo, C. Yan, G. Chen, J. Sep. Sci. 28 (2005) 2210.
[33] J.A. Hemandez-Arteseros, J. Barbosa, R. Compano, M.D. Prat, J. Chromatogr. A 945 (2002) 1.
[34] N. Ortega, S.M. Albillos, M.D. Busto, Food Control 14 (2003) 307.
[35] K.D. Altria, Capillary Electrophoresis Guidebook, Humana Press, Totwa, New Jersy, 1996.
[36] E.D. Morgan, Chemometrics: Experimental Design, ACOL, John Wiley and Sons, London, 1991.
[37] A.G. Ewing, R.A. Wallingford, T.M. Oliferowicz, Anal. Chem. 61 (1989) 292.

Review

Determination of vanadium in petroleum and petroleum products using atomic spectrometric techniques

Fábio A.C. Amorim [a,b], Bernhard Welz [a,c], Antônio C.S. Costa [a], Fábio G. Lepri [c], Maria Goreti. R. Vale [d], Sérgio L.C. Ferreira [a,*]

[a] *Universidade Federal da Bahia, Instituto de Química, Grupo de Pesquisa em Química Analítica, Campus Universitário de Ondina, Salvador, BA 40170-290, Brazil*
[b] *Universidade Federal da Bahia, Instituto de Ciências Ambientais e Desenvolvimento Sustentável, Av. José Seabra s/n, Barreiras, BA 40805-100, Brazil*
[c] *Universidade Federal de Santa Catarina, Departamento de Química, Campus Trindade, Florianópolis, SC 88040-900, Brazil*
[d] *Universidade Federal do Rio Grande do Sul, Instituto de Química, Av. Bento Gonçalves 9500, Porto Alegre, RS 91501-970, Brazil*

Abstract

Vanadium is recognized worldwide as the most abundant metallic constituent in petroleum. It is causing undesired side effects in the refining process, and corrosion in oil-fired power plants. Consequently, it is the most widely determined metal in petroleum and its derivatives. This paper offers a critical review of analytical methods based on atomic spectrometric techniques, particularly flame atomic absorption spectrometry (FAAS), electrothermal atomic absorption spectrometry (ET AAS), inductively coupled plasma optical emission spectrometry (ICP OES), inductively coupled plasma mass spectrometry (ICP-MS). In addition an overview is provided of the sample pretreatment and preparation procedures for vanadium determination in petroleum and petroleum products. Also included are the most recent studies about speciation and fractionation analysis using atomic spectrometric techniques.
© 2007 Published by Elsevier B.V.

Keywords: Vanadium determination; Crude oil; Petroleum products; Atomic spectrometric techniques; Speciation analysis

Contents

* Corresponding author. Fax: +55 71 2355166.
E-mail addresses: slcf@ufba.br, sergio1057@hotmail.com (S.L.C. Ferreira).

1. Introduction

Vanadium is a transition metal that is widely distributed in the earth's crust with an average abundance of $0.14\,mg\,kg^{-1}$; it is the 20th most abundant element and the 5th among the transition metals. It is naturally found in minerals (varnotite, patronite, roscoelite and vandinite), and also combined with coal and petroleum. In its compounds it occurs in oxidation states from -1 to $+5$, but the most common ones are $+3$, $+4$ and $+5$. The most stable oxidation state is the tetravalent salt (VO^{2+}, vanadyl) [1–3].

Vanadium is categorized as an essential trace element for plants and animals, which stimulates the synthesis of chlorophyll and promotes the growth of young animals. Its role as an essential trace element for humans has not yet been established, as no deficiency-related diseases have been identified. Food is the major intake of vanadium for the general population ($<10\,\mu g\,dia^{-1}$). Vanadium might also have some therapeutic effect. Studies indicate some promise in the area of diabetes by lowering blood sugar levels in diabetic animals and patients. There are also vanadium compounds that exhibit chemotherapeutic significance in the treatment of leukemia [4,5].

A recently published review presents several methods for determination of vanadium species in environmental samples [6]. In general, the toxicity of vanadium compounds is considered to be low, however, exposure to vanadium dust results in upper respiratory tract irritation characterized by rhinitis, wheezing, nasal hemorrhage, cough, sore throat, and chest pain [7]. These effects are observed on workers exposed to vanadium-rich ash from crude oil and other fossil fuels, especially of fuel oil that is available for the concentration of vanadium in blood, serum, urine, and hair [8–10]. High air concentrations might occur in the occupation setting during boiler-cleaning operations as a result of the presence of vanadium oxides in the dust, and by burning fossil oils and coal.

2. Vanadium in petroleum and petroleum products

Study of concentration of metallic elements present in crude oil has been used in geochemical interpretations related to thermal maturity, oil–oil and oil–rock correlation, in primary and secondary migration studies; the trace metal content is a characteristic of the geographic location of where the oil was produced [11]. Trace metals can have a negative influence on the refining process and degrade the quality of intermediate and end products. Besides that, there is concern about the potential contamination of the environment, because metals enter the environment through combustion products of the refined oil. All of these factors point towards the need to characterize petroleum based on its trace metal content.

Vanadium is usually the most abundant trace metal in petroleum samples; it might be found in concentration levels up to $1500\,mg\,kg^{-1}$, although some crude oils contain less than $0.1\,mg\,kg^{-1}$. Its occurs predominantly as the vanadyl ion (VO^{2+}) in the form of organometallic complexes with porphyrins (vanadyl porphyrins), which originate from the formation of crude oil, for the substitution of the Mg of plant chlorophylls

with the trace element, and with other largely unknown non-porphyrins or as the cation of organic acids. In the porphyrin complexes, vanadium is bound by four nitrogen donor atoms while in the non-porphyrin compounds nitrogen, oxygen and sulfur can all act as donor atoms in various combinations such as in β-diketones, β-ketoimines, salicylaldimines, monothio- and dithio-β-diketones, mono- and dithio-carbamates, etc. [12,13]. The chemical structure of some typical vanadyl porphyrin and non-porphyrin complexes is shown in Fig. 1.

There is a need for the quantification of vanadium in crude oil and its derivatives since it is a serious catalyst poison, and may cause undesirable side reactions in refinery operations. Pore blocking, fouling of active sites and change in catalysts selectivity are typical problems [14]. Vanadium compounds also cause corrosion problems that derive from the formation, e.g., in the combustion chamber of power plants, of sodium vanadates, which have low melting points; the molten vanadates react with the metal surface of the super heaters and form the metal oxide [15]. In addition, the knowledge of the concentration ratio of vanadium to other metals, particularly the V/Ni ratio in petroleum, provides useful geological information about the maturation and evaluation of the paleo-environmental conditions of sedimentation [16]. The V/Ni ratio is actually bore-hole specific and can be used to identify the geographic origin of a crude oil, for example in case of an oil spill.

3. Vanadium determination using atomic spectrometric techniques

A variety of atomic spectrometric techniques have been used for the determination of vanadium, among which are atomic absorption spectrometry (AAS) with flame and graphite tube atomizers, inductively coupled plasma optical emission spectrometry (ICP OES), inductively coupled plasma mass spectrometry (ICP-MS) and X-ray fluorescence spectrometry (XRF). It is beyond the scope of this review to describe these analytical techniques, and the reader is referred to several excellent text books and review articles for a detailed description [3,17,18].

This review includes a retrospect from the early to the most recent significant contributions in the fields of sample preparation, direct analysis and studies of characterization and distribution of vanadium in petroleum and petroleum products using the spectroanalytical techniques mentioned above. Other techniques might be used, but they are not widely found in the literature.

3.1. Methods for sample preparation

For the determination of vanadium in petroleum and petroleum products using spectroanalytical techniques it is necessary to use an appropriate sample preparation in order to avoid measurement errors. Nowadays, the selection of a sample preparation procedure involves the task to obtain the best results in the shortest time, with minimum contamination, using the smallest quantities of reagents and samples, and having little residue and waste generation. In addition it is of importance to maintain the integrity of the sample and the traceability of the results, to have
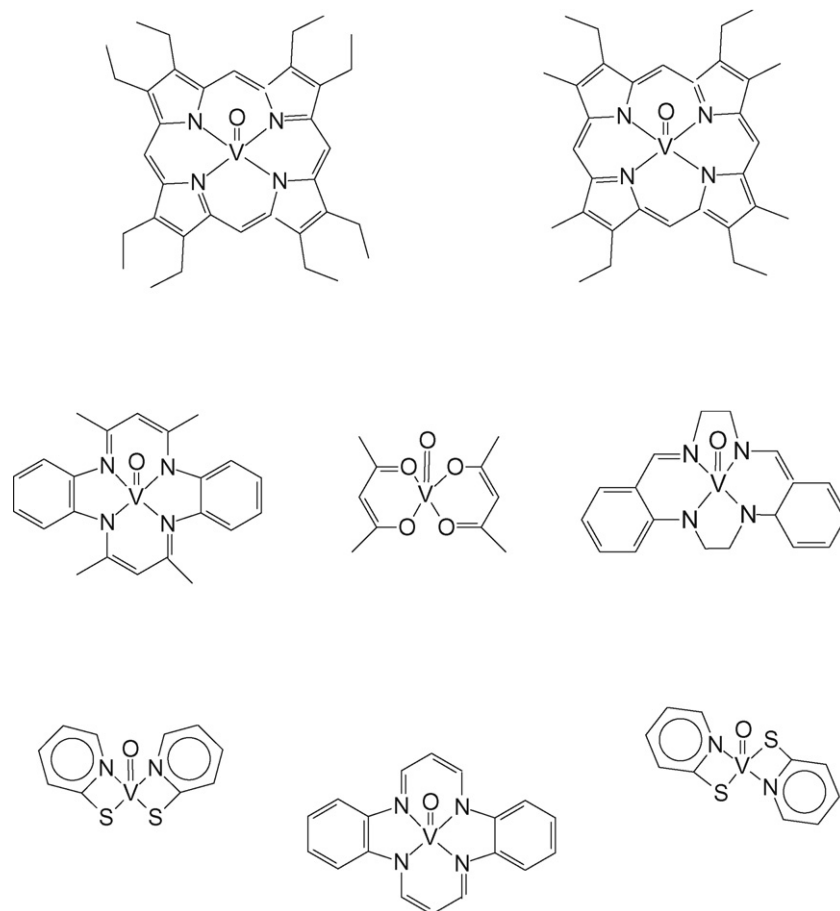
Fig. 1. Chemical structures of typical vanadyl porphyrin and non-porphyrin complexes in crude oil.

quality and confidence in the measurements. This task involves parameters, such as choice of the proper analytical technique, number of samples, desired accuracy and precision, availability of equipment, and the applicable dilution factor [19,20].

The principal sample preparation methods used for vanadium determination in petroleum and petroleum products by spectro-analytical techniques, besides direct analysis, are dilution with organic solvents, dilution in three-component systems (emulsion or micro-emulsion), dry ashing, and wet acid digestion.

Direct analysis using little or no sample preparation is most suitable for electrothermal (ET) AAS with a graphite tube furnace [21] and XRF [22]. The main advantage of direct analysis is obviously the time saving and the minimum risk of analyte loss. The main problem might be in calibration, as standards might behave differently from the samples, an effect that cannot be compensated for by matrix matching or the analyte addition technique.

Dilution with organic solvents is an attractive preparation method because it is rapid and simple; it can be used for all analytical techniques mentioned in this review. The solvents used most frequently are xylene, kerosene and methyl isobutyl ketone (MIBK), but dimethylbenzene, propan-1-ol, heptane, *n*-pentane, and mixtures of these solvents have been used as well. This procedure does not minimize the high organic load, which is mostly a problem for the ICP-based techniques, and necessarily requires the use of expensive metal-organic calibration solutions prepared in the same way. At the microgram-per-liter range such calibration solutions may change in concentration rapidly by evaporation and/or sorption of the analyte on the walls of the storage container, resulting in analytical errors [23,24]. In addition, various organic compounds of vanadium have been found to exhibit different sensitivity, particularly in flame AAS, which makes the choice of the proper organic compound used for calibration particularly difficult.

Alternatively, the oil sample might be modified by formation of an emulsion or micro-emulsion (three-component system). Whenever two immiscible liquids are stirred, a macro-emulsion is obtained, either oil-in-water (O/W, droplets of oil in water) or water-in-oil (W/O, droplets of water in oil), depending on the dispersed phase. The kind of emulsion that is formed is mainly related to the formulation and to a lesser degree to the W/O ratio. In this case, a co-solvent allows the formation of a homogeneous system containing both the aqueous and the organic phase, resulting in a homogeneous and long-term stable three-component solution [25,26]. An emulsion, a cloudy mixture, is prepared agitating a mixture of water, oil and one or more surfactants under controlled experimental conditions. A micro-emulsion is kind of an emulsion in which the droplets are much smaller, thus the light passes through without much scattering, i.e., it appears as a clear solution. Micro-emulsions are formed by a mixture of water, oil and an organic co-solvent, such as a short-chain alcohol (i.e. propan-1-ol), because its molecules

are inserted in between the surfactant molecules and push them apart, with a corresponding reduction in polar interactions and rigidity. However, micro-emulsions are dynamic systems that form, disintegrate and reform in fractions of milliseconds. As a rule, a hydrophilic surfactant is needed to produce an O/W emulsion, a hydrophobic surfactant to make a W/O emulsion, and a surfactant of intermediate hydrophilic property results in a micro-emulsion. The main advantage of micro-emulsions is their long-term stability although they require a high amount of surfactant (about five times the one needed to form an emulsion) and are very sensitive to temperature changes [27].

Emulsions and micro-emulsions have been successfully applied for the preparation of oil samples, due to the homogeneous dispersion and stabilization of the oil micro-droplets in the aqueous phase, which reduces oil viscosity and the organic load of the system. For ET AAS, it has been demonstrated that the use of emulsions of fuels (gasoline and kerosene), acidified with HNO_3, made possible direct correlation between the signals of the analyte in the sample in aqueous standard solutions [28,29]. The introduction of oil samples as emulsions has been used for the determination of metals in techniques that use nebulization systems, such as FAAS, ICP OES and ICP-MS. The details of these procedures will be discussed in connection with each of these techniques. Comparison with established methods (acid digestion or dilution in an organic solvent) shows that the emulsion or micro-emulsion methodology presents clear advantages in terms of simplicity of sample preparation, total analysis time, long-term sample stability and the use of inorganic standards for calibration instead of expensive metal-organic standards [30,31].

Organic solvents and O/W emulsions used in an ICP might require specially designed torches, nebulizers, modifications to the argon flow, and addition of oxygen as an auxiliary gas due to the volatile nature of organic solvents as opposed to aqueous solutions, and in order to maximize carbon combustion and minimize background. One concern for nebulization systems (FAAS and ICP) is the difference in viscosity between samples and calibration solutions, causing different uptake rates and aerosol configuration. The resulting transport interferences can be detected and compensated through the use of the analyte addition or reference element (internal standard) techniques.

Sample digestion is performed for partial or total decomposition of the organic matter. The digestion systems were evaluated in terms of accuracy and precision, reagents and time saving, residual organic carbon content and the resulting limits of detection (LOD). Dry or wet digestion procedures may be used for petroleum and petroleum products [32].

Dry ashing is used for the almost complete elimination of organic materials prior to analyte determination, and consists of the ignition of the organic matrix in air or in a stream of oxygen, followed by dissolution of the residue in an acid medium. The time required for this procedure is one of the disadvantages of this method. Another one is the risk of losses of volatile elements and their compounds. This method has also been applied for vanadium [33], however, although this element is usually considered to be thermally stable, some compounds have been found to be volatile at relatively low-temperature, as will be discussed in detail later.

For wet digestion, oxidizing agents are used to decompose the organic constituents prior to analyte determination. Normally concentrated acids are applied under heating, and the important aspects to consider are the strength of the acids, their oxidizing and complexing power, their boiling points, the solubility of the resulting salts, safety in manipulation, and purity. The acids and oxidizing agents used for oil samples include mixtures of nitric, hydrochloric and sulfuric acids and hydrogen peroxide. Wet digestion procedures for oil samples can be performed in closed or open vessels, using thermal energy or microwave radiation. Microwave heating offers a considerable advantage in time over thermal heating. Many microwave-assisted sample preparation systems offer multi-sample preparation with temperature and pressure control features. For wet digestion procedures it is important to consider the time consumption (several hours) and the amount of reagents used, in comparison to the dilution methods.

3.2. Flame atomic absorption spectrometry (FAAS)

Vanadium determination by FAAS requires the use of a nitrous oxide–acetylene flame. The characteristic concentration at the 318.5-nm analytical wavelength is about $2\,mg\,L^{-1}$, a sensitivity that is considered not to be sufficient for most applications. Kragten [34] observed that the sensitivity for vanadium depended on the oxidation state, and the pentavalent state exhibited the best sensitivity. The effect of added alkali metals and of halogen to the vanadium determination in organic solutions and petroleum samples has been studied by Lang et al. [35,36].

There were several publications about the determination of vanadium in petroleum products using FAAS in the 1970s [37], however, little has been published in later years. The main advantage of this technique appears to be that a direct determination of the analyte in the hydrocarbon matrix might be possible after corresponding dilution with an organic solvent or after formation of an O/W emulsion.

A direct method for the determination of V in fuel oils by FAAS has been developed by Bettinelli and Tittarelli [38]. Fifty-four European laboratories participated in a round-robin test, which was carried out on six fuel oil samples in order to evaluate the accuracy and precision of the method, using various procedures and instrumental techniques. The control of accuracy and the comparison of results obtained by independent techniques allowed validation of the proposed method.

Platteau and Carrillo [39] developed a method for the determination of V and other metals in highly stable O/W emulsions using FAAS. The emulsions were prepared with the sample (fuel, lubricating and crude oils), linear alkylbenzene, sulfonic acid and ethanol. Recoveries ranged from 95 to 104% with relative standard deviations lower than 4%. Lakatos et al. [40] investigated the proportion of aerosol desolvatation in sample introduction in different systems and the possibility of solvent-independent sample introduction based on nebulization of O/W emulsions. It was found that desolvatation governs sample intro-

duction if the volatility of the solvent is high and the aerosol concentration in the chamber is small.

Hydraulic high-pressure nebulization (HHPN) has been employed for sample introduction of petroleum and lubricating oil samples in FAAS and FOES for the determination of vanadium and a number of other analytes. Using this technique an aerosol is produced by means of an HPLC pump. With this system LOD decreases by a factor of 2–4 in comparison with sample dilution required by pneumatic nebulization [41]. The behavior of a single-bore high-pressure pneumatic nebulizer (SBHPPN) as a tool for the analysis of lubricating oils was investigated by Mora et al. [42]. A pneumatic concentric nebulizer (PCN) was used for comparison. The SBHPPN provided higher sensitivity and a lower LOD than the PCN. Moreover, the SBHPPN provided results similar to those obtained using a previous acid digestion step.

Other methods proposed for vanadium determination in petroleum products using FAAS are synergistic extraction with organic acids (5,5′-methylene-disalicylohydroxamic acid) [43]; ashing, microwave-assisted digestion and burning in a modified calorimetric bomb [44,45].

3.3. Electrothermal atomic absorption spectrometry (ET AAS)

In spite of its relatively high meting point of 1929 °C, vanadium can be determined very well by ET AAS. The atomization mechanism in the graphite tube is most likely via the thermal decomposition of the carbide [46,47]. Pyrolysis temperatures around 1200–1500 °C can be applied in several situations; however, low-temperature losses of volatile vanadium compounds have been reported in the absence of a modifier, as will be discussed below. An atomization temperature of at least 2650 °C and wall atomization is necessary in a longitudinally heated atomizer; platform atomization and a somewhat lower atomization temperature may be used with a transversely heated atomizer. The characteristic mass is around 30–40 pg, varying with the tube dimensions and the modifier or tube surface treatment.

Electrothermal AAS might be able to analyze oil samples directly if low-temperature losses of volatile vanadium compounds are avoided. In the pyrolysis stage, the sample is treated for elimination of the majority of the organic matrix, resulting in a shorter sample preparation time, reduced risk of sample contamination and elimination of hazards due to the use of acids and organic solvents. Several methods for the determination of vanadium in petroleum products have been developed using ET AAS.

A procedure has been described for the digestion of crude oil by microwave heating in the presence of a 1 + 3 mixture of HNO_3 and H_2SO_4. The solutions obtained were analyzed for V, Cr, Cu, Fe, Mn and Ni by ET AAS, using platform atomization. This microwave-assisted sample treatment produced solutions ready for analysis in approximately 25–30 min [48].

Barrera et al. [49] studied the determination of vanadium in petroleum samples employing three procedures of sample preparation: dilution with xylene, dry calcination and wet digestion

with sulfuric acid and hydrogen peroxide, and the xylene dilution and dry calcination were found to be the best procedures.

Aucelio et al. [50] developed a method for the analysis of diesel and asphaltene, where samples were stabilized as detergentless micro-emulsions by mixing with propan-1-ol and nitric acid. No modifier was used and wall atomization was applied. For diesel, aqueous analytical solutions could be used for calibration. For asphaltene, calibration was performed with analytical solutions prepared in dichloromethane + propan-1-ol + nitric acid medium, spiked with inorganic standard solution. Good recoveries were obtained for diesel samples spiked with V-cyclohexanebutyrates, and coherent results were found for the asphaltene fraction of the certified reference material NIST 1634c (trace elements in fuel oil). dos Santos et al. [51] proposed an alternative method to determine vanadium and molybdenum in multiphase gasoline emulsions. Samples were prepared by mixing gasoline with a nitric acid solution (0.1%, v/v) and two cationic surfactants (N-cetylpiridineum bromide and cetyltrimethylammonium bromide). The mixture was sonicated, resulting in an emulsion. Calibration was carried out using the same solutions with added analyte. The accuracy was evaluated by the analysis of samples spiked with a metal-organic standard, and a characteristic mass of 123 pg was reported, which is clearly inferior to literature data.

A variety of modifiers, including magnesium nitrate, palladium and platinum have been proposed for the determination of vanadium [3], although most vanadium compounds are thermally quite stable. The efficiency of the magnesium nitrate and platinum as chemical modifiers was tested and compared in the analysis of oil standards diluted with MIBK. It was found that 1 μg of Pt increased the pyrolysis temperature from 1000 to 1400 °C and decreased the characteristic mass from 27.5 to 15.3 pg, measuring the peak height absorbance with a new graphite tube. Magnesium nitrate was inadequate for this type of sample. The ageing of the graphite tube surface affected the vanadium determination; a slow drift in sensitivity appeared with increasing atomization cycles [52]. These results, however, are not representative as wall atomization and peak height was used for signal evaluation. This drift would most likely not have been observed if integrated absorbance would have been used for signal evaluation.

The use of pyrolytic graphite-coated tubes treated or coated with refractory elements such as tungsten, zirconium, lanthanum and boron have also been recommended. Meeravali and Kumar [53] investigated the use of W, W–Rh and W–Ir as permanent chemical modifiers for the determination of vanadium and nickel in emulsified fuel oils and naphtha in a transversely heated graphite furnace. In the case of vanadium, best results were obtained using an untreated, pyrolytic graphite-coated tube with an integrated platform. Tungsten-coated tubes with or without Ir or Rh not only gave poor sensitivity but also increased the memory effect. The characteristic mass values were 80, 125, 100 and 150 pg, respectively, for untreated, W, W–Rh and W–Ir-coated tubes. These values are also inferior to literature data and were in addition affected by the relatively short graphite tube used in this study. Nakamoto et al. [54] proposed a simple and rapid method for the direct determination of vanadium in heavy oil
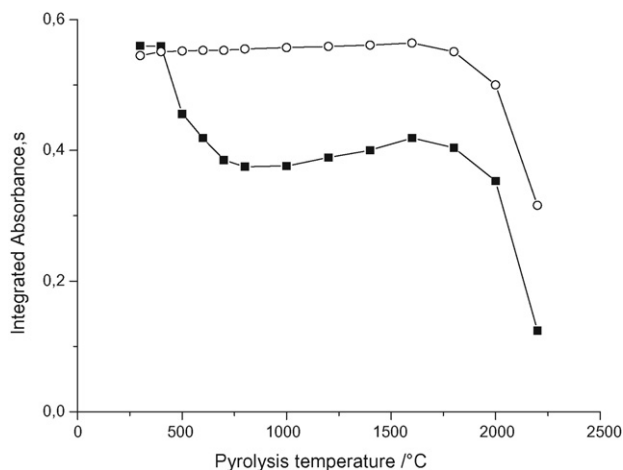
Fig. 2. Pyrolysis curves for vanadium in a crude oil sample (■) without modifier and (○) with 20 μg Pd as chemical modifier using HR-CS GF AAS (from Ref. [57]).

samples using a tungsten-coated graphite tube. A pyrolysis temperature of 1450 °C was used in order to completely decompose or remove the organic matrix.

Using high-resolution continuum source atomic absorption spectrometry (HR-CS AAS), Vale et al. [55] discovered that up to 50% of nickel was lost from petroleum samples already at pyrolysis temperature above 400 °C, and soon after the same phenomenon was found as well for vanadium [56]. The authors proposed that it is most likely the non-polar nickel and vanadyl-porphyrin complexes that are known to be rather volatile and could be lost already at relatively low-temperatures. The rest of the analyte, which was present as non-porphyrins and polar, salt-like compounds, was stable up to at least 1200 °C. These authors also investigated the use of a chemical modifier in order to avoid these low-temperature losses. Oil-in-water emulsions, using Triton X-100 as surfactant, were used for easy sample handling. A mass of 20 μg of Pd, introduced into the graphite tube and thermally pretreated prior to the injection of the emulsion, was found to efficiently prevent any low-temperature losses of vanadium from crude oil samples up to pyrolysis temperatures of 1450 °C, as is shown in Fig. 2.

The authors also succeeded to quantify different fractions by determining total vanadium in the presence of palladium, the thermally stable fraction without a modifier, and the volatile analyte fraction by difference. Lepri et al. [57] succeeded later to do the same approach for fractionation analysis without the addition of a modifier using HR-CS AAS and pyrolysis temperatures of 400 and 1000 °C to determine the total and the thermally stable fraction, respectively. These authors report a best characteristic mass of $m_0 = 10$ pg and a LOD of 0.04 μg g^{-1} of vanadium in the undiluted crude oil Obviously, this discovery of low-temperature losses of a volatile vanadium fraction sheds doubt on all data published about the determination of this element by ET AAS without sample preparation and without the addition of an appropriate modifier. Spike recoveries carried out with salt-like vanadium compounds, such as cyclohexanebutyrates, are inadequate to discover this problem and cannot be used for validation purposes. In a recent manuscript

[58] a procedure has been proposed to use direct 'solid sampling' for the determination of vanadium in crude oil without any sample pretreatment. The approach to use a permanent modifier for this kind of application did not work out as analytes such as nickel and vanadium were apparently poisoning the modifier. Hence, the previously established palladium modifier had to be applied prior to each determination. But the results obtained with this very simple procedure were in good agreement with those obtained for emulsified samples.

Table 1 gives a survey about several additional publications for the determination of V in petroleum products [59,60] using ET AAS.

3.4. Inductively coupled plasma optical emission spectrometry (ICP OES)

Compared to AAS, ICP OES offers a wider linear dynamic range (4–6 orders of magnitude) and has multielement detection capability, while AAS is basically a monoelement technique. The main emission lines of vanadium are: V II 309.311 nm, V II 310.230 nm, V II 292.402 nm, V II 290.882 nm and V II 311.071 nm. The line at 292.402 nm is used most frequently, as it has the highest sensitivity and the greatest freedom from interference effects, using equipment with good resolution. The estimated instrumental detection limit is in the range of 0.01 mg L^{-1} [64], which obviously has to be qualified because of the inevitable dilution of oil samples and the effect of the organic matrix on the overall performance of ICP OES. The high viscosity of petroleum and many petroleum products and the flammability of the lighter fractions cause a number of difficulties when these samples are analyzed by ICP OES. Nevertheless, many schemes have been developed to overcome these problems; several examples are cited below.

Although alternative procedures have been proposed for sample introduction, such as electrothermal vaporization, the introduction of samples in the form of solutions is still the most frequently used approach for ICP OES. An aerosol composed of small droplets is provided by using an efficient nebulizer/spray chamber system. One way to introduce oil samples into the ICP is dilution with an organic solvent [65,66]. Studies on physico-chemical fundamentals of plasma-organic solvent interactions can be found in the literature [67,68].

Nakayama et al. [69] developed a simple and rapid method for the determination of nickel, vanadium and sulfur in crude oils by ICP OES using dilution with organic solvents (dimethylbenzene, 1,2-dimethylbenzene, 4-methyl-2-pentanone and kerosene). 1,2-Dimethylbenzene provided the LOD. Kuokkanen et al. [70] optimized the analytical conditions for the quantitative determination of vanadium and other heavy metals in waste lubricating oils by sequential ICP OES using a simple dilution with kerosene. Anderau et al. [71] described an analytical method for the determination of wear metals in engine lubricating oils, including wavelengths and operating conditions of the ICP OES. Results are presented based on the analysis of NIST SRM 1085 Wear Metals in Lubricating Oil. This procedure does not minimize the problems associated with the high organic load (destabilization of the plasma, decreasing the

Table 1
Selected publications on the determination of vanadium in petroleum products using ET AAS

Sample	Method	LOD	m_0[a] (pg)	Reference
Petroleum fractions	Dilution with xylene and MIBK	$0.10\ \mu g\ g^{-1}$	–	[61]
Diesel oil	Wet mineralization acid in heating block, employing $Mg(NO_3)_2$ as chemical modifier	$12\ ng\ L^{-1}$	–	[62]
Heavy oil	Wet digestion with HNO_3–H_2SO_4 in a three-necked round-bottomed flask	$21\ ng\ L^{-1}$	–	[63]
Crude oil	Dilution with xylene	$47\ \mu g\ L^{-1}$	–	[49]
Crude oil	Dry calcinations at 600 °C and dilution with HNO_3–H_2SO_4 1%	$15\ \mu g\ L^{-1}$	–	[49]
Crude oil	Wet digestion with H_2SO_4–H_2O_2 in a Kjeldhal flask	$58\ \mu g\ L^{-1}$	–	[49]
Diesel	Detergentless micro-emulsions by mixing with propan-1-ol and nitric acid	$5\ \mu g\ L^{-1}$	–	[50]
Asphaltene	Detergentless micro-emulsions by mixing with propan-1-ol and nitric acid	$4\ \mu g\ g^{-1}$	–	[50]
Gasoline	Multiphase emulsions prepared by mixing gasoline with a nitric acid solution (0.1%, v/v) and two cationic surfactants	$4.7\ \mu g\ L^{-1}$	123	[51]
Oil standards	Dilution with MIBK and use the Pt as modifier	$2.8\ \mu g\ L^{-1}$	15.3	[52]
Naphtha and residual fuel oil	Sample emulsified and use of transverse heated untreated tube with an integrated platform	$6\ ng\ g^{-1}$ and $0.1\ \mu g\ g^{-1}$	80	[53]

[a] Characteristic mass.

energy available for analyte ionization/excitation and increasing background emission), and necessitates the use of expensive and unstable metal-organic standards for calibration. The application of ultrasonic nebulization (USN) coupled to a microporous membrane desolvator (MMD) in the direct analysis of petroleum and volatile hydrocarbons such as toluene, naphtha, isopropanol, etc., by ICP OES is an alternative that provides additional sensitivity, tending to offset degradation in performance due to residual solvent loading and organic spectral background effects. USN permitted further improvement in organic solvent introduction, because of two effects: a more efficient nebulization and a desolvation of the organic aerosol by a heater and cooler system. In this system, LOD for toluene solutions and other solvents are similar to aqueous solutions with USN [72,73].

Acid digestion of the oil samples has also been applied and makes possible the use of aqueous standards for calibration. An analytical method using microwave-assisted high-pressure decomposition in HNO_3–HCl was certified for the analysis of metals, particularly vanadium, in crude petroleum and petroleum products, using residual fuel oil SRM and checking the method against an independent procedure [74]. The measured results were in agreement, however, the procedures involving acid digestion are labor intensive and time consuming, resulting in a low sample throughput.

The use of emulsions or micro-emulsions is well described in the literature as a strategy for sample preparation and introduction into the ICP. A study of the plasma discharge was carried out in order to evaluate the possible effects of the introduction of emulsified samples, measuring several plasma parameters such as excitation temperature, electron number density, ionic-to-atomic and atomic-to-molecular carbon intensity ratios [75]. Organic solvents with different evaporation factors and crude oil were used as the organic phase in the emulsion. Typical operating conditions for ICP OES were employed for all the experiments. Generally, the results show that an organic phase such as xylene in the emulsion can perturb the plasma discharge processes. Also, an evaluation of the diagnostic parameters shows

that a crude-oil-in-water emulsion has a similar effect on the plasma discharge as an aqueous solution. This result confirms that plasma emission is mainly perturbed by the volatility of the organic material in the emulsion.

Wang et al. [76] proposed a simple method for the simultaneous determination of up to 21 elements, including vanadium, in organic matrices. Organic samples are simply dispersed in concentrated nitric acid by sonication, and the resulting emulsions/suspensions are directly aspirated into an ICP OES, previously calibrated with aqueous standards. The results obtained using this method for waste oil and the NIST SRM Wear Metals in Lubricating Oil were comparable with those from a method that utilized microwave-assisted digestion for sample preparation. They were also comparable with results obtained by dilution in an organic solvent followed by ICP OES determination with an ultrasonic nebulizer equipped with a membrane desolvator.

Zoltan et al. [77] described a new nebulizer system that extended the analytical capability of the ICP technique to include the simultaneous determination of two hydride-forming elements (antimony and tin) with two conventionally nebulized elements, vanadium and zinc. The main advantage of this system is its simultaneous determination of elements that form volatile hydrides and elements that do not, without any instrumental changes. Spike recovery experiments were performed on the NIST SRM 1643c Residual Fuel Oil and results were in agreement with the certified values. Thiem and Watson [78] studied the effect of acid on extraction efficiency of emulsions for 21 elements in oil and transmission fluids. Four different acid combinations were investigated in this study, namely, HCl, HNO_3, H_2SO_4, and HCl/HNO_3 in a 75/25 ratio. For vanadium, extraction efficiencies near to 100% could be realized for all the acids.

de Souza et al. [79] optimized a procedure to prepare crude oil samples as detergentless micro-emulsions and applied it for the determination of vanadium and 10 additional elements. Propan-1-ol was used as a co-solvent allowing the

formation of a homogeneous and stable system containing crude oil and water. The optimum composition of the micro-emulsion was crude oil/propan-1-ol/water/concentrated nitric acid, 6/70/20/4 w/w/w/w. This simple sample preparation together with an efficient sample introduction (using a Meinhard K3 nebulizer and a twister cyclonic spray chamber) allowed a fast quantification of the analytes using calibration with inorganic standards. Scandium was used as internal standard to correct for signal fluctuations and matrix effects. Oxygen was used in the complementary nebulizer gas flow in order to maximize the carbon combustion and minimize background. The method was tested analyzing one standard reference material (NIST 1634c Residual Fuel Oil) with recoveries of 97.9–103.8%. The method was also applied to two crude oil samples and the results were in good agreement with those obtained using an acid digestion procedure.

de Souza et al. [80] compared a Triton X-100 emulsion and a detergentless emulsion for sample preparation and introduction into the ICP to determine vanadium, molybdenum, chromium and titanium in diesel and in used fuel oil. A 2^3 factorial design was applied to elucidate and establish the relationship between three experimental variables: presence of HNO_3, amount of diesel fuel oil (between 5 and 25%) and the presence of O_2 in the Ar plasma gas. Results indicated that best performance was achieved using 10% sample (w/w) together with concentrated HNO_3 (0.5 mL) and 0.047 L min^{-1} O_2 as auxiliary gas. The use of O_2 minimized carbon deposits at the injector tip and plasma background. The addition of HNO_3 resulted in good correlation between inorganic standards used for calibration, and metal-organic standards used for sample enrichment. Analyte-enriched diesel and SRM 1634b were analyzed using the optimized conditions. Recoveries from 90.1 to 106.5% were obtained, with better results for detergent emulsions, which enabled LOD in the ng g^{-1} range for all analytes and a lower background.

The emulsification of used lubricating oil as a method of sample preparation, preceding the determination of wear metals in the oil was compared with an ashing and dilution method [81]. The oil samples were treated with acid and emulsified in water (1%, w/w) using tetralin as a solvent and Triton X-100 as a surfactant. The results for the emulsion method compared favorably with the traditional methods of sample preparation. The LOD for the emulsion method were lower in certain cases than those for ashing and dilution. Murillo and Chirinos [82] described a rapid procedure for the determination of sulfur, nickel and vanadium in crude oil by ICP OES by emulsifying crude oil in water. Aqueous inorganic solutions with the same amount of emulsifier and solvent were used as calibration standards. The standard reference materials sulfur in residual fuel oil and trace elements in fuel oil were analyzed to evaluate the accuracy of the method. Heavy crude oil samples were analyzed and the results were compared with those obtained by a digestion method.

Souza et al. [83] presented a method for the determination of vanadium and other refractory elements in used lubricating oil samples, aiming at the introduction of such organic samples into the ICP as emulsions. Several nebulization systems were tested with clear advantage for Meinhard K3 coupled with a cyclonic

spray chamber. The carbon deposition on the injector tip as well as the plasma background were minimized through careful optimization of the Ar and O_2 gas flow rates to the plasma. The optimization of instrumental and experimental parameters allowed quantification using calibration curves prepared with inorganic standards. Scandium was used as an internal standard to correct for matrix effects and signal fluctuations. The method was validated through the analysis of an SRM with good recoveries. Comparison against established ICP OES methods (acid digestion or direct dilution in an organic solvent) showed that the proposed method had clear advantages in terms of simplicity of sample preparation, overall analysis time, and the use of inorganic standards for calibration instead of expensive metal-organic standards.

Other relevant applications of ICP OES to V determination in petroleum products are found in the literature [84,85].

3.5. Inductively coupled plasma mass spectrometry (ICP-MS)

More recently, ICP-MS has been applied for trace metal determination in oil and derivatives due to the known advantages of this technique, such as very low LOD, multielement and isotopic-ratio measurement capability. Current LOD for the isotope ^{51}V in direct analysis of solution is in the range of 10 ng L^{-1}. Polyatomic interferences might be observed in the presence of chloride due to $^{35}Cl^{16}O$. In ICP-MS, the presence of solvent vapor in the plasma causes carbon deposition on the cooler surfaces of the sampler and skimmer cones and on the ion lenses, affecting the transport efficiencies of ions. In order to minimize these problems adequate sample preparation and special introduction tools have to be applied, such as flow injection and USN. The methods for introduction of samples in ICP-MS are in general similar to those presented above for ICP OES. Relevant applications of ICP-MS to the determination of vanadium in petroleum products are discussed below.

Determination of trace elements in fuel oils and residual fuel oil SRM by ICP-MS after acid mineralization of the sample were realized employing a microwave oven with high-pressure vessel [86], and in closed digestion vessels or in open-refluxed microwave digestion flasks with good accuracy and precision [87]. AlSwaidan [88] found that the addition of 8-hydroxyquinoline to oil samples increased the efficiency of vanadium extraction, resulting in recoveries of 98–102%.

Direct analysis was proposed for petroleum condensate and naphtha [89,90], and also for crude oil fractions after dissolution in toluene [91] with subsequent ultrasonic nebulization and desolvation.

Determination of vanadium using water-in-oil emulsions as sample preparation procedure has been proposed for several sample types, as such naphtha [92], Saudi Arabian petroleum [93,94], crude oils [95,96], commercial gasoline and crude oil [97]. The coupling of sequential injection with ICP-MS as an analytical tool for vanadium detection was described by AlSwaidan [98], using micro-emulsion oil sampling and analyte addition for the analysis of crude oil and SRM residual fuel oil with good agreement.

3.6. Other spectrometric techniques

Other techniques can be used, but they are not widely found in the literature. Iwasaki and Tanaka [99] and Denoyer and Siegel [100] used XRF for vanadium determination. Alvarez et al. [101] described radioisotope XRF spectroscopy as an analytical procedure for the analysis of geological materials, including oil. Zeng and Uden [102,103] used high-temperature gas chromatography coupled with microwave-induced plasma OES for the determination of vanadyl, nickel and iron porphyrins in crude oils. The use of laser-induced breakdown spectroscopy (LIBS) in jets has also been investigated for quantitative analysis of used lubricating and engine oils [104,105]. The thermal behavior of vanadyl porphyrins was studied by electron spin resonance (ESR) during heating of the kerogens isolated from the bituminous rocks at 150 and 250 °C for 1–20 days in the presence of air [106].

4. Speciation and characterization

One of the most interesting areas of petroleum research is studies directed towards the isolation and identification of vanadyl compounds in heavy crude oils. In the majority of these studies, the focus has been on the vanadyl porphyrin compounds, and relatively little is known yet about the non-porphyrin compounds, even though they comprise 50–80% of the total vanadium present. The molecular characterization of vanadyl (and nickel) non-porphyrin compounds is necessary in order to design innovative trace metal removal methods. In addition, knowledge of the molecular environment associated with both vanadium and nickel in heavy crude oils and asphaltenes is also required to provide an improved understanding of the biogeochemical mechanisms responsible for the inclusion of these metals during the diagenesis and maturation process of petroleum formation. Fish et al. [107,108] accomplished several studies about the characterization and identification of vanadyl compounds in petroleum. Márquez et al. [109] developed three extraction methods to isolate and characterize vanadium porphyrins from a heavy crude oil. Investigations about the distribution of vanadium and several other trace metals in heavy crude oils and oil products are also found in the literature [110,111]. The isotopic study and origin of the vanadium in petroleum asphaltenes and source kerogens was investigated by Premovic et al. [112,113].

Recent investigations using high-resolution continuum source atomic absorption spectrometry (HR-CS AAS) with a graphite furnace have shown that kind of a speciation analysis can also be carried out with ET AAS, taking advantage of the dramatically higher volatility of the vanadyl porphyrin complexes, compared to the non-porphyrins [55–57]. As already mentioned in Section 3.3, using conventional ET AAS, the total vanadium content could be determined with the addition of palladium as a modifier to avoid low-temperature losses and the thermally stable non-porphyrin fraction was determined without a modifier. Using HR-CS AAS, total vanadium could be determined using a pyrolysis temperature of 400 °C, whereas the thermally stable fraction was determined with a pyrolysis temperature >800 °C. The volatile porphyrin fraction was determined in both cases by

difference. This selective determination of the volatile fraction is considered to be of particular importance, as it is for sure predominantly this type of species that is transported in the distillation process to intermediate products, and acts as catalyst poison. A clear indication for this poisoning effect was found in recent work, where iridium has been investigated as permanent chemical modifier for vanadium determination in crude oil. The stabilizing action of this modifier for the volatile porphyrin fraction was completely lost after only two atomization cycles [58]. The quality of a crude oil might therefore be much better characterized by its content of volatile vanadium than by its total vanadium content, which is not correlated to the former one.

5. Conclusion

Considering the importance of vanadium and the relatively high concentration of this element in petroleum and petroleum products, analytical methods published during the last 25 years, involving atomic spectrometric techniques such as FAAS, ET AAS, ICP OES, ICP-MS, have been presented in a detailed way. Nevertheless, each technique has its pros and cons and should therefore be chosen according to the type of product, considering that the concentration of vanadium is significantly lower in the lighter fractions. The most frequently used sample preparation methods are digestion in microwave oven and dilution with three-component systems (emulsion and micro-emulsion), as they have been found to provide precise and accurate results in a relatively simple and fast way.

References

[1] N.N. Greenwood, A. Earnshaw, Chemistry of the Elements, 2nd ed., Butterworth-Heinemanm, 1997.
[2] J.D. Lee, Concise Inorganic Chemistry, Chapmar & Hall, 1996.
[3] B. Welz, M. Sperling, Atomic Absorption Spectrometry, 3rd ed., Wiley–VCH, Weinheim, New York, 1999.
[4] K. Schwartz, D.B. Milne, Science 174 (1971) 426.
[5] D.G. Barceloux, J. Toxicol. Clin. Toxicol. 37 (1999) 265.
[6] K. Pyrzynska, T. Wierzbicki, Talanta 64 (2004) 823.
[7] M.A. Woodin, Y.C. Liu, D. Neuberg, R. Hauser, T.J. Smith, D.C. Christiani, Am. J. Ind. Med. 37 (2000) 353.
[8] M. Kiviluoto, O. Rasanen, A. Rinne, M. Rasanen, Scand. J. Work Environ. Health 5 (1979) 50.
[9] J.P. Buchet, E. Knepper, R. Lauwerys, Anal. Chim. Acta 136 (1982) 243.
[10] M.W. Arbouine, N.J. Smith, At. Spectrosc. 12 (1991) 54.
[11] T.F. Yen, in: T.F. Yen (Ed.), The Role of Trace Metals in Petroleum, Ann Arbor Science Publishers, Ann Arbor, MI, 1975.
[12] G. Sebor, I. Land, P. Vavrecka, V. Sychra, O. Weisser, Anal. Chim. Acta 78 (1975) 99.

[13] F.E. Dickson, C.J. Kunesh, E.L. Mcginnis, L. Petrakis, Anal. Chem. 44 (1972) 978.

[14] J.F. Branthaver, in: R.H. Filby, J.F. Branthaver (Eds.), ACS Symposium Series, vol. 344, American Chemical Society, Washington, DC, 1987.

[15] W.T. Reid, External Corrosion and Deposits—Boilers and Gas Turbines, Elsevier, Amsterdam, 1971.

[16] L. López, S.L. Mónaco, Fuel 83 (2004) 365.

[17] F. Settle, Handbook of Instrumental Techniques for Analytical Chemistry, Prentice Hall PTR, New York, 1997.

[18] K.W. Jackson, Anal. Chem. 72 (2000) 159R–167R.

[19] E. Oliveira, J. Braz. Chem. Soc. 14 (2003) 174.

[20] F.J. Krug, Métodos de Preparo de Amostras, 6ª ed., VI Workshop sobre Preparo de Amostras, UFSM, 2006.

[21] J.A.A. Amaro, S.L.C. Ferreira, J. Anal. At. Spectrom. 19 (2004) 1.

[22] J.K. Vilhunen, A. von Bohlen, M. Schmeling, R. Klockenkamper, D. Klockow, Spectrochim. Acta B 52 (1997) 953.

[23] H. Tao, A. Miyazaki, K. Bansho, Y. Umezaki, Anal. Chim. Acta 156 (1984) 156.

[24] I. Silva, R.C. Campos, A.J. Curtius, S.M. Sella, J. Anal. At. Spectrom. 8 (1993) 749.

[25] D.G. Smith, J. Colloid Interf. Sci. 60 (1977) 488.

[26] E. Pelizzeti, E. Pramauro, Anal. Chim. Acta 169 (1985) 1.

[27] J.L. Burguera, M. Burguera, Talanta 64 (2004) 1099.

[28] R.Q. Aucélio, A.J. Curtius, B. Welz, J. Anal. At. Spectrom. 15 (2000) 1389.

[29] R.Q. Aucélio, A.J. Curtius, J. Anal. At. Spectrom. 17 (2002) 242.

[30] M.V. Reboucas, S.L.C. Ferreira, B.B. Neto, J. Anal. At. Spectrom. 18 (2003) 1267.

[31] R.J. Cassella, B.A.R.S. Barbosa, R.E. Santelli, A.T. Rangel, Anal. Bioanal. Chem. 379 (2004) 66.

[32] R. Bock, A Handbook of Decomposition Methods in Analytical Chemistry, International Text Book Company, London, 1979.

[33] Method UOP 391-91—Trace Metals in Petroleum Products or Organics by AAS, Universal Oil Products Company, 1991.

[34] J. Kragten, At. Spectrosc. 2 (1981) 135.

[35] I. Lang, G. Sebor, O. Weissere, V. Sychara, Anal. Chim. Acta 88 (1977) 313.

[36] G. Sebor, I. Lang, Anal. Chim. Acta 89 (1977) 221.

[37] A. Varma, Handbook of Atomic Absorption Analysis Part I, CRC Press, Inc., 1989.

[38] M. Bettinelli, P.E. Tittarelli, J. Anal. At. Spectrom. 9 (1994) 805.

[39] O. Platteau, M. Carrillo, Fuel 74 (1995) 761.

[40] J. Lakatos, I. Lakatos, G. Bagdi, Microchem. J. 54 (1996) 303.

[41] H. Berndt, G. Schaldach, S.H. Kägler, Fresenius J. Anal. Chem. 355 (1996) 37.

[42] J. Mora, J.L. Todoli, F.J. Sempere, A. Canals, V. Hernandis, Analyst 125 (2000) 2344.

[43] G. Bagur, D. Gazquez, M. Sanchez, A.M. Martin, Anal. Lett. 26 (1993) 125.

[44] J.M. Guidroz, J. Sneddon, Microchem. J. 73 (2002) 363.

[45] Z. Czovek, A. Gaspar, M. Braun, J. Posta, ACH-Models Chem. 136 (1999) 95.

[46] W. Wendl, G. Müller-Vogt, Spectrochim. Acta B 39 (1984) 237.

[47] Z. Benzo, T. Montero, M. Quintal, J. Anal. At. Spectrom. 11 (1999) 445.

[48] J. Alvaro, A.R. Picon, C.M. Vecchi, Acta Cientifica Venezolana 41 (1990) 306.

[49] P.B. Barrera, C.P. Calvo, F.B. Martinez, Anal. Lett. 24 (1991) 447.

[50] R.Q. Aucelio, A. Doyle, B.S. Pizzorno, M.L.B. Tristao, R.C. Campos, Microchem. J. 78 (2004) 21.

[51] D.S.S. dos Santos, A.P. Teixeira, M.G.A. Korn, L.S.G. Teixeira, Spectrochim. Acta B 61 (2006) 592.

[52] N.S. Thomaidis, E.A. Piperaki, Analyst 121 (1996) 111.

[53] N.N. Meeravali, S.J. Kumar, J. Anal. At. Spectrom. 16 (2001) 527.

[54] Y. Nakamoto, T. Ishimaru, N. Endo, K. Matsusaki, Anal. Sci. 20 (2004) 739.

[55] M.G.R. Vale, I.C.F. Damin, A. Klassen, M.M. Silva, B. Welz, A.F. Silva, F.G. Lepri, D.L.G. Borges, U. Heitmann, Microchem. J. 77 (2004) 131.

[56] I.C.F. Damin, M.G.R. Vale, M.M. Silva, B. Welz, F.G. Lepri, W.N.L. dos Santos, S.L.C. Ferreira, J. Anal. At. Spectrom. 20 (2005) 1332.

[57] F.G. Lepri, B. Welz, D.L.G. Borges, A.F. Silva, M.G.R. Vale, U. Heitmann, Anal. Chim. Acta 558 (2006) 195.

[58] M.M. Silva, I.C.F. Damin, M.G.R. Vale, B. Welz, Talanta, in press.

[59] A. Akinlua, N. Torto, Anal. Lett. 39 (2006) 1993.

[60] T. Shimizu, Y. Shijo, K. Sakai, Bunseki Kagaku 29 (1980) 685.

[61] M.C. Gonzalez, A.R. Rodriguez, V. Gonzalez, Microchem. J. 35 (1987) 94.

[62] R.C.S. Luz, L.M.S. da Silva, G.S. Lopes, A.B. Marques, E.P. Marques, Revista Analytica 07 (2003) 48.

[63] M. Turunen, S. Peraniemi, M. Ahlgren, H. Westerholm, Anal. Chim. Acta 311 (1995) 85.

[64] R.K. Winge, V.A. Fassel, V.J. Peterson, M.A. Floyd, Inductively Coupled Plasma-Atomic Emission Spectroscopy: An Atlas of Spectral Information, Elsevier, The Netherlands, 1985.

[65] E.B.M. Jansen, J.H. Knipscheer, M. Nagtegaal, J. Anal. At. Spectrom. 7 (1992) 127.

[66] R.I. Botto, Spectrochim. Acta Rev. 14 (1991) 141.

[67] P.C. Hauser, M.W. Blades, Appl. Spectrosc. 42 (1988) 595.

[68] J.F.A. Chirinos, J. Franquiz, J. Anal. At. Spectrom. 13 (1998) 995.

[69] K. Nakayama, S. Okada, S. Tanaka, Bunseki Kagaku 46 (1997) 599.

[70] T. Kuokkanen, P. Peramaki, I. Valimaki, H. Ronkkomaki, Int. J. Environ. Anal. Chem. 81 (2001) 89.

[71] C. Anderau, K.J. Fredeen, M. Thomsen, D.A. Yates, At. Spectrosc. 16 (1995) 79.

[72] R.I. Botto, J. Anal. At. Spectrom. 8 (1993) 51.

[73] R.I. Botto, J.J. Zhu, J. Anal. At. Spectrom. 11 (1996) 675.

[74] G. Knapp, M. Zischka, P. Kettisch, A. Schalk, in: B. Welz (Ed.), CANAS '95 Colloquium Analytische Atomspektroskopie, Bodenseewerk Perkin-Elmer, Überlingen, 1995, p. 221.

[75] M. Murillo, J. Chirinos, J. Anal. At. Spectrom. 11 (1996) 253–257.

[76] T.B. Wang, K.J. Jia, J. Wu, J. Pharm. Biomed. Anal. 33 (2003) 639.

[77] T. Zoltan, Z. Benzo, M. Murillo, E. Marcano, C. Gomez, J. Salas, M. Quintal, Anal. Bioanal. Chem. 382 (2005) 1419.

[78] T.L. Thiem, J.D. Watson, Microchem. J. 57 (1997) 245.

[79] R.M. de Souza, A.L.S. Meliande, C.L.P. da Silveira, R.Q. Aucelio, Microchem. J. 82 (2006) 137.

[80] R.M. de Souza, B.M. Mathias, I.S. Scarminio, C.L.P. da Silveira, R.Q. Aucélio, Microchim. Acta 153 (2006) 219.

[81] J.L. Fischer, N.B. Krusberski, S. Afr. J. Chem. -Suid-Afrikaanse Tydskrif Vir Chemie 58 (2005) 131.

[82] M. Murillo, J. Chirinos, J. Anal. At. Spectrom. 9 (1994) 237.

[83] R.M. Souza, C.L.P. da Silveira, R.Q. Aucélio, Anal. Sci. 20 (2004) 351.

[84] A.L. Molinero, J.R. Castillo, Anal. Lett. 31 (1998) 903.

[85] H.J. Wei, D.L. Guan, P.T. Sun, H.Z. Wang, Z.E. Wang, Z.P. Luo, S.H. Li, Spectrosc. Spect. Anal. 26 (2006) 340.

[86] M. Bettinelli, S. Spezia, U. Baroni, G. Bizzarri, J. Anal. At. Spectrom. 10 (1995) 555.

[87] T. Wondimu, W. Goessler, Bull. Chem. Soc. Ethiopia 14 (2000) 99.

[88] H.M. AlSwaidan, Anal. Lett. 26 (1993) 141.

[89] S.D. Olsen, S. Westerlund, R.G. Visser, Analyst 122 (1997) 1229.

[90] R.I. Botto, Can. J. Anal. Sci. Spectrosc. 47 (2002) 1.

[91] C. Duyck, N. Miekeley, C.L.P. da Silveira, P. Szatmari, Spectrochim. Acta B 57 (2002) 1979.

[92] S.J. Kumar, S. Gangadharan, J. Anal. At. Spectrom. 14 (1999) 967.

[93] H.M. AlSwaidan, Anal. Lett. 21 (1988) 1487.

[94] H.M. AlSwaidan, At. Spectrosc. 14 (1993) 170.

[95] C.J. Lord, Anal. Chem. 63 (1991) 1594.

[96] S.D. Olsen, R.H. Filby, T. Brekke, G.H. Isaksen, Analyst 120 (1995) 1379.

[97] R.A. Reimer, A. Miyazaki, Anal. Sci. 9 (1993) 157.

[98] H.M. AlSwaidan, Talanta 43 (1996) 1313.

[99] K. Iwasaki, K. Tanaka, Anal. Chim. Acta 136 (1982) 293.

[100] E.R. Denoyer, L.A. Siegel, Anal. Chim. Acta 192 (1987) 361.

[101] M. Alvarez, J. Alvarado, A.R. Cristiano, L.M. Marco, M.M. Perez, J. Radioanal. Nucl. Chem. 144 (1990) 327.

[102] Y.D. Zeng, P.C. Uden, J. High Resolut. Chromatogr. 17 (1994) 223.

[103] Y.D. Zeng, P.C. Uden, J. High Resolut. Chromatogr. 17 (1994) 217.
[104] P. Yaroshchyk, R.J.S. Morrison, D. Body, B.L. Chadwick, Spectrochim. Acta B 60 (2005) 1482.
[105] P. Yaroshchyk, R.J.S. Morrison, D. Body, B.L. Chadwick, Spectrochim. Acta B 60 (2005) 986.
[106] P.I. Premovic, I.R. Tonsa, M.T. Pajovic, L. Lopez, S.L. Monaco, D.M. Dordevic, M.S. Pavlovic, Fuel 80 (2001) 635.
[107] R.H. Fish, J.J. Komlenic, B.K. Wines, Anal. Chem. 56 (1984) 2452.
[108] R.H. Fish, J.J. Komlenic, Anal. Chem. 56 (1984) 511.
[109] N. Márquez, F. Ysambertt, C. De La Cruz, Anal. Chim. Acta 395 (1999) 343.
[110] M.M. Barbooti, E.Z. Said, E.B. Hassan, Fuel 68 (1989) 84.
[111] D. Ugarkovic, D. Premeri, Fuel 66 (1987) 1431.
[112] P.I. Premovic, D.M. Dordevic, M.S. Pavlovic, Fuel 81 (2002) 2009.
[113] P.I. Premovic, I.R. Tonsa, L. Lopez, S.L. Mônaco, D.M. Dordevic, M.S. Pavlovic, J. Inorg. Biochem. 80 (2000) 153.

Evaluation of the atmospheric pressure photoionization source for the determination of benzidines and chloroanilines in water and industrial effluents by high performance liquid chromatography–tandem mass spectrometry

Alessandro Bacaloni [a], Chiara Cavaliere [a], Angelo Faberi [a], Patrizia Foglia [a], Alessandra Marino [b], Roberto Samperi [a], Aldo Laganà [a,*]

[a] *Department of Chemistry, "La Sapienza" University, Piazzale Aldo Moro 5, 00185 Roma, Italy*
[b] *ISPESL/DIPIA, Via Urbana 167, 00184 Roma, Italy*

Abstract

A solid phase extraction-high performance liquid chromatography–tandem mass spectrometry based analytical method suitable for simultaneous analysis of benzidine, 3,3′-dichlorobenzidine, mono-, di-, and tri-chloroanilines has been developed.

Normal phase separation by liquid chromatography was performed using a cyano propyl methyl silica column, and atmospheric pressure photoionization was employed as interface with mass spectrometer.

The developed method was evaluated in terms of limit of detection, accuracy, and precision. The quantification limit for all the compounds ranged between 7 and 112 ng L^{-1}, while recovery for all the compounds was higher than 94%. The method was tested by analyzing different industrial wastes, showing residual contamination by most of the analytes.
© 2006 Elsevier B.V. All rights reserved.

Keywords: Atmospheric pressure photoionization; LC/APPI-MS; APPI-MS/MS; Benzidine; Chloroaniline; Industrial waste water analysis

1. Introduction

Aromatic amino compounds comprise a wide group of substances that are fundamental to industries producing pharmaceuticals, synthetic rubbers and dyes. This group of chemicals exhibits a specific toxic effect related to the production of methemoglobin and bladder carcinoma.

Among aromatic amino compounds, the most dangerous are benzidine and 3,3′-dichlorobenzidine; although their use has been reduced [1], they can be found in the environment because are intermediates in manufacturing of dyes and pigments. Being potent human carcinogens, they are included worldwide in the list of the priority pollutants. Moreover, concern exists over the release of chloroanilines into the environment during production processes or improper treatment of industrial waste streams. Aromatic chloroamines can also enter the environment as result of some commonly used herbicide degradation [2]. The European Water Framework Directive (WFD) 2000/60/EC [3] requires member states to regularly monitor environmental waters for priority contaminants, including benzidines and chloroanilines.

Various methods have been developed for determination of chloroanilines and benzidines in aqueous samples at low concentration. The extraction of aqueous samples can be performed via liquid–liquid extraction (LLE), as in EPA method 605 [4,5], or via solid phase extraction (SPE), that is the technique of choice because it requires less amount of organic solvents and it is more rapid than LLE [1,6,7]. Recently, as alternative, solid phase microextraction (SPME) technique has been proposed. This technique allows to perform the extraction and the concentration of several organic compounds without solvents. The SPME has found some applications in waste water analysis, and

* Corresponding author at: Dipartimento di Chimica, Università "La Sapienza", Box no 34, Roma 62, Piazzale Aldo Moro 5, 00185 Roma, Italy. Tel.: +39 06 49913679; fax: +39 06 490631.

E-mail address: aldo.lagana@uniroma1.it (A. Laganà).

it has been applied to benzidine and chloroaniline determination [8,9].

Concerning separation techniques, these are mostly based on gas chromatography (GC) and high performance liquid chromatography (LC). The use of GC is complicated by analyte thermal degradation tendency and by the need of derivatization step before injection into the GC apparatus, thus reproducibility is affected and possible biases are introduced. On the contrary, LC does not need many preliminary sample manipulations, and methods for determining chloro-amino compounds have been developed coupled with UV, diode-array, fluorimetric or electrochemical detector [10]. These compounds, however, must be often determined in complex matrices at low concentrations, then a more specific detection technique has to be preferred.

At present, the use of LC coupled to mass spectrometry (LC/MS) has been limited because di-chlorobenzidine, di- and tri-chloroaniline, that are non-polar compounds, do not give any signal with electrospray ionization (ESI) interface, while give a very weak signal with atmospheric pressure chemical ionization (APCI) interface [6].

Atmospheric pressure photoionization (APPI) source was recently introduced for coupling MS to LC separation systems. Even if photoionization detection has been proposed from the middle '70 in combination with both GC [11] and LC [12], some severe practical limitations have delayed its use as source for analytical mass spectrometry. Nowadays, two different APPI sources for LC/MS are commercially available: the open orthogonal source designed to enhance direct photoionization [13,14], and a closed axial source where a dopant is added to increase the efficiency of ion formation [15]. Due to high sample density in the region close to nebulizer, APPI can lead to a sensitivity much higher than that of APCI [14,16]. Since the APPI mechanism is based on a multitude of equilibriums, mobile phase composition, dopant nature, and concentration influence directly the analyte ionization process and thus sensitivity [17–19].

The aim of the present work has been the development of a rapid, sensitive and accurate analytical methodology, based on LC/APPI-MS/MS, for simultaneous determination of mono- di- and tri-chloroanilines, 3,3′-dichlorobenzidine and benzidine in surface water and industrial effluents. For this purpose, a normal phase (NP) chromatographic separation was developed and optimized, and a simple and rapid extraction procedure, compatible with the non-polar mobile phase, was developed. Moreover, the influence of various solvent combinations over APPI signal intensity has been studied.

2. Experimental

2.1. Chemicals and reagents

Benzidine, 3,3′-dichlorobenzidine (3,3′-DCB), 2-chloroaniline (2-MCA), 3-chloroaniline (3-MCA), 4-chloroaniline (4-MCA), 2,3-dichloroanline (2,3-DCA), 2,4-dichloroaniline (2,4-DCA), 2,5-dichloroaniline (2,5-DCA), 2,6-dichloroaniline (2,6-DCA), 3,4-dichloroaniline (3,4-DCA), 3,5-dichloroaniline (3,5-DCA), 2,3,4-trichloroaniline (2,3,4-TCA), 2,4,5-trichloroaniline (2,4,5-TCA), 2,4,6-trichloroaniline (2,4,6-TCA) and 2,4-

dibromoaniline (internal standard) were purchased from Sigma (Milan, Italy).

A standard stock solution of each compound was prepared by dissolving the pure analytical standard in isopropanol to achieve a concentration of $1.0 \, \text{mg mL}^{-1}$. Composite working standard solutions were prepared by combining aliquots of each of the individual stock solutions and diluting with isopropanol or isooctane/toluene 1:1 (v/v) to obtain the required concentration. All the above solutions were kept at $-20 \, ^\circ\text{C}$, in the dark, and allowed to equilibrate at room temperature before use.

Methanol, isooctane, isopropanol and toluene, all HPLC grade, were supplied by Carlo Erba (Milan, Italy). Toluene (residual analysis grade) was supplied by Panreac (Spain) and Fluka (Fluka Chemie, GmbH, Buchs, Switzerland). Deionized water was further purified using a Milli-Q (Millipore, Bedford, MA, USA) apparatus. For solid phase extraction, Amberchrom CG161M styrene-divinylbenzene resin (SDVB), 3 mL polypropylene tubs, polyethylene frits and a vacuum manifold (all from Supelco, Bellefonte, IL, USA) were used.

2.2. Sample collection

Three different types of water were sampled: tap water, river water and industrial effluent. Five industrial effluents were analyzed: Sample 1, untreated effluent from galvanic plant; Sample 2, untreated effluent from photo printing plant; Sample 3, inker washing waste; Sample 4 and Sample 5, respectively, waste water treatment plant (WWTP) influent and effluent of a paint production factory. Twenty-four-hour composite samples of raw and treated sewage were obtained by using flow proportional samplers.

In order to eliminate residual chlorine, 0.5 g/L of sodium thiosulphate were added to tap water samples. Samples of river water and industrial effluents were kept unfiltered at room temperature in a brown bottle. Prior to the analysis, they were filtered using a Millipore filtering system with two different kinds of filter: a 1 μm WhatmanGF/C glass microfiber filter and a 0.45 μm regenerated cellulose filter.

2.3. Sample extraction method

Amberchrom CG161 was supplied as ethanolic suspension. Dried resin was prepared by decantation and paper filtration, then the filtered particles were washed several times with Milli-Q water and air dried. Finally, the resin was placed in a beaker and let dried in a ventilated oven at $100 \, ^\circ\text{C}$ for 48 h.

A 3 mL polypropylene tube was filled with 100 mg of resin and the cartridge was fitted with a bottom and a top polypropylene frit. Prior to use, the cartridge was soaked for about 10 min in methanol, then sequentially washed prior to use with 3 mL of dichloromethane, 3 mL of methanol, and 5 mL of Milli-Q water. After addition of an appropriate amount of IS, 400 mL of sample were vacuum forced through the cartridge at a flow rate of 5 mL min^{-1}. Then, the cartridge was washed with 10 mL of Milli-Q water and air-dried for 5 min. As a further precaution to reduce the presence of water in the final eluate, 50 μL of isopropanol were slowly passed through the cartridge. This vol-

ume showed to be suitable for removing most of residual water, without eluting out analytes, but then this amount of isopropanol was present in the final extract. The elution was performed with 2 mL of toluene:isooctane 1:1 (v/v). Finally, in order to eliminate residual water, 1 g of anhydrous sodium sulphate was added to the solution into the vial. The vial was then vortex mixed, centrifuged (3000 rpm for 5 min) and the supernatant transferred into a clean vial; 10 μL of this solution were directly injected into the LC-MS/MS apparatus.

2.4. LC-MS/MS analysis

The LC system was a Perkin-Elmer series 200 (Norwalk, CT, USA) consisting of a binary LC micropump, and a vacuum degasser, equipped with a Rheodyne injector with a 10 μL loop. The chromatographic column was a 250 mm × 2.0 mm i.d. cyano propyl methyl silyl Luna 5 μm CN 100 Å (Phenomenex, Torrace, CA, USA) equipped with a CN 4.0 mm × 2.0 mm i.d. guard column (Phenomenex). The flow rate was set at 200 μL/min, and the column was maintained in an oven (Timberline Instruments, Inc., Boulder, CO, USA) at 40 °C.

For fractionation of the analytes, phase A was toluene/isooctane 1:1 (v/v) and phase B was toluene/isopropanol 99:1 (v/v). After an isocratic step at 100% A for 12 min, B was linearly increased to 100% in 1 min, then held constant for 13 min. An equilibrium time of 15 min was necessary for restoring the initial conditions.

An API 2000 (Applied Biosystems/MDS SCIEX, Concord, ON, Canada) triple quadrupole mass spectrometer equipped with a PhotoSpray^{TM} (APPI) probe was operated in the positive ion mode.

Best responses were recorded with the source block voltage set at 1.5 kV and a heated nebulizer temperature of 350 °C. Concerning gasses, ultrapure air was used as API gas and pure nitrogen was used as collision gas and lamp cooling gas. Curtain gas was set at 20 (arbitrary units), while nebulizing (GS1) and turbo spray gas (GS2) were set at 25 and 65, respectively. Mass calibration and resolution adjustment on the resolving quadrupoles were automatically performed by using a 10^{-5} mol/L solution of poly(propylene glycol) introduced via a model 11 Harvard infusion pump (Harvard apparatus, Hollison, MA, USA). For each analyte, full scan spectra and product ion scan spectra in the range of m/z 50–300 were obtained by infusing a 10 ng/μL solution of each analyte by a syringe pump at a flow rate of 200 μL/min.

Quantitative analysis was performed in multiple reaction monitoring (MRM) mode. Proton adduct $[M+H]^+$ or radical cation $[M]^{\bullet+}$ were selected as precursor ion. Collision energies, MRM transitions and instrumental optical parameters used for each monitored transition are reported in Table 1. To allow longer

Table 1
Retention times and mass spectrometric parameters utilized for analyte detection

Analyte	Retention time (min)	Q1 mass (m/z)	Precursor ion type	Q3 mass (m/z)	CE (eV)
Period 1	0–4.9 min				
2,4,6-TCA	4.2	196	$[M+H]^+$	160, 124	39
2,6-DCA	4.5	162	$[M+H]^+$	126, 90	30
Period 2	4.9–6.0 min				
2,5-DCA	5.2	162	$[M+H]^+$	126, 99, 90	30
2,4-DBA	5.2	252	$[M+H]^+$	143, 91	48
2,4,5-TCA	5.3	196	$[M+H]^+$	161, 133, 125	39
2,4-DCA	5.6	162	$[M+H]^+$	99, 90	32
		161	$[M]^{\bullet+}$	99, 90	32
2-MCA	5.7	128	$[M+H]^+$	92, 65	33
2,3-DCA	5.8	162	$[M+H]^+$	126, 90	32
2,3,4-TCA	5.8	196	$[M+H]^+$	134, 125	41
Period 3	6.0–7.7 min				
3,5-DCA	6.3	162	$[M+H]^+$	127, 109	48
3-MCA	7.2	128	$[M+H]^+$	111, 93	55
3,4-DCA	7.4	162	$[M+H]^+$	127, 109	40
		161	$[M]^{\bullet+}$	99, 90	40
Period 4	7.7–9.0 min				
4-MCA	8.3	128	$[M+H]^+$	111, 93	33
		127	$[M]^{\bullet+}$	92, 65	33
Period 5	9.0–15.0 min				
3,3′-DCB	10.3	253	$[M+H]^+$	182	55
		252	$[M]^{\bullet+}$	154	55
Period 6	15.0–24.0 min				
BEN	21.1	185	$[M+H]^+$	167	44
		184	$[M]^{\bullet+}$	166	44

dwell times and therefore a better sensitivity, the total acquisition time was divided in six acquisition periods. Retentions times of compounds were reproducible within 2%.

2.5. Quantitative analysis, method performance and matrix effect

Calibration solutions were prepared by diluting the working composite solution containing all the analytes with toluene:isooctane 1:1 (v/v) to achieve the desired concentrations and by adding the internal standard. A five point calibration curve was constructed by plotting the ratio between the observed peak areas and the internal standard area. The combined ion current profile for both transitions was extracted from the LC MRM dataset. Quantification was made by relating the ratio between the peak area of the analytes and that of the internal standard in the sample to those obtained from a standard solution. To calculate matrix effect in environmental and waste water samples, the peak area ratio of extracted sample spiked post-extraction, after blank subtraction, were compared to those obtained from a solvent procedural blank. Due to unpredictable matrix effect, quantification in industrial waste and WWTP influent and effluent was done by the standard addition method (three points). Quantitative data analysis was performed with Analyst software (Applied Biosystems/MDS SCIEX).

2.6. Safety considerations

Benzidine and 3,3′-DCB are carcinogenic compounds and chloroanilines are dangerous compounds. Consequently, standards, solutions and extracts should be handled with extreme care. Gloves and other protective clothing were worn as safety precaution during the handling of the compounds. Residual solutions and contaminated glassware were treated with sodium hypochlorite in order to detoxify them.

3. Results and discussion

3.1. Mass spectrometry

3.1.1. Solvent effect on APPI

In APPI, solvents must be selected carefully because they can heavily affect the response of analytes [17,18]. On the basis of previous experiments conducted in our laboratory [19], we selected a limited number of solvents. To test the photoionization yield for the compounds of interest isopropanol, toluene, isooctane and isooctane/isopropanol mixture were used. In Fig. 1 is reported, in arbitrary units, the total ion signal intensity in positive APPI for 2-chloroaniline, obtained in flow injection mode (10 μL, 10 ng/μL) at a flow rate of 200 μL/min. In all cases, 30 μL/min of toluene as dopant were added. Response in acetonitrile is reported for comparison. As can be seen, the non-polar solvent combination gave the highest signal intensity (the signal intensity for isooctane was about half without dopant addition). The differences in response between non-polar and polar solvents increased for di- and tri-chloroanilines, while decreased for benzidines. In Fig. 2, two histograms are reported
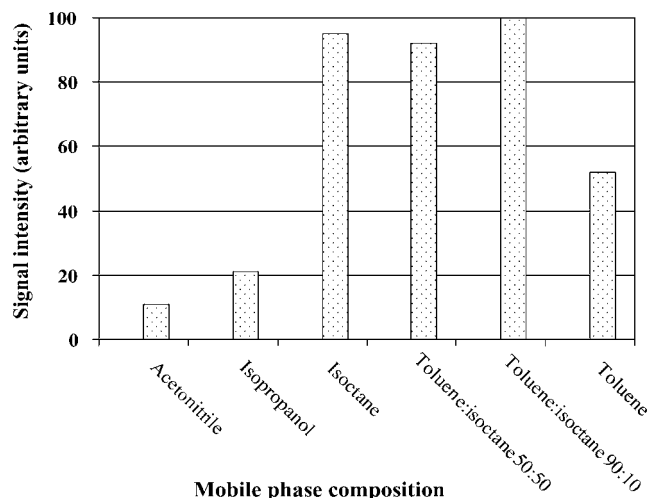
Fig. 1. Total ion signal intensity in positive APPI (arbitrary units) for 2-chloroaniline, obtained with different solvents in flow injection (10 μL, 10 ng/μL) at a flow rate of 200 μL/min and using 30 μL/min of toluene as dopant.

showing the different behaviors of 2-chloroaniline and 3,3′-dichlorobenzidine when increasing percentages of isopropanol were added to a mixture isooctane/toluene 1:1 (v/v); other conditions are as in Fig. 1.

For investigating the effect of solvent purity grade on total ion signal, we prepared four isooctane/toluene 1:1 (v/v) mixtures in which isooctane was in all cases HPLC grade and toluene varied as follows: toluene 1: HPLC grade (Carlo Erba); toluene 2: residue grade (Fluka); toluene 3: residue grade (Panreac); toluene 4: residue grade fortified with 10 ng/mL of *p*-cresole. The experiment was conducted by flow injection of 2,4,5-TCA (10 μL, 10 ng/μL) and by monitoring the total ion intensity. As a result, we measured for the two residue grade toluene a signal about two-fold higher than that obtained using the less pure or the purposely contaminated solvents. This demonstrates that not
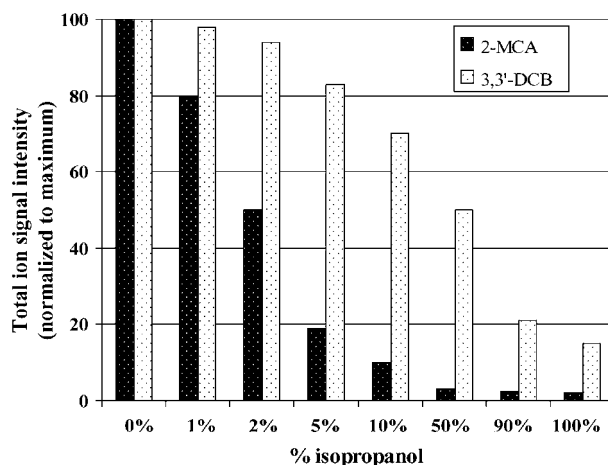
Fig. 2. Total ion signal intensity variation in positive APPI (arbitrary units) for 2-chloroaniline and 3,3′-dichlorobenzidine, obtained when increasing percentages of isopropanol were added to a toluene:isooctane 1:1, v/v mixture. The analyte signals were obtained by injecting in flow injection analysis 10 μL of a 10 ng/μL solution prepared in the same solvents.

only the nature, but also the purity grade of the solvents used may deeply influence the analyte response in APPI.

3.1.2. Mass spectra of MCAs, DCAs, TCAs, DCB and BE

In Table 2, relative intensities of the signals for radical cation $[M]^{\bullet+}$, proton adduct $[M+H]^+$ and principal ions formed by MS/MS are reported. Standards of chloroanilines and benzidines (10 ng/μL) were ionized either in flow injection mode, by using the 1:1 (v/v) isooctane/toluene mixture at a flow rate of 200 μL/min as carrier, and by injecting on column water extract fortified after extraction at the same level; 10 μL were injected in both cases. At this time, the mass spectrometer was operated in single MS mode and declustering potential was maintained low to reduce in source fragmentation.

There are three main ways of photoionization reported in literature [20]: direct photoionization; electron transfer via dopant; proton transfer with the dopant or other protonated molecules.

As it can be seen in Table 2, fourth column, an abundant $[M]^{\bullet+}$ precursor ion was observed for all the investigated compounds. In addition, even if photoionization energies of analytes (8.18 eV for 4-chloroaniline) suggest that direct photoionization may be involved, weaker signals were observed for both kind of ions without the use of toluene as dopant. Then, as noticed by Traldi and coworkers [21], probably a cascade of

Table 2
Observed precursor ions and fragments obtained using atmospheric pressure photoionization for target analytes (chloroanilines and benzidines)

Compound	Observed precursor ion (Q1 SCAN)	m/z	Relative intensities[a]	Relative intensities[b]	Observed fragments (Q3 SCAN) m/z[c]
Monochloroanilines					
2-MCA	$[M]^{\bullet+}$	127	100	45	100, 99, 92, 91, 79, **65**, 64
	$[M+H]^+$	128	20	100	93, 92, **65**
3-MCA	$[M]^{\bullet+}$	127	100	100	100, **92**, 65
	$[M+H]^+$	128	50	3	111, **93**, 75
4-MCA	$[M]^{\bullet+}$	127	100	100	100, 92, **65**
	$[M+H]^+$	128	23	70	111, **93**, 75
Dichloroanilines					
2,3-DCA	$[M]^{\bullet+}$	161	80	4	134, 126, 125, 99, **90**, 63
	$[M+H]^+$	162	100	100	127, 126, 99, **90**
2,4-DCA	$[M]^{\bullet+}$	161	100	65	134, 126, 125, 99, **90**
	$[M+H]^+$	162	55	100	127, 126, **99**, 91, 90
2,5-DCA	$[M]^{\bullet+}$	161	100	12	126, 125, 105, 99, **90**, 63
	$[M+H]^+$	162	75	100	127, 126, **99**, 91, 90
2,6-DCA	$[M]^{\bullet+}$	161	80	10	126, 125, 105, 99, 98, **90**
	$[M+H]^+$	162	100	100	127, 126, 99, **90**, 63
3,4-DCA	$[M]^{\bullet+}$	161	75	43	134, 126, 125, **99**, 90, 63
	$[M+H]^+$	162	100	100	145, **127**, 109, 100, 99, 91, 90
3,5-DCA	$[M]^{\bullet+}$	161	100	15	134, 126, 125, **99**, 90
	$[M+H]^+$	162	25	100	**127**, 109, 100, 92
Trichloroanilines					
2,3,4-TCA	$[M]^{\bullet+}$	195	100	12	160, 159, 133, **124**, 97, 88
	$[M+H]^+$	196	20	100	161, 160, 134, **125**
2,4,5-TCA	$[M]^{\bullet+}$	195	100	5	160, 159, **133**, 124, 97
	$[M+H]^+$	196	15	100	161, 160, **133**, 125
2,4,6-TCA	$[M]^{\bullet+}$	195	100	25	160, 159, 133, 132, **124**, 97, 88
	$[M+H]^+$	196	45	100	161, 160, **124**
Benzidines					
BEN	$[M]^{\bullet+}$	184	20	80	183, 182, 167, **166**, 156, 130, 117
	$[M+H]^+$	185	100	100	168, **167**, 151, 141, 93
3,3′-DCB	$[M]^{\bullet+}$	252	100	100	215, 190, 182, 181, 164, **154**, 127
	$[M+H]^+$	253	75	50	217, 216, 191, 190, **182**, 181, 154
Internal standard					
2,4-DBA	$[M]^{\bullet+}$	251	100	55	172, 170, 145, 143, 91, **90**
	$[M+H]^+$	252	50	100	173, 171, 145, 143, 92, **91**

[a] Flow injection of 10 μL of a 10 ng μL^{-1} solution of each analyte using toluene:isooctane 1:1, v/v at a flow rate of 200 μL^{-1} min.

[b] Injection on column of 10 μL of a water extract fortified after extraction at 10 ng μL^{-1}. Gradient separation, as described in Section 2.

[c] Base peak in bold.

other photo induced reactions must be involved. On the other hand, formation of proton adduct reflects gas phase basicity of analytes. When a small quantity (<1%) of isopropanol was added to mobile phase, the intensity of the radical ion was lowered in favor of protonated molecule. Moreover, it must be said that the ratio $[M]^{•+}/[M+H]^+$ was susceptible to vary in a great extent also depending on the compound. As shown in Table 2, fifth column, the ratio $[M]^{•+}/[M+H]^+$ dramatically changes when the water extract fortified after extraction was injected on column. This phenomenon may be likely due to slight variation in mobile phase composition caused by the small amount of isopropanol (about 2%) contained in the water extract, since all the other experimental conditions were the same. In addition, the use of a toluene/isooctane mixture, previously passed through the chromatographic column for flow injection experiments, did not modify the ratio between molecular ion and proton adduct. What originates this phenomenon is not clear, and until now little is known about analyte interaction with low polarity solvents in this type of interface, and more experiments are needed for elucidating mechanisms. Signals of $[M+H]^+$ ions, not only were less influenced by mobile phase than signals of $[M]^{•+}$, but also give rise to a greater fragment yield and therefore were chosen as precursors for further MRM experiments for MCAs, 2,6-DCA, 2,5-DCA, 2,3-DCA, 3,5-DCA, TCAs and IS. 3,4-DCA, benzidine and 3,3′-dichlorobenzidine showed a more stable ratio between radical and proton adduct, likely because of the longer retention times than those of the other selected analytes (see later), and the most intense transition of both ions can be selected for MRM. The choice of transitions for 2,4-DCA monitoring was more complex and it will be discussed in the next paragraph.

As far as negative APPI was concerned, only $[M−H]^−$ ions were abundant. Although the signal intensity was much lower than in positive APPI, the signal-to-noise ratios for DCA and TCA were similar. However, the only intense ion formed after collisional fragmentation (with the exception of 2,4,5-TCA) was $Cl^−$.

3.2. LC-APPI-MS/MS

The low polarity solvents, required to obtain high signal intensity for all the analytes, implied the choice of a normal phase separation. The best compromise between chromatographic separation and low limit of detection (LOD) was achieved by using a cyano propyl methyl silica column and a gradient elution with toluene/isooctane 1:1 (v/v) and toluene/isopropanol 99:1 (v/v) as mobile phases. Although there are many overlapping among analytes, they can be resolved by properly selecting the MRM transitions. Only 2,3-DCA and 2,4-DCA were poorly resolved and have qualitatively very similar CID spectra of protonated molecule. This problem has been overcame, with an acceptable loss in terms of LOD, by selecting for MRM acquisition of 2,4-DCA two specific transitions of molecular ion. When 2,4-DCA is found while 2,3-DCA is not present, four transitions can be used for its quantification and LOD decreases by a factor about 4.

In a previous work [19], we selected a 4.6 mm i.d. column for operating with LC/APPI-MS/MS, since with a mobile phase

Table 3
Absolute limit of detection and r^2 coefficient of the five point regression equation in the range 0.5–50 ng for the analytes under investigation

Analytes	LOD (ng)	r^2 coefficient
Monochloroanilines		
2-MCA	0.007	0.9978
3-MCA	0.007	0.9984
4-MCA	0.003	0.9941
Dichloroanilines		
2,3-DCA	0.02	0.9977
2,4-DCA	0.02	0.9972
2,5-DCA	0.03	0.9938
2,6-DCA	0.007	0.9958
3,4-DCA	0.06	0.9979
3,5-DCA	0.2	0.9893
Trichloroanilines		
2,3,4-TCA	0.04	0.9972
2,4,5-TCA	0.04	0.9923
2,4,6-TCA	0.05	0.9947
Benzidines		
3,3′-DCB	0.003	0.9995
BEN	0.013	0.9923

flow rate of 1.0 mL/min, due to a very low background noise, the most favorable signal-to-noise ratio was achieved. In this work, however, we preferred to use a 2 mm i.d. column because, dealing with environmental samples, the advantage of selecting a higher flow rate was almost entirely lost due to chemical noise.

In these conditions, the linear range and instrumental LODs were estimated from the five point calibration curve, constructed as reported in Section 2, in the range 0.5–50 ng. In Table 3 are reported the r^2 coefficients and the LODs calculated as three times the standard deviation of the regression line intercept.

3.3. Extraction of the analytes

Simultaneous extraction of compounds with a broad range of polarity by SPE generates many issues: since benzidine is polar, it is prone to breakthrough; on the other hand, the volatility of the other analytes, especially TCAs, may generate losses if the eluates are evaporated for the purpose of solvent exchange and analyte concentration.

Two considerations suggested the choice of a high-surface SDVB material for sample extraction. The first one was that, for avoiding a solvent exchange step, a non-polar solvent has to be used for analyte recovery; the second one was that, when extracting target compounds from aqueous samples containing a high total organic carbon (TOC) content, an adsorbent with a high surface area avoids early breakthrough due to overloading generated by co-extracted compounds [6].

A 3 mL tube filled with 100 mg of resin was able to extract all the target analytes from 400 mL of high-polluted water without loss of benzidine, which is the compound having the lowest breakthrough volume. Moreover, 2 mL of the very low polarity mixture isooctane/toluene 1:1 (v/v) recovered more than 75% of all the compounds. Even if recovery was better than 90% by increasing to 3 mL the elution volume, on the other hand

Table 4
Absolute recovery, recovery relative to surrogate standard (S.S), within day precision (R.S.D.%) and MQLs for analytes under investigation

Analytes	Tap water (spike level 0.5 µg L^{-1})			River water (spike level 0.5 µg L^{-1})			MQLs (ng L^{-1})
	Absolute recovery %	Recovery (S.S.) %	R.S.D.%	Absolute recovery %	Recovery (S.S.) %	R.S.D. %	
Monochloroanilines							
2-MCA	79	100	7	78	95	5	16
3-MCA	74	94	7	84	102	5	16
4-MCA	71	90	8	81	99	3	7
Dichloroanilines							
2,3-DCA	80	101	5	91	111	4	22
2,4-DCA	78	99	6	85	104	3	112
2,5-DCA	76	96	8	86	105	6	38
2,6-DCA	81	103	5	88	107	4	16
3,4-DCA	74	94	11	84	102	7	45
3,5-DCA	75	95	10	83	101	5	74
Trichloroanilines							
2,3,4-TCA	83	105	7	91	111	4	45
2,4,5-TCA	78	99	8	89	109	7	38
2,4,6-TCA	81	103	7	88	107	4	74
Benzidines							
3,3'-DCB	72	91	5	83	101	5	4
BEN	76	96	6	87	106	5	5
Standard							
2,4-DBA	79		3	82		4	

Recoveries ($n=6$) were calculated for 400 mL of spiked tap water (0.5 µg L^{-1}) and river water (0.5 µg/L^{-1}; TOC = 16 mg/L).

there was a reduction of the method detection limit (MDL), due to dilution. To avoid the evaporation step and thus the probable degradation of the most volatile compounds, a 2 mL elution volume was chosen.

3.4. Analytical performance evaluation

Absolute recovery, recovery relative to surrogate standard, within day precision (R.S.D.%) and MDLs are reported in Table 4. Recoveries were calculated for 400 mL of spiked tap water and river water (TOC = 16 mg/L) at the spiking level of 0.5 µg/L ($n=6$). As can be seen, the values obtained without the surrogate standard (absolute recovery) were in the range 69–91%, while the use of a surrogate standard with chemical and physical characteristics similar to those of the target compounds (2,4-dibromoaniline) improved both accuracy and precision.

The method quantification limits (MQLs) were extrapolated calculating the amount of each compound that gives a signal-to-noise ratio equal to 10 in the river water sample spiked at 0.5 µg/L. The sum of at least two selected transitions for MRM was used for all the analytes.

Table 5
Analyte concentration (ng L^{-1}) found in the analyzed samples

Analytes	Sample 2 (photo printing plant waste)	Sample 3 (typography inker washing waste)	Sample 4 (paint production factory WWTP influent)	Sample 5 (paint production factory WWTP effluent)
Monochloroanilines				
2-MCA	n.d.	990	140	98
3-MCA	n.d.	81	69	n.d.
4-MCA	n.d.	81	25	n.d.
Dichloroanilines				
2,4-DCA	n.d.	n.d.	26	21
2,5-DCA	n.d.	n.d.	47	134
2,6-DCA	n.d.	n.d.	12	n.d.
3,4-DCA	n.d.	n.d.	100	20
Trichloroanilines				
2,4,5-TCA	n.d.	n.d.	192	189
Benzidines				
3,3'-DCB	9	n.d.	n.d.	n.d.

n.d. = not detected; WWTP = waste water treatment plant

3.5. Industrial waste water survey

The method described above was tested in a short survey concerning four industrial effluent typologies: Sample 1, galvanic plant waste; Sample 2, photo printing plant waste; Sample 3, typography inker washing waste; Sample 4, paint factory WWTP influent; Sample 5, paint factory WWTP effluent. Due to a matrix effect present in each sample in an unpredictable extent (recoveries relative to IS ranged from 69 to 123%), quantification was achieved by the standard addition method. After extraction, the eluate was subdivided in four aliquots, and three of them were spiked with an amount of standard, respectively, one, two and four times the concentration initially estimated.

In Table 5 the results of the survey are summarized. Sample 1 is not reported since all the compounds were under the MDLs. As can be seen, in Sample 2 only 3,3′-DCB is present in a very little amount, whereas in Sample 3 there is a remarkable amount of MCAs. In Sample 4 and Sample 5, 2,3,4-TCA is the compound found at the highest concentration and remains constant after waste treatment. Data for these samples are not easy to rationalize. 3-MCA, 4-MCA and 2,6-DCA were undetectable after waste treatment and 3,4-DCA concentration was drastically reduced. On the contrary, 2-MCA and 2,4-DCA were poorly removed (note: being 2,3-DCA under MDL, the low concentration found for 2,4-DCA were over MDL since four transitions could be used for quantification). Finally, 2,5-DCA concentration increased after waste treatment. Both influent and effluent from this WWTP contained abundant suspended solid particles. Methanolic extracts of the filters used for these samples, analyzed by LC-APPI-MS/MS, showed high 2,3,4-TCA content. This finding may suggest that in the water treatment plant this compound is degraded to 2-MCA via 2,5-DCA and, in lesser extent, via 2,4-DCA and a continuous equilibrium mobilizes the adsorbed 2,3,4-TCA.

4. Conclusions

A rapid, sensitive and highly selective method for the simultaneous determination of benzidine, 3,3′-DCB, MCAs, DCAs, and TCAs by LC-MS/MS has been developed for the first time and evaluated using spiked and real samples. Normal phase LC separation coupled with an APPI interface permitted to overcome the limitation in ionizing the less polar among these compounds experienced with both ESI and APCI, and low LODs have been attained for all the compounds. Shortcoming of this method is that it lacks robustness, because small changes in ionization environment may provoke substantial change in ionization yield and ion type formation. This drawback can be avoided by using the standard addition method for quantification.

References

[1] M.C. Nyman, A.K. Nyman, L.S. Lee, L.F. Nies, E.R. Blatchley, Environ. Sci. Technol. 31 (1997) 1068.
[2] A. Di Corcia, A. Costantino, C. Crescenzi, R. Samperi, J. Chromatogr. A 852 (1999) 465.
[3] Directive 2000/60/EC of the European Parliament and of the Council of 23 October 2000 establishing a framework for Community action in the field of water policy, Official Journal, L 327; 22/12/2000: P. 0001–0073.
[4] E.P.A. Method 605–Benzidines; available at http://www.epa.gov/waterscience/methods.
[5] S. Chiron, A. Fernandez-Alba, D. Barcelò, Environ. Sci. Technol. 27 (1993) 2352.
[6] S. Lacorte, M.C. Perrot, D. Fraisse, D. Barcelò, J. Chromatogr. A 833 (1999) 181.
[7] S.-L. Zhao, F.-S. Wei, H.-F. Zou, X.-B. Xu, Chemosphere 36 (1998) 73.
[8] L. Muller, E. Fattore, E. Benfenati, J. Chromatogr. A 791 (1997) 221.
[9] W.-Y. Chang, Y.-H. Sung, S.-D. Huang, Anal. Chim. Acta 495 (2003) 109.
[10] L.E. Vera-Avila, A. Garcia-Ac, R. Covarrubias-Herrera, J. Chrom. Sci. 39 (2001) 302.
[11] J.N. Driscol, Am. Lab. 8 (1976) 71.
[12] J.T. Schermund, D.C. Locke, Anal. Lett. 8 (1975) 611.
[13] J.A. Syage, M.D. Evans, K.A. Hanold, Am. Lab. 32 (2000) 24.
[14] K.A. Hanold, S.M. Fisher, P.H. Cormia, C.E. Miller, J.A. Syage, Anal. Chem. 76 (2004) 2842.
[15] D.B. Robb, T.R. Covey, A.P. Bruins, Anal. Chem. 72 (2000) 3653.
[16] C.K. Meng, Agilent technologies Publication EN 2002: 59886635EN.
[17] J.P. Rauha, H. Vuorela, R. Kostiainen, J. Mass Spectrom. 36 (2001) 1269.
[18] T.J. Kauppila, T. Kuuranne, E.C. Meurer, M.N. Eberlin, T. Kotihao, R. Kostiainen, Anal. Chem. 74 (2002) 5470.
[19] C. Cavaliere, P. Foglia, E. Pastorini, R. Samperi, A. Laganà, J. Chromatogr. A 1101 (2006) 69.
[20] A. Raffaelli, A. Saba, Mass Spectrom. Rev. 22 (2003) 318.
[21] E. Marotta, R. Seraglia, F. Fabris, P. Traldi, Int. J. Mass Spectrom. 228 (2003) 841.

Micelle-mediated extraction for simultaneous spectrophotometric determination of aluminum and beryllium using mean centering of ratio spectra

Morteza Bahram [a], Tayyebeh Madrakian [b], Elaheh Bozorgzadeh [b], Abbas Afkhami [b,*]

[a] *Department of Chemistry, Faculty of Science, Urmia University, Urmia, Iran*
[b] *Department of Chemistry, Faculty of Science, Bu-Ali Sina University, Hamadan, Iran*

Abstract

A new micelle-mediated extraction method for preconcentration of ultra-trace quantities of beryllium and aluminum as a prior step to their simultaneous spectrophotometric determination has been developed. Chrome Azurol S (CAS), cetyltrimethylammonium bromide (CTAB) and Triton X-114 were used as chelating agent, cationic surfactant for extraction and co-extraction agent, respectively. Mean centering (MC) of ratio spectra has been used for simultaneous analysis of beryllium and aluminum. The optimal extraction and reaction conditions were studied, and the analytical characteristics of the method (e.g., limit of detection, linear range, preconcentration, and improvement factors) were obtained. Linearity was obeyed in the range of 5–40 ng mL^{-1} of beryllium and 3–100 ng mL^{-1} of aluminum. The detection limit of the method is 0.98 and 0.52 ng mL^{-1} for beryllium and aluminum, respectively. The interference effect of some anions and cations was also tested. The method was applied to the simultaneous determination of beryllium in water samples.
© 2006 Published by Elsevier B.V.

Keywords: Beryllium; Aluminum; Micelle-mediated extraction; CAS; Mean centering

1. Introduction

The toxicity of beryllium and aluminum as well as the need for sensitive and selective methods for determining these elements is well documented. The toxicity of beryllium could be accounted for through its effect on lysosomes with release of cell destroying enzymes [1]. There is considerable evidence that aluminum is neurotoxic in experimental animals, although there is considerable variation among species. In susceptible species, toxicity following parenteral administration is characterized by progressive neurological impairment, resulting in death with status epilepticus. Osteomalacia, as it presents in man, is observed consistently in larger species (e.g., dogs and pigs) exposed to aluminum; a similar condition is observed in rodents. Absorption via the gastrointestinal tract is usually less than 1%. Aluminum is distributed in most organs within the body with accumulation occurring mainly in bone at high dose levels. To a limited extent, aluminum passes the blood–brain barrier and is also distributed to the fetus. Aluminum is eliminated effectively by urine [2].

In comparison with sophisticated laboratory methods for the analyzing of metals such as inductivity coupled plasma (ICP), atomic absorption spectrometry (AAS), electro thermal atomic absorption spectrometry (ETAAS) and HPLC; spectrophotometric determination has a great attraction for its simplicity, low cost, high sensitivity and sometimes its selectivity.

Spectrophotometric determination of aluminum and beryllium in mixtures is difficult because these two elements mutually interfere in the method owing to a considerable overlap of the spectra. Numerous complexes of Be(II) and Al(III) with azo reagents for example eriochrome cyanine R (ECR) [3,4] and Chrome Azurol S (CAS) [5,6] have been proposed for the spectrophotometric determination of both the elements individually. Several spectrophotometric methods have also been proposed for the simultaneous determination of Al(III) and Be(II) ions. A derivative spectrophotometric method for simultaneous determination of Al(III) and Be(II) was reported based on their

* Corresponding author. Tel.: +98 811 8272404; fax: +98 811 8272404.
 E-mail address: afkhami@basu.ac.ir (A. Afkhami).

complexes with 5,8-dihydroxy-1,4-naphoquinone [7]. Valencia et al. [8] reported a method for simultaneous determination of Al(III) and Be(II) by solid phase extraction and first derivative spectrophotometric method based on their complexation reaction with erichrome cyanine R. The difference between the rate of the complexation reactions of Al(III) and Be(II) with CAS in cetyltrimethylammonium bromide (CTAB) micellar media was used to the simultaneous kinetic spectrophotometric determination of these cations using H-point standard addition method [9]. Al(III) and Be(II) could be determined in the range of 10–200 and 10–300 ng mL^{-1}, respectively. Recently, we developed a partial least-squares regression (PLS) method for the simultaneous spectrophotometric determination of aluminum and beryllium in geochemical samples by xylenol orange as the chromogenic reagent in water media and in micellar media [10]. The concentration range in this method was obtained 0.1–1.0 mg L^{-1} and 0.05–1.0 mg L^{-1} for both the metal ions in water and micellar Triton X-100 media, respectively.

Cloud-point extraction (CPE), based on the clouding phenomena of surfactants, has become more and more attractive. As a new separation technique, the CPE offers many advantages over traditional liquid–liquid extraction [11].

For charged micelles, the phenomenon rarely occurs, presumably because electrostatic repulsion prevents phase separation in most cases. In the presence of salt, long-tailed cationic surfactants can self-assemble in aqueous solution into long, flexible wormlike micelles, thus rendering the solution viscoelastic [12,13]. Salts with hydrophobic counterions, such as sodium salicylate (NaSal) and sodium tosylate (NaTos), are particularly effective in inducing micellar growth even at low concentrations. With increasing salt content, complex variations occur in the rheological properties [12–14].

High concentrations of salt also cause cationic surfactant solutions to separate into immiscible surfactant-rich and surfactant-poor phases [15]. This phenomenon, originally termed coacervation, has been investigated since the 1940s and was first observed for mixtures of the cationic surfactant Hyamine 1622 with salts such as potassium thiocyanate (KSCN) and potassium chloride (KCl) [16,17]. The phase separation is typically of the upper consolute type, i.e., it occurs on cooling below a characteristic temperature T_c, which, in turn, increases with salt content [15].

More recently we have presented some new approaches for simultaneous analysis of binary and ternary mixtures that called mean centering of ratio spectra [18–21]. These methods have been inspired from successive ratio derivative spectra method which is based on the successive derivatives of ratio spectra in two steps [22]. The mean centering methods uses mean centering of ratio spectra instead of derivative of them. By eliminating derivative steps, signal-to-noise ratio is enhanced dramatically.

Recently we proposed a new micelle-mediated phase preconcentration method for preconcentration of ultra-trace quantities of beryllium as a prior step to its determination by spectrophotometry has been developed. CAS and cetyltrimethylammonium bromide (CTAB) were used as chelating agent and cationic surfactant, respectively [23]. The method evaluates and eliminates the blank bias error present in such procedures using mean cen-

tering of ratio spectra. This procedure gives more accurate results than by traditional approach using absorbance values against reagent blank.

The purpose of this study is to propose a method for the simultaneous spectrophotometric determination of beryllium and aluminum after preconcentration in a simple cloud point extraction process. The method is based on the color reaction of beryllium and aluminum with CAS and mixed micell mediate extraction of produced complexes. A cationic surfactant, cetyltrimethylammonium bromide (CTAB) and a non-ionic one, Triton X-114, were chosen as extraction agent and co-sorfactant, respectively. Mean centering of ratio spectra was used for simultaneous analysis of mentioned analytes after CPE. A satisfied preconcentration factor and improvement factor were obtained in the proposed method for the determination of beryllium and aluminum.

2. Theory of mean centering of ratio spectra

Consider a mixture of three compounds X, Y and Z. If there is no interaction among the compounds and Beer's low is obeyed for each compound, it can be written:

$$A_m = \alpha_x C_x + \alpha_y C_Y + \alpha_z C_z \tag{1}$$

where A_m is the vector of the absorbance of the mixture, α_x, α_Y, and α_z are the molar absorptivity vectors of X, Y and Z and C_x, C_Y and C_z are the concentrations of X, Y and Z, respectively.

If Eq. (1) is divided by α_z corresponding to the spectrum of a standard solution of Z in ternary mixture, the first ratio spectrum is obtained in the form of Eq. (2) (for possibility of dividing operation, the zero values of α_z should not be used in the divisor):

$$B = \frac{A_m}{\alpha_z} = \frac{\alpha_x C_x}{\alpha_z} + \frac{\alpha_Y C_Y}{\alpha_z} + C_z \tag{2}$$

If the Eq. (2) is mean centered (MC), since the mean centering of a constant (C_z) is zero, Eq. (3) will be obtained:

$$MC(B) = MC\left[\frac{\alpha_X C_X}{\alpha_Z}\right] + MC\left[\frac{\alpha_Y C_Y}{\alpha_Z}\right] \tag{3}$$

By dividing Eq. (3) by MC (α_Y/α_Z), corresponding to the mean centering of the ratio of the spectra of the standard solutions of Y and Z the second ratio spectrum is obtained as Eq. (4) (for possibility of dividing operation, the zero values of MC(α_Y/α_Z) should not be used in the divisor):

$$D = \frac{MC(B)}{MC(\alpha_y/\alpha_z)} = \frac{MC[\alpha_X C_X/\alpha_Z]}{MC(\alpha_y/\alpha_z)} + C_Y \tag{4}$$

Now if the Eq. (4) is mean centered, since the mean centering of a constant (C_Y) is zero, Eq. (5) would be obtained:

$$MC(D) = MC\frac{MC[\alpha_X C_X/\alpha_Z]}{MC(\alpha_y/\alpha_z)} \tag{5}$$

Eq. (5) permits the determination of concentration of each of the active compounds in the solution (X in this equation) without interfering from the other compounds of the ternary system (Y

and Z in these equations). As Eq. (5) shows there is a linear relation between the amount of MC(*D*) and the concentration of X in the solution.

A calibration curve could be constructed by plotting MC(*D*) against concentration of X in the standard solutions of X or in the standard ternary mixtures. For more sensitivity the amount of MC(*D*) corresponding to maximum or minimum wavelength should be measured.

Calibration graphs for Y and Z could also be constructed as described for X.

In this work the blank of system has been assumed an interferent (Z) in order to eliminate blank bias error [23].

3. Experimental

3.1. Apparatus

A Perkin-Elmer Lambda 45 UV–vis spectrometer was used for recording absorbance spectra. Absorption measurements at λ_{max} wavelength were performed using a Shimadzu UV-mini-1240 V spectrophotometer with 1-cm quartz cells (0.5 mL). A Metrohm pH meter (model 713) with a combined glass electrode was used for pH measurements. A centrifuge with 10-mL calibrated tubes (Superior, Germany) was used to accelerate the phase separation process. All calculations in the computing process were done in Matlab 6.5 and Microsoft Excel for windows. A simple program was written for this purpose in Matlab 6.5.

3.2. Reagents

All the solutions were prepared using reagent grade substances and triply distilled water. A $1.000\,\mathrm{g\,L^{-1}}$ stock solution of Be^{2+} was prepared in $0.10\,\mathrm{mol\,L^{-1}}$ sulfuric acid using $BeSO_4 \cdot 4H_2O$ (Merck). A $1.000\,\mathrm{g\,L^{-1}}$ stock solution of Al^{3+} was prepared using $Al(NO_3)_3 \cdot 3H_2O$ (Merck). Working solutions were prepared by appropriate dilution of the stock solution every day. A $4.0 \times 10^{-4}\,\mathrm{mol\,L^{-1}}$ CAS solution was prepared by dissolving an appropriate amount of CAS (Merck) in water. Triton X-114 stock solution (1% v/v) was prepared by dissolving 1 mL of concentrated solution (Merck) in hot distilled water. A $0.15\,\mathrm{mol\,L^{-1}}$ iodide solution in water was prepared. A 0.1% CTAB solution in water was prepared. Acetate buffer solution of pH 6 was prepared from $0.5\,\mathrm{mol\,L^{-1}}$ acetic acid and $0.5\,\mathrm{mol\,L^{-1}}$ sodium acetate solutions.

3.3. Procedure

3.3.1. Individual calibration

An aliquot of the solution containing 50–400 ng of beryllium ion or 30–1000 ng of aluminum ion, 0.9 mL of $1.0 \times 10^{-4}\,\mathrm{mol\,L^{-1}}$ CAS solution, 2 mL of pH 6 acetate buffer solution, 1 mL of $0.15\,\mathrm{mol\,L^{-1}}$ iodide solution and 1 mL of 0.1% (w/v) CTAB solution was transferred into a 10-mL tube. The solution was diluted to approximately 9 mL with water and allowed to stand for 10 min in room temperature. Then 1 mL of 0.10% (v/v) Triton X-114 solution was added and made up to the mark with water. Separation of two phases was acceler-

ated by centrifugation for 5 min at 3000 rpm. The aqueous phase was easily decanted by simply inverting the tube. The surfactant rich phase of this procedure was dissolved and diluted to 0.5 mL with the mixture of acetonitril/pH 6 acetate buffer (4:1) and transferred into a 0.5-mL quartz cell. The absorbance spectrum of the solution was recorded and stored in the range of 350–750 nm.

The blank solution was submitted to the same procedure and its spectrum was recorded and stored.

3.3.2. Mean centering of ratio spectra

A calibration graph for beryllium is obtained by recording and storing the spectra of standard solutions containing different concentrations of Be(II) and using Al(III) and blank spectra. The stored spectra of the solutions of Be(II) are divided by standard spectrum of Al(III) according to Eq. (2). Then mean centering of these vectors with respect to wavelength are obtained according to Eq. (3) After that residual vector is divided by MC($\alpha_{Blank}/\alpha_{Al}$) corresponding to the MC of the ratio of the spectra of blank and Al(III) according to Eq. (4). The minimum or maximum of the mean centering of later vectors with respect to wavelength is used for the construction of calibration graph for Be(II). For the prediction of concentration of Be(II) in synthetic ternary mixtures and real samples the same procedure was used except that the spectra of the mixture were used instead of the spectra of standard solution of Be(II).

For construction of calibration curves for Al(III), the stored spectra of the standard solutions of Al(III) are divided by standard spectrum of Be (II) according to Eq. (2). Then mean centering of these vectors with respect to wavelength are obtained according to Eq. (3). After that residual vector is divided by MC($\alpha_{Blank}/\alpha_{Be}$) corresponding to the MC of the ratio of the spectra of blank and Be(II) according to Eq. (4). The minimum or maximum of the mean centering of later vectors with respect to wavelength is used for the construction of calibration graph for Al(III). For the prediction of concentration of Al(III) in synthetic ternary mixtures and real samples the same procedure was used except that the spectra of the mixture were used instead of the spectra of standard solution of Al(III).

4. Results and discussion

Triphenylmethane dye Chrom Azurol S ($3''$-Sulfo-$2''$,$6''$-dichloro-$3,3'$-dimethyl-4-hydroxyfuchsone-$5,5'$-dicarboxylic acid, trisodium salt; (CAS)) reacts with beryllium and aluminium to form the anionic complex $Be(CAS)_2$ and $Al(CAS)_3$ [5,6,23]. Surfactants can interact with dye and/or the metal–dye complex as an individual molecule or aggregates. For example, cationic surfactants react by ion pair formation with the anionic $Be(CAS)_2$ and $Al(CAS)_3$ to form a ternary complex involving surfactant monomers.

The absorption spectra of Al(III) and Be(II) complexes with CAS are shown in Fig. 1. As Fig. 1 shows, the spectra of the CAS and the complexes overlap with each other, and therefore each compound interferes in the spectrophotometric determination of the others. But simultaneous determination of Al(III) and Be(II) is possible by using mean centering of ratio profiles.
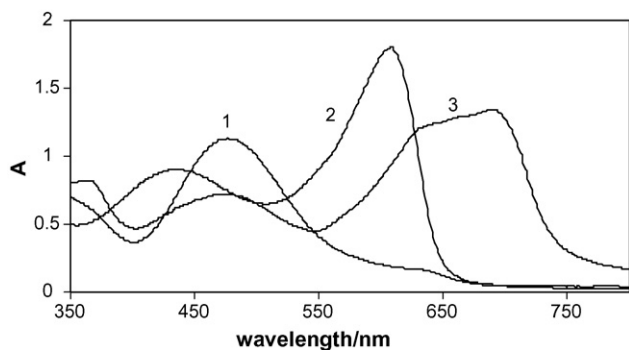
Fig. 1. The ordinary spectra of a 5×10^{-5} mol L^{-1} CAS solution (1), its complexes with 25 ng mL^{-1} Be^{2+} (2) and 70 ng mL^{-1} Al^{3+} (3) at pH 6 after CPE.

4.1. Optimization of the system

To take full advantage of the procedure, the reagent concentrations and reaction conditions must be optimized. Various experimental parameters were studied in order to obtain optimized system. These parameters were optimized by setting all parameters to be constant and optimizing one each time.

In order to find the optimum conditions, the effect of pH on the spectrum of a constant concentration of each complex was investigated. Although there was no significant changes in the spectra of Be(II) and Al(III) complexes with CAS in the pH range 3–8, but the results showed that the pH of 5 and 6.5 gives the highest sensitivity for determination of Al(III) and Be(II), respectively. In order to have a moderate sensitivity, pH 6 has been selected as the suitable one for simultaneous analysis of Be(II) and Al(III).

Effect of CAS concentration on the extraction and determination of beryllium was investigated in the range 2.0×10^{-6} to 1.1×10^{-5} mol L^{-1}. The sensitivity of the method increased by increasing CAS concentration up to 9.0×10^{-6} mol L^{-1} and decreased at higher concentrations. It was expected that increasing CAS causes an increase in absorbance because increasing in CAS concentration caused an increase in Be(CAS)$_2$ and Al(CAS)$_3$ concentration. At concentrations higher than 9.0×10^{-6} mol L^{-1} the concentration of complex did not change significantly but the concentration of uncomplexed CAS increases significantly. Therefore, much probably decrease of absorbance at concentrations higher than 9.0×10^{-6} mol L^{-1} decreases is due to this fact that the free CAS competes with the complexes in extraction to surfactant rich phase. A concentration of 9.0×10^{-7} mol L^{-1} of CAS was selected as the optimum.

Effect of CTAB concentration on the extraction and determination of beryllium and aluminum was investigated in the range 0.003–0.03% (w/v). The amount of the absorbance for sample increased by increasing in CTAB concentration up to 0.01% (w/v) and remained constant at higher concentrations. Therefore, 0.01% (w/v) CTAB was chosen as the optimum.

Effect of Triton X-114 as a co-extraction agent in CPE procedure was also investigated in the range 0–0.02% (v/v). The absorbance of the complexes was increased by increasing Triton X-114 and remains constant in the range upper than 0.01(v/v).

Therefore, a concentration of 0.01% (v/v) Triton X-114 was selected for further works.

As described above, addition of salt can cause cationic surfactant solutions to separate into immiscible surfactant-rich and surfactant-poor phases. Therefore, iodide was added to induce micelle growth and extraction of complex. The effect of iodide concentration was studied in the range 0.002–0.02 mol L^{-1}. The results showed that at zero point the micellization process does not take place and the amount of ΔA is zero. Addition of 0.002 mol L^{-1} iodide sufficed for maximum extraction of the complex and the signal remained constant at higher concentrations. A concentration of 0.015 mol L^{-1} iodide was selected for further works.

Effect of time on the reaction and also on the CPE procedure was investigated. The results showed that complexation reactions were completed in 10 min. Also a 10 min centrifugation at 3000 rpm was found to be enough for successful CPE.

In order to select the proper dilution solvent for the surfactant-rich phase, different solvents were tried so as to select the one producing the optimal results regarding sensitivity. A mixture of pH 6 buffer solution with different solvents was used. As the complexes did not form in pure solvent buffer solution was added to the solvent to provide proper conditions for complex formation. Among methanol, ethanol, DMF, acetone and acetonitril the last one (acetonitril) gave the best results due to high sensitivity and low overlapping of spectra of components. Therefore, a mixture of acetonitril/pH 6 acetate buffer (4:1) solution was added to surfactant-rich phase after CPE in order to facilitate its transfer into spectrophotometric cell. A 0.3 mL acetonitril/pH 6 acetate buffer (4:1) was chosen in order to have appropriate amount of sample for transferring and measurement of the absorbance of the sample and also a suitable preconcentration factor. Therefore, a preconcentration factor of 20 was archived using the proposed method.

4.2. Mean centering of ratio spectra

The absorption spectra of the standard solutions of Be(II) with different concentrations were recorded in the wavelength range of 350–800 nm (Fig. 2a) and divided by the normalized spectrum of the Al(III) and the ratio spectra were obtained. Mean centering (MC) of the ratio spectra were obtained in the range 565–590 nm. After that these vectors (MC of ratio spectra) were divided by MC($\alpha_{Blank}/\alpha_{Al}$) corresponding to the MC of the ratio of the normalized spectra of blank and Al(III) and second ratio spectra (according to Eq. (4)) were obtained. MC of these vectors was obtained (Fig. 2b). The amount of Be(II) was determined by measuring the amplitude at 570 nm corresponding to a maximum wavelength in the MC of second ratio spectra as shown in Fig. 2b. For the prediction of concentration of Be(II) in synthetic ternary mixtures and real samples the same procedure was used except that the spectra of the mixture were used instead of the spectra of standard solution of Be(II).
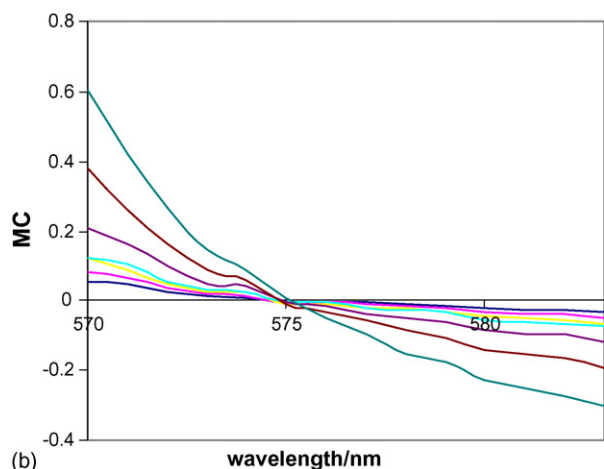
In the same way, the absorption spectra of the standard solutions of Al(III) with different concentrations were recorded in the wavelength range of 350–850 nm (Fig. 3a) and divided by the normalized spectrum of the Be(II) and the ratio spectra
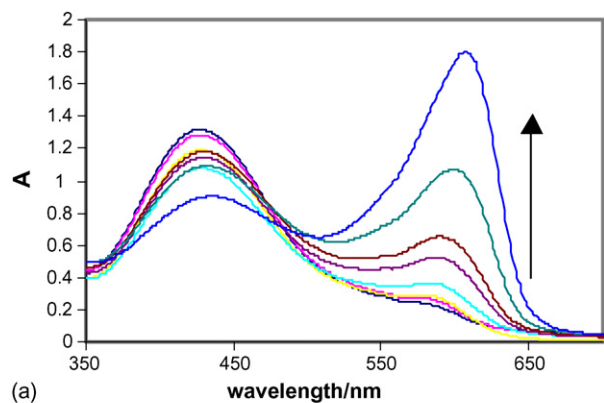
Fig. 2. The zero order spectra of different concentrations of beryllium (a) and MC of their ratio spectra obtained with according to Eq. (3) (b).

Fig. 3. The zero order spectra of different concentrations of aluminum (a) and MC of their ratio spectra obtained with according to Eq. (3) (b).

were obtained. Mean centering (MC) of the ratio spectra were obtained in the wavelength range of 370–445 nm. After that these vectors (MC of ratio spectra) were divided by $MC(\alpha_{Blank}/\alpha_{Be})$ corresponding to the MC of the ratio of the normalized spectra of blank and Be(II) and second ratio spectra (according to Eq. (4)) were obtained. MC of these vectors was obtained (Fig. 3b). The amount of Al(III) was determined by measuring the amplitude at 380 nm corresponding to a maximum wavelength in the MC of second ratio spectra as shown in Fig. 3b. For the prediction of concentration of Al(III) in synthetic ternary mixtures and real samples the same procedure was used except that the spectra of the mixture were used instead of the spectra of standard solution of Al(III).

Table 1 summarizes the analytical characteristics of the optimized method, including regression equation, linear range, limit of detection and limit of quantification (LOQ). Because the amount of analytes in 10 mL of sample solution is measured

after preconcentration by CPE in a final volume of 0.5 mL, the solution is concentrated by a factor of 20. The improvement factor, defined as the ratio of the slope of the calibration graph for the CPE method to that of the calibration graph in micellar media without preconcentration, was 40.3 and 33.4 for Al(III) and Be(II), respectively. The limit of detection, defined as $C_L = 3S_B/m$ [24], where C_L, S_B, and m are the limit of detection, standard deviation of the blank and slope of the calibration graph, respectively, was 0.98 and 0.52 ng mL^{-1} for Be(II) and Al(III), respectively.

The limit of quantification, defined as $C_Q = 10S_B/m$ [24], where C_Q is limit of quantification was 3.27 and 1.73 ng mL^{-1} for Be(II) and Al(III), respectively.

In order to obtain the accuracy and precision of the method, several synthetic mixtures with different concentration ratios of Al(III) and Be(II) were analyzed using the proposed method. The results are given in Table 2. The prediction error of a single component in the mixtures was calculated as the relative

Table 1
Analytical characteristics of the optimized method

Analyte	Wavelength (nm)	Calibration equation[a]	R^2 ($N=8$)	Linear range/ng mL^{-1}	LOD/ng mL^{-1}	LOQ/ng mL^{-1}
Be	570	$Y = 0.0153C + 0.01$	0.9956	5–40	0.98	3.27
Al	380	$Y = 0.0726C - 0.1142$	0.9934	3–100	0.52	1.73

[a] C is the concentration of analyte in ng mL^{-1}.

Table 2
Results for several experiments for analysis of Be–Al binary mixture by mean centering of ratio spectra

Taken/ng mL^{-1}		Found/ng mL^{-1}		Recovery (%)	
Be	Al	Be	Al	Be	Al
5	3	5	3.2	100	106.6
10	10	10.1	10.3	101	103
10	10	10.4	9.5	104	95
25	3	25.4	2.8	101.6	93.3
25	70	25.5	70.4	102	100.6
30	40	30.7	40.6	102.3	101.5
30	50	30.5	49.1	101.7	98.2
40	50	39.5	50.5	98.8	101
40	25	40.1	25.4	100.2	101.6
15	100	14.5	100.4	96.7	100.5
Mean recovery				100.8	100.1
R.S.E. signal (%)				1.65	1.04
R.S.E.$_t$ total (%)					1.21

standard error (R.S.E) of the prediction concentration [25]:

$$R.S.E.(\%) = \left(\frac{\Sigma_{j=1}^{N}(\hat{C}_j - C_j)^2}{\Sigma_{J=1}^{N}(C_j)^2} \right)^{1/2} \times 100 \qquad (6)$$

where N is the number of samples, C_j the concentration of the component in the jth mixture and $\hat{C}_j$ the estimated concentration. The total prediction error of N samples is calculated as follows:

$$R.S.E._t(\%) = \left(\frac{\Sigma_{i=1}^{M}\Sigma_{j=1}^{N}(\hat{C}_{ij} - C_{ij})^2}{\Sigma_{i=1}^{M}\Sigma_{J=1}^{N}(C_{ij})^2} \right)^{1/2} \times 100 \qquad (7)$$

where C_{ij} is the concentration of the ith component in the jth samples and $\hat{C}_{ij}$ its estimation. Table 2 also shows the reasonable single and total relative errors for such system.

To check the repeatability of the method, five replicate resolving of Al(III) and Be(II) in their binary mixtures were performed. The relative standard deviation (R.S.D.) for five replicate determinations of binary mixtures containing 70.0 ng mL^{-1} of Al(III) and 25.0 ng mL^{-1} of Be(II) was obtained as 2.85 and 2.41%, respectively. The mean recoveries for simultaneous determination of these species in binary mixtures were obtained as 98.8 and 101.8% for Al(III) and Be(II), respectively.

4.3. Selectivity

In order to study the selectivity of the proposed method, we tested the effect of various cations and anions on the preconcentration and determination of a mixture of 10 ng mL^{-1} of Be^{2+} and 10 ng mL^{-1} of Al^{3+} by the proposed method under the optimum conditions. The results are summarized in Table 3. The tolerance limit was defined as the concentration of added ion that caused less than $\pm 3\%$ relative error. The ions Cd^{2+}, Co^{2+}, Cu^{2+}, Mn^{2+}, Fe^{2+}, Pb^{2+}, Zn^{2+}, V(IV), Zr(IV), Mo(VI), Fe^{3+} and V(V) interfered at 50 ng mL^{-1}. The interfering effects of Cd^{2+}, Co^{2+}, Cu^{2+}, Mn^{2+}, Fe^{2+}, Pb^{2+}, Zn^{2+}, V(IV), Zr(IV), Mo(VI) up to 5000 ng mL^{-1} were completely removed by the addition of

Table 3
Tolerance ratios of diverse ions on the determination of 10 ng mL^{-1} of Be^{2+} and 10 ng mL^{-1} of Al^{3+}

Ion	Tolerance limit/ng mL^{-1}
Na$^+$, K$^+$, NH$_4^+$, Br$^-$, Cl$^-$, NO$_3^-$, SO$_4^{2-}$, CO$_3^{2-}$, Mg^{2+}, Ca^{2+}, ClO$_3^-$	5000
Cd^{2+}, Co^{2+}, Cu^{2+}, Mn^{2+}, Fe^{2+}, Pb^{2+}, Zn^{2+}, V(IV), Zr(IV), Mo(VI), Fe^{3+}, V(V)	5000^a
PO$_4^{3-}$, F$^-$, Citrate	200

^{a} After removing as described in text.

Table 4
Determination of Al(III) and Be(II) added to water samples by the mean centering of ratio spectra

Sample	Amount added/ng mL^{-1}		Amount found/ng mL^{-1}		Recovery (%)	
	Al(III)	Be(II)	Al(III)	Be(II)	Al(III)	Be(II)
Tap water	15.0	25.0	15.5	25.2	103.3	100.8
	30.0	40.0	29.9	40.2	99.7	100.5
	40.0	70.0	40.1	70.0	100.3	100.0
Well water	20.0	10.0	19.5	10.2	97.5	102.0
	40.0	20.0	40.2	19.9	100.5	99.5
	60.0	30.0	60.0	30.2	100.0	100.7

0.5 mL of 0.1% EDTA solution. The interfering effects of Fe^{3+} and V(V) up to 5000 ng mL^{-1} were completely removed by the addition of ascorbic acid to the solution.

4.4. Application

The proposed method was successfully applied to the determination of aluminum and beryllium ion in water samples. The results are shown in Table 4. The recoveries are close to 100% and indicate that both proposed methods were helpful for the determination of these cations in the real samples.

5. Conclusion

The proposed procedures give selective, very sensitive, and low-cost spectrophotometric procedure for simultaneous analysis of beryllium and aluminum that can be applied to real samples. The surfactant has been used for preconcentration of beryllium and aluminum, and thus toxic solvent extraction, has been avoided. Mean centering of ratio spectra has been used to obtain pure analyte response free from absorbent reagent blank. To the best of our knowledge this is the first report on the cloud point extraction for simultaneous analysis of beryllium and aluminum.

References

[1] G.D. Clayton,. And, F.E. Clayton (Eds.), Patty's Industrial Hygiene and Toxicology, vol. 2a, 2b, 2c: toxicology, third ed., John Wiley sons, New york, 1981–1982, p. 1547.
[2] World Health Organization/International Programme on Chemical Safety. Environmental Health Criteria 194. Aluminium. pp. 1–13 (1997).
[3] U.T. Hill, Anal. Chem. 30 (1958) 521.

[4] U.T. Hill, Anal. Chem. 31 (1959) 429.

[5] K. Hayashi, Y. Sasaki, S. Tagashira, E. Kosaka, Anal. Chem. 58 (1986) 1444.

[6] Z. Marczenko, M. Jarosz, Analyst 107 (1982) 1431.

[7] N.K. Agnihotri, H.B. Singh, R.L. Sharma, V.K. Singh, Talanta 40 (1993) 415.

[8] M.C. Valencia, S. Boudra, J.M. Bosque-Sendra, Anal. Chim. Acta 327 (1996) 73.

[9] A. Afkhami, A.R. Zarei, Anal. Sci. 20 (2004) 1711.

[10] T. Madrakian, A. Afkhami, M. Borazjani, M. Bahram, Spectrochim. Acta, Part A 61 (2005) 2988.

[11] J. Liang Li, C.B. Hung, J. Colloid Interface Sci. 263 (2003) 625.

[12] H. Rehage, H. Hoffmann, Mol. Phys. 74 (1991) 933.

[13] H. Hoffmann, in: C.A. Herb, R. Prudhomme (Eds.), Structure and Flow in Surfactant Solutions, ACS Symposium Series 578, American Chemical Society, Washington, DC, 1994, p. 2.

[14] V.K. Aswal, P.S. Goyal, P. Thiyagarajan, J. Phys. Chem. B 102 (1998) 2469.

[15] A.E. Vassiliades, in: E. Jungerman (Ed.), Cationic Surfactants, Marcel Dekker, New York, 1970, p. 387.

[16] H.L. Booij, in: H.R. Kruyt (Ed.), Colloid Science, Elsevier, Amsterdam, 1949, p. 681.

[17] I. Cohen, C.F. Hiskey, G. Oster, J. Colloid Sci. 9 (1954) 243.

[18] A. Afkhami, M. Bahram, Talanta 66 (2005) 712.

[19] A. Afkhami, M. Bahram, Anal. Chim. Acta 526 (2004) 211.

[20] A. Afkhami, M. Bahram, Talanta 68 (2006) 1148.

[21] A. Afkhami, T. Madrakian, M. Bahram, J. Haz. Mater. 123 (2005) 250.

[22] A. Afkhami, M. Bahram, Spectrochim. Acta, Part A 61 (2005) 869.

[23] A. Afkhami, T. Madrakian, E. Bozorgzadeh, M. Bahram, Talanta, in Press.

[24] V. Thomsen, D. Schatzlein, D. Mercuro, Spectroscopy 18 (2003) 112.

[25] H. Abdollahi, Anal. Chim. Acta 442 (2001) 327.

Ultra-trace level determination of hydroquinone in waste photographic solutions by UV–vis spectrophotometry

Sirajuddin *, M. Iqbal Bhanger, Abdul Niaz, Afzal Shah, Abdul Rauf

National Center of Excellence in Analytical Chemistry, University of Sindh, Jamshoro, Pakistan

Abstract

A simpler UV–vis spectrophotometric method was investigated for hydroquinone (HQ) determination using $KMnO_4$ as oxidizing agent for conversion of HQ to p-benzoquinone (BQ) as well as signal enhancer. Various parameters such as analytical wavelength, stability time, temperature, pH, solvent effect and interference of chemicals were checked and parameters optimized by using $1\,\mu g\,ml^{-1}$ standard solution of HQ. Beer's Law was applicable in the range of 0.07–$2\,\mu g\,ml^{-1}$ and 0.005–$0.05\,\mu g\,ml^{-1}$ at 245.5 nm and at 262 nm for aqueous standard solutions of HQ with linear regression coefficient value of 0.9978 and 0.9843 and detection limit of $0.021\,\mu g\,ml^{-1}$ and $0.0016\,\mu g\,ml^{-1}$ HQ, respectively. Standard deviation of 1.7% and 2.4% was true for $1\,\mu g\,ml^{-1}$ and $0.03\,\mu g\,ml^{-1}$ HQ solution ($n = 11$) run at respective wavelengths. The method was successfully applied to dilute waste photographic developer samples for free HQ determination.
© 2006 Elsevier B.V. All rights reserved.

Keywords: UV–vis spectrophotometry; Hydroquinone; $KMnO_4$; Oxidation/reduction

1. Introduction

Hydroquinone (HQ) is used as a developer in black and white photography, an antioxidant for fats and oils, a polymerization inhibitor, a stabilizer in paints, varnishes, motor fuels, oils, an intermediate for rubber processing chemicals in the production of mono and dialkyl ethers and as de-pigmenting agent [1].

Besides its positive and beneficial utilization, it bears some harmful and toxic aspects as well, which may produce serious health complications due to its release especially in water and air from mentioned and other sources. The possible health problems include irritation of skin, eyes, nose and throat, dizziness, headache, unconsciousness, tinnitus, breathing difficulties and others [2]. It has also been reported as a nephrocarcinogenic reagent [3]. According to other report [4] mononuclear compounds such as benzene metabolites, caffeic acid and o-toluidine should express their carcinogenicity through oxidative DNA damage.

Various authors [5–7] have determined HQ by various techniques such as high performance liquid chromatography (HPLC), gas chromatography–mass spectrometry (GC–MS) and voltammetry [8,9] in different types of samples. Colorimetric analysis of small amount of HQ in styrene has also been reported [10]. Spectrophotometric determination of HQ has also been cited elsewhere [11–14]. All the workers employing these techniques have tried to modify sensitivity of the method after optimization of the relative parameters.

Each of the above methods for HQ determination is however, somewhat complicated, costly and more hazard producing due to utilizing many expensive and toxic materials and reagents. In contrast, our newly developed method is very fast, simple, economical and environmental friendly. Moreover, it has lower detection limits, better sensitivity and better application range for dilute aqueous samples where matrix effect minimizes the interfering effect of ions or reagents.

2. Experimental

2.1. Instrumentation

Spectrophotometric analysis of HQ was performed with a Lambda 2 UV–vis spectrometer of Perkin-Elmer company. Temperature related observations were carried out with the help of a controlled temperature Water Bath, Model, GMBH D-7633,

---

* Corresponding author. Tel.: +92 22 2771379; fax: +92 22 2771560.
E-mail address: drsiraj03@hotmail.com (Sirajuddin).

Julabo HC5, Germany, to which was attached a double wall flow-type cell having a thermometer dipped in the test tube containing the analyte solution.

2.2. Reagents and solutions

Analytical grade HQ and potassium permanganate of E. Merck (Germany) were used for most of preparations. Other chemicals and salts used in this study were also of analytical grade with greater than 99% purity purchased from different popular companies. Preparation of solutions and final washings of all glassware were performed with doubly distilled water. Fresh solutions of HQ with required strengths were prepared each day for routine work.

2.3. Procedure

According to procedure, after optimization studies a standard HQ solution was prepared by taking first 0.3 ml of 0.0001 M KMnO$_4$ solution in a 10 ml volumetric flask. To this was then added appropriate volume of HQ from a 100 μg ml^{-1} solution of HQ, shaken thoroughly and made to the mark with doubly distilled water. Same procedure was repeated for preparing blank but without HQ. The instrument was set at zero in air with appropriate range and the absorbance of HQ solution was read at 245.5 nm against the blank put in the reference compartment. The diluted samples of waste photographic developer solution were similarly treated and the unknown concentration of HQ determined from calibration plot.

3. Results and discussion

HQs are thermodynamically less stable at neutral pH than the corresponding quinones (Qs) [15]. In a buffered aqueous solution, HQ is slowly oxidized to BQ via a semiquinone (SQ) radical [16]. The same is true for HQ by a Cu(II)-mediated oxidation to corresponding SQ radicals which are then oxidized to *p*-benzoquinone [4] leading to DNA damage according to following mechanism (Fig. 1).
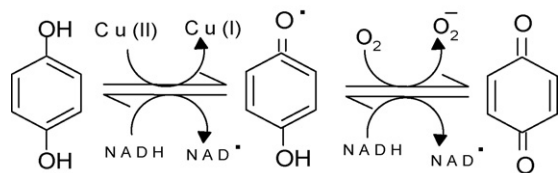

Fig. 1. Conversion of HQ to BQ with Cu(II)-mediation.

The same type of conversion is true for other metal ions capable of oxidizing HQ to BQ via SQ formation. Being a strong oxidizing agent, KMnO$_4$ has tremendous capability of oxidizing HQ to BQ in the same fashion as true in case of Cu(II), however the role of Mn(VII) in DNA damage has not been reported so far.

Fig. 2 describes the conversion of 1 μg ml^{-1} aqueous HQ into HQ (λ_{max}, 288 nm), SQ (λ_{max}, 222 nm) and BQ (λ_{max}, 245.5 nm) in the absence and presence of KMnO$_4$ solution. It is evident from the figure that after dissolution of HQ in water, the
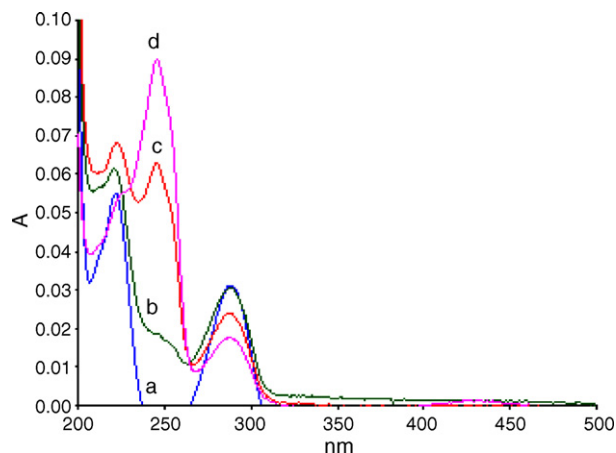

Fig. 2. UV spectra showing formation of: (a) HQ (288 nm) and SQ (222 nm) in water without KMnO$_4$ and (b), (c) and (d) BQ (245.5 nm) in presence of 0.1, 0.5 and 1.0 μM KMnO$_4$, respectively.

formation of SQ radical occurs which is due to photo-oxidation of HQ. BQ is also formed but after a very long time [17].

For aqueous solution of 1 μg ml^{-1} HQ, the absorption spectra of SQ increases with subsequent appearance and increase in BQ spectrum while that of HQ decreases in the presence of 0.1 and 0.5 μM KMnO$_4$ solution. As soon as the concentration of KMnO$_4$ reaches to 1 μM or more, the spectra of HQ and SQ are nearly completely transformed into a single spectrum of BQ. It means that KMnO$_4$ addition leads to catalytic oxidation of HQ into a final product BQ at 245.5 nm. The BQ absorption at this wavelength (245.5 nm) was confirmed by spiking the BQ solution to aqueous solution of HQ free of KMnO$_4$. The same wavelength of 288 nm has been described [18] for HQ determination in reversal first developer. The wavelength of 248 and 290 nm has been described by Jiahai et al. [19] for BQ and HQ, respectively. Their quoted values are a little bit higher due to pH value of 2.9 they used for recording the UV spectra.

This conversion of HQ into BQ was taken as the basis for ultra-trace determination of HQ in aqueous solutions where the formation of yellowish solution is responsible for absorption in UV region due to catalytic oxidation of the HQ into BQ by KMnO$_4$. In other words the HQ is determined at the cost of BQ formation. The formation of yellow colored solution is the indication of BQ formation. Moreover, the conversion of HQ into BQ brings structural changes from benzenoid to quinoid ring according to chromophore theory [20]. HQ has also been determined by HPLC in air as BQ after oxidation on a permanganate-impregnated glass–fiber filter, trapping BQ on an XAD-2 adsorbent and desorbing it with acetonitrile [21].

From Figs. 1 and 2, a possible proposed mechanism for conversion of HQ into BQ via SQ can be worked out for Mn(VII) of KMnO$_4$ as shown in Fig. 3.

It is clear from Fig. 2 that before adding KMnO$_4$ the formation of HQ into SQ takes place but no BQ is formed. It means that SQ formation from HQ can occur in the presence of O$_2$. After using KMnO$_4$ up to 0.5 μM there is an increase in the spectrum of SQ with subsequent decrease in that of HQ. It means that KMnO$_4$ enhances the conversion of HQ into SQ. So it proves the
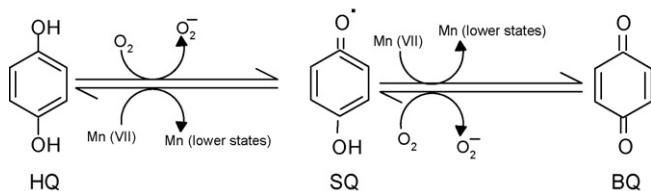
Fig. 3. Proposed mechanism for conversion of HQ into SQ and BQ.

participation of permanganate in the first step which oxidizes HQ into SQ. The formation of spectrum of BQ after continuous use of permanganate from 0.1 to 0.5 μM proves its role in conversion of HQ into BQ via SQ. Further use of permanganate solution up to 1 μM or greater speeds up conversion of HQ into BQ at such a rate as the SQ radical formation seems absent. With still further addition of the former the spectrum of HQ also disappears and the spectrum of BQ dominates. This proves the involvement of Mn(VII) of permanganate for oxidation of HQ into BQ with subsequent reduction of Mn(VII) into lower state. The reduction of Mn(VII) into lower state is also evident from the lowering and the disappearance of Mn(VII) spectrum which is present at lower concentration of analyte in a range of 400–500 nm. The role of O_2 in second step is not essential but can assist Mn(VII) for its catalytic action. According to literature [22], a significant portion of Mn is reduced to Mn(II) by reaction with HQ.

3.1. Optimization of parameters

Among the parameters which are often crucial for accurate analysis are pH, time for color development, stability of color, solvent composition and order of adding reagent.

3.2. Optimization of analytical wavelength

In the absence of interferences, the wavelength chosen for a quantitative determination is the wavelength of maximum absorbance. Sometimes the adding coloring reagent may absorb very close to the same region where the determining substance does. To avoid big errors in the wavelength (λ_{max}) of the species, it is essential to use a reagent which gives zero absorption at maximum absorbance value for analyte [23]. (Fig. 4) describes the absorbance of 1 μg ml^{-1} HQ solution as BQ at different wavelengths after 5 min mixing with 10 μM KMnO$_4$ solution.
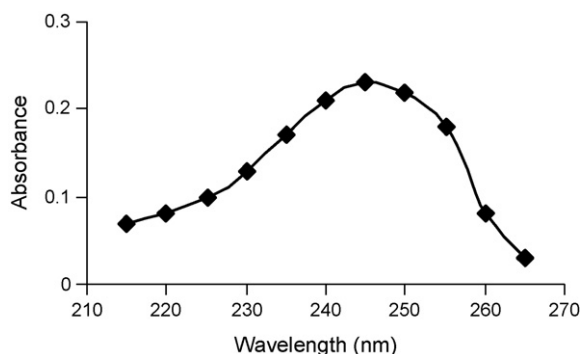

Fig. 4. Change of absorbance with wavelength.

It is evident that maximum absorbance of 0.23 occurs at a wavelength of 245 nm. However, the actual central value of 245.5 nm was chosen as λ_{max} which is nearly same as reported earlier [19].

3.3. Optimization of mixing amount of KMnO$_4$ solution

The effect of adding various amount of KMnO$_4$ solution on absorbance of 1 μg ml^{-1} HQ solution is given in Fig. 5. Observations were made after 5 min mixing of the two solutions at λ_{max} value of 245.5 nm.
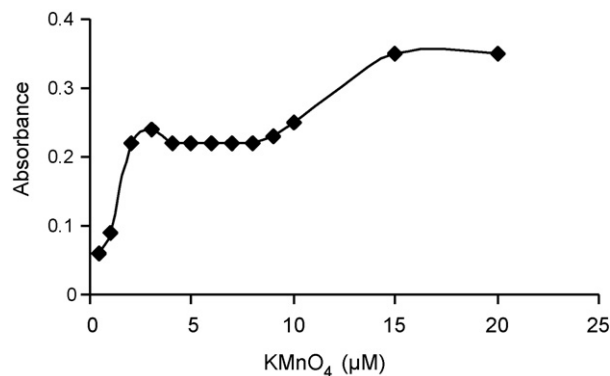
Fig. 5. Effect of KMnO$_4$ addition on absorbance of HQ.

It is seen that the maximum absorbance of 0.35 occurs in the presence 15 and 20 μM solution of KMnO$_4$ but the concentration of 3 μM KMnO$_4$ solution showing an absorbance of 0.24 was taken as optimum amount for further study because a calibration plot check of HQ in case of former solution did not result in better absorbance value at lower HQ concentration. Although it is clear that the volume of 15 μM KMnO$_4$ is sufficient enough to make the reaction first order in favor of 1 μg ml^{-1} HQ but it produces poor response at lower HQ concentration. This may be due to re-oxidation of lower state Mn ions to higher state by the formed BQ and conversion of later to SQ because SQ spectra were observed after addition of greater amount of KMnO$_4$. However, at lower concentration (3 μM KMnO$_4$ solution) such problem does not exist due to limited amount of Mn present. According to literature [24], application of a higher KMnO$_4$ concentration would facilitate the determination of analyte in a higher concentration range. A reverse behavior of formation of SQ with subsequent formation of HQ and hydroxyl-HQ from BQ by a metal in lower state such as Fe(II) has also been reported earlier [25] where no complex formation was reported between Fe(III) formed and BQ. Chemiluminescence study for determination of HQ [26] and chemiluminescence combined with HPLC for simultaneous determination of catechol, resorcinol, HQ and 1,2,4-benzenetriol [27] have also been reported by using its oxidation properties with the system sulfuric acid–potassium permanganate.

3.4. Effect of order of adding reagent

As mentioned earlier, order of adding reagent plays very important role in accuracy of results and peak enhancement.

In the present study it was observed that the addition of 0.3 ml of 0.0001 M $KMnO_4$ (to make 3 μM $KMnO_4$ solution) to 1 μg ml^{-1} HQ solution (taken as 0.1 ml from 100 μg ml^{-1} HQ) and dilution with water up to 10 ml resulted in a lower absorbance value. Taking the water first and adding $KMnO_4$ and HQ also gave poor absorbance value. The greatest absorbance value was observed when we first took 0.3 ml of 0.0001 M $KMnO_4$ then added HQ solution (from 100 μg ml^{-1} HQ standard solution) with thorough mixing and diluting this to 10 ml mark with doubly distilled water. Such studies have also been carried out by other workers [28].

3.5. Optimization of time for development of stable color

In UV–vis spectrophotometry the main problem is the instability of the absorbance value. The researchers try to choose a proper time for the formation of a stable colored complex or chromophore as the case may be to assign stability to the process and get maximum absorbance value for a particular analyte.

Keeping in view the above point, the effect of time on absorbance of 1 μg ml^{-1} HQ solution in the presence of 3 μM $KMnO_4$ solution was checked at 245.5 nm from 1 to 60 min and the results are presented in Fig. 6.
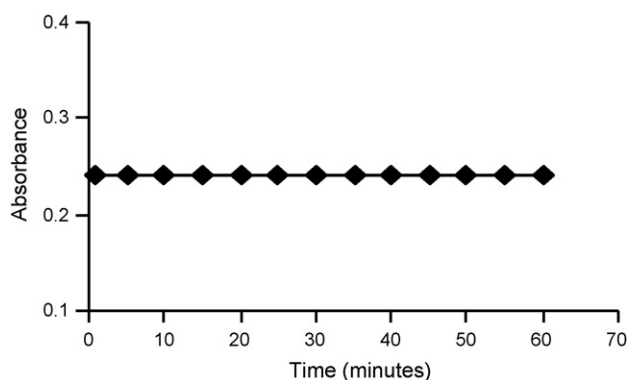

Fig. 6. Dependence of absorbance on mixing time.

It is evident from figure that the solution is quite stable within the range studied. However, 2–5 min after mixing was chosen as optimum time for further study so that one could prepare, mix and process the solution according to his analytical skill. The stable color development in lesser time is due to tremendous oxidizing power of $KMnO_4$ for conversion of HQ into BQ. In comparison to our results, an optimum time of 3 min for color development in case of HQ and catechol each and 13 min in case of resorcinol (including 10 min after addition of other reagents plus 3 min after addition of coloring reagent) has been reported for getting maximum absorbance values [11].

3.6. Temperature optimization

Tells about the effect of temperature on absorbance in the range of 10–60 °C for 1 μg ml^{-1} HQ solution at previously optimized parameters (Fig. 7).
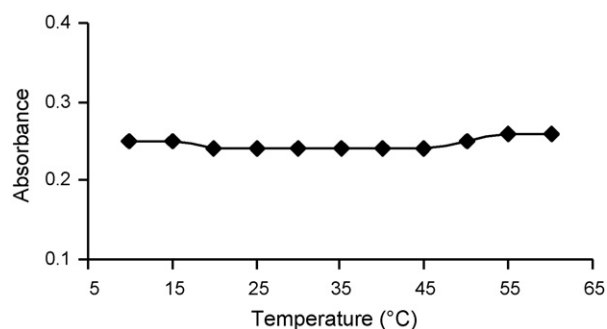
Fig. 7. Effect of temperature on absorbance.

It is seen that at lower and very higher temperature value the absorbance is enhanced while in the range of 20–45 °C it is lower. At lower temperature of 10 and 15 °C the increase in absorbance may be due to the condensation of water vapors from surrounding air and/or adsorption of analyte on the wall of the quartz cell while at higher temperature of 50–60 °C it may be due to evaporation of solvent particles which increases the concentration of analyte. In order to avoid the variation in concentration and hence absorbance of analyte by the mentioned effects, 25 °C was chosen as optimum temperature for further study. The effect of temperature on absorbance of resorcinol, catechol and HQ has also been studied [11] in a range of 5–40 °C, where 25 °C has been selected as optimum temperature.

3.7. Solvent effect

It was aimed to check the better combination of a polar solvent with aqueous solution of HQ containing optimum amount of $KMnO_4$ so that the method could also be applied for water insoluble samples such as creams, gels, etc. after HQ extraction, which could then be mixed with the aqueous solution. The effect of various solvents with different volumes was thus investigated on the absorbance of 1 μg ml^{-1} HQ (as BQ) after mixing with aqueous solution of HQ per 10 ml in 3 μM $KMnO_4$ and the results are given in the Table 1.

It is obvious from the data that 2-propanol is the best solvent with minimum or no effect on the absorbance of analyte and can thus be used in combination with aqueous HQ solution containing optimum amount of $KMnO_4$. So this solvent can be employed for determining HQ in the water insoluble samples such as creams, gels, etc. after extracting it and mixing with water.

3.8. Effect of acidic and basic solutions

The effect of adding various amounts of 0.1 M of various strong and weak acids and bases on the absorbance of 1 μg ml^{-1} HQ solution per 10 ml at already optimized conditions has been studied and the results are shown in Table 2.

It is evident from the table that 0.1 M NaOH produces the greatest % effect of −54.2% with the sole shift of λ_{max} to 257 nm after addition of its 1 ml volume to HQ solution. However, its lower amount produces very little effect. This may be its competition at higher concentration with $KMnO_4$ for oxidizing HQ to

Table 1
Effect of mixing amount of various polar solvents to aqueous solution of 1 µg ml^{-1} HQ per 10 ml

Solvent	Volume (ml)	Absorbance	Effect (%)
Methanol	0.01	0.23	−04.2
	0.10	0.18	−25.0
Ethanol	0.01	0.16	−33.3
	0.10	0.16	−33.3
2-propanol	0.01	0.24	±00.0
	0.10	0.23	−04.2
N-dimethyl formamide	0.01	0.14	−41.7
	0.10	0.12	−50.0

Table 2
Effects of various volumes of acid/base per 10 ml on absorbance of 1 µg ml^{-1} HQ solution

Acid/base (0.1 M)	Volume of acid/base (ml)	Effect (%)	pH of HQ solution	λ_{max} (mid point) (nm)
HCl	0.1	−25.0	3.0	245.5
	1.0	−04.2	2.2	245.5
CH$_3$COOH	0.1	−50.0	4.0	245.5
	1.0	−25.0	3.6	245.5
NH$_3$	0.1	+8.3	9.1	245.5
	1.0	0.0	9.3	245.5
NaOH	0.1	−4.2	10.0	245.5
	1.0	−54.2	11.0	257.0

BQ because according to a report [29] auto-oxidation of HQ to BQ is pH dependent, occurring very rapidly at alkaline pH to produce a brown color but very slowly in acidic solution. The effect of −25.0% by 0.1 ml of 0.1 M HCl and −25.0 and 50.0% by 0.1 and 1 ml of 0.1 M CH$_3$COOH may be due to the reducing effect of these acids on KMnO$_4$ whose capacity of converting HQ to BQ is thus reduced hence resulting in reduced absorbance value. However, the little negative effect of −4.2 by addition of greater volume of 1 ml of 0.1 M HCl may be due to inhibition of reducing effect and hence resuming of the oxidizing properties of KMnO$_4$ as is true in most cases. There is an effect of +8.3% on absorbance of analyte in case of 0.1 ml NH$_3$ addition, however its higher concentration has no effect. The slightly greater effect after NH$_3$ addition may be due to its efficiency of accepting protons to form NH$_4^+$ ions from acidic HQ to help it in its rapid and more enhanced conversion into BQ by KMnO$_4$ assisted oxidation of HQ. The greater amount of 0.1 M NH$_3$ may produce some hindrance to this effect by provision of some electrons to Mn(VII) to convert it to lower state and slowing its capacity for conversion of HQ to BQ, however, not much enough to minimize it.

3.9. Interference study

The percent interference effect of various chemicals used in photographic developer (D-76) solution on 1 µg ml^{-1} HQ solution containing 3 µM KMnO$_4$ at 25 °C is listed below. The values are according to the proposed mixing ratio of these chemicals in the mentioned solution [18] (Table 3).

It is evident from the table that the interference effect is within the acceptable limit of ±5% for all the interferents present in a

waste photographic solution. This study can be compared with the interference study carried out elsewhere [9] who studied the effect of same compounds as we did. However, in that case, the interference was studied in more acidic solution using cyclic voltammetry while we conducted the study by using UV–vis spectrometry in less acidic solution. Such studies of various interfering agents for the analysis of HQ and related compounds have also been reported in another citation [11].

3.10. Calibration plots

HQ can be determined at a concentration ≥1 µg ml^{-1} in any freshly prepared aqueous solution without using any reagent on the basis of UV absorption at λ_{max}, 288 nm as HQ or at λ_{max}, 222 nm as SQ. UV spectra and calibration plots based on such criteria are shown for 1–10 µg ml^{-1} freshly prepared aqueous solution of HQ in Fig. 8. As reported earlier [15] at least traces of BQ are necessary to start the process of auto-oxidation of HQ into BQ via SQ radical formation and this seems to be always realistic since small amounts of BQ are present even in thoroughly purified HQ samples. However, it is seen that there is no UV spectrum in the BQ absorption region (243–247 nm).

Table 3
Interference effect of various salts during HQ determination

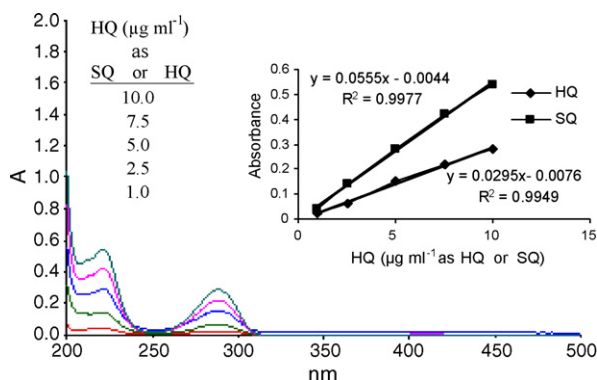| Salt added	Added chemical (µg ml^{-1})	Interference (%)
Metol (*para*-(methylamino)phenol)	0.4	+4.2
Na$_2$SO$_3$	20.0	+4.2
Na$_2$B$_4$O$_7$	0.4	−4.2

Fig. 8. HQ determination as HQ at 288 nm and as SQ at 222 nm in water.

This is due to the presence of BQ at ultra-trace level (below its detection limit).

For older aqueous samples containing HQ one must take care of formed BQ after long time where HQ cannot be determined as HQ or SQ as described in Fig. 8.

For increasing rate of auto-oxidation of HQ, a suitable oxidizing agent or transition metal ion with higher oxidation state such as Cu^{2+} or Fe^{3+} [30] has been used. This is essential for determination of HQ at lower concentration. So HQ must be converted to BQ after addition of proper amount of oxidant to get a single UV spectrum of BQ rather than taking two spectra. This overcomes possible errors due to increase or decrease in SQ and/or HQ spectral height with time in the absence of strong oxidant.

Fig. 9 shows the linear calibration plot of HQ at the extent of BQ formation versus absorbance at optimum amount
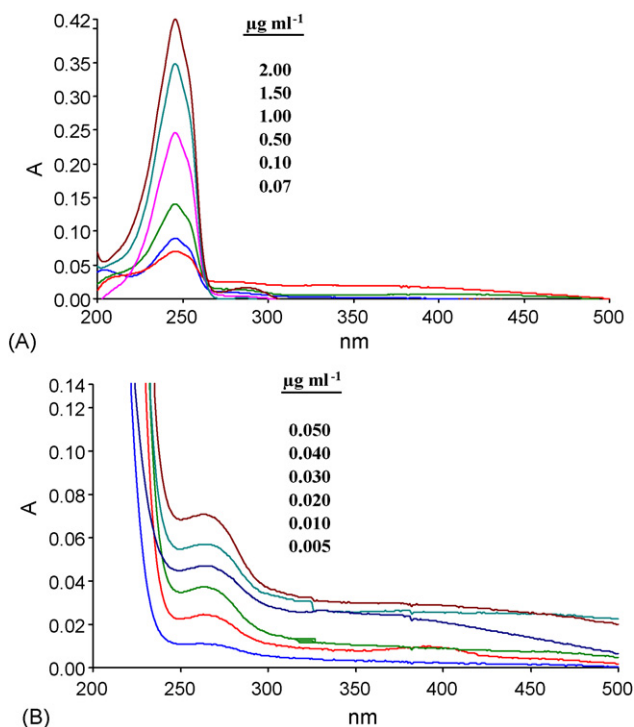

Fig. 9. Calibration plots of standard HQ solutions, (A): 0.07–2 µg ml^{-1} and (B): 0.005–0.05 µg ml^{-1}.

(3 µM) $KMnO_4$ solution in the range of 0.07–2 µg ml^{-1} and 0.005–0.05 µg ml^{-1} HQ at 245.5 and 262 nm having linear regression coefficient value of 0.9978 and 0.9843 with detection limit of 0.021 µg ml^{-1} and 0.0016 µg ml^{-1}, respectively. The standard deviation of 1.7% and 2.4% was obtained for 1 µg ml^{-1} and 0.03 µg ml^{-1} solution of HQ ($n = 11$) at former and later wavelength, respectively.

In case of lower calibration range of 0.005–0.05 µg ml^{-1} HQ, it was observed that initially there was no well-organized UV spectrum for ≥ 0.05 µg ml^{-1} HQ processed by the method described in the experimental section. But when the solution of analyte was thoroughly shaken for 40 s with 10 s interval after each 10 s shaking (optimized for 0.03 µg ml^{-1} HQ but not shown) in Teflon caped 3/4th filled quartz cell, then cap removed and UV spectrum taken after putting it in the sample compartment with blank in the reference compartment, the peak of analyte appeared with a shift in λ_{max}, from 245.5 to 262 nm with a changed shape. This shift may be due to the conversion of formed BQ to some other metabolite with mixed characters of *ortho*, *meta* and *para* BQ because the spectra of catechol and resorcinol were observed in the range of 271–277 nm after addition of $KMnO_4$ solution. However, this transformation was responsible for setting the lowest calibration range and lower detection limit of 0.0016 µg ml^{-1} for HQ determination. One possibility of absorption at 262 nm may indicate the formation of 2-hydroxy-1-4-BQ absorbing above 250 nm [31] which is possible due to excessive shaking of analyte solution for incorporation of OH ion from water to BQ in the presence of oxygen. However such transformations have not been reported in the literature.

These results are better than the range of 0.05–1.2 µg ml^{-1} and detection limit of 0.008 µg ml^{-1} observed [11] and upper and lower ranges of 0.28–0.54 µg ml^{-1} and 0.04–0.18 µg ml^{-1}, respectively with the detection limits of 0.007 µg ml^{-1} HQ as reported [13] using spectrophotometric method.

HQ was also determined in higher concentration ranges, 3–10 µg ml^{-1} and 5–10 µg ml^{-1} as HQ and SQ, respectively after treating with 3 µg $KMnO_4$ solution as shown in Fig. 10.
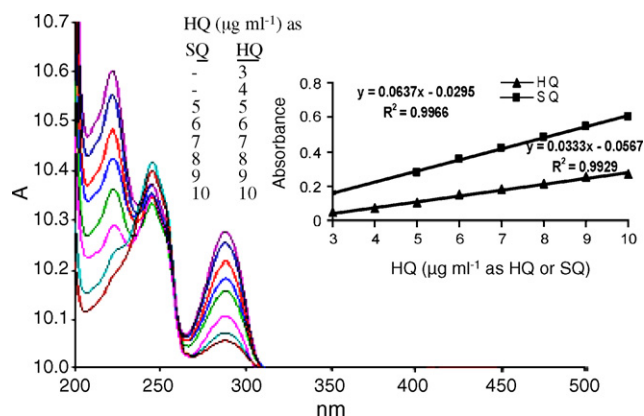

Fig. 10. HQ as HQ at 288 nm and as SQ at 222 nm after treating with 3 µM KMNO$_4$ solution.

This determination of HQ is more feasible than that shown in Fig. 8 because in this case the errors of increase or decrease in concentration of HQ or SQ does not occur and remains constant

Table 4
Analysis of HQ in waste photographic developer samples by newly investigated method

Sample no.	HQ$^{n=11}$ (μg ml^{-1})			
	New method		Reported method	
	Observed value ($D_f = 10,000$)	Actual value	Observed value ($D_f = 500$)	Actual value
1	0.01600 ± 0.00047	160.00 ± 4.70	0.3100 ± 0.0074	155.00 ± 3.70
2	0.02100 ± 0.00034	210.00 ± 3.40	0.4100 ± 0.0054	205.00 ± 2.70
3	0.02400 ± 0.00034	240.00 ± 3.40	0.4800 ± 0.006	240.00 ± 3.00
4	0.02600 ± 0.00054	260.00 ± 5.40	0.5100 ± 0.0087	255.00 ± 4.35
5	0.01000 ± 0.00020	100.00 ± 2.00	0.2100 ± 0.0067	105.00 ± 3.35
6	0.03300 ± 0.00040	330.00 ± 4.00	0.6800 ± 0.0121	340.00 ± 6.05
7	0.01100 ± 0.00013	110.00 ± 1.30	0.2100 ± 0.0034	105.00 ± 1.70
8	0.00900 ± 0.00020	90.00 ± 2.00	0.1800 ± 0.0040	90.00 ± 2.00

Values expressed as, 95% confidence limits; n, no. of replications; D_f, dilution factor.
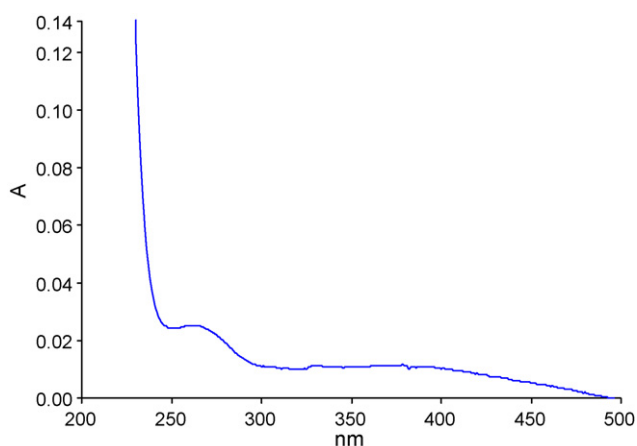

Fig. 11. Spectrum of 10,000-fold diluted waste photographic developer sample.

due to the presence of sufficient amount of BQ in the medium. So this could be applied for determining HQ at higher concentration range.

3.10.1. HQ determination in photographic developer solutions

Fig. 11 shows the UV spectrum of a representative sample of 10,000-fold diluted waste photographic developer solution at optimized conditions by the currently developed method.

The shape of the UV spectrum and $\lambda_{\max}$ of the sample are identical to that of lower range 0.005–0.05 μg ml^{-1} HQ shown in Fig. 9(B).

Table 4 gives the comparison between average results of various waste developer solutions from photographic shops by current method (10,000 times diluted samples) and reported method [11] (500 times diluted samples) within average range of 0.009–0.033 μg ml^{-1} and 0.18–0.68 μg ml^{-1} HQ, respectively. The results are presented as 95% confidence limits, μ [32] by the following equation:

$$\mu = \bar{x} \pm t \left(\frac{s}{\sqrt{n}} \right)$$

where $\bar{x}$, t, s and n represent mean, Student's distribution coefficient, standard deviation and number of replications, respectively.

After calculations, the actual concentration of HQ in the bulk samples ranges from 90 to 330 μg ml^{-1} in case of current method and 90–340 μg ml^{-1} in case of reported method. The closeness of values obtained by two methods proves that the validity of present is quite better and more promising due to its highly reproducible results with extended ranges of application and lower detection limits.

4. Conclusions

Using KMnO$_4$ as reagent for conversion of HQ to BQ and analysis of the former at the extent of formation of the later is very useful for analysis of HQ at ultra-trace level. It is a very good example of redox reaction and may be employed in situation involving useful oxidation products of such types. This method has a clear edge over other methods employing expensive and/or hazardous reagents. Moreover, the lower detection limit achieved by this method which is not possible by other methods can be helpful for presence and source investigation of HQ at ultra-trace level especially in environmental monitoring strategies. Such reaction can also be employed for DNA damage studies in the bacterial cells and others where these studies are considered important.

References

[1] S. Emma, A.G. John, Ann. Occup. Hyg. 43 (1999) 131.
[2] Methods for the Determination of Hazardous Substances (MDHS) Health and Safety Laboratory, Method No. 98, 2003. p 1.
[3] M.M. Peter, T.W. Jones, T.J. Monks, S.S. Lau, Carcinogenesis 18 (1997) 2393.
[4] K. Shosuke, H. Yusuke, M. Mariko, O. Shinji, Free Radic. Biol. Med. 32 (2002) 822.
[5] J. Wittig, S. Wittemer, M. Veit, J. Chromatogr. B 761 (2001) 125.

[6] H. Shou-Chieh, L. Cheng-Chin, H. Ming-Chuan, W. Kuo-Ching, J. Food Drug Anal. 12 (2004) 13.

[7] W. Suramya, R. Nathaniel, L. Guilan, T.S. Martyn, Y. Songnian, M.R. Stephen, Anal. Biochem. 327 (2004) 184.

[8] W. Shengfu, D. Dan, Sensors 2 (2002) 41.

[9] I.D.C. Vieira, O.F. Filho, L. Angnes, Anal. Chim. Acta 398 (1999) 145.

[10] S.M.A. Whettem, Analyst 74 (1949) 185.

[11] A. Afkhami, H.A. Khatami, J. Anal. Chem. 56 (2001) 429.

[12] L.P. Jia, A.M. Zhang, Anal. Abstr. No 5 (2004) 05G156.

[13] X.Y. Huang, C.X. Xu, Anal. Abstr. No. 3 (2004) 03G157.

[14] S. Shahine, R. Mahmoud, Microchem. Acta 70 (1978) 431.

[15] R. Vitaly, B. Tatyana, B. J. Chem. Soc., Perkin Trans. 2 (2000) 1575.

[16] P. Soucek, G. Ivan, S. Pavel, Chem. Biol. Interact. (2000) 45.

[17] Q. Bartolomé, C.C. María del, Proceedings of the 6th Internet World Congress for Biomedical Sciences, Poster #55, Institute for Rehabilitation, Slovenia, 14–25 February, 2000.

[18] Processing KODAK Motion Picture Films, Analytical Procedures, 2003. Module 3.

[19] M. Jiahai, M. Wanhong, S. Wenjing, C. Chuncheng, T. Yalint, Z. Jincai, Environ. Sci. Technol. 40 (2006) 618.

[20] S.F. James, H.S. George, Quantitative Analytical Chemistry, Allyn and Bacon Inc., Boston, London, Sydney, Toronto, 1979, p. 91.

[21] L. Jan-Olof, L. Chemosphere 17 (1988) 671.

[22] U. Bergmann, M.M. Grush, C.R. Horne, P. DeMarois, J.E. Penner-Hahn, C.F. Yocum, D.W. Wright, C.E. Dube, W.H. Armstrong, G. Christou, H.J. Eppley, S.P. Cramer, J. Phy. Chem. B 102 (1998) 8350.

[23] V. Alexeyev, Quantitative Analysis, Mir Publishers/CBS Publishers & Distributers, Moscow/Delhi, 1979 (Translated from Russian by Uvarov).

[24] D. Easwaramoorthy1, Y. Yueh-Chuan, H. Hsuan-Jung, Anal. Chim. Acta 439 (2001) 95.

[25] A.I. Ononye, A.R. McIntosh, J.R. Bolton, J. Phys. Chem. 90 (1986) 6266.

[26] B.G. Corominas, M.C. Icardo, L.L. Zamorab, Talanta 64 (2004) 618.

[27] F. Shun-Li, Z. Li-Ke, L. Jin-Ming, Talanta 68 (2006) 646.

[28] X. Chunli, L. Baoxin, Spectrochem. Acta 60 (2004) 1861.

[29] National Institute for Occupational Safety and Health, "Occupational Exposure to HQ", No. 78, (1978) pp. 182.

[30] Z. Luoping, B. Brian, J.D. Allan, Free Radic. Biol. Med. 20 (1996) 495.

[31] G. Helmut, J. Phys. Chem. A 107 (2003) 11587.

[32] J.C. Miller, J.N. Miller, Statistics for Analytical Chemistry, 2nd edn., Halsted Press, England, 1988, p. 42.

ELSEVIER

Study of reaction processes by in-line near-infrared spectroscopy in combination with multivariate curve resolution Esterification of myristic acid with isopropanol

Marcelo Blanco [a,*], Miguel Castillo [a], Rafael Beneyto [b]

[a] *Department of Chemistry, Faculty of Sciences, Universitat Autònoma de Barcelona, 08193 Bellaterra, Barcelona, Spain*
[b] *Development and Quality Assurance Department, ICI Spain S.A. (Mevisa Site), Ctra Hostalric and Tossa km 1.8,*
08495 Fogars de la Selva, Barcelona, Spain

Abstract

The acid-catalysed esterification of myristic acid with isopropanol was studied by using near-infrared spectroscopy (NIR) in combination with soft-modeling curve resolution (MCR) methodology with a view to establishing the effect of experimental variables on the reaction kinetics. The reaction was conducted at temperatures above the boiling point of the alcohol, with continuous addition of an isopropanol/water mixture to the reactor. Spectral and concentration profiles were determined by applying soft-modeling curve resolution methodology to a column-wise augmented data matrix containing the spectra for the pure components. MCR profiles were compared with reference values and found to depart from then by less than 3% as %RSE for concentrations and to exhibit correlation above 0.999 for spectra.

The reaction kinetics as estimated from the concentration profiles was found to be *pseudo*-first-order. Also, the *pseudo*-first-order rate constant was found to depend on the flow-rate of the isopropanol/water mixture and its water content; although the constant decreased with increase in the proportion of water, a content of *ca.* 15% could be used without important retarding effects on the kinetics. The proposed NIR-MCR method allows the rate constant and the influence of the initial water content to be determined with a view to minimizing consumption of the raw materials and optimizing the experimental conditions.
© 2007 Elsevier B.V. All rights reserved.

Keywords: Near-infrared spectroscopy; Multivariate curve resolution; In-line measurements; Monitoring; Optimization

1. Introduction

The esters of fatty acids and lower alcohols are usually obtained by direct esterification of the acid or transesterification of natural oils with an alcohol, at a relatively high temperature. The low boiling point of the alcohol requires using temperatures below such a point, high pressures in order to increase it or adding the alcohol continuously during the reaction if substantial losses through evaporation are to be avoided. Continuously adding the alcohol requires using a considerably overstoichiometric amount of this reactant and produces a large volume of alcohol/water distillate that must be recovered for subsequent use. However, the reuse of distillates containing much water decreases the final yield to a great extent by displacing equilibrium and altering the rate of the main reaction:

$$R\text{–COOH} + R' - OH \rightleftarrows R - COO - R' + H_2O$$
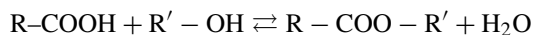
It is therefore essential to determine the effect of the water content on the reaction rate and yield. By monitoring the reaction, one can identify the variation pattern of the composition of the reaction mixture in order to optimize the reaction time, alcohol consumption and distillate reuse, all with a view to reducing consumption of the alcohol and production of waste.

In this work, we studied the esterification at a high temperature (130 °C) of myristic acid with isopropanol – the latter of which was slowly added – and *p*-toluenesulphonic acid as catalyst to obtain isopropyl myristate and water. The water was distilled together with residual isopropanol, the two forming an azeotrope of boiling point 80.4 °C with a water content of 12.3%.

Esterification reactions under homogeneous catalysis are usually second-order in the acid (Ac) and alcohol (Al):

$$v = -\frac{d[Ac]}{dt} = k \cdot [Ac][Al] \tag{1}$$

In the presence of a large excess or a constant understoichiometric amount of alcohol, however, the reaction kinetics can be approximated to a *pseudo*-first-order law for the acid [1,2]:

$$v = -\frac{d[Ac]}{dt} = k' \cdot [Ac] \tag{2}$$

where

$$k' = k \cdot [Al] \tag{3}$$

Eq. (2) can be expressed in integral form as

$$Ln\,[Ac] = Ln\,[Ac]_0 - k' \cdot t \tag{4}$$

where k' is the *pseudo*-first-order rate constant, which depends of various experimental variables including temperature, and the water content and rate of addition of the alcohol, and can be readily determined from a plot of Ln [Ac] *versus* time.

Although this type of esterification reaction under acid catalysis [1–3] has been the subject of several studies, monitoring the process entails withdrawing a large number of samples from the reaction mixture and performing an also large number of analyses. Near infrared spectroscopy (NIR) [4] provides a practical tool for monitoring chemical processes [5–9]; in combination with multivariate calibration techniques such as multivariate curve resolution-alternating least squares methodology (MCR-ALS) [10], it allows the concentration profiles for the reactants as a function of time to be obtained from spectral information for the process and little additional external information [11].

2. A brief introduction to multivariate curve resolution (MCR)

In multivariate curve resolution-alternating least squares (MCR-ALS), the spectral data matrix, $\mathbf{D}$ $(I \times J)$, is resolved into the product of a concentration matrix, $\mathbf{C}$ $(I \times N)$, and a spectrum matrix, $\mathbf{S}$ $(N \times J)$, according to:

$$\mathbf{D} = \mathbf{CS^T} + \mathbf{E} \tag{5}$$

where $\mathbf{E}$ $(I \times J)$ is the residual matrix which contains all information not explained by matrices $\mathbf{C}$ and $\mathbf{S^T}$; being I the number of samples, J the number of wavelengths and N the number of compounds in the samples. Eq. (5) can be resolved iteratively by using alternating least squares methodology. The process starts with the initial estimation of matrix $\mathbf{C}$ or $\mathbf{S}$, each iteration producing a refined estimate, and is stopped when the difference between the root mean square error,

$$RMS = \sqrt{\frac{\sum_i \sum_j e_{ij}^2}{n}} \tag{6}$$

between two consecutive iterations falls below a preset threshold, being e_{ij} the residual between two consecutive iterations for sample i at wavelength j.

The goodness of fit of the resulting model was assessed in terms of the percent calculated variance between the estimated $\mathbf{D}$ matrix (calculated as $\mathbf{C \cdot S^T}$) and the original $\mathbf{D}$ matrix:

$$\%Var = \frac{\sum_i \sum_j \hat{d}_{ij}^2}{\sum_i \sum_j d_{ij}^2} \times 100 \tag{7}$$

Because of rotational and intensity ambiguity [12], this multivariate methodology cannot provide a unique solution. In order to reduce the number of potential solutions and solve Eq. (5) accurately, computations are done under non-negativity, unimodality or closure constraints [10]. Augmenting the data matrix with the spectra for absorbing species involved in the reaction [11,13] and/or introducing quantitative values (concentration values) in the iterative process [10] as equality constraints, also helps suppress ambiguity.

By assuming the physico-chemical conditions between batches (such as temperature, or initial molar ratio) to remain constant, one can predict the analyte concentrations at any time during it [12] for new batches. To this end, one must first calculate the *pseudo*-inverse of the $\mathbf{S^T}$ matrix obtained by MCR-ALS:

$$P = (S^T)^+ \tag{8}$$

where the plus sign denotes *pseudo*-inverse. The concentrations corresponding to any new spectrum or matrix can be calculated via matrix $\mathbf{P}$:

$$c_{pred} = s \cdot P \tag{9}$$

where s denotes the spectrum for a new sample.

3. Experimental

3.1. Apparatus and software

Esterification processes were conducted in a LabMax Mettler Toledo laboratory reactor that was governed via the software Camile Tg 3.06 from Sagian Inc. The instrument allows the reactor, jacket and distillation temperatures, and the stirring and reactant addition rates, to be controlled (Fig. 1).

NIR in-line transflectance spectra were recorded on a FOSS NIRSystems 5000 spectrophotometer equipped with an OptiProbe™ analyser module allowing in-line spectra in the region 1100–2498 nm to be recorded by using a fiber-optic probe immersed in the reaction mixture. NIR at-line transflectance spectra were recorded on a FOSS NIRSystems 6500 spectrophotometer equipped with an RCA module in the same region as the in-line spectra. Both spectrophotometers were governed via the software Vision v. 2.51.

Multivariate curve resolution-alternating least squares computations were done by using the software GUIPRO [14,15] as implemented in Matlab v. 7 [16].

3.2. Catalysed esterification of myristic acid with isopropanol

The raw materials for the reaction were myristic acid (Uniqema, ICI Spain, 98–100% pure, AV 244–248 mg
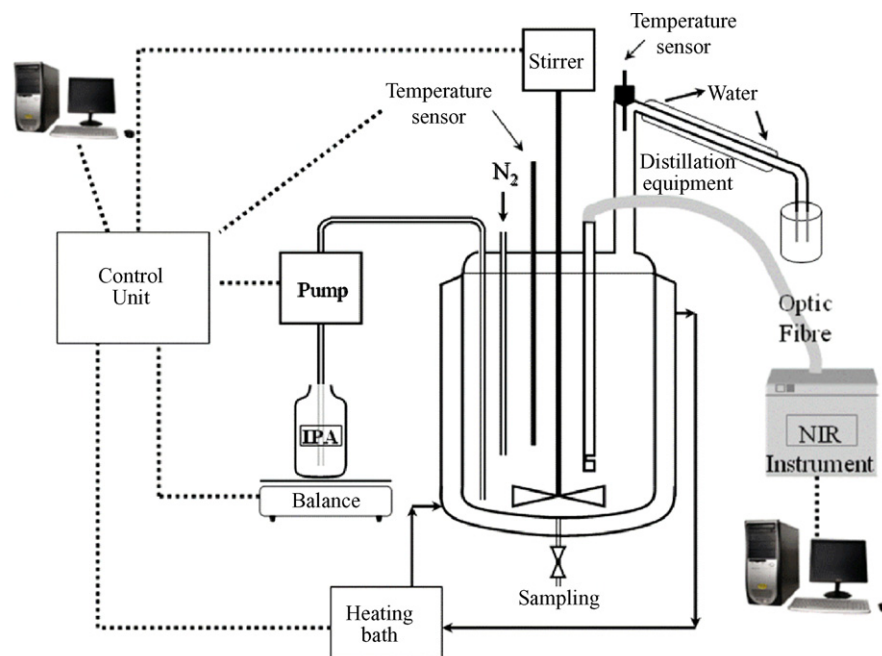
Fig. 1. Schematic drawing of the lab-scale reactor.

KOH/g), isopropanol (Uniqema, ICI Spain, 99.5% pure) and *p*-toluenesulphonic acid (50% in water). All processes were conducted in the LabMax reactor and according to the following procedure: under a continuous stream of N$_2$, the reactor was loaded with 500 g of acid and heated to the reaction temperature (130 °C), after which the catalyst (2.6 g) was incorporated and addition of the isopropanol/water mixture at a rate of 0.5 g/min started—by exception, a rate of 1 g/min was used in process 7. The water content in the mixtures ranged from 0 to 25%. Table 1 summarizes the characteristics of each process.

At intervals of roughly 60 min, 2–3 g samples of the reaction mixture were withdrawn in order to quantify unreacted acid by titration with 0.1 M KOH in ethanol and aliquots of the distillates were used to determine the composition of the isopropanol–water mixture by NIR spectroscopy. The process was monitored for about 700 min (before completion of the esterification process); by exception, process 4 had to be stopped after 580 min due to experimental problems.

3.3. Recording of NIR spectra

Fig. 1 depicts the reactor used; as can be seen, the probe was placed far from the isopropanol and nitrogen inlets, and close to the stirrer, in order to ensure homogeneity in the mixture and facilitate the removal of any nitrogen bubbles potentially formed. Transflectance spectra were recorded at 3 min intervals by using a light path of 0.4 mm (2 mm × 0.2 mm), each spectrum being the average of 32 scans over the wavelength range 1100–2498 nm with a resolution of 2 nm.

3.4. Processing of experimental data

Spectral data were subjected to the multiplicative scatter correction (MSC) treatment in order to suppress scatter. A baseline-offset correction was also used in order to exclude negative spectral values and facilitate application of the spectral non-negativity constraint in the MCR-ALS calculations.

Experimental matrices were subjected to rank analysis by using singular value decomposition (SVD) methodology; both singular values and the profile of the corresponding eigenvectors were considered in determining ranks.

MCR-ALS methodology was applied to the individual data matrix augmented (column-wise) with the spectra for the pure components (myristic acid, isopropyl myristate and isopropanol) used as the initial estimates prior to the ALS iterative process. The sole equality constraint used during the iterative process was the concentration of the pure myristic acid scaled to 1, which allowed the MCR-ALS concentration profiles to be correctly scaled. All calculations were done under the non-negativity constraint in both spectral and concentration profiles. The goodness of the results was determined by comparing the concentration of

Table 1
Experimental data for the eight processes conducted in the LabMax reactor

Process	Water in Al (%)	Al (g/min)	Unreacted acid (%)	Total time (min)
1	0	0.5	4.2	753
2	5	0.5	7.3	771
3	10	0.5	23.3	582
4	15	0.5	20.9	768
5	20	0.5	33.9	756
6	25	0.5	38.7	711
7	10	1.0	7.6	636
8	0	0.5	8.0	714

unreacted acid by MCR-ALS ($\hat{y}$) with that obtained by titration with KOH (y) in order to calculate the relative standard error,

$$\%RSE = \sqrt{\frac{\sum_{i=1}^{n}(\hat{y}_i - y_i)^2}{\sum_{i=1}^{n} y_i^2}} \tag{10}$$

and root mean square error (RMSE),

$$RMSE = \sqrt{\frac{\sum_{i=1}^{n}(\hat{y}_i - y_i)^2}{n}} \tag{11}$$

where n is the number of samples.

4. Results and discussion

Fig. 2a shows the NIR spectra for myristic acid, isopropanol and isopropyl myristate. The most important differences between the spectra lie in the 1800–2200 nm region, where the acid absorption is virtually constant in the 1900–2100 nm region, with a slight increase between 2100 and 2200 nm. Isopropanol and the ester exhibit a band peaking at 2088 and 2136 nm, respectively. The acid and ester also exhibit some differences in the 2300–2500 nm region that are due to combination bands of C–H bonds. Fig. 2b shows the variation of the NIR spectra during a reaction process; the spectral variation is due to the disappearance of myristic acid and formation of an equivalent amount of ester.
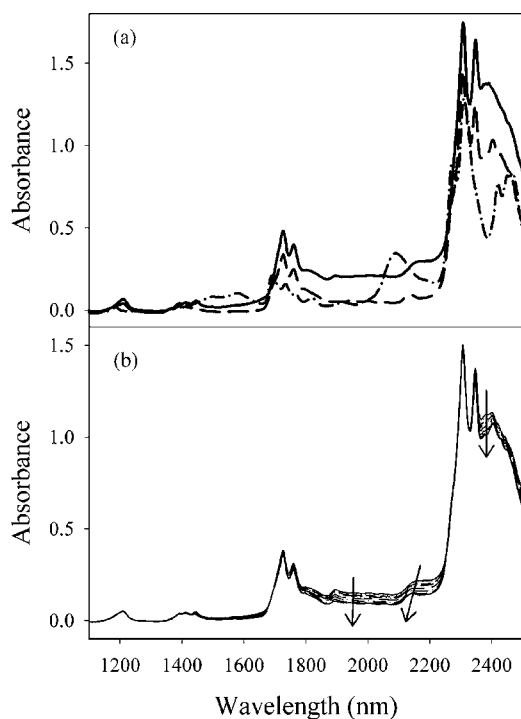

Fig. 2. (a) Spectra for the pure compounds involved in the reaction. Solid line: myristic acid; dash line: isopropyl myristate; dash-dot line: isopropanol. (b) Spectra for the evolving components. Arrowheads indicate temporal variation.

4.1. Application of multivariate curve resolution methodology

The MCR study was conducted on the first six processes shown in Table 1. For each data matrix, which contained the NIR spectra recorded in each process, we estimated the mathematical range (number of chemical components that could be extracted from the data) by examining the corresponding eigenvalues and eigenvectors, using singular value decomposition (SVD) methodology. The first four SVD eigenvalues for process 1 were 3.5×10^6, 283, 1.4 and 0.7—those for the other processes were similar in magnitude. Since the fourth eigenvalue was less than 1, the number of significant chemical components was 3. Applying MCR required the significant components to be previously identified; myristate ester and myristic acid were clearly two such components, and isopropanol or water might be the third. The alcohol was added in a continuous manner and the water, which was added in the mixture with the alcohol or produced in the reaction, was removed by distillation (the reactor temperature was 130 °C), so its concentration was very low throughout the process. An MCR-ALS computation with the four components and a data matrix augmented with four spectra in order to offset the rank deficiency allowed the methodology described in Section 3.4 to provide the concentration profiles for the four components. The concentration profile for water was near-zero, which suggests a very low concentration of this component in the reaction medium—much lower than that of isopropanol; also, the MCR concentration profile for myristic acid was inconsistent with the concentration determined by titration, with errors (%RSE) of 15% for processes 4–6 (*viz* those involving the highest water contents in the isopropanol–water mixture, and hence the highest concentration of water in the reaction medium). Therefore, water was not a significant component of the reaction medium, so the three components finally chosen for the MCR-ALS study were myristic acid, isopropyl myristate and isopropanol.

With three components, MCR-ALS was implemented by augmenting the spectral matrix for the process with the spectra of the three pure compounds for processes 1–6. The variance accounted for was 100% and the coefficient of determination, R^2, of the spectral profiles estimated for each process using the corresponding spectra for the pure compounds exceeded 0.999, in all six cases; this testifies to the good fitting of the spectral data. As can be seen from the concentration profiles of Fig. 3, myristic acid and isopropyl myristate evolved virtually inversely. On the other hand, the isopropanol concentration was always low (0.5–2% depending on the particular process) and increased slightly as the reaction developed in some cases by effect of this reactant being continuously added to the medium and the net reaction rate decreasing with time.

Fig. 3 compares the concentration profile for myristic acid with its reference concentrations as determined by titration—which were not used in the calculations; as can be seen, the two were quite consistent. As can be seen from Table 2, the %RSE and RMSE values obtained from the MCR and titration data were accurate—by exception, process 1 gave some spurious results that were ascribed to inappropriate standardiza-
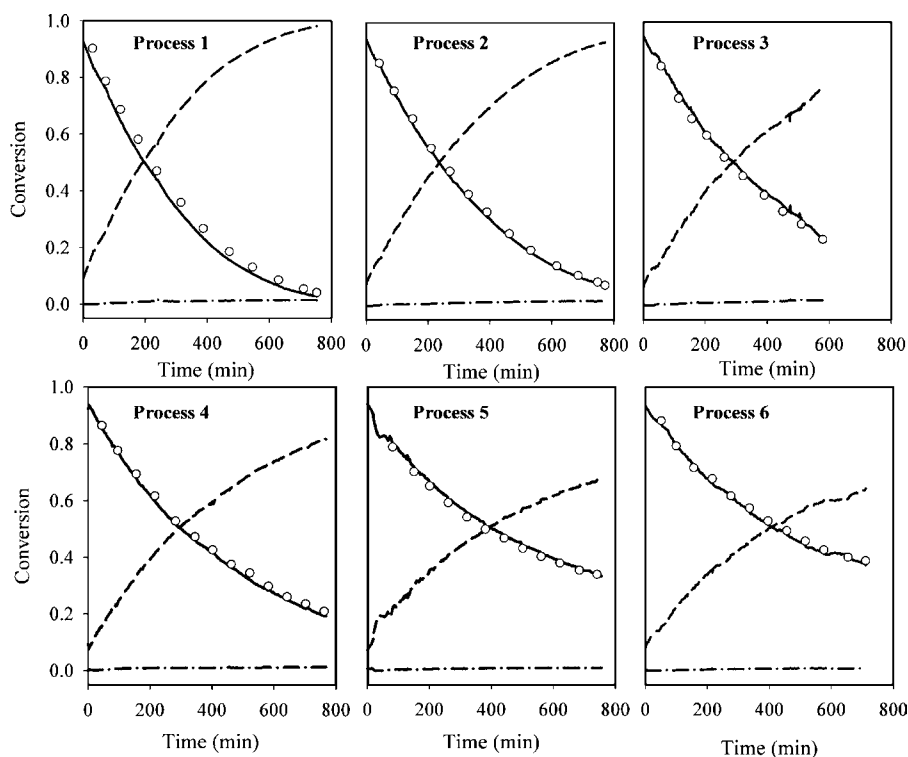
Fig. 3. MCR–ALS estimated concentration profiles for processes 1–6. Solid line: myristic acid; dash line: isopropyl myristate; dash-dot line: isopropanol; (○): acid concentrations obtained by titration.

tion of the KOH solution. The goodness of fit of the MCR-ALS results is reflected in the high correlation between the MCR spectral profiles and the spectra for the pure components ($R^2 = 0.99$), and also in the low %RSE values for the concentration profiles.

4.2. Estimation of kinetic constants

A plot of the natural logarithm of the MCR concentration profile for the acid as a function of time, Eq. (4), was used to calculate the reaction rates for processes 1–6. As can be seen from Fig. 4, the reaction profiles obtained during the first four hours fitted a *pseudo*-first-order law. Linearity was very good in the six processes—the correlation coefficient of the least-squares fit exceeded 0.997 in the six. The interval from 18 to 72 min in process 5 was excluded owing to oscillations in the spectral recording possibly caused by the presence of bubbles in

the light path. Table 3 shows the slope values (k') obtained, which decreased with increasing water content in the isopropanol mixture.

Constant k can be calculated by applying Eq. (3), where [Al] is the alcohol concentration in the reaction medium. Assuming that we do not know the alcohol concentration in the reaction medium, we can estimate it as the average of the concentration profile obtained by MCR-ALS for this compound. Also, in order to check whether the isopropanol MCR-ALS values were accurate, we analysed 7 samples from processes 1 and 7 by gas chromatography. The average concentration (g/g) by chromatography for process 1 was 0.97×10^{-2} (1.03×10^{-2} with MCR) and that for process 7 was 1.66×10^{-2} (2.14×10^{-2} with MCR); therefore, the average MCR values were quite accurate. Table 3 lists k', average isopropanol concentrations and k values ($k = k'/[\text{Al}]$) for each process. The k values obtained for processes 2–5 were very similar to one another, which confirm the accuracy of the proposed methodology for estimating reaction

Table 2
Correlation, relative standard error and root mean square error between MCR–ALS and reference values for the myristic acid concentration

Process	Concentration		
	R^2	%RSE	RMSE
1	0.9996	7.2	0.034
2	0.9998	2.3	0.010
3	0.9992	3.1	0.017
4	0.9997	2.7	0.014
5	0.9997	1.8	0.010
6	0.998	2.1	0.012

Table 3
Kinetic data for processes 1–6

Process	Water (%)	k' ($\times 10^3$ min^{-1})	[Isopropanol] ($\times 10^3$ mean)	k (min^{-1})
1	0	3.16 ± 0.03	10.3 ± 0.5	0.31
2	5	2.63 ± 0.02	12.4 ± 0.6	0.21
3	10	2.24 ± 0.03	11.4 ± 0.7	0.20
4	15	2.11 ± 0.01	9.4 ± 0.3	0.22
5	20	1.66 ± 0.04	7.3 ± 0.3	0.23
6	25	1.61 ± 0.02	5.2 ± 0.3	0.31

k' and [isopropanol] include confidence interval (95%)
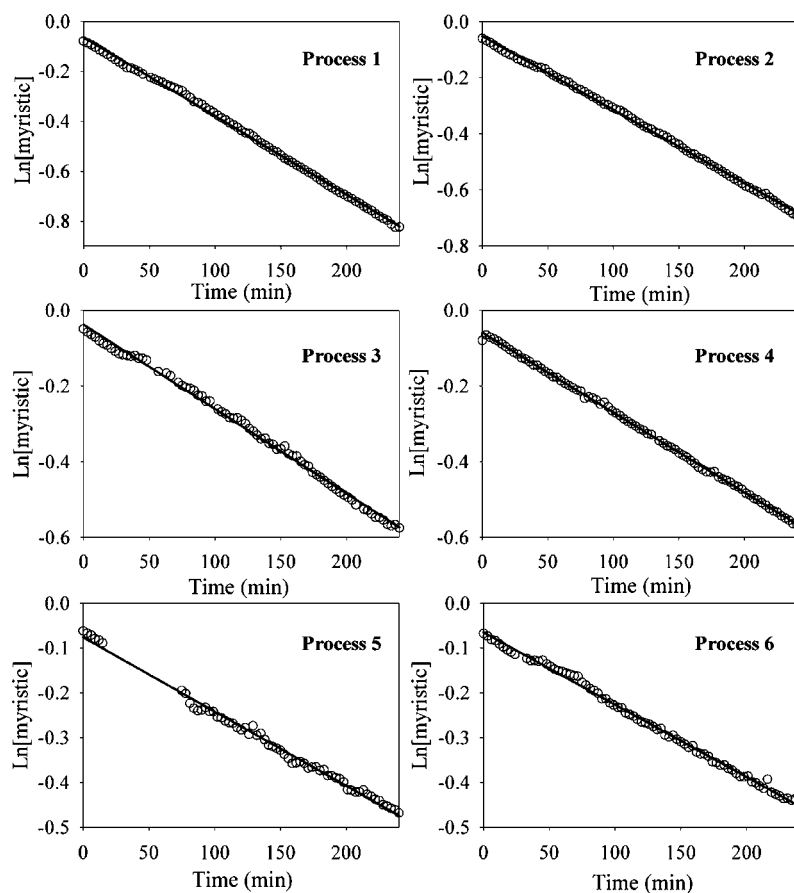
Fig. 4. Plot of Ln [myristic] *vs.* time for processes 1–6. Solid line: regression line.

constants; spurious estimates of *k* as seen for processes 1 and 6 could be caused by deviations in the estimated isopropanol concentration.

4.3. Study of the esterification process

Once concentration profiles and kinetic data were obtained, the process was evaluated in terms of yield and reaction rate as a function of the proportion of water in the alcohol mixture. A comparison of the concentration profiles of myristic acid in Fig. 3 reveals that the reaction rate decreases and the profile appears to level off at a higher asymptote, all of which results in a decreased reaction yield. The effective rate constant (k', Table 3) halved from pure isopropanol to a mixture containing 20% water, the decrease being only 35% in the presence of less water (15%). Therefore, reusing distillates with substantial water contents is industrially viable, albeit at the expense of a decreased reaction rate and yield. This requires the knowledge of the composition of the distillates during the reaction, which was monitored by NIR spectroscopy here. Previously, a PLS calibration model was constructed from 21 laboratory samples containing 50–100% isopropanol (and 0–50% water) at 5% intervals. The calibration models for isopropanol and water were constructed from second-derivative values, using two PLS factors over the wavelength range 1100–2498 nm for isopropanol and 1350–2150 nm for water. The %RSE between the predicted

and reference values for the 21 calibration samples was 0.6% or isopropanol and 1.5% for water.

Fig. 5 shows the variation of the isopropanol concentration in the distillates of processes 1, 2, 4 and 6; as can be seen, it increased with time, to the level in the mixture fed to the reactor. This can be ascribed to an increased esterification rate during the first few minutes of the process that subsequently decreased as the reaction completed. The distillates obtained at the end of the process can be directly reused untreated as feed mixtures in subsequent processes; those collected at an

Fig. 5. Concentration of isopropanol in distilled samples from process 1 (●), 2 (■) 4 (♦) and 6 (▲).

Fig. 6. MCR–ALS estimated concentration profiles for processes 3 and 7. Solid line: myristic acid; dash line: isopropyl myristate; dash-dot line: isopropanol.

early stage, however, must previously be re-distilled in order to concentrate the alcohol.
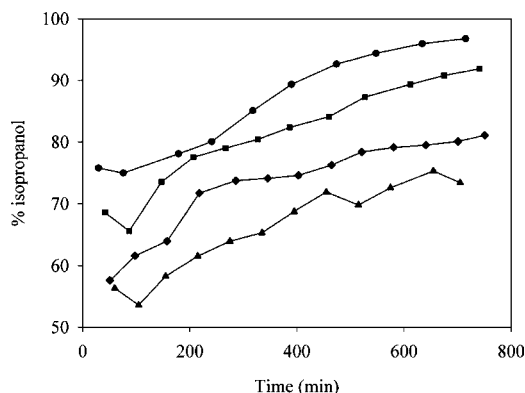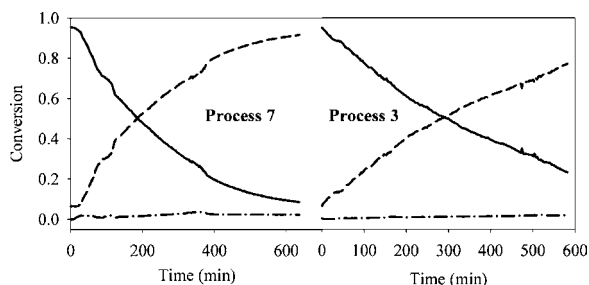
One other way of increasing the reaction rate with reused distillates is by increasing the rate of addition of isopropanol. In order to assess the effect, we applied MCR-ALS methodology to a process involving an increased rate of addition of the alcohol-water mixture (process 7, addition rate = 1 g/min) and compared the resulting profiles with those for process 3, which was conducted at 0.5 g/min; both used a feed mixture containing 10% water. As can be seen from the concentration profiles of Fig. 6, the increased addition rate resulted in an increased reaction rate and in decreased acid concentrations. Experimentally, increasing the addition rate raises the isopropanol concentration in the medium, and hence the reaction rate. This approach entails increasing the volume of isopropanol–water distillate and reactant consumption as a result. Thus, the proportion of unreacted acid at the end of process 7 (7.6%) was similar to that for process 2 (7.3%); however, the amount of isopropanol–water mixture consumed in process 7 was roughly twice that used in process 2.

The ability to predict the concentration profiles for new processes allows their monitoring in real time. Thus, by using Eqs.
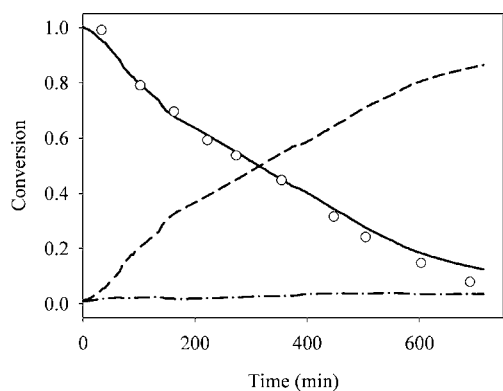
(8) and (9) in combination with the estimated spectral profiles for process 1 (that shows the high reacted acid), we obtained the concentration profiles for process 8, which was not used in previous calculation. Fig. 7 shows the resulting concentration profiles and the acid concentrations obtained by titration; as can be seen, the fit was similarly good to that of Fig. 3 (%RSE = 6.8).

5. Conclusions

The application of soft-modeling MCR-ALS methodology to in-line NIR data allows estimating the variation of the reactant concentrations from spectra recorded during the process; the sole source of external information is the pure spectra of the species involved in the reaction. This avoids the need to withdraw and analyse samples of the reaction mixture in order to elucidate the kinetics of the process and/or develop calibration models. Our results in terms of %RSE and RMSE are as good as those provided by other chemometric calibration techniques such as PLS or PCR, with the advantage that the proposed alternative involves less laboratory work.

Estimating kinetic constants from MCR concentration profiles allows one to establish the effect of experimental variables on the reaction rate and yield; also, the information thus obtained allows one to take steps towards minimizing consumption of raw materials and optimizing parameters such as temperature or the rate of addition of the reactants. Although its industrial implementation would require a previous upscaling study at a pilot plant, the process methodology has proved viable for monitoring industrial processes.

References

[1] T. Kocsisová, J. Cvengros, J. Lutisan, Eur. J. Lipid Sci. Technol. 107 (2005) 87–92.
[2] R. Aafaqi, A.R. Mohamed, S. Bhatia, J. Chem. Technol. Biotechnol. 79 (2004) 1127–1134.
[3] E. Sendzikiene, V. Makareviciene, P. Janulis, S. Kitrys, Eur. J. Lipid Sci. Technol. 106 (2004) 831–836.
[4] M. Blanco, I. Villaroya, Trends Anal. Chem. 21 (4) (2002) 240–1240.
[5] A. Cherfi, G. Févotte, Macromol. Chem. Phys. 203 (2002) 1188–1193.
[6] C. Pasquini, S.H.F. Scafi, Anal. Chem. 75 (2003) 2270–2275.
[7] S.E. Barnes, E.C. Brown, M.G. Sibley, H.G.M. Edwards, I.J. Scowen, P.D. Coates, Appl. Spectrosc. 59 (5) (2005) 611–619.
[8] M. Watari, Y. Ozaki, Appl. Spectrosc. 59 (5) (2005) 600–610.
[9] M. Blanco, D. Serrano, Analyst 125 (2000) 2059–2064.
[10] A. De Juan, R. Tauler, Anal. Chim. Acta. 500 (2003) 195–210.
[11] R. Tauler, A. Smilde, B. Kowalski, J. Chemometr. 9 (1) (1995) 31–58.
[12] R. Tauler, B. Kowalski, S. Flemming, Anal. Chem. 65 (1993) 2040–2047.
[13] M.S. Larrechi, F.X. Rius, Appl. Spectrosc. 58 (1) (2004) 47–53.
[14] P. Gemperline, E. Cash, Anal. Chem. 75 (2003) 4236–4243.
[15] http://personal.ecu.edu/gemperlinep/Research/gemper_software.html. P. Gemperline, East Carolina University.
[16] MATLAB, version 7.0, The MathWorks, 2004.

Fig. 7. Predicted concentration profiles for process 8. (—) myristic acid; (- -) isopropyl myristate; (-.-) line: isopropanol; (◯): acid concentrations obtained by titration.

ELSEVIER

An improved flow system for chloride determination in natural waters exploiting solid-phase reactor and long pathlength spectrophotometry

Viviane G. Bonifácio, Luiz C. Figueiredo-Filho, Luiz H. Marcolino Jr.,
Orlando Fatibello-Filho *

Departamento de Química, Centro de Ciências Exatas e de Tecnologia, Universidade Federal de São Carlos, São Carlos, SP, Brazil

Abstract

A single and sensitive spectrophotometric method for chloride ions determination based on a commuted flow system with a 100 cm optical path flow cell and a solid-phase reactor containing immobilized silver chloranilate was proposed. This procedure exploited the AgCl formation in the solid-phase reactor leading the chloranilate ions, monitored spectrophotometrically at 530 nm. The analytical signals were 75-fold higher and the sensitivity was 12-fold than that achieved with a 1 cm flow cell, allowed a chloride determination in the 0.5–100 mg l^{-1} range. The R.S.D. was 1.1% ($n = 20$) with a sample throughput of 80 h^{-1} and a waste generated of *ca.* 100 ng of chloranilate ions per determination. Four samples of natural waters from São Carlos and Araraquara cities were evaluated using the proposed method. Results agreed with the obtained by a reference method at the 95% confidence level.
© 2006 Elsevier B.V. All rights reserved.

Keywords: Flow analysis; Long pathlength; Chloride; Solid-phase reactor; Silver chloranilate

1. Introduction

Environmental-friendly analytical procedures are in demand for today's analytical chemistry. The new concept of "green chemistry" concerns the development of methods using non-toxic chemicals, with smaller amounts of reagent and hence less waste generated. Moreover, a high throughput analysis with a high degree of automation and portability is required [1].

In this way, spectrophotometric procedures coupled with commuted flow system can be improved by increasing the measurement optical path [2–7]. These procedures are based in the use of liquid-core waveguides in which the light propagation is constrained within a liquid medium with a higher refractive index than the surrounding material [2,3]. This strategy allowed the attainment of detection limits in the nanomols per litre range for determination of iron [2,4], chromium(VI) and molybdenium(VI) [5], nitrate and nitrite [6] and phenols [7] in natural waters.

Chloride is one of the most widespread analytes and its determination using simple, fast and sensitive methods is necessary in different types of samples. Spectrophotometric procedures developed for chloride determination have been based in the reaction between mercury(II) thiocyanate and chloride leads the displacement of thiocyanate yielding an intensely colored complex of Fe(III) [8]. Although several procedures reported [9,10], these methods have some unfavorable analytical characteristics like the use of a high Hg(II) concentration, not desirable from the viewpoint of green chemistry.

The application of various metal chloranilates for the spectrophotometric determination of chloride and other ions has already been investigated using silver [11], mercury(II) [12,13] and barium chloranilates [14]. In this paper, a flow-injection method for the spectrophotometric determination of chloride ion in natural waters, using a solid-phase reactor with immobilized silver chloranilate, exploiting commutation and a 100 cm optical path flow cell is presented. The immobilization of silver chloranilate is based on the physical entrapment of the reagent via polymerization reactions of linear polystyrene chains. This procedure is simple and quick to prepare.

* Corresponding author at: PO Box 676, 13560-970 São Carlos, SP, Brazil.
Tel.: +55 16 3351 8098; fax: +55 16 3351 8350.
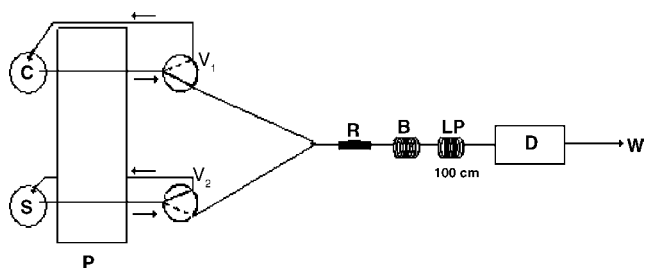 *E-mail address:* bello@dq.ufscar.br (O. Fatibello-Filho).

Fig. 1. Flow diagram of the system for determination of chloride ion in natural water: P, peristaltic pump; C, water carrier ($2.0\,ml\,min^{-1}$); S, sample ($2.0\,ml\,min^{-1}$); V_1 and V_2, three-way solenoid valves; R, solid phase reactor with immobilized silver chloranilate; B, reaction coil (50 cm); LP, long path-length flow cell (100 cm optical path); D, spectrophotometer USB2000 (Ocean Optics); W, waste. Dashed lines represent the flow paths when the valves are switched on.

2. Experimental

2.1. Apparatus

The flow injection assembly is depicted in Fig. 1. An Ismatec IPC peristaltic pump equipped with Tygon® tubes was employed to propel the carrier and solutions. Two three-way solenoid valves (Nresearch, 161T031) were used to commutation. A Pentium 166 MHz equipped with an electronic interface (Advantech Corp. PCL-711S) was employed to control the commutation devices. An extern power interface (12 V) was used to supply the electric potential difference and electric current intensity required to drive the solenoid valves. Signals were measured with a multi-channel USB-2000 fiber-optic spectrophotometer with an LPC-FL flow cell with 100 cm optical path and *ca*. 280 µl inner volume (Ocean Optics). Optical fibers were used to link the tungsten–halogen radiation source to the detection system through the flow cell. The software for system controlling was developed in Visual Basic (Microsoft). Data acquisition and processing were made through an Ocean Optics software and a Pentium 4 microcomputer.

2.2. Reagents and solutions

All solutions were prepared with distilled and deionized water and analytical grade chemicals.

Silver chloranilate was prepared by dropwise addition of $0.15\,mol\,l^{-1}$ of silver nitrate (100 ml) to an aqueous solution of $6.0\,mmol\,l^{-1}$ chloranilic acid (1.5 l), followed by continuous stirring for 24 h. The resulting precipitate, a dark violet-brown powder, was filtered, washed with water and dried under vacuum. This procedure was carried out on absence of light.

Single $200\,mg\,l^{-1}$ stock solutions were prepared from NaCl, $NaNO_3$, Na_2CO_3, $NaHCO_3$, Na_2SO_4 and Na_3PO_4. Reference solutions were prepared by appropriated dilutions.

2.3. Immobilization of silver chloranilate

The immobilization of silver chloranilate was made using a polyester resin solution (Resapol T-208, Resana, SP, Brazil) and

methylethyl ketone (Ibere, Ramires and Cia, Taboão da Serra, SP, Brazil) as catalyst as described elsewhere [15,16].

Several ratios of polyester resin and silver chloranilate were transferred to a polyethylene flask and after manual homogenization, 0.5 ml of the catalyst (methylethyl ketone) were added and stirred until an increase of viscosity. After 3–4 h, a rigid solid was obtained, which was broken with a hammer and ground in a Tecnal mill (model TE 631/1, Piracicaba, SP, Brazil). The particle size was selected by passing the pulverized material through sieves with different mesh sizes.

The solid-phase reactors were prepared by packing *ca*. 350 mg of immobilized silver chloranilate particles size of 350–500 µm into PTFE tubings (2.0 mm i.d.) of different lengths by means of suction with a syringe and fixed in the column with small pieces of glass wool. The solid-phase reactor was inserted in the flow system between the valves and the reactor coil.

2.4. Flow system and procedure

The diagram of the system is shown in Fig. 1. In the initial status, the sample valve is switched off and the carrier solution controlled by the valve V_1 is flowing through the analytical path while sample solution is recycling to its vessel. Sample solution is introduced by switching on the valve V_2 for 1.5–3.5 s. In this step, the valve V_1 is switched off and the carrier solution is recycled to its vessel. Afterwards, valves are switched off and data acquisition is started. Measurements were carried out at 530 nm. There are no troubles with memory effect caused by the remaining sample portion previously monitored, since the valve and the confluence were washed with the carrier solution after each sample measurement.

The principle of this method is based on the following chemical reaction:

$$2Cl^-(aq) + Ag_2Ch(s)$$
$$\rightleftharpoons 2AgCl(s) + Ch^{2-}(aq) \quad \lambda = 530\,nm$$
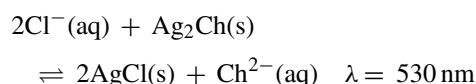
where Ch^{2-} represents the chloranilate anion.

Natural river an lake waters were collected in São Carlos and Araraquara cities, SP, Brazil, in polyethylene bottles and filtered.

3. Results and discussion

3.1. Preliminary studies

Several parameters had to be optimized in order to achieve the optimal conditions to promote the AgCl formation releasing chloranilate ions spectrophotometrically monitored at 530 nm.

A comparison between the absolute absorbance signals obtained with 1 and 100 cm optical path flow cells showed a 75-fold increase. The increasing in the absolute absorbance signal is lower than the theoretical value (100-fold) probably due to radiation power attenuation after passing the solution through a 100 cm optical flow cell.

3.2. Choice of carrier solution

One requirement for prolonged stability of the solid-phase reactor is the low solubility of the immobilized reagent in the solvent employed. Thus, the stability and variations of the peak height as function of the carrier solution were measured. The response was examined in the presence of different carrier solutions such as deionized water and $0.01 \, mol \, l^{-1}$ acetate buffer solutions (pH 3.2–5.8). In these experiments were employed a carrier and reagent flow rate of $1.7 \, ml \, min^{-1}$, sampling time of 2.4 s, reactor coil length of 50 cm and a silver chloranilate solid-phase reactor of 5.0 cm (2.0 mm i.d.).

Deionized water was selected as the optimum carrier solution due to the highest response, good reproducibility and long-term stability of the reactor.

3.3. Solid-phase reactor

The effects of the column length, particle size and internal diameter on the performance of the solid-phase reactor containing silver chloranilate were studied. All columns tested were previously conditioned by passing the carrier solution 10 min before starting the first injection in order to minimize compaction of the particles in the column. At least five injections were necessary to obtain reproducible absorbance signals after the system was started. Six different ratios of silver chloranilate/polyester resin were used in the preparation of the solid-phase reactors: 1:4, 1:3, 1:2, 1:1, 2:1 and 3:1 (m/m). An increase of the sensitivity was observed with an increase of the silver chloranilate:polyester ratio up to (2:1) with the polyester solution used. Thus, a ratio of 2:1 was adopted as being satisfactory.

The uniformity of the column packing affects the column efficiency. Thus, selection of uniform particle size fractions is desirable. The effect of particle size was studied in two size ranges (100–350 and 350–500 mm) selected by passing the particles through known mesh sieves. The 100–350 mm particle size presented a highest absorbance signal, but the 350–500 mm particle size was chosen for further studies as a compromise between sensitivity and minimum difficulties of operating conditions (operation at lower hydrodynamic pressure).

The influence of the column length on the analytical signal was studied in the 3–12 cm range at a carrier flow rate of $1.7 \, ml \, min^{-1}$. Fig. 2 shows the absorbance signals obtained in this study. Best results were obtained with the 10 cm column length. Beyond this length the absorbance decreased with the increase of the column length, probably due to the dispersion of the sample zone.

3.4. Flow system

The flow system was designed exploiting the commutation approach in order to minimize the reagent consumption producing effects on both reduction of effluent generation and minimization in the contact time with the 100 cm optical path flow cell. The effect of flow variables such as total flow rate, sampling time and reactor coil length were investigated searching the best compromise conditions among absorbance magnitude,
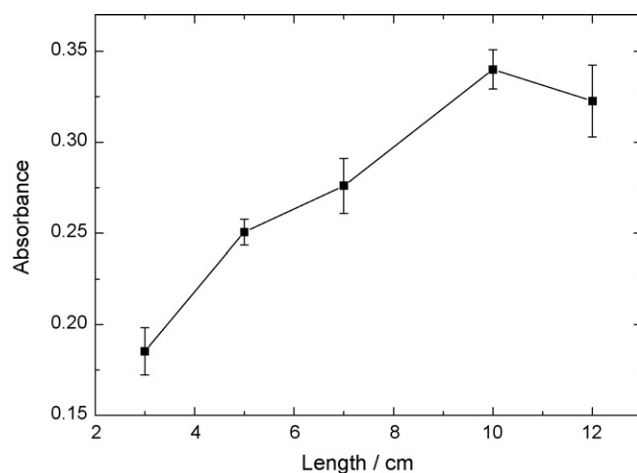
Fig. 2. Effect of the column length on the analytical signal for 83 μl of $20 \, mg \, l^{-1}$ chloride solution (sampling time of 2.4 s at a flow rate of $1.7 \, ml \, min^{-1}$).

repeatability and sample throughput. Table 1 shows the ranges studied and the optimum values for each parameter.

The effect of the total flow rate was investigated in the range of 0.8–$3.3 \, ml \, min^{-1}$. It was found that the sensitivity decreased with the increase of the flow rate due to the decrease in the contact time between the sample zone and the silver chloranilate particles into the solid-phase reactor. Nevertheless, a flow rate of $2.0 \, ml \, min^{-1}$ was selected for the carrier stream in order to obtain a good repeatability and sample throughput.

The effect of the sampling time was investigated in the range of 1.5–3.5 s. The absorbance signals increased with the increase of the sampling time due to the higher volume of the chloride solution. In this way, measurements were carried out with 2.5 s sampling time (83 μl) for a best compromise between sensitivity and repeatability.

The influence of the reactor coil length was studied in the 30–120 cm range. The sensitivity decreased continuously with increasing coil length, probably due to dispersion of the sample zone. Thus, a 50 cm reactor coil length was chosen for further experiments.

3.5. Analytical features

The precision of the proposed method was tested by repeated runs of $20 \, mg \, l^{-1}$ chloride solution. The R.S.D. was 1.1% ($n = 20$) with a sample throughput of $80 \, h^{-1}$. Under optimized experimental conditions, a quantification limit of $0.5 \, mg \, l^{-1}$ (10 times the standard deviation of the blank/slope) and detection limit (3 times the standard deviation of the blank/slope) of $0.3 \, mg \, l^{-1}$ chloride can be obtained.

Table 1
System optimization for chloride determination

Parameter	Evaluated range	Selected value
Column length (cm)	3–12	10
Flow rate (ml min^{-1})	0.8–3.3	2.0
Sampling time (s)	1.5–3.5	2.5
Reactor coil length (cm)	30–120	50
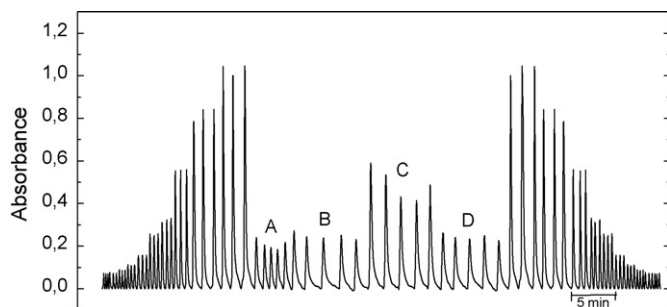
Fig. 3. Typical transient signals for reference and sample solutions. On the left, is shown a triplicate of reference chloride solutions of 0.5–100 mg l^{-1} range, four water sample solutions (A, B C and D) and triplicate of reference chloride solutions again. Experimental conditions reported on the Fig. 1.

Typical transient signals corresponding to a linear calibration graph (100 cm cell) for chloride are shown in Fig. 3. Adopting the conditions recommended in Table 1, a linear response ($r = 0.9997$) within 0.5–100 mg l^{-1} (Abs = 0.0614 + 0.00989 [Cl^{-}], where Abs is the absorbance value and [Cl^{-}] is a chloride concentration in mg l^{-1}) with a detection limit of 0.3 mg l^{-1}, chloride was verified, which is suitable for chloride determinations in natural water samples according to the limits established by the CONAMA [17]. The sensitivity estimated by considering the slopes of the analytical curves was 12-fold higher than that achieved with a 1 cm flow cell, those allowed a chloride determination in the 5–50 mg l^{-1} range (Abs = 0.0678 + 0.000839 [Cl^{-}], with a detection limit of 2 mg l^{-1}). In order to investigate the selectivity of the proposed method, the effect of several anions (SO_4^{2-}, PO_4^{3-}, CO_3^{2-}, HCO_3^{-}, NO_2^{-} and NO_3^{-}) were investigated by the analysis of 20 mg l^{-1} chloride reference solution in the presence of these anions at a 10-fold and at the same chloride concentration (Table 2). None of these substances caused significant interference in this method.

Additionally, the long-time stability of the column was investigated measuring the absorbance of solutions containing 0.5–100 mg l^{-1} chloride. The calibrations were done at regular intervals during an 8-h working period. The columns prepared by the described procedure gave reproducible results after the injection of at least 500 samples with a variation of 8–10% of the analytical curve slope.

Table 2
Effect of several anions by the analysis of 20 mg l^{-1} chloride reference solution in natural water samples

Anions	[interferent]:[Chloride]	% Interference
SO_4^{2-}	1:1	+3.8
SO_4^{2-}	10:1	+5.5
PO_4^{3-}	1:1	−3.1
PO_4^{3-}	10:1	−3.9
HCO_3^{-}	1:1	−0.7
HCO_3^{-}	10:1	+1.1
CO_3^{2-}	1:1	−1.2
CO_3^{2-}	10:1	+2.2
NO_3^{-}	1:1	−1.0
NO_3^{-}	10:1	−1.6
NO_2^{-}	1:1	−2.4
NO_2^{-}	10:1	−2.8

Table 3
Determination of chloride in natural water samples

Sample	Chloride (mg l^{-1})		Relative error[a] (%)
	Official method	Proposed method	
A	15.1 ± 0.7	14.9 ± 0.2	−1.3
B	41.8 ± 0.4	43.2 ± 0.4	+3.3
C	26.8 ± 0.4	24.4 ± 0.3	−8.9
D	17.9 ± 0.6	18.4 ± 0.4	+2.8

[a] Relative error between proposed method *vs*. official procedure value [16].

3.6. Application to natural waters

Table 3 shows the results for four samples of natural waters from São Carlos and Araraquara cities, SP, Brazil, using the proposed method and the results obtained using the official standard method [18]. Appling *t*-test for paired data, it was found that all results are in agreement at the 95% confidence level and within acceptable range of errors, confirming the precision and accuracy of the proposed method.

4. Conclusion

In comparison to previously reported chloride determination procedures, the proposed method yielded better analytical features associating the sensitivity, sample throughput, reagent consumption and toxic-waste production. The consumption of chloranilate ions displaced from the solid phase reactor was of *ca*. 100 ng per determination. In this sense, a waste of *ca*. 70 μg of chloranilate ions was generated for an 8 h working period. Although the proposed method is easy and very useful for the rapid determination of chloride in natural waters dispensing any sample pre-treatment. The detection limit is suitable for determining chloride in natural waters, attending the requirements of environmental controlling agencies.

Acknowledgements

References

[1] J. Jakmunee, L. Patimapornlert, S. Suteerapataranon, N. Lenghor, K. Grudpan, Talanta 65 (2005) 789.
[2] R.D. Waterbury, W. Yao, R.H. Byrne, Anal. Chim. Acta 357 (1997) 99.
[3] J. Li, P.K. Dasgupta, Z. Genfa, Talanta 50 (1999) 617.
[4] J. Zhang, C. Kelble, F.J. Millero, Anal. Chim. Acta 438 (2001) 49.
[5] W. Yao, R.H. Byrne, Talanta 48 (1999) 277.
[6] W. Yao, R.H. Byrne, R.D. Waterbury, Environ. Sci. Technol. 32 (1998) 2646.
[7] K.O. Lupetti, F.R.P. Rocha, O. Fatibello-Filho, Talanta 62 (2004) 463.
[8] C.R. Silva, H.J. Vieira, L.S. Canaes, J.A. Nobrega, O. Fatibello-Filho, Talanta 65 (2005) 965.
[9] F.J. Krug, L.C.R. Pessenda, E.A.G. Zagatto, B.F. Reis, Anal. Chim. Acta 130 (1981) 409.

[10] S.T. Chalk, J.F. Tyson, Anal. Chim. Acta 366 (1998) 174.

[11] F. Sagara, T. Tsuji, I. Yoshida, D. Ishii, U. Keihei, Anal. Chim. Acta 270 (1992) 217.

[12] R.E. Humprey, W. Hinze, Anal. Chem. 43 (1971) 1100.

[13] J.E. Barney, R.J. Bertolacini, Anal. Chem. 29 (1957) 1187.

[14] H.N.S. Shafer, Anal. Chem. 39 (1967) 1719.

[15] A.V. Pereira, O. Fatibello-Filho, Anal. Chim. Acta 366 (1998) 55.

[16] A.V. Pereira, O. Fatibello-Filho, Talanta 46 (1998) 11.

[17] CONAMA, Ministério do Desenvolvimento Urbano e Meio Ambiente, Conselho Nacional do Meio Ambiente, Resolução 37, 2005.

[18] A.E. Greenberg, L.S. Clesceri, A.D. Eaton, Standard Methods for the Examination of Water and Wastewater, American Public Health Association, Washington, 1992, pp. 4-48–4-52.

Resolution of phenol, and its di-hydroxyderivative mixtures by excitation–emission fluorescence using MCR-ALS Application to the quantitative monitoring of phenol photodegradation

M. Bosco, M.P. Callao, M.S. Larrechi *

*Department of Analytical and Organic Chemistry, Faculty of Chemistry, Rovira i Virgili University,
Campus Sescelades, Marcelli Domingo s/n, 43007 Tarragona, Spain*

Abstract

The photodegradation of phenol using TiO_2 as catalyst was studied and monitored by fluorescence excitation–emission matrix (EEM). Hydroquinone, catechol and resorcinol were the dihydroxyderivative intermediates although in lower concentrations than phenol. The data were analyzed using a three-way multivariate curve resolution alternating least squares method (MCR-ALS) and augmented matrices. The procedure was assessed using synthetic samples prepared with a {4,3} Simplex-lattice design that considered a representative range of analyte concentrations. The results were analyzed in terms of overall RMSEP for the overall data set. A detailed study was made of how the analytes behaved at each concentration level and how the concentration of the other species affected the process. The method was used to quantify phenol in photodegradation samples with an overall prediction error of 5.37%. The conversion values were fitted to pseudo first-order kinetics and the apparent rate constant was calculated to be $-4.9 \times 10^{-4} \pm 5.2 \times 10^{-5} \, min^{-1}$.

1. Introduction

Phenol is widely used in the chemical industry for various purposes [1]. It is found in a wide range of effluents and has a direct or indirect effect on the ecosystem [2]. Photodegradation is one of the most effective advanced oxidation processes for treating organic pollutants such as phenol [2–5]. Through the process of degradation, phenol completely decomposes to CO_2 and H_2O following a mechanism of hydroxylation of the aromatic ring [1,2,6]. Hydroquinone, catechol and resorcinol are the habitual intermediates although in lower concentrations than phenol. The habitual methods of analysis usually involve time-consuming analytical procedures: for example, extraction and/or preconcentration, followed by such separation processes as gas chromatography (GC) [6,7] or high performance liquid chromatography (HPLC) [2].

Phenolic compounds can be determined by molecular fluorescence, which is highly sensitive and has moderate selectivity. However, in complex mixtures, spectral overlapping is often a serious drawback and separation techniques must be used before univariate spectrofluorimetric techniques can be used.

Collecting a two-dimensional total fluorescence spectrum, known as an excitation–emission matrix (EEM) spectrum, increases selectivity. In EEM spectroscopy a total fluorescence spectrum is obtained by systematically varying the excitation and emission wavelengths and collecting the resulting $i \times j$ data matrix [8].

The principal advantage of EEM is that it can use potent, multiway deconvolution methods on all the available data to increase the information content extracted from a data set. This makes it possible to develop instrumentation that can be applied in real time. In this field, JiJi et al. have developed a battery of instrumental methods that use fluorescence spectroscopy and EEM for accurate remote, in situ, and field screening for pesticides and PAHs in the environment [9,10].

* Corresponding author. Tel.: +34 977 559559; fax: +34 977 559563.
E-mail address: mariasoledad.larrechi@urv.cat (M.S. Larrechi).

Nowadays, developing catalysts that can be used to degrade organic polluting agents and optimizing these processes is a subject of particular interest in the field of catalysis. The degradation kinetics of a polluting agent and the yield of the degradation process require the polluting agent to be quantitatively determined. UV–vis spectrophotometry with univariate calibration is the common method for analysing organic pollutants, but this methodology requires previous sample pretreatment. In the particular case of phenol photodegradation, the analytical signal is largely caused by phenol but its hydroxyderivatives – hydroquinone, catechol and resorcinol – also make a small contribution [1,6,11]. Obtaining the results in this way, then, can lead to erroneous conclusions about the reality of the process, particularly as far as quantification is concerned.

The present study is part of our research group's general objective, which is to develop analytical methods based on EEM and curve resolution methods, and to find practical uses for quantitative, in situ monitoring of photodegradation reactions of organic pollutant agents such as phenol.

Parallel factor analysis (PARAFAC) [12–14] is one of several methods for deconvoluting multiway data and has been used by our research group to analyse phenol [11]. It assumes an underlying trilinear structure, and yields a single solution. However, the single profiles obtained are not necessarily the true profiles if the data set is not trilinear. This study discusses the ability of another method for deconvoluting multiway data: multivariate curve resolution-alternating least squares (MCR-ALS) [15–17]. This method has some important features that differentiate it from other three-way data analysis methods. Firstly, it can be used for three-way data with different data structures: trilinear and not trilinear. Methods which do not assume trilinearity may provide more ambiguous solutions, although they are more flexible at modelling the profile shape. Secondly, it has a simple algorithmic implementation based on matrix inversion. Thirdly, eigenvalue–eigenvector decomposition of the experimental data matrix is used to determine the number of independent contributions. And finally, it means that several constraints can be simply applied during the ALS optimization with increasing reliability of the solutions obtained [18].

In the present study, synthetic mixtures were prepared with a {4,3} Simplex-lattice design [19] for quaternary mixtures so that they represented the concentration intervals of the problem being studied. First, the ability of MCR-ALS to resolve highly overlapped spectra was evaluated in terms of overall prediction error (root mean square error of prediction, RMSEP) for each analyte, and the effect of the analyte concentrations in the mixtures on the error. Next, the phenol in the photodegradation process was quantified using TiO_2 as catalyst. The results were fitted to a pseudo first-order kinetics so that the rate constant could be calculated.

The study of these concentration mixtures and the use of phenol degradation is a practical example that has not yet been documented among the applications of MCR-ALS to spectroscopic data.

2. Background

2.1. Application of MCR-ALS to EEM data

MCR is based on a linear model that assumes the response additivity of all fluorescent components in the samples measured [20]. MCR-ALS is a flexible method which can be used to analyze: (a) a single data matrix containing data recorded throughout an individual experiment, (b) a column-wise augmented data matrix containing data recorded over several experiments or techniques, (c) a row-wise data matrix, and (d) a simultaneous column and row-wise augmented data matrix. In excitation–emission fluorescence data, all the data matrices for the EEM spectra of each measured sample can be aligned to one another to obtain an augmented data matrix [21]. Both excitation-wise and emission-wise matrix augmentations are possible in fluorescence. In the excitation-wise augmentation used here, the matrices are put on top of one other and the common excitation wavelengths are kept in the same column. Using this resolution method, the excitation-wise (column wise) augmented data matrices are modeled with the equation:

$$\mathbf{D}_{aug}^{ex} = \mathbf{Y}_{aug}\mathbf{X}^T + \mathbf{E}_{aug} \tag{1}$$

where $\mathbf{D}_{aug}^{ex}$ is the excitation-wise augmented response data matrix, $\mathbf{Y}_{aug}$ the augmented matrix of emission spectra, $\mathbf{X}^T$ the transposed matrix of excitation spectra and $\mathbf{E}_{aug}$ is the matrix of residuals. The quantitative information is contained in the relative intensities of the emission spectra $\mathbf{Y}_{aug}$.

2.1.1. Rank analysis

Before the alternating least squares iterative process begins, the number of compounds in a particular experiment (matrix) is estimated. This is usually done by principal component analysis (PCA) [22] or singular value decomposition (SVD) [23,24]. It is assumed that the variance explained by chemical compounds is larger than noise variance and, therefore, that only larger principal components will sufficiently explain the experimental data.

In this study, we estimated the rank analysis of the data matrices (augmented matrices) by SVD and used the indicator proposed by Malinowski [25] to determine the number of significant values. This indicator is based on an empirical function called the factor indicator function (IND) defined as

$$\text{IND} = \frac{\text{RE}}{(c-n)^2} \tag{2}$$

where c is the number of columns of the data matrix and n is the number of factors. RE is the real error (or residual standard deviation) defined by

$$\text{RE} = \left(\frac{\sum_{j=n+1}^{c}\lambda_j^0}{r(c-n)}\right)^{1/2} \tag{3}$$

where λ_j^0 is the value of the eigenvalue.

2.1.2. ALS optimization

The ALS optimization began by using initial estimates. This can be done in many different ways. It is sensible to start with the best possible estimates available (i.e. the component spectra if they are known). In this case, these initial estimates of the fluorescence excitation spectra were chosen by analysing the excitation spectra with the maximum fluorescence of the standard matrices of the analytes and choosing the most representative spectra of each one. These estimates were initially used to calculate the emission spectra as:

$$\mathbf{Y}_{aug} = \mathbf{D}_{aug}((\mathbf{X}^T\mathbf{X})^{-1}\mathbf{X}^T) \tag{4}$$

From this new emission spectra matrix $\mathbf{Y}_{aug}$, the excitation spectra were updated using the equation:

$$\mathbf{X}^T = ((\mathbf{Y}_{aug}\mathbf{Y}_{aug}{}^T)^{-1}\mathbf{Y}_{aug})\mathbf{D}_{aug} \tag{5}$$

These two steps were repeated until convergence was achieved.

The constraints applied to get physically meaningful solutions during the ALS optimization were: (a) the excitation and emission spectra had to be non-negative, (b) there had to be a correspondence between common species in the different data matrices, (c) the excitation spectrum of each species had to be the same in all matrices where that species was present and (d) the emission spectrum shape of each species had to be the same in all runs where that species was present.

The relative concentrations of a particular species were simply obtained from the quotient between the areas below the emission spectra of the analyte in the standard and in the unknown sample:

$$C_{unk} = \left(\frac{A_{unk}}{A_{std}}\right) = C_{std} \tag{6}$$

where C_{unk} and C_{std} were the concentrations of the analyte in the unknown and standard samples, respectively; and A_{unk} and A_{std} were the areas below the excitation or emission spectra profiles in the unknown and in the standard samples, respectively.

The overall prediction error was calculated by the root mean squares error of prediction (RMSEP):

$$\text{RMSEP} = \sqrt{\frac{\sum_{i=1}^{m}(C_{i\,\text{true}} - \hat{C}_{i\,\text{calc.}})^2}{m}} \tag{7}$$

where $C_{i\,\text{true}}$ and $\hat{C}_{i\,\text{calc.}}$ were the true and calculated concentrations of each analyte in the ith prediction sample, and m is the number of prediction samples.

2.1.3. Kinetic calculations

The kinetic constants of photodegradation processes, assuming that they normally fit pseudo first-order kinetics [5,8], and the half lives of the analytes are calculated using the following equation:

$$\ln\frac{C_0}{C_i} = kt \tag{8}$$

where C_0 and C_i (calculated by MCR-ALS) are the concentrations at time zero and time t, respectively, and k is the velocity constant.

3. Experimental

3.1. Chemicals

All reagents were of analytical grade: phenol, catechol, hydroquinone, and resorcinol were used as received from Sigma–Aldrich (99%) and glacial acetic acid (100%) was provided by Merck. Stock solutions were prepared by weighing the appropriate amounts of the reagents and dissolving them in Millipore water. All solutions were prepared in an acidic medium of 1% (v/v) acetic acid, so the analytes remained in molecular form, and were stored in dark bottles at 4 °C. They remained stable for 1 week. Working solutions were prepared by diluting stock solutions with Millipore water, and maintaining a concentration of 1% (v/v) acetic acid. TiO$_2$ in the anatase form (99.8%) (Sigma–Aldrich) was used as the photocatalyst without further treatment.

3.2. Samples

Individual standards of 5 ppm of each analyte were prepared in aqueous solution.

A set of 20 mixtures was also prepared following a {4,3} Simplex-lattice design for quaternary mixtures so that the ability of the model to resolve and quantify these analytes could be evaluated. The set of mixtures was prepared in duplicate. The design took into account the relation between the concentrations of the species during the degradation process and the linearity interval of the fluorescent measurements. Fig. 1 shows the content of the samples prepared in detail.

The photodegradation process was similar to one used in a previous study [11] as can be seen in Scheme 1. A total of 23 samples corresponding to the photodegradation of phenol (Scheme 2) were analyzed.

3.3. Measurements

The spectrofluorimetric data were acquired on an Aminco–Bowman Series 2 Luminescence spectrometer (SLM Aminco, Rochester, NY, USA) equipped with a 150 W continuous xenon lamp and a PMT detector. The instrument was interfaced by a GPIB card and driver with a PC Pentium microcomputer provided with the AB2 software version 1.40 for spectral acquisition.

All solutions (individual standards, mixtures, samples and solvent) were measured in the same conditions. Three-dimensional excitation-emission spectra were recorded from 270 to 350 nm in the emission domain and from 231 to 291 nm in the excitation domain, both at regular steps of 3 nm. The scanning rate of the monochromators was maintained at 30 nm s^{-1}. The excitation and emission monochromator slit widths were set to 4 nm. All measurements were made in a 10 mm quartz cell at 620 V.
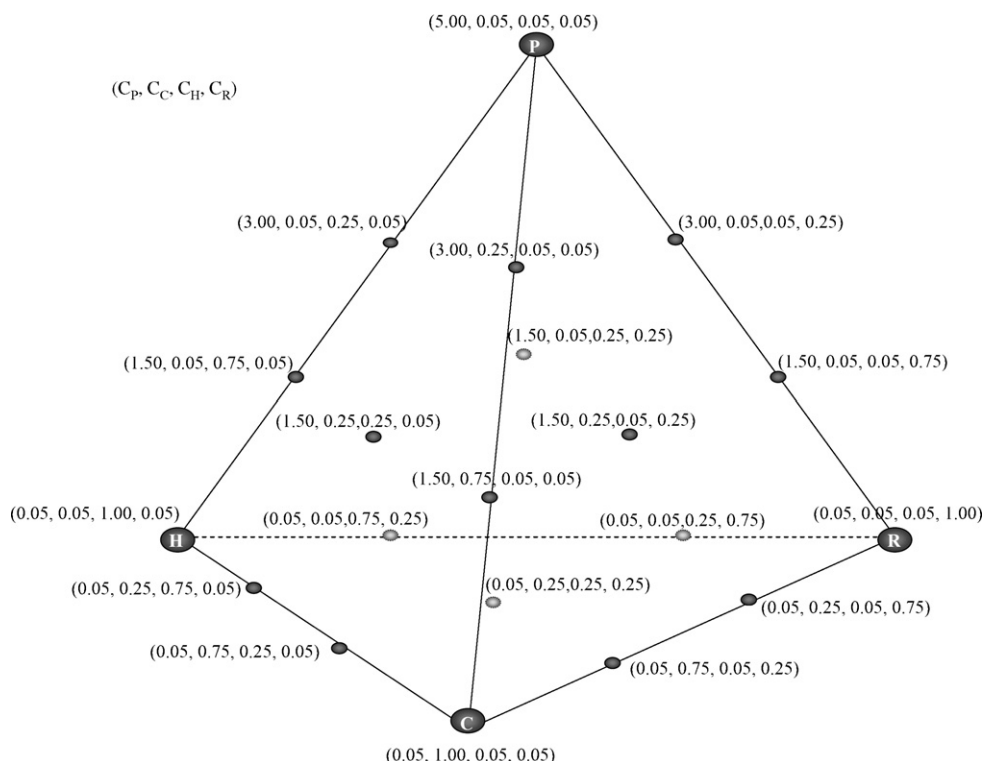
Fig. 1. Set of samples prepared following a {4,3} Simplex-lattice design. Concentration values of phenol (P), hydroquinone (H), catechol (C) and resorcinol (R) in ppm.

4. Data set and data analysis

A data matrix of 28×21 in size was obtained for each sample analyzed. The augmented data matrix was arranged by setting one matrix on top of the other and keeping the common excitation wavelengths in the same column (excitation-wise).

Four data sets are involved in this study: (a) augmented matrix **A** (112×21) built with the four individual standards, (b) augmented matrix **B** (1120×21) built with the synthetic samples, (c) augmented matrix **C** (1232×21), built with the four individual standards and synthetic samples, (d) augmented matrix **D** (1876×21), built with the four individual standards, the synthetic samples and the photodegradation samples. The fluorescence spectra were exported in ASCII format from the AB2 software to MATLAB [26,27].

5. Results and discussion

Fig. 2 shows, as an example, the emission and excitation spectra for the particular maximum of each analyte obtained from a 5 ppm sample of phenol, catechol, resorcinol and hydroquinone. Only the excitation and emission maxima for hydroquinone ($\lambda_{em} = 328$ nm and $\lambda_{ex} = 288$ nm) are significantly different from the maxima of the other three analytes ($\lambda_{em} = 294$ nm and $\lambda_{ex} = 270$ nm for phenol, $\lambda_{em} = 311$ nm and $\lambda_{ex} = 276$ nm for catechol, $\lambda_{em} = 302$ nm and $\lambda_{ex} = 274$ nm for resorcinol) and the emission and excitation spectra of catechol and resorcinol are embedded in the spectrum of phenol. It should also be pointed out that the analytical technique is more sensitive to variation in phenol concentration than to variation in any other analyte; it is least sensitive to catechol. Therefore, it is very difficult to mathematically resolve these components by individually analysing a mixture of these analytes at the same concentration [28].
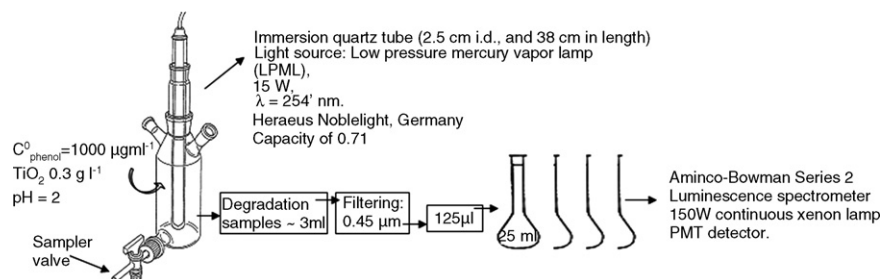
Scheme 1. Photodegradation process.
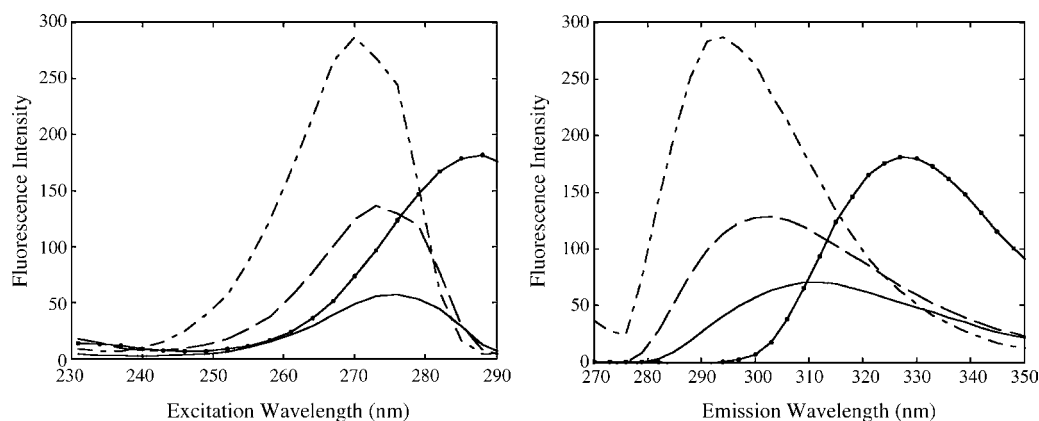
Fig. 2. Excitation (231–291) nm and emission (270–350 nm) spectra obtained for 5 ppm phenol (– - –), catechol (—), resorcinol (– –) and hydroquinone (– ○ –). Scanning rate: 30 nm s^{-1}; monochromator slit widths: 4 nm; 620 V.

As can be seen in Fig. 3, the EEM spectra for a mixture of the four analytes present a diagonal signal (270–290 nm in both modes) which rarely provides any additional chemical information. More specifically, it is in the corner and is produced by the first-order Rayleigh scatter. This dispersion does not have any chemical meaning, and takes place at all wavelengths when the excitation and emission fluorescence radiation are close together [29]. This Rayleigh scattering becomes more pronounced for less sensitive analytes such as catechol and resorcinol and is very difficult to eliminate by blank subtraction because the intensity of the dispersion is not constant for all the measured samples. However, blank subtraction can minimize Rayleigh scattering quite considerably.

The effects of the Raman scattering were minimized by subtracting the mean blank from all spectra.

Table 1 shows the results of the rank analysis of augmented matrices by singular value decomposition. As can be seen by visual inspection, for matrix **A** the rank is lower than the total
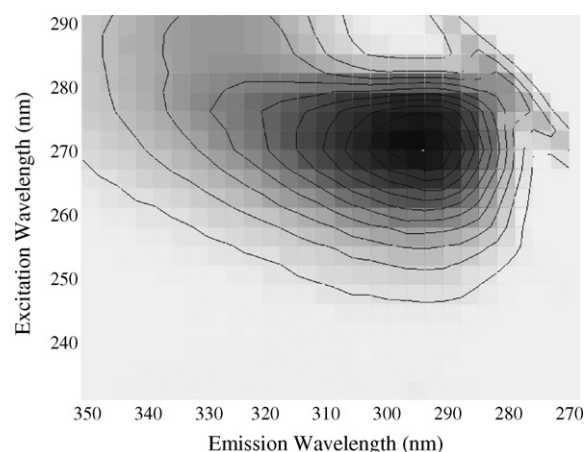
Fig. 3. EEM spectra of a mixture of the four analytes recorded from 270 to 350 nm in the emission domain and from 231 to 291 nm in the excitation domain (steps of 3 nm); scanning rate: 30 nm s^{-1}; monochromator slit widths: 4 nm; 620 V.

number of absorbing species present (apparent rank deficiency). This matrix contains the four analytes, at the same concentration, and only three eigenvalues seem to have significant values. This can be attributed to the fact that the sensitivity of phenol is higher than that of catechol and resorcinol at the same concentration, and their spectra are embedded within the phenol spectrum in both the emission and excitation modes (see Fig. 2). In a previous study [11] in which we worked with the same data set (i.e. a cube
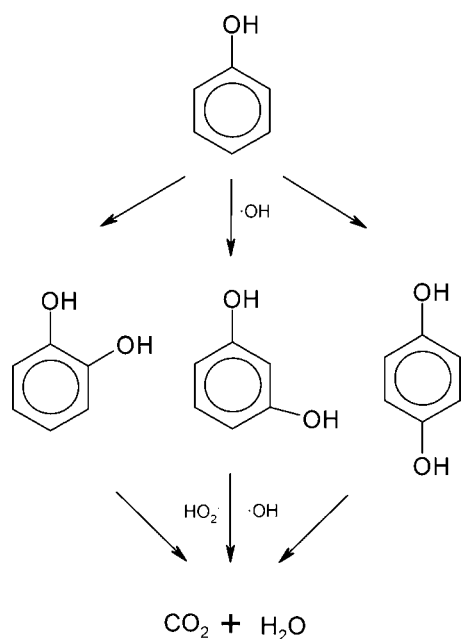
Scheme 2. Process of mineralizing phenol.

Table 1
Results of rank analysis of augmented matrices by singular value decomposition

Singular values	Data matrix			
	A	**B**	**C**	**D**
s1	2267.2	4425.2	4955.0	7087.6
s2	995.5	615.8	1237.5	1262.8
s3	218.9	349.4	355.6	357.4
s4	47.2	242.0	293.9	303.8
s5	39.9	115.1	198.7	204.6
s6	32.3	85.2	88.9	92.4
s7	21.3	40.7	60.2	71.5
s8	16.0	32.4	40.0	45.6
s9	12.3	28.8	34.3	39.5
s10	9.6	24.9	31.6	38.5

Table 2
Real error (RE) and indicator function (IND) [25] values for the singular values of the augmented data matrices

Singular values	Data matrix							
	A		B		C		D	
	RE	IND ($\times 10^{-3}$)	RE	IND ($\times 10^{-3}$)	RE	IND ($\times 10^{-3}$)	RE	IND ($\times 10^{-3}$)
s1	0.798	1.996	0.426	1.066	0.268	0.669	0.273	0.683
s2	0.450	1.248	0.323	0.894	0.193	0.534	0.199	0.552
s3	0.325	1.003	0.274	0.846	0.166	0.514	0.174	0.537
s4	0.295	1.021	0.227	0.784	0.139	0.479	0.147	0.509
s5	0.265	1.035	0.192	0.752	0.115	0.448	0.125	0.486
s6	0.236	1.049	0.171	0.759	0.103	0.456	0.114	0.506
s7	0.215	1.096	0.157	0.803	0.094	0.478	0.104	0.532
s8	0.197	1.164	0.147	0.872	0.087	0.517	0.098	0.581
s9	0.181	1.257	0.137	0.952	0.081	0.564	0.092	0.642
s10	0.167	1.382	0.126	1.043	0.074	0.614	0.085	0.704

built by PARAFAC with the four individual standards) we found four significant contributions. However, in the rank analysis of data matrices **B**, **C** and **D**, where the fluorescence intensities are for different concentrations (and concentration combinations) of the four analytes, the number of significant contributions difficulties not so easy to decide only after visual inspection. Table 2 gives the results of the indicator function proposed by Malinowski [25] for the augmented matrices. The indicator function gives a minimum value for the number of independently detected chemical species or chemical rank. Five significant contributions were found for data matrices **B**, **C** and **D**. Four were interpreted as the variability yield by the chemical rank (i.e. for the absorbing species present in the data analysis). The other contributions were attributed to the Rayleigh scattering. Here, the rank deficiency is overcome since we are working with data matrices with different concentrations and combinations of the analytes.

From this first analysis, we concluded that for this particular problem, the quantitative determination of phenol in the presence of its di-hydroxyderivatives, the MCR-ALS application requires four factors.

Therefore, the MCR-ALS method was applied to augmented matrix **C** to evaluate the prediction error (to quantify the analytes properly we needed a simultaneous analysis that included the four standard data matrices in addition to the mixtures). Non-negativity and unimodality constraints were applied in excitation and emission modes. In this particular case we used an excitation-wise augmented data matrix with excitation spectra as initial estimates that we had obtained by individually analysing standard matrices and choosing the most representative spectra of each analyte (see Section 2).

The optimal solution with four components was obtained in the seventh iteration, with a fitting error (lack of fit, lof) at the optimum of 12.71%. The percent of variance explained at the optimum was 98.38%. The recoveries of the emission spectra were measured as the dissimilarity between the ALS recovered spectra and the true spectra (those obtained from the matrices of the pure analytes). In all cases the recoveries were good: the dissimilarities were 0.0451 for phenol, 0.0263 for hydroquinone, 0.1108 for catechol and 0.0722 for resorcinol. They were higher than those found by PARAFAC [11]: 0.0045 for phenol, 0.0026 for hydroquinone, 0.0118 for catechol and 0.0132 for resorcinol. This is because the method used strictly trilinear data and because it is better to use a dissimilarity measure such as the *sin* of the angle between two vectors than the *cos* of the angle between vectors since, for very similar profiles, the discrimination power is greater. Dissimilarity equal to 0.1 means a correlation equal to 0.995 and dissimilarity equal to 0.01 means a correlation equal to 0.9999.

In the quantification step, the overall prediction errors (Eq. (7)) for each analyte were: 5.37% for phenol, 4.67% for hydroquinone, 28.52% for catechol and 13.24% for resorcinol. The percent of variance explained by PARAFAC for a model with four factors was 99.98% [11]. The RMSEPs for phenol were practically the same (5.22%) and slightly better for hydroquinone (3.84%), catechol (16.78%) and resorcinol (9%). We consider that these results are comparable since the determination of these analytes by other techniques such as high performance liquid chromatography (HPLC) gave coefficients of variation of 10.4% for phenol, 14.9% for hydroquinone, 14.9% for catechol and 70.5% for resorcinol [30].

It should also be pointed out that the main advantage of MCR-ALS is that PARAFAC needs to pre-treat the data matrix because the data need to be strictly trilinear. So, before PARAFAC is used, the sources of variability present in the spectra that are not caused by variation in the concentrations of the analytes need to be eliminated. PARAFAC needs the experimental data to preserve their trilinear structure if it is to work correctly. MCR-ALS, however, only requires the data set *to tend* to trilinearity, but it is not a hard condition. In our case, when we minimized the scatter effect by blank subtraction, results were good.

Tables 1 and 2, then, show that the relative concentration between the analytes is very influential when evaluating the resolution possibilities of EEM and MCR-ALS. Therefore, we believe that a detailed analysis of the results should be made considering the different concentration levels of each analyte.

Fig. 4a–d represents the values of the error in each analyzed sample following the design of Fig. 1. To facilitate the interpretation of the results, the tetrahedron in Fig. 1 has been turned, so that the planes that contain the same concentration value of the analyte being studied can be viewed more easily.
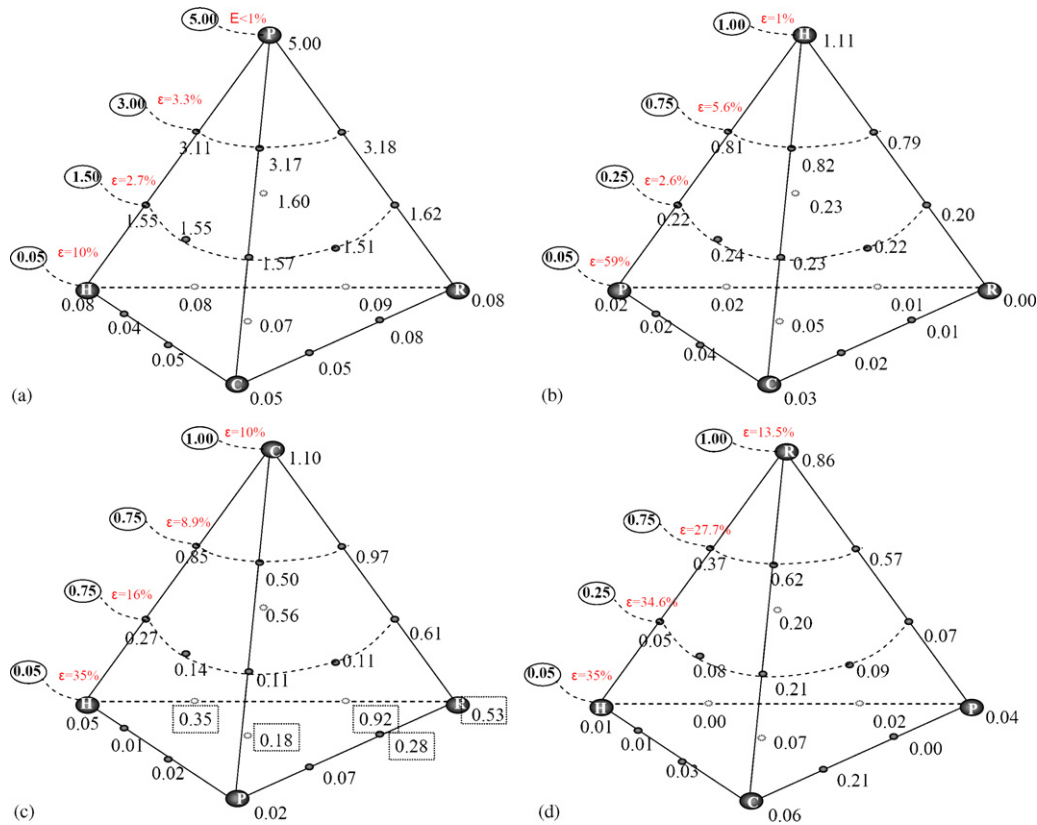
Fig. 4. Average values (ppm) found by MCR-ALS for phenol (P), hydroquinone (H), catechol (C) and resorcinol (R) for the 20 samples prepared in duplicate. Real concentration values (ppm) are surrounded by a solid line ◯.

The error values were calculated using a variation coefficient for each concentration level. Fig. 4a shows the results for the quantification of phenol in which the major error was when its concentration in the mixtures was 0.05 ppm, and the error was never above 10%. This conclusion is independent of the concentration values of the other analytes. Fig. 4b shows the results for hydroquinone. At low concentrations the error is very large but at overall RMSEP this error was not observed. The values for catechol and resorcinol are shown in Fig. 4c and d, respectively. As can be seen for catechol, the error is always above 9%. At low concentrations and when the resorcinol concentration in the mixture is increased, the error is above 100%. Errors are only lower than 10% if there is no resorcinol in the mixture and its concentration is higher than 0.25 ppm. Error values are always high for resorcinol. This analysis shows that phenol is the only analyte that can be quantified with an acceptable error and hydroquinone can only be quantified if the concentration is higher than 0.05 ppm.

As the purpose of this work is to follow the quantitative monitoring of the photodegradation of phenol, a model with four factors was applied to matrix **D**. The results are shown in Fig. 5. These values were fitted to pseudo first-order kinetics (Eq. (8)). The data was fitted using weighted least squares considering the error committed at each concentration. It could be assumed that in the interval of values in which we have measured the degradation samples the error was between 1 and 3%. The value of slope, representative of the apparent rate constant, was of -4.9×10^{-4} min^{-1} and his standard deviation of

5.2×10^{-5} min^{-1}. This value could be considered an estimation of the error for the apparent rate constant. As can be seen (Fig. 5) the values obtained by MCR-ALS for the photodegradation are in acceptable agreement with the calculated rate constant (solid line). Indeed, most of the values are within the confidence bands related to the estimated error for the apparent rate constant (broken lines). However, the later values (from 1100 to
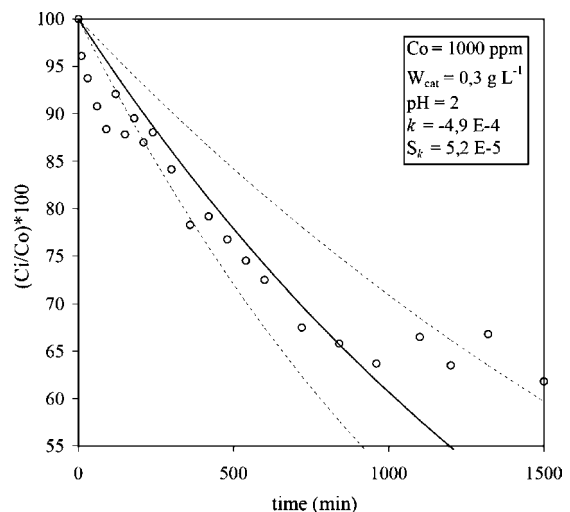

Fig. 5. Variation of phenol throughout the photodegradation of phenol (circle); fitted concentrations according to the calculated apparent rate constant (solid line); confidence bands related to the estimated error for the apparent rate constant (broken lines).
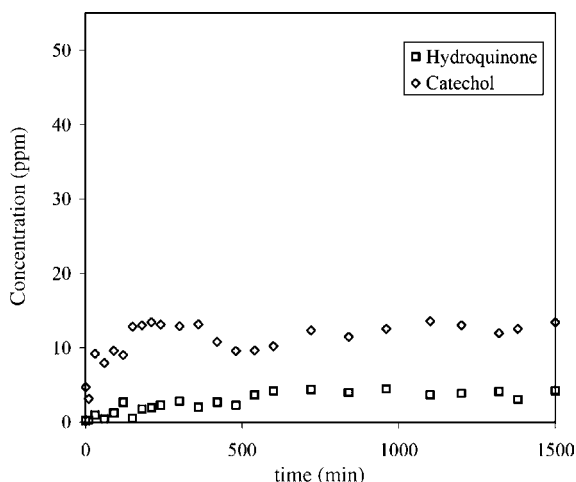
Fig. 6. Variation in hydroquinone and catechol concentration (calculated by MCR-ALS) throughout the photodegradation of phenol.

1500 min) show a little deviation from the solid line. One explanation for this fact is that, from the catalytic point of view, the photocatalytic degradation did not work in optimal conditions. Nevertheless the objective of this work is to show the advantages of the developed analytical method rather than to optimize the appropriate conditions of the photodegradation.

Fig. 6 shows the degradation concentration values obtained for hydroquinone and catechol by MCR-ALS. These results are slightly different to those obtained by PARAFAC in a previous work [11], but the kinetic behaviour is conserved.

The analytical method developed is faster than HPLC, which is normally used to monitor this sort of reaction. This methodology makes it possible to obtain rapidly and valuable information for the future optimization of the degradation process.

6. Conclusions

EEM and MCR-ALS are good tools for quantitatively monitoring the degradation of phenol.

It has been shown that, for quantification to be correct, the contribution of the hydroxyderivatives of phenol must be separated. Hydroquinone can be quantified when concentrations are higher than 0.05 ppm. Catechol and resorcinol can be differentiated from phenol and hydroquinone but their quantification errors are very high.

In the light of the results, this methodology could be a fast, cheap alternative for the quantitative monitoring of the phenol photodegradation process.

References

[1] M. Peiró, J.A. Ayllón, J. Peral, X. Doménech, Appl. Catal. B 30 (2001) 359.
[2] G. Sivalingam, M.H. Priya, G. Madras, Appl. Catal. B 51 (2004) 67.
[3] Ö.E. Kartal, M. Erol, H. Oğuz, Chem. Eng. Technol. 24 (2001) 645.
[4] M. de1 Olmo, C. Diez, A. Molina, I. de Orbe, J.L. Vilchez, Anal. Chim. Acta 335 (1996) 23.
[5] S. Lathasree, A. Nageswara Rao, B. SivaSankar, V. Sadasivam, K. Rengaraj, J. Mol. Catal. A 223 (2004) 101.
[6] A. Mylonas, E. Papaconstantinou, V. Roussis, Polyhedron 15 (1996) 3211.
[7] Ö.E. Kartal, M. Erol, H. Oğuz, Chem. Eng. Technol. 24 (2001) 645.
[8] M.L. Nahorniak, K.S. Booksh, J. Chemometr. 17 (2003) 608.
[9] R.D. JiJi, G.A. Cooper, K.S. Booksh, Anal. Chim. Acta 397 (1999) 61.
[10] R.D. JiJi, G.G. Andersson, K.S. Booksh, J. Chemometr. 14 (2000) 171.
[11] M.V. Bosco, M. Garrido, M.S. Larrechi, Anal. Chim. Acta 559 (2006) 240.
[12] R. Bro, Chemometr. Intell. Lab. Syst. 38 (1997) 149.
[13] K.S. Booksh, A.R. Muroski, M.L. Myrick, Anal. Chem. 68 (1996) 3539.
[14] R. Bro, Multiway Analysis in the Food Industry: Models, Algorithms, and Applications, Ph.D. Thesis, University of Amsterdam, 1998 (http://www.mli.kvl.dk/staff/foodtech/brothesis.pdf).
[15] R. Tauler, A. Smilde, R. Kowalsky, J. Chemometr. 9 (1995) 31.
[16] E. Casassas, I. Marqués, R. Tauler, Anal. Chim. Acta 310 (1995) 473.
[17] R. Tauler, I. Marqués, E. Casassas, J. Chemometr. 12 (1998) 55.
[18] R. Tauler, Chemometr. Intell. Lab. Syst. 30 (1995) 133.
[19] A.I. Khuri, J.A. Cornell, Response Surfaces, Marcel Dekker Inc., New York, 1987, p. 335.
[20] J. Saurina, R. Tauler, Analyst 125 (2000) 2038.
[21] J. Saurina, C. Leal, R. Compañó, M. Granados, R. Tauler, M.D. Prat, Anal. Chim. Acta 409 (2000) 237.
[22] S. Wold, K. Esbensen, P. Geladi, Chemometr. Intell. Lab. Syst. 2 (1987) 37.
[23] G.H. Golub, Ch.F. van Loan, Matrix Computations, 2nd ed., The John Hopkins University Press, London, 1989.
[24] D.L. Massart, B. Vandeginste, L. Buydens, S. de Jong, P. Lewi, J. Smeyers-Verbeke, Handbook of Chemometrics and Qualimetrics: Part A, Elsevier, Amsterdam, 1997.
[25] E.R. Mallnowski, Anal. Chem. 49 (1977) 612.
[26] The Mathworks, MATLAB, Version 6.1, South Natick, MA, 1999.
[27] The Mathworks, Optimization Toolbox, Version 2.0, Natick, MA, 1998.
[28] R. Tauler, E. Casassas, A. Izquierdo-Ridorsa, Anal. Chim. Acta 248 (1991) 447.
[29] A. Garrido Frenich, D. Picón Zamora, J.L. Martínez Vidal, M. Martínez Galera, Anal. Chim. Acta 449 (2001) 143.
[30] www.hc-sc.gc.ca, Health Canada-Official method "Determination of phenolic compounds in sidestream tobacco smoke", December 1999.

ELSEVIER

An optical immunosensor for rapid vitellogenin detection in plasma from carp (*Cyprinus carpio*)

E. Bulukin [a], V. Meucci [b], M. Minunni [a], C. Pretti [c], L. Intorre [b], G. Soldani [b], M. Mascini [a],∗

[a] *Dipartimento di Chimica, Polo Scientifico, Università degli Studi di Firenze, via della Lastruccia 3, 50019 Sesto Fiorentino, Italy*
[b] *Dipartimento di Clinica Veterinaria e, Profilassi e Igiene degli Alimenti, Università degli Studi di Pisa, viale delle Piagge 2, 56124 Pisa, Italy*
[c] *Dipartimento di Patologia Animale, Profilassi e Igiene degli Alimenti, Università degli Studi di Pisa, viale delle Piagge 2, 56124 Pisa, Italy*

Abstract

Vitellogenin (vtg) has proven to be a sensitive and simple biomarker for assessing exposure of fish to environmental estrogens. The aim of this work was to develop a rapid, in the order of minutes, screening method for the detection of fish vtg. The surface plasmon resonance technique (Biacore X™) was coupled with immunodetection for the determination of fish vtg in plasma and mucus from carp (*Cyprinus carpio*). Monoclonal anti-vtg antibodies were linked on the sensor surface through chemical cross-linking via a capturing antibody. A simple regeneration process allowed the reuse of the sensor surface. Sensor optimisation was carried out using carp vtg. The developed immunosensor was tested with vtg spiked samples and with plasma and mucus from fish exposed to 17β-estradiol (E2). Vitellogenin could be detected in the ppm range in buffer as well as in plasma and mucus. Good discrimination between control and exposed samples was obtained. The results were compared with ELISA and a correlation coefficient of $R^2 = 0.85$ ($n = 9$) between the two methods indicated that the immunochemical biosensor could be used for the analysis of vtg in fish plasma samples. The assay time was 20 min hence allowing for rapid sample screening.
© 2006 Elsevier B.V. All rights reserved.

Keywords: Optical immunosensor; Vitellogenin; Surface plasmon resonance; Carp

1. Introduction

There is growing evidence and concern of the impact of endocrine disrupting chemicals (EDCs) in the environment. Endocrine disruptors are exogenous agents that alters functions of the endocrine system consequently causing adverse effects of the reproductive health of organisms [1]. A large range of EDCs have been identified, making the detection of a single compound or group of compounds difficult. Consequently, the development of analytical techniques using specific biomarkers have shown to be a promising route for evaluating EDC contamination in the aquatic environment. Among these, the detection of the phospholipoglycoprotein vitellogenin (vtg) has been commonly reported.

vtg is produced as the yolk protein precursor in the liver of oviparous vertebrates such as fish. The transcription of the vtg gene takes place as a result of circulating 17β-estradiol (E2) produced in the gonads of female fish during sexual maturation. The E2 enters the liver cells by diffusion and is retained in the target cells through binding to a specific receptor protein (estrogen receptor) hence inducing the activation of the vtg loci [2]. Although naturally present only in female fish, the expression of the protein has been observed to be induced in male and immature fish through the exposure to xeno-estrogens [3]. Consequently, the presence of vtg in plasma and sera of male and sexually immature fish has proven to be a sensitive and simple biomarker for assessing exposure to environmental estrogens [4–6].

Several analytical approaches for vtg determination have been reported such as separation techniques and immunoassays. Allner et al. [7] used an electrophoretic method for the determination of estrogen-induced proteins in fish exposed to synthetic and naturally occurring chemicals. Similarly, Song et al. [8] reported about the separation and detection of vitellogenin in fish plasma by capillary zone electrophoresis. Chromatographic and mass spectrometry methods have also been described [9–11]. In addition a range of immunochemical methods such as enzyme linked immunosorbent assays (ELISAs), radioimmunoassay

---

(RIA) and Western Blotting have been studied. For quantitative detection of vtg the most widely used techniques are based on heterogeneous competitive ELISAs or sandwich ELISAs. In the last decade a range of ELISAs for measuring vtg concentrations in various fish species have been developed, such as sole (*Solea vulgaris*) [12], striped bass (*Morone saxatilis*) [13], eelpout (*Zoarces viviparus*) [14], Artic charr (*Salvelinus alpinus*) [15], fathead minnow (*Pimephales promelas*) [16,17], rainbow trout (*Oncorhynchus mykiss*) [18], zebrafish (*Danio rerio*) [19], Japanese medaka (*Oryzias latipes*) [20] and carp (*Cyprinus carpio*) [21]. Despite showing high sensitivities, ELISAs used for vitellogenin detection are multistage processes with long overall analysis times varying from 1 to 4 days [22].

Biosensors have in recent years shown to represent interesting alternatives for developing rapid screening techniques. However, only very few studies report the development of biosensors for vtg detection. In Oshima et al. [23] the use of a quartz crystal microbalance for the determination of plasma vitelllogenin was described. Darain et al. [24] reported the detection of vitellogenin using impedance spectroscopy. The same author has also reported about a separation-free amperometric immunosensor for vitellogenin detection based on screen-printed carbon assays modified with a conductive polymer [25]. Despite demonstrating sensitivities in the ppm or sub-ppm vitellogenin range, these methods show long incubation times for the preparation of the sensor surfaces. Darain, et al. [25] reported a total time for the fabrication of the immunosensor array of 28 h. Similarly, long incubation times for the modification of the electrode surface used for impedance spectroscopy have been reported [24]. Likewise, the preparation of the quartz crystal microbalance involves long incubation times as well as large sample volumes [23].

The present study was aimed at developing an optical-label free sensor for rapid, in the order of minutes, vtg detection in fish. The surface plasmon resonance technique (Biacore X^{TM}) was coupled to immunodetection for the determination of fish vtg in plasma. The analytical parameters (specificity, sensitivity, reproducibility, analysis time, matrix effects) of the system were evaluated. Hence, the developed immunosensor was tested with vtg spiked samples and with plasma and mucus from fish exposed to E2. The obtained results were compared with the ELISA test used as a reference method.

2. Materials and methods

2.1. Reagents

Vitellogenin (vtg) from carp (*C. carpio*) was purchased from Biosense Laboratories A/S, (Bergen, Norway). The product had been obtained through the purification of plasma from 17β-estradiol-induced fish by selective precipitation with MgCl$_2$, in the presence of EDTA. Rabbit polyclonal antibodies (pab) (purified IgG fraction) against vitellogenin from carp and monoclonal mouse anti-carp vtg antibodies (mab) were also purchased from Biosense Laboratories (Bergen, Norway). *N*-Hydroxysuccinimide was from FLUKA (Milan, Italy), anti-mouse antibodies, *N*-(3-dimethylaminopropyl)-*N*′-

ethylcarbodiimide, bovin serum albumin (BSA), sodium hydroxide (NaOH) and ethanolamine were obtained from Sigma (Milan, Italy). Saline phosphate buffer, PBS (0.1 M pH 7.0) was prepared from di-sodium hydrogen phosphate dihydrate (Na$_2$HPO$_4$·2H$_2$O), sodium dihydrogen phosphate monohydrate (NaH$_2$PO$_4$·H$_2$O) and sodium chloride (NaCl) purchased from Merck (Milan, Italy). Acetate buffer (0.01 M, pH 5.0) was prepared from sodium acetate (CH$_3$COONa) and acetic acid (CH$_3$COOH) from Merck. The running buffer employed in all experiments was HBS-EP containing [4-(2-Hydroxyethyl)piperazine-1-ethanesulonic acid] (HEPES, 0.1 M), sodium chloride (0.15 M), polyoxyethylene-sorbital monolaurate (Tween 20, 0.005%) and ethylenediaminetetraacetic acid (EDTA, 3 mM) from Sigma. All aqueous solutions were prepared with Milli-Q water, obtained from a Milli-Q system (Millipore, Milford, USA). The running buffer was filtered (0.2 μm) and degassed before use.

2.2. Instrumentation

Surface plasmon resonance measurements were performed with the Biacore X^{TM} instrument (Biacore AB, Uppsala, Sweden). The measurements were carried out using CM5 chips (carboxymethylated dextran covalently attached to a gold surface) with HBS-EP as running buffer (5 μl/min). The SPR signal was expressed in resonance units (RU).

2.3. Immobilisation of antibodies

2.3.1. Capturing antibodies

Mouse monoclonal anti-carp vtg antibodies (mab) were immobilised with anti-mouse as capturing antibodies. The sensor chip was activated using a solution of *N*-hydroxysuccinimide (NHS) (50 mM) and *N*-(3-dimethylaminopropyl)-*N*′-ethylcarbodiimide (EDAC) (200 mM) in water [26]. The solution was passed over the sensor surface for 7 min at a flow rate of 5 μl/min. Thereafter the anti-mouse antibodies were allowed to flow over the chip surface (50 μg/ml in acetate buffer, 15 min interaction time). Remaining active sites were blocked using ethanolamine (1 M). Hence, a mab solution 18 μg/ml in phosphate buffer (PBS, 0.1 M, pH 7.0) was allowed to flow over the sensor surface (interaction time 15 min).

2.3.2. Capturing antibodies with cross-linking

The mouse monoclonal anti-carp vtg antibodies (mab) were immobilised using cross-linking with anti-mouse antibodies. Firstly, the activation of the sensor surface was carried out as described in Section 2.3.1. Hence, the mouse-monoclonal anti-carp vtg antibodies (mab) were immobilised with anti-mouse as capturing antibodies. In order to achieve cross-linking between the two types of antibodies a solution of NHS/EDAC was used. In this case aminocoupling between the carboxylic and aminogroups of the two types of antibodies was achieved. Subsequently remaining activated sites were blocked with ethanolamine (1 M).

2.4. Measuring assay

The measuring cycle consisted of the following steps; (i) surface with immobilised capturing antibodies (anti-mouse) binding the anti-vtg mab with running buffer 5 μl/min (baseline), then (ii) addition of the analyte vtg; (iii) washing with buffer to remove excess analyte; primary response recorded; hence (iv) surface regeneration by dissociation of the immunochemical reaction and return to the baseline.

2.5. Surface regeneration

For surface reuse it was necessary to return to the baseline. For this purpose the dissociation of the formed immunocomplex was achieved using sodium hydroxide (NaOH) at different concentrations (0.5–10 mM, 2 μl).

2.6. Quantitative ELISA analysis of vtg

Using a procedure modified from Specker and Anderson [22], a quantitative vtg ELISA was performed using the monoclonal carp vtg antibody (Biosense Laboratories). Purified carp vtg protein (Biosense Laboratories) was used to coat the plates and for preparation of the standard curve. Briefly, purified carp vtg was serially diluted to obtain standard concentrations between 8 and 1000 ng/ml. Standards and diluted samples were incubated for 1 h at 37 °C with an equal volume of the primary antibody (diluted 1:1000). Triplicate aliquots of standards and samples (200 μl) were added to 96-well microtiter plates previously coated with vtg (100 ng/ml overnight at 4 °C) and incubated for 1 h at 37 °C. The plates were washed with tween-phosphate buffered saline (TPBS) and a 1:1000 dilution of sheep anti-mouse peroxidaseconjugated secondary antibody (Gibco-Invitrogen Life Technologies, Carlbad, CA, USA) was added and incubated for 1 h at 37 °C. Levels of vtg in samples were measured colorimetrically at 492 nm using o-phenylenediamine dihydrochloride as substrate with a Microplate Reader Model 550" from Bio-Rad Laboratories (Richmond, CA, USA). vtg ELISA Absorbance values (expressed as optical density, OD) were converted to the proportion of antibody bound (B) expressed as a percentage in the zero standard by the following equation: $B(\%) = (OD - NSB/OD_0 - NSB) \times 100$ (where OD is the absorbance of a given sample or standard, OD_0 is the absorbance of the zero standard and NSB is the non-specific binding absorbance value). In evaluating the detection limit of the ELISA assay, the minimum amount of vtg that produced a response significantly different from OD_0 was estimated around 15 ng/ml. The linear range of the standards obtained from the sigmoidal curve was between 125 and 1000 ng/ml. The sample concentration was obtained from the sigmoidal curve at a sample dilution of 1:50,000 and 1:5000 for the mucus.

2.7. Fish samples

In this study carp (*C. carpio*) was selected as test species. The carp is a freshwater cyprinid present both in the wild and as farmed species. Adult carps were purchased from ErreCi (Pisa, Italy). The fish was stored in 500 l oxygenated fish tanks, supplied with fresh water in a closed recirculating system with controlled temperature (20 ± 1 °C). Fish were kept under normal laboratory illumination with a daily photoperiod of 12 h, and were acclimatised to laboratory conditions for 1 week. Procedures for the care and management of animals were performed in accordance with the provisions of the EC Council Directive 86/609 EEC, recognised and adopted by the Italian Government (DL 27.01.1992, no. 116). Blood was collected from the caudal vein of adult male carp ($t = 0$) and this represented the negative control samples. Mucus was collected by scraping the tail surface with a plastic spatula into microcentrifuge tubes. Hence, the fish were injected i.p. with 2.5 mg/kg body weight of 17β-estradiol (E2) dissolved in corn oil. On days 5, 10 and 14 ($t = 5$, 10 and 14 days, respectively) after the E2 injection, blood was collected from the caudal vein from three fish species ($n = 3$). Plasma was separated by centrifugation at $1500 \times g$ for 20 min (4 °C) and frozen (-80 °C) until further analysis was undertaken. The mucus was weighed and homogenized in one volume of PBS (pH 7.4). The homogenates were centrifuged at $10,000 \times g$ for 15 min at (4 °C), supernatants were collected and used for vtg analysis.

3. Results and discussion

3.1. Immobilisation using capturing antibodies

Direct immobilisation of the analyte specific antibodies showed an analytical detection range in the order of 10–100 ppm. For increased sensitivity of the sensors (0.1–10 ppm) the use of capturing antibodies was attempted since this strategy allowed to control the orientation of the specific anti-vtg antibodies (mab). The sensor was thereafter tested for its ability to recognise the relative antigen. The vtg standard was diluted in PBS. A calibration curve was obtained by subsequent injections of vtg without regenerating the surface by dissociating the immunocomplex. A linear range was observed between 1 and 10 ppm vtg ($R^2 = 0.98$, $y = 3.9x - 2.2$) demonstrating that the sensor was able to recognise the antigen. Specificity was tested by injecting BSA (100 ppm). No response was observed. The interaction time was 15 min. However, the process was tedious and expensive as it was not possible to regenerate the sensor surface after the calibration. The absence of the dissociation step was due to the fact that the linking between the capturing and mab antibodies is a reversible, non-covalent affinity binding. Hence, treatment of the mab/anti-vtg/vtg complex with a dissociating agent also caused the dissociation of the mab from the capturing antibodies. Consequently, requiring reimmobilisation of mab prior to further measurements. Subsequently, cross-linking between the capturing and analyte specific antibodies was attempted.

3.2. Immobilisation using cross-linking

By using NHS/EDAC cross-linking between the aminogroups and carboxylic groups of the capturing and anti-vtg antibodies was obtained. The cross-linking of the two types of
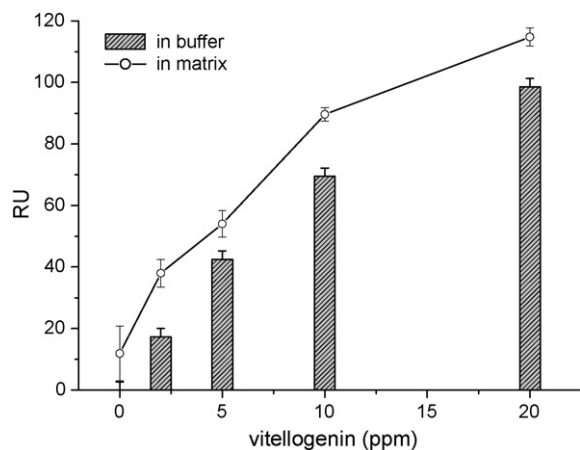
Fig. 1. Calibration curve of vitellogenin in buffer and in matrix (plasma, diluted 1:500).

Fig. 2. Typical sensorgram recorded during the injection of a sample from an E2 treated carp.

antibodies significantly improved the method in terms of costs and analysis time since it was not necessary to reinject the mab anti-vtg (15 min). Moreover, it was possible to dissociate the mab/vtg complex leaving on the surface both the capturing and the mab antibodies. The amount of immobilised mab on the sensor chip surface was estimated from the RU signal obtained where 1000 RU represents a change in surface protein concentration of $1 \, ng/mm^2$ (instrument handbook). In the present study the immobilisation of the mab anti-vtg antibodies resulted in a RU shift of $2220 \pm 70 \, RU$ ($n = 3$), hence corresponding to a surface coverage of $2.2 \, ng/mm^2$. Furthermore, the affinity constant between the vtg and the mab was evaluated using the Biaevaluation software following a 1:1 Langmuir association model. Three standard curves were used for the evaluation. The affinity constant K_D was found to be $(4.5 \pm 1.2) \, 10^{-10} \, M$. Selectivity of the sensor was tested using BSA (100 ppm). No binding was observed demonstrating that the sensor was specific for the antigen. With this assay scheme a calibration curve was carried out in the ppm range. The binding between the immobilised mab and the vtg obey a Langmuir type adsorption isotherm. However, for quantification purposes, only the linear part of the sigmodial curve
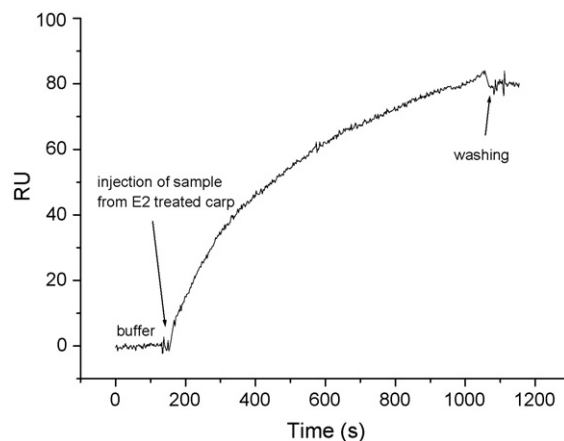
was considered. A linear range from 1 to 10 ppm was obtained ($R^2 = 0.98$, $y = 6.9x + 2.9$) with an average CV of 7% ($n = 3$ for each concentration). The limit of detection (L.O.D.) was estimated to be 1 ppm (three times the standard deviation of the blank).

3.3. Matrix effects

Since the applicability would be the vtg detection in fish plasma, the influence of this matrix on the signal was tested using plasma samples from fish not exposed to any estrogenic compounds (negative controls). Different dilutions as well as the effect of filtration were studied. The samples were diluted in PBS. Filtration using a 0.22 μm filter did not appear to have an effect on reducing aspecific adsorption. Despite the fact that the non-exposed fish (reference) resulted in an aspecific response it was possible to detect the presence of vtg (standard additions) to the matrix (Table 1). A calibration curve of the vtg in the matrix was thereafter carried out at a matrix dilution of 1:500. The RU signal obtained for the vtg at different concentrations in the matrix was comparable with that obtained in buffer (Fig. 1).
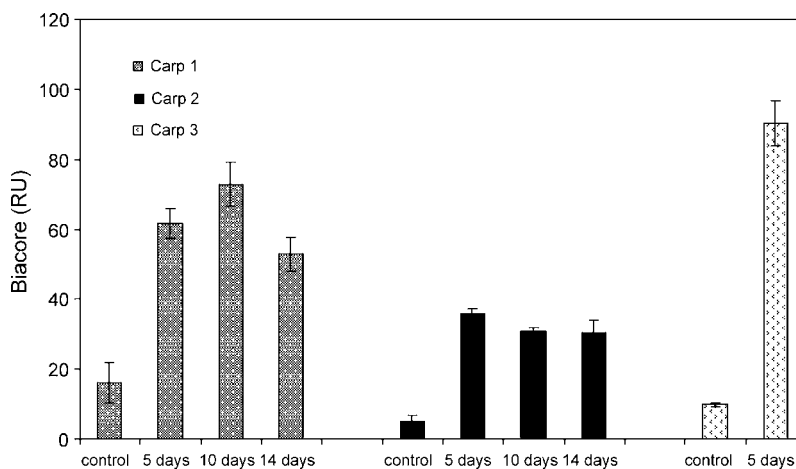
Fig. 3. Results of the analysis of control and E2 treated carp plasma samples.

Table 1
Plasma matrix effects

Dilution	Matrix (RU)	matrix + vtg 10 ppm (RU)	vtg signal/matrix
1:10	93 ± 9 (n = 3)	102	1.1
1:25	61 ± 10 (n = 3)	92	1.5
1:50	54 ± 10 (n = 5)	76	1.4
1:500	12 ± 9 (n = 3)	90 ± 2 (n = 3)	7.5

Table 2
Mucus matrix effects

Dilution	filtration	vtg (ppm)	RU
1:20	-	-	75
1:20	Yes	-	41
1:50	Yes	-	55
1:100	Yes	-	45
1:100	Yes	10	93
Buffer	Yes	10	91

3.4. Analysis of plasma samples

The analysis of E2 exposed fish using the optical immunosensor was carried out using the previously described protocol. The samples were diluted 1:1000 in PBS. A typical sensorgram recorded during the injection of a sample from an E2 treated carp is shown in Fig. 2. Despite obtaining some aspecific absorption from the negative control samples, a good discrimination between the control and E2 treated fish could be obtained (Fig. 3). Furthermore, a good reproducibility was obtained with an average CV of 12.9% ($n = 10$). High RU values were observed for the sample obtained after 5 days of E2 treatment indicating a fast vtg response in the fish. The results were compared with ELISA. The sample concentrations were estimated from the ELISA sigmoidal curve (Fig. 4). For the immunochemical biosensor the sample concentration was estimated by subtracting the RU value of the control sample from the exposed sample and hence estimating the concentration from the vtg calibration curve. A relative good correlation between the two methods was obtained ($R^2 = 0.85$, $n = 9$) indicating that the immunochemical biosensor could be used for the rapid analysis of vtg in fish plasma samples.

3.5. Analysis of mucus samples

An interesting matrix for the non-invasive vtg detection is represented by mucus. The mucus can be obtained from the fish by simple scraping on the fish surface (see Section 2.7). Mucus was obtained from one carp not treated with any estradiol (negative control). Hence, after the fish had been treated with E2, mucus was sampled on 3 different days ($t = 5$, 10 and 14). The biosensor analysis was carried out as previously described. The mucus showed some matrix effects that

improved using filtration. A good compromise between the lower expected vtg concentrations in this matrix [27] and the dilution factor was found to be 1:100. At this dilution the matrix was spiked with 10 ppm. A signal comparable to that in buffer could be obtained (Table 2). vtg could be detected in the mucus after 14 days (Fig. 5). Compared to the plasma it appeared that a longer time period is required for the vtg to be detectable in the mucus [27]. Despite being close to the detection limit of the sensor the results show that this matrix might offer interesting future possibilities for non-invasive vtg detection.

3.6. Enhancing the primary response

To increase the sensitivity of the sensor, the use of polyclonal antibodies was employed [28]. The vtg is likely to have several epitopes and it is in this case possible to enhance the primary response using anti-vtg polyclonal anti-rabbit antibodies (pab). After measuring the vtg standard the secondary response is obtained (without regeneration of the surface) by adding pab directly to the bound vtg with subsequent washing of the surface to remove excess pab (Fig. 6). The amplification was effective as the primary response was increased by about 30%. Furthermore, the regeneration process remained a simple and fast step as the formed immunocomplex could be easily dissociated using sodium hydroxide at different concentrations for 30 s leaving on the sensor surface the capturing and anti-vtg antibodies. This type of enhancement could prove to be important for the analysis of matrices such as mucus where the expected vtg concentration is lower compared to that found in plasma.

Fig. 4. Dose-response curve obtained by ELISA.
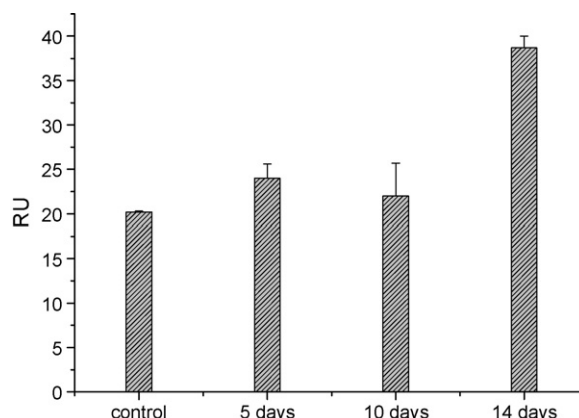
Fig. 5. Results of the analysis of control and E2 treated carp mucus samples.
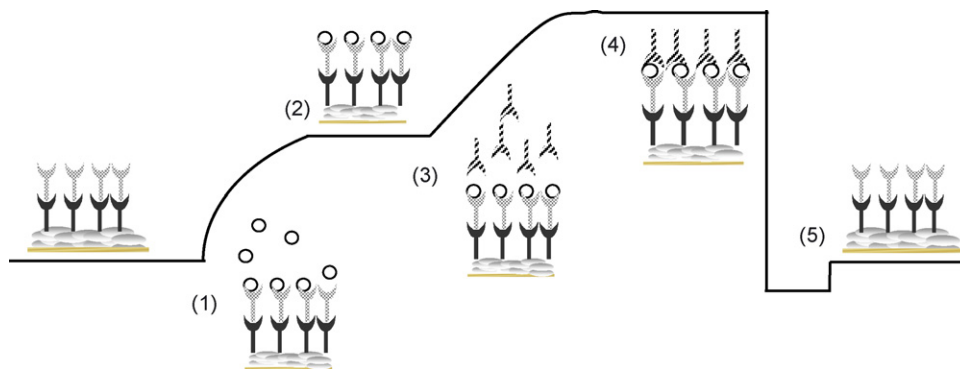
Fig. 6. Measuring assay using secondary antibodies for signal magnification. Surface with immobilised capturing Ab (anti-mouse Pab) binding the anti-vtg Mab with flowing buffer 5 μl/min (baseline), hence (1) addition of vtg; (2) washing with buffer to remove the analyte excess. Primary response recorded; thereafter (3) a secondary antibody (rabbit anti-vtg, Pab anti-vtg), specific for a different epitope of the vtg protein was added to enhance the analytical signal; (4) washing of the surface to remove the excess of secondary Pab; secondary response recorded; (5) surface regeneration by dissociation of the immunochemical reaction and return to the baseline.

4. Conclusions and future work

In the present study an optical immunosensor was developed for the rapid screening of vtg in plasma from carp (*C. carpio*). The sensor was assembled linking the analyte specific antibodies using capturing antibodies. The two types of antibodies were cross-linked which significantly improved the method as it allowed the reuse of the sensor surface. The sensor was able to detect vtg in the ppm range both in buffer and in plasma from carp. The preparation of the sensor surface took less than 1 h and the analysis of sample and standards 20 min, hence allowing for rapid screening. The optimised sensor was used for the analysis of 17β-estradiol-treated carp. Good discrimination between 17β-estradiol and control carp could be obtained, demonstrating that the sensor could be used for the rapid screening of vtg in this sample matrix. The analysis of vtg in mucus showed that this matrix could offer interesting future applications for the non-invasive vtg detection. Future work will involve the analysis of vtg in plasma and mucus from field exposed samples.

References

[1] J.G. Vos, E. Dybing, H.A. Greim, O. Ladefoged, C. Lambré, J.V. Tarazona, I. Brandt, A.D. Vethaak, Crit. Rev. Toxicol. 30 (2000) 71.
[2] T.P. Mommsen, P.J. Walsh, Vitellogenesis and oocyte assembly, in: W.S. Hoar, V.J. Randall (Eds.), Fish Physiology, vol. XIA, Academic Press, San Diego, CA, USA, 1988, pp. 347–406.
[3] G. Flouriot, G. Monod, Y. Valotaire, A. Devaux, J.-P. Travedi, Mar. Environ. Res. 39 (1995) 293.
[4] J.P. Sumpter, S. Jobling, Environ. Health Perspect. 103 (1995) 173.
[5] P.-D. Hansen, H. Dzer, B. Hock, A. Marx, J. Sherry, M. McMaster, Ch. Blaise, Trends Anal. Chem. 17 (1998) 448.
[6] D.E. Kime, J.P. Nash, A.P. Scott, Aquaculture 177 (1999) 345.
[7] B. Allner, G. Wegener, T. Knacker, P. Stahlschmidt-Allner, Sci. Total Environ. 233 (1999) 21.
[8] M. Song, J. Wang, J. Shao, B. He, G. Jiang, G. Shi, J. Chromatogr. B 821 (2005) 38.
[9] J. Shao, G. Shi, J. Liu, G. Jiang, Anal. Bioanal. Chem. 378 (2004) 615.
[10] J. Banoub, A. Cohen, A. Mansour, P. Thibault, Eur. J. Mass Spectrom. 10 (2004) 121.
[11] D. Wunschel, I. Schultz, A. Skillman, K. Wahl, Aquat. Toxicol. 73 (2005) 256.
[12] J.N. Rodriguez, O. Kah, M. Geffard, F. Le Menn, Comp. Biochem. Physiol. B: Biochem. Mol. Biol. 92 (1989) 741.
[13] M. Kishida, T.R. Anderson, J.L. Specker, Gen. Comp. Endocrinol. 88 (1992) 29.
[14] B. Korsgaard, K.L. Pedersen, Comp. Biochem. Physiol. C: Pharmacol. Toxicol. 120 (1998) 159.
[15] H.K. Johnsen, H. Tveiten, N.P. Willassen, A.M. Biochem. Physiol. B: Biochem. Mol. Biol. 124 (1999) 355.
[16] L.G. Parks, A.O. Cheek, N.D. Denslow, S.A. Heppell, J.A. McLachlan, G.A. LeBlanc, C.V. Sullivan, Comp. Biochem. Physiol. C: Pharmacol. Toxicol., 123 (1999) 113.
[17] E. Mylchreest, S. Snajdr, J.J. Korte, G.T. Ankley, Comp. Biochem. Physiol. C: Pharmacol. Toxicol., 134 (2003) 251.
[18] E. Bon, U. Barbe, J.N. Rodriguez, B. Cuisset, C. Pelissero, J.P. Sumpter, F. Le Menn, Biochem. Physiol. B: Biochem. Mol. Biol. 117 (1997) 75.
[19] H. Holbech, L. Anderson, G. Peterson, B. Korsgaard, K.L. Pedersen, P. Bjerregaard, Comp. Biochem. Physiol. C: Pharmacol. Toxicol. 130 (2001) 119.
[20] K. Nishi, M. Chikae, Y. Hatano, H. Mizukami, M. Yamashita, R. Sakakibara, E. Tamiya, Comp. Biochem. Physiol. C: Pharmacol. Toxicol. 123 (2002) 161.
[21] M. Hennies, M. Wiesmann, B. Allner, H. Sauerwein, Sci. Total Environ. 309 (2003) 93.
[22] L.L. Specker, T.R. Anderson, Developing an ELISA for a model protein-vitellogenin, in: P.W. Hochanchka, T.P. Mommsen (Eds.), Biochemistry and Molecular Biology of Fishes, Elsevier, Amsterdam, The Netherlands, 1994, pp. 567–579.
[23] K. Oshima, H. Nakajima, S. Takahashi, Y. Kera, M. Shimomura, S. Miyauchi, Sens. Actuators, B 105 (2005) 473.
[24] F. Darain, D.-S. Park, J.-S. Park, Y.-B. Shim, Biosens. Bioelectron. 19 (2004) 1245.
[25] F. Darain, D.-S. Park, J.-S. Park, Y.-B. Shim, Biosens. Bioelectron. 20 (2005) 1780.
[26] S. Löfås, B. Johnsson, J. Chem. Soc., Chem. Comm. 21 (1990) 1526.
[27] V. Meucci, A. Arukwe, Aquat. Toxicol. 73 (2005) 1.
[28] M. Minunni, Anal. Lett. 28 (1995) 933.

Speciation of chromium in waste water using ion chromatography inductively coupled plasma mass spectrometry

ZuLiang Chen [a,*], Mallavarapu Megharaj [a], Ravendra Naidu [a,b]

[a] *University of South Australia, Mawson Lakes Boulevard, Mawson Lakes, South Australia 5095, Australia*
[b] *CRC for Contamination Assessment and Remediation of Environments, Mawson Lakes Boulevard, Mawson Lakes, South Australia 5095, Australia*

Abstract

Ion chromatography (IC) coupled with inductively coupled plasma mass spectrometry (ICP–MS) was systematically investigated for determining the speciation of chromium in environmental samples. Firstly, the stability of complexes formed by Cr(III) with various aminopolycarboxylic acids was studied by electrospray ionization mass spectrometry (ESI–MS). The results showed that $[Cr(EDTA)]^-$ was stable in solution. Secondly, various mobile phases were examined to separate Cl^- from chromium species by IC to avoid Cl^- interference. The separation of $[Cr(EDTA)]^-$ and Cr(VI) was achieved on a new anion-exchange column (G3154A/102) using a mobile phase containing 20 mM NH_4NO_3 and 10 mM $NH_4H_2PO_4$ at pH 7.0 without Cl^- interference. Detection limits for chromium species were below 0.2 µg/L with a direct injection of sample and without prior removal of interferences from the matrix. Finally, the proposed method was used for the determination of chromium species in contaminated waters.
© 2006 Elsevier B.V. All rights reserved.

Keywords: Chromium speciation; ESI–MS; IC–ICP–MS; Waste water

1. Introduction

There is an increasing demand for techniques capable of providing accurate information on heavy metal speciation. This is because it is now recognised that the toxicity of many elements depends not on the total amount of metal present but rather on the specific toxic species present. Different species of the same element may have different oxidation states and exhibit different behaviour or potential for toxicity within environmental and biological systems [1]. In the case of chromium (Cr), the two most environmentally important oxidation states are Cr(III) and Cr(VI), where Cr(VI) has a greater water solubility and potential for toxicity [2]. Environmental contamination by chromium chiefly results from industrial processes such as electroplating, paint production, leather tanneries and metallurgy [2–4]. Since chromium toxicity is species-specific, determining the total chromium concentration in environmental samples is insufficient for a toxicity assessment of chromium. For this reason,

many papers concerned with analytical techniques for chromium speciation in environmental samples have increased in recent years. Analytical techniques include atomic spectrometric (AS), inductively coupled plasma mass spectrometry (ICP–MS) and their hyphenated techniques [5].

In hyphenated approaches, liquid chromatography (LC) coupled with ICP–MS has been developed for chromium speciation because ICP–MS offers both multi-element and multi-isotope detection with high sensitivity [6–8]. Ion chromatography (IC) is also compatible with ICP–MS for metal speciation analysis if the eluent contains minimal amounts of organic solvent. The simultaneous separation of chromium cannot normally be conducted since Cr(VI) typically exists as cationic aqua-hydroxo complexes while Cr(VI) exists typically as an anionic chromate species. However, this problem can be resolved using two approaches. The first of these approaches uses an anion-exchange column and a cation-exchange guard column in series or a mixed-mode column to retain both species [9–12]. The second of these approaches involves a derivitization process whereby Cr(III) is complexed with a ligand to form an anionic complex, which can be subsequently separated from Cr(VI) by anion-exchange chromatography [13–18]. The ligand is a nec-

essary component of the mobile phase to stabilize the Cr(III) as the chelate complex [16]. Cr(III) reacts to form a complex while Cr(VI) species does not complex with the ligand. However, the above analytical methods only provide elemental information. As a supplementary technique, electrospray ionization mass spectrometry (ESI–MS) has become popular for elemental speciation studies in recent years, as it gives structural information on the analyte [19]. For this reason, one objective of the present study was to characterize the form of the Cr(III) aminopolycarboxylate complexes in aqueous solutions by ESI–MS in order to determine whether these complexes were stable in solution. The stability of the formed complexes provides the basis for simultaneous separation of chromium species because Cr(III) complexes formed must be stable during chromatographic separation [16].

Determination of chromium using ICP–MS detection has some limitations. If the matrix contains high levels of chloride (Cl$^-$) or carbon (C) then the formation of $^{35}Cl^{16}OH^+$ or $^{40}Ar^{12}C^+$ in the plasma may be significant. These compounds have the potential to interfere with the determination of chromium because they have the same mass as the chromium isotope commonly used for ICP–MS detection of chromium (^{52}Cr). ^{52}Cr is preferred for detection by ICP–MS since it is the more abundant isotope (83.8%). To overcome this limitation, one approach is the removal of interferences of the target analyte by using various eluents, followed by ICP–MS detection. Therefore, in this study, we report on the effectiveness of the use of various mobile phases to reduce Cl$^-$ interferences. In addition, the new application of anion-exchange column (G3154A/102, provided by Agilent) has not been reported previously. To achieve these aims, the presented work includes: (1) the examination of the stability of anionic complexes by IC–ICP–MS and ESI–MS, (2) the removal of Cl$^-$ interference from the target analyte by ion chromatography using various ammonium salt eluents and (3) a new application for an anion-exchange column for the determination of chromium speciation.

2. Experimental

2.1. Chemicals and solutions

All chemicals used in this study were analytical grade reagents from Sigma and Aldrich (Sydney, Australia). Milli-Q water (18.2 MΩ/cm, Milli-Q Plus System, Millipore, Bedford, MA, USA) was used for preparing all solutions and standards. Standard solutions (K$_2$Cr$_2$O$_7$ and CrCl$_3$·6H$_2$O) were prepared daily from 10 mM aqueous stock solutions. The complexation of Cr(III) with EDTA was achieved by adding the appropriate amounts of Cr(III), EDTA and water into 15 mL polypropylene tubes and heating the tubes in a water bath set to at 80 °C for 20 min. Eluents required for IC–ICP–MS, were prepared by dissolution of the appropriate amount of ammonium salts in Milli-Q water and were filtered through a disposable 0.45 μm cellulose acetate membrane filter and degassed in an ultrasonic bath prior to use. Eluent pH was adjusted with 0.1 M ammonium hydroxide. Waste waters, contaminated with chromium, were filtered through a 0.45 μm membrane filter prior to analysis.

Table 1
Optimised operational conditions for IC–ICP–MS

ICP–MS	Agilent 7500c
RF power	1450 W
Plasma gas flow	Ar, 15 L/min
Auxiliary gas flow	Ar, 1.0 L/min
Carrier gas flow	Ar, 1.15 L/min
Sampling depth	7.5 mm
Monitoring mass (TRA)	*m/z* 52
Integration time	1 s
Dwell time	0.5 s/mass
IC	Agilent 1100
Column	G3154A/102 (Agilent)
Mobile phase	20 mM NH$_4$NO$_3$, 10 mM NH$_4$H$_2$PO$_4$ at pH 7.0
Flow rate	1.0 L/min
Injection volume	50 μL
Column temperature	30 °C

2.2. FIA–ESI–MS system

Flow injection analysis was carried out using an Agilent 1100 series (Agilent, Waldbornn, Germany) instrument equipped with an injector. The carrier solution contained 0.1% formic acid and the flow-rate was 0.5 mL/min with an injection volume of [Cr(EDTA)]$^-$ of 20 μL. The MS system was an Agilent 1100 series quadrupole equipped with an electrospray ionization (ESI) source. The instrument was operated in the negative ionization mode. The operating conditions for ESI were: nebulizer gas (nitrogen), 40 psi; drying gas (nitrogen) flow-rate, 12 L/min; capillary voltage, 4000 V; gas temperature, 350 °C; the fragmentor voltage was set at 80 V.

2.3. IC–ICP–MS conditions

An Agilent 1100 liquid chromatography module (Aglient, Tokyo, Japan) equipped with a guard column (G3154A/102) and a separation column (G3154A/101) was used. The separation column was based on a porous polymethacrylate resin with 10 μm particle size and had an exchange capacity of 50 μeq/g. Samples (50 μL) were injected using an 1100 auto-sampler. The eluent flow-rate was 1.0 mL/min. The outlet of the separation column was connected directly, via Polyetheretherketone (PEEK) tubing (70 cm, 0.13 mm i.d.) to a Babington nebulizer of an Agilent 7500c ICP–MS (Agilent, Tokyo, Japan), which served as the element-specific mass detector. Chromium was detected at *m/z* 52. The IC–ICP–MS system was controlled and data processed using Agilent Chemstation software. The ICP–MS and HPLC operating conditions are given in Table 1.

3. Results and discussion

3.1. Stability of Cr(III)–ligand complexes

Simultaneous separation of cations and anions using anion-exchange chromatography require conversion of cations to anionic metal-complexes. Successful separation required the anionic complex to be stable and to not readily undergo ligand exchange during the chromatographic process [16]. In
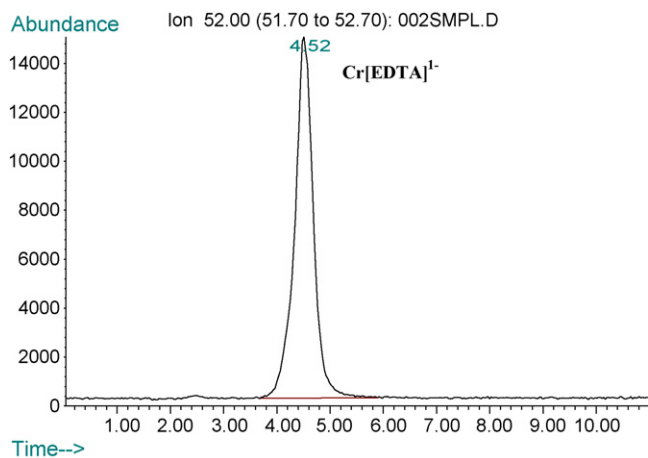
Fig. 1. Typical chromatogram obtained using IC–ICP–MS with 150 μg/L [Cr(EDTA)]⁻. Ion chromatography and ICP–MS condition used are described in Table 1.

this study, three ligands were investigated for their suitability to complex with Cr(III). The ligands tested were ethylenediaminetetraacetic acid (EDTA), diethylenetriaminepentaacetric acid (DTPA) and 2,6-pyridinedicarboxylic acid (PDCA). Stabilities were examined by IC–ICP–MS using a mobile phase containing 15 mM NH_4NO_3 and 10 mM $NH_4H_2PO_4$ at pH 6.0. For all three ligands, only [Cr(EDTA)]⁻ was observed as shown Fig. 1. This indicates that during chromatographic process [Cr(EDTA)]⁻ did not undergo ligand-exchange with competing ions in the eluent, such as NO_3^- and $H_2PO_4^-$, because the Cr(III) complex formed with EDTA is kinetically stable [13–15]. In contrast, small responses were observed for both [Cr(DTPA)]²⁻ and [Cr(PDCA)₂]⁻, which could be a result of poorer stability, since the eluent used in this case was not added to the ligand [16] and may have resulted in interconversion during the separation [13,14]. The conditions affecting formation of [Cr(EDTA)]⁻, such as solution pH, temperature and the concentration ratio of Cr(III)/EDTA, were also investigated. The maximum complex formation was obtained at pH 6.0, when the concentration ratio was [Cr(III)/EDTA = 1:3] and the samples were reacted at 80 °C for 20 min.

ESI–MS spectra for both [EDTA]⁴⁻ and [Cr(EDTA)]⁻ in the negative ion mode [M−H]⁻ were investigated to determine whether ESI–MS could be used to confirm formation of [Cr(EDTA)]⁻. A 0.1% (v/v) formic acid solution was used as the carrier solution because formic acid is volatile and, therefore, compatible with ESI–MS [20–22]. Firstly, a standard [EDTA]⁴⁻ solution (5 mg/L) was injected into the ESI–MS system under the optimised conditions for ionization (fragmentor 70 V and capillary voltage 3000 V). The ESI–MS spectrum of [EDTA]⁴⁻ shows a single peak at *m/z* 291.3 (Fig. 2a) [20–22]. Secondly, to understand the complexation of [EDTA]⁴⁻ with Cr^{3+}, a mixed solution of Cr^{3+} with [EDTA]⁴⁻ (5 mg/L, Cr(III)/EDTA, 1:1) was injected into the FIA–ESI–MS system. The spectrum (Fig. 2b) shows a prominent ion at *m/z* 340.2, corresponding to [EDTA + Cr−4H⁺]⁻, with a similar mass spectra obtained following ESI–MS detection of Fe[EDTA]⁻ [23,24]. In addition, the mass spectrum attributable to [EDTA]⁴⁻ is absent in

Fig. 2b indicating that all EDTA were completely converted into the Cr(III) complex. The ESI–MS detection of [Cr(EDTA)]⁻ is specific since chromium has four stable isotopes [⁵⁰Cr(4.35%), ⁵²Cr(83.8%), ⁵³Cr(9.50%) and ⁵⁴Cr(2.37%)]. Therefore, the Cr(III) complexes have very distinctive isotope patterns, corresponding to *m/z* 338.2, 340.2, 341.2 and 342.2, respectively, making it relatively easy to locate unknown compounds which contain chromium. The results indicated that the [Cr(EDTA)]⁻ complex was stable in solution and the use of IC for the separation of [Cr(EDTA)]⁻ was possible without adding EDTA to the mobile phase.

3.2. Retention behaviour using different mobile phases

One of the approaches for removing Cl⁻ interferences is via chromatographic separation prior to introduction into the ICP–MS detector system. In this approach interferences such as C and Cl⁻ can be separated from chromium species by ion chromatography through the use of different separation modes and mobile phases [25,26]. In anion-exchange chromatography, the retention of a target anion depends on the nature of the competing ion, its concentration in solution and the pH of the mobile phase [26]. Among these variables, the nature of the competing ions is the main parameter determining whether target anions are eluted as these compete with target ions on the anion-exchange column. In order to separate Cl⁻ from chromium species with reasonable resolution, these parameters can be manipulated by using various eluting systems.

A mobile phase containing 20 mM NH_4NO_3 at pH 5.80 was used for an injected mixture of 50 μg/L [Cr(EDTA)]⁻, 50 μg/L Cr(VI) and 500 mg/L Cl⁻. The retention times of [Cr(EDTA)]⁻ and Cr(VI) were 4.28 and 8.43 min, respectively, while Cl⁻ eluted at 3.52 min. However, the Cl⁻ peak overlapped the [Cr(EDTA)]⁻ peak since the difference in retention between Cl⁻ and [Cr(EDTA)]⁻ was only 0.66 min. This indicated the possibility of Cl⁻ interfering in the determination of [Cr(EDTA)]⁻. As the NO_3^- competing ion is unaffected by pH, changes in the pH of the mobile phase would not affect the measured concentration of NO_3^- or significantly influence the retention. Therefore, changes in pH would not be expected to improve resolution.

For this reason, an alternative mobile phase that would be affected by pH was assessed. A mobile phase containing 20 mM $NH_4H_2PO_4$ at pH 4.60 was initially examined as the eluent but neither [Cr(EDTA)]⁻ nor Cr(VI) were observed and only Cl⁻ was detected at 12.39 min. A longer retention time resulted for all the target analytes because the target anions were being retained more strongly on the anion-exchange site and $H_2PO_4^-$ has a weaker affinity compared with the target anions for anion-exchange sites [25,26]. However, changes in the mobile phase pH could now influence the retention, as the speciation of the mobile phase was pH-dependent. A mobile phase containing 20 mM $(NH_4)_2HPO_4$ at pH 7.90 reduced the retention time for Cl⁻ to 6.29 min, but [Cr(EDTA)]⁻ and Cr(VI) were still not observed within the time frame for the run (<20 min). The reduction of Cl⁻ retention was due to the pH-induced changes in the nature of the competing ion, and consequently led to an increased eluting power. Considering the results from both
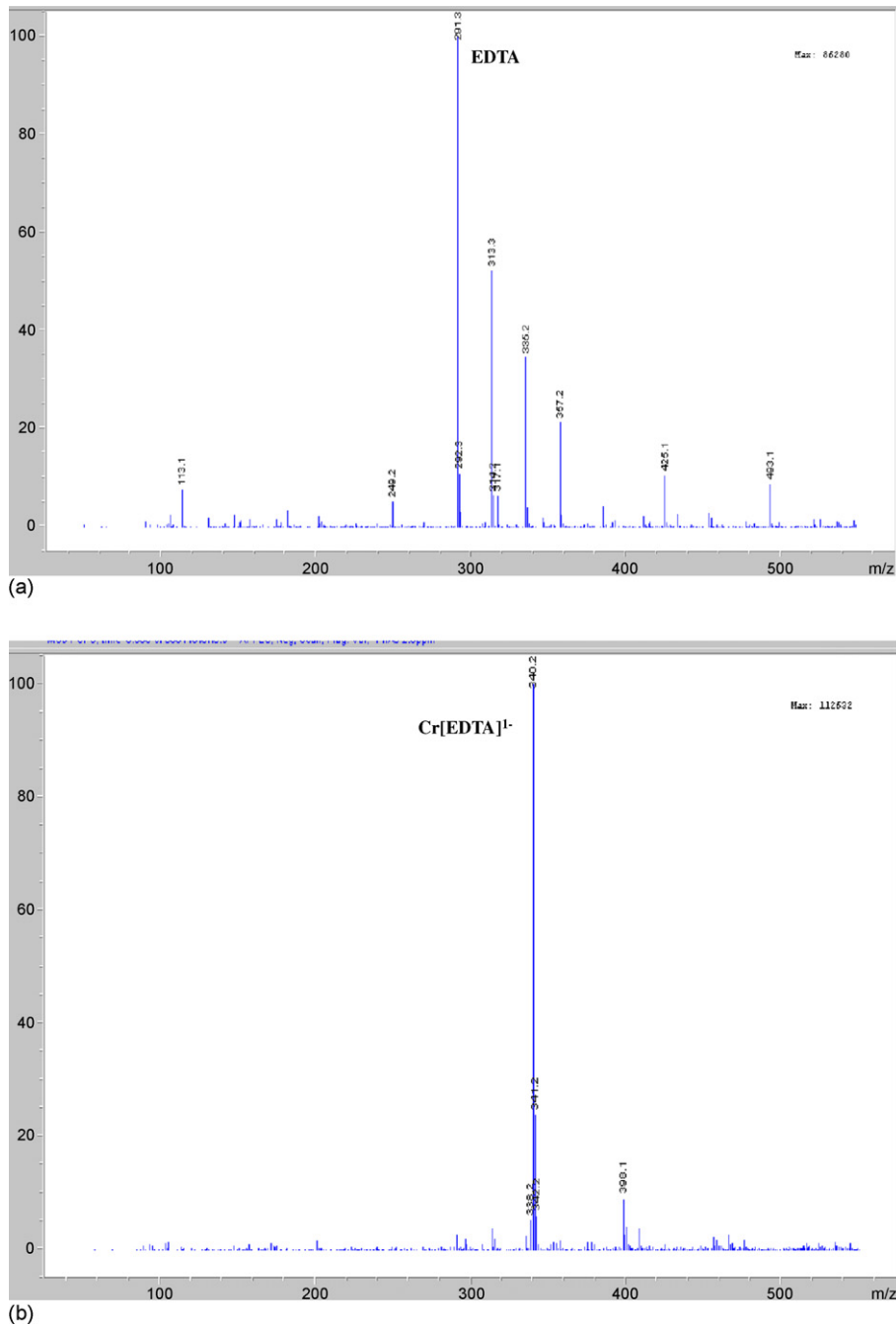
Fig. 2. Negative ESI–MS spectra of: (a) [EDTA]$^{4-}$ and (b) [Cr(EDTA)]$^-$. Each spectra corresponds to a concentration of 5 mg/L and was collected under the conditions described in Section 2.

eluents tested so far, a mixed mobile phase containing 10 mM NH$_4$NO$_3$ and 10 mM NH$_4$H$_2$PO$_4$ at pH 6.0 was tested because of its dual buffering capacity (NH$_4$H$_2$PO$_4$) and strong eluting power (NH$_4$NO$_3$). This eluent could be useful for the analysis of samples at varying pH values. Using this eluent, Cl$^-$, [Cr(EDTA)]$^-$ and Cr(VI) were all observed to elute, with retention times of 3.90, 5.92 and 9.80 min, respectively. While Cl$^-$ was now separated from [Cr(EDTA)]$^-$ by 1.72 min, the peak attributed to [Cr(EDTA)]$^-$ had a poor peak shape. However, the peak shape can be improved by changes in both the concentration of NO$_3^-$ and the pH of the mobile phase.

Various mobile phase NO$_3^-$ concentrations were tested in the range of 10–20 mM. The retention time decreased with increasing NH$_4$NO$_3$ concentration (Fig. 3) and, consequently, the peak shapes was improved. Good peak shape and resolution were obtained using a mobile phase containing 20 mM NH$_4$NO$_3$ and 10 mM NH$_4$H$_2$PO$_4$ at pH 6.0. The rationale behind this is that the higher the concentration of competing ions in the eluent, the more effectively the eluent displaces target ions from the stationary phase and the target ions are more rapidly eluted from the column [25,26]. Slow elution of target ions over a long period results in poor peak shape due to
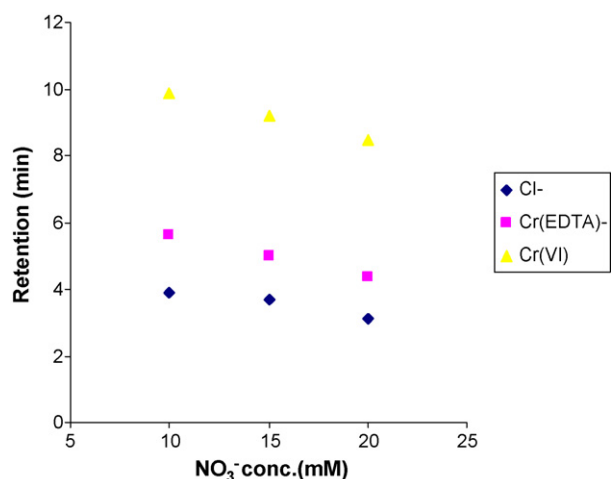
Fig. 3. The influence of competing ion (NO_3^-) concentration on the retention time of chromium species and chloride at constant pH 6.0. Other conditions are as described in Table 1.

Fig. 4. The influence of eluent pH on the retention time of chromium species and chloride at a constant concentration of NH_4NO_3 (20 mM) and $NH_4H_2PO_4$ (10 mM). Other conditions are as described in Table 1.

tailing of resilient target anions as they are slowly eluted from the column. Further peak shape improvement can be obtained by small changes in mobile phase pH, as the mobile phase pH influences the charges on both competing and solute ions. The retention of target anions decreased with increasing eluent pH. That is, when the mobile phase pH increased from 6.0 to 8.0, for a mobile phase containing 20 mM NH_4NO_3 and 10 mM $NH_4H_2PO_4$ (Fig. 4), the peak shape was consequently improved. The best peak shape and resolution was observed at pH of 7.0, where Cl^- was well separated from $[Cr(EDTA)]^-$ and Cr(VI) and therefore did not interfere with the determination of $[Cr(EDTA)]^-$ (Fig. 5). When the eluent pH was raised from 7.0 to 8.0, poor resolution between $[Cr(EDTA)]^-$ and Cr(VI) was observed and the peaks attributable to $[Cr(EDTA)]^-$ and

Cr(VI) overlapped. The reduction in retention with increasing pH was due to an increase in charge on the competing ion and the phosphate ions ($[H_2PO_4]^-$ to $[H_2PO_4]^{2-}$, while the charge on the target ions also changed. As a consequence, the eluting power was increased from a combination of these two effects [25]. Thus, the optimal conditions for the composition of the mobile were 20 mM NH_4NO_3 and 10 mM $NH_4H_2PO_4$ at pH 7.0.

3.3. Analytical performance and analysis of waste water samples

Calibration curves for quantification were obtained by plotting peak area versus the concentration of the corresponding
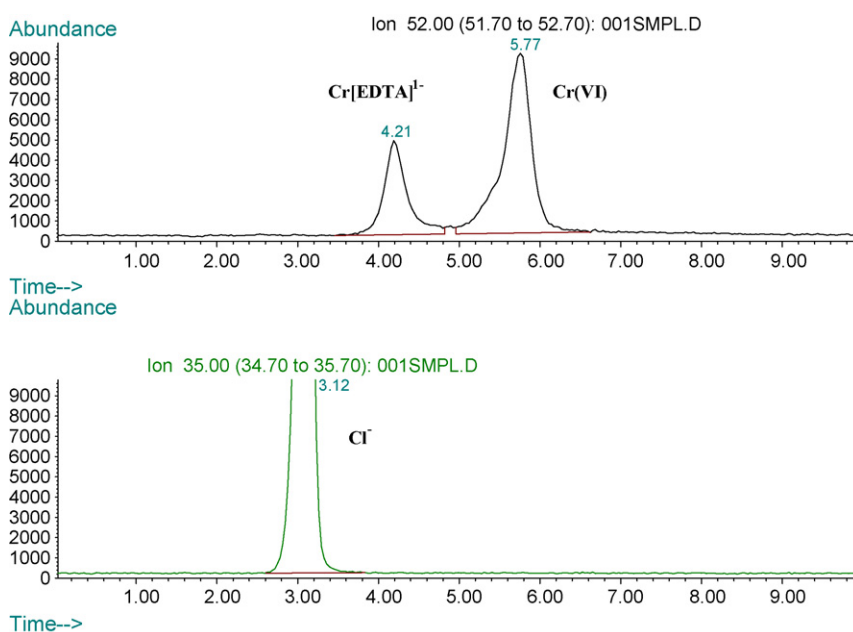
Fig. 5. Chromatogram of chromium species and chloride obtained from the eluent containing 20 mM NH_4NO_3 and 10 mM $NH_4H_2PO_4$ at pH 7.0. Other conditions are as described in Table 1.

Table 2
Characteristics for chromium speciation determined using the proposed method

Species	Regression line	Coefficient	Detection limit (µg/L)	Reproducibility ($n = 5$, R.S.D.%)
Cr(III)	$y = 1.73 \times 10^3 x + 1.43 \times 10^4$	0.999	0.2	2.8
Cr(VI)	$y = 3.27 \times 10^3 x + 3.08 \times 10^4$	1.000	0.1	1.9

The conditions are as in Fig. 5; detection limit—signal/noise = 3.

target anion. All calibrations were linear over a concentration range of 1–1000 µg/L with correlation coefficients greater than 0.999 when a 50 µg/L standards was injected. Detection limits (S/N = 3) ranged from 0.1 to 0.2 µg/L. The reproducibility from multiple injections ($n = 5$) of a 10 µg/L standard solution, containing a mixture of [Cr(EDTA)]$^-$ and Cr(VI), showed that the R.S.D. was <2.8%. Analytical performance characteristics of the proposed method are summarised in Table 2. In order to test the applicability of the method for the speciation of chromium, water samples were spiked with a mixture of 10 µg/L mixed standards. Recoveries for individual chromium species ranged from 91.5 to 104.3%.
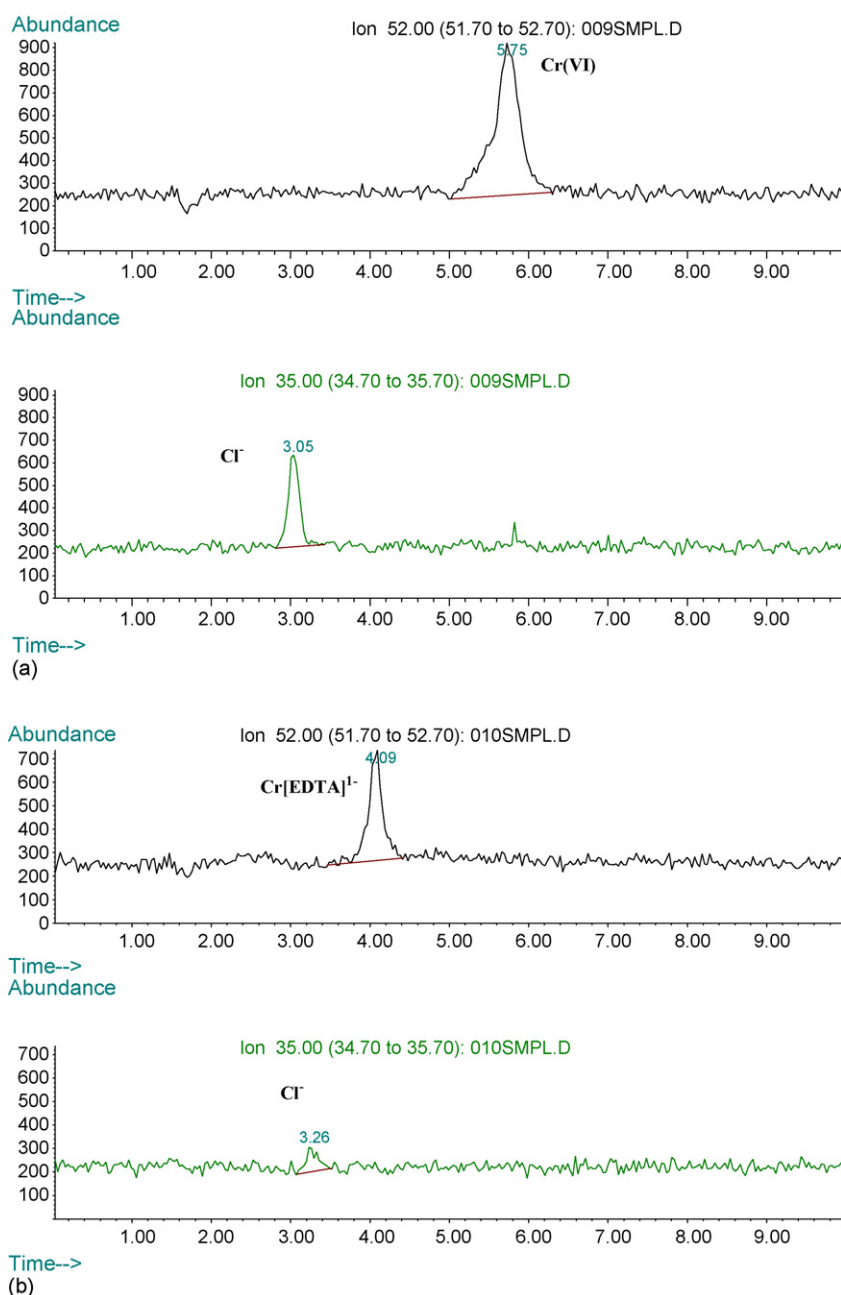
Fig. 6. The typical chromatograms of chromium species and chloride obtained from real samples. The conditions are as in Fig. 5.

The proposed method was tested using real samples to determine if it could be used for monitoring speciation of chromium in contaminated waters and soils. Fig. 6 shows two typical chromatograms from waste waters. Chromium species were found at concentrations of $26.2 \pm 1.6\,\mu$g/L for Cr(III) and 48.0 ± 2.3 for Cr(VI) ($n = 3$) in contaminated waste waters.

4. Conclusion

In this work, ESI–MS was used to confirm that a stable chromium-chelate complex, Cr(EDTA)]$^-$, was formed in solution and that this complex formation could be used as a basis for the simultaneous ion chromatographic separation of Cr(III) and Cr(VI). Chloride interference in the determination of chromium was eliminated through separation by ion chromatography. A new anion-exchange column (G3154A/102, provided by Agilent) can be used to elucidate chromium speciation with a mobile phase of 20 mM NH_4NO_3 and 10 mM $NH_4H_2PO_4$ at pH 7.0 within 7 min. The proposed method was demonstrated for the analysis of chromium species in waste water.

References

[1] D.E. Kimbrough, Y. Cohen, A.M. Winer, L. Creelman, C. Mabuni, Crit. Rev. Environ. Sci. Technol. 29 (1999) 1.
[2] S. Avudainayagam, M. Megharaj, G. Owens, R.S. Kookana, D. Chittleborough, R. Naidu, Rev. Environ. Contam. Toxicol. 178 (2003) 53–91.
[3] J.R. Pretty, E.A. Blubaugh, J.A. Caruso, T.M. Davidson, Anal. Chem. 66 (1994) 1540.
[4] D. Oktavec, J. Lehotay, E. Hornackova, At. Spectrosc. 8 (1995) 92.
[5] M.J. Marqués, A. Salvador, A. Morales-Rubio, M. de la Guardia, Fresenius J. Anal. Chem. 367 (2000) 601.
[6] C. CaEmara, R. Cornelis, P. Quevauviller, Trends Anal. Chem. 19 (2000) 189.
[7] C.A. Ponce de Leon, M. Montes-Bayon, J.A. Caruso, J. Chromatogr. A 947 (2002) 1.
[8] B. Michalk, Trends Anal. Chem. 21 (2002) 142.
[9] M. Pantsar-Kallio, P.K.G. Manninen, Anal. Chim. Acta 318 (1996) 335.
[10] M. Pantsar-Kallio, P.K.G. Manninen, J. Chromatogr. A 750 (1996) 89.
[11] M. Pantsar-Kallio, P.K.G. Manninen, Fresenius J. Anal. Chem. 355 (1996) 716.
[12] B. Barnowski, N. Jakubowski, D. Stuewer, J.C. Broekaert, J. Anal. At. Spectrom. 12 (1997) 1155.
[13] M.J. Tomlinson, L.S. Wang, J.A. Caruso, J. Anal. At. Spectrom. 9 (1994) 957.
[14] F.A. Byrdy, L.K. Olson, N.P. Vela, J.A. Caruso, J. Chromatogr. A 712 (1995) 311.
[15] H. Gurleyuk, D. Wallschlager, J. Anal. At. Spectrom. 16 (2001) 926.
[16] Y. Inoue, T. Sakai, H. Kumagai, J. Chromatogr. A 706 (1995) 127.
[17] A.P. Vonderheide, J. Meija, K. Tepperman, A. Puga, A.R. Ponhas, J.C. States, J.A. Caruso, J. Chromatogr. A 1924 (2004) 129.
[18] M. Nowak, A. Seubert, Anal. Chim. Acta 359 (1998) 193.
[19] E. Rosenberg, J. Chromatogr. A 1000 (2003) 841.
[20] T. Reemtsma, J. Chromatogr. A 1000 (2003) 477.
[21] C. Zwier, F.H. Frimmel, Anal. Bioanal. Chem. 378 (2004) 851.
[22] C. Zwier, F.H. Frimmel, Anal. Bioanal. Chem. 378 (2004) 862.
[23] A. Dodi, V. Monier, J. Chromatogr. A 1032 (2004) 87.
[24] T.P. Knepper, A. Werner, G. Bogenschutz, J. Chromatogr. A 1085 (2005) 240–246.
[25] J. Weiss, Ion Chromatography, second ed., VCH, Weinheim, 1995.
[26] C. Sarzanini, M.C. Bruzzoniti, Trends Anal. Chem. 20 (2001) 304.

Determination of carbonyl compounds in the atmosphere by DNPH derivatization and LC–ESI-MS/MS detection

Yuguang Chi [a,b], Yanli Feng [c,*], Sheng Wen [a], Huixiong Lü [a], Zhiqiang Yu [a], Wenbing Zhang [a], Guoying Sheng [a,c], Jiamo Fu [a,c]

[a] *State Key Laboratory of Organic Geochemistry, Guangzhou Key Laboratory of Environment Protection and Resources Utilization, Guangzhou Institute of Geochemistry, Chinese Academy of Sciences, Guangzhou 510640, China*
[b] *Graduate School of Chinese Academy of Sciences, Beijing 100049, PR China*
[c] *Institute of Environmental Pollution and Health, School of Environmental and Chemical Engineering, Shanghai University, Shanghai 200072, China*

Abstract

A method of determination of 32 carbonyl compounds by high performance liquid chromatography (HPLC) and electrospray ionization (ESI) tandem mass spectrometry (MS/MS) after derivatization with 2,4-dinitrophenylhydrazine (DNPH) was developed and successfully applied to the atmosphere sample of a residential area of Liwan District (S1) and a research institute of Tianhe District (S2) in Guangzhou, China. Some operation conditions of ESI-MS/MS in the negative ion mode including selection of parent and daughter ions, declustering potential (DP), entrance potential (EP), collision energy (CE), collision cell exit potential (CXP) and effect of buffer in ESI-MS/MS process were optimized. The regression coefficient of the calibration curves (R^2), recovery, reproducibility (R.S.D., $n = 5$) and limit of detection (LOD) were in the range of 0.9938–0.9999, 90–104%, 1.7–11% and 0.4–9.4 ng/m³, respectively. Among most of the samples, acetone was the most abundant carbonyl in two sampling sites and formaldehyde, acetaldehyde and butyraldehyde/2-butanone were also abundant carbonyls. In contrast to LC–UV method, the LOD, the separation of some co-eluting compounds and the precision (mainly to higher molecular weight carbonyls) are all improved by LC–ESI-MS/MS.
© 2006 Elsevier B.V. All rights reserved.

Keywords: LC–ESI-MS/MS; Carbonyl compounds; 2,4-Dinitrophenylhydrazine; Derivatization

1. Introduction

Carbonyl compounds in air are important photochemical oxidation products of virtually all hydrocarbons and precursors of free radicals, ozone, and peroxyacyl nitrates [1–3]. Moreover, several carbonyls also have received regulatory attention as toxic air contaminants, mutagens, eye irritants and carcinogens, such as formaldehyde, acetaldehyde, and acrolein [4,5]. Therefore, it is essential to develop a method for the determination of carbonyl compounds.

The quantitative method most frequently used for measuring carbonyls in air samples is based on derivatization with 2,4-dinitrophenylhydrazine (DNPH) in acid medium during sampling. The formed 2,4-dinitrophenylhydrazones are separated by reversed-phase liquid chromatography and detected by UV [6–10]. This method was widely used as an international standard and mainly applied to the determination of C1–C5 aldehydes and ketones in the United States and Europe [5,11]. The reasons were the low content of higher molecular weight (HMW) carbonyls in air and the interference of the sample matrices. In order to solve the problem, LC–MS and LC–MS/MS were applied for quantitive analysis and identification of carbonyl-DNPHs (in our knowledge, few studies focused on quantitative analysis of carbonyls by LC–MS/MS) [12–21]. In these studies, the best detection method was atmospheric pressure chemical ionization in the negative ion mode (APCI−), and the detection for carbonyls could achieve low-picogram quantities. However, there are also other ion sources and ion modes were used for the detection. Karst and coworkers found APCI and ESI in the positive mode were suitable to

* Corresponding author: Tel.: +86 21 56334184; fax: +86 21 56334184.
E-mail address: fengyanli@shu.edu.cn (Y. Feng).

determine aldehydes and ketones derivatized by the Hantzsch reaction [22–24]. Van den Bergh et al. [25] considered that both ESI and APCI in the negative ion mode were suitable for the detection of the DNPH derivatives of carbonyls and found ESI (−) in combination with single ion monitoring (SIM) detection showed the lowest detection limits. Moreover, Richardson et al. [26] determined polar disinfection by-products in water by LC–ESI-MS. Zwiener et al. [27] optimized some conditions of determination carbonyls and identified several carbonyls from swimming pool water by LC–ESI-MS/MS in the negative ion mode, and the detection limits were achieved µg/L degree by SIM measurements without sample preconcentration. Recently, Karst et al. [12] also applied APPI-MS in the negative ion mode method for the determination of aldehydes and ketones after DNPH derivatization and LC separation. Compared to APCI-MS, the lower detection limits were obtained under the same conditions. At present, the studies of carbonyls were mainly focused on air [6–19,22–25,28,29], water [26,27] and plants [30,31]. Due to the special action of carbonyls in air (important photochemical oxidation products of virtually all hydrocarbons and precursors of free radicals, ozone, and peroxyacyl nitrates), people were much more attention to the detection of carbonyls in air.

In our work, we extend the method of Zwiener et al. [27] and develop a method of quantitative analysis of 32 carbonyl compounds by DNPH derivatization and LC–ESI-MS/MS detection. This method is successfully applied to the air samples of a residential area and a research institute of Guangzhou, China. In contrast to other methods, some new target compounds are quantitative determine and much lower LOD are achieved by LC–ESI-MS/MS. Study shows that the negative ion mode is suitable for determining carbonyl-DNPHs. The influence of several operation conditions in quantitive process is explored, and a description of the process of their values optimized is provided. We detail the development of sensitive, selective, and dependable methods to quantify carbonyl compounds in air by LC–ESI-MS/MS.

2. Experimental

2.1. Reagents and materials

All solvents employed were HPLC grade. Water was double distilled and filtered by Milli-Q. The acetonitrile (ACN) and the 2,4-dinitrophenylhydrazine (DNPH) were purchased from Merck (Germany) and Fluka (USA). Ammonium acetate (Analytical grade) was purchased from Tianjin Chemical Reagent No. 1 Plant (Tianjin, China). Standard solutions containing 21 kinds of carbonyl-DNPHs (DNPH derivatives of formaldehyde, acetaldehyde, acetone, acrolein, benzaldeyde, butyraldehyde, crotonaldehyde, valeraldehyde, isvaleraldehyde, propionaldehyde, o-tolualdehyde, m-tolualdehyde, p-tolualdehyde, 2-butanone, cyclohexanone, heptaldehyde, octylaldehyde, nonanaldehyde, decylaldehyde, 2,5-dimethylbenzaldehyde, hexaldehyde) were purchased from ChemService (West Chester, USA). Other standard solutions including 12 DNPH derivatives of the following

carbonyls were synthesized in our lab: 2-hexanone, 2-nonanone, methacrolein, cyclopentanone, acetophenone, 4-methyl-2-pentanone, 2-pentanone, undecanal, dodecanal, tridecanal, and 2-OH-benzaldehyde.

2.2. DNPH derivatization of some carbonyls

The derivatives of carbonyls were prepared according to the method described in other literatures [32–34]. Proceed as follows. Firstly, 0.4 g DNPH (recrystallization in HPLC grade ACN twice) was dissolved in 2 mL H_2SO_4, and then 3 mL water and 10 mL ethanol were slowly added to this solution, respectively. Secondly, 50% molar excess of the respective carbonyls was dissolved in 20 mL ethanol and then the solution of carbonyl was slowly added to the solutions of DNPH. Finally, the precipitate formed was filtered off, recrystallized from 30 mL hot ethanol or ACN, washed with ethanol and dried in a desiccator. Purities of the products were identified by LC–MS, and no impurity peaks were found.

2.3. Sample preparation and sampling sites selection

The sampling method for carbonyls was described in our previous reports [8,9]. The sampling medium was a Sep-Pak Silica Gel cartridge (waters, Millipore Corp.). DNPH was recrystallized from ACN (HPLC grade) three times. Each cartridge was rinsed by 10 mL of ACN, and then coated with 7 mL of the freshly made coated solution, which contained 60 mL DNPH-ACN-saturated solution and 4 mL concentrated ortho-phosphoric acid in 500 mL ACN. When there was no more solution flowing out, they were dried with a gentle flow of high-purity nitrogen. Each cartridge was wrapped in a piece of filter paper, which impregnated with the DNPH-ACN solution to prevent contamination before use, wrapped in an aluminum foil, and sealed in a Teflon bag. All the processes were carried out in the high-purity nitrogen-filled glovebox. Finally, cartridges were stored in refrigerator at 4 °C [35,36] until use.

Samples were collected by drawing the air with a sampling pump (Thomas, USA) through the cartridge. A potassium iodide (KI) denuder was connected to the upstream of the cartridge to prevent the interference of ozone [37]. Before sampling, two cartridges in series were tested for breakthrough under the same sampling conditions and no compounds were detected in the back cartridge. After sampling, each cartridge was wrapped in an aluminum foil, resealed in a new Teflon bag, taken back to the laboratory and stored in the refrigerator.

The sampled cartridges were eluted with 2 mL of ACN into a 2 mL volumetric flask. This eluted solution was directly injected into the LC–MS system.

2.4. Instrument analysis

The LC–MS/MS system included an Agilent 1100 HPLC system equipped with quaternary Pump, on-line vacuum degassing system, autosampler and Variable Wavelength Detector (VWD, at 360 nm) and an API 4000 triple quadrupole mass spectrometer

(Applied Biosystems, Foster City, CA, USA) equipped with electrospray ionization (ESI).

LC separation of carbonyls was conducted by using a mixture of acetonitrile (ACN), water and 1 mmol/L ammonium acetate solution as mobile phase. The gradient program was as follows: constant 65% ACN and 35% water during 0–27 min, then changes of 65–80% ACN, 35–0% water and 0–20% ammonium acetate solution were taken in 27–30 min. The content of ACN increased to 95% in 30–35 min and kept constant until 50 min, and then restored to 80% at 55 min, in these times (30–55 min) constant 0% water was kept. During 55–60 min, changes of 80–65% ACN, 0–15% water and constant 20% ammonium acetate solution were taken. Changes of 15–35% water, 20–0% ammonium acetate solution and constant 65% ACN were taken in 60–61 min, and then followed by a 5 min equilibration time. An Agilent Zorbax Eclipse XDB-C18 column (250 mm × 4.6 mm, particle size 5 μm) was used as the analytical column. Flow rate was 0.6 mL/min and injection volumes were 5 μL. The mass spectra (MS) scanning from $m/z = 0$ to 500 was applied for the determination of m/z values. Electrospray mass data were acquired in the negative mode with a spray voltage of −4.5 kV. The source temperature was 450 °C. Nitrogen was used as the curtain gas (setting 10), nebulizer gas (setting 15) and turbo gas (setting 40). MS/MS was performed using nitrogen as collision gas (CAD gas setting 6). Other operating conditions of MS/MS were shown in Table 1. The data were acquired with the Sciex Analyst software, version 1.3.1 (Applied Biosystems, Foster City, CA, USA).

3. Results and discussion

3.1. Operating conditions of ESI-MS/MS

The optimized numerical values of some parameters (spray voltage, source temperature, curtain gas, nebulizer gas and turbo gas) of ESI-MS/MS have been described already in Section 2. These parameters were of the same numerical values for all carbonyl compounds in the experiment. In addition, declustering potential (DP), entrance potential (EP), collision energy (CE) and collision cell exit potential (CXP) were also important parameters of ESI-MS/MS. For these parameters, different carbonyl compounds need different numerical values and the results are shown in Table 1. Because the stability to collision-induced dissociation (CID) of ion source increased with the aldehyde carbon-chain length [27], the DP of the higher aldehydes was larger than those of the lower aldehydes. Aromatic aldehydes and ketones had the most stable molecular structure among all carbonyls and provided the largest DP values (setting 50). Moreover, the intensity of the CE also acquired the same behavior. CE was important parameter of the product ion spectra and the intensities of CE affected the formation of daughter ions and the degree of parents ions reduced. In general, the more stable the compounds were, the larger intensities of CE needed. The same conclusion also had been acquired in other literature [27]. For EP and CXP, there had not found any obvious influences in the experiment.

The selection of fragment ions is also an important condition in the quantitative process of carbonyls. The processes of frag-

Table 1
Operating conditions for MS/MS analysis of different carbonyl-DNPHs

Carbonyl compounds	DNPH derivative [M − H] (m/z)	Fragment ion for quantification (m/z)	Declusre-ring potential DP (V)	Entrance potential EP(V)	Collision energy CE (rel. units)	Collision cell exit potential CXP (V)
Formaldehyde	209.1	162.9	−25	−6	−16	−6
Acetaldehyde	223.1	163.1	−27	−6	−18	−6
Propionaldehyde	236.8	162.9	−30	−6	−18	−6
Butyraldehyde/2-butanone	251.1	152.1	−30	−10	−21	−6
Valeraldehyde	265	162.9	−30	−6	−20	−5
Hexaldehyde/2-hexanone	279	151.8	−35	−10	−20	−6
Heptaldehyde	293.0	162.6	−35	−12	−21	−6
Octylaldehyde	306.9	162.9	−35	−13	−22	−6
Nonanaldehyde/2-nonanone	321	151.8	−30	−12	−23	−6
Decylaldehyde	335.0	162.9	−40	−10	−23	−6
Undecanal	349.1	162.8	−40	−14	−24	−12
Dodecanal	362.9	163.4	−40	−14	−25	−12
Tridecanal	376.8	162.8	−50	−13	−26	−10
2-OH-benzaldehyde	301.1	181.6	−30	−10	−24	−6
Acetone	237.1	206.6	−27	−6	−21	−8
Acrolein	235.1	162.9	−27	−8	−20	−10
Methacrolein	249.1	162.4	−28	−11	−21	−8
Crotonaldehyde	248.9	172.1	−30	−11	−20	−6
Cyclopentanone	263.0	232.6	−30	−13	−20	−6.0
Cyclohexanone	276.9	230.8	−30	−13	−23	−6
Acetophenone	299	254.1	−50	−13	−25	−8
4-Methy-2-pentanone	279	151.6	−35	−10	−21	−6
Benzaldehyde	285	162.8	−50	−13	−23	−10
$o/m/p$-Tolualdehyde	299	162.6	−50	−14	−25	−10
2,5-Dimethylbenzalde-hyde	313	162.6	−50	−12	−25	−10
Isovaleraldehyde/2-pentanone	265.0	151.6	−30	−6	−23	−10

ment ions selected were based on product ion spectra of each DNPH derivative of carbonyls. m/z 163 is a typical fragment ion for all aldehyde-DNPHs. Aldehyde and ketone-DNPHs show a typical fragment ion at m/z 152. The formations of ion m/z 163 and m/z 152 have already been explained by Kölliker [13]. Moreover, under the conditions listed in Table 1, acetone, croton-aldehyde, cyclopentanone, cyclohexanone, 2-OH-benzaldehyde and acetophenone also show a high signal intensity fragment ion at m/z 207, 172, 233, 231, 182 and 254, respectively (see Table 1). These fragment ions have much higher signal intensities than typical fragment (m/z 163 and 152). Therefore, these ions were selected as the quantitative daughter ions in the next experiment.

3.2. Selection of mobile phases

Since some conditions of the mobile phase such as pH and ionic strength, influence ion formation in the electrospray process [27], the ammonium acetate as a buffer solution was introduced in this experiment. Zwiener et al. [27] compared ammonium acetate in both mobile phase with no buffer addition and buffer addition, and found both mobile phase addition got maximum signal intensity. However, little differences were found in our experiment.

The experiments demonstrated that ammonium acetate in both mobile phases was abandoned, because it was found difficult to completely dissolve ammonium acetate into 100% ACN. The peak areas of 10–20 µg/L aldehydes using 1 mmol/L ammonium acetate solution/ACN as mobile phases were compared with the peak areas of H_2O/ACN as mobile phases. The results are shown in Fig. 1. From the figure we could see that the buffered mobile phases provided larger peak area for higher aldehydes. However, for <C6 aldehydes, the peak areas
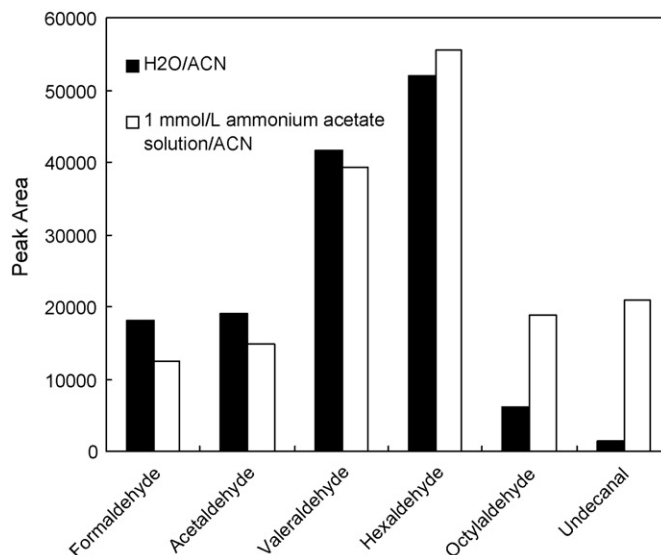
Fig. 1. Effect of buffer solution on the peak area of several aldehydes.

of the buffered were similar or little lower than those of non-buffered. Therefore, ammonium acetate solution as the third mobile phase was introduced into detection system at 27 min in the next experiment. Under the conditions of LC separation, 18 kinds of them were baseline separated among 32 kinds of carbonyl-DNPHs. The result is shown in Fig. 2. Fig. 2 demonstrated the total ion current chromatogram of a standard mixture of 32 carbonyl-DNPHs. The concentrations of standard solution were 200 µg/L for formaldehyde, acetaldehyde, propionaldehyde, butyraldehyde, hexaldehyde and crotonaldehyde, and 100 µg/L for other carbonyls. Due to the different parents and daughter ions between co-eluting compounds, the separation of some co-eluting compounds, such as valeraldehyde,
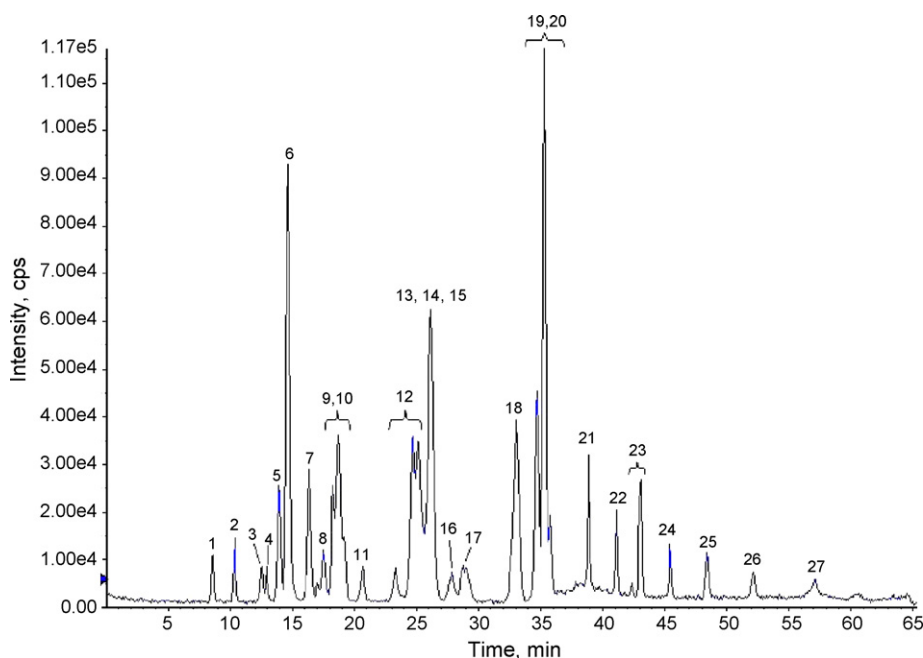
Fig. 2. Total ion current chromatogram of a standard mixture of 32 carbonyl-DNPHs. The peak numbers were consistent with the compound numbers of Table 3.

Table 2
Some analytical performance dates of the proposed method and 32 carbonyl compounds contents in two sample site

Compounds	Limit of detection (ng/m^3)	Reproducibility (R.S.D.%, $n = 5$)	Recovery (%, mean $\pm$ S.D., $n = 3$)	Concentrations (μg/m^3)	
				S1	S2
Formaldehyde	1.9	3	100 $\pm$ 3	4.10	5.25
Acetaldehyde	5.2	2	92 $\pm$ 4	4.80	7.11
Acrolein	2.5	2.8	96 $\pm$ 2	0.11	0.07
Acetone	4.3	1.7	103 $\pm$ 3	6.99	8.92
Propionaldehyde	5.3	1.8	102 $\pm$ 4	1.24	0.85
2-OH-benzaldehyde	0.4	3.3	100 $\pm$ 3	0.05	0.02
Crotonaldehyde	3.4	2.2	95 $\pm$ 1	0.17	0.05
Methacrolein	3.5	9.3	97 $\pm$ 7	0.78	0.27
Butyraldehyde/2-butanone	3.3	4.3	94 $\pm$ 8	4.02	3.52
Cyclopentanone	4.0	2.2	98 $\pm$ 1	0.04	0.03
Benzaldehyde	2.1	11	104 $\pm$ 4	0.50	0.31
Isovaleraldehyde/2-pentanone	2.2	5.2	99 $\pm$ 3	3.99	0.69
Valeraldehyde	2.7	2.2	96 $\pm$ 6	6.00	0.36
Cyclohexanone	2.0	7.3	90 $\pm$ 2	0.74	0.28
Acetophenone	7.6	5.7	92 $\pm$ 4	0.11	0.46
p-Tolualdehyde	4.8	8.7	96 $\pm$ 5	0.02	0.01
o/m-Tolualdehyde	4.9	9.3	97 $\pm$ 1	0.13	0.07
4-Methy-2-pentanone	2.0	3.0	90 $\pm$ 1	0.11	0.08
Hexaldehyde/2-hexanone	3.3	4.6	97 $\pm$ 7	1.39	0.64
2,5-Dimethyl-benzaldehyde	6.0	5.7	90 $\pm$ 6	0.04	0.02
Heptaldehyde	2.5	4.6	103 $\pm$ 8	0.18	0.31
Octylaldehyde	1.7	5.7	93 $\pm$ 6	0.16	0.48
Nonanaldehyde/2-nonanone	5.2	4.7	92 $\pm$ 3	0.95	1.08
Decylaldehyde	9.0	5.2	97 $\pm$ 1	0.16	0.38
Undecanal	5.4	5.2	96 $\pm$ 1	0.05	0.56
Dodecanal	8.3	5.5	94 $\pm$ 3	0.07	0.09
Tridecanal	9.4	6.5	95 $\pm$ 6	0.04	0.13

cyclohexanone and acetophenone, were also achieved by ESI-MS/MS. Some carbonyls have the same molecular weight were still not separated by ESI-MS/MS, including butyraldehyde/2-butanone, *o/m*-tolualdehyde, isovaleraldehyde/2-pentanone, hexaldehyde/2-hexanone, and nonanaldehyde/2-nonanone.

3.3. Method evaluation

In order to evaluate the proposed method, some parameters were determined under the above optimized conditions and results are shown in Table 2.

Linearity was investigated over a concentration range of 10–450 μg/L. Good linearities with correlation coefficients (R^2) ranging from 0.9938 to 0.9999 were obtained. The recoveries were determined as follows. Firstly, the standard solutions were directly added to the blank sampled cartridges. Secondly, the cartridges were eluted with 2 mL ACN. Finally, the eluted solutions were determined by LC–ESI-MS/MS. The added quantities of carbonyl-DNPHs were 8 μg for formaldehyde and acetaldehyde, 4 μg for acetone, 0.3 μg for butyraldehyde/2-butanone and hexaldehyde/2-hexanone, 0.2 μg for propionaldehyde, isovaleraldehyde/2-pentanone, crotonaldehyde and nonanaldehyde/2-nonanone, and 0.1 μg for other carbonyls. Recoveries were in the range of 90–104%. Reproducibilities (R.S.D., $n = 5$) were in the range of 1.7–11% which were measured by repeated determination of standard solutions containing 30 μg/L

butyraldehyde/2-butanone and hexaldehyde/2-hexanone, 20 μg/L propionaldehyde, isovaleraldehyde/2-pentanone, crotonaldehyde and nonanaldehyde/2-nonanone, and 10 μg/L other carbonyl-DNPHs. Limit of detection (LOD) was determined by using seven replicate analyses of the working standards at the lowest concentration (signal-to-noise ratio, S/N = 3), for which an approach was described in detail in 40 CFR Part 136B (Code of Federal Regulation, 2001). The LOD of the proposed method were in the range of 0.4–9.4 ng/m^3 for various carbonyls assuming a sampling volume of 180 L air and these values were about 1–2 order of magnitude better than LC–UV detection. Brombacher et al. [14] reported a LOD range of 1–15 ng/m^3 on a quadrupole ion-trap system (LCQ classic, ThermoFinnigan, San Jose, CA, USA) in APCI (−). In the study of Grosjean [15], the LOD of formaldehyde was 20 pg. In the present study, a 6 pg LOD of formaldehyde could be achieved.

3.4. Application to air samples

The samples collected in two sampling sites (a residential area of Liwan District (S1) and a research institute of Tianhe District (S2) in Guangzhou, China), were determined by the proposed method. Thirty-two target carbonyl compounds were all identified and quantified, in which butyraldehyde/butanone, isovaleraldehyde/2-pentanone hexaldehyde/2-hexanone, nonanaldehyde/2-nonanone and *o/m*-tolualdehyde could not be separated by LC–ESI-MS/MS

Table 3
Comparison of ESI-MS/MS and UV detection

Compounds	S_a concentration ($\mu g/m^3$) mean ± S.D., $n = 6$	S_b concentration ($\mu g/m^3$) mean ± S.D., $n = 6$	S_c concentration ($\mu g/m^3$) mean ± S.D., $n = 6$
Formaldehyde			
UV	6.37 ± 0.10	6.95 ± 0.06	7.13 ± 0.04
ESI-MS/MS	6.13 ± 0.10	6.32 ± 0.06	6.45 ± 0.38
Acetaldehyde			
UV	9.50 ± 0.20	8.50 ± 0.07	9.32 ± 0.05
ESI-MS/MS	8.97 ± 0.14	8.04 ± 0.16	8.89 ± 0.21
Acetone			
UV	8.14 ± 0.11	7.17 ± 0.05	7.73 ± 0.05
ESI-MS/MS	8.11 ± 0.13	7.92 ± 0.08	6.97 ± 0.18
Propionaldehyde			
UV	0.89 ± 0.05	0.94 ± 0.04	0.83 ± 0.01
ESI-MS/MS	0.97 ± 0.02	0.88 ± 0.01	0.89 ± 0.02
Heptaldehyde			
UV	0.32 ± 0.02	0.34 ± 0.03	0.31 ± 0.03
ESI-MS/MS	0.36 ± 0.01	0.41 ± 0.01	0.35 ± 0.03
Octylaldehyde			
UV	0.62 ± 0.03	0.78 ± 0.01	0.57 ± 0.02
ESI-MS/MS	0.58 ± 0.02	0.62 ± 0.03	0.55 ± 0.05
Decylaldehyde			
UV	0.62 ± 0.02	0.88 ± 0.06	0.46 ± 0.07
ESI-MS/MS	0.43 ± 0.01	0.73 ± 0.03	0.43 ± 0.04

S.D.: standard deviation.

method. Therefore, their sum concentrations were determined in this study. The concentrations of carbonyl compounds are listed in Table 2.

3.5. Compare to LC–UV method

The LC–ESI-MS/MS method was compared with the LC–UV detection at 360 nm method described in our previous work [8,9]. Three samples (S_a, S_b and S_c) in S2 were detected six times by the both methods, respectively. The results of seven carbonyls: formaldehyde, acetaldehyde, acetone, propionaldehyde, heptaldehyde, octylaldehyde and decylaldehyde, are listed in Table 3.

Table 3 shows that for low molecular weight (LMW) carbonyls, such as formaldehyde, acetaldehyde, acetone and propionaldehyde, good agreement existed between the two detection methods and the deviations between the two methods were 3.9–10%, 4.8–5.9%, 0.4–11% and 7–9%, respectively. But for HMW carbonyls (such as heptaldehyde, octylaldehyde and decylaldehyde), since most of their concentrations were below 0.6 $\mu g/m^3$, small difference maybe resulted in a large deviation. The deviations of heptaldehyde, octylaldehyde and decylaldehyde were in the range of 11–20%, 7–42%, and 7–44%, respectively. The R.S.D. of the studied seven carbonyls detected by LC–UV method were all <9.7% and <9.3% by ESI-MS/MS, and results were both acceptable.

The LOD of LC–ESI-MS/MS method was already described in method evaluation. The 32 carbonyls LOD of LC–ESI-MS/MS were in the range of 0.4–9.4 ng/m^3 and were much lower than those of UV detection [8], which were in the range

of 50–150 ng/m^3 for 21 carbonyls. Because of the lower LOD, the determination of low concentration carbonyls in air samples (mainly HMW carbonyls) was much more precise by LC–ESI-MS/MS than that by UV.

Compared with UV detection, more carbonyls were identified and quantified by LC–ESI-MS/MS method and study shows that if more carbonyls standards were applied, much more carbonyls also could be determined by the method. Moreover, other disadvantages of LC–UV detection, such as the HMW carbonyls (because of the low concentrations in air sample and the interference of the sample matrix) [5,11] and the co-eluting compounds (with different molecular weight, but same property), were also overcame by LC–ESI-MS/MS. This was mainly due to the lower LOD and the higher selectivity of LC–ESI-MS/MS.

4. Conclusions

This study demonstrated that DNPH derivatization and LC–ESI-MS/MS detection is an better analytical method for determination of HMW carbonyl compounds in air sample. Good Linearity, reproducibility and recovery are all obtained. Compared with LC–UV detection, the proposed method obtained much lower LOD and could detect more carbonyl compounds. The application of the method to air samples also achieved excellent result. Thirty-two carbonyl compounds were all identified and quantified in the samples of two sampling sites of Guangzhou. Among most of the samples, acetone was the most abundant carbonyls, followed by formaldehyde, acetaldehyde and butyraldehyde/2-butanone. Study shows that if more carbonyls standards were applied, much more carbonyls

also could be analyzed by the proposed method. Moreover, the identification of the unknown carbonyls in air samples will be an interesting direction.

Acknowledgements

References

[1] P. Carlier, H. Hannachi, G. Mouvier, Atmos. Environ. 20 (1986) 2079–2099.
[2] W.P.L. Carter, Atmos. Environ. 29 (1995) 2513–2527.
[3] D. Grosjean, E.L. Williams, E. Grosjean, Environ. Sci. Technol. 27 (1993) 110–121.
[4] P.B. Shepson, T.E. Kleindienst, E.O. Edney, C.M. Nero, Environ. Sci. Technol. 20 (1986) 1008–1013.
[5] E. Grosjean, D. Grosjean, M.P. Fraser, G.R. Cass, et al., Environ. Sci. Technol. 30 (1996) 2687–2703.
[6] K. Fung, D. Grosjean, Anal. Chem. 53 (1981) 168–171.
[7] K. Kuwata, M. Uerobi, H. Yamasaki, Y. Kuga, Anal. Chem. 55 (1983) 2013–2016.
[8] Y.L. Feng, S. Wen, X.M. Wang, G.Y. Sheng, Q.S. He, J.H. Tang, J.M. Fu, Atmos. Environ. 38 (2004) 103–112.
[9] Y.L. Feng, S. Wen, Y.J. Chen, X.M. Wang, H.X. Lü, X.H. Bi, G.Y. Sheng, J.M. Fu, Atmos. Environ. 39 (2005) 1789–1800.
[10] Gy. Kiss, B. Varga, Z. Varga Puchony, A. Gelencsér, Z. Krivácsy, J. Hlavay, Talanta 48 (1999) 755–762.
[11] W. Pötter, U. Karst, Anal. Chem. 68 (1996) 3354–3358.
[12] S.M. van Leeuwen, L. Hendriksen, U. Karst, J. Chromatogr. A 1058 (2004) 107–112.
[13] S. Kölliker, M. Oehme, Anal. Chem. 70 (1998) 1979–1985.
[14] S. Brombacher, M. Oehme, C. Dye, Anal. Bioanal. Chem. 372 (2002) 622–629.
[15] E. Grosjean, P.G. Green, D. Grosjean, Anal. Chem. 71 (1999) 1851–1861.
[16] A. Sakuragawa, T. Yoneno, K. Inoue, T. Okutani, J. Chromatogr. A 844 (1999) 403–408.
[17] V. Van den Bergh, I. Vanhees, et al., J. Chromatogr. A 896 (2000) 135–148.
[18] G. Zurek, H. Luftmann, U. Karst, Analyst 124 (1999) 1291–1295.
[19] V. Van den Bergh, H. Coeckelberghs, I. Vanhees, R. De Boer, F. Compernolle, C. Vinckier, Anal. Bioanal. Chem. 372 (2002) 630–638.
[20] T.I. Williams, M.A. Lovell, B.C. Lynn, Anal. Chem. 77 (2005) 3383–3389.
[21] S. Brombacher, M. Oehme, J.A. Beukes, J. Environ. Monit. 3 (2001) 311–316.
[22] G. Zurek, U. Karst, J. Chromatogr. A 864 (1999) 191–197.
[23] G. Zurek, A. Büldt, U. Karst, J. Fresenius, Anal. Chem. 366 (2000) 396–399.
[24] C. Kempter, G. Zurek, U. Karst, J. Environ. Monit. 1 (1999) 307–311.
[25] V. Van den Bergh, H. Coeckelberghs, H. Vankerckhovenm, F. Compernolle, C. Vinckier, Anal. Bioanal. Chem. 379 (2004) 484–494.
[26] S.D. Richardson, T.V. Caughran, T. Poiger, Y. Guo, F.G. Crumley, Ozone Sci. Eng. 22 (2000) 653–675.
[27] C. Zwiener, T. Glauner, F.H. Frimmel, Anal. Bioanal. Chem. 372 (2002) 615–621.
[28] P. Sritharathikhun, M. Oshima, S. Motomizu, Talanta 67 (2005) 1014–1022.
[29] C.A. Jakober, M.J. Charles, M.J. Kleeman, P.G. Green, Anal. Chem. 78 (2006) 5086–5093.
[30] E. Sánchez-Palomo, M.C. Díaz-Maroto, M.S. Pérez-Coello, Talanta 66 (2005) 1152–1157.
[31] J.F. Liu, J.F. Peng, Y.G. Chi, G.B. Jiang, Talanta 65 (2005) 705–709.
[32] C.F.H. Allen, J.H. Richmondm, J. Org. Chem. 2 (1937) 222–226.
[33] M. Behforouz, J.L. Bolan, M.S. Flynt, J. Org. Chem. 50 (1985) 1186–1189.
[34] R. Schulte-Ladbeck, R. Lindahl, J.O. Levin, U. Karst, J. Environ. Monit. 3 (2001) 306–310.
[35] J.O. Levin, K. Anderson, R. Lindahl, C.A. Nilsson, Anal. Chem. 57 (1985) 1032–1035.
[36] C.M. Druzik, D. Grosjean, A. Van Neste, S.S. Parmar, Int. J. Environ. Anal. Chem. 38 (1990) 495–512.
[37] A. Sirju, P.B. Shepson, Environ. Sci. Technol. 29 (1995) 384–392.

Short communication

A novel application of Onyx™ monolithic column for simultaneous determination of salicylic acid and triamcinolone acetonide by sequential injection chromatography

Petr Chocholouš, Pavel Holík, Dalibor Šatínský, Petr Solich *

*Department of Analytical Chemistry, Faculty of Pharmacy, Charles University,
Heyrovského 1203, Hradec Králové 500 05, Czech Republic*

Abstract

A novel and fast simultaneous determination of triamcinolone acetonide (TCA) and salicylic acid (SA) in topical pharmaceutical formulations by sequential injection chromatography (SIC) as an alternative to classical high performance liquid chromatography (HPLC) has been developed. A recently introduced Onyx™ monolithic C18 (50 mm × 4.6 mm, Phenomenex®) with 5 mm monolithic precolumn were used for the first time for creating sequential injection chromatography system based on a FIAlab® 3000 with a six-port selection valve and 5.0 mL syringe pump in study. The mobile phase used was acetonitrile/water (35:65, v/v), pH 3.3 adjusted with acetic acid at flow rate 0.9 mL min^{-1}. UV detection provided by fibre-optic DAD detector was set up at 240 nm. Propylparaben was chosen as suitable internal standard (IS). There is only simple pre-adjustment of the sample of topical solution (dilution with mobile phase) so the analysis is not uselessly elongated. Parameters of the method showed good linearity in wide range, correlation coefficient >0.999; system precision (relative standard deviation, R.S.D.) in the range 0.45–1.95% at three different concentration levels, detection limits (3σ) 1.00 µg mL^{-1} (salicylic acid), 0.66 µg mL^{-1} (triamcinolone acetonide) and 0.33 µg mL^{-1} (propylparaben) and recovery from the pharmaceutical preparations in the range 97.50–98.94%. The chromatographic resolution between peaks of compounds was more than 4.5 and analysis time was 5.1 min under the optimal conditions. The advantages of sequential injection chromatography against classical HPLC are discussed and showing that SIC can be a method of option in many cases.
© 2006 Elsevier B.V. All rights reserved.

Keywords: Sequential injection chromatography, SIC; ONYX™ monolithic column; Salicylic acid; Triamcinolone acetonide; Spectrophotometric determination

1. Introduction

Chromatographic columns are widely used in separation of mixtures in almost all branches of science. Sequential injection chromatography (SIC) based on integration of short monolithic column into flow manifold is a new generation of flow methods analysis and extending the possibilities of sequential injection analysis (SIA) technique enabling determination of simple multi-compound samples in one step without pretreatment of sample.

SIA—high versatile technique based on a programmable flow [1] has been proposed by Ruzicka and Marshall as an efficient tool for automated liquid handling [2]. The "single-line" technique is based on forward and reverse movement of a piston of syringe pump, which together with a multi-position selection valve enables precise sampling of liquid chemicals into the system and propelling of the sequenced zones to the reactors and detector [3]. Automation, speed of the analysis and low consumption of sample and reagents are the most important features that favour the SIA technique for application in many fields of analysis, primarily by more complicated operations such as sample pre-treatment, derivatisation reactions or monitoring of long lasting processes [4–6].

On the other side, SIA technique itself has generally one important drawback—it cannot primary provide the separation procedure and analysis of multi-component samples. This weak point was solved by coupling of short monolithic column [7] with SIA manifold and created method called sequential injection chromatography. It was recently successfully applied in the analysis of relatively simple multi-component samples [8–13].

---

* Corresponding author. Fax: +420 495 210 718.
  E-mail address: solich@faf.cuni.cz (P. Solich).

The use of monolithic columns (formed by "Sol–gel" technology from a single piece of porous silica gel) enabling operation at high flow rates with lower back-pressure [14]). This feature can be used for integrating these columns into a SIA manifold and for extending the possibilities of SIA technique (the back-pressure limit range of the syringe pump in SIA apparatus is about 2.5 MPa).

Salicylic acid (SA) is the traditional pharmaceutical substance. It has antiseptic and antifungal properties. It shows keratoplastic and keratolytic effect, which is often used in the topical preparations in combination with other substances, e.g. prednisolone, estradiol, betamethasone, triamcinolone, etc. It is also a product of decomposition of acetylsalicylic acid, which is a common antiinflammatory, analgesic and antipyretic drug used in topical preparations and tablets. Triamcinolone acetonide (TCA) is an antiflogistic and antiallergic drug used frequently in therapy of rheumatic, allergic and dermatologic symptoms.

There have been recently a number of reports in literature dealing with various analytical methods for the determination of SA [15–16] and TCA [17–19], mainly by HPLC methods, but there is no analytical method in literature for simultaneous determination of TCA in the presence of SA.

2. Experimental

2.1. Apparatus

2.1.1. Sequential Injection system and monolithic column

A commercially available instrument FIAlab® 3000 system (FIAlab® Instruments Inc., Bellevue, USA) with a syringe pump (syringe reservoir 5.0 mL) and a six-port selection Cheminert® valve (Valco Instrument Co., Houston, USA) was used. The manifold was equipped with fibre-optic UV–VIS diode array detector USB 2000 (Ocean Optics Inc., Dunedin, USA), 10 mm Z-flow cell (Avantes, Colorado, USA) and UV light source D-1000-CE (Analytical Instrument Systems Inc., Flemington, USA). The whole SIC system was controlled by the program FIAlab® for Windows 5.0. Flow lines were made of 0.75 mm I.D. PTFE tubing. Mobile phases and samples were aspirated through the six-port multi-position valve then delivered to the monolithic column and to the detector. Direct sample separation was performed on C-18 monolithic column Onyx^{TM} Monolithic C18 (50 mm × 4.6 mm) (Phenomenex®, USA) coupled with monolithic precolumn (5 mm × 4.6 mm) (Phenomenex®). The monolithic column with precolumn was placed between the multi-position valve and flow cell of the detector [9].

2.1.2. HPLC apparatus

Preliminary experiments concerning the composition of mobile phase for precise separation and comparative measurement of pharmaceutical product samples were performed on HPLC system Shimadzu Prominence 20 series with DAD detector. Analyses were performed on the same above-mentioned column. Mobile phases of different composition were tested at flow rate 0.9 mL min^{-1} and the detector was set on 240 nm.

2.2. Reagents

Salicylic acid was obtained from Herbacos-Bofarma Ltd. (Czech Republic, Ph.Eur.3 grade quality), triamcinolone acetonide was obtained from Sicor (Milan, Italy, Ph.Eur.3 grade quality), propylparaben was obtained from Zentiva, a.s. (Czech Republic, Ph.Eur.3 grade quality) and organic modifiers for mobile phase preparation were obtained from Sigma–Aldrich. Acetonitrile (Chromasolv, for LC) was obtained from Sigma–Aldrich. All other used chemicals were of analytical grade quality. Millipore Milli-Q RG (Millipore s.r.o., Czech Republic) ultra pure water was used for preparing the solutions. Mobile phases were degassed by helium before use. Stock standards were solved in acetonitrile 60% (v/v) at concentration of 20 mg mL^{-1} (SA), 2 mg mL^{-1} (TCA) and 4 mg mL^{-1} (PP)—all were stored at 5 °C for 1 month. The final concentrations of the sample working standard solutions or reference standards for pharmaceutical preparations analysis were prepared by diluting the stock solution in the mobile phase.

2.3. Method and sample preparation

2.3.1. Mobile phase

The optimal mobile phase for separation of SA, TCA and internal standard (IS) propylparaben (PP) was acetonitrile–water (35:65, v/v), pH 3.3 adjusted with acetic acid; flow rate 0.9 mL min^{-1} at ambient temperature. Volume of mobile phase used for one analysis was 4.0 mL.

2.3.2. Solutions and sample preparation

The tested pharmaceutical preparation was Triamcinolon-IVAX (IVAX, Czech Republic) containing 20 mg of SA and 2 mg of TCA in 1.0 mL of topical solution. Sample adjustment was done by the following procedure: 100.0 μL of Triamcinolon-IVAX solution was transferred to 10.00 mL calibrated flask; then 100.0 μL stock solution of internal standard propylparaben was added and the flask was filled to the mark with mobile phase and mixed. The sample was homogenized and dissolved by 5 min sonication. The comparative standard solution was same for all the analysis and it was prepared diluting stock standard solution in 10.00 mL calibrated flask and the flask was filled to the mark with mobile phase and mixed. The final concentrations of the analytes in comparative standard solution were 200.0 μg mL^{-1} of SA, 20.0 μg mL^{-1} of TCA and 40.0 μg mL^{-1} of PP. Standards and samples were measured in triplicates and the mean peak height values were used for data acquisition.

3. Results and discussion

3.1. Method development and optimization

Applications of SIC has already been introduced in our previous papers [7–13]. In this work for the first time has been used Onyx^{TM} (Phenomenex®) column instead of Chromolith^{TM} (Merck®) column in the SIC method. The optimization of mobile phase was started with Onyx^{TM} Monolithic C18

Table 1
Characterization of SIC process

	Salicylic acid		Triamcinolone acetonide		Propylparaben	
	SIC	HPLC	SIC	HPLC	SIC	HPLC
Retention time (min)	1.46	1.65	2.64	2.63	3.45	3.59
Peak symmetry	1.95	2.03	1.65	1.23	1.64	1.19
Number of theoretical plates	1475	812	2188	2620	3135	3085
Peak resolution	$R_{SA/TCA} = 6.03$	$R_{SA/TCA} = 4.51$	$R_{TCA/PP} = 4.52$	$R_{TCA/PP} = 4.06$		

(50 mm × 4.6 mm, Phenomenex®) with 5 mm monolithic pre-column and acetonitrile/water (50:50, v/v) mobile phase. The mobile phases containing acetonitrile as organic part have shown better separation of peaks and peak symmetry than methanol containing mobile phases. The optimization was focused to make a proposal appropriate ratio of acetonitrile/water composition and optimal pH of mobile phase to achieve a sufficient symmetry of the peaks together with a good separation of compounds and a short retention time. The optimal mobile phase for the separation of SA, TCA and internal standard was found acetonitrile/water (35:65, v/v), pH adjusted to 3.3 by means acetic acid. Flow rate was set to 0.9 mL min^{-1}. Propylparaben fulfills the requirements so was chosen as a suitable internal standard. The sample injection volume was 10.0 μL. Due to very different quantity of SA and TCA in pharmaceutical formulation (sample of pharmaceutical solution contains ten time more SA than TCA) only one wavelength (240 nm, absorption maximum of TCA in mobile phase) was used to ensure high absorption response of TCA and lower response of SA (not exceed range of detector). The proposed system enabled successful separation of target analytes in the time 5.1 min (0.66 min for aspiration of mobile phase, 0.0016 min for aspiration of sample and 4.43 min for elution of sample) and total volume of mobile phase for one analysis was 4.0 mL. Peak height evaluation was performed using the FIAlab® software.

3.2. Parameters of sequential injection chromatography process

The target compounds were successfully separated using the proposed procedure. Basic chromatographic parameters were calculated from experimental data, such as retention times, peak symmetry, number of theoretical plates and peak resolution; they are given in Table 1 in comparison to HPLC results.

3.3. Validation and analytical parameters of the method

The validation and analytical parameters (linearity, sensitivity, repeatability, recovery, selectivity, precision and accuracy) have shown good results. Linearity was established with a series of working solutions prepared by diluting the stock solution with mobile phase to the final concentrations. Each concentration was injected in triplicate and the mean value of peak height was used for the calibration curve. The calibration graphs involved seven experimental points for SA (concentration range 3.1, 6.3, 12.5, 25.0, 50.0, 100.0 and 300.0 μg mL^{-1}) and it is described by the following equation: $A = (0.0035 \pm 0.00001)c + (0.0018 \pm 0.0011)$ (where A is the absorbance and c the analyte concentration), the correlation coefficient was 0.9999; for TCA and PP nine experimental points (concentration range 6.2, 12.3, 18.5, 27.7, 41.6, 83.0, 125.0, 166.0 and 250.0 μg mL^{-1}) and they are described by following equations: TCA $A = (0.0034 \pm 0.00003)c - (0.0096 \pm 0.0031)$, the correlation coefficient was 0.9998; and for internal standard PP: $A = (0.0029 \pm 0.00002)c - (0.0062 \pm 0.0027)$, the correlation coefficient was 0.9998. The limit of detection (LOD) was calculated by comparison of the three-fold variation of signal to noise ratio (3 S/N) obtained from analysis of the standards, and the limit of quantification (LOQ) was defined as the lowest measured quantity above which the analyte can be quantified at a given statistical level of (3 LOQ). The system precision

Table 2
Analytical parameters and method validation results

	Salicylic acid	Triamcinolone acetonide	Propylparaben
Calibration range (μg mL^{-1})	3.1–300.0	6.2–250.0	6.2–250.0
Correlation coefficient	0.9999	0.9998	0.9998
Limit of detection 3σ (μg mL^{-1})	1.00	0.66	0.33
Limit of quantification (μg mL^{-1})	3.00	2.00	1.00
System precision–concentration 200 μg mL^{-1} (%)[a]	0.64	0.47	0.44
System precision–concentration 100 μg mL^{-1} (%)[a]	0.91	0.96	0.50
System precision–concentration 10 μg mL^{-1} (%)[a]	1.28	1.49	1.95
Repeatability of T_R (%)[a]	0.46	0.42	0.47
Method precision (%)[b]	1.73	3.43	
Accuracy–spike recovery (%)[c]	98.9	97.5	

[a] Relative standard deviation (R.S.D.) values were calculated for repeated standard injections ($n = 8$).
[b] R.S.D. for repeated injections of multiple sample preparations ($n = 6$).
[c] Spiked sample solutions.

of the method was determined by preparing the standards of SA, TCA and PP at three concentration levels (200.0, 100.0 and $10.0\,\mu g\,mL^{-1}$ of all standards) and peak heights for each compound were determined after processing each standard eight times. The method validation results obtained under the final conditions are shown in Table 2. The method was found to fulfill common requirements of accuracy, precision and linearity (calibration range with correlation coefficient >0.999, R.S.D. for repeated standard injections at three concentration levels ($n = 8$) was less than 1.6%). To validate the precision of the method a number of six different pharmaceutical sample solutions were used, which were prepared from the same batch and analyzed consecutively. This approach provides a means of covering the precision of the entire method, from sample preparation to data handling. The precision of the method calculated as R.S.D. of six sample determination, including sample preparation, was 1.73% for SA and 3.43% for TCA. The mean values of found amount were 99.41% of SA and 97.29% of TCA. The accuracy of the method was carried out measuring of the pharmaceutical samples fortified with known quantity of the analytes (addition of 20% amount of SA standard and 100% amount of the TCA and PP standards to pharmaceutical preparation). Spiked sample solutions and un-spiked sample solutions were compared for recovery evaluation. The method accuracy results—mean values of the recoveries were found as 98.9% for SA and 97.5% for TCA. Assay values of recoveries show that the method allows direct determination of SA and TCA in commercial dosage forms in the presence of other adjuvants (analysis of blank solution of matrix showed no interferences in measurement, depicted in Fig. 1).

3.4. Determination in pharmaceutical product

The novel method developed has been applied to the determination of SA and TCA in topical solution Triamcinolon-IVAX. The pharmaceutical was commercially available on the Czech market. The interference effect of adjuvants (EDTA and carbethopendecinii bromidum) was not observed. The samples were prepared just by dilution hundred times with mobile phase containing IS. For analysis, a loop of three loads of comparative standard solution was programmed and three loads
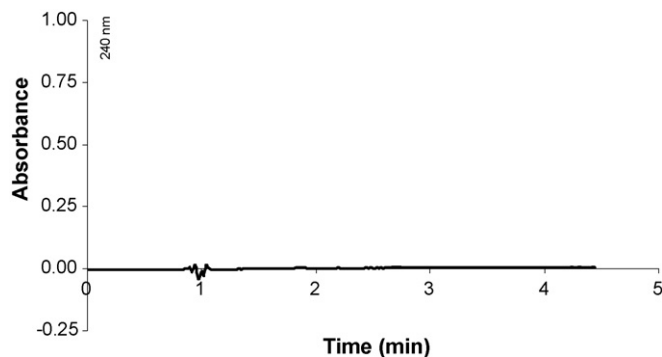

Fig. 1. SI chromatogram of blank solution of matrix of Triamcinolon-IVAX. Mobile phase: acetonitrile/water (35:65, v/v), pH 3.3 adjusted with acetic acid, flow rate $0.9\,mL\,min^{-1}$ at ambient temperature, UV detection at 240 nm.
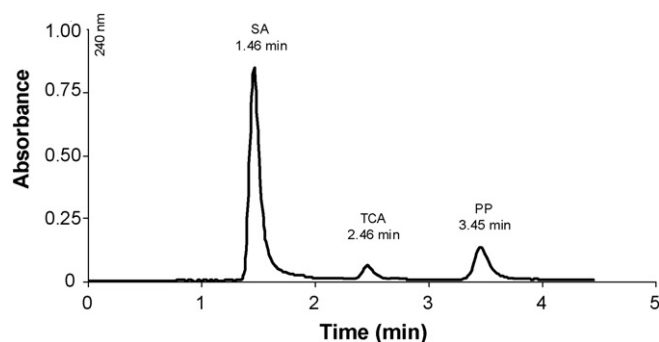
Fig. 2. SI chromatogram of the separation of active substances of Triamcinolon-IVAX topical solution. Mobile phase: acetonitrile/water (35:65, v/v), pH 3.3 adjusted with acetic acid, flow rate $0.9\,mL\,min^{-1}$ at ambient temperature, UV detection at 240 nm.
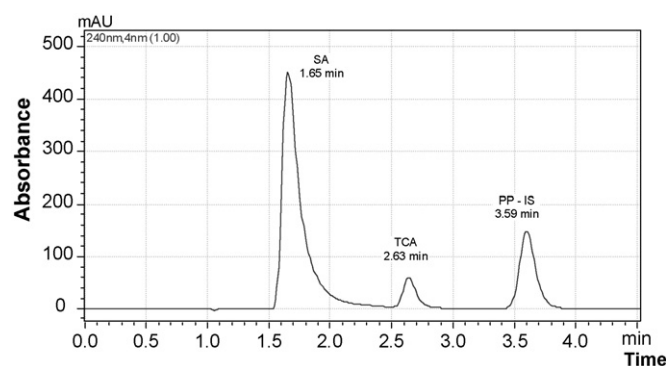
Fig. 3. HPLC chromatogram of the separation of active substances of Triamcinolon-IVAX topical solution. Mobile phase: acetonitrile/water (35:65, v/v), pH 3.3 adjusted with acetic acid, flow rate $0.9\,mL\,min^{-1}$ at ambient temperature, UV detection at 240 nm.

of sample solution. The results of determination of six samples (different batch) were in range (99.32–101.43%; R.S.D. 1.83) for SA and (100.32–107.50%; R.S.D. 2.55) for TCA of declared value. The procedure of sample preparation was simple, fast and achieving high precision and low sample and reagent consumption. Representative sequential injection chromatogram showing successful separation of active substances of Triamcinolon-IVAX including internal standard is shown in Fig. 2.

After the SIC determination was done comparative HPLC measurement of mentioned six samples of Triamcinolon-IVAX solution with comparable results (SA 99.61–102.77%; R.S.D. 1.20% and TCA 100.64–104.18%; R.S.D. 1.32%) at the same conditions. Representative HPLC chromatogram showing successful separation of active substances of Triamcinolon-IVAX including internal standard is shown in Fig. 3.

4. Conclusion

Recently it has been shown that the novel SIC system as the solution-handling and automation system enables fast determination of simple mixtures and gives additional possibilities in chromatographic measurements compared with the conventional HPLC. An Onyx^{TM} Monolithic C18 (50 mm × 4.6 mm,

Phenomenex[®]) column with 5 mm monolithic precolumn incorporated first time into SIC manifold was proved to be a convenient and efficient tool for the separation and determination of salicylic acid and triamcinolone acetonide in pharmaceutical preparation (topical solution). Even in case of diametrical difference of amount of both compounds (proved solution contains ten times more SA than TCA) the analysis was achieved simultaneously only with simple pre-treatment of sample (dilution with mobile phase). Results of many chromatographic parameters for determination SA and TCA in pharmaceutical solution were compared to HPLC measurements. SIC technique shows several advantages as short time of analysis, easy handling with sample and low consumption of sample and solvents and low production of the waste (due to discontinual flow). These features enable reduction of cost per analysis. Easy liquid manipulation not attainable by classical HPLC set up, dimensions of the SIC system and portability of analyzer provides the opportunity for analysis "on field".

On the other hand, SIC is limited by column (at present only short monolithic reverse phased) and limited amount of mobile phase available for one analysis due to the use of 5.0 mL syringe pump. Commercial program for data processing can only height of peaks evaluate. Recent development results in commercially available SIChrom[TM] liquid chromatography analyzer by FIAlab[®] Instruments [20] that can solve several weak points of the present SIC system—equipped with more powerful pump (enables use of higher flow rates and longer columns) and chemical resistant Lab-On-Valve system for variable sample handling.

In summary, the SIC system renders a useful alternative to existing chromatographic methods and can be an important tool for the rapid separation and quantification of several compounds not only in pharmaceutical analysis.

Acknowledgement

References

[1] C.E. Lenehan, N.W. Barnett, S.W. Lewis, Analyst 127 (2002) 997.
[2] J. Ruzicka, G. Marshall, Anal. Chim. Acta 237 (1990) 329.
[3] T. Gübeli, G.D. Christian, J. Ruzicka, Anal. Chem. 63 (1991) 2407.
[4] R.W. Min, J. Nielsen, J. Villadsen, Anal. Chim. Acta 312 (1995) 149.
[5] X.Z. Liu, S.S. Liu, J.F. Wu, Z.L. Fang, Anal. Chim. Acta 392 (1999) 273.
[6] P. Solich, H. Sklenářová, J. Huclová, D. Šatínský, U.F. Schaefer, Anal. Chim. Acta 499 (2003) 9.
[7] D. Šatínský, P. Solich, P. Chocholouš, R. Karlíček, Anal. Chim. Acta 499 (2003) 205.
[8] D. Šatínský, J. Huclová, P. Solich, R. Karlíček, J. Chromatogr. A 1015 (2003) 239.
[9] P. Chocholouš, D. Šatínský, P. Solich, Talanta 70 (2006) 408.
[10] J. Huclová, D. Šatínský, R. Karlíček, Anal. Chim. Acta 494 (2003) 133.
[11] D. Šatínský, L. Santos, H. Sklenářová, P. Solich, M.C. Montenegro, A. Araújo, Talanta 68 (2005) 214.
[12] D. Šatínský, J. Huclová, R.L.C. Ferreira, M.C. Montenegro, P. Solich, J. Pharm. Biomed. Anal. 40 (2006) 293.
[13] J. Klimundová, D. Šatínský, H. Sklenářová, P. Solich, Talanta 69 (2006) 730.
[14] H. Minakuchi, K. Nakanishi, N. Soga, N. Ishizuka, N. Tanaka, J. Chromatogr. A 762 (1997) 135.
[15] S. Croubels, A. Maes, K. Baert, P. De Backer, Anal. Chim. Acta 529 (2005) 179.
[16] R. Pirker, C.W. Huck, M. Popp, G.K. Bonn, J. Chromatogr. B 809 (2004) 257.
[17] A.M. Di-Pietra, V. Andrisano, R. Gotti, V. Cavrini, J. Pharm. Biomed. Anal. 14 (1996) 1191.
[18] P.R. Rege, V.D. Vilivalam, C.C. Collins, J. Pharm. Biomed. Anal. 17 (1998) 1225.
[19] Y.M. Xu, G.Y. Wong, J. Liq. Chromatogr. Related Technol. 22 (1999) 2071.
[20] http://www.sichrom.com/.

Electrochemical behavior of dopamine at a 3,3′-dithiodipropionic acid self-assembled monolayers

Lucia Codognoto[a], Eduardo Winter[a], Jonas A.R. Paschoal[a], Hugo B. Suffredini[b],
Murilo F. Cabral[c], Sergio A.S. Machado[c], Susanne Rath[a,*]

[a] Institute of Chemistry, Department of Analytical Chemistry, State University of Campinas, P.O. Box 6154, 13084-971 Campinas, SP, Brazil
[b] Federal University of ABC, Rua Santa Adélia, 166, 09.210-170 Santo André, SP, Brazil
[c] Institute of Chemistry of São Carlos, USP, Av. Trabalhador Sãocarlense 400, 13566-590 São Carlos, SP, Brazil

Abstract

Monolayers of 3,3′-dithiodipropionic acid (DTDPA) were prepared on a polycrystalline gold electrode through a self-assembly procedure to produce a gold 3,3′-dithiodipropionic acid self-assembled monolayer (AuDTDPA) modified electrode. The characterization of the AuDTDPA electrode was investigated by cyclic voltammetry and *ac* impedance using the $[Fe(CN)_6]^{3-/4-}$ redox couple. The electrochemical behavior of DA on the modified electrode AuDTDPA was studied by cyclic and square-wave voltammetries, using phosphate buffer as supporting electrolyte. The oxidation peak current for DA increases linearly with concentration in the range of 0.35×10^{-5} to 3.4×10^{-5} mol L^{-1}. The performance of the AuDTDPA modified electrode was evaluated for the electroanalytical determination of dopamine (DA) in a pharmaceutical formulation. The AuDTDPA modified electrode showed a stable behavior and the presence of surface-COOH groups avoided the passivation of the electrode surface during the dopamine oxidation.
© 2006 Elsevier B.V. All rights reserved.

Keywords: Self-assembled monolayers; 3,3′-Dithiodipropionic acid; Dopamine; Square-wave voltammetry; Gold electrode

1. Introduction

Dopamine (DA) is the most important and most studied neurotransmitter and is often used as a model compound to evaluate novel electrochemical sensors and methodologies [1]. Nevertheless, the electrochemical determination of phenolic compounds presents some problems due to the loss of electrode activity of some solid state electrodes during the oxidation process [2–4]. The electrochemical oxidation of DA in aqueous solutions occurs as a two-electron process forming, initially, *o*-dopaminoquinone. In a second step, this molecule may be converted to leucodopaminochrome. This species undergoes further oxidation (two electrons) to form dopaminochrome. However, polymerization of the oxidation product of DA leads to polymer deposition on the electrode surface, thus promoting a gradual loss of activity (electrode poisoning or fouling) [5–7].

A previous work verified that by adding carboxylic compounds to the supporting electrolyte, the polymerization process due to the oxidation of phenolic compounds at the solid state electrode is inhibited and, as a consequence, electrode passivation is avoided [8]. In addition, it was verified that on a Hg electrode at potentials more positive than 250 mV DA and Hg are oxidized yielding, in the presence of citrate, dopaminoquinone (DQ) and Hg(II). The Hg(II) reacts with the DA forming DQ, leucodopaminochrome (LDC) and dopaminochrome (DC). DQ undergoes further reduction at 200 mV. Citrate, in the form of Cit^{3-}, stabilizes the DC formed and this new electroactive compound undergoes further reduction at −250 mV [9]. The LDC is stabilized by the citrate ions (Cit^{3-}) in solution, where the interaction occurs, probably, between the three carboxylic groups of the citrate and the hydrogens from the hydroxyls of the catechol group [10]. These results attracted our attention and initiated an investigation of the electrochemical behavior of DA when a carboxylic acid is immobilized on the solid electrode surface.

Carboxylic acid terminated thiols can be easily immobilized on gold electrodes using self-assembled monolayers (SAM)
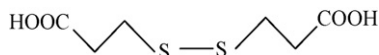

Fig. 1. Molecular structure of DTDPA.

[11]. The self-assembly procedure is the precise modification of the surface structure on a nanometer-scale [12] and has been employed recently in many applications, such as sensors [13–17] and biosensors [18,19]. The stable, well-organized and compact self-assembled monolayers (SAM) formed by thiols on gold electrodes offer advantages such as selectivity, sensitivity, short response time and small overpotential in electrocatalytic reactions. Self-assembly using ω-mercaptocarboxylic acid monolayers to separate the oxidation potentials of ascorbic acid (AA) and DA was employed for the first time by Malem and Mandler [20]. Li and coworkers used various SAM for studying DA [21]. Osaka and coworkers reported electroanalysis of DA using charged monolayers and gold nanoparticles [22] and focused on the determination of DA in the presence of AA. It has been shown that by changing the charge state of the electrodes the electrochemical properties of the surface, such as inhibition from fouling effects of the redox active molecules, can be controlled.

This paper describes the development of a COOH-terminated SAM electrode formed by 3,3′-dithiodipropionic acid (Fig. 1) on a gold electrode surface to evaluate the influence of carboxyl group on the DA electrochemical response. Moreover, the electrochemical characteristics of the new modified gold electrode were evaluated using cyclic voltammetry and electrochemical impedance spectroscopy. A square-wave voltammetric method was developed and validated for DA determination in pharmaceuticals.

2. Experimental

2.1. Chemicals and solutions

Analytical grade disodium hydrogenphosphate, sodium hydroxide, phosphoric acid, sodium ethylenediaminetetraacetate, sulfuric acid and phosphoric acid were purchased from Merck (Brazil). Methanol and ethanol, HPLC-grade solvents, were purchased from Tedia (USA) and Mallinckrodt (USA), respectively.

The 99% 3,3′-dithiodipropionic acid and 99% dopamine were from Sigma–Aldrich, USA. Standard solutions of 1.0×10^{-2} mol L^{-1} DTDPA were prepared in ethanol (HPLC-grade) those for 1.0×10^{-2} mol L^{-1} DA were prepared in water.

The supporting electrolyte was 0.10 mol L^{-1} phosphate buffer. The pH of the solutions was adjusted with 0.1 mol L^{-1} H_3PO_4 or 0.1 mol L^{-1} NaOH. Working standard solutions of 1.0×10^{-3} mol L^{-1} $K_3Fe(CN)_6$ (Sigma–Aldrich, USA) and 1.0×10^{-3} mol L^{-1} $K_4Fe(CN)_6$ (Sigma–Aldrich, USA) were prepared in 0.5 mol L^{-1} sulfuric acid.

Throughout the study, water was obtained from a Milli-Q system from Millipore (USA).

Three commercial samples of dopamine hydrochloride injections from different batches were used in the analyses of real samples.

2.2. Instrumentation

The electrochemical measurements were carried out on a computer controlled potentiostat Autolab® PGSTAT30, with GPES and FRA software (Eco Chemie B.V.; The Netherlands). A three-electrode system, with a bare gold electrode (diameter 1 mm, sealed in a Teflon tube) or a 3,3′-dithiodipropionic acid self-assembled monolayer modified electrode as the working electrode, a Ag/AgCl, 3.0 mol L^{-1} KCl, as the reference electrode and a platinum wire as the auxiliary electrode were used in all measurements.

Measurements of pH were made with a DM-20 pH-meter from Digimed (Brazil), using a combined glass electrode.

The HPLC-experiments were performed using a binary solvent gradient chromatographic system from Waters (USA), model 1525, coupled to a Waters PDA 2996 detector and a Rheodyne injector 7725 (sample loop of 20 µL). Data acquisitions were performed by the Millenium³² 4.0 software. The chromatographic column was an octadecyl Microsorb-MV column (250 mm × 4.6 mm, 5 µm particle size, Varian).

2.3. Preparation of self-assembled monolayer modified electrode

The bare gold electrode was polished with 0.05 µm Al_2O_3 slurry on micro-cloth pads before modification. Then it was rinsed with water and sonicated in absolute ethanol and water for 10 min, respectively. After rinsing with water, the electrode was pretreated by heating in a Piranha solution containing concentrated sulfuric acid/30% hydrogen peroxide, 5:1 (v/v) for 15 min in order to remove possible contaminants. Finally, the electrode was activated by cyclic sweepings from 0 to 1.55 V in 0.5 mol L^{-1} sulfuric acid until a constant background cyclic voltammogram was obtained [23,24].

The freshly pretreated electrode was immersed in 1.0×10^{-2} mol L^{-1} ethanolic DTDPA solution for 24 h. Before use, the electrode was rinsed with water to remove the physically adsorbed species.

The self-assembled monolayer modified electrode was characterized using cyclic voltammety and electrochemical impedance spectroscopy.

2.4. Dopamine determination in samples

Dopamine hydrochloride injection samples were diluted 10 and 25 times with water before SWV and HPLC analyses, respectively. All analyses were performed in triplicate.

2.4.1. Square-wave voltammetry

A volume of 200 µL of the previously diluted sample was transferred to the voltammetric cell containing 20 mL of the supporting electrolyte (0.10 mol L^{-1} phosphate buffer, pH 7.0). After dearation, DA was determined by SWV through the standard addition method, using the AuDTDPA working electrode. The voltammetric parameters comprise: frequency (f): 100 s^{-1}, the pulse amplitude (a): 100 mV and the scan increment (ΔE_s): 2 mV. The current–potential curves were registered in the

potential interval of 0–0.6 V and quantitation was performed at 0.25 V.

2.4.2. High performance liquid chromatography

DA was determined by an external calibration. The calibration graph was obtained at five levels, in triplicate, in the concentration range of 1×10^{-4} to 1×10^{-3} mol L^{-1} DA.

The mobile phase used, at a flow rate of 1 mL min^{-1}, was 0.050 mol L^{-1} phosphate buffer, pH 4.5 + 20 mg L^{-1} EDTA/methanol (85/15, v/v). Quantitation was performed at a retention time of 4.5 min at 280 nm.

3. Results and discussion

3.1. Electrochemical characterization of the SAM

3.1.1. Cyclic voltammetry

The electron transfer kinetics of a redox couple in solution on the SAM modified electrode depends on the compactness and thickness of the monolayer. The characterization of the AuDT-DPA self-assembled monolayer modified gold electrode was conducted using the hydrophilic redox probe [Fe(CN)$_6$]$^{3-/4-}$. Fig. 2 shows the cyclic voltammetric responses for a bare gold electrode and for the AuDTDPA modified electrode in 1.0×10^{-3} mol L^{-1} [Fe(CN)$_6$]$^{3-/4-}$ + 0.5 mol L^{-1} H$_2$SO$_4$. The $E^{0'}$ of the redox pair [Fe(CN)$_6$]$^{3-/4-}$ on the bare gold (curve a) and the AuDTDPA modified electrodes (curve b) are 450 and 480 mV, respectively. The formal potential shifts towards positive potentials, as well as the decrease in peak currents, indicate the modifications induced by SAM deposition on the gold surface [25].

In order to evaluate the effect of the proton concentration on the electron transfer rate of [Fe(CN)$_6$]$^{3-/4-}$ on the AuDT-DPA modified electrode, cyclic voltammograms were scanned in 0.10 mol L^{-1} KNO$_3$ at pH 2.0, 4.0 and 9.0 (Fig. 3). It was verified that when the pH was increased from 2.0 to 4.0, the ΔE_p value increased from 95 to 395 mV and the peak current decreased. In alkaline solution, pH 9.0, no changes in the voltam-
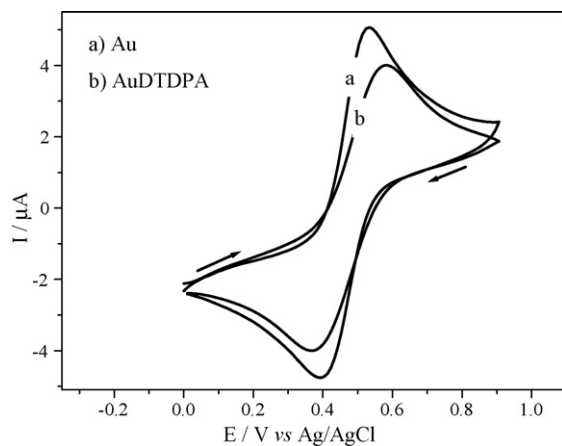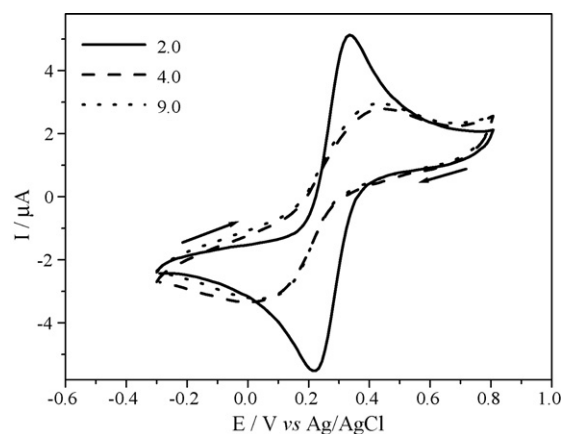

Fig. 3. Cyclic voltammograms of 1.0×10^{-3} mol L^{-1} [Fe(CN)$_6$]$^{3-/4-}$ in 0.1 mol L^{-1} KNO$_3$ solution at different pH values with the AuDTDPA modified electrode. Scan rate: 100 mV s^{-1}.

mogram in relation to that obtained in pH 4.0 was observed. At pH 2.0 a reversible voltammetric response ($\Delta E_p = 95$ mV and $I_{pa}/I_{pc} = 0.95$) was observed. This behavior could be explained due to the fact that in acidic medium (pH 2.0) the carboxyl groups of DTDPA, which present a pK_a value of 3.9 [11], are protonated and, therefore, no electrostatic repulsion between the molecules of the monolayer and the negatively charged [Fe(CN)$_6$]$^{3-/4-}$ occurs. At higher pH values (pH > 4) the terminal groups of the monolayer are deprotoned and become negatively charged and a repulsive force between the SAM modified electrode surface and the electroactive anion in solution is established. The increase in ΔE_p indicates that the electron rate transfer becomes slower.

3.1.2. Electrochemical impedance spectroscopy

In order to get more information about the surface, electrochemical impedance spectroscopy was employed. The *ac* impedance method is based upon a measurement of the response of the electrochemical cell to a small amplitude alternating potential. The procedure is performed over a range of frequencies. The response is established through the complex-impedance plot and the result can be interpreted in terms of an equivalent electrical circuit. If the surface changes, the impedance signal will modify and the differences in the signal before and after modification of the electrode with the SAM can be used to understood the electrode/solution behavior. Using a simplified circuit that represents an electrochemical cell (Randles equivalent circuit) [26], the electrode coverage can be estimate by the charge-transfer resistances.

The impedance plots of Fig. 4 are characterized by two distinct regions: (1) a semicircle in high frequencies, related to charge-transfer process, which was electrically described by a resistance in parallel with a capacitor related to the charge transfer and electrode/SAM double-layer, respectively; (2) a 45° line in the complex-impedance plot defining a region of semi-infinite diffusion of species in the modified electrode. Our attention is focused on the more interesting part of the spectrum, at a high frequency, where the electrode reaction is controlled purely kinetically, and the heterogeneous charge-transfer resistance is

Fig. 2. Cyclic voltammograms for 1.0×10^{-3} mol L^{-1} [Fe(CN)$_6$]$^{3-/4-}$ in 0.5 mol L^{-1} H$_2$SO$_4$, scan rate 100 mV s^{-1} at (a) bare gold electrode and (b) AuDTDPA modified electrode.
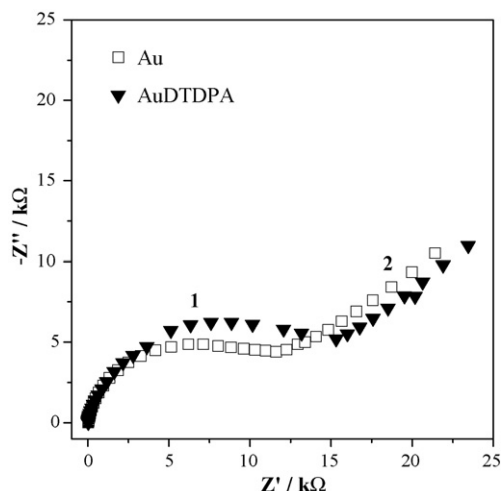
Fig. 4. *ac* impedance plots in 1.0×10^{-3} mol L^{-1} [Fe(CN)$_6$]$^{3-/4-}$ + H$_2$SO$_4$ 0.5 mol L^{-1} with a frequency of 0.1–40 kHz for AuDTDPA modified electrode (▼) and bare gold electrode (□). Potential 0.45 vs. Ag/AgCl, 3.0 mol L^{-1} KCl.

expected to increase due to inhibition of electron transfer by the monolayer on the electrode surface [27]. The electrode coverage (θ) is a key factor, which can be used to estimate the surface state of the electrode, and the charge-transfer resistance is also related to it. Assuming that all the current is passed by pinholes on the electrode, the electrode coverage can be calculated as

$$1 - \theta = \frac{R_{ct}^0}{R_{ct}} \tag{1}$$

where R_{ct}^0 is the charge-transfer resistance using bare gold and R_{ct} is the charge-transfer resistance with the monolayer-covered electrode under the same conditions.

Fig. 4 shows the complex-impedance plot of the gold bare electrode and the Au/DTDPA modified electrode for 1.0×10^{-3} mol L^{-1} [Fe(CN)$_6$]$^{3-/4-}$ in 0.5 mol L^{-1} sulfuric acid. The charge-transfer resistance for the gold bare electrode and for the AuDTDPA modified electrode, established through the impedance plot, is 9.2 and 16.5 kΩ, respectively. Using these values and Eq. (1), the electrode coverage value was estimated to be 45%. The incomplete coverage of the electrode surface could be related to steric effects of the terminal carboxyl groups of the DTDPA molecules.

3.2. Electrochemical behavior of dopamine on AuDTDPA modified electrode

3.2.1. Cyclic voltammetry

Fig. 5 shows the cyclic voltammograms of 1.0×10^{-3} mol L^{-1} DA on a bare gold electrode (curve a) and on a AuDT-DPA modified electrode (curve b). It is verified that the presence of the SAM at the electrode surface reduces the overpotential of DA oxidation, shifting the $E^{0'}$ value by −48 mV. The peak current was enhanced about two-fold. The ratio of anodic to cathodic peak currents remains unchanged and close to 1. The ΔE_p of DA was 140 and 66 mV for the bare gold electrode and the AuDTDPA modified electrode, respectively.
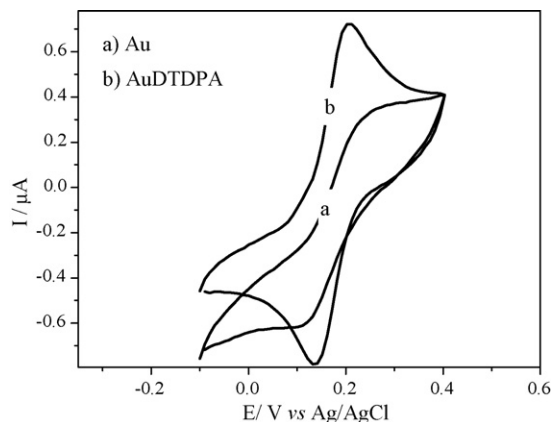
Fig. 5. Cyclic voltammograms of 1.0×10^{-3} mol L^{-1} dopamine in 0.1 mol L^{-1} phosphate buffer at pH 7.0. (a) On the bare gold electrode and (b) on the AuDTDPA modified electrode. Scan rate: 100 mV s^{-1}.

At pH 7.0 the monolayer of the AuDTDPA modified electrode is negatively charged and the DA, due to the presence of the amino group (p$K_a = 8.9$), positively charged. The electrostatic interaction facilitates the oxidation of DA. The current enhancement due to an increase in the electron transfer rate could be attributed to a catalytic process [28,29].

The effect of pH on E_p and I_p was evaluated for 1.0×10^{-3} mol L^{-1} DA using the AuDTDPA electrode in a 0.10 mol L^{-1} phosphate buffer medium varying the pH in the range of 2.0–8.0. The peak potential shifts negatively with the increase of pH (Fig. 6). The relationship between peak potential and pH results in the following linear regression equation: $E^0 = 0.619 - 0.064$ pH. This result shows that the overall process is proton-dependent and that the electron transfer is accompanied by the transfer of an equal number of protons, i.e., for the oxidation of DA two electrons and two protons are involved.

The anodic peak current increases between pH 4.0 and 8.0 (Fig. 6). The change of the anodic peak current of DA with the pH can be explained in terms of the electrostatic attraction between DTDPA and DA. At lower pH, the surface-COOH groups are fully protonated. When the pH gradually increases, the surface of the AuDTDPA electrode becomes negatively charged (pH > 4.0)

Fig. 6. Influence of the pH on peak potential (■) and peak current (●) for cyclic voltammetry on the AuDTDPA modified electrode (1.0×10^{-3} mol L^{-1} DA in 0.1 mol L^{-1} phosphate buffer, with scan rate of 100 mV s^{-1}).

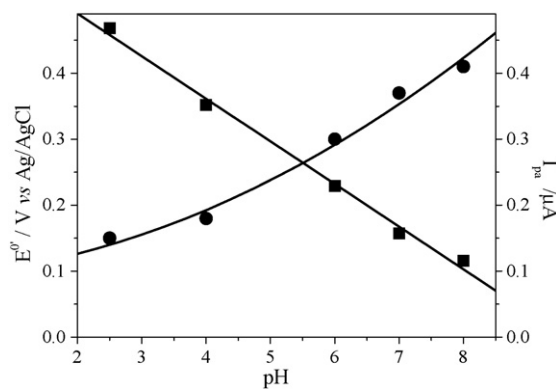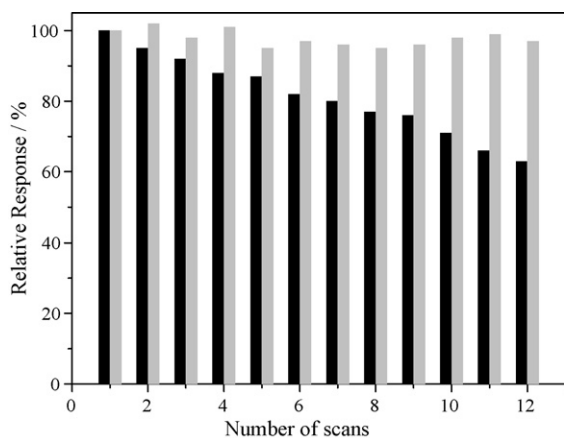Fig. 7. Relative responses of the anodic peak current for DA oxidation during successive cyclic voltammetric scans recorded with a bare gold electrode (■) and with a AuDTDPA modified electrode (□) to 1.0×10^{-3} mol L^{-1} dopamine in 0.1 mol L^{-1} phosphate buffer, pH 7.0. Scan rate: 100 mV s^{-1}.

due to the dissociation of protons of the surface-COOH groups. At pH < 8.5, the NH$_2$ group in the DA molecule is positively charged and the hydroxyls of catechol are already protonated. The same phenomenon was observed when the carboxylate was in solution. The interaction of DA in the presence of citrate was previously reported [10].

3.2.2. Passivation and stability

The electrochemical oxidation of DA leads to deposition of polymeric films on the surfaces of solid electrodes, decreasing electrode activity. However, the literature shows that the addition of carboxylic compounds to the medium produces a significant enhancement in the electrochemical behavior of phenolic compounds, avoiding electrode passivation [8].

The relative responses of the anodic peak current for DA oxidation during successive cyclic voltammetric scans with the bare gold and AuDTDPA modified electrodes is shown in Fig. 7. Subsequent scanning with the bare gold electrode leads to a decrease in the anodic peak current with the AuDTDPA modified electrode. This phenomenon was not observed, indicating that interaction of surface-COOH groups with DA avoids the passivation of the electrode surface. These results are similar to those observed in previous works [8,9,10], where carboxylates present in supporting electrolyte interact with DA and stabilize the intermediate products of the electrochemical reactions of DA, which lead to deposition of polymerized films on the surfaces of solid electrodes and induce loss of electrode activity [8,30].

The stability of the AuDTDPA modified electrode was evaluated in relation to the applied potential in successive scanning. The AuDTDPA modified electrode was shown to be stable in the potential range of −0.3 to 0.7 V in phosphate buffer solution, where no voltammetric peaks were observed. After successive scanning (10 cycles) the peak current for the oxidation of DA remains unchanged. These indicate that the SAM succeeded to avoid electrode fouling using the experimental conditions employed here.

3.2.3. Square-wave voltammetry (SWV)

Among the electroanalytical techniques presently used, square-wave voltammetry (SWV) has proved to be extremely useful for the detection of organic molecules in low concentrations and in complex matrices [31]. It also allows to obtain information about the electrochemical mechanism.

The square-wave voltammogram for DA on the AuDTDPA modified electrode presents similar features to those obtained from cyclic voltammetry, showing a single reversible process for DA with a peak potential of 0.25 V.

Optimization of the analytical procedure involved a systematic study of the voltammetric parameters that affect the SWV response, namely, the frequency (*f*), the pulse amplitude (*a*) and the scan increment (ΔE_s).

The oxidation peak current of the DA on the AuDTDPA modified electrode increases linearly with the square root of the frequency in the range from 10 to 100 s^{-1}. These results indicate that the electro-oxidation of DA is occurring by a diffusion-controlled process. For further studies a frequency of 100 s^{-1} was chosen.

It was also verified that the peak current increases linearly with the amplitude in the range of 10–100 mV and, for the subsequent analytical applications, a value of 100 mV was chosen. Finally, increasing the potential step in the base staircase potential program (ΔE_s) from 1 to 10 mV showed no influence on the peak current; a value of 2 mV was used in further studies.

3.3. Analytical applications

The performance of the AuDTDPA electrode was evaluated for the determination of DA in pharmaceutical formulations, using square-wave voltammetry.

The developed SWV method was *in-house* validated for the analyses of the DA in pharmaceutical formulations by evaluation of the following parameters: linear range, linearity, sensitivity, detectability and intra-assay precision. The accuracy was evaluated by comparing the results obtained from the analysis of pharmaceutical formulations by the proposed SWV method with a previous HPLC developed method.

The linearity, linear range and sensitivity were obtained from calibration graphs using an external standard at seven concentration levels, in triplicate, between 0.35×10^{-5} and 3.4×10^{-5} mol L^{-1} DA, at pH 7.0 in 0.10 mol L^{-1} phosphate buffer (Fig. 8). The linearity was tested using a pure error lack of fit test with simple regression, which was not significant at the 5% level. The sensitivity (slope of the calibration graph) and linearity (linear regression coefficient) are calculated as 0.098 A/mol L^{-1} and 0.999, respectively.

The inter-assay precision, expressed as the estimated relative standard deviation, established through analyses of a 1.7×10^{-6} mol L^{-1} DA solution (*n* = 10) was 1.8%.

The detectability (*D*) established as 1.1×10^{-6} mol L^{-1} DA represents the lowest concentration of an analyte in sample solutions that can be detected in the voltammetric cell and was calculated by the following expression $D = 3s_{y/x} b^{-1}$, where $s_{y/x}$ is the residual standard deviation of the regression line and *b* is the slope of the calibration graph [32]. The detection and the
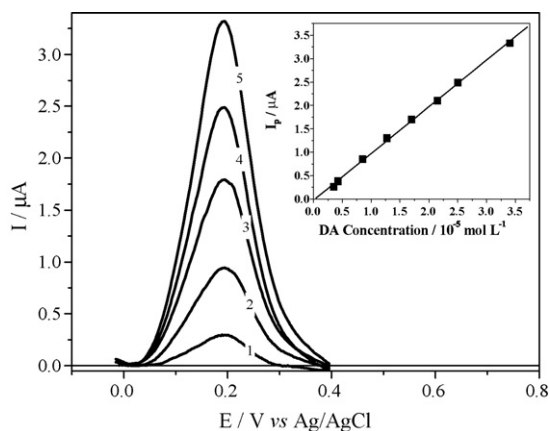
Fig. 8. SWV response of the AuDTDPA modified electrode for different DA concentrations: (1) 0.35×10^{-5} mol L^{-1}, (2) 0.85×10^{-5} mol L^{-1}, (3) 1.7×10^{-5} mol L^{-1}, (4) 2.5×10^{-5} mol L^{-1} and (5) 3.4×10^{-5} mol L^{-1} in 0.1 mol L^{-1} phosphate buffer, pH 7.0, with $a = 100$ mV, $\Delta E_s = 2$ mV, $f = 100$ s^{-1}. *Insert*: linear dependence of the peak current with DA concentration.

Table 1
Determination of DA in dopamine hydrochloride injection solutions (DA nominal value 5 mg mL^{-1})

Sample	SWV ($n = 3$) (DA mg mL^{-1})	HPLC ($n = 3$) (DA mg mL^{-1})
1	4.75 ± 0.10	4.82 ± 0.04
2	4.76 ± 0.06	4.90 ± 0.03
3	4.85 ± 0.05	4.89 ± 0.02

quantitation limits of the method are not presented, due to the fact that the active compound is the major constituent of the formulation and this parameter is not required for method validation for the quality control of pharmaceutical products. Furthermore, these limits would depend on sample dilution before analysis.

The accuracy of the method was evaluated through analyses of three samples of dopamine injectable formulations by the proposed square-wave voltammetric method with the AuDTDPA modified electrode and by a reversed phase HPLC-method, using the procedure described in Section 2.4. The results are shown in Table 1. The mean values obtained using the proposed voltammetric method and the HPLC-method, for all samples, do not differ significantly ($P < 0.05$). The concentrations determined in the samples varied between 4.74 and 4.85 mg mL^{-1} of DA. Considering that the active ingredient needs to be in the range of 95–105% [33], all of the samples analyzed were in accordance with their specifications.

4. Conclusion

In the present paper, a stable 3,3′-dithiodipropionic acid modified gold electrode was prepared. A $[Fe(CN)_6]^{3-/4-}$ redox probe was used to characterize the AuDTDPA modified electrode using cyclic voltammetry and impedance techniques.

The anodic peak current of DA with the AuDTDPA modified electrode is higher than that at a bare gold electrode. The overpotential decreased by 100 mV at AuDTDPA electrode. These results indicate that DTDPA is an effective mediator in the elec-

trocatalytic oxidation of DA. The gold SAM modified electrode is stable in the conditions studied and avoids passivation of the electrode surface, probably due the interaction of surface-COOH groups with DA. The interaction between the SAM of DTDPA and DA is pH-dependent and faster kinetics for DA oxidation was obtained at pH values higher than 4.0. The interaction of DA with the immobilized carboxylic acid on the gold electrode surface confirm the previously reported results for the electrochemical behavior of phenolic compounds in the presence of carboxylic acids in solution, using solid state electrodes [8–10].

Furthermore, the results indicate that the AuDTDPA modified electrode could be employed for the determination of DA in pharmaceutical formulations, with adequate selectivity and precision. Furthermore the proposed method is simple, rapid, dispenses with the use of organic solvents and presents lower costs in comparison with chromatographic methods.

Acknowledgements

References

[1] B.J. Venton, K.P. Troyer, M. Wightman, Anal. Chem. 74 (2002) 539.
[2] S.H. Duvall, R.L. McCreery, J. Am. Chem. Soc. 122 (2002) 6759.
[3] T.M. Vergheese, S. Berchmans, J. Electroanal. Chem. 570 (2004) 35.
[4] J.W. Kang, L. Zhuo, X.Q. Lu, X.Q. Wang, J. Solid State Electrochem. 9 (2005) 114.
[5] R. Lapuente, F. Cases, P. Garcés, E. Morallón, J.L. Vásquea, J. Electroanal. Chem. 45 (1998) 163.
[6] H. Yi, K. Wu, S. Hu, D. Cui, Talanta 55 (2001) 1205.
[7] Y. Li, M. Liu, C. Xiang, Q. Xie, S. Yao, Thin Solid Film 497 (2006) 270.
[8] R.M. Carvalho, L.T. Kubota, S. Rath, J. Electroanal. Chem. 19 (2003) 548.
[9] E. Winter, R.M. Carvalho, L.T. Kubota, S. Rath, J. Braz. Chem. Soc. 14 (2003) 564.
[10] E. Winter, L. Codognoto, S. Rath, Electrochim. Acta 51 (2006) 1282.
[11] S. Berchmans, R.G. Nirmal, G. Prabaharan, A.K. Mishra, V. Yegnaraman, J. Solid State Electrochem. (2005) 15 (online first).
[12] J.C. Love, L.A. Estroff, J.K. Kriebel, R.G. Nuzzo, G.M. Whitesides, Chem. Rev. 105 (2005) 1103.
[13] D. Mandler, I. Turyan, Electroanalysis 8 (1996) 207.
[14] Y.X. Sun, S.F. Wang, X.H. Zhang, Y.F. Huang, Sens. Actuators B: Chem. 113 (2006) 156.
[15] P. Morf, F. Raimondi, H.G. Nothofer, B. Schnyder, A. Yasuda, J.M. Wessels, T.A. Jung, Langmuir 22 (2006) 658.
[16] I. Kubo, K. Yoshimura, E. Ohashi, Electrochemistry 74 (2006) 149.
[17] T. Weiss, K.D. Schierbaum, W. Göpel, U. Thoden van Velzen, D.N. Reinhoudt, Sens. Actuators B: Chem. 26 (1995) 203.
[18] J.J. Gooding, P. Erokhin, D. Losic, W. Yang, V. Policarpio, J. Liu, F.M. Ho, M. Situmorang, D.B. Hibbert, J.G. Shapter, Anal. Sci. 17 (2001) 3.
[19] C.L. Boozer, Q. Yu, S. Chen, C.Y. Lee, J. Homola, S.S. Yee, S. Jiang, Sens. Actuators B: Chem. 90 (2003) 22.
[20] F. Malem, D. Mandler, Anal. Chem. 65 (1993) 37.
[21] H.M. Zhang, N.Q. Li, Z. Zhiwei, Microchem. J. 64 (2000) 277.
[22] C.R. Raj, T. Okajima, T. Osaka, J. Electroanal. Chem. 543 (2003) 127.
[23] C.M. Whelan, M.R. Smyth, C.J. Barnes, J. Electroanal. Chem. 441 (1998) 109.
[24] U.K. Sur, R. Subramanian, V. Lakshminarayanan, J. Colloid Interf. Sci. 266 (2003) 175.
[25] R.C. Raj, S. Behera, J. Electroanal. Chem. 581 (2005) 61.

[26] X. Zhang, S. Wang, Q. Shen, Microchim. Acta 149 (2005) 37.
[27] H.S. Silva, V. Garcia-Morales, C. Moura, J.A. Manzanares, F. Silva, Langmuir 21 (2005) 7461.
[28] P.R. Roy, T. Okajima, T. Ohsaka, Bioelectrochemistry 59 (2003) 11.
[29] T. Liu, M. Li, Q. Li, Talanta 63 (2004) 1053.
[30] R.M. Carvalho, R.S. Freire, S. Rath, L.T. Kubota, J. Pharm. Biomed. Anal. 34 (2004) 871.

[31] D. de Souza, L. Codognoto, A.R. Malagutti, R.A. Toledo, V.A. Pedrosa, R.T.S. Oliveira, L.H. Mazo, L.A. Avaca, S.A.S. Machado, Quim. Nova 27 (2004) 790.
[32] J.C. Miller, J.N. Miller, Statistics for Analytical Chemistry, 3rd ed., Ellis Horwood Limited, New York, 1993.
[33] The United States Pharmacopoeia, The National Formulary, 28th ed., United States Pharmacopeial Convention, Rockville, 2005, pp. 690–691.

ELSEVIER

A study of the analytical behaviour of selected psycho-active drugs using liquid chromatography, ion trap mass spectrometry, gas chromatography and polarography and the construction of an appropriate database for drug characterisation

Bernadette Doherty[a], Fionnuala O'Donnell[a], W. Franklin Smyth[a], Julian C. Leslie[b], Venkataraman N. Ramachandran[a], Neil S. Boyd[a], Catherine J. Hack[a], Edmund O'Kane[a], Stephen McClean[a],*

[a] *School of Biomedical Science, University of Ulster, Coleraine BT52 1SA, Northern Ireland*
[b] *School of Psychology, University of Ulster, Coleraine BT52 1SA, Northern Ireland*

Abstract

This paper provides analytical chemical information on a range of psycho-active drugs. This analytical chemical information on liquid chromatography–electrospray ionisation-mass spectrometry (HPLC–ESI-MS), ion trap mass spectrometry (ESI–MS^n), gas chromatography–flame ionisation detection (GLC–FID) and polarographic behaviour is then incorporated into a database which is of use in drug characterisation. Application is found in the determination of selected drug compounds in hair samples.
© 2006 Elsevier B.V. All rights reserved.

Keywords: Psycho-active drugs; Ion trap mass spectrometry (ESI–MS^n); Liquid chromatography–electrospray ionisation-mass spectrometry (HPLC–ESI-MS); Gas chromatography–flame ionisation detection (GLC–FID); Polarography; Database

1. Introduction

For people diagnosed with severe depression, the lifetime risk of suicide may be as high as 6% compared with 1.3% in the general population [1]. It is the third leading cause of death among 15–24 year olds [2]. In recent times particular concerns have been raised about suicide as a potential side effect of commonly prescribed antidepressants, namely the selective serotonin reuptake inhibitors (SSRIs). It is thought that these drugs may increase the risk of suicidal thoughts and self-harm, in particular for those under the age of 19 [3–5]. The Food and Drug Administration (FDA) has requested manufacturers of the following drugs: Prozac (fluoxetine), Zoloft (sertraline), Paxil (paroxetine), Celexa (citalopram), Effexor (venlafaxine), Remeron (mirtazapine), Lexapro (escitalopram) and Wellbutrin (bupropion) to include in their labelling a warning statement

that describes the increased risk of suicide in patients given such antidepressants.

Joyce et al. [6] have investigated the characterisation of selected drugs with amine-containing side chains, such as the psycho-active chlorpromazine, methadone and amphetamine, using electrospray ionisation and ion trap mass spectrometry (ESI–MS^n). From this study, certain rules were formulated with respect to the ESI–MS^n behaviour of drugs with amine-containing side chains. Smyth et al. [7] have carried out a study of the ESI–MS^n behaviour of some 12 selected drugs with nitrogen-containing saturated ring structures such as the psycho-active risperidone, cocaine and olanzapine. Fragmentation of these drugs with nitrogen-containing saturated ring structures using ESI–MS^n was commonly found to involve loss of certain functional groups with the aromatic entities in the drug structures being predictably resistant to fragmentation. Smyth [8] has reviewed selected publications for the period 1993–2003 concerning the ESI-MS analysis of drugs and their metabolites in order to investigate the generality of such rules of fragmentation. The drugs were chosen according to selected structural classes

---

* Corresponding author. Tel.: +44 28 7032 4406; fax: +44 28 7032 4965.
  E-mail address: s.mcclean@ulster.ac.uk (S. McClean).

in which the molecules gave ESI signals primarily as $[M+H]^+$ ions, i.e., drugs with amine-containing side chains, drugs with *N*-containing saturated ring structures, 1,4-benzodiazepines etc. by various mass spectrometric analysers. Where possible, the molecular structures of product ions from MS/MS experiments were assigned. The characterisation of citalopram, fluoxetine, mirtazepine, paroxetine, sertraline and venlafixine by ion trap and QTOF mass spectrometry has also been described by Smyth et al. [10].

This paper follows on from these earlier studies by investigating the ESI–MS^n behaviour of some 26 selected antidepressant drugs and other relevant psycho-active compounds. In addition, their HPLC–ESI-MS behaviour has also been studied with a view to the identification of these drugs simultaneously in mixtures at ng/ml concentrations which would ultimately be of value in their determination in biological matrices with particular reference to human hair. A few studies have appeared in the literature regarding the simultaneous analysis by HPLC–MS

of some of these antidepressants, but these have generally involved the use of the less specific selected ion monitoring of the pseudo-molecular ions and the analyses have been directed towards biological fluids such as serum [11] and plasma [12,13]. Hair samples of psychiatric patients and hair samples of suicide cases have been analysed by HPLC–ESI-MS for antidepressants, including citalopram and its desmethyl-metabolite, and neuroleptics [14]. The SSRI antidepressant drugs chosen for this study were fluoxetine, citalopram, paroxetine and sertraline (Fig. 1). Also chosen were mirtazapine and venlafaxine (Fig. 1) which are serotonin–noradrenergic reuptake inhibitors, SNRIs). This new generation of antidepressants has similar efficacy and better-tolerated side effects when compared with classical antidepressants such as the tricyclics. Determinations of some of these drugs have been made by the use of LC–UV [15,16], gas chromatography with electron capture or mass-spectrometric detection [16–18], micellar electrokinetic capillary chromatography [19] and recently cap-
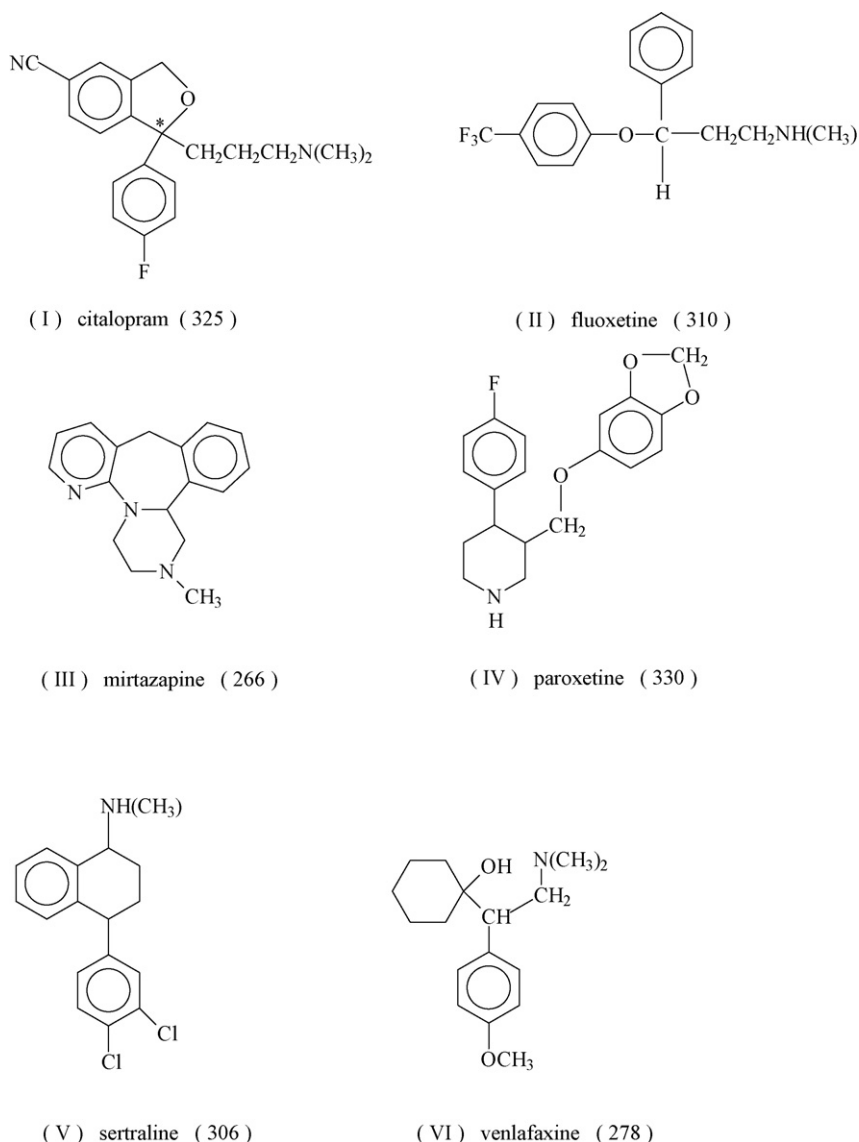

Fig. 1. Structures of the six antidepressant compounds with pseudomolecular ion masses in brackets. Taken from [10] Copyright John Wiley & Sons Limited. Reproduced with permission.

illary electrophoresis with quadrupole and TOF detection [20]. However, these techniques have not been used for the rapid identification of these antidepressant drugs and other relevant psycho-active drugs. In addition to this current study of the ESI–MS^n and HPLC–ESI-MS behaviour of the selected psycho-active drugs, the latter were also subjected to investigation by gas chromatography–flame ionisation detection (GLC–FID) and polarography.

The aim of this paper is therefore to provide analytical chemical information on these antidepressants and other relevant psycho-active drugs. This analytical chemical information using ESI–MS^n, HPLC–ESI-MS, GLC–FID and polarography is then incorporated into a database for drug characterisation. The paper by Philainen et al. [21] has described the production of a database for 14 drugs of forensic significance using HPLC–ESI-MS/MS. It is intended that the production of the database as described herein will ultimately be of value in the investigation of the possible association between self harm/suicide in young men and these drugs. Application of this method is made to the analysis of SSRIs and other psycho-active drugs in hair samples by LC–MS/MS following automated Soxhlet extraction, a method successfully used by our group for the analysis of 1,4-benzodiazepines in hair samples [24].

2. Experimental—chemicals, drugs, instrumentation and methodology

Methanol, acetic acid and formic acid were obtained from BDH (Poole, Dorset, UK). The antidepressant drug compounds were obtained from Alphapharm (Queensland, Australia), Gerard Laboratories (Dublin, Ireland), PPG-SIPSY (Avrille, France), H. Lundbeck A/S (Copenhagen, Denmark) and N.V. Organon (Oss, The Netherlands). Other psycho-active drugs were obtained from the Forensic Science Agency, Carrickfergus, Northern Ireland. Stock solutions of the drugs were prepared by dissolving an appropriate mass in 25 ml of methanol to provide a concentration of 1.0×10^{-3} mol l^{-1}. Dilutions were then made to provide working standards.

2.1. ESI–MS^n studies

MS^n characterisation of the psycho-active drugs was achieved using a LCQ^{TM} "Classic" quadrupole ion trap mass spectrometer (Finnigan MAT, San Jose, California, USA) utilising electrospray ionisation (ESI). Drugs at a concentration of 1.0×10^{-5} mol l^{-1} in methanol were infused into the ESI probe at a rate of 10 μl min^{-1}. The collision energy was kept at the instrument default value of 25% (arbitrary unit set by the software). The sheath gas flow was set to 50 and the auxiliary gas to 5 (arbitrary units defined by the software). Nitrogen gas for the LCQ^{TM} was delivered from a Whatman nitrogen generator (Whatman Inc., Haverhill, MA, USA), while the helium damping gas present in the ion trap was obtained from BOC Gases (Guildford, Surrey, UK). The capillary temperature was set to 250 °C and the spray voltage to 4.5 kV for the MS^n studies. For MS^n characterisation of the compounds, the most intense peak in the mass spectrum, i.e. [M + H]$^+$, was chosen for MS^2

analysis, providing first generation product ions in this mode. The most intense peak from MS^2 analysis was chosen for further characterisation at the MS^3 stage and so on until no further reproducible signals were obtained.

2.2. HPLC–ESI-MS studies

HPLC–ESI-MS was carried out using a Luna 5 μ C18 column (150 mm × 4.6 mm). A gradient mobile phase was used with solvent A being 20/80 (methanol/water) + 0.1% formic acid and solvent B being 90/10 (methanol/water) + 0.1% formic acid. The gradient went from 100% A to 100% B over 25 min at a flow rate of 0.5 ml min^{-1}. Injections of the drugs were made at a concentration of 10^{-5} mol l^{-1} with an injection volume of 25 μl. Experiments were conducted at room temperature.

2.3. GLC–FID studies

GLC–FID was carried out using a Perkin-Elmer 8600 Gas Chromatograph (Perkin-Elmer Ltd., Beaconsfield, Buckinghamshire, UK) in conjunction with a Zebron ZB-5 (Phenomenex, Macclesfield, Cheshire, UK) column (30 m × 0.25 μm). The oven was initially set to 80 °C, with a ramp rate of 15 °C min^{-1} until a temperature of 180 °C was reached. At this point, the ramping rate was increased to 30 °C min^{-1} until a final temperature of 300 °C was achieved. This final temperature was held for 5 min to give an overall run time of 15.66 min. For each drug, a 1 μl injection was made of a 10^{-3} mol l^{-1} solution in methanol. R.S.D. values ($n = 6$) of retention time were calculated on standard solutions of the compounds at a concentration of 1.67×10^{-4} M.

2.4. Polarographic studies

Polarographic analysis was carried out using a Metrohm 646 VA processor in conjunction with a 675 VA sample changer, a 683 pump unit and a 677 drive unit (Metrohm, Herisau, Switzerland). The current axis was set from 0 to -160 nA and cathodic scans were initiated from -0.4 V to -1.6 V using 0.1 M acetate buffer (pH 4.47) as background electrolyte and a standard Ag/AgCl 3 M KCl electrode system. Each solution was purged with nitrogen gas for 300 s prior to analysis.

2.5. Database and web interface

A database was constructed to contain the available ESI–MS^n, HPLC–ESI-MS, GLC–FID and polarographic data for the 26 psycho-active drugs. In order to account for variations in chromatographic retention time tolerances of ± 1.0 min are automatically applied in any search query. Similarly for MS/MS data tolerances of ± 0.5 Th are applied and ± 50 mV for the polarographic data. For each compound, the following extra information is available—molecular weight, chemical formula, image of the chemical structure and synonyms. The database is implemented in mySQL and run on a central server in the Bioinformatics Research Group at the University of Ulster, http://bioinformatics.ulster.ac.uk/~kay/. The database may be

browsed via a web interface or interrogated using standard web forms.

2.6. Analysis of antidepressants in human hair samples

To test the use of the database, HPLC–ESI-MS/MS was performed on drug compounds that were extracted from hair samples using automated Soxhlet extraction (Tecator Soxtec System HT12 with a 1046 Soxtec Service unit Tecator, HOGANAS, Sweden). Samples of hair weighing 150 mg, 200 mg and 105 mg, respectively were obtained from volunteers being treated with sertraline (50 mg per day) and risperidone (2.5 mg per day), paroxetine (20 mg per day), and escitalopram (10 mg per day), though the exact durations of the treatments were not known. In addition, a sample of hair weighing 200 mg was obtained from a volunteer being treated with trimipramine (100 mg per day), flurazepam (30 mg per day) and diazepam (4 mg daily). In each case, the sample was washed by five consecutive washes with 5 ml of methanol to remove exogenous compounds. After being dried, the sample was cut into approximately 1 mm lengths and transferred into a thimble compatible with the Soxtec extraction system. Fifty milliliters of methanol were used for the extraction and the temperature control was set to 160 °C. Tap water was supplied to the condenser at an approximate rate of 2 l min^{-1}. The sample was boiled for 3 h with the thimble in contact with the solvent, after which the thimble was raised to the rinsing position for 2 h during which time the solvent dropped through the sample from the condenser. After the extraction process, the solvent was evaporated and the residue reconstituted in 500 µl of HPLC-solvent (78.8% water, 20% methanol, 0.1% formic acid and 0.1% TFA). The sample was then subjected to HPLC–ESI-MS/MS analysis, 20 µl being injected each time. Prior to analysis of hair samples, the injection system was washed with methanol, the column equilibrated with mobile phase to ensure that the system was free from all traces of drug standards from previous analyses. The drugs were identified based on a comparison of their chromatographic retention times and mass spectral fragmentation characteristics with those of psycho-active drug standards.

3. Results and discussion

This paper deals with analytical chemical properties of a total of 26 psycho-active drugs which were investigated using ESI–MS^n, HPLC–ESI-MS, GLC–FID and polarography. All data gathered such as retention times, molecular ions, fragment ions, polarographic reduction peak potentials etc., were used to populate a searchable database that could be used to rapidly characterise unknown drugs from generated data.

3.1. ESI–MS^n studies

McClean et al. [22] have investigated the ESI–MS^n characterisation of selected anti-psychotic drugs such as flupenthixol and their detection and determination in human hair samples by HPLC–ESI-MS. Smyth et al. [23] have made a study of the ESI of pharmacologically significant 1,4-benzodiazepines

such as oxazepam, lorazepam and temazepam and their subsequent fragmentation using an ion trap mass spectrometer. Joyce et al. [6] have investigated the characterisation of selected drugs with amine-containing side chains, such as the psycho-active chlorpromazine, methadone and amphetamine, using ESI–MS^n. Smyth et al. [7] have carried out a study of the ESI–MS^n behaviour of some 12 selected drugs with nitrogen-containing saturated ring structures such as the psycho-active risperidone, cocaine and olanzapine. A further paper [9] followed on from these studies by investigating the ESI–MS^n behaviour of selected hypnotic drugs and their metabolites, i.e., zopiclone and its N-desmethyl metabolite, zolpidem, flunitrazepam and its 7-amino, N-desmethyl and 3-hydroxy metabolites. More recently, Smyth et al. [10] have studied the fragmentation pathways of citalopram, fluoxetine, mirtazepine, paroxetine, sertraline and venlafixine by ion trap and QTOF mass spectrometry.

The relevant fragmentation data of the 21 psycho-active drugs discussed in the preceding paragraph is included in Table 1 for the purpose of completion of the database. ESI–MS^n characterisation of the three other drugs, namely pentobarbitone, 3,4-methylenedioxymethamphetamine (MDMA, Ecstasy) and methamphetamine which were not included in previous studies, is discussed below.

(i) Pentobarbitone

The nitrogen atoms in pentobarbitone do not protonate due to the adjacent and electron withdrawing carbonyl groups. As such no ESI–MS^n behaviour is observed. Future work may investigate negative mode ionisation of this compound to produce $[M - H]^-$. However, the mobile phase conditions for HPLC separation would also have to be adjusted to include appropriate modifiers to enhance deprotonation. As such, this may cause suppression effects of the other compounds within this study and so was not pursued at this time.

(ii) Methylenedioxymethamphetamine, MDMA, Ecstacy

The pseudo-molecular ion at *m/z* 194.1 loses CH_3NH_2 at the MS^2 stage, followed by the loss of 30 u at MS^3 corresponding to CH_2=O from the methylenedioxy ring. MS^4 results in the loss of 28 u to give a signal at *m/z* 105.1.

(iii) Methamphetamine

The pseudo-molecular ion at *m/z* 150.0 again loses CH_3NH_2 at the MS^2 stage, followed by the loss of 28 u at MS^3 generating the tropylium cation, $C_7H_7^+$, at *m/z* 91.

3.2. HPLC–ESI-MS studies

The results from the analysis of the 26 psycho-active drugs are tabulated and displayed in Table 1. Using the mobile phase conditions specified, good chromatographic resolution of the drugs was achieved. Under these mobile phase conditions, the retention time of the solvent front was difficult to determine accurately and so retention time of eluting molecules is presented instead of capacity factor. This analytical selectivity is further enhanced by the use of precursor (MS) or product ion (MS/MS) mass scans in the mass spectrometry software to specifically locate the presence of each compound with reference to its retention

Table 1
MS^n characterisation data for the psycho-active drugs and HPLC–ESI-MS/MS retention time

Compound name	Molecular weight	[M + H]$^+$	MS^2	MS^3	MS^4	MS^5	HPLC–ESI-MS/MS retention time (min)
Amphetamine	135	136	119	91	–	–	11.33
Chlorpromazine	319	320	274	246	214	–	18.07
Citalopram	324	325	262	234	216	–	14.78
Cocaine	303	304	182	150	122	–	12.04
Diazepam	284	285	257	228	193	167	16.67
Ecstasy	193	194	163	133	105	–	11.23
Escitalopram	324	325	262	234	220	–	14.98
Flunitrazepam	313	314	268	239	222	–	17.28
Fluoxetine	309	310	148		–	–	17.23
Flupenthixol	434	435	307	265	–	–	18.37
Flurazepam	387	388	315	272	244	217	14.62
Lorazepam	321	321	303	275	239	–	18
Methadone	309	310	265	247	219	204	16.74
Methamphetamine	149	150	119	91	–	–	10.96
Mirtazapine	265	266	195	–	–	–	9.14
Olanzapine	312	313	256	213	198	146	10.11
Oxazepam	286	287	269	241	–	–	17.31
Paroxetine	329	330	192	70	–	–	16.3
Pentobarbitone	226	–	–	–	–	–	–
Risperidone	410	411	191	163	–	–	12.56
Sertraline	306	306	275	159	123	–	17.7
Temazepam	300	301	283	255	–	–	18.47
Trimipramine	294	295	100	58	–	–	16.93
Venlafaxine	277	278	260	215	159	–	14.31
Zolpidem	307	308	263	248	220	–	12.45
Zopiclone	388	389	345	–	–	–	11.99

(–): no signal obtained.

time and *m/z* characteristics as demonstrated by Smyth et al. [10].

3.3. GLC–FID studies

The results from the GLC analysis of the of the 26 psycho-active drugs are presented in Table 2. In general, good resolution of the drugs is achieved apart from citalopram and paroxetine which co-elute with identical retention times. The benzodiazepines, diazepam and lorazepam also have similar retention times under the analytical conditions employed. Notwithstanding, the data presented for GLC–FID compliments that obtained from the other analytical techniques when used to qualitatively profile psycho-active drugs in a biological matrix such as hair. Table 2 provides R.S.D. values (*n* = 6) based on retention time for standard solutions of the compounds under investigation. Values of less than 2% are reported for the majority of compounds apart from risperidone that had an R.S.D. value of 3.16%.

3.4. Polarographic studies

Voltammetric techniques have proved useful if the determination of 1,4-benzodiazepines which give signals due to the reduction of the −C=N− bond when a cathodic scan is initiated [25,26]. Table 3 shows the data from these electroanalytical studies confirming that flurazepam, flunitrazepam, lorazepam, diazepam, temazepam and oxazepam exhibit reduction waves in the range −853 to −890 mV. Trimipramine and zopiclone

Table 2
Comparison of retention times for psycho-active drugs using GLC–FID analysis

Compound name	GC retention time (min)	GC retention time (% R.S.D.)
Amphetamine	3.44	1.82
Chlorpromazine	11.76	0.41
Citalopram	11.31	0.12
Cocaine	10.59	0.13
Diazepam	11.55	0.13
Ecstasy	8.7	0.92
Escitalopram	11.21	0.34
Flunitrazepam	12.34	0.13
Fluoxetine	9.29	0.4
Flupenthixol	14.69	0.17
Flurazepam	13.07	0.15
Lorazepam	11.34	0.12
Methadone	10.37	0.35
Methamphetamine	3.57	1.02
Mirtazapine	10.82	0.13
Olanzapine	12.88	0.05
Oxazepam	11.04	0.13
Paroxetine	12	0.11
Pentobarbitone	8.48	0.2
Risperidone	9.59	3.16
Sertraline	11.77	0.24
Temazepam	11.91	0.08
Trimipramine	10.65	0.08
Venlafaxine	10.08	0.18
Zolpidem	13.35	0.54
Zopiclone	11	0.7

R.S.D. values for retention time are also included (*n* = 6) on standard solutions at a concentration of 1.67×10^{-4} M.

Table 3
Comparison of peak potentials for the psycho-active drugs using polarographic analysis

Compound name	Differential pulse polarography Ep value (mV)
Amphetamine	–
Chloropromazine	–
Citalopram	–
Cocaine	–
Diazepam	−856
Ecstacy	–
Escitalopram	–
Flunitrazepam	−863
Fluoxetine	–
Flupenthixol	–
Flurazepam	−853
Lorazepam	−877
Methadone	–
Methamphetamine	–
Mirtazapine	–
Olanzapine	–
Oxazepam	−890
Paroxetine	–
Pentobarbitone	–
Risperidone	–
Sertraline	–
Temazepam	−890
Trimipramine	−1086
Venlafaxine	–
Zolpidem	–
Zopiclone	−666

(−): no signal obtained.

were the only two other compounds to give reduction signals under these analytical conditions. DPP is a useful voltammetric technique that may be available in some analytical labs. The data presented here, which will form part of the online database, may therefore be useful to other workers in the field.

3.5. Database and web interface

Data from these analytical studies were used to populate the database described above.

3.6. Analysis of antidepressants in human hair samples

The analysis of sertraline, risperidone, escitalopram, paroxetine, trimipramine, flurazepam and diazepam in hair samples was investigated using HPLC–ESI-MS/MS analysis. As shown in Table 4, sertraline and risperidone were readily identified and quantified in hair based on their retention times on the HPLC column and fragmentation characteristics using mass spectrometry. Quantitation was achieved by virtue of an external calibration method. A typical HPLC–ESI-MS/MS chromatogram is shown in Fig. 2. Repeatability of the MS method was confirmed for four extracts of the same hair sample. The coefficient of variation for the retention time of the four extracts was 0.2% and 6.78% for the peak area for sertraline and 0.3% for the retention time and 17.1% for the peak area for risperidone. Escitalopram, paroxetine, trimipramine, flurazepam and diazepam were also readily detected in hair samples (Table 4).
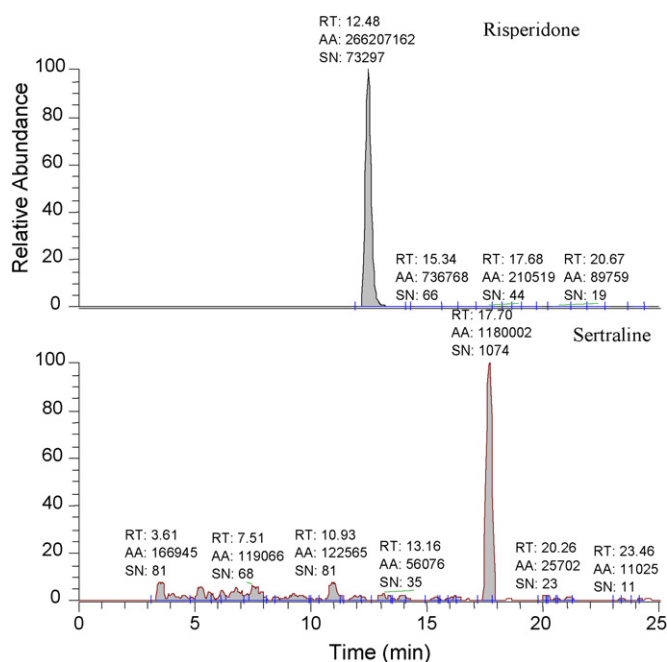

Fig. 2. HPLC–MS/MS chromatogram of risperidone and sertraline from a hair sample.
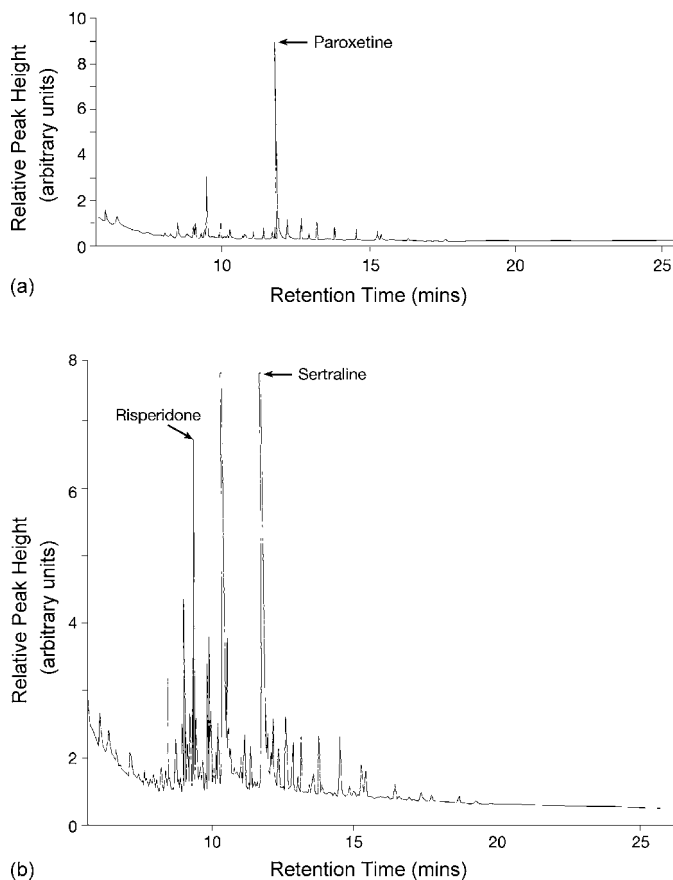

Fig. 3. (a) GC–FID chromatogram of an extracted hair sample positive for paroxetine. (b) GC–FID chromatogram of an extracted hair sample positive for sertraline and risperidone.

Table 4

Detection and determination of diazepam, escitalopram, flurazepam, paroxetine, risperidone, sertraline and trimipramine in human hair using HPLC–MS/MS with an external calibration method

Compound	MS	MS/MS	LC–MS/MS retention time (min)	Concentration in hair as determined by LC–MS/MS (ng mg^{-1})	GC retention time (min)
Diazepam	285	257	16.99	0.11	11.68
Escitalopram	325	262	14.85	0.03	11.84
Flurazepam	388	315	14.63	0.0019	13.29
Paroxetine	330	192	16.66	0.26	11.79
Risperidone	411	191	12.48	6.8	9.38
Sertraline	306	275	17.7	0.64	11.76
Trimipramine	295	100	16.89	0.23	10.68

GC–FID retention times are also included though no quantitation took place by this method.

The psycho-active drugs were also detected in these hair samples using GC–FID based on retention times (Table 4) though no quantitation was attempted by this method. Examples of GC–FID chromatograms of hair-extract samples are shown in Fig. 3.

A hair sample extract positive for trimipramine, diazepam and flurazepam was analysed by differential pulse polarography but the current method was not sufficiently sensitive to detect the 1,4-benzodiazepines present. Future work may consider the use of stripping voltammetry to enhance the sensitivity of the method.

With hair samples extraction yields are very difficult to determine based on the nature of the matrix and no attempt to quantify extraction yields was made in the current study.

4. Conclusions

The ESI–MS^n, HPLC–ESI-MS, GLC–FID and polarographic results obtained from this study have been compiled into a database for use within the University of Ulster Pharmaceutical Biotechnology Research Group. It is envisaged that this database will aid in the characterisation of unidentified drugs in biomatrices such as hair. In addition, confirmation of the validity of the database was obtained from the HPLC–ESI-MS/MS analysis of hair samples that tested positive for the drugs sertraline, risperidone, escitalopram, paroxetine, trimipramine, flurazepam and diazepam. Hair analysis as an indicator for drug use has emerged as a new tool for drug screening. From the results obtained to date, it is concluded that HPLC–ESI-MS/MS and GLC can provide rapid, selective and sensitive methods for detecting and quantifying psycho-active drugs in hair samples following therapeutic administration.

Acknowledgements

References

[1] H.M. Inskip, E.C. Harris, B. Barraclough, Br. J. Psychiatry 172 (1998) 35.
[2] R. Anderson, Natl. Vital. Stat. Rep. 49 (2001) 14.
[3] C.J. Whittington, T. Kendall, P. Fonagy, D. Cottrell, A. Cotgrove, E. Boddington, Lancet 363 (2004) 1341.
[4] D. Fergusson, S. Doucette, K.C. Glass, S. Shapiro, D. Healy, P. Hebert, B. Hutton, Br. Med. J. 330 (2005) 1.
[5] C. Martinez, S. Rietbrock, L. Wise, D. Ashby, J. Chick, J. Moseley, S. Evans, D. Gunnell, Br. Med. J. 330 (2005) 1.
[6] C. Joyce, W.F. Smyth, V.N. Ramachandran, E. O'Kane, D.J. Coulter, J. Pharm. Biomed. Anal. 36 (2004) 465.
[7] W.F. Smyth, V.N. Ramachandran, E. O'Kane, D. Coulter, Anal. Bioanal. Chem. 378 (2004) 1305.
[8] W.F. Smyth, Anal. Chim. Acta 492 (2003) 1.
[9] C. Joyce, W.F. Smyth, V.N. Ramachandran, E. O'Kane, D.J. Coulter, Anal. Chim. Acta 506 (2004) 203.
[10] W.F. Smyth, J.C. Leslie, S. McClean, B. Hannigan, H.P. McKenna, B. Doherty, C. Joyce, E. O'Kane, Rapid Commun. Mass Spectrom. 20 (2006) 1637.
[11] U. Gutteck, K.M. Rentsch, Clin. Chem. Lab. Med. 41 (2003) 1571.
[12] J. He, Z.L. Zhou, H.D. Li, J. Chromatogr. B 820 (2005) 33.
[13] C. Pistos, M. Koutsopoulou, I. Panderi, Anal. Chim. Acta 514 (2004) 15.
[14] C. Muller, S. Vogt, R. Goerke, A. Kordon, W. Weinmann, Forensic Sc. Int. 113 (2000) 415.
[15] G. Tournel, N. Houdret, V. Hedouin, M. Deveau, D. Gosset, M. Lhermitte, J. Chromatogr. B 761 (2001) 147.
[16] L. Kristoffersen, A. Bugge, E. Lundanes, L. Slordal, J. Chromatogr. B 734 (1999) 229.
[17] A. Lucca, G. Gentilini, S. Lopez-Silva, A. Soldarini, Ther. Drug Monit. 22 (2000) 271.
[18] E. Lacassie, J.M. Gaulier, P. Marquet, J.F. Rabatel, G. Lachatre, J. Chromatogr. B 742 (2000) 229.
[19] L. Labat, M. Deveaux, P. Dallet, J.P. Dubost, J. Chromatogr. B 773 (2002) 17.
[20] M. Himmelsbach, C.W. Klampfl, W. Buchberger, J. Sep. Sci. 28 (2005) 1735.
[21] K. Philainen, E. Sippola, R. Kostiainen, J. Chromatogr. A 994 (2003) 93.
[22] S. McClean, E. O'Kane, W.F. Smyth, J. Chromatogr. B 740 (2000) 141.
[23] W.F. Smyth, S. McClean, V.N. Ramachandran, Rapid Commun. Mass Spectrom. 14 (2000) 2061.
[24] S. McClean, E. O'Kane, J. Hillis, W.F. Smyth, J. Chromatogr. A 838 (1999) 273.
[25] G.B. El-Hefnawey, I.S. El-Hallag, E.M. Ghoneim, M.M. Ghoneim, J. Pharm. Biomed. 34 (2004) 75–86.
[26] M.M. Correia dos Santos, V. Famila, M.L.S. Simoes Goncalves, Anal. Bioanal. Chem. 374 (2002) 1074–1081.

ELSEVIER

Development of membrane electrodes for the selective determination of hyoscine butylbromide

Y.S. El-Saharty [*], F.H. Metwaly, M. Refaat, S.Z. El-Khateeb

Analytical Chemistry Department, Faculty of Pharmacy, Cairo University, El-Kasr El-Aini Street, ET-11562 Cairo, Egypt

Abstract

Four polyvinyl chloride (PVC) membrane sensors for the determination of hyoscine butylbromide are described and characterized. The sensors are based on the use of the ion association complexes of hyoscine cation with ammonium reineckate counter anions as ion exchange sites in the PVC matrix. The membranes incorporate ion association complexes of hyoscine with dibutylsebathete (sensor 1), dioctylphthalate (sensor 2), nitrophenyl octyl ether (sensor 3) and β-cyclodextrin (sensor 4). The performance characteristics of these sensors were evaluated according to IUPAC recommendations, which reveal a fast, stable and linear response for hyoscine over the concentration range of 10^{-5}–10^{-2} M for sensors 1 and 2 and 10^{-6}–10^{-2} for sensors 3 and 4 with cationic slopes of -53.19, -55.17, -51.44 and -51.51 mV per concentration decade for the four sensors, respectively. The direct potentiometric determination of hyoscine butylbromide using the proposed sensors gave average recoveries % of 99.92 ± 1.11, 99.93 ± 1.00, 99.94 ± 1.18 and 99.87 ± 1.39 for the four sensors, respectively. The sensors are used for determination of hyoscine butylbromide in laboratory prepared mixtures, pharmaceutical formulations in combination with ketoprofen and in plasma. Validation of the method shows suitability of the proposed sensors for use in the quality control assessment of hyoscine butylbromide. The developed method was found to be simple, accurate and precise when compared with a reported HPLC method.
© 2007 Published by Elsevier B.V.

Keywords: Hyoscine butylbromide; Ion selective electrodes; PVC membranes; Ammonium reineckate

1. Introduction

Hyoscine butylbromide, (1S,3s,5R,6R,7S,8r)-6,7-epoxy-3-[(S)-(3-hydroxy-2-phenylpropionyl)oxy]-8-butyl-8-methyl-8-azoniabicyclo[3.2.1] octane bromide (Fig. 1) is used as an antispasmodic in treating peptic ulcer, gastritis and various disorders of the gastrointestinal tract which are characterized by spasm. It has also found employment for the relief of spasmodic conditions of the bile duct and urinary tract and for the treatment of dysmenorrhoea [1].

Hyoscine butylbromide is a white or almost white powder, freely soluble in water, in methylene chloride and sparingly soluble in ethanol. It melts at 142–144 °C and it should be protected from light [2,3].

Various methods have been developed for the determination of hyoscine butylbromide, including titrimetric methods [3,4],

spectrophotometric [5–10], comprising derivative techniques [5–8] and colorimetric procedures [11,12].

The degradations products of hyoscine butylbromide were identified in presence of the drug alone or in mixture with ethaverine, dipyrone and papaverine in injection or oral drops by two chromatographic techniques, paper chromatography and TLC [13,14].

The drug was determined in its pharmaceutical preparations and biological fluids using a reversed phase HPLC [15–18]. The studied drug was assayed in pharmaceutical dosage forms by capillary electrophoresis [19,20].

Hyoscine butylbromide was analyzed by a potentiometric method using liquid membrane electrode impregnated with graphite rods [21]. Buschmann [22] described a potentiometric titration for the determination of hyoscine butylbromide. In this method the drug in suppositories was titrated with sodium dodecyl sulphate using bis(2,2′-bipyridyl) iron as indicator.

Li et al. [23] used an ion selective sensor for direct potentiometric determination of hyoscine butylbromide. The method depends on formation of association complex of the drug with
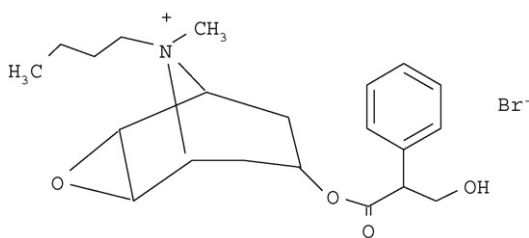
Fig. 1. Chemical structure of hyoscine butylbromide. Molecular formula: $C_{21}H_{30}BrNO_4$; molecular weight, 440.4.

sodium tetraphenylborate, the complex was dissolved in dibutyl phthalate and incorporated in polyvinyl chloride matrix.

A novel bromide PVC-based membrane sensor, based on using either bis(4-hydroxyphenyl)1,4-diaza-1,3-butadiene-Hg(II) complex [24] or iron(III)-salen [25] as an electroactive materials were used for direct potentiometric determination of hyoscine butylbromide. The first sensor was also used as an indicator electrode in the potentiometric titration of the bromide with silver ions [25].

The rapid growth in the analytical chemistry techniques is necessary to match the development of a wide variety of science and technology approaches. In the last three decades, being commercially and not expensive, ion selective electrodes have become an item of general equipment of analytical work. This result happens because ion selective electrodes have rapid, simple, low cost and give accurate measurements of ionic species.

The key to constructing such an electrode is to produce a sensitive and selective membrane that responds to a particular drug. Such a membrane is usually prepared by incorporating an appropriate ion-exchanger and solvent mediator into a poly(vinyl chloride) (PVC) membrane matrix.

The present work originates from the fact that hyoscine butylbromide (HYOB) behave as cation, as it is a quaternary ammonium compound. This fact suggests the use of anionic type of ion exchangers, forming water insoluble ion association complexes. Ammonium reineckate as an anionic exchanger was used for construction of water insoluble ion-association complex with HYOB. The high lipophilicity and remarkable stability of this complex suggested its selective use as electroactive materials in PVC matrix membrane sensors for the determination of HYOB, without interference in laboratory prepared mixtures, pharmaceutical formulations in combination with ketoprofen and in plasma.

2. Experimental

2.1. Instrument

Potentiometric measurements were made at 25 ± 1 with a Hanna (Model 211) pH/mV meter. A single junction calomel reference electrode (Model HI 5412) was used in conjunction with the drug sensor. A WPA pH combined glass electrode Model CD 740 was used for pH measurements. Bandelin sonorex, RK 510 S, magnetic stirrer and a silver wire (3 mm diameter) immersed in the internal solutions were also applied.

2.2. Reagents

All chemicals were of analytical grade and bidistilled water was used. Tetrahydrofuran (THF) 99% (Lab Scan), high molecular weight (10,000) polyvinyl chloride (PVC) powder (Aldrich), nitrophenyl octyl ether (o-NPOE) and dioctylphthalate (DOP) were obtained from Aldrich, dibutylsebathete, ammonium reineckate (R) and β-cyclodextrin (β-CD) were obtained from Sigma. Phosphate buffer pH 7 and pH 8 were prepared [26].

2.3. Samples

2.3.1. Pure sample

HYOB and ketoprofen (KET) were kindly supplied by Amriya Pharmaceutical Industries, Alexandria, Egypt. Their purities were found to be 100.28 ± 0.77 and 99.89 ± 0.61, respectively, according to the HPLC and direct spectrophotometry manufacturer procedures [27].

2.3.2. Pharmaceutical dosage form

Spasmofen ampoules (Amriya Pharm. Ind., Alexandria, Egypt) batch no. 866926. Each ampoule claimed to contain 100 mg of ketoprofen and 20 mg of hyoscine butylbromide.

2.4. Prepared solutions

2.4.1. Stock standard solutions

HYOB stock solution (10^{-2} M) in either water or phosphate buffer pH 7 or 8 were prepared by transferring 0.4404 g of HYOB into three separate 100 ml measuring flasks. Fifty millilitres of either water or phosphate buffer pH 7 or 8 were added, shacked for few minutes and completed to volume with the same solvent.

2.4.2. Working standard solutions

HYOB working solutions (10^{-7}–10^{-3} M) were prepared by suitable dilution from its stock solution using either water or phosphate buffer pH 7 or 8.

2.4.3. Laboratory-prepared mixtures

2.5 ml HYOB from its stock solution (10^{-2} M) was transferred accurately to a series of 25 ml measuring flasks. Aliquots from KET (10^{-2} M) solution were added to prepare mixtures containing 1:0.5, 1:1, 1:2 and 1:5 of HYOB and KET, respectively.

2.5. Procedures

2.5.1. Precipitation-based technique for the preparation of PVC-membrane sensor (sensors 1–3)

Ten millilitres of 10^{-2} M HYOB aqueous solution was mixed with 10 ml of a saturated aqueous solution of ammonium reineckate. The resulting precipitate was filtered, washed with cold water, allowed to dry at room temperature and grounded to fine powder. Elemental analysis for carbon, hydrogen and nitrogen were carried to study the formation of the complex.

In three glass Petri dishes (5 cm diameter), 10 mg of the previously prepared ion association complex were mixed thoroughly

with 0.35 ml of either dibutylsebathete (sensor 1) or dioctylphthalate (sensor 2) or nitrophenyl octyl ether (sensor 3) then add 0.19 g of poly(vinyl chloride) (PVC). These mixtures were dissolved in 5 ml tetrahydrofuran (THF). The dishes were covered with a filter paper and left to stand overnight to allow slow evaporation of the solvent at room temperature forming master membrane with 0.1 mm thickness [28].

Sensors were assembled using a disk of an appropriate diameter (about 8 mm) were cut from the previously prepared master membranes and cemented to the flat end of PVC tubing with THF. A mixed solution consisting of equal volumes of 10^{-2} M HYOB and 10^{-2} M sodium chloride was used as an internal reference solution. Ag/AgCl coated wire (3 mm diameter) was employed as an internal reference electrode. The sensors were conditioned by soaking for 24 h in a solution of 10^{-2} M of drug and stored in the same solution when not in use.

2.5.2. β-CD-based technique for the preparation of PVC-membrane sensor (sensor 4)

β-CD, 0.04 g, was mixed with 0.4 g of nitrophenyl octyl ether and with 0.01 g of ammonium reineckate. PVC, 0.18 g, previously dissolved in 6 ml THF was added and the procedures were completed as under Section 2.5.1 starting from "with a filter paper and leave to stand overnight...".

2.5.3. Study of the experimental conditions

2.5.3.1. Identification of slope, response time and lifetime of the studied electrodes.
The electrochemical performance characteristics of the four studied HYOB-selective electrodes (sensors 1–4) were evaluated according to IUPAC standards [28]. Sensors calibration was carried out by measuring the potential of 10^{-7}–10^{-2} M drug solutions starting from low to high concentrations. The potentials were plotted as a function of drug concentrations. Sensor life span was examined by repeated monitoring of the slope of the drug calibration curve periodically. The detection limit was taken at the point of intersection of the extrapolated linear segment of the drug calibration graph.

The dynamic response times of the electrodes were tested for the concentrations 10^{-6}–10^{-2} M HYOB solutions. The sequence of measurements was from low to high concentrations.

The time required for the electrodes to reach value within ± 2 mV from the final equilibrium potential after increasing HYOB concentration level by ten folds was measured.

2.5.3.2. Effect of pH on the electrode response.
The effect of pH on the potential values of the four electrode systems was studied over pH range of 1–12 at 1-pH interval by immersing electrodes in 10^{-3} and 10^{-4} M HYOB solutions. The pH was gradually increased or decreased by adding aliquots of diluted sodium hydroxide or hydrochloric acid solutions, respectively. The potential obtained at each pH was recorded.

2.5.3.3. Effect of foreign compounds on the electrode selectivity.
The response of the four studied electrodes was also examined in the presence of a number of other related substances. The potentiometric selectivity coefficients ($K_{\mathrm{HYOB,I}}^{\mathrm{Pot}}$) were evaluated according to IUPAC guidelines using the separate solutions

method [28,29] in which the potential of cell compromising the membrane electrode and a reference electrode is measured with two separate solutions, A and B where A (HYOB ions) and B (interfering ion) at the same activity aA = aB. Selectivity coefficients were calculated by the separate solutions method, where potentials were measured for 10^{-3} M HYOB solution and then for 10^{-3} M interfering solution, separately, then potentiometric selectivity coefficients were calculated using the following equation:

$$\log K_{\mathrm{A,B}}^{\mathrm{Pot}} = \frac{(\mathrm{EB} - \mathrm{EA})}{S} + \left(1 - \frac{\mathrm{ZA}}{\mathrm{ZB}}\right) \log \mathrm{aA}$$

where $K_{\mathrm{A,B}}^{\mathrm{Pot}}$ is the potentiometric selectivity coefficient, S the slope of the calibration plot, aA the activity of HYOB, and ZA and ZB are the charges on HYOB and the interfering ion, respectively.

2.5.4. Construction of calibration graphs for direct potentiometric determination of hyoscine butylbromide using the proposed sensors

The sensors were conditioned by soaking in 10^{-2} M HYOB solution for 24 h. Storage was in the same solution when not in use. The conditioned electrodes were immersed in conjunction with the single junction calomel reference electrode in solutions of HYOB in the range of 10^{-7}–10^{-2} M. They were allowed to equilibrate whilst stirring and recording the e.m.f. readings within ± 1 mV. The membrane sensors were washed between measurements with water. The mV–concentration profiles were plotted. The regression equations for the linear part of the curves were computed and used for subsequent determination of unknown concentrations of HYOB.

2.5.5. Application to laboratory prepared mixtures

The membrane sensor was immersed in conjunction with the single junction calomel reference electrode in the different laboratory prepared mixtures. The membrane sensor was washed with water between measurements. The e.m.f. produced for each mixture was measured by the four proposed electrodes then the concentration of HYOB was determined from the corresponding regression equation.

2.5.6. Application to pharmaceutical dosage form

The contents of six spasmofen ampoules were mixed. An amount of this solution equivalent to 22.02 mg HYOB was accurately transferred separately to a 50 ml volumetric flask and the volume was completed to the mark with phosphate buffer (pH 7 for sensors 1–3 and pH 8 for sensor 4) to prepare 10^{-3} M solution of HYOB. The e.m.f. produced by immersing the prepared electrodes in conjunction with single junction calomel reference electrode in the prepared solutions were determined then the concentration of HYOB was calculated from the regression equation of the corresponding electrode.

2.5.7. Application to plasma sample

4.5 ml plasma were placed into two stoppard shaking tubes, then 0.5 ml of 10^{-2} and 10^{-3} M HYOB were added separately

and shacked. Each membrane sensor was immersed in conjunction with the single junction calomel reference electrode in these solutions. The membrane sensor was washed with water between measurements. The e.m.f. produced for each solution was measured by the four proposed electrodes then the concentration of HYOB was determined from the corresponding regression equations.

3. Results and discussion

The development and application of ion-selective electrodes (ISEs) continue to be of interest for pharmaceutical analysis because these sensors offer the advantages of simple design and operation, fast response, reasonable selectivity, low detection limit, high accuracy, wide concentration range applicability to colored and turbid solutions, and possible interfacing with automated and computerized systems [29].

HYOB reacted with ammonium reineckate to form stable 1:1 water insoluble ion association complex, with low solubility product and suitable grain size precipitate, having the following suggested composition:
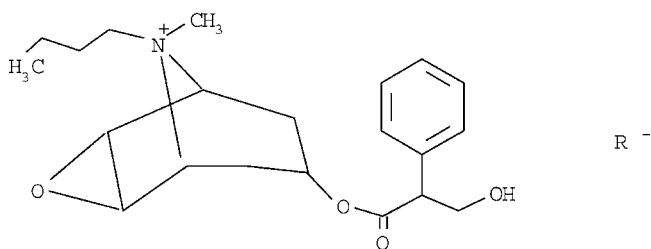
Sensor 1, 2 and 3

Sensor 4

This ratio was confirmed by the elemental analysis data (Table 1) and by the Nernestian response of the suggested sensors, which was about 60 mV; the typical value for monovalent drugs [28].

The introduction of high molecular PVC, as regular support matrix and traps for the sensed ions, creates a need for a plasticizer [30]. In the present investigation, dibutylsebathete

Table 1
Elemental analysis of hyoscine butylbromide–reineckate complex

Parameters	Analysis%		
	Carbon	Hydrogen	Nitrogen
Calculated%	44.19	5.30	14.43
Found%	45.21	5.88	13.97

*Calculated according to 1:1 ratio.

and dioctylphthalate were chosen from diesters of dicarboxylic acids and nitrophenyl octyl ether was chosen as an example of the nitroaromatic group. They gave responses similar to each other with no noise but the membrane with nitrophenyl octyl ether was more sensitive as calibration range from 10^{-6} to 10^{-2} M. With PVC, they plasticize the membrane, dissolve the ion association complex, and adjust both permittivity of the final organic membrane and mobility of the ion exchange sites. Such adjustments influence the partition coefficient of the studied drug with subsequent effect on electrode selectivity.

Cyclodextrins are optically active oligosaccharides that form inclusion compounds in the aqueous and in solid state with organic molecules. They were previously applied as sensor ionophores to potentiometric ISEs for the determination of protonated amines [31] and chiral molecules incorporating aryl rings [32]. β-CD-based sensors showed accurate results in both response and selectivity.

The electrochemical cell of the suggested membrane electrodes for the determination of HYOB can be illustrated diagrammatically as follows:

Electrochemical performance characteristics of the proposed sensors were evaluated according to the IUPAC recommendation data [28] (Table 2). It was found that the electrodes displayed constant and stable potential readings within 2 mV from day-to-day and the calibration slopes did not change by more than 2 mV per decade over a period of 1 month for the four sensors.

The response time of the electrodes were tested for concentrations of the drug from 10^{-6} to 10^{-2} M. The measurements

Table 2
Response characteristics of the four investigated hyoscine butylbromide electrodes

Parameter	Sensor 1	Sensor 2	Sensor 3	Sensor 4
Slope (mV/decade)	−53.19	−55.17	−51.44	−51.51
Intercept (mV)	209.89	201.62	204.74	148.34
Correlation coefficient	0.9992	0.9993	0.9992	0.9992
Detection limit [M]	4.5×10^{-6}	4.3×10^{-6}	5.2×10^{-7}	4.9×10^{-7}
Limit of quantitation (LOQ)	0.8×10^{-5}	0.7×10^{-5}	0.6×10^{-6}	0.9×10^{-6}
Response time (s)	20–30	20–30	20–30	20–30
Working pH range	6–8	6–8	6–8	7–9
Concentration range [M]	10^{-5}–10^{-2}	10^{-5}–10^{-2}	10^{-6}–10^{-2}	10^{-6}–10^{-2}
Life span (weeks)	6–8	6–8	5–6	5–6
Average recovery (%)	99.92	99.93	99.94	99.87
R.S.D.%[a]	1.11	1.00	1.18	1.39

[a] Results of four determinations.
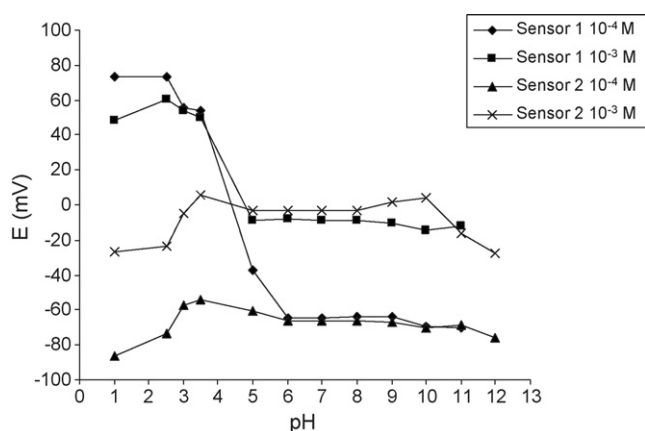
Fig. 2. Effect of pH on the response of sensors 1 and 2.

Fig. 4. Profile of the potential in mV to the −log concentration of sensors 1–4.

was characterized by a fast stable response within 20–30 s for concentrations less than 10^{-4} M and 10–20 s for concentrations more than 10^{-4} M.

The effect of pH on the electrode potential was investigated and it was found that the electrodes gave a stable potential over a pH range from 6 to 8 for sensors 1–3 and 7–9 for sensor 4 (Figs. 2 and 3). Above and below this pH range, the potentials displayed by the electrodes were noisy.
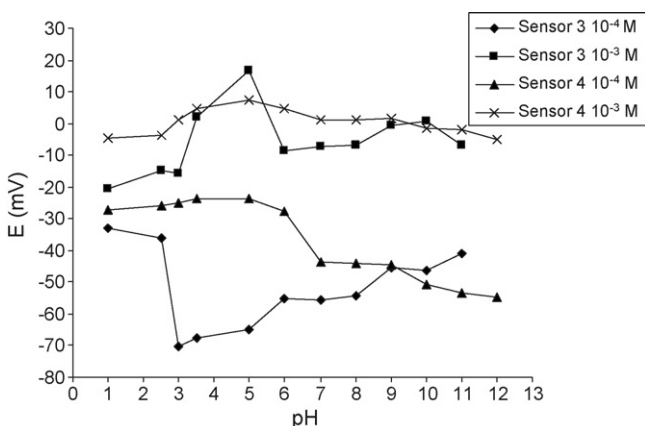

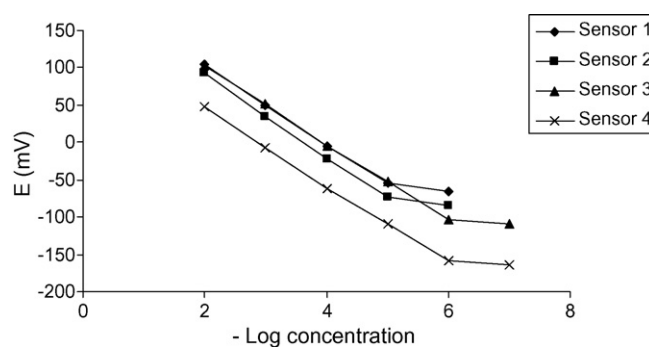Fig. 3. Effect of pH on the response of sensors 3 and 4.

The potentiometric response of the four studied electrodes at the optimum pH were linear with constant slopes over a drug concentration range of 10^{-5}–10^{-2} M for sensors 1 and 2 and in the concentration range of 10^{-6}–10^{-2} M for sensors 3 and 4 (Fig. 4).

The accuracy of the proposed membrane sensors for the quantification of blind samples of HYOB was assessed by using the four sensors. The results showed average recoveries of 99.92 ± 1.11, 99.93 ± 1.00, 99.94 ± 1.18 and 99.87 ± 1.39 for sensors 1–4, respectively.

The performance of the four electrodes in the presence of ketoprofen was assessed. Selectivity coefficient values ($K_{HYOB, I}^{Pot}$) were measured using a fixed concentration of the interfering (10^{-3} M). The results obtained by the developed sensors (Table 3) showed reasonable selectivity of the four sensors for HYOB in presence of ketoprofen.

HYOB was analyzed in different laboratory prepared mixtures with ketoprofen and good recoveries were obtained (Table 4).

Pharmaceutical additives such as argenine and citric acid did not show any interference. Thus, analysis was carried out without prior treatment or extraction. The four sensors were successfully used for the determination of HYOB in spasmofen ampoules (Table 5).

On application to the biological fluids, plasma electrolyte did not show any interference. It has been found that the four electrodes gave stable results as revealed by high precision and accuracy of recoveries of the spiked plasma samples (Table 6).

Table 3
Potentiometric selectivity coefficients ($K_{HYOB,I}^{Pot}$) for the four proposed electrodes

Interfering substance	Selectivity coefficient			
	Sensor 1	Sensor 2	Sensor 3	Sensor 4
Ketoprofen	1.82×10^{-3}	7.94×10^{-3}	2.81×10^{-3}	5.45×10^{-3}
Citric acid	3.64×10^{-3}	6.24×10^{-3}	4.57×10^{-3}	5.74×10^{-3}
Na^+	2.52×10^{-3}	7.19×10^{-3}	3.61×10^{-3}	6.43×10^{-3}
K^+	1.90×10^{-3}	5.02×10^{-3}	2.22×10^{-3}	5.52×10^{-3}
NH_4^+	1.70×10^{-3}	6.21×10^{-3}	2.28×10^{-3}	5.02×10^{-3}
Mg^{2+}	2.16×10^{-3}	9.20×10^{-3}	6.14×10^{-3}	5.90×10^{-3}
Ca^{2+}	3.50×10^{-3}	9.73×10^{-3}	5.92×10^{-3}	5.38×10^{-3}
Glucose	1.63×10^{-3}	6.28×10^{-3}	3.41×10^{-3}	4.99×10^{-3}
Lactose	1.62×10^{-3}	5.74×10^{-3}	3.16×10^{-3}	5.57×10^{-3}
Sucrose	1.67×10^{-3}	5.89×10^{-3}	3.25×10^{-3}	5.47×10^{-3}
Urea	1.52×10^{-3}	5.24×10^{-3}	2.68×10^{-3}	5.19×10^{-3}
L-Phenyl alanine	1.33×10^{-3}	4.89×10^{-3}	2.56×10^{-3}	4.68×10^{-3}
Argenine	3.24×10^{-3}	7.06×10^{-3}	4.21×10^{-3}	6.07×10^{-3}

Table 4
Analysis of hyoscine butylbromide in different laboratory prepared mixtures with ketoprofen by the four electrodes

Ratio of HYOB:KET	Recovery%[a] of hyoscine butylbromide			
	Sensor 1	Sensor 2	Sensor 3	Sensor 4
1:0.5	101.63	100.17	99.01	101.29
1:1	100.29	100.33	100.20	100.01
1:2	101.09	99.49	99.38	101.38
1:5	101.79	99.83	99.80	100.64
Mean ± S.D.%	101.20 ± 0.68	99.96 ± 0.37	99.60 ± 0.52	100.83 ± 0.64

[a] Average of four determinations.

Table 5
Determination of hyoscine butylbromide in spasmofen ampoules by the proposed four electrodes

Dosage form	Recovery%[a]			
	Sensor 1	Sensor 2	Sensor 3	Sensor 4
Spasmofen ampoules (batch no. 866926)	99.03 ± 0.28	98.66 ± 0.63	100.60 ± 0.61	100.23 ± 0.34

[a] Average of three determinations.

Table 6
Determination of hyoscine butylbromide in spiked human plasma by the proposed four electrodes

Concentration [M]	Recovery%[a]			
	Sensor 1	Sensor 2	Sensor 3	Sensor 4
1×10^{-3}	98.12 ± 2.13	101.01 ± 1.41	98.76 ± 1.56	98.61 ± 2.22
1×10^{-4}	101.14 ± 2.42	99.01 ± 1.12	100.97 ± 1.06	101.76 ± 1.86

[a] Average of three determinations.

Table 7
Statistical analysis of the results obtained by the proposed method and the manufacturer method [27] for the analysis of hyoscine butylbromide in pure powder form

Item	Sensor 1	Sensor 2	Sensor 3	Sensor 4	Manufacturer method [27]
Mean	99.92	99.93	99.94	99.87	100.28
R.S.D.	1.11	1.00	1.18	1.39	0.77
N	4	4	4	4	5
Variance	1.232	1.000	1.392	1.932	0.593
t-Test (2.365)[a]	0.576	0.596	0.524	0.566	–
F-Test (6.59)[a]	2.078	1.686	2.347	3.258	–

[a] The values between parenthesis are the corresponding theoretical values of t and F at the 95% confidence level.

Statistical evaluation of the results of analysis of pure HYOB by the proposed electrodes and the manufacturer method [27] showed that there is no significant difference between the proposed and reported method in terms of accuracy and precision (Table 7).

Validation of the proposed potentiometric methods for determining HYOB was made by measuring the range, lower limit of detection (LOD), lower limit of quantitation (LOQ), accuracy (recovery), trueness, precision, repeatability (inter- and intra-day variability) linearity and sensitivity (slope). Results obtained on four batches are depicted in Table 2.

4. Conclusion

The use of the proposed sensors offers the advantages of fast response, elimination of drug pretreatment or separation steps, low detection limit and direct determination of drugs in turbid and colored solutions. They can therefore be used for routine analysis of the HYOB in quality control laboratories.

References

[1] J. Crossland (Ed.), Lewis's Pharmacology, 5th ed., Churchill Livingstone Inc., New York, 1980, pp. 224–234.

[2] J. O' Neil Maryadele, Merck Index, 13th ed., Merck, Darmstadt, 2001, pp. 609, 610.

[3] British Pharmacopoeia, Her Majesty Stationary Office, London, 2001, pp. 882–883, 1102–1103.

[4] R.F. Falcao, M.J. Vianna, Rev. Port. Farm. 29 (1979) 201.

[5] N. Erk, F. Onur, Anal. Lett. 29 (1996) 369.

[6] N. Karali, S. Ozkirimli, A. Gursoy, IL Farmaco 53 (1998) 62.

[7] M.I. Toral, M.A. Munoz, S.L. Orellana, J. AOAC Int. 88 (2005) 1173.

[8] M.S. Mahrous, H.G. Daabees, Y.A. Beltagy, Spectrosc. Lett. 25 (1992) 389.

[9] P.B. Issopoulos, E.P. Zervou, IL Farmaco 49 (1994) 205.

[10] K.M. Thomos, D.A. Dabholkar, C.L. Jain, Indian Drugs 31 (1994) 391.

[11] A.M. Taha, M.A. Abdelkader, S. Abdelfattah, Pharmazie 35 (1980) 93.

[12] T. Altinkurt, Eczacilik Bull. 24 (1982) 9.

[13] K.C. Guven, T. Altinkurt, U. Terzioglu, Eczacilik Bull. 21 (1979) 29.

[14] T. Altinkurt, K.C. Guven, U. Terzioglu, Eczacilik Bull. 21 (1979) 46.

[15] I. Papadoyannis, A. Zotou, V. Samanidou, M. Georgarakis, Instrum. Sci. Technol. 22 (1994) 83.

[16] M. Parissi-Poulou, I. Panderi, J. Liq. Chromatogr. Relat. Technol. 22 (1999) 1055.

[17] Y. Nakagawa, T. Shimazu, Y. Ishii, M. Ishibashi, Y. Hashimoto, J. Mass Spectrom. Soc. Jpn. 48 (2000) 42.

[18] T.T. Wang, R. Zhu, Yaowu Fenxi Zazhi 20 (2000) 392.

[19] S. Cherkaoui, L. Mateus, P. Christen, J.-L. Veuthey, J. Pharm. Biomed. Anal. 21 (1999) 165.

[20] Y.S. Chang, Y.R. Ku, K.C. Wen, L.K. Ho, J. Liq. Chromatogr. Relat. Technol. 23 (2000) 2009.

[21] M.S. Ionescu, D. Negoiu, V.V. Cosofret, Anal. Lett. 16 (1983) 553.

[22] N. Buschmann, Fresen. Z. Anal. Chem. 326 (1987) 123.

[23] B. Li, Z. Zhang, X. You, T. Lu, G. Yin, Analyst 113 (1988) 57.

[24] M.R. Ganjali, M. Tahami, T. Poursaberi, A.R. Pazoukian, M. Javanbakht, M. Shamsipur, M.R. Baezat, Anal. Lett. 36 (2003) 347.

[25] M.R. Ganjali, P. Norouzi, M. Golmohammadi, M. Rezapour, M. Salavati-Niasari, J. Electroanal. 16 (2004) 910.

[26] British Pharmacopoeia, Her Majesty Stationary Office, London, 2001 (Appendix 1D A119).

[27] Direct spectrophotometry and HPLC manufacturer procedure (Amriya Pharm. Ind., Alexandria, Egypt), personal communication.

[28] IUPAC, Pure Appl. Chem. 72 (2000) 1852.

[29] T.S. Ma, S.S.M. Hassan, Organic Analysis using Ion Selective Electrodes, vols. 1 and 2, Academic Press, London, 1982.

[30] J. Zyka, Instrumentation in Analytical Chemistry, vol. 2, Ellis Horwood, Chichester, UK, 1994.

[31] J. Lima, M. Montenegro, Mikrochim. Acta 131 (1999) 187.

[32] J. Lima, M. Montenegro, A. Silva, J. Pharm. Biomed. Anal. 8 (1990) 701.

Determination of pK_a values of some hydroxylated benzoic acids in methanol–water binary mixtures by LC methodology and potentiometry

F.Z. Erdemgil [a], S. Şanli [b], N. Şanli [b], G. Özkan [b],
J. Barbosa [c], J. Guiteras [c], J.L. Beltrán [c,*]

[a] *Anadolu University, BIBAM, 26470 Eskişehir, Turkey*
[b] *Department of Chemistry, Faculty of Science and Literature, Süleyman Demirel, University, 32260 Isparta, Turkey*
[c] *Department of Analytical Chemistry, Barcelona University, Diagonal 647, 08028 Barcelona, Spain*

Abstract

An accurate estimation of pK_a values in methanol–water binary mixtures is very important for several separation techniques such as liquid chromatography and capillary electrophoresis that use these solvent mixtures. In this study, the pK_a values of 11 polyphenolic acids have been determined in methanol–water binary mixtures (10%, 20% and 30% (v/v)) by potentiometry, liquid chromatography (LC) and LC-DAD methodology.

The results show a similar trend for the pK_a values of all the studied compounds, as they increase with increasing concentration of organic modifier, which allows a linear relationship between pK_a values and mole fraction of methanol to be obtained. The pK_a values obtained in aqueous medium have been compared with those given in the literature, and also with the values predicted by the SPARC on-line pK_a calculator. The data obtained have been used to test the feasibility of an estimation of dissociation constants in a methanol–water medium from the relationship between pK_a values and the organic cosolvent fraction in the mixtures.
© 2006 Elsevier B.V. All rights reserved.

Keywords: Dissociation constants; Polyphenolic acids; Methanol–water mixtures; Liquid chromatography

1. Introduction

The ionization constant is an important physico-chemical parameter of a substance, and the knowledge of this parameter is of fundamental importance in a wide range of applications and research areas. The chromatographic retention and electrophoretic behavior of ionizable compounds strongly depend on the pK_a of the compound and the mobile phase pH. A satisfactory knowledge of the acid–base behavior of substances in hydro-organic media such as methanol–water is therefore essential to predict the influence of pH on selectivity and on retention in liquid chromatography (LC) and also to optimize analytical procedures for the separation of ionizable compounds by different techniques [1–3].

There are several methods for the determination of dissociation constants. Traditionally, potentiometry and UV–vis

absorption spectrometry have been the most useful techniques for the determination of equilibrium constants [4,5], because of their accuracy and reproducibility. Moreover, the use of computer programs for the refinement of equilibrium constants allows the different pK_a values in polyprotic substances to be determined, even when they are very close [6–8].

In the last decade, some alternative techniques, based on separation methods such as liquid chromatography (LC) [9] and capillary zone electrophoresis (CZE) [10], have been developed. The last, based on the dependence of electrophoretic mobility with respect to the pH of the electrophoretic buffer, provides fast and accurate pK_a determination in a wide pH range for mono- and polyprotic substances.

The determination of pK_a values by liquid chromatography is based on the relationships between the capacity factors and the pH values of the mobile phase [11,12]. This procedure is limited by the working pH range of the LC column, the optimum conditions being when the pK_a corresponds to the equilibrium between a neutral species and a charged species (this is, $H_2A^+ \leftrightarrow HA$, $HA \leftrightarrow A^-$, or $B \leftrightarrow HB^+$), but as the main

objective of pK_a determination by LC is the optimization of chromatographic separations, this method is perfectly adequate for its purpose.

In recent years, a new procedure has been developed when LC and CZE methodologies are used for pK_a determination in combination with a diode array detector (DAD) for absorbance measurements [13–15]. In these cases, the pK_a values can be determined from the absorbance spectra obtained at the maxima of the chromatographic or electrophoretic peaks. In this way, pK_a values can be obtained from two independent methods: mobility/pH data and spectra/pH data in CZE procedures (CZE-DAD), and capacity factor/pH data and spectra/pH data in LC procedures (LC-DAD).

Polyphenolic compounds include a large range of bioactive substances occurring widely in plants. Many phenolic compounds are good sources of natural antioxidants, and there is a growing interest in the characteristics and behavior of this kind of compounds, because some of them have inhibitory effects on mutagenesis and carcinogenesis [16]. The determination of these compounds in matrices such as fruits and plants is carried out by means of chromatographic (LC) or electrophoretic separations [17–20], using different detection systems, mainly UV–vis absorption or mass spectrometry. Although most liquid chromatography separation procedures are based on reversed phase columns and water–methanol or water–acetonitrile mobile phases [20], the dissociation constants of phenolic acids have been determined mainly in water and water–acetonitrile mixtures [12,15].

In order to overcome the lack of information related with the acid–base equilibria of this kind of compounds in water–methanol medium, the pK_a values of some hydroxybenzoic and hydroxycinnamic acids in water and methanol–water binary mixtures have been determined by means of potentiometric and chromatographic (LC and LC-DAD) measurements. For practical reasons, the potentiometric determinations were carried out at 0%, 10%, and 20% methanol content (v/v), whereas the chromatographic determinations of pK_a were at 10%, 20%, and 30% methanol content (v/v). The pK_a values obtained will be useful for the development and optimization of separation methods of phenolic acids based on liquid chromatography in methanol–water mixtures. Additionally, some attempts have been made to try and predict pK_a values in the different water–methanol mixtures from the values obtained in aqueous medium.

The results obtained for pK_a in water have been compared with those predicted by the SPARC on-line Calculator [21]. This program estimates several physico-chemical properties of organic compounds on the basis of their molecular structure. One of these properties is the dissociation constant: the pK_a value of an acid group in a molecule is estimated as the sum of two terms, the first corresponding to the pK_a of the acid group or reaction center C (pK_a)$_C$, and the second indicates the change in the ionization behavior as consequence of a perturber structure P, δ_P(pK_a)$_C$, meaning any molecular structure appended to C:

$$pK_a = (pK_a)_C + \delta_P(pK_a)_C = (pK_a)_C + \delta_{RES}(pK_a)_C$$

$$+ \delta_{ELE}(pK_a)_C + \delta_{SOLV}(pK_a)_C + \delta_{H\text{-}BOND}(pK_a)_C \quad (1)$$
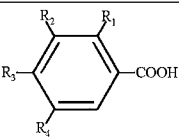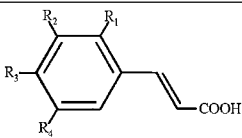

Fig. 1. Structures of the phenolic acids studied.

The second term is factored into mechanistic components, describing the differential resonance, electrostatic, solvation and hydrogen bonding of P with the protonated and unprotonated states of C, respectively. This approach has been rigorously tested by the comparison between the experimental and estimated pK_a of more than 4300 ionization constants [22].

The phenolic compounds selected for this study are seven hydroxybenzoic acids (gallic, protocatechuic, gentisic, *p*-hydroxybenzoic, vanillic, isovanillic and syringic) and four hydroxycinnamic acids (caffeic, *p*-coumaric, ferulic and sinapinic). Their structures are shown in Fig. 1.

2. Experimental

2.1. Chemicals and reagents

Analytical reagent grade chemicals were used, unless otherwise stated. Phenolic acids were purchased from Sigma and used without further purification. Water, with conductivity lower than 0.05 μS cm^{-1}, was obtained with a Milli-Q water purification system (Millipore Corp.).

Methanol was of HPLC grade. Potassium hydrogen phthalate (dried at 110 °C before use, Fluka), sodium hydroxide, hydrochloric acid, potassium bromide, formic acid and diethylmalonic acid were supplied by Merck.

Potassium hydroxide and potassium chloride were also purchased from Merck and used in potentiometric studies. Potassium hydroxide solutions (0.025 mol L^{-1}) were prepared in each methanol–water mixtures by suitable dilution of a 1.000 mol L^{-1} Merck Titrisol. Hydrochloric acid solutions were also prepared in each methanol–water mixtures by dilution of a 1.000 mol L^{-1} Merck Titrisol. The ionic strength was adjusted to 0.1 mol L^{-1} with potassium chloride.

2.2. Apparatus

In the potentiometric titrations for the determination of pK_a values, emf was measured with a precision of ± 0.1 mV, using a Mettler-Toledo MA 235 pH/ion analyzer equipped with a Hanna HI 1332 combination glass electrode. All titrations were carried out in a double-walled cell, externally thermostatted at $25.0 \pm 0.1\,^\circ C$ with a cooling system consisting of a HETO CBN 8-30 water bath and a HETO HMT 200 temperature control unit. Test solutions were magnetically stirred under a continuous stream of pure nitrogen (chromatography grade).

The chromatographic system consisted of a Shimadzu LC 10 ADVP pump, a SIL 10 ADVP auto injector and a SPD-M10A DAD diode array detector system; it also included a CTO 10 AVP column oven and a DGU 14 A degasser system. A Thermo ODS Hypersil RP C-18 column (250 mm × 4,6 mm i.d., 5 μm) was used throughout and all separations were carried out at 25 °C.

2.3. Procedures

2.3.1. Potentiometric method

The standardization of the electrode system in methanol–water mixtures was carried out by the Gran's method [23]. For the determination of the cell standard potential (E^0), the electrode was immersed in the methanol–water mixture (20 mL and 0.1 mol L^{-1} ionic strength), and then 0.1 mol L^{-1} hydrochloric acid was added to this solution; about 10 or 12 titration points of this solution were enough for an accurate determination of the cell E^0. A suitable amount of a polyphenolic acid was then added to obtain an approximate concentration of 0.003 mol L^{-1}, and the final solution was titrated with a strong base (KOH) at the same ionic strength and solvent composition.

The data pairs (emf/titrant volume) thus obtained were processed by the program PKPOT [7] to determine the pK_a values. This program refines the thermodynamic equilibrium constants in order to minimize the sum of squared differences (U_{emf}) between the experimental e.m.f. values and those calculated on the basis of the mass balances for hydrogen and polyphenolic acid, the equilibrium constants, the cell standard potential and the activity coefficients:

$$U_{emf} = \sum_i^m \sum_j^n (emf_{i,j,exp} - emf_{i,j,calc})^2 \tag{2}$$

where m is the number of titrations and n the number of experimental points in each titration.

2.3.2. Chromatographic method

Stock standard solutions of the different phenolic acids to be tested were prepared in water at 200 mg L^{-1} concentration and stored in a deep freezer. Working solutions (20 mg L^{-1}) were obtained by suitable dilution of stock standard solutions with the corresponding mobile phase and stored at 4 °C in the dark.

The flow rate was maintained at 1 mL min^{-1}. Throughout this study, the mobile phases assayed were methanol–water at 10%, 20% and 30% (v/v), containing 0.1% (w/v) formic or diethyl-
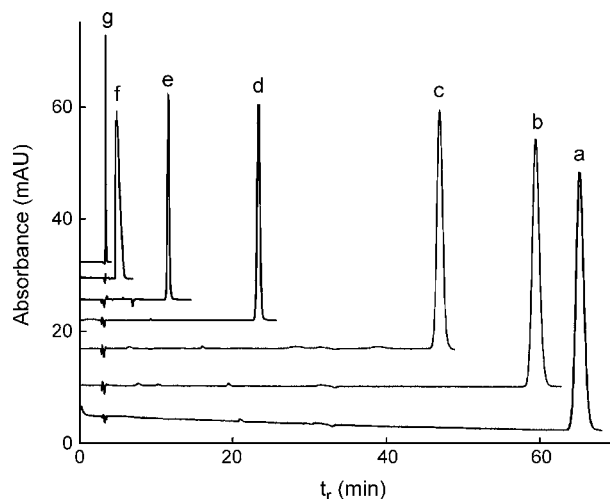

Fig. 2. Chromatograms of syringic acid in 10% methanol (v/v) obtained at the pH values: (a) 3.0; (b) 3.5; (c) 4.1; (d) 4.5; (e) 5.1; (f) 6.1; (g) 7.1. Absorbance is measured at 280 nm.

malonic acid. The pH of the mobile phase was adjusted between 2.75 and 7.00 by the addition of sodium hydroxide. For gentisic acid, pH 2.45 was also investigated.

In general, for each methanol content the chromatographic retention was studied from acid to neutral pH. The column was pre-conditioned during at least 1 h at low flow-rate (0.4 mL min^{-1}) with mobile phase at the corresponding pH before the first injection.

The pH of the mobile phase (pH_x) was determined in accordance with the IUPAC commendations [24,25], by comparison between the measured electromotive forces E_X and E_S of the mobile phase and a standard reference solution of known pH, respectively. Thus, the pH is determined from:

$$pH_X = pH_S - \frac{E_X - E_S}{g} \tag{3}$$

where g is the Nernst coefficient of the potentiometric cell ($g = (\ln 10)RT/F$). In our case, the operational pH scale has been established using potassium hydrogen phthalate (0.05 mol kg^{-1}) as standard reference solution, as its corresponding pH_s values in the appropriate methanol content are already known [26].

For each polyphenolic compound, mobile phase composition and pH, the retention time values, t_R, were determined from three replicate injections. An example is given in Fig. 2, in which the chromatograms of syringic acid obtained at 10% methanol and different pH values are plotted. The changes in the retention times at the different pH values are clearly shown, the higher value corresponding to acidic medium, where the neutral species (H_2A) of syringic acid predominates; the lower retention time, close to hold-up time, corresponds to pH 7.1, where the predominant form is the anionic species (HA^-).

Capacity factors (or retention factors) were calculated as

$$k' = \frac{t_R - t_M}{t_M} \tag{4}$$

where t_M indicates the retention time of potassium bromide (hold-up time), which was measured by injection of a 0.01%

potassium bromide solution in water for each mobile phase composition and pH studied.

In the study of dissociation equilibria by reversed phase liquid chromatography, the compounds under study can be considered to be monoprotic acids throughout the working pH range. The observed retention factors at different pH values can thus be described [12] as a function of the retention factors of the neutral and anionic species (k'_{HA} and k'_{A^-}) and their corresponding mole fractions (χ_{HA} and χ_{A^-}):

$$k' = k'_{HA}\chi_{HA} + k'_{A^-}\chi_{A^-} \tag{5}$$

The mole fractions can be expressed as function of the dissociation constants, the hydrogen ion activity and the activity coefficient, and Eq. (5) can be rewritten as

$$k' = k'_{HA}\frac{a_{H^+}\gamma_{H^+}}{K_a + a_{H^+}\gamma_{H^+}} + k'_{A^-}\frac{K_a}{K_a + a_{H^+}\gamma_{H^+}}$$
$$= \frac{k'_{HA}a_{H^+}\gamma_{H^+} + k'_{A^-}K_a}{K_a + a_{H^+}\gamma_{H^+}} \tag{6}$$

The pK_a values associated with the carboxylic acid function were first determined from k'/pH data pairs by means of the non-linear regression program NLREG [27]. This is a general-purpose program, where the function to be minimized and the parameters to be estimated can be defined by means of the built-in program editor. In our case, the input data include the experimental retention factors (k'_{exp}), the measured pH and the calculated activity coefficients, whereas the dissociation constants and the retention factors of the neutral and anionic species are treated as parameters to be optimized. Starting values for these parameters must be also included. The activity coefficients were calculated by the Debye–Hüquel equation, in which the A and a_0B values for each methanol content were taken from Ref. [28]:

$$-\log \gamma = \frac{Az^2\sqrt{I}}{1 + a_0B\sqrt{I}} \tag{7}$$

The ionic strength (I) was determined from the amount of sodium hydroxide added to obtain the desired pH of the mobile phase, and from the dissociation constant of the buffer in the more acidic solutions (corresponding to formic acid buffers).

In this way, NLREG refines the parameters until a minimum in the function $U_{k'}$ (defined as the sum of squared differences between the experimental and calculated capacity factors) is reached:

$$U_{k'} = \sum_{i=1}^{p}(k'_{i,exp} - k'_{i,calc})^2 \tag{8}$$

where p is the number of data points, and $k'_{i,exp}$ and $k'_{i,calc}$ the experimental and calculated capacity factors for each data point, respectively. The calculated values are obtained from equation (6). In Fig. 3, the experimental data pairs k'/pH for some of the phenolic compounds studied (in 20% (v/v) methanol–water) are shown, together with the corresponding calculated from the refined parameters pK_a, k'_{HA} and k'_{A^-}.

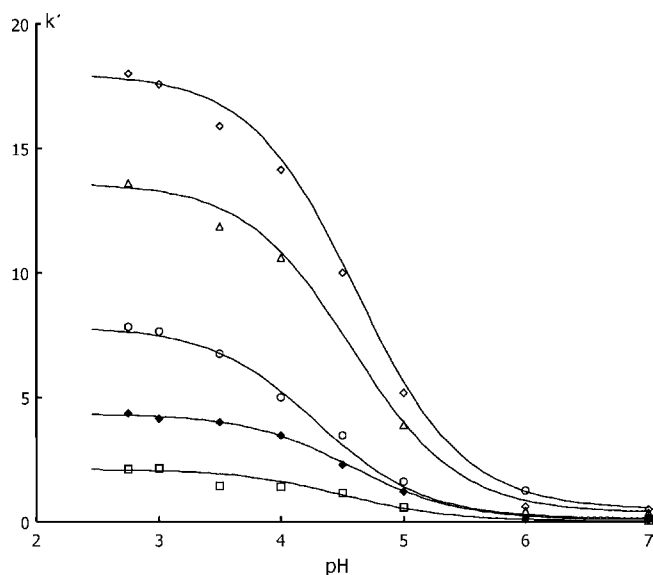
Fig. 3. Plot of capacity factors against the pH of the mobile phase (20% methanol–water v/v). Symbols indicate: (◇) ferulic acid; (△) coumaric acid; (◯) syringic acid; (◆) *p*-hydroxybenzoic acid; (□) protocatechuic acid. Lines indicate the calculated retention factors.

Independent determinations of the corresponding pK_a values were also obtained from the absorbance spectra recorded between 190 and 800 nm at the maximum of the chromatographic peaks; the acquired data (absorbance spectra and pH) were processed with the program STAR [13,15,29]. This is a non-linear regression program specifically developed for the study of complex equilibria from spectrometric data. It can be applied to complex systems, including acid–base and complex formation equilibria, described by experimental data containing until 150 spectra, measured at 50 wavelengths.

The program refines the equilibrium constants, using the Gauss–Newton algorithm, until a minimum value in the sum of the squared differences between the experimental and calculated absorbance values for each spectra and wavelength (U_{abs}) is obtained:

$$U_{abs} = \sum_{i=1}^{ns}\sum_{i=1}^{nw}(A_{i,j,exp} - A_{i,j,calc})^2 \tag{9}$$

where ns and nw indicate the number of spectra and wavelengths, respectively. $A_{i,j,exp}$ and $A_{i,j,calc}$ are the experimental and calculated absorbance values for the wavelength j in the spectrum i. The calculated absorbances are obtained in three steps: the program first solves the mass balances for each spectrum according to the guessed equilibrium constants and experimental conditions (using a procedure similar to that in PKPOT program); then, a multiple linear regression procedure is applied in order to determine the molar absorbances of each unknown species, and finally the individual absorbance values are re-calculated from the guessed species concentration and the corresponding molar absorbances.

The comparison between pK_a values obtained from retention and absorbance allows a better understanding of dissociation equilibria to be reached, with the additional advantage that both
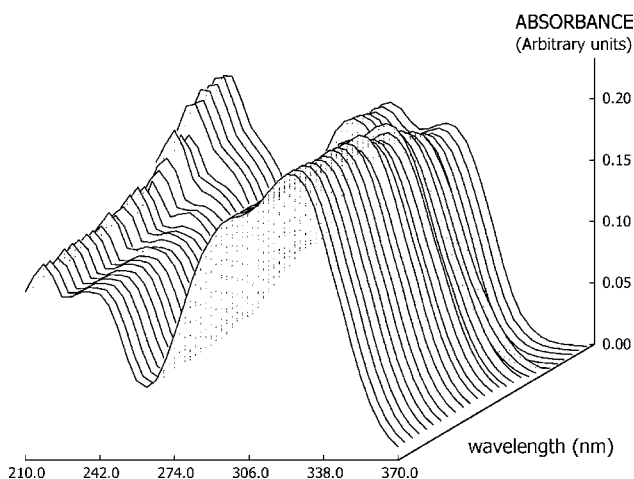
Fig. 4. Absorption spectra of caffeic acid, in 30% (v/v) methanol–water, obtained from the maxima of the chromatographic peaks at different pH values of the mobile phase.

kinds of data can be obtained in the same experimental run. The spectral data corresponding to the pK_a determination of caffeic acid in 30% methanol–water are presented in Fig. 4.

3. Results and discussion

The results obtained by the different methodologies, together with literature data and the values predicted by SPARC, are summarized in Table 1. The values obtained in this work by potentiometry, LC and LC-DAD for the first pK_a (attributed to the carboxylic group) are in good agreement, as the differences are usually lower than 0.2 pK_a units.

However, we must take into account that the potentiometric methodology gives better accuracy and precision than any of the other two methods used. This is due, mainly, to the fact that the electrode system is calibrated before each potentiometric titration [23], and the electrode remains into the solution during all the titration, so that the calibration parameters are the same for all titration data corresponding to the same experimental run. By comparison, in LC methodology the pH of the mobile phase is measured against the pH of a standard; the drawback of this procedure is the possibility of small changes in the electrode response every time it is immersed in a different solution. Moreover, small errors in the preparation of the standard will be noted as systematic deviations. Additionally, the retention factors (k') used to estimate the pK_a are derived from the retention time of the solute and the hold-up time, giving lower precision. The LC-DAD procedure does not use retention factors; instead of them it uses the spectra measured by the diode-array detector, but the procedure will be affected by the errors in the pH measurement.

A further comparison between the pK_a values obtained in this work in aqueous medium and those given in the literature (where available) and predicted by SPARC shows that the values corresponding to the first pK_a are generally in good agreement. The remarkably good results obtained by SPARC should be mentioned, because, except in the case of syringic acid, predicted values are within 0.2 pK_a units from real experimental values.

Results are not so good for the dissociation constants of the phenolic groups (pK_{a2} and pK_{a3}), as the differences between the results obtained in this work and those available in the literature or predicted by SPARC are higher, particularly for pK_{a3}, in which case they may exceed one pK_a unit.

The influence of methanol on the dissociation constants was as expected: pK_a values increase with increasing percentage of organic cosolvent. Although the variations of the physico-chemical properties of solutes in mixed solvents can be described by the Kamlet–Taft solvatochromic parameters [30] or the Dimroth–Reichardt E_T polarity parameter [31], it has been found that in several water–organic cosolvent mixtures, such as acetonitrile–water [32] (up to 70% acetonitrile) or methanol–water (up to 50% methanol) [33,34], pK_a values of a given substance show a linear relationship with the mole fraction of organic cosolvent. This is indicated by the following expression:

$$pK_{a,\varphi} = pK_{a,w} + \varphi \Delta_{pK} \tag{10}$$

where $pK_{a,w}$ indicates the dissociation constant in water, φ the mole fraction of organic cosolvent, Δ_{pK} the slope of the linear relationship, and $pK_{a,\varphi}$ the pK_a at the corresponding composition.

This equation was only applied to pK_{a1} and pK_{a2} values obtained by potentiometry, because of the higher precision of the methodology, although the maximum possible methanol proportion was limited to 20% (about 0.1 mole fraction). Regression results are listed in Table 2, where intercept (corresponding to $pK_{a,w}$), slope (Δ_{pK}) and correlation coefficient are given. These results indicate that, in general, the assumption of a linear relationship between pK_a and mole fraction of organic cosolvent is a good approximation within this interval.

The mean slope of pK_{a1} values listed in Table 2 was 2.92, with a relative standard deviation s_R (%) = 29.7%. This was in good agreement with available data for other carboxylic acids in different methanol–water mixtures (including formic, acetic, propionic, butyric, benzoic, and the first pK_a of citric and phtalic) [33,34], which gave a mean value $\Delta_{pK} = 2.78$ (s_R (%) = 19.6%), showing a similar behavior against increasing methanol content. In the case of pK_{a2}, the slopes for polyphenolic acids were higher (as was to be expected) and with higher dispersion (mean slope is 4.51, s_R (%) = 52.3%).

As was mentioned in the introduction, the knowledge of the dissociation constants of ionizable compounds in different water–organic cosolvent mixtures is a valuable tool in the development of separation methods based on reversed phase liquid chromatography, but, as the number of compounds to be separated increases, the determination of such pK_a values become, in the best of cases, a long and tedious work. However, an exact pK_a value is not usually required: in most cases, an approximated value is enough for a substantial reduction of the experimental work required to develop a good separation method. For this reason, linear extrapolation from the pK_a value in water is a simple and straightforward procedure to estimate pK_a in methanol–water mixtures, and the more so as, usually, only pK_{a1} value is of importance in liquid chromatography separations.

Table 1
Summary of the pK_a values for the phenolic acids studied (the estimated standard deviations are given in parentheses)

Compound	pK_a number	SPARC[a] prediction	Method	Literature values	Methanol content (% v/v)[b]			
					0	10	20	30
Gallic acid	1	4.09	Potentiometry	4.26[c]	4.24 (0.04)	4.48 (0.03)	4.72 (0.08)	–
	2	7.3		8.70[c]	8.27 (0.06)	8.67 (0.01)	8.81 (0.07)	–
	3	12.17		11.45[c]	9.23 (0.20)	9.94 (0.03)	10.15 (0.05)	–
	1		LC	–	–	4.56 (0.06)	4.41 (0.08)	4.79 (0.18)
	1		LC-DAD	–	–	4.18 (0.06)	4.57 (0.03)	4.48 (0.03)
Protocatechuic acid	1	4.19	Potentiometry	4.35[d]	4.38 (0.02)	4.44 (0.04)	4.72 (0.06)	–
	2	7.86		8.79[d]	8.74 (0.05)	8.86 (0.03)	9.13 (0.05)	–
	3	13.22		13.00[d]	10.67 (0.03)	11.05 (0.03)	10.86 (0.05)	–
	1		Spectrometry	4.26[c]				
	2			8.64[c]				
	1		LC		–	4.50 (0.03)	4.51 (0.16)	4.91 (0.10)
	1		LC-DAD		–	4.25 (0.04)	4.63 (0.03)	4.98 (0.02)
Gentisic acid	1	2.98	Potentiometry		2.77 (0.04)	2.89 (0.03)	2.98 (0.03)	–
	2	10.29			10.01 (0.05)	10.07 (0.02)	10.48 (0.02)	–
	3				10.80 (0.17)	10.79 (0.02)	10.94 (0.06)	–
	1		LC		–	2.75 (0.13)	2.77 (0.10)	3.36 (0.09)
	1		LC-DAD		–	2.82 (0.03)	2.83 (0.11)	2.95 (0.11)
p-Hydroxybenzoic acid	1	4.3	Potentiometry	4.58[d], 4.47[e]	4.38 (0.02)	4.50 (0.01)	4.66 (0.01)	–
	2	8.68		9.49[d], 9.06[e]	8.97 (0.01)	8.97 (0.01)	9.16 (0.01)	–
	1		LC		–	4.50 (0.07)	4.58 (0.08)	4.60 (0.09)
	1		LC-DAD		–	4.49 (0.08)	4.58 (0.04)	5.00 (0.02)
Vanillic acid	1	4.08	Potentiometry		4.31 (0.03)	4.36 (0.01)	4.56 (0.01)	–
	2	8.54			8.81 (0.08)	9.07 (0.01)	9.25 (0.01)	–
	1		Spectrometry	4.16[f]				
	2			8.96[f]				
	1		LC		–	4.40 (0.04)	4.44 (0.06)	4.64 (0.07)
	1		LC-DAD		–	4.44 (0.08)	4.85 (0.04)	4.90 (0.01)
Isovanillic acid	1	4.33	Potentiometry		4.24 (0.08)	4.50 (0.04)	4.57 (0.02)	–
	2	9.9			9.58 (0.09)	9.47 (0.03)	9.90 (0.01)	–
	1		LC		–	4.36 (0.05)	4.47 (0.04)	4.65 (0.13)
	1		LC-DAD		–	4.40 (0.12)	4.50 (0.07)	4.82 (0.02)
Syringic acid	1	3.86	Potentiometry		4.20 (0.06)	4.30 (0.01)	4.47 (0.02)	–
	2	7.76			9.00 (0.08)	9.10 (0.01)	9.34 (0.01)	–
	1		LC		–	4.27 (0.04)	4.30 (0.06)	4.68 (0.05)
	1		LC-DAD		–	4.28 (0.09)	4.33 (0.02)	4.68 (0.02)
Caffeic acid	1	4.3	Potentiometry	4.43[g]	4.47 (0.04)	4.60 (0.13)	4.86 (0.15)	–
	2	8.14		8.69[g]	8.32 (0.01)	8.41 (0.09)	8.87 (0.12)	–
	3	13.16						
	1		LC		–	Not eluted	4.64 (0.06)	4.72 (0.10)
	1		LC-DAD		–	Not eluted	4.66 (0.04)	4.85 (0.01)
p-Coumaric acid	1	4.32	Potentiometry		4.39 (0.04)	4.49 (0.01)	4.62 (0.08)	–
	2	8.97			8.37 (0.02)	9.13 (0.05)	9.45 (0.13)	–
	1		Spectrometry	4.36[f]				
	2			8.98[f]				
	1		LC		–	Not eluted	4.58 (0.11)	4.55 (0.10)
	1		LC-DAD		–	Not eluted	4.57 (0.08)	4.70 (0.05)
Ferulic acid	1	4.27	Potentiometry	4.52[d]	4.56 (0.05)	4.60 (0.10)	4.78 (0.02)	–
	2	8.83		9.39[d]	8.65 (0.02)	8.74 (0.10)	8.89 (0.06)	–

Table 1 (*Continued*)

Compound	pK_a number	SPARC[a] prediction	Method	Literature values	Methanol content (% v/v)[b]			
					0	10	20	30
	1		LC		–	Not eluted	4.62 (0.01)	4.55 (0.03)
	1		LC-DAD		–	Not eluted	4.60 (0.04)	4.81 (0.02)
Sinapinic acid	1	4.21	Potentiometry	4.47[h]	4.40 (0.10)	4.50 (0.03)	4.60 (0.08)	–
	2	8.04		9.21[h]	9.21 (0.08)	9.35 (0.08)	9.58 (0.06)	–
	1		Spectrometry	4.19[f]				
	2			9.40[f]				
	1		LC		–	Not eluted	4.57 (0.04)	4.44 (0.06)
	1		LC-DAD		–	Not eluted	4.57 (0.08)	4.71 (0.03)

[a] Ref. [21].
[b] This work.
[c] Ref. [35].
[d] Ref. [36].
[e] Ref. [37].
[f] Ref. [15].
[g] Ref. [38].
[h] Ref. [39].

Table 2
Linear relationships between pK_{a1} and pK_{a2} of polyphenols and the mole fraction of methanol in methanol–water media (from potentiometric data, methanol content between 0 and 20% (v/v))

Compound	pK_{a1}			pK_{a2}		
	Intercept	Slope	Correlation coefficient	Intercept	Slope	Correlation coefficient
Gallic acid	4.24	4.81	0.999	8.32	5.36	0.954
Protocatechuic acid	4.34	3.45	0.948	8.72	3.93	0.983
Gentisic acid	2.78	2.10	0.993	9.95	4.77	0.932
p-Hydroxybenzoic acid	4.38	2.81	0.999	8.94	1.94	0.883
Vanillic acid	4.29	2.53	0.955	8.83	4.39	0.990
Isovanillic acid	4.28	3.27	0.938	9.49	3.31	0.740
Syringic acid	4.19	2.72	0.993	8.98	3.43	0.980
Caffeic acid	4.45	3.93	0.988	8.26	5.58	0.944
p-Coumaric acid	4.39	2.31	0.999	8.46	10.73	0.965
Ferulic acid	4.54	2.23	0.950	8.64	2.41	0.994
Sinapinic acid	4.40	2.00	0.999	9.20	3.72	0.994

Two different procedures have been used for this extrapolation, both based in the mean value of Δ_{pK} obtained for several carboxylic acids in methanol–water mixtures [33,34] (which means that the Δ_{pK} corresponding to phenolic acids are not used), one of them makes use of $pK_{a,w}$ of phenolic acids determined in this work, while the other uses the values predicted by the SPARC on-line pK_a calculator [21]; this latter is of particular interest, as in this case no experimental work is required to reach an estimation of pK_a values in methanol–water mixtures.

The validity of the predictions offered by both procedures is measured by the root-mean-squared error (RMSE) and the percentage of relative root-mean-squared error (RRMSE%):

$$RSME = \sqrt{\frac{\sum_{i=1}^{n}(pK_{a,exp,i} - pK_{a,calc,i})^2}{n}} \qquad (11)$$

$$RRMSE\% = \sqrt{\frac{\sum_{i=1}^{n}(pK_{a,exp,i} - pK_{a,calc,i})^2}{\sum_{i=1}^{n}pK_{a,exp,i}^2}} \qquad (12)$$

where n indicates the number of pK_a values in each case.

Table 3
Errors in the pK_{a1} estimation in methanol–water mixtures from experimental and SPARC predicted pK_{a1} in water

Compound	From experimental pK_{a1}[a]		From predicted pK_{a1}[b]	
	RMSE	RRMSE%	RMSE	RRMSE%
Gallic acid	0.16	3.43	0.23	5.06
Protocatechuic acid	0.13	2.77	0.21	4.46
Gentisic acid	0.18	6.03	0.35	12.02
p-Hydroxybenzoic acid	0.11	2.35	0.12	2.50
Vanillic acid	0.13	2.83	0.26	5.76
Isovanillic acid	0.07	1.61	0.09	1.98
Syringic acid	0.09	2.01	0.30	6.77
Caffeic acid	0.11	2.34	0.15	3.13
p-Coumaric acid	0.14	3.07	0.09	2.05
Ferulic acid	0.24	5.24	0.15	3.26
Sinapinic acid	0.19	4.11	0.13	2.84

[a] This work.
[b] Ref. [21].

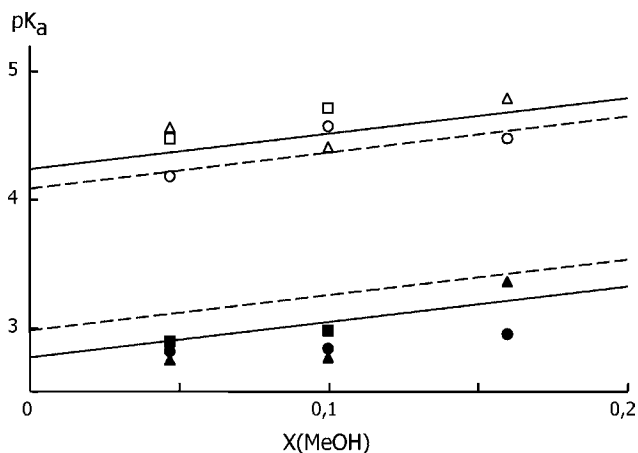Fig. 5. Plot of experimental and estimated pK_{a1} values of polyphenolic acids against the mole fraction of methanol. Experimental methods are: (□) potentiometric; (△) LC; (◯) LC-DAD. Open and filled symbols correspond to gallic and gentisic acids, respectively. Lines indicate the estimated pK_{a1} from experimental data (continuous lines) and from SPARC prediction (dashed lines).

Table 3 lists the RMSE and RRMSE% values obtained in each case, applied to all results of pK_a in methanol–water mixtures (10%, 20% and 30%, obtained by the different methodologies: potentiometric, LC and LC-DAD). An example of the results is given in Fig. 5, in which the experimental pK_{a1} values are plotted for gallic and gentisic acids, together with those obtained from both of estimation procedures.

The results presented in Table 3 show that, in most cases, RMSE values are in the range 0.1–0.2, and, as was to be expected, overall fit is better when experimental pK_a values are used. However, and with the exception of gentisic acid, estimated values from the SPARC prediction are usually good enough to be useful for the optimization of the pH of mobile phase in the separation of acid solutes by reversed-phase HPLC, as the differences between predicted and real pK_a values are in most cases lower than 0.2 units.

Acknowledgment

References

[1] C.F. Poole, S.K. Poole, Chromatography Today, Elsevier, Amsterdam, 1991.
[2] P.J. Schoenmakers, R. Tijsen, J. Chromatogr. A 656 (1993) 577.
[3] S. Hakkinen, S. Kareniampi, H. Mykkanen, I. Heinonen, A. Torronen, Eur. Food Res. Technol. 212 (2000) 75.
[4] M. Meloun, J. Havel, E. Högfeldt, Computation of Solution Equilibria: A Guide to Methods in Potentiometry, Extraction and Spectrophotometry, Ellis Horwood Limited, Chichester, 1988.
[5] R. Wrobel, L. Chmurzynski, Anal. Chim. Acta 405 (2000) 303.
[6] A.B. Martell, R.J. Motekaitis, Determination and Use of Stability Constants, 2nd ed., VCH, 1992.
[7] J. Barbosa, D. Barron, J.L. Beltran, V. Sanz-Nebot, Anal. Chim. Acta 317 (1995) 75.
[8] P. Gans, A. Sabatini, A. Vacca, Talanta 43 (1996) 1739.
[9] P. Janos, J. Chromatogr. A 1037 (2004) 15.
[10] S.K. Poole, S. Patel, K. Dehring, H. Workman, C.F. Poole, J. Chromatogr. A 1037 (2004) 445.
[11] J.E. Hardcastle, I. Jano, J. Chromatogr. B 717 (1998) 39.
[12] N. Sanli, G. Fonrodona, D. Barrón, G. Özkan, J. Barbosa, J. Chromatogr. A 975 (2002) 299.
[13] M. Pérez-Urquiza, J.L. Beltrán, J. Chromatogr. A 917 (2001) 331.
[14] E. Jiménez-Lozano, I. Marqués, D. Barrón, J.L. Beltrán, J. Barbosa, Anal. Chim. Acta 464 (2002) 37–45.
[15] J.L. Beltrán, N. Sanli, G. Fonrodona, D. Barrón, G. Özkan, J. Barbosa, Anal. Chim. Acta 484 (2003) 253.
[16] F. Shahidi, C.T. Ho (Eds.), ACS Symposium Series 909. American Chemical Society, Washington DC, USA, 2005.
[17] A. Escarpa, M.C. Gonzalez, J. Chromatogr. A 830 (1999) 301.
[18] A. Schieber, P. Keller, R. Carle, 3. Chromatogr. A 910 (2001) 265.
[19] Y.H. Cao, Y. Wang, Q. Yuan, Chromatographia 59 (2004) 135.
[20] R.J. Robbins, J. Agric. Food Chem. 51 (2003) 2866.
[21] http://ibmlc2.chem.uga.edu/sparc/.
[22] S.H. Hilal, S.W. Karickhoff, L.A. Carreira, Quant. Struct. Acta Relat. 14 (1995) 348.
[23] G. Gran, Analyst 77 (1952) 661.
[24] T. Mussini, A.K. Covington, P. Longhi, S. Rondinini, Pure Appl. Chem. 57 (1985) 865.
[25] S. Rondinini, P.R. Mussini, T. Mussini, Pure Appl. Chem. 59 (1987) 1549.
[26] J. Barbosa, I. Marqués, D. Barron, V. Sanz-Nebot, Trends Anal. Chem. 18 (1999) 543.
[27] http://www.nlreg.com.
[28] I. Canals, F.Z. Oumada, M. Rosés, E. Bosch, J. Chromatogr. A 911 (2001) 191–202.
[29] J.L. Beltrán, R. Codony, M.D. Prat, Anal. Chim. Acta 276 (1993) 441.
[30] M.J. Kamlet, J.L.M. Abboud, R.W. Taft, Progr. Phys. Org. Chem. 13 (1981) 485.
[31] C. Reichardt, Solvents and Solvent Effects in Organic Chemistry, 2nd ed., VCH Verlagsgesellschaft, Weinheim, 1988.
[32] J. Barbosa, J.L. Beltrán, V. Sanz-Nebot, Anal. Chim. Acta 288 (1994) 271.
[33] A.L. Bacarella, E. Grunwald, H.P. Marshall, E.L. Purlee, J. Org. Chem. 20 (1955) 747.
[34] I. Marques, G. Fonrodona, S. Buti, J. Barbosa, TrAC - Trends Anal. Chem. 18 (7) (1999) 472.
[35] IUPAC Stability Constants of Metal-Ion Complexes. Part B. Organic Ligands. Pergamon Press. Oxford, 1979.
[36] M. Smith, E. Martell, Critical Stability Constants, vol. 6, (supplement section), Plenum Press, New York, 1989.
[37] Y. Ishihama, Y. Oda, N. Asakawa, J. Pharm. Sci. 83 (1994) 1500.
[38] IUPAC Ionization Constants of Organic Acids in Aqueous Solutions, Pergamon Press, Oxford, 1979.
[39] B. Smyk, R. Drabent, Analyst 114 (1989) 723.

ELSEVIER

Speciation analysis of platinum antitumoral drugs in impacted tissues

D. Esteban-Fernández [a], M.M. Gómez-Gómez [a,*], B. Cañas [a], J.M. Verdaguer [b],
R. Ramírez [b], M.A. Palacios [a]

[a] *Department of Analytical Chemistry, Faculty of Chemistry, University Complutense of Madrid, Ciudad Universitaria s/n, 28040 Madrid, Spain*
[b] *Servicio de Otorrinolaringología, Hospital Universitario Puerta de Hierro, C/San Martín de Porres 4, 28035 Madrid, Spain*

Abstract

Chemical compounds containing platinum have been employed since 1978 as drugs to beat certain type of tumours. Nevertheless, besides of their exceptional antitumoral properties, these drugs also have important deleterious side effects, such as, nephrotoxicity and ototoxicity.

A study of Pt accumulation and a speciation analysis has been performed by ICP-MS in samples from kidney and inner ear in a controlled population of Wistar rats treated with, either, cisplatin, carboplatin or oxaliplatin. The results on Pt accumulation point out to drug structure and not only to Pt content as the responsible for the alteration of organ functionality.

Speciation studies in the samples from kidney and inner ear were performed coupling two-dimensional liquid chromatography (2D-LC) to ICP-MS. Size exclusion (SEC) and anion exchange fast protein liquid chromatography (FPLC) was employed for 2D orthogonal separation. After these separations, free drug peaks were not observed in any of the samples.

The binding of Pt to biomolecules was demonstrated by SEC and, independently of the drug used, Pt eluted as two main bands with molecular weights of 12 kDa and 25–65 kDa for inner ear samples, and as two different bands with 20 kDa and 50–60 kDa in the samples from kidney. However, the relative band intensity presented important differences for the three drugs. Using the same chromatographic conditions, it was shown that a metallothionein (MT) standard eluted in the same position as some of the cytosolic Pt-biomolecules.

High Pt-containing fractions eluting from the SEC column were analysed by anion exchange FPLC after a preconcentration step. Among the different preconcentration methods tested, sample focusing on the head of the FPLC column shows main advantages. In this way, the separation by 2D chromatography of the high molecular Pt-species has been considerably improved.
© 2006 Elsevier B.V. All rights reserved.

Keywords: Pt-based drugs; Rats; LC–ICP-MS; 2D chromatographic separations; Sample focusing; Pt-biomolecules; Kidney and inner ear toxicity

1. Introduction

Since 1978 cisplatin (*cis*-diaminedichloroplatinum(II)), is widely used for the treatment of many cancers. Severe side effects like nephrotoxicity, ototoxicity, etc., limit the maximum dosage to $100 \, mg/(m^2 \, 21 \, days)$ [1]. Besides, some tumors present an intrinsic resistance to cisplatin, while others develop resistance only when the treatment begins. Because of these drawbacks, other Pt containing antitumoral compounds have been synthesized and tested with the aim of finding a related drug with increased treatment efficacy and reduced toxic side-effects. Higher dosages, of $300 \, mg/(m^2 \, 21 \, days)$

and $135 \, mg/(m^2 \, 15 \, days)$, were allowed, respectively, with two of these new generation drugs: carboplatin (*cis*-diamine(1,1-cyclobutanedicarboxylato)platinum(II)) and oxaliplatin (*trans*-L-1,2-diaminocyclohexaneoxalatoplatinum(II)) [2,3]. The most important side effects of these drugs were myelo-suppression and neuropathy, respectively.

The study of the accumulation, distribution and biotransformation of a drug in the affected organs is the first step to understand the physiological behaviour that produces organ injury. Previous accumulation and distribution studies carried out with laboratory rats treated with cisplatin revealed a maximum accumulation of Pt around the first week of post-treatment for all the organs under study (kidney, liver, brain and inner ear) [4]. The drug persists longer in the kidney and inner ear. The damage produced in the affected organs is probably due to the

* Corresponding author. Tel.: +34 913945146; fax: +34 913944329.
 E-mail address: mmgomez@quim.ucm.es (M.M. Gómez-Gómez).

association of Pt (or the parent drug metabolites) to important proteins of the impacted organ.

The current concept of bioinorganic speciation analysis involves metallomic studies of real samples like plasma, urine or tissues [5,6]. In this way, some interesting elements like selenium have been extensively studied employing hyphenated techniques combining different types of chromatography, like SEC, anion exchange, etc., and powerful detectors, such as ICP-MS (inductively coupled plasma mass spectrometry) or structural mass spectrometry techniques like ESI-MS (electrospray ionisation mass spectrometry) or MALDI-MS (matrix-assisted laser desorption/ionisation mass spectrometry) [7]. Few studies have been done in real samples such as, serum or urine for the bioinorganic speciation analysis of Pt-based drugs [8,9]. The coupling of HPLC to ICP-MS is the first essential step to perform these studies [10].

Most of the studies related to speciation of Pt-based drugs are related to cisplatin [11]. The transformation of the drug in different media [12,13], their interaction with HPLC mobile phases [14,15], or their incubation with small biomolecules like aminoacids or thiol compounds [16,17], even with small proteins like metallothioneins (MTs) [18,19], have been studied. Similar speciation studies with other Pt-based drugs, like carboplatin or oxaliplatin, have also been reported [20]. It is known that MTs, a group of small cysteine-rich proteins that form metal-thiolate clusters with metals, have important functions in metal detoxification processes with Cd, Hg and Ag [21]. The synthesis of apo-thionein is induced by high concentrations, within the cells, of heavy metals. Probably, likewise mechanisms may be involved in Pt detoxification after a high uptake [22,23].

Present work is focused on the development of an analytical methodology for the separation and characterization of the different Pt-biomolecules present in kidney and inner ear cells cytosol from rats, which were previously treated with mono-doses of, either cisplatin, carboplatin or oxaliplatin equivalent to that used for human disease treatments. Up to our knowledge, it is the first time that this type of speciation studies is performed in tissues. These studies are of paramount importance to improve the understanding of the mechanisms related to the side effects produced by these drugs.

2. Experimental

2.1. Instrumentation and chromatographic materials

For the determination of Pt, a Quadrupole ICP-MS Thermo X-Series (Thermo Electron, Windsford, Cheshire, UK) equipped with a Meinhard nebulizer, a Fassel torch and an Impact Bead Quartz spray chamber cooled by a Peltier system, was employed. For total analysis of Pt, sample introduction was performed in continuous mode, and single ion monitoring of m/z 191 (Ir), 194 (Pt) and 195 (Pt), was used to collect data. Quantification of Pt was carried out by external calibration of ^{195}Pt isotope with 200 μg L^{-1} Ir as internal standard.

For speciation studies by chromatographic separations, a high-pressure quaternary gradient pump (Jasco PU-2089), equipped with an injection valve (Rheodine, USA) was used as

Table 1
ICP-MS and LC–ICP-MS operating conditions

ICP-MS operating conditions	
Forward power (W)	1250
Plasma gas (Ar, L min^{-1})	15
Auxiliary gas (Ar, L min^{-1})	7.3
Nebuliser gas (Ar, L min^{-1})	0.76
Spray chamber	Impact bead quartz
Nebuliser	Meinhard
Skimmer cone	Nickel
Sampling cone	Nickel
Acquisition mode	Continuous and transient
Channels per AMU	10
Integration time (ms)	0.6
Internal standard	^{191}Ir 200 μg L^{-1}
SEC	
Analytical column	Superdex 75 10/300 GL
Mobile phase	10 mM Tris–HCl, 25 mM NaCl (pH 7.4)
Injection volume (μL)	250
Flow rate (mL min^{-1})	0.8
FPLC	
Analytical column	Mono Q H/R 5/5
Mobile phase	A: 4 mM Tris–HCl (pH 7.4); B: A + 400 mM ammonium acetate (pH 7.4)
Time (min)	B (%)
0	0
10	20
15	50
20	85
25	100
Injection volume (μL)	250 (6 mL for head focusing)
Flow rate (mL min^{-1})	0.6

a sample delivery system. Separation of Pt-biomolecules was performed by SEC using a Superdex 75 10/300 GL column (Pharmacia, Amersham, Uppsala, Sweden, separation range of 3–70 kDa) and with a strong anion exchange FPLC column Mono-Q H/R 5/5 (Pharmacia, Amersham, Uppsala, Sweden). The operating conditions used for chromatographic separations and instrumental parameters employed for ICP-MS analysis are summarised in Table 1.

Digestions for total Pt determination were carried out in a high-pressure microwave oven (CEM MSP 1000, Matthews, USA). An acid distiller (Berghof B BSB-939IR, Eningen, Germany) was used for HCl and HNO$_3$ purification. For Pt-biomolecules speciation analysis the homogenisation of the tissues was performed with a Polytron PT 1200 (Kinematica AG, Switzerland) and a 10 mL Potter (Deltalab, Barcelona, Spain). Samples were centrifuged in a centrifuge 5804 R (Eppendorf, Hamburg, Germany). A Turbo Vap II evaporation system (Caliper Life Science, USA), Centricon centrifugal filters YM-3 (3 kDa NMWL, Millipore, USA) and a freeze-dryer (Lioalfa 6, Tesla, Spain) were used for preconcentration of the samples.

2.2. Standards and reagents

All solutions were prepared with deionized water (Milli-Q Ultrapure water systems, Millipore, USA). High-purity nitric

and hydrochloric acids were obtained by distillation of the analytical-grade reagents (Merck, Darmstadt, Germany). H_2O_2, 30% (w/v) (Panreac Química SA, Barcelona, Spain) was used for sample digestion.

The Pt-based drugs used were cisplatin (Sigma–Aldrich Chemie), carboplatin (EBEWE Pharma, Austria) and oxaliplatin (Sanofi-Synthelabo, France).

Stock solutions of Pt (1000 mg L^{-1} in HCl 0.5 mol L^{-1}, Spectrosol BDH Limited Poole, England) and Ir (1000 mg L^{-1} in HCl 8%, Merck, Darmstadt, Germany) were diluted with HCl 0.24 mol L^{-1} to prepare standard solutions. Working solutions for Pt analysis were prepared daily and then diluted with HCl 0.24 mol L^{-1} to final concentration.

Extraction reagents for the cytosol preparation were tris-(hydroxymethyl)aminomethane (Fluka Chemie), NaCl (Panreac Quimica SA) and Protease Inhibitor Cocktail for mammalian cell and tissue extracts (Sigma–Aldrich Chemie).

Proteins used for SEC calibration were blue dextran (>2000 kDa), bovine albumin (66 kDa), carbonic anhydrase (29 kDa), cytochrome *C* (12.4 kDa) and aprotinine (6.5 kDa) (Sigma–Aldrich Chemie). Metallothionein from rabbit liver (Sigma–Aldrich Chemie, around 6 kDa) was also used.

2.3. Drug administration

All drugs administrations and sacrifices of the rats were carried out under laboratory controlled conditions at the Hospital Universitario Puerta de Hierro (Madrid). The animals were handled following the guidelines of the National Council for the Care of the Laboratory Animals. The drugs were administrated by intraperitoneal injections. The weight of the rats was around 200 g and the dosages were related to their corporal area. The administration guidelines and dosages of the three drugs used in this study are equivalent to those applied in humans and usually employed for laboratory rats under clinical trials. It consisted of the administration of one dosage of cisplatin (16 mg/m^2), carboplatin (450 mg/m^2) or oxaliplatin (80 mg/m^2) to different groups of seven rats each, corresponding to 10.4 mg/m^2, 236.5 mg/m^2 and, 39.3 mg/m^2 as Pt, respectively. The sacrifice was carried out 3 days after administration and kidney and inner ear extracted for analysis.

2.4. Total Pt determination

Inner ear and kidney samples were dried in a conventional oven up to constant weight (6 h at 55 °C followed by 3 h at 105 °C). After that, samples were homogenised by agate mortar grinding. Dried samples (0.1 g) were placed in PFA advanced composite vessels and digested in a microwave oven with 2 mL of HNO_3 and 0.6 mL of H_2O_2 [24]. The microwave digestion program used for 12 vessels was: 1 min at 250 W, 1 min at 0 W, 5 min at 400 W, 6 min at 600 W and 8 min at 750 W.

The digested samples were evaporated to dryness in Teflon vessels. Two more evaporation steps were performed adding 2 mL of aqua regia and 1 mL of HCl, respectively. The samples were diluted to 5 mL with HCl 0.24 mol L^{-1} for ICP-MS analysis.

2.5. Pt-biomolecules speciation analysis

2.5.1. Cytosol preparation

About 0.250 g of kidney tissue was dissected and homogenised with a Potter homogenisator in 3 mL of a solution (pH 7.4) containing 10 mM Tris–HCl, 25 mM NaCl and an inhibitor protease cocktail. In the case of inner ear, the entire organ (about 0.2–0.4 g) was homogenised with a polytron in the same extraction solution. The homogenates were centrifuged at 15,000 × *g* for 20 min at 4 °C to minimise the risk of species degradation or transformation. The supernatant cytosol was filtered through a 0.22 µm Nylon filter.

2.5.2. Monodimensional chromatographic separation

Pt-biomolecules separation was performed by injection of the cytosol in the tandem LC–ICP-MS (SEC) under the conditions indicated in Table 1. The SEC column was calibrated with standards of proteins.

2.5.3. Preconcentration for two-dimensional chromatographic analysis

A pool of cytosol sample from five inner ears was prepared and its volume reduced to 2.5 mL by evaporation under N_2 stream. This sample was injected into the SEC column and fractions with high Pt content were collected (1 mL each). The pool of four identical fractions was subjected to the following preconcentration methods:

- *Evaporation*: 1 mL was evaporated under N_2 stream at ambient temperature for 1 h until a final volume of 400 µL.
- *Freeze-drying*: 1 mL was freeze-dried and the final volume was made up with 400 µL of H_2O.
- *Cut-off filters*: 1 mL was filtered through Centricon YM-3 cut-off filters at 6500 g and 4 °C for 1 h. The retentate was made up to 400 µL with H_2O.

In the three preconcentration methods 250 µL of the preconcentrated samples were injected into the FPLC–ICP-MS system under the conditions shown in Table 1.

- *Focusing*: 1 mL were diluted with water to 2 mL to reduce the ionic strength of the sample and preconcentrated by chromatographic focusing in the head of the Mono-Q H/R 5/5 column, using as mobile phase Tris–HCl 4 mM. The low ionic strength of this mobile phase allowed the preconcentration of the sample in a small band around the first section of the column (focusing). The elution of the focused compounds was performed by increasing the ionic strength under the gradient conditions indicated in Table 1.

3. Results and discussion

3.1. Pt accumulation

Three different drugs, cisplatin, carboplatin and oxaliplatin, have been tested for Pt accumulation and speciation in rat kidney and inner ear. The dosages administered in this study were the

Table 2
Platinum relative concentration in kidney and inner ear from rats treated with monodoses of cisplatin, carboplatin and oxaliplatin

	Inner ear	Kidney
Cisplatin	5.4 ± 1.5	33 ± 7
Carboplatin	0.26 ± 0.05	10 ± 3
Oxaliplatin	1.7 ± 0.3	57 ± 4

Results expressed as (mg Pt/kg dried sample)/mg Pt administered (mean ± s_{n-1}), $n = 7$.

equivalent to those used for regular human treatments. Therefore, the amount of Pt injected is different depending on the drug. For data comparison, results are given as Pt concentrations found in the tissue (mg Pt/kg dried tissue) per mg of Pt administrated. Table 2 shows the mean of the relative Pt concentration in both organs, after 3 days of each drug administration.

These results are interesting from a pharmacokinetic point of view. It is important to highlight that cisplatin produces the highest accumulation of Pt in the inner ear, but not in the kidney. Considering that cisplatin has been reported as strong ototoxic drug, this may indicate that ototoxicity and Pt accumulation could be related. Pt accumulation after carboplatin administration is the lowest for both tissues. Oxaliplatin shows high accumulation capability for kidney (1.7 times) with respect to the values obtained for cisplatin.

The fact that oxaliplatin, a drug structurally similar to cisplatin, presents higher tendency to be accumulated in kidney, but does not produce the same side effect (as reported in the literature), suggests that the particular drug structure more than the Pt content could be the responsible of alterations in the normal functionality of organs. Therefore, the Pt-biomolecule interactions and the different species formed (speciation) have to be studied in order to understand the causes of the adverse effects.

3.2. Pt-biomolecules speciation

3.2.1. Monodimensional chromatographic separation

The Pt-biomolecule complexes formed in the two target organs have been firstly separated by SEC-ICP-MS. Fig. 1 shows the SEC chromatogram of the prepared inner ear cytosol for the three drugs under study. As can be seen, the main chromatographic peaks for the three samples present similar retention times and are grouped around two molecular weight regions of 25–65 kDa and 12 kDa according to the SEC calibration. However, the relative intensity of both groups (mass balance) present important differences among the different drugs. For cisplatin, most species are present in the 12 kDa region, while with carboplatin the species are mostly present in the 25–65 kDa region. When oxaliplatin is administrated, species produced are similarly distributed in both molecular weight groups, being observed a third peak of 8 kDa.

Fig. 2 shows the SEC-ICP-MS chromatogram of kidney cytosol from rats treated with each of the three drugs. Most chromatographic peaks for Pt bound molecules present similar retention times in all three samples and the species found are also distributed in two molecular bands in the regions of 50–60 kDa
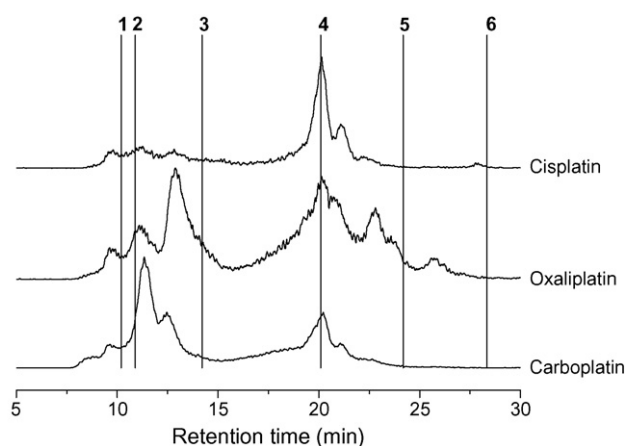

Fig. 1. SEC-ICP-MS chromatograms of inner ear cytosol from rats treated with cisplatin, oxaliplatin or carboplatin. Numbers correspond to molecular weight calibration markers: (1) 70 kDa, (2) 66 kDa, (3) 29 kDa, (4) 12.4 kDa, (5) 6.5 kDa and (6) 3 kDa.

and 20 kDa. However, in this case, the bands present similar relative mass balance profiles for the three drugs, being the intensity for the low molecular weight band higher. In oxaliplatin treated samples, a third peak at 8 kDa appears as described earlier for the inner ear sample (Fig. 1).

To check whether low molecular weight Pt binding proteins could correspond to MTs, a standard solution of rabbit liver MT was injected on the SEC column under the same chromatographic conditions. Fig. 3 shows the comparative chromatograms of the MT standard ([66]Zn and [111]Cd were monitored), and from the inner ear and kidney cytosols from rats treated with cisplatin ([66]Zn and [195]Pt were monitored). In the case of kidney cytosols a wide peak of a Pt-biomolecule elutes in the MT region, however the Zn signal is not present, suggesting the possible replacement of Zn by the Pt drug. In the case of the inner ear cytosols, although a small fraction of Pt could be bound to the MTs, most of the drug is bounded to other biomolecules with a higher molecular weight.
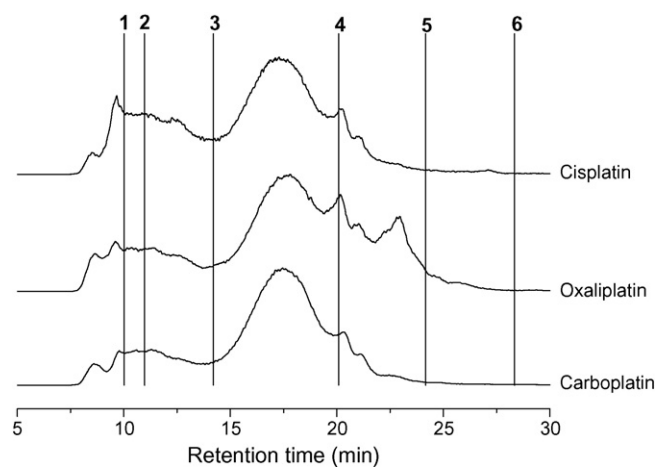

Fig. 2. SEC-ICP-MS chromatograms of kidney cytosol from rats treated with cisplatin, oxaliplatin or carboplatin. Numbers correspond to the molecular weight calibration markers: (1) 70 kDa, (2) 66 kDa, (3) 29 kDa, (4) 12.4 kDa, (5) 6.5 kDa and (6) 3 kDa.
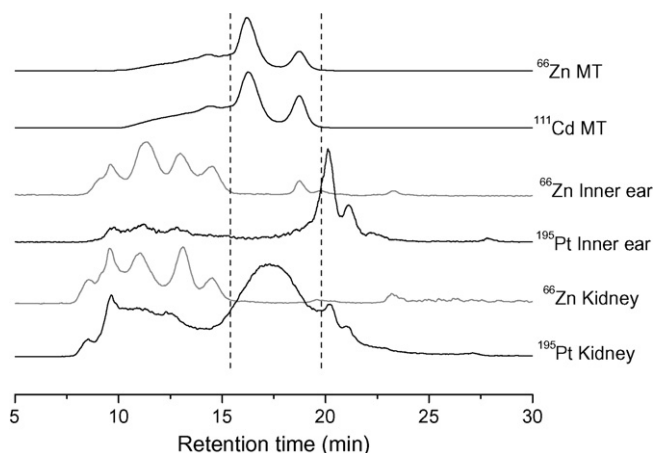
Fig. 3. SEC-ICP-MS chromatograms of rabbit liver MT standard, and inner ear and kidney cytosol from rats treated with cisplatin.

Low amounts of Pt-species have been found above 70 kDa (top of the calibration range) for both tissues. It is important to point out that the chromatograms obtained by SEC fractionation for both organs show the absence of free-drug (elution time about 50 min). This means that the drug present in the cytosol is mostly bound to biomolecules. These results agree with those reported by Szpunar et al. [8], which show that very low amounts of free cisplatin remained in blood after 24 h incubation.

3.2.2. Preconcentration for two-dimensional chromatographic analysis

The poor resolution attained by the SEC column made necessary to resolve the different Pt-species, present in these wide peaks, by a second chromatographic dimension (2D). Before this 2D separation could be performed, a preconcentration step of the SEC fractions of interest was imperative.

A systematic study to check the efficiency of four different methods for Pt-biomolecules preconcentration has been carried out. Established methodologies such as, evaporation, freeze-drying, filtration through cut-off filters [25] and focusing on the head of the ion exchange column were tested.

Identical fractions representative of compounds with high and low molecular weight (fraction 9 and 17 with retention times of 11.25 and 21.25 min, respectively), of inner ear cytosol from rats treated with cisplatin, were subjected to the preconcentration methodology reported in Section 2 and resolved by FPLC–ICP-MS. Fig. 4a shows the comparative ion exchange chromatograms obtained by the four preconcentration methods for the fraction 9. A similar peak distribution is observed for the four methods tested. However, column-head focusing shows the highest sensitivity and also a slight improvement on resolution, probably due to the lower salt content of the sample. In this case, there is a delay on the retention time of the peaks, also due to the different salt content of the focused sample. When cut-off filters were used, an important loss of sensitivity (especially for compounds of low retention time) was observed. This was, probably, due to adsorption of the Pt-biocompounds in the filter, so, it was discarded for further experiments.
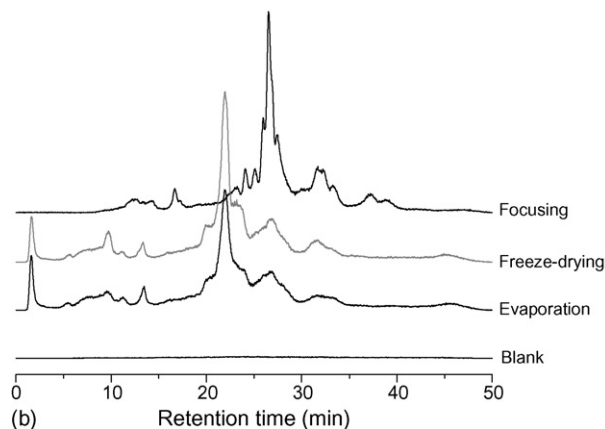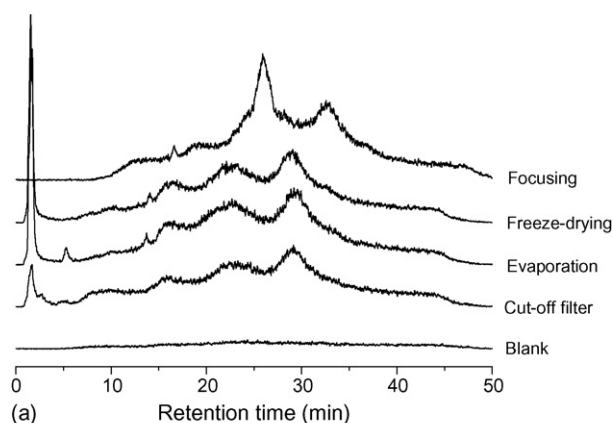

Fig. 4. Two-dimensional FPLC–ICP-MS chromatograms of SEC fractions of inner ear cytosol from rats treated with cisplatin, obtained by four different preconcentration methods: chromatographic focusing, cut-off filters, evaporation and freeze-drying. (a) Fraction 9 (11.25 min retention time) and (b) fraction 17 (21.25 min retention time).

Fig. 4b presents the ion exchange chromatograms obtained for fraction 17 where again head focusing shows the best results.

It was observed that at least three fractions coming from the SEC column could be simultaneously preconcentrated by focusing without over-loading the FPLC ion exchange column used and without producing any peak widening. The main advantages of focusing on the column head are high pre-concentration capacity, simplicity, fast procedure, low sample manipulation and no need of additional instrumentation. Besides, the risk of species transformation involved in this preconcentration technique is significantly reduced in comparison with others. Thus, it was selected for further experiments.

Fig. 5 shows the chromatogram for the second dimension of the highest Pt containing fractions (retention time 20 min, 12 kDa) eluting from the SEC column. After the SEC separation (Fig. 1), three samples from cisplatin treated inner ear cytosol were pooled and focused in the head of the anion exchange column. This chromatogram still presents a high degree of complexity, although the resolution was improved. At least seven well resolved Pt-species were found. Owing to that complexity it is necessary to develop new dimensions to purify these species for further identification.
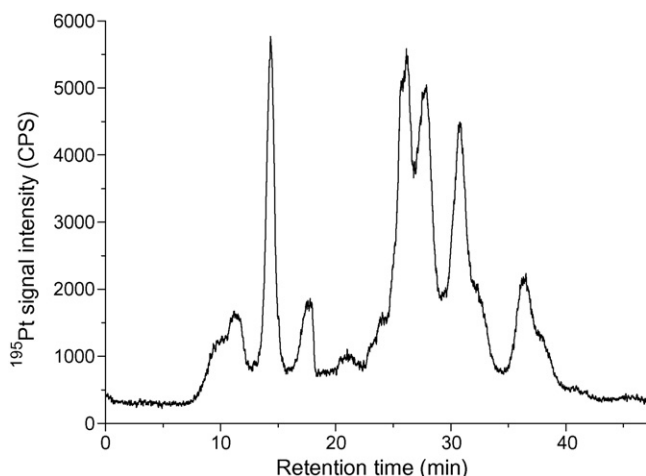
Fig. 5. Two-dimensional FPLC–ICP-MS chromatogram, after sample focusing on the head of the column of the 12 kDa fraction (20 min retention time) of SEC separated inner ear cytosol from rats treated with cisplatin.

There are Pt-compounds which are not retained in the FPLC column used in the second dimension, and therefore were lost in the focusing. These compounds elute all together in the death volume, as it can be observed in Fig. 4a and b for non-focusing preconcentration methods. Different types of chromatographic separations, like cation exchange or reverse phase, will be of use for such compounds.

4. Conclusions

The bioaccumulation studies of Pt-based drugs in rat inner ear and kidney shows a sound difference between these two organs and for the different drugs administrated. The relative accumulation of cisplatin metabolites is higher than that of oxaliplatin metabolites for inner ear, but not for kidney. The establishment of a direct relation between Pt accumulation and toxicity could be true for the inner ear. The relative accumulation of carboplatin is the lowest in both organs. Thus, metallomic studies are necessary to explain the interactions causing the toxic effects of these drugs. In kidney cytosol, MTs seem to be present in the low molecular weight fraction of SEC separated Pt-biomolecules.

The combination of SEC and anion exchange chromatography can highlight the differences between the species found in kidney and inner ear when the rats have been treated with cisplatin. The focusing of the Pt-biocompounds on the head of the anion exchange column has demonstrated several advantages over other preconcentration methods: higher preconcentration capacity, lower sample manipulation and therefore lower risk of species transformation.

The two-dimensional use of LC techniques improved the separation of Pt-biospecies for future identifications. The identification of target Pt bound biocompounds will be the result of a combination of multidimensional orthogonal separations and structural mass spectrometry techniques using ionization techniques like ESI and MALDI.

Acknowledgements

References

[1] M.J. Zelefsky, D.H. Kraus, D.G. Pfister, A. Raben, J.P. Shah, E.W. Strong, R.H. Spiro, G.J. Bosl, L.B. Harrison, Head Neck 18 (1996) 405.
[2] N.D. Doolittle, L.L. Muldoon, R.E. Brummett, R.M. Tyson, C. Lacy, J.S. Bubalo, D.F. Kraemer, M.C. Heinrich, J.A. Henry, E.A. Neuwelt, Clin. Cancer Res. 7 (2001) 493.
[3] L. Alinari, G. Musuraca, M. Tani, V. Stefoni, A. Gabriele, E. Marchi, M. Fina, A. De Vivo, S. Pileri, M. Baccarani, P.L. Zinzani, Leuk. Lymphoma 46 (2005) 1437.
[4] D. Esteban-Fernández, M.M. Gómez-Gómez, J.M. Verdaguer, R. Ramírez, M.A. Palacios, J. Anal. Toxicol., submitted for publication.
[5] J. Szpunar, Anal. Bioanal. Chem. 378 (2004) 54.
[6] J. Szpunar, Analyst 130 (2005) 442.
[7] J. Ruiz Encinar, L. Ouerdane, W. Buchmann, J. Tortajada, R. Lobinski, J. Szpunar, Anal. Chem. 75 (2003) 3765.
[8] J. Szpunar, A. Makarov, T. Pieper, B.K. Keppler, R. Lobinski, Anal. Chim. Acta 387 (1999) 135.
[9] V. Vacchina, L. Torti, C. Allievi, R. Lobinski, J. Anal. At. Spectrom. 18 (2003) 884.
[10] J. Szpunar, Analyst 125 (2000) 963.
[11] R.R. Barefoot, J. Chromatogr. B 751 (2001) 205.
[12] M. Verschraagen, K. van der Born, T.H. Ursula Zwiers, W.J.F. van der Vijgh, J. Chromatogr. B 772 (2002) 273.
[13] A. Andersson, H. Ehrsson, J. Chromatogr. B 652 (1994) 203.
[14] O. Heudi, A. Cailleux, P. Allain, Chromatographia 44 (1997) 19.
[15] M. El-Khateeb, T.G. Appleton, B.G. Charles, L.R. Gahan, J. Pharmacol. Sci. 88 (1999) 319.
[16] Z. Zhao, K. Tepperman, J.G. Dorsey, R.C. Elder, J. Chromatogr. B 615 (1993) 83.
[17] J.C. Dabrowiak, J. Goodisman, A. Souid, Drug Metab. Dispos. 30 (2002) 1378.
[18] D. Hagrman, J. Goodisman, J.C. Dabrowiak, A. Souid, Drug Metab. Dispos. 31 (2003) 916.
[19] A. Pattanaik, G. Bachowski, J. Laib, D. Lemkuil, F. Shaw, D.H. Petering, A. Hitchcock, L. Saryan, J. Biol. Chem. 267 (1992) 16121.
[20] Y. Zhao, R. Mandal, X. Li, Rapid Commun. Mass Spectrom. 19 (2005) 1956.
[21] M. Nordberg, Talanta 46 (1998) 243.
[22] K. Wang, J. Lu, R. Li, Coordin. Chem. Rev. 151 (1996) 53.
[23] R. Lobinski, H. Chassaigne, J. Szpunar, Talanta 46 (1998) 271.
[24] S.V.M. Maharaj, Anal. Bioanal. Chem. 380 (2004) 84.
[25] A. Rodríguez-Cea, M.R. Fernández de la Campa, E. Blanco González, B. Andón Fernández, A. Sanz-Medel, J. Anal. At. Spectrom. 18 (2003) 1357.

ELSEVIER

The role of various binding materials for trace elemental analysis of powder samples using laser-induced breakdown spectroscopy

M.A. Gondal [a,*], T. Hussain [b], Z.H. Yamani [a], M.A. Baig [b]

[a] *Laser Research Laboratory, Physics Department, King Fahd University of Petroleum & Minerals, Dhahran 31261, Saudi Arabia*
[b] *Institute of Environmental Science & Engineering, National University of Sciences and Technology (NUST), Tamiz Ud din Road, Rawalpindi, Pakistan*

Abstract

Study of various binding materials like potassium bromide, poly(vinyl alcohol), starch, silver and aluminum has been carried out using laser-induced breakdown spectroscopy (LIBS). The role of matrix effects using these five binders on LIBS signal intensity was investigated for better performance of LIBS technique as a quantitative analytical tool. For comparative study of different binders, the signal intensity of different Mg lines at 518.3, 517.2, 383.8 and 279.5 nm wavelengths were recorded for pellets prepared with known concentrations of Mg in these binders. The influence of laser energy on ablated mass under different binding materials and its correlation with LIBS signal intensity has been explored. Optical scanning microscopy images of the ablated crater were studied to understand the laser ablation process. The study revealed that the binding material plays an important role in the generation of LIBS signal. The relative signal intensity measured for a standard Mg line (at 518.3 nm) were 735, 538, 387, 227 and 130 for potassium bromide, starch, poly(vinyl alcohol), silver and aluminum as binders, respectively. This indicates clearly that potassium bromide is better as a binder for LIBS studies of powder samples.
© 2006 Elsevier B.V. All rights reserved.

Keywords: Laser-induced break down spectroscopy (LIBS); Binding materials; Trace element detection; Crater effect; LIBS applications; Matrix effects; Analytical techniques; Environmental pollution

1. Introduction

Laser-induced breakdown spectroscopy (LIBS) is useful for analysis of solid samples of environmental and geological interest. Most of these samples are investigated for bulk analysis and are therefore need to be processed properly to obtain compact targets prior to analysis using LIBS technique. In LIBS, the interaction between laser beam and the solid sample is a complicated [1–3]. It depends on physical and chemical characteristics of the sample material, laser parameters, surrounding atmosphere and the binder material used for the pellet formation especially for the analysis of samples in powder forms [4–6].

The process of conforming and binding the samples into a specific shape is generally known as pelletizing. The homogeneity is an important factor for accurate analysis of powder samples. In addition, such target samples (pellets) must show adequate mechanical strength for LIBS analysis. This is due to

the fact that when a laser beam interacts with the sample material, the sample disintegrates during laser ablation by mechanical shocks. This usually results either in the target breaking or crumbling into original particulate material. For geological and environmental analysis, soil and rock samples are the primary focus for processing of such target samples. Generally speaking, the soil and rock samples are not naturally homogeneous and so it is mandatory that these samples be processed into homogeneous pellets. This, in turn, requires the selection of a proper binding material [7,8]. For homogenous pellet formation, the soil and rock samples must first be broken down into unconsolidated particles by grinding to an extremely fine powder with a grinding machine. Then, pellets of specific shapes are prepared using binding materials.

In order to achieve higher sensitivity and more delicate analysis with LIBS, the binding material should be appropriately selected. This can be achieved by mixing the actual powder material with suitable binders, such as cellulose, Ag, Al, potassium bromide (KBr), starch or poly(vinyl alcohol) and then pressing in a special die. One of the parameters of binding material is called "bond strength" which is a measure of strength between

* Corresponding author. Tel.: +966 3 8602351; fax: +966 3 8602293.
E-mail address: magondal@kfupm.edu.sa (M.A. Gondal).

particles that bind a sample together and resist ablation. Bond strength is one factor influencing the matrix of the sample. Higher particle bond strength causes resistance to both scaling and conformation geometry changes and thereby increases the analytical stability of the samples. Also, the uniformity of particle bond strength throughout the pellet is essential for the measurements of different LIBS samples [8–18].

In this study, we prepared various samples in the form of pellets of Mg in different binders, such as Ag, KBr, poly(vinyl alcohol), Al and starch. For comparison of the effect of different binders on LIBS signal intensity, we measured the LIBS signal intensity of Mg lines at 518.3, 517.2, 383.8 and 279.5 nm wavelength. In addition, we measured the ablated mass and the crater depth in pelletized powder samples prepared with different binders.

2. Experimental setup details

Fig. 1 depicts the schematic diagram of the experimental setup used in this study. A Nd:YAG laser (Spectra-Physics Lasers, Model GCR 100) at a wavelength of 1064 nm (20 mJ Q-switched, 10 Hz pulses of 8 ns pulse width) was applied as a radiation sources. The experimental setup applied in this study has been discussed in detail in earlier publications [19–22]. In brief, the laser beam was focused on the targets with a lens of 30 mm focal length. The target pellets were prepared by mixing 8 g of binding material with 0.8 g of Mg. The emission from the plasma spark was collected by a collimating lens using UV graded fused silica 1 m, multimode sampling fiber with an SMA connector and was transferred to an optical spectrometer (Ocean Optics Model, 2000$^+$). This system has four spectrometer modules to provide high resolution (~0.1 nm) in the 200–620 nm wavelength region. The detector has a gated CCD camera having 14,336 pixels. The plasma emission was observed at a 45° angle to the laser pulse. Software built in the spectrometer read the data from the chip and reconstructed the spectra.

Pellets prepared in different binders were placed on a rotary stainless steal cup of 20 mm diameter and 10 mm depth. These samples were positioned such that the focal volume of the laser pulse was centered in the cup holding these samples. Twenty laser pulses were directed into the cup to complete one measurement and the average was taken in order to improve on shot-to-shot variations in the laser plasma. For comparison and validity of LIBS data, the Mg concentrations from identical binder samples were also measured by a conventional standard technique; namely, inductively coupled plasma (ICP).

2.1. Reagent used and sample preparation for binding material studies

The pellets in different binders, such as Al, poly(vinyl alcohol), Ag, starch and KBr having the same amount of Mg were prepared. Care was taken to avoid any contamination due to mixing of other species during the pellet formation process. The samples were accurately weighed, according to standard procedures. The samples were first dried and grinded in Spectro Mill Ball Pestle impact Grinder (Model 1100-11, Chemplex Industries, Inc., USA) to suitable mesh size for preparation of pellets. The pellets were made in a die of cylindrical form having diameter 20 mm and thickness 10 mm using a hydraulic press (Carver Laboratory Press Model, C Sterling USA). The applied load was 12,500 psi for 15 min. The samples were stored in desiccators to avoid any moisture and humidity effects.

Analytical-reagent grade chemicals, without further purification, were used for calibration, and as binding materials for ICP and LIBS studies. The binding materials (matrix) were of high purity (99.99%) procured from Fluka, Germany. The magnesium metal was in powder form of high purity (99.99%) and procured from Fisher Scientific, USA. For the parametric dependence of LIBS signal intensity on the concentration of Mg, different stoichiometric samples comprising Mg metal were prepared. For this purpose, pure Mg in powder form was mixed with
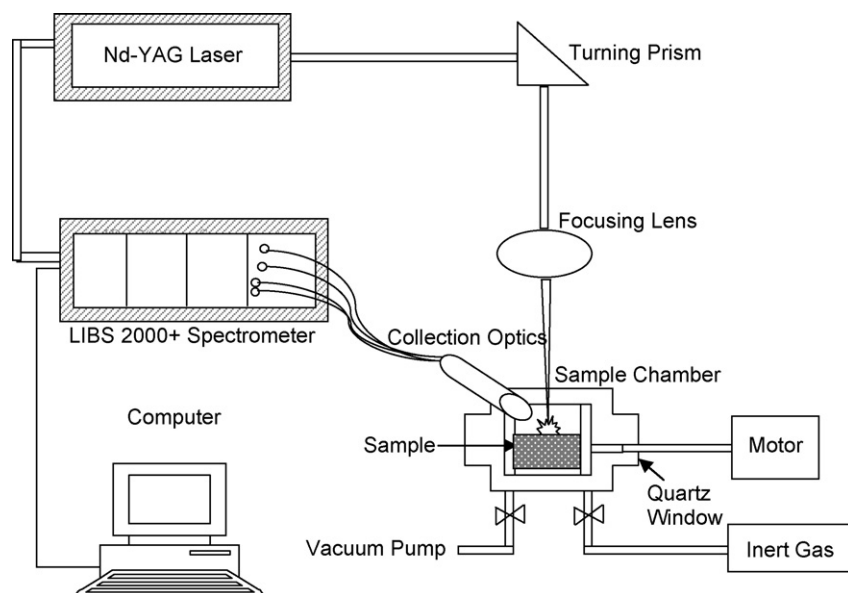

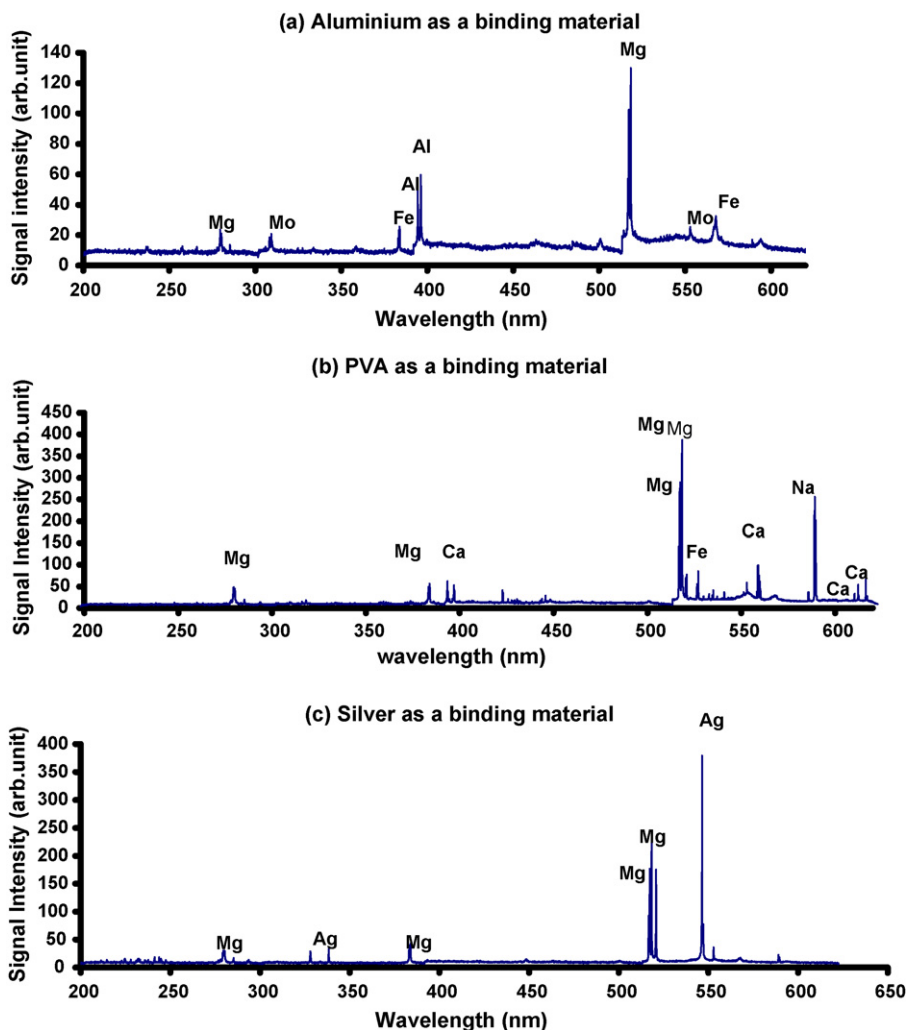Fig. 1. Schematic diagram of LIBS system applied for comparative study of different binding materials.

Fig. 2. LIBS spectrum of Mg mixed in various binding materials recorded in 200–620 nm region at a delay time = 4.5 μs and laser pulse energy = 20 mJ. (a–c) Representative spectra of Mg with aluminum, poly(vinyl alcohol) and silver as a binding materials.

the matrix material KBr in a ball milling apparatus in order to ensure good mixing and homogeneity.

3. Results and discussion

3.1. Laser-induced breakdown spectra of Mg in various binding materials

LIBS spectra of the pellets prepared by mixing 0.8 g Mg in 8 g of binder materials, such as Al, poly(vinyl alcohol), Ag, starch

and KBr powders were recorded in the 200–620 nm spectral region. Typical spectra of five binder samples indicating the Mg signal intensity at wavelengths 518.3, 517.2, 279.5 and 383.8 nm are depicted in Figs. 2(a–c) and 3(a and b). The wavelengths and the signal intensities of Mg at these peak wavelengths are presented in Table 1. These emission lines were specifically selected due to their minimal interference with other emission lines and do not involve the ground state so that self-absorption is almost absent. Hence, these lines authentically represent the Mg content in the different samples. Similar behavior has been noticed

Table 1
Comparison of signal intensity of different Mg lines in various binding materials

Peak wavelength (nm) of Mg lines	Binding material									
	Aluminum		KBr		PVA		Silver		Starch	
	S.I.	SNR	S.I.	SNR	S.I.	SNR	S.I.	SNR	S.I.	SNR
518.3	130	15	735	105.0	387	55	227	45.4	538	77
517.2	ND	–	634	84	289	38	177	24	470	63
383.8	ND	–	ND	–	57	7	43	5	65	7
279.5	24	3	54	8	ND	–	24	3.5	45	5

Laser energy = 20 mJ/pulse, *Q* switch delay = 4.5 μS and averaged for 20 laser shots. ND: not detected; S.I.: signal intensity (arb. units); SNR: signal to noise ratio.
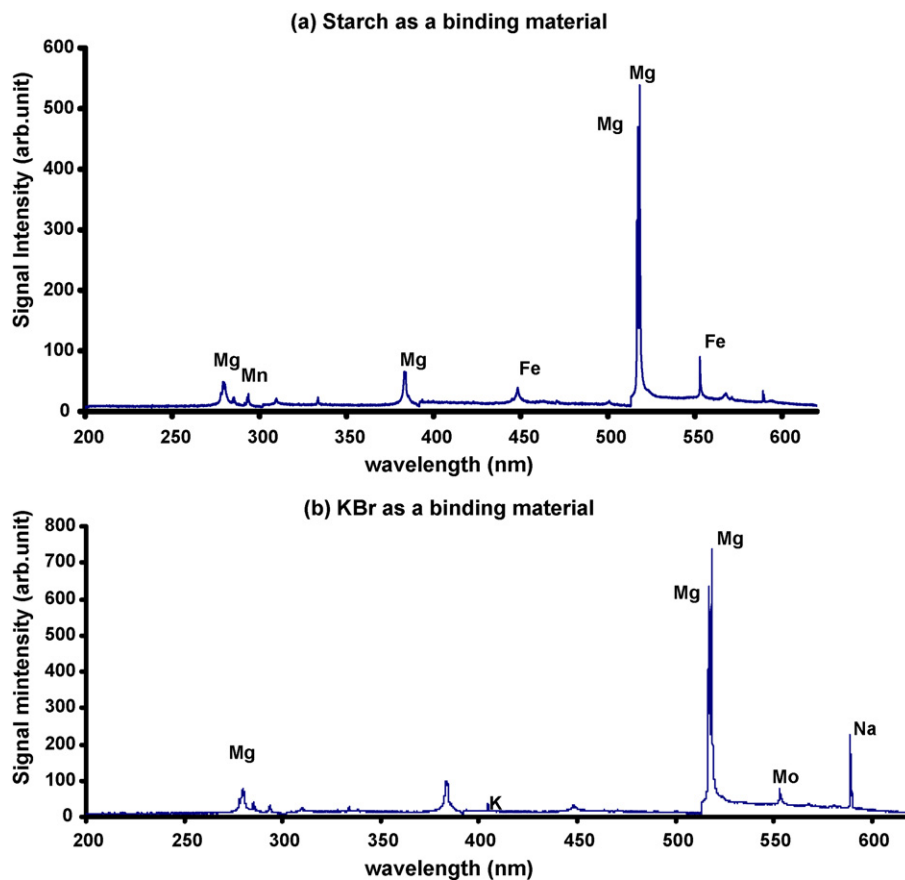
Fig. 3. LIBS spectrum of Mg mixed in various binding materials recorded in 200–620 nm region at a delay time = 4.5 µs and laser pulse energy = 20 mJ. (a and b) Representative spectra of Mg with starch and potassium bromide as binding materials.

for other elements, such as Ca and Cu whose emission lines have no interference and are free from self-absorption by the binding materials. In addition to Mg lines, some additional emission lines have been recorded in the spectral region 200–620 nm (see, for example, Figs. 2 and 3). These lines are due to the impurities in the applied reagents. For example, one can notice the presence of Mo and Fe in Fig. 2(a) which is due to the impurities in the aluminum powder used for this study. Similarly Fe, Ca and Na are indicated in Fig. 2(b) and are due to impurities in the poly(vinyl alcohol). Fe is recorded in Fig. 3(a) and is due to impurities in starch.

As clear from Table 1, the signal intensity for Mg lines is largest for KBr as a binding material while Mg/starch matrix is second and the lowest signal intensity was recorded for Mg/aluminum matrix.

It is well reported that in LIBS analysis, the physical and chemical properties of the sample can affect the plasma composition. The so-called matrix effect becomes important for LIBS sensitivity enhancement [14–26]. Matrix effects are related to complicated phenomena involved in plasma formation and sample ablation. Many of the involved processes are highly nonlinear and are not fully understood [24–29]. We have performed a series of experiments to understand the role of various binding materials rather than a theoretical approach. Our study has experimentally revealed that the proper choice of binding material is of vital significance. One of the unsolved problems related

to laser-induced plasma spectroscopy analysis is its sensitivity to matrix effects and their influence on the results. Due to this problem only relative concentrations are often obtained based on an internal standard of constant concentration. There are several possible reasons for sensitivity (line intensity) enhancement due to matrix effects. It can be due to simple geometrical factors, or it can be due to differences in grain size distributions of Mg in different binding materials. Also, there could be spectral line interference due to line overlap of Mg with binder material absorption lines, and thereby self-absorption could reduce the overall LIBS signal intensity for Mg lines.

In order to understand the matrix effect on signal intensity of Mg, we also measured the crater depth of all pellets after laser irradiation. In addition, for comparative study of the effect of binder under investigation, we optimized the experimental parameters such as incident laser energy, in addition to time delay between the initiation of plasma (arrival of the laser pulse) and the collection of plasma emission (activation of the detector).

3.2. Laser energy and crater depth

The crater depth is an important parameter for the understanding of the laser ablation process and eventually the LIBS signal intensity enhancement on Mg lines in various binding materials. The craters created by the laser beam are affected by many parameters. Of greatest influence are: (1) the magnitude of
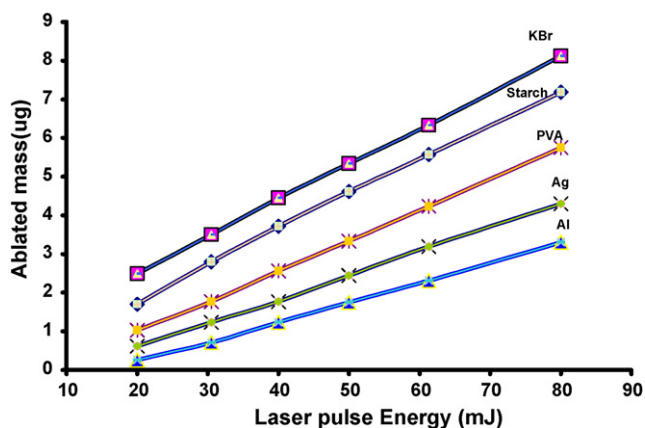
Fig. 4. Influence of incident laser pulse energy on ablated mass for different binding materials.

the incident laser energy, (2) the geometry of the incident radiation and (3) the particle bond strength of the sample. Studies of laser-induced breakdown spectroscopy by laser ablation through material removal and crater depth have been investigated by researchers [23–29]. The mass–ablation rate "m (kg s^{-1} cm^{-2})" with absorbed laser intensity (I_a), laser wavelength λ and atomic number Z based on experimental data for laser energies lower than 10^{13} W cm^{-2} is given by [23]:

$$m \text{ (kg s}^{-1} \text{ cm}^{-2}) = 65 \frac{(I_a)^{5/9} \text{ (W cm}^{-2})}{10^{13}} \lambda^{-4/9} \text{ (μm) } Z^{1/4}$$
(1)

In our work, the ablated mass was measured using a very sensitive (microgram resolution) balance at different laser pulse energies emitted at 1064 nm fundamental wavelength of the Nd:YAG laser. The ablated mass was recorded at 20, 30, 40 and 50 mJ/pulse laser energy. The experimental curves obtained for the binding materials under investigation are shown in Fig. 4. This figure shows the effect of laser pulse energy on mass ablated for these binding materials.

The experimental values show reasonable agreement with the values predicted by the abovementioned equation.

The crater depth, "d", in terms of the crater radius "r", is given by [23]:

$$d = \frac{J(A_i)}{K_i C(A_i) \pi r^2 (1-x)}$$
(2)

where A_i represents a matrix element and $C(A_i)$ is volume concentration in the binder matrix, K_i is a constant that represents the emission affectivity, and x is Mg percentage. In all the cases of various binding materials the crater depths were measured after irradiation of the binder samples with 20 laser pulses. Fig. 5 depicts images recorded using optical scanning microscopy. A central tiny crater is surrounded by a ring shaped structure originating from residues of the melted material pushed out of the interaction region by the pressure of the laser-induced plasma and the accompanying shock wave.

The values of crater depth measured with scanning electron microscope for Mg/KBr matrix, Mg/poly(vinyl alcohol),

Mg/starch matrix, Mg/aluminum matrix and Mg/Ag matrix were 80, 70, 25, 10 and 40 μm, respectively, and are listed in Table 2.

The binding material (matrix) plays an important role in efficiently coupling the laser energy into the sample, ablating a measurable quantity of mass, reducing fractionation, and minimizing relative standard deviation (R.S.D.) values. However, the fundamental physical processes of laser ablation are not fully understood. In this context, several recent articles and conference proceedings have been devoted to this issue [24–29].

The measurement of ablated mass and crater depth could be good indications for understanding the enhancement of LIBS signal intensity in various binders. Indeed, as is clear from Table 2, for binders in which more material is ablated, the crater is deeper and the LIBS signal intensity for Mg lines and the signal to noise ratio (SNR) is high. In our study, the deepest craters, maximum ablated material and the highest LIBS signal intensity and SNR were recorded for KBr. Hence, the greatest LIBS sensitivities may be achieved by using KBr as a binder amongst the binders in our study.

The increase in crater depth for KBr matrix could be due to various factors, such as the grain size of the KBr powder and the bond strength amongst the grains. The ablated material and the crater depth are dependent on the thermal process. Electrons absorb the laser light, transferring this energy into the atomic lattice. Melting and vaporization of the target material occurs during this process. Because of the difference in latent heat of vaporization for different chemical materials (or elements in binding materials), a thermal mechanism may induce strong fractionation. Moreover, if the incident laser photon energy is higher than the bonding energy between neighboring atoms in the solid matrix, the electromagnetic laser radiation can directly break the atomic lattice, inducing ion and atom ejection without traditional heating effects. This would principally result different numbers of vaporized atoms for different matrices and would be the cause for the variations in the Mg line signal intensity observed between different matrices in this study. Hence, the number of vaporized atoms (proportional to ablated mass or crater depth) is the driving parameter which varies between KBr, poly(vinyl alcohol), Ag, Al and starch matrices.

In addition to abovementioned facts, the sample (pellets) preparation method is very important and could influence the LIBS signal intensity significantly. The pellet quality depends on the grain size of the matrix material which mainly depends how much the sample is finely milled, roughly ball-milled and/or not milled. By fine milling, one can reduce the grain size. Due to this milling procedure, the grain size in different pellets could vary, resulting in variation of the ablation diameter under same experimental conditions (laser energy, laser wavelength, beam shape, etc.). The range of grain sizes attained after fine milling of our binding materials are listed in Table 2. Another effect of grain size could be on crater diameter and R.S.D. In the case of samples having larger grain size, rough crater bottom surfaces were detected with a larger crater diameter and depth. The R.S.D. values also vary for different grain sizes. In the case of the finely ball-milled (smallest grain size) sample pellets, the R.S.D. values recorded for respective line intensity were lower

(a) Binding material KBr,
crater depth 80μm

(b) Binding material poly(vinyl alcohol)
crater depth 70μm

(c) Binding material starch,
crater depth 25μm

(d) Binding material aluminum
crater depth 10μm

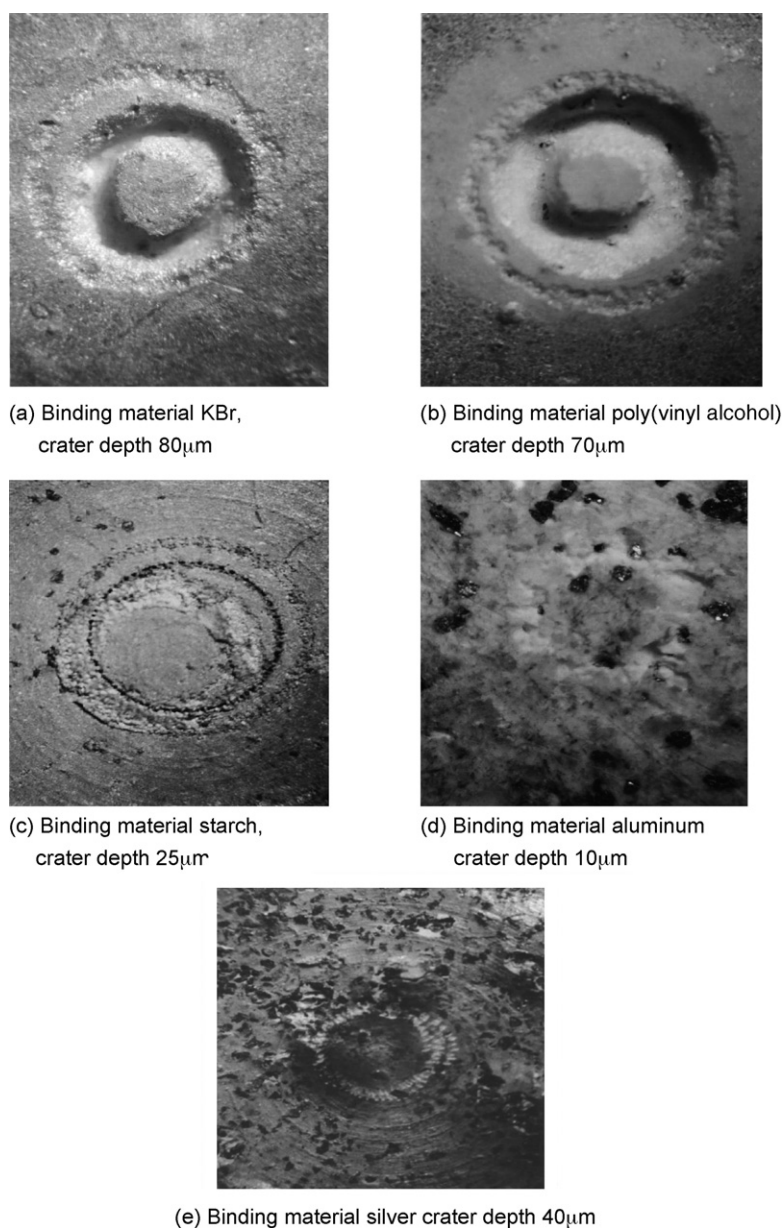(e) Binding material silver crater depth 40μm

Fig. 5. Optical scanning microscopy images of the laser ablated crater under different binding materials: (a) KBr, (b) poly(vinyl alcohol), (c) starch, (d) aluminum and (e) silver.

than for those having larger grain sizes. The reason of low R.S.D. values for smaller grain size could be the homogeneous mixing of the trace metal and the binding material. The homogeneity of pallet could enhance the reproducibility of LIBS signal emission intensity of Mg lines and thus reduce the R.S.D. values. In this study, the improvement in standard deviation of the LIBS results was also noticed with an increasing number of accumulations.

Table 2
Comparison of crater depth and mass ablated (theoretical and experimental values) at laser pulse energy of 20 mJ and Nd:YAG laser at 1064 nm

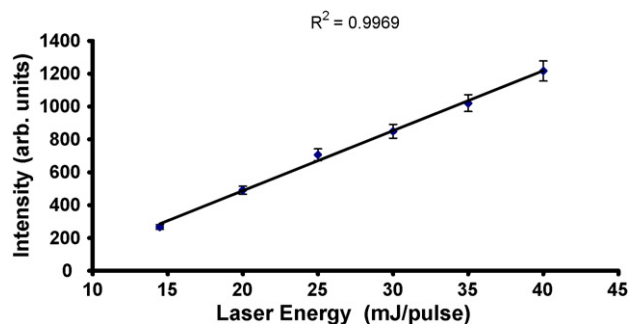| Binding material	Crater depth (μm)		Mass ablated (μg)			Grain size range (μm)
	Measured	Standard deviation	Measured	Theoretical	Standard deviation	
KBr	80	2.2	2.7	3.1	0.4	100–600
PVA	50	3.8	1.2	1.35	0.21	20–100
Starch	70	5.02	1.9	2.2	0.38	80–400
Al	45	4.4	0.5	0.7	0.15	10–200
Ag	10	4.53	0.6	0.8	0.18	10–300

Fig. 6. Plot of dependence of the intensity of the Mg 518.36 nm emission line on laser energy with KBr as a binding material.

3.3. Influence of laser energy on binding materials

The dependence of Mg signal intensity on the incident laser energy and the binding material was also studied in this work. The dependence of Mg signal on laser pulse in the matrix of KBr is presented in Fig. 6. The LIBS signal for Mg 518.36 nm line intensity is plotted as a function of incident laser energy. It is clear from Fig. 6 that the LIBS signal is linearly dependent on the incident laser energy. This is indicated by the least square fit with $R^2 = 0.994$.

With higher irradiation laser energy, more material is ablated from the pellet and thus the LIBS signal intensity is higher. This can be explained by a theoretical model [19,23] where the LIBS signal intensity (*I*) is given by [19]:

$$I = h\nu_{ji} A_{ji} N g_j Q^{-1} \; \exp\left(\frac{-E_j}{kT}\right) \tag{3}$$

where ν_{ji} is the frequency of the transition from state j → i, A_{ji} the Einstein coefficient for spontaneous emission between states j and I, *N* the population density of the ground state, *h* Planck's constant, g_j and E_j the statistical weight and energy of upper level j, *Q* the partition function of the relevant species, *k* the Boltzmann's constant and *T* is the electron temperature of the plasma.

From Eq. (3), the population density *N* which is excited from the ground state to the upper level j depends on the mass of the ablated material which eventually depends on the incident laser energy as indicated by the graph depicted in Fig. 6.

3.4. Dependence of LIBS signal on Mg concentration in KBr matrix

As clear from Eq. (3), the LIBS signal intensity depends on the number of the particles "*N*" of Mg excited to the higher state "j", which de-excite to lower state "i" to emit the 518.3 nm wavelength. In order to verify this, we studied the dependence of LIBS signal intensity at 518.3 nm for various concentrations of Mg prepared in KBr binder. Four samples of concentrations 10, 1, 0.1 and 0.01% corresponding to 10^5, 10^4, 10^3 and 10^2 mg kg^{-1} of Mg were prepared in the matrix of KBr. The LIBS spectra were recorded for these four concentrations. All these spectra were recorded at three different locations on the sample surface with an average of 20 laser pulses. This averaging of the
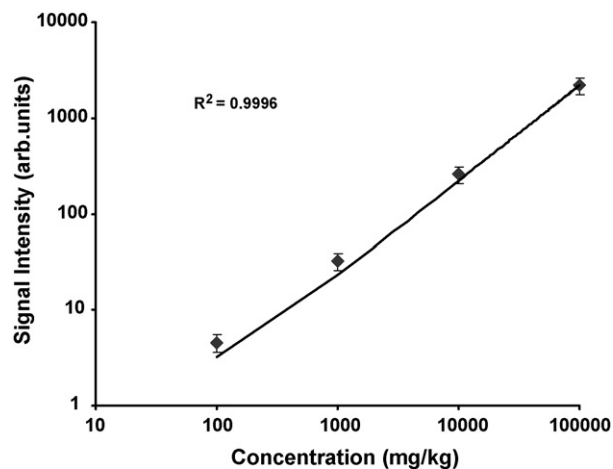

Fig. 7. The LIBS signal intensity of the Mg 518.36 nm emission line at various known concentrations of magnesium mixed with KBr as a binding material.

spectra reduces the background noise to a great extent when compared to the single shot spectrum of the sample. The signal intensities were recorded at 518.3 nm and plotted as a function of concentration of Mg as depicted in Fig. 7.

The signal intensity increases linearly with the increases in concentration of Mg which is clear from the least square fit $R^2 = 0.9996$.

This linear dependence of LIBS signal intensity agrees well with the predictions of Eq. (3) which shows that LIBS signal intensity is proportional to the number density of magnesium atoms "*N*" excited through the laser ablation process.

4. Conclusions

Various materials like KBr, poly(vinyl alcohol), silver, aluminum and starch were investigated as binding materials for LIBS analysis of powder samples. The masses ablated and crater depths were measured. By comparing the signal intensity recorded of selected Mg line in different binders, KBr matrix proved to be the best binder. The values obtained for crater depths and ablated mass also support the above findings.

Acknowledgements

References

[1] L.J. Radziemski, D.A. Cremers, in: L.J. Radziemski, D.A. Cremers (Eds.), Applications of Laser-Induced Plasmas, Marcel Dekker, New York, 1989, pp. 295–325.
[2] D.A. Cremers, M.J. Ferris, M. Davies, Proc. Soc. Photo Opt. Instrum. Eng. 2835 (1996) 190.
[3] M. Kuzuya, H. Matsumoto, H. Takechi, Appl. Spectrosc. 47 (1993) 1659.
[4] K.Y. Yamamoto, D.A. Cremers, M.J. Ferris, L.E. Foster, Appl. Spectrosc. 50 (1996) 222.

[5] M.Z. Martin, M.D. Cheng, Appl. Spectrosc. 54 (2000) 1279.

[6] D. Gunther, S.E. Jackson, H.P. Longerich, Spectrochim. Acta B 54 (1999) 381.

[7] G.A. Latif, H. Imam, Spectrochim. Acta B 57 (2002) 1155.

[8] J.A. Bolger, Appl. Spectrosc. 54 (2000) 181.

[9] M. Noda, Y. Deguchi, S. Iwasaki, N. Yoshikawa, Spectrochim. Acta B 57 (2002) 701.

[10] D.A. Cremers, J.E. Barefield, A.C. Koskelo, Appl. Spectrosc. 49 (1996) 857.

[11] J. Leon, L.J. Radziemski, Spectrochim. Acta Part B 57 (2002) 1109.

[12] S. Sjostrom, P. Mauchien, Spectrachim. Acta B 15 (1991) 153.

[13] A.A. Hauer, H.A. Baldis, in: L.J. Raziemski, D.A. Cremers (Eds.), Laser-Induced Plasmas and Applications, Marcel Dekker, New York, 1989, p. 1109.

[14] C.J. Lorenzen, C. Carlholf, U. Hahn, M. Jogwich, J. Anal. At. Spectrom. 7 (1992) 1029.

[15] R. Noll, H. Bette, A. Brysch, M. Kraushwar, I. Monch, L. Peter, V. Strum, Spectrochim. Acta Part B 56 (2001) 637.

[16] K. Song, Y.I. Lee, J. Sneddon, Appl. Spectrosc. Rev. 32 (1997) 187.

[17] Y.I. Lee, K. Song, J. Sneddon, Laser-Induced Plasma in Analytical Atomic Spectroscopy, VCH Publishers, New York, 1997, pp. 197–236.

[18] P.W. Boumans, Inductively Coupled Plasma Emission Spectroscopy (Part 1), Wiley, New York, 1987.

[19] M.A. Gondal, T. Hussain, Talanta (available online, 28 April 2006), in press.

[20] M.A. Gondal, T. Hussain, Z.H. Yamani, Talanta 69 (2006) 1072.

[21] T. Hussain, M.A. Gondal, Z.H. Yamani, Environ. Monit. Assess. (available online, 6 September 2006), in press.

[22] M.A. Gondal, T. Hussain, Z.H. Yamani, Energy Sources, in press.

[23] G. Bekefi, C. Deutsch, B. Yaakobi, Principal of Laser Plasma, Wiley, New York, 1976.

[24] H.T. Buscher, R.G. Tomlinson, E.K. Damon, Phys. Rev. Lett. 15 (1965) 847.

[25] R.A. Bingham, P.L. Salter, Anal. Chem. 48 (1976) 1735.

[26] N. Omenetto, J. Anal. At. Spectrom. 13 (1998) 385.

[27] S. Amoruso, R. Bruzzese, N. Spinelli, R. Velotta, J. Phys. B 32 (1999) R131.

[28] R.E. Russo, D.B. Geohegan, R.F. Haglund Jr., K. Murakami, Proceedings of the Fourth International Conference on Laser Ablation, Elsevier, Amsterdam, 1998.

[29] J.S. Horwitz, H.U. Krebs, K. Murakami, M. Stuke, Proceedings of the Fifth International Conference on Laser Ablation, Springer, Heidelberg, 1999.

ELSEVIER

Effect of oxidant type on the chemiluminescence intensity from the reaction of tris(2,2′-bipyridyl)ruthenium(III) with various organic acids

Bree A. Gorman [a], Kieran F. Lim [a], Conor F. Hogan [b], Neil W. Barnett [a],*

[a] *School of Life and Environmental Sciences, Deakin University, Geelong, Victoria 3217, Australia*
[b] *Department of Chemistry, La Trobe University, Victoria 3086, Australia*

Abstract

An investigation into the chemiluminescence of fourteen organic acids and tris(2,2′-bipyridyl)ruthenium(II) was undertaken. Particular emphasis was placed upon the method of production of the reagent, tris(2,2′-bipyridyl)ruthenium(III), with cerium(IV) sulfate, potassium permanganate, lead dioxide and electrochemical generation. Analytically useful chemiluminescence was observed when Ce(IV) or potassium permanganate were employed as oxidants. The kinetics of analyte oxidation was related to the intensity of the chemiluminescence emission, which increased by three orders of magnitude for tartaric acid after 40 h of oxidation.
© 2006 Elsevier B.V. All rights reserved.

Keywords: Tris(2,2′-bipyridyl)ruthenium(II) chemiluminescence; Organic acids; Ce(IV); Electrochemiluminescence

1. Introduction

Low-molecular mass organic acids are found in many natural and synthetic matrices [1–4]. They are often metabolites of biochemical pathways including the citric acid cycle, carbohydrate fermentation and ethanol oxidation [5]. Commonly, they are found in food products including juices [2], wine [2], honey [3] and also as vitamin supplements. Determination of organic acids in urine and other bodily fluids has facilitated the diagnosis of central nervous system diseases, neuroblastoma and nephrolithiasis [5]. Current analytical techniques include capillary electrophoresis [5,6], HPLC [7,8], gas chromatography [9] and enzymatic procedures [10,11]. Various organic acids have been determined using tris(2,2′-bipyridyl)ruthenium(II) chemiluminescence [12–17]. Due to the poor sensitivity and slow kinetics of these reactions this type of chemiluminescence has not been exploited or investigated with these analytes to the same extent as those containing amine moieties [18,19].

Electrochemical oxidation is by far the most common method used to generate tris(2,2′-bipyridyl)ruthenium(III).
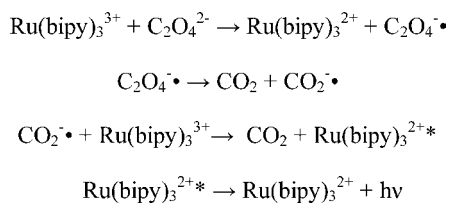
Seventy percent of papers published since 1998 on tris(2,2′-bipyridyl)ruthenium(II) chemiluminescence have utilised this method of generation [18]. However, organic acid determinations have predominantly been achieved through the use of cerium(IV) sulfate as the oxidant [13–15,20]. Rubinstein and Bard investigated the electrochemiluminescence of oxalate and some organic acids with tris(2,2′-bipyridyl)ruthenium(II) [21] and proposed the reaction mechanism shown in Scheme 1.

These authors [21] also proposed that tris(2,2′-bipyridyl)ruthenium(III) did not have the oxidising strength to produce a radical intermediate from pyruvate and other organic acids [21]. However, upon the addition of the auxiliary oxidant Ce(IV) they postulated the reactions shown in Scheme 2:

The final product in Scheme 2 (CH$_3$CO$^\bullet$) is a strong reducing agent which reacts with tris(2,2′-bipyridyl)ruthenium(III) to produce the excited species in a similar fashion to the carbon dioxide anion radical in Scheme 1. Knight and Greenway [17] used Ce(IV) to determine pyruvate by electrochemiluminescence. Other groups employed Ce(IV) to oxidise tris(2,2′-bipyridyl)ruthenium(II) for the determination of oxalate [22], tartaric acid [15,22], pyruvic acid [13,15] and citrate [13] *via* simple chemiluminescence. All authors [13,15,22] reported a strong dependence upon sulfuric acid and cerium(IV) concen-

---

* Corresponding author. Tel.: +61 3 52271409.
  E-mail address: barnie@deakin.edu.au (N.W. Barnett).

$$Ru(bipy)_3^{3+} + C_2O_4^{2-} \rightarrow Ru(bipy)_3^{2+} + C_2O_4^{-}\bullet$$

$$C_2O_4^{-}\bullet \rightarrow CO_2 + CO_2^{-}\bullet$$

$$CO_2^{-}\bullet + Ru(bipy)_3^{3+} \rightarrow CO_2 + Ru(bipy)_3^{2+}*$$

$$Ru(bipy)_3^{2+}* \rightarrow Ru(bipy)_3^{2+} + h\nu$$

Scheme 1. Electrochemiluminescence reaction mechanism for the reaction between oxalate and tris(2,2′-bipyridyl)ruthenium(III) [21].

$$Ce^{4+} + CH_3COCO_2^{-} \rightarrow Ce^{3+} + CH_3COCO_2\bullet$$

$$CH_3COCO_2\bullet \rightarrow CH_3CO\bullet + CO_2$$
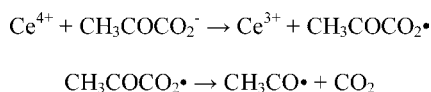
Scheme 2. Reaction of Cerium(IV) and pyruvate [21].

trations and noted that the reaction kinetics were different for each analyte.

To date, there has been no systematic investigation of the relationship between oxidant and analyte in tris(2,2′-bipyridyl)ruthenium(II) chemiluminescent reactions. In this work, fourteen organic acids were subjected to oxidation both electrochemically and chemically in the presence of tris(2,2′-bipyridyl)ruthenium(II).

2. Experimental

2.1. Flow injection analysis

The FIA was constructed from a Gilson Minipuls^{TM} 3 Peristaltic pump (John Morris Scientific Pty. Ltd., Australia) and a six port injection valve (Valco Instruments Company, Model E60-220) using PVC pump tubing (1.02 mm i.d., Protech Group Pty. Ltd., Coolum Beach, QLD, Australia). A spiral PTFE tubing flow cell constructed in-house was positioned directly in front of a photomultiplier tube (Electron Tubes, UK) biased at 900 V (Thorn EMI power supply, Electron Tubes, UK). Signals were recorded on a strip chart recorder (Yokogawa Electric Works Ltd., Tokyo, Japan). The instrument was enclosed in a light-tight box made in-house.

2.1.1. Procedure 1

A simple two-line manifold was employed with a 70 µL injection loop. The organic acids (0.01 M) were injected into a running stream of tris(2,2′-bipyridyl)ruthenium(II) (0.1 mM), which merged with either cerium(IV) sulfate (1 mM) or potassium permanganate (1 mM) at the point of detection.

2.1.2. Procedure 2

Cerium(IV) sulfate (10 mL of 1 mM) was added to 20 mL of organic acid (0.01 M). Samples were taken at different time intervals and injected into a sulfuric acid (0.05 M) carrier stream. Tris(2,2′-bipyridyl)ruthenium(III) was prepared off line by the addition of cerium(IV) sulfate, before merging with the sample at the point of detection.

2.1.3. Procedure 3

Tris(2,2′-bipyridyl)ruthenium(III) (0.1 mM in 0.05 M sulfuric acid) was prepared off-line by the addition of solid lead dioxide (4 g in 100 mL). The solution was filtered on line prior to merging with a sulfuric acid carrier (0.05 M) into which the sample (10 mM in deionised water) was injected.

2.1.4. Procedure 4

All electrochemical experiments were carried out using a µ-Autolab Type II (Eco Chemie) potentiostat. 3 mm diameter glassy carbon disk electrodes embedded in a 6 mm diameter teflon body (CH instruments) were used as working electrodes with a 1 cm^2 platinum gauze and an Ag/AgCl (3 M KCl) electrode as counter and reference electrodes, respectively. Light emission during the electrochemiluminescence experiments was detected using a 9828SB photomultiplier tube (Electron Tubes, UK) positioned underneath the cell. A specially designed holder and quartz glass cell was used to position the working electrode opposite the PMT in a reproducible manner. The PMT was biased at +500 V using a high voltage supply (Electron Tubes, UK) and signal amplification was performed using an amplifier constructed in house. The entire electrode assembly was housed inside a light-tight box which also served as a Faraday cage. Data acquisition and manipulation were performed using the auxiliary channel of the potentiostat and GPES software package (Eco Chemie, Netherlands). Organic acids (1 mM) were added to tris(2,2′-bipyridyl)ruthenium(II) (1 mM in appropriate buffer solution) in a 2.5:1 molar ratio. The electrochemiluminescent reaction was initiated in each case by scanning the potential between 0 V and 1.35 V.

2.2. Reagents

All chemicals were supplied by Sigma–Aldrich unless otherwise noted. Tris(2,2′-bipyridyl)ruthenium(II) (0.1 mM), cerium(IV) sulfate (1 mM) and potassium permanganate were prepared in 0.05 M sulfuric acid. All organic acids (See Fig. 1) were dissolved in deionised water at a concentration of 0.01 M. Buffer solutions used for pH range experiments were glycine/hydrochloric acid (pH 2–3.5), sodium acetate/acetic acid (pH 4–5.5) and potassium dihydrogen phosphate/ sodium hydrogen phosphate (pH 6–8) at 0.1 M.

3. Results and discussion

3.1. Cerium(IV) sulfate

The use of Ce(IV) in tris(2,2′-bipyridyl)ruthenium(II) chemiluminescence has been restricted due to its low solubility at greater than pH 3 and its oxidising strength [23]. The latter restriction is a benefit for the determination of organic acids as oxidation of the analyte is necessary to produce a species that reacts with tris(2,2′-bipyridyl)ruthenium(III) to emit light. Table 1 presents the emission intensities of fourteen organic acids upon reaction with tris(2,2′-bipyridyl) ruthenium(II)/cerium(IV) (utilising procedure 1).
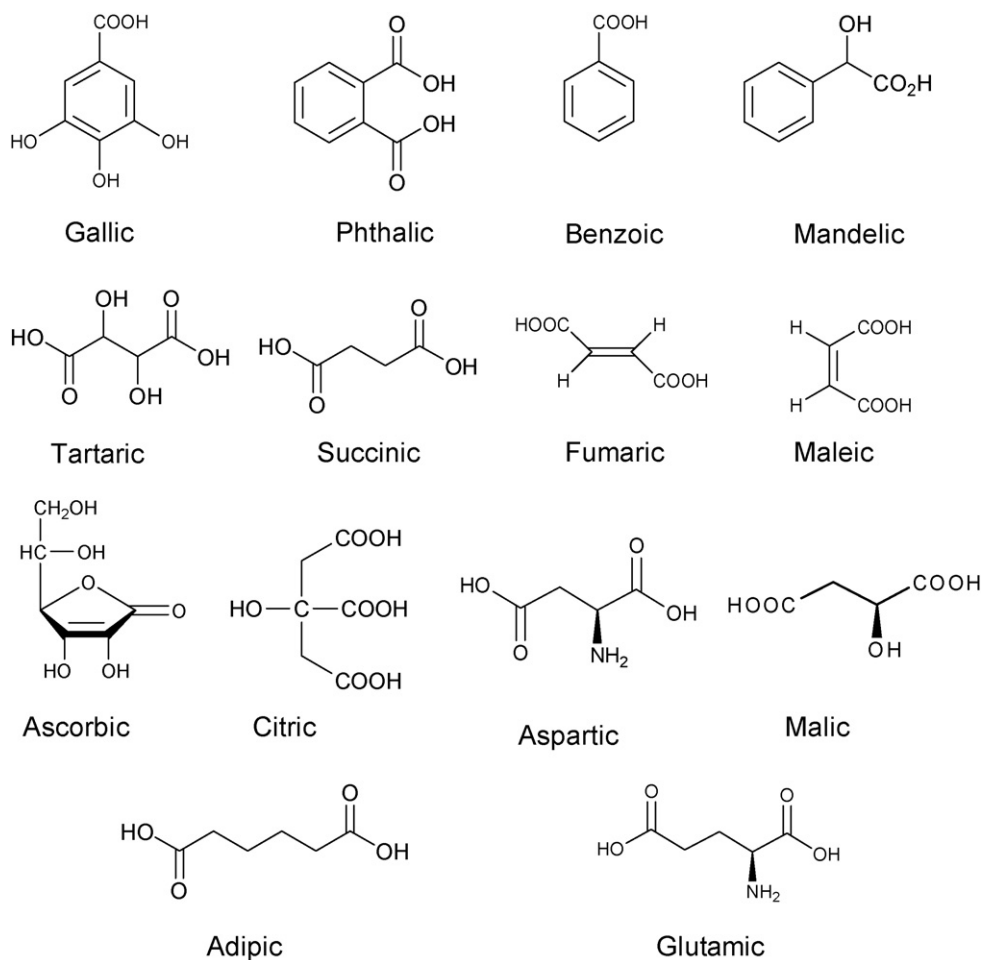
Fig. 1. Structures of fourteen organic acids investigated in this study.

The choice of aqueous medium was vital to the generation of chemiluminescence; for example perchloric acid quenched the emission observed with ascorbic acid. Conversely, tartaric and malic acid exhibited an increase in emission intensity in the presence of perchloric acid. Four of the six organic acids that produced light upon reaction with tris(2,2′-bipyridyl)ruthenium(III) in the presence of Ce(IV) contained a hydroxyl moiety alpha to a carboxylic acid.

Table 1
Emission intensities of 14 organic acids upon reaction with tris(2,2′-bipyridyl)ruthenium(II) oxidised by Ce(IV), $KMnO_4$ and electrochemistry

Organic acid	Intensity (Ce(IV) in sulfuric acid[a])	Intensity (Ce(IV) in perchloric acid)	Intensity ($KMnO_4$ as oxidant)	Intensity (ECL[b])
Mandelic	3	2	0	0.7
Aspartic	0	0	0	0
Malic	0	0.4	0	0.3
Tartaric	0	0.2	0	0.5
Maleic	0	0	0.35	0.4
Fumaric	0	0	2	0
Gallic	1.2	1.4	0.5	0
Ascorbic	5	0.1	4.5	0.2
Citric	22.5	11	0	1.1
Benzoic	0	0	0	0.3
Glutamic	0	0	0	0.3
Adipic	0	0	0	0.3
Succinic	0	0	0	0.2
Phthalic	0	0	0	0.7

All intensities are displayed in V.
  [a] Sulfuric acid (0.05 M), perchloric acid (0.5 M).
  [b] Due to the use of a different instrument and different PMT bias, intensities are not directly comparable to chemiluminescence emission intensities.

Much has been published on the oxidation of organic acids using Ce(IV) in sulfuric acid [24–29]. Singh et al. stated that the maleic acid/cerium(IV) oxidation was sluggish by nature but resulted in the production of glyoxylic acid [24]. The oxidation of fumaric acid by cerium(IV) perchlorate was described also as being relatively slow [28]. All papers published reported the transient formation of a cerium(IV)/organic acid complex. The kinetics of the reaction between tartaric acid and cerium(IV) have been investigated by Sengupta [25] and Ali and Aziz [27]. It was shown that the final products of oxidation are formic acid and carbon dioxide. Initially, the formation of a red tartrate-Ce(IV) complex was observed [25]. In the current study, cerium(IV) sulfate was added to each acid in a 5:1 molar ratio and the results were monitored both visually and with UV-visible spectrometry. In the case of tartaric acid the aforementioned red complex [25] was observed, and some of the other acids also exhibited a colour change upon mixing. Following initial reaction most of the solutions became colourless albeit at different rates. This is postulated [25] to coincide with the decomposition of the red complex to form an intermediate radical followed by reaction with more Ce(IV) to afford, in the case of tartaric acid, glyoxylic acid [25]. Hydration and oxidation then occurs resulting in formic acid formation [25].

The complex formation of tartaric acid was followed using UV-Visible spectrometry at 430 nm after the method of Drake and Nutt [26] and was found to be complete within five minutes. The chemiluminescence was observed to increase in intensity over the same five-minute period. The emission intensities for all acids were then monitored after addition of cerium(IV) sulfate over a period of one hundred and 40 h utilising procedure 2 (see Fig. 2). The chemiluminescence of tartaric acid increased dramatically in the first 25 h. The experiment was repeated for all acids resulting in similar trends. The control showed no fluctuation in intensity over the time period studied. Temperature remained constant throughout the experiment.

The chemiluminescence was possibly due to the reaction of the products of oxidation, formic or glyoxylic acid, with tris(2,2′-bipyridyl)ruthenium(III). These postulated intermedi-
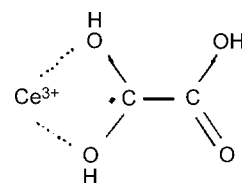

Fig. 3. Proposed structure of the radical species produced upon the oxidation of glyoxylic acid with Ce(IV) [31].

ates were then subjected to procedure 1 and while no light was observed from formic acid, the glyoxylic acid produced an intense response (e.g. 1 mM resulted in 160 V signal) that could be seen with the naked eye. The responses from formic acid and glyoxylic acid did not change over time (140 h).

Mehrotra et al. disagreed with the proposal by Sengupta [25] that glyoxylic acid was an intermediate in this reaction and proposed a different intermediate species; HOOC–CH(OH)–CH(OH)$^•$ [30]. This species may also produce chemiluminescence with tris(2,2′-bipyridyl)ruthenium(III) but is not likely to be long-lived, therefore precluding the observation of the intense emission seen from the tartaric acid/cerium(IV) solution after twenty hours of reaction. Hence, the formation of glyoxylic acid from the Ce(IV) oxidation of tartaric acid may be a likely source of the increase in chemiluminescence. Neumann and co-workers attempted to identify the radical species produced by the oxidation of glyoxylic acid with Ce(IV) using rapid-flow EPR measurements [31]. They postulated a structure for the radical species based on evidence of Ce(III) complexation (see Fig. 3). Vijai and co-workers proposed the existence of a radical in the mechanism of the reaction between tris(2,2′-bipyridyl)ruthenium(III) and glyoxylic acid with peroxodisulfate as the oxidant, however no evidence was provided to support this postulation [32]. Sengupta showed that the rate constant of the reaction increased with an increase in temperature [25]. Consequently, the reaction mixtures were heated at 70 °C for 1 h and as expected, this substantially increased the emission intensities (see Table 2).

Three calibrations of tartaric acid were performed at different concentrations of Ce(IV) over a period of 90 h. The molar ratios of Ce(IV) to analyte and chemiluminescence intensities were calculated and are shown in Table 3. The results obtained for low concentrations of tartaric acid ($1 \times 10^{-7} - 1 \times 10^{-5}$ M) followed a different trend and therefore possibly a different mechanism to those of 1×10^{-4} M to 1×10^{-3} M. Low concentrations of analyte exhibited minimal intensities, increases
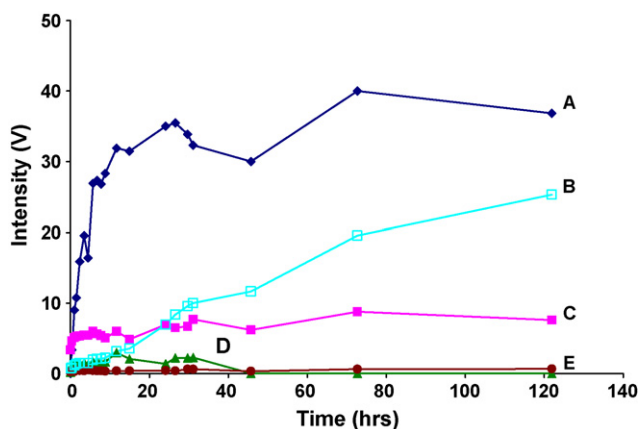

Fig. 2. Intensity vs. time profiles, utilizing procedure 2, for (A) tartaric acid (B) ascorbic acid (C) citric acid (D) mandelic acid (E) gallic acid. Cerium(IV) sulfate was added in a 1:2 volume ratio oxidant to acid. Temperature remained constant throughout the experiment.

Table 2
Effect of heating upon the emission intensities of organic acids mixed with cerium(IV) sulfate prior to detection

Organic Acid	Intensity prior to heating (V)	Intensity after heating (V)
Citric	1.2	5.3
Ascorbic	5.2	6.5
Malic	0	1.3
Tartaric	0	6.8

Prior to heating: the analytes were mixed with Ce(IV) and then reacted with tris(2,2′-bipyridyl)ruthenium(II), After heating: the same solutions were then heated for one hour at 70 °C.

Table 3
Increases in tris(2,2′-bipyridyl)ruthenium(II) chemiluminescence observed for two different tartaric acid concentrations upon reaction with Ce(IV) over time

Molar ratio[a]	Time = 0 h	Time = 20 h	Time = 44 h	Time = 92 h
1×10^{-7} M tartaric acid				
5.6:1	8	10	10	0
56:1	0	10	0	0
560:1	0	0	0	0
1×10^{-6} M tartaric acid				
0.56:1	8	13	13	0
5.6:1	8	17	12	12
56:1	0	0	0	0
1×10^{-5} M tartaric acid				
0.056:1	78	20	20	7.5
0.56:1	27	133	115	112
5.6:1	5	0	0	0
1×10^{-4} M tartaric acid				
0.0056:1	13	37	33	28
0.056:1	38	212	178	165
0.56:1	463	1940	1990	PMT overloaded
1×10^{-3} M tartaric acid				
0.00056:1	35	87	85	93
0.0056:1	84	445	408	397
0.056:1	668	1880	2070	PMT overloaded

[a] The molar ratio is the number of moles of Ce(IV) present to the number of moles of analyte present.

were observed over time and with increases in molar ratios for the first two calibration sets. High concentrations of tartaric acid exhibited significant increases in emission intensity, possibly a consequence of the oxidation of tartaric acid to glyoxylic acid followed by the formation of a radical species. The signal intensities of the high concentrations improved as the number of moles of Ce(IV) increased relative to tartaric acid. The responses recorded were reproducible at constant temperature, with no variation in intensity observed in the controls.

3.2. Potassium permanganate

Acidic potassium permanganate has been shown to elicit chemiluminescence upon reaction with some organic acids [33,34]. It has also been utilised as the oxidising agent in tris(2,2′-bipyridyl)ruthenium(II) chemiluminescence [35,36]. Emission intensities of the fourteen acids upon reaction with potassium permanganate and tris(2,2′-bipyridyl)ruthenium(II)/potassium permanganate are presented in Table 1 (procedure 1).

Of particular interest were the results for two geometric isomers (see Fig. 1) maleic and fumaric acids. Initially, fumaric acid produced light upon reaction with tris(2,2′-bipyridyl)ruthenium(II) in the presence of potassium permanganate, whereas the majority of the maleic acid emission from the tris(2,2′-bipyridyl)ruthenium(II)/potassium permanganate system was actually resulting from potassium permanganate (emission intensity with and without tris(2,2′-bipyridyl)ruthenium(II) was 0.35 V). This result demonstrated, for the first time, a degree of selectivity between two stereoisomers possibly due to the differing kinetics of the respective initial analyte oxidations.

To investigate the affect the reaction of potassium permanganate with the organic acids had on the chemiluminescence, oxidant and acid were mixed prior to detection. Only four of the

acids exhibited an increase in response over time (see Fig. 4). Citric acid which had previously exhibited no light emission in the presence of potassium permanganate was found to emit light with high sensitivity after approximately five hours. The responses for all four acids increased dramatically in the first five hours, with tartaric acid as an exception each acid then proceeded to decrease in intensity with time.

Unlike cerium(IV), potassium permanganate is soluble at most pH values. Therefore, the chemiluminescence of organic acids was investigated from pH 1.5 to pH 8.5. Above pH 8.5 the blank response, from the reaction of tris(2,2′-bipyridyl)ruthenium(III) with hydroxide ions, was more intense than the analyte signal [37]. Increasing the pH afforded chemiluminescence that had not been previously observed, for example; succinic acid and aspartic acid, albeit at low intensities. The pH
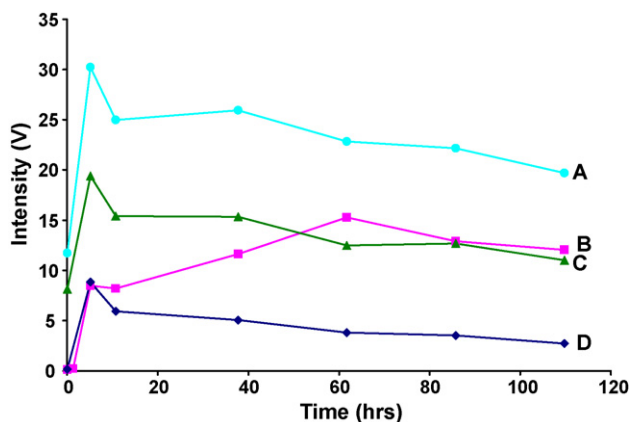

Fig. 4. Intensity vs. time profiles for (A) fumaric; (B) tartaric; (C) maleic; and (D) citric acids in the presence of potassium permanganate and tris(2,2′-bipyridyl)ruthenium(II).

profile for succinic acid showed increases in intensity at pH 4 and pH 6, which corresponds to the pK_a values of 4.16 and 5.61. A relationship between emission intensities and pK_a values did not exist for all of the analytes studied.

3.3. Lead dioxide

Lead dioxide has been used as an oxidant to generate tris(2,2′-bipyridyl)ruthenium(III) for the sensitive determination of various analytes including codeine, thebaine, proline, glyphosate, and ranitidine [38–41]. The reagent is filtered prior to injection to prevent valve damage, however this also precludes analyte oxidation due to the presence of residual lead dioxide [42]. Not surprisingly, the responses obtained from all fourteen analytes upon reaction with the lead dioxide-generated tris(2,2′-bipyridyl)ruthenium(III), were significantly poorer than those obtained when either Ce(IV) or potassium permanganate were employed as oxidants (procedure 3). For example, the intensity of the citric acid signal was six orders of magnitude less than that obtained with Ce(IV). The results illustrate the necessity for the pre-oxidation of these particular analytes in order to achieve analytically useful chemiluminescence upon reaction with tris(2,2′-bipyridyl)ruthenium(III).

3.4. Electrochemiluminescence

In situ electrochemiluminescence facilitates the oxidation of both analyte and reagent in close proximity to the detector [18]. Consequently, this approach potentially offers advantages similar to those seen above with either Ce(IV) or potassium permanganate. Specifically the oxidative modification of certain analytes to afford species that will elicit chemiluminescence from their reaction with tris(2,2′-bipyridyl)ruthenium(III). Table 1 shows the results achieved using electrochemical oxidation, which proved to be less selective towards the analytes than either Ce(IV) or potassium permanganate. The change in selectivity most probably resulted from a greater variety of oxidation pathways that exist for the acids in electrochemiluminescence than those of the chemical oxidants [43]. Although the ECL intensities cannot be directly compared with the CL intensities, the fact that the emission from the CL reactions could, in some cases, be seen with the naked eye suggests a higher level of sensitivity for the chemiluminescence method, at least under the conditions used in this study. Oxidant strength may have been a contributing factor in relation to the measured chemiluminescence intensities given that Ce(IV) ($E^\circ = 1.72$ V) [44] and potassium permanganate ($E^\circ = 1.5$ V) [44] are stronger oxidants than tris(2,2′-bipyridyl)ruthenium(III) [19]. Notably the electrochemiluminescence maximum was observed in each case close to 1.2 V, which is close to the oxidation potential for the reagent. It should be noted that the electrochemiluminescence results were obtained in quiescent solutions using a potential scan lasting only a few seconds for each measurement (see procedure 4). As a consequence only a very small quantity of tris(2,2′-bipyridyl)ruthenium(III) reagent is generated relative to the chemiluminescence experiment and the reactions leading to light emission are diffusion limited.

4. Conclusion

The choice of oxidant in the chemiluminescence of tris(2,2′-bipyridyl)ruthenium(II) is vital to selectivity and sensitivity. The variation in response could be a result of oxidant strength, products of oxidation, and the stability of an intermediate radical species. For example, the isomeric species fumaric and maleic acids showed different reactivity's with the tris(2,2′-bipyridyl)ruthenium(II)/potassium permanganate system. The reaction of some organic acids with oxidant prior to reaction with tris(2,2′-bipyridyl)ruthenium(III) increased signal intensity and, in the case of tartaric acid, by approximately three orders of magnitude. The dependence of the oxidation and chemiluminescence, upon the molar ratios of Ce(IV) to analyte and the identification of the species present in solution over time, are currently being investigated to assist in applying the increases in signal intensity to real samples.

References

[1] A. Moreno-Cid, M.C. Yebra, X. Santos, Talanta 63 (2004) 509–514.
[2] I. Mato, S. Suarez-Luque, J.F. Huidobro, Food Res. Int. 38 (2005) 1175–1188.
[3] I. Mato, J.F. Huidobro, J. Simal-Lozano, M.T. Sancho, Crit. Rev. Anal. Chem. 36 (2006) 3.
[4] C.W. Klampfl, W. Buchberger, P.R. Haddad, J. Chromatogr. A 881 (2000) 357–364.
[5] V. Galli, A. Garcia, L. Saavedra, C. Barbas, Electrophoresis 24 (2003) 1951–1981.
[6] M.-E. Yue, T.-F. Jiang, Y.-P. Shi, J. Anal. Chem. 61 (2006) 365–368.
[7] R.N. Collins, J. Chromatogr. A 1059 (2004) 1–12.
[8] S.-F. Chen, R. Mowery, V.A. Castleberry, G.P. van Walsum, C.K. Chambliss, J. Chromatogr. A 1104 (2006) 54–61.
[9] C. Dong, Y. Mei, L. Chen, J. Chromatogr. A 1117 (2006) 109–114.
[10] M.L. Tourn, A. Lombard, F. Belliardo, M. Buffa, J. Apicult. Res. 19 (1980) 144–146.
[11] F. Corradini, R. Pellegrini, Vini Ital. 20 (1978) 225–230.
[12] T. Perez-Ruiz, C. Martinez-Lozano, V. Tomas, J. Martin, J. Chromatogr. A 1026 (2004) 57–64.
[13] T. Perez-Ruiz, C. Martinez-Lozano, V. Tomas, J. Fenoll, Anal. Chim. Acta 485 (2003) 63–72.
[14] Z. He, X. Li, H. Meng, S. Lu, G. Song, L. Yuan, Y.e. Zeng, Anal. Lett. 31 (1998) 1553–1561.
[15] X. Li, L. Ling, Z. He, G. Song, S. Lu, L. Yuan, Y.e. Zeng, Microchem. J. 64 (2000) 9–13.
[16] X. Chen, W. Chen, Y. Jiang, L. Jia, X. Wang, Microchem. J. 59 (1998) 427–436.
[17] A.W. Knight, G.M. Greenway, Analyst 120 (1995) 2543–2547.
[18] B.A. Gorman, P.S. Francis, N.W. Barnett, Analyst 131 (2006) 616–639.
[19] R.D. Gerardi, N.W. Barnett, S.W. Lewis, Anal. Chim. Acta 378 (1999) 1–41.
[20] H. Han, Z. He, X. Li, Y. Zeng, Wuhan Univ. J. Nat. Sci. 4 (1999) 326–330.
[21] I. Rubinstein, A.J. Bard, J. Am. Chem. Soc. 103 (1981) 512–516.
[22] Z. He, H. Gao, L. Yuan, Q. Luo, Y.e. Zeng, Analyst 122 (1997) 1343–1345.
[23] S. Budavari (Ed.), Merck Index, Merck and Co. Inc., Whitehouse Station, N.J., 1996.
[24] A. Singh, R.A. Singh, Oxid. Comm. 29 (2006) 110–114.
[25] K.K. Sengupta, J. Indian Chem. Soc. 41 (1964) 427–431.
[26] E.N. Drake, J.L. Nutt, Tex. J. Sci. 22 (1971) 133–137.
[27] S.M. Ali, A. Aziz, Pak. J. Sci. Ind. Res. 9 (1965) 113–116.
[28] M. Ignaczak, J. Dziegiec, J. Sawicki, Acta Universitatis Lodziensis 11 (1976) 33–44.
[29] U.R. Chaudhary, B. Madhava Rao, Z. Phys. Chemie, Leipzig 270 (1989) 412–420.

[30] R.M. Mehrotra, S. Ghosh, Phys. Chem. 57 (1963) 224–239.
[31] B. Neumann, O. Steinbock, S.C. Muller, N.S. Dalal, J. Phys. Chem. 100 (1996) 12342–12348.
[32] N. Vijai, Suniti, C.L. Khandelwal, P.D. Sharma, J. Chem. Res. (2005) 813–816.
[33] J.W. Costin, P.S. Francis, S.W. Lewis, Anal. Chim. Acta 224273 (2003) 1–11.
[34] B.J. Hindson, N.W. Barnett, Anal. Chim. Acta 445 (2001) 1–19.
[35] A. Townshend, W. Ruengsitagoon, C. Thongpooon, S. Liawruangrath, Anal. Chim. Acta 541 (2005) 103–109.
[36] C.E. Lenehan, N.W. Barnett, S.W. Lewis, K.M. Essery, Aust. J. Chem. 57 (2004) 1001–1004.
[37] D.M. Hercules, F.E. Lytle, J. Am. Chem. Soc. 88 (1966) 4745.
[38] N.W. Barnett, B.J. Hindson, S.W. Lewis, S.D. Purcell, Anal. Comm. 35 (1998) 321–324.
[39] J.W. Costin, N.W. Barnett, S.W. Lewis, Talanta 64 (2004) 894–898.
[40] J.L. Adcock, N.W. Barnett, R.D. Gerardi, C.E. Lenehan, S.W. Lewis, Talanta 64 (2004) 534–537.
[41] N.W. Barnett, B.J. Hindson, S.W. Lewis, Anal. Chim. Acta 384 (1999) 151–158.
[42] R.D. Gerardi, N.W. Barnett, P. Jones, Anal. Chim. Acta (1999) 1–10.
[43] A.J. Bard, Electrogenerated Chemiluminescence, Marcel Dekker, New York, 2004.
[44] D.R. Lide (Ed.), Handbook of Chemistry and Physics, CRC Press, Boca Raton, 2002–2003.

Matrix-assisted laser desorption/ionization mass spectrometry (MALDI TOF MS) study of Huperzine A, a natural anti-Alzheimer's disease product, its derivatization and its detection by highly sensitive laser induced fluorescence (LIF)

A. Ben Hameda [a], P. Táborský [b], E.M. Peña-Méndez [a,b], J. Havel [a,*]

[a] *Department of Analytical Chemistry, Faculty of Science, Masaryk University, Kotlářská 2, CZ-611 37 Brno, Czech Republic*
[b] *On the leave from: Department of Analytical Chemistry, Nutrition and Food Science, University of La Laguna, 38071-La Laguna, Tenerife, Spain*

Abstract

Huperzine A, a reversible acetylcholinesterase inhibitor for the treatment of Alzheimer disease (HupA), was studied using an (MALDI TOF MS) instrument in MALDI mode. The formation of a HupA dimmer in a vacuum was observed and several matrices were found that were able to inhibit its formation. The structures of the neutral and protonated form of the HupA molecule were calculated and optimized using a Hyperchem program. Detection limit using MALDI TOF MS in the model sample was 5.3 pg. MALDI TOF MS was also applied to the direct detection of the drug in medical preparations and in human serum. The limit of detection in plasma was 14.2 pg with a signal-to-noise ratio of 3:1. However, the sensitivity was not as high as it usually is in MALDI. Therefore, a new method for the derivatization of HupA was developed using fluorescent labelling with rhodamine B isothiocyanate (RBITC). A limit of detection using capillary electrophoresis laser induced fluorescence detection (CE-LIF) equal to $4 \times 10^{-9} \, \mathrm{mol \, l^{-1}}$ was reached.
© 2007 Elsevier B.V. All rights reserved.

Keywords: Huperzine A; Derivatization; MALDI TOF MS; CE-LIF

1. Introduction

Alzheimer's disease (AD) affects the elderly population worldwide and is a major health problem. The illness is in third place after cancer and heart problems. AD causes dysfunction in the cholinergic system associated with a deficit in the neurotransmitter acetylcholine. Different compounds, such as tacrine, galanthamine, donepezil and rivastigmine have been used to enhance the central cholinergic neurotransmission activity [1–4]. However, many undesirable effects of these drugs have been described (hepatoxicity, gastrointestinal upset, etc.) and their effectiveness is highly dependent on accurate drug doses. On the other hand, HupA seems to be very promising as a natural anti-Alzheimer's disease product.

The *Huperzia serrata* plant has traditionally been used in Chinese medicine for the treatment of contusion, strain, haematuria, and swelling [5]. From this plant, HupA, an alkaloid with pharmaceutical uses was obtained and shown to be a potent reversible inhibitor or acetyl cholinesterase (AchE) and butyryl cholinesterase (BuChE). It was first isolated and named selagine from *Lycopodium selago* and later named as Huperzine from *Huperzia serrata* [6]. Synthesis, properties and the use of this drug are described in several reviews [7–9]. The structure of huperzine was first described by Valenta et al. [10] and later revised by Kozikowski et al. [11]. HupA is an unsaturated sesquiterpenic compound with pyridone moiety and belongs to the primary amino group. Generally, the drug has been shown to be promising for the palliative treatment of Alzheimer's disease as well as for memory loss, inhibiting AchE activity in the brain and increasing the acetylcholine levels [1]. The loss of acetylcholine is directly related to several diseases connected with disorders of the brain, of which Alzheimer's disease is included. The compound also improves learning and retrieval processes

---

and facilitates memory retention. In this sense it belongs to a group of so called "smart drugs" with similar biological activity. Recently, the use of HupA contra nerve gas poisoning was studied by Lallement et al. [12].

Several analytical methods have already been published for the determination of HupA. The use of reverse-phase HPLC to follow HupA in plasma was described by Qian et al. [13] and Ye et al. [14] while Wang et al. [15] have applied HPLC to test HupA in tablets. Peña-Méndez et al. [17] and Ben Hameda et al. [18] have applied capillary zone electrophoresis (CZE) with spectrophotometric detection for the rapid and efficient determination of the levels of HupA in medical preparatives. Recently, a very sensitive LC–MS/MS method has been developed and applied to the determination of HupA in dog plasma by Wang et al. [16] with a limit of detection (LOD) $0.01 \, ng \, ml^{-1}$. Also, Ye et al. [14] have used an ion-pair reverse-phase high performance liquid chromatography for the determination of HupA in beagle dog serum, with a limit of quantification (LOQ) of $4 \, ng \, ml^{-1}$ in serum.

MALDI TOF MS is a powerful tool routinely used in the analysis of biomolecules and low detection limits like femtomoles up to attomoles can be reached. To our knowledge, there is no MALDI-TOF MS method for the detection of HupA. The aim of this work therefore was to study the behaviour of HupA in MALDI TOF MS and to examine the possibility of this promising technique being used for the sensitive detection of HupA. As CE-LIF also usually offers a very high level of sensitivity, another aim was to examine the possibility of HupA derivation using this technique.

2. Experimental

2.1. Reagents

The compounds: 2,5-dihydroxybenzoic acid (DHB); 3,4,5-trihydroxybenzoic acid (HBA); 4-hydroxy-3-methoxybenzoic acid (HMA); 5-methoxysalicylic acid (5 MS); 3,5-dimethoxy-4-hydroxycinnamic acid (DHC); α-cyano-4-hydroxycinnamic acid (CHC), and 4-hydroxy-3-methoxycinnamic acid (MHC) used as matrices were purchased from Sigma–Aldrich (Steinhein, Germany). Sodium azide was from Pliva-Lachema a.s. (Brno, Czech Republic). Rhodamine B isothiocyanate (RBITC) was from Sigma–Aldrich (Steinhein, Germany). HPLC-grade acetonitrile, trifluoroacetic acid (TFA), hydrochloric acid, ethanol, acetone, acetonitrile (ACN) and methanol were from Merck (Darmstadt, Germany). Ammonium citrate, ammonium chloride, disodium phosphate and ammonium acetate (all pro analysis) were from Sigma–Aldrich (Prague, Czech Republic). All solutions were prepared using double distilled water from a quartz apparatus of Heraeus Quarzschmelze (Hanau, Germany). Standard of (-)-Huperzine A (HupA) M.W. 242.31 was purchased from Panorama Research Inc. (Mountain View, CA, USA). All other chemicals were of analytical grade purity.

2.2. Sample preparation and derivatization procedure

Stock solutions of HupA were prepared by dissolving the compound in 50 mM hydrochloric acid and watered up to the final volume. The HupA stock solution (1×10^{-3} mM) was further diluted with double distilled water to working solution ranges. All solutions were stored in a refrigerator.

The matrices for MALDI measurements were prepared by dissolving the matrix compound in acetonitrile:water (1:1, v/v), while TFA was added up to 0.5%.

Lyophilised serum (Boehringer, Mannheim, Germany) was de-proteinized by two different methods: (a) serum (200 μl) was mixed with acetonitrile in ratio 2:3 (v/v) (serum:acetonitrile) and mixed for 15 s; the mixture was then centrifuged for 1 min at 4000 r.p.m. and the supernatant was taken for the analysis (b) serum was mixed with dichloromethane in a ratio 1:5 (v/v). The mixture was shaken for 5 min and, after being centrifuged, the HupA was re-extracted from the organic phase into the aqueous one using 0.01 M HCl [19].

2.3. Derivatization procedure

RBITC labelling reagent was dissolved in acetone (stock solution of $5 \times 10^{-4} \, mol \, l^{-1}$). Different ratios of this reagent were tested to derivatize HupA and the optimal ratio between RBITC and HupA was found to be 1:12 (HupA:RBITC). HupA was subjected to derivatization with RBITC in 20 mM phosphate buffer (pH 9.5) at 50 °C for 5 h.

2.4. Mass spectrometry of Huperzine A using MALDI TOF

The mass spectra were measured using an Axima-CFR mass spectrometer (Manchester, UK); controlled by Kratos Kompact V5.2.0. Launchpad 1.2.0 software was used for data acquisition. The Axima-CFR mass spectrometer was equipped with a nitrogen laser (wavelength 337 nm, pulse duration $\tau = 4$ ns, pulse energy 300 μJ) from Laser Science Inc. (Franklin, MA, USA). The energies of the laser were in the range of 0–180 (arbitrary units). There were 100 up to 1000 laser shots used for each sample. The signals were averaged and smoothed by the Savitzky-Golay algorithm. Peak maxima were determined via the gradient-centroid procedure.

Sample preparation: (a) 1 μl of a matrix solution was added to a target, allowed to dry and then 1 μl of HupA solution was added and dried in an air stream. (b) 1 μl of matrix solution was applied onto the target and mixed with HupA solution and dried in an air stream at room temperature.

2.5. Separation and detection by CE-LIF

A home-built CE-LIF instrument optimized for the detection of rhodamine derivatives was used in this work. Excitation source in the CE-LIF system was a diode pumped, frequency doubled Nd:YAG excitation laser (model LCS-DTL382QT) with a wavelength of 532 nm and a power 5 mW (Laser Compact, Russia), $4 \times f$ using a DPGL-3005F (CASIX, China). The laser beam was focused on an optical window of the uncoated silica capillary (37 cm, 75 μm i.d.). Fluorescence emission signals were collected by a photomultiplier model 6356 (Hamamatsu, photonics, Germany) through a set of filters and a microscope
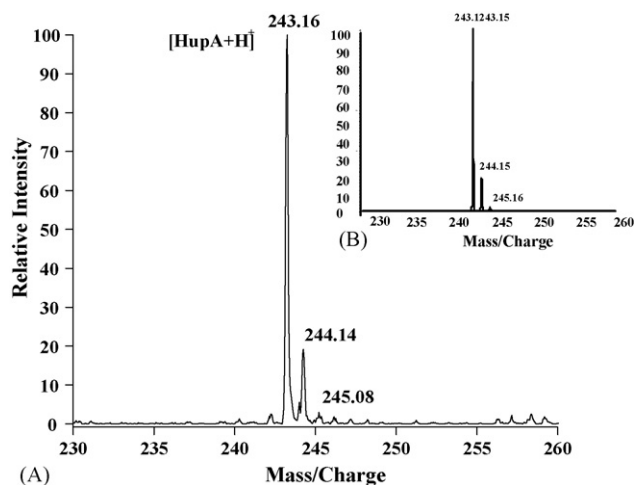
Fig. 1. MALDI-TOF mass spectrum of (A) [HupA + H]⁺, and (B) the theoretical model of [HupA + H]⁺. Experimental conditions: 1 μl of 14.21 ng of HupA, DHB was used as the matrix. The measurement was done in the linear positive mode.

objective 60× (Edmund Scientific, USA). A signal from the photomultiplier was converted into a voltage by an RC circuit and digitised. Obtained data was stored on a Pentium PC. More details about this instrument are described elsewhere [23]. CE conditions: electromigration injection (10 s, 5 kV), t 25 °C.

3. Results and discussion

Huperzine A is a rigid molecule with endo- and exocyclic-double bonds. The amino group can be protonated in acid solution. The protonation constant (∼7.4) was determined by capillary electrophoresis, as found by Peña-Méndez et al. [17].

3.1. MALDI-TOF MS

Because MALDI TOF MS is so promising with respect to reaching low limits of detection of biomolecules, ionization of HupA was studied here. Different matrices, such as CHC, DHB, 5-MS, and MHC were tested to improve the limit of detection (LOD). When MHC and CHC were used as matrices, no improvement was observed for the LOD of the mass spectra for HupA. The DHB matrix was found to be the most suitable matrix for the analysis of HupA. Two different sample preparation protocols for the ionization of HupA were used. First, a saturated solution of the matrix in acetonitrile: water (1:1, v/v), was allowed to dry on the sample plate prior to the application of the sample. Second, a method involving co-crystallation of the matrix and the analytes together on the sample plate. The first method, where 1 μl of saturated solution of DHB matrix was applied onto the target and mixed with HupA solution and dried in an air stream at room temperature, yielded the best signal-to-noise ratio and was therefore selected for all the experiments. Fig. 1 shows the mass spectra of HupA obtained under the optimized experimental conditions. The major peak corresponds to the protonated molecular ion of HupA [M + H]⁺ at *m/z* 243.16 (theoretical *m/z* value 243.15). Low intensity peaks, corresponding to the adducts of HupA with sodium and potassium,

respectively, were observed; the [M + Na]⁺ at *m/z* 265.15 (theoretical *m/z* value 265.13) and [M + K]⁺ at *m/z* 281.10 (theoretical *m/z* value 281.11). When the laser power was increased, a peak at *m/z* 226.17 corresponding to the split of –NH₂ from the HupA was observed in mass spectra. The loss of –NH₂ has already been described in the literature [14]. Formation of the dimmer of HupA was also found [(HupA)₂ + H]⁺ at *m/z* 485.15 (theoretical *m/z* value 485.29). The formation of a dimmer in a vacuum may potentially result from non-covalently bound monomers [20]. This dimmer is completely different from the "dimmer" of HupA described in the literature [21], where a new drug was designed by dimmerizing an inactive fragment of (-)-huperzine A via chemical (covalent) bonds.

In the commercial HupA product used in this work the content of potassium (0.46% rel.) was found and determined by flame photometry [17]. The potassium in the preparation most probably comes from the extraction procedure when the drug is extracted from the plant material using potassium hydroxide. This is also the possible explanation of the formation of a HupA adduct with potassium.

In order to suppress adduct formation during the MALDI process, due to the presence of potassium and sodium in the sample, the effect of different ammonium salt additions to the matrix was studied. It was found that ammonium salts did not eliminate the formation of adducts. On the other hand, acidification of the matrix by TFA 0.5% in the matrix solution suppressed both adducts and the dimmer formation during the analysis.

Taking 1 μl of the different aqueous standard solutions with different concentrations of HupA, the limit of MALDI TOF MS detection, calculated as a signal-to-noise ratio 3:1, was found to be about 5.3 pg.

3.1.1. Detection of HupA in biological matrices using MALDI TOF MS

The possibility to detect HupA in serum using MALDI TOF MS was studied. Detection of the compound in serum was carried out by using DHB as a matrix under the experimental conditions described above. Serum (5 ml) was spiked with different concentrations of HupA and the extraction of HupA from the serum was done following the procedures described in the Section 2, applying de-proteination and consecutive liquid–liquid extraction under acidic conditions. The detection limit (LOD) for the MALDI-TOF MS detection of HupA, calculated as a signal-to-noise ratio 3:1 was calculated by taking 1 μl of the extract containing HupA and was found to be around 14.2 pg.

3.2. Laser induced fluorescence

Fluorescent spectroscopy is a very sensitive analytical method for the analysis of biomolecules. Measuring native fluorescence gives information about the structure and quantity of the analysed compound. Small molecules, such as amino-acids, small peptides or other biologically important compounds including drugs without fluorophores can be determined after labelling them with a suitable fluorophore [22]. The labelling of HupA by rhodamine B with isocyanate binding group (RBITC)
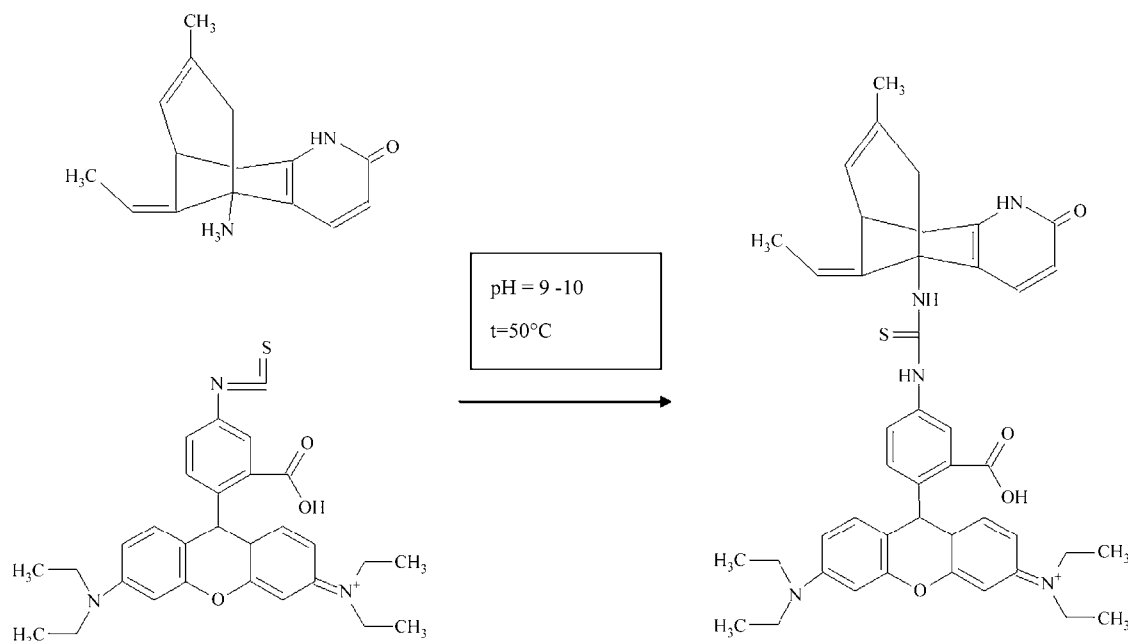
Fig. 2. Scheme of the derivatization procedure of HupA by RBITC.

was studied in an attempt to decrease the LOD of HupA. Rhodamine B is a highly fluorescing agent from the family of xanthen dyes with an excitation maximum, when near to an excitation source (532 nm), of about 580 nm (in phosphate buffer, pH 9.5). The isothiocyanate group of RBITC reacts with deprotonated amino groups (protonation constant of HupA is pKa 7.7 [17]. The CE-LIF system was first optimized for the detection of low concentrations of rhodamine B and LOD for the pure dye was found to be 2×10^{-13} mol l^{-1}. The derivatization buffer was used as a separation buffer (20 mM phosphate buffer, pH 9.5) with the addition of 10% (vol.) methanol. The scheme of the derivatization procedure of HupA by RBITC is shown in Fig. 2.

Two LODs of the analyte can be calculated on CE-LIF after derivatization. The first possibility is the LOD calculation from the lowest concentration of the labelled molecule (LOD$_1$). Second, reagents react in high concentrations with a high level of reaction recovery and the formed compound is determined after dilution. This LOD$_2$ is very similar to the LOD of pure RBITC and many authors present this number to be the LOD or interchange these numbers. However, this number is very important as in immunoassay analysis, fluorescence microscopy, fluorescence resonance energy transfer, and other methods where labelled biomolecules in low concentration are needed. From the analytical point of view it is more important to know the LOD from the direct conjugation of a sample with a low concentration of analyte.

The samples with concentrations of HupA from 10^{-5} to 10^{-8} mol l^{-1} were tested on the CE-LIF. The total limit of detection (LOD$_2$) of HupA labelled by RBITC (HupA-RBITC) was calculated from a sample with a concentration of HupA 10^{-5} mol l^{-1} (cRBITC $= 10^{-4}$ mol l^{-1}, in 20 mM phosphate buffer, pH 9.5) as being $1.8\,10^{-11}$ mol l^{-1}. LOD$_1$ was estimated to be 4.1×10^{-9} mol l^{-1}, Fig. 3. These LODs are comparable with results from a derivatization and determination of

normorphine, morphine, 6-acetyl morphine, and codeine using fluorescein isothiocyanate [22].

3.3. MALDI–TOF MS of labelled HupA

After the derivatization procedure, the sample was analysed, also using MALDI-TOF MS, to confirm the structure of the
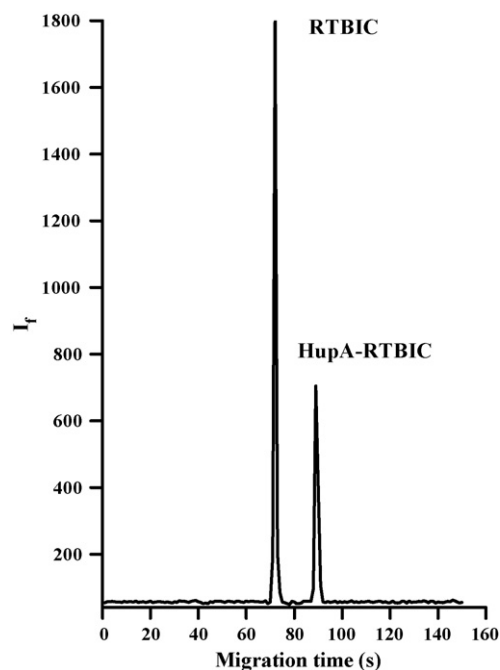

Fig. 3. Electropherogram concerning the separation of HupA labelled by RBITC. Experimental conditions: C_{HupA} 1.0×10^{-7} mol l^{-1}, C_{RBITC} 1.2×10^{-6} mol l^{-1}, buffer 20 mM phosphate + 10% methanol (pH 9.5). Uncoated silica capillary (45 cm total length, 37 cm to detector), injection (10 s, 5 kV), and separation voltage 15 kV.
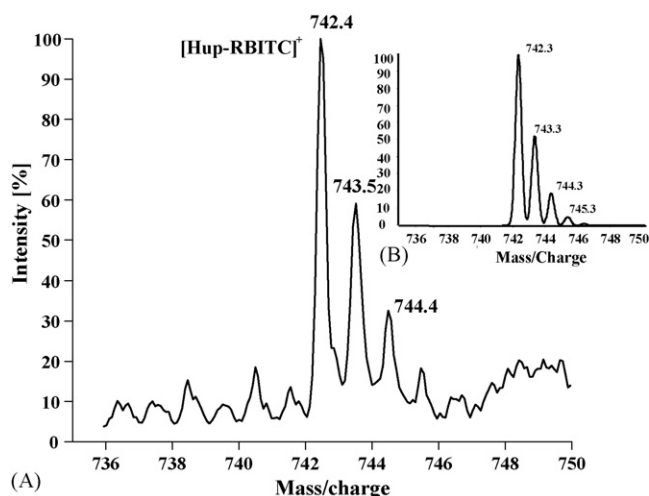
Fig. 4. (A) MALDI-TOF spectra of labelled HupA by RBITC, [HupA-RBITC]⁺ or [HupA-RBITC + H]⁺ and (B) theoretical model of HupA-RBITC. Experimental conditions: 1 μl of the mixture containing: 14.21 pg HupA, 0.643 ng RBITC was given to the target. DHB was used as the matrix. The measurements were done in the linear positive mode.

formed derivatives. Several matrices were tested (CHC, DHB, and MHC). The best results were obtained when DHB was used. Fig. 4 shows the mass spectra obtained from HupA derivatized with RBITC. The protonated form of HupA labelled with RBITC [HupA-RBITC]⁺ was observed in positive linear and reflectron modes. The peak observed at *m/z* 742.4 is related to [HupA-RBITC]⁺ species. The isotopic pattern observed for [HupA-RBITC]⁺ is in an excellent agreement with the calculated theoretical model. Also, species related to unlabelled HupA and RBITC itself were observed in mass spectra.

The limit of detection was estimated to be $\sim 2 \times 10^{-8}$ mol l^{-1} (the limit of quantification $\sim 8 \times 10^{-8}$ mol l^{-1}). So, CE-LIF is ~ 5 times more sensitive.

4. Conclusions

It was found that, in MALDI TOF MS, HupA can be ionized to an [HupA + H]⁺ cation using several matrices, although DHB was found as the most suitable. A reliable method for HupA extraction from serum has been developed and thus the MALDI TOF MS method can be used for the fast identification of HupA in biological liquids, e.g. in serum. The LOD reached applying this methodology is adequate for determining the pharmacokinetic profile of HupA at a high dosage. The disadvantage of the method is the rather low sensitivity but, in any case, it can be applied for the Quality Control of HupA in commercial products and for pharmaceutical products in general.

It was found that HupA can be derivatized by RBITC and a highly fluorescent product HupA-RBITC is formed. Its structure has been confirmed by MALDI TOF mass spectrometry. After capillary electrophoretic separation of the reagent and the derivatized product, HupA with RBITC allows for a highly sensitive

determination with laser induced fluorescence detection. This CE-LIF method was optimized and a super sensitive and rapid CE-LIF method was developed. The procedure can be used for the highly sensitive determination of HupA in biological liquids, such as serum.

Recently, we have developed extraction method which allows separation of HupA from serum and shows excellent recovery (92%) [18]. Therefore, the derivatization procedure developed here offers due to its low DL the possibility to quantify HupA in serum, e.g. for pharmaceutical purpose. However, careful verification is still needed.

References

[1] Y. Foricher, J. Mann, Tetrahedron Lett. 41 (2000) 2007.
[2] L. Pokorná, A. Revilla, J. Havel, J. Patočka, Electrophoresis 20 (1999) 1993.
[3] M.G. Vargas, J. Havel, J. Patočka, J. Chromatogr. A. 802 (1) (1998) 121.
[4] M.G. Vargas, J. Havel, J. Patočka, Am. Clin. Lab. 17 (1998) 22.
[5] Z. Da-Yuan, B. Dong-Lu, T. Xi-Can, Drug Dev. Res. 39 (1998) 147.
[6] W.A. Ayer, L.M. Browne, H. Orszanska, Z. Valenta, J. Liu, Can. J. Chem. 67 (1989) 1538.
[7] J.-S. Liu, Y.L. Zhu, C.M. Yu, Y.Z. Zhou, Y. Yhan, W. WuF, B.F. Qi, Can. J. Chem. 64 (1986) 837.
[8] V. Rajendran, K.R.C. Prakash, S.V. Haresh, A.P. Saxena, A.P. Kozikowski, Bioorg. Med. Chem. Lett. 10 (2000) 2467.
[9] S. Kaneko, T. Yoshino, T. Katoh, S. Terashima, Tetrahedron 54 (1998) 5471.
[10] Z. Valenta, H. Yoshimura, E.F. Rogers, M. Ternbah, K. Wiesner, Tetrahedron Lett. 1 (1960) 26.
[11] A.P. Kozikowski, Y. Xia, E. Rajarathnam Reddy, I. Hanin, W. Tückmantel, X.C. Tang, J. Org. Chem. 56 (1991) 4636.
[12] G. Lallement, V. Baille, D. Baubichon, P. Carpentier, J.M. Collombet, P. Filliat, A. Foquin, E. Four, C. Masqueliez, G. Testylier, L. Tonduli, F. Dorandeu, Neurotoxicology 23 (2002) 1.
[13] B.C. Qian, M. Wang, Z.F. Zhou, K. Chen, R.R. Zhou, G.S. Chen, Acta Pharmacol. Sin. 16 (1995) 396.
[14] J. Ye, S. Zeng, W. Zhang, G. Chen, J. Chromatogr. B 817 (2005) 187.
[15] G.-F. Wang, F. Zeng, Z.-D. Zheng, Chin. J. Pharm. Anal. 21 (2001) 85.
[16] Y.W. Wang, D.F. Chu, J.K. Gu, J.P. Fawcett, Y. Wu, W. Liu, J. Chromatogr. B 803 (2004) 375.
[17] E.M. Peña-Méndez, T. Hottmar, J. Havel, J. Patočka, J. Appl. Biomed. 1 (2003) 99.
[18] A. Ben Hameda, S. Elosta, J. Havel, J. Chromatogr. A 1084 (2005) 7.
[19] S. Malovaná, D. Gajdošová, J. Benedík, J. Havel, J. Chromatogr. B 760 (2001) 37.
[20] M. Dey, J. Grotemeyer, Eur. J. Mass Spectrom. 1 (1995) 95.
[21] P.R. Carlier, D.-M. Du, Y.-F. Han, J. Liu, E. Perola, I.D. Williams, Y.-P. Pang, Angew. Chem. Int. Ed. 39 (2000) 1775.
[22] S. Alnajjar, J.A. Butcher, B. McCord, Electrophoresis 25 (2004) 1592.
[23] P. Vrábel, P. Táborský, M. Ryvolová, J. Havel, J. Preisler, J. Lumin. 118 (2006) 283.

ELSEVIER

Synthesis of a novel bistriazene reagent 4,4′-*bis*[3-(4-phenylthiazol-2-yl)triazenyl]biphenyl and its highly sensitive color reaction with mercury(II)

Xiao-Ling He [a,*], Yong-Qiu Wang [a], Ke-Qing Ling [b,*]

[a] *Department of Chemistry, Huaibei Coal Industry Teacher's College, Huaibei, Anhui 235000, China*
[b] *Department of Chemistry, Case Western Reserve University, Cleveland, OH 44106, USA*

Abstract

We report the synthesis of a novel *bistriazene*, 4,4′-*bis*(3-(4-phenylthiazol-2-yl)triazenyl)biphenyl (BPTTBP), and its highly sensitive color reaction with Hg^{2+}. The new reagent was synthesized in good yield by coupling 2-amino-4-phenylthiazole with 4,4′-biphenyldiamine bisdiazonium salt. Using a blend of surfactants N-cetylpyridinium chloride (CPC) and polyethylene glycol n-octanoic phenyl ether (OP) as a micelle sensitizer, the *red* colored reagent assembles with Hg^{2+} in pH 9.8 borate buffer according to a 1:1 stoichiometry, forming a *blue* oligomeric/polymeric chelating complex with a high apparent stability constant ($1.1 \times 10^8 \, M^{-1}$). Whereas the maximum absorption of reagent occurs at 510 nm with an extinct coefficient of $1.35 \times 10^4 \, M^{-1} \, cm^{-1}$, the complex absorbs at 611 nm, with an apparent extinct coefficient of $1.04 \times 10^5 \, M^{-1} \, cm^{-1}$. Beer's law is obeyed in the range of 0–15 µg/25 mL Hg^{2+}, and Sandell's sensitivity is 1.92×10^{-3} µg/cm². In the presence of thiourea and $Na_4P_2O_7$ as masking agents, the method was found free from interferences of foreign ions commonly occurring with mercury. The optimized protocol has been successfully applied to spectrophotometric determination of mercury in waste water samples. The features of the new reagent associated with its special structure were discussed, and an unprecedented *"domino effect"* was proposed to account for its unique chelating stoichiometry with Hg^{2+}.
© 2006 Elsevier B.V. All rights reserved.

Keywords: *bis*(Phenylthiazolyltriazenyl)biphenyl; Mercury(II); Spectrophotometry; Waste water samples; Colorimetric probe; Domino effect

1. Introduction

Mercury is one of the most toxic heavy metals on earth. The toxicity of mercury depends on its occurring forms; organomercurials such as methylmercury are more toxic than elemental mercury and other inorganic mercury compounds [1]. Symptoms of methylmercury poisoning include instantaneous and permanent neurological damages, paralysis, insanity, impaired vision and blindness, chromosome damage, birth defects, sensory loss of limbs, loss in hearing and mental retardation [1,2]. Since the well known "Minamata disaster", which occurred in Japan in 1950s and 1960s, there has been an increasing concern about the impact of sea food mercury contamination on human health [3]. Mercury and mercury compounds have been listed

as high priority pollutants globally, and various regulations and guidelines have been developed to limit their levels in food, medicine, water and sediments [4]. It is therefore important to develop fast, simple, and sensitive assays to measure mercury levels in environmental and biological samples.

Numerous instrumental methods for micro mercury determination have been developed, including cold vapor atomic absorption spectroscopy [5], potentiometry [6], fluorimetry [7] and liquid chromatography [8]. These methods are usually sensitive and accurate, but in the meantime are inconvenient and time consuming. Several spectrophotometric methods have also been reported for estimation of trace mercury using various reagents such as dithizone [9], Cadion 2B [10], and potassium iodide [11]. Although most of these methods are quite sensitive, they suffer from several drawbacks such as need of extraction with toxic organic solvents, as well as poor selectivity.

Triazene reagents have received considerable attention in the past two decades due to their highly sensitive color reactions with

* Corresponding author.
  E-mail addresses: hbhxl111@hotmail.com (X.-L. He),
kxl56@case.edu (K.-Q. Ling).
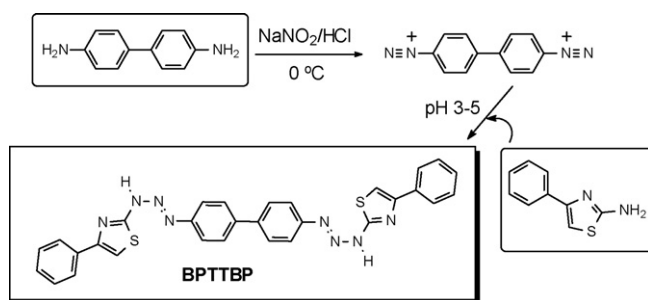
Scheme 1. Synthetic route for the new reagent BPTTBP.

a number of metal ions [12]. Several protocols for spectrophotometric determination of Hg(II) based on these reagents have also been developed [13]. However, one general drawback associated with triazene reagents is the interference of reagent background due to spectral overlap between reagents and their Hg^{2+} complexes, which may cause loss of sensitivity [14]. Although this problem can be partly solved by dual-wavelength spectrophotometry [15], structural modification of triazene reagents remains the best approach to improve their analytical properties *without sacrificing simplicity and convenience.* In this regard, it is worth mentioning that there have been tremendous research interests recently in colorimetric probes, or the so-called "naked-eye chemosensors" of Hg^{2+}, which are being developed for fast detection of Hg^{2+} in biological and environmental samples *without use of any instrumentation* [16].

Aiming to improve the analytical properties of triazene reagents, we were the first to study *bis*triazenes as opposed to the normal *mono*triazenes [17]. Our initial consideration was that, by coupling two aromatic monotriazenes into a single aromatic system, not only could the absorptions of the reagent and its metal complex be shifted to longer wavelength (perhaps also be intensified) due to extended conjugation, but the spectral overlap between reagent and metal complex may also be improved because *double* chelating within a *single* reagent molecule, if it happens, might cause larger red shift in absorption spectrum. Indeed, by choosing appropriate surfactants as micelle sensitizers, chelating of bistriazene reagents with Hg^{2+} usually showed large red shifts in absorption spectrum ($\Delta\lambda_{max}$ 100–130 nm), though sensitivity remains to be improved ($\varepsilon < 10^5\,M^{-1}\,cm^{-1}$) [17]. As part of our ongoing research in this effort, we hereby report the synthesis of a novel bistriazene reagent 4,4′-*bis*(3-(4-phenylthiazol-2-yl)triazenyl)biphenyl (BPTTBP, Scheme 1), and its color reaction with Hg^{2+}. This new reagent is by far *the most sensitive bistriazene for Hg^{2+}* ($\varepsilon > 10^5\,M^{-1}\,cm^{-1}$). An optimized protocol based on this reagent was successfully applied to spectrophotometric determination of mercury in waste water samples.

2. Experimental

2.1. Apparatus and reagents

IR spectrum was recorded on a 470 FT-IR spectrophotometer. ^1H NMR spectrum was obtained on a Varian Inova 400 instrument (at 399.75 MHz), with chemical shifts being referenced to

the solvent peak. Elemental analysis was performed on a Perkin Elmer analyzer. UV–vis spectra were obtained using a double beam spectrophotometer (Beijing General Instrument Company Ltd). pH was measured with a pHS-3D pH meter equipped with a combination glass electrode (Chengdu Analytical Instrument Company). 2-Amino-4-phenylthiazole was synthesized according to a literature method [18]. All the commercially available reagents are of A.R. grade. All aqueous solutions were prepared using double distilled deionized water.

Stock solution of Hg^{2+} (0.5 g/L, 2.49×10^{-3} M) was prepared using $HgCl_2$, which was then diluted to 10 mg/L (4.99×10^{-5} M) as working solution. The surfactants used were 1% polyethyleneglycol *n*-octanoic phenyl ether (OP) aqueous solution and 0.2% *N*-cetylpyridinium chloride (CPC) aqueous solution. The pH 9.8 borate buffer solution was prepared by mixing appropriate volumes of 0.10 M aqueous $Na_2B_4O_7$ and 0.10 M aqueous NaOH as monitored by a pH meter. Stock solution of BPTTBP (0.20 g/L, 3.58×10^{-4} M) was prepared by dissolving 0.10 g of analytically pure BPTTBP (see below) in a minimum volume of *N,N*-dimethylformamide (DMF), followed by dilution with absolute ethanol to 500 mL.

2.2. Synthesis of 4,4′-bis(3-(4-phenylthiazol-2-yl)triazenyl)biphenyl

The synthetic route is shown in Scheme 1. To a solution of 4,4′-biphenyldiamine (0.92 g, 5 mmol) in 10 mL of 6 N aqueous HCl was added within 30 min a solution of $NaNO_2$ (0.69 g, 10 mmol) in 5 mL of water under electromagnetic stirring, during which time the temperature was maintained at 0–2 °C. After further stirring for 15 min, the resulting 4,4′-biphenyldiamine bisdiazonium salt solution was slowly added to a solution of 2-amino-4-phenylthiazole (1.76 g, 10 mmol) in 60 mL of ethanol under stirring at 0–2 °C. The mixture was maintained at pH 3–5 by adding appropriate amount of 20% cold aqueous Na_2CO_3. The mixture was stirred at 10–15 °C for 1.5 h, and then was allowed to stand overnight at room temperature. Filtration of the mixture, followed by washing with water and ethanol afforded 2.44 g of crude product (4.37 mmol, 87.4% yield), which was further purified by crystallization in 3:1 (v/v) ethanol–water to give pure product as a dark purple solid: m.p. > 280 °C dec; IR (KBr) 3357.4 (NH), 3286.8 (NH), 3061.5 (ArH), 1633.2, 1598.9,1517.5, 1474.3 cm^{-1}; ^1H NMR (DMSO-d_6) δ 7.45–7.54 (6H, ArH), 7.52 (s, 2H), 7.73 (d, 4H, J = 8.8 Hz), 7.88 (d, 4H, J = 8.8 Hz), 8.21 (dd, 4H, J = 1.2 8.4 Hz), 8.45 (br, 2H, NH); Anal. Calcd. for $C_{30}H_{22}N_8S_2$: C, 64.52; H, 3.94; N, 20.07, found: C, 64.94; H, 4.12; N, 19.87.

2.3. Typical procedure

To a 25 mL calibrated tube were added sequentially 8.0 mL of pH 9.8 borate buffer, 1.5 mL of 1% OP aqueous solution (final concentration 0.06%), 3.0 mL of 0.2% CPC aqueous solution (final concentration 0.024%) and 2.0 mL of 0.20 g/L BPTTBP enthanolic solution (final concentration 2.86×10^{-5} M). After

mixing thoroughly, an aliquot of standard solution containing 10 μg of Hg^{2+} (final concentration 2×10^{-6} M) was added, and the solution was brought to mark with water. Upon further mixing, the solution was allowed to stand at room temperature for 10 min, and then subjected to spectrophotometric measurement at 611 nm using 1 cm cuvettes with the same concentration of reagent solution as reference.

2.4. Optimized protocol for determination of Hg(II) in waste water samples

To a 25 mL beaker were added an appropriate volume of waste water sample, 5 mL of 3 M aqueous H_2SO_4 and 5 mL of concentrated aqueous HNO_3. The mixture was heated at a steam bath for 2 h and then cooled in air for 10 min. To the mixture was carefully added 5 mL of 10% aqueous hydroxylamine hydrochloride under stirring and the resulting solution was heated in a steam bath for another 10 min to decompose any residual HNO_3. The solution was adjusted to pH 3–4 with aqueous NaOH, transferred to an appropriate volume of volumetric flask and then brought to mark with water. An aliquot of this solution was taken into a 25 mL calibrated tube, to it was added an aqueous solution containing 1.0 mg thiourea and 3.0 mg sodium pyrophosphate ($Na_4P_2O_7$) as masking agents, and the mixture was further treated following the typical procedure. The final results are listed in Table 3.

3. Results

3.1. Absorption spectra

BPTTBP forms a red solution in pH 9.8 borate buffer in the presence of OP (0.06%) and CPC (0.024%). Upon titration with Hg^{2+}, a sharp color change from red to blue was observed. Following the typical procedure, the absorption spectra of reagent and its complex with Hg^{2+} were recorded (Fig. 1). The maximum absorption of reagent occurs at 510 nm, with an extinct coefficient of $1.35 \times 10^4\,M^{-1}\,cm^{-1}$. The complex absorbs at 611 nm, with an apparent extinct coefficient of $1.04 \times 10^5\,M^{-1}\,cm^{-1}$. We thus chose 611 nm as the working wavelength for the spectrophotometric measurements.

3.2. Chelating stoichiometry

The apparent molar ratio of the chelating complex of BPTTBP with Hg^{2+} was determined as 1:1 using both molar ratio method and Job's method. Based on the Job's plot (Fig. 2), where the total concentration of reagent and Hg^{2+} was maintained at 1×10^{-5} M, the apparent stability constant of the complex was calculated as $1.1 \times 10^8\,M^{-1}$ [19].

3.3. Effect of pH

Following the typical procedure but using borate buffer solutions with different pH values, the absorbance at 611 nm was found to reach maximum and become stable in the range of pH 9.2–10.4 (Fig. 3). Also, best results were obtained
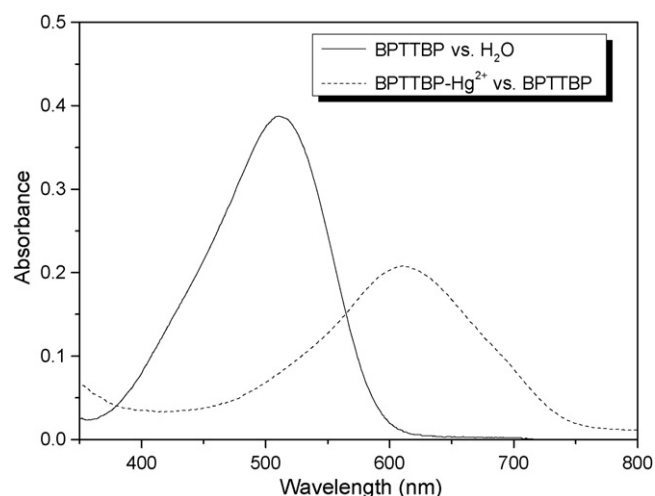

Fig. 1. Absorption spectra of BPTTBP (2.86×10^{-5} M, against water) and its chelating complex with Hg^{2+} (2×10^{-6} M, against BPTTBP) in pH 9.8 borate buffer in the presence of OP (0.06%) and CPC (0.024%) at room temperature. The BPTTBP–Hg^{2+} complex was generated from 2.86×10^{-5} M of BPTTBP and 2×10^{-6} M of Hg^{2+}, and the reference was 2.86×10^{-5} M of BPTTBP.

when the total volume of buffer solution was controlled in the range of 7.0–9.0 mL. We thus chose 8.0 mL of pH 9.8 borate buffer.

The pK_a values of aromatic triazenes usually fall in the range of 12–13 [20], with the conjugate base form showing a deeper color background, whereas metal chelating requires full dissociation of the triazene group [21]. Thus, at low pH, A_{611} is low due to incomplete metal chelating. At high pH, the reagent background increases, resulting in decrease of A_{611} and in turn loss of sensitivity. Metal hydroxide formation is another cause, at least in part, for the low A_{611} at high pH. Therefore, the optimum pH represents a compromise where the thermodynamically favorable metal chelating is able to
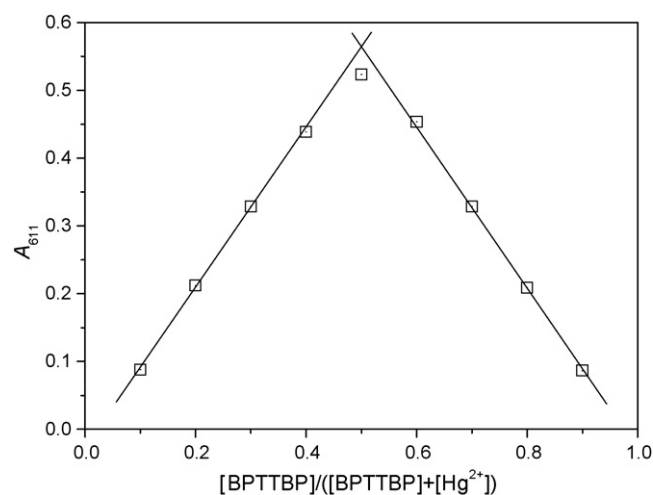

Fig. 2. Job's plot obtained in pH 9.8 borate buffer in the presence of OP (0.06%) and CPC (0.024%) at room temperature by varying the ratio of [BPTTBP] and [Hg^{2+}] while the total concentrations ([BPTTBP]+[Hg^{2+}]) being maintained at 1×10^{-5} M.
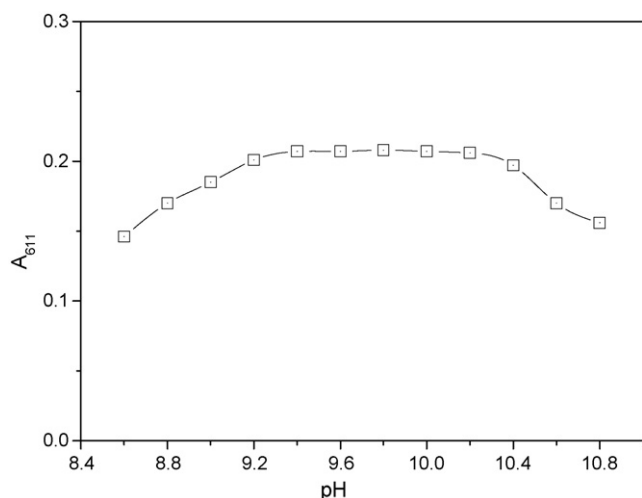
Fig. 3. Effect of pH on the color reaction of BPTTBP (2.86×10^{-5} M) with Hg^{2+} (2×10^{-6} M) in borate buffer in the presence of OP (0.06%) and CPC (0.024%) at room temperature.

complete without significant dissociation of free triazene group and formation of metal hydroxide.

3.4. Selection of surfactants and effects of their concentrations

BPTTBP is insoluble in water such that the solution became cloudy in the absence of a surfactant. Following the typical procedure, we examined the effects of several surfactants, both individually and in combination with each other, on the color reaction between BPTTBP and Hg^{2+}. Our data showed that common surfactants such as 4-(1,1,3,3-tetramethylbutyl)phenyl polyethylene glycol (TritonX-100), polyethylene glycol n-octanoic phenyl ether (OP), polyethylene glycol sorbitan monooleate (Tween-80), N-cetylpyridinium bromide (CPB), N-cetylpyridinium chloride (CPC) and cetyltrimethylammonium bromide (CTB) all improved the solubility of reagent and sensitized the color reaction to varying degrees, among which a combination of CPC and OP gave the best results. Using a blend of 1.0–2.0 mL of 1% OP aqueous solution and 2.0–4.0 mL of 0.2% CPC aqueous solution, the absorbance at 611 nm reached maximum and became stable as well. Therefore, we chose 1.5 mL of 1% OP aqueous solution plus 3.0 mL of 0.2% CPC aqueous solution.

3.5. Effect of reagent concentration

Following the typical procedure with varying volumes of 0.20 g/L BPTTBP solution, the absorbance at 611 nm reached maximum and became stable when 1.5–3.0 mL reagent solution (final concentration $2.15–4.30 \times 10^{-5}$ M) was utilized (Fig. 4). We chose 2.0 mL of 0.20 g/L reagent solution.

3.6. Effect of reaction time and color stability

Following the typical procedure but with varying reaction time, we found that the absorbance at 611 nm reached maximum
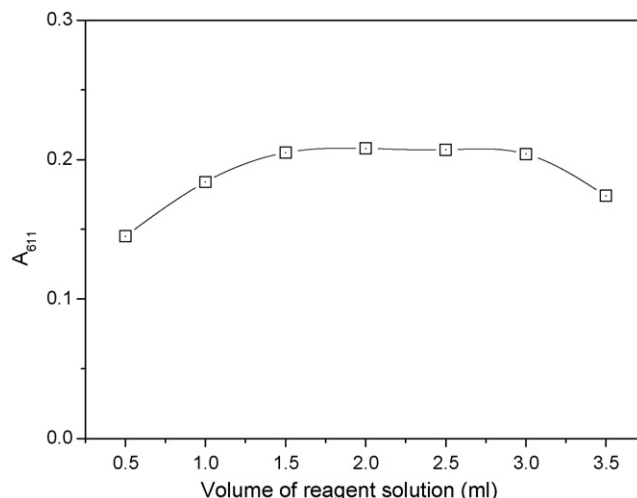
after standing at room temperature for 10 min, which was stable at least for 4 h. It should be noted that the color stability here is different from the thermodynamic stability of chelating complex. Color stability mainly depends on the stability of micelle which not only improves solubility of reagent and the chelating complex, but also participates in metal chelating.

3.7. Calibration plot

Following the typical procedure with varying amount of Hg^{2+}, the calibration curve was constructed (Fig. 5). The linear regression equation was $A = 0.0208C - 0.0016$ ($C = \mu g/25$ mL Hg), and the correlation coefficient was 0.9996. The Sandell's sensitivity was calculated as 1.92×10^{-3} $\mu g/cm^2$. The apparent extinct coefficient (1.04×10^5 M^{-1} cm^{-1}) calculated from the calibration plot is identical with that obtained directly from the absorption spectrum (Fig. 1).

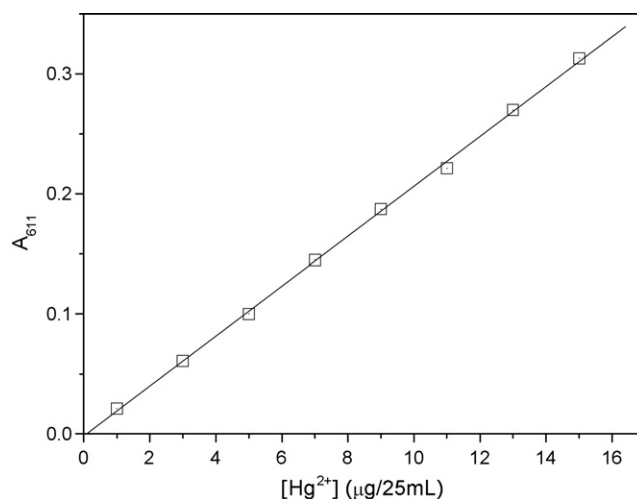Fig. 4. Effect of reagent concentration on the color reaction of BPTTBP with Hg^{2+} (2×10^{-6} M) in pH 9.8 borate buffer in the presence of OP (0.06%) and CPC (0.024%) at room temperature.

Fig. 5. Calibration plot constructed for the reaction of BPTTBP (2.86×10^{-5} M) with varying concentrations of Hg^{2+} in pH 9.8 borate buffer in the presence of OP (0.06%) and CPC (0.024%) at room temperature.

Table 1
Effects of foreign species on Hg^{2+} measurements[a]

Foreign species	Tolerance limit ($\mu g/25\,mL$)[b]
K^+, Na^+, NH_4^+, Li^+, CO_3^{2-}, NO_3^-, F^-, Cl^-, Br^-	5000[c]
$Na_4P_2O_7$, citrate, tartrate, $C_2O_4^{2-}$, PO_4^{3-}, I^-	3000
thiourea, salicylate, Mg^{2+}, Ca^{2+}, Ba^{2+}	1000
Bi^{3+}, Ni^{2+}, Co^{2+}, Pb^{2+}	250
Mn^{2+}	150
Cr^{3+}, Pd^{2+}	100
Al^{3+}, Fe^{3+}	80
Ag^+	50
Zn^{2+}	25
Cd^{2+}	10 (170[d])
Cu^{2+}	5 (30[d])

[a] All the measurements were conducted with a 25 mL water sample containing 10 μg of Hg^{2+} (2×10^{-6} M, 0.4 ppm) following the typical procedure.
[b] Tolerance limit is the amount of foreign species that causes an error of $\pm 5\%$.
[c] The upper limits were not determined.
[d] Tolerance limits in the presence of 1.0 mg/25 mL thiourea and 3.0 mg/25 mL of $Na_4P_2O_7$ as masking agents.

3.8. Effects of foreign species

The effects of foreign species on determination of Hg^{2+} (10 μg) in 25 mL water samples were examined (Table 1). Whereas the interferences from Cu^{2+} and Cd^{2+} can be masked by thiourea and $Na_4P_2O_7$, the method is free from interferences of most foreign species commonly occurring with Hg(II).

3.9. Validation of the method

The new method was validated by determination of Hg^{2+} in commercially available artificial water samples, which were prepared according to the national standard of ground water quality, but the concentrations of various species have been amplified appropriately. In short, the water samples used contain Hg^{2+}, Co^{2+}, Ni^{2+} and Cr^{3+} (0.2 mg/L each); Mn^{2+}, Cu^{2+} and Fe^{3+} (0.5 mg/L each); Zn^{2+}, Pb^{2+} and Cd^{2+} (1.0 mg/L each); and Mg^{2+} and Ca^{2+} (50 mg/L each). A 5.0 mL aliquot was taken and the amount of Hg^{2+} was determined according to the typical procedure (Table 2), showing excellent recovery values and very small relative standard deviations (R.S.D.).

3.10. Analytical applications

The method was applied to the determination of micro Hg(II) in waste water samples. Following the optimized protocol in Section 2, the Hg(II) contents of two industrial waste water

Table 3
Determination of Hg(II) in waste water samples[a]

Sample #	Dithiazone method (mg/L)	This method (mg/L)	R.S.D. (%)
1	0.094	0.095	1.9
2	0.131	0.132	1.1

[a] Reported as means of five replicate measurements.

samples obtained in the local manufacturing companies were determined (Table 3). Not only do the results agree well with those determined by the standard dithiozone method (which requires extraction with toxic organic solvent), but our method also showed small R.S.D. values.

4. Discussion

4.1. Structure of the complex

Monotriazenes usually form 2:1 chelating complexes with Hg^{2+} [10,12,13]. The crystal structures of 1,3-diaryltriazenes with Hg(II) showed that Hg^{2+} coordinates with two *deprotonated* triazene anions in a quasi-planar geometry [21], with two primary N–Hg covalent bonds, and two secondary N–Hg coordinate bonds being formed in the opposite position from each other. Our finding that BPTTBP forms an apparent 1:1 chelating complex with Hg^{2+} is inherently consistent with this stoichiometry. However, one may immediately realize that a *real* 1:1 complex between BPTTBP and Hg^{2+} would be geometrically impossible due to the linear structure of the reagent that is not able to fold to allow for intramolecular chelating. Likewise, although it is tempting to imagine a 2:2 complex to account for the 1:1 stoichiometry, computational simulation (MOPAC) indicated that such a macrocyclic structure can only accommodate the two primary N–Hg bonds to avoid bad ring strains (Fig. 6). Moreover, the energy minimized structure also suffers from lack of conjugation between the triazenes and aromatic rings, thereby
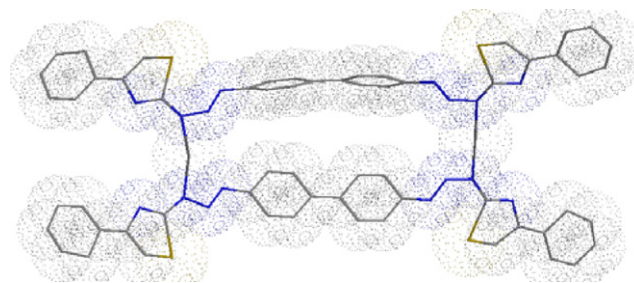

Fig. 6. Energy-minimized (MOPAC) structure of a postulated 2:2 chelating complex of BPTTBP with Hg^{2+}.

Table 2
Determination of Hg(II) in artificial water samples

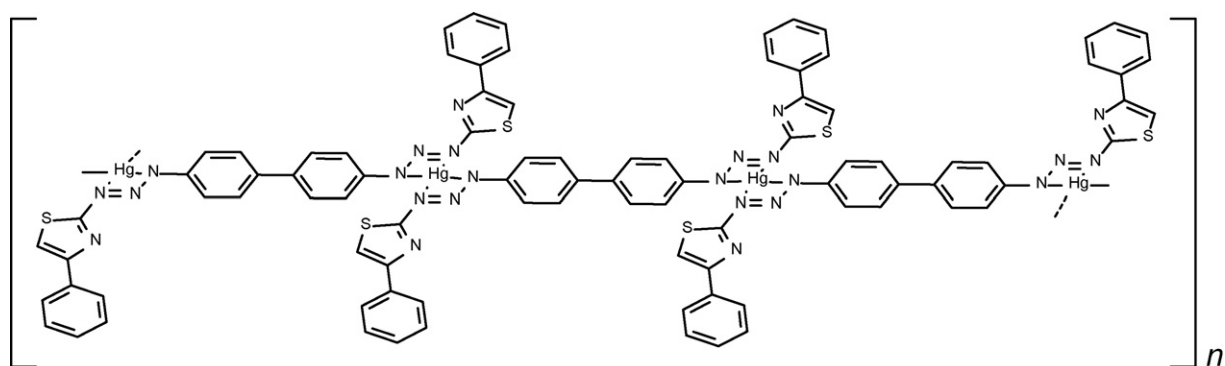| Sample #	Hg(II) (μg)			Recovery (%)	R.S.D. (%)
	Theoretical	Hg(II) added	Experimental[a]		
1	1.00	2.00	2.94	98	1.2
2	1.00	4.00	5.03	101	0.7

[a] Mean of five replicate measurements.

Fig. 7. Proposed structure of the apparent 1:1 chelating complex of BPTTBP with Hg^{2+}.

further decreasing its stability. Similar situations also exist for macrocyclic 3:3 and 4:4 chelating complexes (not shown). All these findings point to the *noninvolvement of a close chelating ring structure*.

Based on the above discussion, we propose that BPTTBP and Hg^{2+} could possibly assemble into oligomeric or polymeric *n:n* chelating complexes, which do not suffer from any unfavorable steric effects while conjugations of triazenes and the aromatic rings are fully allowed (Fig. 7). Such an assembly structure may also account for its high apparent stability constant as compared to the 2:1 chelating complex in monotriazene cases [22]. It is interesting to note that, even though more than 10-fold excess of reagent was used in all the color reactions, chelating between BPTTBP and Hg^{2+} still followed a 1:1 rather than 2:1 stoichiometry. This abnormal phenomenon suggests that, whatever structures the complex might have, *chelating of the first triazene on the reagent molecule with Hg^{2+} must significantly enhance the chelating strength of the other*. This so-called *"domino effect"* is unprecedented in metal chelating of monotriazenes [12]. One possible interpretation is that chelating of the first triazene group on BPTTBP with Hg^{2+} imposes an electron-withdrawing effect on the other triazene through the biphenyl conjugate system, thereby decreasing its pK_a and promoting its chelating with the next Hg^{2+}.

4.2. Features of the new bistriazene reagent

It is well known that the analytical properties of triazene reagents largely depend on the choice of surfactants, which not only promote solubility, but also sensitize the color reactions. However, given that the optimized protocols reported in literature with triazene reagents all utilized similar surfactants as ours, some features of the new reagent independent of surfactant usage can be discussed. First, while data in literature indicated that most monotriazenes showed relatively small red shift ($\Delta\lambda_{max}$ 80–90 nm) in absorption spectra upon chelating with Hg^{2+} [15], the $\Delta\lambda_{max}$ between BPTTBP and its Hg^{2+} complex (101 nm) is relatively large such that absorption of reagent at the λ_{max} of complex is small (Fig. 1). Second, unlike some of the monotriazenes, where reagents and complexes showed comparable absorption intensities [15], the extinct coefficient of BPTTBP ($1.35 \times 10^4\,M^{-1}\,cm^{-1}$) is almost an order

of magnitude *smaller* than the apparent extinct coefficient of its Hg^{2+} complex ($1.04 \times 10^5\,M^{-1}\,cm^{-1}$). These features suggest that the interference from reagent background should be very small in our case. Given that large excess of reagent was used and the chelating stoichiometry had already been determined, the real molar absorption spectrum of the complex can be *simulated* (using Origin 7.5) simply by linear combination of the *molar* absorption spectra of reagent (versus water) and its Hg^{2+}complex (versus reagent) according to the 1:1 chelating stoichiometry to compensate for the absorption cancellation of the complex by the fraction of reagent participating in metal chelating (Fig. 8). The calculated *real* extinct coefficient of BPTTBP–Hg^{2+} complex is $1.044 \times 10^5\,M^{-1}\,cm^{-1}$, which corresponds to only 0.4% of loss in sensitivity due to interference from reagent background. We point out that *excess (unreacted) reagent does not interfere with any spectrophotometric determinations even though the reagent blank absorbance is high* [14,23]; the interference actually arises not from excess reagent, but from the *fraction* of reagent participating in metal chelating.
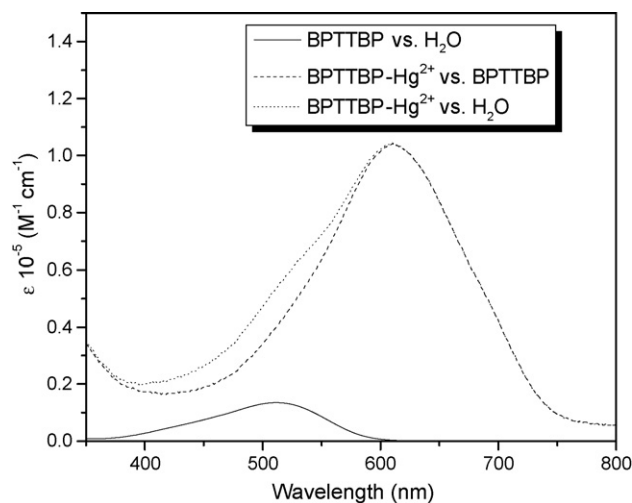

Fig. 8. Molar absorption spectra of BPTTBP and its 1:1 chelating complex with Hg^{2+}. The real molar absorption spectrum of the complex vs. water (dotted line) was obtained by linear combination of the molar spectra of reagent vs. water (solid line) and the complex vs. reagent blank (dashed line) according to the 1:1 chelating stoichiometry.

4.3. Comparison with other methods

A survey of reported methods for spectrophotometric determination of Hg^{2+} reveals several advantages of our optimized protocol. First, the use of surfactants in our method allows for omission of toxic organic solvents, which were required for such reagents as dithizone [9], Cadion 2B [10], 2-(8-quinolylazo)-4,5-diphenylimidazole [24], 5,6-diphenyl-2,3-dihydro-asym-triazine-3-thione [25], tetraphenylpyridium [26], 1-salicylidene-5-(2-pyridylmethylidene)isothiocarbonohydrazide [27], and benzyl-2-pyridylketone 2-quinolylhydrazone [28]. These traditional methods were also less sensitive than our new protocol. Second, the sensitivity and selectivity of BPTTBP for Hg^{2+} are comparable with those of *o*-carboxyphenyldiazoamino-*p*-azobenzene [13b], which is by far the most sensitive and selective triazene reagent in terms of *solution-phase single-wavelength spectrophotometry*, despite that the color change of this latter reagent with Hg^{2+} was not reported, and the chelating chemistry was also not well studied. Third, a recent report showed that the sensitivity and selectivity of a known triazene reagent with Hg^{2+} could be significantly improved by *solid-phase dual-wavelength spectrophotometry* combined with a solid-phase *enrichment* technique based on polymer-supported β-cyclodextrin [29], which was claimed to have the potential of automation. We argue that, while such effort may reflect the trend of analytical instrumentation and automation, there is also an increasing demand for cheap, simple, convenient, sensitive and selective single-wavelength spectrophotometric methods, and the ultimate goal along this line is to develop highly sensitive and selective "naked-eye" chemosensors of Hg^{2+} without any instrumentation [16]. Given that the quality of a colorimetric probe not only depends on the color contrast ($\Delta\lambda_{max}$) between the reagent and its metal complex, but also depends on the stability of the metal complex (large stability constant may help reduce the requisite reagent concentration and eliminate the reagent background), the sharp color change of reaction of BPTTBP with Hg^{2+} (red → blue) and the large stability constant of the BPTTBP–Hg^{2+} complex suggest that our new bistriazene reagent may serve as a valuable lead compound for further development into novel colorimetric probes of Hg^{2+}.

5. Conclusion

We have presented a comprehensive study on the color reaction of Hg^{2+} with a novel bistriazene reagent, BPTTBP, which showed a large red shift ($\Delta\lambda_{max}$ 101 nm) in absorption spectrum upon chelating with Hg^{2+}. The improved spectral overlap, the light color of reagent and the deep color of the complex all helped reduce the interference from reagent background significantly such that our method was able to exploit nearly full strength of the reaction (99.6% of the theoretical sensitivity) without imposing the inconvenience of dual-wavelength spectrophotometry and complicated mathematic manipulations [14,15]. The sensitivity is very high and the selectivity is also good. The optimized protocol has been successfully applied to the spectrophotometric determination of micro Hg(II) in environmental samples with remarkable reproducibility. More importantly, our novel design of bistriazenes as opposed to monotriazenes, especially the observed "*domino effect*" which not only results in a unique chelating stoichiometry, but also helps stabilize the chelating complex significantly, may provide new insight into strategies in designing other chromogenic reagents for spectrophotometric analysis of trace metals. Further development of bistriazene reagents should be a worthwhile objective.

Acknowledgement

References

[1] (a) L. Magos, T.W. Clarkson, Ann. Clin. Biochem. 43 (2006) 257;
(b) D. Ibrahim, B. Froberg, A. Wolf, D.E. Rusyniak, Clin. Lab. Med. 26 (2006) 67;
(c) D. Saint-Phard, B. Van Dorsten, Orthopedics 27 (2004) 394;
(d) J.F. Risher, H.E. Murray, G.R. Prince, Toxicol. Ind. Health 18 (2002) 109.

[2] (a) C. Sanfeliu, J. Sebastia, R. Cristofol, E. Rodriguez-Farre, Neurotox. Res. 5 (2003) 283;
(b) F. Gobba, A. Cavalleri, Neurotoxicology 24 (2003) 693.

[3] (a) C.W. Levenson, D.M. Axelrad, Nutr. Rev. 64 (2006) 139;
(b) H.M. Chan, G.M. Egeland, Nutr. Rev. 62 (2004) 68.

[4] See, for example, the US EPA regulations of mercury http://www.epa.gov/mercury/regs.htm.

[5] J.R. Otero-Rey, J.M. Lopez-Vilarino, J. Moreda-Pineiro, E. Alonso-Rodriguez, S. Muniategui-Lorenzo, P. Lopez-Mahia, D. Prada-Rodriguez, Environ. Sci. Technol. 37 (2003) 5262.

[6] A.M. Othman, Int. J. Environ. Anal. Chem. 86 (2006) 367.

[7] C.L. He, F.L. Ren, X.B. Zhang, Z.X. Han, Talanta 70 (2006) 364.

[8] P. Tajes-Martinez, E. Beceiro-Gonzalez, S. Muniategui-Lorenzo, D. Prada-Rodriguez, Talanta 68 (2006) 1489.

[9] H. Irving, E. Andrew, E.J. Risdon, J. Chem. Soc. (1949) 541.

[10] (a) N.K. Ch'en, W.K. Ch'ao, T.J. Tung, Shangyi Xuebao (1958) 155; Chem. Abstr. 53 (1958) 82409;
(b) G. Popa, A.F. Danet, M. Popescu, Talanta 25 (1978) 546.

[11] S.M. Park, H.S. Choi, Anal. Chim. Acta 459 (2002) 75.

[12] Z. Li, Q. Zhang, J. Pan, Rev. Anal. Chem. 22 (2003) 191; Chem. Abstr. 140 (2004) 433275.

[13] (a) R.K. Banjare, M.K. Deb, J. Indian Chem. Soc. 83 (2006) 702;
(b) S. Chatterjee, A. Pillai, V.K. Gupta, Talanta 57 (2002) 461.

[14] H.W. Gao, Zhurnal Prikladnoi Spektroskopii 63 (1996) 951; Chem. Abstr. 126 (1997) 161837.

[15] (a) M. Yang, Y. Zheng, A. Chen, H. Lu, Lihua Jianyan, Huaxue Fence 38 (2002) 415; Chem. Abstr. 138 (2003) 313483.;
(b) C. Gong, M. Yang, Z. Hu, C. Jin, Lihua Jianyan, Huaxue Fence 36 (2000) 551, 554; Chem. Abstr. 134 (2001) 187539.

[16] (a) S. Tatay, P. Gavina, E. Coronado, E. Palomares, Org. Lett. 8 (2006) 3857;
(b) E.M. Nolan, M.E. Racine, S.J. Lippard, Inorg. Chem. 45 (2006) 2742;
(c) H. Zheng, Z.H. Qian, L. Xu, F.F. Yuan, L.D. Lan, J.G. Xu, Org. Lett. 8 (2006) 859;
(d) A. Caballero, R. Martinez, V. Lloveras, I. Ratera, J. Vidal-Gancedo, K. Wurst, A. Tarraga, P. Molina, J. Veciana, J. Am. Chem. Soc. 127 (2005) 15666;
(e) Y.K. Yang, K.J. Yook, J. Tae, J. Am. Chem. Soc. 127 (2005) 16760.

[17] (a) X.L. He, Q.L. Liu, L. Jia, Fenxi Shiyanshi 18 (1999) 46; Chem. Abstr. 131 (1999) 266258.;
(b) Y.Q. Wang, Q.L. Liu, X.L. He, P.Y. Yang, Fenxi Shiyanshi 19 (2000) 66; Chem. Abstr. 133 (2000) 271224.;

(c) Y.Q. Wang, X.L. He, Guangpu Shiyanshi 17 (2000) 364; Chem. Abstr. 133 (2000) 124798.;

(d) X.L. He, Y.Q. Wang, L. Wang, Fenxi Ceshi Xuebao 21 (2002) 80; Chem. Abstr. 137 (2002) 209994.;

(e) X.L. He, Y.Q. Wang, Fenxi Shiyanshi 24 (2005) 29; Chem. Abstr. 144 (2006) 10968.;

(f) X.L. He, Y.Q. Wang, Yankuang Ceshi 25 (2006) 42; Chem. Abstr. 145 (2006) 341568.

[18] R.M. Dodson, L.C. King, J. Am. Chem. Soc. 67 (1945) 2242.

[19] P. Job, Ann. Chim. 9 (1928) 113.

[20] L. Wang, P.P. Sun, Huaxue Xuebao 53 (1995) 923; Chem. Abstr. 124 (1996) 74888.

[21] M. Horner, G.M. de Oliveira, J.A. Naue, J. Daniels, J. Beck, J. Organomet. Chem. 691 (2006) 1051.

[22] The stability constant of the 2:1 complex of a monotriazene, 1-(p-nitrophenyl)-3-(p-sodiosulfophenyl)triazene, with Hg^{2+} was reported as 1022.93, see A.F. Danet, M. Tiron, Rev. Chim. (Bucharest, Romania) 30 (1979) 376, Chem. Abstr. 91 (1979) 133437.

[23] J. Kobylecka, A. Cyganski, Chem. Anal. (Warsaw) 44 (1999) 567; Chem. Abstr. 131 (1999) 110547.

[24] S. Miwa, M. Furukawa, S. Shibata, Anal. Chim. Acta 120 (1980) 405.

[25] M. Edrissi, Microchem. J. 27 (1982) 323.

[26] T. Perez-Ruiz, J.A. Ortuno, M.C. Torrecillas, Anal. Chim. Acta 165 (1984) 275.

[27] D. Rosales, L.G.A. Jose, Anal. Chem. 57 (1985) 1411.

[28] J. Medinilla, F. Ales, F. Garcia Sanchez, Talanta 33 (1986) 329.

[29] Y. Liu, X. Chang, X. Hu, Y. Guo, S. Meng, F. Wang, Anal. Chim. Acta 532 (2005) 121.

Short communication

Filtration through nylon membranes negatively affects analysis of arsenic and phosphate by the molybdenum blue method

A.C. Heimann *, R. Jakobsen

Institute of Environment & Resources, Technical University of Denmark, Bygningstorvet, Building 115, DK-2800 Lyngby, Denmark

Abstract

Filtering synthetic arsenic- or phosphate-containing solutions (1.5–47.6 µmol/L) with nylon syringe filters significantly reduced absorbances (by 6–74%) when analyzed with the colorimetric molybdenum blue method. Filtering the same solutions with cellulose acetate syringe filters yielded no significant differences as compared to unfiltered controls. The detrimental effect of nylon membranes was also observed when pure Milli-Q water was filtered and subsequently spiked with arsenic(III) or phosphate suggesting that some compound(s) eluting from the filter membranes interfere with the color formation in the assay. Consequently, we caution against using nylon filters when filtering water samples for the determination of arsenic or phosphate with the molybdenum blue method.
© 2006 Elsevier B.V. All rights reserved.

Keywords: Molybdenum blue; Nylon membranes; Arsenic; Phosphate; Groundwater; Syringe filters

1. Introduction

The colorimetric molybdenum blue method is widely used for the determination of inorganic phosphate, arsenic, and silicate in natural and contaminated water [1–7]. Typical applications include flow-injection analysis [8–13] and microbiological studies of arsenate-respiring bacteria [14–17]. Filtering environmental water samples prior to analysis is a standard sampling technique for removing colloids and/or microorganisms, thereby conserving important redox parameters such as dissolved As(III/V) ratios [18,19]. Sample filtration is also recommended for removing interfering turbidity prior to analysis [20]. We here demonstrate that using nylon filters for this purpose can significantly reduce the absorbance in the colorimetric analysis of synthetic, arsenic- and phosphate-containing solutions.

2. Experimental

2.1. Instrumentation and procedure

Absorbances were read on a Thermo Spectronic Helios ε spectrophotometer using Plastibrand disposable cuvettes (1.5 mL, semi-micro, Brand). Reagents were prepared according to the procedure of Johnson and Pilson [1], as modified and downscaled by Anderson and Cook [15]. Acid-washed glassware was used for preparation of reagent stock solutions while new plastic ware was used in all other steps. Pure, previously autoclaved (20 min at 121 °C) Milli-Q water was used to prepare all reagents and analyte solutions. The mixed color reagent was prepared freshly for use by mixing the following stock solutions: (i) 4 mL of a 24.3 mM ammonium molybdate tetrahydrate solution; (ii) 10 mL of a 2.5 M sulfuric acid solution; (iii) 4 mL of a 307 mM ascorbic acid solution (defrosted from frozen stock solution); (iv) 2 mL of a 4 mM potassium antimony(III)oxide tartrate hemihydrate solution. For the analysis of phosphate, 1.2 mL of standard or sample were pipetted into a 2 mL plastic tube (Eppendorf), and amended with 120 µL of the mixed color reagent. After a reaction time of 15 min the absorbance was read at 865 nm. For the analysis of arsenite (As(III)), 1.2 mL of standard or sample were pipetted into a 2 mL plastic tube (Eppendorf), amended with 30 µL 1 M HCl and 2 µL of a 215 mM potassium iodate solution, and were left to oxidize for 10–15 min at room temperature. After oxidation, 120 µL of the mixed color reagent was added. After 4 h reaction time, the absorbance was read at 865 nm. Samples for arsenate (As(V)) were analyzed in the same way, even though sample oxidation is not a prerequisite for purely As(V) contain-

---

* Corresponding author. Tel.: +45 4525 2172; fax: +45 4593 2850.
E-mail address: axh@er.dtu.dk (A.C. Heimann).

ing solutions. The detection limit was 0.5 μmol/L. All results presented here are from synthetic solutions containing one of the three analytes (P, As(III) or As(V)). Therefore, no corrections between an untreated, oxidized, and reduced set-up were necessary. Standards for P, As(III), and As(V) were prepared in pure, previously autoclaved (20 min at 121 °C) Milli-Q water using the following salts: sodium dihydrogen phosphate monohydrate ($NaH_2PO_4 \cdot H_2O$, P.a.), sodium arsenite ($NaAsO_2$), and di-sodium hydrogen arsenate heptahydrate ($AsHNa_2O_4 \cdot 7H_2O$, puriss P.a.).

2.2. Filters and sampling solutions

Three different types of syringe filters were tested (two types with a nylon membrane and one type with a cellulose acetate membrane): (i) 13 mm Cameo 13N, nylon, 0.22 μm pore size (Osmonics Inc.), (ii) 13 mm, nylon, 0.45 μm pore size (Whatman), and (iii) 26 mm, sterile, wetting agent-free cellulose acetate, 0.20 μm pore size (Sartorius Minisart). Sampled solutions were either pure Milli-Q water or standards of phosphate, arsenite, or arsenate (between 1.5 and 48 μmol/L). Filtered volumes were typically 2–3 mL, no pre-washing of the filters was performed. A fresh filter was used for each replicate (i.e. $n = 3$, indicating three individual syringe filters). In some experiments, Milli-Q water was filtered and subsequently spiked with a stock solution of interest. In other experiments, the housing of the 0.22 μm nylon syringe filters was broken apart, the membranes were removed and placed into 20 mL plastic vials containing 5 mL Milli-Q water (1–3 membranes per vial). These vials were then stored either stagnantly or on a horizontal shaker (400 rpm) for about 14 h. Between 1.185 and 1.2 mL of this solution was then pipetted into 2 mL Eppendorf tubes, spiked with a stock solution of interest (5–15 μL), and analyzed as described above. The significance of differences between filtered and unfiltered samples was verified through Student's t-test ($\alpha = 0.05$; two-tail).

3. Results and discussion

Table 1 summarizes the results from filtering As(III) standards, phosphate standards, or Milli-Q water (subsequently spiked with analyte stock solution) using different filters. Nylon syringe filters reduced the signal of filtered solutions by 6–74% as compared to unfiltered solutions (Table 1). Differences between absorbances of nylon-filtered samples and unfiltered controls were significant in all experiments. The fact that this effect was also observed with filtered Milli-Q water strongly suggests that some compound(s) are eluted from the nylon membrane interfering with the color formation in the photometric assay.

This is also supported by the experiments in which the membranes were removed from the housing and submerged in Milli-Q water for several hours before the solutions were amended with As(III) (Fig. 1). Again, the difference between Milli-Q water (i) in contact with the membranes and (ii) without membranes was 13–21%. A similar experiment was conducted with As(V), at a final concentration of about 8 μmol/L. Solutions prepared with Milli-Q water in contact with nylon filters

Table 1

Arsenic and phosphate concentrations of various synthetic solutions after filtering with different types of filters (as compared to unfiltered controls)

Filtered solution	Analyte	Filter[a]	n	Concentration (μmol/L)		Δ (%)
				Filtered	Unfiltered	
Standard	As(III)	NY 0.22	1	∼0.4 (< d.l.)	1.5	∼74
Standard	As(III)	NY 0.22	1	9.2	23.9	−61
Standard	As(III)	NY 0.22	1	23.3	47.6	−51
Standard	As(III)	NY 0.22	3	7.7 ± 0.03	8.4 ± 0.03	−7
Standard	As(III)	NY 0.22	3	1.5 ± 0.03	2.9 ± 0.05	−46
Standard	As(III)	NY 0.45	3	7.2 ± 0.03	8.2 ± 0.03	−12
Standard	As(III)	NY 0.45	3	2.6 ± 0.08	3.3 ± 0.03	−21
MQ water	As(III)	NY 0.22	3	5.7 ± 0.11	6.3 ± 0.05	−10
MQ water	As(III)	NY 0.22	3	2.6 ± 0.06	3.1 ± 0.06	−16
Standard	P	NY 0.22	3	10.0 ± 0.03	10.6 ± 0.03	−6
Standard	P	NY 0.45	3	10.0 ± 0.00	10.6 ± 0.11	−6
MQ water	P	NY 0.45	3	7.5 ± 0.20	8.2 ± 0.18	−9
Standard	P	NY 0.45	3	3.5 ± 0.00	4.1 ± 0.03	−17
Standard	As(III)	CA 0.2	3	8.3 ± 0.06	8.2 ± 0.03	+1
Standard	As(III)	CA 0.2	3	4.2 ± 0.05	4.1 ± 0.03	0
Standard	P	CA 0.2	3	10.7 ± 0.03	10.6 ± 0.03	0

[a] NY: nylon membrane; CA: cellulose acetate membrane; number indicates pore size in micrometers.

showed significantly lower absorbances than solutions prepared from pure Milli-Q water (8–9%), both in non-oxidized samples and samples that were oxidized with potassium iodate before adding the color reagent.

The stability of the color complex also decreased over time as exemplified in Fig. 2. After 15 min of reaction, the difference between nylon-filtered and unfiltered Milli-Q (spiked with phosphate after filtration) was about 17%, while it increased to over 30% after 85 min.

This again indicates the presence of one or more unknown interfering compounds originating from the nylon membrane and interacting with reagents from the assay. Filtering and subsequent spiking of Milli-Q water with phosphate or As(III) showed the same adverse effect when the nylon filters (0.45 μm pore size) had been kept at 60 °C for several days (in a preliminary attempt to simulate filter aging).
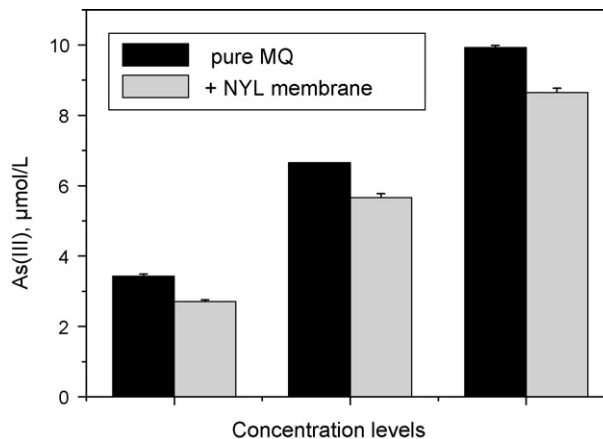

Fig. 1. As(III) concentrations in synthetic solutions made from (i) pure Milli-Q water and (ii) Milli-Q water that had been in contact with nylon membranes, respectively.
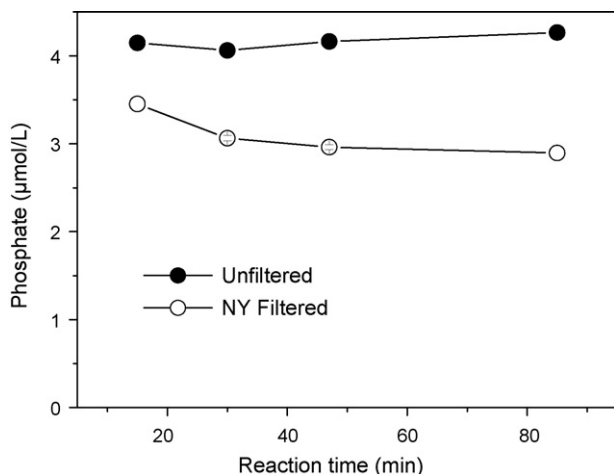
Fig. 2. Phosphate concentrations over time determined in synthetic solutions that were unfiltered or filtered with a nylon syringe filter, respectively, prior to analysis ($n = 3$, S.D. < size of symbols).

From these findings we can only speculate about the nature of this interference. If the compound(s) eluting from the membrane are redox-active they could potentially interfere with the final step in the procedure, the reduction of the antimony–phosphomolybdate complex with ascorbic acid. Other known interfering compounds include hexavalent chromium and nitrite [20]. Both decrease measured concentrations, however, they are probably not likely to be found in nylon filter membranes. Washing the filters prior to use might improve the recovery. A more detailed investigation of this phenomenon is warranted.

References

[1] D.L. Johnson, M.E.Q. Pilson, Anal. Chim. Acta 58 (1972) 289.
[2] R.E. Stauffer, Anal. Chem. 55 (1983) 1205.
[3] R. Ramachandran, P.K. Gupta, Anal. Chim. Acta 172 (1985) 307.
[4] L.H.M. Carvalho, T. de Koe, P.B. Tavares, Ecotoxicol. Environ. Restor. 1 (1998) 13.
[5] C.X. Galhardo, J.C. Masini, Anal. Chim. Acta 417 (2000) 191.
[6] V. Lenoble, V. Deluchat, B. Serpaud, J.-C. Bollinger, Talanta 61 (2003) 267.
[7] R.K. Dhar, Y. Zheng, J. Rubenstone, A. van Geen, Anal. Chim. Acta 526 (2004) 203.
[8] W. Frenzel, F. Titzenthaler, S. Elbel, Talanta 41 (1994) 1965.
[9] J. Floch, S. Blain, D. Birot, P. Treguer, Anal. Chim. Acta 377 (1998) 157.
[10] M.C. Giacomelli, O. Largiuni, G. Piccardi, Anal. Chim. Acta 396 (1999) 285.
[11] J.Z. Zhang, C.H. Fischer, P.B. Ortner, Talanta 49 (1999) 293.
[12] K. Grudpan, P. Ampan, Y. Udnan, S. Jayasvati, S. Lapanantnoppakhun, J. Jakmunee, G.D. Christian, J. Ruzicka, Talanta 58 (2002) 1319.
[13] S. Karthikeyan, S. Hashigaya, T. Kajiya, S. Hirata, Anal. Bioanal. Chem. 378 (2004) 1842.
[14] L. Kuai, A.A. Nair, M.F. Polz, Appl. Environ. Microbiol. 67 (2001) 3168.
[15] C.R. Anderson, G.M. Cook, Curr. Microbiol. 48 (2004) 341.
[16] D. Ahmann, A.L. Roberts, L.R. Krumholz, F.M.M. Morel, Nature 371 (1994) 750.
[17] D.K. Newman, E.K. Kennedy, J.D. Coates, D. Ahmann, D.J. Ellis, D.R. Lovley, F.M.M. Morel, Arch. Microbiol. 168 (1997) 380.
[18] R.B. McCleskey, D.K. Nordstrom, A.S. Maest, Appl. Geochem. 19 (2004) 995.
[19] C.A.J. Appelo, D. Postma, Geochemistry, Groundwater and Pollution, 2nd ed., A.A. Balkema Publishers, Leiden, The Netherlands, 2005, p. 649.
[20] A.D. Eaton, L.S. Clesceri, A.E. Greenberg, Standard Methods for the Examination of Water and Wastewater, 19th ed., American Public Health Association, 1995, p. 1325.

A new and selective and sensitive nanogold-labeled immunoresoance scattering spectral assay for trace prealbumin

Ming Hou [a], Shuangjiao Sun [b], Zhiliang Jiang [a,b,*]

[a] *Department of Material and Chemical Engineering, Guilin University of Technology, Guilin 541004, China*
[b] *School of Environment and Resource, Guangxi Normal University, Guilin 541004, China*

Abstract

A gold-labeled immunoresonance scattering spectral probe for trace prealbumin (PA) was prepared by using gold nanoparticles in size of 9.0 nm to label goat anti-human prealbumin polyclonal antibody. The immune reaction between the gold-labeled antibody and prealbumin took place in pH 7.6 Na_2HPO_4–NaH_2PO_4 buffer solution. In the presence of polyethylene glycol PEG-10000, the labeled gold nanoparticles were released and aggregated which brought the resonance scattering intensity (I_{RS}) at 580 nm to enhance greatly. The ΔI_{RS} is proportional to the prealbumin concentration in the range from 16.67 to 666.67 ng/mL, with a detection limit of 4.1 ng/mL. This simple, sensitive and selective assay was applied to determination of prealbumin in human plasma, with satisfactory results.
© 2007 Published by Elsevier B.V.

Keywords: Gold nanoparticle labeling; Immunological resonance scattering spectral probe; Prealbumin

1. Introduction

Prealbumin (PA) was the precursor of serum albumin and synthesized by liver [1]. It is one of value indexes for evaluating liver function because its half-life only has 1.9 day and could reflect liver function sensitively and idiosyncraticly [2,3]. Wu et al. [4] reported that serum PA would decrease greatly when people have acute hepatitis, cirrhosis or severe hepatitis. It [5] was also reported that PA is a value index when calculating the survival time of terminal cancer. In addition, malnutrition would lead serum PA to decrease, and the determination of PA could work as a good indicator to judge the nutrition condition [6]. Therefore, it is very significant to found a highly sensitive, good selective method for assaying PA in clinical medicine. The reported methods for determining PA are mainly electrophoresis [7–9], radial immunodiffusion [10], radioactivity immunoanalysis [11], immunonephelometricssays [12], immunoturbidimetric assays [13] and ELISA [14]. In electrophoresis analysis, the PA components are separated by isoelectric focusing in agarose gel,

especially radio-immunoisoelectric focusing has better sensitivity, but it costs long time, has much influence factors and it could not assay massive samples at the same time [7,9]. Radial immunodiffusion is also time-consuming [10]. Polyethyleneglycol was used to separate bound from free PA in a 2 h radioimmunoassay (RIA), compared with electroimmunoassay; the method relativity is good, but owing to the half-life of isotope, the results always changed [11]. Immunonephelometric assays were used to determine 50–400 μg/mL PA with a detection limit of 8 μg/mL [12]. Nephelometry is simple, but its sensitivity is low, with a detection limit of 12 mg/L [13]. An ELISA method basing on peroxidase-labeled antibody was used, with a linear range of 1–4 ng per well, antisera needs small amounts, but enzyme is expensive and some reagents are harmful [14]. Light scattering is a common phenomenon, and resonance scattering (RS) or resonance light scattering (RLS) is the resonance between the incident photon and the interface electron on the particle surface, which cause the scattering signal enhanced greatly. RS spectral method, with high sensitivity, rapidity and simplicity, has been applied to analysis of trace protein, nucleic acid and inorganic ions [16–21]. Immunoreaction is based on special interaction between the antigen and antibody, with better selectivity than other interaction. Recently, Jiang [22] and Huang and Li [23] have proposed a highly selective immunoresonance

* Corresponding author at: School of Environment and Resource, Guangxi Normal University, Guilin 541004, China.

E-mail address: zljiang@mailbox.gxnu.edu.cn (Z. Jiang).

scattering spectral assay for the determining IgG. However, a highly sensitive and good selective immunoresonance scattering spectral assay for PA has not reported. It is known that immunogold labeling technique is fourth labeled technique after radioactive, enzymatic and fluorescence labeling. It overcomes the disadvantages of the radioactive hazard, the carcinogenicity of enzymatic substrate and the complex of fluorescence labeling, has sensitivity, simplicity, rapidity, accuracy and non-pollution, with tiny effect in bioactivity [24]. Recently, our group have found that small gold particles have weak RS effect and it is stronger when they aggregate [25]. In this work, we combined the immune reaction between gold-labeled PA antibody and PA with RS effect of gold particles to establish a gold-labeled immune resonance scattering spectral assay for PA in human serums, with good selectivity and high sensitivity and simplicity.

2. Experimental

2.1. Reagents and apparatus

HAuCl$_4$ was obtained from the National Pharmaceutical Group Chemical Reagents Company, China. Goat anti-human PA antisera, PA were purchased from Shanghai Jiemen Bio-tech Company, Shanghai, China. A 0.20 mol/L solution of Na$_2$HPO$_4$ and NaH$_2$PO$_4$ was used to prepare different pH phosphate buffer solutions (PB). Tri-sodium citrate, polyethylene glycol 6000 (PEG-6000), PEG-4000, PEG-10000, PEG-20000 and KCl were used. All reagents were of analytical grade, and the water used was double distilled.

A model RF-540 spectrofluorometer (Shimadzu), spectrophotometer (Puxi General Istrumental Company, Beijing), model 79-1 magnetic heat agitator (Zhongda Instrumental Plant), model SK8200LH ultrasonic reactor (Kedao Ultrasonic Instrument Limited Company) and a model H-600 transmission electron microscope (Electronic Stock Limited Company) were used.

2.2. Preparation and identification of colloidal gold

We used the improved method [26] to prepare colloidal gold by adding HAuCl$_4$ solution to a boiled solution of tri-sodium citrate while stirring. With this procedure, we obtained gold colloid with consistent particle size of 9.0 nm. We used transmission electron microscope to observe the size and uniformity of the gold particles. Examination of the gold nanoparticles revealed that the diameter was 9 nm, and the distribution and size were uniform and consistent.

2.3. Preparation of the immunogold probe

2.3.1. Pretreatment of goat anti-human PA antibody
Excessive salt matter lowers Zeta potentiometry of gold particles, influences the absorption of goat antihuman PA on gold surfaces and can lead to colloidal gold aggregation. We eliminated the redundant electrolytes from the PA antibody before labeling by dialysis for 30 h in doubly distilled water.

2.3.2. Selection of the pH of the colloidal gold labeling
Because the combination of colloidal gold with PA antibody is done by physical force, the successful combination depends on the pH. When the pH value is less than its isoelectric point, the adsorbability decrease and the bad stability results in aggregation. In suitable pH condition at isoelectric point, combination could stabilize [27]. In this experiment, we used a resonance scattering method to test the influence of different pH conditions on colloidal gold labeling. We adjusted the pH of 1.0 mL 58 μg/mL colloidal gold solution to different value by adding 0.20 mol/L K$_2$CO$_3$ or 0.10 mol/L HCl and adding 25 μg of PA antibody. After 5 min, added 0.10 mL of 100 mg/mL KCl solution, 2 h later, then diluted the solution with distilled water to 3.0 mL. Second, we recorded the resonance scattering intensity (I_{RS}) at 580 nm [25]. The results showed that when the pH was less than 7.0, the addition of the antibody did not stabilize the gold nanoparticles, the RS intensity was bigger. When the pH was more than 7.0, the RS intensity decreased and the system stabilized because better combination of gold nanoparticles and antibody prevented colloidal gold from aggregation by KCl solution.

2.3.3. Selection of the ratio between colloidal gold and the antibody
Too much antibody in solution, which could not connect with gold anoparticles, resulted in the poor sensitivity in assay; we should find the minimum level of PA antibody for stabilizing certain gold nanoparticles [27]. Different quantities (0, 5, 10, 15, 20, 25, 30, 35, 40, 45, 50 and 55 μg) of PA antibody were added into 1.0 mL of 58 μg/mL colloidal gold solution. The pH of the colloidal gold solution had been adjusted to 7.0–7.5. After 5 min, 0.10 mL of 10% KCl solution added and mixed well. After 2 h, we recorded the RS intensities in each tube. Results showed that the RS intensity was stronger for the tubes with 0–30 μg antibody than in the tubes with 35–55 μg PA antibody, which remained stable. Thus, the minimum level of antibody that stabilized a 1.0 mL colloidal gold solution was a 35 μg.

2.3.4. Preparation of gold-labeled goat anti-human PA antibody
A 100 mL colloidal gold solution was adjusted to pH 7.0–7.5. During magnetic stirring, a 2.0 mL of the PA antibody (3.5 mg) was added to a 100 mL colloidal gold, maintaining the dropping time for 5 min, and a 1.75 mL of 3% PEG-20000 was added as stabilizer to a final concentration of 0.05% PEG-20000. The mixture was stirred for 15 min and kept at 4 °C. The gold-labeled PA antibody concentration is 33.73 μg/mL. The gold-labeled antibody was not purified by centrifugation, and the results were consistent with those for the purified. Micrographs of gold-labeled PA antibody (Fig. 1) show that the gold nanoparticles were not clearly observable because they were coated tightly by antibody.

2.4. Procedure of the immunoresonance scattering

A 0.30 mL of pH 7.6 phosphate-buffer solution, 1.2 mL gold-labeled PA antibody, a certain quantity of PA and 0.50 mL of
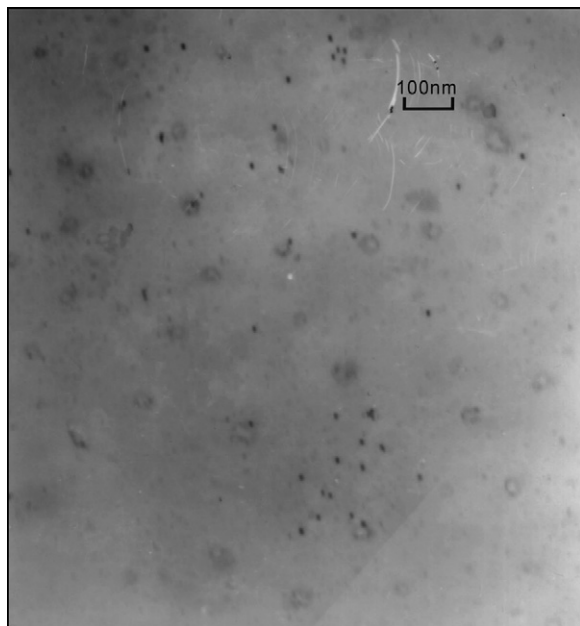
Fig. 1. Transmission electron micrograph of gold-labeled PA antibody.

300 mg/mL PEG-10000 were successively added to 10 mL graduated tubes. The mixed solutions were diluted to 3.0 mL with distilled water, mixed well, and then incubated in an ultrasonic reactor (59 kHz) for 25 min. Suitable volumes of the prepared solutions were transferred into a quartz cell. Low sensitive files and a longitudinal coordinate scale of 6 were set, and the synchronous scattering spectrum of the system was recorded by means of synchronous scanning of excited wavelength λ_{ex} and emission wavelength λ_{em} ($\lambda_{ex} - \lambda_{em} = \Delta\lambda = 0$) on the model RF-540 spectrofluorophotometer. Then the resonance scattering intensity at 580 nm was recorded. The RS intensities of the blank solution with no PA [$(I_{RS})_b$] were also measured. The $\Delta I = I_{RS} - (I_{RS})_b$ value was calculated.

3. Results and discussion

3.1. Principles

PA antibody could combine with PA to form immunocomplexes (IC). The sensitivity is relatively low when it was used to determine PA. The I_{RS} of colloidal gold has close correlation with the size of gold particles [25]. In gold-labeled goat anti-human AP system, gold particles connecting with goat anti-human PA could stably exist in 50 mg/mL PEG-1000 solution. After the immune reaction between goat anti-human PA and PA, the gold particles would be released and aggregated in the action of PEG-10000. It was identified by the absorption spectra which the maximum absorption wavelength has red-shift changed from 516 to 528 nm, and also proved by transmission electron microscope (Fig. 2). The aggregated gold particles resulted in the enhancement of I_{RS} at 580 nm. In a certain PA concentration range, the RS intensity enhanced linearly with PA concentration. Therefore, we founded an immune RS assay for PA with gold-labeled technique.

3.2. Resonance scattering spectrum (RSS)

Gold colloidal has two RS peaks at 320 and 580 nm and a synchronous scattering peak at 470 nm, where the apparatus has the strongest emission [28]. When gold particle is small, its RS intensity at 320 and 580 nm is weak, but the RS intensities at 580 nm enhanced greatly when it aggregated [23]. The gold nanoparticles in small size connecting with the PA antibody could exist stably in 50 mg/mL PEG-10000 solution and the RS intensities were weak at 320 and 580 nm. After the immune reaction took place, the coated gold nanoparticles was released from goat anti-human PA and aggregated at the action of 50 mg/mL PEG-10000, then the I_{RS} enhanced greatly, especially the I_{RS} at 580 nm (Fig. 3). In this work, a 580 nm was selected for use.

3.3. Selection of the pH, type and volume of buffer solution

The influence of PB (pH 5.8–8.0) and Tris–HCl (pH 7.0–8.5) buffer solution on the I_{RS} was tested. PB had better effect and was chosen for use. The maximum I_{RS} occurred at pH 7.6 PB solutions. It is owing to that the isoelectric point of PA is at pH 7.5. As a result of tests for buffer solution concentration, a 0.020 mol/L PB solution was chosen.

3.4. Effect of different PEG concentration

PEG is a kind of linear molecular polysaccharide and the polymer of ethylene with no charge and it can lead to aggregation of IC, causing the release of gold particles. This aggregation is reversible, and the deposited proteins have no effect on bioactivity [29]. Our results demonstrated that I_{RS} increased greatly with increased PEG concentrations (Fig. 4) owing to the gold
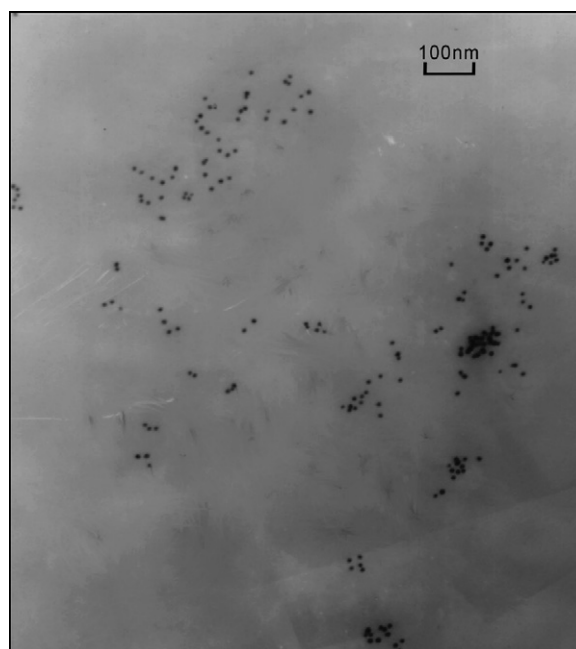

Fig. 2. Transmission electron micrograph of PA–gold-labeled PA antibody system: pH 7.6–13.50 μg/mL gold-labeled PA–0.17 μg/mL PA–50 mg/mL PEG-10000.
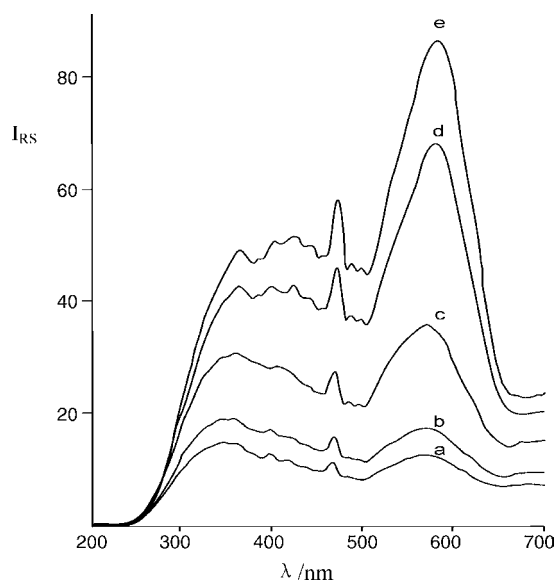
Fig. 3. RS spectra of gold-labeled goat anti-PA antibody and AP: (a) pH 7.6–13.50 µg/mL gold-labeled PA antibody–50 mg/mL PEG-10000; (b) a–0.067 µg/mL PA; (c) a–0.17 µg/mL PA; (d) a–0.33 µg/mL PA; (e) a–0.50 µg/mL PA.

aggregating nanoparticles. The maximum I_{RS} for the system occurred at 50 mg/mL PEG-10000 solution.

3.5. Effect of gold-labeled AP antibody concentrations

The influence on I_{RS} of different concentration of gold-labeled antibody was considered. In range of 0–5.8 µg/mL gold-labeled PA antibody, the I_{RS} value increase with its concentration. The I_{RS} value changed weakly, when the gold-labeled antibody is in range of 5.8–17.5 µg/mL. This does not like the immunoreaction between PA and PA antibody that the RS intensity decreased considerably when one of both is excessive. It is owing to gold nanoparticles were in negative charges. A 13.50 µg/mL gold-labeled PA antibody, giving a maximum I_{RS}, was chosen for use.

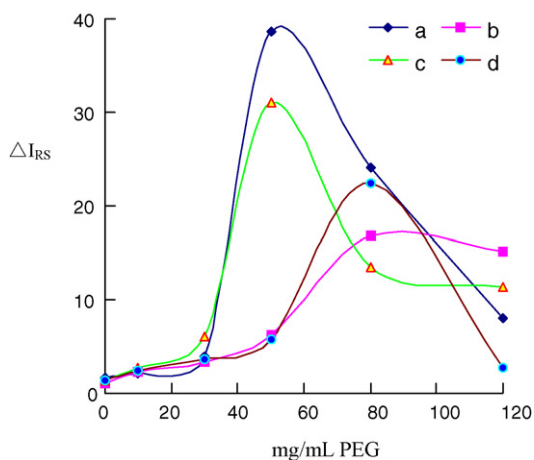### 3.6. Effect of ultrasonic irradiation incubation time

The influence of ultrasonic irradiation incubation time from 0 to 60 min on the I_{RS} was considered. Under the condition of ultrasonic irradiation, when the reaction lasted 30 min, the reactions completed and the I_{RS} held constantly. A 30 min ultrasonic irradiation time was chosen.

3.7. Linear range

According to the procedure, its RS intensities corresponding different concentration of PA were measured. The linear range, linear regression equation, correlation coefficient, and detection limit were 16.67–666.67 ng/mL PA, $\Delta I = 0.1532c$–2.03, 0.9985, 4.1 ng/mL PA, respectively. Compared with other immune methods [11–14], this method accomplished in one step without separation, has better selectivity, sensitivity, high-speed and simplicity. The reagents are innocuous.

3.8. Effect of foreign substance

The effect of foreign substances on the measurement of PA was considered. When PA concentration was 0.57 mg/L with a relative error of ±6%, 700 mg/L sodium oxalate, 400 mg/L urea, 210 mg/L EDTA, 167 mg/L glucose, 83 mg/L cane sugar, 60 mg/L ascorbic acid, 33 mg/L L-Tyr and Vitamin B_1, 30 mg/L Trp, 20 mg/L Asp, 17 mg/L nicotine, 13 mg/L Gly, 7 mg/L HSA and BSA, 3 mg/L His, L-Cys, Met and L-Arg, 2 mg/L human IgA, human IgG, human IgM and Vitamin B did not interfere with the assay. It showed that this assay has good selectivity, owing to the specific immunoreaction.

3.9. Analysis of samples

Fifteen serum samples from apparently healthy men were analyzed (Table 1). It was obtained from No. 5 Hospital of Guilin City. The samples were also assayed by immunoturbidimetry
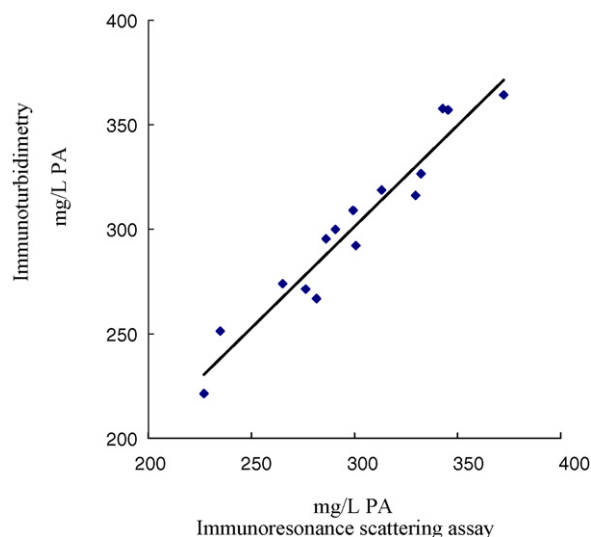

Fig. 4. Influence of PEG on the ΔI_{RS} pH 7.6 PB–13.50 µg/mL gold-labeled PA antibody–0.26 µg/mL PA–PEG. (a) PEG-10000; (b) PEG-4000; (c) PEG-20000; (d) PEG-6000.

Fig. 5. Linear regression analysis for PA.

Table 1
Results for AP in serum samples

Samples	Content (mg/L)					Mean value (mg/L)	R.S.D. (%)	Immunoturbidimetry (mg/L)
1	298.2	305.6	302.4	284.1	306.3	299.3 ± 9.1	3.04	308.9
2	328.9	334.3	323.5	329.2	331.1	329.4 ± 3.9	1.20	316.1
3	340.9	340.9	357.9	338.3	349.4	345.5 ± 8.1	2.35	356.9
4	263.9	272.4	267.8	257.1	250.3	265.3 ± 6.5	2.44	274.3
5	230.6	221.7	218.9	237.1	226.3	226.9 ± 7.3	3.20	221.5
6	289.1	275.8	282.2	275.6	286.5	281.9 ± 6.1	2.17	267.1
7	301.3	295.5	290.9	303.6	312.8	300.8 ± 8.3	2.78	292.4
8	277.9	289.6	286.0	278.1	299.7	286.3 ± 9.1	3.16	295.5
9	309.1	321.1	304.7	311.9	318.6	313.1 ± 6.8	2.16	319.1
10	331.4	345.7	323.4	328.5	330.8	332.0 ± 8.3	2.50	326.4
11	228.9	235.8	241.3	240.7	227.8	234.9 ± 6.4	2.71	251.2
12	347.8	358.9	346.1	326.6	333.7	342.6 ± 12.7	3.69	357.7
13	293.1	277.4	291.5	289.7	303.4	291.0 ± 9.3	3.19	299.7
14	373.1	382.4	365.2	371.6	369.5	372.3 ± 6.4	1.71	364.3
15	287.7	269.9	268.6	277.5	279.1	276.6 ± 7.7	2.80	271.7

[13]. The linear regression analysis of the both was shown in Fig. 5. The correlation coefficient, slope and intercept are 0.966, 0.969 and 10.986, respectively. We could see the results of the both methods are consistent on the whole.

4. Conclusions

Without phase separation in assay course, a new immune RS for determination of 16.67–666.67 ng/mL PA was developed, with simplicity, high sensitivity and good selectivity. In the presence of PEG, owing to the aggregated gold nanoparticles, the RS intensity increased greatly. Furthermore, different from most immunoassay, the enhanced RS intensity is linear to the PA concentration and the range is wide, which was used in PA assay in human plasma, with satisfactory results.

References

[1] Y.Y. Jin, Clinical Biochemistry Laboratory Science, Ocean Press, Beijing, 1993.
[2] Y.G. Lin, Clin. Biochem. Lab. Med. Foreign Med. Sci. 17 (1996) 113.
[3] D.C. Hu, H.J. Liu, D.Q. Xia, J. Chin. Inter. Med. 24 (1985) 723.
[4] J.Q. Wu, S.F. Fan, H.B. He, J. Jiangxi, Lab. Med. 18 (2000) 79.
[5] Y. Inoue, R. Nezu, H. Matsuda, Surg. Today 25 (1995) 948.
[6] K. Yu, T.Y. Chen, S.Y. Zhang, Parenter. Enter. Nutrit. 12 (1995) 201.
[7] R.J. Chen, J. Chin. Lab. Med. 8 (1985) 151.
[8] J.Y. Wei, Q.S. Xu, H.M. Chen, C.J. Guo, Y.Z. Gou, J. Prev. Med. Chin. People's Liberation Army 9 (1991) 437.
[9] J.L. Longbottom, J. Immunol. Methods 68 (1984) 297.
[10] D.R. Hutchison, Clin. Chim. Acta 114 (1981) 96.
[11] D.M. Cowley, Clin. Chim. Acta 143 (1983) 69.
[12] L.X. Guo, J. Chin. Lab. Med. 14 (1991) 84.
[13] T.S. Guo, F.W. Wang, J. Chin. Lab. Med. 14 (1991) 133.
[14] G.T. Vatassery, H.T. Quach, W.E. Smith, B.A. Benson, J.H. Eckfeldt, Clin. Chim. Acta 197 (1991) 19.
[16] P.F. Pasternack, P.J. Collings, A. Gianncttd, J. Am. Chem. Soc. 115 (1993) 5393.
[17] H. Zhong, J.J. Xu, H.Y. Chen, Talanta 67 (2005) 749.
[18] S.P. Liu, H.Q. Luo, N.B. Li, Anal. Chem. 73 (2001) 3907.
[19] C.Y. Kang, D.L. Xi, S.M. Zhou, Z.L. Jiang, Talanta 68 (2006) 974.
[20] P. Francois, M. Bento, P. Vaudaux, J. Microbiol. Method 55 (2003) 755.
[21] P. Bao, A.G. Frutos, C. Greef, J. Lahiri, Anal. Chem. 74 (2002) 1792.
[22] Z.L. Jiang, Spectrosc. Spec. l Anal. 26 (2006) 1487.
[23] C.Z. Huang, Y.F. Li, Talanta 70 (2006) 609.
[24] X.F. Chen, S.Z. Liu, Pharm. Biotechnol. 11 (2004) 278.
[25] Z.L. Jiang, H.C. Pan, W.E. Yuan, Chem. Res. Chin. Univ. 20 (2004) 523.
[26] X. Chen, T. Li, Clinical Immunological and New Immunological Technique, People's Military Medical Press, Beijing, 2002.
[27] L.P. Zhu, X.Q. Chen, Common Experimental Method for Immunology, People Military Medicial Press, Beijing, 2000.
[28] Z.L. Jiang, Nanoparticle and Resonance Scattering Spectrosopy, Guangxi Normal University Press, Guilin, 2003.
[29] J.G. Wu, Application Clinical Immunology Test, Jiangsu Scientific Technology Press, Nanjing, 1990.

ELSEVIER

Sensitive detection of clozapine using a gold electrode modified with 16-mercaptohexadecanoic acid self-assembled monolayer

Fei Huang, Song Qu, Song Zhang, Baohong Liu, Jilie Kong[*]

Department of Chemistry, Fudan University, Shanghai 200433, PR China

Abstract

Clozapine, an effective antipsychotic drug, was found generating a pair of redox peaks at about 0.33–0.4 V (versus SCE) at 16-mercaptohexadecanoic acid (i.e. MHA) self-assembled monolayer (SAM) modified gold electrode (i.e. MHA/Au) in $0.05 \, mol \, L^{-1}$ Tris–HCl (pH 8.1) buffer solution. Sensitive and quantitative measurement of clozapine based on anodic peak was established under optimum conditions. The anodic peak current was linear to clozapine concentration in the range from 1×10^{-6} to $5 \times 10^{-5} \, mol \, L^{-1}$ with the detection limit of $7 \times 10^{-9} \, mol \, L^{-1}$. This method was successfully applied to the detection of clozapine in drug tablets and proved to be reliable compared with ultraviolet spectrophotometry (UV). The MHA SAM was characterized by Fourier transform infrared spectroscopy (FT-IR), X-ray photoelectron spectroscopy (XPS), contact angle goniometry, electrochemical impedance spectroscopy (EIS) and electrochemical probe.
© 2006 Elsevier B.V. All rights reserved.

Keywords: Clozapine; 16-Mercaptohexadecanoic acid; Self-assembled monolayer; Detection; Gold electrode; Characterization

1. Introduction

Clozapine (Scheme 1) is an effective antipsychotic drug treating schizophrenia [1]. Owing to its importance, researchers used many analytical methods to study it, including capillary zone electrophoresis [2], high-performance liquid chromatography [3], spectrophotometry [4], mass spectrometry, etc. [5]. There were some reports about electrochemical study of clozapine due to its electroactivity. Blanket et al. [6], Hernandez et al. [7], and Ozakn et al. [8], respectively, used horseradish peroxidase (HRP) modified carbon paste electrode, sepiolite modified carbon paste electrode and activated glassy carbon electrode to determine clozapine. The detection limits obtained were 1.7×10^{-7}, 1×10^{-7} and $2 \times 10^{-7} \, mol \, L^{-1}$, which seemed somewhat unsatisfactory. Jarbawi and Heineman [9] determined clozapine using wax-impregnated graphite electrode and got a satisfactory detection limit of $5 \times 10^{-9} \, mol \, L^{-1}$. Nevertheless, the 15 min preconcentration was somewhat time-consuming.

Self-assembled monolayer (SAM) is a useful and promising technique in electroanalytical chemistry. This technique makes it possible for modifying electrodes surfaces conveniently and controllably and improving greatly the characteristics of the electrodes, including selectivity, sensitivity and reproducibility [10]. It has been reported that SAM modified electrodes were successfully applied to study and determine some biological and organic molecules, inorganic ions such as cytochrome c [11], dopamine [12], Hg^{2+} [13]. However, there is no report about the application of self-assembled monolayer modified electrodes in the detection of clozapine.

In this paper, the electrochemical behavior of clozapine at 16-mercaptohexadecanoic acid self-assembled monolayer modified gold electrode was studied. Furthermore, a more sensitive and simpler determination method for clozapine was proposed.

2. Experimental

2.1. Reagents

Clozapine ($C_{18}H_{19}ClN_4$) was purchased from Sigma. Its stock solution ($0.01 \, mol \, L^{-1}$) was prepared with ethanol and stored at $4 \, °C$. $0.01 \, mol \, L^{-1}$ 16-mercaptohexadecanoic acid ($HS(CH_2)_{15}COOH$, Aldrich) stock solution was prepared with ethanol. Buffer solution was a $0.05 \, mol \, L^{-1}$ Tris–HCl (pH 8.1) aqueous solution. The drug tablets came from Sine JiuFu

---

* Corresponding author. Tel.: +86 21 6564 2405; fax: +86 21 6564 1740.
E-mail address: jlkong@fudan.edu.cn (J. Kong).
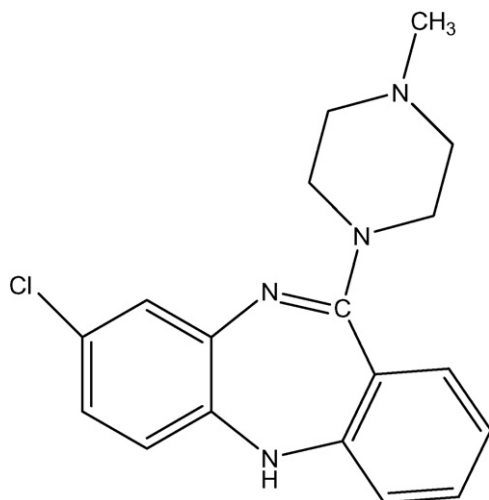
Scheme 1. Molecular structure of clozapine.

Pharmaceutical Company of Shanghai (Shanghai, China). Prior to determination, they were ground into powder, dissolved in ethanol, filtered into a container and then diluted to certain volume. Other reagents used were of analytical grade or chemical grade, and their solutions were prepared with twice distilled water or ethanol.

2.2. Apparatus

Electrochemical measurements were carried out on a CHI 440 electrochemical analytical instrument (Chenhua Instrument company, Shanghai, China). A three-electrode system was used, including a bare gold electrode ($\Phi = 2.0$ mm) or modified electrode as working electrode, a saturated calomel electrode (SCE) as reference electrode and a platinum wire electrode as counter electrode. EIS measurements were performed on an EG&G PAR Model 273 A bipotentiostat (Princeton, USA) in conjunction with a lock-in amplifier. A 5 mV amplitude sine wave was applied to the electrode under potentiostatic control and the frequency range was from 0.1 Hz to 100 kHz. FT-IR measurements were performed on NEXUS 470 FT-IR spectrometer (Nicolet company, USA). XPS measurements were performed on PHI5000C ESCA system (Perkin-Elmer company, USA). Contact angle measurements were performed on OCA15 contact angle goniometer (Dataphysics company, Germany). UV measurements were performed on HP8453 ultraviolet–visible spectrophotometer (Agilent company, USA). Solution pH was measured with a Mettler-Toledo 320-s pH meter (Shanghai, China). All experiments were carried out at 22 °C.

2.3. Preparation of MHA/Au modified electrode

The bare gold electrode was first polished to a mirror-like surface with 0.3 and 0.05 μm α-alumina slurry, then rinsed and ultrasonicated for 2 min with twice distilled water, and dried in air. If necessary, the electrode was immersed in a Piranha solution (a mixed solution of 30% H_2O_2 and concentrated H_2SO_4 with the ratio of volume of 1/3) for 1 min before washing with

water. The electrode was then cycled between 0 and +1.5 V in 0.5 mol L^{-1} H_2SO_4 until a stable cyclic voltammogram was obtained. According to the cathodic peak area of the gold electrode, the effective area of the electrode was calculated to be 0.0565 cm^2. MHA/Au modified electrode was prepared by soaking the clean gold electrode in a 0.01 mol L^{-1} MHA solution for about 2 min. Then the modified electrode was taken out and washed thoroughly with water to remove the physically adsorbed MHA.

2.4. Procedure

The three-electrode system was immersed in a 10 mL cell containing proper amount of clozapine and 0.05 mol L^{-1} Tris–HCl (pH 8.1) buffer solution. After accumulating for 60 s at open circuit under stirring and following quiet for 10 s, potential scan was initiated and cyclic voltammograms were recorded between −0.2 and +0.8 V with a scan rate of 100 mV s^{-1}. After potential cycling, the electrode was polished and modified again for the next measurement. The determination was carried out using differential pulse voltammetry (DPV) within the same potential window, the major parameters were as following: pulse amplitude was 50 mV; pulse width was 50 ms; pulse period was 0.2 s; potential increment was 4 mV. As to the chronocoulometric experiment, the potential step was from 0.3 to 0.5 V.

3. Results and discussion

3.1. The characterization of hydrophobic and dense MHA SAM formed on Au electrode

The spectral characteristics of MHA SAM were investigated by FT-IR and XPS. Fig. 1A shows the IR spectra of MHA. The strong peaks at 2970, 2870, 1470 cm^{-1} are attributed to $(-CH_2-)_n$, while the peak at 3100, 2560 and 1740 cm^{-1} is attributed to −OH, −SH and C=O, respectively. However, when MHA assembled on gold surface, the peak at 2560 cm^{-1} disappeared (Fig. 1B), indicating the formation of S–Au bond. Fig. 2
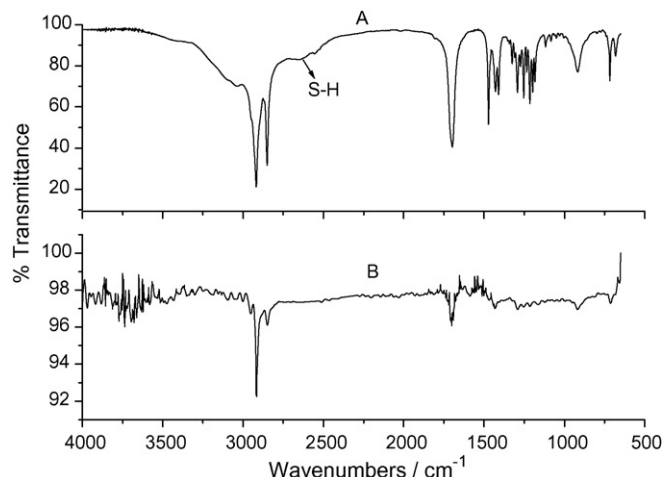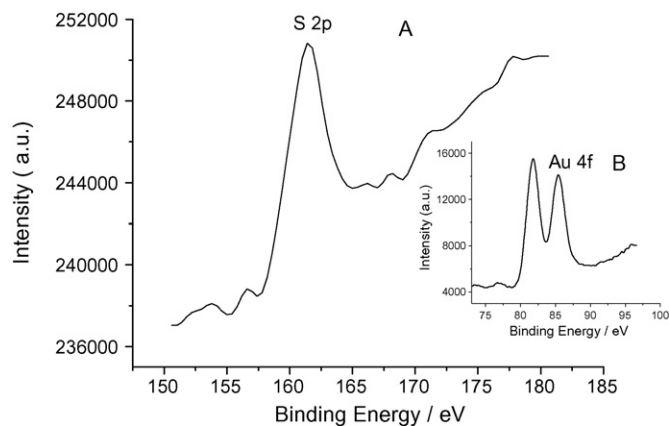

Fig. 1. FT-IR spectra of MHA (A) and MHA SAM (B).

Fig. 2. XPS spectra of S 2p region (A) and Au 4f region of MHA SAM (B).

Fig. 4. EIS spectra of Au (A) and MHA/Au (B). Frequency used: 0.1 Hz to 100 kHz. Solution: 2 mmol L^{-1} K$_3$Fe(CN)$_6$/K$_4$Fe(CN)$_6$ containing 0.1 mol L^{-1} KNO$_3$. The insert was the amplification of (A).

shows the XPS spectra of MHA SAM. The MHA SAM gave a strong peak at 161.9 eV. According to the literature [14], S 2p chemical shift of a thiolate in alkanethiol SAM on gold (RS–Au), a thiol in polycrystalline sample (RSH) and a sulfonate (SO$_3{}^{2-}$) are in the ranges of 161.8–162.6, 163.5–163.8, and >167 eV, respectively. Therefore, the peak at 161.9 eV corresponded to the S–Au bond. Furthermore, the smaller peak at 168 eV resulted from the oxidation of MHA to sulfonate when it was exposed to air for some time.

The electrochemical characteristics of MHA SAM were also studied by electrochemical probe and EIS. As shown in Fig. 3, K$_3$Fe(CN)$_6$ exhibited a pair of quite reversible redox peaks at bare gold electrode. However, the redox peaks disappeared completely at the modified electrode. This was due to the strong blocking action of MHA SAM to K$_3$Fe(CN)$_6$. MHA is hydrophobic, when it assembled at the bare gold electrode, the dense monolayer restrained hydrophilic K$_3$Fe(CN)$_6$ arriving at the electrode surface. Fig. 4 shows the EIS spectra of bare gold electrode and MHA/Au modified electrode in the given solution. The resistor of the modified electrode (R'_{ct}) was much larger than the bare electrode (R_{ct}), also suggesting that the MHA SAM had strong hindrance to the transfer of Fe(CN)$_6{}^{4-/3-}$.

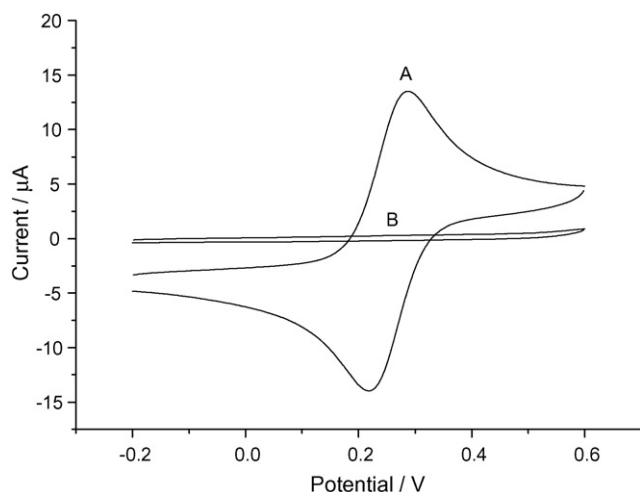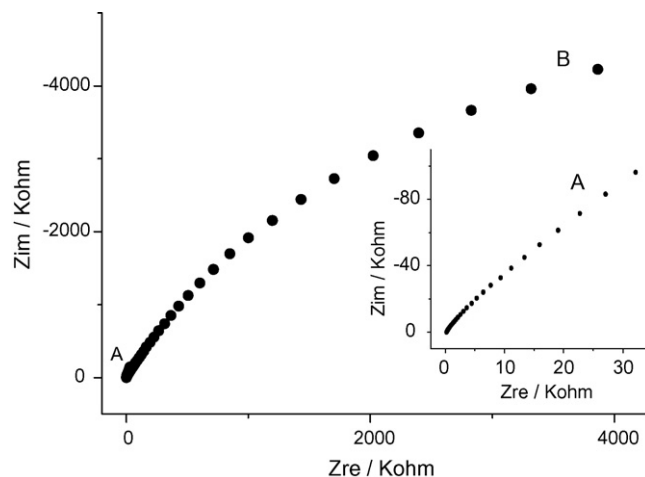According to the impedance of the two electrodes in high frequency range, the coverage (θ) of the monolayer was estimated to be 99.9% ($R_{ct} = 2.5$ kΩ, $R'_{ct} = 4000$ kΩ, $\theta = 1 - R_{ct}/R'_{ct}$ [15]), indicating the electrode surface was almost completely covered with MHA.

The wettability of MHA SAM was determined by contact angle goniometry. It was found that after gold surface was modified with MHA, the contact angle varied from 70° to 104°, suggesting the surface became more hydrophobic. The strong hydrophobicity of MHA SAM results from its long alkyl chain, in spite that it has hydrophilic −COOH.

3.2. Cyclic voltammograms of clozapine at MHA/Au

As shown in Fig. 5, at bare gold electrode, clozapine generated two pairs of poor-defined redox peaks at 0.13–0.21 V and
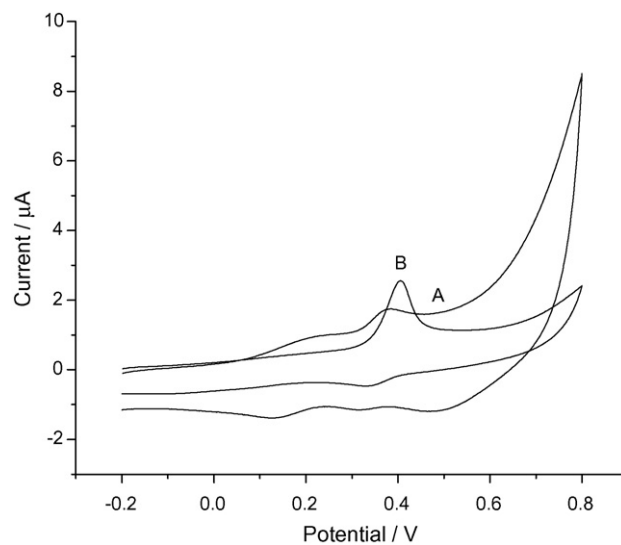

Fig. 3. Cyclic voltammograms (CV) of 2 mmol L^{-1} K$_3$Fe(CN)$_6$ at Au (A) and MHA/Au (B). Supporting electrolyte: 0.5 mol L^{-1} KNO$_3$.

Fig. 5. CVs of Au (A) and MHA/Au (B) in a 3×10^{-5} mol L^{-1} clozapine solution. Scan rate: 100 mV s^{-1}; supporting electrolyte: 0.05 mol L^{-1} Tris–HCl (pH 8.1); accumulation time: 60 s (at open circuit).

0.32–0.4 V, respectively. However, only one pair of well-defined redox peaks occurred at MHA/Au modified electrode. The sensitive anodic peak was at about 0.4 V and the small cathodic peak was at about 0.33 V, the difference of peak potential (ΔE_p) was about 70 mV. This suggested the electrochemical process was partially reversible. In addition, the anodic peak current was about 3.5 times as high as that of bare gold electrode. Apparently, the MHA SAM improved the sensitivity to some extent and the anodic peak was favorable for detection. According to the literature [16], the pK_a of clozapine was about 4.5, thus it was neutral charged in the given solution due to the deprotonation. On the other hand, owing to its poor solubility in water [17], clozapine was hydrophobic. Additional, the MHA SAM was also almost neutral (pK_a = 8.0 [18]) and hydrophobic (described in Section 3.1). Therefore, it was probably the hydrophobic interaction between them that responsible for the enhancement of response. Generally, voltammograms corresponding to the first cycle were recorded.

3.3. Effect of scan rate and chronocoulometric investigation

With scan rate increasing, both anodic peak and cathodic peak grew (Fig. 6). It was found that anodic peak current was linear to the square root of scan rate in the range of 50–500 mV s^{-1}, the regression equation was $I_p = -1.438 + 0.337v^{1/2}$ (I_p (μA), v (mV s^{-1}), $r = 0.997$), indicating the electrode process was diffusion-controlled. In addition, the anodic peak potential shifted positively about 60 mV while the cathodic peak potential remained almost unchanged, ΔE_p varied from 58 to 120 mV, indicated the electrode process became irreversible. The anodic peak potential and the logarithm of scan rate showed a linear relationship, following the equation: $E_p = 0.264 + 0.0296 \ln v$ (E_p(V), $r = 0.997$). According to the equation [19]: $E_p = E^\Phi + m[0.78 + \ln(D^{1/2}/k_s) - 0.5 \ln m] + 0.5m \ln v$ ($m = RT/(1-\alpha)nF$), the $n(1-\alpha)$ was calculated to be 0.43. Generally, the charge-transfer coefficient α is within the range 0.3–0.7, therefore, n was estimated to be
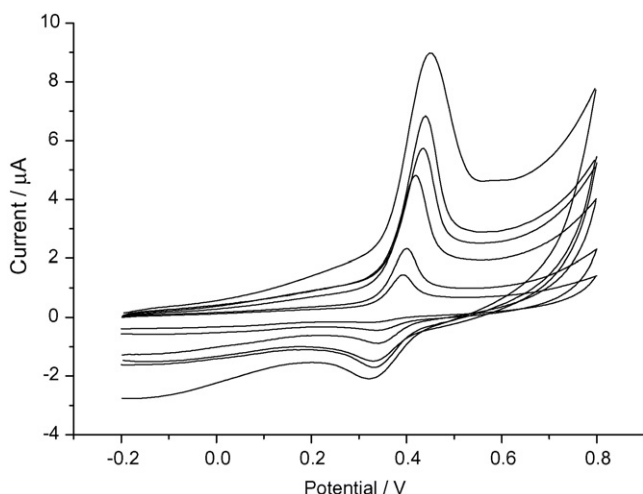

Fig. 6. Influence of scan rate on anodic peak. Scan rate: 50, 100, 200, 300, 400, 500 mV s^{-1} (from bottom to top). Other conditions as in Fig. 5.
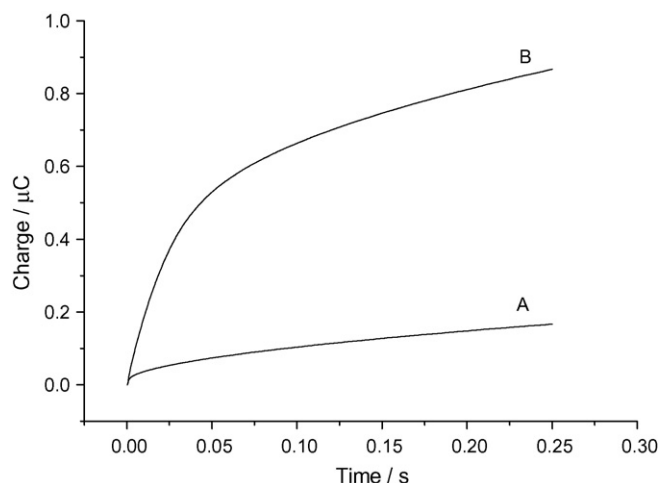

Fig. 7. Chronocoulomertric response of MHA/Au in 0.05 mol L^{-1} Tris–HCl (pH 8.1) solution without (A) and with (B) 3×10^{-5} mol L^{-1} clozapine. The potential step was from 0.3 to 0.5 V. Other conditions as in Fig. 5.

1 and α was 0.57 in this case. This suggested one electron was lost during the oxidation process, which was probably related to the formation of a relatively stable cation radical [6,16].

Fig. 7 shows the chronocoulometric response curves. After subtracting the background charge, the plot of Q against $t^{1/2}$ was made. It was a straight line and the regression equation was $Q = 2.868 + 8.442t^{1/2}$ ($Q(1 \times 10^{-7}$ C), t(s), $r = 0.996$). According to the integrated Cottrell equation [20]: $Q = 2nFAD^{1/2}Ct^{1/2}/\pi^{1/2} + Q_{dl} + nFA\Gamma_0$, the diffusion coefficient (D) of clozapine was calculated to be 2.09×10^{-5} cm^2/s.

3.4. Optimization of the analytical conditions

3.4.1. Influence of modification time and mercaptans

With the modification time varying from 1 min to 12 h, it was found that the anodic peak current kept almost constant, which was due to the effect of the long alkyl chain. In general, the alkanethiol with longer alkyl chain can form dense SAM easier and faster [21]. Hence, 2 min was chosen as modification time.

Besides 16-mercaptohexadecanoic acid, some other mercaptans such as L-cysteine, L-glutathione, dithiothreitol, 2-mercaptoethanol, thioine, 2-mercaptobenzothiazole, thiosalicylic acid and thioctic acid were tested as modifier (modification for 12 h). Owing to its electroactivity, clozapine could produce electrochemical response on these SAMs. However, compared with bare gold electrode, these SAMs could not enhance the sensitivity. This indicated that the hydrophobic interaction between clozapine and MHA SAM was stronger than the other tested SAMs. The hydrophobic interaction between clozapine and MHA SAM led to the enrichment of the analyte on the surface of the modified electrode, thus resulted in the enhancement of electrochemical response. The strength of this interaction was probably related to the surface characteristics of SAMs, such as hydrophilicity/hydrophobicity, pK_a, charge, coverage, structure, etc. The exact nature of the interaction is currently under
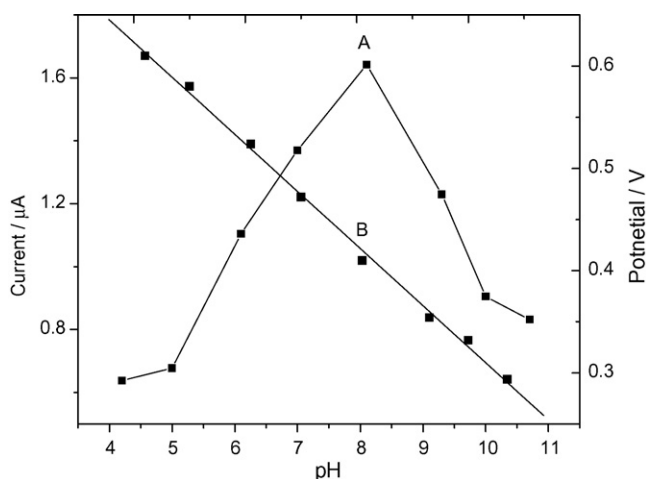
Fig. 8. Influence of pH on anodic peak current (A) and peak potential (B). Supporting electrolyte: 0.05 mol L^{-1} phosphate. Other conditions as in Fig. 5.

investigation. Thus, MHA was chosen as the modifier in this work.

3.4.2. Influence of pH and buffer solution

Within the range of pH 4–11, the peak potential shifted negatively with pH increasing, following the linear equation: $E_p = 0.822{-}0.0497$ pH (E_p(V), $r = 0.999$), meaning H$^+$ was involved in the oxidation. Meanwhile, the peak current increased until it attained the maximum at pH 8.1, then it decreased (Fig. 8). Generally, when pH of solution was lower than 4, the repulsion of hydrophobic MHA SAM to positive charged clozapine resulted in the suppression of current; with pH increasing gradually, owing to the deprotonation of clozapine, the hydrophobic interaction between them strengthened and led to the enhancement of electrochemical response; if the pH increased further and exceeded 11, the cathodic peak was obvious and the redo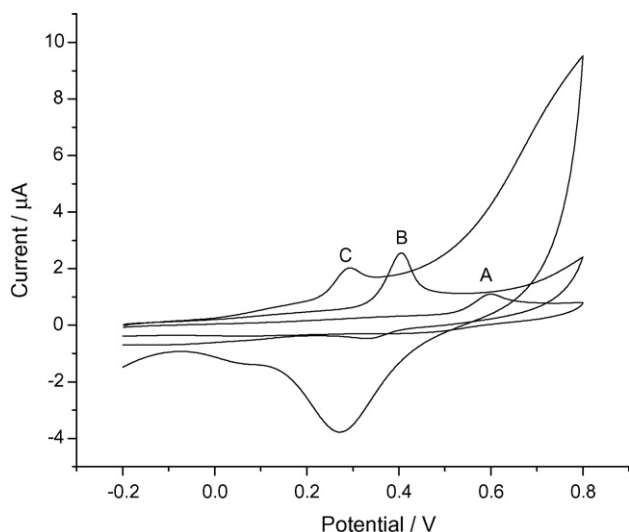x peaks became deformed (Fig. 9), indicating there was probably some alteration in the electrochemical mechanism [7,16]. Owing to the ill-defined and complicated shape, the cathodic peak at pH > 9 was not employed as the quantitative criterion in the detection of clozapine. Therefore, pH 8.1 was chosen as the optimum pH value. Furthermore, several different supporting electrolytes such as NH$_3$–NH$_4$Cl, Na$_2$B$_4$O$_7$–HCl, Tris–HCl, NaH$_2$PO$_4$–Na$_2$HPO$_4$ were tested. The best electrochemical response of clozapine was obtained in Tris–HCl buffer solution. In addition, the response kept almost unchanged with the concentration of buffer solution increasing from 0.01 to 0.4 mol L^{-1}. In general, 0.05 mol L^{-1} Tris–HCl was selected as the buffer solution.

3.4.3. Influence of accumulation time and potential

For a 5×10^{-6} mol L^{-1} clozapine solution, the anodic peak current remained almost constant with accumulation time increasing, indicating accumulation had no effect and the diffusion dominated the surface kinetic process. However, when the concentration of clozapine was much lower, the electrode process might exhibit adsorptive characteristics and suitable accumulation could contribute to the enhancement of sensitivity. Therefore, considering the need for the detection of lower concentration samples, 60 s was chosen as accumulation time. Additional, compared with at open circuit, the effect of accumulation potential was negligible due to the neutrality of clozapine in the given solution. Hence, accumulation at open circuit was selected.

3.5. Calibration curve and interference

DPV is considered sensitive and simple for detection. The major parameters were described in Section 2. Under the selected analytical conditions, the determination of clozapine with different concentrations was performed. The anodic peak current was linear to concentration from 1×10^{-6} to 5×10^{-5} mol L^{-1} and the regression equation was $I_p = 0.927 + 0.0485c$ (I_p (μA), c (μmol L^{-1}), $r = 0.996$), the detection limit was 7×10^{-9} mol L^{-1} (S/N = 3). For eight parallel determination of a 1×10^{-5} mol L^{-1} clozapine solution, the R.S.D. of peak current was calculated to be 2.5%.

The influence of foreign compounds was tested. It was found that several kinds of surfactants such as Tween-20, Triton X-100, sodium dodecyl sulfate (SDS) did not interfere, while cetylpyridinumbromide (CPB), cetyltrimethylammonium bromide (CTAB) made the peak current decrease. Additional, 100-fold antipyrine, norfloxacin, allopurinol, thiamine, hydrochlorothiazide, hydroxyzine, captopril, 50-fold sulpiride,

Fig. 9. Influence of pH on the shape of anodic peak. pH: 4.2 (A), 8.1 (B) and 10.7 (C). Other conditions as in Fig. 5.

Table 1
Measurement results of clozapine in drug tablets

Sample (2.55 μmol L^{-1}) number	Add (μmol L^{-1})	Found (μmol L^{-1})	Recovery (%)
1	2.55	5.00	96.1
2	5.10	7.80	102.9
3	7.65	10.06	98.2
4	10.20	12.61	98.6

Table 2
Measurement results of parallel determinations of drug tablets

Sample (2.55 μmol L^{-1})	n					
	1	2	3	4	5	6
UV	2.54	2.54	2.56	2.51	2.60	2.48
EC	2.49	2.57	2.55	2.60	2.63	2.63

Statistical analysis results: $F_{exp} = 1.71$, smaller than the F_{crit} value (5.05, at the 5% probability level); $t_{exp} = 1.44$, smaller than the corresponding t_{crit} value (2.23, at the 95% confidence level).

phenylephrine, propranolol, isoniazid, riboflavine, folic acid had no obvious effect on the determination. Some heavy metal ions such as Cu^{2+}, Pb^{2+}, Zn^{2+}, Fe^{3+}, Cd^{2+} also did not interfere owing to the deposition in basic solution. This suggested the MHA/Au modified electrode had certain resistance to some interference. However, uric acid and epinephrine interfered severely.

3.6. Applications

This method was applied to the detection of clozapine in drug tablets. The pretreatment and determination procedure were the same as described in Section 2. The analytical results were shown in Table 1, the recovery was 96.1–102.9%. According to Table 1, the clozapine contents could be calculated, which was 24.7 mg per tablet (its declared content was 25 mg per tablet). In order to examine the accuracy of this method, the drug sample was also measured by UV and the analytical results were shown in Table 2. By means of F-test and t-test [22], the calculated F-value (1.71) and t-value (1.44) did not exceed the theoretical values (5.05 and 2.23, respectively, 95% confidence level). It suggested that the determination method proposed was reliable.

4. Conclusions

The MHA/Au modified electrode could enhance the electrochemical response of clozapine due to the hydrophobic interaction between them. When potential was made to move, clozapine generated a sensitive anodic peak at about 0.4 V and a small cathodic peak at 0.33 V in 0.05 mol L^{-1} Tris–HCl (pH 8.1) buffer solution. Under the selected conditions, the anodic peak current was linear to clozapine concentrations over a certain range. The MHA/Au modified electrode had certain resistance to some interference. This method proposed could be successfully applied to the determination of clozapine in drug tablets and proved to be reliable.

References

[1] T. Sharma, C. Hughes, W. Soni, V. Kumari, Psychopharmacology 169 (2003) 398.
[2] W.R. Jin, Q. Xu, W. Li, Electrophoresis 21 (2000) 1415.
[3] Y.L. Shen, H.L. Wu, W.K. Ko, S.M. Wu, Anal. Chim. Acta 460 (2002) 201.
[4] C.S.P. Sastry, T.V. Rekha, A. Satyanarayana, Microchim. Acta 128 (1998) 201.
[5] M. Kollroser, C. Schober, Rapid Commun. Mass. Spectrom. 16 (2002) 1266.
[6] B. Blankert, O. Dominguez, W.El. Ayyas, J. Arcos, J.M. Kauffmann, Anal. Lett. 37 (2004) 903.
[7] L. Hermandez, E. Gonzalez, P. Hernandez, Analyst 113 (1988) 1715.
[8] S.A. Ozkan, Z. Senturk, Analysis 24 (1996) 73.
[9] T.B. Jarbawi, W.R. Heineman, Anal. Chim. Acta 186 (1986) 11.
[10] R.K. Shervedani, M.K. Babadi, Talanta 3 (2006) 741.
[11] Y.H. Wu, S.S. Hu, Bioelectrochemistry 68 (2006) 105.
[12] T. Liu, M.X. Li, Q.Y. Li, Talanta 4 (2004) 1053.
[13] S. Berchmans, S. Arivukkodi, V. Yegnaraman, Electrochem. Commun. 2 (2000) 226.
[14] M.H. Schoenfisch, J.E. Pemberton, J. Am. Chem. Soc. 120 (1998) 4502.
[15] K. Bandyopadhyay, K. Vijayamohanan, G.S. Shekhawat, R.P. Gupta, J. Electroanal. Chem. 447 (1998) 11.
[16] J.M. Kauffmann, G.J. Patriacrche, G.D. Christian, Anal. Lett. 12 (1979) 1217.
[17] Chinese Pharmacopoeia Commission, Chinese Pharmacopoeia, 1st ed., Chemical Industry Press, Beijing, 2005, 772 pp.
[18] Z. Dai, H.X. Ju, Phys. Chem. Chem. Phys. 3 (2001) 3769.
[19] E. Laviron, J. Electroanal. Chem. 101 (1979) 19.
[20] A.J. Bard, L.R. Faulkner, Electrochemical Methods: Fundamentals and Applications, 1st ed., John Wiley& Sons, New York, 1980, 200 pp.
[21] C.D. Bain, E.B. Troughton, Y.T. Tao, J. Evail, G.M. Whitesides, R.G. Nuzzo, J. Am. Chem. Soc. 111 (1989) 321.
[22] H. David, Modern Analytical Chemistry, 1st ed., McGraw-Hill Higher Education, 2000, pp. 85–95, 726–727.

Quantification of tripdiolide in human whole blood by liquid chromatography coupled with atmospheric pressure chemical ionization tandem mass spectrometry

Micong Jin [a,b], Xiaokun OuYang [a], Yiwen Yang [a], Qilong Ren [a,*]

[a] *Department of Chemical and Biochemical Engineering, Zhejiang University, Hangzhou 310027, China*
[b] *Ningbo Municipal Center for Disease Control and Prevention, Ningbo 315010, China*

Abstract

A liquid chromatographic-tandem mass spectrometric (LC–MS/MS) assay was developed and validated to determine tripdiolide in human whole blood using dexamethasone acetate as an internal standard (I.S.). Liquid–liquid extraction with ethyl acetate was used to isolate them from the biological matrix. Detection was performed on a mass spectrometer coupled with a negative atmospheric pressure chemical ionization (APCI) in the multiple-reaction monitoring (MRM) mode. The calibration curve was linear ($r^2 = 0.9973$) in the concentration range of 0.5–100.0 ng/mL in human whole blood with a lower limit of quantification of 0.5 ng/mL. Intra-day and inter-day relative standard deviations (R.S.D.s) were less than 7.0 and 10.1%, respectively. Extraction recoveries of tripdiolide ranged from 80.5 to 90.1%. This assay can be used to determine trace tripdiolide in human whole blood.

1. Introduction

Tripdiolide (Fig. 1) is one of the major diterpene bioactive compounds existed in *Tripterygium wilfordii* Hook. f. (TWHF), a traditional Chinese medicinal herb. The extract of TWHF has been widely used for various immune and inflammatory diseases and autoimmune disorders, e.g., rheumatoid arthritis, systemic lupus erythematosus and skin diseases, in China [1–3]. Tripdiolide has also been reported to be effective in the treatment of leukaemia [4,5], and to have anti-cancer [6] and anti-fertility activities [7]. Although tripdiolide had a wider therapeutic index [8] than most of the other diterpenoids, e.g., triptolide, in TWHF, the concentration in blood circulatory system during the treatment or test period is still much lower due to its severe toxicities. Therefore, a sensitive and accurate method for the quantification of tripdiolide in human whole blood samples is essential from a safety or further study points of view.

So far, only one chromatographic method has been proposed for the quantification of tripdiolide [9]. That method was devel-

oped to determine the content of tripdiolide in the ethyl acetate extract of TWHF using high-performance liquid chromatography (HPLC) with ultraviolet (UV) detection, which was not suitable for the determination of tripdiolide in the blood matrices owing to its lack of sensitivity and selectivity. With the advent of multiple-reaction monitoring (MRM) technique, tandem mass spectrometry (MS/MS) has played an important role in the analyses of drugs in biological fluids because of its excellent specificity, speed and sensitivity [10–18]. To the best of our knowledge, a LC–MS/MS method for the determination of tripdiolide in biological fluids has not been reported. The purpose of this study is to develop and validate a rapid, sensitive and specific LC–MS/MS method by a negative atmospheric pressure chemical ionization (APCI) in MRM mode using dexamethasone acetate (Fig. 1) as an internal standard (I.S.) for the determination of tripdiolide in human whole blood.

2. Experimental

2.1. LC–MS/MS system

The LC–MS/MS system for development and validation was an Agilent 1100 series LC/MSD Trap SL mass spectrometer

---

* Corresponding author. Tel.: +86 571 87952773; fax: +86 571 87952773.
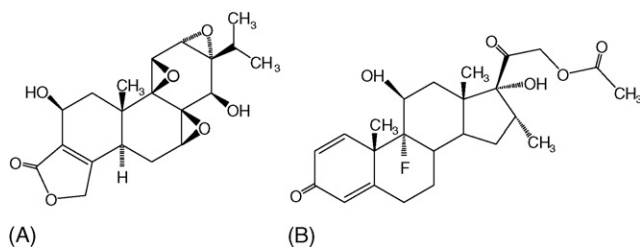*E-mail address:* Renql@zju.edu.cn (Q. Ren).

Fig. 1. Chemical structures of tripdiolide (A) and dexamethasone acetate (B).

system (Agilent Technologies, Germany), consisting of a quaternary gradient pump (G1311A), a column thermostat (G1316A), a degasser unit (G1379A), an autosampler (G1313A), a diode array detector (G1315B) and an ion trap mass spectrometer with an APCI interface. The LC–MS/MS system was controlled, and data were analyzed, on a computer equipped with LC/MSD Trap Software 4.2 (Bruker). All tubing used for connection was PEEK (polyetheretherketone) (0.25 mm ID, Agilent Technologies, Germany).

2.2. Solvents and materials

Methanol (MeOH), acetonitrile (MeCN), acetic acid and ethyl acetate (Merck, Darmstadt, Germany) were HPLC grade. Pure water was supplied by a Milli-Q water purification system from Millipore (Molsheim, France). Tripdiolide (>98%) was purified by our laboratory, which was identified by HPLC–MS and NMR, and quantified by HPLC-UV. Dexamethasone acetate (>99.5%) was purchased from the National Institute for the Control of Pharmaceutical and Biological Products (Beijing, China). Blank human whole blood was supplied by Ningbo Blood Center (Ningbo, Zhejiang, China). Samples A–E were collected from five volunteer patients who were treated in Ningbo Traditional Chinese Medical Hospital (Ningbo, Zhejiang, China) for the disease of rheumatoid arthritis, and had taken the tablets of TWHF extractions more than 2 days.

2.3. Preparation of standard stock solutions

Tripdiolide standard and I.S. were accurately weighed, transferred to volumetric flasks and dissolved in MeCN to make individual stock solutions of 1.0 mg/mL. These solutions were thoroughly mixed and stored at 4 °C in tightly closed bottles until use. Interim standard solutions of 10.0 μg/mL for tripdiolide and I.S. were diluted from the stock solutions with MeCN. Working solutions of 0.5, 1.0, 2.0, 5.0, 15.0, 50.0 and 100.0 ng/mL for tripdiolide, wherein the I.S. concentrations were 100.0 ng/mL, were diluted from the interim standard solution with MeCN, which were used for spiking human whole blood.

2.4. Preparation of spiked human whole blood samples

The standard working solutions (200 μL) were taken to a 2 mL polypropylene centrifuge tube, and evaporated to dryness under a gentle stream of nitrogen. The residues were recon- stituted with 200 μL of blank human whole blood, which was thawed to room temperature in advance, to give final trip- diolide concentrations of 0.5, 1.0, 2.0, 5.0, 15.0, 50.0 and 100.0 ng/mL, wherein the I.S. concentrations were 100.0 ng/mL. These sequences of spiked human whole blood solutions were considered as the matrix-matched calibration standards and three concentration levels of 2.0, 15.0 and 100.0 ng/mL of tripdiolide in human whole blood were considered as quality control (QC) samples.

2.5. Preparation of sample

Human whole blood sample (200 μL) that had been thawed to room temperature and 2.0 μL of the interim I.S. solution (10.0 μg/mL) were added into a 2 mL polypropylene centrifuge tube before analysis, vortex-mixed by Vortex-Genie-2 (Scientific Industries, USA) and extracted using 1.0 mL ethyl acetate for 5 min. After centrifugation for 5 min at 7800 rpm, the upper organic layer was transferred to a disposable glass tube and liquid–liquid extraction was repeated once. The organic layer was combined in the disposable glass tube and evaporated to dryness under a stream of nitrogen on a heating block at 50 °C. Prior to analysis, the residues were dissolved in 200 μL mobile phase. The tubes were immerged into a KQ 500DB ultrasonic cleaning bath (Kunshan Ultrasonic, Jiangsu, China) which were contained 5 cm depth of water, and ultrasonicated for 2 min to facilitate dissolution and centrifuged before injection.

2.6. LC–MS/MS analysis

The separation was performed on a Waters AccQ.Tag C_{18} column (150 mm × 3.9 mm ID, 5 μm particle size, Waters, Milford, MA, USA) protected by a Zorbax XDB-C_{18} guard column (12.5 mm × 4.6 mm ID, particle size 5 μm, Agilent Technologies, USA) using 0.05% acetic acid in water/MeCN/MeOH (60:30:10 v/v/v) as isocratic mobile phase at a constant flow rate of 0.60 mL/min. The column was held at a constant temperature of 35 °C and the injection volume was 20.0 μL. Detection was carried out on an Agilent 1100 series LC/MSD Trap SL mass spectrometer in the negative mode with a cycle time of 1 s, a corona current of 4.0 μA, a capillary voltage of 3.5 kV, a capillary exit voltage of −135 V, a dry temperature of 325 °C, a vaporizer temperature of 425 °C, a high purity (99.999%) dry nitrogen gas of 5.0 L/min, a nitrogen nebulizer pressure of 60.0 psi and a dwell time of 200 ms. The APCI interface and mass spectrometer parameters were optimized by direct infusion of the target compounds (1.0 mg/L) at 0.5 mL/h to obtain maximum sensitivity. To determine the product ions of tripdiolide and I.S., both the deprotonated precursor ion $[M - H]^-$ at m/z 375 for tripdiolide and fragment ion 341 $[M-F-C_3H_6O_2]^-$ for I.S. were isolated, helium gas was introduced into the trap to induce collision with analyte precursor ions. Throughout all the measurements tripdiolide and I.S. were detected by MRM of m/z 375 → 357 for tripdiolide, 341 → 179 for I.S., respectively. Table 1 outlines the MRM parameters for tripdiolide and I.S.

Table 1
The MRM parameters for tripdiolide and I.S.

Item	Tripdiolide	I.S.
Precursor ion (m/z)	375	341
Product ion for detection and quantification (m/z)	357	179
Additional ions for confirmation (m/z)	313, 229	161
Width (m/z)	2.0	2.0
Cutoff mass	98	93
Collision induced dissociation (CID) (V)	1.65	1.40
Retention time (min)	2.61	1.89

3. Results and discussion

3.1. Chromatographic separation

In order to speed up the analysis without compromising the reliability of this method, we adopted the mobile phase wherein the analytes have small capacity factors. Meanwhile, a high selective MS/MS strategy was employed to ensure the specificity of detection. Recently, Shao [19] reported that triptolide, a homolog of tripdiolide, was separated by a mobile phase composed of acetonitrile/methanol/0.05% triethylamine aqueous solution (30:50:20 v/v/v) at a flow rate of 0.75 mL/min on Zorbax Extend-C18 analytical column (150 mm × 4.6 mm ID, particle size 5 μm, Agilent Technologies, USA) with APCI-MS detection in the negative mode, and obtained a well separation and a good quantitative result. However, this method was not preferentially recommended in many laboratories owing to the use of triethylamine that could contaminate the PEEK tubes when used for a long time and result in a persistent and strong molecular ion peak m/z $[M+H]^+$ 102 in the positive ESI mode, which not only increased the base line noise but also seriously interfered with the detection of the ion near m/z 102. Initially, we found that tripdiolide and I.S. were completely separated by water/MeCN (60:40 v/v) on Waters AccQ.Tag C$_{18}$ column (150 mm × 3.9 mm ID, 5 μm particle size, Waters, Milford, MA,

USA). However, for a longer run time, a bad precision and a lower intensity of mass signal existed under APCI conditions when monitoring the signal by MRM for the transition of m/z $375 \rightarrow 357$ for tripdiolide, m/z $341 \rightarrow 179$ for I.S., respectively. Fortunately, when we added 10% (v/v) MeOH in the mobile phase, the intensity of the signal of tripdiolide or I.S. increased about 100%, the run time decreased to 5 min, a well separation for tripdiolide and I.S. was obtained, and moreover, the relative standard deviations (R.S.D.s) of the MRM peak areas for both analyte and I.S. were significantly reduced and the peaks become more symmetrical. These phenomena could be considered that tripdiolide was more easily deprotonated in water/MeCN/MeOH (60:30:10 v/v/v) than in water/MeCN (60:40 v/v). The low concentration of acetic acid (0.05%) could improve the stability of the transition of m/z $375 \rightarrow 357$ for tripdiolide, and m/z $341 \rightarrow 179$ for I.S.

3.2. MS/MS detection

Under APCI conditions, sensitivity of tripdiolide and I.S. was favorable in negative-ion detection mode. Fig. 2(A) and (B) shows the full-scan MS negative ion spectra of I.S. and tripdiolide, respectively. Thus, formed fragment precursor ion at m/z 341 as the base peak for I.S. and deprotonated precursor ion $[M-H]^-$ at m/z 375 as major ion peak for tripdiolide. Fig. 2(C) and (D) shows the MS/MS spectra from ion trap CID of the precursor ion at m/z 341 for I.S. and m/z 375 for tripdiolide. Tripdiolide produced a deprotonated precursor ion ($[M-H]^-$) at m/z 375 with a major product ion at m/z 357 (loss of H$_2$O from $[M-H]^-$), and I.S. produced a fragment precursor ion at m/z 341 $[M–F–C_3H_6O_2]^-$ with a major product ion at m/z 179 $[C_{12}H_{19}O]^-$. The pseudomolecular $[M-H]^-$ of the I.S. is not stable in both acidic solution and water/MeCN/MeOH (60:30:10 v/v/v), therefore the relative abundance of the $[M-H]^-$ peak is too small to be observed in Fig. 2A. The precursor ions and major product ions of tripdiolide
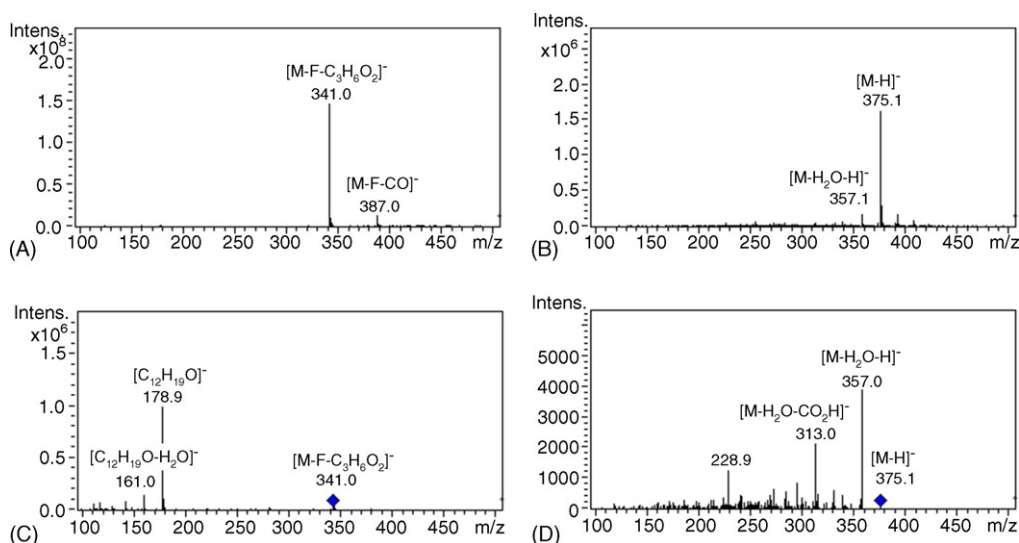

Fig. 2. Mass spectra by negative APCI mode for I.S (A) and tripdiolide (B), and MS/MS spectra from ion trap CID of the ion at m/z 341 for I.S (C) and m/z 375 for tripdiolide (D). The diamond in this figure marked the precursor ion.
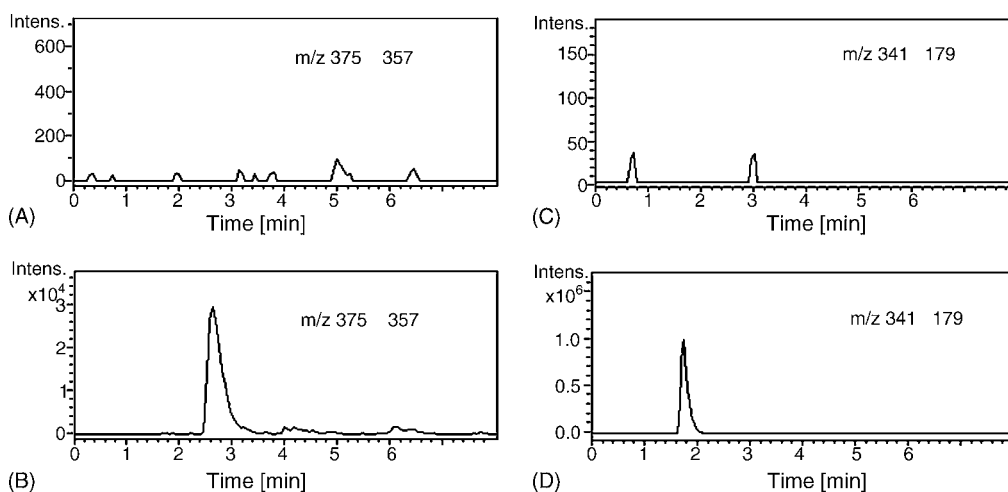
Fig. 3. Typical MRM chromatograms of tripdiolide and I.S.: (A) blank human whole blood of a transition of *m/z* 375 → 357 for tripdiolide; (B) blank human whole blood spiked with 10.0 ng/mL tripdiolide of a transition of *m/z* 375 → 357; (C) blank human whole blood of a transition of *m/z* 341 → 179 for I.S.; (D) blank human whole blood spiked with 100.0 ng/mL I.S. of a transition of *m/z* 341 → 179.

and I.S. were monitored in the multiple-reaction mode. Fig. 3 shows the representative chromatograms of the blank human whole blood and blank human whole blood spiked with tripdiolide (10.0 ng/mL) and I.S. (100.0 ng/mL). It can be seen that the mean retention times for tripdiolide and I.S. under the optimal conditions were 2.61 and 1.89 min, respectively, with an overall chromatographic run time of 5 min. The selectivity for the analysis is shown by symmetrical resolution of the peaks, with no significant chromatographic interference around the retention times of the tripdiolide and I.S. in blank specimens.

3.3. Specificity, selectivity and internal standard

To examine the effect of the human whole blood on ionization efficiency, we compared the peak areas of tripdiolide and I.S. in QC samples of three concentration levels with those in standard solutions that had been prepared in the same way as the QC samples except that water replaced the blank human whole blood. For tripdiolide the mean peak areas from the three QC samples had relative errors of −3.5%, when compared with that for these standard solutions. For the I.S., the relative error was −4.3%. These indicated that there were little endogenous substances to significantly influence the ionization of tripdiolide and I.S.

In order to ensure the accuracy of the analytical method, an internal standard having similar ionization efficiency and similar polarity to the analyte is needed. Triptolide, a homolog of tripdiolide, was firstly evaluated as the internal standard. However, it was not suitable for the intended purpose, since triptolide is one of the metabolite of tripdiolide in vivo. Dexamethasone acetate (Fig. 1), which has similar polarity to tripdiolide, was chosen as an internal standard. However, dexamethasone acetate is a hormone of synthetical compound, some similar structures maybe exist in vivo which maybe interfere the analysis. Six different sources of human whole blood specimens were investigated for interferences from endogenous compounds. Fig. 3 shows the typical MRM chromatogram of blank and spiked human whole blood for tripdiolide and I.S. It indicated that no

matrix effects or interferences from endogenous substances were detected.

3.4. Method validation

Calibration curve for tripdiolide was obtained by a series of spiked human whole blood at the concentrations of 0.5, 1.0, 2.0, 5.0, 15.0, 50.0 and 100.0 ng/mL, respectively, wherein the I.S. concentrations were 100.0 ng/mL. Three replicates of standards at each concentration were performed. Calibration curve was constructed by using the ratio of area (*Y*, tripdiolide peak area to I.S. peak area) to the concentration (*C*, ng/mL) in human whole blood. The typical equation of the calibration curve was $C = 346.15Y - 0.38120$. It was linear in the tested concentration range of 0.5–100.0 ng/mL with coefficient of determination $r^2 = 0.9973$ and consistent slope (3.3%) and intercept values (2.9%).

The limit of quantification for tripdiolide was determined using a blank human whole blood sample spiked at low of 2.0 ng/mL standard solutions, extraction with ethyl acetate, detection in MRM mode for 10 replicates and evaluation by the criterion that the signal to noise ratio (S/N) should be >10, for quantification purposes. The limit of quantification was 0.5 ng/mL for tripdiolide in the whole human blood.

The intra-day precision was evaluated by performing five replicates of three spiked QC samples (2.0, 15.0 and 100.0 ng/mL) including extraction procedures. The inter-day precision was evaluated by performing five replicates of the three spiked QC samples on each of five different days within a 7-day period. The intra-day precision (R.S.D.) on the basis of peak area was less than 7.0% and the inter-day precision (R.S.D.) on the basis of peak area was less than 10.1%, as shown in Table 2.

The extraction recoveries of tripdiolide were determined by comparing the peak area of tripdiolide at three QC levels in the human whole blood samples that had been spiked with tripdiolide at three different concentrations (2.0, 15.0 and 100.0 ng/mL) before and after extraction. The intra- and inter-

Table 2
The recovery and precision of the method for spiked blank whole blood samples

Compound	Added (ng/mL)	Intra-day			Inter-day		
		Found (ng/mL)[a]	Recovery (%)	R.S.D. (%)	Found (ng/mL)[b]	Recovery (%)	R.S.D. (%)
	2.0	1.68 ± 0.10	84.0	6.0	1.61 ± 0.14	80.5	8.7
Tripdiolide	15.0	13.01 ± 0.91	86.7	7.0	13.52 ± 1.36	90.1	10.1
	100.0	82.13 ± 3.89	82.1	4.7	86.22 ± 7.16	86.2	8.3

[a] Determined in 1 day, $n = 5$, expressed as mean ± S.D.
[b] $n = 5$ replicates × 5 days within a 7-day period, expressed as mean ± S.D.

Table 3
Assessment of stability in spiked blank whole blood for tripdiolide ($n = 3$)

Condition	Concentration change[a]		
	2.0 ng/mL	15.0 ng/mL	100.0 ng/mL
Freeze–thaw stability (−20 °C)			
Cycle 1	97.1	95.7	96.1
Cycle 2	97.3	92.9	93.9
Cycle 3	96.8	93.4	92.5
Short-term stability (room temperature 25 °C)			
Time = 0.5 h	98.2	99.1	96.3
Time = 2.0 h	97.2	96.7	97.5
Time = 12.0 h	98.7	97.5	97.8
Time = 48.0 h	96.2	92.4	94.7

[a] Expressed as the mean concentration change percentage from time zero.

day recoveries were 82.1–86.7% and 80.5–90.1%, respectively, as shown in Table 2.

3.5. Stability

The stability of tripdiolide was assessed using the QC samples of three different concentrations (2.0, 15.0 and 100.0 ng/mL) at two circumstances, ambient stability and freeze/thaw stability. The ambient stability was assessed by leaving the QC samples at room temperature (25 °C) in autosampler vials for up to 48 h. The freeze/thaw stability was assessed over three cycles thawed at room temperature and refrozen at −20 °C. Three replicates were performed at every condition. Table 3 shows the assessment of stability in the human whole blood under several conditions. It can be seen that tripdiolide in human whole blood was stable for up to 48 h at 25 °C with the maximal loss of 7.6% and that it was also stable over at least three freeze/thaw cycles with no significant loss (<7.5%).

3.6. Application to the real samples

Samples A–E were analyzed by above established method of LC-APCI/MS/MS. The results indicated that the concentrations of tripdiolide in human whole blood were 1.7–25.9 ng/mL, and there were little interferences for the determination of tripdiolide in the real whole blood samples. The significant difference of the tripdiolide concentration in blood from the five patients comes out of taking various dosages of TWHF tablets owing to their different states of illness. The male patient who took the maximal

dosage has the highest concentration of 25.9 ng/mL in the whole blood, and the female patient who took the minimal dosage has the lowest concentration of 1.7 ng/mL in the whole blood.

4. Conclusions

In this paper, a highly sensitive and selective method for the quantification of tripdiolide in human whole blood was developed and validated by high-performance liquid chromatographic separation with tandem mass spectrometric detection. The new assay required only small sample amount and simple extraction without additional clean-up procedures. The described method offers high sensitivity with a lower limit of quantification of 0.5 ng/mL, wide linearity, and specificity without interferences from endogenous substances, therefore it could be applied in clinical and toxicological investigations.

References

[1] C.P. Zhang, X.Y. Lu, P.C. Ma, Y. Chen, Y.G. Zhang, Z. Yan, G.F. Chen, Q.T. Zheng, C.H. He, D.Q. Yu, Acta Pharm. Sin. 28 (1993) 110.
[2] X. Tao, P.E. Lipsky, Rheum. Dis. Clin. North Am. 26 (2000) 29.
[3] X. Tao, J. Younger, F.Z. Fan, B. Wang, P.E. Lipsky, Arthritis Rheum. 46 (2002) 1735.
[4] Y.J. Lou, J. Jin, Leuk. Lymphoma 45 (2004) 373.
[5] S.M. Kupchan, W.A. Court, R.G. Dailey Jr., C.J. Gilmore, R.F. Bryan, J. Am. Chem. Soc. 94 (1972) 7194.
[6] T. Panichakul, T. Wanun, V. Reutrakul, S. Sirisinha, Asian Pac. J. Allergy Immunol. 20 (2002) 167.
[7] S.A. Matlin, A. Belenguer, V.E. Stacey, S.E. Qian, Y. Xu, J.W. Zhang, J.K.M. Sanders, S.R. Amor, C.M. Pearce, Contraception 47 (1993) 387.
[8] P.E. Lipsky, X. Tao, J. Cai, W.J. Kovacs, J. Oisen, USA Patent 5,616,458 (1997).
[9] J.J. Cai, X. Tao, P.E. Lipsky, J. Liq. Chromatogr. 17 (1994) 4479.
[10] J.F. Van Bocxlaer, K.M. Clauwaert, W.E. Lambert, D.L. Deforce, E.G. Van den Eeckhout, A.P. de-Leenheer, Mass Spectrom. Rev. 19 (2000) 165.
[11] P. Marquet, Ther. Drug Monit. 24 (2002) 255.
[12] H.H. Maurer, Anal. Bioanal. Chem. 381 (2005) 110.
[13] K.H. Yoon, S.Y. Lee, M. Jang, S.H. Ko, W. Kim, J.S. Park, I. Park, H.J. Kim, Talanta 66 (2005) 831.
[14] B. Delmulle, S. De Saeger, A. Adams, N. De Kimpe, C. Van Peteghem, Rapid Commun. Mass Spectrom. 20 (2006) 771.
[15] S.A. Chan, S.W. Lin, K.J. Yu, T.Y. Liu, M.R. Fuh, Talanta 69 (2006) 952.
[16] B.K. Matuszewski, M.L. Constanzer, C.M. Chavez-Eng, Anal. Chem. 70 (1998) 882.
[17] M.C. Jin, X.H. Chen, Rapid Commun. Mass Spectrom. 20 (2006) 2741.
[18] M. Gros, M. Petrović, D. Barceló, Talanta 70 (2006) 678.
[19] F. Shao, G.J. Wang, J.G. Sun, H.T. Xie, H. Li, Y. Liang, R. Zhang, X.Y. Zhu, J. Pharma. Bio. Anal. 41 (2006) 341.

Characterization of aniseed-flavoured spirit drinks by headspace solid-phase microextraction gas chromatography–mass spectrometry and chemometrics

J.M. Jurado [a], O. Ballesteros [b], A. Alcázar [a], F. Pablos [a,*],
M.J. Martín [a], J.L. Vílchez [b], A. Navalón [b]

[a] *Department of Analytical Chemistry, Faculty of Chemistry, University of Sevilla, C/Profesor García González, 1, E-41012 Sevilla, Spain*
[b] *Research Group of Analytical Chemistry and Life Sciences, Department of Analytical Chemistry,*
University of Granada, Avda. Fuentenueva, s/n, E-18071 Granada, Spain

Abstract

The volatile composition of aniseed-flavoured spirit drinks was studied by headspace solid-phase microextraction (HS-SPME) coupled with gas chromatography–mass spectrometry (GC–MS). The influence of the time, temperature, volume of sample and ionic strength on the extraction were considered. Several aniseed-flavoured spirit drinks, such as pastis, sambuca, anis and raki were analyzed. The major compounds found were *trans*-anethole (41.22–98%), *cis*-anethole (0.77–18.65%) and estragole (0.1–17.96%). γ-Himachalene (0–28.07%) and α-himachalene (0–4.8%) were also present in anis and raki beverages. The compounds determined were used as chemical descriptors to differentiate the four types of beverages considered. Principal component analysis (PCA), linear discriminant analysis (LDA) and artificial neural networks (ANN) were used as chemometric tools for characterization purposes.
© 2006 Elsevier B.V. All rights reserved.

Keywords: Beverages analysis; Aniseed-flavoured spirit drinks; Solid-phase microextraction; Gas chromatography–mass spectrometry; Chemometrics; Principal component analysis; Linear discriminant analysis; Artificial neural networks

1. Introduction

Aniseed-flavoured spirit drinks are produced by flavouring and distilling ethyl alcohol of agricultural origin with natural extracts of star anise (*Illicium verum*), anise (*Pimpinella anisum*), fennel (*Foeniculum vulgare*), or any other plant which contains the same principal aromatic constituent [1]. The main flavouring constituent is anethole, but other components like estragole, α- and γ-himachalene and terpene hydrocarbons [2–5] are also present. Aniseed-flavoured spirit drinks are produced in several countries like France, Greece, Italy, Spain and Turkey, with different names such as pastis, ouzo, sambuca, anis and raki, respectively.

The analysis of the volatile compounds in alcoholic beverages is usually carried out by gas chromatography (GC) though requires enrichment as a basis for identification and quantification. Thus, liquid–liquid extraction, static and dynamic headspace (HS) and solid-phase extraction have been commonly used for the analysis of spirits [6–11]. Solid-phase microextraction (SPME) is an alternative to these techniques that is easy to use, provides high sensitivity, good reproducibility and low cost. This technique eliminates use of organic solvents and substantially shortens the time of analysis. [12,13]. It has been successfully applied in studies for the characterization of wines and spirits [8,14–21].

The characterization of samples, using their chemical composition as input data, is of great interest for the identification of the geographical origin and authenticity of food products. Assessment of food samples origin has been mostly conducted through multivariate analysis in combination with pattern recognition techniques [22–24]. Multivariate analysis methods for data visualization, dimensionality reduction and sample classification include principal component analysis (PCA) and linear discriminant analysis (LDA), respectively. Artificial neural net-

* Corresponding author. Tel.: +34 95 4557173; fax: +34 95 4557168.
E-mail address: fpablos@us.es (F. Pablos).

works (ANN) are also powerful tools, especially when other statistical techniques are not able to predict complicated phenomena [25].

In this work, a HS-SPME/GC–MS method is used to determine the volatile components of aniseed-flavoured spirit drinks. These components have been used as input variables to apply pattern recognition techniques to differentiate several types of these beverages.

2. Experimental

2.1. Reagents and materials

All reagents were analytical grade unless specified otherwise. Water was purified with a Milli-Q plus system (Millipore, Bedford, USA).

Ethanol and sodium chloride were supplied from Panreac (Barcelona, Spain). Menthol (Merck, Darmstadt, Germany) was used as internal standard. A standard solution of $1000 \, \text{mg} \, \text{L}^{-1}$ was prepared in ethanol.

A manual fiber holder for SPME was purchased form Supelco (Bellefonte, PA, USA). Four types of fibers were used: 100 μm polydimethylsiloxane (PDMS), 65 μm polydimethylsiloxane–divinylbenzene (PDMS/DVB), 75 μm carboxen–polydimethylsiloxane (CAR/PDMS) and 50 μm divinylbenzene–carboxen–polydimethylsiloxane (DVB/CAR/PDMS). These fibers were obtained from the same manufacturer and were conditioned under their specifications before use.

Samples ($N = 76$) were obtained from local stores, belonging to four different types of aniseed-flavoured spirit drinks: anis ($N = 46$), pastis ($N = 12$), sambuca ($N = 6$) and raki ($N = 12$). All samples were contained in glass bottles and stored at 4 °C until analysis.

2.2. HS-SPME procedure

The influence of the variables, extraction temperature and time, volume of sample and salt concentration, was studied using a central composite experimental design. The extraction temperature was varied from 25 to 45 °C, the extraction time between 10 and 50 min, the amount of NaCl from 0 to 0.5 g and the volume of sample percentage from 10% to 90%, for a total volume of 10 mL. Each variable had five levels and the experiments were divided in three blocks. A central point at 35 °C, 30 min, 60% of sample volume and, 0.3 g of NaCl was done by duplicate in each of the three blocks considered. The HS-SPME conditions were established according to the results obtained in this study. Then, each sample was prepared taking a volume of 6 mL of aniseed drink, 0.18 g of NaCl and 1 mL of menthol solution into a 10-mL standard flask, adding water till the mark. The content of the standard flask was transferred to a 20-mL vial containing a magnetic stirring bar. The vial was hermetically sealed with PTFE faced silicone septum and placed in a thermostated block at 34 °C on a magnetic stirrer (Agimatic-N, Selecta, Spain). The CAR/PDMS fiber was exposed to the headspace of the sample for 35 min. During this time, the sample was stirred at a constant speed of 300 rpm. After sampling, the fiber was removed

from the sample vial and inserted into the injection port of the GC, where thermal desorption of the analytes was carried out at 270 °C during 2 min. Quantitative analysis was performed by using the internal normalization method.

2.3. Apparatus

Chromatographic analysis was performed using an Agilent 6890 gas chromatograph interfaced to an Agilent 5973 *Network* mass spectrometer (Agilent Technologies, Little Falls, DE, USA). A capillary column ZB-5 (30 m × 0.25 mm i.d.; 0.25 μm film thickness) from Phenomenex (Jasco, Madrid, Spain) was used. Oven temperature program started at 40 °C, heated at 5 °C/min up to 150 °C and held for 5 min. Helium (purity 99.999%) was used as carrier gas at a flow rate of $1 \, \text{mL} \, \text{min}^{-1}$. A split ratio 10:1 was fitted. The injection was made in splitless mode for 2 min using a 0.75 mm liner at a temperature of 270 °C, a SPME inlet guide and pre-drilled Thermogreen LB-2 septa from Supelco (Bellefonte, PA, USA).

Transfer line temperature was 270 °C. All mass spectra were acquired in electron impact mode (EI) at 70 eV using full scan with a scan range of 50–400 amu at a rate of 2.5 scans/s. Data acquisition and integration were carried out with the ChemStation chromatography software. The identification of the peaks was achieved through mass spectrometry by comparing mass spectra of the unknown peaks with those stored in the Wiley GC–MS library.

2.4. Multivariate analysis

The ratio of the analyte area/internal standard area of the compounds was used as input data. A data matrix whose rows are the cases and columns the variables was prepared and used in the chemometric calculations. Statistica 7.0 software package (StatSoft Inc., 2004) was used for the statistical data analysis.

3. Results and discussion

3.1. Optimization of HS-SPME conditions

To develop a suitable HS-SPME method optimization of several variables such as SPME fiber selection, extraction time and temperature, volume of sample and salt concentration is required. SPME is a process which depends on the equilibrium process involving partitioning of the analytes from the sample into the stationary phase. The type of coating was the first variable considered. Four different coatings were compared, 100 μm PDMS, 65 μm PDMS/DVB, 75 μm CAR/PDMS and 50 μm DVB/CAR/PDMS. All extractions were carried out using an extraction time of 30 min at 30 °C. Higher recoveries and abundances for most of the target compounds were obtained with the fiber CAR/PDMS. The fiber maintained its performance for >100 extractions with between-day precision below 10%.

To optimize extraction time and temperature, volume of sample and salt concentration a central composite experimental design was carried out. Values and intervals of the considered variables were included in Section 2.2. Response obtained for

trans- and *cis*-anethole, estragole, α- and γ-himachalene was considered. Taking into account the ANOVA results obtained from the experimental design, the influence of the variables on the response for *trans*-, *cis*-anethole and estragole was not significant. In the case of α- and γ-himachalene a significant influence of the variables was observed and maximum responses were obtained at 35 min, 34 °C, 60% of volume of sample and 0.18 g of NaCl. Consequently, these were the selected extraction conditions.

3.2. Analysis of volatile composition of aniseed-flavoured spirit drinks

Quantitation of the compounds present in the volatile fraction of the aniseed drinks was performed on the basis of their peak areas. All samples were analyzed three times. The ranges of percentages of the compounds in each type of aniseed drink are included in Table 1. Chromatograms of samples of pastis, sambuca, raki and anis are depicted in Fig. 1. More than 40 compounds were detected including propenyphenols, monoterpenes, sesquiterpenes and hydrocarbons. Propenylphenols like *trans*-anethole (41.22–98%), *cis*-anethole (0.77–18.65%) and estragole (0.10–17.96%) were the main components. Monoterpenes and sesquiterpenes like α- and β-pinene, limonene, β-bisabolene, zingiberene, α-, β- and γ-himachalene were also

detected. α- and β-himachalene were present in anis and raki samples and traces of γ-himachalene and *p*-anisaldehyde were detected in pastis.

Taking into account these results, differences in the composition of the volatile fraction of the aniseed-flavoured spirit drinks types can be assumed, and the detected compounds were used chemical descriptors to characterize the samples.

3.3. Characterisation of aniseed-flavoured spirit drinks

PCA-based display methods allow a detailed study of the data trends. The three first PCs were calculated explaining up to 72.6% of the total variance. PC1 explains 39.2%, PC2 accounts for 24.8% and PC3 for 8.6%. Fig. 2 shows the scores plot of the samples in the three-dimensional space constructed with the three first PC. As can be seen, pastis, anis and raki samples appear almost grouped, and no clear separation can be observed. Otherwise, sambuca samples are grouped at the negative scores of PC1. Considering the factor loadings of the variables the most contributing ones were decane, limonene, α-terpinene, *p*-vinylanisole, dodecane, anisylacetone, (*E*)-5-tetradecene, *n*-tetradecane, (*EXO*)-α-bergamotene, β-caryophyllene, (*ENDO*)-α-bergamotene, α-humulene, ledene, bicyclogermacrene, δ-cadinene, *Z*-3-hexadecene, *Z*-7-hexadecene, hexadecane, *trans*-anethole, δ-elemene, α-longipinene, α-ylangene, β-elemene,

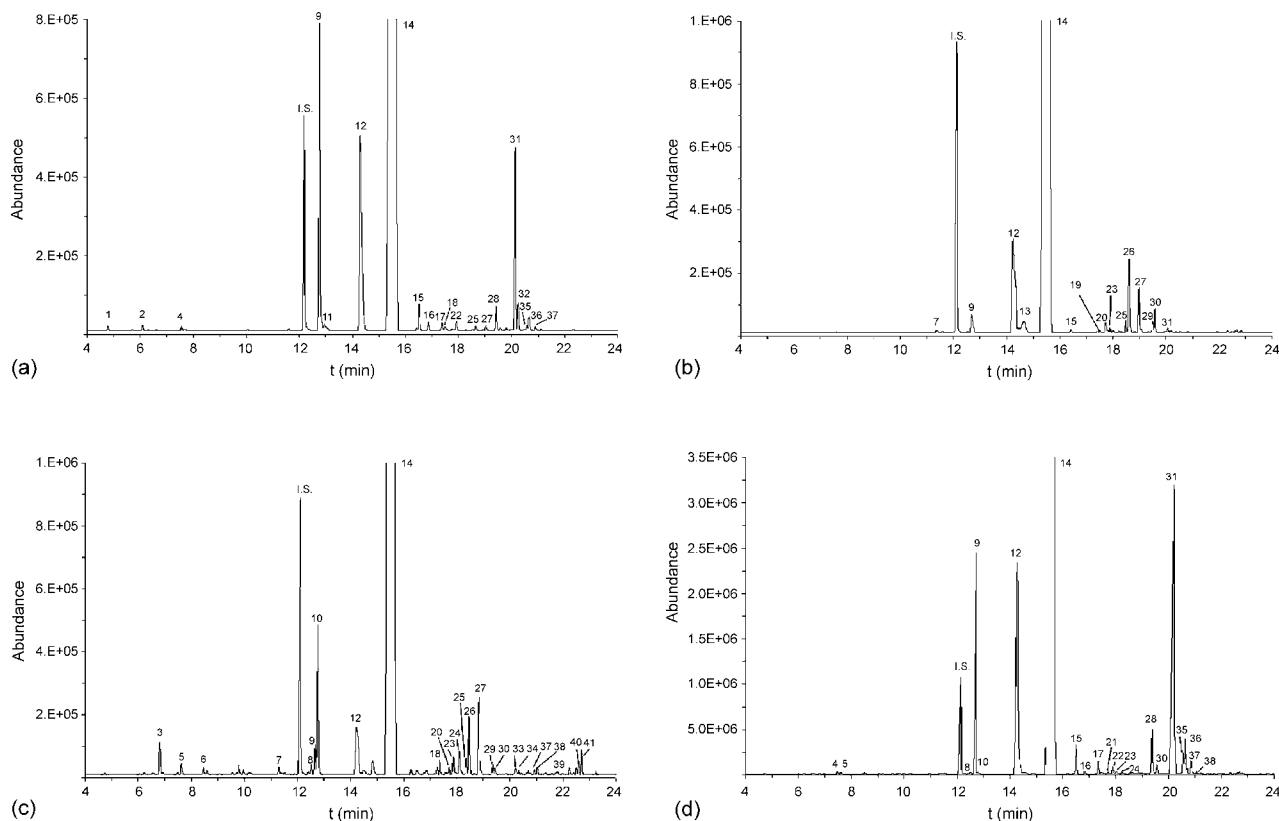

Fig. 1. Chromatograms corresponding to (a) anis, (b) pastis, (c) sambuca and (d) raki samples. See chromatographic conditions in Section 2.2. (1) α-Pinene; (2) β-pinene; (3) *n*-decane; (4) *p*-cymene; (5) limonene; (6) α-terpinene; (7) *p*-vinylanisole; (8) (*Z*)-2-dodecene; (9) estragole; (10) dodecane; (11) *p*-*n*-propilanisole; (12) *cis*-anethole; (13) *p*-anisaldehyde; (14) *trans*-anethole; (15) δ-elemene; (16) α-longipinene; (17) α-ylangene; (18) α-copaene; (19) α-cubebene; (20) anisylacetone; (21) β-bourbonene; (22) β-elemene; (23) (*E*)-5-tetradecene; (24) tetradecane; (25) (*EXO*)-α-bergamotene; (26) β-caryophyllene; (27) (*ENDO*)-α-bergamotene; (28) α-himachalene; (29) α-humulene; (30) *trans*-β-farnesene; (31) γ-himachalene; (32) *Ar*-curcumene; (33) ledene; (34) bicyclogermacrene; (35) zingiberene; (36) β-himachalene; (37) β-bisabolene; (38) δ-cadinene; (39) (*Z*)-3-hexadecene; (40) (*Z*)-7-hexadecene; (41) hexadecane.

Table 1
Composition (%) of volatile fraction of aniseed-flavoured spirit drinks

Peak number[a]	Compound	Retention index[b]	Samples			
			Anis	Pastis	Sambuca	Raki
1	α-Pinene	769	0.00–0.26	–	–	–
2	β-Pinene	888	0.00–0.15	–	–	–
3	*n*-Decane	1000	–	–	0.94–1.44	–
4	*p*-Cymene	1033	t	–	–	t
5	Limonene	1040	0.00–0.39	–	0.30–0.66	t
6	α-Terpinene	1074	–	–	0.22–0.38	–
7	*p*-Vinylanisole	1160	–	0.00–0.27	0.18–0.23	–
8	(Z)-2-Dodecene	1194	–	0.00–0.36	0.36–0.51	0.00–0.48
9	Estragole	1198	0.27–17.96	0.10–1.37	1.54–2.01	0.97–8.34
10	Dodecane	1200	–	–	3.96–6.86	t
11	*p-n*-Propilanisole	1209	0.00–0.82	–	–	–
12	*cis*-Anethole	1312	1.68–18.65	0.77–10.36	6.57–10.12	7.50–11.39
13	*p*-Anisaldehyde	1322	–	0.28–8.86	–	–
14	*trans*-Anethole	1343	41.22–98.00	79.22–97.52	66.16–73.02	56.78–89.95
15	δ-Elemene	1363	0.00–2.65	0.00–0.16	–	0.00–0.84
16	α-Longipinene	1371	0.00–1.08	–	–	t
17	α-Ylangene	1382	0.00–1.41	–	–	0.00–0.44
18	α-Copaene	1386	0.00–0.54	–	0.50–0.68	–
19	α-Cubebene	1387	–	0.00–0.11	–	–
20	Anisylacetone	1390	–	0.08–0.41	0.17–0.56	–
21	β-Bourbonene	1390	–	–	–	0.00–0.11
22	β-Elemene	1393	0.00–1.16	0.00–0.18	0.00–0.13	0.00–0.26
23	(E)-5-Tetradecene	1396	–	0.00–0.66	0.50–0.98	0.00–0.85
24	Tetradecane	1400	–	t	0.46–1.29	0.06–0.30
25	(EXO)-α-Bergamotene	1413	t	0.00–0.54	0.56–0.73	–
26	β-Caryophyllene	1418	t	0.00–2.97	2.08–2.77	–
27	(ENDO)-α-Bergamotene	1435	0.00–1.17	0.00–2.09	2.83–3.81	–
28	β-Himachalene	1450	0.00–4.80	–	–	0.00–1.88
29	β-Humulene	1456	–	0.00–0.37	0.38–0.50	–
30	*trans*-β-Farnesene	1460	0.00–1.68	0.00–0.30	0.23–0.31	0.00–0.34
31	γ-Himachalene	1482	0.00–28.07	t	–	0.00–18.25
32	*Ar*-Curcumene	1486	0.00–2.02	–	–	–
33	Ledene	1493	–	–	0.26–0.32	–
34	Bicyclogermacrene	1498	–	–	0.11–0.15	–
35	Zingiberene	1501	0.00–11.09	–	–	0.00–0.63
36	β-Himachalene	1504	0.00–2.52	–	–	0.00–1.32
37	β-Bisabolene	1515	0.00–2.46	–	0.19–0.24	0.00–0.49
38	δ-Cadinene	1525	t	–	0.27–0.34	t
39	(Z)-3-Hexadecene	1563	–	t	0.12–0.26	0.00–0.24
40	(Z)-7-Hexadecene	1595	–	0.00–0.36	0.26–0.41	0.00–0.59
41	Hexadecane	1600	–	–	0.44–0.87	–

t, traces (<0.06%).

[a] See chromatograms of Fig. 1. For experimental conditions see Section 2.

[b] Relative to C_7–C_{16} *n*-alkanes determined using ZB-5 capillary column.

α-himachalene, *trans*-β-farnesene, γ-himachalene, zingiberene, β-himachalene, β-bisabolene, α-cubebene, α-pinene, β-pinene, β-bourbonene.

Considering that highly correlated variables provide similar information a Pearson correlation study was carried out to find out variables that were strongly correlated. From this study, the variables limonene, anisylacetone, (E)-5-tetradecene, *n*-tetradecane, (ENDO)-α-bergamotene, δ-cadinene, *trans*-anethole, *trans*-β-farnesene, γ-himachalene, β-pinene, α-cubebene and β-bourbonene were considered as the most significant ones.

In order to obtain suitable classification rules forward LDA was carried out by using the above mentioned variables. Three discriminant functions (DF) were obtained. Fig. 3 shows the distribution of the samples in the plane generated by the two first DF. As can be seen, a good separation of sambuca class was achieved. For pastis, raki and anis classes some tendencies can be seen, though there is not a clear separation. The recognition ability, according to the *a posteriori* probabilities was of 100% for sambuca and anis, 83.3% for pastis and 91.7% for raki. The leave one out method [26] was used as cross-validation procedure to evaluate the classification performance. The prediction ability of the constructed model was 100% for sambuca and anis, 91.7% for raki and 83.3% for pastis. According to LDA results the most discriminant variables were δ-cadinene, anisylacetone, β-bourbonene, *E*-5-tetradedecene, α-cubebene, *n*-tetradecane,
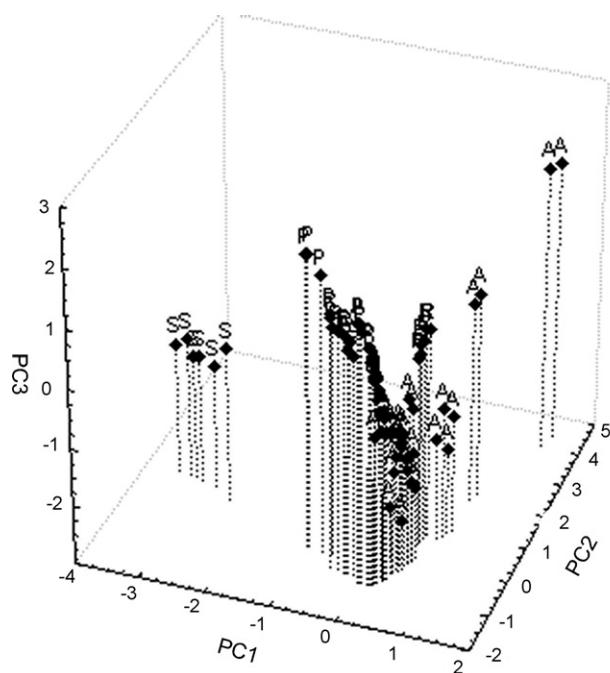
Fig. 2. Scores plot of the aniseed-flavoured spirit drinks in the three-dimensional space of the firsts PCs: (P) pastis; (S) sambuca; (R) raki; (A) anis.

limonene, (*ENDO*)-α-bergamotene, γ-himachalene and *trans*-anethole.

Considering that the linear model did not provide a complete solution to the classification problem, non-linear approach such as ANN was used. Using the most discriminant variables extracted from LDA as inputs and the class of each case as output, a multilayer perceptron ANN (MLP) [27] was used to solve the classification problem. The data set was divided in three subsets, training ($N = 38$), verification ($N = 19$) and test ($N = 19$) sets, respectively. A three layer MLP was applied. The architecture was 10 neurons in the input layer, 13 in the hidden and four in the output one. The network was trained by back propagation during 1000 epochs with a learning rate and momentum of 0.16 and 0.52, respectively. The classification procedure was validated by
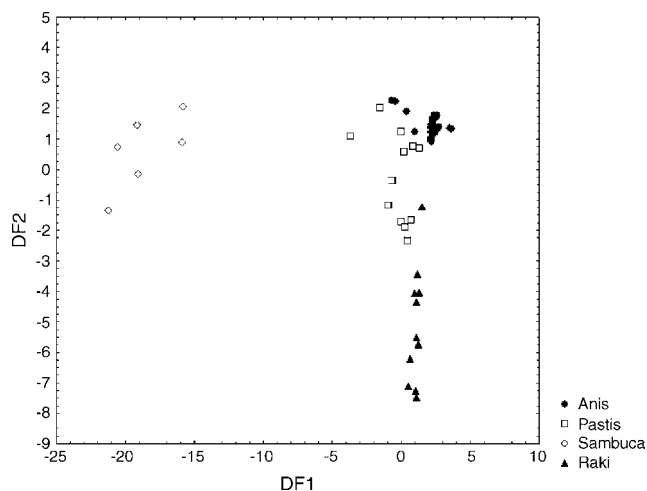

Fig. 3. Scatter plot of the aniseed-flavoured spirit drinks in the plane of the two first discriminant functions.

applying the sensitivity and specificity parameters [28,29] to the test set. Both parameters were 100% indicating that MLP models the class distribution better than LDA. The possible cause of this behaviour can be the intrinsically non-linear nature of the class distribution.

4. Conclusions

HS-SPME/GC–MS has been used to analyze the volatile fraction of aniseed-flavoured spirit drinks. CAR/PDMS SPME fiber was used and the extraction conditions were optimized using a central composite experimental design. Pastis, sambuca, raki and anis samples were analyzed. Propenylphenols, monoterpenes, sesquiterpenes and hydrocarbons were present. Propenylphenols such as *trans*-anethole, *cis*-anethole and estragole were the main components. Other components like monoterpenes, sesquiterpenes and hydrocarbons were also present. Using a chemometric approach, the volatile fraction provides a suitable method to differentiate aniseed beverages, the best results being obtained with MLP.

References

[1] Council Regulation (EC) No. 1576/89 of 29 May 1989, Official Journal L160, 12/06/1989, P. 0001.
[2] V.M. Rodrigues, P.T.V. Rosa, M.O.M. Marques, A.J. Petenate, M.A.A. Meireles, J. Agric. Food Chem. 51 (2003) 1518.
[3] A. Besharati-Seidani, A. Jabbari, Y. Yamini, Anal. Chim. Acta 530 (2005) 155.
[4] P.M. Santos, A.C. Figueiredo, M.M. Oliveira, J.G. Barroso, L.G. Pedro, S.G. Deans, A.K.M. Younus, J.J. Scheffer, Phytochemistry 48 (1998) 455.
[5] N. Tabanca, B. Demirci, T. Ozek, N. Kirimer, K.H. Can Baser, E. Bedir, I.A. Khan, D.E. Wedge, J. Chromatogr. A 1117 (2006) 194.
[6] O. Lablanquie, G. Snakkers, R. Cantagrel, G. Ferrari, Anal. Chim. Acta 458 (2002) 191.
[7] H. Guichard, S. Lemesle, J. Ledauphin, D. Barillier, B. Picocheid, J. Agric. Food Chem. 51 (2003) 424.
[8] S.E. Ebeler, M.B. Terrien, C.E. Butzke, J. Sci. Food Agric. 80 (2000) 625.
[9] T. Fernández-García, M.E. Martín, A. Casp, Z. Lebens. Unter. Forsch. 206 (1998) 414.
[10] V. Andrea, N. Nadia, R.M. Teresa, A. Andrea, J. Agric. Food Chem. 51 (2003) 4978.
[11] S.C. Diéguez, M.L.G. de la Peña, E.F. Gómez, J. Agric. Food Chem. 51 (2003) 7385.
[12] H. Lord, J. Pawliszyn, J. Chromatogr. A 885 (2000) 153.
[13] C. Dietz, J. Sanz, C. Camara, J. Chromatogr. A 1103 (2006) 183.
[14] R.F. Alves, A.M.D. Nascimento, J.M.F. Nogueira, Anal. Chim. Acta 546 (2005) 11.
[15] V.A. Watts, C.E. Butzke, R.B. Boulton, J. Agric. Food Chem. 51 (2003) 7738.
[16] W. Wardencki, P. Sowinski, J. Curylo, J. Chromatogr. A 984 (2003) 89.
[17] B. Vallejo-Córdoba, A.F. González-Cordova, M.C. Estrada-Montoya, J. Agric. Food Chem. 52 (2004) 5567.
[18] J. Pino, M.P. Martí, M. Mestres, J. Pérez, O. Busto, J. Guasch, J. Chromatogr. A 954 (2002) 51.
[19] G. Fitzgerald, K.J. James, K. MacNamara, M.A. Stack, J. Chromatogr. A 896 (2000) 351.
[20] C. Da Porto, L. Pizzale, M. Bravin, L.S. Conte, Flavour Frag. J. 18 (2003) 66.
[21] E.A. Nonato, F. Carazza, F.C. Silva, C.R. Carvalho, Z.L. Cardenal, J. Agric. Food Chem. 49 (2001) 3533.

[22] M.S. Valdenebro, M. León-Camacho, F. Pablos, A.G. González, M.J. Martin, Analyst 124 (1999) 999.

[23] D. González-Arjona, V. González-Gallero, F. Pablos, A.G. González, Anal. Chim. Acta 381 (1999) 257.

[24] J.M. Jurado, A. Alcázar, F. Pablos, M.J. Martín, A.G. González, Talanta 66 (2005) 1350.

[25] J. Zupan, J. Gasteiger, Neural Networks in Chemistry and Drug Design, Wiley–VCH, Weinhein, 1999.

[26] R. Henrion, G. Henrion, Überwatchte Klassifikation in Multivariate Dateanalysen, Springer-Verlag, Berlin, 1995.

[27] C. Bishop, Neural Networks for Pattern Recognition, University Press, Oxford, 1995.

[28] M. Forina, C. Armanino, R. Leardi, G. Drava, J. Chemometr. 5 (1991) 435.

[29] D. González-Arjona, G. López-Pérez, A.G. González, Chemometr. Intell. Lab. Syst. 57 (2001) 133.

Dual WO$_3$ based sensors to selectively detect DMMP in the presence of alcohols

Sofian M. Kanan [a,*], Anil Waghe [b,c], Bruce L. Jensen [c], Carl P. Tripp [b,c]

[a] *American University of Sharjah, Department of Biology and Chemistry, P.O. Box 26666, Sharjah, United Arab Emirates*
[b] *Laboratory for Surface Science and Technology (LASST), University of Maine, Orono, ME 04469, United States*
[c] *Department of Chemistry, University of Maine, Orono, ME 04469, United States*

Abstract

A size selective approach to improving selectivity in semiconducting metal oxides (SMO) sensors was obtained by tailoring the architecture of WO$_3$ powders. The key for achieving high selectivity is based on using a dual sensor configuration where the response on a porous WO$_3$ powder sensor was compared to the response on a nonporous WO$_3$ powder sensor. Detection selectivity between methanol and dimethyl methylphosphonate (DMMP) is obtained because the access of a gas molecule in the interior pore structure of WO$_3$ is size dependent leading to a size dependant magnitude change in the conductivity of SMO sensor.
© 2006 Elsevier B.V. All rights reserved.

Keywords: SMO sensor(s); WO$_3$; DMMP; Porous; FTIR; Selectivity

1. Introduction

Although semiconducting metal oxide (SMO) based sensors have demonstrated high sensitivity in detecting low levels of gaseous compounds, they suffer from lack of detection selectivity. Poor detection selectivity can be traced to the fact that there is very little information content in the sensor response other than an increase in conductivity occurs when a gas molecule is oxidized and a corresponding decrease occurs when a gas molecule is reduced. This leads to unacceptably high false alarm rates and this is the biggest technical hurdle preventing the widespread use of this technology. The current approaches to improve selectivity in SMO sensing involve a combination of filtration [1], concentration [2], and array based detection [3,4].

Use of prefilters/concentrators tackles the problem by reducing the number of components in the gas stream impinging on the SMO detector element. Materials such as inorganic membranes, zeolites, and other adsorbents are used to selectively preconcentrate and prefilter interferent molecules from the gas stream. For example, we have recently shown that silica based material can be used to selectively adsorb organophosphonates from a gas stream [5,6]. Work by others has shown that silicalite (A-zeolite) can be used for size and polarity based separation of isoprene and NO$_2$ from NO [1].

An array-based approach increases the information content of the response signal because each element of the array produces a different response characteristic to the gas matrix. In this case, a bank of sensors is used in which each sensor element produces a different response to the various components of the gas stream. Variables such as metal oxide composition and morphology, impregnation with metal catalysts and operational temperature are a few approaches that are under investigation to achieve distinguishable sensor array elements [7–12]. Neural network methodologies are then used to process the complex response signal.

The threat of terrorism has increased the need for nerve agent detection systems and this application requires stringent tolerances in detection selectivity as high false alarm rates are not tolerated. As a result, this has prompted several studies aimed at obtaining a basic understanding of the fundamental chemical reactions occurring between organophosphonate compounds and metal oxide surfaces [13–23]. For obvious safety reasons, research on nerve agent detection in academia is accomplished with benign analogues. The choice of the simulant depends on

---

* Corresponding author. Tel.: +971 6 515 2409; fax: +971 6 515 2450.
E-mail address: skanan@aus.edu (S.M. Kanan).

the particular nerve agent characteristic to be mimicked, and by far, the most common molecule used as a simulant is dimethyl methyl phosphonate (DMMP).

On most oxides such as Al_2O_3, [13,24–26] TiO_2, [26–29] WO_3, [26,27] La_2O_3, [13] MgO, [13,14,16,26,30,31] Fe_2O_3, [13,23,32,33] and Ag_2O, [19] DMMP adsorbs through the P=O functionality and decomposes via elimination of the methoxy groups at elevated temperatures producing a stable methyl phosphonate (phosphate in the case of Fe_2O_3) on the surface. This is in contrast to the adsorption behavior on silica, where DMMP adsorbs via a hydrogen bond between the methoxy modes and the surface SiOH groups with subsequent evacuation at elevated temperature resulting in the complete desorption of intact DMMP molecules from the surface [5,6] (Scheme 1).

The decomposition of DMMP on a WO_3 based SMO sensor liberates methanol in the process, and it is the subsequent oxidation of methanol to formaldehyde that leads to a change in conductivity [30]. Since the mechanism of signal generation for DMMP and methanol are the same (i.e., oxidation of methanol) developing a method that can distinguish between DMMP and methanol has been a critical goal and benchmark for demonstrating detection selectivity for toxic nerve agents by this technology.

In this article, we demonstrate an approach to achieving detection selectivity in SMO sensors that occurs by tailoring the architecture of WO_3 powders. Detection selectivity between methanol and DMMP is obtained because the access of a gas molecule in the interior pore structure of the WO_3 is size dependent leading to a size dependent magnitude change in conductivity of the SMO sensor. In essence, use of the porous WO_3 incorporates a filtering approach directly into the sensor element itself. Specifically, gas pulses of various alcohols and DMMP are exposed to side-by-side sensors fabricated with a porous and nonporous WO_3 powders mounted on the same platform. By ratioing the change in conductivity measured on the porous WO_3 sensor to that obtained on the nonporous WO_3 counterpart, a unique signal is obtained based on the size of the molecule. Complementary IR spectroscopic studies show that the difference in conductivity is primarily due to the amount adsorbed on each material and not to differences in reaction chemistry.
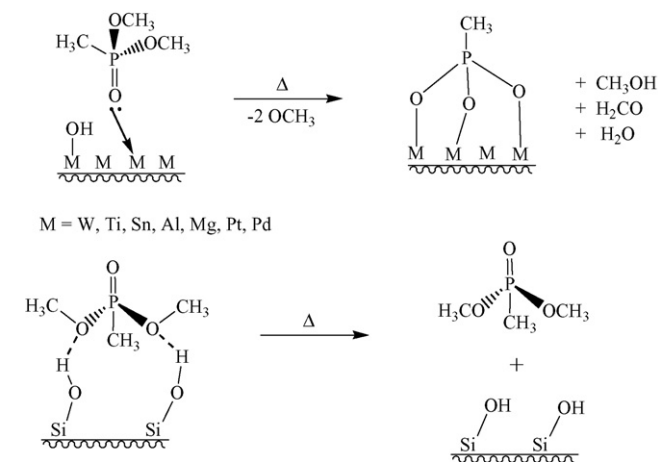
Scheme 1.

2. Experimental

2.1. Materials

DMMP, methanol, ethanol, isopropanol, *tert*-butanol, hexanol (HPLC grades) and *N*-cetyl trimethyl ammonium bromide (CTAB) were purchased from Alrdrich Chemical Company and were used without any further purification.

2.2. Synthesis of porous and noporous WO_3 powders

Tungstic acid (H_2WO_4) was prepared by passing Na_2WO_4 through an ion exchange resin. A 35.0 g sample of the resin (DOWEX 50X2-200) was loosely packed into a standard 50.0 mL burette and repeatedly washed with deionized water until the effluent was neutral to pH paper. Then 25.0 mL of a 25% Na_2WO_4 solution in distilled water was passed through the ion exchange column at a rate of about 0.3 mL/min. A 50 mL aliquot of the effluent was collected when the pH of effluent dropped below 4. The freshly eluted solution of H_2WO_4 was immediately added to the solutions described below.

The nonporous sample (sample A) was prepared by emulsion polymerization and the procedure is described in detail elsewhere [34] whereas, the two porous samples were prepared using two different protocols (labeled as samples B and C) as previously reported [35,36]. In brief the nonporous sample (sample A) was prepared by stirring a solution of Span 60 (a nonionic surfactant) and toluene at 1000–1600 rpm and the exiting tungstic acid was added at a rate of 0.5 mL/min. The solution was stirred for 5 min after adding the necessary amount of tungstic acid. The final solution was stirred at 300 rpm for 72 h until a single cloudy phase suspension was observed. The surfactant was removed during the calcinations process at 500 °C for 6 h. Sample B was prepared by adding the H_2WO_4 effluent to an aqueous CTAB solution. In brief, 0.6 g of CTAB was dissolved in 5.0 mL of deionized water and stirred with mechanical stirrer at 800 rpm until the solution was homogeneous and clear. Then, 2.0 mL of NH_4OH (32 wt%) was added to the CTAB solution and the solution was stirred for an additional 5 min. A 25.0 mL sample of a freshly eluted solution of H_2WO_4 was then added to CTAB solution; the solution was stirred for 24 h and then allowed to continue the sol–gel polymerization process at ambient temperature for an additional 48 h. The resulting yellow powder was filtered, then washed sequentially with ethanol and deionized water. The powder was then calcinated at 500 °C for 5 h. The temperature was raised at 1 °C/min to 500 °C and was decreased at a rate of 20 °C/min.

Sample C was prepared by mixing 4.4 mmol CTAB in 7.0 mL distilled water with 33.0 mL of technical grade ethanol (0.58 mol) and 8.5 mL of aqueous NH_4OH (29.2 wt%, 0.14 mol). The solution was stirred for 10 min and then 25 mL of eluted H_2WO_4 solution was added. The mixture was stirred for 24 h and then left undisturbed at room temperature for an additional 48 h. The precipitate that formed was filtered, washed with ethanol and then with deionized water and the calcination protocol was the same as used in generating sample B. The surface areas for

the three WO_3 samples (A–C) were determined to be 22, 120, and 150 m^2/g, respectively.

2.3. Fabrication of sensor platforms

Sensor platforms were prepared using photolithographic lift-off techniques [37]. The sensor platform, a 6 mm square device, is composed of an interdigitated electrode pattern composed of 300 nm of platinum on 20 nm of zirconium as an adhesion layer. The substrate is R-cut sapphire. The reverse side contains a serpentine heater and a resistance temperature device (RTD) of the same material as the electrode.

A suspension of WO_3 powders (25 mg) in 1 mL of deionized water was prepared and sonicated for 30 min. A drop of the suspension was placed on the sensor platform to cover the electrodes and dried in a nitrogen environment. WO_3 powder films produced with this simple deposition procedure were remarkably robust, stable, and routinely generating sensor data over months of operation at temperatures above 300 °C. Furthermore, the powder based sensors showed good sample-to-sample reproducibility as the response signal was insensitive to variations in powder film thickness. Above a minimum threshold thickness, the rapidity and magnitude of the sensors response to target gas pulse showed little, if any, thickness dependence. Both the nano-sized nonporous and porous powder sensor show very fast response to a gas pulse because the migration of bulk lattice oxygen to the surface is dictated by particle size (or wall thickness in porous materials) and not the thickness of the powder layer deposited on the sensor platform. Below a minimum thickness the devices usually failed because the films were not contiguous with large cracks appearing leading to an equivalent electrical open circuit. It is also noted that the powder-based sensors have been shown to be equal in sensitivity with thin film based sensors. Therefore, any improvement in selectivity obtained by using the porous WO_3 powder sensors would occur without a sacrifice in sensitivity.

The RTD of each sensor was then calibrated at various temperatures up to 400 °C. The response of the film was measured at the same time. After RTD calibration, the sensors were then placed in a test chamber and heated using a Watlow temperature controller.

Once bonded into a header package, the sensors were placed in a stainless steel test chamber where four sensors can be tested simultaneously to the same gas pulse. The entire test system is composed of eight Tylan General mass flow controllers, each mixed and plumbed into one inlet for the test chamber. The operating temperature was fixed at 360 °C and target gas flow rate was 100 sccm. The test protocol for each compound consists of first flowing zero air (hydrocarbon removed) for 20 min to establish a baseline. Second, the target gas is switched on for 5 min, followed by a 2-min purge of the target gas line. Third, the system flows zero air over the sensors for either 20 or 40 min to again establish a baseline. The input line was then switched to the next target gas.

Methanol was supplied at 30 psig from a premixed bottle with zero air. For all other gases, the input line was placed above the liquid level in a bottle containing the alcohol or DMMP. The bottle was then sealed with the gas line inside.

The sensors were tested against a series of random pulses of the five alcohols and DMMP with a minimum of three separate pulses per alcohol (at least 15 random alcohol pulses in total). The alcohol pulses were performed before DMMP because the alcohols do not poison the sensor enabling repeated measurements. The last gas pulse was reserved for DMMP as this led to poisoning of the sensor (by forming stable methylphosphate on the surface of the sensor), and thus ending its usefulness for further testing.

2.4. Instrumentation

N_2 adsorption–desorption isotherms were measured with Micromeritics Gemini 2360 instrument equipped with a Micromeritics Flowprep 060 degasses attachment. Surface areas, pore volumes and pore size distributions were calculated from the N_2 adsorption data.

FTIR spectra were recorded on a Bomem MB-Series spectrometer with a liquid N_2 cooled mercury cadmium telluride (MCT) detector. Typically 200 scans were co-added at a resolution of 4 cm^{-1}. Spectra were recorded in transmission using a thin film technique [38]. In brief, a thin film of WO_3 powder was spread on a 1.0 inch in diameter KBr disc (referred to as a WO_3 film) and the reference spectrum was recorded through the WO_3 thin film. The WO_3 film was evacuated and then exposed to an excess amount of DMMP and/or alcohol vapors for 5 min followed by evacuation at room temperature. All spectra were recorded at ambient temperature.

3. Results and discussion

The space filling models of DMMP and methanol depicted in Scheme 2 shows that the largest diameter of DMMP is about 5.71 and 2.8 Å for methanol. Thus, obtaining size selectivity in detection between methanol and DMMP, would require a microporous material with pores larger than 2.8 Å and less than 5.71 Å. At first glance, the use of a porous WO_3 samples with pore sizes between 3 and 5.5 Å will operate as a selective sensor for methanol rather than the target DMMP or the even larger sized nerve agents. This is in an opposite direction to our goal. The intent is to detect the larger DMMP or nerve agents whereas methanol is an interferent giving rise to false alarms. While methanol would penetrate inside 3–5.5 Å pores, the larger DMMP (5.71 Å diameter) would

2.8 Å   5.71 Å

Methanol   DMMP
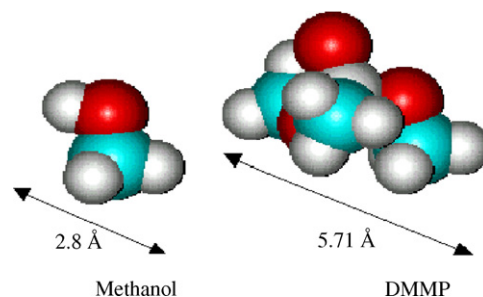
Scheme 2.

Scheme 3.
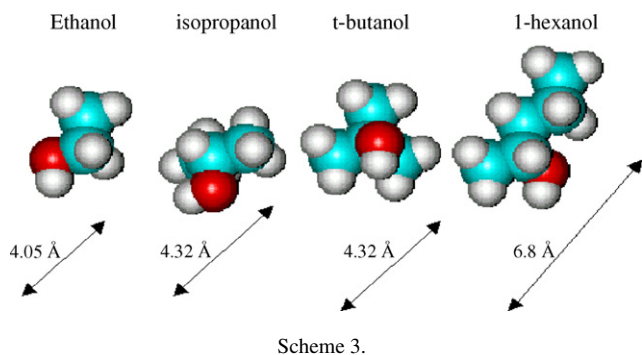
be excluded from the inner pore area and this exclusion would be more severe for the even larger nerve agents. The solution to this problem is to operate the sensor in a difference detection mode where the response of a target molecule on the porous WO_3 is compared to a second sensor containing the nonporous WO_3 powder.

On the nonporous WO_3 sensor, there should be minimal, if any size dependence in the availability of surface sites to the target gas. In contrast, a molecule too big to enter a pore will result in a lower amount adsorbed on the porous based sensor. This leads to a lower change in resistance relative to the same signal measured on the reference sensor (sample A).

To fully explore size dependence in selectivity, we have performed conductivity measurements with the two test molecules of methanol and DMMP along with a series of alcohols of different shapes and sizes. The additional alcohols used were ethanol, isopropanol, t-butanol and 2-hexanol and their structures and relative size are shown in Scheme 3.

Fig. 1 shows a typical sensor response curve to three consecutive gas pulses of methanol, t-butanol, and DMMP. The lower curve is the response obtained from the sample A and the upper curve is the data obtained from the porous sample C sensor. The curves are on the same coordinate scale and are offset for clarity.

It is noted that the gas pulses were done without strict controls on the dosing protocol. The carrier gas was simply passed over

a vial containing the alcohol for a period of about 2 min. This means that each pulse was ill defined with no control in concentration and mixing with the carrier gas. While this would account for pulse-to-pulse differences in the magnitude and shape of the sensor response on the same detector, it is noted that the shape including the fine features of the response of each element in the dual sensor platform for the same pulse was very similar. This is not surprising as both sensors are in contact with the same ill-defined gas pulse at the same time. While the initial slope of the change in resistance was rapid for both porous and nonporous sensors, the slope was always steeper on the nonporous oxide and this is indicative of a slower diffusion of the gas in the porous oxide. However, the variation in the initial slope showed large pulse-to-pulse variations in value for repeated measurement to the same target gas. Therefore, no trend was discernable from the initial slopes for different gases. Given the ill-defined nature of the gas pulse, the result is consistent with recent work by Frederick and co-workers [39] that showed the pulse-to-pulse variation in the initial sensor response is controlled by the gas delivery system.

By far, the biggest difference in sensor response to a given gas pulse was the relative change in magnitude in resistance. While the magnitude of the resistance change for methanol is about the same on both sensors in Fig. 1, the magnitude of the response is clearly lower for both t-butanol and DMMP on the porous sensor (sample C) relative to the nonporous material (sample A). For each pulse, we calculated the change in conductivity (ΔC) with Eq. (1):

$$\Delta C = \frac{1}{R_{Pulse}} - \frac{1}{R_{Base}} \tag{1}$$

where R_{Pulse} is the resistance measured in the plateau region of the pulse and R_{Base} is the based resistance measured just prior to the gas pulse. An example of the selection points for R_{Base} and R_{Pulse} are indicated for the methanol pulse in Fig. 1.

The value of ΔC is proportional to the number of carriers generated in the WO_3 which is related to kinetics of the redox reaction of the surface with the gaseous molecule. The ΔC obtained on each mesoporous WO_3 sensor is then ratioed to the corresponding ΔC obtained on the nonporous WO_3 sensor ($\Delta C_{porous}/\Delta C_{nonporous}$). A plot of this ratio versus volume of the molecule is given in Fig. 2 and these curves clearly point to a selective detection method for distinguishing methanol from DMMP. The error bars in Fig. 2 represent the 95% confidence level.

It is possible that the difference in $\Delta C_{porous}/\Delta C_{nonporous}$ arises from different reaction chemistry on the nonporous and porous materials. This would alter the kinetics of the surface reduction and hence change the number of charge carriers under steady state conditions. However, our infrared data suggests that there is very little difference in the adsorption behavior of the various alcohols on sample C relative to the nonporous sample A. Fig. 3 shows the FTIR spectra methanol adsorbed on of samples A and B. Of particular note is the similarity in the intensity ratio of the two bands at 1394 and 1124 cm^{-1} on both materials which indicates the same relative amount of undissociated and dissociative adsorption on both materials. The band at 1394 cm^{-1} is
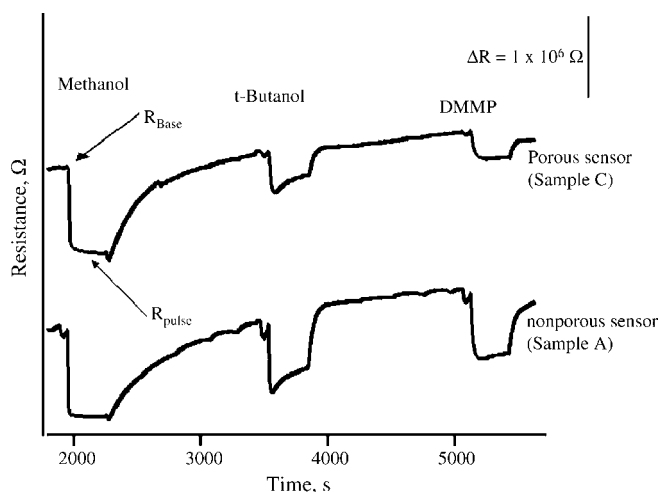

Fig. 1. Sensor response to a three pulse sequence of methanol, t-butanol and DMMP for samples A and C based sensors.
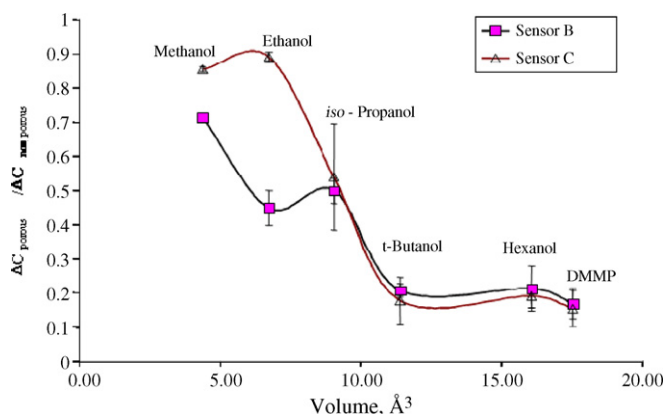
Fig. 2. $\Delta C_{porous}/\Delta C_{nonporous}$ values as a function of size of the target molecule.

the O–H bending mode of molecularly adsorbed methanol and the band at 1124 cm^{-1} is the O–C mode of adsorbed OCH$_3$ group on the surface [39,40].

This similarity in the IR spectra of methanol on the samples A and B is also observed for other alcohols used in this study (not shown). On the other hand, several differences were observed for DMMP adsorption on the three different powders. The infrared spectra of adsorbed DMMP on samples A–C evacuated at 25 °C are shown in Fig. 4. The infrared spectrum of DMMP adsorbed on sample A has been previously reported [5,6,13,27]. In brief, two O–CH$_3$ stretching modes appear at 1068 and 1043 cm^{-1} (Fig. 4a) and they are slightly shifted to lower frequency compared to the corresponding bands of the gaseous DMMP (1075 and 1049 cm^{-1}) showing that there is little, if any interaction between the methoxy groups and the surface. On the other hand, DMMP adsorbs on WO$_3$ through the P=O and WO$_3$ surface sites as evidenced by the shift to lower frequency in the P=O stretching modes from the frequencies of their gaseous counterparts. In Fig. 4a, three P=O stretching modes at 1243, 1223, and 1205 cm^{-1} (shifted from the gaseous DMMP by 39, 54, and 70 cm^{-1}, respectively) are assigned for P=O bonded to the surface through Bronsted, H-bonded, and Lewis sites. A fourth band at 1189 cm^{-1} in this region is assigned to the O–CH$_3$ rocking mode [5,6,27].
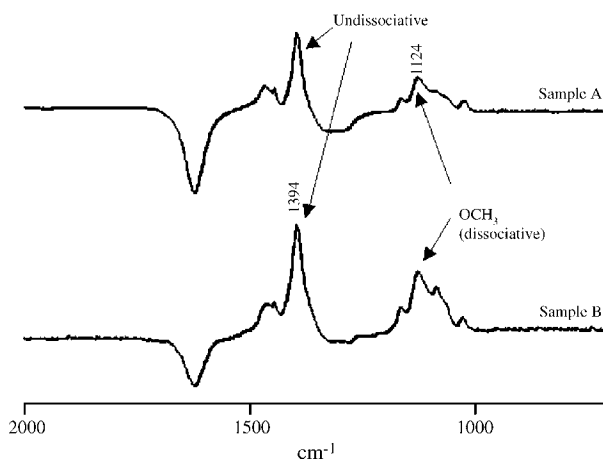

Fig. 3. Infrared spectra of methanol adsorbed on samples A and B powders.
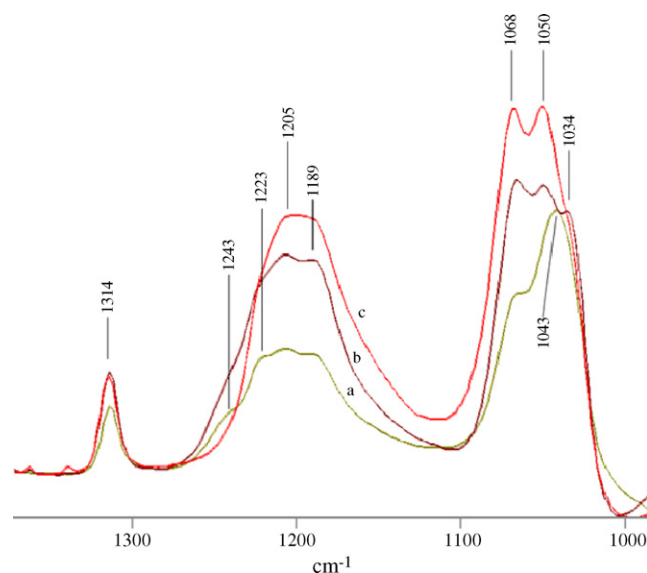

Fig. 4. Infrared spectra after addition of excess DMMP at room temperature for 1 min followed by evacuation for 2 min on (a) sample A (b) sample B, and (c) sample C. All spectra are normalized for same amount WO$_3$.

Interestingly, the DMMP adsorbed on the porous samples B and C show the same three P=O modes albeit in different intensity ratio compared to sample A. Furthermore, the OCH$_3$ modes in the spectra of samples B and C are similar (i.e., three bands at 1068, 1050, and 1034 cm^{-1}) whereas the spectrum of sample A clearly shows two bands at 1060 and 1043 cm^{-1}. This shows that the adsorbed species on the porous powders are generally the same and differs in the relative number of each species compared to sample A. It is noted that changes in the conductivity can arise from minute changes in the surface kinetics. Thus, the IR data do not eliminate the possibility that the difference in sensor response to DMMP is due to differences in reaction kinetics arising from subtle differences in surface chemistry.

On the other hand, the IR data do support a size selectivity explanation for the detection selectivity. The spectra shown in Fig. 4 were recorded for the same amount of WO$_3$ powder probed by the IR beam. Given that the surface areas for the three samples were determined to be 22, 120, and 150 m^2/g, the amount of DMMP adsorbed on sample B would be expected to be at least 6 times of the DMMP adsorbed on an equal mass of sample A (i.e., DMMP is able to freely access the internal surface area of sample B). The intensity of the P–CH$_3$ modes at 1314 cm^{-1} is structure insensitive and therefore can be used to provide an estimated of the relative amount of DMMP adsorbed on each sample. As shown in Fig. 4, the amount of the DMMP adsorbed on samples B or C is only 1.3 times higher than the amount of DMMP adsorbed on sample A. This shows that DMMP has limited access to the internal pore structure.

Further evidence of a size exclusion effect was provided by a series of thin film infrared experiments in which samples A–C were evacuated at room temperature and exposed to the saturation vapor pressure of various alcohols. Each alcohol produces unique bands that could be used to measure the amount of each alcohol adsorbed on the three powders. A plot of the amount of each alcohol adsorbed on samples B and C relative to sample A
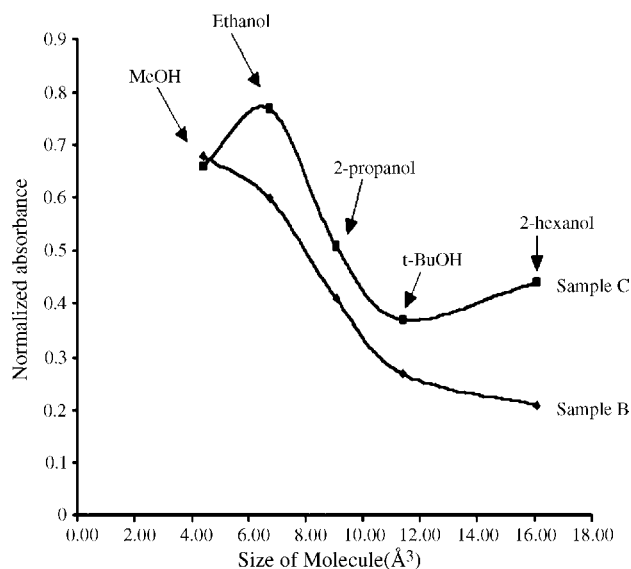
Fig. 5. Amount of various alcohols adsorbed on samples B and C relative to sample A as determined by IR spectroscopy.

as a function of the size of the alcohol is shown in Fig. 5. The trend obtained from the infrared measurements clearly show the strong correlation between the relative amount of alcohol adsorbed and the $\Delta C_{porous}/\Delta C_{nonporous}$ values plotted in Fig. 2.

We recall that, our initial intent was to develop a strategy for distinguishing between methanol and DMMP in SMO detection. This is clearly demonstrated as the $\Delta C_{porous}/\Delta C_{nonporous}$ for methanol on sensors B and C is about 0.72 and 0.86, respectively, and for DMMP is about 0.17 and 0.14, respectively (see Fig. 2). This is 4 and 6 times in magnitude between methanol and DMMP on the two porous sensors (sensors C and B, respectively) relative to the corresponding response on the nonporous sample A and same factor is obtained when comparing methanol to t-butanol on each sensor. Similarly, the IR also shows a large difference in adsorbed amounts of methanol relative to t-butanol. The adsorbed amount ratio for t-butanol is a factor of 2.5 times lower than the value obtained from methanol.
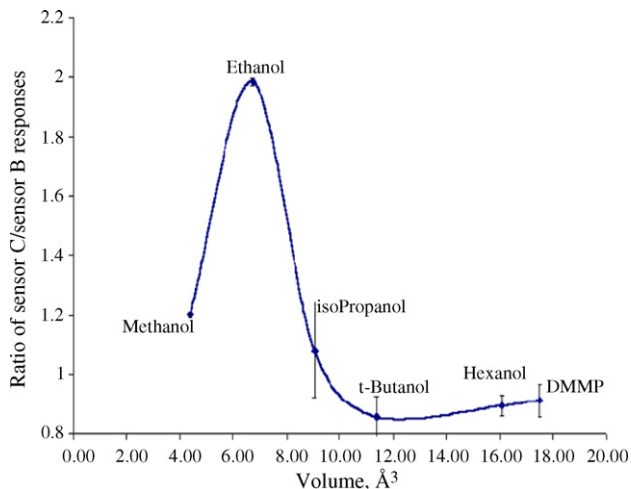

Fig. 6. $\Delta C_{sample\ C}/\Delta C_{sample\ B}$ values as a function of size of the target molecule.

Perhaps more interesting is that the results point to a strategy for developing a very narrow "Notch" detection system. For example, the data in Fig. 2 show that by ratioing the sensor response from two closely related porous powders (i.e., $\Delta C_{sample\ C}/\Delta C_{sample\ B}$, we have a system that can detect ethanol. This is shown in Fig. 6. A possible explanation for this effect is that a slight difference in the pore size distribution between the two porous materials enhances the capillary condensation of ethanol over methanol. This produces a higher relative adsorbed amount of ethanol leading to highly selective "Notch" detector. In principle, this concept could be applied to any size molecule. In the case of DMMP, we predict that two porous materials with average pore size distribution near 5.7 Å and different pore size distribution would lead to a DMMP notch detector.

4. Conclusions

Use of porous WO_3 materials in SMO detection has been shown to provide a route to achieve detection selectivity between methanol and DMMP. The key to achieving detection selectivity is to perform measurements on a dual detection system in which the response of a sensor based on porous powder is compared to that of a nonporous counterpart. IR adsorption measurements show that the difference in sensor response is due to a size dependent difference in the adsorbed amount of the target compound on the surface of the porous WO_3 relative to the amount adsorbed on a nonporous WO_3 powder.

In summary, we believe the strength of this approach is in its simplicity. Identification of a particular molecule is not done by comparing the response of different gases on a single sensor, but rather the same gas pulse on two different detectors. While each pulse has different pressures and gas delivery characteristics and different gases would have different reaction rates, these differences are normalized in calculating the values for the curves in Figs. 3 and 6.

References

[1] B. Fruhberger, N. Stirling, F.G. Grillo, S. Ma, D. Ruthven, R.J. Lad, B.G. Frederick, Sens. Actuators B 76 (2001) 226–234.
[2] S.M. Kanan, C.P. Tripp, Langmuir 18 (2002) 722.
[3] S. Semancik, R. Cavicchi, M.C. Wheeler, J.E. Tiffany, G.E. Poirier, R.M. Walton, J.S. Suehle, B. Panchapakesan, D.L. DeVoe, Sens. Actuators B 77 (2001) 579.
[4] R. Menzel, J. Goschnick, Sens. Actuators B 43 (2000) 235–238.
[5] S.M. Kanan, Z. Lu, C.P. Tripp, J. Phys. Chem. B 106 (2002) 9576.
[6] S.M. Kanan, C.P. Tripp, Langmuir 17 (2001) 2213.
[7] D.F. Cox, T.B. Fryberger, S. Semancik, Surf. Sci. 224 (1989) 121–142.
[8] D.F. Cox, T.B. Fryberger, S. Semancik, J. Vac. Sci. Technol. A 6 (1988) 828–829.
[9] S. Semancik, D.F. Cox, Sens. Actuators B 12 (1987) 101–106.
[10] T.B. Fryberger, S. Semancik, Sens. Actuators B 2 (1990) 305–309.
[11] D.F. Cox, T.B. Gryberger, S. Semancik, Phys. Rev. B 38 (1988) 2072–2082.
[12] R.E. Cavicchi, S. Semancik, J.S. Suehle, M. Gaitan, US Patent Number 5,356,756 (1994).
[13] M.B. Mitchell, V.N. Sheinker, E.A. Mintz, J. Phys. Chem. 101 (1997) 11192–11203.
[14] N.U. Zhanpeisov, G.M. Zhidomirov, I.V. Yudanov, K.J. Klabunde, J. Phys. Chem. 98 (1994) 10032–10035.
[15] M.A. Henderson, J.M. White, J. Am. Chem. Soc. 110 (1988) 6939–6947.

[16] Y.X. Li, J.R. Schlup, K.J. Klabunde, Langmuir 7 (1991) 1394–1399.
[17] L. Bertilsson, I. Engquist, B. Liedberg, J. Phys. Chem. B 101 (1997) 6021–6027.
[18] V.S. Smentkowski, P. Hagans, J.T. Yates Jr., J. Phys. Chem. 92 (1988) 6351–6357.
[19] N. Taranenko, J.-P. Alarie, D.L. Stokes, T. Vo-Dinh, J. Raman Spectrosc. 27 (1996) 379–384.
[20] K.Y. Lee, M. Houalla, D.M. Hercules, W.K. Hall, J. Catal. 145 (1994) 223–231.
[21] L. Bertilsson, K. Potje-Kamloth, H.D. Liess, I. Engquist, B. Liedberg, J. Phys. Chem. 102 (1998) 1260–1269.
[22] I.D. Gay, A.J. McFarlan, B.A. Morrow, J. Phys. Chem. 95 (1991) 1360–1368.
[23] M.A. Henderson, T. Jin, J.M. White, J. Phys. Chem. 90 (1986) 4607–4611.
[24] L. Cao, S.R. Segal, S.L. Suib, X. Tang, S. Satyapal, J. Catal. 194 (2000) 61–70.
[25] M.K. Templeton, W.H. Weinberg, J. Am. Chem. Soc. 107 (1985) 97–108.
[26] B. Blajeni-Aurian, M.M. Boucher, Langmuir 5 (1989) 170–174.
[27] C.S. Kim, R.J. Lad, C.P. Tripp, Sens. Actuators B 76 (2001) 442.
[28] C.N. Rusu, J.T. Yates Jr., J. Phys. Chem. B 104 (2000) 12292–12298.
[29] T.N. Obee, S. Satyapal, J. Photochem. Photobiol. A 118 (1998) 45–51.
[30] L. Bertilsson, K. Potje-Kamloth, H.-D. Liess, Langmuir 15 (1999) 1128–1135.
[31] Y.X. Li, K. Klabunde, Langmuir 7 (1991) 1388–1393.
[32] R.I. Hedge, J.M. White, Appl. Surf. Sci. 28 (1987) 1–10.
[33] T.M. Tesfai, V.N. Sheinker, M.B. Mitchell, J. Phys. Chem. B 102 (1998) 7299–7302.
[34] Z. Lu, S.M. Kanan, C.P. Tripp, J. Mater. Chem. 12 (2002) 983–989.
[35] A.B. Waghe. Synthesis of porous monoclinic tungsten oxides and their application in sensors, Ph.D Thesis, University of Maine, 2003.
[36] D. Kumar, K. Schumacher, C. du Fresne von Hohenesche, M. Grun, K.K. Unger, Colliods Surf. A: Physicochem. Eng. Aspects 187–188 (2001) 109–116.
[37] S.C. Moulzolf, L.J. LeGore, R.J. Lad, Thin Solid Films 400 (2001) 56–63.
[38] C.P. Tripp, M.L. Hair, Langmuir 7 (1991) 923.
[39] R.S. Pilling, G. Bernhardt, C.S. Kim, J. Duncan, C.B.H. Crothers, D. Kleinschmidt, D.J. Frankel, R.J. Lad, B.G. Frederick, Sens. Actuators (2003) 200–204.
[40] C. Cantalini, W. Wlodarski, Y. Li, M. Passacantando, S. Santucci, E. Comini, G. Faglia, G. Sberveglieri, Sens. Actuators B 64 (2000) 182–188.

ELSEVIER

Fabrication of a novel immunosensor using functionalized self-assembled monolayer for trace level detection of TNT by surface plasmon resonance

Toshikazu Kawaguchi [a],[*], Dhesingh Ravi Shankaran [a],[b],[*], S.J. Kim [a],
K. Vengatajalabathy Gobi [a], Kiyoshi Matsumoto [c], Kiyoshi Toko [d], Norio Miura [a]

[a] *Art, Science and Technology Center for Cooperative Research, Kasuga-shi, Fukuoka 816-8580, Japan*
[b] *Japan Society for the Promotion of Science, Tokyo 102-8471, Japan*
[c] *Graduate School of Agriculture, Kyushu University, Fukuoka 812-8581, Japan*
[d] *Graduate School of Information Science and Electrical Engineering, Kyushu University, Fukuoka 812-8581, Japan*

Abstract

We have developed a new immunosensor based on self-assembly chemistry for highly sensitive and label-free detection of 2,4,6-trinitrotoluene (TNT) using surface plasmon resonance (SPR). A monolayer of amine terminated poly(ethylene glycol) hydrazinehydrochloride (PEG-NH$_2$) thiolate was constructed on an activated gold surface and immobilized with trinitrophenyl-β-alanine (TNPh-β-alanine) by amide coupling method. The binding interaction of a monoclonal anti-TNT Ab (M-TNT Ab) with TNPh-β-alanine immobilized thiolate monolayer surface was monitored and evaluated for detection of TNT based on the principle of indirect competitive immunoreaction. Here, the competition between the self-assembled TNT derivative and the TNT in solution for binding with antibody yields in the response signal that is inversely proportional to the concentration of TNT in the linear detection range. With the present immunoassay format, TNT could be detected in the concentration range from 0.008 ng/ml (8 ppt) to 30 ng/ml (30 ppb). The response time for an immunoreaction was 2 min and one immunocycle could be done with in 4 min including surface regeneration. Bound antibodies could be easily eluted from the self-assembled immunosurface at high recoveries (more than 100 cycles) using pepsin solution without any damage to the TNT derivatives immobilized on the surface. The compact self-assembled monolayer was highly stable and prevented the non-specific adsorption of proteins on the surface favoring error free measurement.
© 2006 Elsevier B.V. All rights reserved.

Keywords: TNT; Surface plasmon resonance; Immunosensor; Self-assembly; Poly(ethylene glycol) hydrazinehydrochloride; Monoclonal anti-TNT antibody

1. Introduction

In the recent years, surface plasmon resonance (SPR) based immunosensors enjoy expanding recognition as a high-throughput screening tool in environmental and biomedical analysis [1–5]. One of the key factors for success of an immunoassay is the construction of highly effective recognition surface capable of fast and reliable interaction with its binding partner or analyte of interest. It is important to create robust sensor surface with specific binding properties and minimal background interference to improve the screening capabilities in a variety of complex analytical matrices. Over the

years, a number of different approaches have been demonstrated for immobilization of biomolecules on transducer surface such as, physical adsorption [6–8], embedding in polymers or membranes [9,10], sol–gel [11,12] and self-assembly [13–15]. Among them, self-assembly method received a great interest for fabrication of sensing surfaces, because it allows remarkable flexibility with respect to terminal functionality, size and orientation of the recognition molecules on the transducer surface [16–18]. In addition, the good stability under extreme conditions of pH and temperature, as well as the re-use and applicability in flow system makes self-assembled monolayer (SAM) surface a preferred, versatile tool in immunoassays. Considerable attention has been drawn in the recent years to functionalize the transducer surfaces by ultra-thin organic films containing free anchor groups such as thiols, amines, silanes or acids [13–19]. Despite many organic functional compounds, poly(ethylene gly-

* Corresponding authors. Tel.: +81 92 583 7886; fax: +81 92 583 8976.
  E-mail address: kawa@astec.kyushu-u.ac.jp (T. Kawaguchi).

cols) (PEG) attracted considerable interest as a robust platform for stable immobilization of a variety of receptor molecules with good control over size and orientation for various applications [20–22].

In the present work, we aimed to develop a stable and reliable immunosensor platform using PEG based self-assembled layer for detection of TNT. TNT is a well-known explosive compound used in the preparation of landmines for military and terrorist activities [23,24]. Contamination of soil and ground water with TNT is of the major concern because of its biological persistence, toxicity and mutagenicity [25]. Thus, detection of TNT is of tremendous importance in wide areas including landmine detection, environmental monitoring and homeland security. Recently, a number of immunosensors have been demonstrated for detection of TNT. Charles et al. [26] developed a microcapillary reversed-displacement immunosensor for TNT using 3-aminopropyltriethoxysilane as a functional layer for immobilization of trinitrobenzene. An electrochemiluminescence based enzyme immunoassay with a detection of 0.11 ng/ml was reported by Wilson et al. [27]. Bowen et al. [28] employed a 11,11′-dithio-bis(succinimidoylundecanoate) self-assembled monolayer for covalent attachment of antibody for gas-phase detection of TNT. Sapsford et al. [29] developed an array biosensor with a detection limit of 1, 20 and 10 ng/ml TNT based on direct, indirect competitive and displacement assays, respectively. Green et al. [30] reported a reversed-displacement immunosensor with a detection limit of 2.5 ng/ml TNT using a microcolumn containing an Aff-Gel resin derivatized with a TNB and a fluorophore labeled anti-TNT Ab. Zeck et al. [31] reported a detection limit of 0.06 ng/ml TNT using ELISA method. A fluorescent displacement immunoassay with a detection limit of 0.05 ng/ml was developed by Goldman et al. [32]. Despite the good sensing characteristics for TNT detection, most of the immunoassays have difficulties with respect to labelling of the reagents and time consuming procedures. Moreover, most of the methods involve the immobilization of antibodies on the sensor surface, which may result in loss of activity during immobilization and surface regeneration. Thus, the search for new approaches to increase the sensitivity and simplicity of the biosensor continues with a special attention towards the improvement in the mode of immobilization of biological molecules on transducer surface.

In our laboratory, we have been developing SPR immunosensor for TNT in the last few years. We have reported few immunosensors for TNT, which were constructed by simple physical adsorption method [8,33,34]. In the present work, we developed a simple and stable immunosensor surface by self-assembly for highly sensitive and label-free detection of TNT using SPR. Here, an amine terminated PEG monolayer was created as a nonfouling sensor platform on a transducer surface and functionalized with a TNT derivative, trinitrophenyl-β-alanine based on amide coupling method. This strategy allowed the stable immobilization of TNT with good control over the prevention of non-specific adsorption. The biomolecular interaction of the resulting TNT immobilized self-assembled surface with a monoclonal anti-TNT antibody was monitored

and evaluated for detection of TNT using SPR technique based on the principle of indirect competitive immunoreaction. The indirect inhibition method is compatible for highly sensitive detection of small analytes compared to sandwich and displacement methods and has been utilized for analysis of compounds of biomedical and environmental interest in our laboratory [6–8,13,33–36]. The performance of the present immunoassay was evaluated with respect to sensitivity, stability, and reproducibility. Furthermore, the cross-reactivity towards several TNT analogues was investigated. The proposed immunoassay showed highly promising sensing characteristics for rapid and reliable detection of TNT with good sensitivity and selectivity.

2. Experimental

2.1. Material and reagents

TNPh-β-alanine was received form Research Organics, USA, PEG-6-hydrazine alkanethiol was purchased form Sensopath Technologies, USA. Monoclonal anti-TNT Ab (mouse IgG, clone A1.1.1) was obtained from Strategic Biosolutions, USA. All other reagents and solvents (analytical grade) were obtained from Sigma, USA and Wako chemicals, Japan. Standard TNT solution was adjusted from TNT solution (Chugoku Kayaku Co. Ltd., Japan.) with PBS buffer (pH 7.2, contained 1% ethanol). *N*-(3-dimethylaminopropyl)-*N*′-ethylcarbodiimide hydrochloride (EDC) and *N*-hydroxysuccinimide (NHS) were received from Sigma USA. RDX, HMX, 2-A-4,6-DNT and 4-A-2,6-DNT were purchased from Accustandard, USA. DNT was received from Wako Chemicals, Japan. BSA and pepsin were obtained from Sigma, USA. Deionized water ($\rho = 18\,M\Omega$) was used for preparing all buffer solution. All experimental solutions were prepared with phosphate buffered saline (PBS, 0.1 M, pH 7.2). Tris buffer (pH 8.0) was used during immobilization TNPh-β-alanine. Pepsin solution (0.2 M) was prepared with glycine with the pH adjusted to 2.0 using 1 M HCl. Refractive index matching fluid (refractive index = 1.518) was obtained from Cargille Labs, USA.

2.2. Instrumentation

The immunoassay studies were carried out with an SPR 670 M instrument (Moritex Co., Japan) with home-made gold-chips. The SPR instrument was equipped with an automatic flow injection system. The loop volume of the flow cell is 200 μl. Through out the experiment, the room temperature was maintained at 25.0 ± 0.1 °C.

2.3. SPR gold-chip fabrication

Microscopic glass slides (BK7 type, 20 mm × 13 mm × 0.7 mm) were sonicated in soap water (20% Contrad 70), distilled water, and ethanol for 30 min. Then these glass substrates were dried with pure-nitrogen gas after rinsing with plenty of distilled water. 5 nm of chromium and 50 nm of gold were sputtered onto these glass substrates under a vacuum at room tempera-
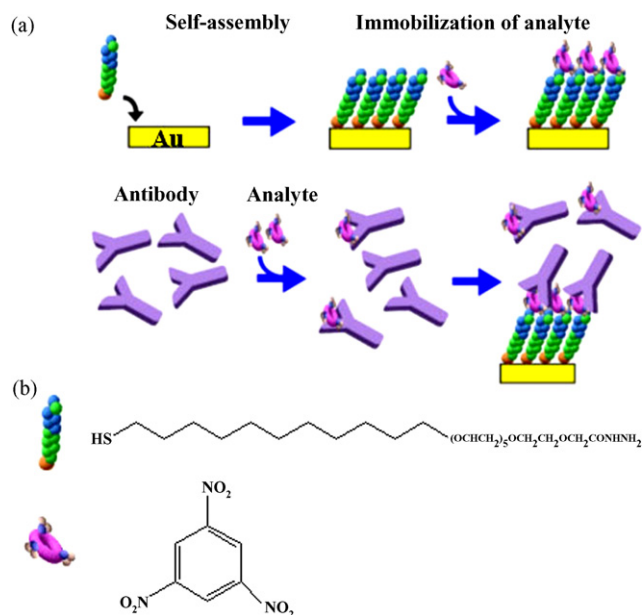
Fig. 1. Scheme of (a) the construction of immunosurface by self-assembly and (b) the principle of indirect competitive inhibition for TNT detection.

ture. Thus, prepared gold-chips were used immediately after sputtering.

2.4. Immunoassay principle and procedure

Fig. 1 shows the scheme of the present SAM based immunoassay for the detection of TNT. The first step of the immunosensor fabrication is the formation of an amine terminated self-assembled layer of PEG-NH$_2$ on a well cleaned activated gold surface. In the second step, TNPh-β-alanine was immobilized over the PEG-NH$_2$ SAM surface by amide coupling reaction. Thus, produced self-assembled layer consisting of TNPh-β-alanine outer layer was allowed for binding interaction with M-TNT antibody. This binding interaction was evaluated for detection of TNT based on the principle of indirect competitive immunoreaction.

In the indirect competitive inhibition method, different concentrations of free analyte (TNT) were mixed with a fixed (optimized) concentration of antibody (M-TNT Ab) and allowed for incubation at room temperature for 10 min. This standard TNT solutions were injected over the TNT immobilized self-assembled surface and the corresponding immunoreactions were monitored by SPR. It is expected that during incubation, free TNT couples with antibody in the sample solution and hence only the remaining antibody in the standard sample solution can bind to the TNT immobilized PEG-NH$_2$ SAM surface. Thus, as the amount of free TNT increased, the number of antibody available for interaction with TNT immobilized SAM surface is decreased and vice versa. Based on this dependence, free TNT in the sample solution can be quantified. The immunoassay conditions were carefully optimized for sensitivity, selectivity, and reproducibility.

3. Results and discussion

3.1. Immunosensor fabrication by self-assembling method

The self-assembling process was carried out using methanol as a carrier solution, and was flowed over the gold surface until a stable base line response was reached. Once a stable baseline was reached, 1 mM PEG-NH$_2$ in methanol solution was allowed to flow over the gold surface at a rate of 15 μl/min (flow duration ≈ 14 min). Fig. 2 depicts the SPR sensorgram for the formation of a self-assembled monolayer of PEG-NH$_2$ on a gold surface. A good linear increase in the resonance angle clearly indicates the formation of well-ordered monolayer on the gold surface. As can be seen (curve a), the resonance angle increased with time during the flow of PEG-NH$_2$ over the gold surface, and reached almost saturation in approximately 14 min. The observed resonance angle shift was $0.1345 \pm 0.0099°$ ($n = 5$) and was reproducible on repeated experiments. Further injections of PEG-NH$_2$ showed only a small increase in resonance angle (curve b), which suggested that a saturated monolayer of PEG-NH$_2$ was formed in the first injection. From the resonance angle shift, the surface concentration of the PEG-NH$_2$ was calculated as $2.5 \pm 0.2 \times 10^{-10}$ mol cm^{-2} ($0.01° = 10$ ng/cm^2). We simulated the molecular structure of PEG-NH$_2$ thiolate by using "Chem Office 2004". This software can calculate the molecular structure by simulation using approximation of energy between atoms. By the results of minimized energy, the molecular structure of PEG-NH$_2$ thiolate was calculated by Gaussian approximation as shown in Fig. 3. We assumed that the orientation of the alkyl chain in the molecule was 60°, which was the same angle as the ordinary alkanethiolate. The height of this molecule was calculated to 21.9 Å. It is well known that thiolate forms the close packed monolayer on gold surface. The close packed monolayer was used to be the structure as shown in Fig. 1. The coverage of PEG-NH$_2$ thiolate was calculated to 95.4 Å^2/molecule, which corresponds to 1.74×10^{-10} mol cm^{-2}. This calculated coverage was higher than the surface coverage calculated from the observed SPR angle change ($0.1345 \pm 0.0099°$), which corresponded to $2.5 \pm 0.2 \times 10^{-10}$ mol cm^{-2}.
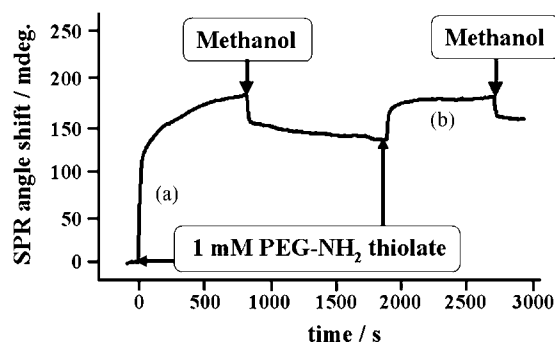

Fig. 2. Construction of self-assembled monolayer of PEG-NH$_2$ thiolate. SPR response for the flow of 1 mM PEG-NH$_2$ thiolate in methanol over the activated gold surface. Carrier solution: methanol, flow rate: 15 μl/min, flow duration 14 min.
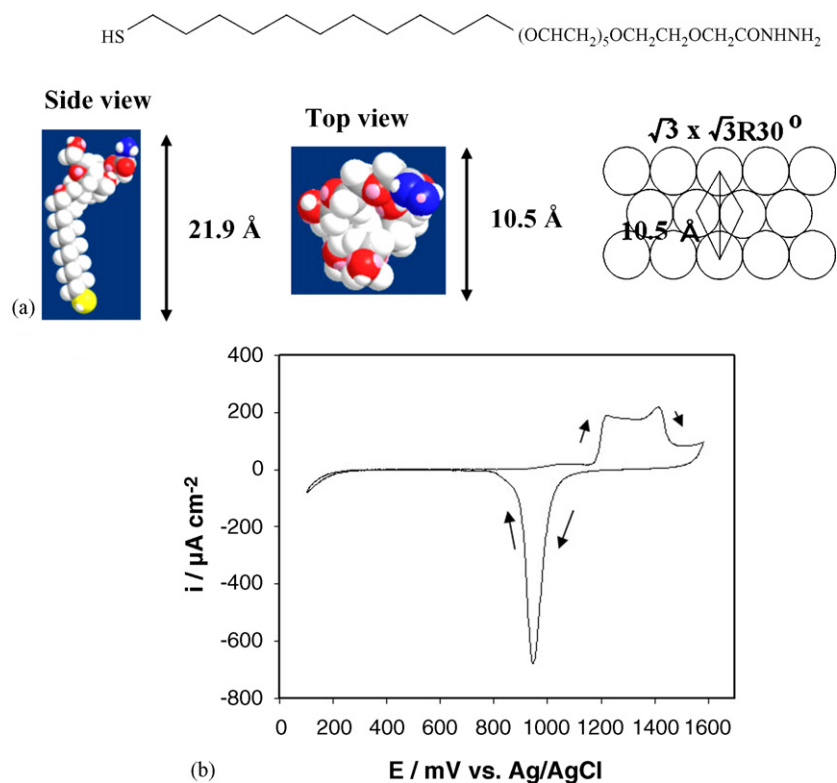
Fig. 3. (a) Molecular structure of PEG-NH$_2$ thiolate simulated by using Chem. Office 2004. (b) A cyclic voltammogram of a bare gold substrate in 1 M sulfuric acid. Sweep rate was 0.1 V s^{-1}.

It is believed that the surface concentration of a closest packed monolayer of alkanethiolate is 7.6×10^{-10} mol cm^{-2} [37]. The surface coverage of thiolate observed by SPR was slightly higher than that calculated from the simulation. This difference used to be corrected with the surface roughness. To estimate the true surface area, we used the electrochemical technique. Fig. 3 shows cyclic voltammogram in 1.0 M H$_2$SO$_4$ to determine the surface roughness. The reduction peak of oxygen–gold at +0.960 V was integrated to calculate the reduction charge, which was 626.2 μC cm^{-2}.

From the comparison between this charge and the reduction charge on an atomically flat surface, the surface roughness factor was estimated to 1.33.

By the correction with roughness factor (1.33), the true surface coverage of PEG-NH$_2$ thiolate observed by SPR after activation ($1.87 \pm 0.15 \times 10^{-10}$ mol cm^{-2}) was the same as the simulated value (1.74×10^{-10} mol cm^{-2}), which was within the error bar of the observed surface coverage. Thus, the observed surface coverage of the PEG-NH$_2$ was reasonable considering the fact that the molecular size of PEG thiolate (0.86 nm^2) was larger than alkanethiolate.

3.2. Immobilization of TNPh-β-alanine

After the formation of the PEG-NH$_2$ SAM on the gold surface, the carrier solution was changed to 10 mM Tris buffer (pH 8.0) for immobilization of TNPh-β-alanine. Prior to the injection, the TNPh-β-alanine was activated with *N*-(3-dimethylaminopropyl)-*N'*-ethylcarbodiimide hydrochloride and

N-hydroxysuccinimide (NHS) in 10 mM Tris buffer (pH 8.0) for effective immobilization on the amine-terminated thiolate (PEG-NH$_2$) monolayer surface. Here, 2.5 μg/ml of TNPh-β-alanine was mixed with 1000 μg/ml each of EDC and NHS and the mixture was allowed to flow over the PEG-NH$_2$ SAM surface at a rate of 15 μl/min. Fig. 4 shows the immobilization of TNPh-β-alanine over the self-assembled surface. An increase in the resonance angle indicates the immobilization of TNPh-β-alanine on the SAM surface (curve a). The resonance angle dropped down after switching the sourcing solution from TNPh-β-alanine solution to Tris buffer solution. This decrement was caused due to the difference in the refractive index
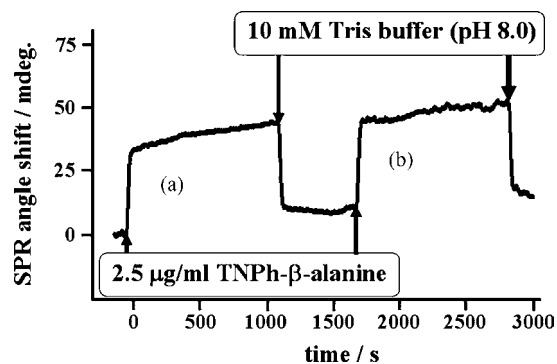

Fig. 4. SPR response for the immobilization of TNPh-β-alanine via amide reaction. 2.5 μg/ml TNPh-β-alanine was flowed over the PEG-NH$_2$ SAM surface. Carrier solution: 10 mM Tris buffer (pH 8.0), flow speed: 15 μl/min, flow duration: 14 min.

between TNPh-β-alanine solution and Tris buffer solution. The resonance angle change for TNPh-β-alanine immobilization was $0.0179 \pm 0.0002°$ ($n = 5$), which corresponds to a surface coverage of $3.92 \pm 0.01 \times 10^{-11}$ mol cm^{-2}. Further injection of the same concentrations of the TNPh-β-alanine mixture did not show any appreciable increase in the resonance angle (curve b). This is due to the saturation of TNPh-β-alanine with in 14 min during first injection. From the results, it is expected that the ratio of PEG-NH$_2$ and TNPh-β-alanine was 1:6. In order to evaluate the effect of the surface density of the PEG-NH$_2$ monolayer on the immobilization of TNPh-β-alanine and corresponding TNT sensing, the SPR gold-chips were functionalized with different concentrations of PEG-NH$_2$ and TNPh-β-alanine. It was observed that as the concentration of the PEG-NH$_2$ increased, increase in surface density of TNPh-β-alanine was observed. Similarly, the surface concentration of TNPh-β-alanine was low in the case the low surface concentration of PEG-NH$_2$ (data not shown). However, ratio remains same even in low surface concentrations of both PEG-NH$_2$ and TNPh-β-alanine. The possible reason for this behavior is that the PEG-NH$_2$ interacted with each other, resulting in a domain structure on the surface, which was partially the same surface concentration of PEG-NH$_2$. It is expected that the partial monolayer structure remains same always, but the inactive bare gold existed in the case of low surface concentration of PEG-NH$_2$ SAM on gold substrate. Therefore we used only the substrate highly covered with PEG-NH$_2$ SAM for TNT detection.

3.3. Antigen–antibody immunoreaction and surface regeneration

The immunoreaction of TNPh-β-alanine immobilized PEG-NH$_2$ SAM surface with monoclonal anti-TNT antibody was studied by SPR. For the immunoreaction experiments, PBS buffer (pH 7.2) was used as a carrier solution and was flowed over the sensor surface continuously. Fig. 5 depicts the SPR response observed for the flow of 10 μg/ml of M-TNT Ab over the TNPh-β-alanine immobilized surface at a rate of 100 μl/min for 2 min. A shift in the resonance angle of $0.0283 \pm 0.0005°$ ($n = 12$) indi-

cates the good interaction between the M-TNT Ab and the TNT on the TNPh-β-alanine immobilized surface, which can also be evidenced from the stable response angle during the flow of PBS after completion of the antibody flow.

The regeneration of the sensor surface was achieved by the flow of pepsin solution (5 μg/ml in glycine–HCl buffer) as shown in Fig. 5. As the pepsin solution injected, the resonance angle jumped up due to the difference in the refractive index between pepsin solution and PBS buffer. After completion of the pepsin injection and the flow switched to PBS buffer, the response angle decreased to the original level (before antibody injection), which indicates the good surface regeneration process favoring multiple analyses.

3.4. Detection of TNT by indirect competitive immunoassay

Detection of TNT was carried out by indirect competitive immunoreaction method. Standard TNT solutions (in the range from 10^{-2} to 10^6 pg/ml) incubated with 10 μg/ml of M-TNT Ab were allowed to flow over the TNT immobilized SAM surface. Fig. 6 shows the SPR responses for the binding interaction between TNT immobilized SAM surface and M-TNT Ab in the absence and in the presence of different concentrations of TNT. As can be seen, the response angle decreased progressively with increasing free TNT concentration, which clearly indicates that TNT in solution inhibited the binding interaction between M-TNT Ab and the TNT immobilized PEG-NH$_2$ SAM surface. After each immunoreaction, the surface was regenerated by a brief injection of pepsin solution. Each TNT concentration was measured at least five time and the response showed good reproducibility.

The relationship between the concentration of free TNT and the percentage of inhibition was shown in Fig. 7. With the present self-assembled immunoassay format, TNT can be detected in the concentration range from 0.008 ng/ml (8 ppt) to 30 ng/ml (ppb). The linear dose-response range was considered between 10% and 90% of inhibition. This sensitivity is highly comparable to most of the other immunoassays demonstrated for TNT (noted in the introduction part). The high sensitivity observed here is possibly due to the surface chemistry of the self-assembled PEG-
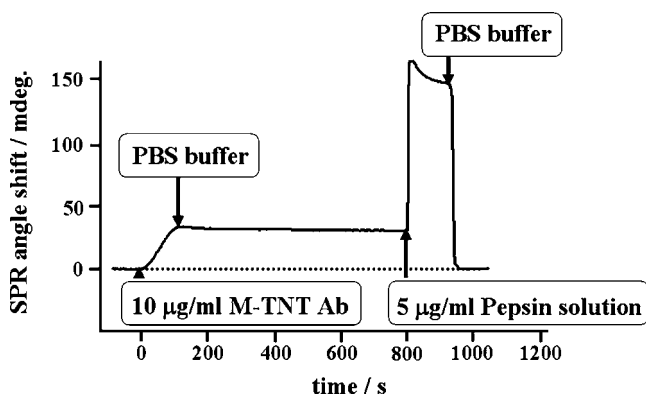

Fig. 5. SPR response for the flow of 10 μg/ml M-TNT Ab over TNT immobilized PEG-NH$_2$ SAM surface followed by elution with pepsin solution. Carrier solution: PBS, flow speed: 100 μl/min, flow duration: 2 min.
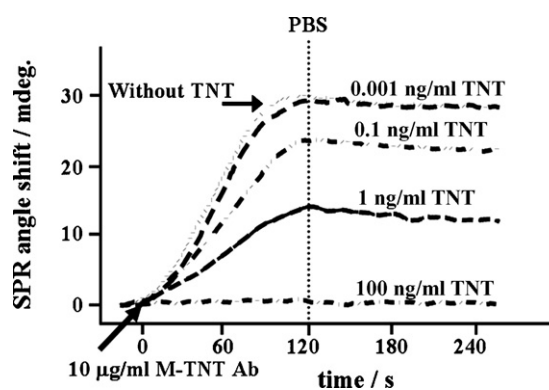

Fig. 6. SPR response for the immunoreaction between M-TNT Ab and TNT immobilized PEG-NH$_2$ SAM surface in the absence and in the presence of TNT. Carrier solution: PBS, flow rate: 100 μl/min, flow duration: 2 min.
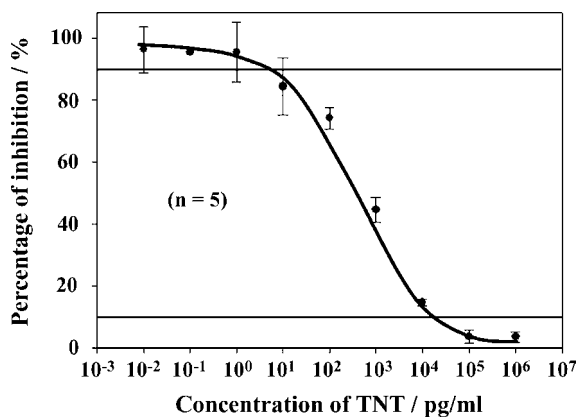
Fig. 7. The sensitivity curve of TNT detection.

NH_2 layer, which maintained the activity of the immobilized TNT towards M-TNT Ab and also diminished the non-specific adsorption.

3.5. Stability of the immunosensor

It is highly desirable to produce stable and regenerable sensor surface for multiple analysis. We evaluated the stability and reproducibility of the present sensor for detection of TNT. Fig. 8 depicts the stability response of the immunosensor surface on multiple regeneration cycles. We observed that the TNT immobilized PEG-NH_2 SAM surface was highly robust and reproducible for more than 100 cycles without any significant change in the original activity. This stability is highly advantageous compared to other immunosensors reported for TNT including our previous study using the immunoreaction of a home-made polyclonal antibody with a physically immobilized TNP–BSA conjugate [33]. Moreover, the self-assembled PEG surface is highly effective in the prevention of the non-specific adsorption. These characteristics are highly appreciable for cost and time effective use of the proposed immunosensor for reliable and error free measurement of TNT.
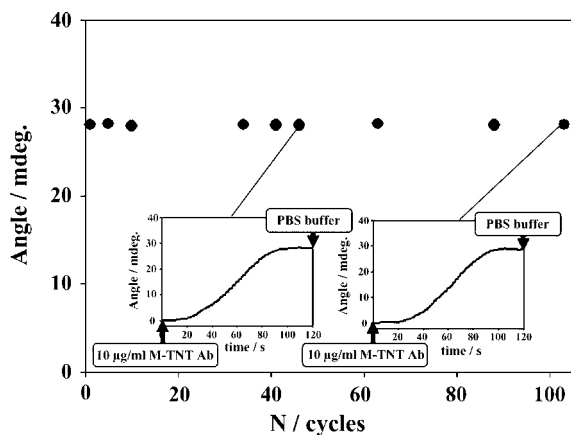

Fig. 8. The stability of the immunoreaction between TNT immobilized PEG-NH_2 SAM surface and M-TNT Ab on multiple cycles. Carrier solution: PBS, flow rate: 100 μl/min, flow duration: 2 min.

3.6. Cross-reactivity studies

Cross-reactivity is an important analytical parameter regarding specificity and reliability of immunoassays. We studied the interference effect from the TNT analogues for the detection of TNT to evaluate the suitability of the proposed systems for possible application to the real sample analysis. Several TNT related compound such as, 2,4-DNT, 2-A-4,6-DNT, 4-A-2,6-DNT, and RDX were mixed with standard TNT samples and the resulting interference effects were monitored by indirect inhibition method. The results showed the cross-reactivity values of 0.92, 1.15, 0.11, and 0.035% for 2,4-DNT, 2-A-4,6-DNT, 4-A-2,6-DNT, and RDX, respectively. The cross-reactivity values are calculated using the formula; cross-reactivity $= (C_0/C) \times 100$, where, C_0 is the concentration of TNT at 50% inhibition and C is the concentration of the cross-reacting analyte at 50% inhibition. These values indicate that most of the TNT analogues showed small interference effect on TNT detection in the present immunoassay.

4. Conclusions

As immunosensors continues to develop as a promising tool for future explosive detection system, great efforts are under progress around the world to optimize the system components that provide enhanced sensitivity and selectivity for development of field portable systems. In this context, we demonstrated a simple and robust approach for functionalization of sensor surfaces based on self-assembly for detection of TNT. The present immunoassay exhibited a good sensitivity with a detection limit of 0.008 ng/ml for TNT. A single immunocycle could be done within 4 min including surface regeneration, favoring rapid detection of TNT. Besides the good stability and reproducibility, the sensor surface was highly effective in avoiding the non-specific adsorption and is an excellent platform for rapid and reliable detection of TNT. The performance of the newly developed platform has shown promising results with good options for possible expansion to multianalyte detection in complex matrices, which is currently under progress in our laboratory.

References

[1] P.B. Luppa, L.J. Sokoll, D.W. Chan, Clin. Chim. Acta 314 (2001) 1.
[2] E.M.D. Barcelo, C.B.G. Gauglitz, R. Abuknesha, Trends Anal. Chem. 20 (2001) 124.
[3] J. Homola, S. Yee, D. Myszka, in: S. Ligler, C.A.R. Taitt (Eds.), Surface Plasmon Resonance Biosensors, Elsevier, The Netherlands, 2002, pp. 207–251.
[4] C.L. Baird, D.G. Myszka, J. Mol. Recognit. 14 (2001) 261.

[5] M.A. Cooper, Nat. Rev. Drug Discov. 1 (2002) 515.

[6] N. Miura, H. Higobashi, G. Sakai, A. Takeyasu, T. Uda, N. Yamazoe, Sens. Actuators B 13–14 (1993) 188.

[7] N. Miura, K. Ogata, G. Sakai, T. Uda, N. Yamazoe, Chem. Lett. 26 (1997) 713.

[8] D.R. Shankaran, K.V. Gobi, T. Sakai, K. Matsumoto, K. Toko, N. Miura, Biosens. Bioelectron 20 (2005) 1750.

[9] S. Cosnier, Biosens. Bioelecton 14 (1999) 443.

[10] D.A. Buttterfield, J. Colvin, J.L. Liu, J.Q. Wang, L. Bachas, D. Bhatacharrya, Anal. Chim. Acta 470 (2002) 29.

[11] E.H. Lan, B. Dunn, J.I. Zink, Chem. Mater. 12 (2000) 1874.

[12] R. Liang, J. Qiu, P. Cai, Anal. Chim. Acta 534 (2005) 223.

[13] K.V. Gobi, C. Kataoka, N. Miura, Sens. Actuators B 108 (2005) 784.

[14] W. Lee, B.K. Oh, Y.M. Bae, S.H. Paek, W.H. Lee, J.W. Choi, Biosens. Bioelectron 19 (2003) 185.

[15] S.S. Mark, N. Sandhyarani, C. Zhu, C. Campagnolo, C.A. Batt, Langmuir 20 (2004) 6808.

[16] W. Senaratne, L. Andruzzi, C.K. Ober, Biomacromolecules 6 (2005) 2427.

[17] N.K. Chaki, K. Vijayamohanan, Biosens. Bioelectron 17 (2002) 1.

[18] E.A. Smith, M.J. Wanat, Y. Cheng, S.V.P. Barreira, A.G. Frutos, R.M. Corn, Langmuir 17 (2001) 2502.

[19] Q. Yu, S. Chen, A.D. Taylor, J. Homola, B. Hock, S. Jiang, Sens. Actuators B 107 (2005) 193.

[20] K. Uchida, H. Otsuka, M. Kaneko, K. Kataoka, Y. Nagasaki, Anal. Chem. 77 (2005) 1075.

[21] S. Herrwerth, T. Rosendahl, C. Feng, J. Fick, W. Eck, M. Himmelhaus, R. Dahint, M. Grunze, Langmuir 19 (2003) 1880.

[22] H.B. Lu, C.T. Campbell, D.G. Castner, Langmuir 16 (2000) 1711.

[23] J. Yinon, Trends Anal. Chem. 21 (2002) 292.

[24] A.M. Rouhi, Chem. Eng. News 75 (1997) 1.

[25] Environmental Protection Agency, Health Advisory for TNT. Criteria and Standard Division. Office of Drinking Water, Washington, DC, 1989.

[26] P.T. Charles, J.G. Rangasammy, G.P. Anderson, T.C. Romanoski, A.W. Kusterbeck, Anal. Chim. Acta 525 (2004) 199.

[27] R. Wilson, C. Clavering, A. Hutchinson, Anal. Chem. 75 (2003) 4244.

[28] J. Bowen, L.J. Noe, B.P. Sullivan, K. Morris, V. Martin, G. Donnelly, Appl. Spectrosc. 57 (2003) 906.

[29] K.E. Sapsford, P.T. Charles, C.H. Patterson, F.S. Ligler, Anal. Chem. 74 (2002) 1061.

[30] T.M. Green, P.T. Charles, G.P. Anderson, Anal. Biochem. 310 (2002) 36.

[31] A. Zeck, M.G. Weller, R. Niessner, Fres. J. Anal. Chem. 364 (1999) 113.

[32] E.R. Goldman, G.P. Anderson, N. Lebedev, B.M. Lingerfelt, P.T. Winter, C.H. Patterson, J.M. Mauro, Anal. Bioanal. Chem. 375 (2003) 471.

[33] D.R. Shankaran, K. Matsumoto, K. Toko, N. Miura, Sens. Actuators B 114 (2006) 71.

[34] D.R. Shankaran, K.V. Gobi, T. Sakai, K. Matsumoto, T. Imato, K. Toko, N. Miura, IEEE Sens. J. 5 (2005) 616.

[35] N. Miura, H. Higobashi, G. Sakai, A. Takeyasu, T. Uda, N. Yamazoe, Proceeding of the Technical Digest of the 4th International Meeting on Chemical Censors, Tokyo, 1992, p. 228.

[36] N. Miura, M. Sasaki, K.V. Gobi, C. Kataoka, Y. Shoyama, Biosens. Bioelectron 18 (2003) 953.

[37] T. Kawaguchi, H. Yasuda, K. Shimazu, M.D. Porter, Langmuir 16 (2000) 9830.

Preparation and characterization of a new organic–inorganic nano-composite poly-*o*-toluidine Th(IV) phosphate: Its analytical applications as cation-exchanger and in making ion-selective electrode

Asif Ali Khan*, Anish Khan, Inamuddin

Analytical and Polymer Research Laboratory, Department of Applied Chemistry, Faculty of Engineering and Technology,
Aligarh Muslim University, Aligarh 202002, India

Abstract

An organic–inorganic hybrid poly-*o*-toluidine Th(IV) phosphate was chemically synthesized by mixing *ortho*-tolidine into the gel of Th(IV) phosphate in different mixing volume ratios, concentration of inorganic reactant with a fixed mixing volume ratios of organic polymer. The physico-chemical characterization was carried out by elemental analysis, TEM, SEM, XRD, FTIR and simultaneous TGA–DTA studies. The ion-exchange capacity, chemical stability, effect of eluant concentration, elution behavior and pH titration studies were also carried out to understand the ion-exchange capabilities. The distribution studies revealed that the cation-exchange material is highly selective for Hg^{2+}, which is an important environmental pollutant. Due to selective nature of the cation-exchanger ion-selective membrane electrode was fabricated for the determination of Hg(II) ions in solutions. The analytical utility of this electrode was established by employing it as an indicator electrode in electrometric titrations.
© 2006 Elsevier B.V. All rights reserved.

Keywords: Organic–inorganic hybrid; Cation-exchanger; Poly-*o*-toluidine Th(IV) phosphate

1. Introduction

Organic–inorganic hybrid, a new class of materials is attractive for the creating high performance or high functional polymeric behaviors that are expected to provide many possibilities. Hybrid can be used to modify organic polymeric material or to modify inorganic materials that exhibit very different properties from their original component. The inorganic ion-exchange materials besides other advantages are important in being more stable to high temperature and radiation field than the organic ones [1]. In order to obtain a combination of these advantages associated with polymeric and inorganic materials as ion-exchangers, attempts have been made to develop polymeric-inorganic composite ion-exchangers by incorporation of organic monomers in the inorganic matrix [2]. Few such excellent ion-exchange materials have been developed in our laboratory and successfully being used in chromatographic techniques [3–5]. An inorganic precipitate ion-exchanger based on

organic polymeric matrix must be an interesting material, as it should possess the mechanical stability due to the presence of organic polymeric species and the basic characteristics of an inorganic ion-exchanger regarding its selectivity for some particular metal ions [6–12]. It was therefore considered to synthesize such hybrid ion-exchangers with a good ion-exchange capacity, high stability, reproducibility and selectivity for heavy metal ions, indicating its useful environmental application.

Mercury is responsible for causing poisoning through water, food and smoking. Mercury contamination in drinking water inhibits the function of certain enzymes necessary for the formation of haem in bone marrow, the pigment that combines with protein to form haemoglobin. Its vapor, on inhalation, enters the brain through the blood stream and causes severe damage to the central nervous system. Inorganic mercuric compounds mainly attack liver and kidney. Mercuric chloride is corrosive and, when ingested, precipitates proteins of the mucous membrane causing ashen appearance of the mouth, pharynx and gastric mucus. Organic mercurial are the mist toxic substances; the CH_3Hg^+ can pass through the placental barrier and enter the foetal tissues. Hg(II) is therefore a potential pollutant in the environment. Heavy metal ion removal from

---

* Corresponding author. Tel.: +91 571 2720323.
E-mail address: asifkhan42003@yahoo.com (A.A. Khan).

waters has been the subject of extensive technological research [13].

The ion-exchange membranes obtained by embedding ion-exchangers as electroactive materials in a polymer binder, i.e. PVC, has been extensively used as potentiometric sensors, i.e. ion sensors, chemical sensors or more commonly ion-selective electrodes. In our present studies attempt has been made to obtain a new heterogeneous precipitate based membrane electrode by using the poly-o-toluidine Th(IV) phosphate, a nano-composite cation-exchanger as an electroactive material for the determination of Hg(II) ion present in the sample solution.

2. Experimental

2.1. Reagents and instruments

The main reagents used for the synthesis of the material were obtained from CDH, Loba Chemie, E-Merck and Qualigens (India Ltd., used as received). All other reagents and chemicals were of analytical grade. Following instruments were used during present research work: a FTIR spectrophotometer (Perkin-Elmer, USA, model Spectrum-BX); digital pH-meter (Elico Li-10, India); X-ray diffractometer—Phillips (Holland), model PW 1148/89; UV/VIS spectrophotometer—Elico, model EI 301E; a thermal analyzer—V2.2A DuPont 9900; an elemental analyzer—Elementary Vario EL III, Carlo-Erba, model 1108; a digital potentiometer (Equiptronics EQ 609, India); accuracy ± 0.1 mV with a saturated calomel electrode as reference electrode; an electronic balance (digital, Sartorius-21OS, Japan) and an automatic temperature controlled water bath incubator shaker—Elcon (India) were used.

2.2. Preparation of reagents

Thorium nitrate $Th(NO_3)_4 \cdot 5H_2O$ and phosphoric acid, H_3PO_4 solutions of different molarities were prepared in 1 M HNO_3 and demineralised water (DMW), respectively.

2.3. Preparation of poly-o-toluidine Th(IV) phosphate composite

2.3.1. Synthesis of poly-o-toluidine

The polymerization of the monomer ortho-tolidine was initiated by the addition of oxidizing agent, i.e. ammonium persulphate in 1:1 ratio under constant stirring at room temperature for 2 h [14]. After 2 h a brown colored poly-o-toluidine polymer was obtained.

2.3.2. Synthesis of thorium(IV) phosphate

The method of preparation of the inorganic precipitate of Th(IV) phosphate ion-exchanger was very similar to that of Alberti and Constantino with slight modification [15] by mixing a solution of 0.1 M $Th(NO_3)_4 \cdot 5H_2O$ prepared in 1 M HNO_3 at the flow rate at 0.5 ml min^{-1} to a solution of H_3PO_4 in different molarities. Constant string was done during mixing using a magnetic stirrer at a temperature of 85 °C, white gel type slurries

were obtained. After digestion of the mixture for several hours, it was cooled to room temperature in each case.

2.3.3. Synthesis of poly-o-toluidine Th(IV) phosphate

The composite cation-exchanger was prepared by the sol–gel mixing of poly-o-toluidine an organic polymer into the inorganic precipitate of thorium(IV) phosphate. In this process, when the gels of poly-o-toluidine were added to the white inorganic precipitate of thorium(IV) phosphate with a constant stirring, the resultant mixture was turned slowly into brown colored slurries. The resultant brown colored slurries were kept for 24 h at room temperature.

Now, the poly-o-toluidine based composite cation-exchanger gels were filtered off, washed thoroughly with DMW to remove excess acid and any adhering trace of ammonium persulphate. The washed gels were dried over P_4O_{10} at 30 °C in an oven. The dried products were immersed in DMW to obtain small granules. They were converted to the H$^+$ form by keeping it in 1 M HNO_3 solution for 24 h with occasionally shaking intermittently replacing the supernatant liquid. The excess acid was removed after several washing with DMW. The material was finally dried at 40 °C and sieving to obtain particles of particular size range ($\sim 125 \mu m$). Hence, a number of poly-o-toluidine thorium(IV) phosphate nano-composite cation-exchanger samples were prepared and on the basis of Na$^+$ exchange capacity (i.e.c.), percent of yield and physical appearance, sample S-3 was selected for further studies.

2.4. Ion-exchange capacity (i.e.c.)

The ion-exchange capacity, which is generally taken as a measure of the hydrogen ion liberated by neutral salt to flow through the composite cation-exchanger was determined by standard column process. One gram of the dry cation-exchanger sample S-3 in the H$^+$-form was taken into a glass column having an internal diameter (i.d.) ~ 1 cm and fitted with glass wool support at the bottom. The bed length was approximately 1.5 cm long. One molar alkali and alkaline earth metal nitrates as eluants were used to elute the H$^+$ ions completely from the cation-exchange column, maintaining a very slow flow rate (~ 0.5 ml min^{-1}). The effluent was titrated against a standard 0.1 M NaOH using phenolphthalein indicator.

2.5. Effect of eluant concentration

To find out the optimum concentration of the eluant for complete elution of H$^+$ ions, a fixed volume (250 ml) of sodium nitrate (NaNO$_3$) solutions of varying molar concentration were passed through a column containing 1 g of the exchanger in the H$^+$-form with a flow rate of ~ 0.5 ml min^{-1}. The effluent was titrated against a standard alkali solution of 0.1 M NaOH for the H$^+$ ions eluted out. A maximum elution was observed with the concentration of 1.6 M NaNO$_3$ as indicated in Fig. 1.
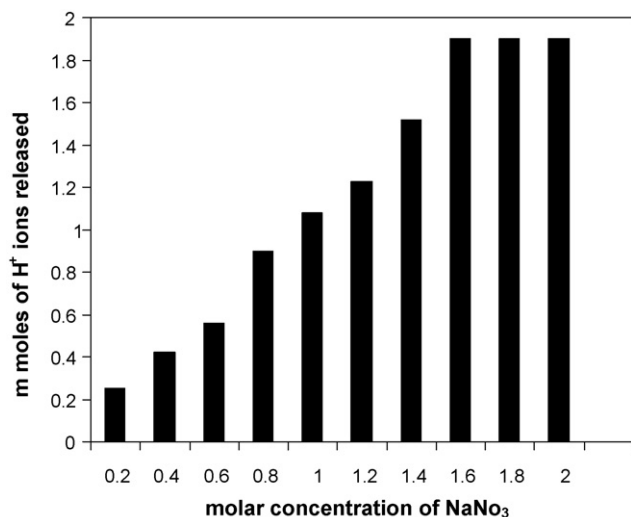
Fig. 1. Concentration plot of poly-*o*-toluidine Th(IV) phosphate.

2.6. Elution behavior

Since an optimum concentration Fig. 2 for a complete elution was observed to be 1.6 M for sample S-3, a column containing 1 g of the exchanger in H$^+$-form was eluted with NaNO$_3$ solution of this concentration in different 10 ml fractions with minimum flow rate as described above and each fraction of 10 ml effluent was titrated against a standard alkali solution for the H$^+$ ions eluted out.

2.7. pH-titration

pH-titration studies of poly-*o*-toluidine Th(IV) phosphate nano-composite cation-exchanger (S-3) was performed by the method of Topp and Pepper [16]. A total of 500 mg portions
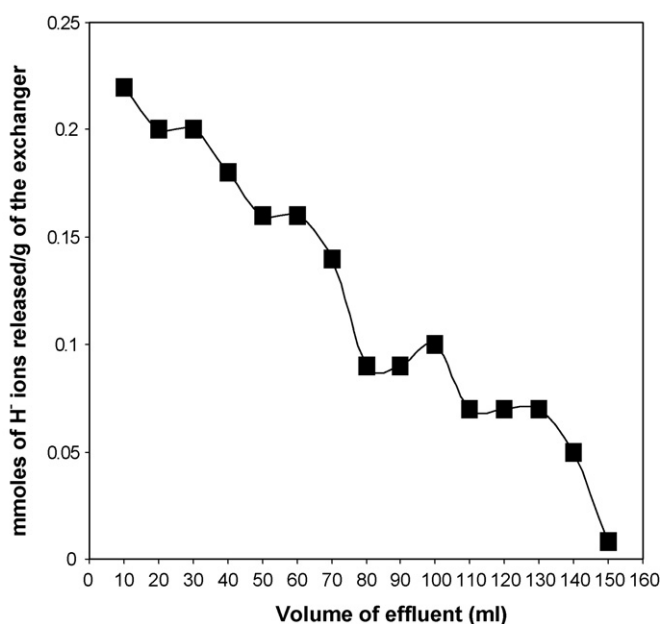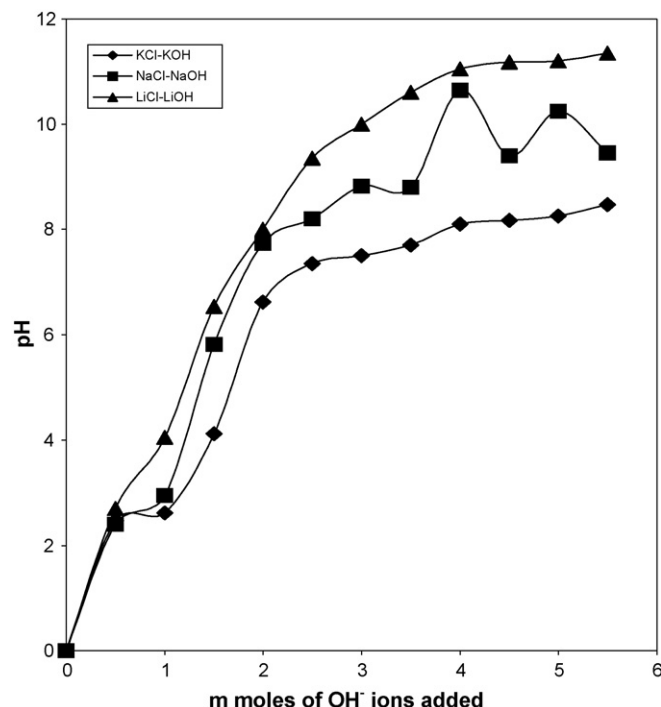

Fig. 3. pH-titration curves for poly-*o*-toluidine Th(IV) phosphate nano-composite cation-exchanger.

of the cation-exchanger in the H$^+$-form were placed in each of the several 250 ml conical flasks, followed by the addition of equimolar solutions of alkali metal chlorides and their hydroxides in equal volume ratio, the final volume is being 50 ml to maintain the ionic strength constant. The pH of the solution was recorded every 24 h until equilibrium was attained which needed 5 days. The pH at equilibrium was plotted against the *m* moles of OH$^-$ ions added (Fig. 3)

2.8. Chemical dissolution

Two hundred fifty milligrams portions of the composite cation-exchanger (poly-*o*-toluidine Th(IV) phosphate, S-3) in H$^+$-form were treated with 20 ml each of different acids such as HCl, HNO$_3$, H$_2$SO$_4$, HClO$_4$, different bases such as NaOH, KOH, NH$_4$OH, salt (NaNO$_3$) and organic solvents such as dimethyl sulphoxide (DMSO), acetone, *n*-butyl alcohol, and also with double distilled water (DMW) for 24 h with occasional shaking.

2.9. Chemical composition

The chemical composition of poly-*o*-toluidine Th(IV) phosphate nano-composite cation-exchanger (sample S-3) was determined by using elemental analyzer, inductively coupled plasma mass spectrophotometer and UV–vis spectrophotometer for CHN, Th and phosphorous, respectively. The weight percent composition of C, H, N, Th, P and O in the material was found to be 38.85, 4.579, 8.26, 36.62 and 1.88 and 9.81, respectively.

Fig. 2. The elution behavior of poly-*o*-toluidine Th(IV) phosphate cation-exchange material.

2.10. Thermal studies

To study the effect of temperature on the i.e.c., 1 g samples of the composite cation-exchange material (S-3) in the H^+-form were heated at various temperatures in a muffle furnace for 1 h and the Na^+ ion-exchange capacity was determined by column process after cooling them at room temperature.

Simultaneous TGA and DTA studies of the composite cation-exchange material (poly-o-toluidine Th(IV) phosphate, S-3) in original form were carried out by an automatic thermo balance on heating the material from 10 to 1000 °C at a constant rate (10 °C min^{-1}) in the air atmosphere (air flow rate of 400 ml min^{-1}).

2.11. Fourier transform infra red (FTIR) studies

The FTIR spectrum of poly-o-toluidine (sample S-4); Th(IV) phosphate (sample S-5) and poly-o-toluidine Th(IV) phosphate (sample S-3) in the original form dried at 40 °C were taken by KBr disc method at room temperature.

2.12. X-ray analysis

Powder X-ray diffraction (XRD) pattern was obtained in an aluminum sample holder for the sample S-3 in the original form using a PW 1148/89 based diffractometer with Cu Kα radiations.

2.13. Transmission electron microscopy (TEM) studies

TEM studies were carried out to know the particle size of the poly-o-toluidine Th(IV) phosphate composite cation-exchange material.

2.14. Scanning electron microscopy (SEM) studies

Microphotographs of the original form of poly-o-toluidine (S-4); inorganic precipitate of Th(IV) phosphate (S-5); and organic–inorganic composite material poly-o-toluidine thorium(IV) phosphate (S-3); were obtained by the scanning electron microscope at various magnifications.

2.15. Selectivity (sorption) studies

The distribution coefficient (K_d values) of various metal ions on poly-o-toluidine Th(IV) phosphate nano-composite were determined by batch method in various solvent systems. Various 200 mg of the composite cation-exchanger beads (S-3) in the H^+-form were taken in Erlenmeyer flasks with 20 ml of different metal nitrate solutions in the required medium and kept for 24 h with continuous shaking for 6 h in a temperature controlled incubator shaker at 25 ± 2 °C to attain equilibrium. The initial metal ion concentration was so adjusted that it did not exceed 3% of its total ion-exchange capacity. The metal ions in the solution before and after equilibrium were determined by titrating against standard 0.005 M solution of EDTA [17]. The alkaline earth metal ion [Ca^{2+}] was determined by flame photometry and some heavy metal ions such as [Pb^{2+}, Cd^{2+}, Cu^{2+}, Hg^{2+}, Ni^{2+},

Zn^{2+}] were determined by atomic absorption spectrophotometry (AAS). The distribution quantity is given by the ratio of amount of metal ion in the exchanger phase and in the solution phase. In other words, the distribution coefficient is the measure of a fractional uptake of metal ions competing for H^+ ions from a solution by an ion-exchange material and hence mathematically can be calculated using the formula given as:

$$K_d = \frac{m \, \text{mol metal ions/g ion-exchanger}}{m \, \text{mol metal ions/ml solution}} (\text{ml g}^{-1}) \qquad (1)$$

i.e.

$$K_d = \left[\frac{I - F}{F}\right] \left[\frac{V}{M}\right] (\text{ml g}^{-1}) \qquad (2)$$

where I is the initial amount of metal ion in the aqueous phase, F the final amount of metal ion in the aqueous phase, V the volume of the solution (ml) and M is the amount of cation-exchanger (g).

2.16. Preparation of poly-o-toluidine Th(IV) phosphate cation-exchange membrane

Ion-exchange membrane of poly-o-toluidine Th(IV) phosphate was prepared as the method reported by Khan and Inamuddin [18] in earlier studies. To find out the optimum membrane composition, different amounts of the composite material was grounded to a fine powder and mixed thoroughly with a fixed amount (200 mg) of PVC dissolved in 10 ml tetrahydrofuran. The resultant slurries were poured to cast in glass tube having 10 cm in length 5 mm in diameter. These glass tubes were left for slow evaporation for several hours. In this way, three sheets of different thicknesses 0.15, 0.17 and 0.22 mm were obtained. A fixed area of the membranes was cut using sharp edge blade.

2.17. Characterization of membrane

The important factors to check the performance of the membrane, three parameters were determined as reported earlier [19–22].

2.17.1. Water content (% total wet weight)
First the membranes were soaked in water to elute diffusible salt, blotted quickly with Whatmann filter paper to remove surface moisture and immediately weighted. These were further dried to a constant weight in a vacuum over P_2O_5 for 24 h. The water content (total wet weight) was calculated as:

$$\% \, \text{Total wet weight} = \frac{W_w - W_d}{W_w} \, 100$$

where W_w is the weight of the soaked/wet membrane and W_d is the weight of the dry membrane.

2.17.2. Porosity
Porosity (ε) was determined as the volume of water incorporated in the cavities per unit membrane volume from the water

content data:

$$\varepsilon = \frac{W_w - W_d}{AL\rho_w}$$

where W_w is the weight of the soaked/wet membrane, W_d the weight of the dry membrane, A the area of the membrane, L the thickness of the membrane and ρ_w is the density of water.

2.17.3. Thickness and swelling

The thickness of the membrane was measured by taking the average thickness of the membrane by using screw gauze. Swelling is measured as the difference between the average thicknesses of the membrane equilibrated with 1 M NaCl for 24 h and the dry membrane.

2.18. Fabrication of ion-selective membrane electrode

The membrane sheet of 0.17 mm thickness as obtained by the above procedure was cut in the shape of disc and mounted at the lower end of a Pyrex glass tube (o.d. 0.8 cm, i.d. 0.6) with araldite. Finally, the assembly was allowed to dry in air for 24 h. The glass tube was filled with 0.1 M mercuric nitrate solution. A saturated calomel electrode was inserted in the tube for electrical contact and another saturated calomel electrode was used as external reference electrode. The whole arrangement can be shown as:

Internal reference electrode (SCE) | internal

    electrolyte 0.1 M Hg^{2+} | membrane | sample solution |

    external reference electrode (SCE)

Following parameters were evaluated to study the characteristics of the electrode such as lower detection limit, electrode response curve, response time and working pH range.

2.19. Electrode response or membrane potential

To determine the electrode response, a series of standard solutions of varying concentrations ranging from 10^{-1} to 1^{-10} were prepared. External electrode and ion-selective membrane electrode are plugged in digital potentiometer and the potentials were recorded.

For the determination of electrode potential the membrane of the electrode was conditioned by soaking in 0.1 M Hg(NO$_3$)$_2$ solution for 5–7 days and for 1 h before use. When electrode was not in use electrode must be kept in 0.1 M Hg(NO$_3$)$_2$ solution. Potential measurement was plotted against selected concentration of the respective ion in aqueous solution.

2.20. Effect of pH

pH solutions ranging from 1 to 13 were prepared at constant ion concentration, i.e. (1×10^{-2} M). The value of electrode potential at each pH was recorded and plot of electrode potential versus pH was plotted.

2.21. The response time

The method of determining response time in the present work is being outlined as follows.

The electrode is first dipped in a 1×10^{-3} M solution of Hg(NO$_3$)$_2$ and 10-fold higher concentration. The potential of the solution was read at 0 s; just after dipping of the electrode in the second solution and subsequently recorded at the intervals of 5 s. The potentials were then plotted versus time.

2.22. Determination of Hg^{2+} by potentiometric titrations using poly-o-toluidine Th(IV) phosphate nano-composite membrane electrode

The practical utility of the proposed membrane sensor assembly was tested by its use as an indicator electrode in the potentiometric titration of Hg(II) with EDTA.

2.23. Life span of the membrane

For this study, the electrode responses were noted for one or more weeks over weak and response curve is drawn for the data. The electrode response curve showed that the response remains constant over a period of time. After this period the electrode starts behaving irregular, therefore cannot be used for any measurements. This period in which the electrode response is constant can be termed as life of electrode.

3. Results and discussion

Various samples of a new and novel organic–inorganic composite cation-exchange material have been developed by the incorporation of electrically conducting polymer poly-o-toluidine into the inorganic matrices of fibrous Th(IV) phosphate. Due to the high percentage of yield, better ion-exchange capacity, reproducible behavior, chemical and thermal stabilities, sample S-3 (Table 1) was chosen for the details of the ion-exchange studies.

The composite cation-exchange material possessed a better Na$^+$ ion-exchange capacity (1.90 meq g^{-1}) as compared to inorganic precipitate of fibrous type Th(IV) phosphate (0.72 meq g^{-1}) [15].

The ion-exchange capacity of the composite cation-exchanger for alkali metal ions and alkaline earth metal ions increased according to the decrease in their hydrated ionic radii (Table 2). The ion-exchange capacity of dried composite cation-exchanger sample (S-3) decreased as the temperature increased. The ion-exchange capacity of the material was found stable upto 150 °C and it retained about 61% of the initial ion-exchange capacity by heating upto 250 °C (Table 3).

It is evident from Fig. 1 that minimum molar concentration of NaNO$_3$ as eluant for sample (S-3) was found to be 1.6 M for maximum release of H$^+$ ions from 1 g of the cation-exchanger column. The elution behavior indicates that the exchange is quite fast because only 250 ml of sodium nitrate solution (1.6 M) is enough to release the total H$^+$ from 1 g sample of poly-

Table 1
Conditions of preparation and the ion-exchange capacity of poly-o-toluidine Th(IV) phosphate composite cation-exchange materials

| Sample no. | Mixing volume ratios (v/v) | | Heating time (h) | Heating temperature (°C) | Mixing volume ratios (v/v) | | Appearance of the sample | Na$^+$ ion-exchange capacity (meq dry g^{-1}) |
	Th(NO$_3$)$_4$·5H$_2$O in 1 M HNO$_3$	H$_3$PO$_4$			0.1 M (NH$_4$)$_2$S$_2$O$_8$ in 1 M HCl	10% ortho-toluidine in 1 M HCl		
S-1	1 (0.1 M)	1 (1 M)	2	85	1	1	Fibrous brown	1.26
S-2	1 (0.1 M)	1 (1 M)	4	85	1	1	Fibrous brown	1.60
S-3	1 (0.1 M)	2 (1 M)	4	85	1	1	Fibrous brown	1.90
S-4	–	–	–	–	1	1	Reddish	0.11
S-5	5 (0.1 M)	2 (2 M)	4	85	–	–	White sheet	0.72
S-6	2 (0.1 M)	1 (1 M)	4	85	1	1	Fibrous brown	1.15
S-7	3 (0.1 M)	1 (1 M)	4	85	1	1	Fibrous brown	1.18
S-8	3 (0.1 M)	1 (2 M)	4	85	1	1	Fibrous brown	1.24
S-9	3 (0.1 M)	1 (2.4 M)	4	85	1	1	Fibrous brown	1.04
S-10	5 (0.1 M)	1 (2.5 M)	4	85	1	1	Fibrous brown	0.95
S-11	1 (0.2 M)	4 (1 M)	4	85	1	1	Fibrous brown	1.60
S-12	1 (0.2 M)	2 (1 M)	4	85	1	1	Fibrous brown	1.52
S-13	1 (0.2 M)	2 (2 M)	4	85	1	1	Fibrous brown	1.44

Table 2
Ion-exchange capacity of various exchanging ions on poly-o-toluidine Th(IV) phosphate composite cation-exchanger

Exchanging ions	pH of the metal solution	Ionic radii	Hydrated ionic radii	Ion-exchange capacity (meq g^{-1})
Na$^+$	4.99	0.97	2.76	1.90
K$^+$	6.50	1.33	2.32	1.76
Li$^+$	3.30	0.68	3.40	0.40
Mg^{2+}	4.87	0.78	7.00	0.97
Ca^{2+}	6.20	1.06	6.30	0.83
Sr^{2+}	6.02	1.27	–	1.40
Ba^{2+}	6.50	1.43	5.90	1.70

o-toluidine thorium(IV) phosphate cation-exchange material (Fig. 2).

The pH titration curves for poly-o-toluidine Th(IV) phosphate (S-3) were obtained under equilibrium conditions with NaOH/NaCl, KOH/KCl and LiOH/LiCl, systems indicated bifunctional behavior of the material as shown in Fig. 3. For the sample S-3, the rate of H$^+$–Na$^+$ exchange was faster than those of H$^+$–K$^+$ and H$^+$–Li$^+$ exchangers. The solubility experiments showed that the material has good chemical stability, as it is resistant to DMW, 1 M HCl, 0.5 M NaOH, 2 M NH$_4$NO$_3$, buffer pH 10 and 3.75. The chemical dissolution in 1.5 M HNO$_3$, 1 M tetrahydrofuran, 20% alcohol and 0.5 M NaOH is almost

negligible. The percent composition of C, H, N, Th, P and O in the material was found to be 38.85, 4.579, 8.26, 36.62, 1.88 and 9.81, respectively.

It is clear from the thermogravimetric analysis (TGA) curve (Fig. 4) of the material that upto 100 °C only 5.82% weight loss was observed, which may be due to the removal of external H$_2$O molecules present at the surface of the composite [23]. Further weight loss of mass approximately 7% between 100 and 250 °C may be due to the slight conversion of inorganic phosphate into pyrophosphate. Slow weight loss of mass about 5% in between 250 and 600 °C may be due to the slight decomposition of organic part of the material. The thermo-gravimetric analysis

Table 3
Effect of temperature on ion-exchange capacity of poly-o-toluidine Th(IV) phosphate composite cation-exchanger on heating time for 1 h

Serial no.	Heating temperature (°C)	Na$^+$ ion-exchange capacity (meq dry g^{-1})	% Retention of ion-exchange capacity
1	50	1.90	100
2	100	1.90	100
3	150	1.90	100
4	200	1.16	63
5	250	0.92	61
6	300	0.84	48
7	350	0.52	27
8	400	0.20	10.52
9	500	0.08	4.02
10	600	0.00	0.00
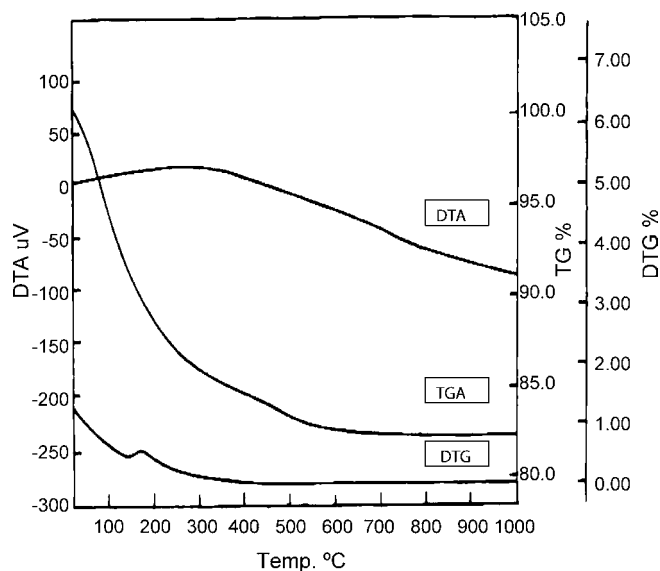
Fig. 4. Simultaneous TGA–DTA curves of poly-*o*-toluidine Th(IV) phosphate (as prepared).

Fig. 6. Power X-ray diffraction pattern of poly-*o*-toluidine Th(IV) phosphate nano-composite.

of the composite exchanger indicates that the composite cation-exchanger is thermally stable because only 18% of mass was lost upto 1000 °C.

The peak values of the FTIR spectra (Fig. 5) of poly-*o*-toluidine Th(IV) phosphate composite material indicates that the band centered at 3367 cm^{-1} results for the characteristics of free N–H stretching vibration, suggest the presence of secondary amino group (–NH–) [14]. The peak at 1640–1560 cm^{-1} represents the free water molecule (water of crystallization) and

strongly bonded –OH group in the matrix [24]. An assembly of two peaks at 980–1072 cm^{-1} may represent the presence of ionic phosphate groups [25]. The I.R. spectrum of composite material can be compared with the spectra of Th(IV) phosphate (S-5) and poly-*o*-toluidine (S-4).

The X-ray diffraction pattern of this materials (S-3 as prepared) recorded in powdered sample exhibited some small peaks in the spectrum (Fig. 6) which suggest semi-crystalline nature of the composite material. From the TEM studies it is clear (Fig. 7) that the poly-*o*-toluidine Th(IV) phosphate cation-exchange material shows particles size in range of 11.0, 10.0, 15.0, 3.0 and 18.0 nm. Thus, the material particle size shows the nano-range. The scanning electron microphotograph (SEM) of poly-*o*-toluidine, Th(IV) phosphate and poly-*o*-toluidine Th(IV) phosphate are represented in Fig. 8. It is clear from the photographs that after binding of organic polymer poly-*o*-toluidine with inorganic precipitate of Th(IV) phosphate. The morphology of the material has been changed with the formation of organic inorganic composite material poly-*o*-toluidine Th(IV) phosphate.

In order to explore the potential of the composite material (S-3) in the separation of metal ions, distribution studies for 15 metal ions were performed in 15 solvent systems, it was observed from the data given in Table 4 that the K_d-values vary with the nature of the contacting solvents. It was also observed from the (K_d) values that Hg^{2+} was strongly adsorbed Zn^{2+}, Ba^{2+}, Ca^{2+} and Al^{3+} are significantly adsorbed while the remaining are partially adsorbed on the surface of ion-exchange material.

The separation capability of the material has been demonstrated by achieving some important binary separations involving Hg^{2+}, viz. Hg^{2+}–Cu^{2+}, Hg^{2+}–Zn^{2+}, Hg^{2+}–Ce^{4+}, Hg^{2+}–Ni^{2+}, Hg^{2+}–Mg^{2+}, Hg^{2+}–Co^{2+}, Hg^{2+}–Ag^{2+}, Pb^{2+}–Ni^{2+} and Pb^{2+}–Fe^{2+} (Table 5). The sequential elution of the ions from the column depends upon the stability of the metal-eluting ligand (eluant). The order of elution and eluant used separation are given in Fig. 9. The separations are quite sharp and recovery is quantitative and reproducible.

Fig. 5. FTIR spectra of as prepared Th(IV) phosphate S-5, poly-*o*-toluidine S-4, and poly-*o*-toluidine Th(IV) phosphate nano-composite cation-exchanger S-3.
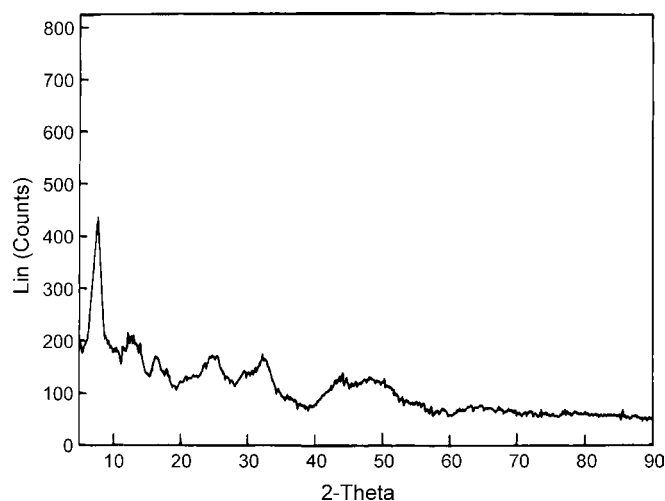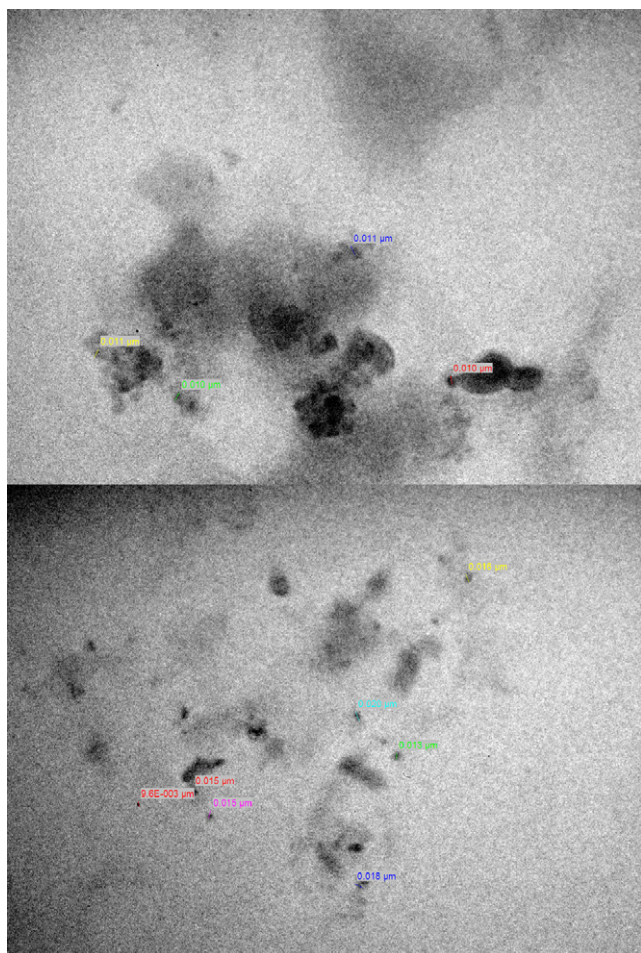
Fig. 7. Transmission electron microphotographs (TEM) of poly-*o*-toluidine Th(IV) phosphate showing different particle sizes.

In this study, organic–inorganic composite cation-exchanger poly-*o*-toluidine Th(IV) phosphate was also used for the preparation of heterogeneous ion-selective membrane electrode.

Sensitivity and selectivity of the ion-selective electrodes depend upon the nature of electro-active material, membrane composition and physico-chemical properties of the membranes employed. A number of samples of the poly-*o*-toluidine Th(IV) phosphate composite membrane were prepared with different amounts of composite material and PVC and checked for the mechanical stability, surface uniformity, materials distribution, cracks and thickness, etc. But the membranes obtained with 33% PVC (w/w) were found to be good.

The results of thickness, swelling, porosity and water content capacity of poly-*o*-toluidine Th(IV) phosphate nano-composite cation-exchanger membrane are summarized in Table 6. The membrane sample M-2 (thickness 0.17 mm) was selected for further studies. Thus, low order of water content, swelling and porosity with less thickness of this membrane suggests that interstices are negligible and diffusion across the membrane would occur mainly through the exchange sites.

The heterogeneous precipitate Hg(II) ion-selective membrane electrode obtained from poly-*o*-toluidine Th(IV) phosphate cation-exchanger material gives linear response in the range 1×10^{-1} and 5×10^{-5} M. Suitable concentrations were chosen for sloping portion of the linear curve. The limit of detection determined from the intersection of the two extrapolated segments of the calibration graph [26] was found to be 5×10^{-5} M, and thus the working concentration range is found to be 1×10^{-1} to 5×10^{-5} M (Fig. 10) for Hg^{2+} ions with a lower Nerstian slope of 26.97 mV per decade change in Hg^{2+} ion concentration, the slope value is blow to Nerstian value, 29.6 mV per concentration decade for divalent cation [27].

pH effect on the potential response of the electrode were measured for a fixed (1×10^{-2} M) concentration of Hg^{2+} ions in different pH values. It is clear that electrode potential remains unchanged within the pH range 4.0–8.0 (Fig. 11), known as working pH for this electrode.

Another important factor is the promptness of the response of the ion-selective electrode. The average response time is defined [28] as the time required for the electrode to reach a stable poten-
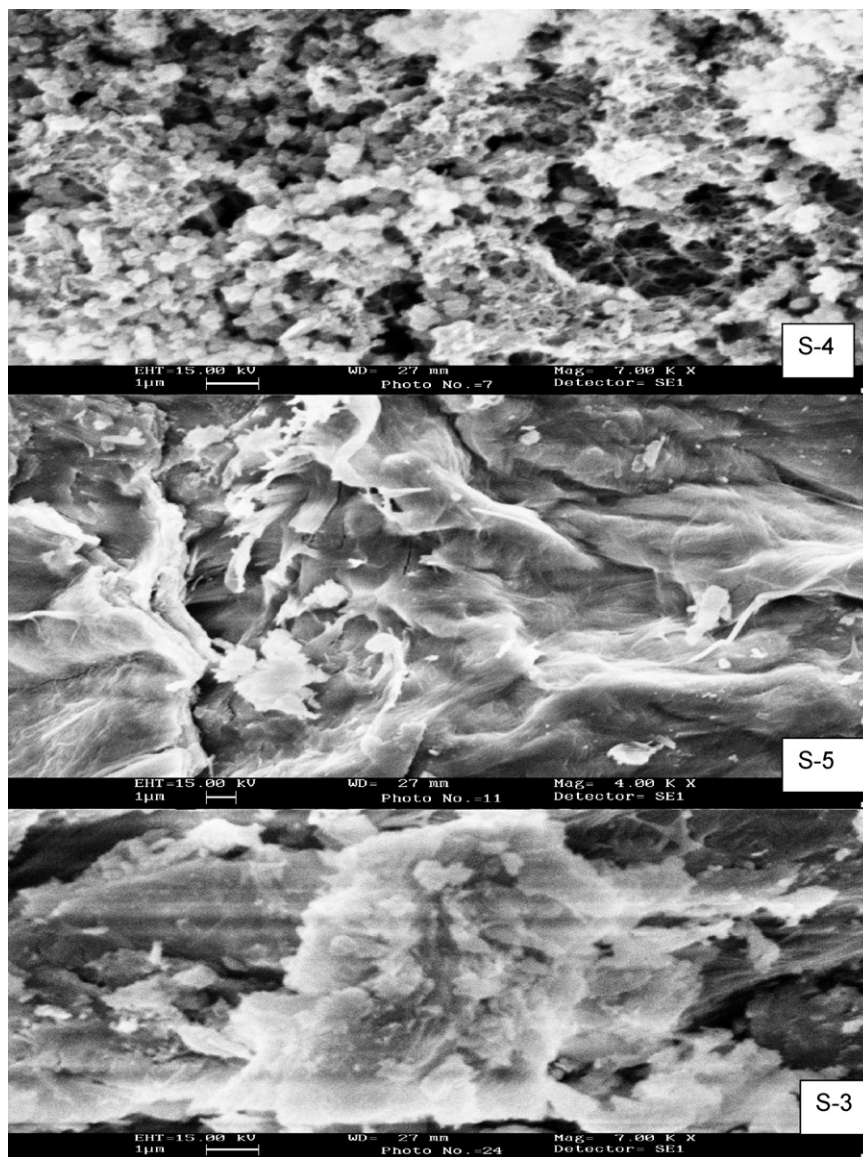
Table 4

K_d-values of some metal ions on poly-*o*-toluidine Th(IV) phosphate nano-composite cation-exchanger column in different solvent system

Solvents	Metal ions														
	Mg^{2+}	Ba^{2+}	Ca^{2+}	Tl^+	Pb^{2+}	Hg^{2+}	Al^{2+}	Ni^{2+}	Fe^{2+}	Ce^{4+}	Co^{2+}	Zn^{2+}	Ag^+	Cu^{2+}	Cd^{2+}
DMW	–	200	100	8	425	66	57	20	200	33	20	400	25	25	25
10^{-3} M HNO$_3$	14	50	36	–	260	200	100	140	300	26	50	10	45	43	43
10^{-2} M HNO$_3$	–	15	13	20	150	116	25	33	–	90	25	50	66	25	25
10^{-1} M HNO$_3$	–	600	50	70	–	–	–	–	–	25	–	100	10	–	–
10^{-3} M HClO$_4$	–	66	33	14	25	300	80	11	57	25	25	–	44	43	43
10^{-2} M HClO$_4$	14	27	70	40	113	150	9	20	–	–	23	400	18	–	–
10^{-1} M HClO$_4$	–	16	13	40	140	140	500	600	66	100	43	150	33	–	–
10^{-3} M CH$_3$COOH	100	67	60	400	260	400	43	40	40	80	–	50	116	50	50
10^{-2} M CH$_3$COOH	100	50	58	90	116	400	1000	16	–	50	50	275	120	63	63
10^{-1} M CH$_3$COOH	–	116	50	40	180	87	–	36	66	100	63	250	200	67	67
CH$_3$COOH + CH$_3$COONa	134	180	200	100	375	275	120	150	60	66	87	150	5	100	100
10% DMSO	56	700	57	200	300	223	43	30	100	80	50	366	18	–	–
10% Acetone	70	45	50	–	200	400	60	16	66	130	60	233	80	–	–
20% Formic acid	–	–	–	160	166	–	100	150	33	–	–	–	–	20	20
10^{-1} M H$_2$SO$_4$	20	17	160		75	400	200	300	60	100	–	–	7	50	50

Fig. 8. Scanning electron microphotographs (SEM) of poly-*o*-toluidine at the magnifications of 7.00k× (S-4), Th(IV) phosphate at the magnification of 4.00k× (S-5) and poly-*o*-toluidine Th(IV) phosphate (S-3) at the magnification of 7.00k×.
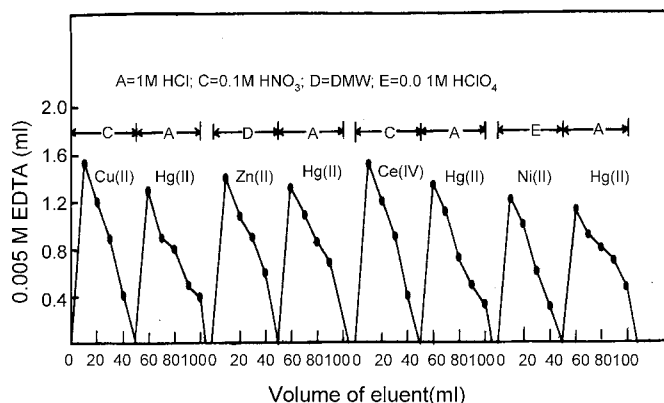

Fig. 9. Binary separations of Hg(II) from Cu(II), Zn(II), Ce(IV), Ni(II) on poly-*o*-toluidine Th(IV) phosphate nano-composite columns.

tial. It is clear (Fig. 12) that the response time of the membrane sensor is found to be ∼25 s.

The membrane could be successfully used upto 7 months without any notable drift in potential during which the potential slope is reproducible within ±1 mV per concentration decade. Whenever a drift in the potential is observed, the membrane is re-equilibrated with 0.1 M Hg(NO$_3$)$_2$ solutions for 3–4 days.

The selectivity coefficients, $K_{\mathrm{Hg\,M}}^{\mathrm{pot}}$ of various differing cations for the Hg(II) ion-selective poly-*o*-toluidine Th(IV) phosphate composite membrane electrode were determined by the mixed solution method [29]. The selectivity coefficient indicates the extent to which a foreign ion (M^{n+}) interferes with the response of the electrode towards its primary ions (Hg^{2+}). By examine the selectivity coefficient data given in Table 7, it is clear that the electrode is selective for Hg(II) in presence of interfering cations.

Table 5
Some binary separations of metal ions achieved on poly-o-toluidine Th(IV) phosphate composite column (A = 1 M HCl; C = 0.1 M HNO$_3$; D = DMW; E = 0.01 M HClO$_4$; F = 0.1 M HClO$_4$)

Separation achieved	Eluant used	Volume of eluant (ml)	Amount of metal loaded (μg)	Amount of metal found (μg)	Error (%)
Hg(II)	A	40	4011.80	4011.80	0.00
Cu(II)	C	40	1271.00	1271.00	0.00
Hg(II)	A	40	4011.80	3961.65	−1.25
Zn(II)	D	40	1307.40	1307.40	0.00
Hg(II)	A	50	4011.80	3961.65	−1.25
Ce(IV)	C	40	2802.30	2802.30	0.00
Hg(II)	A	40	4011.80	3961.65	−1.25
Ni(II)	E	40	880.65	895.33	+1.66
Hg(II)	A	40	300.90	3018.87	−0.33
Mg(II)	E	40	486.10	492.18	+1.25
Hg(II)	A	50	4011.80	3961.65	−1.25
Co(II)	E	50	1001.80	1031.28	+2.94
Hg(II)	A	50	4011.80	3967.65	−1.25
Ag(I)	F	40	1921.62	1968.44	+1.38
Hg(II)	C	40	3315.20	3367.00	+1.56
NI(II)	F	50	1174.20	1174.20	0.00
Hg(II)	C	40	4144.00	4195.00	+1.25
Fe(II)	E	50	1117.00	1103.03	−1.25

Table 6
Characterization of ion-exchange membrane

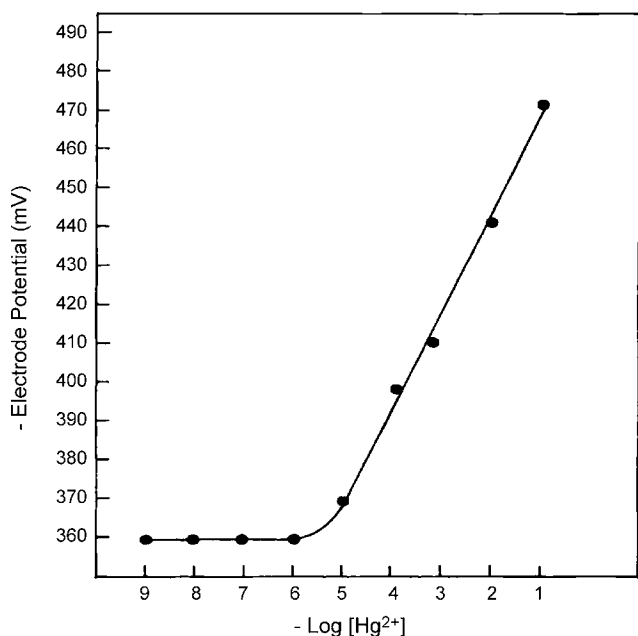| Poly-o-toluidine Th(IV) phosphate composite material	Thickness of the membrane (mm)	Water content as % weight of wet membrane	Porosity	Swelling of % weight of wet membrane
M-1	0.15	0.02517	2.16×10^{-4}	No swelling
M-2	0.17	0.01957	1.85×10^{-4}	No swelling
M-3	0.22	0.13397	2.16×10^{-3}	No swelling

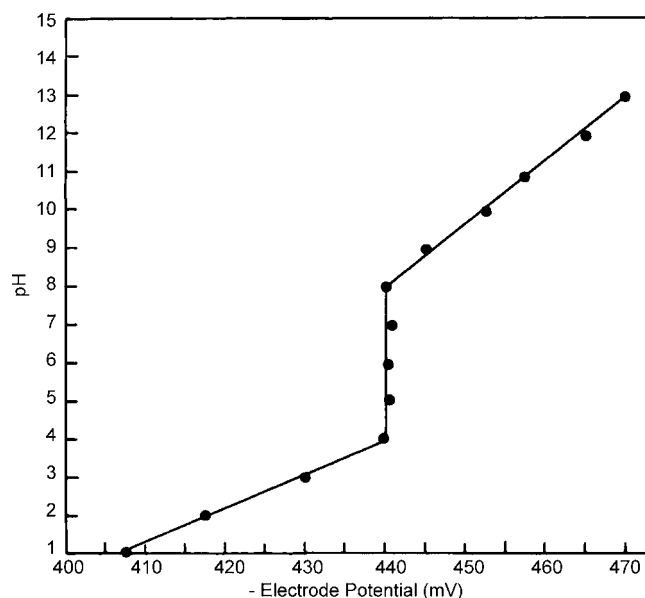Fig. 10. Calibration curve of poly-o-toluidine Th(IV) phosphate membrane electrode in aqueous solutions of Hg(NO$_3$)$_2$.

Fig. 11. Effect of pH on the potential response of the poly-o-toluidine Th(IV) phosphate membrane electrode at 1×10^{-2} M Hg^{2+} concentration.
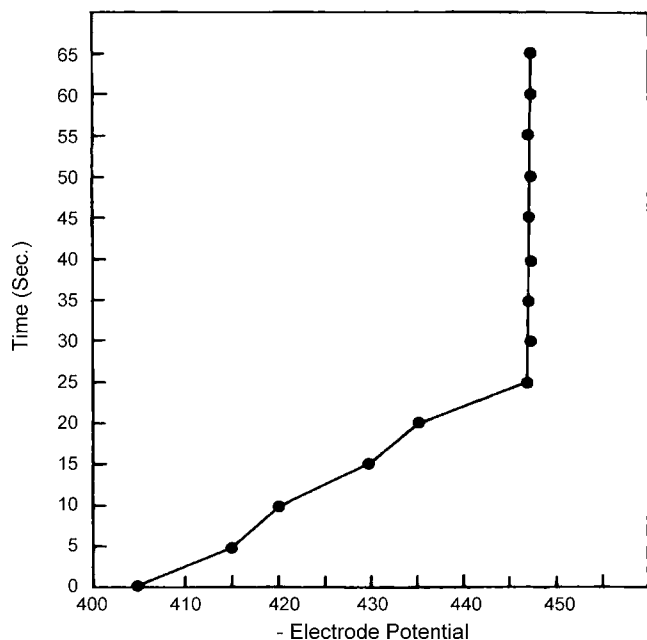
Fig. 12. Time response curve of poly-*o*-toluidine Th(IV) phosphate membrane electrode.

Table 7
Selectivity coefficient values for Hg^{2+} selective poly-*o*-toluidine Th(IV) phosphate membrane electrode of mercury ions

Interfering ions (M^{n+})	Selectivity coefficient values
Zn^{2+}	0.025
Cd^{2+}	0.055
Cu^{2+}	0.040
Mg^{2+}	0.035
Co^{2+}	0.020
Na^+	0.85
K^+	0.9500
Fe^{2+}	0.400
Cr^{3+}	0.910
Mn^{2+}	0.900
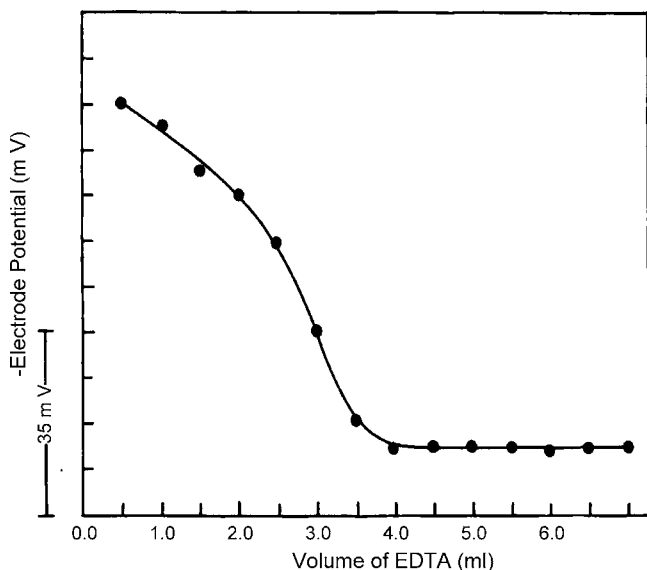
Fig. 13. Potentiometric titration of Hg(II) against EDTA solution using poly-*o*-toluidine Th(IV) phosphate PVC membrane electrode.

The practical utility of the proposed membrane sensor assembly was tested by its use as an indicator electrode in the potentiometric titration of Hg(II) with EDTA. The addition of EDTA causes a decrease in potential as a result of the decrease in the free Hg(II) ions concentration due to its complexation with EDTA (Fig. 13). The amount of Hg(II) ions in solution can be accurately determined from the resulting neat titration curve providing a sharp rise in the titration curve at the equivalence points.

4. Conclusion

In the present study, a mercury selective composite cation-exchanger poly-*o*-toluidine Th(IV) phosphate having good ion-exchange capacity (1.90) as compared to Th(IV) phosphate (0.72) have been prepared successfully. As shown in TEM photograph the particle size of the composite material are within the range of 11.00, 10.00, 15.00 and 18.00 nm. Thus material can be considered as nano-composite material. This composite material was also utilized as an electroactive component for the preparation of ion-selective membrane electrode for the determination of Hg(II) ions in aqueous solution. The membrane electrode showed a working concentration range $10^{-1} - 5 \times 10^{-5}$ M, response time 25 s, 4–8 pH range, and selectivity in presence of other metal ions. The practical utility was determined as potentiometric sensor for the titration of Hg(II) using ethylenediaminetetra-acetic acid (EDTA) as a titrant.

Acknowledgements

References

[1] C.B. Amphlett, Inorganic Ion Exchangers, Elsevier, Amsterdam, 1964.
[2] A. Clearfield, Solv. Extrn. Ion Exch. 18 (2000) 655.
[3] A.A. Khan, M.M. Alam, Anal. Chim. Acta 504 (2004) 253.
[4] A.A. Khan, Inamuddin, React. Funct. Polym. 66 (2006) 1649.
[5] A.A. Khan, Inamuddin, M.M. Alam, React. Funct. Polym. 63 (2005) 119.
[6] A.A. Khan, M.M. Alam, React. Funct. Polym. 55 (2003) 277.
[7] K.G. Varshney, N. Tayal, A.A. Khan, R. Niwas, Colloid Surf. A: Physicochem. Eng. Asp. 181 (2001) 123.
[8] A.P. Gupta, H. Agarwal, S. Ikram, J. Indian Chem. Soc. 80 (2003) 57.
[9] R. Niwas, A.A. Khan, K.G. Varshney, Colloid Surf. A: Physicochem. Eng. Asp. 150 (1999) 7.
[10] K.G. Varshney, N. Tayal, U. Gupta, Colloid Surf. A: Physicochem. Eng. Asp. 145 (1998) 71.
[11] B. Zhang, D.M. Poojary, A. Clearfield, G. Peng, Chem. Mater. 8 (1996) 1333.
[12] G. Alberti, M. Casciola, C. Dionigi, R. Vivani, Proceedings of International Conference on Ion-Exchange ICIE'95, Takamtsu, Japan, 1995.
[13] D. Perez-Quintanilla, I. del Hierro, M. Fajardo, I. Sierra, J. Hazard. Mater. B134 (2006) 245.
[14] Xin-Guili, M.-R. Hung, R. Liu, React. Funct. Polym. 2 (2005) 285.
[15] A.K. De, K. Chowdhury, J. Chromatogr. 101 (1974) 63.

[16] N.E. Topp, K.W. Pepper, J. Chem. Soc. (1949) 3299.

[17] C.N. Reiliy, R.W. Schmidt, F.S. Sadek, J. Chem. Educ. 36 (1959) 555.

[18] A.A. Khan, Inamuddin, Sen. Actuat. B: Chem. 120 (2006) 10.

[19] A. Craggs, G.J. Moody, J.D.R. Thomas, J. Chem. Educ. 51 (1974) 541.

[20] S.K. Srivastava, A.K. Jain, S. Agarwal, R.P. Singh, Talanta 25 (1978) 157.

[21] S. Amarchand, S.K. Menon, Y.K. Agarwal, Indian J. Chem. Technol. 5 (1998) 99.

[22] H.P. Gregor, H. Jacobson, R.C. Shair, D.M. Weston, J. Phys. Chem. 61 (1957) 141.

[23] C. Duval, Inorganic Thermogravimetric Analysis, Elsevier, Amsterdam, 1963, p. 315.

[24] C.N.R. Rao, Chemical Applications of Infrared Spectroscopy, Academic Press, New York, 1963, p. 355.

[25] C.N.R. Rao, Chemical Applications of Infrared Spectroscopy, Academic Press, New York, 1963, p. 338.

[26] M.K. Amini, M. Mazloum, A.A. Ensaf, Fresenius J. Anal. Chem. 364 (1999) 690.

[27] A. Demirel, Dogan, E. Canel, Shahabuddin, Talanta 62 (2004) 123.

[28] IUPAC Analytical Chemistry Division, Commission on Analytical Nomenclature, Pure Appl. Chem. 66 (1994) 2527.

[29] G.J. Moody, J.R.D. Thomas, Selective Ion Sensitive Electrode, Marrow, Watford, 1971.

ELSEVIER

Quantitative determination of Malathion in pesticide by modified attenuated total reflectance-Fourier transform infrared spectrometry applying genetic algorithm wavelength selection method

M. Khanmohammadi [a,*], M.A. Karimi [b,c], K. Ghasemi [b], M. Jabbari [d], A. Bagheri Garmarudi [a]

[a] Department of Chemistry, Faculty of Science, Imam Khomeini International University, Qazvin, Iran
[b] Department of Chemistry, Faculty of Science, Payam e Noor Ardakan University, Ardakan, Iran
[c] Department of Chemistry, Faculty of Science, Shahid Bahonar University, Kerman, Iran
[d] Department of Mathematics, Faculty of Science, Imam Khomeini International University, Qazvin, Iran

Abstract

A simple and environment friendly method was developed for determination of Malathion content of analytical and commercial insecticide samples with no special preparation. Attenuated total reflectance-Fourier transform infrared (ATR-FTIR) spectra were characterized and $1000–2000\,cm^{-1}$ region was selected for quantitative analysis utilizing partial least square (PLS) and two wavelength selection methods: (a) principal component regression (PCR) and (b) genetic algorithm (GA). Relative error of prediction (REP) was calculated in PLS, PCR-PLS and GA-PLS methods and was 3.536, 1.656 and 0.188, respectively. Proposed method is successfully applicable for quantification of Malathion in commercial grade samples and reliable results in comparison with known methods, confirms this idea.
© 2006 Elsevier B.V. All rights reserved.

Keywords: Fourier transform infrared; Malathion; Genetic algorithm; Chemometrics

1. Introduction

Malathion (*S*-(1,2-dicarbethoxyethyl) *O*,*O*-dimethyl dithio phosphate) is an organophosphate (OP) insecticide, which was introduced in 1950 by American Cyanamid Company as a new generation. It has a wide range of applications, e.g. in vegetable producing crofts, farms and fly dopes.

Organophosphates are environment pollutants and thus the insecticides based on these compounds would be harmful especially when they have widespread applications [1]. Detailed analysis of the incident data identified specific use patterns which are more likely to be associated with pesticide poisoning. According to the type of use, risk mitigation measurements are recommended to reduce the associated effects of poisoning [2].

Some methods for determination of Malathion in pesticides have been published in Collaborative International Pesticide Analytical Council (CIPAC) reference book, e.g. gas chromatography with flame ionization detection (GC-FID) [3] or photometric determination procedure at 420 nm. Other procedures which have been proposed for Malathion quantification in pesticide are based on using GC with mass spectrometry as the detector [4], screen-printed enzyme electrodes [5], photometric determination with molybdenum at 825 nm [6] and indirect determination by atomic absorption spectrometry [7]. One of the most important drawbacks of foresaid methods is the use of solvent in most of them which is environmentally concerning.

In present research a simple procedure for quantification of analytical and commercial Malathion in presence of spectral interference relating to diethyl maleate (as a residue of production process), TF-XN10 and TF-7438 (product additives in commercial samples) has been developed. Commercial Malathion is 30–90% (w/v) concentrated in pesticide emulsion. The main aim of this study was to develop a procedure based on FTIR spectroscopy for fast, accurate and direct determination of Malathion, which could be used in the quality control of its

* Corresponding author at: Department of Chemistry, Faculty of Science, Imam Khomeini International University, P.O. Box 288, Qazvin, Iran. Tel.: +98 281 3780040; fax: +98 281 3780040.

E-mail addresses: mrkhanmohammadi@gmail.com, mkhanmohammadi@ikiu.ac.ir (M. Khanmohammadi).

commercial products, being an eco-friendly method trying to reduce the organic solvents' waste, as much as possible.

Partial least squares (PLS) was used to extract the relevant part of information and produce reliable models. Nowadays, this concept is applied by several researchers, according to Martens and Neas algorithm [7,8]. The choice of wavelength would critically affect the future predictive ability of the model. Recently, several selection methods have been developed, e.g. artificial neural network (ANN) [9], Tabu search [10], hybrid linear analysis (HLA) [11], and successive projection algorithm (SPA) [12].

In this study, PCR and GA techniques were used for wavelengths selection. In PCR method, wavelengths with minimum "relative error of prediction" (REP) were selected for calibration model by introducing them into the regression iteratively and evaluating the relative error of models [9]. Genetic algorithms (GA) are widely applied including an extraordinary increment in calculation power and being applicable for extremely complex problems. There are some publications dealing with genetic algorithms [13–15].

2. Experimental

2.1. Materials and apparatus

An AB-Bomem (Quebec, Canada) MB100, FTIR spectrometer equipped with a di-triglycerine sulfate (DTGS, DC3IB) mid-range detector, a Ge/Sb_2S_3 coated KBr beam splitter and a SiC source, was employed for IR spectrometry. Spectratech (Warrington, UK) in-compartment contact with a sampler and a horizontal attenuated total reflector (with a 45° ZnSe trough plate) were used. GRAMS/32 software (Galactic Ind. Co.) was utilized for spectral analysis. A GBC UV–vis (Cintra 6) spectrophotometer, attached to a Pentium (IV) computer, with 10 cm glass cell was used as reference method at 420 nm.

All FTIR absorptions spectra were recorded at 1000–2000 cm^{-1} region with spectral resolutions of 3.85 cm^{-1}. All spectra were processed by MATLAB software (ver.7.00) consisting of PLS and GA m.files (copyright 1989–1992 by Math Works, Inc.). The PCR algorithm was also formatted as an m.file. Purity of analytical grade Malathion was determined by reference method, i.e. absorption at 420 nm. Standard solution of Malathion with 95.2% purification of stock solution (Chemservice, USA) was applied. Diethyl maleate (DEM) reagent, TF-XN10 and TF-7438 additives (Omnic.chem., Belgium) were of commercial grade, solvent used was xylene (Merck, Germany). Chemical reagents and solvent used in reference method were anhydrous ethanol, sodium hydroxide, ferric chloride solution (0.2 g $FeCl_3 \cdot 6H_2O$ in 8 ml hydrochloric acid), cupric sulfate solution (1.0 g $CuSO_4 \cdot 5H_2O$ in 1000 ml double distilled water) and carbon tetrachloride, all in analytical grade (Merck, Germany).

2.2. Classic reference procedure for determination of Malathion

About 0.2 g of Malathion is weighted, dissolved by anhydrous ethanol in a 200 ml volumetric flask. A 20 ml portion of solution is transferred to another 200 ml volumetric flask and anhydrous ethanol is added up to the volume mark. Using pure ethanol, 1, 2, 5, 10, 15, 20 and 25 ml of diluted solution is transferred into seven separating funnels and sufficient ethanol is added to make an exactly 20 ml mixture, followed by mixing the contents of funnels. Then sodium hydroxide solution (2 ml, 0.5 M) is added and stirred. After 2 min ferric chloride reagent (75 ml, 0.001 M) is added and mixed for 5 min. Then carbon tetrachloride (50 ml) and cupric sulfate solution (2 ml, 0.066 M) are added, funnel's stopper is tightened, and funnel is agitated, exactly 1 min. Then organic phase (carbon tetrachloride) is separated and absorbance of the yellow solution is measured at 420 nm immediately.

2.3. Proposed procedures for quantification of analytical malathion

Standard solutions were prepared in concentration range of 1.567–0.166 mg ml^{-1} with xylene as solvent. In this way, 30 samples were prepared for calibration set. To decrease the difference of matrix effect between standard and real sample solutions, other interfering components were added to them in different concentration levels (0.10–1.20 mg ml^{-1} for DEM, 0.15–1.00 mg ml^{-1} for TF-XN10 and 0.14–1.01 mg ml^{-1} for TF-7438). Foresaid standard solutions were applied in calibration model, also for assessment of the model and for quantitation of real samples.

3. Results and discussion

3.1. Solvent selection

A suitable solvent dissolves the analytical samples without reacting and has the least interference at spectral region of the analyte. Carbon tetrachloride and chloroform have been mentioned in the reference methods as solvent. According to the high solubility of Malathion in xylene, commercial samples are diluted by this organic solvent. Thus, xylene has been selected as an appropriate solvent in proposed method. Fig. 1 shows the absorption spectra of solvent and standard Malathion solution
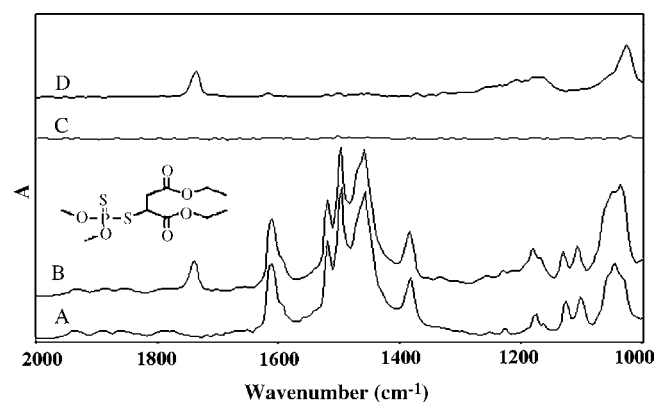

Fig. 1. Absorbance spectra of the solvent and Malathion standard with air background (A and B), solvent and Malathion standard with solvent background (C and D).
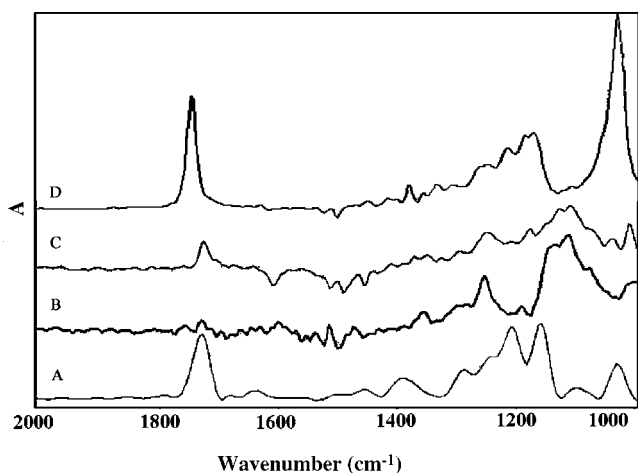
Fig. 2. Absorbance spectra of $1.02\,\mathrm{mg\,ml^{-1}}$ concentrated DEM (A), $3.10\,\mathrm{mg\,ml^{-1}}$ concentrated TF-7438 (B) and $3.00\,\mathrm{mg\,ml^{-1}}$ of concentrated TF-XN10 (C) and $1.00\,\mathrm{mg\,ml^{-1}}$ concentrated malathion (D).

with air background (A and B) and with solvent background (C and D).

3.2. FTIR spectra of malathion

The FTIR absorption spectrum of Malathion indicates that the wave number region of $1000–2000\,\mathrm{cm^{-1}}$ could be selected to carry out its determination. The bands located at $1720–1770\,\mathrm{cm^{-1}}$ and $1000–1060\,\mathrm{cm^{-1}}$ are the most intensive ones. The signal at $1720–1770\,\mathrm{cm^{-1}}$ is due to the carbonyl stretching of the ester group. The P–OCH$_3$ group has two closer bands located at $1018–1047\,\mathrm{cm^{-1}}$ region. Absorptions around $1450\,\mathrm{cm^{-1}}$ are according to –CH$_2$ and –CH$_3$ groups while the band at $1375\,\mathrm{cm^{-1}}$ indicates the –CH$_3$ group [16–17].

3.3. Spectral region of interferences

As can be seen in Fig. 2, the ATR-FTIR absorption spectrum of DEM in xylene (A) shows an intensive band at $1047–1070\,\mathrm{cm^{-1}}$ which causes an interference with Malathion in this region.

On the other hand, the absorption spectra of additives (TF-XN10 and TF-7438) show the spectral interferences at $1727–1731\,\mathrm{cm^{-1}}$ and $1050–1175\,\mathrm{cm^{-1}}$ with the analyte.

3.4. Calibration model and validation step

Multivariate calibration models are suitable for the analysis of large number of samples. However, they are not advisable for the determination of large numbers of analytes because of the complexity of the calibration matrix. Multivariate calibration methods such as PLS require a suitable experimental design of the standards belonging to the calibration set in order to provide a good prediction [18,19].

In order to find the best regions for quantification of Malathion, 4 regions were evaluated ($1000–1180\,\mathrm{cm^{-1}}$, $1180–1350\,\mathrm{cm^{-1}}$, $1350–1780\,\mathrm{cm^{-1}}$ and also the combination of both $1000–1180\,\mathrm{cm^{-1}}$ and $1350–1780\,\mathrm{cm^{-1}}$), according to the

Table 1
Quantification of Malathion by PLS calibration model using different spectra region

Area (cm^{-1})	RMSEC	REP	R^2
1000–1180	0.561	6.160	0.990
1180–1350	0.737	8.089	0.924
1350–1780	1.568	17.212	0.959
1000–1180 and 1350–1780	0.341	3.741	0.993

absorbance signals of Malathion and spectral interference of other components. The analytical quantification results of PLS model at mentioned regions are shown in Table 1. The results of this evaluation showed these regions ($1000–1180\,\mathrm{cm^{-1}}$ and $1350–1780\,\mathrm{cm^{-1}}$) are more suitable for analysis.

3.5. Variable selection methods

One important goal in multivariate method is increasing the prediction ability of the calibration model. Therefore, two wavelength selection methods were applied. In order to select the modified wavelengths, 22 variables were selected at first by PCR. Results of calculation errors in iterative application of wavelengths in regression have been illustrated in Fig. 3 and Fig. 4 shows the selected wavelengths.

GA is an evolutionary computing technique which uses an algorithm known as a fitness function to assess the robustness of the model proposed by each individual. GA usually takes the form of a minimization function; therefore the fittest individuals are those with the lowest fitness value. The genetic process will produce individuals with better performance than the previous ones, and thus the individual in the terminal generation can be considered as the approximate optimal solution. GA parameters are shown in Table 2.

GA was performed on spectral data set using a PLS regression method with maximum number of factors as the optimal number of components which were determined by cross-validation on the model containing all of the variables, using selected variables for PLS performing. The selected variables which were used in GA-PLS calibration set are about 40. Fig. 5 shows the GA selected variables. The present study shows that the GA-PLS
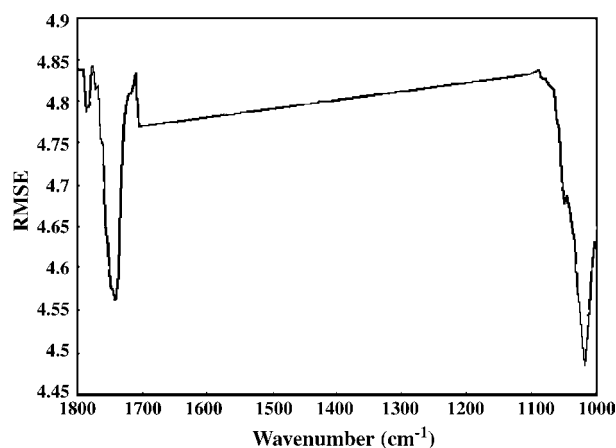

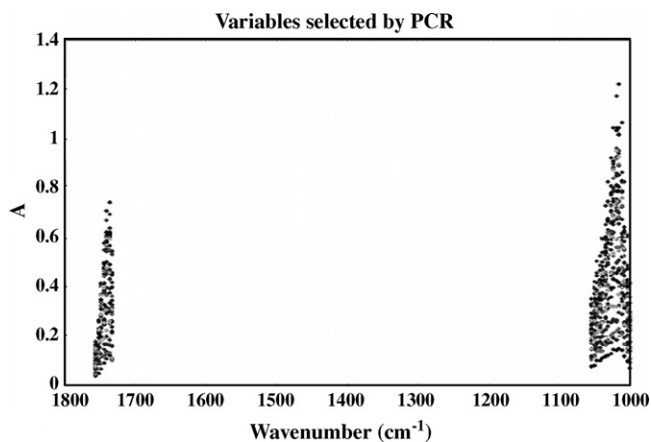Fig. 3. Errors according to the total wavelengths calculated by the PCR method.

Fig. 4. Selected wavelength by proposed PCR method.

could be a good method for feature selection in spectral data sets. As a result, the prediction ability of the model has been modified and the results are so much better than the use of PLS or PCR-PLS only.

3.6. Number of significant factors

PLS is often presented as the major regression technique for multivariate data. An important feature of PLS is that it takes into account errors in both the concentration estimates and the spectra.

Using a set of 30 spectra, the PLS calibration was performed on 29 spectra and concentration of the compounds in the left out sample was predicted. This process was repeated 30 times until each calibration sample left out once. The predicted concentration of analyte in each sample was compared with its known concentration and the root mean square of cross-validation (RMSECV) was calculated. One reasonable choice for optimum number of factors would be the number of factor which yields minimum RMSECV. Various PLS calibration models have been calculated for the samples of the training set using different data wavelength selection methods and "number of factors". The validation error (RMSECV) for different models was obtained, using the leave-one-out validation procedure. For the final model we must use the lowest "number of factors" which gives a minimal RMSECV. Including a large number of factors often leads to deterioration in prediction ability (over fitting) for the samples of the test set. The criteria of lowest RMSECV and an optimal number of PLS-factors were used to calculate PLS models, but location of the minimum RMSECV is not always

Table 2
Parameters used in GA methodology

Population size	64
Windows with	3
Maximum generation	100
Mutation rate	0.05
Crossover	Double
Regression choice	PLS
Cross-validation	Contiguous

well defined as a result of when the minimum is very shallow; one might trade in a few factors for a simpler and probably more robust model with almost the same prediction error. The criterion to add an additional factor to the model, in order to build the final model, is our need to reduction of the RMSECV to 3% or lower.

Fig. 6 illustrates the results of RMSECV according to the factors. As can be seen, there is no significant difference between the factors 6–10, thus there is no good reason to select a "number of factors" as an optimum one.

Another choice for the optimum number of factors would be that number which yields the minimum prediction error sum of square (PRESS). PRESS is obtained in cross-validation process. However using the number of factors ($h*$) that yields minimum PRESS usually leads to some over fitting. A better criterion for selecting the optimum number of factors involves the comparison of PRESS from models with fewer than ($h*$) factors. We used F-statistic to make the significance determination. Haaland and Thomas empirically determined that an F-ratio probability of 0.75 is a good choice [20]. We selected 6, 8 and 10 factors according to these 2 processes for PLS, PCR-PLS and GA-PLS, respectively.

The root mean square error (RMSE) is an indication of average error for each of components in analysis [21] and thus was calculated. The results obtained by applying PLS algorithm to an independent data set consisting of 12 samples are listed in Table 3 for each method. Root mean square error of calibration (RMSEC) for PLS calibration model was 0.322 and root mean square error of test (RMSET) for independent data set was 0.420 which are quite acceptable.

The square of the correlation coefficient (R^2) [22] indicates the linearity of data. The RMSE values estimate the absolute errors of prediction for each component. The prediction ability of each method for each component can also be described in term of the relative error of prediction (REP) [23]. RMSEC, R^2 and REP values for each method (according to the optimum factor) have been summarized in Table 4.
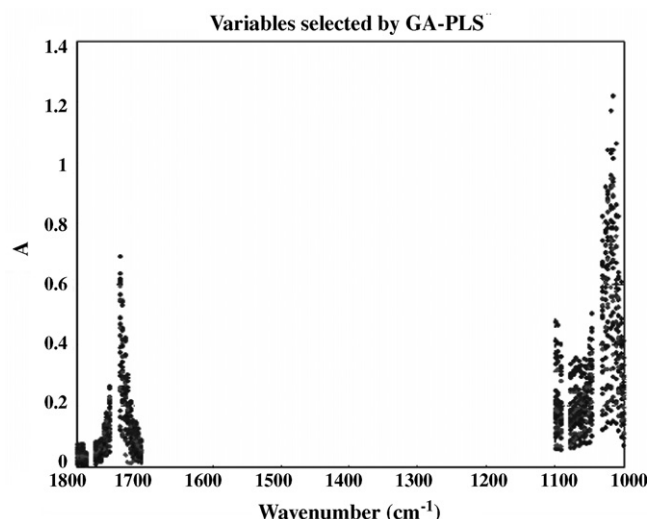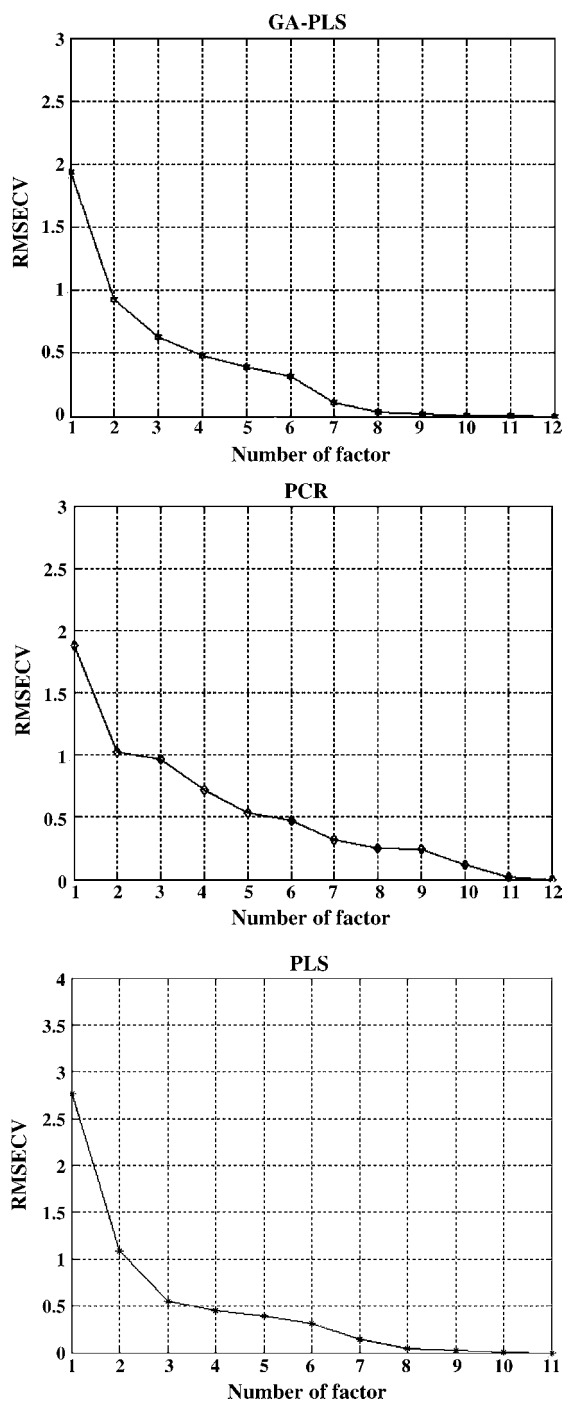

Fig. 5. Selected wavelengths by GA-PLS method.

Fig. 6. RMSECV attributed to number of factors in different methods (GA-PLS, PCR-PLS and PLS).

Table 3
The results of validation of calibration models by independent data set solution

Sample	Actual concentration (mg ml^{-1})	PLS predicted concentration (mg ml^{-1})	GA-PLS predicted concentration (mg ml^{-1})
1	1.491	1.483	1.493
2	1.162	1.153	1.167
3	0.271	0.279	0.272
4	1.092	1.145	1.093
5	1.326	1.356	1.325
6	1.073	1.039	1.074
7	0.557	0.644	0.539
8	0.656	0.677	0.656
9	0.641	0.615	0.644
10	0.835	0.906	0.839
11	0.369	0.388	0.365
12	1.328	1.326	1.333
RMSET	–	0.4200	0.0593

Table 4
Statistical parameters of the calibrations using PLS, PCR-PLS and GA-PLS method with the best number of factors

Method	NC[a]	RMSEC	REP	$R2$
PLS	6	0.322	3.536	0.994
PCR-PLS[b]	8	0.151	1.656	0.997
GA-PLS[c]	10	0.017	0.188	0.999

[a] Number of significant factors.
[b] Results by 22 selected variables.
[c] Results by 40 selected variables.

Table 5
Comparison of the actual concentrations of Malathion measured by UV–vis with GA-PLS predicted concentrations

Samples	UV–vis, reference concentration (mg ml^{-1})	GA-PLS, predicted concentration (mg ml^{-1})
1	0.545	0.519
2	0.712	0.680
3	0.818	0.793
4	1.160	1.159

applying a method such as PLS regression for whole spectral region. A wavelength selection method such as GA is helpful to find more capability of prediction. Present study shows that GA is a reliable method for feature selection in a spectral data set.
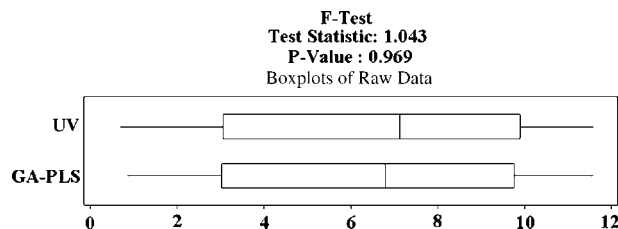
3.7. Quantification of the commercial malathion

Four samples in different concentration levels were provided in order to compare the recommended methods with reference method and PLS model. Results of analyzing these samples by UV–vis and GA-PLS are shown in Table 5. *F*-ratio statistic of GA-PLS and reference method in comparison, declares that these results are reliable with 96% of confidence limit (Fig. 7). Results of experimental procedure are modified by

Fig. 7. Box plot obtained by *F*-test, comparing the results made of the reference and proposed GA-PLS method.

4. Concluding remarks

Attenuated total reflectance-Fourier transform infrared (ATR-FTIR) is a reliable technique for determination of Malathion content of insecticide samples. The GA-PLS wavelength selection method has the lowest "relative error of prediction" in comparison with other methods, we had applied. This procedure is also fast and environment friendly as the amount of organic solvents used during its quantitative determination process is reduced significantly.

References

[1] M.A. Gallo, N.J. Lawry, in: J.W. Hayes (Ed.), Handbook of Pesticides Toxicology, Academic, E.R. Laws Press, New York, 1991, p. 3.

[2] US Public Health Service, Hazardous Substance Data Bank, Washington DC, 1995, p. 5.

[3] Collaborative International Pesticides Analytical Council (CIPAC) Handbook, vol. 1B, CIPAC Ltd., Cambridge, UK, 1994, p. 1849.

[4] Y.W. Lin, S.S.Q. Hee, J. Chromatogr. A 814 (1998) 181.

[5] A.L. Hart, W.A. Collier, D. Janssen, Biosens. Bioelectron. 12 (1997) 645.

[6] U.V. Naidu, T. Gangaiah, P. Ramadevi, K. Seshaiah, G.R.K. Naidu, Talanta 37 (1990) 761.

[7] J. Hernández-Méndez, O. Jiménez de Blas, A. Lozano Garcia, Microchem. J. 38 (1988) 355.

[8] H. Martens, T. Neas, Multivariate Calibration, John Wiley, New York, 1991, pp. 116–228.

[9] D. Svozil, V. Kvasnicka, J. Pospichal, Chemomet. Intelligent Lab. Syst. 39 (1997) 43.

[10] J.A. Hageman, M. Strepal, R. Wehrensand, L.M.C. Buydens, J. Chemomet. 17 (2003) 427.

[11] H.C. Goicoechea, A.C. Oliviera, Analyst 124 (1999) 725.

[12] M. Cesar, T. Cristina, R. Kawakami, T. Yoneyama, Chemomet. Intelligent Lab. Syst. 57 (2001) 65.

[13] H. Ghasemi, A. Niazi, R. Leardi, Talanta 59 (2003) 311.

[14] R. Leadri, R. Boggia, M. Terrile, J. Chemomet. 6 (1992) 267.

[15] R. Leadri, J. Chemomet. 8 (1994) 65.

[16] G. Quitas, S. Garrigues, M. Guardia, Talanta 63 (2004) 345.

[17] G. Quitas, A. Morales, S. Amenta, Anal. Chim. Acta 502 (2004) 213.

[18] P. Geladi, B.R. Kowalski, Anal. Chim. Acta 185 (1996) 1.

[19] L. Kooistra, R. Wehrens, R.S.E.W. Leuven, L.M.C. Budens, Anal. Chim. Acta 446 (2001) 97.

[20] D.M. Haaland, E.V. Thomas, Anal. Chem. 60 (1988) 1193.

[21] R.G. Brerton, Chemometrics, John Wiley, Canada, 2003, p. 284.

[22] A. Espinosa-Mansilla, F. Salinas, I. De Orbe Paya, Anal. Chim. Acta 313 (1995) 103.

[23] I. Duran-Meras, M. De Orbe Paya, A. Espinosa-Mansilla, F. Salinas, Analyst 118 (1993) 807.

Turbulent flow and ternary column-switching on-line clean-up system for high-throughput quantification of risperidone and its main metabolite in plasma by LC–MS/MS Application to a bioequivalence study

Constantinos Kousoulos, Yannis Dotsikas, Yannis L. Loukas *

Laboratory of Pharmaceutical Analysis and Bioequivalence Services (GLP Compliant), Department of Pharmaceutical Chemistry, School of Pharmacy, University of Athens, Panepistimioupoli Zografou, GR-157 71 Athens, Greece

Abstract

A high-throughput LC–MS/MS method was developed for the simultaneous determination of Risperidone and 9-OH-risperidone in human plasma. A semi-automated sample preparation procedure was applied, including protein precipitation after addition of ACN, via a robotic system, and subsequent sub-zero temperature extraction of the latter. Injections of the ACN extractants were performed on a turbulent flow ternary column-switching system, consisted of dual extraction columns in parallel for on-line purification of samples and an analytical column. Toggling with the assistance of two valves provided a run cycle time of 3 min and the whole procedure minimized carry-over effect. On-line clean-up procedure along with sub-zero temperature extraction increased sample purification and extended column life. The analytical range of the method was 0.1–200 ng mL^{-1} for both analytes with excellent linearity and very good accuracy and precision. The proposed method was employed in a bioequivalence study after per os administration of a 2 mg tablet of risperidone and allowed the completion of the study (>1400 samples) in only 4 days time.
© 2007 Elsevier B.V. All rights reserved.

Keywords: Risperidone; Column-switching; Mass spectrometry; 96-Well; Sub-zero extraction; Bioequivalence

1. Introduction

Risperidone (RIS) is an atypical antipsychotic drug used in the treatment of schizophrenia and other psychotic disorders [1–4]. 9-Hydroxy-risperidone (9-OH-RIS) is the main metabolite of RIS formed in liver by cytochrome P450 isoenzymes [5]. 9-OH-RIS has a similar pharmacological activity as the parent compound and the sum of both molecules constitutes the total active moiety responsible for the pharmacological responses to RIS administration. Typical oral doses of RIS in the treatment of chronic schizophrenia range from 2 to 6 mg per day resulting in plasma levels of 5–100 nM of RIS and 9-OH-RIS [6,7].

Numerous HPLC methods with UV or electrochemical detection [8–13] have been described for the quantitative deter-

mination of RIS and its hydroxy-metabolite in human plasma. Such methods usually lack the combined sensitivity and selectivity needed to analyze complex mixtures. Liquid chromatography coupled with atmospheric pressure ionization tandem mass spectrometry is nowadays the method of choice for the quantitative determination of pharmaceutical substances in complex biological matrices. Few methods have been reported for the determination of RIS and 9-OH-RIS that employ mass spectrometric detectors. Three of them [14–16] apply conventional extraction protocols, while recently [17] a LC–MS/MS method using column switching with one extraction column for on-line clean-up has been presented.

Plasma protein precipitation (PPP), liquid–liquid extraction (LLE) and solid-phase extraction (SPE), are the sample preparation techniques most commonly used for processing plasma and tissue samples. These processes are labor-intensive and time-consuming and constitute the rate-limiting step in high-throughput pharmacokinetic studies. The introduction however

---

* Corresponding author. Tel.: +30 210 7274224; fax: +30 210 7274224.
  E-mail address: loukas@pharm.uoa.gr (Y.L. Loukas).

of several liquid workstations for the parallel processing of samples has greatly facilitated this task, resulting in the development of numerous automated methodologies for the determination of drugs and their metabolites in biological fluids during the last few years [18–24]. An alternative approach to automated sample extraction is the use of turbulent flow chromatography (TFC) with column-switching [25–30]. By using this approach sample pre-treatment is minimized. The biological sample can be injected directly onto a narrow-bore large particle size extraction column where the sample matrix is rapidly washed away using a high flow rate aqueous mobile phase while analytes are retained. After the load and wash steps are completed, the composition is changed to high organic solvent for the elution of the analytes in the backflush mode from the extraction column onto an analytical column, under laminar flow rate conditions, and finally into the mass spectrometer for detection. In most cases only a single extraction column is utilized in such procedures [31–34]. These single extraction column systems are simple and quite fast and have been applied to the analyses of numerous clinical samples. However, in such approaches the time for column equilibration between injections is often added to the respective run time. Utilization of dual extraction columns in parallel for purification and an analytical column for analysis results in a system with increased sample throughput.

In the present study we report the development and validation of the first method combining semi-automated sample pre-treatment with turbulent flow chromatography and column-switching for the determination of RIS and 9-OH-RIS. Plasma proteins are initially precipitated with ACN containing the internal standard in order to achieve cleaner extracts and thus increase the life of both extraction and analytical columns. Following the example of a previously presented protocol [35] the resulting samples are injected onto a ternary column on-line system with dual extraction columns. However, the use of a single valve in this protocol (10-port switching valve) resulted in significant carry-over problem. In the current protocol we added a six-port valve and such phenomena along with the appropriate wash solvent selection were minimized. With this system, two on-line processes can be staggered on the two extraction columns. While one column is in the wash, load or equilibration step, the other is in the elution step. Thus, the equilibration time does not add to the run time and the sample throughput is significantly increased. All liquid transfer steps including preparation of calibration standards and quality control samples (QCs), transfer of study samples and addition of ACN containing the internal standard were performed automatically via robotic systems.

The proposed method enabled the automated high-throughput and reliable determination of RIS and 9-OH-RIS in a bioequivalence study after per os administration of a 2 mg tablet in 30 healthy volunteers.

2. Experimental

2.1. Chemicals and reagents

Risperidone, hydroxy-risperidone and the compound R68808 (Fig. 1) used as the internal standard were obtained from
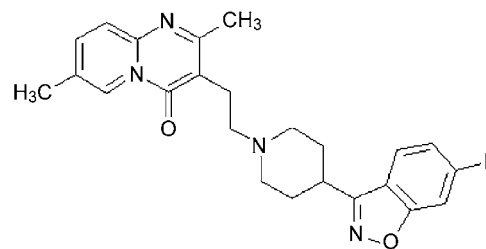

Fig. 1. Molecular structure of IS (R68808).

HELP Pharmaceutical Company (Athens, Greece). Methanol (HPLC grade), Acetonitrile (HPLC grade), were obtained from Sigma–Aldrich (Athens, Greece). Glacial acetic acid (analysis grade) and ammonium acetate (analysis grade) were purchased from Metrolab (Athens, Greece). All aqueous solutions and buffers were prepared using de-ionized and doubly distilled water (resistivity > 18 MΩ) from a Millipore Milli-Q Plus System (Malva, Athens, Greece). Pooled human control plasma (heparinized) was kindly donated from Ippokrateio hospital (Athens, Greece).

2.2. Instrumentation

A PerkinElmer Multiprobe® II HT-EX workstation (Perkin-Elmer, Downers Grove, IL) equipped with an eight-tip robotic arm coordinated x-, y- and z-axis was employed for transferring the plasma samples from 2 mL eppendorf microfuge tubes (Lab Supplies, Athens, Greece) into 2.2 mL square 96-deep-well plate (Sigma–Aldrich, Athens, Greece) as well as for the addition of ACN containing the internal standard. The workstation was controlled by WinPrep Software. Conductive disposable tip-boxes (1000 μL) were purchased from E&K Scientific Products (Cambell, CA, USA), a tipchute, reagent troughs and a tip flush/wash station were purchased from PerkinElmer. A Tomtec Quadra 96 model 320 robotic liquid-handling system equipped with a 96-tip pipetting head (Bidservice, NJ, USA) was used for transferring the supernatant organic layer, after protein precipitation, into a new 2.2 mL 96-deep-well plate. An Eppendorf 5810 R (Bacakos, Athens, Greece) centrifuge that could accommodate 96-well plate as well as Eppendorf microfuge tubes was also utilized during sample preparation. The HPLC system included two Agilent 1100 series binary pumps, a degasser and a column oven/cooler (Hellamco, Athens, Greece). The CTC PAL autosampler (Hellamco) could accommodate six 96-deep-well plates allowing an automated measurement of a big amount of samples. The PAL 2-Valve drive module consisted of two individually controlled valve drives, a six-port injection valve and a 10-port switching valve. The Oasis HLB extraction columns (S-25 μm, 20 mm × 2.1 mm i.d.) used were from Waters (Milford, MA, USA) while the Cyano (CN) analytical column (S-5 μm, 50 mm × 4.0 mm i.d.) was from YMC (Schermbeck, Germany). A PE Sciex API 3000 triple quadrupole mass spectrometer (Biosolutions, Athens, Greece) interfaced with the HPLC via a turbo ionspray source was used for the mass analysis and detection, operating under Analyst 1.4.1 software. Eppendorf deepwell mats for covering the 96-well plates were purchased

Configuration A
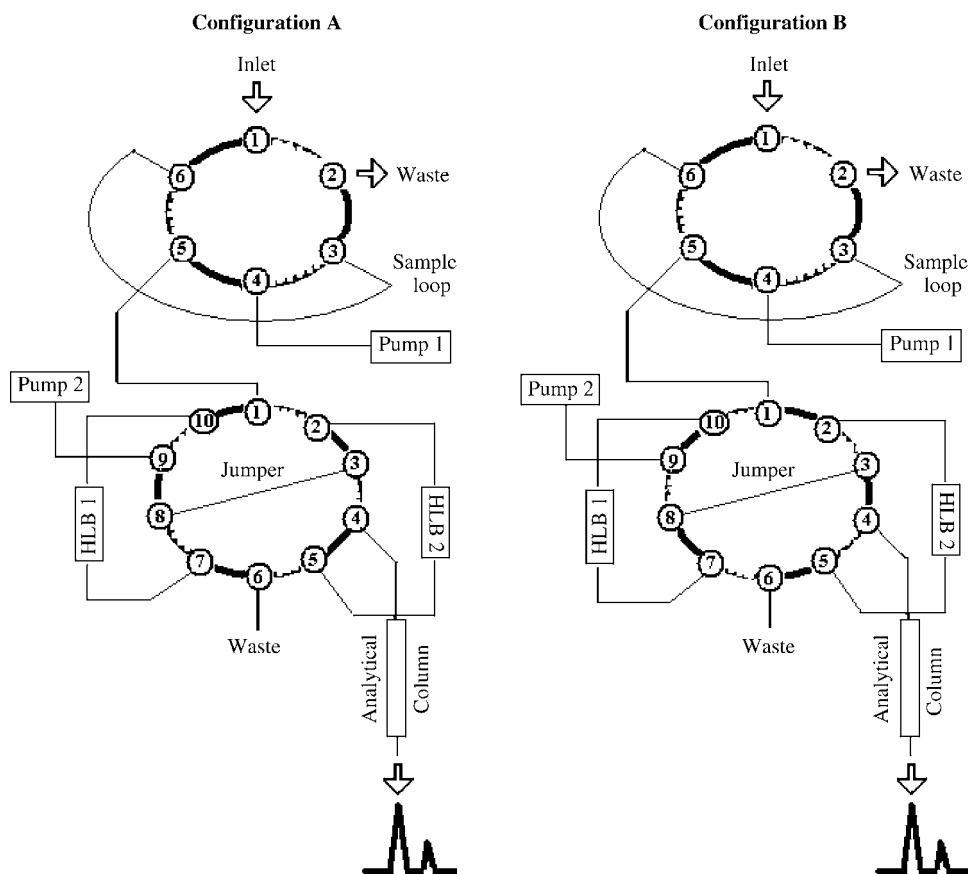
Configuration B

Fig. 2. Schematic representation of the dual extraction column-switching system.

from Sigma–Aldrich. Finally, a 96-well plate vortex-mixer (MS1 Minishaker) was obtained from Metrolab (Athens, Greece).

2.3. Chromatographic conditions and column-switching configuration

As shown in Fig. 2, the column-switching system consisted of two binary pumps (pump1 and pump2), an autosampler equipped with two valves, a six-port injection valve and a 10-port switching valve, two HLB extraction columns (HLB_1 and HLB_2), an analytical column (column) and a triple quadrupole mass spectrometer (detector). The protocol applied for the on-line sample clean-up was as follows:

- Loading and clean-up phase (0.00–0.70 min): A 20 μL portion of the processed human plasma standard or QC/MV sample is injected by the autosampler onto the HLB_1 column, using a mobile phase of 5% methanol and 95% water (Solvent A), delivered from pump1, at a flow rate of 5.0 mL min^{-1}, with the effluent directed to waste (Configuration A). At the same time an isocratic elution mobile phase delivered from pump2 is introduced through HLB_2, the analytical column and into the mass spectrometer at a flow rate of 0.8 mL min^{-1}.
- Elution and purification stage (0.80–2.40 min): At 0.80 min the 10-port valve is switched so that the HLB_1 column is in line with the analytical column and the mass spectrometer, which now receives the isocratic elution mobile phase (75%

acetonitrile, and 25% aqueous 10 mM ammonium acetate pH 4.0) from pump2 at a flow rate of 0.8 mL min^{-1} (Configuration B). The analytes are eluted from HLB_1 column to the analytical column for detection by the mass spectrometer. During the same period HLB_2 receives the flow from pump1 whose composition has changed from 100% solvent A (5/95, methanol/water) to 100% solvent B (0.1% formic acid in methanol/acetonitrile 80/20) for column purification.
- Reconditioning stage (2.50–3.00 min): Conditioning of the extraction column HLB_2 with the mobile phase composition used in the loading stage. The total run time was 3.0 min.

It is worth noting that the next injection was performed while the system was still in Configuration B. At 0.70 min, the system switches back to Configuration A and all the following odd-numbered injections were loaded onto HLB_1 while the even-numbered injections onto HLB_2. The gradient program followed by pump1 during the chromatographic run can be seen in Table 1.

2.4. Mass spectrometric conditions

The turbo ionspray of the API 3000 mass spectrometer operated in the positive ionization mode. The tuning parameters for RIS, 9-OH-RIS and IS were optimized by infusing a 100 ng mL^{-1} standard solution containing all compounds in mobile phase at 20 μL/min via an external syringe pump (Harvard 11 plus) directly connected to the mass spectrometer. The

Table 1
Pump 1 gradient table

Total time (min)	Flow rate (mL min^{-1})	Solvent A (%)	Solvent B (%)
0.00	5	100	0
0.70	5	100	0
0.80	5	0	100
2.40	5	0	100
2.50	5	100	0
3.00	5	100	0

turbo ionspray source temperature was maintained at 500 °C and the turbo ionspray voltage was set at 3000 V. The curtain gas was set at 10 (arbitrary units), the Declustering potential (DP) at 36 V for RIS, 41 V for 9-OH-RIS and 61 V for the internal standard. The nebulizer gas (GS$_1$) was set at 10 (arbitrary units) while the turbo ionspray gas (GS$_2$) at 7 L min^{-1}. The analytes were detected by monitoring the precursor → product ion transition using multiple reaction monitoring (MRM) scan mode with 150 ms dwell time and 5 ms pause time for each transition. The MRM was performed at m/z 411.3 → 191.4 for RIS, 427.2 → 207.3 for 9-OH-RIS and 421.1 → 201.2 for the IS. The collision-induced dissociation (CID) gas was set at 8 (arbitrary units) while the collision energy was set at 41 V, for RIS and 9-OH-RIS and 33 V for the IS, respectively. Data were acquired using the Analyst 1.4.1 software.

2.5. Preparation of standard and quality control/method validation samples

Initially, standard working solutions, containing both RIS and 9-OH-RIS, at concentrations of 2, 4, 10, 20, 40, 100, 200, 400, 1000, 2000 and 4000 ng mL^{-1} in MeOH/H$_2$O 50/50 (v/v) were prepared. A 100 μg/mL IS working solution was also prepared in the same solvent mixture. Further dilution resulted in the final IS solution (20 ng mL^{-1}).

Quality Control/Method Validation (QC/MV) stock solutions (100 μg mL^{-1}) were prepared from a separate weighing. Dilutions were used to prepare four levels of QC/MV working solutions at 2, 6, 1500 and 3000 ng mL^{-1} for both RIS and 9-OH-RIS. All these solutions were stored at 4 °C and were brought to room temperature before use. Calibration standards, QC/MV samples were prepared in the same biological matrix (human plasma) as the samples to be analyzed, utilizing the Multiprobe II HT-EX workstation. All Eppendorf tubes were capped and stored at −30 °C until required for assay.

The calibration curve consisted of a blank sample (matrix sample processed without internal standard), a zero sample (matrix sample processed with internal standard) and 11 non-zero standards covering the expected range of concentrations to be quantified. The above spiking procedure resulted in final concentrations for the calibration standards of 0.1, 0.2, 0.5, 1, 2, 5, 10, 20, 50, 100 and 200 ng mL^{-1} for RIS and 9-OH-RIS. Similarly, the following concentration levels of QC/MV samples were achieved: MV$_L$ (0.1 ng mL^{-1}), MV$_1$/QC$_1$ (0.3 ng mL^{-1}), MV$_2$/QC$_2$ (15 ng mL^{-1}) and MV$_3$/QC$_3$ (150 ng mL^{-1}). QC and

MV samples have two distinct purposes: the results for QC samples provide the basis for accepting or rejecting analytical runs, while the results for MV samples are used to calculate bias and precision of the assay methodology.

2.6. Sample preparation

Initially, all plasma samples were thawed at room temperature, vortexed and centrifuged at 3500 rpm for 5 min at approximately 4 °C. Each of the calibration, quality control and subject samples (300 μL) were transferred from the Eppendorf tubes into the appropriate wells of a 96-well plate. Then, to each plasma sample, 300 μL of the final IS solution in ACN, were added. The deep-well plates were covered with a mat and vortex mixed for 10 min. The plates were frozen at −30 °C for 5 min in order to aid protein precipitation and centrifuged for 15 min, at 3600 rpm and 4 °C. Subsequently, the samples were frozen for 20 min at −30 °C to separate ACN and aqueous phase [36]. The mats were carefully removed and 200 μL of the supernatant acetonitrile layer were transferred, using the Tomtec workstation, from the original sample plates, into the respective positions of new 2.2 mL 96-deep-well plates. The height of the transfer stage was carefully chosen so that only organic layer was aspirated. Finally the resulting samples were transferred into the PAL CTC autosampler for on-line clean-up and analysis.

3. Results and discussion

3.1. Detection

According to a previously published paper [15], the protonation of RIS occurs at the nitrogen on the 1-position of pyrimidinone group rather than at the 5-position nitrogen which belongs to a cyclic amide. The molecular ions of RIS (427.2), 9-OH-RIS (427.2) and IS (421.1) produced intense product ion signals at m/z 191.4, 207.3 and 201.2, respectively, due to cleavage of the ethyl-piperidinyl nitrogen bond and the subsequent loss of the benzisoxazole group with its piperidine substituent. Optimization of the signal intensity allowed reliable determination of the analytes of interest at the lower limit of quantification (LLOQ).

3.2. Sub-zero temperature extraction

As mentioned above, all plasma samples were diluted 1:1 (v/v) with ACN containing the IS. However, this ratio cannot be considered sufficient in order to achieve complete denaturation and precipitation of proteins. Additionally, the high miscibility of ACN with water, especially at room temperature, prevents phase separation, resulting in an organic-aqueous mixture containing a significant load of matrix components. The presence of endogenous plasma compounds was considered responsible for the major signal suppression and the poor reproducibility of results during preliminary experiments.

Therefore, all samples after precipitation and centrifugation were frozen at −30 °C for 20 min to achieve separation between the organic and the aqueous layers. After freezing, an interme-

diate layer between the ACN and aqueous phase was observed and the height of the transfer stage was carefully adjusted so that only the ACN layer would be aspirated and transferred. The volume of recoverable ACN was 200 μL, when 300 μL were added initially.

3.3. Semi-automated sample pre-treatment and TFC with ternary column-switching

Application of Multiprobe robotic workstation allowed rapid plasma sample transfer from properly labeled Eppendorf tubes into 96-well plate. This conversion into the 96-well format was a critical step in the automation process as all samples could be further processed in a batch-wise fashion by the Tomtec Quadra 96 workstation that is able to process all 96 samples in parallel. This resulted in an extremely fast and accurate transfer of the supernatant ACN phase after sub-zero temperature extraction. The proposed method's throughput was remarkably high considering that in only 3 h time, 500 samples were ready to be submitted for analysis.

During the TFC column-switching step, a highly aqueous mobile phase (MeOH/H_2O, 5/95) was employed at the loading step with a flow rate of 5 mL min^{-1}. This resulted in a plug-type flow profile allowing large protein molecules to easily pass through the HLB columns and directly to the waste while the compounds of interest were retained. It was also found during method development that a flow rate of 5 mL min^{-1} resulted in increased signal response and improved peak shape compared to that of 4 mL min^{-1} while a period of 0.7 min proved to be the optimum loading time. The next step involved switching of the 10-port valve into Configuration B and back-flushing of the analytes from the extraction into the analytical column and the mass detector with elution mobile phase under a laminar flow rate of 0.8 mL min^{-1}.

The use of two extraction columns in parallel has the advantage of reduced run time as the equilibration time does not add to the chromatographic time. During the elution step of analytes from HLB$_1$ into the analytical column, HLB$_2$ is initially being "purified" with 0.1% $CH_3CO_2NH_4$ (w/v) in MeOH/ACN (80/20) under a flow rate of 5 mL min^{-1} for 1.6 min and re-equilibrated for 0.5 min with the loading mobile phase in order to "receive" the next injection.

3.4. Carry-over minimization protocol

A major problem encountered during assay development was carry-over contamination. Carry-over effect [37] tends to be more of an issue in on-line sample preparation than in conventional off-line methods. The large amount of proteins present in plasma can be adsorbed onto the surface of the (i) injector; (ii) transfer lines; (iii) column frits; (iv) column packing material through various mechanisms. Since most of the drug-like compounds are highly protein-bound, a small portion of them can remain in the system.

Initially in the current study, this phenomenon occurred in a large extent and was intense when injections of blank samples followed high concentrated samples. Their area reached in many

Table 2
Optimum on-line clean-up conditions for carry-over minimization

Loading mobile phase	MeOH/H_2O (5/95)
Purification mobile phase	0.1% ammonium acetate in MeOH/ACN (80/20)
Purification time	1.6 min
Turbulent flow	5 mL min^{-1}

cases 0.20% of the highest calibrator area value (200 ng mL^{-1}) for both RIS and 9-OH-RIS, which was four times higher than the respective of the first calibrator (0.1 ng mL^{-1}).

Our first attempts were focused on replacing needle and syringe tubing, without any change. Then, the initial loop (20 μL) was replaced with a 50 μL one, without changing the injection volume, while the injection speed was reduced from 50 to 20 μL s^{-1}. These factors often affect the hydrodynamic flow pattern of the solvent front reaching the loop inlet and outlet and can influence carry-over, however, in our case only a slight decrease of the phenomenon for 9-OH-RIS took place. Numerous experiments dealing with the composition of needle and valve wash solvents were also performed. All different solution mixtures of MeOH, ACN, H_2O and formic acid were tested, but had no effect on the phenomenon.

Consequently, it was concluded that HLB columns were the main source for carry over. The factors influencing on-line clean-up were the composition of loading and purification mobile phase, the turbulent flow rate and the duration of the HLB column purification stage. An experimental design was conducted and the obtained optimum conditions for on-line clean-up were the ones described in Table 2. Under these conditions carry-over was minimized to <0.01% for both compounds and it could not be discriminated from noise. At this point it should be noted that the presence of ACN in purification mobile phase was of great importance for this dramatic decrease. Without ACN carry-over could not be reduced <0.05% and 0.07% for 9-OH-RIS and RIS, respectively.

3.5. Chromatographic conditions

CN analytical column provided the best peak shape (more symmetrical and less tailing) with consistent retention times for both analytes and the internal standard. Typical LC–MS/MS MRM chromatograms of blank plasma and plasma spiked with RIS, 9-OH-RIS and IS are shown in Fig. 3 with retention times of 2.16, 2.08 and 2.20 min, respectively. The compounds were not chromatographically fully resolved, since LC–MS/MS provides the required selectivity for their reliable and accurate quantitation. These retention times were very short considering the additional stages for loading, purification and equilibration.

The efficiency of the on-line clean-up purification had a positive impact on column life duration. After three consecutive overnight runs of totally >1400 samples, the column backpressure measured during the loading step increased approximately 4% compared to the initial values (780 → 811 psi for pump1 and 531 → 554 psi for pump2). Furthermore, the retention times of all analytes were consistent throughout the study.
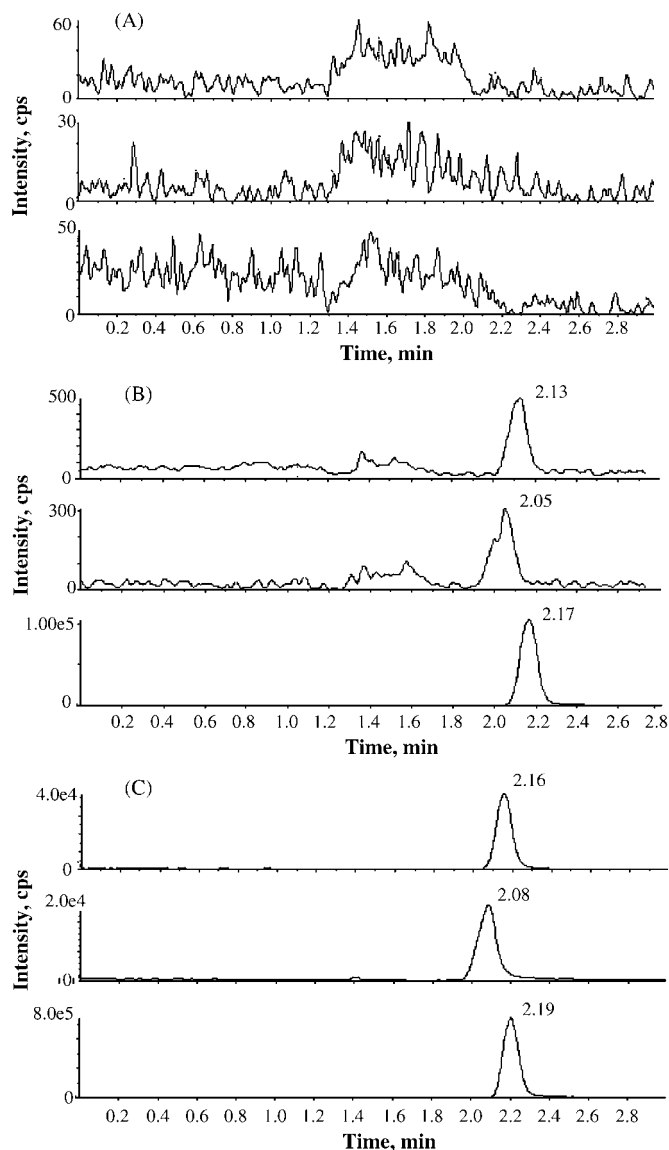
Fig. 3. Representative MRM chromatogram of RIS (top), 9-OH-RIS (middle) and IS obtained from a blank (A), MV$_L$ (B) and MV$_2$ (C) sample.

3.6. Standard curves

In order to define the relationship between concentration and response, a calibration curve, containing 11 non-zero standards, ranging from 0.1 to 200 ng mL^{-1} for both RIS and 9-OH-RIS,

was prepared for each analytical run. Peak area ratios of RIS and 9-OH-RIS to IS were used for regression analysis. The calculated concentrations were determined from linear regression using $1/x^2$ weighting. Individual standard curve data from five runs met all of the preset criteria.

The regression coefficients (*R*-squared) for the five runs were greater than 0.9800 for both analytes, the average linear slope was 0.0430 ($S_b = 0.0007$) for RIS and 0.0163 ($S_b = 0.0004$) for 9-OH-RIS while the average intercept was 0.0003 ($S_a = 0.0002$) for RIS and 0.000014 ($S_a = 0.0001$) for OH-RIS. However, before applying a statistical hypothesis test to the regression line coefficients it is essential to check whether "lack of fit" exists. This test is based on the analysis of the variance of the residuals from the regression line [38,39]. The ANOVA table (Table 3) divides the total variability of the residuals in *y* ($y = ax + b$) into two pieces: (i) A pure error piece, which measures the variability between replicate values of *y* at the same *X*. Since the variability among these replicates has nothing to do with the fitted model, it is a "pure" estimate of the noise in the data. (ii) A lack-of-fit piece, which estimates groups of replicates variation from the fitted line.

The table also shows the results of an *F* test comparing the estimated lack-of-fit to pure error through *F* ratio = lack-of-fit mean square/pure error mean square. These mean squares values result from dividing the sum of squares due to lack of fit and the sum of squares due to pure error by the corresponding degrees of freedom. Of primary interest is the *P*-value associated with the test. Small values of *P* (<0.05) indicate significant lack-of-fit at the 5% significance level. From *P* values listed in the table, it is obvious that there is no significant lack of fit and that the automated on-line SPE procedure employed in this method was capable of producing satisfactory concentration data for RIS and 9-OH-RIS standard samples.

3.7. Accuracy and precision

During method validation, the precision and accuracy were also assessed by analyzing method validation samples in five runs on three separate days. The % accuracy was determined by calculating the deviations of the predicted concentrations from their nominal values. In all cases the values were within the acceptable range. The intra-assay precision was assessed by analyzing six replicates at each MV level, while inter-assay precision was determined over five runs conducted in 3 days, by analyzing 30 samples. Data for both types of accuracy and pre-

Table 3
ANOVA results for lack of fit

	Degrees of freedom	Sum of squares	Mean square	*F* ratio	Probability level
Risperidone					
Error	49	9.70E−04	1.98E−05		
Lack of fit	9	1.05E−04	1.17E−05	0.54	0.83
Pure error	40	8.65E−04	2.16E−05		
9-OH-risperidone					
Error	44	2.32E−04	5.27E−06		
Lack of fit	9	3.60E−05	3.99E−06	0.71	0.69
Pure error	35	1.96E−04	5.60E−06		

Table 4
Intra- and inter-assay accuracy and precision results for RIS

MV sample	Intra-run accuracy (%)[a]	Inter-run accuracy (%)[b]	Intra-run precision (%CV)[c]	Inter-run precision (%CV)[b]
MV_L	106.9	101.7	13	6.8
MV_1	111.2	110.1	4.6	1.4
MV_2	108.1	102.3	5.2	3.8
MV_3	103.8	100.2	2.7	3.6

[a] Expressed as $100 \times$ (mean calculated concentration)/(nominal concentration) ($n = 6$).
[b] Values obtained from all 5 runs ($n = 30$).
[c] $n = 6$.

Table 5
Intra- and inter-assay accuracy and precision results for 9-OH-RIS

MV sample	Intra-run accuracy (%)[a]	Inter-run accuracy (%)[b]	Intra-run precision (%CV)[c]	Inter-run precision (%CV)[b]
MV_L	117.1	99.6	14	13
MV_1	108.7	106.4	9.5	4.8
MV_2	106.2	103.4	6.5	3.9
MV_3	110.7	105.7	8.2	4.3

[a] Expressed as $100 \times$ (mean calculated concentration)/(nominal concentration) ($n = 6$).
[b] Values obtained from all 5 runs ($n = 30$).
[c] $n = 6$.

cision (expressed as CV%) are presented in Tables 4 and 5 for RIS and 9-OH-RIS, respectively.

3.8. Recovery and matrix effect

The extraction efficiency of the analytical method was assessed using data from five runs. Recovery values were determined by comparing the absolute peak areas of the analytes spiked in human plasma which had undergone the sub-zero temperature extraction procedure with the peak areas of the analytes spiked in ACN at three QC concentration levels (QC_1, QC_2 and QC_3). Mean values of extraction recovery for RIS in QC_1, QC_2 and QC_3 were 55.7%, 40.0% and 43.6%, respectively, while for 9-OH-RIS the corresponding values were 40.9%, 32.2% and 35.6%. Mean extraction recovery for the I.S was 106.5%. IS was selected so as to have very small structural differences with RIS and 9-OH-RIS. However, it seems that even these small differences led to significantly different behavior (probably during HLB washing) between the molecules of interest and IS. However, the above recovery values were consistent and more than adequate for the specific concentration range, and therefore no problems with RIS and 9-OH-RIS quantification were observed. The current procedure takes into account possible ion suppression caused by matrix endogenous components which may have remained after the loading phase during on-line clean-up. However, the fact that both accuracy and precision of the samples at all concentration levels were within the acceptance criteria ($\leq 20\%$ for LLOQ and $\leq 15\%$ for the rest levels) suggests that the endogenous materials should have been effectively removed.

3.9. Assay application to a bioequivalence study

A crossover bioequivalence study of risperidone comparing a test formulation (HELP Pharmaceutical Company, sponsor: Chepharma) versus a reference formulation (Risperdal®/

Table 6
Pharmacokinetic parameters (mean values) of risperidone and 9-hydroxy-risperidone after oral administration of a single dose of 2 mg in 30 volunteers

Parameter		Values
AUC_{0-96h} (ng h/mL)[a]	RIS	117.9
	9-OH-RIS	280.2
$AUC_{0-\infty}$ (ng h/mL)	RIS	241.0
	9-OH-RIS	298.7
C_{max} (ng/mL)	RIS	19.15
	9-OH-RIS	12.54
T_{max} (h)	RIS	1.13
	9-OH-RIS	4.35
$t_{1/2}$ (h)	RIS	5.35
	9-OH-RIS	23.6

[a] Area under (concentration) curve.

Janssen-Cilag), after the administration of a single dose of each formulation (2 mg/tab) in 30 healthy volunteers, was conducted according to the approved protocol, the ethical principles that have origins in the Declaration of Helsinki and the Good Laboratory Practice (GLP) regulatory requirements. Blood samples collected at designated times were analyzed with the current method. Mean pharmacokinetic parameters obtained from concentration data are presented in Table 6. All calculations were performed using Pharsight WinNonLin 5.0.1 statistical software and based on these parameters we concluded that the two formulations were bioequivalent.

4. Conclusions

We have presented a high-throughput ternary column on-line clean-up LC–MS/MS method for the simultaneous determination of risperidone and its co-active metabolite, 9-hydroxy-risperidone, in human plasma. This system employed

two parallel extraction columns and an analytical one allowing the equilibration of one extraction column while the analysis is taking place on the other extraction column. This resulted in a total run time of 3 min compared to run times of 4 min or more, required for other off-line and on-line methods reported for the determination of RIS and 9-OH-RIS.

Despite the fact that this approach cannot be considered as a direct injection technique the use of two liquid-handling robotic workstations greatly simplified the sub-zero temperature extraction process, not only compensating for the extra time required for extraction but resulting in significant advantages over existing methods with manual sample treatment, in terms of throughput and efficiency. Furthermore, the precipitation–extraction step provided cleaner extracts with a relatively low content of proteins, especially with application the sub-zero temperature protocol. The latter, in combination with the use of two extraction columns instead of one allowed for longer column lifetime compared to traditional direct injection methods. Furthermore, the proposed method had high selectivity, sensitivity and wide linear range of 0.1–200 ng mL^{-1}.

The present method was applied to a bioequivalence study of risperidone after per os administration of a 2 mg tablet of the test and reference formulation and allowed its completion in just 4 days time. The described high-throughput method possessed excellent precision and accuracy and proved to be reliable. It is expected that this approach can be applied for the extraction and analysis of other pharmaceutical compounds from biological samples.

References

[1] J.E. Leysen, W. Gommeren, A. Eens, D. de Chafoy de Courcelles, J.C. Stoof, P.A.J. Janssen, J. Pharmacol. Exp. Ther. 247 (1988) 661.
[2] G. Chouinard, W. Arnott, Can. J. Psychiatry 38 (1993) S89.
[3] G. Chouinard, B. Jones, G. Remington, D. Bloom, D. Addington, W. MacEwan, A. Labelle, L. Beauclair, W. Arnott, J. Clin. Psychopharmacol. 13 (1993) 25.
[4] A. Schotte, P.F.M. Janssen, A.A.H.P. Megens, J.E. Leysen, Brain Res. 631 (1993) 191.
[5] G. Mannens, M.L. Huang, W. Meuldermans, J. Hendrickx, R. Woestenborghs, J. Heykants, Drug Metab. Dispos. 21 (1993) 1134.
[6] G. Chouinard, L. Kopala, A. Labelle, L. Beauclair, S.V. Johnson, K.I. Singh, Can. J. Psychiatry 43 (1998) 1018.
[7] O.V. Olesen, R.W. Licht, E. Thomsen, T. Bruun, J.E. Viftrup, K. Linnet, Ther. Drug Monit. 20 (1998) 380.
[8] M. Aravagiri, S.R. Marder, D. Wirshing, W.C. Wirshing, Pharmacopsychiatry 31 (1998) 102.
[9] R. Woestenborghs, W. Lorreyne, F. Van Rompaey, J. Heykants, J. Chromatogr. 583 (1992) 223.
[10] J.P. Le Moing, S. Edouard, J.C. Levron, J. Chromatogr. 614 (1993) 333.
[11] A. Avenoso, G. Facciolà, M. Salemi, E. Spina, J. Chromatogr. B 746 (2000) 173.
[12] A. LLerena, R. Berecz, P. Dorado, C. Sanz de la Garza, M.J. Norberto, M. Càceres, J.R. Gutiérez, J. Chromatogr. B 783 (2003) 213.
[13] O.V. Olesen, K. Linnet, J. Chromatogr. B 698 (1997) 209.
[14] M. Aravagiri, S.R. Marder, J. Mass Spectrom. 35 (2000) 718.
[15] S. McClean, E.J. O'Kane, W.F. Smyth, J. Chromatogr. B 740 (2000) 141.
[16] B.M.M. Remmerie, L.L.A. Sips, R. de Vries, J. de Jong, A.M. Schothuis, E.W.J. Hooijschuur, N.C. van de Merbel, J. Chromatogr. B 783 (2003) 461.
[17] J. Flarakos, W. Luo, M. Aman, D. Snivarov, N. Gerber, P. Vouros, J. Chromatogr. A 1026 (2004) 175.
[18] G. Basileo, M. Breda, G. Fonte, R. Pisano, C.A. James, J. Pharm. Biomed. Anal. 32 (2003) 591.
[19] Y. Dotsikas, C. Kousoulos, G. Tsatsou, Y.L. Loukas, Rapid Commun. Mass Spectrom. 19 (2005) 2055.
[20] N. Zhang, A. Yang, J.D. Rogers, J.J. Zhao, J. Pharm. Biomed. Anal. 34 (2004) 175.
[21] S. Barattè, S. Sarati, E. Frigerio, C.A. James, C. Ye, Q. Zhang, J. Chromatogr. A 1024 (2004) 87.
[22] J. Zhang, W. Zeng, C. Kitchen, A.Q. Wang, D.G. Musson, J. Chromatogr. B. 806 (2004) 167.
[23] C. Kousoulos, G. Tsatsou, C. Apostolou, Y. Dotsikas, Y.L. Loukas, Anal. Chim. Acta 551 (2005) 177.
[24] C. Kousoulos, G. Tsatsou, C. Apostolou, Y. Dotsikas, Y.L. Loukas, Anal. Bioanal. Chem. 384 (2006) 199.
[25] J.T. Wu, H. Zeng, M. Qian, B.L. Brogdon, S.E. Unger, Anal. Chem. 72 (2000) 61.
[26] D. Zimmer, V. Pickard, W. Czembor, C. Müller, J. Chromatogr. A 854 (1999) 23.
[27] W. Zeng, A.Q. Wang, A.L. Fisher, D.G. Musson, Rapid Commun. Mass Spectrom. 17 (2003) 2475.
[28] X. Xu, K.X. Yan, H. Song, M.-W. Lo, J. Chromatogr. B 814 (2005) 29.
[29] Y.-J. Xue, K.C. Turner, J.B. Meeker, J. Pursley, M. Arnold, S. Unger, J. Chromatogr. B 795 (2003) 215.
[30] K. Heinig, F. Bucheli, J. Chromatogr. B 769 (2002) 9.
[31] M. Tanaka, H. Yamazaki, Anal. Chem. 68 (1996) 1513.
[32] X. Ye, Z. Kuklenyik, L.L. Needham, A.M. Calafat, Anal. Chem. 77 (2005) 5407.
[33] J.-T. Wu, H. Zeng, M. Qian, B.L. Brogdon, S.E. Unger, Anal. Chem. 72 (2000) 61.
[34] M. Zell, C. Husser, G. Hopfgartner, J. Mass Spectrom. 32 (1997) 23.
[35] Y.-Q. Xia, D.B. Whigan, M.L. Powell, M. Jemal, Rapid Commun. Mass Spectrom. 14 (2000) 105.
[36] M. Yoshida, A. Akane, Anal. Chem. 71 (1999) 1918.
[37] D. Wells, High Throughput Bioanalytical Sample Preparation, Elsevier Science, New York, 2003, p. 539.
[38] A. Martínez, J. Riu, F.X. Rius, Chemometr. Intell. Lab. Syst. 54 (2000) 61.
[39] M. Analla, Agric. Syst. 57 (1998) 115.

Part-per-trillion determination of chlorobenzenes in water using dispersive liquid–liquid microextraction combined gas chromatography–electron capture detection

Reyhaneh Rahnama Kozani [c], Yaghoub Assadi [a,b,*], Farzaneh Shemirani [c], Mohammad-Reza Milani Hosseini [a,b], Mohammad Reza Jamali [d]

[a] *Department of Analytical Chemistry, Faculty of Chemistry, Iran University of Science and Technology, Tehran, Iran*
[b] *Electroanalytical Chemistry Research Center, Faculty of Chemistry, Iran University of Science and Technology, Tehran, Iran*
[c] *School of Chemistry, University College of Science, University of Tehran, Tehran, Iran*
[d] *Department of Chemistry, Payame Noor University, Behshahr, Iran*

Abstract

In this study, a simple, rapid and efficient method, dispersive liquid–liquid microextraction (DLLME) combined gas chromatography–electron capture detection (GC–ECD), for the determination of chlorobenzenes (CBs) in water samples, has been described. This method involves the use of an appropriate mixture of extraction solvent (9.5 µl chlorobenzene) and disperser solvent (0.50 ml acetone) for the formation of cloudy solution in 5.00 ml aqueous sample containing analytes. After extraction, phase separation was performed by centrifugation and the enriched analytes in sedimented phase were determined by gas chromatography–electron capture detection (GC–ECD). Our simple conditions were conducted at room temperature with no stiring and no salt addition in order to minimize sample preparation steps. Parameters such as the kind and volume of extraction solvent, the kind and volume of disperser solvent, extraction time and salt effect, were studied and optimized. The method exhibited enrichment factors and recoveries ranging from 711 to 813 and 71.1 to 81.3%, respectively, within very short extraction time. The linearity of the method ranged from 0.05 to 100 $\mu g\,l^{-1}$ for dichlorobenzene isomers (DCB), 0.002–20 $\mu g\,l^{-1}$ for trichlorobenzene (TCB) and tetrachlorobenzene (TeCB) isomers and from 0.001 to 4 $\mu g\,l^{-1}$ for pentachlorobenzene (PeCB) and hexachlorobenzene (HCB). The limit of detection was in the low $\mu g\,l^{-1}$ level, ranging between 0.0005 and 0.05 $\mu g\,l^{-1}$. The relative standard deviations (R.S.D.s) for the concentration of DCB isomers, 5.00 $\mu g\,l^{-1}$, TCB and TeCB isomers, 0.500 $\mu g\,l^{-1}$, PeCB and HCB 0.100 $\mu g\,l^{-1}$ in water by using the internal standard were in the range of 0.52–2.8% ($n = 5$) and without the internal standard were in the range of 4.6–6.0% ($n = 5$). The relative recoveries of spiked CBs at different levels of chlorobenzene isomers in tap, well and river water samples were 109–121%, 105–113% and 87–120%, respectively. It is concluded that this method can be successfully applied for the determination of CBs in tap, river and well water samples.
© 2006 Elsevier B.V. All rights reserved.

Keywords: Dispersive liquid–liquid microextraction (DLLME); Chlorobenzenes; Gas chromatography; Water samples

1. Introduction

Chlorobenzenes (CBs) that are widely used as industrial solvents, pesticides, dielectric fluids, deodorant and chemical intermediates can enter the aquatic environment through solid and liquid effluents and atmospheric discharges. These compounds have high octanol–water partition coefficient [1], so biological accumulation can be expected in the aquatic ecosystem. Due to their acute toxicity [2] and potential harmfulness to the aqueous environment [3], these compounds have been ranked as priority pollutants by United States Environmental Protection Agency (USEPA) [4]. Thus, excessive exposure to these compounds can exert effects on the central nervous system, irritation of the eyes, irritation of the upper respiratory tract, hardening of skin, and hematological disorders including anemia [5]. Therefore, research is directed towards developing inexpensive, simple and efficient sample preparation and analytical techniques for the

* Corresponding author at: Department of Analytical Chemistry, Faculty of Chemistry, Iran University of Science and Technology, Tehran, Iran.
Tel.: +98 21 77491204; fax: +98 21 77491204.
E-mail address: y_assadi@iust.ac.ir (Y. Assadi).

detection of trace quantities of these compounds in water samples. In order to determine trace or ultra-trace CBs in water samples, a chemical separation and preconcentration step is often necessary prior to analysis. There have been many reports on the application of a preconcentration and separation method prior to the analysis of CBs such as liquid–liquid extraction (LLE) [1,6], solid phase extraction (SPE) [7–9], headspace solid phase microextraction (HS-SPME) [4,10–15], liquid phase microextraction (LPME) [16,17], headspace liquid phase microextraction (HS-LPME) [18–20] and microwave extraction [21].

Recently, we have developed a simple and rapid preconcentration and microextraction method, dispersive liquid–liquid microextraction (DLLME), which was initially used for determination of polycyclic aromatic hydrocarbons (PAHs) and organophosphorous pesticides (OPPs) in water samples [22,23]. This method consists of two steps: (1) the injection of an appropriate mixture of extraction and disperser solvent into aqueous sample containing analytes: In this step extraction solvent was dispersed into the aqueous sample as very fine droplets and analytes were enriched into it. Because of infinitely large surface area between extraction solvent and aqueous sample, the equilibrium state is achieved quickly and extraction is independent of time. This is the most important advantage of this method. (2) The centrifugation of cloudy solution: After centrifugation, the determination of analytes in sedimented phase can be performed by instrumental analysis. Rapidity, high enrichment factor, simplicity of operation and low cost are some of the advantages of this method.

The object of the present work is to investigate the possibility of using DLLME combined gas chromatography–electron capture detection (GC–ECD) for the analysis of 11 CBs in water samples. The proposed method was optimized by controlling various parameters. The results indicated that DLLME is an efficient extraction technique to analyze CBs in water samples.

2. Experimental

2.1. Reagents and standards

1,2-Dichlorobenzene (1,2-DCB), 1,3-dichlorobenzene (1,3-DCB), 1,4-dichlorobenzene (1,4-DCB), 1,2,3-trichlorobenzene (1,2,3-TCB), 1,2,4-trichlorobenzene (1,2,4-TCB), 1,3,5-trichlorobenzene (1,3,5-TCB), 1,2,3,4-tetrachlorobenzene (1,2,3,4-TeCB), 1,2,4,5-tetrachlorobenzene (1,2,4,5-TeCB), 1,2,3,5-tetrachlorobenzene (1,2,3,5-TeCB), pentachlorobenzene (PeCB) and hexachlorobenzene (HCB) were supplied by Riedel-de Haën (Seelze-Germany). 1,4-Dibromobenzene (internal standard), acetone (suprasolv for gas chromatography), acetonitrile (hyper grade for liquid chromatography), methanol (for spectroscopy), carbon disulfide (for spectroscopy) and chlorobenzene, were obtained from Merck (Darmstadt-Germany). For more purification, chlorobenzene was distillated four times before use.

Stock standard solutions were prepared in acetone (10 ml), with concentration levels of $10,000\,mg\,l^{-1}$ for DCB isomers, $1000\,mg\,l^{-1}$ for TCB and TeCB isomers and $200\,mg\,l^{-1}$ for

PeCB and HCB and were stored in a freezer at $-20\,°C$. Working solutions were obtained by appropriate dilution.

2.2. Instrumentation

The analysis of CBs was performed on a Shimadzu GC-2010 gas chromatograph equipped with an electron capture detector (GC-ECD). The GC was fitted with ZB-1701 capillary column (15 m × 0.25 mm, i.d., 0.25 μm phase thickness, 86% dimethyl–14% cyanopropyl silicone) from Phenomenex (USA). The injection port was held at 250 °C and used in the splitless mode with splitless time of 0.50 min. Ultra pure helium (99.9999%, Air Products, UK) passes through a molecular sieve trap and oxygen trap (Crs, USA) was used as the carrier gas at constant linear velocity of $30\,cm\,s^{-1}$. The analysis was performed with an initial column temperature of 70 °C held for 5 min followed by heating to 125 °C at $5\,°C\,min^{-1}$, followed by heating to 200 °C at $15\,°C\,min^{-1}$ (held 4 min), and finally, followed by heating to 280 °C at $40\,°C\,min^{-1}$ and holding at 280 °C for 3 min to clean the column. The ECD temperature was maintained at 300 °C. Ultra pure nitrogen (99.9999%, Air Products) as a makeup gas for ECD was passed through molecular sieve trap and oxygen trap (Crs) at the flow of $30\,ml\,min^{-1}$. The Centurion Scientific Ltd. (model 2010D, UK) was used for centrifuging.

All of the 10 ml screw cap glass test tube with conical bottom (extraction vessel) was maintained at 500 °C in furnace (Carbolite, model CWF 1200, UK) for cleaning of any organic compounds and good sedimentation of fine droplets of extraction solvent (chlorobenzene) in the centrifugation step.

2.3. Extraction procedure

For the DLLME, an aliquot of 5.00 ml of a aqueous solution containing $5.00\,μg\,l^{-1}$ of DCB isomers, $0.500\,μg\,l^{-1}$ of TCB and TeCB isomers, $0.100\,μg\,l^{-1}$ of PeCB and HCB, and $1.00\,μg\,l^{-1}$ of 1,4-dibromobenzene (IS) was placed in a 10 ml screw cap glass test tube with conical bottom. Then the injection of 0.500 ml acetone (disperser solvent) containing 9.5 μl chlorobenzene (extraction solvent) was performed by using 0.50 ml syringe (gastight, Hamilton, USA), rapidly. By the injection of mentioned mixture, a cloudy solution that consists of very fine droplets of chlorobenzene dispersed into aqueous sample was formed. After centrifugation for 2.0 min at 5000 rpm, extraction solvent was sedimented in the bottom of the conical test tube. The volume of the sedimented phase was determined using a 10.0-μl microsyringe which was about 5.0 μl. The 0.50 μl of sedimented phase was removed using a 1.00-μl microsyringe (zero dead volume, cone tip needle, SGE, Australia) and injected into GC.

3. Result and discussion

It is necessary to investigate the effect of all parameters that can probably influence the performance of extraction. In DLLME method these parameters are the kind and volume of extraction solvent, the kind and volume of disperser solvent,

extraction time and salt addition that were investigated and optimized in order to achieve high recovery and enrichment factor of CBs from water samples. We selected five compounds as representative of the CBs, and showed their behavior under these extraction conditions.

3.1. Effect of the kind of extraction solvent

In the selection of extraction solvent, some properties must be considered: it should have (a) higher density than water, (b) good chromatographic behavior, (c) extraction capability of interested compounds and (d) low solubility in water. Most of the heavy solvents are halogenated compounds. According to the strong response with a high peak tailing of the halogenated solvents in ECD, there are some restrictions for choosing an extraction solvent. Among all solvents, carbon disulfide (CS_2) (density: $1.2\,g\,ml^{-1}$, boiling point: $46\,°C$), that had all of these properties, and chlorobenzene (density: $1.1\,g\,ml^{-1}$, boiling point: $131.6\,°C$), that had much lower response factor than analytes in ECD [1], were selected as extraction solvent and investigated for DLLME of CBs from water samples. For this purpose, a series of sample solution were studied by using 0.50 ml acetone containing 9.5 and 19.5 μl of chlorobenzene and CS_2, respectively, to achieve 5.0 μl volume of sedimented phase. According to results in Table 1, chlorobenzene has a little higher extraction efficiency than CS_2 that is because of similarity with analytes. Also, standard deviations by using chlorobenzene as extraction solvent are lower than CS_2 because repeatability in the volume of sedimented phase with chlorobenzene is better than CS_2. Therefore chlorobenzene was selected as extraction solvent.

3.2. Effect of the kind of disperser solvent

Solvents that are miscible in extraction solvent and aqueous solution can be used as disperser solvents. These solvents can disperse extraction solvent as very fine droplets in aqueous phase. Therefore, acetone, acetonitrile and methanol were selected as disperser solvent and the effect of these solvents on the performance of DLLME was investigated. For this purpose, various experiments were performed using 0.50 ml of each disperser solvent containing 9.5 μl extraction solvent (chlorobenzene) and the recoveries were investigated. Results are shown in Table 2. As can be seen, recoveries with acetonitrile (63.4–74.3%) and methanol (64.7–74.4%) are almost equal and recoveries with acetone (71.1–81.3%) are a little more. Thus, we chose acetone among these solvents because of higher recoveries, less toxicity and low cost.

3.3. Effect of volume of extraction solvent

In order to evaluate the effect of extraction solvent volume on extraction efficiency, additional experiments were performed using 0.50 ml acetone containing different volumes of chlorobenzene (9.5, 14.5, 19.5 and 24.5 μl). Figs. 1–3 show the curves of volume of sedimented phase, enrichment factor and recovery of CBs versus volume of extraction solvent (chlorobenzene), respectively. By increasing the volume of extraction solvent (chlorobenzene) from 9.5 to 24.5 μl, the volume of sedimented phase increases (5.0–19.5 μl) (Fig. 1) therefore, enrichment factor decreases from 710–816 to 210–246.6 (Fig. 2). Also, extraction recovery is almost constant (from 71.0–81.6% to 81.9–96.2%) (Fig. 3) because of quantity extraction and high distribution coefficient of CBs in this condition. Thus, 9.5 μl of chlorobenzene was selected in order to obtain high enrichment factor, low detection limit and good recovery.

3.4. Effect of volume of disperser solvent

After choosing acetone as disperser solvent, it is necessary to optimize the volume of it. Because at low volume, acetone

Table 1
Efficiency of different extraction solvents evaluated for extraction of CBs by DLLME[a]

Compounds	Recovery (%)	
	Chlorobenzene, mean ± S.D. ($n=3$)	Carbon disulfide, mean ± S.D. ($n=3$)
1,3-DCB	73.0 ± 0.37	71.4 ± 4.9
1,4-DCB	71.1 ± 0.34	70.5 ± 4.8
1,2-DCB	71.3 ± 0.44	66.7 ± 4.6
1,3,5-TCB	80.1 ± 1.14	71.2 ± 5.9
1,2,4-TCB	78.5 ± 0.70	69.4 ± 5.4
1,2,3-TCB	79.1 ± 0.99	70.6 ± 5.2
1,2,3,5-TeCB	81.3 ± 0.46	69.3 ± 5.9
1,2,4,5-TeCB	79.1 ± 0.81	67.4 ± 4.9
1,2,3,4-TeCB	78.8 ± 0.35	71.1 ± 4.6
PeCB	72.3 ± 1.05	63.3 ± 4.8
HCB	73.7 ± 1.53	66.5 ± 5.5

[a] Extraction conditions—water sample volume: 5.00 ml; disperser solvent (acetone) volume: 0.50 ml; extraction solvent volumes: 9.5 μl chlorobenzene and 19.5 μl carbon disulfide; sedimented phase volume: 5.0 ± 0.2 μl; room temperature; concentration of DCB isomers: 5.0 μg l^{-1}; TCB and TeCB isomers: 0.5 μg l^{-1}; PeCB and HCB: 0.1 μg l^{-1}.

Table 2
Efficiency of different disperser solvents evaluated for extraction of CBs by DLLME[a]

Compounds	Recovery (%)		
	Acetone, mean ± S.D. ($n=3$)	Acetonitrile, mean ± S.D. ($n=3$)	Methanol, mean ± S.D. ($n=3$)
1,3-DCB	73.0 ± 0.4	69.3 ± 3.9	69.0 ± 1.9
1,4-DCB	71.1 ± 0.3	67.4 ± 4.2	67.6 ± 2.4
1,2-DCB	71.3 ± 0.4	74.3 ± 4.2	68.5 ± 1.5
1,3,5-TCB	80.1 ± 1.1	73.2 ± 3.7	74.0 ± 2.3
1,2,4-TCB	78.5 ± 0.7	71.2 ± 3.8	72.4 ± 2.0
1,2,3-TCB	79.1 ± 1.0	72.3 ± 3.8	73.7 ± 2.1
1,2,3,5-TeCB	81.3 ± 0.5	73.3 ± 3.6	74.4 ± 2.8
1,2,4,5-TeCB	79.1 ± 0.8	72.0 ± 3.7	71.5 ± 1.3
1,2,3,4-TeCB	78.8 ± 0.3	71.1 ± 3.3	71.8 ± 2.0
PeCB	72.3 ± 1.0	63.4 ± 3.1	64.7 ± 1.5
HCB	73.7 ± 1.5	64.7 ± 2.1	66.3 ± 2.0

[a] Extraction conditions—water sample volume: 5.00 ml; disperser solvent (acetone, acetonitrile and methanol) volume: 0.50 ml; extraction solvent (chlorobenzene) volume: 9.5 μl; sedimented phase volume: 5.0 ± 0.2 μl; room temperature; concentration of DCB isomers: 5.0 μg l^{-1}; TCB and TeCB isomers: 0.5 μg l^{-1}; PeCB and HCB: 0.1 μg l^{-1}.
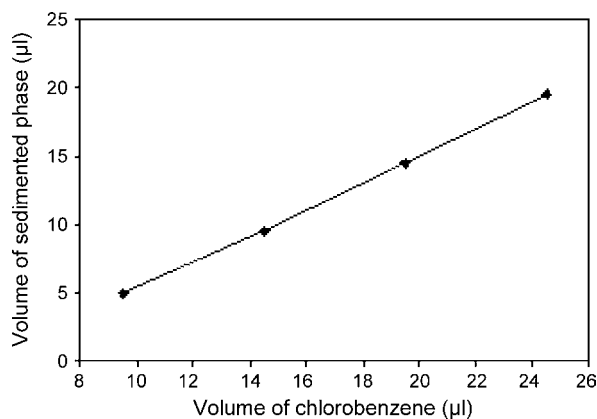
Fig. 1. Effect of the volume of extraction solvent (chlorobenzene) on the volume of sedimented phase in DLLME. Extraction conditions: water sample volume, 5.00 ml; disperser solvent (acetone) volume, 0.50 ml; room temperature.
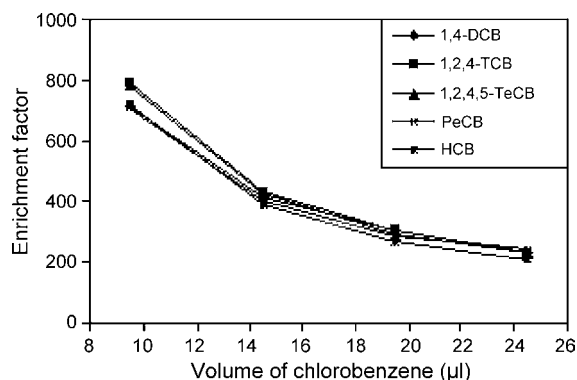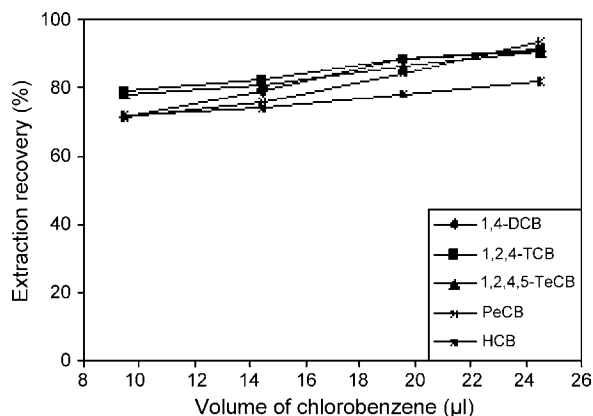

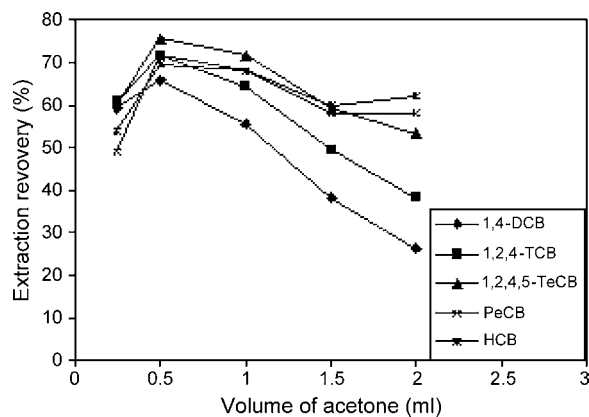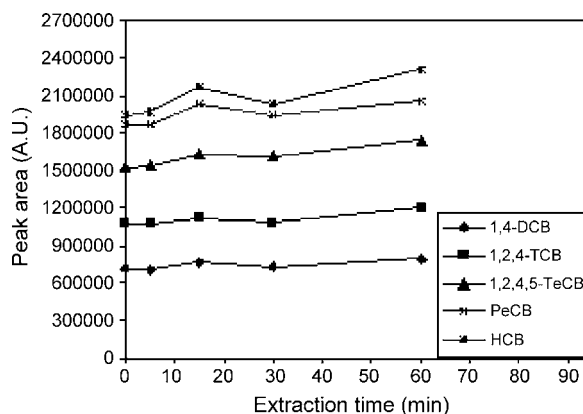Fig. 2. Effect of the volume of extraction solvent (chlorobenzene) on the enrichment factor of CBs obtained from DLLME. Extraction conditions: as with Fig. 1; concentration of DCB isomers, $5.0 \, \mu g \, l^{-1}$, TCB and TeCB isomers, $0.5 \, \mu g \, l^{-1}$, PeCB and HCB $0.1 \, \mu g \, l^{-1}$.

cannot disperse extraction solvent properly and cloudy solution is not formed completely and at high volume, the solubility of CBs in water increases, therefore, the extraction efficiency decreases, too. For obtaining optimized volume of acetone, various experiments were performed by using different volumes of acetone (0.25, 0.5, 1.0, 1.5 and 2.0 ml) containing 9.0, 9.5, 12.5,

Fig. 3. Effect of the volume of extraction solvent (chlorobenzene) on the recovery of CBs obtained from DLLME. Extraction conditions: as with Fig. 2.

Fig. 4. Effect of the volume of acetone on the recovery of CBs obtained from DLLME. Extraction conditions: water sample volume, 5.00 ml; sedimented phase volume, $5.0 \pm 0.2 \, \mu l$; room temperature; concentration of DCB isomers, $5.0 \, \mu g \, l^{-1}$, TCB and TeCB isomers, $0.5 \, \mu g \, l^{-1}$, PeCB and HCB $0.1 \, \mu g \, l^{-1}$.

Fig. 5. Effect of extraction time on the peak area of CBs obtained from DLLME. Extraction conditions, as with Fig. 2; extraction solvent (chlorobenzene) volume, 9.5 μl.

16.2 and 22.4 μl chlorobenzene, respectively. It is necessary to change the volume of chlorobenzene by changing the volume of acetone in order to obtain constant volume of sedimented phase ($5.0 \pm 0.2 \, \mu l$) in all experiments. Fig. 4 shows the curves of recoveries of CBs versus the volume of acetone. According to the results, a 0.50 ml acetone was chosen as the optimum volume.

3.5. Effect of extraction time

The effect of extraction time (interval time between the injection of a mixture of disperser solvent and extraction solvent, before starting to centrifuge) on the performance of DLLME is considered as a key factor which must be studied and evaluated. Therefore, for evaluating this parameter, different extraction times (ranged from 0 to 60 min) with constant experimental conditions were studied. According to the results (Fig. 5), this extraction method is time-independent, that is because of an infinitely large surface area between extraction solvent and aqueous phase. Therefore, this method is very fast and this is the most important advantage of DLLME technique.
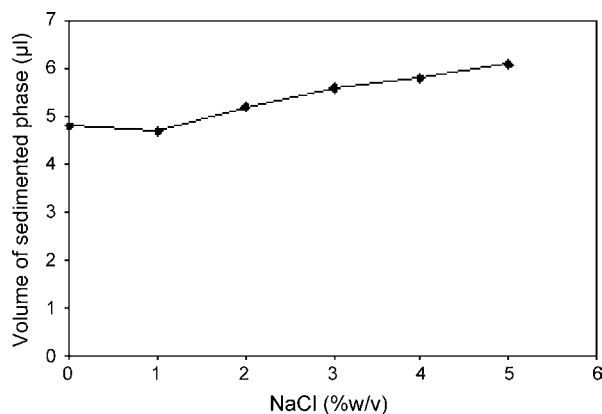
Fig. 6. Effect of salt addition on the volume of sedimented phase obtained from DLLME. Extraction conditions, as with Fig. 5.
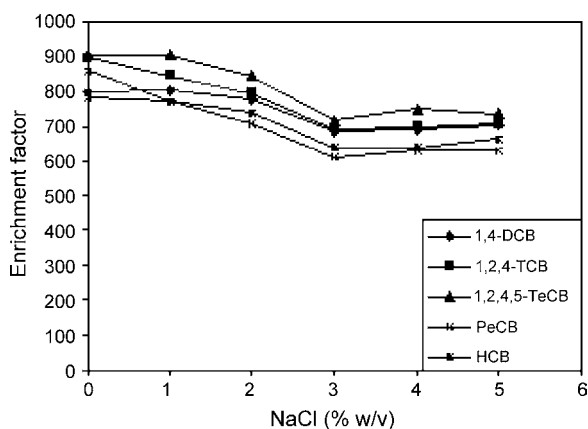

Fig. 7. Effect of salt addition on the enrichment factor obtained from DLLME. Extraction conditions, as with Fig. 5; concentration of DCB isomers, 5.0 μg l^{-1}, TCB and TeCB isomers, 0.5 μg l^{-1}, PeCB and HCB 0.1 μg l^{-1}.

3.6. Effect of salt

For investigating the influence of ionic strength on the performance of DLLME, various experiments were performed by adding different amounts of NaCl (0–5%). Other experimental conditions were kept constant. Figs. 6–8, show the effect of
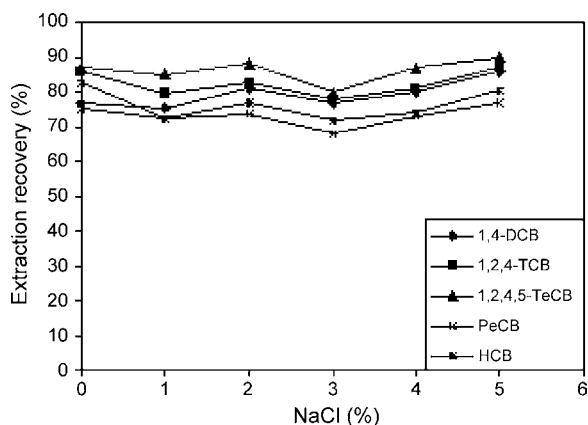
Fig. 8. Effect of salt addition on the recovery obtained from DLLME. Extraction conditions, as with Fig. 7.

increasing the ionic strength on the volume of sedimented phase, enrichment factor and the recovery of CBs. By increasing the ionic strength (from 0 to 5%) the solubility of extraction solvent in aqueous phase decreases, therefore, the volume of sedimented phase increases (from 4.8 to 6.1 μl) (Fig. 6). As a result, the enrichment factor decreases (from 780–924 to 630–752) (Fig. 7). According to Fig. 8, extraction recovery is almost constant (from 74.9–88.7 to 76.9–91.7%).

3.7. Quantitative analysis

The characteristics of calibration curves shown in Table 3 were obtained under optimized conditions. Linearity was observed in the range 0.05–100 μg l^{-1} for DCB isomers, 0.002–20 μg l^{-1} for TCB and TeCB isomers, and 0.001–4 μg l^{-1} for PeCB and HCB (more than three orders of magnitude) for most of analytes. Correlation coefficient (r^2) ranged from 0.9990 to 0.9998 with the internal standard and from 0.9990 to 0.9995 without the internal standard. The repeatability study was carried out by extracting a spiked (concentration of DCB isomers, 5.0 μg l^{-1}, TCB and TeCB isomers, 0.5 μg l^{-1}, PeCB and HCB 0.1 μg l^{-1}) water sample. The relative standard deviations (R.S.D.s) were calculated to be between 0.52 and 2.8% with the internal standard ($n = 5$) and between 4.6 and 6.0% without the internal standard ($n = 5$). The limit of detections (LODs), based on signal-to-noise ratio (S/N) of three ranged from 0.0005 to 0.05 μg l^{-1}. The enrichment factors and recoveries of CBs were from 711 to 813 and 71.1 to 81.3%, respectively [22].

3.8. Real water analysis

During the present investigation, matrix effects on the extraction were also evaluated by investigating the applicability of the proposed method to determine CBs concentration in river, tap and well water samples. River water was collected from Ziarat River (Gorgan, Iran) tap and well water from Tehran (Iran). These samples were extracted using DLLME method and analyzed by GC–ECD. The results from tap, river and well water samples showed that they were free of CBs contamination. These samples were spiked with CBs standards at different concentration levels to assess matrix effects. Fig. 9 shows the chromatograms obtained for well water and spiked well water at the concentration level of 10.0 μg l^{-1} for DCB isomers, 1.0 μg l^{-1} for TCB and TeCB isomers, and 0.2 μg l^{-1} for PeCB and HCB. The results of relative recovery of river, tap and well water samples are shown in Table 4. Relative recoveries for all CBs in tap, well and river water were between 109–121%, 105–113% and 87–120%, respectively. These results demonstrate that the tap, well and river water matrices, in our present context, had little effect on DLLME.

3.9. Comparison of DLLME with other methods

We compare DLLME–ECD of CBs from water samples with other methods such as LLE-GC–ECD [1], SPE-GC–MS [7,9], HS-SPME-GC–MS [4], LPME-GC–MS [16] and HS-LPME-

Table 3
Quantitative results of DLLME and GC-ECD of CBs from water sample[a]

Compounds	R.S.D.%[b] ($n = 5$)	R.S.D.%[c] ($n = 5$)	EF[d]	R[e] (%)	LR[f] ($\mu g\,l^{-1}$)	r^2 [g]	r^2 [h]	LOD[i] ($\mu g\,l^{-1}$)
1,3-DCB	0.73	4.8	730	73.0	0.05–100	0.9997	0.9995	0.02
1,4-DCB	2.8	5.4	711	71.1	0.1–100	0.9990	0.9990	0.05
1,2-DCB	0.52	4.6	713	71.3	0.05–100	0.9997	0.9994	0.02
1,3,5-TCB	1.4	5.0	801	80.1	0.005–20	0.9991	0.9990	0.002
1,2,4-TCB	1.1	5.0	785	78.5	0.005–20	0.9992	0.9991	0.002
1,2,3-TCB	0.9	4.9	790	79.0	0.002–20	0.9995	0.9993	0.001
1,2,3,5-TeCB	1.4	5.6	813	81.3	0.002–20	0.9994	0.9991	0.001
1,2,4,5-TeCB	1.5	5.3	791	79.1	0.005–20	0.9990	0.9990	0.002
1,2,3,4-TeCB	1.1	5.4	788	78.8	0.002–20	0.9992	0.9991	0.001
PeCB	2.7	6.0	723	72.3	0.001–4	0.9998	0.9995	0.0005
HCB	1.8	5.6	737	73.7	0.001–4	0.9996	0.9992	0.0005

[a] Extraction conditions—water sample volume: 5.00 ml; disperser solvent (acetone) volume: 0.50 ml; extraction solvent (chlorobenzene) volume: 9.5 μl; sedimented phase volume: 5.0 ± 0.2 μl; room temperature; concentration of internal standard (1,4-dibromobenzene): 1.00 $\mu g\,l^{-1}$.

[b] R.S.D.% by using internal standard at a concentration of DCB isomers: 5.0 $\mu g\,l^{-1}$; TCB and TeCB isomers: 0.5 $\mu g\,l^{-1}$; PeCB and HCB: 0.1 $\mu g\,l^{-1}$.

[c] R.S.D.% without using internal standard at a concentration of DCB isomers: 5.0 $\mu g\,l^{-1}$; TCB and TeCB isomers: 0.5 $\mu g\,l^{-1}$; PeCB and HCB: 0.1 $\mu g\,l^{-1}$.

[d] Enrichment factor.

[e] Recovery.

[f] Linear range.

[g] r^2 by using internal standard.

[h] r^2 without using internal standard.

[i] Limit of detection for a S/N = 3.

Table 4
Relative recoveries and standard deviations of CBs from spiked tap, well, river water samples[a]

Compounds	Tap water			Well water			River water		
	Added ($\mu g\,l^{-1}$)	Found (S.D.[b], $n = 3$) ($\mu g\,l^{-1}$)	Recovery (%)	Added ($\mu g\,l^{-1}$)	Found (S.D.[b], $n = 3$) ($\mu g\,l^{-1}$)	Recovery (%)	Added ($\mu g\,l^{-1}$)	Found (S.D.[b], $n = 3$) ($\mu g\,l^{-1}$)	Recovery (%)
1,3-DCB	1.0	1.09 (0.04)	109	10.0	11.01 (0.07)	110	100.0	120.0 (1.9)	120
1,4-DCB	1.0	1.09 (0.08)	109	10.0	10.80 (0.07)	108	100.0	111.5 (2.1)	111
1,2-DCB	1.0	1.14 (0.04)	114	10.0	11.20 (0.07)	112	100.0	111.6 (2.5)	112
1,3,5-TCB	0.1	0.115 (0.005)	115	1.0	1.080 (0.009)	108	10.0	10.7 (0.4)	107
1,2,4-TCB	0.1	0.121 (0.005)	121	1.0	1.076 (0.009)	108	10.0	10.7 (0.3)	107
1,2,3-TCB	0.1	0.114 (0.005)	114	1.0	1.07 (0.01)	107	10.0	10.6 (0.3)	106
1,2,3,5-TeCB	0.1	0.114 (0.003)	114	1.0	1.09 (0.02)	109	10.0	9.7 (0.9)	97
1,2,4,5-TeCB	0.1	0.115 (0.003)	115	1.0	1.05 (0.01)	105	10.0	9.9 (0.8)	99
1,2,3,4-TeCB	0.1	0.109 (0.004)	109	1.0	1.130 (0.014)	113	10.0	9.9 (0.8)	99
PeCB	0.02	0.023 (0.001)	115	0. 2	0.215 (0.005)	107	2.0	1.86 (0.23)	93
HCB	0.02	0.023 (0.001)	115	0.2	0.214 (0.003)	107	2.0	1.74 (0.16)	87

[a] Extraction conditions—water sample volume: 5.00 ml; disperser solvent (acetone) volume: 0.50 ml; extraction solvent (chlorobenzene) volume: 9.5 μl; sedimented phase volume: 5.0 ± 0.2 μl; room temperature; concentration of internal standard (1,4-dibromobenzene): 1.00 $\mu g\,l^{-1}$.

[b] Standard deviation.

Table 5
Comparison of DLLME with other methods for determination of CBs

Method	LOD[a] ($\mu g\,l^{-1}$)	R.S.D.[b] (%)	Extraction time (min)	Sample volume (ml)	Reference
LLE-GC–ECD	0.00001–0.001	10	>240	4000	[1]
SPE-GC–MS	0.010–0.042	<10	About 60	200	[7]
SPE-GC–MS	0.08–0.6	3–8	About 60	100	[9]
HS-SPME-GC–MS	0.003–0.006	1.19–8.19	30	5	[4]
LPME-GC–MS	0.02–0.05	3.62–9.26	3.5	4	[16]
HS-LPME-GC–MS	0.003–0.031	2.1–13.2	5	10	[19]
DLLME-GC–ECD	0.0005–0.05	0.52–2.8	A few second	5	Represented method

[a] Limit of detection.

[b] Relative standard deviation.
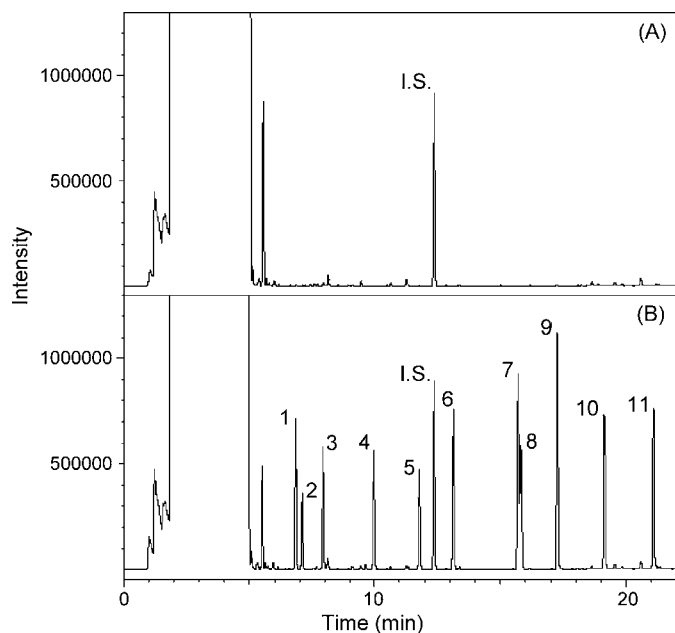
Fig. 9. Chromatograms of well water (A) and spiked well water at concentration level of 10.0 µg l^{-1} DCB isomers, 1.0 µg l^{-1} TCB and TeCB isomers and 0.2 µg l^{-1} PeCB and HCB (B) obtained by using DLLME combined GC–ECD. Extraction conditions: water sample volume, 5.00 ml; disperser solvent (acetone) volume, 0.50 ml; extraction solvent (chlorobenzene) volume, 9.5 µl; sedimented phase volume, 5.0 ± 0.2 µl; room temperature. Peak identification: (1) 1,3-DCB, (2) 1,4-DCB, (3) 1,2-DCB, (4) 1,3,5-TCB, (5) 1,2,4-TCB, (6) 1,2,3-TCB, (7) 1,2,3,5-TeCB, (8) 1,2,4,5-TeCB, (9) 1,2,3,4-TeCB, (10) PeCB, (11) HCB, (IS) 1,4-dibromobenzene, concentration of IS 1.00 µg l^{-1}.

GC–MS [19] from the viewpoint of the limit of detection (LOD), relative standard deviation (R.S.D.), extraction time and sample volume (Table 5). As can be seen, LODs of DLLME-GC–ECD with a sample volume of only 5.00 ml are better than other methods. R.S.D.s in DLLME are very low and extraction time is very short. All these results indicate that DLLME is a sensitive, rapid and reproducible technique that can be used for the preconcentration of CBs from water samples.

4. Conclusion

This paper describes a DLLME method combined with GC–ECD that is applied to the analysis of 11 chlorinated benzenes in environmental water samples. The results of this study demonstrate that the proposed method give acceptable relative recoveries and repeatabilities for CBs from tap, river and well water samples.

The proposed method is linear over a wide range. Detection limits at the ng l^{-1} level were achieved with a sample volume of only 5.00 ml. In this method sample preparation time as well as consumption of toxic organic solvents was minimized without affecting the sensitivity of the method. Compared with other extraction methods such as liquid–liquid extraction, solid phase extraction, liquid phase microextraction and solid phase microextraction, the present method has lower detection limits and R.S.D.s within very short extraction time. This method is also simple, convenient, sufficiently sensitive, precise, cost-effective and rapid.

References

[1] B.G. Oliver, K.D. Bothen, Anal. Chem. 52 (1980) 2066.
[2] A. Belfroid, W. Seinen, K. Vangestel, J. Hermens, Chemosphere 26 (1993) 2265.
[3] M.E. Stephenson, in: R. Haque (Ed.), Dynamics, Exposure Acknowledgements and Hazard Assessment of Toxic Chemicals, Ann Arbor Science, Ann Arbor, MI, 1980.
[4] Y. He, Y. Wang, H.K. Lee, J. Chromatogr. A 874 (2000) 149.
[5] B.G. Oliver, K.D. Bothen, Int. J. Environ. Anal. Chem. 12 (1982) 131.
[6] R.G. Melcher, P.L. Morabito, Anal. Chem. 62 (1990) 2183.
[7] Y. Wang, H.K. Lee, J. Chromatogr. A 803 (1998) 219.
[8] R. Barro, S. Ares, C. Garcia-Jares, M. Llompart, R. Cela, J. Chromatogr. A 1045 (2004) 189.
[9] G. Liu, J. Wang, Y. Zhu, X. Zhang, Anal. Lett. 37 (2004) 3085.
[10] M. Giardina, L.H. Ding, S.V. Olesik, J. Chromatogr. A 1060 (2004) 215.
[11] H.A. Leslie, J.L.M. Hermens, M.H.S. Kraak, Environ. Toxicol. Chem. 23 (2004) 2017.
[12] A. Paschke, P. Popp, J. Chromatogr. A 1025 (2004) 11.
[13] D.H. Wang, J. Xing, J.G. Peng, C.Y. Wu, J. Chromatogr. A 1005 (2003) 1.
[14] Z. Takats, K. Torkos, Chromatographia 48 (1998) 74.
[15] J. Liu, K. Hara, S. Kashimura, T. Hamanaka, S. Tomojiri, K. Tanaka, J. Chromatogr. B 731 (1999) 217.
[16] Y. Wang, Y. Chian Kwok, Y. He, H.K. Lee, Anal. Chem. 70 (1998) 4610.
[17] A. Tor, J. Chromatogr. A 1125 (2006) 129.
[18] M. Khajeh, Y. Yamini, J. Hassan, Talanta 69 (2006) 1088.
[19] L. Vidal, A. Canals, N. Kalogerakis, E. Psillakis, J. Chromatogr. A 1089 (2005) 25.
[20] G. Shen, H.K. Lee, Anal. Chem. 75 (2003) 98.
[21] F.I. Onuska, K.A. Terry, J. Microcolumn Sep. 7 (1995) 319.
[22] M. Rezaee, Y. Assadi, M.R. Milani Hosseini, E. Aghaee, F. Ahmadi, S. Berijani, J. Chromatogr. A 1116 (2006) 1.
[23] S. Berijani, Y. Assadi, M. Anbia, M.R. Milani Hosseini, E. Aghaee, J. Chromatogr. A 1123 (2006) 1.

ELSEVIER

Antioxidants determination with laccase

Juozas Kulys [a,b,*], Irina Bratkovskaja [a]

[a] *Institute of Biochemistry, Department of Enzyme Chemistry, Mokslininku 12, LT-08662 Vilnius, Lithuania*
[b] *Vilnius Gediminas Technical University, Faculty of Fundamental Sciences, Department of Chemistry and Bioengineering,
Sauletekio Avenue 11, LT-10223 Vilnius, Lithuania*

Abstract

The spectrophotometric method of antioxidants determination using recombinant laccase *Polyporus pinsitus* (rPpL) and *Myceliophthora thermophila* (rMtL) was developed. The method includes simultaneous oxidation of the antioxidant and high reactive laccase substrate producing chromophoric radical cation. As laccase substrates ABTS and other high reactive phenoxazine derivatives: 2-phenoxazin-10-yl-ethanol (PET), 3-phenoxazin-10-yl-propane-1-sulfonic acid (PPSA) and 3-phenoxazin-10-yl-propionic acid (PPA) were used. The kinetic data were analysed using a scheme of simultaneous oxidation of the antioxidant and the substrate.

In a range of $(0.9–7.3) \times 10^{-6}$ M of Trolox the measurings recovered 91 and 99% of the antioxidant if ABTS and both laccases were used. The recovery varied between 82 and 124% if phenoxazine derivatives were used. The antioxidant activity determined in rich with antioxidants food samples, i.e. date-palm, black raisin, golden raisin, skin of red grape, dice of red grape, fitted the literature data.
© 2006 Elsevier B.V. All rights reserved.

Keywords: Antioxidant; Trolox; Laccase; ABTS; Phenoxazine; Radical cation

1. Introduction

The exposure of living organisms to reactive oxygen, nitrogen, chlorine, and bromine species (RSs) is common in aerobic life [1,2]. RSs fall into two groups, i.e. those that contain unpaired electrons ($O_2^{\bullet-}$, $OH^{\bullet}$, $NO^{\bullet}$), and those that have the ability to extract electrons from other molecules (H_2O_2, HOCl, and HOBr). These species may damage biomolecules directly, or initiate chain reactions resulting in extensive damage of cell structures. It was recognized that natural antioxidants, due to their RS scavenging activity, might have beneficial effects in protection against these damages. Consequently, considerable interest has been focused on the analytical methods for determination of antioxidants in biological samples. Determination of antioxidants in the biological samples usually requires the use of high-resolving analytical techniques, such as high-performance liquid chromatography and capillary electrophoresis [3]. However, the information about the number and the concentration of antioxidants present in the sample is not sufficient to obtain biologically relevant information about the antioxidant activity of the sample, primarily due to the synergistic interaction between different antioxidants. For this reason methods for measuring the overall antioxidant activity have been introduced which provide the parameter of the cumulative action of all antioxidants present in the sample.

Two types of analytical methods are currently used for evaluation of the antioxidant activity [3]: (i) inhibition methods, in which the inhibition of oxidative damage of the target molecule is measured in the presence of antioxidants and related to a known standard, and (ii) methods based on direct measurement of scavenging stable free radicals by antioxidants present in the sample. The most popular scavenging method is 6-hydroxy-2,5,7,8-tetramethylchroman-2-carboxylic acid (Trolox) equivalent antioxidant capacity (TE) decolourisation assay based on the scavenging of stable 2,2′-azinobis(3-ethylbenzothiazoline-6-sulfonic acid) radical cation ($ABTS^{\bullet+}$) [4–6] or 2,2-diphenyl-1-picrylhydrazyl radical ($DPPH^{\bullet}$) [7]. The $ABTS^{\bullet+}$ typically is prepared under action of peroxidase or myoglobin [4,5], chemically [6] or electrochemically [3], whereas the main source of $DPPH^{\bullet}$ is a chemical

* Corresponding author at: Vilnius Gediminas Technical University, Faculty of Fundamental Sciences, Department of Chemistry and Bioengineering, Sauletekio Avenue 11, LT-10223 Vilnius, Lithuania. Tel. +370 5 2729176; fax: +370 5 2729196.

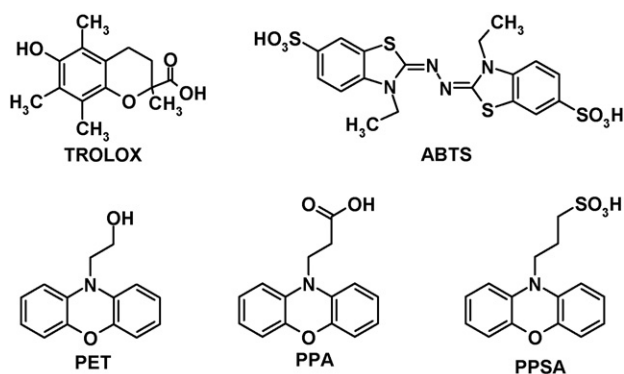*E-mail addresses:* jkulys@bchi.lt, juozas.kulys@fm.vtu.lt (J. Kulys).

Fig. 1. Structure of Trolox and high reactive laccase substrates.

synthesis [7]. When a sample containing an antioxidant (AH) is added into the solution of the ABTS$^{\bullet+}$ or the DPPH$^{\bullet}$ the amount of the radical scavenged is measured by the decrease of an absorbance. This decrease of absorbance is compared with the decrease of absorbance produced by the addition of a known amount of Trolox. TE decolourisation assay is widely used for the evaluation of the antioxidant activity of pure compounds, mixtures of antioxidants, and complex samples such as medicinal plants, blood plasma and organic tissue, food or beverages [8,9].

The merit of antioxidant capacity of peroxidase (myoglobin) based method was simple *lag*-time assay formed during the ABTS$^{\bullet+}$ formation in presence of an oxidant [4]. The application of peroxidase or myoglobin, however, requires hydrogen peroxide that itself can react with AH.

Laccases are classified as polyphenol oxidases, and perform the reduction of oxygen to water while oxidizing the substrate [10]. Laccases show broad substrate specificity and catalyse the oxidation phenol derivatives, inorganic and organic metal complexes and other substrates [10]. It was shown that the ABTS and other heterocyclic aromatic compounds are oxidized with the rate approaching a diffusion of substrates [11]. For this reason laccases are promising for radical cations production. Moreover, making the radical cations does not require any additional oxidizers with exception of dissolved oxygen. Laccases to the best of our knowledge had not been used for antioxidants determination.

The task of this investigation was to develop a method of antioxidants determination with laccases. As laccase substrates ABTS and other high reactive phenoxazine derivatives: 2-phenoxazin-10-yl-ethanol (PET), 3-phenoxazin-10-yl-propane-1-sulfonic acid (PPSA) and 3-phenoxazin-10-yl-propionic acid (PPA) were used (Fig. 1).

2. Experimental

2.1. Materials

Recombinant forms of laccases *Polyporus pinsitus* (rPpL) and *Myceliophthora thermophila* (rMtL) expressed in an *Aspergillus oryzae* and purified as described in [12–14] were received from Novozymes A/S (Copenhagen, Denmark) and

used without further purification. Recombinant peroxidase from *Coprinus cinereus* (rCiP) was received from Novozymes A/S (Copenhagen, Denmark). The concentration of laccases and peroxidase was determined spectrophotometrically. The extinction coefficient for rPpL, was used $7.8 \times 10^4 \, M^{-1} \, cm^{-1}$ at 280 nm [13]. The extinction coefficient of rMtL was $1.34 \times 10^5 \, M^{-1} \, cm^{-1}$ at 276 nm [14]. The extinction coefficient for rCiP, was used $1.08 \times 10^5 \, M^{-1} \, cm^{-1}$ at 405 nm [15]. The catalase *Aspergillus niger* was a product of Novozymes A/S, and the concentration of the enzyme was determined spectrophotometrically using absorbance at 280 nm. The extinction coefficient was assumed $150 \, mM^{-1} \, cm^{-1}$ [16]. The solutions of H$_2$O$_2$ were prepared from perhydrol (30%) and concentration was calculated using an extinction coefficient of $39.4 \, M^{-1} \, cm^{-1}$ at 240 nm. Diammonium salt of 2,2′-azinobis(3-ethylbenzothiazoline-6-sulfonic acid) (ABTS) was obtained from Boehringer Mannheim GmbH (Germany), 6-hydroxy-2,5,7,8-tetramethylchroman-2-carboxylic acid (Trolox) was purchased from Aldrich, 2-phenoxazin-10-yl-ethanol (PET), 3-phenoxazin-10-yl-propane-1-sulfonic acid sodium salt (PPSA), 3-phenoxazin-10-yl-propionic acid (PPA) were synthesized as described in [17]. Sodium acetate, acetic and hydrochloric acid were "chemically pure" and were received from Reachim (Moscow, Russia). Methanol (purity 99.9%) was received from Fluka, the highest purified argon was from Aga (Latvia).

2.2. Apparatus and methods

The spectral measurements were performed by using a computer-controlled "Nicolet evolution 300" spectrophotometer (Thermo electron corporation, USA) in 1 cm thermostated quartz cuvette at $(25.0 \pm 0.1) \, °C$.

The kinetic measurements were performed in 20 mM acetate buffer solution pH 5.5. The formation of ABTS radical cation was monitored at 414 nm using extinction coefficient $3.5 \times 10^4 \, M^{-1} \, cm^{-1}$ [18]. The formation of PET and PPA radical cation was monitored at 530 nm using extinction coefficient $1.6 \times 10^4 \, M^{-1} \, cm^{-1}$ [11]. The concentration of PPSA radical cation was measured at 530 nm. The extinction coefficient determined with peroxidase $(1.0 \times 10^{-9} \, M)$ and hydrogen peroxide $(1.0 \times 10^{-4} \, M)$, and it was $9.5 \times 10^3 \, M^{-1} \, cm^{-1}$. During antioxidants determination the reaction mixture contained $1.1 \times 10^{-5} \, M$ of ABTS, $1.3 \times 10^{-5} \, M$ of PET $(1.3–2.5) \times 10^{-5} \, M$ of PPSA, $1.5 \times 10^{-5} \, M$ of PPA $(0.6–7.6) \times 10^{-6} \, M$ of Trolox and $1.0 \times 10^{-9} \, M$ of rPpL or $1.0 \times 10^{-8} \, M$ of rMtL. The mixture contained 5% (v/v) of methanol. The concentration of laccase and substrate was chosen to perform measurements during 3–10 min and to get 0.1–0.2 absorbance change at desired wavelength in 1 cm optical path length cell. The reaction started with addition of the enzyme solution. The concentration of the antioxidants in the real samples was determined using instead of Trolox solution the diluted extract of the samples.

For radical cations titration with Trolox the radical cations were synthesized using peroxidase. The solution of ABTS $(1.3 \times 10^{-4} \, M)$, PET $(6 \times 10^{-4} \, M)$, PPSA $(9 \times 10^{-4} \, M)$ and PPA $(9 \times 10^{-4} \, M)$ was incubated with $1.0 \times 10^{-4} \, M$ of

hydrogen peroxide and 2.0×10^{-8} M of rCiP during 5 min. The reaction was stopped by adding 2.0×10^{-8} M of catalase. The solution of radicals was diluted with buffer solution and fixed amount of Trolox solution was added. The amount of consumed radical was calculated after 1 min.

2.3. Preparation of solutions

The solutions of PET and PPA were prepared in methanol with the subsequent dissolution with deionised water. The concentration of methanol was 5% (v/v). The solutions of other reagents were prepared in deionised water and were diluted to the desired concentration immediately before the use. For the removal of oxygen the solutions were bubbled with argon during 5 min.

The extracts of real samples, i.e. date-palm, black raisin, golden raisin, skin of red grape, dice of red grape, were prepared by incubating 0.6–1.5 g of a sample with 1.2–3.0 ml of methanol during 3 days at anaerobic conditions. The mixture was permanently mixed with magnetic stirrer at room temperature. The extract was diluted 800–102,400 times with methanol. For the measurements 100 µl of the diluted sample was added into 1.85 ml of thermostated buffer solution containing ABTS. The reaction started by addition 50 µl of laccase solution.

2.4. Calculations and modelling

To process the data the programs MathCAD 2001 Professional and GraFit 3.01 were used. A complex kinetic scheme of simultaneous substrate and antioxidants oxidation was modelled by Euler's method [19]. A standard deviation of the parameters found, i.e. the concentration of an antioxidant and the kinetic constants varied between 4 and 11%.

3. Results and discussion

3.1. Reaction of antioxidants with radical cations

The radical cations of ABTS, PET, PPA and PPSA produced in presence of peroxidase showed strong absorbance in visible area of spectrum (Fig. 2).

The radical cations of phenoxazine derivatives (PET, PPA and PPSA) demonstrated remarkable stability during weeks in water solution. The addition of Trolox solution to the solution of the radical cation followed immediate decrease of absorbance in visible area of spectrum. The amount of consumed radical cation was linearly proportional to the added Trolox (Fig. 3).

The calculated consumption of the radical cation of ABTS corresponded almost to 2 mol per 1 mol of Trolox since the slope of linear dependence was 1.91 ± 0.07 (Table 1). The stoichiometry of reaction for radical cations of PET, PPA and PPSA was more than two (Table 1). The reason of this apparent stoichiometry increase is unknown. This can be explained by difference of correct and used for the calculations extinction coefficients. A more complex reaction scheme of the radical cations with Trolox
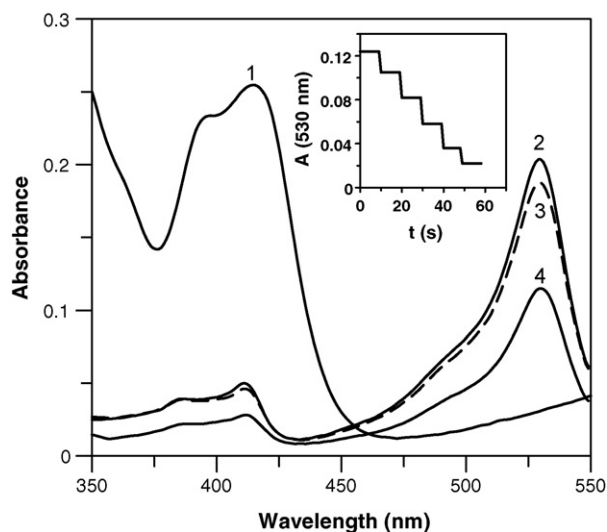
Fig. 2. Absorbance of radical cation of ABTS (1), PET (2), PPA (3) and PPSA (4) at pH 5.5. Concentrations of ABTS$^{\bullet+}$ 7.3×10^{-6} M, PET$^{\bullet+}$ 1.3×10^{-5} M, PPA$^{\bullet+}$ 1.2×10^{-5} M and PPSA$^{\bullet+}$ 1.2×10^{-5} M. Inset show the titration graph of PET with Trolox. Each step corresponds the addition of 6×10^{-7}, 1.2×10^{-6}, 1.8×10^{-6}, 2.3×10^{-6} and 2.9×10^{-6} M of Trolox.
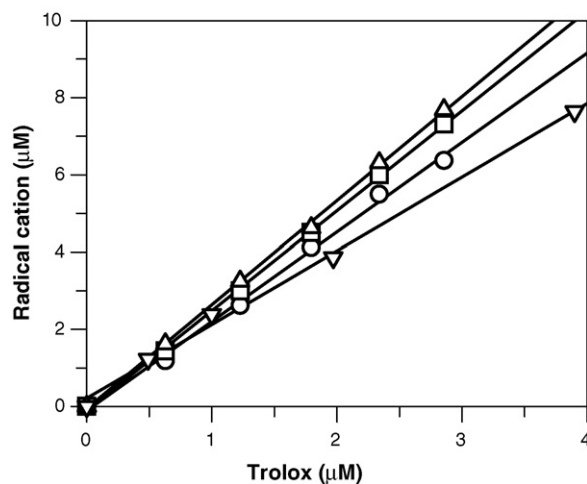
Fig. 3. The titration of radical cation of ABTS ($\triangledown$), PET ($\square$), PPA ($\bigcirc$) and PPSA ($\triangle$) with Trolox at pH 5.5.

also may origin this difference. This inconsistency was simply eliminated by calibration with Trolox during TE determination of real samples.

The generation of the radical cation of ABTS in presence of 1 nM of rPpL is shown in Fig. 4. The addition of Trolox stimulated the appearance of *lag*-period of the

Table 1
The parameters of radical cations titration with Trolox at pH 5.5

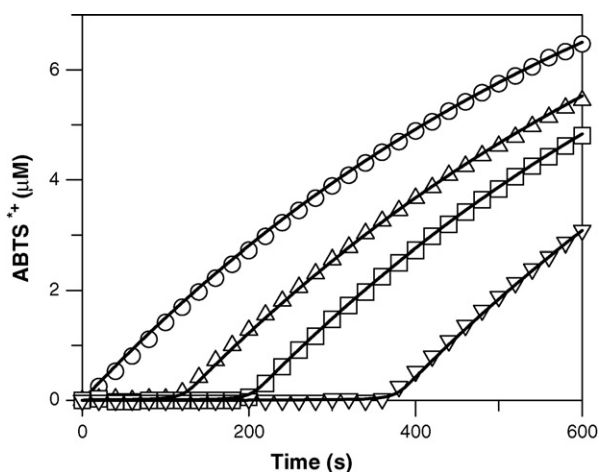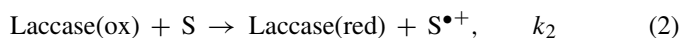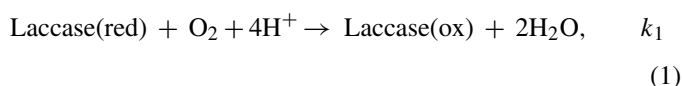| Radical cation	Slope	Standard error	Correlation coefficient
ABTS$^{\bullet+}$	1.91	0.07	0.9981
PET$^{\bullet+}$	2.58	0.03	0.9996
PPA$^{\bullet+}$	2.32	0.07	0.9982
PPSA$^{\bullet+}$	2.69	0.04	0.9996

Fig. 4. The kinetics of laccase-catalysed radical cation of ABTS production in presence of Trolox. Curves correspond to data fitting following a scheme of laccase action (Eq. (1)–(4)). About 20 mM acetate buffer solution, pH 5.5, 1.1×10^{-5} M of ABTS, 1.1×10^{-9} M of rPpL, 25 °C; concentration of Trolox 0 M ($\bigcirc$), 1.0×10^{-6} M ($\triangle$), 1.7×10^{-6} M ($\square$), and 3.5×10^{-6} M ($\triangledown$).

kinetics curve (Fig. 4). The period was larger at bigger Trolox concentration.

The reactivity of other substrates was similar to ABTS. However, a similar rate of radical cations production was indicated at 10 times larger thermostable laccase (rMtL) concentration (Fig. 5). In presence of rMtL Trolox also induced *lag*-period that was proportional to the antioxidant concentration.

The appearance of *lag*-period and a sharp absorbance change is associated with a fast radical cations reaction. In principal the *lag*-period can be used for antioxidants concentration determination [4], however, for laccase-catalysed process this is not correct since: (i) production of radical cation is not linear in absence of an antioxidant; (ii) antioxidant reacts with laccase as well as high reactive laccase substrate. For this reason a scheme
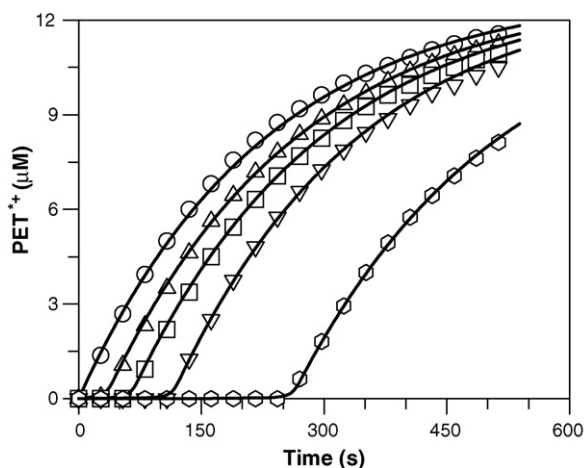
Fig. 5. The kinetics of laccase-catalysed radical cation production of PET in presence of Trolox. Curves correspond to data fitting following a scheme of laccase action (Eq. (1)–(4)). About 20 mM acetate buffer solution, pH 5.5, 1.3×10^{-5} M PET, 1.0×10^{-8} M of rMtL, 25 °C; concentration of Trolox 0 M ($\bigcirc$), 7×10^{-7} M ($\triangle$), 1.4×10^{-6} M ($\square$), 2.8×10^{-6} M ($\triangledown$), and 6.9×10^{-6} M ($\Diamond$).

of simultaneous antioxidants and substrates oxidation was built and the antioxidant concentration was determined by data fitting of kinetic curves.

3.2. Kinetic scheme of simultaneous antioxidants and substrates oxidation

ABTS and phenoxazine derivatives used in this work are oxidized with high rate in presence of laccases [11]. Trolox and other antioxidants as phenol derivatives were also oxidized with laccase [20]. Therefore the kinetic scheme of substrates and Trolox oxidation should include simultaneous oxidation of both types of substrates. In addition, the reaction of the radical cation with antioxidant (Eq. (4)) should be considered. A formal redox potential of Trolox is 0.39 V [21] while of ABTS it is 0.66 V [18], and of phenoxazine derivatives it is 0.63 V versus NHE [17]. Therefore the reaction of the radical cation with antioxidant (Eq. (4)) is exothermic and fast.

The simples kinetic scheme of laccase-catalysed simultaneous substrates oxidation can be written:

$$\text{Laccase(red)} + \text{O}_2 + 4\text{H}^+ \rightarrow \text{Laccase(ox)} + 2\text{H}_2\text{O}, \qquad k_1 \tag{1}$$

$$\text{Laccase(ox)} + \text{S} \rightarrow \text{Laccase(red)} + \text{S}^{\bullet+}, \qquad k_2 \tag{2}$$

$$\text{Laccase(ox)} + \text{Trolox} \rightarrow \text{Laccase(red)} + \text{P}, \qquad k_3 \tag{3}$$

$$\text{S}^{\bullet+} + \text{Trolox} \rightarrow \text{S} + \text{P}, \qquad k_4 \tag{4}$$

where Laccase(red) and Laccase(ox) – reduced and oxidized forms of laccase, S or $\text{S}^{\bullet+}$ – ABTS, PET, PPA and PPSA or respective radical cation, k_1, k_2, k_3, and k_4 – the rate constants.

The fitting of experimental data in absence of antioxidant (Trolox) produced k_1 and k_2 values. Due to high concentration of oxygen (2.5×10^{-4} M) and large k_1 value (10^6 M^{-1} s^{-1} [22]) reaction (Eq. (1)) is fast and the fitting permits to calculate k_2. In presence of an antioxidant three parameters (k_3, k_4 and antioxidant concentration) are unknown. The constant k_4 corresponding to chemical reaction (Eq. (4)) depends on free energy of reaction following Marcus theory, and for exothermic reactions can be as large as 10^8 M^{-1} s^{-1} [23]. The fitting of experimental data showed that k_4 did not influence significantly k_3 and calculated antioxidant concentration at k_4 $>10^6$ M^{-1} s^{-1}. Therefore this reaction does not limit a process and k_3 and the antioxidant concentration can be found by data fitting.

At Trolox concentration $(0.9–7.6) \times 10^{-6}$ the following parameter were found from the calculations (Table 2). The results demonstrate that for rPpL the substrate showing the largest oxidation rate is PET, whereas ABTS and PPA are the best substrates for thermostable laccase rMtL. Unexpected was low reactivity of PPSA with rMtL indicating some specificity of laccase. A comparison of k_2 and k_3 values shows that Trolox reactivity is similar or just 2–5 times less in comparison to high active substrates.

Table 2
Kinetic characteristics of laccase-catalysed oxidation of high reactive substrates and Trolox in 20 mM acetate buffer solution pH 5.5 at 25 °C

Substrate	$c_{substrate}$ (M)	Laccase	$c_{laccase}$ (M)	k_2 (M^{-1} s^{-1})	k_3 (M^{-1} s^{-1})
ABTS	1.1×10^{-5}	rPpL	1.1×10^{-9}	1.4×10^6	6.4×10^5
PET	1.3×10^{-5}	rPpL	1.0×10^{-9}	3.6×10^6	6.4×10^5
PPA	1.5×10^{-5}	rPpL	1.0×10^{-9}	2.5×10^6	6.4×10^5
PPSA	1.3×10^{-5}	rPpL	1.0×10^{-9}	2.0×10^6	6.4×10^5
ABTS	1.4×10^{-5}	rMtL	1.0×10^{-8}	1.2×10^6	2.2×10^5
PET	1.3×10^{-5}	rMtL	1.0×10^{-8}	4.3×10^5	2.2×10^5
PPA	1.5×10^{-5}	rMtL	1.0×10^{-8}	9.5×10^5	2.2×10^5
PPSA	2.3×10^{-5}	rMtL	1.0×10^{-8}	1.5×10^5	2.2×10^5

Table 3
Trolox determination using laccase-catalysed oxidation of ABTS, PET, PPA and PPSA in 20 mM acetate buffer solution, pH 5.5, 25 °C

Substrate	Laccase	Trolox added (M)	Trolox found (M)	Recovery (mean ± S.D.) (%)
ABTS	rPpL	$(0.95–7.6) \times 10^{-6}$	$(1.0–6.1) \times 10^{-6}$	91 ± 9
ABTS	rMtL	$(1.8–7.3) \times 10^{-6}$	$(1.9–6.3) \times 10^{-6}$	99 ± 8
PET	rPpL	$(0.91–7.3) \times 10^{-6}$	$(1.0–8.3) \times 10^{-6}$	114 ± 1
PET	rMtL	$(0.91–7.3) \times 10^{-6}$	$(0.7–6.9) \times 10^{-6}$	82 ± 7
PPA	rPpL	$(0.91–7.3) \times 10^{-6}$	$(1.2–8.3) \times 10^{-6}$	124 ± 6
PPA	rMtL	$(0.91–7.3) \times 10^{-6}$	$(0.8–6.4) \times 10^{-6}$	87 ± 1
PPSA	rPpL	$(0.91–3.6) \times 10^{-6}$	$(0.6–2.6) \times 10^{-6}$	69 ± 3
PPSA	rMtL	$(0.91–7.3) \times 10^{-6}$	$(0.7–6.7) \times 10^{-6}$	78 ± 7

Trolox recovery determination was performed by fitting kinetic curves in absence and in presence of different concentrations of the antioxidants. The results demonstrate that Trolox can be determined with recovery of 100% at less than 10^{-6} M concentration (Table 3). If ABTS was used the recovery of Trolox was about 100% for both laccases used.

Trolox recovery varied between 82 and 124% if phenoxazine derivatives were used.

3.3. Antioxidants determination in real samples

The antioxidant activity (TE) in real samples was determined by samples treatment with methanol and dilution of the extract with the same solvent. Three dilutions were used, and standard deviation of TE was calculated from the measurements of these samples. A typical kinetic curves of radical cation of ABTS quenching in presence of the date-palm extract is depicted in Fig. 6.

The largest antioxidant activity was found in raisins and a dice of red grape (Table 4). The determined values fitted TE described in the literature [24].

Table 4
Antioxidant activity of real samples

Sample	TE per 100 g of sample
Date-palm	$(1.9 ± 0.1) \times 10^2$
Black raisin	$(3.6 ± 0.3) \times 10^2$
Golden raisin	$(1.0 ± 0.1) \times 10^3$
Skin of red grape	$(2.4 ± 0.1) \times 10^3$
Dice of red grape	$(5.0 ± 0.5) \times 10^3$
Trolox	$(3.6 ± 0.4) \times 10^5$

TE (mean ± S.D.) was determined using 1.1×10^{-5} M of ABTS and 1.0×10^{-9} M of rPpL.
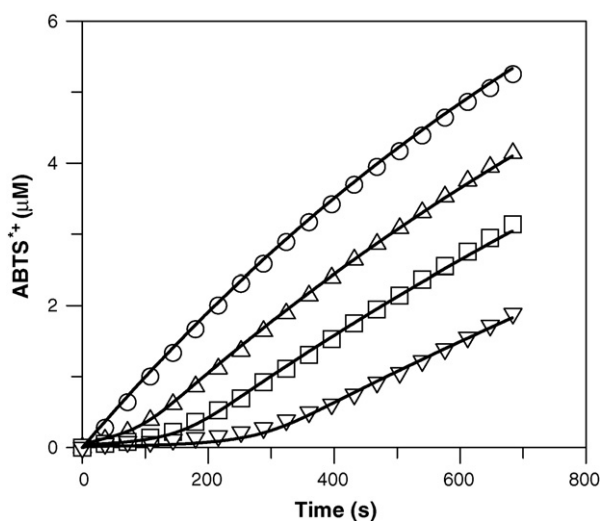

Fig. 6. The kinetics of laccase-catalysed radical cation of ABTS production in presence of the date-palm extract. Curves correspond to data fitting following a scheme of laccase action (Eq. (1)–(4)). About 20 mM acetate buffer, pH 5.5, 1.1×10^{-5} M of ABTS, 1.0×10^{-9} M of rPpL, 25 °C; TE 0 M (○), 3×10^{-7} M (△), 6×10^{-7} M (□), 1.1×10^{-6} M (▽).

4. Conclusions

The experiments performed show that laccases can be used for antioxidant activity determination with spectrophotometer in presence of high active chromophoric substrates. The use of laccases expands the enzymatic method of antioxidants determination, and can be used if the application of peroxidases is unfavourable. As laccase substrate commercially available ABTS was used. New N-substituted phenoxazine derivatives demonstrate versatility of the suggested method. The determined Trolox equivalent of real samples fitted described in

the literature for both types of substrates. The method permits to measure submicromole concentration of an antioxidant. The optimisation of the method may significantly increase the sensitivity.

Acknowledgement

References

[1] B. Halliwell, Plant Physiol. 141 (2006) 312.
[2] M.D. Temple, G.G. Perrone, I.W. Dawes, Trends Cell Biol. 15 (2005) 319.
[3] D. Ivekovic, S. Milardovic, M. Roboz, B.S. Grabaric, Analyst 130 (2005) 708.
[4] T.-W. Yu, Ch. Nam Ong, Anal. Biochem. 275 (1999) 217.
[5] D. Villano, M.S. Fernandez-Pachon, A.M. Troncoso, M.C. Garcia-Parrilla, Anal. Chim. Acta 538 (2005) 391.
[6] R. Re, N. Pellegrini, A. Proteggente, A. Pannala, M. Yang, C. Rice-Evans, Free Radical Biol. Med. 26 (1999) 1231.
[7] J.A. Vinson, Y. Hao, X. Su, L. Zubik, J. Agri. Food Chem. 46 (1998) 3630.
[8] C.C. Wang, C.Y. Chu, K.O. Chu, K.W. Choy, K.S. Khaw, M.S. Rogers, C.P. Pang, Clin. Chem. 50 (2004) 952.
[9] R.T.P. Correia, P. Mccue, M.M.A. Magalhaes, G.R. Macedo, K. Shetty, J. Food Biochem. 28 (2004) 404.
[10] P. Baldrian, FEMS Microbiol. Rev. 30 (2006) 215.
[11] J. Kulys, K. Krikstopaitis, A. Ziemys, J. Biol. Inorg. Chem. 5 (2000) 333.
[12] P. Schneider, M.B. Caspersen, K. Mondorf, T. Halkier, L.K. Skov, P.R. Ostergaard, K.M. Brown, St.H. Brown, F. Xu, Enzyme. Microb. Technol. 25 (1999) 502.
[13] D.S. Yaver, F. Xu, E.J. Golightly, K.M. Brown, S.H. Brown, M.W. Rey, P. Schneider, T. Halkier, K. Mondorf, H. Dalboge, Appl. Environ. Microbiol. 62 (1996) 834.
[14] F. Xu, R.M. Berka, J.A. Wahleithner, B.A. Nelson, J.R. Shuster, S.H. Brown, A.E. Palmer, E.I. Solomon, Biochem. J. 334 (1998) 63.
[15] Z.S. Farhangrazi, B.R. Copeland, T. Nakayama, T. Amachi, I. Yamazaki, L.S. Powers, Biochemistry 33 (1994) 5647.
[16] J. Kulys, K. Kriauciunas, R. Vidziunaite, J. Mol. Catal. B: Enzym. 3 (2003) 79.
[17] J. Kulys, R. Vidziunaite, R. Janciene, A. Palaima, Electroanalysis 18 (2006) 1771.
[18] M. Solis-Oba, V.M. Ugalde-Saldivar, I. Gonzalez, G. Viniegra-Gonzalez, J. Electroanal. Chem. 579 (2005) 59.
[19] J. Kulys, Nonlinear Anal. Model. Contr. 1 (1997) 67.
[20] J. Kulys, R. Vidziunaite, P. Schneider, Enzyme Microb. Technol. 32 (2003) 455.
[21] J. Vrba, J. Hrbac, J. Ulrichova, M. Modrianski, Chem. Biol. Interac. 147 (2004) 35.
[22] H. Goldberg, O. Farver, I. Pecht, J. Biol. Chem. 255 (1980) 7353.
[23] G. Merenyi, J. Lind, M. Jonsson, J. Am. Chem. Soc. 115 (1993) 4945.
[24] A. Prakash, Medallion Lab. Anal. Prog. 19 (2001) 1.

Short communication

Myoglobin/arylhydroxylamine film modified electrode: Direct electrochemistry and electrochemical catalysis

S. Ashok Kumar, Shen-Ming Chen *

*Electroanalysis and Bioelectrochemistry Lab, Department of Chemical Engineering and Biotechnology,
National Taipei University of Technology, No. 1, Section 3, Chung-Hsiao East Road, Taipei 106, Taiwan, ROC*

Abstract

The adsorption processes and electrochemical behavior of 4-nitroaniline (4-NA) adsorbed onto glassy carbon electrodes (GCE) have been investigated in aqueous 0.1 M nitric acid (HNO_3) electrolyte solutions using cyclic voltammetry (CV). 4-NA adsorbs onto GCE surfaces, and upon potential cycling past -0.2 V, is transformed into the arylhydroxylamine (ArHA) derivative which exhibits a well-behaved pH dependent redox couple centered at 0.32 V at pH 1.5. It is noted as arylhydroxylamine modified glassy carbon electrodes (HAGCE). This modified electrode can be readily used as an immobilization matrix to entrap proteins and enzymes. In our studies, myoglobin (Mb) was used as a model protein for investigation. A pair of well-defined reversible redox peaks of Mb (Fe(III)–Fe(II)) was obtained at the Mb/arylhydroxylamine modified glassy carbon electrode (Mb/HAGC) by direct electron transfer between the protein and the GCE. The formal potential ($E^{0'}$), the apparent coverage (Γ^*) and the electron-transfer rate constant (k_s) were calculated as -0.317 V, 8.26×10^{-12} mol/cm² and 51 ± 5 s^{-1}, respectively. Dramatically enhanced biocatalytic activity was exemplified at the Mb/HAGC electrode by the reduction of hydrogen peroxide (H_2O_2), trichloroacetic acid (TCA) and oxygen (O_2). The Mb/arylhydroxylamine film was also characterized by UV–visible spectroscopy (UV–vis), scanning electron microscope (SEM) indicating excellent stability and good biocompatibility of the protein in the arylhydroxylamine modified electrode. This new Mb/HAGC electrode exhibited rapid electrochemical response (2 s) for H_2O_2 and had good stability in physiological condition, showing the potential applicability of the films in the preparation of third generation biosensors or bioreactors based on direct electrochemistry of the proteins.
© 2006 Elsevier B.V. All rights reserved.

Keywords: Nitroaniline; Myoglobin; Directelectrochemistry; Arylhydroxylamine; Biosensors

1. Introduction

There has been increasing interest in studying metalloproteins in order to achieve direct electron transfer applications in mediator-free biosensors, bioreactors, and mimicking catalytic roles in living systems [1,2]. Many electron-transfer metalloproteins are membrane-associated, and efficient electron transfer for proteins can only be accomplished within the membrane environment [3]. Myoglobin (Mb) is a single-chain protein of 153 amino acids, containing a heme (iron-containing porphyrin) group in the center. Mb is found in mammalian skeleton and muscle tissues, which functions in the storage of oxygen and in the enhancement of the rate of oxygen diffusion [4,5]. Because the heme group in Mb is much more buried with respect to the protein surface than in cytochrome, its interaction with the electrode surface is hindered [6]. To explore methods to increase the electron transfer between Mb and the electrode, great efforts have been devoted to the characterization of the electrochemistry of Mb using electrodes modified with films such as surfactants [7–13], polymers [14–17], distal histidine [18,19], and inorganic materials [20–31]. Recently, the adsorption of enzymes on multiwall carbon nanotube has been reported [32–34]. These films provide the friendly microenvironment for enzyme loading and improve the stability of the entrapped enzymes. Mb in these films facilitated relatively faster electron transfer and catalytic activity than that between Mb in the solution and bare electrodes [7–13,21]. To date, most studies on immobilization of protein were focused on layered or mesoporestructured materials due to their higher specific surface area [26–31]. In most cases, the reason for the interaction between the matrix and enzyme is not clear [35].

* Corresponding author. Tel.: +886 2 27017147; fax: +886 2 27025238.
E-mail addresses: sakumar80@gmail.com (S.A. Kumar),
smchen78@ms15.hinet.net (S.-M. Chen).

NH$_2$

N$^+$

O$^-$ O
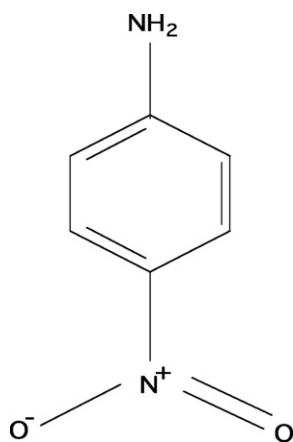
Scheme 1. Structure of 4-nitroaniline.

During recent years much attention has been paid to electrochemical investigations of monosubstituted benzenes and substituted anilines by both electrochemical and spectroelectrochemical techniques [36]. 4-Nitroaniline (4-NA) (Scheme 1) is a particularly prominent member of the family of isomeric nitroanilines has attracted much attention because of the specific effects of an electron withdrawing nitro group and an electron-donating amino group being in the para position of an aromatic ring system [37]. These results in low-energy electronic transitions with charge migration within the molecule [38] and greater nonlinear susceptibility [39–41] making this molecule interesting as material for nonlinear optics [42–46]. Its use as an end-group in thiol-based self-assembled monolayers has been reported [47]. Pre-resonance and resonance Raman spectra for nitroanilines have been investigated [48,49]. To the best of our knowledge, the electrochemical studies of nitroaniline in HNO$_3$ medium using GCE was not yet available. Furthermore, for the first time we are used the nitroaniline derivative as a matrix for enzyme and protein immobilization.

In this communication, we attempt to immobilize Mb onto the hydroxylamine modified GCE. Interestingly the direct electron transfer between Mb and electrode was achieved without aid of any electron mediator. A pair of well-defined and nearly symmetrical redox peak was achieved for Mb (Fe(III)–Fe(II)), which suggested the enhanced, reversible electron-transfer between Mb and GCE. The adsorption of Mb on HAGCE film retained its native structure as characterized by ultraviolet visible spectroscopy. Subsequently, the direct electrochemical behavior of Mb/HAGC electrode and its electrocatalytic properties for reduction of hydrogen peroxide (H$_2$O$_2$), trichloro acetic acid (TCA) and oxygen (O$_2$) were studied using cyclic voltammetry (CV). We hope this new Mb/HAGC modified electrode can find potential application in the preparation of third generation biosensors or bioreactors.

2. Experimental

2.1. Apparatus and chemicals

Electrochemical measurements were performed with CH Instruments Model-1200A with conventional three-electrode

cell. A BAS glassy carbon and platinum wire are used as the working electrode and counter electrode, respectively. All the cell potentials were measured with respect to an Ag/AgCl [KCl (sat)], reference electrode. HITACHI Model S-3000H Scanning Electron Microscope was used for surface image measurements. The UV–vis absorption spectra were checked by using a U3300 Spectrophotometer (HITACHI). All experiments were carried out at room temperature.

4-Nitroaniline, myoglobin (source: horse heart) and hemin (chloro(protoporphyrinato) iron(III)) (source: bovine) were purchased from Sigma chemical company, used without further purification. Other chemicals were of analytical grade. Supporting electrolytes used for electrochemical experiments were 0.1 M H$_2$SO$_4$, 0.1 M HNO$_3$, 0.2 M phosphate and 0.1 M acetate buffer solutions. The aqueous solutions were prepared by using doubly distilled deionized water, and before each experiment the solutions were deoxygenated by purging with pre-purified nitrogen gas.

2.2. Fabrication of Mb/HAGC modified electrodes

The GCE was polished with 0.05 μm alumina on Buehler felt pads, rinsed in water and then ultrasonicated for 1 min in distilled water, and then the GCE was cycled in the potential range between 0.5 and −0.2 V at 50 mV s^{-1} for 25 cycles in 1 mM 4-NA containing aqueous HNO$_3$ solution (pH 1.5). After that, the electrode was thoroughly rinsed with doubly distilled water; this process was used to remove any loosely bound, un-reacted material from the electrode surface. Finally, the HAGCE was immersed in pH 5.0 buffer solution containing 0.1 mM Mb for an hour; in such a way the Mb attached HAGCE (Mb/HAGC) electrode was obtained. Thus, the driving force for Mb to enter HAGCE films would be mainly hydrophobic interaction between macromolecule Mb and HAGCE films, in which the long hydrocarbon backbone of HAGCE film constitutes the hydrophobic region of the films. The adsorption of positively charged Mb protein at pH below their isoelectric point (pH 6.8) [50] with the arylhydroxylamine modified GC electrode mainly occurs by electrostatic interactions [51,52].

3. Results and discussion

3.1. Electrochemical synthesis of HAGC modified electrodes

The electrochemical reduction was carried out in the potential range between 0.5 and −0.2 V in 0.1 M HNO$_3$ acidic solution (pH 1.5) containing 1 mM 4-NA using GCE. The results are presented in Fig. 1. On the first cathodic scan irreversible reduction peak was observed at peak potential about −0.10 V due to the electroreduction of nitro group present in 4-NA. Upon scan reversal, an anodic wave with a peak potential centered at 0.33 V was observed. On the second and subsequent potential scans, an additional cathodic peak was observed at 0.31 V which is the cathodic counterpart to the anodic wave at 0.33 V. This appears to indicate that the first cathodic sweep gives rise to a reversible redox couple with a formal potential of 0.32 V.
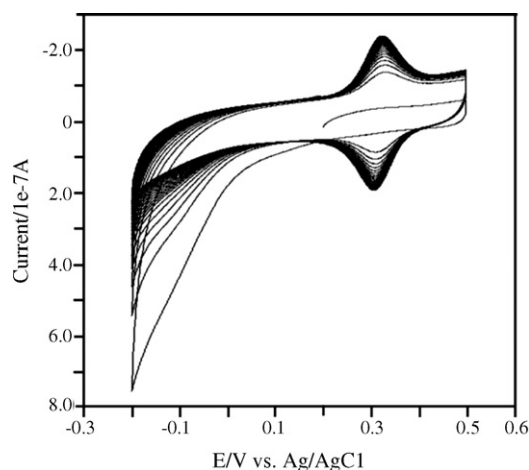
Fig. 1. Repeated cyclic voltammograms of a glassy carbon electrode modified with 1 mM 4-NA in 0.1 M HNO$_3$ solution (pH 1.5). Scan rate = 0.05 V/s.

In addition, the peak current of the cathodic waves at −0.20 V decreased significantly on the second and on subsequent cycles, then GC electrodes are thoroughly washed using background solution and transferred into the pH 1.5 buffer (absence of 4-NA) solution. The above modified GC electrodes showed a very stable reversible redox couple centered at 0.32 V (figures not shown). It is indicated that 4-NA and its reduced product was strongly adsorbed onto the electrode surfaces in acidic condition.

In this protic medium an irreversible reduction wave (Fig. 1) corresponds to the four-electron, four protons nitro reduction to form the arylhydroxylamine derivative. Consequently, the overall mechanism at acid media is described in following equation and also previously proposed by Stutts and Wlghtman [53], Shi et al. [54] and Casero et al. [55].

$$H_2N–C_6H_4–NO_2 + 4H^+ + 4e^-$$
$$\rightarrow H_2N–C_6H_4–NHOH + H_2O \qquad (1)$$
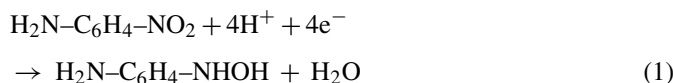
An adsorption of 4-NA onto the electrode surface in acidic medium occurs because it has three different anchoring sites (the nitro, the amino function, and the aromatic ring system). Recently, the oxidative and reductive electrochemistry of the three isomeric nitroanilines has been investigated in neutral and acidic aqueous electrolyte solution by CV. A variety of modes of interaction between adsorbed 4-NA and the electrode surface are reported and may involve the aromatic electron system of benzene ring, hydrogen atoms on the ring, or substituent groups [36]. In acidic medium the attachment of 4-NA and its reduced product occurs onto the GC electrode surface through the anilinium cation and π-electrons of an aromatic ring [36].

The reversible redox couple of hydroxylamine modified electrodes centered at 0.32 V is thus ascribed to

$$H_2N–C_6H_4–NO + 2H^+ + 2e^- \rightleftarrows H_2N–C_6H_4–NHOH \qquad (2)$$
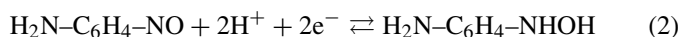
In such a way the HAGCE was prepared and used to study the direct electrochemistry of Mb. The effect of anions onto the film formation of ArHA was also performed; results suggested that the nitrate ion highly enhanced the ArHA generation according
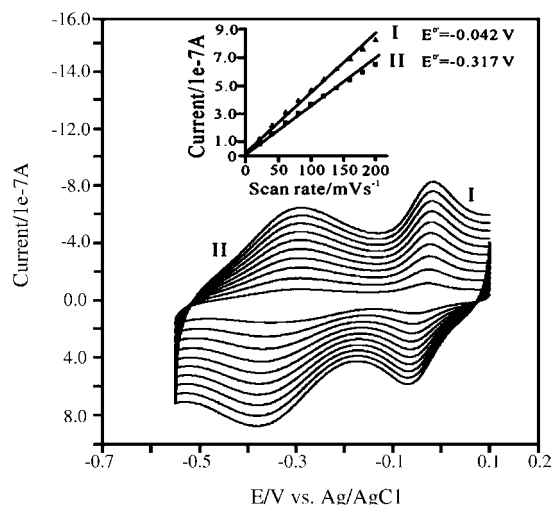
Fig. 2. Cyclic voltammograms of Mb/HAGCE in pH 6.9 PBS at different scan rates. The scan rates from inner to outer are 0.02, 0.04, 0.06, 0.08, 0.10, 0.12, 0.14, 0.16, 0.18, and 0.20 V/s, respectively. Inset is the plot of anodic peak currents of: (I) hydroxylamine/nitroso redox couple and (II) Mb (Fe(III)–Fe(II)) redox couple vs. scan rates.

to the literature report [56]. Sulphate, chloride and perchlorate anions had no any effect on synthesis of HAGCE film preparation in acidic medium. Hence, we used the 0.1 M HNO$_3$ as supporting electrolyte for all experiments.

3.2. Direct electrochemistry of Mb on HAGCE film

The Mb/HAGC electrode was prepared as described in Section 2.2. When the Mb/HAGC electrode was transferred into the phosphate buffer solution (pH 6.9), two redox waves are observed, as shown in Fig. 2. Which are corresponds to hydroxylamine/nitroso radical and another reversible redox wave due to the adsorbed Mb Fe(III)/Fe(II) protein, respectively. The reversible redox peak of arylhydroxylamine was observed only after the reduction of 4-NA and the reduced product (arylhydroxylamine) was strongly adsorbed onto the electrode surface in acidic solutions. Even, after the immobilization of Mb onto the HAGC modified electrode the arylhydroxylamine/nitroso redox peak was observed along with Mb Fe(III)/Fe(II) redox waves. The formal potentials ($E^{0'} = E_{pa} + E_{pc}/2$) are −0.042 and −0.317 V for hydroxylamine and Mb (Fe(III)/Fe(II)) reversible redox waves at pH 6.9, respectively. The $E^{0'}$ of Mb is very close to other reported film modified electrodes [21]. The shapes of the cathodic and anodic waves were nearly symmetric, and the reduction and oxidation peaks have the same heights. This behavior suggests that all of the electroactive Mb Fe(III) within the films are converted to Mb Fe(II) on the forward scan to negative potentials and that the Mb Fe(II) produced is reoxidised to Mb Fe(III) on the reverse scan.

The dependence of peak currents and peak potentials on the scan rate was showed in Fig. 2. It is suggested that the peak current (I_p) increased linearly with the scan rate (v) from 10 to 200 mV/s, as expected for thin layer electrochemistry [57,58]. The slope of the plot of log (I_p) versus log(v) is 0.91 with a correlation coefficient of 0.999, which is closed to

the theoretical slope of 1 for thin layer voltammetry [58,59]. According to the slope of the $I_p - \upsilon$ curve and the surface coverage (Γ) was estimated from integration of the reduction peak in the CVs according to $\Gamma = Q/nFA$, where Q is the charge involved in the reaction, n the number of electron transferred, F the Faraday's constant and A is the electrode area (0.0707 cm^2). The surface concentration (Γ) of Mb entrapped on HAGCE was 8.26×10^{-12} mol/cm^2, this value is just about 10% or less of the total amount of Mb deposited on the electrode surface. However, this value is only 1.9 times lower than theoretical monolayer coverage (counting in one heme-containing chain) of 1.58×10^{-11} for Mb [60], which is estimated taking into account the crystallographic dimensions of 6.4 nm × 5.5 nm × 5.0 nm for it, assuming one molecule with the long axis parallel to the electrode surface, a few layers of the proteins that are close to the electrode surface bring the electrochemical responses [60]. The lower value of surface coverage than other Mb film modified electrodes [17,21,62] reflected that only those Mb molecules in the inner layers of the hydroxylamine film closed to the electrode could transfer electrons with the electrode to contribute the observed redox peaks in buffer solutions.

On the other hand, the anodic peak potentials shifted to the positive direction and the cathodic peak potentials shifted to the negative direction at higher scan rate, which resulted in an increase of the peak separation between anodic and cathodic peak. The peak separation at higher scan rate could be used to estimate the heterogeneous electron transfer rate constant. According to the method of Laviron [61,62], taking charge transfer coefficient α as 0.5, and a scan rate >200 mV/s with peak separation (ΔE_p), the average values of electron-transfer rate constant (k_s) was determined to be about $51 \pm 5\,\mathrm{s}^{-1}$, indicating a fast electron transfer reaction of Mb at HAGC-modified electrode. This rate constant value is nearly equal to Mb/agarose hydrogel film electrode [60]. The $E^{0\prime}$, k_s and Γ of various Mb film modified electrode were compared with Mb/HAGC electrode in Table 1.

At below isoelectric point (pH 6.8) of Mb shows positive surface charges, while HAGC electrode is essentially neutral on the whole with no charges. Thus, the driving force for Mb to enter on HAGC electrode would be mainly hydrophobic interaction between macromolecule Mb and HAGC electrode, in which the long hydrocarbon backbone of hydroxylamine constitutes the hydrophobic region of the films [63–65]. As previously suggested by other researchers for organic film such as poly-
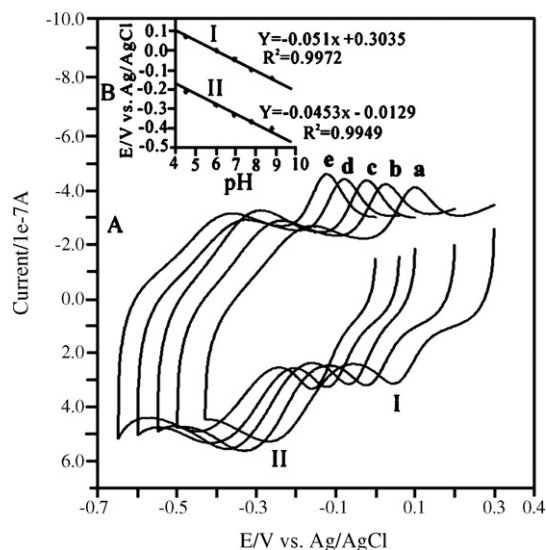
Fig. 3. (A) Cyclic voltammograms for Mb/HAGCE film modified electrode at different pH values: (a) 4.5 (b) 6.0 (c) 6.9 (d) 7.8, and (e) 8.8 at a scan rate of 0.05 V/s. (B) Formal potentials as a function of pH at scan rate of 0.05 V/s.

acrylamide hydrogel films [65], agarose hydrogel [60] modified electrodes had hydrophobic interaction with heme containing proteins and this interaction would also be mainly responsible for the retention of native structure of proteins in the modified electrodes. In the case of Mb/HAGC modified electrodes, arylhydroxylamine is also an organic film covered on electrode surface and its strong interaction with Mb shows existence of hydrophobic interaction between arylhydroxylamine and Mb protein. Although the exact reason for good stability and Mb-exhibited enhanced electrochemistry in HAGC modified electrode is unclear yet and need further studies to understand it. The $E^{0\prime}$ of the Mb Fe(III)/Fe(II) redox couples in HAGC electrode were little more negative than Mb-DDAB system [63,64] and polyacrylamide hydrogel films [65].

3.3. Effect of pH on Mb/HAGC modified electrodes

To ascertain the effect of pH, the voltammetric response of Mb/HAGC electrode was obtained in solutions of varying pH 3–10. As can be seen in Fig. 3A, the formal potentials of both redox couples were pH dependent, with a slope of 51 mV per pH for arylhydroxylamine/nitroso couple and 45.3 mV per pH for Mb Fe(III)/Fe(II) redox couple (Fig. 3B), which are very close

Table 1

Comparison of apparent heterogeneous electron transfer rate constants, formal potentials and surface concentration of various Mb films and Mb/HAGCE films

Films	Average $E^{0\prime}$ (CV)	Average k_s (s^{-1})	Γ (×10^{-11} mol cm^{-2})	Reference
Mb/ArHA	−0.317	51 ± 5	0.826	tw
Mb/AQ	−0.362	52 ± 6	0.256	[10]
Mb/agarose	−0.293	47 ± 3	5.18	[62]
Mb/PAM	−0.335	86 ± 19	0.198	[65]
[Mb − 1]/PSS$_7$	−0.356	20 ± 3	11.9	[17]
Mb/sol–gel film	−0.298	0.0012	137	[21]
Myb/MWNT	−0.248	5.4	42 ± 0.4	[34]
Mb-MWNT	−0.347	50 ± 6	14	[32]

tw: this work; AQ: poly(ester sulfonic acid) Eastman; PAM: polyacrylamide.
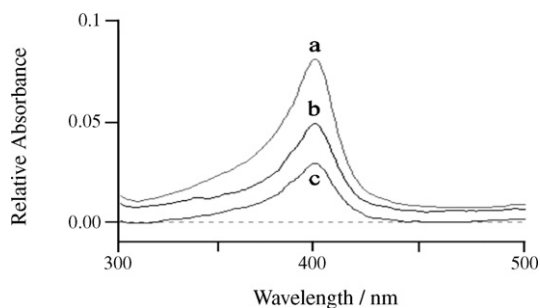
Fig. 4. UV–vis spectra of Mb and Mb/ArHA films on ITO glass slides: (a) 0.1 mM Mb solution, (b) Mb dry films, and (c) dry Mb/ArHA films.

to the anticipated nernstian value of 59 mV for electrochemical processes involving the same number of protons and electrons, the values of the slopes were smaller than 59 mV/pH perhaps because of the influence of the protonation states of trans ligands to the heme iron and amino acids around the heme, or the protonation of the water molecule coordinated to the central iron [60]. In addition, no significant variations in the slope were observed, suggesting that the ArHA groups remain protonated over the entire pH range studied, which is indicating both redox process is stable over the entire range of pH. Thus, the simplified equation for the electrochemical reaction of Mb can be expressed as

$$MbFe(III) + H^+ + e^- \leftrightarrow MbFe(II) \tag{3}$$

3.4. UV–vis spectroscopy and SEM measurements of Mb/ArHA films

The Soret band of heme protein is usually an indicator of the microenvironment where heme center locates. The peak will be diminished if the protein is denatured [50]. The band for Mb in the solution is located at 406 nm (Fig. 4a). The dry films of only Mb and Mb/ArHA film were prepared onto the ITO glass electrodes, both dry films showed Soret bands at 406 nm (Fig. 4b and c), suggesting that Mb in dry ArHA films has a secondary structure nearly the same as the native state of Mb in solution. It is well known, acidification of solution causes unfolding of hemeproteins consequently causes large change in the heme crevice [66]. But the change is reversible. The Soret band of Mb in ArHA film was confirmed by using UV–vis spectroscopy measurement after the Mb adsorbed onto the ArHA modified ITO coated glass electrode in acidic condition, the results suggested that the protein retains native secondary structure after glass Mb/ArHA was transferred to a pH 6.9 buffer solution. The reversibility of change in conformation should be attributed to highly specific and tightly folding conformation of proteins. According to the previous report [67], addition of denaturants such as acid or base could induce unfolding of the protein to a largely disordered conformation, but most proteins spontaneously would refold to their native state when the denaturants were removed.

The control experiment, hemin (heme redox cofactor) adsorption onto arylhydroxylamine modified GCE and ITO electrodes were also carried out as did for Mb immobilization, the CV indicated, no adsorption of hemin takes place onto the HAGC
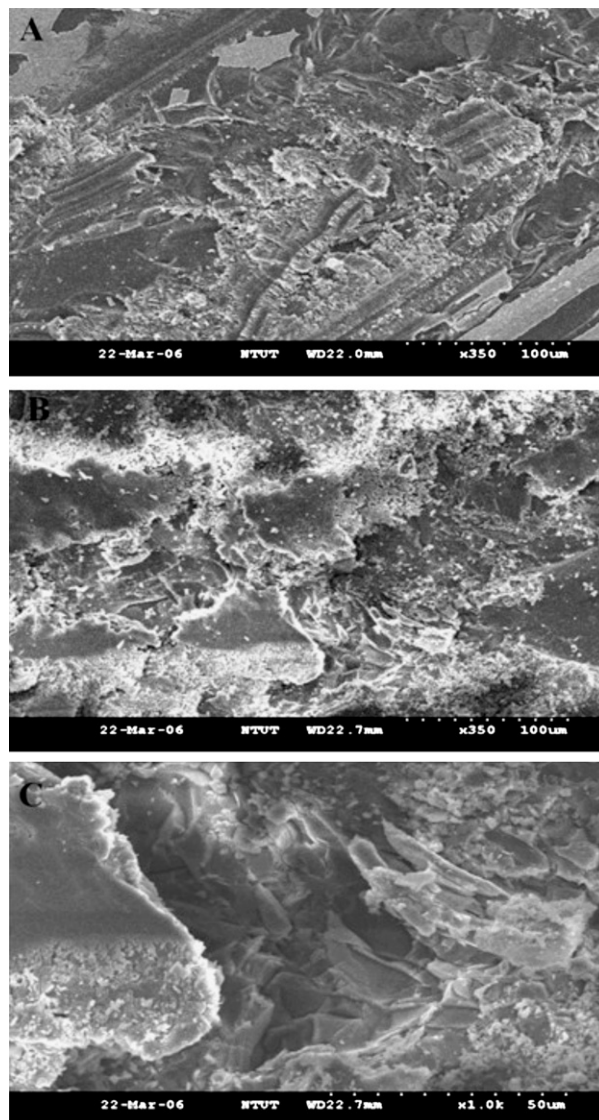
Fig. 5. SEM images of (A) ArHA film, (B) Mb/ArHA film and (C) Mb/ArHA film (high magnification (1k)) on ITO electrodes.

modified electrodes (figures not shown), it is suggested that only proteins like structure Mb can be adsorbed onto the ArHA modified electrodes [8].

For SEM measurements, ArHA and Mb/ArHA modified films are prepared onto the ITO electrodes surface. Morphological Characterization of both dry films was measured. The ArHA film revealed a coral-like pattern (Fig. 5A), while the Mb/ArHA film showed evenly distributed small spots of 0.3–0.4 μm diameter (Fig. 5B). This difference suggested interactions between ArHA and Mb, which governed the morphology of the dry films. The high magnification image of Mb/ArHA film shows the small Mb particles on the surface of sponge like thin film of ArHA (Fig. 5C).

3.5. Electrocatalytic activity of Mb/HAGC electrode

It was reported that proteins containing heme groups, such as HRP, cytochrome c, hemoglobin, myoglobin and hemin, are
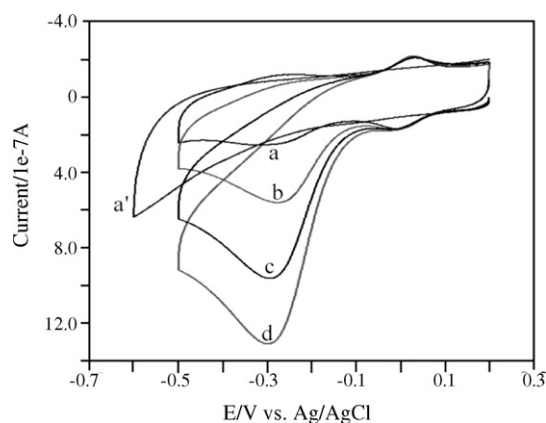
Fig. 6. Cyclic voltammograms at 0.05 V/s in pH 6.0 PBS: (a) Mb/HAGCE film without H$_2$O$_2$, (b) 2.02 μM, (c) 4.01 μM, (d) 5.81 μM H$_2$O$_2$ and (a') bare GCE with 5.81 μM H$_2$O$_2$.

capable to reduce H$_2$O$_2$ electrocatalytically [21]. In order to survey the activity of Mb/HAGC electrode, its response to the reduction of H$_2$O$_2$ was studied. When H$_2$O$_2$ was added to a pH 6.0 buffer solution, an increase in the reduction peak at about −0.3 V is seen with the decrease of the oxidation peak for Mb Fe(II) (Fig. 6). The reduction peak current increases with the concentration of H$_2$O$_2$ in the solution. However, direct reduction of H$_2$O$_2$ is not distinct at only the HAGC electrode film in the potential range of 0.2 to −1.0 V. The linear relationship of the electrocatalytic reduction peak current and H$_2$O$_2$ concentration is observed between 6.67×10^{-6} and 9.33×10^{-4} M. The linear regression equation is I (A) = 6.0×10^{-2} [H$_2$O$_2$] (M) + 4.0×10^{-7} with a correlation coefficient of 0.999. The calibration curve gradually tended to a plateau and then dropped down with adding H$_2$O$_2$, implying a progressive enzyme inactivation in the presence of higher concentration of H$_2$O$_2$.

As is well known, TCA is an important organohalide environmental pollutant. To detect the concentration of TCA in the environment is of great importance for controlling pollution. The electrocatalytic reduction of TCA by the Mb/HAGC electrode in pH 6.0 phosphate buffer solution is shown in Fig. 7. When TCA was added to buffer solution, a reduction peak was
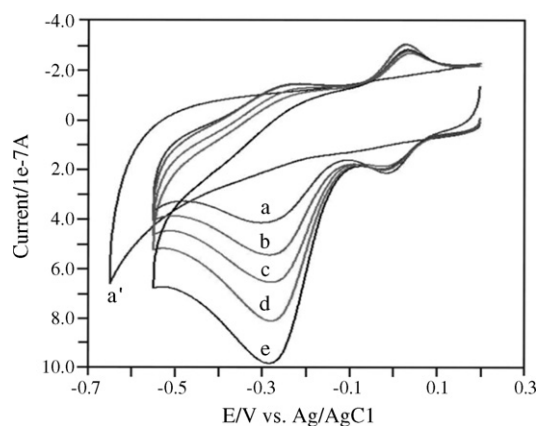
Fig. 7. Cyclic voltammograms at 0.05 V/s in pH 6.0 PBS: (a) Mb/HAGCE film without TCA, (b) 1.02 μM, (c) 2.08 μM, (d) 3.17 μM, (e) 4.25 μM TCA and (a') bare GCE with 4.25 μM TCA.
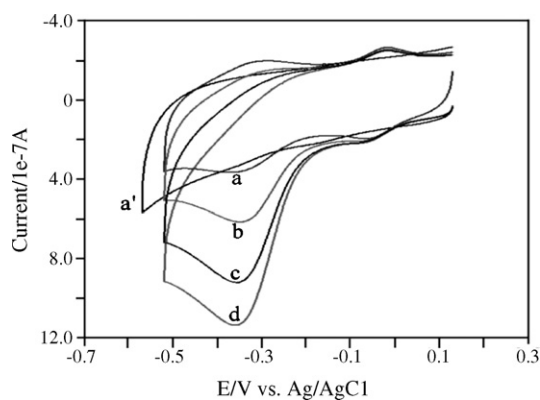
Fig. 8. Cyclic voltammograms at 0.05 V/s in pH 6.0 PBS: (a) Mb/HAGCE film without O$_2$, injection of air (b) 10 ml, (c) 20 ml, (d) 25 ml, and (a') bare GCE with injection of 25 ml air.

observed at about −0.288 V, accompanying the decrease of the oxidation peak of Mb. No electrochemical reduction peak was observed when the cyclic voltammetric scan was performed at bare GC or HAGCE under the same conditions. The reduction peak currents increased linearly with concentrations of TCA, as shown in Fig. 7. The Mb/HAGC electrode may be used to detect organohalide pollutants in the environmental samples.

The mechanism of bioelectrocatalytic reduction of TCA by myoglobin might be schematically expressed as follows [68]:

$$MbFe(III) + H^+ + e^- \leftrightarrow MbFe(II) \tag{4}$$

$$CCl_3COOH \leftrightarrow CCl_3COO^- + H^+, \quad pK_a = 0.89 \tag{5}$$
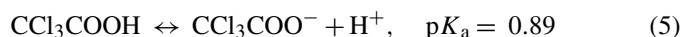
The overall reaction would be:

$$2(MbFe(II)) + CCl_3COOH + H^+ + 2e^-$$
$$\rightarrow 2(MbFe(III)) + HCCl_2COOH + Cl^- \tag{6}$$
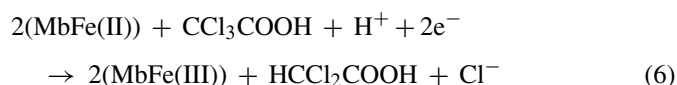
Fig. 8 shows the cyclic voltammograms of Mb/HAGC modified electrode in phosphate buffer solution (pH 6.9) containing different O$_2$ concentrations. When a volume of air was injected, a significant increase in the cathodic peak at about −0.36 V was observed. The increase in the reduction peak is accompanied by a decrease of oxidation peak of Mb Fe(II), suggesting that Mb Fe(II) had reacted with oxygen. An increase in the amount of oxygen in solution increases the reduction peak current. The catalytic efficiency expressed as the ratio of reduction peak current of Mb(III) in the presence of (I_c) and absence of oxygen (I_d), I_c/I_d, decreases with the increase of scan rate, which is also a characteristic of electrochemical catalytic reduction of oxygen at Mb/HAGC film electrode. The mechanism of catalytic reduction of oxygen at Mb/HAGC can be elucidated by the pathway suggested by Hu and Rusling [10]. On Mb-DDAB film modified pyrolytic graphite electrode, direct electrochemical reduction of Mb Fe(III) to Mb Fe(II) occurred at the electrode, followed by a fast reaction of Mb Fe(II) with oxygen. The product of Mb Fe(II)–O$_2$ could then undergo electrochemical reduction at the potential of Mb Fe(III) reduction, producing hydrogen peroxide and Mb Fe(II) again.
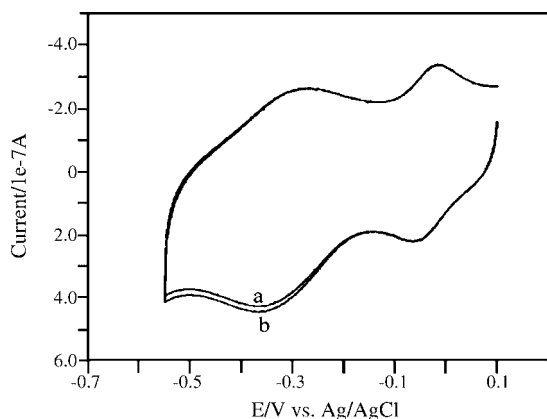
Fig. 9. Cyclic voltammograms of the Mb/HAGCE modified electrode in pH 7.0 PBS (a) 1st and (b) 100th cycle at a scan rate of 0.1 V/s.

3.6. Stability, reproducibility of Mb/HAGC electrode

To ascertain the stability, reproducibility of Mb/HAGC film electrode, CV studies showed that this modified electrode is very stable, after several initial scans, the CV remains nearly unchanged for about 100 cycles (Fig. 9). The flow injection analysis of H_2O_2 was studied at Mb/HA modified carbon paste electrode with successive additions of $2 \mu M$ H_2O_2 (PBS, pH 7) at an applied potential of -0.35 V. It is shown in Fig. 10, upon continuous injection of an aliquot of H_2O_2 to the moving buffer solution, the reduction current increases steeply to reach a stable value. This modified electrode reaches 95% of the steady-state current in less than 2 s, which indicates that the electrocatalytic response is very fast and reproducible results were obtained for continuous injection of fourteen times the same concentration of H_2O_2 (Fig. 10). The reproducibility catalytic response for $2 \mu M$ H_2O_2 solution at Mb/HAGC was estimated (pH 7), and the relative standard deviation (R.S.D.) is 0.3% ($n = 13$). It is suggested the Mb/HAGC electrode shows fast response and also very stable at physiological pH. This also implied that the present modified electrode exhibited a higher affinity for H_2O_2.

When compared to other modified electrode systems reported for immobilization of Mb such as carbon nanotubes, the activity of carbon nanotubes are mainly depended on the method of
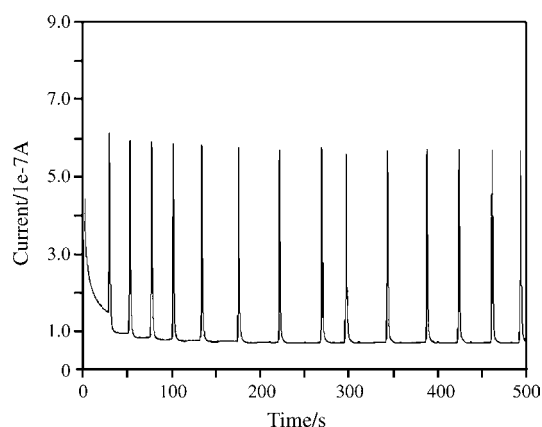
Fig. 10. Flow injection analysis of $2 \mu M$ H_2O_2 for every 25 s at Mb/HA modified carbon paste electrode at constant potential of -0.35 V in PBS (pH 7.0).

preparation, dispersing agents, and casting of CNT onto the electrode surface have substantial effect on the stability of modified electrode [65,69,70] such factors limits the cost, duration of the CNT modified electrodes and higher background current also limit it is use in electrocatalysis, So this new Mb/HAGC electrode is simple one for electrode fabrication; the time required for electrode preparations is less than 70 min and electron transfer rate constant (k_s) value 51 ± 5 s^{-1} higher than the CNT modified electrode (5.4 s^{-1}) reported for Mb [32–34], hence, the HAGCE modified electrode is a prompted material for the immobilization of Mb and it is use in the preparation of biosensors are evident. Here we have demonstrated only Mb as a model protein for investigation; furthermore it is possible to study about other proteins and enzymes using this kind of modified electrodes. So we hope this Mb/HAGC modified electrode can find potential application in the preparation of third generation biosensors or bioreactors.

4. Conclusions

We explored a new HAGC film modified electrode. The HAGC film can be readily used as an immobilization matrix to entrap proteins and enzymes. We were chosen redox-active Mb as a model protein to investigate the HAGC electrode. A simple and general method was used to prepare the bioactive Mb/HAGC film electrode. The obtained results revealed that direct electron transfer between redox proteins and the underlying electrode can be easily performed at Mb/HAGC electrode. This new modified electrode had dramatically enhanced electrocatalytic activity toward H_2O_2, O_2 and TCA along with good stability in solution. This unique Mb/HAGC film can provide a good electrochemical sensing platform for redox proteins and enzymes, and thus it is expected to have widely potential applications in direct electrochemistry, biosensors, and electrocatalysis.

References

[1] F.A. Armstrong, H.A. Hill, N.J. Walton, Acc. Chem. Res. 21 (1988) 407.
[2] M.K. Beissenhirtz, F.W. Scheller, F. Lisdat, Anal. Chem. 76 (2004) 4665.
[3] I. Hamachi, A. Fujita, T. Kunitake, J. Am. Chem. Soc. 119 (1997) 9096.
[4] J.F. Stargardt, F.M. Hawkridge, H.L. Landrum, Anal. Chem. 50 (1978) 930.
[5] D.P. Hildebrand, H.-I. Tang, Y. Luo, C.L. Hunter, M. Smith, G.D. Brayer, A.G. Mauk, J. Am. Chem. Soc. 118 (1996) 12909.
[6] E. Stellwagen, Nature 275 (1978) 73.
[7] J.F. Rusling, A.-E.F. Nassar, J. Am. Chem. Soc. 115 (1993) 11891.
[8] A.-E.F. Nassar, J.M. Bobbitt, J.D. Struart, J.F. Rusling, J. Am. Chem. Soc. 117 (1995) 10986.
[9] R. Lin, M. Bayachou, J. Greaves, P.J. Farmer, J. Am. Chem. Soc. 119 (1997) 12689.
[10] N. Hu, J.F. Rusling, Langmuir 13 (1997) 4119.
[11] M. Bayachou, R. Lin, W. Cho, P.J. Farmer, J. Am. Chem. Soc. 120 (1998) 9888.
[12] S. Boussaad, N.J. Tao, J. Am. Chem. Soc. 121 (1999) 4510.
[13] C.E. Immoos, J. Chou, M. Bayachou, E. Blair, J. Greaves, P.J. Farmer, J. Am. Chem. Soc. 126 (2004) 4934.

[14] N.K. Kawahara, W. Ohkubo, H. Ohno, Bioconjugate Chem. 8 (1997) 244.

[15] Y.M. Lvov, Z. Lu, J.B. Schenkman, X. Zu, J.F. Rusling, J. Am. Chem. Soc. 120 (1998) 4073.

[16] V. Panchagnula, C.V. Kumar, J.F. Rusling, J. Am. Chem. Soc. 124 (2002) 12515.

[17] H. Liu, N.J. Hu, Phys. Chem. B 109 (2005) 10464.

[18] B.R. Van Dyke, P. Saltman, F.A. Armstrong, J. Am. Chem. Soc. 118 (1996) 3490.

[19] M. Feng, H.J. Tachikawa, J. Am. Chem. Soc. 123 (2001) 3013.

[20] Q. Gao, S.L. Suib, J.F. Rusling, Chem. Commun. (2002) 2254.

[21] Q. Wang, G. Lu, B. Yang, Langmuir 20 (2004) 1342.

[22] E. Topoglidis, A.E.G. Cass, G. Gilardi, S. Sadeghi, N. Beaumont, J.R. Durrant, Anal. Chem. 70 (1998) 5111.

[23] Q. Li, G. Luo, Feng, J. Electroanal. Chem. 13 (2001) 359.

[24] E. Topoglidis, C.J. Campbell, A.E.G. Cass, J.R. Durrant, Langmuir 17 (2001) 7899.

[25] C. Grealis, E. Magner, Chem. Commun. (2002) 816.

[26] G.A. Garwood, M.M. Mortland, T.J. Pinnavaia, J. Mol. Catal. 22 (1983) 153.

[27] C.V. Kumar, A. Chaudhari, J. Am. Chem. Soc. 122 (2000) 830.

[28] Y.J. Han, J.T. Watson, G.D. Stucky, A. Butler, J. Mol. Catal. B: Enzymol. 17 (2002) 1.

[29] X. Xu, B.Z. Tian, J.L. Kong, S. Zhang, B.H. Liu, D.Y. Zhao, Adv. Mater. 15 (2003) 1932.

[30] S. Peng, Q. Gao, Q. Wang, J. Shi, Chem. Mater. 16 (2004) 2675.

[31] V.V. Shumyantseva, Y.D. Ivanov, N. Bistolas, F.W. Scheller, A.I. Archakov, U. Wollenberger, Anal. Chem. 76 (2004) 6046.

[32] L. Zhao, H. Liu, N. Hu, J. Colloid Interface Sci. 296 (2006) 204.

[33] L. Zhao, H. Liu, N. Hu, Anal. Bioanal. Chem. 384 (2006) 414.

[34] G.C. Zhao, L. Zhang, X.W. Wei, Z.S. Yang, Electrochem. Commun. 5 (2003) 825.

[35] A. Liu, A. Wei, I. Honma, H. Zhou, Anal. Chem. 77 (2005) 8068.

[36] A.A. Jbarah, R. Holze, J. Solid State Electrochem. 10 (2006) 360.

[37] H. Nobutoki, H. Koezuka, J. Phys. Chem. 101 (1997) 3762.

[38] F. Bertinelli, P. Palmieri, A. Brillante, C. Taliani, Chem. Phys. 25 (1977) 333.

[39] M. Stahelin, D.M. Burland, J.E. Rice, Chem. Phys. Lett. 191 (1992) 245.

[40] J.N. Woodford, M.A. Pauley, C.H. Wang, J. Phys. Chem. A 101 (1997) 1989.

[41] F.L. Huyskens, P.L. Huyskens, A.P. Persoons, J. Chem. Phys. 108 (1998) 8161.

[42] L. Turi, J.J. Dannenberg, J. Phys. Chem. 100 (1996) 9638.

[43] M.M. Szostak, B. Kozankiewicz, G. Wojcik, J. Lipinski, J. Chem. Soc., Faraday Trans. 94 (1998) 3241.

[44] M. Hurst, R.W. Munn, Special Publication, Roy. Soc. Chem. (Org. Mater. Non-linear Opt.) 69 (1989) 3.

[45] J. Hutter, G. Wagniere, J. Mol. Struct. 175 (1988) 159.

[46] J.J. Dannenberg, ACS Symp. Ser. (Mater. Nonlinear Opt.) 455 (1991) 457.

[47] A. Wesch, O. Dannenberger, C. Woll, J.J. Wolff, M. Buck, Langmuir 12 (1996) 5330.

[48] E.D. Schmid, M. Moschallski, W.L. Peticolas, J. Phys. Chem. 90 (1986) 2340.

[49] K. Kumar, P.R. Carey, J. Phys. Chem. 63 (1975) 3697.

[50] L. Shen, N. Hu, Biomacromolecules 6 (2005) 1475.

[51] D. Mansuy, J.C. Chottard, G. Chottard, Eur. J. Biochem. 76 (1977) 617.

[52] R.F. Eich, T. Li, D.D. Lemon, D.H. Doherty, S.R. Curry, J.F. Aitken, A.J. Mathews, K.A. Johnson, R.D. Smith, G.N. Phillips, J.S. Olson, Biochemistry 35 (1996) 6976.

[53] K.J. Stutts, R.M. Wlghtman, Anal. Chem. 55 (1983) 1576.

[54] C. Shi, W. Zhang, R.L. Birke, J.R. Lombardi, J. Phys. Chem. 94 (1990) 4766.

[55] E. Casero, M. Darder, K. Takada, H.D. Abruna, F. Pariente, E. Lorenzo, Langmuir 15 (1999) 127.

[56] L.I. Halaoui, H. Sharifian, A.J. Bard, J. Electrochem. Soc. 148 (2001) E386.

[57] A.J. Bard, L.R. Faulkner, Electrochemical Methods, Wiley, New York, 1980.

[58] R.W. Murray, in: A.J. Bard (Ed.), Electroanalytical Chemistry, vol. 13, Marcel Dekker, New York, 1984, pp. 191–368.

[59] E. Laviron, in: A.J. Bard (Ed.), Electroanalytical Chemistry, vol. 12, Marcel Dekker, New York, 1982, pp. 53–157.

[60] H.H. Liu, Z.Q. Tian, Z.X. Lu, Z.X. Lu, Z.L. Zhang, M. Zhang, D.W. Pang, Biosens. Bioelectron. 20 (2004) 294.

[61] E. Laviron, J. Electroanal. Chem. 52 (1974) 355.

[62] E. Laviron, J. Electroanal. Chem. 101 (1979) 19.

[63] S.M. Chen, C.C. Tseng, J. Electroanal. Chem. 575 (2005) 147.

[64] S.M. Chen, C.C. Tseng, Electrochim. Acta 49 (2004) 1903.

[65] L. Shen, R. Huang, N. Hu, Talanta 56 (2002) 1131.

[66] Z. Chi, S.A. Asher, Biochemistry 37 (1998) 2865.

[67] O.O. Sogbein, D.A. Simmons, L. Konermann, J. Am. Soc. Mass Spectrosc. 11 (2000) 312.

[68] X. Lu, J. Hu, X. Yao, Z. Wang, J. Li, Biomacromolecules 7 (2006) 975.

[69] N.S. John, T.-W. Yeow, IEEE Trans. Nanobiosci. 4 (2005) 180.

[70] N.S. Lawrence, R.P. Deo, J. Wang, Electroanalysis 17 (2005) 65.

Hollow-fibre liquid phase microextraction for separation and preconcentration of vanadium species in natural waters and their determination by electrothermal vaporization-ICP-OES

Li Li, Bin Hu [*]

Department of Chemistry, Wuhan University, Wuhan 430072, China

Abstract

For separation and determination of vanadium(IV/V) species, a fast and sensitive method by combining hollow-fibre liquid phase microextraction (HF-LPME) with electrothermal vaporization (ETV)-ICP-OES has been developed. Two vanadium species (V(IV) and V(V)) were separated by HF-LPME with the use of ammonium pyrrolidinecarbodithioate (APDC) as chelating agent for complexing with different V species and carbon tetrachloride as the extraction solvent, and the vanadium in the post-extraction organic phase was injected into the graphite furnace for ETV-ICP-OES detection, in which APDC was acted as the chemical modifier. At pH 5.0, both V(IV)-APDC and V(V)-APDC were extracted quantitatively into CCl$_4$ for determination of total V. For speciation studies, 1,2-cyclohexanediaminetetraacetic acid (CDTA) was added to the sample for masking V(IV), so that only V(V)-APDC was extracted and determined. The concentration of V(IV) was calculated by subtracting the V(V) concentration from the total concentration of V. Under the optimized experimental conditions, the enrichment factor was 74 and the detection limits for V(IV) and V(V) were 86 pg mL^{-1} and 71 pg mL^{-1}, respectively. The proposed method has been applied to the speciation of V in environmental water samples, and the recovery was in the range of 94%–107%. The results show that V(V) is the dominant existence form in oxygenic water and V(IV) could not been detected. In order to validate the developed procedure, a NIES No.8 vehicle exhaust particulates certified reference material was analyzed, and the results obtained for total vanadium are in good agreement with the certified values. The proposed method is simple, rapid, selective, and sensitive and no oxidation/reduction is required, it is applicable to the speciation of vanadium in environmental samples with the complicated matrix.
© 2006 Elsevier B.V. All rights reserved.

Keywords: Hollow-fibre liquid phase microextraction; Vanadium; Speciation; Electrothermal vaporization-ICP-OES; APDC; CDTA; Water

1. Introduction

Increasing emission of vanadium into the environment has been related to industrial sources, especially iron, oil refineries and power plants using vanadium-rich fuel oil and coal. And the environmental pollution from vanadium has subsequently endangered the health of human [1,2]. Vanadium has many existing forms, among which V(IV) and V(V) are the dominant oxidation forms. It has been approved that V(V) is largely responsible for the restraining effect to adenosine triphosphatase in the biological bodies, while V(IV) has little effect [3]. Therefore, the speciation analysis of V(IV) and V(V) in environmental samples has drawn much more attention in recent years.

The effective method for vanadium speciation analysis is to combine the simple and selective separation/preconcentration step with the sensitive detection techniques. Taking the stability of the oxidation forms and their concentration difference into accounts, an ideal pretreatment technique should possess qualities such as high analysis speed, good selectivity and low matrix interference. The separation/preconcentration methods including solvent extraction [4], solid phase extraction (SPE) [5], high performance liquid chromatography (HPLC) [6], ion-exchange resins [1], capillary electrophoresis (CE) [7], flow-injection microcolumn [8] and so on, have been applied widely to the speciation of vanadium until to present. Among the above-mentioned methods, column or microcolumn based SPE separation/preconcentration is the most common used one.

* Corresponding author. Tel.: +86 27 87218764; fax: +86 27 68754067.
  E-mail address: binhu@whu.edu.cn (B. Hu).

Based on the selective sorption onto the column, the two species of vanadium can be separated in a certain pH range. In most cases, the column has been modified by chelating reagents, such as quinoline [9], thenoyltrifluoroacetone (TTA) [10], 4,5-imidazole dicarboxylic acid [5], etc. However, these methods often suffer from such disadvantages as large consumption of sample and eluent solution, and slow analysis speed.

It has been studied that trans-1,2-cyclohexanediamine-tetraacetic acid (CDTA) can form complex with V(IV) selectively, and the lgK for V(IV)-CDTA is 20.1 [11]. Based on this character, CDTA has been used as masking agent for V(IV) in many studies [8,12–15]. Pyrzyńska and Wierzbicki [8] used cellulose with phosphonic acid exchange groups (Cellex P) for enrichment of both vanadium(IV) and vanadium(V). Both species could be simultaneously eluted using EDTA solution with recoveries of 94–101% and determined by atomic adsorption spectrometry (AAS). The speciation study of vanadium has been tested using CDTA added to the sample or as a selective eluent for V(IV). Another report [15] used amberlite IRA-904 resin modified with tetrakis (*p*-carboxyphenyl) porphyrin (TCPP) to preconcentrate vanadium species, and CDTA was added to the sample to mask V(IV), which was not retained on the microcolumn.

Hollow-fibre liquid phase microextraction (HF-LPME) [16–19] is an attractive and novel pretreatment method qualified with high concentration factor, rapid analysis time, simple setup and low cost. As an environmental-friendly technique, it has been successfully employed for the determination of polycyclic aromatic hydrocarbons [16], phthalate esters [17], basic drugs [18], and organochlorine pesticides [19] in environmental samples, food and biological samples.

Many detection techniques, such as neutron activation analysis (NAA) [20], AAS [21], inductively coupled plasma optical emission spectrometry (ICP-OES) [9,10] and inductively coupled plasma mass spectrometry (ICP-MS) [22], have been employed so far for the speciation analysis of vanadium. Of all these methods, ICP-OES/MS has been proven to be one of the most powerful techniques for trace vanadium determination. In ICP-OES/MS, sample introduction techniques play a key role not only in improving the sensitivity and the selectivity, but also in extending the application of analytical methods. Conventional pneumatic nebulization (PN) has disadvantages of low intake efficiency (less than 2%), large sample consuming and difficult to analyze the high salt-containing and viscous samples. Electrothermal vaporization (ETV), as a means of sample introduction for ICP-OES/MS, has been demonstrated to have the distinct merits of high transport efficiency, low sample consumption, low matrix effect and being able to analyze solid samples directly, which leads to extensive application in analysis of trace elements. As a microvolume sample introduction technique, ETV is apt to effectively combine with various modes of microextraction techniques. The combination of newly developed liquid phase microextraction (LPME) technique with ETV-ICP-OES/MS has been recently studied for trace elements and their species analysis [23–27].

Although the detection sensitivity of vanadium in ETV-ICP-OES is satisfying, rather high vaporization temperature is needed to vaporize vanadium from the graphite furnace due to its refractory character (vanadium metal: 1890 °C m.p., 3380 °C b.p.). In addition, the memory effect of vanadium is usually remarkable. Lots of the research has shown that the use of chemical modifier can make the analytes efficiently vaporized in graphite furnace and transported to ICP-OES, and thereby improve analytical performance of the method. Although inorganic compounds and polytetrafluoroethene (PTFE) have been developed as chemical modifiers for a long time, they are difficult to use directly in the process of separation/preconcentration steps. So analysts have been attempting to use organic chelating reagents as chemical modifier, and thus have proposed the low temperature ETV technique.

A number of organic chelating reagents have been reported, such as quinoline [28], β-diketone [29] and dithiodicarbamates [30], for the use as chemical modifier. Such reagents can form chelates with metals, which possess good volatility and thermal stability and improve the vaporization behavior of the analytes in the graphite furnace. The successful application of these chelating reagents as chemical modifiers and meanwhile extractants indicates that the exploitation and research of organic chelating reagents has a prospective potentiality in combination of separation/preconcentration steps and ETV-ICP-OES/MS.

In this work, a simple and efficient method by combining HF-LPME with ETV-ICP-OES was proposed for the speciation of V(IV) and V(V). CDTA was used as the masking agent for V(IV) and ammonium pyrrolidine dithiocarbamate (APDC) was employed as both the extractant for the HF-LPME separation of different V species and the chemical modifier for ETV-ICP-OES determination of vanadium. The proposed method was applied to analyze the vanadium species in environmental waters.

2. Experimental

2.1. Apparatus and experimental conditions

2.1.1. Microextraction system
The homemade "U"-shaped setup of HF-LPME is illustrated in Fig. 1. The sample solution was filled into a 4-mL glass vial with a rubber top. An infundibular plastic was served as both the injection guide of organic solvent and the holder of the hollow fibre. A capillary was served as another holder and made an open channel in order to avoid forming air bubbles in the fibre. The Q3/2 Accurel KM polypropylene hollow fibre (Akzo Nobel, Wuppertal, Germany) was cut into 8-cm long pieces. The inner diameter of the hollow fibre was 600 μm, the thick-
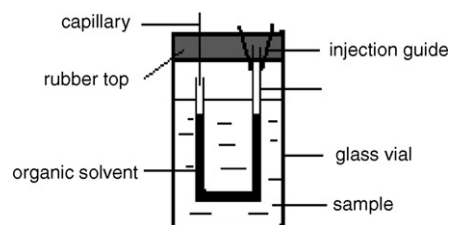

Fig. 1. The homemade "U"-shaped setup of HF-LPME.

ness of the wall was 200 μm, and the pore size was 0.2 μm. A 10-μL microsyringe (Gaoxin, Shanghai, China) was used to inject and withdraw the organic solvent into and from the fibre.

Besides, an MM-1 minivibrator (Qingpu huxi Instrument Factory, Shanghai, China), an MDS-2003F (Sineo Microwave Chemical Technology Co. Ltd., Shanghai, China) and a DELTA-320 pH meter (Mettler Toledo, Switzland) were used in the work.

2.1.2. ETV-ICP-OES apparatus

A modified commercially WF-4C graphite furnace (Beijing Second Optics, Beijing, China) was available as an electrothermal vaporizer and the details on the modification of the graphite furnace and its connection with ICP-OES have been described previously [10]. An ICP spectrometric system (Beijing Broadcast Instrument Factory, Beijing, China) with 2-kW plasma generator was used with a conventional silica plasma torch. A WF-1B type heating device with a matching graphite furnace (Beijing Second Optics, Beijing, China) was used for the sample introducing. Pyrolytic graphite-coated tubes were used throughout. The radiation from the plasma was focused as a 1:1 image on the entrance slit of a WDG 500-1A type monochromator (Beijing Second Optics, Beijing, China) having a reciprocal linear dispersion of 1.6 nm mm^{-1}. The transient emission signals from plasma were detected with a R456 type photomultiplier tube (Hamamatsu, Japan) fitted with a laboratory-built direct current amplifier, and recorded by a U-135C recorder (Shimadzu, Kyoto, Japan). The used operating conditions for ETV-ICP-OES and the wavelength were summarized in Table 1.

Table 1

Operation conditions of ICP-OES/ICP-MS and temperature programs of graphite furnace

	Optimized condition
ETV-ICP-OES parameters	
Wavelength (nm)	V 309.311
Incident power (kW)	1.0
Carrier gas (L min^{-1})	0.6
Coolant gas (L min^{-1})	16
Plasma gas (L min^{-1})	0.8
Observation height (mm)	12
Entrance slit-width (μm)	25
Exit slit-width (μm)	25
ICP-MS parameters	
Incident power (kW)	1.3
RF matching (V)	1.6
Carrier gas (Ar) flow rate (L min^{-1})	1.16
External gas (Ar) flow rate (L min^{-1})	15
Sampling depth (mm)	7
Sample uptake rate (mL min^{-1})	0.4
Monitored isotope (m/z)	51
Integration time (s)	0.1
Temperature programs of graphite furnace for ETV-ICP-OES	
Drying temperature	100 °C, ramp 10 s, hold 15 s
Vaporization temperature	1700 °C, hold 6 s
Cleaning temperature	2500 °C, hold 3 s
Sample volume	5 μL

2.1.3. ICP-MS apparatus

An Agilent 7500a ICP-MS (Hewlett-Packard, Yokogawa Analytical Systems, Tokyo, Japan) with a Babington nebulizer was used for the determination of the total V in lake water and tap water to test the accuracy of the developed method, and peak height was used for quantification. The operating conditions for ICP-MS were also given in Table 1.

2.2. Standard solutions and reagents

The stock standard solution of 1000 μg mL^{-1} vanadium(V) was prepared by dissolving 0.2297 g of analytical reagent grade (AR) NH$_4$VO$_3$ (99.99%) (Shanghai Reagent Factory, Shanghai, China) in 100 mL 0.01 mol L^{-1} HCl; the stock standard solution of 1000 μg mL^{-1} vanadium(IV) was prepared by dissolving 0.4968 g of analytical reagent grade VOSO$_4$·5H$_2$O (99.99%) (Merck, Darmstadt, Germany) in 100 mL 0.01 mol L^{-1} HCl. Buffer solutions used were 0.01 mol L^{-1} KH$_2$PO$_4$-K$_2$HPO$_4$. The solution of ammonium pyrrolidine dithiocarbamate (AR, Shanghai Reagent Third Factory, Shanghai, China) was prepared in high purity deionized water and stored in refrigerator at 4 °C against light. All containers were dipped in 10% HNO$_3$ over 24 h and washed by high purity deionized water prior to usage. High purity deionized water was used throughout the all experiments.

2.3. Collection and preparation of samples

2.3.1. Environmental waters

Lake water (pH 7.48, East Lake, Wuhan, China) and sea water (pH 7.70, Star Gulf, Dalian, China) were collected in the 50-mL polyethylene containers and directly filtrated with 0.45-μm membrane filter (Tianjin Jinteng Instrument Factory, Tianjin, China) and immediately adjusted to pH of 5.0. Tap water (pH 7.17, Wuhan, China) was adjusted to pH of 5.0 prior to analysis. A 3.5-mL filtered aliquot of sample was used for further analysis. High purity deionized water was used as blank, and the blank experiments were carried out through the same procedure.

2.3.2. Certified reference material (NIES No.8, vehicle exhaust particulates)

In order to validate the developed method, a certified reference material (NIES No.8, vehicle exhaust particulates) was employed. 50.0 mg of dry vehicle exhaust particulates was accurately weighed into a clean and dry PTFE digest vessel, and then 4.0 mL ultrapure nitric acid, 1.0 mL ultrapure perchloric acid and 1.0 mL ultrapure hydrofluoric acid were added into the vessel. After digested according to a certain microwave digestion program, and cooled down to room temperature, the clear sample was adjusted to pH of 5.0 and diluted to 25 mL with high purity deionized water for subsequent microextraction and determination. Blank experiments were carried out through the same procedure without the certified reference material.

The microwave digestion program was performed in three steps: (1) 8 atm for 2 min, heating power 600 W; (2) 12 atm for 3 min, heating power 800 W; (3) 16 atm for 8 min, heating power 800 W.

2.4. Analysis procedure

2.4.1. HF-LPME procedure

An aliquot of 3.5 mL sample solution was filled into a 4-mL glass vial with a homemade rubber top. An 8-cm hollow fibre was cut and fixed into U-shape with the homemade rubber top. After dipped into CCl_4 for 1 min, both the inner channel and the pores of the U-shaped hollow fibre were filled with CCl_4. And then it was immersed in the sample solution for further extraction. The enrichment was performed under vibration and by this means about 12 samples can be pretreated at the same time. After a period of extraction, the organic solvent in the fibre was withdrawn by the microsyringe from the infundibular plastic guide and was then injected into the graphite furnace for further ETV-ICP-OES analysis.

2.4.2. ETV-ICP-OES procedure

After the ICP-OES system was stabilized, the detection wavelength for vanadium was adjusted. And then the ETV unit was connected to the ICP-OES system followed by stabilizing for a while. Afterwards, the post-extraction solvent withdrawn in the microsyringe was directly introduced into the graphite furnace for analysis. The dosing pole was open to remove the water and organic solvent during the drying step of the temperature program, and it was sealed with a graphite probe 6 s prior to the vaporization step. At the same time, the emission signal was recorded, and the peak heights were measured for quantification.

2.4.3. Speciation of V(IV) and V(V)

(1) Total V: When total vanadium was to be determined, HF-LPME was performed at pH 5.0 with only APDC (final concentration of 6.0×10^{-3} mol L^{-1}) added into the sample. The post-extraction organic phase was introduced into the graphite furnace for ETV-ICP-OES determination.
(2) V(V): For determination of V(V), 1,2-cyclohexanediamine-tetraacetic acid (CDTA) was added to the sample for masking V(IV), so that only V(V)-APDC was extracted and the post-extraction organic phase was introduced into the graphite furnace for ETV-ICP-OES determination.
(3) V(IV): The content of V(IV) was calculated by subtraction of V(V) from the total V.

All experiments were corrected against the reagent blank. For testing the accuracy of the developed method, the total V of lake water and tap water was directly determined by means of ICP-MS.

3. Results and discussion

3.1. Vaporization behavior of vanadium in graphite furnace

3.1.1. Chemical modification of APDC to vanadium

The APDC complexes of metals are often volatile compounds with good thermal stability, so the vaporization behavior of APDC chelate of vanadium in graphite furnace was investigated in this work. Fig. 2 is the typical signal profiles of vanadium with
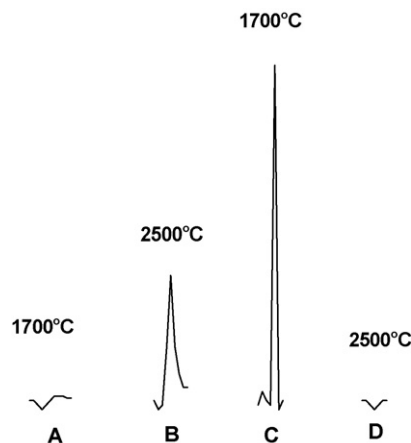
Fig. 2. Signal profiles. (A) A 10 ng V(V) at ETV. *Conditions*: drying, 100 °C, ramp 10 s, hold 15 s; vaporization, 1700 °C, 6 s. (B) The residual signals of empty firing at 2500 °C, 3 s for (A). (C) A 10 ng V(V) with APDC as chemical modifier at ETV. *Conditions*: drying, 100 °C, ramp 10 s, hold 15 s; vaporization, 1700 °C, 6 s. (D) The residual signals of empty firing at 2500 °C, 3 s for (C).

and without APDC as the chemical modifier. As could be seen, without the addition of APDC, no emission signal of vanadium was detected at 1700 °C while a severe memory signal occurred at 2500 °C. It was because vanadium is a refractory element and can be partly vaporized only when the vaporization temperature is above 2000 °C without chemical modifiers. On the contrary, an intense and sharp emission signal could be observed at 1700 °C in the presence of APDC as the chemical modifier, and only a very weak memory signal was found at 2500 °C. This indicated that vanadium could be vaporized quantitatively from the graphite furnace as the form of V-APDC chelate at a relatively lower vaporization temperature.

In order to validate the thermal stability of V(V)-APDC chelate, thermal gravimetric (TG) analysis of the synthetic metal chelate has been carried out. Fig. 3 was the profile of the thermal gravimetric analysis of the V(V)-APDC chelate. It can be seen that V(V)-APDC chelate shows a weight loss between 270 and 510 °C in one step, indicating that V(V)-APDC chelate possesses good thermal stability and volatility.
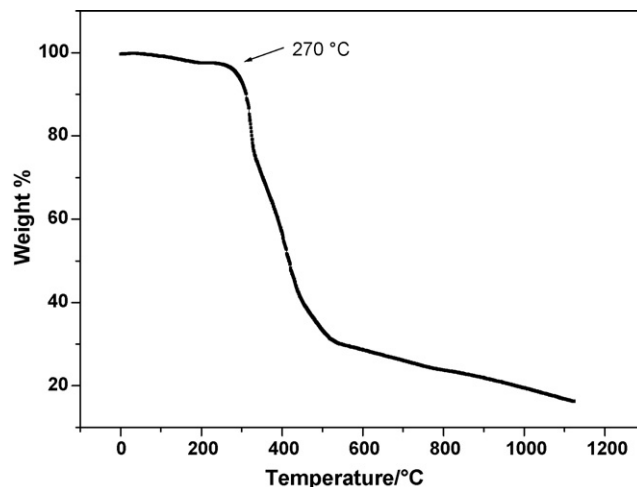

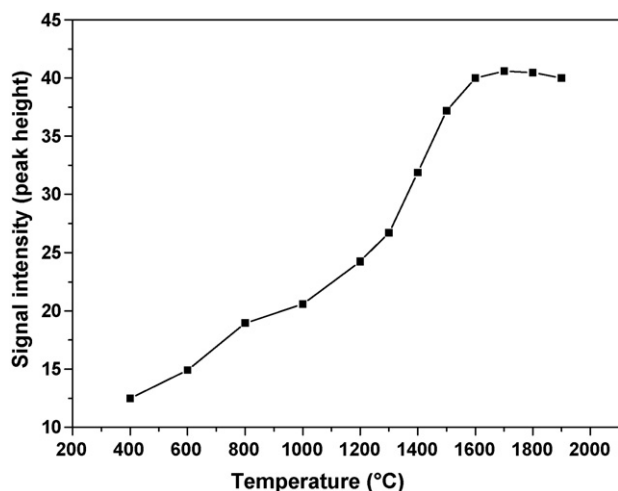Fig. 3. Thermo gramps (TG) of V(V)-APDC chelate.

Fig. 4. Effect of vaporization temperature on signal intensity of V(V). *Conditions*: 10 ng V(V) with 6.0×10^{-3} mol L^{-1} APDC as chemical modifier; drying, 100 °C, ramp 10 s, hold 15 s; vaporization time, 6 s; cleaning, 2500 °C, 3 s.

It was also found that V(IV) behaved the same as V(V) in the graphite furnace. The possible reason is that V(V) is reduced to V(IV) in the heating process. Similar results were obtained in reference [10].

3.1.2. Optimization of the ETV temperature program

The temperature program of graphite furnace has been optimized to get the highest sensitivity. Fig. 4 shows the effect of vaporization temperature on the emission signal of V(V)-APDC chelate. As could be seen, a weak signal could be observed at 400 °C, and the signal intensity was increased with the increase of the vaporization temperature. The maximum signal intensity was obtained at 1600 °C and kept constant in the range of 1600 °C–1900 °C. With the further increase of the vaporization temperature above 1900 °C, the emission signal started to decrease. So 1700 °C was selected as the vaporization temperature in further work.

The effect of vaporization time on the emission signal of V(V)-APDC chelate was also investigated at the vaporization temperature of 1700 °C. The experimental results indicated that the maximum analytical signal was obtained and kept constant when the vaporization time was longer than 5 s, so 6 s was chosen in this work.

3.2. Optimization of the microextraction conditions

The type of organic solvent immobilized within the pores of the hollow fibre and filled in the inner channel was of high importance in order to achieve efficient preconcentration within reasonable time. In this work, four kinds of organic solvent: toluene, 1-octanol, chloroform and carbon tetrachloride were tested as extraction solvent, and the experimental results demonstrated that carbon tetrachloride yielded a reproducible enrichment associated with a moderate loss into the sample solution. Therefore, carbon tetrachloride was employed as the organic extraction solvent for HF-LPME.
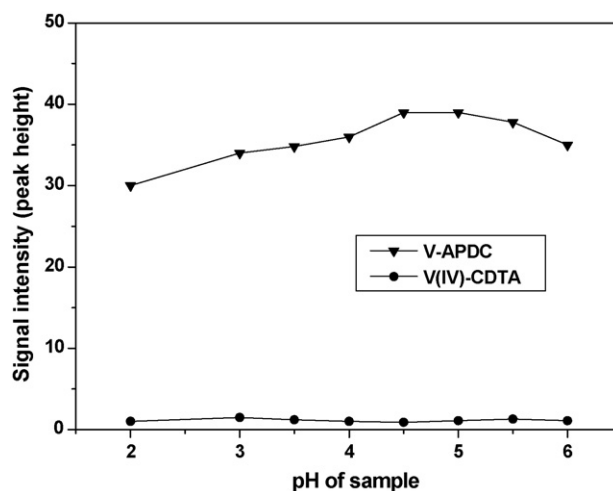
Fig. 5. Effect of sample pH on the signal intensity of vanadium. *Conditions*: V(V) and V(IV), 2.0 ng mL^{-1}; APDC concentration, 6.0×10^{-3} mol L^{-1}; CDTA concentration, 5.0×10^{-5} mol L^{-1}; sample volume, 3.5 mL; extraction time, 8 min; drying, 100 °C, ramp 10 s, hold 15 s; vaporization, 1700 °C, 6 s; cleaning, 2500 °C, 3 s.

The other factors which influenced the extraction efficiency and analytical signal intensity, such as pH of sample, extraction time, concentrations of APDC and CDTA have been studied with the use of carbon tetrachloride as the extraction solvent.

3.2.1. Influence of sample pH

Sample pH has a significant effect on the formation of V-APDC chelate and the extraction efficiency. Fig. 5 shows the influence of sample pH on analytical signal intensity. It was found that V(V)-APDC chelate could be extracted into CCl$_4$ in the pH range of 2.0–6.0 and the maximum extraction efficiency was obtained in pH 4.5–5.5. Similar results were obtained for V(IV)-APDC chelate. In another word, two species of vanadium cannot be separated merely by means of adjusting sample pH. However, this situation has been changed completely after the masking agent of CDTA was added into the sample. No emission signal of V(IV) was detected if excessive amount of CDTA was added into the sample prior to the addition of APDC. The possible reason is that CDTA served as the masking agent for V(IV) and the formation of V(IV)-CDTA restrained the formation of V(IV)-APDC. But no influence of CDTA on the extraction of V(V) was found under the same conditions showing that no masking effect of CDTA on V(V) was available. Based on these experimental results, sample pH of 5.0 was selected for further experiments.

3.2.2. Influence of extraction time

To investigate the influence of extraction time on the analytical signal, aqueous samples of V(V)-APDC chelate were extracted within time range of 2–20 min under the sample pH of 5.0. Fig. 6 shows the influence of extraction time on analytical signal intensity. As could be seen, the signal intensity of V(V) increased rapidly to the highest with the increase of extraction time from 2 to 7 min, then leveled off with the extraction time prolonging from 7 to 12 min, which indicated the considerable
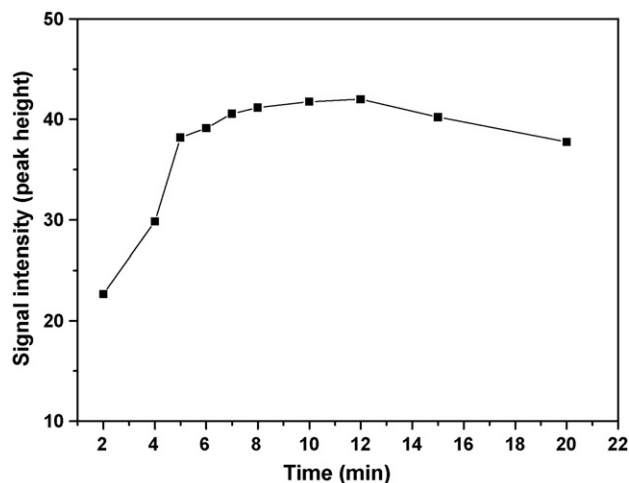
Fig. 6. Effect of extraction time on the signal intensity of V(V). *Conditions*: V(V), 2.0 ng mL^{-1}; APDC concentration, 6.0×10^{-3} mol L^{-1}; sample pH, 5.0; sample volume, 3.5 mL; drying, 100 °C, ramp 10 s, hold 15 s; vaporization, 1700 °C, 6 s; cleaning, 2500 °C, 3 s.

transferring speed of V(V)-APDC from aqueous phase to CCl$_4$. When the extraction time was more than 12 min, the analytical signal intensity decreased with the further increase of extraction time. Taking the loss of organic solvent into accounts, long extraction time would lead to the decrease of analytical sensitivity, so 8 min was selected as the extraction time in the subsequent experiment.

3.2.3. Concentration of APDC and CDTA

It was reported [28] that the excess of chelating reagent could promote the formation of chelates and effectively restrict the decomposition of chelates in the vaporization and transportation processes. Therefore, the influence of APDC on the signal intensity was studied with its concentration varying between 6.0×10^{-4} mol L^{-1} and 1.2×10^{-2} mol L^{-1} at the V(V) concentration of 2.0 ng mL^{-1}. As shown in Fig. 7, the strong
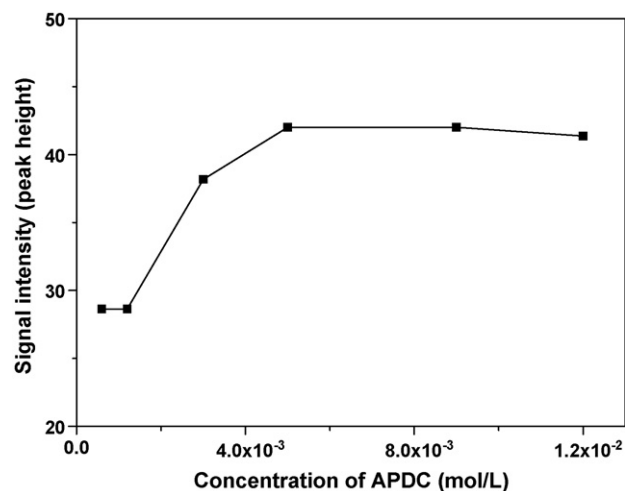
Fig. 7. Effect of concentration of APDC on the signal intensity of V(V). *Conditions*: V(V) 2.0 ng mL^{-1}; sample pH, 5.0; sample volume, 3.5 mL; extraction time, 8 min; drying, 100 °C, ramp 10 s, hold 15 s; vaporization, 1700 °C, 6 s; cleaning, 2500 °C, 3 s.

analytical signals of vanadium were found when the concentration of APDC was above 5.0×10^{-3} mol L^{-1}. Considering the possible competitive reaction of coexisting metal ions with APDC, the APDC concentration of 6.0×10^{-3} mol L^{-1} was preferred.

The influence of CDTA on the signal intensity was also studied in this work. The results showed that 5.0×10^{-5} mol L^{-1} CDTA was sufficient to mask several ng mL^{-1} V(IV) and no significant influence on the extraction of V(V)-APDC was found. Since the actual concentration of V(IV) in environmental samples is often very low, 5.0×10^{-5} mol L^{-1} of CDTA was selected for the separation of vanadium species.

Based on the above argumentations, the optimum extraction conditions were: sample pH of 5.0, 8 min of extraction time, 6.0×10^{-3} mol L^{-1} of APDC, 5.0×10^{-5} mol L^{-1} of CDTA.

3.3. Coexistiong ions interference

The coexisting ions commonly found in environmental samples were added individually to the samples and the effects of coexisting ions on the analytical signal intensity were investigated under the optimized conditions. The results indicated that at least 2000 μg mL^{-1} Na$^+$, K$^+$, Ca^{2+}, Mg^{2+}; 10 μg mL^{-1} Cu^{2+}, Al^{3+}; and 5 μg mL^{-1} Zn^{2+}, Fe^{2+}/Fe^{3+} had no obvious influence on the signal intensity of analyte (error <10%). This indicated that the developed method is applicable to the analysis of vanadium species in environmental samples.

3.4. Analytical performance

Under the optimum experimental conditions abovementioned, the LODs of V(IV) and V(V) were 86 pg mL^{-1} and 71 pg mL^{-1}, respectively. As shown in Table 2, the enrichment factor, defined as the ratio of calibration slope after and before HF-LPME, was 74. The relative standard deviation (R.S.D.) is 5.3% ($C_{V(V)} = 2.0$ ng mL^{-1}, $n = 7$). Linearity was obtained between 0.75 and 75 ng mL^{-1} with $r^2 > 0.99$. A comparison of detection limit obtained in this work and other previous works was also made in Table 2. It could be seen that the LODs of the proposed method are fairly better than that obtained by other previous works.

3.5. Sample analysis

The proposed method was applied to the speciation analysis of vanadium in different environmental waters and the analytical results together with the recovery for the spiked samples were given in Table 3. As could be seen, the recoveries for the spiked samples were in the acceptable range (94–107%), and the results showed the dominant oxidation form of vanadium in environment is V(V).

The accuracy of the present procedure was examined by determination of total vanadium in a NIES No.8 vehicle exhaust particulates certified reference material and the analytical result is given in Table 4. As could be seen, a satisfying agreement between the determined values and the certified values was obtained.

Table 2
Analytical performance for speciation of vanadium

Wavelength (nm)	Enrichment factor (fold)	R.S.D.[a] (%)	Linear range (ng mL^{-1})	Limit of detection (3σ) (ng mL^{-1})	
				This work	Literature[b]
309.311	74	5.3	0.75–75, $r^2 > 0.99$	0.086 for V(IV)	1.8 [31][c]
				0.071 for V(V)	0.072 [9][d]

[a] $C_{V(V)} = 2.0$ ng mL^{-1}, $n = 7$.
[b] Determination of V(V).
[c] By ETAAS.
[d] By FETV-ICP-OES.

Table 3
Analytical results (Mean $\pm$ S.D., $n = 5$) for V species in real water samples

Sample	Vanadium(IV)			Vanadium(V)		
	Added (ng mL^{-1})	Found (ng mL^{-1})	Recovery (%)	Added (ng mL^{-1})	Found (ng mL^{-1})	Recovery (%)
Lake water	0	N.D.[a]		0	4.20 $\pm$ 0.26	
					3.96 $\pm$ 0.11[b]	
	5	5.15 $\pm$ 0.23	103	5	8.93 $\pm$ 0.46	98
Tap water	0	N.D.[a]		0	2.41 $\pm$ 0.19	
					2.27 $\pm$ 0.13[b]	
	5	4.93 $\pm$ 0.18	99	5	7.52 $\pm$ 0.40	103
Sea water	0	N.D.[a]		0	2.80 $\pm$ 0.11	
	5	4.71 $\pm$ 0.22	94	5	8.35 $\pm$ 0.56	107

[a] Not detected.
[b] Total concentration of vanadium determined by ICP-MS.

Table 4
Analytical results (Mean $\pm$ S.D., $n = 5$) for V species in reference sample (NIES No.8)

Sample	Total V certified (μg g^{-1})	Found (μg g^{-1})		
		Total V	V(IV)	V(V)
NIES No.8 vehicle exhaust particulates	17 $\pm$ 2	18.16 $\pm$ 1.12	N.D.	18.16 $\pm$ 1.12

4. Conclusion

A new method by combining hollow-fibre liquid phase microextraction (HF-LPME) and electrothermal vaporization (ETV)-ICP-OES has been developed for the speciation of vanadium in environmental waters. The developed method has the merits of considerable analysis speed, good separation efficiency, notable precision and high sensitivity. CDTA served as the masking agent and meanwhile strengthened the stability of V(IV) in analysis procedures. Additionally, APDC was used as the chemical modifier for vanadium, remarkably decreasing the vaporization temperature of vanadium from the graphite furnace, thus the life of the graphite furnace was lengthened and the analytical sensitivity was improved greatly.

Acknowledgments

References

[1] L. Minelli, E. Veschetti, S. Giammanco, G. Mancini, M. Ottaviani, Microchem. J. 67 (2000) 83.
[2] B. Venugopal, T.D. Luckey, Metal Toxicity in Mammals, vol. 2, Plenum Press, New York, 1979, p. 220.
[3] G.R. Dubyak, A. Kleinzeller, J. Biol. Chem. 255 (1980) 12.
[4] M.J.C. Toylor, J.F. Vanstaden, Anal. Chim. Acta 307 (1995) 1.
[5] D. Banerjee, B.C. Mondal, D. Das, A.K. Das, Microchim. Acta 141 (2003) 147.
[6] M.H. Nagaoka, T. Yamazaki, T. Maitani, Biochem. Biophys. Res. Commun. 296 (2002) 1207.
[7] Z.L. Chen, R. Naidu, Anal. Bioanal. Chem. 374 (2002) 502.
[8] K. Pyrzyńska, T. Wierzbicki, Microchim. Acta 147 (2004) 59.
[9] Y.W. Wu, Z.C. Jiang, B. Hu, Talanta 67 (2005) 854.
[10] Z.F. Fan, B. Hu, Z.C. Jiang, Spectrochim. Acta 60B (2005) 65.
[11] H.Q. Zhang, Z. Chen, Shiyonghuaxueshouce, Science Press, Beijing, 2001, p. 536.
[12] R.G. Wuilloud, J.C. Wuilloud, R.A. Olsina, L.D. Martinez, Analyst 126 (2001) 715.
[13] H. Filik, K.I. Berker, N. Balkis, R. Apaka, Anal. Chim. Acta 518 (2004) 173.
[14] K. Pyrzyńska, T. Wierzbicki, Anal. Sci. 21 (2005) 951.
[15] K. Pyrzyńska, T. Wierzbicki, Anal. Chim. Acta 540 (2005) 91.
[16] M. Charalabaki, E. Psillakis, D. Mantzavinos, N. Kalogerakis, Chemosphere 60 (2005) 690.
[17] E. Psillakis, N. Kalogerakis, J. Chromatogr. A 999 (2003) 145.
[18] S.P. Bjergaard, K.E. Rasmussen, Anal. Chem. 71 (1999) 2650.
[19] C. Basheer, V. Suresh, R. Renu, H.K. Lee, J. Chromatogr. A 1033 (2004) 213.
[20] H. Tavallali, G. Hosseini, Am. Lab. 34 (2002) 40.

[21] T. Shimizu, T. Moteqi, M. Nakano, H. Kawaqauchi, N. Uehara, Bunseki Kagaku 50 (2001) 133.

[22] R.G. Sanchez, J. Bettmer, L. Ebdon, Microchem. J. 76 (2004) 161.

[23] Y.L. Wu, Z.C. Jiang, B. Hu, Chem. J. Chin. Universities-Chin. 24 (2003) 1793.

[24] L.B. Xia, B. Hu, Z.C. Jiang, Y.L. Wu, Y. Liang, Anal. Chem. 76 (2004) 2910.

[25] L.B. Xia, B. Hu, Z.C. Jiang, Y.L. Wu, L. Li, R. Chen, J. Anal. At. Spectrom. 20 (2005) 441.

[26] L.B. Xia, B. Hu, Z.C. Jiang, Y.L. Wu, R. Chen, L. Li, J. Anal. At. Spectrom. 21 (2006) 362.

[27] L. Li, B. Hu, L.B. Xia, Z.C. Jiang, Talanta 70 (2006) 468.

[28] S. Tao, T. Kumamaru, Appl. Spectrosc. 50 (1996) 785.

[29] Y.W. Wu, B. Hu, T.Y. Peng, Z.C. Jiang, Anal. Chim. Acta 439 (2001) 153.

[30] Z.F. Fan, B. Hu, Z.C. Jiang, L. Pan, Microchim. Acta 153 (2006) 211.

[31] R.J. Cassella, E.P. Oliveira, O.I.B. Magalhães, Talanta 69 (2006) 48.

Biocompatible core-shell nanoparticle-based surface-enhanced Raman scattering probes for detection of DNA related to HIV gene using silica-coated magnetic nanoparticles as separation tools

Yi Liang, Ji-Lai Gong, Yong Huang, Yue Zheng, Jian-Hui Jiang*, Guo-Li Shen, Ru-Qin Yu*

State Key Laboratory for Chemo/Biosensing and Chemometrics, College of Chemistry and Chemical Engineering, Hunan University, Changsha 410082, PR China

Abstract

A novel, highly selective DNA hybridization assay has been developed based on surface-enhanced Raman scattering (SERS) for DNA sequences related to HIV. This strategy employs the Ag/SiO_2 core-shell nanoparticle-based Raman tags and the amino group modified silica-coated magnetic nanoparticles as immobilization matrix and separation tool. The hybridization reaction was performed between Raman tags functionalized with 3′-amino-labeled oligonucleotides as detection probes and the amino group modified silica-coated magnetic nanoparticles functionalized with 5′-amino-labeled oligonucleotides as capture probes. The Raman spectra of Raman tags can be used to monitor the presence of target oligonucleotides. The utilization of silica-coated magnetic nanoparticles not only avoided time-consuming washing, but also amplified the signal of hybridization assay. Additionally, the results of control experiments show that no or very low signal would be obtained if the hybridization assay is conducted in the presence of DNA sequences other than complementary oligonucleotides related to HIV gene such as non-complementary oligonucleotides, four bases mismatch oligonucleotides, two bases mismatch oligonucleotides and even single base mismatch oligonucleotides. It was demonstrated that the method developed in this work has high selectivity and sensitivity for DNA detection related to HIV gene.
© 2006 Published by Elsevier B.V.

Keywords: Surface-enhanced Raman scattering; Raman tags; Magnetic nanoparticles; Hybridization

1. Introduction

With worldwide attention to acquired immure deficiency syndrome (AIDS) caused by human immunodeficiency virus (HIV), there is a clear need for researchers to develop sensitive and specific analytical and diagnostic techniques that detect HIV at the earliest possible time following infection. Although serologic tests as standard HIV assays including the enzyme-linked immunosorbent assay (ELISA) and Western blot assay are very sensitive, the ELISA suffers the shortcomings of false positive and false negative results and Western blot assay might be indeterminate or falsely negative if a blood specimen is collected in the time too closed to the infection [1]. Therefore, many researchers are interested in developing a direct nucleic acid-based test which can detect the presence of DNA sequences related to HIV [2–4]. To date, several methods including optical [5–7], gravimetric [8], and electrochemical [9–11] transducers have been developed for the highly sensitive and specific DNA detection in the areas of medicinal diagnosis and biochemical analysis.

Raman spectroscopy containing rich molecular vibration possesses the nature of yielding narrow and highly resolved bands, which minimize the potential overlap of different labels in a given spectral region [12]. Unfortunately, Raman spectroscopy suffers the poor sensitivity because of low Raman scattering cross sections exhibited by most molecules. Surface-enhanced Raman scattering can increase the Raman intensities of molecules adsorbed at rough metal surfaces by about 6 orders or even up to 14 orders of magnitude. Since the pioneer work of Fleischmann who observed intense Raman scattering from pyridine adsorbed onto a roughened silver electrode surface from aqueous solution, surface-enhanced Raman scattering spectroscopy has become a promising method for sensitive biological

* Corresponding authors. Tel.: +86 731 8822577; fax: +86 731 8822782.
  E-mail addresses: jianhuijiang@hnu.cn (J.-H. Jiang), rqyu@hnu.cn
(R.-Q. Yu).

detection [13,14]. SERS has attracted considerable interest for biomedical applications such as immunoassay [15,16], cellular studies [17,18], DNA detection [3,19], and cancer diagnosis [20]. Nevertheless, in some cases, the interaction of the analyte with the reaction system must be traced by the use of labels. To date, the nanoparticle tagging systems such as plasmon-resonant particles [21], quantum dots [7,22] and Raman tags [23] become increasingly popular for amplifying the signal of analytes in biological assay because of their common properties of being able to be excited at appropriate wavelengths, having narrow peak widths in comparison to fluorescence, and without photobleaching. Nanoparticle-based Raman tags have advantages over other nanoparticle tags in that each Raman active molecule provides unique spectrum, therefore hundreds of different tags are available. Nanoparticle-based Raman tags have been developed by some research groups. To our knowledge, there are two kinds of nanoparticle-based Raman tags reported in the literature. One of them is prepared by the direct attachment of both Raman reporter and biomolecule to the nanoparticle [23,24]. The other is prepared by the dye-embedded core-shell nanoparticle-based Raman tags. For example, Natan and co-workers have prepared glass-coated, analyte-tagged nanoparticle Raman tags, where a nanometer-scale Au or Ag core is functioned by Raman dye and encapsulated with a silica layer [25]. On this laboratory, Au/SiO$_2$ nanoparticle-based Raman tags have been prepared without the need of coupling agent. This preparation method avoids the competition between the Raman dyes and the coupling agent thus greatly extending the scope of the Raman tags. Furthermore, we have reported a novel simplified method based on reverse micelle technique for synthesis of surface-enhanced Raman scattering tags which were composed of silver core, Raman active molecules and silica shell. The Raman active molecules absorbed on the silver surface can yield strong SERS. This Ag/SiO$_2$ nanoparticle-based Raman tags exhibited extraordinary stability by encapsulating silica shell [26,27]. It is obvious that nanoparticle-based Raman tags with glass shell is more stable and bio-compatible than those without the glass shell.

Magnetic nanoparticles have been applied to many areas such as the immobilization of proteins and enzymes [28], bioseparation [29], immunoassay [30], drug delivery [31] and biosensors [32]. The pure magnetic particles might have the problems associated with the formation of large aggregates, alteration of magnetic properties and their toxicity in the biological system. The silica-coated core-shell magnetic nanoparticles consisting of cores of superparamagnetic particles and silica shells are much more suitable for practical applications as the silica shells usually possess the properties of biocompatibility and easy functionalization [33–35]. Magnetic separation has become an interesting tool for the biological molecules and cells because the magnetic nanoparticles can enable the isolation or extraction of a target molecule or substance by external magnetic field.

In this paper, we described a novel method combining the biocompatible Ag/SiO$_2$ nanoparticle-based Raman tags functionalized with oligonucleotides as the detection probe and the amino group functionalized silica-coated magnetic nanoparticles with capture strands as immobilization matrix and separation tool for detection of HIV related DNA sequences.

The utilization of magnetic nanoparticles not only possesses the advantage of superparamagnetism, but also preconcentrates the analyte thus efficiently amplifying the Raman signal.

2. Experimental

2.1. Materials and reagents

Igepal CO-520, Triton X-100, and (3-aminopropyl)trimethoxysilane (APTMS) were provided by Aldrich, hydrazine hydrate was purchased from Sigma. Rhodamine B isothiocyanate, N-(3-dimethylaminopropy)-N′-ethylcarbodiimidehydrochloride (EDC) and N-hydroxysuccinmide (NHS) were purchased from Fluka. Succinic anhydride was obtained from ACROS ORGNICS, New Jersey, USA. 2-(N-morpholino)-ethanesulfonic acid (MES) was purchased from Oumai Biotech Corporation (China). Silver nitrate, tetraethoxysilane (TEOS), cyclohexane, ethanol, ammonia, FeCl$_3$·6H$_2$O, FeCl$_2$·4H$_2$O, N,N-dimethylformamide (DMF) and glycine were used as received. Ultrapure water (18.3 MΩ cm^{-1}) was obtained through a nanopure infinity ultrapure water system (Barnstead/thermolyne Corp, Dubuque, Iowa, USA) and was used throughout. All oligonucleotides were obtained from Takara Biotechnology Co. Ltd. (Dalian, China) and had following sequences:

Complementary oligonucleotide: 5′-AGAAGATATTTGGAA-TAACATGACCTGGAT GCA-3′.
Detection oligonucletide: 5′-TTATTCCAAATATCTTCT-3′-C$_6$-NH$_2$.
Capture oligonucleotide: NH$_2$-C$_6$-5′-TGCATCCAGGTCA-TG-3′.
Random oligonucleotide: 5′-ATCGGCATTTACGGGCAAT-CCTACGCATTACGG-3′.
Four bases mismatch oligonucleotide: 5′-AGAA<u>T</u>ATATT<u>A</u>-GGAATAACATGACC <u>A</u>GG<u>T</u>TGCA-3′.
Two bases mismatch oligonucleotide: 5′-AGAAGATATT<u>A</u>-GGAATAACATGACC <u>A</u>GGATGCA-3′.
Single base mismatch oligonucleotide: 5′-AGAAGATATT-TGGAATAACATGACC <u>A</u>GGATGCA-3′.

All the oligonucleotide solutions and the buffers in the experiments were prepared using sterile water.

2.2. Instrumentation

Raman measurements were performed on Jobin Yvon HORIBA Micro-Raman spectrometer (LabRam-010) equipped with an integral Olympus BX 41 microscope attached with Labspec 4.02 software. The slit and pinhole were set at 100 and 1000 μm respectively in a confocal configuration. A holographic grating (1800 g/mm) and an air-cooled He–Ne laser for 632.8 nm excitation with a power of ca. 3 mW were used. UV–vis measurements were performed using MultiSpec-1501 UV–vis spectrometer (Shimadzu Corporation, Japan) equipped with Hyper UV software. Transmission electron micrographs were obtained by using JEM-3010 electron microscope (JEOL,

Japan) with Digitalgraph software at an accelerating voltage of 300 kV.

2.3. Procedure

2.3.1. Synthesis of Ag/SiO₂ nanoparticle-based SERS tags

The synthesis of Ag/SiO_2 nanoparticle-based surface-enhanced Raman scattering tags was accomplished using reverse micelle technology [27]. All glassware used in the following procedure was cleaned by aqua regia freshly prepared prior to use. To obtain microemulsion, 4 ml of Igepal CO-520, 10 ml of cyclohexane, appropriate amount of $AgNO_3$ solution and rhodamine B isothiocyanate solution were mixed in a 250 ml three-neck flask under vigorous stirring. After 5 min, 50 μl of hydrazine hydrate was added followed by the injection of ammonia and TEOS stock solution consisting of 50% of TEOS and 50% of cyclohexane by weight. The reaction was continued for 24 h. After the reaction was complete, the nanoparticles prepared were isolated from the microemulsion using ethanol. And then, the nanoparticles were washed with ethanol for several times. The nanoparticles were dispersed in ethanol and stored in 4 °C when not in use. The final concentration of the nanoparticles is 0.91 mg/ml.

2.3.2. Preparation of silica-coated magnetic nanoparticles

The synthesis of amino group modified silica-coated magnetic nanoparticles included two steps: the preparation of Fe_3O_4 magnetic nanoparticles and the synthesis of silica-coated magnetic nanoparticles. Fe_3O_4 magnetic nanoparticles were prepared according to the method described in the literature [36]. To prepare the silica-coated magnetic nanoparticles, 8.4 mg of magnetic nanoparticles were first diluted with 24 ml of water in a 250 ml three-neck flask. Then, 80 ml of 2-propanol, 20 ml of Triton X-100, 2 ml of ammonia and the mixed solution containing 120 μl of TEOS and 30 μl of APTMS were added successively under vigorous stirring. After 3 h, the resulting magnetic nanoparticles were separated from the mixture by external magnetic field followed by washing with copious ethanol and water. The nanoparticles were dispersed in water and stored in 4 °C when not in use. The final concentration of the nanoparticles is 0.23 mg/ml.

2.3.3. The modification of Ag/SiO₂ nanoparticle-based SERS tags with detection oligonucleotides

The preparation of the Ag/SiO_2 Raman tags functionalized with oligonucleotides included the following processes. The Ag/SiO_2 Raman tags were first modified with amino groups by injecting 20 μl APTMS into the solution of 1 ml of Raman tags dispersed in 7 ml ethanol drop by drop at room temperature for 0.5 h under the conditions of magnetic stirring. Then, the particles were washed using ethanol and water successively by centrifugation an ultrasonication. The amino-modified particles were treated with 5 ml of 10% succinic anhydride in DMF solution under nitrogen atmosphere and stirred for 3 h at room temperature. After centrifugation and washing with water, the resulting particles were dispersed in MES (pH 4.65) followed by the addition of the mixed solution containing 80 μl of EDC

(0.1 M), 40 μl of NHS (0.05 M) and 200 μl of detection oligonucletides (6.1 μM) drop by drop for 4 h under magnetic stirring. After centrifugation, the particles were dispersed in an appropriate amount of glycine (20 mM) for 1 h under magnetic stirring followed by centrifugation and washing with water. The resulting particles were dispersed in 1.8 ml of 0.6 M NaCl PBS buffer containing 0.05% Triton X-100 and were stored at 4 °C until use.

2.3.4. The modification of silica-coated magnetic nanoparticles with capture oligonucleotides

The preparation of silica-coated magnetic nanoparticles functionalized with oligonucleotides included the following processes. Appropriate amount (400 μl) of amino group functionalized silica-coated magnetic nanoparticles was first immersed in 9 ml of 10% succinic anhydride in DMF solution and stirred under nitrogen atmosphere for 3 h at room temperature. After magnetic separation and washing with water, the particles obtained were dispersed in MES (pH 4.65) followed by the addition of mixed solution containing 800 μl of EDC (0.1 M), 400 μl of NHS (0.05 M) and 500 μl of capture oligonucleotides (7.3 μM) drop by drop at room temperature under stirring. Four hours later, the resulting particles were isolated from mixture using permanent external magnetic field followed by addition of an appropriate amount of glycine (20 mM) for 1 h under stirring. After magnetic separation and washing with water for several times, the particles were dispersed in 8 ml of 0.6 M NaCl PBS buffer solution containing 0.05% Triton X-100 and were stored at 4 °C for latter usage.

2.3.5. The procedure of hybridization assay

An aliquot of 50 μl of target oligonucleotides (3 μM) was added to 200 μl of magnetic nanoparticles modified with capture oligonucleotides. After gently mixing for several hours, the magnetic separation and washing with PBS containing 0.6 M NaCl were carried out followed by the addition of 200 μl of the Ag/SiO_2 Raman tags functionalized with detection oligonucleotides. After mixing gently for several hours, the resulting particles were isolated under external magnetic field, washed with the PBS solution containing 0.6 M NaCl and separated by a permanent magnet. The sandwich-type hybridization complexes were stored in 4 °C prior to Raman measurements.

3. Results and discussion

We employed the Ag/SiO_2 nanoparticle-based Raman tags functionalized with oligonucleotides as the detection probes and the amino group modified silica-coated magnetic nanoparticles functionalized with oligonucleotides as capture probes for detection of DNA sequences related to HIV (Fig. 1). The synthesis and characterization of silica-coated silver nanoparticle-based Raman tags have been described in detail in the literature [27]. Ag/SiO_2 nanoparticle-based Raman tags are composed of silver core conjugated with rhodamine B isothiocyanate and an encasing silica shell. rhodamine B isothiocyanate encapsulated in silica shell can form strong chemical bond with silver nanoparticle leading to the generation of surface-enhanced
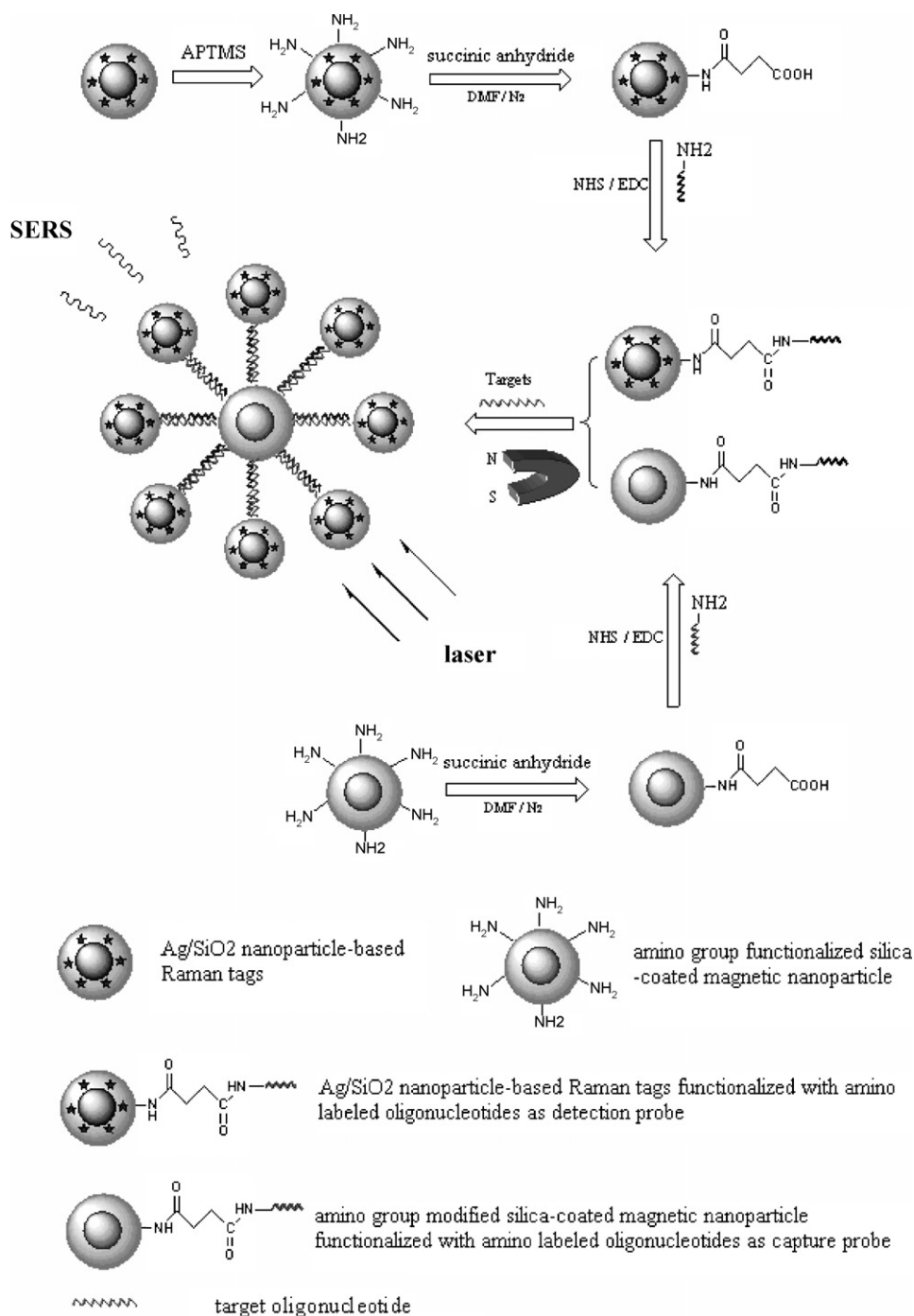
Fig. 1. Schematic diagram of hybridization assay of HIV using Ag/SiO$_2$ nanoparticle-based Raman tags functionalized with oligonucleotides as the detection probes and the amino group functionalized silica-coated magnetic nanoparticles with capture strands as immobilization matrix and separation tool.

Raman scattering phenomenon. Fig. 3 shows the Raman spectra of the Ag/SiO$_2$ nanoparticle-based Raman tags and Ag/SiO$_2$ nanoparticle-based Raman tags modified with oligonucleotides. One notices that there is no change for all peaks location of these nanoparticles. It demonstrated that the Ag/SiO$_2$ nanoparticle-based Raman tags functionalized with oligonucleotides as the detection probes also exhibited SERS spectrum of rhodamine B isothiocyanate molecules conjugated with silver cores and there was no influence on the signal of Raman tags after modification. Fig. 2a is TEM micrograph of Ag/SiO$_2$ nanoparticle-based

Raman tags. It was observed that the 23 ± 1 nm silver cores are encapsulated in 12 ± 1 nm of silica shell. The utilization of Raman tags provides unique spectrum of each Raman reporter and avoids the background signal from the biological system. The silica shells around the silver cores allow Raman tags to exhibit extraordinary easy functionalization. Fig. 2b shows the morphology of amino group modified silica-coated magnetic nanoparticles. Additionally, the UV–vis spectra were recorded to characterize Ag/SiO$_2$ nanoparticle-based Raman tags. The maximum absorption of the Raman tags was around 403 nm.
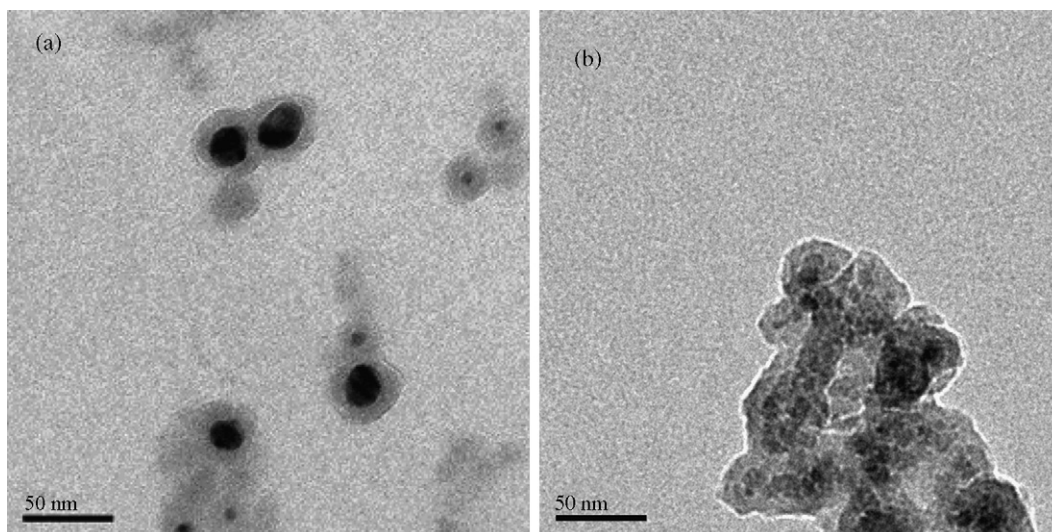
Fig. 2. Transmission electron micrographs of nanoparticles: (a) Ag/SiO$_2$ nanoparticle-based Raman tags; (b) amino group functionalized silica-coated magnetic nanoparticles.

Furthermore, there was no noticeable change for peak location of the Raman tags dispersed in various solvents such as water, methanol, ethanol, and acetone. It implied that the Ag/SiO$_2$ nanoparticle-based Raman tags exhibit extraordinary stability (data not shown).

3.1. Nanoparticles surface modification

The biochemical surface modification of nanoparticles, which adds the desired functions to nanoparticles, is very important to biochemical assay [37,38]. Herein, the Ag/SiO$_2$ nanoparticle-based Raman tags and amino group modified silica-coated magnetic nanoparticles are labeled with detection oligonucleotides and capture oligonucleotides, respectively. All of the nanoparticles used in this work have a functionizable silica surface. APTMS was successfully used for the formation of the amino-modified Ag/SiO$_2$ nanoparticle-based Raman

tags. After the succinic anhydride treatment according to the method reported in the literature [37], nanoparticles including the amino-modified nanoparticles-based Raman tags and amino-modified silica-coated magnetic nanoparticles were carboxylated. Then, carboxyl-modified nanoparticles were used for the preparation of detection probes and capture probes. To prepare the nanoparticle functionalized with oligonucleotides, the carboxyl-modified nanoparticles were first dispersed in MES buffer. We used MES solution as buffer because the MES without carboxyl group would not interfere or compete with the coupling reaction and the nanoparticles could disperse in MES very well. Then, the mixing solution containing EDC, NHS and amino-labeled oligonucleotides was added to the carboxyl-modified nanoparticles in MES solution. In this step, the active ester intermediate was first formed by the reaction between the carboxyl groups on the nanoparticle surface and the EDC, and then the Ag/SiO$_2$ nanoparticle-based Raman tags functionalized oligonucleotides were formed immediately by the reaction between the active ester intermediate and amines on the oligonucleotides. The one-step coupling reactions, whereby the carbodiimide, the biomolecules and nanoparticles are combined in one step, are often problematic for coupling biomolecules. The coupling efficiency was increased in the presence of NHS. Finally, glycine solution was added to decrease the nonspecific reaction in the following experiments. The nanoparticles functionalized oligonucleotides were dispersed very well in the 0.6 M NaCl PBS buffer solution containing 0.05% Triton X-100.

3.2. Hybridization

Hybridization experiments were conducted in 0.6 M NaCl PBS buffer solution (pH 7) at room temperature. The results of the target oligonucleotides hybridization experiments are shown in Fig. 4. It was observed that there were strong SERS signal when target oligonucleotides existed because the Raman tags linked around the magnetic nanoparticles were separated from solution by external magnetic field. At the same time, no obvi-
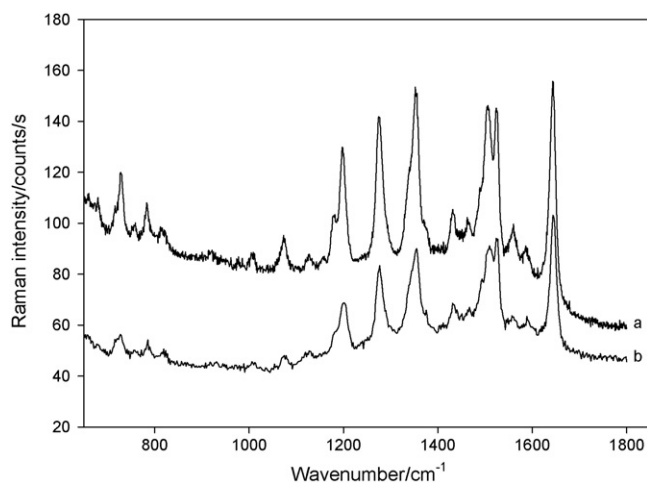
Fig. 3. SERS spectra obtained from: (a) Ag/SiO$_2$ nanoparticle-based Raman tags; (b) Ag/SiO$_2$ nanoparticle-based Raman tags modified with oligonucleotides.
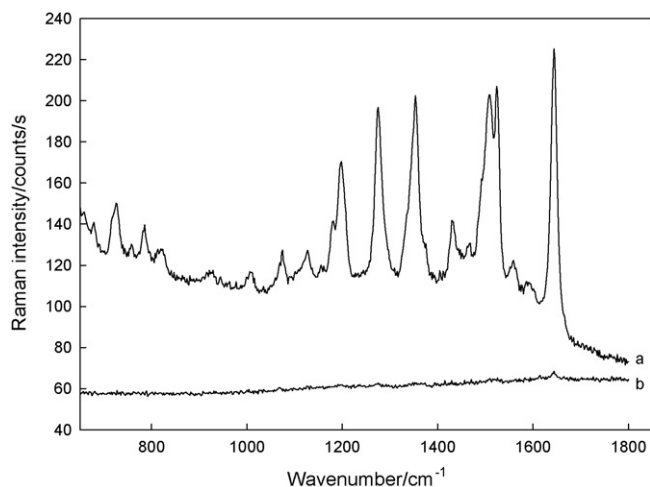
Fig. 4. SERS spectra obtained from the target oligonucleotides hybridization experiments: (a) target oligonucleotides; (b) blank.

ous Raman signal in the blank experiment can be detected due to the failure linkage between Raman tags and magnetic nanoparticles. Therefore, our method can be successfully used for the detection of DNA sequence related to HIV. Fig. 5a and b show that the Raman spectra of Ag/SiO$_2$ nanoparticle-based SERS tags modified with detection oligonucleotides and the hybridization product containing Raman tags and magnetic nanoparticles respectively. One notices that the intensity of Raman spectrum of hybridization product was much stronger than that of Ag/SiO$_2$ nanoparticle-based SERS tags modified with detection oligonucleotides. According to the results of hybridization experiments described above, one could find the main advantages of using silica-coated magnetic nanoparticles as immobilization matrix and separation tool. The magnetic separation technology based on silica-coated magnetic nanoparticles not only avoided time-consuming washing during the experiments, but also amplified
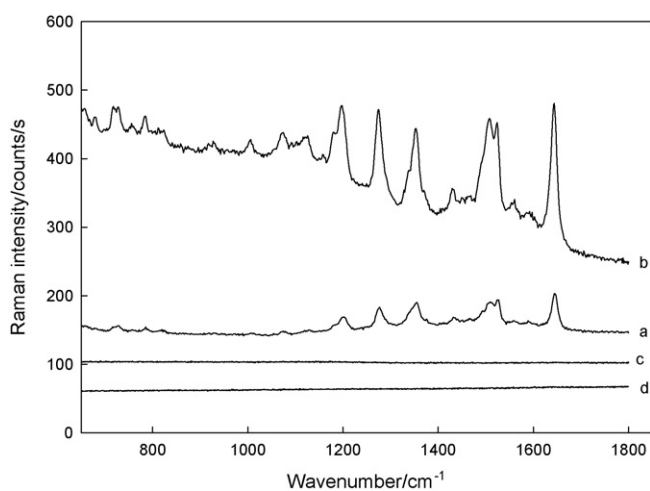
Fig. 5. Surface-enhanced Raman scattering spectroscopy of different nanoparticles: (a) Ag/SiO$_2$ nanoparticle-based Raman tags modified with oligonucleotides; (b) hybridization product containing Raman tags and magnetic nanoparticle; (c) magnetic nanoparticles modified with capture oligonucleotides; (d) the hybridization product of target oligonucleotides and magnetic nanoparticles modified with capture oligonucleotides.
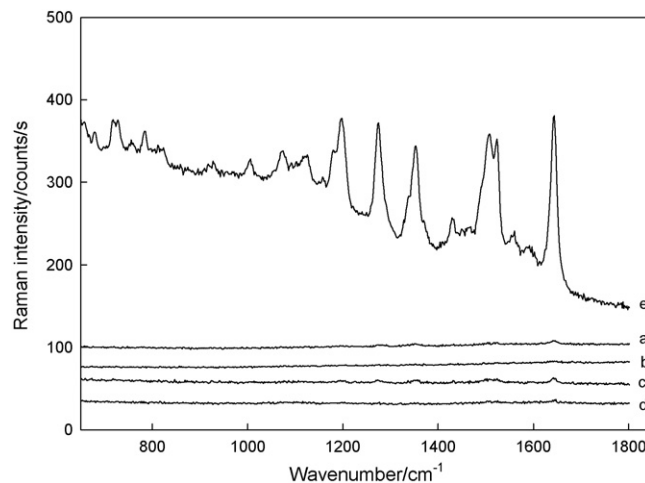
Fig. 6. Raman signal of the hybridization assay conducted in presence of: (a) non-complementary oligonucleotides; (b) four bases mismatch oligonucleotides; (c) two bases mismatch oligonucleotides; (d) single base mismatch oligonucleotides; (e) complementary oligonucleotides.

the signal of hybridization assay. The reason of signal amplification is derived from the preconcentration of the hybridization product in the presence of magnetic nanoparticles. Additionally, the results illustrated in Fig. 5c and d show that no Raman signal was obtained from both magnetic nanoparticles modified with capture oligonucleotides and the hybridization product of target oligonucleotides and magnetic nanoparticles modified with capture oligonucleotides. It was demonstrated that there was no interference with the SERS signal of Raman tags for the oligonucleotides functionalized on the surface of silica-coated magnetic nanoparticles.

We have carried out some control experiments to test the selectivity of this strategy. The results illustrated in Fig. 6 show that no or very low signal was obtained if the hybridization assay was conducted in the presence of DNA sequences other than complementary to the HIV related gene such as random oligonucleotides, four bases mismatch oligonucleotides, two bases mismatch oligonucleotides and single base mismatch oligonucleotides. It was demonstrated that the method developed in this work has high selectivity for HIV DNA sequence detection. High selectivity of our method is due to the utilizing of magnetic separation as well as the condition of hybridization. The magnetic separation not only decreases the sample losing and nonspecific reaction by the greatest extent during the washing, but also concentrates final hybridization product leading to enhance Raman signal. So the Raman spectra in the presence of DNA sequences other than complementary to the HIV related gene were neglectable compared to the signal in the presence of complementary. In addition, we have also studied the effect of hybridization reaction time on the Raman signal. The optimal hybridization time is 60 min (data not shown).

4. Conclusions

We have developed a novel analytical technique, which combined the Ag/SiO$_2$ nanoparticle-based Raman tags with

silica-coated magnetic nanoparticle-based separation technology for detection of DNA sequences related to HIV. Ag/SiO_2 nanoparticle-based Raman tags exhibit strong intensity of SERS, and the silica shells around the silver cores allow Raman tags to exhibit extraordinary and easy functionalization. Besides, compared to other separation and immobilization method, the magnetic nanoparticles possess the advantages including the easy separation and signal amplification. This strategy is very useful for improving sensitivity and selectivity.

Acknowledgements

References

[1] M.R. Proffitt, Anal. Chem. 65 (1993) 396R.
[2] M.B. Wabuyel, T. Vo-Dinh, Anal. Chem. 77 (2005) 7810.
[3] N.R. Isola, D.L. Stokes, T. Vo-Dinh, Anal. Chem. 70 (1998) 1352.
[4] K.B. Lee, E.Y. Kim, C.A. Mirkin, S.M. Wolinsky, Nano Lett. 4 (2004) 1869.
[5] J. Li, X. Chu, Y. Liu, J.H. Jiang, Z. He, Z. Zhang, G. Shen, R.Q. Yu, Nucl. Acids Res. 33 (2005) e168.
[6] Y.C. Cao, R. Jin, C.S. Thaxton, C.A. Mirkin, Talanta 67 (2005) 449.
[7] H.C. Yeh, Y.P. Ho, T.H. Wang, Nanomedicine 1 (2005) 115.
[8] R. Gabl, H.-D. Feucht, H. Zeininger, G. Eckstein, M. Schreiter, R. Primig, D. Pitzer, W. Wersing, Biosens. Bioelectron. 19 (2004) 615.
[9] J. Wang, G. Liu, A. Merkoci, J. Am. Chem. Soc. 125 (2003) 3214.
[10] J. Wang, G. Liu, M.R. Jan, Q. Zhu, Electrochem. Commun. 5 (2003) 1000.
[11] C. Tlili, H. Korri-Youssoufi, L. Ponsonnet, C. Martelet, N.J. Jaffrezic-Renault, Talanta 68 (2005) 131.
[12] D. Pappas, B.W. Smith, J.D. Winefordner, Talanta 51 (2000) 131.
[13] M. Fleischmann, P.J. Hendra, A.J. McQuillan, Chem. Phys. Lett. 26 (1974) 163.
[14] A. Campion, P. Kambhampati, Chem. Soc. Rev. 27 (1998) 241.
[15] X. Dou, T. Takama, Y. Yamaguchi, H. Yamamoto, Y. Ozaki, Anal. Chem. 69 (1997) 1492.
[16] T.E. Rohr, T. Cotton, N. Fan, P.J. Tarcha, Anal. Biochem. 182 (1989) 388.
[17] C.E. Talley, L. Jusinski, C.W. Hollars, S.M. Lane, T. Huser, Anal. Chem. 76 (2004) 7064.
[18] J. Kneipp, H. Kneipp, W.L. Rice, K. Kneipp, Anal. Chem. 77 (2005) 2381.
[19] K. Faulds, W.E. Smith, D. Graham, Anal. Chem. 76 (2004) 412.
[20] L.R. Allain, T. Vo-Dinh, Anal. Chim. Acta 469 (2002) 149.
[21] S.J. Oldenburg, C.C. Genick, K.A. Clark, D.A. Schultz, Anal. Biochem. 309 (2002) 109.
[22] X. Gao, S. Nie, Anal. Chem. 76 (2004) 2406.
[23] Y.C. Cao, R. Jin, J.M. Nam, C.S. Thaxton, C.A. Mirkin, J. Am. Chem. Soc. 125 (2003) 14676.
[24] Y.C. Cao, R. Jin, C.A. Mirkin, Science 297 (2002) 1536.
[25] S.P. Mulvaney, M.D. Musick, C.D. Keating, M.J. Natan, Langmuir 19 (2003) 4784.
[26] J.L. Gong, J.H. Jiang, H.F. Yang, G.L. Shen, R.Q. Yu, Y. Ozaki, Anal. Chim. Acta 564 (2006) 151.
[27] J.L. Gong, J.H. Jiang, Y. Liang, G.L. Shen, R.Q. Yu, J. Colloid Interf. Sci. 298 (2006) 752.
[28] H.H. Yang, S.Q. Zhang, X.L. Chen, Z.X. Zhuang, J.G. Xu, X.R. Wang, Anal. Chem. 76 (2004) 1316.
[29] A. Ito, M. Shinkai, H. Honda, T. Kobayashi, J. Biosci. Bioeng. 100 (2005) 1.
[30] T. Tanaka, T. Matsunaga, Anal. Chem. 72 (2000) 3518.
[31] T. Neuberger, B. Schöpf, H. Hofmann, M. Hofmann, B. Rechenberg, J. Magn. Magn. Mater. 293 (2005) 483.
[32] Z. Liu, Y. Liu, H. Yang, Y. Yang, G. Shen, R. Yu, Anal. Chim. Acta 533 (2005) 3.
[33] S. Santra, R. Tapec, N. Theodoropoulou, J. Dobson, A. Hebard, W. Tan, Langmuir 17 (2001) 2900.
[34] W. Wu, M.A. DeCoster, B.M. Daniel, J.F. Chen, M.H. Yu, D. Cruntu, C.J. O'Connor, W.L. Zhou, J. Appl. Phys. 99 (2006) 08H104.
[35] L. Levy, Y. Sahoo, K.S. Kim, E.J. Bergey, P.N. Prasad, Chem. Mater. 14 (2002) 3715.
[36] Y.S. Kang, S. Risbud, J.F. Rabolt, P. Stroeve, Chem. Mater. 8 (1996) 2209.
[37] M. Qhobosheane, S. Santra, P. Zhang, W. Tan, Analyst 126 (2001) 1274.
[38] N. Zhu, H. Cai, P. He, Y. Fang, Anal. Chim. Acta 481 (2003) 181.

Electrochemical DNA biosensor for the detection of short DNA species of Chronic Myelogenous Leukemia by using methylene blue

Xin-Hua Lin [a], Ping Wu [a], Wei Chen [a,b], Ya-Feng Zhang [a], Xing-Hua Xia [b,*]

[a] *Department of Pharmaceutical Analysis, Faculty of Pharmacy, Fujian Medical University, Fuzhou 350004, China*
[b] *Key Laboratory of Analytical Chemistry for Life Science, School of Chemistry and Chemical Engineering, Nanjing University, Nanjing 210093, China*

Abstract

A novel assay for the voltammetric detection of 18-bases DNA sequences relating to Chronic Myelogenous Leukemia (CML, Type b3a2) using methylene blue (MB) as the hybridization indicator was reported. DNA was covalently attached onto a glassy carbon electrode (GCE) through amines of the DNA bases using *N*-hydroxysulfosuccinimide (NHS) and *N*-(3-dimethylamion)propyl-*N'*-ethyl carbodiimidehydrochloride (EDC). The covalently immobilized single-stranded DNA (ssDNA) could selectively hybridize with its complementary DNA (cDNA) in solution to form double-stranded DNA (dsDNA) on the surface. A significant increase of the peak current for methylene blue upon the hybridization of immobilized ssDNA with cDNA in the solution was observed. This peak current change was used to monitor the recognition of CML DNA sequence. This electrochemical approach is sequence specific as indicated by the control experiments in which no peak current change was observed if a non-complementary DNA sequence was used. Factors, such as DNA target concentration and hybridization conditions determining the sensitivity of the electrochemical assay were investigated. Under optimal conditions, this sensor has a good calibration range between 1.25×10^{-7} and 6.75×10^{-7} M, with CML DNA sequence detection limit of 5.9×10^{-8} M.
© 2006 Elsevier B.V. All rights reserved.

Keywords: Biosensors; DNA; Hybridization; CML; Methylene blue; Sequence-specific electrochemical detection

1. Introduction

Chronic Myelogenous Leukemia (CML) is a clonal myeloproliferative disorder resulting from the neoplastic transformation of the primitive hemopoietic stem cell [1–3]. Generally speaking, the CML patients do not show any observable symptoms in their early stage, and the chronic course can last for 3–5 years. These phenomena bring the difficulties to the diagnosis of CML.

There has been much learned about the clinical disorder and how the chimeric oncogene BCR/ABL generated from the translocation of chromosome 9 to 22 (Philadelphia Ph. Chromosome) can lead to the pathogenesis of CML. BCR/ABL gene is the traditional gene for the disease, and it exists in almost all cases of CML patients [4,5]. There are many types of BCR/ABL genes, and Type b3a2 is one of the most common mutation types, which are often studied in scientific researches. Thus,

the detection of BCR/ABL gene will afford an early diagnosis and monitor of the disease, which in turn improves the facility of detecting minimal residual leukemia cells in the CML patients, especially after the bone marrow transplantation (BMT).

In the recent years, electrochemical DNA biosensors based on nucleic acid hybridization have been rapidly developed due to their increasing importance in the diagnosis of disease. DNA biosensors for recognition of DNA hybridization offer a new approach for rapid, sensitive, simple and low-cost detection of specific nucleic acid sequences [6–11]. Due to the advantages of electrochemical DNA biosensors, we attempted to detect BCR/ABL genes (Type b3a2) using electrochemical methods, which will provide a new way to the diagnosis and monitor of the CML patients.

Some of anticancer drug [12–14], metal complexes [15,16] and organic dyes [17–19] exist as chiral molecules capable of selective recognition of DNA. The changes in electrochemical response of these labels are usually used to monitor the hybridization process. Methylene blue (MB) is an organic dye that belongs to the phenothiazine family. DNA biosensors using MB as chemical indicator have been widely studied [20–23].

* Corresponding author. Tel.: +86 25 83597436; fax: + 86 25 83597436.
E-mail address: xhxia@nju.edu.cn (X.-H. Xia).

According to the spectrophotometric and electrochemical results [24–28], the detection of hybridization was found to be accomplished by the specific interaction of MB with guanine bases in the DNA sequence [29]. Rohs et al. [30] reported a modeling study for MB binding to DNA with alternating guanine-cytosine base sequence. In short, the MB based DNA sensor is sequence dependent.

In this paper, a glassy carbon electrode (GCE) in combination with differential pulse voltammetry (DPV) was used to obtain information about the interaction of MB with CML DNA (Type b3a2). The DNA sensor fabrication method, such as the hybridization method and the conditions control, was modified. Changes in the voltammetric signals resulting from the interaction of MB with dsDNA and ssDNA were used to sequence-specific detection of BCR/ABL gene related to CML. Under optimal performance conditions, the present biosensor can discriminate single-base mismatch well.

2. Experimental

2.1. Apparatus and reagents

DPV measurements were performed by using CHI 660B Electrochemical Workstation (CH Instrument, USA). The electrochemical system consisted of GCE (3 mm diameter) as the working electrode, a platinum wire as the auxiliary electrode, and the reference electrode (Ag/AgCl). All potentials mentioned in this paper refer to this reference electrode.

2.2. Chemicals

The 18-base synthetic oligonucleotides were purchased from Shanghai Chemical Reagents Company (China); their base sequences were:

- immobilized probe(18-base sequence A)-5′-NH$_3$ AGA GTT CAA AAG CCC TTC-3′;
- target (18-base sequence B)-5′-GAA GGG CTT TTG AAC TCT-3′;
- non-complementary(18-base sequence B′)-5′-ACG TGG TCC CCA GCT CTC-3′.

All oligonucleotides, dsDNA and ssDNA stock solutions (100 mg L^{-1}) were prepared with TE solution (10 mM Tris–HCl, 1.0 mM EDTA, pH 8.00) and kept frozen. More dilute solutions were prepared with 20 mM acetate buffer (pH 4.80). MB (AR) was purchased from The Third Agents Factory of Shanghai (China). Stock solutions of MB (1 mM) were prepared with deionized water. *N*-hydroxysulfosuccinimide and *N*-(3-dimethylamion)propyl-*N*′-ethyl carbodiimidehydrochloride were obtained from Sigma. The stock solution of 5 mM DEC and 8 mM NHS was prepared in 50 mM phosphate solution (pH 7.40). Other chemicals were of analytical reagent grade. All the buffer solutions contained 20 mM NaCl. Sterilized and deionized water was used in all solution.

2.3. Experimental procedures

2.3.1. GCE pretreatment

The GCE was polished with 0.3 and 0.05 μm alumina, sonicated in water, and oxidized at 0.5 V for 1 min in 50 mM phosphate buffer solution (pH 7.40). After the oxidation step, the electrode was rinsed with distilled water.

2.3.2. Covalent bond modification

GCE was inverted and 20 μL of solution containing 5 mM DEC and 8 mM NHS in 50 mM phosphate buffer solution (pH 7.40) was pipetted onto the GCE surface. After air-drying of this solution, the electrode was rinsed with distilled water.

2.3.3. Immobilization of DNA on covalently modified GCE

SsDNA (100 μg mL^{-1}, 10 μL) was pipetted onto the GCE surface and air-dried to dryness. The dsDNA modified GCE was prepared by immersing the above electrode into 20 mM Tris–HCl buffer solution (pH 7.00) containing cDNA at 45 °C for 30 min. The electrode was then rinsed with pH 4.80 acetate buffer solution.

2.3.4. MB accumulation and voltammetric transduction

The DNA modified electrode was immersed in 20 mM Tris–HCl buffer (pH 7.00) containing 20 μM MB for 5 min. After this modified electrode was transferred into the blank 20 mM Tris–HCl buffer (pH 7.00), differential pulse voltammograms were collected from 0.1 to −0.6 V with amplitude of 10 mV at 50 mV/s scan rate.

Replicate measurements were performed by renewing the surface and repeating the above assay preparation procedure.

3. Results and discussion

Fig. 1 displays the differential pulse voltammograms of the bare, ssDNA-modified and dsDNA-modified GCE previously accumulated with MB in blank buffer solution. For all these
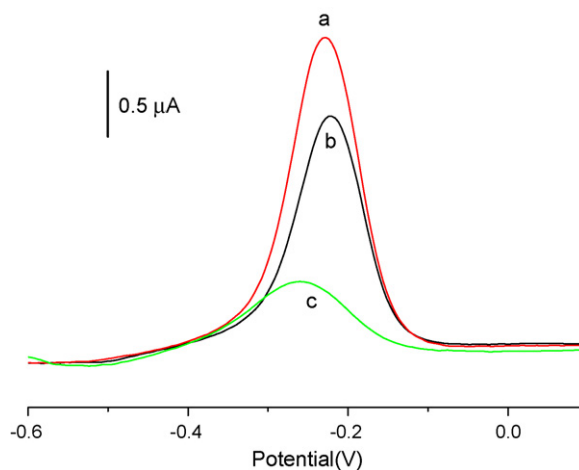

Fig. 1. Differential pulse voltammograms of MB accumulated on the ssDNA (curve a) and dsDNA (curve b) modified electrode in a 0.50 M acetate buffer (pH 4.80) with 20 mM NaCl. For comparison, the DPV of MB accumulated on a bare GCE under the same experimental conditions is also displayed (curve c).

electrodes, a current peak for the reduction of MB appears at
−220 mV. The bare GCE shows the smallest current peak, which
could be due to the specific adsorption of MB at the bare GC
electrode surface (curve c). As the GCEs were modified with
ssDNA (curve a) and dsDNA (curve b), the current peak for the
reduction of MB increased, indicating that MB was successfully
immobilized on the modified GCE due to the interaction between
the MB and the DNA. In addition, the current for the ssDNA-
modified electrode is higher than that for the dsDNA-modified
electrode. This difference should be due to the lesser interaction
between dsDNA and MB than that for ssDNA and MB, result-
ing in decreased intercalation of MB on the dsDNA-modified
electrode. This also indicates that MB has strong affinity to the
free guanine bases, and thus the greatest amount of MB accu-
mulated at this ssDNA-modified electrode [31]. After MB was
intercalated between the base pairs of hybrid, the electrochemi-
cal signal decreased (Fig. 1b). This decrease was attributed to the
steric inhibition of MB packing between the double helix of the
hybrid. Besides the change in peak current, the peak potentials
for the reduction of MB on the ssDNA- and dsDNA-modified
GCEs shift to positive value as compared to that for bare GCE,
which demonstrates the MB interacts with the DNA molecules.

Control experiments were also performed to estimate whether
the biosensor responds selectively via hybridization. The his-
togram of the reduction current of MB intercalated on the ssDNA
modified GCE (1), after hybridization with non-complementary
sequence (2), complementary sequence (3) and one-base mis-
match sequence (4) in solution is shown in Fig. 2. As
expected, there was no significant current difference observed
for the ssDNA modified GCE and its hybridization with non-
complementary sequence, since no successful hybridization
occurs due to the sequence mismatch between the modified
ssDNA and the non-complementary sequence. This means that
the surface properties of the ssDNA modified GCE was not
changed after its interaction with non-complementary sequence.
However, when the ssDNA modified GCE interacted with the
complementary sequence in solution, the peak current for the
MB reduction decreased significantly. This decrease in current
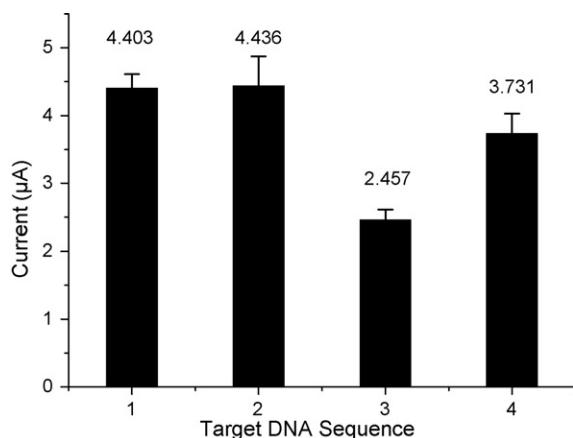
clearly showed that the ssDNA modified on the GCE success-
fully hybridized with its complementary sequence, decreasing
the intercalation amount of MB on the modified GCE due to
the steric inhibition of MB packing. The effective discrimi-
nation against single-base mismatch was also studied. In the
presence of oligonucleotide containing a single-base mismatch,
significant increased voltammetric signal was obtained as com-
pared to the complementary sequence. This difference indicates
that the complete hybridization was not accomplished due to
the base mismatch. A series of three repetitive measurements
resulted in reproducible results. The relative standard devia-
tion is 3.90%, 4.75%, 6.18%, 7.98% and 9.85% for bare GCE,
ssDNA-GCE, dsDNA-GCE, one-base mismatch detection and
non-complementary sequence detection, respectively.

The influence of experimental parameters including MB
accumulation time and concentration, hybridization time and
hybridization temperature on the sensitivity of the present assay
were explored for optimum analytical performance. Fig. 3 shows
that the DPV signals for MB increased as a function of accu-
mulation time. The peak current increased exponentially with
the accumulation time in the first 5 min. Beyond this accumu-
lation time, the MB signal reached constant, which indicated
that intercalation of MB to DNA reached a saturation value.
Thus, accumulation time of 5 min was chosen as the optimal
accumulation time.

The influence of hybridization time and hybridization tem-
perature is shown in Fig. 4. The co-influence of hybridization
time and hybridization temperature was investigated in these
experiments. We can see that hybridization time decreases with
the increase of hybridization temperature due to the fact that
higher temperature speed the movement of DNA molecules. On
the other hand, higher hybridization temperature accelerates the
denaturation of dsDNA, resulting in the decrease of the abso-
lute hybridization number. Taking consideration of the above
two factors, the ssDNA modified electrode reacting with cDNA
in solution is chosen at 45 °C for 30 min, which is the optimal
hybridization condition.

The electrochemical response for the intercalated MB on the
ssDNA modified GCE interacting with different level of the tar-
get DNA in solution was studied and the results are displayed

Fig. 2. Histogram of DPV signals for the electrochemical reduction of MB inter-
calated on the ssDNA/GCE (1); after its hybridization with non-complementary
sequence (2); after its hybridization with complementary sequence (3); after its
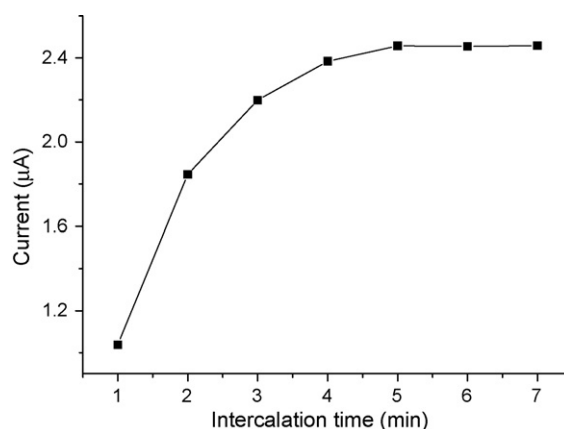hybridization with one-base mismatch sequence (4).

Fig. 3. Plot of the peak current for MB at the modified electrode as a function
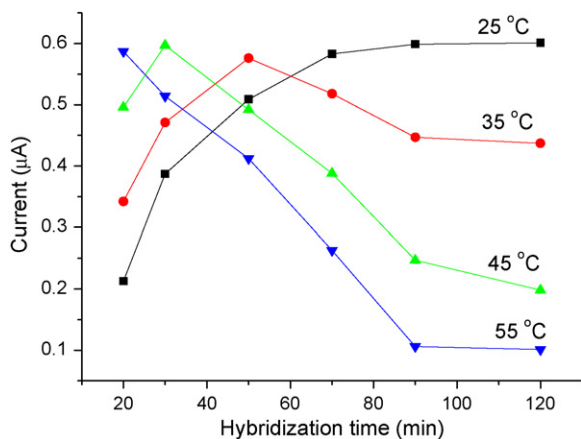of MB accumulation time.

Fig. 4. DPV response as function of hybridization time and temperature using MB as indicator.
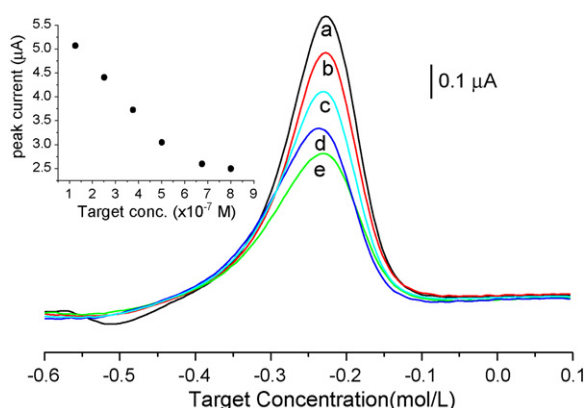

Fig. 5. Differential pulse voltammograms of MB accumulated on the ssDNA after its hybridization with different concentration of the target sequence in a 0.50 M acetate buffer (pH 4.80) with 20 mM NaCl. Target concentration ($\times 10^{-7}$ M): (a) 1.25, (b) 2.5, (c) 3.75, (d) 5.0 and (e) 6.75. Inset shows the plot of the peak current of MB as a function of the target concentration.

in Fig. 5. The signal for the reduction of MB after hybridization with target DNA decreased with the target concentration up to 6.75×10^{-7} M, and then remained constant with further increase of target concentration, which indicates that all the immobilized probes on GCE surface have been involved in hybridization at the concentration of 6.75×10^{-7} M. Before this threadhold concentration, the MB reduction signal decreased accordingly with the increase of the target concentration, which was resulted from more hybrid formation preventing the interaction of guanine bases with MB. The constant MB signal also indicated that all the hybridization sites on the ssDNA GCE have been covered. The reduction peak current of MB was linearly relating to the concentration of the target oligonucleotide sequence of the b3a2 type CML between 1.25×10^{-7} and 6.75×10^{-7} M ($R^2 = 0.9951$). The detection limit was 5.9×10^{-8} M based on the ratio of signal-to-noise of 3.

4. Conclusion

In conclusion, we have reported a new hybridization biosensor for electrochemical detection of sequences specific to CML DNA of Type b3a2. This effort addresses the urgent needs and analytical challenges of detecting BCR/ABL gene in the CML patients. The present method using MB as indicator for the detection of short DNA segments relating to CML (b3a2) is simple, sensitive and rapid and is promising for clinical diagnostic testing for CML.

References

[1] P.J. Fialkow, S.M. Gartler, A. Yoshida, Proc. Natl. Acad. Sci. U.S.A. 58 (1967) 1468.
[2] R.E. Champlin, D.W. Golde, Blood 65 (1985) 1039.
[3] H.M. Kantarjian, A. Deisseroth, R. Kurzrock, Blood 82 (1993) 691.
[4] A. Butturini, B. Ralph, Leuk. Res. 20 (1996) 523.
[5] E.C. Jorge, T. Moshe, K. Hagop, Am. J. Med. 100 (1996) 555.
[6] S.R. Mikkelsen, Electroanalysis 8 (1996) 15.
[7] E. Palecek, E. Fojta, Anal. Chem. 73 (2001) 74A.
[8] J. Wang, Nucleic Acids Res. 28 (2000) 3011.
[9] D. Zhang, Y. Chen, H.Y. Chen, X.H. Xia, Anal. Bioanal. Chem. 379 (2004) 1025.
[10] K.J. Feng, Y.H. Yang, Z.J. Wang, J.H. Jiang, G.L. Shen, R.Q. Yu, Talanta 70 (2006) 561.
[11] C.D. Riccardi, K. Dahmouche, C.V. Santilli, P.I. Costa, H. Yamanaka, Talanta 70 (2006) 637.
[12] M. Fojta, R. Doffkova, E. Palecek, Electroanalysis 8 (1996) 420.
[13] J. Wang, M. Ozsoz, X. Cai, G. Ravis, H. Shiraishi, D.H. Grant, M. Chicarro, J.R. Fernandes, E. Palecek, Bioelectrochem. Bioenerg. 45 (1998) 33.
[14] A. Erdem, M. Ozsoz, Anal. Chim. Acta 437 (2001) 107.
[15] A. Erdem, M. Ozsoz, Turk. J. Chem. 25 (2001) 469.
[16] A. Erdem, K. Kerman, B. Meric, U.S. Akarca, M. Ozsoz, Anal. Chim. Acta 422 (2000) 139.
[17] A. Erdem, K. Kerman, B. Meric, M. Ozsoz, Electroanalysis 13 (2001) 219.
[18] F. Yan, A. Erdem, B. Meric, K. Kerman, M. Ozsoz, O.A. Sadik, Electrochem. Commun. 3 (2001) 224.
[19] G. Marrazza, G. Chiti, M. Mascini, M. Anichini, Clin. Chem. 46 (2000) 31.
[20] A. Erdem, K. Kerman, B. Meric, U.S. Akarca, M. Ozsoz, Anal. Chim. Acta 422 (2000) 139.
[21] B. Meric, K. Kerman, D. Ozkan, P. Kara, S. Erensoy, U.S. Akarca, M. Mascini, M. Ozsoz, Talanta 56 (2002) 837.
[22] D. Ozkan, P. Kara, K. Kerman, B. Meric, A. Erdem, F. Jelen, P.E. Nielsen, M. Ozsoz, Bioelectrochemistry 58 (2002) 119.
[23] K. Kerman, D. Ozkan, P. Kara, B. Meric, J.J. Gooding, M. Ozsoz, Anal. Chim. Acta 462 (2002) 39.
[24] H. Ju, J. Zhou, Electroanalysis 7 (1995) 1165.
[25] D.B. Hall, S.O. Kalley, Biochemistry 37 (1998) 5399.
[26] E.M. Tuite, J.M. Kelley, Photochem. Photobiol. 21 (1993) 103.
[27] T. Friedman, D.M. Brown, Nucleic Acids Res. 5 (1978) 615.
[28] S.O. Kelley, J.K. Barton, Bioconjugate Chem. 8 (1997) 31.
[29] M. Fojta, E. Palecek, Anal. Chim. Acta 12 (1997) 342.
[30] R. Rohs, H. Sklenar, R. Lavery, B. Roder, J. Am. Chem. Soc. 122 (2000) 2860.
[31] A. Erderm, K. Kerman, B. Meric, M. Ozsoz, Anal. Chim. Acta 422 (2000) 139.

Synthesis of porphyrin-appended terpyridine as a chemosensor for cadmium based on fluorescent enhancement

Hong-Yuan Luo, Jian-Hui Jiang, Xiao-Bing Zhang *, Chun-Yan Li, Guo-Li Shen, Ru-Qin Yu *

State Key Laboratory of Chemo/Biosensing and Chemometrics, College of Chemistry and Chemical Engineering, Hunan University, Changsha 410082, China

Received 9 June 2006; received in revised form 10 November 2006; accepted 18 November 2006
Available online 22 December 2006

Abstract

The design and synthesis of a porphyrin-appended terpyridine, 5-(4-([2,2′:6′,2″]-terpyridin-4-yl-carboxyamidyl)phenyl)-10,15,20-triphenylporphyrin (H_2TPPTPy) and its application as potential fluoroionophore for recognition of metal ions are reported. For preparation of the fluoroionophore, a novel simple strategy with improved total yield has been applied for the synthesis of 2,2′:6′,2″-terpyridine-4′-carboxylic acid as a ligand. H_2TPPTPy shows chelation-enhanced fluorescence effect with cadmium ion via the interruption of photoinduced electron transfer (PET) process, which has been utilized as the basis of the fabrication of the Cd(II)-sensitive fluorescent chemosensor. The analytical performance characteristics of the proposed Cd(II)-sensitive chemosensor were investigated. It shows a linear response toward Cd(II) in the concentration range of 3.2×10^{-6} to 3.2×10^{-4} M with a limit of detection of 1.2×10^{-6} M. The chemosensor shows good selectivity for Cd(II) over a large number of cations, such as alkali, alkali earth and transitional metal ions except Cu(II) and Zn(II). The sensor has been used for determination of Cd(II) in water samples with satisfactory recoveries.
© 2006 Elsevier B.V. All rights reserved.

Keywords: Porphyrin-terpyridine; Photoinduced electron transfer; Chelation-enhanced fluorescence effect; Cadmium ions

1. Introduction

Cadmium is widely used in a variety of industrial processes including batteries, alloy, and coloring matters as well as electroplating products. Cadmium is also frequently found in fertilizer production using phosphate minerals and sewage sludge. This element, unfortunately, has detrimental effects on human health as well as the environment accompanying with its wide use. Cadmium can accumulate in organs, such as kidney, thyroid gland and spleen, which can induce physiological disorders, including renal dysfunction, calcium metabolism disorders, and an increased incidence of certain cancer [1]. The development of simple methods for the determination cadmium is, therefore, of considerable research and practical significance.

Past decades have seen increasing interest in the development of fluorescent chemosensors for metal ions [2–6] due to the fact that such sensors demonstrate substantial advantages

in sensitivity, selectivity and costs, and it is possible to perform remote detection with the application of fiber optics. In terms of sensitivity concerns, chemosensors exhibiting fluorescence enhancement on metal ion complexation are favored over those showing fluorescence quenching upon cation binding. Among the many reported fluorescent chemosensors with fluorescence enhancement for metal ions, only a few cases have been explored for Cd(II) [7–10]. Most of such chemosensors for Cd(II) are based on anthrancene derivatives [8,9]. The limited photostability of anthrancene derivatives might cause problems especially in cases where laser is used as the excited source. Additionally, their optical signals are located in wavelength ranges where matrix interference can occur. Moreover, the fluorescence spectrum of anthrancene derivatives became complicated after binding to Cd(II), which is not suitable for high throughput screening.

In this study, we developed a photoinduced electron transfer (PET) chemosensor for cadmium ion based on 5-(4-([2,2′:6′,2″]-terpyridin-4-yl-carboxyamidyl)phenyl)-10,15,20-triphenylporphyrin (H_2TPPTPy). Porphyrin compounds possess fine optical characteristics with strong fluorescence, large Stokes shifts and relatively long excitation (>400 nm) and emission

* Corresponding authors. Tel.: +86 731 8822577; fax: +86 731 8822782.
  E-mail addresses: xbzhang@hnu.cn (X.-B. Zhang), rqyu@hnu.cn
(R.-Q. Yu).

(>600 nm) wavelengths that minimize the effects of the background fluorescence. Pyridine is a good electronic acceptor. Waluk and co-workers have reported that the emission intensity of 1*H*-pyrrolo[3,2-*h*]quinoline (PQ) decreases upon adding pyridine to a nonpolar solution [11,12]. The fluorescence quenching is due to the charge transfer from the PQ moiety to the pyridine ring. At the same time, Clements and Webber have also clarified that the neighboring pyridinium units quench the excited anthrancene [13]. When porphyrin is connected with terpyridine through a linking bridge, it would make up a "donor-spacer-receptor" intramolecular PET transfer system. The fluorescence of porphyrin is quenched by way of transfer of the excited state electron from porphyrin to terpyridine. When terpyridine moiety is bound to cadmium ion, the chelate would abrogate the PET process and the fluorescence of porphyrin is recovered.

2. Experimental

2.1. Reagents

2-Chloro-1-methylpyridinium iodide (CMPI) and 4-dimethylaminopyridine (DMAP) were purchased from Acros (New Jersey). CdCl$_2$, benzaldehyde and pyrrole were supplied by Shanghai Chemical Reagents (Shanghai) and used as received. *N*,*N*-dimethylformamide (DMF) was freshly distilled from CaH$_2$. Except when specified, other chemicals were of analytical reagent grade and used without further purification. Twice-distilled water was used throughout all experiments. 5-(4-Aminophenyl)-10,15,20-triphenylporphyrin was prepared from *meso*-tetraphenylporphyrin according to a literature procedure [14].

2.2. Synthesis of 2,2′:6′,2″-terpyridine-4′-carboxylic acid

2,2′:6′2″-terpyridine-4′-carboxylic acid can be prepared either following a literature procedure from commercially available citrazinic acid [15] or via oxidation of the methyl-

terpyridine [16,17]. These two procedures both need many steps and show low total yield. Inspired by the successful work of Beley and co-worker [18], we synthesized this compound using a simple procedure with high yield via one step oxidation (Scheme 1). The mixture of 4′-(2-furyl)-2,2′:6′,2″-terpyridine (0.2991 g, 1 mmol) and KMnO$_4$ (2.0544 g, 13 mmol) in THF/H$_2$O (1:1) was stirred at room temperature for 24 h. Then the suspension was filtered. The residue was washed with water and ethanol. After that, the residue was recrystallized from DMF to give 2,2′:6′,2″-terpyridine-4′-carboxylic acid. All physical and spectroscopic properties were identical to previously reported data for this compound [15,19]. The yield was up to 80%.

2.3. Synthesis of H$_2$TPPTPy [20]

The synthetic route for H$_2$TPPTPy is shown in Scheme 1. The mixture of 2,2′:6′,2″-terpyridine-4′-carboxylic acid (3.8 mg, 0.014 mmol), 5-(4-aminophenyl)-10,15,20-triphenylporphyrin (7.1 mg, 0.011 mmol), 2-chloro-1-methylpyridinium iodide (10.2 mg, 0.04 mmol) and 4-dimethylaminopyridine (12.9 mg, 0.106 mmol) in DMF was heated at 130 °C for 5 h. The solvent was evaporated, and dichloromethane (100 mL) was added. Then the solution was washed with water (5 mL × 150 mL). The solvent was evaporated, and the residue was purified by chromatography (silica gel, CH$_2$Cl$_2$, then CH$_2$Cl$_2$: methanol, 50:1). The yield was 89.7%. ^{1}H NMR (400 MHz, CDCl$_3$), δ (ppm) 9.04 (s, 2 H, pyridine), 8.92 (d, 2 H, J = 4.8 Hz, β-pyrrol), 8.87 (d, 2 H, J = 4.8 Hz, β-pyrrol), 8.85 (s, 4 H, β-pyrrol), 8.78 (d, 2 H, J = 4 Hz, pyridine), 8.66 (d, 2 H, J = 8 Hz, pyridine), 8.28–8.16 (m, 10 H, ortho triphenyl and 4-aminophenyl), 7.94–7.90 (ddd, 2 H, ^3J = 7.6 Hz, ^4J = 1.6 Hz, pyridine), 7.76 (m, 9 H, meta/para triphenyl); 7.43–7.40 (ddd, 2 H, ^3J = 6.8 Hz, ^4J = 2 Hz, pyridine), −2.77 (s, 2 H, pyrrol NH), ACPI-MS Positive, *m/z* 889.1 ([M + H]$^+$, 40), 812.1 ([M−Py]$^+$, 45), 735.2 ([M−2Py]$^+$, 5), 656.1 (H$_2$TPPCO$^+$, 100), 629 (H$_2$TPP$^+$, 21), 613.1 ([H$_2$TPP−H]$^+$, 15), 277.1 ([TPy + 2H]$^+$, 4).
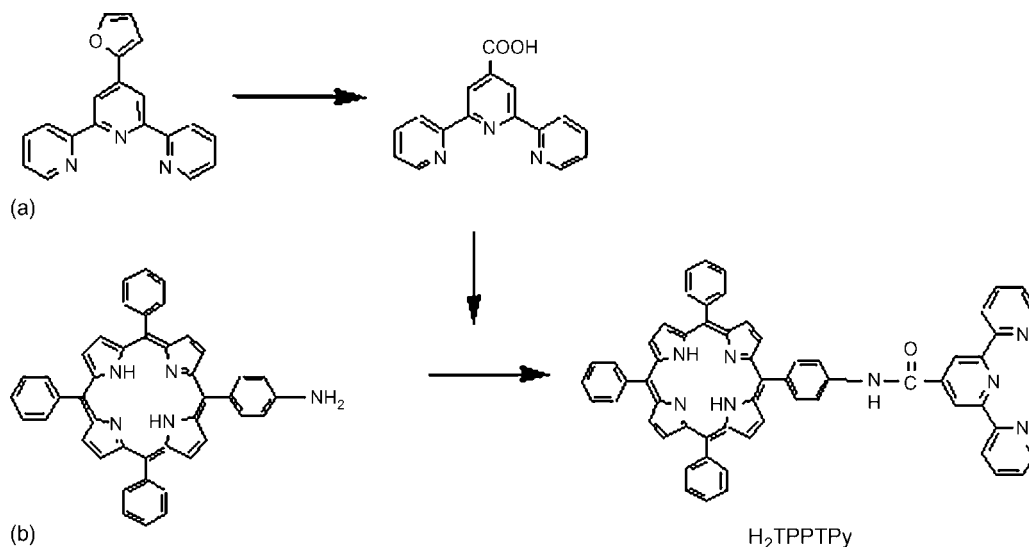
Scheme 1. Scheme for synthetic route. Reagents and conditions: (a) KMnO$_4$, THF/H$_2$O (1:1), RT for 24 h (86%); (b) 2-chloro-1-methylpyridinium iodide, 4-dimethylaminopyridine, DMF, 130 °C, 5 h.

2.4. Preparation of solutions

The standard solution of Cd(II) was obtained by serial dilution of 1.0×10^{-2} M CdCl$_2$ solution with pH 8.62 tris–HCl buffer.

A 1.0×10^{-5} M stock solution of H$_2$TPPTPy was prepared by dissolving it in absolute ethanol.

The wide pH range buffered solution was obtained by adjustment of 0.1 mol L^{-1} NaOAc–HOAc solution with HCl or NaOH solution.

The complex solution of Cd(II) and H$_2$TPPTPy was prepared by adding 2.0 mL of the stock solution of H$_2$TPPTPy and 2.0 mL of the standard solution of Cd(II). In the solution thus obtained, the concentrations were 5×10^{-6} mol L^{-1} of H$_2$TPPTPy and 1×10^{-3}–1×10^{-8} mol L^{-1} of Cd(II). Blank solution of H$_2$TPPTPy was prepared under the same conditions without Cd(II).

2.5. Instrumentation

All fluorescence measurements were carried out on a F4500 luminescence spectrometer (HITACHI) with excitation slit set at 5.0 nm and emission at 10.0 nm. The UV–vis absorbance measurements were made on MultiSpec 1501 (SHIMADZU). The pH measurements were carried out on a Mettler-Toledo Delta 320 pH meter.

2.6. Procedures

The fluorescence intensity was measured with the maximal excitation wavelength of 417 nm and at the maximal emission wavelength of 643 nm. Before each measurement, the solution was allowed to stand for 5 min to allow complete formation of metal–ligand complex.

3. Results and discussion

3.1. Quench effect of terpyridine unit towards porphyrin unit

The fluorescence spectra of H$_2$TPPTPy and *meso*-tetraphenylporphyrin (H$_2$TPP) are shown in Fig. 1, where the H$_2$TPP unit is excited at 417 nm. Compared to the fluorescence intensity of H$_2$TPP, The fluorescence intensity of H$_2$TPPTPy is greatly quenched. The fluorescence quantum yield of H$_2$TPPTPy is 0.029, as determined using the comparative method with H$_2$TPP as the standard ($\Phi = 0.11$ [21]), which is due to the charge transfer from the excited state porphyrin to the pyridine ring [11–13].

The driving force of electron transfer (ΔG_{ET}^0) [22,23] from the single excited state (^{1}H$_2$TPP*) to terpyridine in H$_2$TPPTPy was determined to be -0.24 eV from the one-electron oxidation potential of the H$_2$TPP moiety ($E_{ox}^0 = 1.03$ V versus Ag/AgCl [24]) and the one-electron reduction potential of the terpyridine moiety ($E_{red}^0 = -0.74$ V versus Ag/AgCl [25]), and the ^{1}H$_2$TPPTPy* energy level (2.01 eV). The ^{1}H$_2$TPP* energy level is estimated as the wavelength average of the longest-wavelength
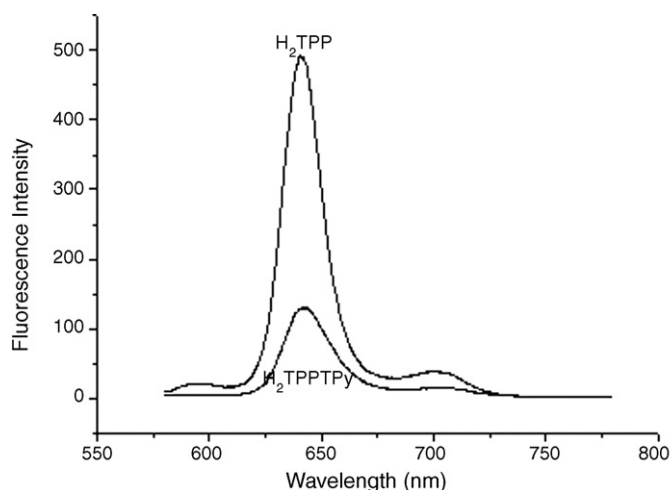
Fig. 1. Fluorescence spectra of 10 μM H$_2$TPPTPy and H$_2$TPP excited at 417 nm in deaerated toluene.

absorption maximum (595 nm) and the shortest-wavelength fluorescence maximum (643 nm).

3.2. Spectral properties

The fluorescence spectrum change of H$_2$TPPTPy when excited at 417 nm under various Cd(II) concentrations is shown in Fig. 2, which are recorded at $\lambda_{ex} = 417$ nm, $\lambda_{em} = 500$–800 nm. The H$_2$TPPTPy exhibits fluorescence emission at 643 nm. As can be observed from Fig. 2 that the fluorescence intensities of the H$_2$TPPTPy increase with increasing concentration of Cd(II), which constitutes the theory for the determination of Cd(II) with the chemosensor proposed in this paper.

For the purpose of studying the response mechanism, the absorption spectra of H$_2$TPPTPy in the absence of Cd(II) and in the presence of Cd(II) were recorded (Fig. 3). Upon addition of Cd(II), the spectra shape remained essentially the same. As can be observed from Fig. 3 that the Q band of H$_2$TPPTPy is almost
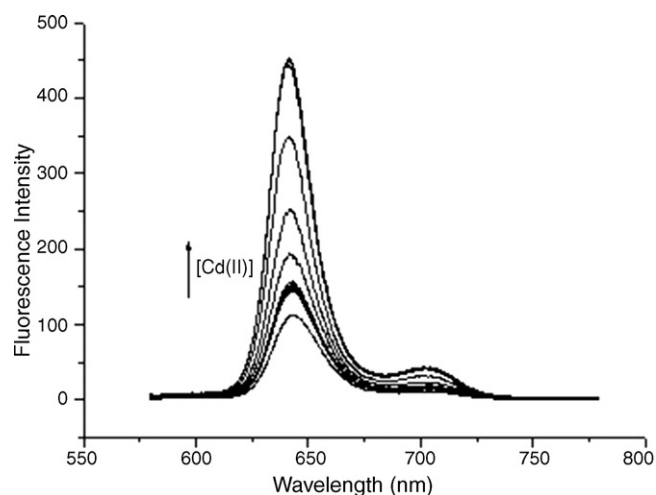

Fig. 2. Changes of the fluorescence spectra of H$_2$TPPTPy ($\lambda_{ex} = 417$ nm) at pH 8.62 as a function of added Cd(II) concentration (0, 1×10^{-8}, 3.2×10^{-8}, 1×10^{-7}, 3.2×10^{-7}, 1×10^{-6}, 3.2×10^{-6}, 1×10^{-5}, 3.2×10^{-5}, 1×10^{-4}, 3.2×10^{-4}, 1×10^{-3}, 1.1×10^{-3} M).
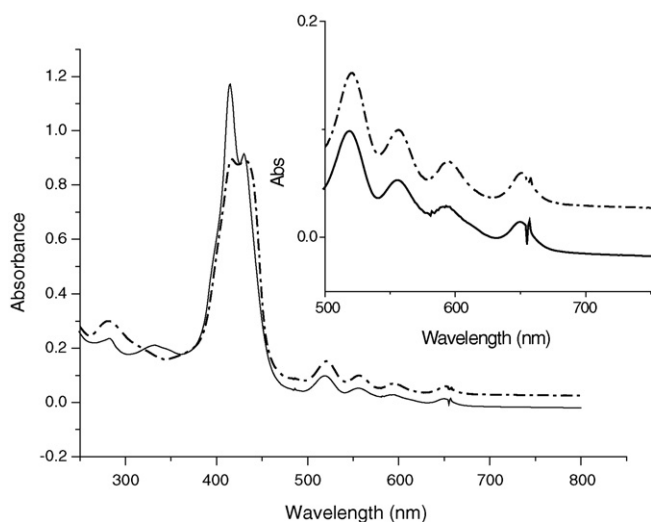
Fig. 3. Changes in the UV-spectra of H_2TPPTPy (10 μM) upon the addition of Cd(II) (10^{-3} M) at pH 8.62 (tris–HCl buffer). Solid line and dashed line spectra relate to the absence and presence, respectively, of Cd(II).

Fig. 4. Plot of log IF as a function of the log [Cd(II)] in EtOH/H_2O(1:1, v/v) solution.

not changed upon addition of Cd(II). Evidently, the porphyrin moiety does not participate in coordination to Cd(II). So, the fluorophore chelates Cd(II) with the terpyridine moiety. At the same time, one also notices that the peak at 417 nm was shifted to 415 nm. The value of the shift is indicative of the degree of the interaction between the fluorophore and Cd(II) [26]. A minor change of absorption spectra was in a usual PET fashion [3,8,27–30]. So, one could expect the fluorescence enhanced effect with Cd(II) is due to the chelate abrogating the PET process. Thus, a binding mode of H_2TPPTPy with Cd(II) is proposed and shown in Scheme 2.

The ability of H_2TPPTPy to recognize Cd(II) was further investigated. A great fluorescence enhancement accompanied with the increase of Cd(II) concentration. According to an equation: log IF = 3.46 + 0.231 log [Cd(II)] (r = 0.9958), a practically usable range for quantitative determination covers a range from 3.2×10^{-6} to 3.2×10^{-4} M. The detection limit is 1.2×10^{-6} M. The response curve of H_2TPPTPy is shown in Fig. 4. The coordination constant (K_a) between the ligand and Cd ion was calculated to be 3.94×10^4 by stern-volmer equation from the fluorescence titration experimental data.

3.3. Effect of pH

The response of H_2TPPTPy with variation of pH was investigated. The pH of solution was adjusted with the hydrochloric
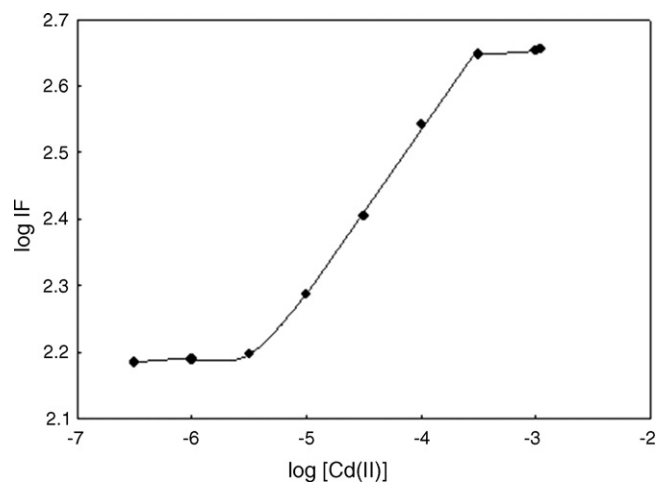
acid or sodium hydroxide in 0.1 M NaOAc–HOAc buffer. The fluorescence spectra of H_2TPPTPy and H_2TPP at different pH (λ_{ex} = 417 nm) are shown in Fig. 5. It can be seen that the spectral profiles of H_2TPPTPy are very similar to those of H_2TPP, but the fluorescence intensity of H_2TPPTPy is much lower than that of H_2TPP, indicating that the terpyridine moiety has substantial quenching effect on the porphyrin ring. One also notices that the emission peaks of H_2TPPTPy and H_2TPP are red-shifted and the fluorescence intensities are declined at low pH (pH ≤ 2). It is engendered possibly owning to protonation of the porphyrin under low pH conditions. The fluorescence spectra of protonated porphyrin are different from those of the free base form. The emission peaks are red-shifted and the fluorescence intensities are declined [31]. In addition, it is observed that the fluorescence intensity of H_2TPP increases with elevated pH in the range of pH 3–12, while H_2TPPTPy shows a declining profile in fluorescence intensity as the pH is elevated in the range, implying that the different pH conditions may influence the quenching effect of terpyridine moiety towards the porphyrin ring. This might be due to the protonation degree of the terpyridine moiety. It is known that 2,2′:6′,2″-terpyridine can accept protons in nonadjacent positions [32,33]. Kim and Nazeeruddin have reported the pK_a values of 2,2′:6′,2″-terpyridine of 3.42 and 4.64 [32,33]. At pH 3 nonadjacent pyridines are protonated. At pH 4 only one pyridine nitrogen is protonated. At pH ≥ 5 the whole terpyridine moiety is not pronated. Therefore, the fluorescence intensity of H_2TPPTPy decreases with increasing pH.
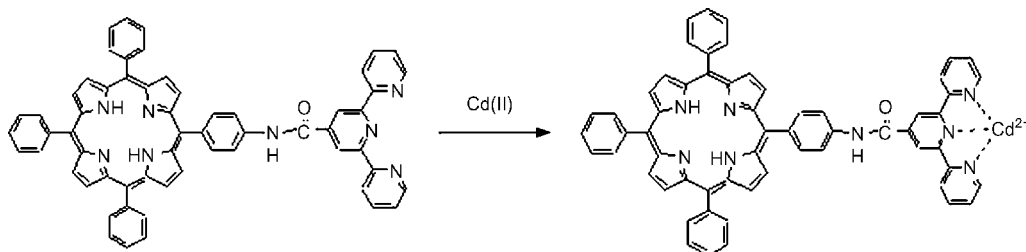
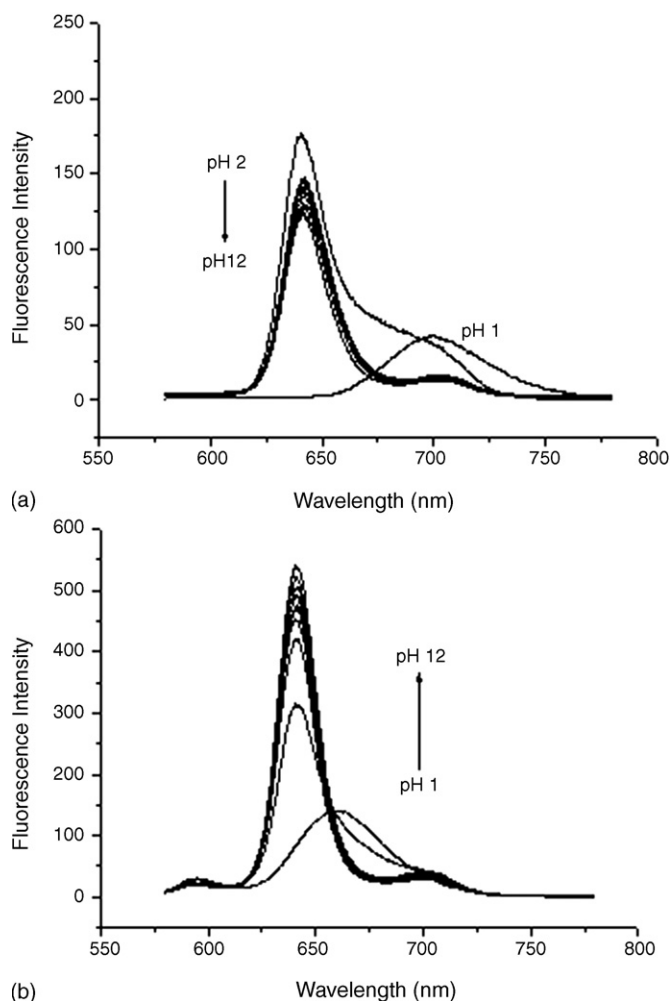Scheme 2. Proposed binding mode of H_2TPPTPy with Cd(II).

(a)

(b)

Fig. 5. The fluorescence spectra ($\lambda_{ex} = 417$ nm) of 10 μM H$_2$TPPTPy (a) and H$_2$TPP (b) recorded at different pH.

Fluorescence enhancement effect of H$_2$TPPTPy upon the addition of Cd(II) at different pH values was investigated. The changes in the fluorescence ($\lambda_{ex} = 417$ nm, $\lambda_{em} = 643$ nm) are shown in Fig. 6. One observes that the fluorescence intensity is almost not changed at low pH (pH ≤ 2), the fluorescence intensity is enhanced clearly at pH 3–6, the fluorescence intensity is enhanced greatly at pH 7–11, and the fluorescence intensity enhancement declines at high pH (pH > 11). It is suggested that at low pH (pH ≤ 2) terpyridine cannot quench the fluorescence of protonated porphyrin, so the fluorescence intensity are almost not changed. At pH 3–6 cadmium ion may not bind the terpyridine moiety completely in acidic condition, which limits the fluorescence enhancement. In basic solution (at pH 7–11) cadmium ion is prone to chelate terpyridine, thus fluorescence is completely recovered. At high pH (pH > 11) the fluorescence enhancement is diminished because cadmium ion is partly hydrolyzed, but terpyridine can still chelate the remaining free cadmium ion. Thereby, we chose pH 8.62 tris–HCl buffer (25 mL 0.2 M tris + 12.5 mL 0.1 M HCl + 62.5 mL H$_2$O) as the determining medium.
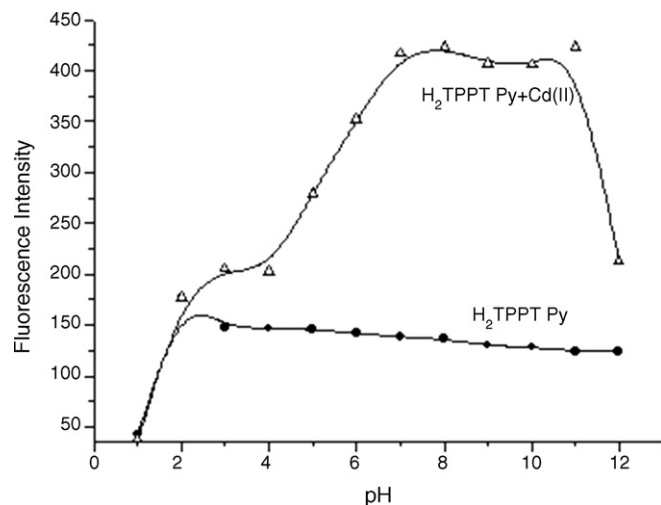
Fig. 6. Changes of the fluorescence intensity ($\lambda_{ex} = 417$ nm, $\lambda_{em} = 643$ nm) of H$_2$TPPTPy (10 μM) upon the addition of 3×10^{-4} M Cd(II) as pH varied.

3.4. Selectivity

The common ions were used to evaluate the fluorescence-enhanced effect of H$_2$TPPTPy. Titration studies were conducted at a pH 8.62 tris–HCl buffer using 10 μM H$_2$TPPTPy, and results are shown in Fig. 7. One notices that the fluorescence was almost not changed in the 10^{-3} M Li(I), Na(I), K(I), Mg(II), Ca(II), Mn(II), Pb(II) and Al(III) solutions. The fluorescence was quenched to some extent in the 10^{-3} M Ag(I), Ni(II), Fe(II), Hg(II) and Fe(III) solutions. When the concentrations of these ions were lowered to 10^{-4} M, the quenching effects were negligible. The fluorescence was quenched completely in the 10^{-3} M Cu(II) and Zn(II). Furthermore, the quenching effects were not negligible in the 10^{-5} M Cu(II) and Zn(II) solutions. For the purpose of studying the response mechanism, the absorption spectra of H$_2$TPPTPy upon the addition of the common ions (10^{-3} M) were recorded (Fig. 8). As can be observed from Fig. 8 that the spectra are changed greatly upon addition of Cu(II) and Zn(II).
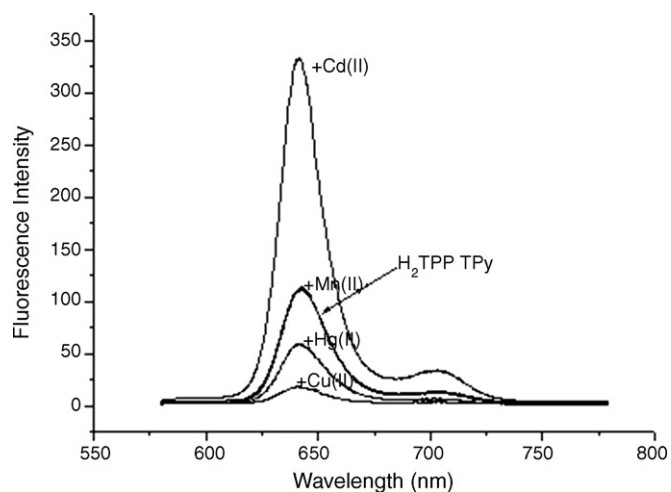

Fig. 7. Changes of the fluorescence intensity ($\lambda_{ex} = 417$ nm) of H$_2$TPPTPy (10 μM) upon the addition of four representative metal ions (10^{-3} M) at pH 8.62 (tris–HCl buffer).
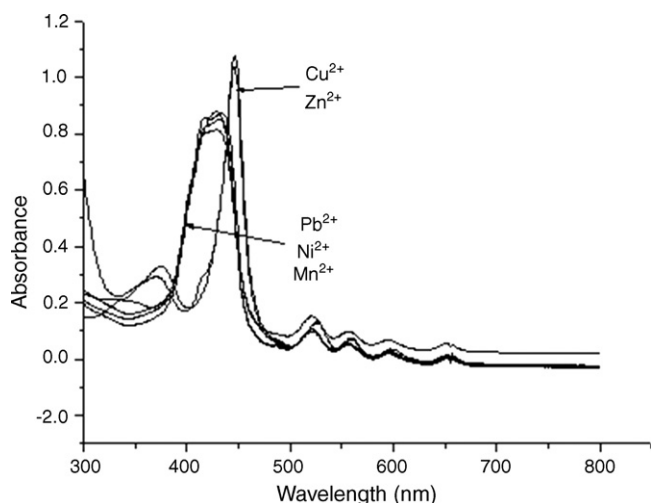
Fig. 8. Changes in the UV-spectra of $H_2TPPTPy$ (10 μM) upon the addition of the other ions (10^{-3} M) at pH 8.62 (tris–HCl buffer).

Fig. 9. Changes of the fluorescence intensity ($\lambda_{ex} = 417$ nm, $\lambda_{em} = 643$ nm) of $H_2TPPTPy$ (10 μM) before and after adding the interferent into the Cd(II) solution. The concentration of Cd(II) is fixed at 3.2×10^{-5} M. The concentrations of Na(I), Li(I), Mg(II), Ca(II), K(I), Al(III), Pb(II), and Mn(II) are at 1×10^{-3} M. The concentration of Ni(II), Fe(II), Fe(III), Ag(I), and Hg(II) are at 1×10^{-4} M. The concentration of Zn(II) and Cu(II) are at 1×10^{-5} M.

Table 1
Recovery study of spiked Cd(II) in water samples of Xiang River

Sample	Cd(II) spiked (M)	Cd(II) recovered[a] (M)	Recovery (%)
Xiang River water 1	4.0×10^{-6}	$(4.08 \pm 0.10) \times 10^{-6}$	102.0
Xiang River water 2	2.0×10^{-5}	$(1.95 \pm 0.05) \times 10^{-5}$	97.5
Xiang River water 3	1.2×10^{-4}	$(1.22 \pm 0.09) \times 10^{-4}$	101.7

[a] Relative standard deviations were calculated with $n = 5$.

The maximal absorption peak of complex with Cu(II) and Zn(II) is red-shifted from 417 to 446 nm. Evidently, the porphyrin moiety participate in coordination to Cu(II) and Zn(II). Binding of the porphyrin moiety with Cu(II) and Zn(II) causes a great fluorescence quenching to the fluorophore. One also notices that the UV–vis spectra shape remain essentially the same upon addition of the other ions. It is shown clearly that these ions bind $H_2TPPTPy$ with the terpyridine moiety. There is little effect on the fluorescence with alkali metal ions and alkaline-earth metal ions, presumably due to the fact that the binding interactions are not strong enough [7]. One also would expect that the structure of terpyridine unit requires a metal ion possessing appropriate ionic radius to be fitted for complexation. Metal ions, such as Ni(II) (0.69 Å) and Fe(III) (0.64 Å), show more serious fluorescence quenching effect as compared to those ions with larger radii, such as Pb(II) (1.19 Å), Ag(I) (1.26 Å) and Hg(II) (1.02 Å). The negligible fluorescence quenching effect of Mn(II) with smallest radius (0.46 Å) is presumably due to the steric effect of the small radius in binding with three nitrogens. Only the radius of Cd(II) is moderate (0.97 Å) for binding with three nitrogens.

To test practical applicability of $H_2TPPTPy$ as a Cd(II)-selective fluorescence chemosensor, competition experiments were carried out. The concentration of Cd(II) was fixed at 3.2×10^{-5} M and then the changes of the fluorescence intensity was recorded before and after adding the interferent into the Cd(II) solution. The results are shown in Fig. 9. Cu(II) shows serious interference, and Zn(II) shows obvious interference with the detection of Cd(II). These results suggested that $H_2TPPTPy$ could be used as a potential Cd(II)-selective fluorescent chemosensor.

3.5. Preliminary analytical application

In order to examine the applicability of the proposed sensor in a practical situation, the sensor was applied in the determination of cadmium ion in water samples of Xiang River. The river water samples were simply fil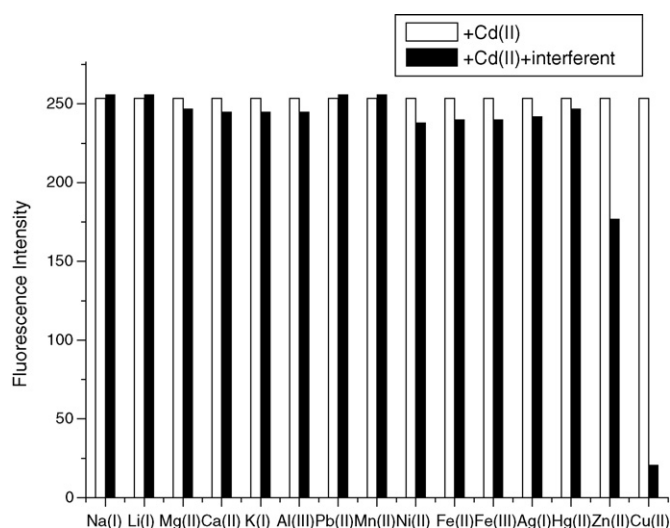tered. No Cd(II) was found in these samples. So they were spiked with standard cadmium solutions and then analyzed with the sensor (Table 1). One can see that the recovery study of spiked Cd(II) determined by the sensor shows satisfactory results. The present sensor seems useful for the determination of Cd(II) in real samples.

4. Conclusion

We have synthesized a new porphyrin-appended terpyridine. Using it, we have developed a fluorescent recognition method for Cd(II) in $EtOH/H_2O$ (1:1, v/v) solution, which shows fluorescent response to Cd(II) in the range of 3.2×10^{-6}–3.2×10^{-4} M with moderate selectivity. The remarkable enhancement of the fluorescence intensity in the presence of Cd(II) is possible for this chelate abrogate the electron from the excited state of porphyrin to the terpyridine. It is a new chemosensor for detecting Cd(II). Compared to the other porphyrin derivatives, this derivative has good solubility in polar solvents, such as ethanol.

References

[1] S. Dobson, Cadmium–Environmental Aspects, World Health Organization, Geneva, 1992.

[2] M.J.R. Rama, A.R. Medina, A.M. Díaz, Talanta 66 (2005) 1333.

[3] Y. Yu, L.R. Lin, K.B. Yang, X. Zhong, R.B. Huang, L.S. Zheng, Talanta 69 (2006) 103.

[4] E. Kimura, T. Koike, Chem. Soc. Rev. 27 (1998) 179.

[5] C.L. He, F.L. Ren, X.B. Zhang, Z.X. Han, Talanta 70 (2006) 364.

[6] N.C. Lim, H.C. Freake, C. Brückner, Chem. Eur. J. 11 (2005) 38.

[7] A.J. Hefley, Anal. Chem. 46 (1974) 2036.

[8] G. Hennrich, H. Sonnenschein, U. Resch-Genger, J. Am. Chem. Soc. 121 (1999) 5073.

[9] T. Gunnlaugsson, T.C. Lee, R. Parkesh, Org. Lett. 5 (2003) 4065.

[10] S. Charles, F. Dubois, S. Yunus, E.V. Donckt, J. Fluoresc. 10 (2000) 99.

[11] J. Herbich, M. Kijak, A. Zielińska, R.P. Thummel, J. Waluk, J. Phys. Chem. A 106 (2002) 2158.

[12] J. Waluk, Acc. Chem. Res. 36 (2003) 832.

[13] J.H. Clements, S.E. Webber, Macromolecules 37 (2004) 1531.

[14] Kruper W.J.JJr., T.A. Chamberlin, M Kochanny, J. Org. Chem. 54 (1989) 2753.

[15] R.A. Fallahpour, Synthesis 8 (2000) 1138.

[16] L. Flamigni, F. Barigelletti, N. Armaroli, J.-P. Collin, J.-P. Sauvage, J.A.G. Williams, Chem. Eur. J. 4 (1998) 1744.

[17] J.-P. Collin, A. Harriman, V. Heitz, F. Odobel, J.-P. Sauvage, J. Am. Chem. Soc. 116 (1994) 5679.

[18] J. Husson, M. Beley, G. Kirsch, Tetrahedron Lett. 44 (2003) 1767.

[19] G.W.V. Cave, C.L. Raston, J. Chem. Soc., Perkin Trans. 1 (2001) 3258.

[20] Y. Yu, J.M. Ostresh, R.A. Houghten, J. Org. Chem. 67 (2002) 5831.

[21] P.G. Seybold, M. Gouterman, J. Mol. Spectrosc. 31 (1969) 1.

[22] K. Okamoto, S. Fukuzumi, J. Am. Chem. Soc. 126 (2004) 13922.

[23] D. Kuciauskas, P.A. Liddell, S.-C. Hung, S. Lin, S. Stone, G.R. Seely, A.L. Moore, T.A. Moore, D. Gust, J. Phys. Chem. B 101 (1997) 429.

[24] D. Reddy, T.K. Chandrashekar, J. Chem. Soc. Dalton Trans. (1992) 619.

[25] M.G. Hill, J.A. Bailey, V.M. Miskowski, H.B. Gray, Inorg. Chem. 35 (1996) 4585.

[26] Y. Zheng, X. Cao, J. Orbulescu, V. Konka, F.M. Andreopoulos, S.M. Pham, R.M. Leblanc, Anal. Chem. 75 (2003) 1706.

[27] A.P. de Silva, H.Q.N. Gunaratne, G.E.M. Maguire, J. Chem. Soc., Chem. Commun. (1994) 1213.

[28] O. Reany, T. Gunnlaugsson, D. Parker, J. Chem. Soc., Perkin Trans. 2 (2000) 1819.

[29] R.A. Bissell, A.P. de Silva, H.Q.N. Gunaratne, P.L.M. Lynch, G.E.M. Maguire, C.P. McCoy, K.R.A.S. Sandanayake, Top. Curr. Chem. 168 (1993) 223.

[30] M.E. Huston, K.W. Haider, A.W. Czarnik, J. Am. Chem. Soc. 110 (1988) 4460.

[31] D.L. Akins, H.-R. Zhu, C. Guo, J. Phys. Chem. 100 (1996) 5420.

[32] K.-Y. Kim, G.H. Nancollas, J. Phys. Chem. 81 (1977) 948.

[33] Md.K. Nazeeruddin, S.M. Zakeeruddin, R. Humphry-Baker, T.A. Kaden, M. Grätzel, Inorg. Chem. 39 (2000) 4542.

Review

Ultrasound-assisted preparation of liquid samples

M.D. Luque de Castro [*], F. Priego-Capote

Department of Analytical Chemistry, Annex C-3, Campus of Rabanales, University of Córdoba, Córdoba, Spain

Abstract

This review intends to show analytical chemists a very little known application of ultrasound for sample preparation: that dealing with liquid samples. The influence of this type of energy on the development of chemical reactions (*e.g.* depolymerization, redox, esterification, alkylation, addition, ethylation of organometallic compounds, complex formation) and that on heterogeneous liquid–liquid processes (*e.g.* liquid–liquid extraction, homogenization, emulsification, liposome formation) deserves to be taken into consideration in the analytical laboratory in order to take profit from its versatile effects to improve, accelerate or make possible a given process.
© 2006 Elsevier B.V. All rights reserved.

Keywords: Ultrasound; Sample preparation; Liquid samples

Contents

[*] Corresponding author. Tel.: +34 957218615; fax: +34 957218615.
E-mail address: qa1lucam@uco.es (M.D. Luque de Castro).

1. Introduction

Ultrasound (US) is simply sound pitched above human hearing that is used at present for a growing variety of purposes in diverse areas. At home, US is typically used for communication with animals (dog whistles), as well as in burglar alarms, anemometers and jewellery cleaners. In hospitals, doctors use US to remove kidney stones without surgery, treat cartilage injuries and image fetal development during pregnancy. Ultrasonic scalpels are used by surgeons to cut precisely where they want without exerting any pressure. In industry, US provides an effective tool for synthesizing fine chemicals, emulsifying cosmetics and foods, welding plastics, cutting alloys, large-scale cleaning and identifying flaws in concrete buildings.

Being a sound wave, US is transmitted through any substance, solid, liquid or gas possessing elastic properties. The transmission produces expansion and compression cycles in which the latter push molecules together, whereas expansion cycles pull them apart and create bubbles or cavities when transmitted in a liquid. The process by which bubbles form, grow and undergo implosive collapse is known as "cavitation". The significance of cavitation to sonochemistry is not so much how the bubbles form, but rather what happens when they collapse. At some point, a bubble can no longer efficiently absorb the energy from the US so it implodes. Rapid adiabatic compression of gases and vapours within the bubbles or cavities produces extremely high temperatures and pressures. The size of the bubbles is very small relative to the total liquid volume, so the heat they produce is rapidly dissipated with no appreciable change in the environmental conditions—this is why cavitation is also known as "cold boiling".

In dealing with sample preparation, the most commonly used analytical effects of US are produced at the kHz frequency and the devices for producing these effects are either baths of probes.

Although the cleaning bath is the piece of ultrasonic equipment most widely used by chemists, it is not necessarily the most effective. Despite the amount of power dissipated from the bath into the analytical system is usually not very large – less than 5 W/cm^2 – maintaining the temperature in the bath is difficult unless the US device is furnished with some automatic thermal control; not all cleaning baths operate at the same frequency; the decline in power with time and the lack of uniformity in the transmission of US typical of inexpensive cleaning baths are two sources of high irreproducibility. For the above reasons, the use of laboratory cleaning baths should be restricted to cleaning operations or the removal of dissolved gases, which are indeed their principal intended uses.

Many of the disadvantages of using a simple cleaning bath in sonochemistry can be avoided by using an ultrasonic probe (also

called a "sonotrode") instead. A sonotrode delivers its energy on a specific zone, cavitation in which is thus dramatically boosted. Also, probes are subject to no exhaustion restrictions, so they are much more suitable for use in Analytical Chemistry than are ultrasonic baths. In addition, ultrasonic probes are more flexible as regards construction, so they can easily be designed for specific purposes.

Ultrasound is being accepted at present in the analytical laboratory for solid sample preparation as a timid alternative to other better established types of energy such as microwaves, superheated liquids or supercritical fluids [1]. It is time to show analytical chemists the potential of US for assisting liquid-sample preparation in the multiple analytical operations (*e.g.* reaction development, liquid–liquid extraction, homogenization and emulsification, liposomes formation) which can be improved, accelerated or made possible by this energy. As this review is focused on the assistance of US to liquid samples, only liquids systems formed by one, two or more liquid phases are deal with; therefore, steps of the analytical process involving systems such as liquid–gas (*e.g.* nebulization) or liquid–solid systems (*e.g.* crystallization) are absent.

2. Ultrasound-assisted chemical reactions

The enormous influence of US on chemical reactions, particularly in organic syntheses, has been widely exploited for more than two decades, as reflected in the large number of books devoted to this specific use of US over this period [2–8]. Industrially, US is largely used to accelerate reactions and also in degradation and hydrolysis reactions. By contrast, US has been only sparingly used to assist reactions involved in analytical processes despite the proven high potential of this form of energy for their acceleration.

Preliminary studies conducted in the 1980s by the authors' research group [9] using continuous flow injection approaches clearly exposed the following effects of US on analytical reactions: (1) homogeneous uncatalysed reactions [*e.g.* the formation of the Co–salicylaldehyde thiosemicarbazone complex, which requires the prior oxidation of Co(II) to Co(III)] are less markedly affected by US than are homogeneous catalysed reactions (*e.g.* the copper-catalysed oxidation of 2,2'-dipyridylketone hydrazone by hydrogen peroxide). The yield of these reactions increases by 28 and 300%, respectively, relative to unsonicated blanks. (2) Heterogeneous reactions are the most strongly influenced by US. One case in point is the Griess reaction, which can be boosted by inserting a redox or catalytic reactor in line in a dynamic system to previously reduce nitrate to nitrite; one other is the above-mentioned oxidation of a hydrazone by hydrogen peroxide, but catalysed in this case by a solid
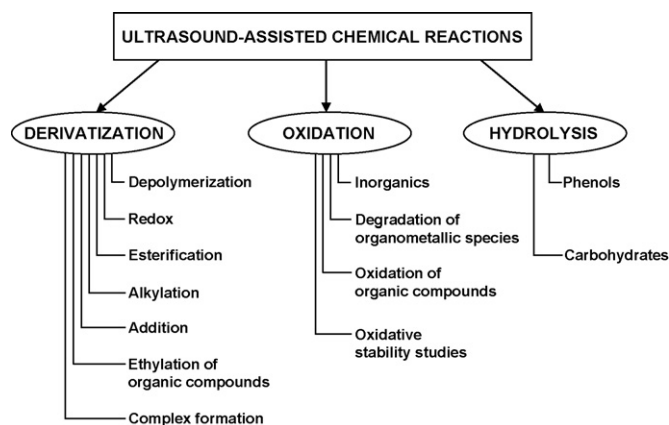
Fig. 1. Scheme of ultrasound-assisted chemical reactions of analytical interest involving liquid samples.

copper reactor instead. In addition, US dramatically increases dispersion of an injected volume in the carrier, which adds to the effects of, especially, the flow-rate, reactor length, inner diameter of the transporting tubes, viscosity and temperature, as the most important.

This section deals with the types of reactions with analytical interest assisted by US summarized in Fig. 1.

2.1. Ultrasound-assisted derivatization

Ultrasound-derivatization reactions involve inorganic, organic and organic–inorganic species, and are implemented in discrete or continuous systems. Most have exploited existing experience in non-analytical areas. They are discussed below according to chemical type.

2.1.1. Depolymerization reactions

The very long experience with the depolymerizing effect of US on high polymers such as starch, gelating and arabic gum [10–12] can be used in Analytical Chemistry to boost reactions involving a slow, limiting depolymerization step (e.g. the determination of phosphate using the Molybdenum Blue method [13]). Molybdenum Blue forms in two steps involving (1) the reaction of o-phosphate with molybdate ions in an acid medium to give molybdophosphoric acid, and (2) reduction to the blue heteropolyacid by a suitable reductant (usually ascorbic acid). Application of US in both steps showed that ascorbic acid was degraded via an oxidation reaction promoted by free radicals formed during irradiation. Also, application of US for 15 min during formation of the heteropolyacid was found to increase the absorbance of the solution by about 20%; however, US application to the molybdate solution for 1 min provided the same improvement, so the limiting step was depolymerization of molybdate ions, which occurred rapidly in the presence of US.

2.1.2. Redox reactions

The formation of OH and H radicals in sonicated aqueous media accelerates or facilitates redox reactions which are slow or unlikely in the absence of US. Such is the case

with the photometric determination of nickel by complexation with dimethylglyoxime, which involves oxidation of Ni(II) by bromine, iodine, hydrogen peroxide or persulphate. The oxidant is mixed with the Ni(II) solution prior to adding the chelating agent; however, replacing the oxidant with US irradiation under reproducible conditions as regards the position of the reaction vessel – in the centre of the US bath – and continuous renewal of the bath water at 400 ml/min substantially increases the absorbance and precision relative to the strongest oxidant among those commonly used for this purpose (viz. persulphate). In addition, the absence of an oxidant reduces interferences from Fe(II), Cu(II), Co(II), particularly when air is continuously bubbled into the solution, as a result of the formation of nitrite and nitrate ions in aqueous solutions saturated with air or nitrogen upon exposure to low-frequency US [14]. As noted earlier, the oxidation of Co(II) to Co(III) prior to complexation with salicylaldehyde thiosemicarbazone in a continuous manifold is also accelerated by US [9].

Not all redox reactions are favoured by US. One that is not is the basis for the determination of polyphenols in extra virgin olive oil by extraction of the target analytes into a basic aqueous medium containing the Folin–Ciocalteu reagent. Mass transfer of the polyphenols to the aqueous phase is doubly displaced by conversion of the analytes into their polyphenolates and subsequent oxidation by the Folin–Ciocalteu reagent. The overall process is greatly enhanced by US irradiation; however, tests examining the influence of US on each step separately by applying US for 3 min in each revealed no difference in the oxidation reaction relative to an insonated blank [15].

2.1.3. Esterification reactions

Resolving enantiomers usually requires using a derivatization reaction that is of the esterification type when α-hydroxy acids are to be derivatized with (+)-1-(9-fluorenyl) ethyl chloroformate. Fransson and Ragnarsson [16] used RPLC to separate the analytes and a US bath to implement the derivatization reaction; however, they provided no details about the gains in using this type of energy.

The conversion of amino acids into N(O,S)-ethoxycarbonyl amino acid ethyl esters is significantly improved by US assistance. The derivatization reaction, developed at a microscale, constitutes the step prior to single-drop microextraction, which is followed by GC–MS. Single-drop microextraction (SDME) is a relatively new sample preparation mode which enables extraction of the analytes or their derivatization products into a small volume of organic solvent. It combines extraction and preconcentration in a single step [17–19], is expeditious and can be implemented with simple equipment usually available in analytical laboratories. The derivatization step involves mixing 1 ml of sample (urine) with 400 μl of 4:1 ethanol–pyridine and 100 μl of ethylchloroformate. The reaction vial is ultrasonicated – no information about the characteristics was reported in the originating paper – for 10 min, followed by addition of 50 mg of NaCl and vigorous stirring for 2 min until all suspended air and CO_2 produced by the reaction are removed. Comparative tests of the derivatization reaction of 12 amino acids assisted by stirring at room temperature and 70 °C, and only under ultrasonication

provided the results which can be summarized as follows: (1) the reaction involving stirring at room temperature took a long time to complete and barely levelled off after 80 min; (2) heating and ultrasonication considerably accelerated the reaction, the latter clearly being a better choice for fast completion of the reaction; (3) ultrasonication can expose subtle interactions and special effects of entropic and enthalpic origin; (4) the efficient removal of bubbles from the bulk solution by US is of paramount importance as bubbles are detrimental to the SDME process—by attaching to drops, they reduce the surface available for extraction and facilitate dislodgement. Ultrasonication for 10 min following 2 min of vigorous stirring increased the yields of the corresponding derivatives by 20–35%, depending on the particular amino acid [20].

2.1.4. Alkylation reactions

Although gas chromatography affords the separation and quantification of phenols, the results are often poor by effect of the high polarity and low vapour pressure of these compounds [21]. Because isomeric compounds with almost identical properties (*e.g. o*-, *m*- and *p*-cresols) are difficult to separate [22,23], derivatization reactions involving the formation of ethers [24] and esters [25], and(or) bromine [26] and silyl derivatives [27] are frequently used to improve the chromatographic characteristics of the analytes [24]. One simple, efficient derivatization reaction is acetylation by acetic anhydride in an alkaline aqueous medium [28,29], which has been used for the automated determination of phenolic compounds (*viz.* phenol and *o*-, *m*- and *p*-cresol), involves three main steps, namely: (a) ultrasound irradiation to accelerate the derivatization reaction; (b) pervaporation [30] to remove the products of the target analytes from the aqueous matrix; and (c) gas chromatography to separate the individual products, followed by flame ionization detection [31]. The reaction time was more than halved relative to the absence of US irradiation and to the use of microwaves under optimal conditions.

2.1.5. Addition reactions

Although the earliest examples of the use of US as a substitute for phase transfer catalysts in organic addition reactions were reported more than two decades ago and a number of such reactions have since been improved as a result [2–8], the sole analytical application exploiting this potential is a method for the determination of paracetamol where the drug is derivatized by hydrolysis to *p*-aminophenol, which reacts with *o*-cresol in an alkaline medium to form the Indophenol Blue dye. The method was developed for determining the analyte in suppositories, so extraction from a toluene solution to an aqueous phase was required prior to hydrolysis and the addition reaction. All these steps were performed in the continuous manifold of Fig. 2A. Fig. 2B compares the results in the presence and absence of US [32] obtained by continuously monitoring the aqueous extractant phase during the liquid–liquid extraction without phase separation; as can be seen, the use of US had an enormous influence on the overall process. A series of tests was conducted with a view to clarifying the influence of US on each of the reactions taking place simultaneously with the extraction process.
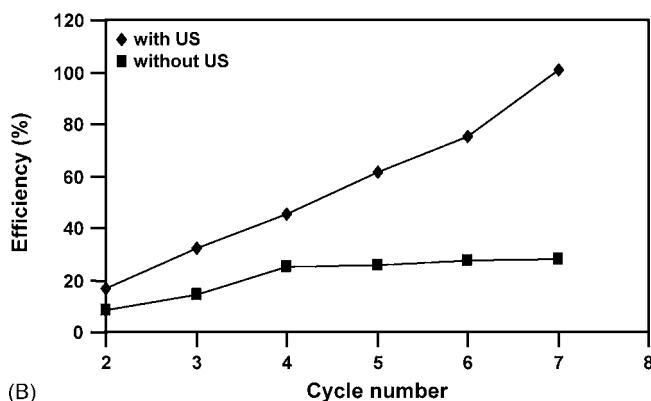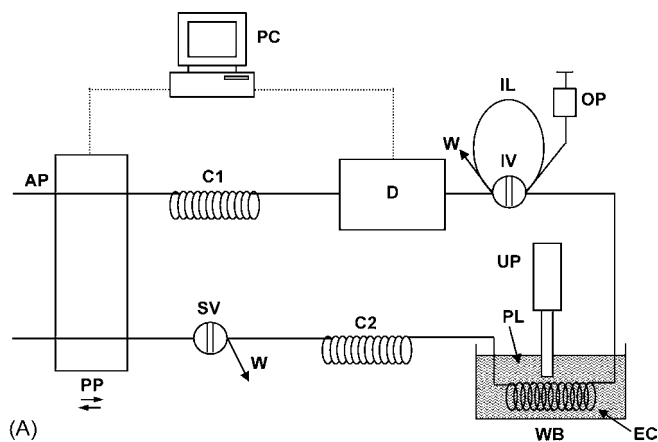

Fig. 2. (A) Flow injection manifold for continuous US-assisted liquid–liquid extraction without phase separation monitoring one interface. AP, aqueous phase; C, coil; D, detection system; EC, extraction coil; IL, injection loop; IV, injection valve; OP, organic phase; PC, personal computer; PL, propagating liquid; PP, peristaltic pump; SV, switching valve; UP, ultrasonic probe; W, waste; WB, water bath. (B) Comparison of the efficiency of continuous liquid–liquid extraction of paracetamol from suppositories previously dissolved in toluene with and without US assistance (reproduced with permission of Elsevier, Ref. [32]).

One of the main advantages of the use of US for enhancing processes implemented in a continuous fashion over that of microwave energy is the small temperature rise involved in the former case, which avoids the presence of undesirable air bubbles in the dynamic system and hence of parasitic signals at the detector.

2.1.6. Ethylation of organometallic compounds

Ethylation by sodium tetraethylborate has become an attractive choice for the speciation analysis of organometallic compounds [33,34]. With this reagent, ethylation takes place even in an aqueous phase, which makes it possible to simplify the pre-treatment process by combining derivatization and extraction in one step. This has been the case with the determination of methylmercury in biological materials by GC–MIP-AES or GC–ICP-MS [35]. Following leaching in an automatic shaker for 5 min, addition of the derivatizing reagent in an appropriate volume of an immiscible phase – nonane – to the suspension and pH adjustment, the system was ultrasonicated in a bath for 40 min. Although the differential effects of US on the derivatization reaction and on liquid–liquid extraction have not

been experimentally established, its combined effect is clearly apparent.

2.1.7. Complex formation

Although US seemingly facilitates complex formation reactions (*e.g.* in the method for Ni determination by formation of the Ni–DMG complex, where US favours Ni(II) oxidation [14], or that for phosphate based on the formation of the heteropolyacid complex, where US accelerates the depolymerization [13]), the potential effect of US on this type of equilibrium has not yet been examined. The only reported example to the authors' knowledge deals with the liquid–liquid extraction of Fe(II) from an aqueous sample to an *o*-phenanthroline–dichloromethane phase, which is not significantly improved by US assistance [15].

2.2. Ultrasound-assisted oxidation reactions

Oxidation reactions in Analytical Chemistry usually constitute a step preceding derivatization, if present, intended to make the analyte amenable to derivatization or, less frequently, direct detection. One can expect US to favour any oxidation reaction taking place in an aqueous medium through the well-known radical formation process. This assumption has been verified with a short, but representative, number of examples. In other cases, aqueous solutions saturated with a solvent of higher vapour pressure than water have been found to favour oxidation reactions. Four major applications of oxidation reactions widely used in Analytical Chemistry have exposed the gains in using US, which include increased efficiency and shortened times in reactions such as those listed in Fig. 1.

2.2.1. Oxidation of inorganic species

Inorganic compounds can be oxidized in an easy, fast, controlled way under the influence of US. This analytical use of US, only examined by Korn et al. [36–38] so far, constitutes an underexplored field which can provide analytical chemists with high benefits. Their work has focused on the generation of species by exploiting the oxidative effect of chlorine radicals formed by sonolysis of CCl_4 in aqueous solutions. The principle behind this use is that when water is sonicated in the presence of a solvent with a higher vapour pressure, preferential sonolysis of the molecules of the latter occurs. Thus, when water saturated with CCl_4 is subject to US, CCl_4 can migrate to the bubbles formed by cavitation and C–Cl bonds be broken by the energy generated in the collapse phenomenon to give $^\bullet CCl_3$ and $^\bullet Cl$. This hypothesis is supported by the proven fact that an aqueous solution saturated with CCl_4 that was irradiated with a US device of 40 kHz and 200 W for 4 min exhibited a pH decrease from 4.6 to 2.6 [39].

Iodine and other oxidized-iodine species have been generated from iodide with US assistance [36], and also exposition of an aqueous solution of Fe(II) to ultrasonication results in its oxidation as the ferrous ion interacts with the OH radicals generated by water sonolysis to form Fe(III) and OH^-. On the other hand, sonication of a CCl_4-saturated aqueous solution prior to mixing with a Fe(II) solution provides quantitative oxidation of Fe(II).

Chromium(III) can also be determined in this way following quantitative oxidation to Cr(VI) by sonication in a carbonated aqueous solution saturated with CCl_4. Under the optimal working conditions, 1 μg of Cr(III) takes less than 60 s to be oxidized. The environmental and health hazards associated to the use of CCl_4 are minimal thanks to the small amount used. Thus, 2000 l of CCl_4-saturated aqueous solution is prepared from 1 l of CCl_4. This solution volume affords more than 50,000 determinations of Cr(III) in water [37].

In addition, US-assisted reagent generation of the strong reductants required to obtain arsine from As(III) can be based on the oxidative effect of CCl_4-saturated water solutions as for the determination of this toxic element in urine. The sample was acidified with 1×10^{-4} to 1×10^{-1} M HCl, placed in a reactor vessel containing 0.1–1 g of Zn and sonicated for 1–10 min while air was circulated through the solution to remove the volatile hydride for transfer to the detector [38].

Analyte oxidation and reagent generation in flow systems using tubular ultrasonic reactors is one underexplored area for analytical chemists.

2.2.2. Degradation of organometallic compounds prior to metal determination

Research in this field, conducted by Capelo et al., has focused on organomercurials in water and urine, and involved US probes and batch approaches in all instances [40–43]. Because these compounds are usually accompanied by inorganic mercury in natural samples, organic and inorganic mercury in water are determined separately. The process is more complex for urine as the presence of other organic matter entails isolating the target analytes after oxidation to ensure proper derivatization and detection.

Organomercurials (*viz.* methylmercury and phenylmercury) in water can be readily oxidized within 3 min by a 100-W power probe of 20 kHz frequency at 40% amplitude in a 1 M HCl medium. The influence of both sonication time and amplitude on the oxidation of both compounds is very similar. Complete oxidation of the target analytes requires the presence of HCl in the medium. Also, replacing US with an oxidant such as H_2O_2 or HNO_3 precludes reaching 100% efficiency [44]. The principal advantage of US assistance to this process is the need for no chemical oxidants, high temperatures or pressures, which avoids the generation of hazardous waste and decrease the risk of Hg loss by volatilization. Oxidation is more efficient – the yield is up to 15% higher – at low temperatures (*viz.* with the sonication cell immersed in an ice-bath) than at uncontrolled temperatures. An additional advantage is the tolerance of concentration up to 1000 mg/l of OH radical scavengers, which facilitates application to wastewater with a chemical oxygen demand of up to 1000 mg/l without diminishing the oxidation efficiency [40].

The determination of total mercury, and that of the organic forms as the difference between total and inorganic mercury, requires the use of a strong oxidant such as $KMnO_4$. The main shortcoming of this reagent is that it forms MnO_2 instead of Mn(II); the MnO_2 forms a film on the walls of vessels or tubing in batch or continuous approaches, respectively, in which mercury is adsorbed [41]. The use of US here avoids precipitation of

manganese dioxide thanks to the low concentration of $KMnO_4$ required (0.01%) and oxidation completes within 30 s and 8 min, depending of the complexity of the urine sample; this is much shorter than the 30 min required in unsonicated media.

The improved oxidation of organomercurials in cold-controlled temperature conditions (usually in ice-baths) has been ascribed to decreased cavitation and an increased risk of Hg volatilization at increased temperature.

Using the word "focused" to designate the action of US on the oxidation of organomecurials with a sonotrode dipped in the transmitting liquid can be misleading as nothing is used to "orientate" US in a given direction.

2.2.3. Oxidation of organic matter for chemical oxygen demand (COD) determination

The digestion of organic matter for COD determination can be assisted by US, which shortens the time required from hours to 3 min [45,46]. A conventional US bath cannot provide the amount of the energy needed, as does a probe dipped in a transmitting liquid; so direct insertion of the probe into the sample is mandatory for proper development of the oxidation. Also, the presence of an oxidant in a very acid medium severely shortens the lifetime of alloy-based probes, so glass probes should be used in their place [47]. Using a plastic or polyethylene round bottomed test tube to accommodate an alloy probe can also be more efficient than using a conventional transmitting bath [48].

As in other oxidation processes, increased temperatures have an adverse effect which also ascribed to the resulting increased vapour pressure leading to easier cavitation, but less violent collapse, as a consequence of the decreased viscosity and surface tension. As the temperature approaches the solvent boiling point, a large number of cavitation bubbles are formed concurrently that act as a barrier to sound transmission and dampen the effective US energy from the source to enter the liquid medium. A temperature close to room level is easy to maintain and ensures proper development of the process.

Bubbling a gas through an oxidizing medium subjected to US had a favourable effect on the process; no differences, however, were observed in the use of monoatomic (*e.g.* Kr, Ar, He) or diatomic gases (*e.g.* N_2, O_2, air), nor in the manner the gas was bubbled (before or during sonication).

Concerning interferences with the oxidation of organic matter in water, US-assisted oxidation tolerates the presence of chloride ions up to 7000 mg/l for 100 mg/l COD as potassium hydrogen phthalate (KHP), which is lower than the levels allowed by FI [49] and Ce(IV)-based methods [50] (*viz.* 30,000 and 10,000, respectively). Unfortunately, as with the conventional method, the ratios of measured and theoretical COD values depend on the particular target compounds.

2.2.4. Fast oxidation of oil for correlation with its oxidative stability

Measuring the resistance to oxidation is one way of establishing oil quality inasmuch as this property determines storage and usage stability. The length of the stability period (*viz.* the interval between oil production and the oil becoming rancid) depends both on intrinsic features (*e.g.* the contents in fatty acids

and natural antioxidants such as tocopherols and phenols) and environmental conditions (temperature, light, air exposure, type and material of the container, trace metal content) and the time the oil is exposed to them.

Chemical and physical tests for oxidative stability are based on the determination of either precusor hydroperoxides or oxidation end-products [51–54], and on oxygen absorption and gravimetric monitoring of the losses of volatile products [55,56]. Some methods based on the peroxide value [57,58] or phenol concentration [59] have been automated.

The stability of edible oils varies widely depending on seed type, one of the most stable being virgin olive oil. Stability also varies widely depending on both the olive variety (*e.g.* picual, manzanilla, arbequina, hojiblanca) and the production process. Because extra virgin olive oil is stable for several months under optimal storage conditions, its stability is traditionally determined in the laboratory using an accelerated oxidation test involving raising the temperature and exposing the oil to oxygen or air bubbled through it as in the Rancimat method [60]. The use of microwaves to accelerate oxidation reduces by 60–68% the time required by the Rancimat method [61] (*e.g.* from 129 to 43 h); however, because the microwave-based method is not automated, monitoring for 43 h is impracticable.

Ultrasound irradiation of an edible oil (particularly direct irradiation of the sample) causes fast oxidation of polyphenols present and produces a rancid smell as a result, mainly with easily oxidized oils such as those from sunflower [62]. Ultrasound energy allows Rancimat times of 129 h to be reduced to 50 min; therefore, the overall time required for the determination of oil stability, even for highly stable virgin olive oils, is less than 1 h [63].

The strong influence of temperature on US-assisted oxidation reactions entails placing the sample containers in a thermostated bath in order to ensure reproducible results.

2.3. Ultrasound-assisted hydrolysis reactions

Hydrolysis reactions in Analytical Chemistry are mainly used to convert the target analytes into easily derivatized and detected forms. Whereas the accelerating effect of US on these reactions has been widely proven and thoroughly studied in Organic Chemistry under different chemical (pH, aqueous–organic media) and US conditions [64–66], few analytical studies on them have been reported. By contrast, US-assisted enzymatic hydrolysis reactions have received considerable attention from analytical and bioanalytical chemists; such reactions, however, are better known as enzymatic digestions.

2.3.1. Hydrolysis of phenol compounds

The US-assisted leaching of phenol compounds from strawberries with an acetone solution containing 0.2 M HCl and 2 g/l *tert*-butyl-hydroquinone facilitates the hydrolysis of the target phenols and their dissolution in the leachant, thus accelerating their removal from the matrix. A titanium alloy probe (2.54 mm in diameter) was used to develop three 30-s cycles; the operating conditions included 50% US amplitude and 0.8-s pulses over 1 s for an overall time of 30 s. The yields resulting were simi-

lar to those obtained by maceration at 85–90 °C for 20 h, with no appreciable degradation [67]—which is one of the greater shortcomings of long leaching times [1]. Also in the case of US-assisted hydrolysis of paracetamol, the absorbances were five times higher than with non-sonicated hydrolysis [32].

2.3.2. Hydrolysis of carbohydrates

One of the most common hydrolysis reactions is that required to convert polysaccharides into monosaccharides prior to the determination of total carbohydrates in food and environmental samples. The use of highly acid media (*e.g.* 12 M sulphuric acid) and elevated temperatures (≈100 °C) for 20 min produces partial oxidation of carbohydrates [68]. Using room temperature to avoid oxidation results in incomplete hydrolysis [69], and so did lowering the concentration of sulphuric acid to 0.5 M while keeping the temperature at 100 °C for 8 h [70–72]. One of the most accurate ways of determining total carbohydrates is by using 1 M HCl at 100 °C for 20 h [73,74].

Existing studies on the US-assisted hydrolysis of carbohydrates have failed to clarify the behaviour of chemical systems upon US irradiation [75]. Thus, Dubois et al. used a US bath at a frequency of 35 kHz – no further details were reported – as, in their opinion, a probe highly increases the temperature of the irradiated system. They found very acid conditions (12 M sulphuric acid) to cause total degradation of carbohydrates—the sonicated solution exhibited no absorption at 485 nm after addition of phenol for development of the Dubois method [76]. They concluded that promoting hydrolysis in an acid medium – it is unclear whether they assayed different acid concentrations – is unavailable and performed the ultrasonicated hydrolysis step in pure water for 3 h, after which they added the acid to develop the derivatizing reaction. Further research on this topic is clearly required in order to clarify such an uncommon behaviour.

The above examples clearly show that the experience on hydrolysis largely acquired in dealing with organic compounds for non-analytical purposes [2–8] has been underexploited in the analytical field.

3. Ultrasound-assisted heterogeneous liquid–liquid systems

Heterogeneous liquid–liquid systems are quite common place in Analytical Chemistry, which uses them for a variety of purposes, including the following in relation to sample preparation: (1) analyte transfer from a phase to another, followed by (a) phase separation in order to feed only the phase enriched with the analyte to the detector or subject it to some other operation step prior to detection, or (b) continuous monitoring of the enriched phase without phase separation; (2) the formation of a heterogeneous medium – small droplets of one phase in another – which is the usual purpose of homogenization and emulsification. Ultrasound has been used to improve the outcome of (1) and (2), albeit with rather disparate results and frequency.

Although mass transfer between two immiscible phases (*i.e.* liquid–liquid) extraction is an old separation technique, the potential and effects of US on it (*viz.* acceleration of the transference and(or) displacement of the equilibrium) have scarcely been studied. By contrast, dispersion of a phase as small droplets into another under US-assistance until the initial heterogeneous liquid–liquid system is made uniform, which is known as "homogenization" or "emulsification", is a well-documented process in both the analytical and industrial fields. Depending on the operating conditions and frequency of ultrasound used, both emulsion formation and destruction can be favoured. One emergent field for US application involves liposomes, the formation of which and(or) their performance can be improved by this type of energy. The peculiar structure of liposomes and the growing interest of analytical chemists in them warrants their discussion here.

3.1. Ultrasound-assisted liquid–liquid extraction

Whether US facilitates mass transfer between two immiscible phases is arguable if one considers the ability of this form of energy to facilitate emulsification. Probably for this reason, analytical chemists have been reluctant to test US as a means for improving liquid–liquid extraction (LLE). In fact, US application most often produces stable emulsions that result in long phase separation times; therefore, US favours mass transfer between phases—provided the partitioning equilibrium involved facilitates the transfer. Efficient, fast liquid–liquid extraction entails avoiding or minimizing the former effect and maximizing the latter. These are several major factors to be optimized in US-assisted liquid–liquid extraction (USALLE).

3.1.1. Variables influencing ultrasound-assisted liquid–liquid extraction

Maximizing the extraction efficiency and minimizing emulsification of the immiscible phases in USALLE entails to optimizing both the typical US-related variables and those characteristic of LLE. In addition, the specific US-related variables to be optimized depend on whether (1) a discrete or continuous experimental approach is implemented, (2) a bath or a probe is used, (3) and direct immersion or a transmitting liquid (if a probe and a discrete approach are used) is employed.

3.1.2. Discrete ultrasound-assisted liquid–liquid extraction (USALLE) approaches

Most reported USALLE approaches are of the discrete type and use an ultrasonic bath. Usually, a vessel containing the sample and the immiscible, acceptor phase is immersed in the transmitting liquid held in a bath and the process involves application of US for a preset time, phase separation and repetition of the extraction cycle, if required. With slight differences, this procedure has been used to extract aroma compounds from must, wine [77–79], aged brandies and aqueous alcoholic wood extracts [80], or specific compound families such as monoterpenoids from wine [81], as well as volatiles [82], pesticides from honey [83] and methylmercury from biological materials [35].

In 1995, Cocito et al. demonstrated the usefulness of USALLE for extracting aromas from wine [77], later used by Hernanz Vila et al. [78] in combination with a factorial design to optimize extraction-related variables but not US-related variables. An interesting comparative study of aroma compounds

in aged brandies and aqueous alcoholic wood extracts involving US-assisted extraction was carried with a view to identifying the components of brandy aroma already present in grapes and wines [79], those formed in the distillation step and those coming from the oak wood [80]. The relative high standard deviations in some cases (0.1–18.4%) can be ascribed mainly to both irreproducibility in the US energy provided by the bath and the low extract volumes. The LLE temperature was controlled in none of the previous methods. This, together with typical decline in power of US baths, might be the origin of the high imprecision.

The discrete USALLE of monoterpenoids has been compared with direct immersion solid-phase microextraction (SPME) of these compounds from wine [81]. Samples were extracted three times under US application for 10 min, using 30, 10 and 10 ml of organic extractant and a constant temperature of 20 °C. For an unconvincing reason (namely, that chromatographic resolution was reduced through overlap of major compounds with minor ones with a greater number of cycles) the authors chose to use only three extraction cycles; however, the adverse effect of using more cycles could have been avoided by diluting the extracts, with the additional advantage that useful information about the extraction kinetics of the different compounds could have been obtained. The conclusions of this study were as follows: (1) both methods are suitable for the extraction of the target compounds from wines with subsequent GC individual separation with a view to classifying wines produced in different geographical zones; (2) both provide similar sensitivity and precision (CV < 5.5%); (3) ultrasound extraction is more efficient (95.1% versus 82.5%) and provides richer qualitative–quantitative flavour profiles; (4) the SPME method is faster (the greatest weakness of US extraction was the long time required to concentrate the extract under an inert atmosphere, 12 h) and uses less sample volume (7 ml versus 100 ml).

The usefulness of US for accelerating the LLE of compounds from honey lies mainly in the ability to operate at ambient temperature; by contrast, some techniques such as simultaneous distillation–extraction and purge and trap [1] are subject to thermal artifacts. Ultrasound-assisted liquid–liquid extraction has been used to extract volatile compounds from citrus flowers and citrus honey with a view to discriminating honey according to botanical origin [82], and also pesticides [83]. In this context, USALLE is faster than conventional methods and has the added advantage that it extracts compounds of molecular weight up to 220, which help to determine the origin of honey; this, however, calls for improved repeatability as the R.S.D. values for some compounds exceed 20%.

Pesticides such as atrazine and simazine have also been extracted from honey with the aid of an ultrasonic bath. In addition to the type of extractant, variables such as the extractant volume, sonication time and number of extraction cycles were optimized, the temperature and the height of the transmitting liquid in the bath being kept constant. A comparison of the ensuing method with its shake-flask extraction counterpart showed the former to be faster and more efficient, and to provide lower relative standard deviations [83].

One major criticism to all previous US-assisted methods is that they have not been compared with their unassisted coun-

terparts, so the influence of US on the results has not been quantified. This, however, is not the case with the method for pesticides in honey and that for the determination of mercury in biological materials proposed by Tu et al., which is based on acid leaching for 5 min, followed by simultaneous in situ derivatization and liquid–liquid extraction for 40 min in the presence of sodium tetraethylborate and nonane, buffered at pH 7.0, under US [35]. The mixture was shaken by hand and sonicated at 40 °C at a fixed US amplitude of 100%; however, the characteristics of the US bath used were omitted. Phase separation was effected by centrifugation at 5400 rpm for 5 min.

Another criticism to the previous methods is that their proponents have failed to state the type of US device used as they seemingly believe that ultrasonic baths are the sole available choice for this purpose. In fact, only one USALLE method using a probe appears to have been reported; the method was used to extract iron from largely organic solvents. Although the proponents gave no optimization details, they specified the depth of the US probe in the extraction system, the ultrasonication and silent periods, and the time required for phase separation. The use of a US probe rather than a conventional US bath was found to significantly improve the rate of emulsification – which was the aim pursued in this case for proper mass transfer – as the system became turbid within few seconds of starting the probe-based sonication step. However, no temperature control was used, nor were the typical variables of US probes (namely, power, pulse duration, amplitude) optimized; also the authors failed to distinguish sample and extract and used the word "sonoemulsification" to refer to the US-assisted step leading to iron extraction. The efficiency of US-assisted extraction (100.2%) was reduced to 21% under silent conditions [84].

Some authors have used US to ensure homogenization of the sample and an acid solution, and found application of this form of energy to dramatically reduce the time needed for conventional extraction in a separatory funnel [85]; others have used US to accelerate an oxidation step preceding or following conventional liquid–liquid extraction [42].

3.1.3. Continuous ultrasound-assisted liquid–liquid approaches

Dynamic approaches to USALLE have scarcely been explored even though manifolds for mass transfer from an organic phase to an aqueous and *vice versa* have been designed (see Fig. 2) and successfully applied [15,32]. Knowledge of the different ways to implement continuous liquid–liquid extraction (*e.g.* using the three usual devices – *viz.* segmenter, extraction coil and phase separator – by using none of them [86,87], or by using a segmenter and an extraction coil [88]) is advisable to understand the manifolds designed for this task. Figs. 2A and 3 show some of these US-assisted manifolds, which differ in the chemical system involved and whether one or both interfaces are monitored. Thus, the manifold in Fig. 2A is appropriate when only one of the interfaces is to be monitored and has been used for the USALLE of paracetamol from suppositories [32]. The time required for development of the method was significantly shorter than that required by the United States Pharmacopoeia (USP) method. In addition, the latter produces

emulsions that need about 30 min for phase separation after extraction.

Sequential monitoring of the two interfaces in each cycle is also possible. This can be exploited for two purposes, namely: (a) the simultaneous monitoring of the extraction process with and without US assistance by using a sample plug long enough to ensure irradiation of only one interface; (b) the simultaneous monitoring of the extraction process under assistance by a different type of energy (*e.g.* US and microwaves) at each interface. The manifold required differs depending on the nature of the donor and acceptor phases. Manifolds of both types have been designed for (a). The manifold in Fig. 3A is an available choice for the sequential monitoring of the two

interfaces in a chemical system involving extraction from an aqueous phase to an organic one. This manifold has been used to develop two methods for the extraction of two analytes from an aqueous phase, with or without a chemical reaction (*viz.* extraction of Fe(II) into a dichloromethane/*o*-phenanthroline phase with formation of the well-known red complex, and extraction of I_3^- into dichloromethane) [15]. The results for iodine reveal that the presence of US results in poorer extraction of this analyte. On the other hand, those for the water Fe(II)/*o*-phenantholine dichloromethane system reveal that the presence of US improves the extraction after several cycles; however, the improvement is very slight, so it does not justify the use of US here.

The manifold in Fig. 3B was designed for the sequential monitoring of the two interfaces of a chemical system involving extraction from an organic phase to an aqueous one. This manifold, the key element of which is an internally coupled valve system, has been used for the extraction and determination of phenols from extra virgin olive oil [15]. The method is based on the standard for this type of analytes and samples, which involves extraction of organic compounds into a Folin–Ciocalteu reagent solution, with monitoring of the product at 725 nm.

Multi-peak recordings can be obtained with manifolds shown in Fig. 3A and B by absorbance changes in the organic or aqueous phase, respectively, from extraction of analytes and monitoring at an appropriate wavelength. Fig. 4 shows the multi-peak recording corresponding to the extraction and determination of polyphenols from extra virgin olive oil. The peaks correspond alternately to sonicated and unsonicated interfaces and show that US is more effective than no sonication.

The reported evidence for USALLE allows the following conclusions to be drawn:

(1) Ultrasound does not always favour mass transfer between two immiscible phases.

Fig. 3. Flow injection manifolds for continuous US-assisted liquid–liquid extraction without phase separation. (A) Sequential monitoring of the two interfaces in a chemical system involving extraction from an aqueous phase to an organic one. (B) Sequential monitoring of the two interfaces in a chemical system involving extraction from an organic phase to an aqueous one. AP, aqueous phase; AS, aqueous sample; AV, auxiliary valve; C, coil; D, detection system; EAP, extractant aqueous phase; EC, extraction coil; IV, injection valve; MV, main valve; OP, organic phase; OS, organic sample; PC, personal computer; PL, propagating liquid; PP, peristaltic pump; SL, sub-loop; SV, switching valve; UP, ultrasonic probe; W, waste; WB, water bath (reproduced with permission of Elsevier, Ref. [15]).
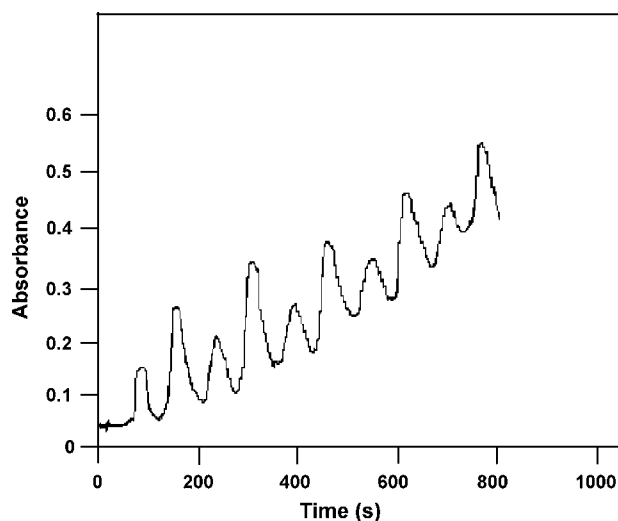

Fig. 4. Multi-peak recording obtained from continuous US-assisted liquid–liquid extraction by monitoring the two interfaces for the extraction of polyphenols from olive oil into a basic aqueous phase (reproduced with permission of Elsevier, Ref. [15]).

(2) Transfer from an organic phase to an aqueous one is more markedly favoured by US than is transfer from an aqueous phase to an organic one, which can be explained by the highest vapour pressure of the organic solvent tested and, therefore, its cushion effect on cavitation.

(3) The effect of US can be more significant when a chemical reaction occurs simultaneously with extraction. The influence of US on mass transfer and chemical reaction should be discriminated in order to select the latter.

(4) Available information is too scant to allow general rules on the behaviour of chemical systems under USALLE to be established.

3.2. Ultrasound-assisted homogenization and emulsification

Homogenization is commonly defined as a chemical or physical treatment by which the composition or structure of a substance (solid, liquid or gas) or mixture of substances is made uniform. The ability of US to effectively stir, mix or agitate a system without altering its chemical characteristics has been widely demonstrated and used in both laboratory and industry. At the laboratory scale, the use of homogenization in the analytical process is restricted to no key or optimized steps as the target system is sonicated for a time exceeding that strictly required to ensure adequate homogenization. However, homogenization of US-assisted processes occurs by virtue of the stirring, mixing and agitating capabilities of US.

Most applications of US-assisted homogenization whether analytical and non-analytical, involve liquid systems. Food processing industries have exploited US homogenization [89] as a key step in the processing of milk, yogurt and ice cream because it helps avoid creaming during incubation and storage. Bioprocesses also benefit from the use of US for continuous homogenization; this, coupled to immobilized metal affinity expanded bed adsorption, provides a new method for on-line purification of histidine-tag enhanced green fluorescent protein with yields close to 100% [90]. The pharmaceutical industry has used US during the tableting of powders [91].

Analytically, the most interesting systems are those formed by two or more immiscible liquids, homogenization of which is known as "emulsification" and dealt with separately on account of its importance.

3.2.1. Emulsification

According to Becher, an emulsion is a heterogeneous system consisting of two immiscible liquids one of which (the dispersed phase) is intimately dispersed in the other (the continuous phase) in the form of small droplets whose diameters generally exceed 0.1 μm [92]. Although emulsions are heterogeneous systems – they consist of two immiscible phases – emulsification is intended to produce a homogeneous system in terms of chemical structure. The type of emulsion formed, normally water-in-oil or oil-in-water, is commonly expressed as w/o or o/w, and determined by the volume ratio of the two liquids and also by the phase addition sequence and the nature of any additives used to promote emulsification [93]. Even if some additive is used,

the assistance of US is usually needed to disperse a liquid phase into the continuous phase and produce metastable mixtures as reducing large droplets to smaller ones involves additional shear forces and the viscous resistance during agitation absorbs most of the applied energy [94].

Ultrasound-assisted emulsification was initially developed by Wood and Loomis [95]. The first patent of an ultrasonic emulsifier was granted in 1944 in Switzerland. Since then, research into US-assisted emulsification and underlying mechanisms has grown in parallel to interest in the process [96]. Several possible mechanisms have been proposed to explain the influence of US energy on droplet formation and disruption. One assumes the formation of droplets as a consequence of unstable oscillations at the liquid–liquid interface ("capillary waves mechanism"). One mechanism similar to that of capillary waves is based on the oscillation and subsequent disruption of droplets under US action [97]. The most widely accepted mechanism for US-assisted emulsification is based on the effects of cavitation, which are deemed crucial for the process to develop [98–100].

3.2.2. Continuous and discrete US-assisted emulsification

Ever since the earliest uses of US energy to assist emulsification were reported, many scientists – analytical chemists included – and industrialists have used various types of US devices to make emulsions in a continuous or discrete manner. Although discrete emulsification can be accomplished with ultrasonic baths, probes are more frequently used for this purpose because they can directly transmit US energy to a liquid–liquid system [101,102].

Ultrasound-assisted emulsification in discrete systems allows the emulsification process to be monitored by withdrawing small portions of the liquid–liquid system [103]. Also, operators require no special training. The main shortcomings of discrete emulsification approaches is that large volumes may not be properly emulsified as a result of US intensity in the liquid–liquid system rapidly decreasing with increasing distance from the ultrasonic emitter. For this reason, many applications require stirring the two-phase system [104]. Thus, discrete approaches are useful for small batches; on the other hand, scale-up is difficult despite the increasing commercial availability of powerful industrial ultrasonic sources. In any case, little research on US emulsification processes with conditions similar to those of industrial practice has been published.

Dynamic US-assisted emulsification can be accomplished in completely continuous and stopped-flow systems. Both use a pre-mixing reservoir circuit in which the two immiscible liquids are pumped, a mixing point and a small reservoir near the flow-cell to sonicate the two-phase system. The dimensions and characteristics of the pre-mixing dictate the differences between stopped-flow and continuous approaches (see Fig. 5A and B, respectively). Thus, in stopped-flow systems, the premixer is a larger vessel furnished with pressure control [105]. In completely continuous approaches, the pre-mixer is a well-stirred glass cell where the two phases merge and are stirred in their way from the inlets to the outlet. The pre-mixing step is particularly important with viscous fluids, which can produce
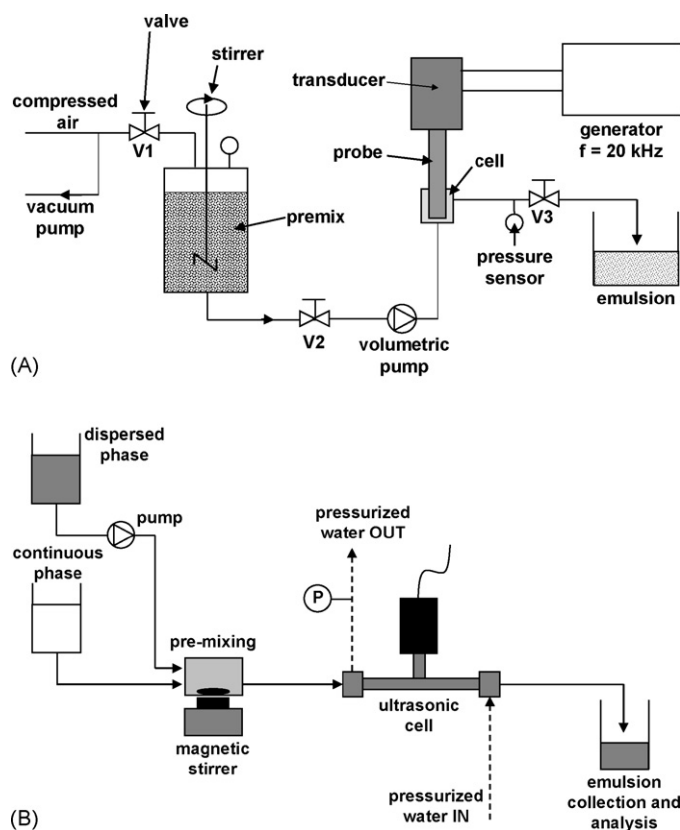
Fig. 5. Stopped-flow (A) and continuous (B) US-assisted emulsification approaches (reproduced with permission of Elsevier, Refs. [108,115]).

unstable interfacial waves [106]. This step provides a coarse emulsion that can be readily broken up further by ultrasonic energy.

In addition, continuous stopped-flow emulsification can be coupled to other physical and chemical operations (*e.g.* previous or subsequent steps of the analytical process). Unlike discrete systems, however, dynamic systems do not allow monitoring of the emulsification process. Similarly to discrete systems, the commonest choice of ultrasonic source in dynamic systems is a probe in direct contact with the two-phase system (see Fig. 5A). Alternative choices use one or several ultrasonic transducers and reflectors accommodated in the walls of the manifold tubing [106].

The efficiency of US-assisted emulsification has been compared with that of other mechanical alternatives in several studies. The most important conclusion is that, with US assistance, the size of emulsions is much smaller than with mechanical agitation under the same conditions; this makes sonicated emulsions more stable [96]. The main drawback of ultrasonic emulsification is the need to take special precautions to avoid surfactant degradation [107,108]; therefore, ultrasonic variables such as irradiation power [103,106], position of the ultrasonic source with respect to the liquid–liquid interface [102], tip diameter and vessel geometry [109], irradiation time [110], volume ratio of phases [109], viscosity [96,106,111], surfactant concentration [109,112], hydrostatic pressure and dissolved gas [113] must be exhaustively optimized and strictly controlled.

3.2.3. Applications of US-assisted emulsification

For the interest of analytical chemists, a large number of methods have been developed where ultrasonic emulsification is a key step in the determination of the target analytes. Most such methods are concerned with the determination of metallic elements in liquid samples by use of an atomic detector. One effective alternative to circumvent the shortcomings of liquid–liquid extraction prior to this type of detector is emulsification of the organic sample with an aqueous phase containing an acid or ligand [114,115].

Ultrasound-assisted emulsification in aqueous samples is the basis for the so-called "liquid membrane process" (LMP). This has been used mostly for the concentration and separation of metallic elements or other species such as weak acids and bases, hydrocarbons, gas mixtures and biologically important compounds such as amino acids [116–119]. Liquid membrane process has aroused much interest as an alternative to conventional liquid–liquid extraction [120–122].

Ultrasonic-assisted emulsification is commonplace in the pharmaceutical, cosmetic, food, chemical and other industries and it can be used in different situations ranging from normal conditions to others requiring manufacturing equipment that can be readily cleaned and sterilized [106].

Analytical applications in which the presence of water is undesirable can also take advantage of non-aqueous emulsions. These emulsions may be of pharmaceutical or cosmetic interest if they are primarily composed of edible and non-toxic ingredients; also, they can be formulated to exhibit a wide range of physical properties. Potential uses are as topical dermatological bases – particularly for labile drugs – as emollient bases for cosmetic preparations and as nutrient preparations. Stable non-aqueous emulsions can be obtained in two general ways. One involves surfactants consisting of two incompatible blocks selectively soluble in each of the immiscible liquids. Thus, diblock copolymers of polystyrene and polyisoprene can stabilize DMF–hexane emulsions for almost 24 h [123]. The main drawback of this approach is the need to develop new surfactants tailored to the particular liquid combination. The other choice is to find an appropriate oil-immiscible polar liquid that can substantially replace water as a surfactant solvent. A liquid capable of replacing water in an emulsion should possess an appreciable polarity to make it immiscible with oils and a good solvent for the solvophilic part of the surfactant molecules [124].

3.3. Joint use of ultrasound and liposomes

Liposomes are spherical vesicles formed by aggregation of amphiphilic phospholipids molecules in a bilayer structure. Liposome formation occurs when phospholipids are dispersed into an aqueous medium – usually water – as a result of interactions between phospholipids and water. The nature and properties of liposomes are directly related to the preparation method used (specifically, to the phospholipid composition) and to the presence of other chemical species in the liposome structure.

Liposomes can play two different roles in Analytical Chemistry [125]: (1) as target analytes or matrices for the target

analytes and (2) as analytical tools for some step of the analytical process.

Some liposomal determinations have exploited the advantages of US energy discussed. Typical examples include the determination of phosphatidylcholine in liposome suspensions using ICP-AES with an ultrasonic nebulizer [126] and that of the phospholipids–lipophilic compound ratio in liposomes by thin-layer chromatography scanning densitometry—which involves US-assisted preliminary extraction [127].

The use of liposomes as analytical tools – the formation of which can be greatly favoured by US – plays major roles towards improving analytical properties such as sensitivity and selectivity in some analytical steps. Applications in this area range from the preparation of liposomes or encapsulation of various types of compounds in the liposome structure to special processes in which US enhances the actuation of liposomes.

Although liposomes can form spontaneously, they are rarely thermodynamically stable, so they usually require some auxiliary energy such as mechanical agitation, electric energy, US, or combination of mechanical treatments. The main advantage of US assistance here is that it does not raise the temperature significantly.

Ultrasound can play a prominent role in the preparation of liposome-based sensors [128]. Encapsulation of water-soluble fluorescent dyes in liposomes assisted by US has also been used to immobilize liposome-encapsulated enzymes in sol–gel matrices for the preparation of biosensors [129].

Acoustically active liposomes have the potential to carry drugs and their acoustic activity allows them to respond to US stimulation by releasing their contents. The effect of US on content release is attributed to the rarefaction phase of the sound wave. Thus, when the negative US wave impinges upon the liposomes, the air pocket expands and stresses the bounding monolayers and also those in the adjacent bilayer. If the pressure drop is large enough, then the stress exceeds the elastic limit of the weakest surface and, at some point, either the bilayer or the monolayers rends. When the integrity of the vesicle is lost, some or all contents are released. If the air in the pocket is expanded faster than it is diffused to the external aqueous phase, then, the monolayer or bilayer reaches the lysis threshold and most liposomes release some contents. The ultrasonic frequency used for compounds delivery is about 1–2 MHz [130].

4. Conclusions

The long time during which research in sonochemistry has been conducted and the fact that no special equipment requirements are involved in using US energy – other, by contrast, "older" technologies such as electrochemistry require a conducting medium, photochemistry the presence of a chromophore and microwaves of dipolar species – have promoted the development of a large number and variety of applications which analytical chemists could exploit for sample preparation. Most such applications have been developed by using US devices present in most analytical laboratories (*e.g.* power ultrasonic devices with frequencies in the range 20–100 kHz); others, however, use unusual frequencies. Careful selection of the type and characteristics of

the US device will always be required as it can be the key to successful development of US-assisted methods, particularly those involving organic reagents [131].

References

[1] M.D. Luque de Castro, J.L. Luque-García, Acceleration and Automation of Solid Sample Treatment, Elsevier, Amsterdam, 2002.
[2] K.S. Suslick (Ed.), Ultrasound: Its Chemical, Physical and Biological Effects, VCH, Weinheim, Germany, 1988.
[3] T.J. Mason, J.P. Lorimer, Sonochemistry. Theory, Applications and Uses of Ultrasound in Chemistry, Ellis Horwood, Chichester, England, 1989.
[4] S.V. Ley, C.M.R. Low, Ultrasound and Synthesis, Springer-Verlag, Heidelberg, Germany, 1989.
[5] T.J. Mason (Ed.), Advances in Sonochemistry, JAI Press, London, England, 1990.
[6] T.J. Mason, Practical Sonochemistry. A Users Guide to Applications in Chemistry and Chemical Engineering, Ellis Horwood, Chichester, England, 1991.
[7] T.J. Mason, Sonochemistry, Oxford University Primer Series, No. 70, Oxford Science Publications, Oxford, England, 1999.
[8] T.J. Mason, J.P. Lorimer, Applied Sonochemistry, Wiley–VCH, Weinheim, Germany, 2002.
[9] P. Linares, F. Lázaro, M.D. Luque de Castro, M. Valcárcel, Anal. Chim. Acta 200 (1987) 51.
[10] E.W. Flosdorf, L.A. Chambers, J. Am. Chem. Soc. 55 (1933) 3051.
[11] A. Szalay, Phys. Chem. A 164 (1933) 234.
[12] A.S. Gyorgi, Nature (London) 131 (1933) 278.
[13] M. Korn, P. Machado Primo, C. Santos de Sousa, Microchem. J. 73 (2002) 273.
[14] C. Santos de Sousa, M. Korn, Anal. Chim. Acta 444 (2001) 309.
[15] J. Ruiz-Jiménez, M.D. Luque de Castro, Anal. Chim. Acta 489 (2003) 1.
[16] B. Fransson, U. Ragnarsson, J. Chromatogr. 827 (1998) 31.
[17] L. Liu, P.K. Dasgupta, Anal. Chem. 68 (1996) 1817.
[18] M.A. Jeannot, F.F. Cantwell, Anal. Chem. 68 (1996) 2236.
[19] E. Psillakis, N. Kalogerakis, Trends Anal. Chem. 21 (2002) 54.
[20] Y.C. Fiamegos, C.G. Nanos, C.D. Stalikas, J. Chromatogr. 813 (2004) 89.
[21] A. di Corcia, J. Chromatogr. 80 (1973) 69.
[22] P. Buryan, J. Macak, J. Hrivna, J. Chromatogr. 137 (1977) 425.
[23] Y. Hoshika, J. Chromatogr. 144 (1977) 181.
[24] J.N. Seiben, D.G. Crosby, H. Fonda, C.J. Soderquist, J. Chromatogr. 73 (1972) 89.
[25] R.J. Agauer, Anal. Chem. 40 (1968) 122.
[26] Y.I. Korenman, I.V. Gruzdev, B.M. Kondratenok, V.N. Fokin, Anal. Chem. 54 (1989) 1134.
[27] S. Nakamura, M. Takino, S. Dasihima, Analyst 126 (2001) 3089.
[28] L.E. Sojo, J. Djauhari, J. Chromatogr. 840 (1999) 21.
[29] I. Turnes, I. Rodríguez, C.M. García, R. Cela, J. Chromatogr. 743 (1996) 283.
[30] M.D. Luque de Castro, A. Jurado López, Anal. Sci. (2004) 538.
[31] E. Priego-López, M.D. Luque de Castro, Chromatographia 57 (2003) 513.
[32] F. Priego-Capote, M.D. Luque de Castro, Anal. Chim. Acta 489 (2003) 223.
[33] S. Rapsomanikis, O.F.X. Donard, J.H. Weber, Anal. Chem. 58 (1986) 35.
[34] N. Bloom, Can. J. Fish. Aquat. Sci. 46 (1989) 1131.
[35] Q. Tu, J. Qian, W. Frech, J. Anal. At. Spectrom. 15 (2000) 1361.
[36] S. da Silva Borges, M. Korn, Quim. Nova 25 (2002) 558.

[37] S. da Silva Borges, M. Korn, J.L.F. Costa Lima, Anal. Sci. 18 (2002) 1361.
[38] M. Korn, M.V.A.S. Andrade, S. da Silva Borges, C.S. Sousa, F.S. Oliveira, J. Braz. Chem. Soc. 14 (2003) 254.
[39] F. Battin-Leclerc, F. Baronnet, G. Paternotte, J.P. Leclerc, R. Gourhan, J. Anal. Appl. Pyrolysis 53 (2000) 95.
[40] J.L. Capelo, I. Lavilla, C. Bendicho, Anal. Chem. 72 (2000) 4979.
[41] J.L. Capelo, C. Maduro, A.M. Mota, J. Anal. At. Spectrom. 19 (2004) 414.
[42] J.L. Capelo, C.D. dos Reis, C. Maduro, A.M. Mota, Talanta 64 (2004) 217.
[43] J.L. Capelo, C. Maduro, A.M. Mota, Ultrason. Sonochem. 13 (2006) 98.
[44] J.T. Creed, T.D. Martin, C.A. Brockholl, J. Anal. At. Spectrom. 10 (1995) 443.
[45] J.M.H. Appleton, J.F. Tyson, R.P. Mounce, Anal. Chim. Acta 179 (1986) 269.
[46] L. Tian, A. Wu, Anal. Chim. Acta 261 (1992) 301.
[47] A. Canals, M.R. Hernández, Anal. Bioanal. Chem. 374 (2002) 1132.
[48] A. Canals, A. Cuesta, L. Gras, M.R. Hernández, Ultrason. Sonochem. 9 (2002) 143.
[49] T. Korenaga, X. Zhou, O. Kimido, T. Moriwake, S. Shinoda, Anal. Chim. Acta 272 (1993) 237.
[50] A. Cuesta, J.L. Todolí, J. Mora, A. Canals, Anal. Chim. Acta 372 (1998) 399.
[51] K. Robards, A.F. Kerr, E. Patsalides, Analyst 113 (1988) 213.
[52] J. Tsaknis, S. Lalas, M. Hole, G. Smith, V. Tychopoulos, Analyst 123 (1988) 325.
[53] T. Chiba, M. Takazawa, K. Fujimoto, JAOCS 66 (1989) 1588.
[54] E.K. Strochkova, Y. Turyan, I. Kuselman, Talanta 54 (2001) 411.
[55] J.A. García-Mesa, M.D. Luque de Castro, M. Valcárcel, Lab. Robotics Autom. 5 (1993) 29.
[56] J.A. García-Mesa, M.D. Luque de Castro, M. Valcárcel, Talanta 11 (1993) 1595.
[57] P.G. Nouros, C.A. Georgiou, M.G. Polissiou, Anal. Chim. Acta 389 (1999) 239.
[58] J.A. García-Mesa, M.D. Luque de Castro, M. Valcárcel, Analyst 118 (1993) 891.
[59] M.P. Cañizares, M.D. Luque de Castro, Anal. Chim. Acta 323 (1996) 55.
[60] M.W. Laubli, P.A. Bruttel, JAOCS 63 (1986) 772.
[61] M.P. Cañizares, J.A. García-Mesa, M.D. Luque de Castro, Anal. Biochem. Chem. 378 (2004) 479.
[62] F. Chemat, I. Grondin, A.S.C. Sing, J. Smadja, Ultrason. Sonochem. 11 (2004) 13.
[63] M.P. Cañizares, J.A. García-Mesa, M.D. Luque de Castro, Anal. Chim. Acta 502 (2004) 161.
[64] J.N. Chen, W.M. Kalback, Ind. Eng. Chem. Fundam. 6 (1967) 175.
[65] S. Fogler, D. Barnes, Ind. Eng. Chem. Fundam. 7 (1968) 222.
[66] E.C. Couppis, G.E. Klinzing, AJChE J. 20 (1974) 485.
[67] M.C. Herrera, M.D. Luque de Castro, Anal. Biochem. Chem. 379 (2004) 1106.
[68] B. Josefsson, L. Uppstrom, G. Ostling, Deep-Sea Res. 19 (1972) 385.
[69] J.D. Pakulsky, R. Benner, Mar. Chem. 40 (1992) 143.
[70] A. Compiano, J. Romano, F. Garabetian, P. Laborde, I. de la Giraudière, Mar. Chem. 42 (1993) 237.
[71] M. Kakuta, A. Misaky, Agric. Biol. Chem. 43 (1979) 993.
[72] M. Kakuta, A. Misaky, Agric. Biol. Chem. 43 (1979) 1269.
[73] S.M. Myklestad, E. Skanoy, S. Hestmann, Mar. Chem. 56 (1997) 279.
[74] C.M. Burney, J.Mc.N. Sieburth, Mar. Chem. 5 (1977) 15.
[75] M. Mecozzi, M. Amici, E. Pietrantonio, R. Acquistucci, Ultrason. Sonochem. 6 (1999) 133.
[76] M. Dubois, K.A. Gilles, J.K. Hamilton, P.A. Rebers, F. Smith, Anal. Chem. 28 (1956) 350.
[77] C. Cocito, G. Caetano, C. Delfini, Food Chem. 5 (1995) 311.
[78] D. Hernanz Vila, F.J. Heredia Mira, R. Beltrán Lucena, M.A. Fernández Recamales, Talanta 50 (1999) 413.
[79] E. Gómez-Plaza, R. Gil-Muñoz, J. Carreño-Espín, J.A. Fernández-López, A. Martínez-Cutillas, Eur. Food. Res. Technol. 209 (1999) 257.
[80] I. Caldeira, R. Pereira, M.C. Clímaco, A.P. Belchior, R.B. de Sousa, Anal. Chim. Acta 513 (2004) 125.
[81] R.M. Peña, J. Barciela, C. Herrero, S. García-Martín, Talanta 67 (2005) 129.
[82] E. Alissandrakis, D. Daferera, P.A. Tarantilis, M. Polissiou, P.C. Harizanis, Food Chem. 82 (2003) 575.
[83] I. Rezic, A.J.M. Horvat, S. Babic, M. Kastelan-Macan, Ultrason. Sonochem. 12 (2005) 477.
[84] A.J. Wain, N.S. Lawrence, J. Davis, R.G. Compton, Analyst 127 (2002) 8.
[85] A. González Casado, E.J. Alonso Hernández, J.L. Vílchez, Water Res. 32 (1998) 3168.
[86] M. Agudo, A. Ríos, M. Valcárcel, Analyst 119 (1994) 2097.
[87] J.M. López-Fernández, A. Ríos, M. Valcárcel, Fresenius J. Anal. Chem. 356 (1996) 49.
[88] F. Ortiz-Boyer, J.A. García-Mesa, M.D. Luque de Castro, Anal. Chem. 66 (1994) 2794.
[89] T.J. Mason, L. Paniwnyk, J.P. Lorimer, Ultrason. Sonochem. 3 (1996) S253.
[90] A.M. Noubhani, W. Dieryck, S. Chevalier, X. Santarelli, J. Chromatogr. 968 (2002) 113.
[91] I. Caraballo, M. Millán, A. Fini, L. Rodríguez, C. Cavallari, J. Control. Release 69 (2000) 345.
[92] P. Becher, Emulsions, Theory and Practice, Reinhold, New York, 1965.
[93] S.E. Friberg, S. Jones, Kirk-Othmer Encyclopedia of Chemical Technology, vol. 9, Wiley, New York, 1994.
[94] P. Walstra, Chem. Eng. Sci. 48 (1993) 333.
[95] R.W. Wood, A.L. Loomis, Philos. Mag. 4 (1927) 417.
[96] O. Behrend, K. Ax, H. Schubert, Ultrason. Sonochem. 7 (2000) 77.
[97] E.S. Rajagopal, Principles of Emulsion Formation: Sonic and Ultrasonic Emulsification, Emulsion Science, Academic Press, London, 1968.
[98] W. Lauterborn, C.D. Ohl, Ultrason. Sonochem. 4 (1997) 65.
[99] M.K. Li, H.S. Fogler, J. Fluid Mech. 88 (1978) 499.
[100] M.K. Li, H.S. Fogler, J. Fluid Mech. 88 (1978) 513.
[101] N.P. Vichare, P.R. Gogate, V.Y. Dindore, A.B. Pandit, Ultrason. Sonochem. 8 (2001) 23.
[102] M. Sivakumar, P. Senthikumar, S. Majumdar, A.B. Pandit, Ultrason. Sonochem. 9 (2002) 25.
[103] B. Abismaïl, J.P. Canselier, A.M. Wilhelm, H. Delmas, C. Gourdon, Ultrason. Sonochem. 7 (2000) 187.
[104] Y.F. Maa, C.C. Hsu, Pharm. Dev. Technol. 4 (1999) 233.
[105] H. Hielscher, UK Patent Application 2,250,930 (1991).
[106] S. Freitas, G. Hielscher, H.P. Merkle, B. Gander, Ultrason. Sonochem. 13 (2006) 76.
[107] A.E. Alegria, Y. Lion, T. Kondo, P. Riesz, J. Phys. Chem. 93 (1989) 4908.
[108] K. Makino, M.M. Mossoba, P. Riesz, J. Am. Chem. Soc. 104 (1982) 8537.
[109] R.S. Juang, K.H. Lin, Colloids Surf. A: Physicochem. Eng. Aspects 238 (2004) 43.
[110] Branson, Fairview Estate, Clayton Road, Hayes, Middlesex UB31AN, UK.
[111] H.B. Briggs, J.B. Johnson, W.P. Mason, J. Acoust. Soc. Am. 19 (1947) 664.
[112] B. Abismaïl, J.P. Canselier, A.M. Wilhelm, H. Delmas, C. Gourdon, Ultrason. Sonochem. 6 (1999) 75.
[113] O. Behrend, H. Schubert, Ultrason. Sonochem. 8 (2001) 271.
[114] M. Murillo, A. González, A. Ramírez, N. Guillén, At. Spectrosc. 15 (1994) 90.
[115] T.B. Wang, X.J. Jia, J. Wu, J. Pharm. Biomed. Anal. 33 (2003) 639.
[116] G. Schulz, Desalination 68 (1988) 191.
[117] C. del Cerro, D. Boey, Chem. Ind. 21 (1988) 681.
[118] M.P. Thien, T.A. Hatton, Sep. Sci. Technol. 23 (1988) 819.
[119] F. Nakashio, J. Chem. Eng. Jpn. 26 (1993) 123.
[120] M. Nakao, H. Matsumiya, M. Hiraide, Bunseki Kagaku 53 (2004) 975.
[121] H. Matsumiya, T. Kageyama, M. Hiraide, Anal. Chim. Acta 507 (2004) 209.
[122] M. Hiraide, K. Hasegawa, Fresenius J. Anal. Chem. 363 (1999) 261.
[123] A. Imhof, D.J. Pine, J. Colloid Interf. Sci. 192 (1997) 368.

[124] T. Sakthivel, V. Jaitely, N.V. Patel, A.T. Florence, Int. J. Pharm. 214 (2001) 43.

[125] A. Gómez-Hens, J.M. Fernández-Romero, Trends Anal. Chem. 24 (2005) 9.

[126] T. Kamidate, T. Suita, H. Watanabe, Anal. Biochem. 241 (1996) 264.

[127] S. Rodríguez, M.V. Cesio, H. Heinzen, P. Moyna, Lipids 35 (2000) 1033.

[128] T. Nguyen, K.P. McNamara, Z. Rosenzweig, Anal. Chim. Acta 400 (1999) 45.

[129] V. Vamvakaki, D. Fournier, N.A. Chaniotakis, Biosens. Bioelectron. 21 (2005) 384.

[130] S.L. Huang, R.C. MacDonald, Biochim. Biophys. Acta 1665 (2004) 134.

[131] J.L. Luche, C. Petrier, J.P. Lansard, A.E. Greene, J. Org. Chem. 48 (1983) 3837.

A pH-stat study of the reaction of some transition metal cations with disodium ethylenedinitrilotetraacetate (EDTA) and its analytical application

Carlo Maccà, Lidia Soldà *, Gabriella Favaro, Paolo Pastore

Department of Chemical Sciences, University of Padua, via Marzolo 1, Padova I-35131, Italy

Abstract

The pH-stat titration technique is an autonomous and very powerful tool for performing and monitoring chelatometric titrations of metal cations with great accuracy, poorly known, however, and seldom exploited. Based on measurement of the amount of strong base required to keep the pH of the test solution at a selected value during stepwise known additions of ethylenedinitrilotetraacetate (EDTA), it requires a glass electrode as the only sensor and is easily implemented on potentiometric titrators. It was introduced a quarter of century ago on an empirical basis for a very peculiar purpose (determination of calcium in diary products), but only very recently it was generalised and its fundamentals were thoroughly examined. In this work, pH-static titrations of some transition metal cations of analytical relevance (Co^{2+}, Cu^{2+}, Mn^{2+}, Zn^{2+}) were thoroughly investigated in the acid pH range between 2.3 and 5 or 7 (the highest pH depending on the metal hydroxide or carbonate solubility). The results at higher acidity showed unsuspected properties of such chelation reactions. At moderately acid pH (generally ≥ 4), indeed, pH-static titrations yield results of high precision and accuracy. On decreasing pH, however, the reaction stoichiomety deviates more and more from the 1:1 ratio between chelating agent and cation, seemingly because of formation of binuclear complexes, an occurrence very seldom mentioned in the current literature. The optimal titration conditions for each metal are defined, and directions for establishing a laboratory protocol for quantitative determinations are given.
© 2006 Elsevier B.V. All rights reserved.

Keywords: Chelatometric titrations; pH-static titrations; Co(II); Cu(II); Mn(II); Zn(II); EDTA complexes

1. Introduction

The automatic control of pH during chemical and biochemical reactions was conceived more than half-a-century ago [1], and the pH-stat operating function is currently available in dedicated instruments as well as in high-performance potentiometric titrators. Monitoring acid-base[2] and complexometric[3] titrations by using the pH-stat data alone, i.e., without measuring any physical quantity other than the control pH and the ongoing volumes of titrants, was also suggested long ago. In pH-stat complexometric titrations of cations with a protonated chelating agent, like disodium ethylenedinitrilotetraacetate (EDTA), the pH is kept at a preselected value by neutralising with a solution of strong base the protons delivered by the titration reaction. In such titrations, the independent or "controlled" variable is, as usual, the volume of chelating agent standard solution; the peculiar dependent or "measured" variable is the volume of strong base solution. The titration course is therefore represented by the plot of the volume V_{OH} of "auxiliary" titrant (the strong base) against the volume V_Y of "primary" titrant (the chelating agent). Inverse titration of a complexing agent with a metal cation can also be performed [4–6] using the same auxiliary titrant.

In suitable conditions, complexometric titrations provide plots composed of two linear segments that converge in correspondence of the equivalence point, which is thus very sharply detected. Therefore, pH-static titration can be considered a technique of choice, particularly when specific sensing devices (indicators, ion-selective electrodes, etc.) are missing, unsatisfactory or too demanding. Indeed, one and the same sensor, the commonly available and inexpensive combined pH electrode, is used for whatever titration.

The direct use of pH-static titration data was also found profitable in investigating multiple complexation equilibria [7]. In the past, however, these opportunities were only very seldom

* Corresponding author.
E-mail address: lidia.solda@unipd.it (L. Soldà).

exploited [8]. Less infrequent, although not widespread, was assisting complexometric titrations with pH-stat apparatus in substitution of pH buffers, particularly for investigating solution equilibria (for instance, by means of ion-selective electrodes) in the absence of any interfering species; however, the valuable pH-static data thus produced was generally neglected.

The fundamentals of the pH-stat monitoring of chelatometric titrations for analytical purpose have been thoroughly discussed in a recent article [9]. A few practical examples (titrations of Ca(II), Cu(II), Mg(II) and Zn(II) with EDTA) [10] have shown that the pH-stat technique provides quantitative determinations of highest accuracy and precision, hardly attainable with common methods, and that it can work finely at more acidic pH values than allowed or prescribed in traditional titrations. It was also shown [9,10] that pH-static titrations can yield considerably improved stability constants of protonated complexes of the type MHY^{m-3}.

The present investigation was undertaken as a part of a research project aiming to study speciation and availability of nutritional cations contained in animal feed supplements. In that project, pH-static titrations are used for the quantitative determination of such cations in commercial products and in their aqueous extracts. More interestingly, they are intended to support potentiometric titrations with ion-selective electrodes when speciation is investigated or must not be disturbed, with the bonus of providing, together with potentiometric data free from buffer interferences, a second useful and largely independent data set. For this aim, a thorough study of the properties of the relevant titrations in a larger pH range than usually considered (and than formerly investigated for Cu(II) and Zn(II)) was deemed essential. It was also wanted to grasp the opportunity for investigating the equilibria between metal cations and protonated forms of EDTA, i.e., for determining the formation constants of MH_iY^{i-2} complexes (where M is a divalent cation).

The results here presented are focused on some transition metal cations of highest interest in animal nutrition, i.e., Co^{2+}, Cu^{2+}, Mn^{2+} and Zn^{2+}. Titrations were made in the pH range between 2.3 and 5 or 7, the higher limit depending on metal hydroxide or carbonate solubility. It was found, as expected [9,10], that protonated complexes do affect the shape of pH-stat titration plots, the more so, the lower is the experimental ("control") pH. Much less expected was, however, an increasing departure of the chelation reaction from the 1:1 stoichiometric ratio with decreasing pH, corresponding to an apparently increasing titre of EDTA. This occurrence can only be assigned to formation of binuclear complexes, seldom, if ever, mentioned in the relevant literature.

Investigation of this matter can have outputs of two different orders. Stating the conditions where chelatometric titrations performed with the pH-stat technique (and possibly with any other technique) can give correct results, unaffected, in particular, by uncertain stoichiometry, is of great concern for analytical applications. Conversely, providing a deeper insight in chelation equilibria and, eventually, determining relevant thermodynamic quantities has a strong fundamental interest. The present report only regards the quantitative aspect of the titrations considered, and gives essential directions for establishing a protocol for

chelatometric analyses monitored with the pH-stat technique. Such a protocol is in current use in our laboratory, in particular for standardising cation solutions to be employed in subsequent experiments. The second aspect, which requires deeper consideration and is possibly of interest for a different audience, will be dealt with in a separate article.

2. Experimental

2.1. Chemicals

All chemicals were analytical grade or better. All solutions were prepared with ultrapure water from a Milli-Q Plus apparatus (Millipore, Bedford, MA, USA).

Stock solutions of metal cations were prepared from analytical grade reagents: Co spherules, $CuSO_4 \cdot 5 H_2O$, $MnSO_4 \cdot H_2O$, ZnO. Zinc oxide was dissolved in perchloric acid; cobalt, after washing in diluted nitric acid and drying, was dissolved in concentrate nitric acid; copper and manganese sulphates were dissolved in water. The ionic strength of all solutions was made 0.1 M with sodium perchlorate. Solutions with lower titre were prepared by dilution with 0.1 M sodium perchlorate. The concentrations obtained by titrating by the pH-stat procedure here described at pH 4–5 (Cu(II)) and 5–7 (Co(II), Mn(II), Zn(II)) were taken as the effective titres.

The primary titrant solution of 0.1 M EDTA was prepared from analytical grade dihydrate disodium salt $Na_2H_2Y \cdot 2 H_2O$ (Titriplex® III Merck, Darmstad, D) and standardised by pH-static titration against primary standard calcium carbonate. A 0.1000 M sodium hydroxide low in carbonate (sodium carbonate <0.2%), BDH Italia (Milano, I) cat. 191503E, was used as the auxiliary titrant. It was kept in the original bottle and protected with a trap against carbon dioxide.

2.2. Apparatus

The measured solution was contained in a 20–90 cm³ jacketed cell (Metrohm Italiana, Origgio, I) thermostated at $25.0 \pm 0.1 °C$, stirred with a PTFE-coated magnetic bar at a fixed speed (400 rpm), and fluxed with carbon dioxide-free nitrogen.

The primary titrant (EDTA standard solution) was dispensed with an 1 cm³ syringe 1001 TLL (Hamilton, Bonaduz, CH) mounted on a computer-controlled motor burette Microbur 2030 (Crison, Barcelona, SP); an home-made computer programme allowed to choose the volume step, a fixed time interval between additions, and the number of additions. The auxiliary titrant (NaOH standard solution) was dispensed with a 2.5 cm³ syringe 1002 TLL (Hamilton) and a second Microbur 2030 connected to a programmable potentiometric titrator MicroTT 2050 (Crison) which operated the pH-stat control and recorded the data list (see Section 2.3, Procedure) by means of an Epson LX-400 printer. The signal from a combined glass electrode with encapsulated Ag/AgCl reference electrode in 3 M KCl and sleeve junction (Ingold, Urdorf, CH, type 405.60.88.E) was measured with a resolution of 0.1 mV. The resolution of the volume delivered by either burette was 1/2500 of the total volume; the accuracy was determined to be better than resolution. The standard perchloric

acid solution used for calibrating the electrode in some experiments, and other solutions for preliminary pH adjustment, were dispensed with similar computer-controlled syringes.

Titrations simultaneously monitored by pH-stat technique and by potentiometry with ion-selective electrode were performed with a potentiometric titrator 836 Titrando (Metrohm) with two galvanically separate measuring interfaces. Reactants were delivered with two motors 800 Dosino with 807 Dosing Units (volume $2\,cm^3$, resolution $2 \times 10^{-5}\,cm^3$). Operation was computer-controlled through the dedicated software Tiamo. The combined pH electrode was LL Ecotrode Plus (all from Metrohm Italiana, Origgio, VA). The copper ISE was F1112Cu Selectrode (Radiometer, Copenhagen, DK) with copper selenide membrane.

2.3. Procedure

When titrations were merely aimed to quantitative determination, preliminary pH calibration was made with buffers at pH 4.0 and 7.0. In order to take advantage of the better resolution of the instrumental reading (0.1 mV against 0.01 pH), the e.m.f. ΔE delivered by the combined glass electrode was measured. The ΔE value corresponding to the wanted operating pH was calculated by linear interpolation.

Test solutions were prepared by mixing a known volume (20 or $25\,cm^3$) of supporting solution containing $0.1\,mol\,dm^{-3}$ of inert electrolyte (sodium perchlorate or potassium nitrate) as ionic strength buffer, a small volume of a suitable pH buffering substance, and an accurately measured volume (generally $5\,cm^3$) of standard solution of the target cation. The buffer, at final concentration not higher than $5 \times 10^{-3}\,M$, has the function of dampening the pH oscillations caused by the primary titrant additions, which would otherwise make the stat action less effective. At $pH \leq 2.5$–2.7, the corresponding concentration of perchloric acid was fit to the purpose; on increasing pH up to 7, chloroacetic acid, acetic acid, hexametilene tetramine and triethanolamine were used in turn as buffering substances.

Operation was started by neutralising the excess acid (coming from the cation's acid solution, from the preliminary calibration in situ, see below, or from the buffer substance) with strong base up to approximately the selected operating pH (i.e., ΔE) by using the titrator's pre-set end-point function. If the resulting pH was near to the selected value, no further adjustment was made, and the measured e.m.f. value was set as the definitive control parameter ΔE_c of the Stat programme. The other instrumental parameters to be set in the titration programme were selected on the basis of a few preliminary experiments or of experience, in order that at every titration step, causing an increase of the ΔE signal, the control value was rapidly and exactly (within not more than 0.1 mV) restored. In practice, such parameters were dependent on the metal cation concentration, on the buffer power of the titrated solution, and on the reaction stoichiometry (mol of acidity delivered per mol of metal reacted), which depends, in turn, on the pH_c value. Finally, titration was started by activating the Stat function and, after 30 or 60 s, a series of constant-volume ($\Delta V_Y = 20$–80 µl) EDTA additions at fixed time intervals (60, 90 or 120 s). The numerical titration report recorded by the pH-stat

apparatus listed, at 10 s intervals, the time elapsed, the measured ΔE and the total volume V_{OH} of sodium hydroxide delivered. The time distance between additions had to be sufficient to reach completion (or equilibrium) of EDTA reaction, as shown by ending NaOH addition as well as by stabilised ΔE.

The pH-stat titration data file, V_{OH} versus the total EDTA volume V_Y, was assembled by selecting from the report the final V_{OH} values that, after each EDTA addition, restored (ideally within ± 0.1 mV) the control ΔE_c, and pairing them with the corresponding V_Y. The equivalence volume of the primary titrant, $(V_Y)_e$, was determined as the abscissa of the intersection between two straight-line segments interpolated, by least-square analysis, between the relevant experimental points. Data was treated with SigmaPlot scientific graphic software (Jandel Scientific, Erkrath, D).

In titrations also intended for determining the stability constants of protonated complexes (in practice, in most titrations at pH <4), the electrode was calibrated to measure the cologarithm of hydronium ion concentration $pH_c = -\log[H^+]$ [11,12]. Calibration was made in the range of about 4.7–2.3 pH_c by stepwise addition of standard perchloric acid directly in the measuring cell filled with 20 or $25\,cm^3$ of 0.1 M sodium perchlorate supporting solution,. Thereafter, the cation solution and (when the operational pH was higher than 2.5–2.7) the pH buffer were added, and operation was started as described above.

3. Results and discussion

3.1. The shape of pH-stat titration plots and the reaction stoichiometry

Solutions containing about 1–5 $mmol\,dm^{-3}$ of Co^{2+}, Cu^{2+}, Mn^{2+} and Zn^{2+} were titrated by the pH-stat technique at pH values from 2.3–2.5 to 5 (for copper) or to 7 (for the other cations). The highest experimental pH was just acid enough to prevent precipitation of metal hydroxide or carbonate in air-saturated solution [13]. Examples of experimental titration plots of solutions containing the same amounts of single metals at different pH are shown in Figs. 1–4.

Previous investigations [9,10] have shown that chelatometric titrations by the pH-stat technique reach their highest precision and accuracy in a defined pH range, depending on the single titrated cation. Obvious factors determining the optimum range are the dependence on pH of cation solubility, which determines the highest exploitable pH, and of the conditional stability constant of its chelate, which sets the lowest pH at which the reaction is still sufficiently although not completely quantitative. Other pH-dependent factors, however, can play a decisive role, and frequently cause the optimum pH range to differ from that prevailing in other techniques [9,10].

The pH-static titrations are represented by plotting against the volume V_Y of primary titrant (the standard solution of chelating agent) against the volume V_{OH} of strong base solution (the auxiliary titrant) delivered by the pH-stat device in order to neutralise the protons set free by the reaction of Na_2H_2Y with the metal cation. As long as the reaction is virtually complete, such plots are composed of two linear segments of different slopes, whose

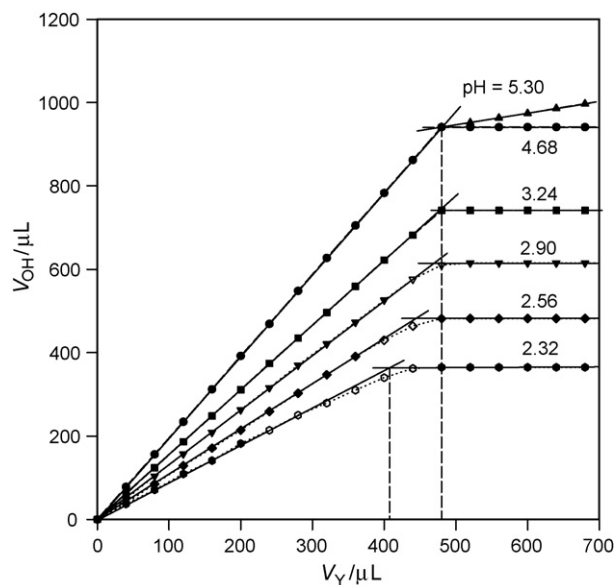Fig. 1. Experimental plots of V_{OH} vs. V_Y for a series of pH-static titrations of 1.5×10^{-3} M Co^{2+} (4.85×10^{-5} mol in about 32 ml of 0.1 M NaClO$_4$) with 0.1 M EDTA and 0.1 M NaOH at various pH (Points with open symbols were not used in linear regression.).
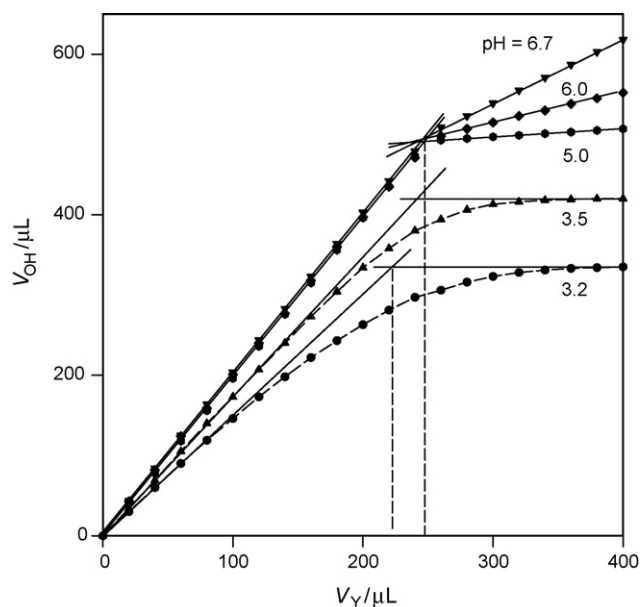

Fig. 3. Experimental plots of V_{OH} vs. V_Y for a series of pH-stat titrations of 0.96×10^{-3} M Mn^{2+} (2.49×10^{-5} mol in about 26 ml of 0.1 M NaClO$_4$) at various pH.

intersection is ideally coincident with the theoretical equivalence point, $N_M = (N_Y)_e = C_Y(V_Y)_e$ where $(V_Y)_e$ is the abscissa of the intersection point, taken as the end-point volume and used to calculate the analyte amount, and the other symbols have obvious meaning.

The molar ratio $\Delta N_{OH}/\Delta N_Y$ of the auxiliary to the primary titrant added at each titration step, and, in practice, the experimental slope

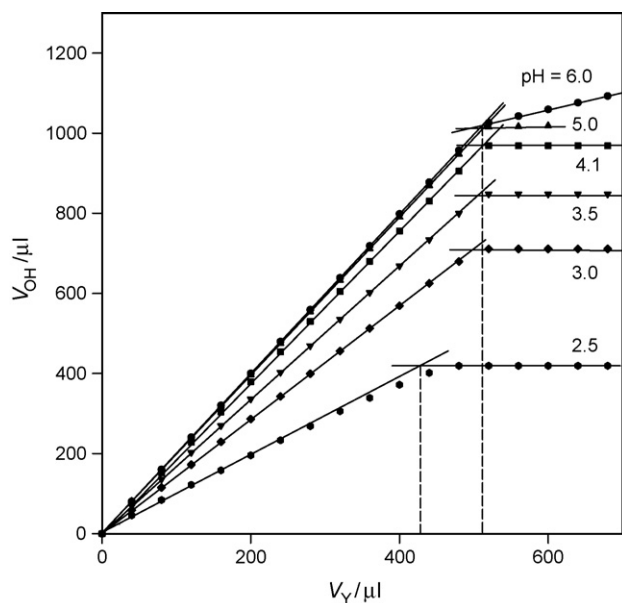$$S = \frac{\Delta V_{OH}}{\Delta V_Y} = \frac{C_Y \Delta N_{OH}}{C_{OH} \Delta N_Y} \tag{1}$$

Fig. 2. Experimental plots of simultaneous potentiometric and pHstatic titrations of 2.4×10^{-3} M Cu^{2+} (4.94×10^{-5} mol in about 21 ml of 0.1 M NaClO$_4$) at pH (●) 5.0 and (■) 2.3. (a) Direct potentiometric plots; (b) Gran linearisation of potentiometric plots (left-hand plots and scale) and pH-static plots (right-hand plots and scale).

Fig. 4. Experimental plots of V_{OH} vs. V_Y for a series of pH-stat titrations of 1.6×10^{-3} M Zn^{2+} (5.10×10^{-5} mol in about 32 ml of 0.1 M NaClO$_4$) at various pH.

of either linear segment composing the titration plot do depend on the experimental pH. The slope at $V_Y < (V_Y)_e$ decreases with decreasing pH because of increasing formation of protonated forms of the metal chelate, of general formula MH_iY^{m+i-4}, with $i \geq 0$. Complexes with $i = 1$ are known for most cations, with $i = 2$ are recorded, among others, for Co^{2+}, Cu^{2+} and Zn^{2+}, with $i = 3$ are reported for very few cations (e.g., Pb^{2+}) [14]. Taking such complexes into account, the titration reaction is written

$$M^{m+} + H_2Y^{2-} + (2-i)H_2O \rightarrow MH_iY^{m+i-4} + (2-i)H_3O^+$$

(2)
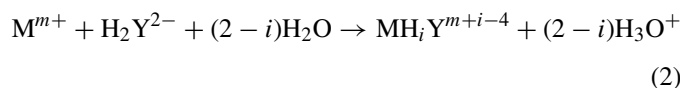
where $i = \bar{n}_{H,MY}$ is the average chelate protonation. At nearly neutral or moderately acid pH, when $\bar{n}_{H,MY} = 0$, the reaction delivers two mol of H_3O^+ for each mol of titrant added; consequently, two mol of base are consumed in order to keep the pH at the initial value. Therefore, the slope corresponds to $\Delta N_{OH}/\Delta N_Y = 2$. When, on decreasing the control pH, $\bar{n}_{H,MY}$ increases, the slope becomes smaller and smaller, because $2 - \bar{n}_{H,MY}$ mol of protons/mol of primary titrant are delivered, and the auxiliary titrant is consumed at the same rate (in the experimental conditions prevailing in this work, hydroxocomplexes of the titrated metal cations, which could cause a similar effect on slope [9], are negligible.).

The slope of the second segment, at $V_Y > (V_Y)_e$, depends on the average number of protons $\bar{n}_{H,Y}$ bound at equilibrium at the operating pH by the excess EDTA. In a narrow range around pH 4.4, $\bar{n}_{H,Y}$ is virtually 2; the protonation of the unreacted titrant does not change and, consequently, the pH-stat device does stop the addition of base, i.e., the slope is null. It is also null at lower pH because, being $\bar{n}_{H,Y} > 2$, the excess EDTA behaves as a base and causes pH to increase out of control, although very slowly. On the other side, when the control pH is set over 4.4, $\bar{n}_{H,Y}$ becomes <2; consequently, the addition of base must continue in order to keep the pH at the control value. Therefore, the slope of the second segment increases the more, the higher the control pH, being obviously independent of the titrated cation. At pH 7, our highest experimental value, $\Delta N_{OH}/\Delta N_Y$ is about 0.8; the difference from the slope 2 of the first segment is thus sufficient to give a sharp intersection, not affecting the end-point volume uncertainty.

The selected plots of Figs. 1–4 aptly illustrate the pH effect and provide a significant test of the experimental relevance of the above predictions. Let us consider the series of Co^{2+} titrations represented in Fig. 1.

At pH 4.68 and 5.30 the plots are composed of two quite straight segments, intersecting at the equivalence volume $(V_Y)_e$. The segments at $V_Y < (V_Y)_e$ are virtually coincident, with slope $V_{OH}/V_Y = 2.00$, corresponding (the concentrations of both titrant solution being the same) to the theoretical ratio N_{OH}/N_Y expected when protonated complexes are negligible. The slope of segments at $V_Y > (V_Y)_e$ increases with pH as expected: it is virtually null at pH 4.68 and quite apparent at 5.30.

At pH 3.24 the slope at $V_Y < (V_Y)_e$ is definitely <2, because protonated complexes form in measure increasing with acidity. Nevertheless, both segments of the Co(II) titration are appre-

ciably straight and the abscissa of their intersection is fairly coincident with the equivalence value.

Under this pH, however, two phenomena, both detrimental for quantitative analysis, begin to become apparent, and worsen with decreasing pH. The first one is a predictable deviation from linearity, due to the loss of reaction quantitativity caused by the adverse effect of increasing acidity on the conditional stability constant of the metal chelate. Nevertheless, complexation of either reagent is still quantitative when the other is in sufficient excess; therefore, linear extrapolation through several experimental points at $V_Y \ll (V_Y)_e$ and $V_Y \gg (V_Y)_e$, respectively, allows to calculate the abscissa of intersection with acceptable uncertainty even at the lowest pH 2.32. This operation, however, gives strong evidence of the second phenomenon, which is much more detrimental and was much less predictable (so much so, that at the beginning of this investigation each series of experiments was repeated with different apparatus and reactants stocks in order to rule out any cause of error not inherent in the chemical system). Under pH about 3.5 the intersection abscissa, i.e., the end-point volume, becomes systematically smaller with decreasing pH, thus deviating more and more significantly from the equivalence volume. At pH 3.24 this deviation is barely appreciable (about-1%), but at pH 2.32 it reaches about −12%. In practice, the reacting power of the chelating agent appears to increase the more, the lower the pH. The only explanation we can devise at this point of our investigation is that binuclear complexes are formed and their importance increases with decreasing pH.

The other cations investigated (Figs. 2–4) show the same kind of behaviour. Obvious differences are related to different stability constants of the primary complex MY^{2-} ($\log K_{MY} = 16.26$, 18.70, 13.81 and 16.44 for cobalt, copper, manganese and zinc, respectively, at $25\,°C$ and 0.1 M ionic strength) [15]. Like for Co(II), the high intrinsic stability of Cu(II) and Zn(II) allows reliable end-point even at the lowest pH; the much smaller intrinsic stability of the Mn(II) complex causes too high deviations under pH 3.2. What is most noteworthy, however, is that, with increasing acidity, all cations show increasing deviations of chelation ratio from the stoichiometric 1:1 value, which are simultaneous with deviations from linearity but independent of them.

In order to be definitely sure that the odd results at low pH are not due to artefacts of the pH-stat end-point, a series of copper titrations at pH 2.3–5.0 was simultaneously monitored pH-statically and potentiometrically with a selective electrode (not available for the other ions investigated). In order to have an efficient pH control, the titrations were performed in the constant addition mode (the default mode of the pH-stat experiments). For clarity, only the results of two experiments at the two extreme pH values (2.3 and 5.0) are shown in Fig. 2. Both the potentiometric and pH-stat plots at pH 2.3 (Fig. 2a and b, respectively) show earlier end-points. Given the relatively large V_Y increments, a precise potentiometric end-point cannot be drawn from the direct plot (Fig. 2a), but can be obtained by linearising the relevant data by means of the Gran function [16–18]

$$G = k(V^\circ + V)10^{E/S}$$

(3)

where E/mV is the measured variable, V° is the initial volume of the titrated solution, $V = V_Y + V_{OH}$ the sum of the primary and auxiliary titrant volumes at the end of each titration step (when E is also measured), S (mV/decade) the experimental response slope of the ion-selective electrode and k is a scale coefficient. The two pairs of plots provide ultimate evidence that at lower pH the reaction stoichiometry fails, the end-point volume at pH 2.3 being more than 10% smaller in comparison with pH 5.0, the phenomenon being independent of the instrumental end-point detection method.

The early stage of deviation from 1:1 stoichiometry was indeed observed in a previous work [10], where pH-static titrations of Cu(II) and Zn(II) were made at 1.0 pH steps between pH 3.0 and 5.0 and 3.0 and 6.0, respectively. At pH ≥ 4.0 both repeatability and reproducibility of the results were excellent (better than 0.2%). At pH 3.0 repeatability was still very good (better than 0.3%), but the apparent amount of copper and zinc was lower by about 0.6 and 1.7%, respectively. At that time, little importance was attached to this rather small systematic error, and its cause was not investigated. The present investigation on an expanded pH range at smaller pH steps shows that this is a structural phenomenon, and that a too low pH is detrimental not only by affecting the reaction quantitativity through its effect on the conditional stability constant, but also by changing the reaction ratio. Fig. 5 shows the dependence on pH of the reaction ratio $(N_Y)_e/N_M$ for the four investigated cations.

As noted above, the titration stoichiometry suggests that binuclear complexes be formed in appreciable amount at low pH. We could find in the literature only two quotations of binuclear complexes with EDTA, both stable at low pH, respectively, of uranyl ion [14] and of cadmium [19], the latter (not taken into consideration in later critical compilations) having an overall formation constant of 17. An investigation of the pH-stat behaviour of Cd(II) (which also gives a very stable 1:1 complex with $\log K_{CdY} = 16.5$) [15] was therefore expedient. A small number of experiments (all shown in Fig. 6) were sufficient to confirm the above general behaviour, in agreement with the previous finding [19]. The $(N_Y)_e/N_{Cd}$ ratio, which at pH 5 has the theoretical value, decreases appreciably at pH $\ll 4$, reaching a difference of about -12% at pH 2.5.
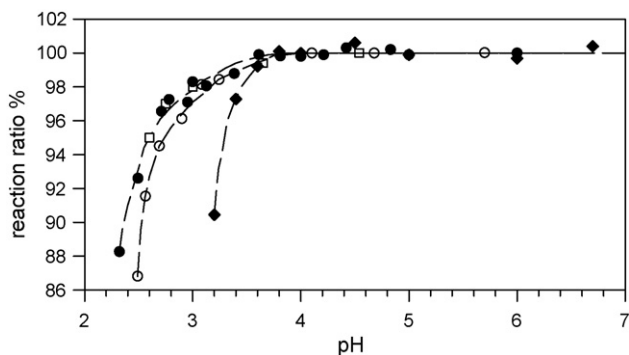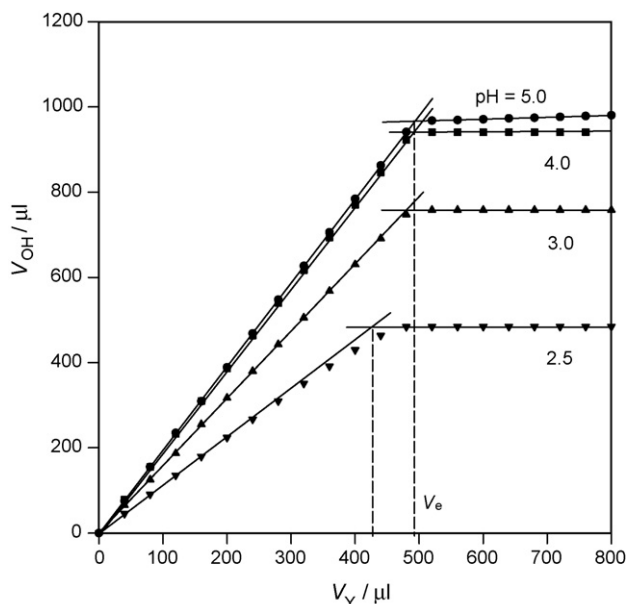

Fig. 6. Dependence on pH of the titration plots of 1.5×10^{-3} M Cd(II).

3.2. Criteria for establishing a pH-static titration protocol

On the basis of the above results, the following optimum pH ranges for pH-static titrations of the elements considered can be defined:

Cobalt(II): pH 7.0–4.0 (3.2);
Copper(II): pH 5.0–4.0 (3.0);
Manganese(II): pH 7.0–5.0 (4.2);
Zinc(II): pH 7.0–4.0 (3.0).

In the above pH ranges, accuracy and precision as good as $\pm 0.2\%$ can be reached. The values in parentheses are the least pH compatible with a systematic error lower than -2% at cation concentration $\geq 10^{-3}$ mol dm^{-3}. High-quality analytical results require, however, carefully set experimental conditions, including the instrumental parameters. The following considerations can help to suit the analytical protocol to the available apparatus, on the trace of the procedure reported in Section 2.3.

As regards the experimental pH, setting an exactly predetermined control value is not important, at condition that it is within the optimum range. A much more important requirement follows from the very principle of pH-static titrations, i.e., that the amount of strong base must exactly neutralise the amount of hydronium ion delivered by the titration reaction. This means that the quantity that must be kept constant during each titration is the initial hydronium ion amount rather than the proton activity, i.e., pH. Since this last is the parameter that rules the operating device, a constant ratio between activity (10^{-pH}), concentration (H_3O^+]) and amount (($V^\circ + V$)[H_3O^+]) should be maintained through each single titration. It is therefore prescribed to keep a constant ionic strength by means of an inert electrolyte and to operate with both titrants concentrated enough to cause negligible dilution. It is not required that the hydronium ion concentration, when kept constant, is exactly

Fig. 5. Dependence on pH of the reaction ratio (mol EDTA/mol cation) $\times$ 100 for titrations of: ●, Co(II); □, Cu(II); ♦, Mn(II); ○, Zn(II). Analyte concentration about 2×10^{-3} M.

known; the combined glass electrode can therefore be calibrated as usual with pH standards, the obvious choice being phthalate at pH 4.0 and phosphate at pH 6.8–7.0.

In order to arrange the test solution for titration, it is sufficient to adjust its pH within the optimum range. For instance, if the test substance (e.g., metallic cobalt, zinc oxide) has been dissolved in acid, this is conveniently neutralised with the auxiliary titrant solution of sodium hydroxide by using the titrator's pre-set end-point function. Before pH adjustment, it is advisable to add a small concentration of a buffer substance suitable to dampen the pH oscillations caused by either titrant's additions, which could hamper the stat action [10]. Moreover, the buffer can help to reach a pH nearer to the pre-set end-point value in the initial pH adjustment, which tends to overact. In our experiments, chloroacetic acid (at pH <4), acetic acid (at pH 4–5), hexamethylene tetramine (at pH 5–6) and triethanolamine (at pH 7–8) at concentration $2–5 \times 10^{-3}$ were used; however, any buffer substance with suitable acidity constant and small complexing ability towards the titrated cation is suitable. The ΔE value measured after the initial pH adjustment can be set as the definitive Stat control value.

As regards the very instrumental parameters, they obviously depend on the type and make of apparatus used. An apparatus composed of a potentiometric titrator with the Stat function for dispensing the auxiliary titrant (the strong base) and a separate PC-controlled burette for dispensing the primary titrant (the EDTA solution) at fixed time intervals was profitably used in a large part of our experiments, with the small inconvenience that the start of pH-stat operation had to be manually synchronised with the first addition of EDTA. Only very recently an apparatus that can automatically co-ordinate all operations was available. At our knowledge, however, instruments directly providing the final pH-static titration plot of V_{OH} versus V_Y are not manufactured. This plot must be manually drawn from the direct data record of V_{OH} against time (see Section 2.3). In order to evaluate

whether the titration has been correctly carried out, the measured ΔE must also be recorded against time; the initial value should accurately be restored (ideally, within 0.1 mV, i.e., 0.002 pH) after each EDTA addition step.

Graphical reports of V_{OH} versus time, like those plotted in Fig. 7, directly provided by the pH-stat apparatus, are also useful. The V_{OH} values to be reported in the titration plot correspond to the final points of each plateau, which should form rapidly but gradually; an abrupt, edged step generally evidences an invalidating initial overshot of base, due to a poor setting of instrumental parameters. Among these, the most important, and most tricky to set correctly, is the one determining the dynamics of compensation of ΔE unbalance after each EDTA addition; in instruments of different makes (where it is variously termed) it obeys to different algorithms, generally conceived for slow pH drifts.

4. Conclusions

The results here reported confirm that the pH-static technique is fit to the purpose of titrating with great accuracy and precision transition cations by using current instrumentation and one and the same potentiometric sensor for whichever analyte. In the suitable pH range the titration points, but, if any, the ones nearest to the intersection point, are finely fitted by two intrinsically linear equations; both their sets are independent each other and statistically homoscedastic, thus quite suitable for least-squares treatment. In comparison, potentiometric titrations with ISEs require specific sensors, readily available only for very few species and rather expensive; moreover, the treatment of their data is affected by variable uncertainty of E, which increases with decreasing distance from the equivalence point and commands weighed least-squares when the end-point is located by curve fitting or by Gran linearisation. In spectrophotometric titrations with indicators, the position of the equivalence point on the plots of transmittance or absorbance versus titrant volume depends on the nature of indicator and the end-point is more conveniently selected by comparison with a known sample titration. When the absorbance of a reactant or product is followed, the uncertainty depends on the measured value; moreover, multiplying absorbance by the dilution factor yields a linear plot, but causes linear least-squares to become invalid.

The time required by a single pH-stat experiment, although not short (typically 15–20 steps of 60–90 s, totalling 15–30 min), is quite acceptable when highest precision and accuracy are wanted, like in standardisation of metal solutions. The measured solution must own a moderately appreciable buffer power, which, however, must not be as high as to dampen the sensitivity to absolute variations of free acidity. This requirement prevents the use of the technique for analysing strongly buffered samples of practical interest, and appears to be the only serious practical limitation. A further inconvenience, the waste of time for translating the direct data sets into V_{OH} versus V_Y sets, could be overcome if the apparatus makers would undertake the not heavy task of implementing the technique in their dedicated software.

The useful range of pH-static titrations has a tendency to expand towards smaller pH than other titration techniques, in
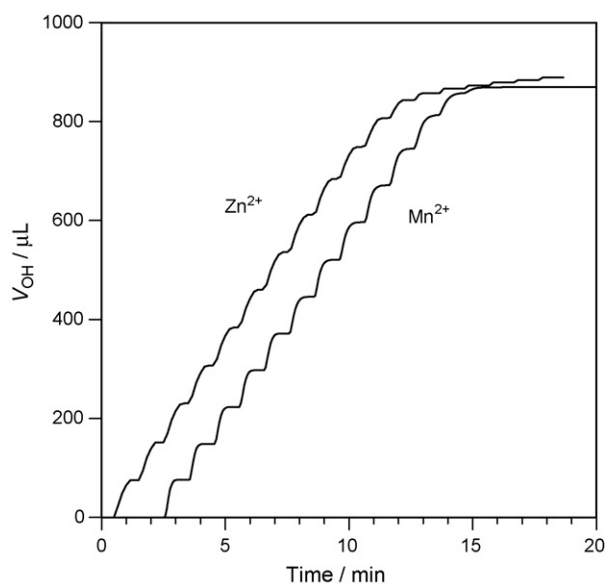

Fig. 7. Direct record of auxiliary titrant volume V_{OH} vs. time for titrations of Mn(II) at pH 4.5 and M Zn(II) at pH 5.2, both 1.5×10^{-3} M.

particular than titrations with chromatic indicators. Unfortunately, this trend is too soon counteracted by the sudden fall of the reaction stoichiometry at pH not extremely acid. This much less expected phenomenon overtakes the effect of decreasing conditional stability constants in setting the practical lower pH limit of application of the technique for the quantitative determination of transition metals. On a more fundamental point of view, it deserves further investigation, which, however, are out of the scope of the present article.

Acknowledgement

References

[1] C.F. Jacobsen, J. Léonis, Compt. Rend. Trav. Lab. Carlsberg, Sér. Chim. 27 (1951) 333.
[2] H.V. Malmstad, E.H. Piepmeier, Anal. Chem. 37 (1965) 34.
[3] F. Di Gregorio, R. Sisto, J. Dairy Res. 47 (1980) 417.
[4] H. Le Nours, J.F. Le Meur, C. Bourgeois, Sci. Aliments 2 (1982) 483.
[5] H. Le Nours, J.F. Le Meur, C. Bourgeois, Lait 63 (1983) 490.
[6] J.F. Le Meur, Analusis 12 (1984) 36.
[7] R. Österberg, in: E. Wänninen (Ed.), Essays on Analytical Chemistry, Pergamon, Oxford, UK, 1977, pp. 103–112, and literature quoted therein.
[8] H. Le Nours, J.F. Le Meur, Analusis 17 (1989) 405.
[9] C. Maccà, Anal. Chim. Acta 456 (2002) 313.
[10] C. Maccà, L. Soldà, M. Zancato, Anal. Chim. Acta 470 (2002) 277.
[11] H. Freiser, G.H. Nancollas, IUPAC Compendium of Analytical Nomenclature, second ed., Oxford, 1987, pp. 13,15.
[12] P.M. May, D.R. Williams, in: D.J. Legget (Ed.), Computational Methods for the Determination of Formation Constants, Plenum, New York, 1985, p. 37.
[13] Kragten, Atlas of Metal-Ligand Equilibria in Aqueous Solution, Ellis Horwood, Chichester, UK, 1978.
[14] R.M. Smith, A.E. Martell, Critical Stability Constants, vol. 6, Plenum, New York, 1989.
[15] A.E. Martell, R.M. Smith, Critical Stability Constants, vol. 1, Plenum, New York, 1974.
[16] G. Gran, Analyst 77 (1952) 661.
[17] C. Maccà, G.G. Bombi, Analyst 114 (1989) 463.
[18] C. Maccà, Analyst 115 (1990) 631.
[19] M. Jawaid, Talanta 27 (1980) 95.

ESI-MS study of the mechanism of glycyl-L-histidyl-L-lysine-Cu(II) complex transport through model membrane of stratum corneum

Lena Mazurowska [*], Mirosław Mojski

Faculty of Chemistry, Warsaw University of Technology, Noakowskiego 3, 00-664 Warsaw, Poland

Abstract

In mammalian organisms copper can be found mainly in the form of complex with specific tripeptide, GHK-Cu (glycyl-L-histidyl-L-lysine-Cu(II)). GHK-Cu is the basic form in which copper is transported in tissues and permeates through cell membranes. The penetration ability of GHK-Cu through the *stratum corneum* and its role in copper ions transport process is the key issue for its cosmetic and pharmaceutical activity. The permeability phenomenon was studied by use *in vitro* model system—Flynn diffusion cell with the liposome membrane.

The earlier studies on the influence of different ligands on the migration rate of copper ions through model membrane provide evidence for hampering role of ligands structure and pH of formulations in this process.

Structures of copper complexes formed in solutions of different pH media were evaluated by use of ESI-MS. The permeability coefficients of copper complexes increase with increasing pH. It was proved that only tripeptide GHK and its complexes with copper: GHK-Cu and (GHK)$_2$-Cu are able to migrate through membrane model of *stratum corneum*.

© 2006 Elsevier B.V. All rights reserved.

Keywords: Copper(II) complexes with glycyl-L-histidyl-L-lysine (GHK); Electrospray MS; Skin penetration

1. Introduction

Tripeptide glycyl-histidyl-lysine (Gly-His-Lys, GHK) is well known peptide isolated from human plasma [1], where it is present at concentration of about 200 ng mL^{-1}. It possesses high affinity for copper(II) ions exhibiting in spontaneous formation of complex GHK-Cu [2]. The equilibrium between GHK-Cu and copper bound to receptor ligands is one of the factors determining biological activity of this metal. GHK also plays a crucial role in regulation of copper content both in certain tissues and organs as well as in the whole body.

This peptide was first described as a growth factor for a variety of differentiated cells but recent data suggested a physiological role related to the process of wound healing and tissue repair [3–5]. It was confirmed that GHK copper peptides: stimulate synthesis of collagen, elastin and glycosaminoglycans (GAGs) as well as the formation of the extracellular cement between cells [6]. Thus, it improves strength, fragility and elasticity of the skin.

In further studies it was recognised that GHK is endowed with a wide range of biological activities including: angiogenesis [7,8], acceleration of bone repair [9], superoxide dismutase-like activity [10] and binding to heparine [11]. A crystal X-ray diffraction structure of a GHK-Cu complex is known and described [12,13].

Biological activity of metal compounds in the skin is always a result of its absorption by the skin. It forms a heterogeneous membrane and absorption is controlled by the outermost layer, the stratum corneum (only 15–20 μm thick). The stratum corneum is the main barrier for skin permeation of drugs and other compounds [14]. Skin penetration by metal ions most often was examined by *in vitro* methods, because their toxicity made *in vivo* experiments too risky [15]. However, the results of experiments performed *in vivo* with volunteers were also reported [16].

Permeation of an exogenous substance through skin layer is a passive diffusion process that depends on a large number of different factors [15] and can be described by Fick's first law of diffusion [16].

The present study was performed by using a Flynn diffusion cell (side-by-side), widely described in the literature [17–19].

* Corresponding author. Tel.: +48 22 234 7719; fax: +48 22 234 7408.
E-mail address: lenka@ch.pw.edu.pl (L. Mazurowska).

The solute is transported through the membrane situated between two aqueous solutions—"donor" phase that initially contains solute and "acceptor" phase in which solute accumulates after crossing the membrane barrier. As a membrane widely accepted "skin barrier model" was used. It is a liquid crystalline system of physicochemical properties similar to the properties of intercellular cement of *stratum corneum* [20–22]. Though surface of the skin is slightly acidic (pH 4.2–5.6), pH of the lower layers of the epidermis is at physiological level 7.4 [23]. For this reason and trying to avoid additional transport process with pH gradient, in the experiments in acceptor and donor cells the physiological pH 7.4 was adjusted. Only penetration ability of copper ions was performed at pH 4.0 because in less acidic solution copper ions precipitate as hydroxide.

Various instrumental techniques have been proposed to study penetration ability of active substances. High-performance liquid chromatography (HPLC) [23–25] and spectrophotometry UV–vis [26] are classical approaches for separation and determination of substances in donor cells. Unfortunately these methods do not provide structural information. The present study is the first (according to the best knowledge of authors) attempt to examine copper tripeptide complexes formed during skin permeation process by electrospray MS [27].

2. Experimental

2.1. Instrumentation

The absorption spectra were recorded using SPECOL 11 spectrophotometer (Zeiss, Jena, Germany) with 5 mm glass cells. The pH measurements were carried out using Elmetron ES24 pH meter (Poland).

The copper peptide complexes were characterized by ESI mass spectrometer LC/MSD 1100 (Agilent Technologies, Wilmington, NC, USA) with quadrupole mass analyzer.

2.2. Reagents, solutions and materials

A stock Cu(II) solution (1 mg mL^{-1}) was obtained by dissolution of copper(II) chloride dehydrate (POCH, Gliwice, Poland) in water.

A GHK-Cu stock solution (0.01 M) was prepared by dissolution of Prezatide copper acetate (ProCyte Corporation, USA) in water.

Buffer solution (pH 4.0) was prepared by dissolution of acetic acid (POCh, Gliwice, Poland), adjustment of pH 7.4 by use of the solution of sodium acetate (POCH, Gliwice, Poland) followed by dilution to 1000 mL with demineralised water.

Buffer solution (pH 7.4) was prepared by dissolution of potassium phosphate (POCh, Gliwice, Poland), adjustment of pH 7.4 by use of the solution of disodium hydrogen phosphate (POCH, Gliwice, Poland) followed by dilution to 1000 mL with demineralised water.

Buffer solution (pH 10.0) was prepared from ammonium chloride (POCh, Gliwice, Poland) solution of pH adjusted to 10.0 by ammonia (POCh, Gliwice, Poland) solution.

A 0.1% biscyclohexanon-oxalyldihydrazone (cuprizon) (Fluka, Buchs, Switzerland) solution was prepared by dissolving 200 mg of cuprizon in 40 mL of 50% hot ethanol. The obtained solution was diluted with ethanol to 200 mL.

2.3. Preparation of model membrane

The lipophilic membrane modeling stratum corneum lipids was prepared by sandwiching 0.125 mL of liposomes—Cerasome (Lipoid GmbH, Germany) composed of the horny layer lipids. The appropriately thick lipid layer (0.125 mL of liposomes) was placed between two membrane (Institute of Chemistry and Nuclear Technique, Warsaw, Poland) discs made of semi-permeable polyester foil (radius, 12 mm; diameter of pores, 0.4 μm; thickness, 12 μm).

The membrane was left for 24 h to evaporate the water. Diffusion cells have been filled with phosphate buffer (pH 7.4) and membrane was stabilised for 24 h.

2.4. Analytical procedures

2.4.1. General procedure for copper determination

In vitro membrane permeation experiments were performed using side-by-side Flynn diffusion cell. The donor medium consisted of 27 mL of phosphate buffer (pH 7.4) containing selected copper complex. The acceptor cell was filled with phosphate buffer solution (pH 7.4). The available diffusion area between cells was 1.77 cm^2. The contents of both cells were stirred at 1000 rpm by use of a magnetic stirrer. Experiments were provided at the room temperature.

Copper was determined spectrophotometrically at 600 nm. One millilitre of the solution from acceptor cell (after 120 h) was transferred into a 10 mL calibrated flask. One millilitres of 0.1% cuprizon solution and 2 mL of buffer solution (pH 10.0) were added. The mixture was diluted to 10 mL with water in calibration flask and the absorbance of it at 600 nm against a reagent blank was measured [28].

The relation between permeability coefficient (K_p) and steady-state flux was calculated by use of equation [29]:

$$K_p = \frac{J}{C_v} \tag{1}$$

where C_v is the initial permeate concentration in donor solution and J is its mass passing through a unit area of the membrane in unit time. The permeability coefficient of Cu(II) ions in the lipid membrane K_p (cm s^{-1}) was calculated by Fick's first diffusion law.

2.4.2. ESI-MS

Electrospray MS was applied to identify copper complexes present in donor and acceptor cell. ESI-MS spectra were acquired in the range 150–1500 amu using 20 ms dwell time and 0.1 U of acquisition step. The ion spray voltage of 4000 V was applied for positive and negative ions mode. The orifice potential 80 V was established as offering the best signal intensity and causing partial fragmentation of molecular ion at the peptide bonds [30].

3. Results and discussion

3.1. Cu(II) permeability through model membrane

The aim of the study was to investigate migration rate of tripeptide copper complex in order to evaluate influence of ligand properties on the permeability coefficient of copper. The influence of GHK on the dynamics of the copper ion diffusion has been investigated by diffusion cell method.

The preliminary experiments comprised evaluation of effect of concentration of the ligand (GHK) on the penetration ability of copper. They were performed at pH 4.0, because in less acidic solution copper ions precipitate as hydroxide. The obtained results ($n = 5$, probability level = 0.95) allowed to calculate permeability coefficient ($K_p \pm$ S.D.): $(0.27 \pm 0.05) \times 10^{-6}$ cm s^{-1} for copper ions and $(0.63 \pm 0.06) \times 10^{-6}$ cm s^{-1} for copper complex with peptide, $(GHK)_2$-Cu. It reveals substantial influence of complexation on the permeation rate of copper ions, as it increases as twice.

Table 1
Ionized species observed in ESI-MS spectra of GHK-Cu solutions of different pH

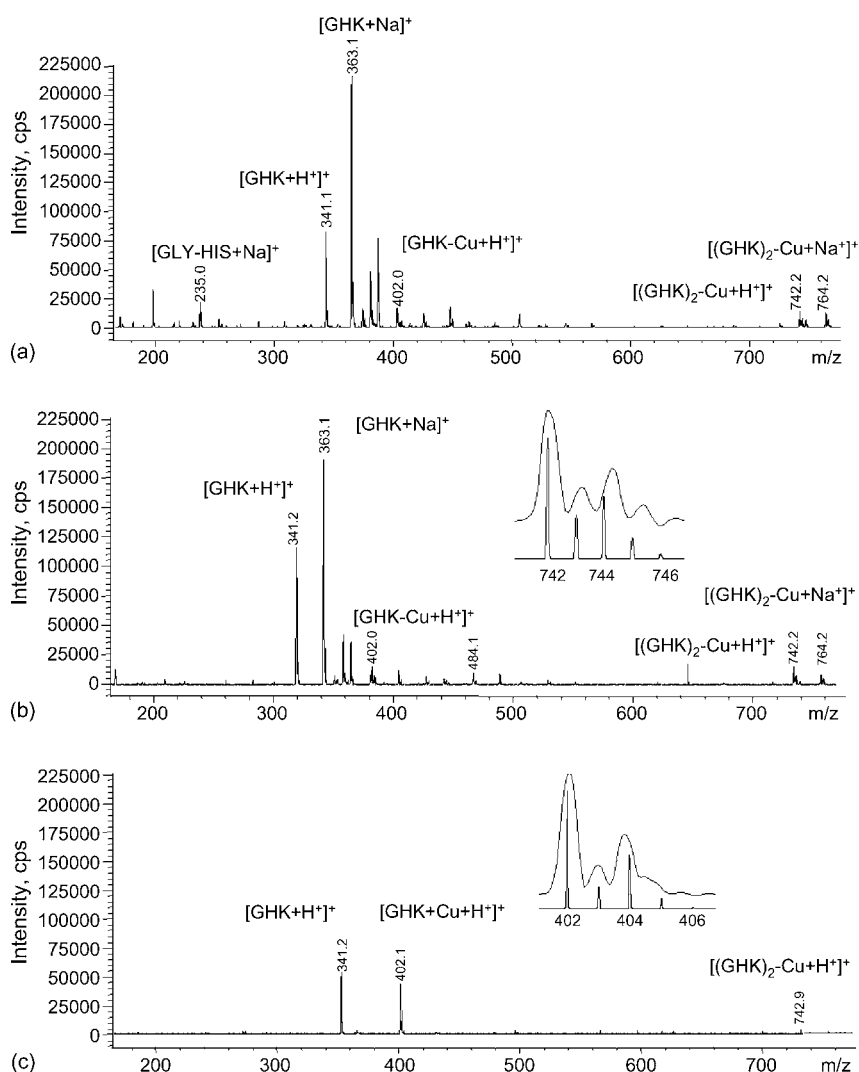| pH	Positive ions mode		Negative ions mode	
	m/z	Proposed ion	*m/z*	Proposed ion
7.4	235	[Gly-His + Na]$^+$	–	–
	341	[GHK + H]$^+$	339	[GHK-H]$^-$
	363	[GHK + Na]$^+$	–	–
	402	[CuGHK + H]$^+$	400	[CuGHK-H]$^-$
	742	[Cu(GHK)$_2$ + H]$^+$	740	[Cu(GHK)$_2$-H]$^-$
	764	[Cu(GHK)$_2$ + Na]$^+$	–	–
5.5	341	[GHK + H]$^+$	339	[GHK-H]$^-$
	402	[CuGHK + H]$^+$	400	[CuGHK-H]$^-$
4.0	341	[GHK + H]$^+$	339	[GHK-H]$^-$
	402	[CuGHK + H]$^+$	400	[CuGHK-H]$^-$
1.8	341	[GHK + H]$^+$	339	[GHK-H]$^-$

Fig. 1. Mass spectra of the solutions of GHK-Cu system of pH 7.4 taken from: (a) donor cell in start point, (b) donor cell after 3 days and (c) acceptor cell after 3 days.

Further increase of permeability coefficient was observed when GHK-Cu(II) system was investigated in solution of pH kept on physiological level, 7.4 [22] under such conditions $K_p \pm$ S.D. was $(3.34 \pm 0.14) \times 10^{-6}$ cm s^{-1} (for five results, probability level 0.95).

3.2. ESI-MS study

The obtained results indicate crucial role played by tripeptide ligand in model membrane transport of copper(II) ions. In order to evaluate species taking part in this phenomenon, solutions from both Flynn cells were examined by electrospray ionisation-mass spectrometry (ESI-MS). It was found that pH essentially influences equilibria existing in solutions. In Table 1 are presented ions registered in positive (PIM) and negative (NIM) ions modes in mass spectra of solutions of the GHK-Cu system in different pH: 1.8, 4.0, 5.5 and 7.4.

The tripeptide GHK was a dominant species in the acidic pH range. Its molecular ion is registered at m/z 341 (PIM) or 339 (NIM). In solution of pH 4.0 and 5.0 GHK and GHK-Cu complex were observed. Signals for these compounds in PIM were registered at m/z 341 for GHK and 402 for GHK:Cu. For solution of almost neutral pH 7.4 (GHK)$_2$-Cu complex is formed but also tripeptide and complex 1:1 were observed. The mass spectrum of the system consists of six signals at m/z: 235, 341, 363, 402, 742 and 764. GHK-Cu complex in which copper ion is bound to N-terminal amino group of glycine, the nitrogen atom of the glycyl-histidyl amide bond and imidazole nitrogen's seems to be dominant and most stable form, as it was suggested in Ref. [31].

Solutions (pH 7.4) taken from donor and acceptor cells of Flynn's set up were examined by ESI-MS (Fig. 1). The mass spectra obtained for the samples from donor cell consist of signals at m/z 341 for tripeptide GHK, 362-sodiated GHK, 402 for GHK-Cu and 742 for (GHK)$_2$-Cu followed by sodiated (GHK)$_2$-Cu at m/z 764. Here also can be observed peak at m/z 235, which can be attributed to the sodiated Gly-His. This can indicate, that the main degradation mechanism of tripeptide GHK lies in breaking of the His-Lys peptide bond [31]. After 3 days of incubation almost the same species (Fig. 1b) were identified in donor cell.

In the mass spectrum of solution taken from the acceptor cell (Fig. 1c) three main ions were observed at m/z 341 for GHK, 402 for GHK-Cu and 742 for (GHK)$_2$-Cu. The isotopic patterns of signals (in the insets to Fig. 1b and c) at m/z 402 and 742 correspond to the species containing only one copper atom.

The lack of the peak at m/z 235 (if it is formed in solution) is not transported through the membrane—after 3 days does not show up in the acceptor cell but on the other hand it also does not show up in the donor cell after 3 days. We could not clearly indicate whether such a species is transported through the membrane or not.

Our earlier investigations (Table 1) confirm that the species observed in the mass spectrum are really reflected the species presented in solution.

The intensity of signals registered in acceptor solution are about five times lower, then those in the spectrum from donor

cell, what nicely corresponds with results obtained in the first part of our study—concerning permeation coefficient (K_p).

4. Conclusions

The obtained results shows that permeability rate of tripeptide copper complexes through model membrane (and probably also through the skin) strongly depend on pH of the donor solution. Moreover they proved that both formed copper species (of composition 1:1 and 1:2) could penetrate skin as well as free ligand. Such complexes exhibit the highest affinity to the lipid structures of a membrane. The molecular specific ESI-MS allows identifying GHK complexes with Cu and allows their specific monitoring in *stratum corneum* model systems.

The presented results provide new information useful to complete the knowledge about copper complexes peptide transport process through the *stratum corneum*. They reveal key role played by pH of the formulations containing copper used as cosmetics, but also proved that process of skin penetration by metals complexes can be controlled by proper selection of other cosmetic additives.

References

[1] L. Pickart, M. Thaler, Nat. New Biol. 243 (1973) 85.
[2] S. Lau, B. Sarkar, Biochem. J. 199 (1981) 649.
[3] F.X. Maquart, L. Pickart, M. Laurent, P. Gillery, J.C. Monboisse, J.P. Borel, FEBS Lett. 238 (1988) 343.
[4] A. Simeon, H. Emonard, W. Hornebeck, F.X. Maquart, Life Sci. 67 (2000) 2257.
[5] L. Pickart, M. Thaler, FEBS Lett. 104 (1979) 119.
[6] A. Simeon, J. Wegrowski, Y. Bontemps, F.X. Maquart, J. Invest. Dermatol. 115 (2000) 962.
[7] P.M. Gullino, EXS 61 (1992) 125.
[8] E.H. Sage, R.B. Vernon, J. Hypertens. Suppl. 12 (1994) S145.
[9] H. Pohunkova, J. Stehlik, J. Vachal, O. Cech, M. Adam, Biomaterials 17 (1996) 1567.
[10] N. Cotelle, E. Tremolieres, J.L. Bernier, J.P. Catteau, J.P. Henichart, J. Inorg. Biochem. 46 (1992) 7.
[11] D.L. Rabenstein, J.M. Robert, S. Hari, FEBS Lett. 376 (1995) 216.
[12] L. Pickart, J.H. Freedman, W.J. Loker, J. Peisach, C.M. Perkins, R.E. Stenkamp, B. Weinstein, Nature 288 (1980) 715.
[13] J.H. Freedman, L. Pickart, B. Weinstein, W.B. Mims, J. Peisach, Biochemistry 21 (1982) 4540.
[14] R.J. Scheuplein, J. Invest. Dermatol. 45 (1965) 334.
[15] J.J. Hostynek, Food Chem. Toxicol. 41 (2003) 327.
[16] R.J. Feldman, H.I. Maibach, Arch. Dermatol. 91 (1965) 661.
[17] R.M. Gudipati, S.A. Stavchansky, Int. J. Pharm. 118 (1995) 41.
[18] K. Sung, J. Fang, J. Wang, O. Hu, Eur. J. Pharm. Sci. 18 (2003) 63.
[19] J. Arct, A. Oborska, M. Mojski, A. Binkowska, B. Świdzikowska, Int. J. Cosm. Sci. 24 (2002) 357.
[20] T. Hatanaka, M. Inuma, K. Sugibayashi, Y. Morimoto, Chem. Pharm. Bull. 38 (1990) 3452.

[21] K. Matsuzaki, T. Imaoka, M. Asano, K. Miyajima, Chem. Pharm. Bull. 41 (1993) 575.

[22] J. Houk, R.H. Guy, Chem. Rev. 88 (1998) 455.

[23] Y.B. Schuetz, A. Naik, R.H. Guy, Y.N. Kalia, Eur. J. Pharm. Sci. 26 (2005) 429.

[24] F.P. Schmook, J.G. Meingassner, A. Billich, Int. J. Pharm. 215 (2001) 51.

[25] R. Wolf, K. Raith, R. Neubert, J. Chromatogr. A 766 (1997) 71.

[26] K.T.E. Kierstan, A.E. Beezer, J.C. Mitchell, J. Hadgraft, S.L. Raghavan, A.F. Davis, Int. J. Pharm. 229 (2001) 87.

[27] H. Lavanant, H. Virelizier, Y. Hoppilliard, J. Am. Soc. Mass Spectrom. 9 (1998) 1217.

[28] L.J.A. Haywood, P. Sutcliffe, Analyst 81 (1956) 651.

[29] H. Schaefer, T.E. Redelmeier, Skin Barrier. Principles of Percutaneous Absorption, S. Karger AG, Basel, 1996.

[30] K. Połeć-Pawlak, R. Ruzik, K. Abramski, M. Ciurzyńska, H. Gawrońska, Anal. Chim. Acta 540 (2005) 61.

[31] C. Conato, R. Gavioli, R. Guerrini, H. Kozłowski, P. Młynarz, C. Pati, F. Pulidori, M. Remelli, Biochim. Biophys. Acta 1526 (2001) 199.

Prediction of humic acid content and respiration activity of biogenic waste by means of Fourier transform infrared (FTIR) spectra and partial least squares regression (PLS-R) models

Katharina Meissl[a], Ena Smidt[a,*], Manfred Schwanninger[b]

[a] Institute of Waste Management, Department of Water, Atmosphere and Environment,
BOKU—University of Natural Resources and Applied Life Sciences, Vienna, Muthgasse 107, 1190 Vienna, Austria
[b] Department of Chemistry, BOKU—University of Natural Resources and Applied Life Sciences, Vienna, Muthgasse 18, 1190 Vienna, Austria

Abstract

Fourier transform infrared (FTIR) spectroscopy has been proven to be an appropriate analytical method for the qualitative assessment of compost stability. This study focuses on quantitative determination of two time-consuming parameters: humic acid (HA) contents and respiration activity. Reactivity/stability and humification were quantified by respiration activities (oxygen uptake) and humic acid contents. These features are also reflected by a specific infrared spectroscopic pattern. Based on this relationship partial least squares regression (PLS-R) models for the prediction of respiration activities and humic acid contents were calculated. Characteristic wavenumber regions that are assigned to the biological/chemical parameter were selected for multivariate data analysis. The coefficient of determination (R^2) obtained for the humic acid prediction model from infrared spectra was 87% with a root mean square error of cross-validation (RMSECV) of 2.6% organic dry matter (ODM). The prediction model for respiration activity resulted in a R^2 of 94% and a RMSECV for oxygen uptake of 2.9 mg g^{-1} dry matter (DM).
© 2006 Elsevier B.V. All rights reserved.

Keywords: FTIR; PLS-R; Humic acid; Respiration activity; Compost

1. Introduction

Biological treatment of biogenic waste materials aims at achieving stabilization of organic matter to reduce environmentally relevant emissions, and to ensure plant compatibility of composts. Definition and criteria of stability are an issue currently undergoing debate in the European Union (HORIZONTAL, CEN BT TF 151, Cluster 7 Biological Parameters).

Respiration activity is a commonly applied biological parameter used to determine stability of organic waste matter. This parameter refers to the measurement of the oxygen uptake by microorganisms in degrading readily degradable fraction of the organic matter under aerobic and standardized conditions [1,2].

Degradation and transformation during the biological process cause significant changes in the complex mixture. Degradation leads partially to emissions of volatile metabolites such as fatty acids and nitrogen containing compounds of low molecular weight, to mineralization, enrichment of scarcely degradable compounds and to humification [3]. Although the mechanisms involved are not yet clear, humification is a favorable means of stabilizing organic matter in view of the environmental benefits provided by carbon sequestration. When composted biogenic materials are applied as soil amendment, humic substances contribute to soil amelioration due to the positive effect exerted on aggregate stability and plant health [4]. Extractable humic acids (HA) that show an increase during composting are an appropriate parameter to describe the humification progress [5] and stability of composts [6].

Infrared spectroscopy has shown to be a valuable tool for the characterization of waste with several application in waste science such as characterization of different waste materials [7] and progressing processes [8,9], and evaluation of sewage sludge composts [10]. Infrared spectra illustrate the plot of absorbed infrared radiation dependent on wavenumbers (wavelengths) caused by interactions of infrared radiation with matter. An infrared spectrum reflects the chemical composition of the whole

---

* Corresponding author. Tel.: +43 1 3189900 343; fax: +43 1 3189900 350.
E-mail address: ena.smidt@boku.ac.at (E. Smidt).

sample supporting their elucidation. Infrared spectroscopy has been applied to describe changes at a molecular level [11] during the biological treatment of organic waste [12]. Moreover, FTIR spectra have also been used in complex materials for quantification of sample components such as lignin in wood using band height ratios [13], single band heights to determine the nitrate content in waste [14], and to follow processes by using the relative absorbance [14]. These techniques are very useful for analyzing main components or single processes but not for the quantification or prediction of complex parameters such as respiration activity or humic acid content in composite samples from different processes or origins. To handle such extensive data sets multivariate statistical methods are necessary.

Multivariate data analysis allows the extraction of additional information from huge data pools generated by spectroscopic analyses. The combination of these methods has been applied in soil science [15] and pharmaceutical industry [16] or to monitor kinetics of adsorption [17]. Based on a mathematical procedure the structure of data pools is revealed and can be applied for a specific purpose [18]. Besides classification, prediction of parameters represents an interesting target. By means of partial least squares regression (PLS-R) a multivariate regression model from a known corresponding X and Y data set is calculated. Based on an established validated model prediction of new data (*Y*-values) is possible only by measuring *X*-values. This approach is advantageous, especially if time-consuming and interference-prone parameters can be overcome by fast methods such as infrared spectroscopy. A combination of these methods was successfully applied in different areas, i.e. wood chemistry for extractives characterization [19], determination of natural durability and lignin composition [20–22] and food technology [23].

The objective of the present study was to develop PLS-R models for the prediction of respiration activity RA$_{4d}$ (oxygen uptake) and humic acid content in composts based on FTIR spectra and reference values. Prediction of these parameters can be established due to the comprehensive information inherent in the spectra. Such approach allows assessing stability of unknown compost samples very fast avoiding time consuming analyses.

2. Experimental

2.1. Materials

Samples originating from different sources were investigated to provide a wide range of respiration activities and humic acid contents. Running processes were included to achieve this target. Compost ingredients of the sample sets used for the calculation of the PLS-R models are compiled in Table 1.

The industrial processes (plants I and II) and the lab-scale process were operated exclusively with biogenic waste. Biogenic waste is separately collected and comprises yard waste (grass clippings, twigs, leaves, plants), market waste (fruits, vegetables) and kitchen waste. Due to the yard waste this mixture always contains a considerable amount of inorganic compounds (clay minerals, carbonates).

From the Austrian point of view composts are the final product of biogenic waste materials, which have undergone aerobic biological processing. These criteria do not apply to all foreign composts. "Composts" from foreign countries also included residues from anaerobic digestion of biogenic waste and leftovers.

2.2. Sampling and sample preparation

Sampling in Austrian composting plants took place according to Austrian Standards ÖNORM S 2123-1 [24]. Representative fresh samples were screened through a 20 mm sieve after shredding. Respiration activity was determined using the fresh sample. For chemical and spectroscopic investigations a representative subsample (about 1 kg of the original fresh sample) was air-dried, ground in an agate mill and screened through 0.63 mm to provide an appropriate particle size according to Austrian Standards for chemical analyses.

The Swiss Research Center Agroscope Reckenholz Tänikon provided representative compost samples (150–200 g, dried, milled and sieved <2 mm). To obtain a uniform particle size samples were ground again in an agate mill and screened through 0.63 mm.

Table 1
Origin and composition of sample sets used for prediction models (numbers in brackets are valid for the model including composts with humic acid contents >40% ODM)

Sample origin	Ingredients	Number of samples used for PLS-R model calculation for	
		HA prediction HA-P	RA$_{4d}$ prediction RA-P
Composts from various Austrian and foreign composting plants	Biogenic waste and additives: leftovers, sewage sludge, poultry manure, clay minerals Residues from anaerobic digestion	92 (101)	18
Samples from an on-going industrial process lasting 280 days in composting plant I	Biogenic waste comprising yard and kitchen waste	28 (29)	8
Parallel lab-scale process of samples from plant I	Biogenic waste comprising yard and kitchen waste	92 (92)	47
Samples from an on-going industrial process lasting 260 days in composting plant II	Biogenic waste comprising yard and kitchen waste	47 (47)	42
Sum		259 (269)	115

2.3. Analyses

Loss on ignition (LOI) was determined according to Austrian Standard Methods ÖNORM S 2023 [25]. Humic acid analysis was carried out according to Gerzabek et al. [5] based on alkaline extraction with 0.1 molar sodium pyrophosphate solution and precipitation with HCl (37%). Based on gravimetric determination humic acid contents were calculated from photometrically measured optical densities and referred to organic dry matter (ODM = LOI). Limit of determination: 4% HA, accuracy: 1.5% and precision: ±0.3%. Extractable humic acids served as parameter to describe progressing humification processes in composts [6,26].

2.4. Biological tests

Respiration activity was measured over a 4-day-period (RA_{4d}) in a Sapromat (Voith Sulzer) according to Binner and Zach [2] recording the oxygen uptake (mg O_2) referring to 1 g of dry matter ($g^{-1}DM$). Limit of determination: 1 mg O_2 g^{-1} DM, accuracy: 0.5 mg O_2 g^{-1} and precision ±0.2 mg.

2.5. Infrared spectroscopic investigations and spectra treatment

FTIR absorbance spectra were recorded on a Bruker (Ettlingen, Germany) FTIR spectrometer (EQUINOX 55) equipped with a DTGS detector. The 2 mg samples were mixed with 200 mg KBr (Aldrich; 22,186-4; FTIR grade), homogenized in a mortar and the 13 mm KBr pellets were prepared under vacuum in a standard device under a pressure of 75 kN cm^{-2} for 3 min. Thirty-two scans per sample were collected in the wavenumber range 4000–400 cm^{-1} in transmission mode at a spectral resolution of 4 cm^{-1}, and the collected spectra were ratioed against air as background.

Spectra of 10 subsamples were recorded to proof the repeatability. The test by the integrated OPUS Software results in an average conformity of 98.4% (range of 96.9–99.2% if each of the 10 spectra is set as a reference).

To illustrate the emerging bands spectra were processed (smoothed and derived) according to Savitzky and Golay [27] by means of a 17-points smoothing filter and a second order polynom to obtain second derivatives (Fig. 1).

For multivariate data analysis spectra were vector-normalized. The procedure is as follows: Y-values of the spectrum are averaged. This average value is then subtracted from the spectrum so that the middle of the spectrum is pulled down to $Y = 0$. The sum of the squares of all Y-values is then calculated and the spectrum is divided by the square root of this sum.

SPSS 12.0 for Windows was used for calculation of confidence intervals and standard deviation of intercepts.

2.6. Multivariate data analysis

Multivariate data analysis (partial least squares regression) was carried out using the OPUS 5 Quant software package (BRUKER Optics, Germany).
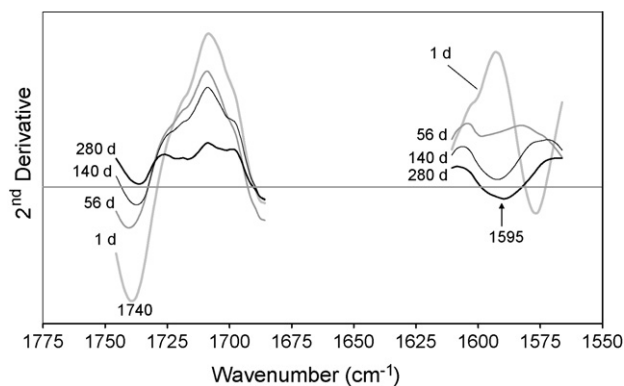

Fig. 1. IR spectroscopic characteristics (second derivative of vector-normalized spectra) of composting days (d): 1 d, 56 d, 140 d and 280 d.

The procedure comprises three steps: in a first step; the preprocessed (vector-normalized) infrared data were regressed against the calibration component, and by means of full cross-validation (CV) with one sample omitted a significant number of PLS components was obtained [21]. CVall stands for calibration and cross-validation for each model using all spectra as described in Table 1.

For model evaluation test set validation (second step) and robustness verification (third step) were performed. For test set validation (TS) the data set was divided and each group was used for both cross-validation and test set validation. Calibration and cross-validation (CV1,3) of the first data set was carried out using the second data set for test set-validation (TS2,4). Then the second data set was used for calibration and cross-validation (CV2,4) and the first data set for test set validation (TS1,3). The same procedure was done by using one-third/two-thirds of the data set. All models were calculated to a maximum rank of 10 and the results of the calibration (R^2 coefficients of determination and root mean square error of estimation, RMSEE) (not shown), the cross-validation (R^2 and RMSECV root mean square error of cross-validation) and the test set validation (R^2 and RMSEP root mean square error of prediction) were compared. Therefore, test set validation was performed not only using the calibration with optimal rank in the cross-validation (as usual in an external validation), but also an optimal rank was defined through test set validation. The comparison of the ranks gives a first indication of the predictive ability of the model, because models with large differences between the ranks determined by CV and TS are never satisfactory [21].

In a third step, the robustness of the model was verified by cross-validation with increasing numbers of samples omitted. The progression of model statistics such as R^2, RMSECV and number of principal components (PCs) in dependence on the number of samples omitted was followed.

3. Results and discussion

Process-originated samples reflected progressing stages of composting and the development of humic acids corresponding to the stage of humification. The variety of humic acid contents in final products (Austrian and foreign composts in

Table 1) can be traced back to process operation and various input materials. The samples covered a wide range (4.5–45.6% ODM) of humic acid contents reachable by composting and respiration activities (oxygen uptake from 60.6 to 1.0 mg g^{-1} DM) usually found in composts and biogenic waste undergoing treatment, respectively. Respiration activity decreased with increasing stabilization and a low oxygen uptake (<7 mg g^{-1} DM) was measured in stabilized materials.

3.1. Infrared spectroscopic characteristics

Infrared spectroscopic characteristics of several samples (composting process plant I) are shown in Fig. 2 to illustrate the changing band heights from the biogenic input material of the first day (1 d) to the final product (280 d) that represents a compost with a high humic acid content. Respiration activity decreased from 60.6 mg O$_2$ g^{-1} DM at the beginning (1 d) to 2.3 mg O$_2$ g^{-1} DM after 280 days. Humic acid content was found to be 45.6% after 280 days.

During composting absorption bands of biogenic waste tend to broaden due to manifold interactions of degrading organic molecules. As these qualitative aspects of spectral changes during composting and the assignment of bands were presented in previous publications [7,14,28], the organic bands mentioned here are limited to the ones used for prediction models.

Bands of inorganic components can be unequivocally assigned to the corresponding functional group, which does not apply to all organic bands due to overlapping. Several "indicator" bands are marked in the spectra (Fig. 2): the aliphatic methylene bands at 2920 and 2850 cm^{-1} representing the skeleton of many biomolecules, the region between 1790 and 1530 cm^{-1} including the 1740 cm^{-1} band (aldehydes, ketons, esters, carboxylic group), the amide II band at about 1540 cm^{-1}, the (aromatic) amine band at 1320 cm^{-1}, the band at 1260–1240 cm^{-1} (C–O vibration of carboxylic acids and C–N of amide III) (Fig. 2). It is not possible to unequivocally assign the 1640 cm^{-1} band due to overlapping of aromatic C=C vibrations, functional group vibrations such as C=O (carboxylates and amides), C=C (alkenes) and OH from water, all contributing to this strong band.
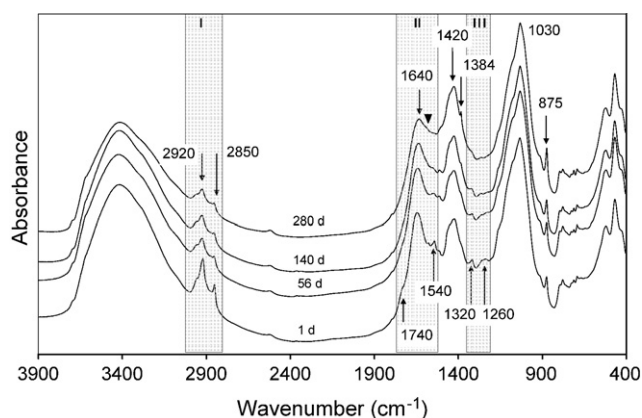

Fig. 2. Infrared spectra of biogenic waste during the composting process in plant I (1 d, 56 d, 140 d, 280 d) indicating the most important bands and the selected areas for the prediction models of respiration activity (I, II, III).
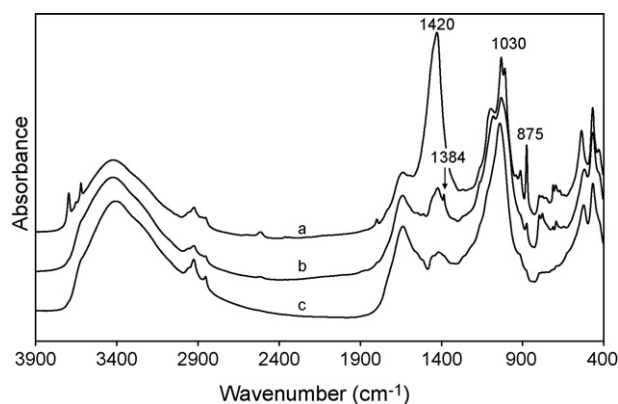

Fig. 3. IR spectroscopic pattern of mineral components in composts a, b and c.

Mineral compounds show a relative increase during composting. Despite increasing intensities during composting their contribution is only significant for a specific process observed. Whereas functional groups attributed to different organic compounds and related metabolic products are present in all compost spectra, inorganic components can differ considerably depending on the geological background and process operation (i.e. addition of clay minerals or carbonates during the process). Nitrate as a mineralization product of organic nitrogen containing molecules indicates an advanced stage of composting. However, the assigned band at 1384 cm^{-1} is not necessarily found in all stabilized composts. Fig. 3 shows the strong bands of different mineral compounds in composts a, b and c. Apart from clay minerals (1030 cm^{-1}) carbonates contribute to the inorganic components of compost a (strong carbonate bands at 1420 and 875 cm^{-1}) and compost b (weak carbonate bands). No carbonates are found in compost c.

3.2. Prediction of the respiration activity

For the prediction model of respiration activity 115 samples were investigated comprising samples from processes and composts. In a first step, PLS-regression was computed including the whole wavenumber range (4000–400 cm^{-1}). X-loadings of the PLS components (not shown) revealed the contribution of both organic and inorganic bands to the variation between the samples according to the bands mentioned above. Focusing on organic bands for the prediction model the inorganic bands of nitrate at 1384 cm^{-1}, carbonate at 1420 and 875 cm^{-1} and silica at 1030 cm^{-1} (Fig. 3) were excluded.

Therefore, data evaluation focused on the following selected regions in the spectrum: 3000–2800 cm^{-1} (I), 1788–1533 cm^{-1} (II) and 1348–1201 cm^{-1} (III) implying that respiration activity should be reflected by highly changing bands assigned to metabolites (Fig. 2). Variance was displayed by seven principal components. Fig. 4 represents the PLS-loadings of the 7 PCs used for the prediction model. PLS-loadings of PC 1 (explained variance 47%) show the strong contribution of the aliphatic methylene bands at 2920 and 2850 cm^{-1}, of the bands at 1540 and 1320 cm^{-1} and a considerable influence of the bands at 1740, 1640 and 1250 cm^{-1}. All PLS-loadings (Fig. 4 a and b)
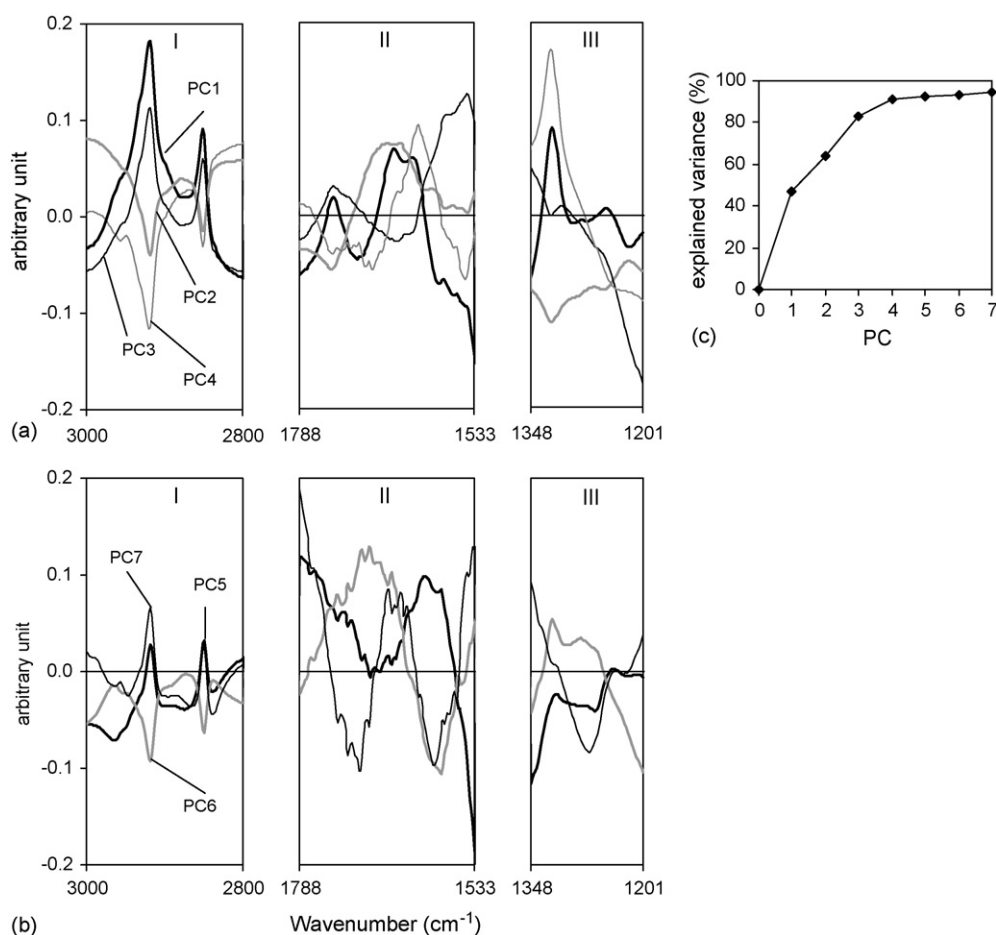
Fig. 4. PLS-loadings of the 7 PCs (a) PC 1–PC 4 and (b) PC 5–PC 7 used for the prediction model show the contribution of the selected wavenumber regions and (c) variance explained by each PC.

confirm the appropriate selection of wavenumber regions for the prediction model. The variance explained by each of the seven PCs is illustrated in Fig. 4c.

For the correlation between measured and predicted respiration activities shown in Fig. 5a, a high coefficient of determination ($R^2 = 94\%$) has been achieved with a RMSECV for oxygen uptake of $2.9 \, \mathrm{mg \, g^{-1}}$ DM. Fig. 5b illustrates the regression line and the standard deviation of slope and intercepts values.

To evaluate the calculated model (CVall) for RA_{4d} prediction (RA-P) the data set was subjected to the procedure described in Section 2. All model statistics are shown in Table 2.

The cross-validation of the models (CV1, CV2 and CVall) and the test set validation (TS1 and TS2) led to nearly the same model statistics (Table 3). That means that all spectra can be used for the computation of a model for prediction of respiration activity. Other authors [21,29] have proven this procedure.

The prediction of respiration activity from the infrared spectrum could constitute a less time-consuming method for the determining of stability in other waste materials such as municipal solid waste in which the same "reactivity" bands are identified [28]. Moreover, this fast prediction serves as a control method if respiration activity determination fails due to

toxic or other inhibiting effects showing no or less oxygen uptake.

3.3. Prediction of extractable humic acids

Based on the fact that aromatic rings are a main constituent of the humic acid molecule skeleton [30], absorption bands in the infrared spectrum are expected in regions of aromatic C=C vibrations. The broadening during composting towards lower wavenumbers shown in Fig. 2 (▼) is revealed by the evolution of a band at $1595 \, \mathrm{cm^{-1}}$ visible in the second derivatives of the vector-normalized spectra (Fig. 1). The observation of the emerging and increasing band gives reason to expect a good correlation of this region with the measured humic acid contents. Slight differences in the vector-normalized spectra are resolved by means of multivariate data analysis. As described by Gossart et al. [31] different states of humic acids that are not visible in the spectra could be assigned to the acid or salt form by multivariate curve resolution. The intensity of the band at $1740 \, \mathrm{cm^{-1}}$ that can be attributed to C=O stretch vibrations of esters, aldehydes and ketones becomes weaker with increasing humic acid contents (Fig. 1). Inclusion of this band in the multivariate evaluation could improve the prediction of humic acid contents. It is hypothesized that the degradation of metabo-
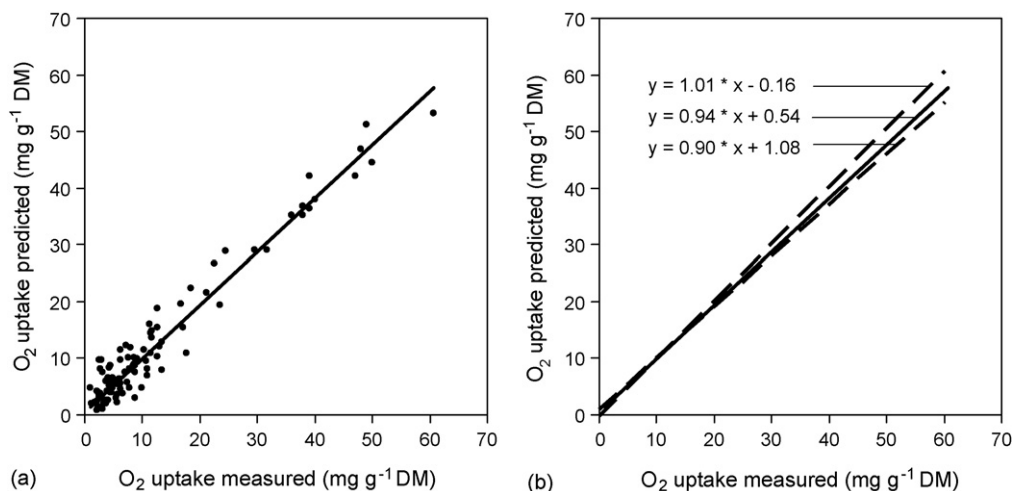
Fig. 5. Predicted vs. measured respiration activities (oxygen uptake) over a 4-day-period (RA$_{4d}$), based on a PLS-R model (RA-P) calculated with infrared spectra and RA$_{4d}$ values of 115 samples (a); regression line, standard deviation of slope and intercepts values are indicated in (b).

Table 2
Parameters of PLS-Regressions for model RA-P

CV/TS	Number of spectra	PCs	R^2 (CV) (%)	R^2 (TS) (%)	RMSECV (mg g^{-1} DM)	RMSEP (mg g^{-1} DM)
CVall	115	7	94	–	2.9	–
CV1	58	7	92	–	3.1	–
TS2	57	5	–	92	–	3.7
CV2	57	7	95	-	3.1	–
TS1	58	6	–	92	–	3.2
CV3	77	7	94	–	3.3	–
TS4	38	7	–	94	–	3.3
CV4	38	6	90	–	3.4	–
TS3	77	4	–	92	–	3.7

lites also indicates advancing humification. Moreover, to avoid a possible influence of water, the water band at 1635 cm^{-1} was excluded.

If the selected wavenumber areas for parameter prediction are compared it becomes visible that the selected regions for humic acid prediction are included in the selected region for respiration activity prediction. It confirms that respiration activity and humic acid content are reciprocally related.

After selection of these bands including the appropriate wavenumber areas (1745–1685 cm^{-1} and 1610–1567 cm^{-1}) for data analysis, PLS-R was carried out using 269 samples for the calculation of the humic acid content prediction model. R^2 of

86% and a RMSECV of 3.1% ODM were obtained. HA contents above 40% ODM are underestimated by this model. Exclusions of samples with HA contents >40% ODM from the model (259 samples) leads to R^2 of 87% and a RMSECV of 2.6% ODM. These results are presented in Fig. 6a that shows the predicted versus measured humic acid contents plot of the cross-validation (CVall). Fig. 6b illustrates the regression line and the standard deviation of slope and intercepts values.

The reason of underestimation is not clear at this moment. Possibly at higher HA contents chemical analyses are interference-prone or unknown effects emerge requiring additional wavenumber ranges for PLS-R. More samples are

Table 3
Parameters of PLS-Regressions for model HA-P (numbers in brackets are valid for the model including composts with humic acid contents >40% ODM)

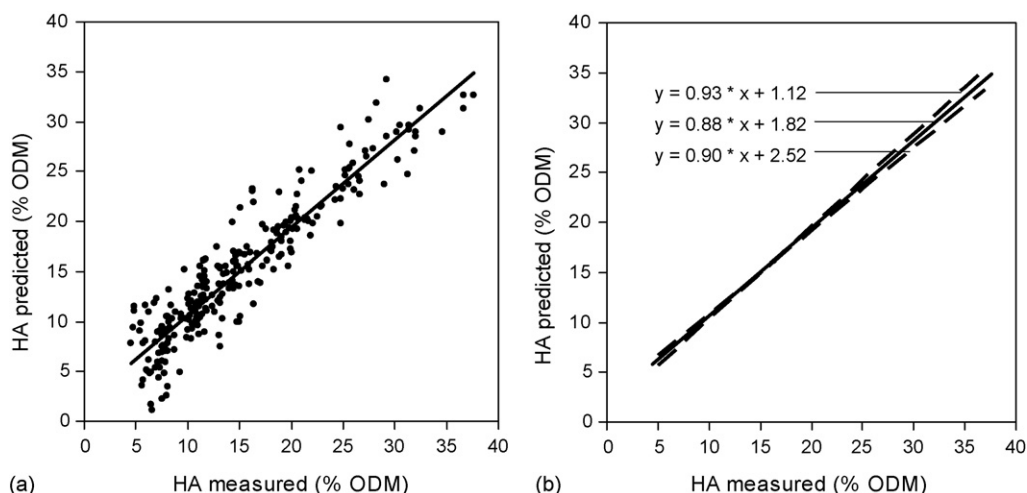| CV/TS	Number of spectra	PCs	R^2 (CV) (%)	R^2 (TS) (%)	RMSECV (% ODM)	RMSEP (% ODM)
CVall	259 (269)	7 (7)	87 (86)	–	2.6 (3.1)	–
CV1	131 (134)	7 (7)	86 (86)	–	2.8 (3.0)	–
TS2	128 (135)	7 (6)	–	87 (84)	–	2.6 (3.2)
CV2	128 (135)	7 (7)	87 (84)	–	2.5 (3.3)	–
TS1	131 (134)	5 (7)	–	84 (85)	–	3.0 (3.1)
CV3	194 (202)	6 (7)	86 (86)	–	2.7 (3.0)	–
TS4	65 (67)	6 (6)	–	90 (87)	–	2.4 (3.1)
CV4	65 (67)	6 (7)	86 (84)	–	2.8 (3.1)	–
TS3	194 (202)	6 (7)	–	82 (81)	–	3.1 (3.8)

Fig. 6. Predicted vs. measured humic acid contents plots of the cross-validation of the PLS-R models calculated with selected infrared spectral areas (wavenumbers: 1745–1685 cm^{-1} and 1610–1567 cm^{-1}) and HA contents based on 259 samples (a); regression line, standard deviation of slope and intercepts values are indicated in (b).

necessary to verify these assumptions being not an easy task to make composts at such high concentrations available.

Evaluation of the calculated models (CVall) for HA prediction (HA-P) was performed as described in Section 2. Validation results and model statistics are shown in Table 3 and in Fig. 7, respectively. The prediction error of model including HA contents >40% ODM (values in brackets) is higher. However, the model stability is not affected.
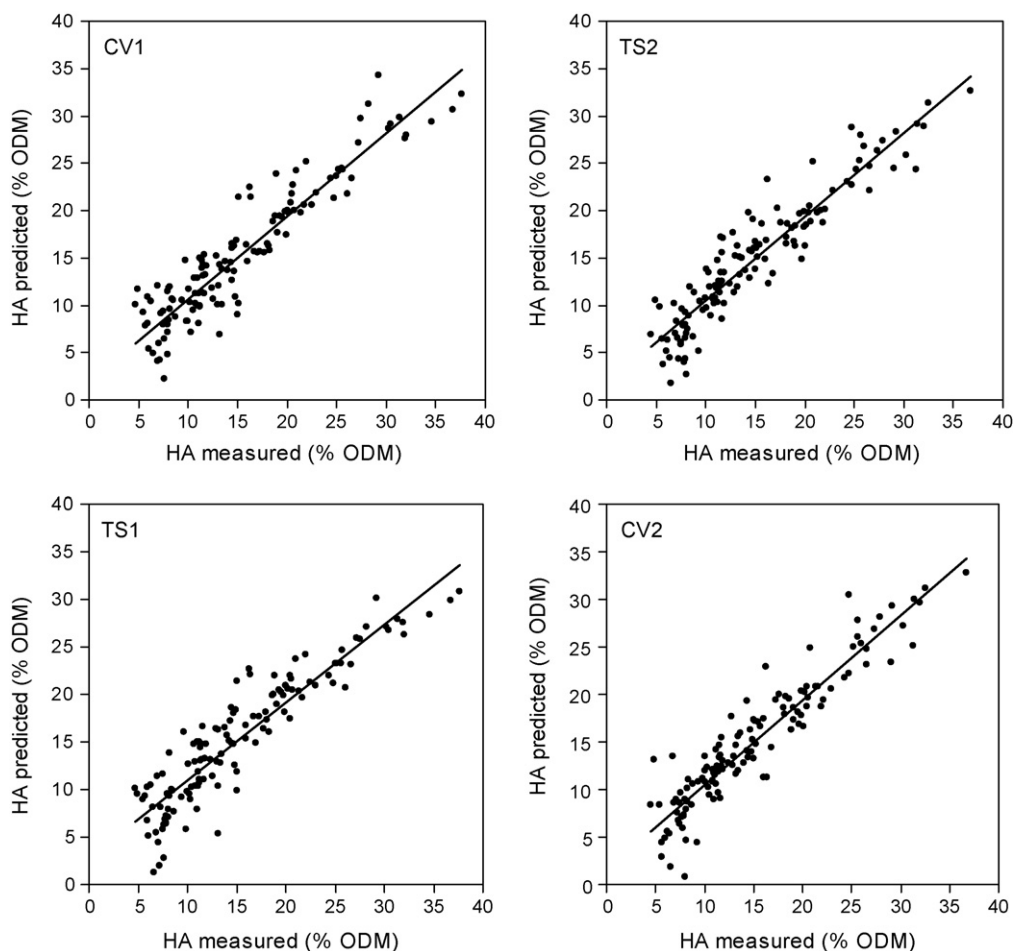
Fig. 7. Cross-validation (CV1 and CV2) and test set validation (TS1 and TS2) results of the divided data set used for model HA–P (CVall) (areas: 1745–1685 cm^{-1} and 1610–1567 cm^{-1}).

Table 4
Measured and predicted values of respiration activity (RA$_{4d}$) and humic acid contents (HA) of 10 replicates of a compost sample, and the confidence intervals at a confidence level of 99%

Subsample Repetition	RA$_{4d}$ measured (mg O$_2$ g^{-1} DM)	RA$_{4d}$ predicted (mg O$_2$ g^{-1} DM)	Deviation (mg O$_2$ g^{-1}DM)	HA measured (%, ODM)	HA predicted (%, ODM)	Deviation (%, ODM)
S1	4.4	2.1	2.3	18.3	17.8	0.5
S2	4.4	6.1	−1.7	18.3	16.9	1.4
S3	4.4	5.5	−1.1	18.3	18.1	0.2
S4	4.4	4.8	−0.4	18.3	17.4	0.9
S5	4.4	4.2	0.2	18.3	17.0	1.3
S6	4.4	4.7	−0.3	18.3	18.0	0.3
S7	4.4	5.8	−1.4	18.3	15.7	2.6
S8	4.4	3.5	0.9	18.3	18.8	−0.5
S9	4.4	4.9	−0.5	18.3	18.3	0.0
S10	4.4	4.8	−0.4	18.3	18.1	0.2
Average		4.6			17.6	
STDEV		1.2			0.9	
Upper CL		5.8			18.5	
Lower CL		3.4			16.7	

STDEV, standard deviation; CL, confidence limit.

Cross-validation of the models (CV1, CV2 and CVall) and test set validation (TS1 and TS2) led to almost the same model statistics. That means that all spectra can be used for the computation of a model for prediction of humic acid content and the same predictive ability is expected.

In the third step, the robustness of the model HA-P (CVall) was proven by increasing the number of samples omitted during cross-validation as applied for other natural samples [21,29]. Fig. 8 shows the minor impact of this procedure on the R^2, the RMSECV and the number of PCs leading to the conclusion that the model is stable.

The extensive procedure to validate the PLS-R models is justified to obtain reliable models. Such as many multivariate statistics PLS-R in spectroscopy implies the risk that indirect correlations can be made with other parameters to a not directly measurable extent. Apart from other quantification problems in spectroscopy such as, e.g. scattering and particle size, peaks in an infrared spectrum are seldom the result of a single molecular moiety or a structural property as mentioned above. These features are additive and unresolved. Underlying inorganic features can have an influence depending on their nature, composition

and content, even if the main bands have been excluded. Therefore, several reasons suggest to divide the sample set in different data sets (TS and CV) and to test them mutually: the number of samples, marginal differences in some cases, the complex varying sample composition, underlying inorganic spectral features and the relatively high number of PCs that are necessary to explain the variance.

To verify the repeatability of spectra and the resulting prediction of both parameters 10 replicates of the same sample were tested. Table 4 shows the prediction of respiration activities and humic acid contents based on these replicates. Standard deviation was found to be 1.2 mg O$_2$ g^{-1} (DM) for RA$_{4d}$ and 0.9% (ODM) for HA contents. The reference values are within the confidence limits, and all predicted values are within the limits of the prediction error (RMSEP).

4. Conclusions

Carefully validated FTIR–PLS-R prediction models for respiration activity and for humic acid content represent an appropriate technique to assess compost stability and allow evaluating unknown compost samples reliably. Inhibiting effects that can influence biological tests such as respiration activity can be well spotted. From an environmental point of view, humification of composts is considered a highly desirable target. The conventional methods of repeated humic acid extraction and respiration activity determination take 5, respectively, 4 days. FTIR spectroscopy combined with multivariate data analysis reduces the expenditure of time drastically. The described methods can be used to evaluate many samples within a short time as well as for the selection of (control-) samples prior starting time-consuming, expensive analyses. Due to the easy handling, the low interference of the technical equipment, and the marginal need of chemicals compared to conventional methods the use of PLS-R models to predict respiration activity and humic acid contents based on FTIR spectra should enhance the application of this fast analytical method in waste management.
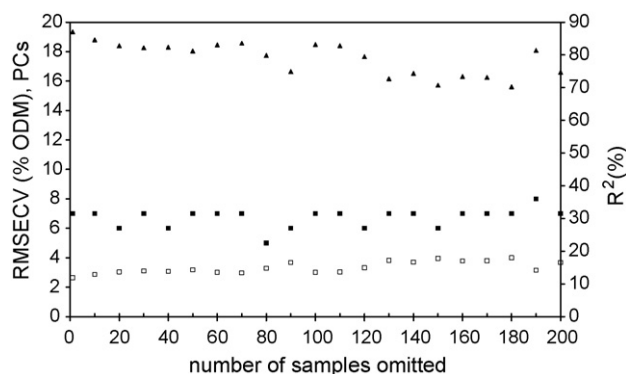

Fig. 8. Progression of the recommended PCs (■), the RMSECV (□) and the R^2 (▲) in dependence on the number of samples omitted during cross-validation (model with 259 samples).

Acknowledgement

References

[1] F. Adani, F. Tambone, A. Gotti, Waste Manage. 24 (2004) 775.

[2] E. Binner, A. Zach, Waste Manage. Res. 17 (1999) 543.

[3] A. Garcia-Gomez, M.P. Bernal, A. Roig, Compost Sci. Util. 13 (2005) 127.

[4] J. Ryckeboer, S. Cops, J. Coosemans, in: S. Klammer (Ed.), Microbiology of Composting, Springer, Berlin, Heidelberg, 2002, p. 527.

[5] M.H. Gerzabek, O. Danneberg, E. Kandeler, in: F. Schinner, R. Öhlinger, E. Kandeler, R. Margesin (Eds.), Bodenbiologische Arbeitsmethoden, Springer Verlag, Wien, 1993, p. 107.

[6] P. Castaldi, G. Alberti, R. Merella, P. Melis, Waste Manage. 25 (2005) 209.

[7] E. Smidt, M. Schwanninger, Spectrosc. Lett. 38 (2005) 247.

[8] E. Smidt, K.U. Eckhardt, P. Lechner, H.R. Schulten, P. Leinweber, Biodegradation 16 (2005) 67.

[9] P. Zaccheo, G. Ricca, L. Crippa, Compost Sci. Util. 10 (2002) 29.

[10] M. Grube, J.G. Lin, P.H. Lee, S. Kokorevicha, Geoderma 130 (2006) 324.

[11] N. Calace, M. Capolei, M. Lucchese, B.M. Petronio, Talanta 49 (1999) 277.

[12] A. Ouatmane, V. D'Orazio, H. Hafizoglu, N. Senesi, Compost Sci. Util. 10 (2002) 39.

[13] M. Schwanninger, B. Hinterstoisser, C. Gradinger, K. Messner, K. Fackler, J. Near Infrared Spec. 12 (2004) 397.

[14] E. Smidt, P. Lechner, M. Schwanninger, G. Haberhauer, M.H. Gerzabek, Appl. Spectrosc. 56 (2002) 1170.

[15] A. Moron, D. Cozzolino, J. Agric. Sci. 142 (2004) 335.

[16] K. Pollanen, A. Hakkinen, S.P. Reinikainen, J. Rantanen, M. Karjalainen, M. Louhi-Kultanen, L. Nystrom, J. Pharm. Biomed. 38 (2005) 275.

[17] A.D. Zhang, W.X. Zeng, T.M. Niemczyk, M.R. Keenan, D.M. Haaland, Appl. Spectrosc. 59 (2005) 47.

[18] K. Esbensen, Alborg University, Esbjerg, 2002.

[19] A. Alves, M. Schwanninger, H. Pereira, J. Rodrigues, Holzforschung 60 (2006) 29.

[20] N. Gierlinger, D. Jacques, M. Schwanninger, R. Wimmer, B. Hinterstoisser, L.E. Pâques, Can. J. Forensic Res. 33 (2003) 1727.

[21] N. Gierlinger, M. Schwanninger, B. Hinterstoisser, R. Wimmer, J. Near Infrared Spec. 10 (2002) 203.

[22] J. Rodrigues, A. Alves, H. Pereira, D. da Silva Perez, G. Chantre, M. Schwanninger, Holzforschung 60 (2006) 402.

[23] R.A. Cocciardi, A.A. Ismail, J. Sedman, J. Agric. Food Chem. 53 (2005) 2803.

[24] ÖNORM S 2123-1, Sampling plans for waste—Part 1: sampling of heaps, 2003.

[25] ÖNORM S 2023, Analytical methods and quality control of compost, 1986.

[26] G.A. Baddi, M. Hafidi, V. Gilard, J.C. Revel, Agronomie 23 (2003) 661.

[27] A. Savitzky, M.J.E. Golay, Anal. Chem. 36 (1964) 1627.

[28] E. Smidt, K. Meissl, Waste Manage. 27 (2007) 268.

[29] M. Schwanninger, B. Hinterstoisser, Proceedings of the 11th International Symposium on Wood and Pulping Chemistry, Nice, III, 2001, p. 641.

[30] K.H. Tan, Humic Matter in Soil and the Environment—Principles and Controversies, Marcel Dekker, New York, Basel, 2003.

[31] P. Gossart, A. Semmoud, C. Ruckebusch, J.P. Huvenne, Anal. Chim. Acta 477 (2003) 201.

Talanta

Review

Biosensors as a tool for the antioxidant status evaluation

L.D. Mello, L.T. Kubota *

Instituto de Química, UNICAMP, P.O. Box 6154, 13083-970 Campinas, SP, Brazil

Abstract

Antioxidants are one of the main ingredients that protect food attributes by preventing oxidation that occurs during processing, distribution and end preparation of food. Physiological antioxidant protection involves a variety of chemical system of endogenous and exogenous origin in a multiplicity of pathways. Associate to this, researches have been directed in the development of methods as biosensors that can characterize antioxidants capable of removing harmful radicals in living organisms in an adequate way. Biosensors have represented a broad area of technology useful for environmental, food monitoring, clinical applications and can represent a good alternative method to evaluate the antioxidant status.

The demonstration of the highlighted current application of biosensor as a potential tool to evaluate the antioxidant status is the main aim of this review.

© 2006 Elsevier B.V. All rights reserved.

Keywords: Antioxidant; Biosensors; Oxidative stress

Contents

1. Introduction

The study of free radicals and antioxidants in biology and food technology has been widely recognized. The prevention of the oxidative reactions in foods, pharmaceutical and cosmetics as well the role of reactive oxygen species (ROS) in chronic degenerative diseases are questions that continue to be investigated due to the difficulties associated to the methods used in the evaluation of antioxidant status in these systems.

Methods for assessing antioxidant properties can be classified basically into two broad categories reflecting the idea on activity in foodstuffs and the antioxidant behavior in human body. In case of food systems, the necessity is the evaluation of the efficacy of an antioxidant in providing protection for the product or the necessity to characterize possible antioxidant compounds. Another category involves the contribution of endogenous antioxidants or nutrients for the modulation of the pathological consequences of ROS *in vivo* activity. In this sense, antioxidants tests can be basically classified in two groups: those assays based on the inhibition of the human low-density lipoprotein oxidation and those assays used to measure oxygen free radical scavenging ability. Several procedures are reported in the literature for measuring the total antioxidant capacity of a biological sample or plant extracts. The principles and the information that these methods provide have been extensively reviewed [1–3].

The evaluation of antioxidant properties is not an easy task. Many methods can be used to determine this activity, however several factors can affect the estimated activity, such as conditions and analytical methods [4,5]. Thus, *in vitro* systems are easier, faster and more cost-effective compared to the traditional bioassays *in vivo*. Therefore, test of the direct antioxidant capacity *in vitro* is useful, because if a substance that is poorly effective *in vitro* will not be better *in vivo*. It can also be evaluated about some possibility of damaging effects [6]. In this context is adequate to define the terms *antioxidant activity* and *antioxidant capacity* whose meanings are quite distinct. The antioxidant activity corresponds to the rate constant of a single antioxidant against a given free radical. The antioxidant capacity is the measurement of moles of a given free radical scavenged by a test solution, independently of the antioxidant present in the mixture [7].

Researches have been directed to the development of methods as biosensors that can characterize antioxidants capable of removing harmful radicals in living organisms in an adequate way. Since the pioneering work of Clark, biosensors have represented a broad area of emerging technology useful for environmental and food monitoring. In clinical applications as diagnostics delivering devices of important diseases and related to the ROS generation in excess such as diabetes. Recently this method has been cited for cancer-related screening testing [8,9]. This progress in potential application of biosensors can be attributed to its inherent characteristics such as rapid and real-time analysis that increase the assay speed and flexibility as well as the possibility of automatic and multi-target analyses with low cost. In this sense, the concept of biosensors also proceeded for a more wide modern definition in comparison to the proposed by Clark and coworkers. Biosensors are a sub-group of chemical sensors and it can be define as a self-contained integrated device, which is able to provide specific quantitative or semi quantitative analytical information using a biological recognition element (biochemical receptor), which is retained in direct and spatial contact with the transduction element [10].

Evaluations of the antioxidant status by means of biosensors have been carried out by measurements of biomarkers. Biomarkers are biological molecules whose chemical structure have been modified as a result of an attack by free radicals or others reactive species and that can be used as indicators to reliably asses oxidative stress status in animals models and in humans.

Developed biosensors employ different strategies ranging since direct analysis of compounds with characteristics antioxidants, measuring the antioxidant enzymes activity and detection of free radicals. Most of them uses immobilized enzymes in combination with electrochemical transducer, in particular, amperometric devices. Enzyme-based biosensors are very suitable since they show excellent selectivity for biological substances and can directly determine and/or monitor antioxidant compound in a complex media such as biological or vegetable samples without needing a prior separation step. Those amperometric transducer combine redox enzymes reactions to measure either consumed oxygen or produced hydrogen peroxide by oxidase enzymes and the reduced form of β-nicotinamide adenine dinucleotide (phosphate) NAD(P)H by dehydrogenase enzymes. During the course of the catalytic reaction on the electroactive substrates the current produced at an applied potential is related to the concentration of the species in solution. The measured concentration is attributed to a specific biomarker, which the biosensor is selective. This species acts like an antioxidant in the normal biological process. Various enzyme systems and simple compound known as endogenous antioxidants are essential to remove (scavenging) reactive oxygen species from the body to prevent their harmful effects. When the antioxidant capacity of a biological system is overwhelmed by the presence of excess free radical reactive species or the concentration of antioxidants are not sufficient to protect against oxidation, the disease processes are accelerated by oxidative damage to cells. In this sense, the biosensor monitoring the biomarker concentration may yield information associated to the degree of disease or disorder state in light of a particular clinical or research interest.

This relation is also applied to the developed biosensors to monitor radical species formed *in vitro* specific system. Oxygen free radicals are very difficult to measure directly because of their highly reactive nature and their very short half-life. The toxic byproducts of these reactions are related to the biomolecules modifications and the concentration of these byproducts as well as some related enzymes are measured by biosensors to reflect the degree of oxidative damage.

An interesting investigation of overall antioxidant status of the biological system is the potential benefit to health caused by the compound with antioxidant action supplied from nutritional supplements or dietary. Epidemiological studies suggest that these nutrients have a positive effect on general health and more specifically on cardiovascular diseases and cancer [11]. Potential antioxidants analyzed by biosensors include among others,

Vitamin C and phenol-derived compounds. The measured concentration of these compounds present in plant-origin samples corresponds to the quality of the dietary used as antioxidant supplement.

An important indicator in oxidative stress research is the identification of specific oxidized protein in human disease. Damage to DNA is the major endogenous type of pathogenic that induces a variety of diseases including cancer [12], which justify the importance of its early detection. DNA-based biosensors have been used in the identification and quantification of DNA molecules in disease diagnostics; detection of pathogenic organism and detection of toxins [9] and also it has been successful used as a screening method to detect DNA damage. The composition of the developed systems so far consist in a DNA layer immobilized on a surface electrode as oxidation target and using a method of inducing damage such as chemical agent or ionizing radiation. Among the modified substrates, the guanine is the most easily oxidized with the lowest oxidation potential of the nucleic acid bases and its oxidation product 8-oxoguanine is considered a clinical biomarker for oxidative DNA damage [13]. The detection principle reflects the fact that the response of DNA (signal relation to changes of guanine base) is strongly dependent on its structure. Samples containing compounds that can neutralize damaging agents that interact with DNA in an irreversible way and as a result maintain almost constant the DNA signal, can be characterized as antioxidant. The application of these biosensors as screening procedure of antioxidant constitute in a great alternative

because the test reduce the time, complexity and cost of the analysis.

In this context, the demonstration of the current application of the biosensors as a method to evaluate the antioxidant status is the main aim to stimulate further investigation in this area.

2. Outline of biology and chemistry of free radicals and antioxidants

Oxidation is a spontaneous process and constitutes in the main deterioration factor in foods, cosmetics and pharmaceutical, causing alteration in its constituents, which result in a key factor in the nutritional and commercial value of these products. These reactions are caused by the atmospheric oxygen or less frequently by ozone, peroxide or oxidant metals and other agents. In biological fluids, the oxidation reactions are involved in important metabolic routes, during the normal metabolism, but an imbalance in the production and/or removal of these primary products induce an oxidative stress condition [14]. The relevant inter-relationships between ROS and antioxidants are shown in Scheme 1.

In case of *in nature* or manufactured products the oxidation reaction usually begins in the lipid fraction, eventhough other components such as proteins, vitamin and pigments are affected in different manner. In living system, the most susceptible targets to the alteration, beyond lipids in cellular membranes are proteins, enzymes and mainly carbohydrates and DNA in tissues [14].
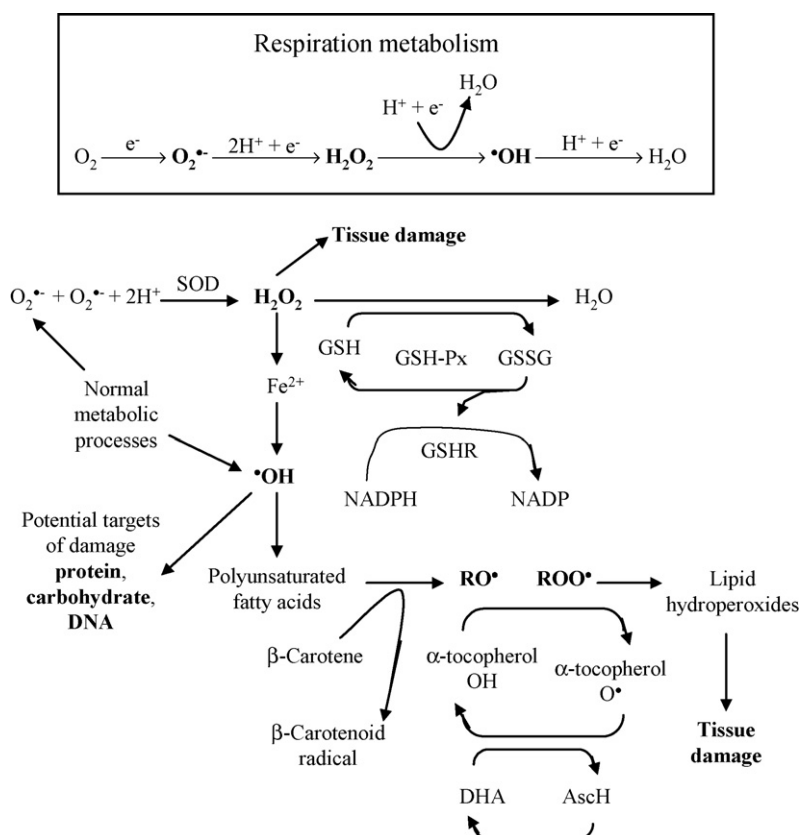
Scheme 1. Relevant relationships between ROS and antioxidants (adapted from [15]).

Table 1
Reactive oxygen species and relevant antioxidants

ROS	Nonenzymatic antioxidants (LMWA)	Enzymatic antioxidants
Singlet O_2	NADPH and NADH	Catalases (CAT)[a]
$O_2^{\bullet-}$ (superoxide radical)	Glutathione (GSH) and thiols	Glutathione peroxidase (GSH-Px)[a]
H_2O_2 (hydrogen peroxide)	Ubiquinol (coenzyme Q)	Superoxide dismutase (SOD)[a]
$^{\bullet}OH$ (hydroxyl radical)	Uric acid	Ceruloplasmin (Cu)[b]
$NO^{\bullet}$ (nitric oxide)	Carotenoids (most commonly β-carotene)[c]	Albumin (Cu)[b]
Lipid peroxide	Vitamin C (ascorbic acid)[c]	Transferin (Fe)[b]
$RO^{\bullet}$ (alkoxyl radical)	Vitamin E (tocopherols)[c]	Ferritin (Fe)[b]
$ROO^{\bullet}$ (peroxyl radical)	Phytochemicals[c]	Myoglobin (Fe)[b]

[a] Free radical scavenging enzymes.
[b] Metal binding proteins.
[c] Dietary antioxidants.

In contrast, the mammalian cells have developed a complex antioxidant defense system to minimize the toxic effect of partially reduced oxygen species. A broader definition of an antioxidant is any substance that when present at low concentration compared to those of an oxidizable substrate significantly delays or prevents oxidation of that substrate [6] and include two classes, primary and secondary antioxidants (Table 1). The primary or chain-breaking antioxidant, AH, include protection by the synthetic and natural origin low-molecular weight antioxidants (LMWA). When it is present in trace amounts, may delay or inhibit the initiation step by reacting with a lipid radical or inhibit the initiation step by reacting with peroxyl or alkoxyl radical resulting in a lesser reactive radical ($A^{\bullet}$) (reactions (1) and (2)). Besides it can act as chain reaction terminators by forming peroxide antioxidant compounds (reactions (3) and (4)) [1].

$$RO^{\bullet} + AH \rightarrow ROH + A^{\bullet} \qquad (1)$$

$$ROO^{\bullet} + AH \rightarrow ROOH + A^{\bullet} \qquad (2)$$

$$RO^{\bullet} + A^{\bullet} \rightarrow ROA \qquad (3)$$

$$ROO^{\bullet} + A^{\bullet} \rightarrow ROOA \qquad (4)$$

Another form of protection is the preventive or secondary antioxidants that retard the rate of oxidation through the enzymatic activities in different mechanisms such as metal chelating, singlet oxygen quenchers or repair systems of damage resulting in oxidation [1].

3. Potential applications of biosensor for evaluation of antioxidant status

Tables 2–9 present the successful application of biosensors for evaluation of antioxidant status. A brief comment about the main aspects of the biology and chemistry of free radicals and antioxidant in the beginning of each topic are also described.

The review was carried out describing works reported in the literature since 2000. In sequence, tables with biosensors applied for characterization of antioxidants based on radical scavenging property, detection/determination of free radicals, antioxidant compounds and enzymatic activity in blood plasma, urine, whole cells, even tissue or natural origin samples, without sample pretreatment. The study is completed with analysis of phytochemicals and synthetic antioxidants that have not recognized as essential nutrients, but apparently play an important antioxidant role in the body. Among the types of biosensors, it is observed those based on electrochemical transducer have dominated this research field. The main reasons are the chain-breaking activity of both electron-transferring and hydrogen-donating antioxidants, in most cases, showing a redox mechanism that is very suitable for the electrochemical measurements.

3.1. DNA as oxidation target

Studies of DNA damage induced by ROS are of special importance because it is the repository of genetic information and it is also present in single copy. It is characterized by a variety of modifications at DNA level that include base and sugar lesions, strand breaks, DNA-protein cross link and base-free sites. However, DNA of all mammalian cells contains trace amounts of modified bases that are indicative of attack by oxidiz-

Table 2
Biosensors applied to detect the antioxidant activity

Target DNA	Intercalator	Transducer[a]	Sample	Precision (as R.S.D.)	Reference
dsDNA (*Calf thymus*)	$[Co(phen)_3]^{3+}$	Voltam. (SPE)	Plant extracts	19% ($n = 8$)	[19]
dsDNA (*Calf thymus*)	$[Co(phen)_3]^{3+}$	Voltam. (SPE)	Yeast	10% ($n = 10$)	[20]
dsDNA (*Calf thymus*)	$[Co(phen)_3]^{3+}$	Voltam. (SPE)	Flavonoids		[21]
dsDNA (Salmon)	MB	Voltam. (ITO)	Gallic acid and glutathione		[22]
dsDNA (*Calf thymus*)	–	Voltam. (SPE)	Tea extracts	16% ($n = 6$)	[23]

[a] Working electrode.

Table 3
Biosensors applied in the superoxide radical detection

Biocomponent	Immobilization	Transducer[a]	Detection range (D.L.)	Stability	Reference
GAO, SOD, tyrosinase	Physical adsorption	Amp. (O_2)	20–250 μmol L^{-1} (1 μmol L^{-1}) (tyr), 100–1200 μmol L^{-1} (10 μmol L^{-1}) (GAO)	3 days (tyr), 3 days (GAO)	[29]
SOD	Physical adsorption	Amp. (H_2O_2)	20–2000 μmol L^{-1} (10 μmol L^{-1})	≥7 days	[30]
Hemin	Physical adsorption	Amp. (PGE)	–	–	[31]
Cyt. *c*	SAM	Amp. (Au)	–	5 days	[32]
SOD	Physical adsorption	Amp. (H_2O_2)	–	–	[33]
SOD	Physical adsorption	Amp. (O_2)	20–1500 μmol L^{-1} (10 μmol L^{-1})	4 days	[34]
SOD	Physical adsorption	Amp. (ME)	–	–	[35]
Cyt. *c*	SAM	Amp. (Au)	–	–	[36]
Cyt. *c*, AOD, XOD	SAM	Amp. (Au)	–	–	[37]
SOD	Chemical cross-linking	Amp. (Pt)	≥100 μmol L^{-1}	–	[38]
Cyt. *c*	SAM	Amp. (Au)	–	–	[39]
Cyt. *c*	SAM	Amp. (Au)	–	–	[40]
SOD	SAM	Amp. (Au)	13–130 nmol L^{-1} (6 nmol L^{-1})	7 days	[41]
SOD	SAM	Amp. (Au)	13–130 nmol L^{-1} (6 nmol L^{-1})	–	[42]
SOD	Physical adsorption	Amp. (H_2O_2)	–		[28]
Cyt. *c*	SAM	Amp. (Au)	0.4–1.5 μmol L^{-1}	–	[43]
SOD	Physical adsorption	Amp. (H_2O_2)	20–2000 μmol L^{-1}	–	[44]
SOD	Physical adsorption	Amp. (H_2O_2)	20–2000 μmol L^{-1}	–	[45]
SOD, HRP	Sol–gel encapsulation	Fluoresc. (glass slide)	<0.02 μmol L^{-1}	–	[46]
SOD	Sol–gel encapsulation	Amp. (Au)	0.2–1.6 μmol L^{-1} (0.1 μmol L^{-1})	>20 days	[47]
Cyt. *c*	SAM	Amp. (SPE –Au)	0.3–1.2 μmol L^{-1}	–	[48]
SOD	Physical adsorption	Amp. (H_2O_2)	20–2000 μmol L^{-1}	–	[49]
SOD	Chemical cross-linking	Amp. (Pt)	20–2000 μmol L^{-1} (10 μmol L^{-1})	30 days	[50]
Cyt. *c*	Physical adsorption	Amp. (ME)	0.86–5.93 μmol L^{-1} (0.50 μmol L^{-1})	30 days	[27]
SOD	SAM	Amp. (CFME)	13–105 nmol L^{-1}	7 days	[51]

[a] Working electrode or transducer.

Table 4
Biosensors applied in the detection of nitric oxide

Biocomponent	Immobilization	Transducer[a]	Detection range (D.L.)	Stability	Reference
HRP	Chemical cross-linking	Amp. (GCE)	2.7–11 μmol L^{-1} (2 μmol L^{-1})	–	[59]
Hemoglobin and DNA	Physical adsorption	Voltam. (PGE)	16.3–163 μmol L^{-1}	–	[60]
Hemoglobin	Physical adsorption	Voltam. (PGE)	<5 μmol L^{-1} (20 pmol L^{-1})	–	[61]

[a] Working electrode.

ing species being removed by excision repairing enzymes and they are known to accumulate with age that can be associated with disease processes [12].

One of the most reactive radical species that induce lesions in DNA is the hydroxyl radical ($^\bullet$OH) generated among other systems by the Fenton reaction (reaction (5)). This species cause cell injury when they are generated in excess or the cellular antioxidant defense is impaired.

$$DNA[Fe(II)] + H_2O_2 \rightarrow DNA[Fe(III)] + OH^- + {}^\bullet OH \quad (5)$$

When $^\bullet$OH is generated adjacent to DNA, it attacks both the deoxyribose sugar and the purine and pyrimidine bases resulting intermediates radicals, which are the immediate precursors for DNA base damage [16]. In living systems many

Table 5
Biosensor applied in the analysis of glutathione and enzyme activity

Biocomponent	Immobilization	Transducer[a]	Sample	Detection range (D.L.)	Stability	Reference
GSH-SOx, HRP	Chemical cross-linking	Amp. (CGE)	–	1–200 μmol L^{-1} (0.50 μmol L^{-1} GSH)	6 days	[71]
GSH-Px	Chemical cross-linking	Amp. (PGE)	Serum	19–240 μmol L^{-1}	60 days	[72]
GSHR	Chemical adsorption	Amp. (GCE)	–	–	–	[73]
Tyrosinase	Physical adsorption	Amp. (CPE)	–	1–8 μmol L^{-1} (100 nmol L^{-1})	–	[74]
Cucumber	Physical cross-linking	Amp. (O_2)	Plant	0.1–2 μmol L^{-1}	60 days	[75]
HRP	Physical cross-linking	Amp. (GCE)	–	0.04–90 μmol L^{-1} (0.3 nmol L^{-1})	30 days	[76]
Biosensor for enzyme activity						
GSHR	Physical adsorption	Amp. (Pt)	Erytrocyte hemolysate	0.08–0.74 IU L^{-1}	–	[77]

[a] Working electrode.

Table 6
Biosensors applied in the uric acid determination

Biocomponent	Immobilization	Transducer[a]	Sample	Detection range (D.L.)	Stability	Reference
UR	Physical adsorption	Conduct. (ME)	Serum	500–1250 mg L^{-1}	–	[88]
UR	Sol–gel encapsulation	CL (sol–gel matrix)	–	1–100 mg L^{-1} (0.1 mg L^{-1})	–	[89]
UOD, HRP	Physical cross-linking	Amp. (O$_2$)	Urine	0.1–0.5 μmol L^{-1}	30 days	[90]
UOD	Sol–gel encapsulation	ECL (sol–gel matrix)	Human serum	1–25 μmol L^{-1}	–	[91]
UR, HRP	Sol–gel encapsulation	Fluoresc. (sol–gel matrix)	Body fluids	<1 μmol L^{-1}	>90 days	[92]
UR	Physical adsorption	Amp. (GCE)	Urine	5–1000 μmol L^{-1} (2 μmol L^{-1})	20 days	[93]
UR	Physical adsorption	Amp. (CPE)	Serum	1–100 μmol L^{-1} (0.19 μmol L^{-1})	–	[94]
UR	Physical adsoprtion	Voltam. (CNT)	Animal tissue	0.1–500 μmol L^{-1} (0.05 μmol L^{-1})	20 days	[95]

[a] Working electrode or transducer.

of the hydroxyl radicals are generated from the metal (M) ion-dependent breakdown of hydrogen peroxide [17,18]. In the presence of ferrous or cupric ions, hydrogen peroxide is converted into the hydroxyl radical by Fenton's reaction. The Fenton-type system is important because it has been implicated as an important mediator of oxidative damage *in vivo* and it is of great interest in terms of reducing the possibility of mutation and consequently the cancer [18].

Mechanisms involving the Fenton system and other way of radical formation like ionizing radiation and nuclease activation have been suggested to evaluate the level of DNA damage that occurs in biological systems and the efficacy of the antioxidant compounds. Procedures based on incubation of calf-thymus DNA with a system producing $^\bullet$OH radicals gives rise the extension of the chemical modifications in the DNA bases evaluating the scavenging property of dietary antioxidants by means of its action as modulators of this degradation process. It is the basic principle used in DNA-based biosensors for characterizing the antioxidants. In many cases are used the Fenton-type reaction as the inducing method to damage the biomolecule. The composition of the system generally consists in a double or single strand DNA layer immobilized on a transducer. Considering that hydroxyl radicals can interact with DNA bases as well as with deoxyribose residues, the antioxidant to be tested is evaluated by changes that occur into DNA layer by means of variation of purine base signal, usually guanine. Table 2 shows screening systems based on DNA-biosensor developed for measuring the antioxidant activity *in vitro* of several types of sample in an adequate and easy way.
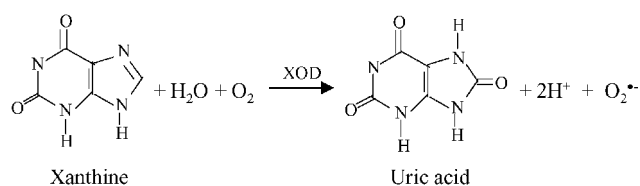
3.2. Monitoring superoxide radical (O$_2$$^{\bullet-}$)

Superoxide anion (O$_2$$^{\bullet-}$) a single-electron reduction product of oxygen is one the most abundant radical produced in biological systems. This cytotoxic species is quite reactive and is easily attacked by other active biomolecules (as nitric oxide), scav-

enged by enzymes (as superoxide dismutase) and antioxidants agents (as ascorbate). Under physiological conditions, superoxide radical is generated in significant quantities, in the nanomolar range, but the variation in its activity occurs in response to neurodegenerative disorders, diabetes, hypertension and others diseases [24,25].

In order to understand the pathological role of superoxides in cellular damage, researches have been leading on the determination of superoxide radical [26].

Electrochemical methods based on biosensors are particularly suitable to determine superoxide anion in a real-time and sensitive way (Table 3) and include two main types. The first group has as mechanism of reduction of cytochrome *c* immobilized on electrode surface by superoxide radical enzymatically produced in solution (reactions (6) and (7)). The superoxide measurement is by means of reaction between superoxide and cytochrome *c* followed by the further oxidation of the later at the electrode surface. The oxidation current is proportional to the superoxide concentration in solution. In this sense, several electrodes configurations have been reported showing the direct or mediated electron transfer between redox protein and the electrode [27].

In solution: Production of superoxide

$$\text{Xanthine} \quad + H_2O + O_2 \xrightarrow{\text{XOD}} \text{Uric acid} \quad + 2H^+ + O_2^{\bullet-} \tag{6}$$

At the electrode: Superoxide detection
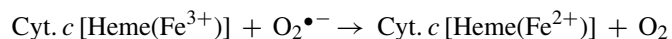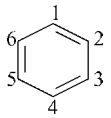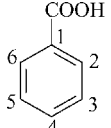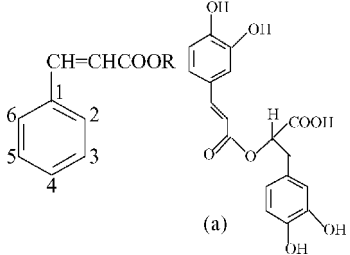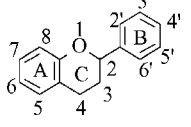
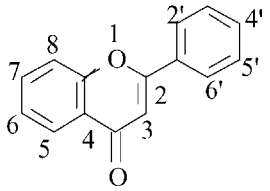$$\text{Cyt. } c\,[\text{Heme}(Fe^{3+})] + O_2^{\bullet-} \rightarrow \text{Cyt. } c\,[\text{Heme}(Fe^{2+})] + O_2 \tag{7}$$
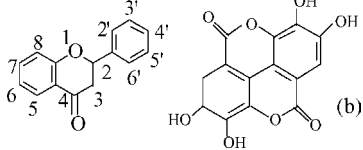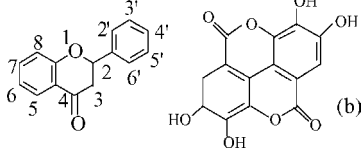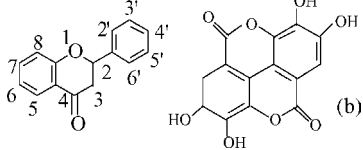
Table 7
Biosensors applied in the ascorbic acid determination

Biocomponent	Immobilization	Transducer[a]	Sample	Detection range (D.L.)	Stability	Reference
POD	Physical adsorption	Amp. (CPE)	Pharmaceutical formulations	200–500 μmol L^{-1} (22 μmol L^{-1})	–	[101]
AOD	Physical adsorption	Amp. (Pt)	Juice fruit	≥3000 μmol L^{-1} (5 μmol L^{-1})	–	[102]
AOD	Physical adsorption	Amp. (SPE)	Fruit	≥7000 μmol L^{-1}	–	[103]
AOD	Physical cross-linking	Amp. (O$_2$)	Commercial pharmaceutical	120–1000 μmol L^{-1}	25 days	[104]

[a] Working electrode.
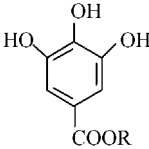
Table 8
Structures of relevant antioxidants in the dietary (adapted from [106])

Compound	Substituent	Structure
Benzenes		
Catechol	1,2-OH	
Resorcinol	1,3-OH	
p-Hydroquinone	1,4-OH	
Pyrogallol	1,2,3-OH	
Benzoic acid		
p-Hydroxybenzoic acid	4-OH	
Vanillic acid	3-OCH$_3$; 4-OH	
Syringic acid	3,5-OCH$_3$; 4-OH	
Gallic acid	3,4,5-OH	
Cinnamic acids		
p-Coumaric acid	4-OH; R = H	
Ferulic acid	3-OCH$_3$; 4-OH; R = H	
Caffeic acid	3,4-OH; R = H	
Chlorogenic acid	3,4-OH; R = quinic acid	
Rosmarinic acid (a)		
Flavans		
(+) - Catechin	3,5,7,3′,4′-OH	
(−) - Epicatechin	3,5,7,3′,4′-OH	
Flavonols		
Quercitin	3,5,7,3′,4′-OH	
Morin	3,5,7,2′,4′-OH	
Rutin	5,7,3′,4′-OH; 3-rutinose	
Kaempferol	3,5,7,4′-OH	
Flavones		
Apigenin	5,7,4′-OH	
Luteolin	5,7,3′,4′-OH	
Flavonones		
Naringenin	5,7,4′-OH	
Hesperetin	5,7,3′-OH; 4′-OCH$_3$	
Tannin		
Ellagic acid (b)		

In the second type of sensors, the superoxide radical is produced by the oxidation in aqueous solution of the xanthine to uric acid by the action of xanthine oxidase. In further step the superoxide dismutase immobilized on electrode surface, catalyses the specific dismutation of superoxide radical producing molecular oxygen (O$_2$) 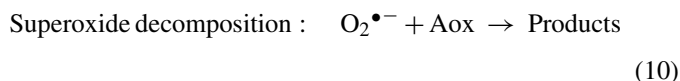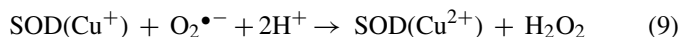and hydrogen peroxide (H$_2$O$_2$) (reactions (8) and (9)). Usually, the electrooxidation of H$_2$O$_2$ at the electrode surface generates the detection signal. This oxidation reaction occurs in a high potential (>0.5 V versus Ag/AgCl), which result in interference problems, limiting the practical applications of superoxide based-biosensors. Strategies to improve the selectivity of the developed sensors include the using H$_2$O$_2$-

Table 9
Naturally derived antioxidant—gallates derivates

Compound	Substituent	
Gallic acid	R = H	
Gallic acid methyl ester (methyl gallate)	R = CH$_3$	
Gallic acid propyl ester (propyl gallate)	R = CH$_2$CH$_2$CH$_3$	
Gallic acid lauryl ester (dodecyl gallate)	R = CH$_2$(CH$_2$)$_3$CH$_3$	

impermeable Teflon membrane or two-channel sensors. The later method allows the simultaneous determination of $O_2^{\bullet-}$ and H_2O_2 [28]. In both mechanisms the effect of the antioxidant substances added in reaction medium is observed by the decomposition of the radical (reaction (10)) resulting in diminished current levels.

Or *at electrode*: Enzymatic dismutation

$$SOD(Cu^{2+}) + O_2^{\bullet-} \rightarrow SOD(Cu^+) + O_2 \qquad (8)$$

$$SOD(Cu^+) + O_2^{\bullet-} + 2H^+ \rightarrow SOD(Cu^{2+}) + H_2O_2 \qquad (9)$$

$$\text{Superoxide decomposition}: \quad O_2^{\bullet-} + Aox \rightarrow \text{Products} \qquad (10)$$

3.3. Monitoring nitric oxide (NO)

Nitric oxide (NO, nitrogen monoxide) was characterized in 1987 as an endothelial-derived relaxing factor [52]. Since then, its biological function as an immune-modulator, neurotransmitter, vasodilator and a potential antioxidant have been studied. NO is a ubiquitous signal transduction molecule, which freely diffuses through cell membranes. Thus, it once formed from cells in different tissues can act as intervention in important biochemistry reactions such as: a mediator in a wide range of both antimicrobial and antitumor activities, an endothelial cell derived vasodilator and anticoagulant, a neurotransmitter with a crucial role in neural communications in the brain and peripheral nervous system [53]. It can also be a toxin in the destruction of pathogens and a precursor to oxidizing and nitrating species mainly at high concentrations or when it reacts with superoxide ($O_2^{\bullet-}$) forming the highly reactive peroxynitrite ($ONOO^-$). On the other hand, some reports carried out in lipid system showed that $NO^\bullet$ can inhibit oxidation, as chain-terminating antioxidant by react with chain-carrying peroxyl radicals during lipid peroxidation [54].

Endogenous NO is produced in a nonenzymatic or enzymatic way. Under specific physiological conditions, it is formed by reduction of NO_2^- promoted by ascorbic acid [55].

$$2NO_2^- + AscH^- + 3H^+ \rightarrow 2NO^\bullet + DHA + 2H_2O \qquad (11)$$

Enzymatic generation of $NO^\bullet$ occurs by action of one of threes isoforms of nitric oxide synthase (NOS). This enzyme mediates the oxidation of guanidine nitrogen of L-arginine to L-citrulline producing $NO^\bullet$. Neuronal NOS_1 and endothelial NOS_3 are constitutively expressed and are estimulated to produce local $NO^\bullet$ concentration in the nanomolar range, whereas NOS_2 activity is inducible and is estimulated to produce concentration of $NO^\bullet$ in the micromolar range, for example in the response to inflammatory stimuli in hepatocytes [56].

Moreover the level of NO production can be varied as well as its functional role between cell types. The interaction of NO and reactive oxygen species (ROS) have assumed greater importance due to the simultaneous generation of both in various pathophysiological conditions [57]. Such interactions follow different pathways resulting either in protection or production of more toxic end products. Thus, the NO determination predicts the cellular state, considering that its abnormal production has been associated to a number of serious clinical conditions.

Measuring NO with high precision *in vitro* and/or biological media is very difficult due to its low concentration, short lifetime and difficulty to prepare standard solution [58]. Therefore, in this sense the recent literature concerning to the developed biosensors present few works and all using electrochemical transducer which present an inherent sensitivity and potential for real time determination of NO [26] as can be seen in Table 4. These biosensors use the property of high affinity of NO to heme group, in proteins such as peroxidase and hemoglobin combined with the redox behavior of NO. In a first approach the signal of the amperometric biosensor is related to the activity of Horseradish peroxidase in the presence of nitric oxide. The decrease in the current intensity associated to the electrocatalytic reduction of H_2O_2 is correlated to the concentration of NO in solution [59]. In the second approach, the biosensor response is due to direct electron transfer between hemoglobin and carbon-based electrodes, which allow the direct detection of NO in solution [60,61].

3.4. Monitoring glutathione (GSH)

Reduced glutathione (GSH) (IUPAC name is 2-amino-5-(2-carboxymethyl)-1-amino) is a low molecular weight tri-peptide found in abundance in all cells compartments along numerous other antioxidants such as urate, ascorbate and α-tocopherol [62]. GSH is the main nonprotein intracellular thiol-containing compound. The term total cellular glutathione refers to the fraction of other disulfides compounds that contain thiol groups such as cysteine, coenzyme A and cysteine residues in proteins [63].

GSH is synthesized from amino acids precursors: L-glutamate, L-cysteine and L-glycine by the consecutive action of γ-glutamylcysteine synthetase and GSH synthetase in two ATP-dependent reactions as shown in Scheme 2. First reaction is the limiting step due to the availability of cysteine maintaining a tight regulation of GSH pool [64]. Once GSH is formed, it could function itself or be degraded to participate in many detoxification and transport processes or metabolic pathways including the synthesis of certain leukotrienes and the reduction of disulfide bonds in proteins and DNA precursors [65].

The antioxidants functions of GSH are associated with its central nucleophilic cysteine residue, which is responsible for its high reductive potential. It is able to directly inactivate the reactive oxygen species $O_2^{\bullet-}$ or $^\bullet OH$ through donation of its hydrogen atom resulting in the formation of glutathione disulfide (GSSG) [66]. The concentration of GSH in mammalian cells is usually in the millimolar concentration range ($0.5–10\ mmol\ L^{-1}$). The depletion in its concentration has been speculated to be an important contributing factor to some serious human diseases directly or indirectly associated with oxidative stress [67,68]. Thus, cited concentration in the organism can be relevant to the clinical diagnosis.

Methods based on enzymatic approaches that use oxido-reductase glutathione enzyme immobilized onto electrode surface or in-column reactors have shown to be very suitable for the determination of reduced thiols-derived intracellular compounds in a sensitive way. Biosensors for glutathione
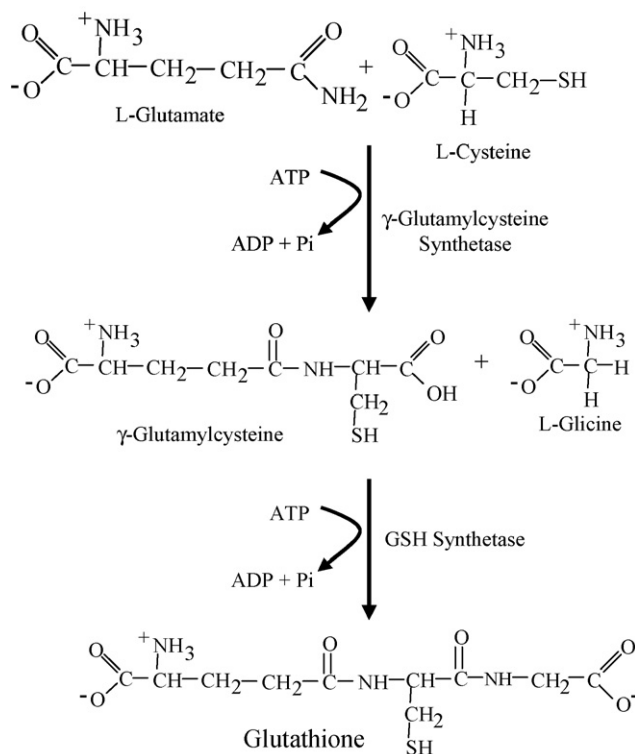
Scheme 2. Biosynthesis of glutathione (GHS).

determination generally use glutathione reductase (GSHR) or glutathione peroxidase (GSH-Px) (Table 5). This later enzyme is specific for GSH as a co-substrate in the reduction of cytotoxic H_2O_2 and other hydroperoxides. GSH-Px enzyme contains four protein sub units, which contains one atom of selenium at its active site and GSH reduces the selenium atom resulting in the formation of GSSG (reactions (12) and (13)). Another biosensor response mechanism is based on formation of glutathione as a product in glutathione reductase (GSHR)-catalyzed reactions. In this case, the oxidized form of glutathione (GSSG) (Fig. 1) is reduced to GSH by glutathione reductase enzyme in the presence of NADPH as a cofactor (reaction (14)). The latter reaction is the great importance when occur in biological system because the reduced form of glutathione, GSH, maintains a redox balance in the cellular compartments. It allows fine-tuning of the cellular redox environment under normal conditions and upon the onset
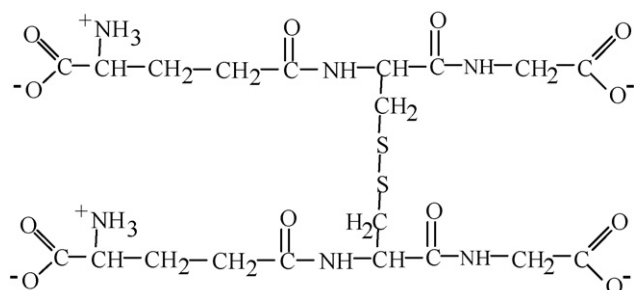
Fig. 1. Structure of oxidized glutathione (GSSG).

of stress and provides the basis for GSH stress signaling [69]. Indeed, the ratio of GSH to GSSG has been used as a marker of oxidative stress and associate to this the measuring of enzyme activity of glutathione reductase is also the great importance in pathological and clinical application to maintain the GSH level [70].

$$2GSH + H_2O_2 \xrightarrow{GSH-Px} GSSG + 2H_2O \qquad (12)$$

$$2GSH + ROOH \xrightarrow{GSH-Px} GSSG + ROH + H_2O \qquad (13)$$

$$GSSG + NADPH + H^+ \xrightarrow{GSHR} 2GSH + NADP^+ \qquad (14)$$
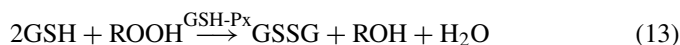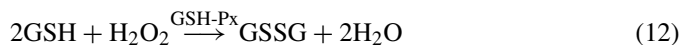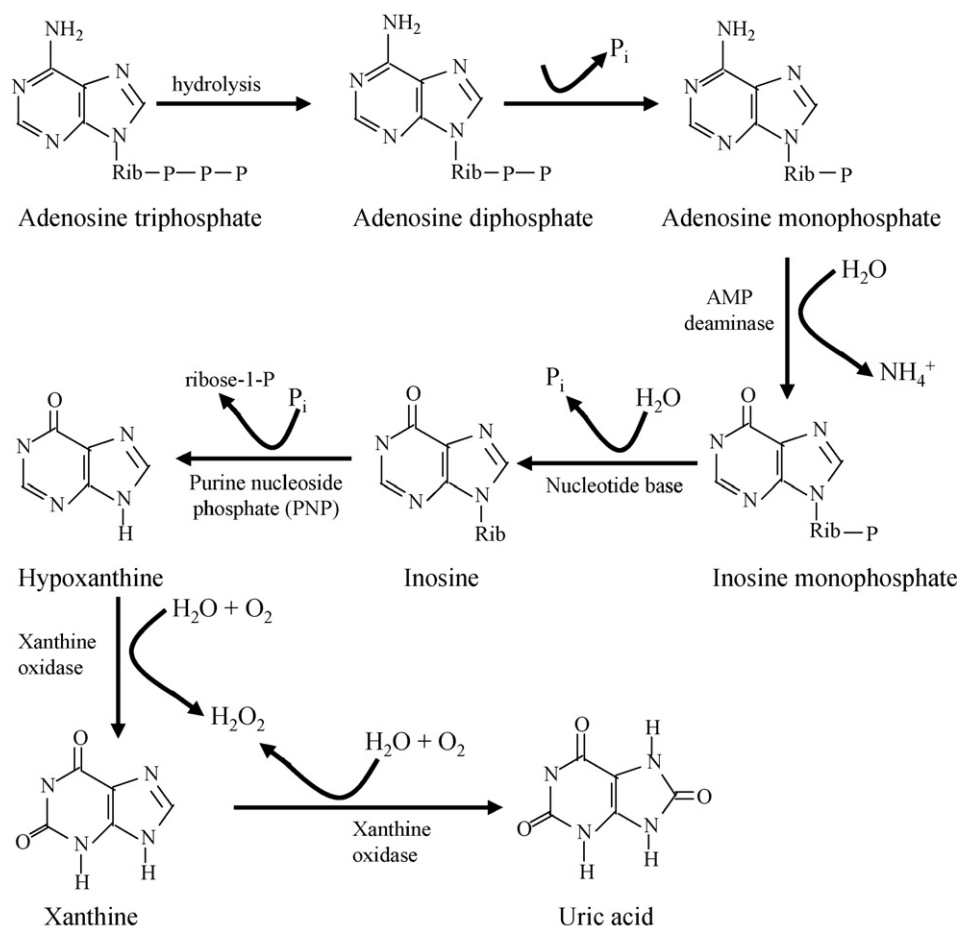
3.5. Monitoring uric acid

Uric acid, 2,6,8-trihydroxypurine is the final product of purine metabolism in humans. It is a weak acid and its dissociated form; the monosodium urate is the compound present in human plasma and extra-cellular liquid [78]. Uric acid precursors as well as the intermediates in purine biosynthesis include xanthine and hypoxanthine. As shown in Scheme 3, the product of the adenosine triphosphate (ATP) decomposition reaction, hypoxanthine (Hx) is converted to xanthine (X) and further undergoes in uric acid through xanthine oxidase (XOD) together with H_2O and O_2. This catabolic reaction was found to be the rate determining step in the overall reaction sequence [80,81].
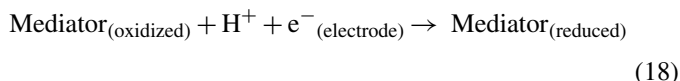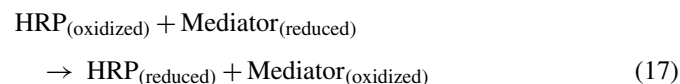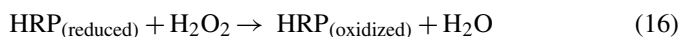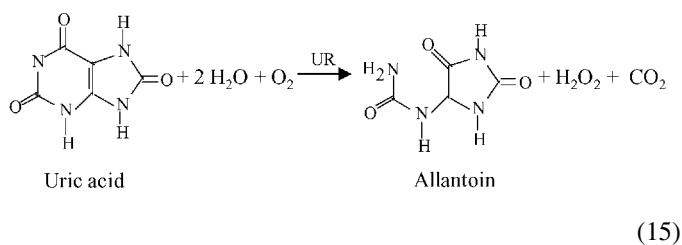
Uric acid is a physiological antioxidant effective inhibitor of the formation of superoxide radical and hydrogen peroxide that are oxygen reactive species formed by the action of xanthine oxidase during the catalysis of xanthine and hypoxanthine [82]. In the past, some studies estimated that uric acid contributes to 35–65% of the total plasma antioxidant capacity [83,84].

Uric acid levels higher than the normal is related to several diseases, being the most common the alteration of the plasma urate concentration known as hyperuricemia (or gout) [85]. Other medical conditions such as muscle damage, leukemia, pneumonia and hypertension have been associated with increased urate levels [86]. Additionally, increasing in purine excretion in urine can also monitor the activity of chemotherapeutic drugs as a result of the nucleoprotein degradation [81]. Thus, monitoring uric acid in human physiological fluids is very important in the diagnosis and therapy of patients suffering from a range of disorders associated with altered purine metabolism [87].Biosensors for uric acid determination are developed involving one (uricase) or two enzymes (uricase and peroxidase) according to Table 6, based on two approaches. In the first approach the use of uricase specifically catalyses the oxidation of urate resulting in the production of allantoin, in a similar mechanism that occurs in animals. The O_2 consumption or the H_2O_2 formed is usually monitored (reaction (15)). In the second method the H_2O_2 produced in the enzymatic oxidation of uric acid is consumed by the peroxidase. This indirect determination of uric acid is commonly observed in a HRP mediated

Scheme 3. Pathways of the formation of uric acid in human system based on purine degradation mechanism (adapted from [79]), Rib: ribose, P: phosphate group.

electrochemical system (reactions (16)–(18)).

$$\tag{15}$$

$$HRP_{(reduced)} + H_2O_2 \rightarrow HRP_{(oxidized)} + H_2O \tag{16}$$

$$HRP_{(oxidized)} + Mediator_{(reduced)}$$
$$\rightarrow HRP_{(reduced)} + Mediator_{(oxidized)} \tag{17}$$

$$Mediator_{(oxidized)} + H^+ + e^-_{(electrode)} \rightarrow Mediator_{(reduced)} \tag{18}$$

3.6. Monitoring ascorbic acid

L-Ascorbic acid (Vitamin C) is a γ-lactone synthesized by plants and many animals (except primates). It is a water-soluble vitamin usually used as an dietary supplement in pharmaceutical preparations and in manufacture food and beverages as an antioxidant, preventing color changes and alterations of aroma and flavor as well as extending the storage time of the products [96]. This vitamin is among the compound of major biological importance, it plays a key role in the protection against biological oxidation processes participating in many metabolic reactions. It has also been used in the treatment and prevention of common cold, mental illness and infertility. Traditionally, ascorbic acid has been used in clinical in the treatment and prevention of scurvy, but it is also important in regulation of the immunological system and in the tissue reconstruction, which assist the formation of collagen. However, an excess of ascorbic acid can cause gastric irritation and diarrhea and it is metabolized to oxalic acid, which can cause renal problems [97]. On the other hand, the ascorbic acid ingestion is associated to increase absorption of metal transition (as inorganic iron and copper), metabolism of folic acid, amino acid and in biosynthesis of suprarenal hormone, minimizing the stress effect [96].

There is a frequent citation about ascorbic acid as an exogenous important antioxidant. Its chemoprotective action is attributed to two mechanisms of action. It is indeed a good scavenger of free radicals and several reactive oxygen species produced during the metabolic pathways of detoxification. It justifies its association to protection against cancer agents by the prevention of formation of carcinogens precursors' compound [98].

Another property is its ability to act as a reducing agent (electron donor). Ascorbic acid (AA) is a reducing agent by donation of one electron giving the semi-dehydroascorbate radical (DHA). It also regenerates tocopherol from tocopheroxyl radical providing membrane protection [99,100]. Thus, Vitamin C determination is very important for biological and food industry.

Ascorbic acid has been measured by biosensors based on ascorbate oxidase enzyme that catalyze the direct oxidation of L-ascorbic acid in the presence of oxygen (reaction (19)) (Table 7). The monitoring of signal can be related to oxygen depletion using a Clark-type electrode. Other option can use a bienzymatic electrode coupled with peroxidase enzyme. In this later method the generated signal is related to the oxidation of ascorbic acid that acts as a mediator compound in the peroxidase catalytic mechanism.

$$2 \text{ L – Ascorbic acid} + O_2 + 2H^+ \xrightarrow{\text{AOD}} 2 \text{ Dehydro-L – ascorbic acid} + 2 H_2O \qquad (19)$$
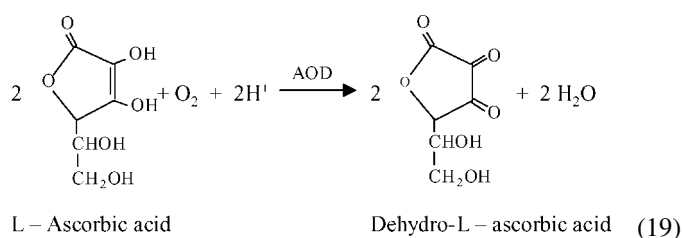
3.7. Monitoring phenol compounds

The active components usually originated from plant-based materials are naturally occurring inhibitors of oxidation. These antioxidants are primary phenolic-derived compounds widely distributed in the vegetable kingdom, mainly in the form of bio-products generated from secondary plant metabolism. Its basic features are the presence of one or more hydroxylated benzene rings and it can be included in three large groups: phenolic acids (hydroxybenzoic acid and hydroxycinnamic acid), flavonoids (anthocyanidins, flavonols, flavononas, flavonas, isoflavonas and chalconas) and tannins (hydrolysable tannins and condensed tannins) [105] (Table 8). As a result, natural sources of phenolics constitutes in integral part of the diet, which are found as a complex mixture of compounds that provide many functional components present in the free, esterified, glycosylated and bound forms. Thus, with few exceptions such as carotene, this fraction is responsible by the majority of the antioxidant capacity of these foods [107].

The protection action mode of phenol may involve multiple mechanisms, depending on the source material and possible presence of synergists and antagonists. In general, the antioxidant activity of the phenolics-derived compounds is determined by its ideal chemical structure in terms of some properties such as: Free-radical scavengers or chain breakers agents, this property related to reducing properties as hydrogen or electron-donating agents, which is determined to its reduction potential. It also, the fact of the resulting antioxidant-derived radical, namely phenoxy radical is relatively stable due to the resonance delocalization and lack of suitable sites for attack by molecular oxygen. The last property, the transition metal-chelating potential, in special iron and copper supports the role of polyphenols as preventive antioxidants in terms of inhibiting transition metal-catalysed free radical formation [108–110].

It has been observed the worldwide growing trend in the usage of natural antioxidants in food industry justified by their health benefits. Thus, efforts have been made in order to find and to characterize substances of natural origin that exert some antioxidant activity. Commercial sources of antioxidants extracted from plant sources are green tea, spices and rosemary extracts. These later two are used as flavoring but exhibit good antioxidant properties in some cases [111].

Other good examples of effective naturally derived antioxidant that have been applied in food formulations are group of gallates (Table 9). Gallic acid often obtained from alkaline or acid hydrolysis of tannins or from hydrolysis of spent broths from *Penicillium glaucum* or *Aspergillus niger* that are used in the manufacturing of dodecyl gallate and propyl gallate, widely used as food antioxidant additive [112].

Table 10
Biosensors applied in the analysis of phenolic antioxidants

Biocomponent	Immobilization	Transducer[a]	Sample	Detection range (D.L.)	Stability	Reference
Tyrosinase	Physical adsorption	Amp. (O$_2$)	Olive oil	0.5–6 (0.04) mg L^{-1} (Catechol)	–	[115]
Tyrosinase	Physical adsoprtion	Voltam. (SPE)	Green tea	–	–	[116]
Catalase	Gel encapsulation	Amp. (O$_2$)	Olive oil	$(9.23–5.04) \times 10^4$ μmol L^{-1} (Cumene hydroperoxide)	16 days	[117]
Tyrosinase	Physical adsorption	FIA (SPE)	Beer	–	–	[118]
Peroxidase	SAM	Amp. (Au)	Wine and tea	<25 (2) μmol L^{-1} (Catechin)	–	[119]
Tyrosinase	Physical adsoprtion	Amp. (CPE)	Wine	1–60 (0.1) mg L^{-1} (Gallic acid)	–	[120]
Peroxidase	Physical adsorption	Amp. (CPE)	Wine and tea	<15 (3) μmol L^{-1} (Catechin)	–	[121]
Laccase	Physical adsorption	Amp. (Pt)	–	10–110 μmol L^{-1} (Catechol)	–	[122]
Laccase	Physical adsorption	Amp. (Pt)	Wine	2.0–14.0 (1) μmol L^{-1} (Catechin and CA)	–	[123]
Peroxidase	Physical cross-linking	Amp. (CPE)	Tea	1–50 (0.7) μmol L^{-1} (CGA)	30 days	[124]
Laccase	Physical assorption	Amp. (SGE)	Plant extract	<10 (0.56) μmol L^{-1} (CA)	–	[125]
Tyrosinase	Physical cross-linking	Amp. (GCE)	Tea	70–400 (2.52) μmol L^{-1} (CGA)	–	[126]
Tyrosinase	Chemical cross-linking	Amp. (SPE)	Wine	10.6–266.0 (10.5) μmol L^{-1} (CA)	–	[127]
Tyrosinase	Physical adsorption	Amp. (GCE)	Wines	25–900 (7) μmol L^{-1} (Gallic acid)	<18 days	[128]

[a] Working electrode.

Table 11
Biosensors applied in the synthetic antioxidant analysis (propyl gallate)

Biocomponent	Immobilization	Transducer[a]	Analyte	Sample	Detection range (D.L.)	Stability	Reference
Hematin	Physical adsorption	CL (fiber-optic)	Propyl gallate	Medicinal plants	$100–1 \times 10^5 \, \mu mol \, L^{-1}$	–	[129]
Tyrosinase	Physical adsorption	Amp. (GTE)	Propyl gallate	Food samples	$2–100 \, (0.9) \, \mu mol \, L^{-1}$	40 days	[130]
Tyrosinase	Physical adsorption	Amp. (GTE)	Propyl gallate	Fatty food samples	$8–200 \, (1.3) \, \mu mol \, L^{-1}$	10 days	[131]

[a] Working electrode or transducer.

The detection of phenolic substances in food samples has been performed for many methods among them biosensor approaches. Phenolic-derived compounds are good substrate for oxidases enzymes, then biosensor modified with tyrosinase, laccase, peroxidase and cellobiose dehydrogenase, have been developed for detection of phenolic compounds since phenols can act as electron donor for these enzymes [113]. In many cases, it is more important to measure the total content of polyphenols compounds than to determine each of them individually [114]. The term "total phenol" refers the all phenols that are responsible by the total antioxidant capacity of a specific sample. Tables 10 and 11 present biosensors developed to determine the total polyphenols content and synthetic antioxidant, respectively. Many biosensors are based on electrochemical transducers that use the redox cycling of enzymes and have as main advantage the low interference.

The essential features of the general analytical system using oxidase or peroxidase enzyme based biosensor are shown schematically in Scheme 4. As observed, phenols oxidases and peroxidases have different enzymatic mechanisms in the electrochemical biosensors. The fundamental reaction is the oxidation of enzymes molecules at the surface of the electrode in the presence of substrate, oxygen (for phenol oxidases) or hydrogen peroxide (for peroxidase), the later being reduced to water. The next step reaction is the regeneration of the enzyme to its original oxidation state, which is carried out by the electron transfer from a suitable mediator, such as phenol compounds in its reduced form. The measured reduction current is due to reduction of the mediator to the original form.

The tyrosinase biosensors are restricted to the monitoring of phenolic compounds with at least one free *ortho*-position. On the other hand, the laccase biosensor can detect free *para*- and *meta*-position, but its catalytic cycle is complicated and in its major part is different from tyrosinase. Also, the formed products during the reaction of the laccase still are not well understood.

Scheme 4. Mechanism for the phenolic compounds detection using biosensors based on peroxidases or oxidases enzymes.

4. Concluding remarks

The idea in the improvement of food quality or prevention of antioxidant stress by means of interaction and synergisms of antioxidants demonstrated *in vitro* studies represents an important research field.

A consideration that must be done is the reliability and practicability of the methods; much of the literature in this field reports the use of a very small amount of sample combined with complex methods to easily generate a significant result.

In this direction, the measurement of the total antioxidant capacity or antioxidant power within biological specimens by biosensors is a challenge to be explored. By virtue of its advantages offered such as ready-to-use, miniaturization and reusable properties with the possibility to combine portable equipment, biosensors have been applied in research related to free radicals and antioxidants in several ways. It can monitor the formation of oxidized products in the first step of degradation of cellular targets. Once the stability, sensitivity and specificity of the biosensor have been demonstrated in several systems, it can be explored to detect radicals in the nanomolar range. In this situation, many times, the radical species, can involved in the beginning of inflammatory, apoptosis and /or vascular diseases.

Another option could be incorporated in manufacturing of food as a simple monitor of lipid food spoilage. Besides, the use of biosensor to classify the diet integrators or drug specialties related to antioxidant properties of the active principles that they contain. The direct measurement of the total antioxidant index of plant origin raw materials related to total content of compounds with antioxidant characteristics is another parameters explored by biosensors.

However, in this context, the biosensors developed so far to evaluate the antioxidant status, are based on direct analyze of specific indicators such as biomarkers or monitoring the free radicals in cells or tissue, without caring to obtain a correlation between, the index obtained of these indicators with the overall condition oxidative stress of sample.

The usefulness of biosensors to evaluate the antioxidant status lies in its ability to provide early indication of some disease and or its progression in a non-invasive way to evaluate the effectiveness of the antioxidant therapy. The results obtained by the biosensor just will be efficient if could be interpreted in terms of these cited parameters.

Acknowledgment
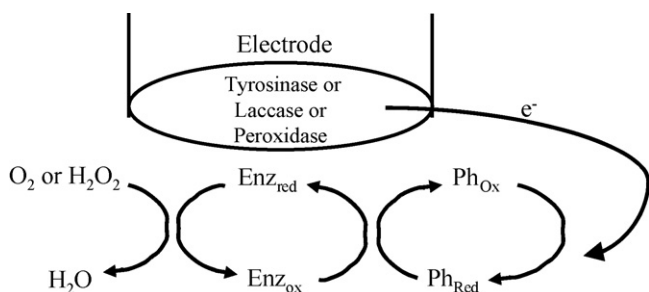
References

[1] M. Antolovich, P.D. Prenzler, E. Ptsalides, S. McDonald, K. Robards, Analyst 127 (2002) 183.

[2] C.S. Moreno, Food Sci. Technol. Int. 8 (2002) 121.

[3] Y. Dotan, D. Lichtenberg, I. Pinchuk, Prog. Lipid Res. 43 (2004) 200.

[4] S. Litescu, G.L. Radu, M. Diaconu, Electroanalysis 13 (2001) 8.

[5] A. Nyska, R. Kohen, Toxicol. Pathol. 30 (2002) 620.

[6] B. Halliwell, R. Aeschbach, J. Löliger, O.I. Aruoma, Food Chem. Toxicol. 32 (1995) 601.

[7] A. Ghiselli, M. Serafini, F. Natella, C. Scaccini, Free Radical Biol. Med. 29 (2000) 1106.

[8] A. Rasooly, J. Jacobson, Biosens. Bioelectron. 21 (2006) 1851.

[9] J. Wang, Biosens. Bioelectron. 21 (2006) 1887.

[10] D.R. Thévenot, K. Toth, R.A. Durst, G.S. Wilson, Biosens. Bioelectron. 16 (2001) 121.

[11] O.I. Aruoma, Mutat. Res. 523–524 (2003) 9.

[12] M. Dizdaroglu, P. Jaruga, M. Birincioglu, H. Rodriguez, Free Radical Biol. Med. 32 (2002) 1102.

[13] ESCODD: European Standards Committee on Oxidation and DNA Damage, Free Radical Res. 32 (2000) 333.

[14] O. Blokhina, E. Virolainen, K.V. Fagerstedt, Annu. Bot. 91 (2003) 179.

[15] O.I. Aruoma, Food Chem. Toxicol. 32 (1994) 671.

[16] P. Jaruga, M. Dizdaroglu, Nucleic Acids Res. 24 (1996) 1389.

[17] H.B. Dunford, Coord. Chem. Rev. 233/234 (2002) 311.

[18] M.J. Burkitt, Prog. React. Kinet. Mech. 28 (2003) 75.

[19] J. Labuda, M. Bucková, L. Heilerová, A.C. Ziaková, E. Brandsteterová, J. Mattusch, R. Wennrich, Sensors 2 (2002) 1.

[20] M. Bucková, L. Labuda, J. Sandula, L. Krizková, I. Stepánek, Z. Duracková, Talanta 56 (2002) 939.

[21] J. Labuda, M. Bucková, L. Heilerová, S. Silhár, I. Stepánek, Anal. Bioanal. Chem. 376 (2003) 168.

[22] J. Liu, C. Roussel, G. Lagger, P. Tacchini, H.H. Girault, Anal. Chem. 77 (2005) 7687.

[23] L.D. Mello, S. Hernandez, G. Marrazza, M. Mascini, L.T. Kubota, Biosens. Bioelectron. 21 (2006) 1374.

[24] F. Auchère, F. Rusnak, J. Biol. Inorg. Chem. 7 (2002) 664.

[25] I. Fridovich, Annu. Rev. Biochem. 64 (1995) 97.

[26] F. Lisdat, F.W. Scheller, Anal. Lett. 33 (2000) 1.

[27] Z. Guo, J. Chen, H. Liu, W. Zhang, Anal. Lett. 38 (2005) 2033.

[28] L. Campanella, A. Bonanni, G. Favero, M. Tomassetti, Anal. Bioanal. Chem. 375 (2003) 1011.

[29] L. Campanella, L. Persi, M. Tomassetti, Sens. Actuators B: Chem. 68 (2000) 351.

[30] L. Campanella, G. Favero, L. Persi, M. Tomassetti, J. Pharm. Biomed. Anal. 23 (2000) 69.

[31] J. Chen, U. Wollenberger, F. Lisdat, B. Ge, F. Scheller, Sens. Actuators B: Chem. 70 (2000) 115.

[32] K.V. Gobi, F. Mizutani, J. Electroanal. Chem. 484 (2000) 172.

[33] L. Campanella, G. Favero, L. Persi, M. Tomassetti, J. Pharm. Biomed. Anal. 24 (2001) 1055.

[34] L. Campanella, S. De Luca, G. Favero, L. Persi, M. Tomassetti, Fresenius J. Anal. Chem. 369 (2001) 594.

[35] S. Descroix, F. Bedioui, Electroanalysis 13 (2001) 524.

[36] K.V. Gobi, F. Mizutani, Anal. Sci. 17 (2001) 11.

[37] K.V. Gobi, Y. Sato, F. Mizutani, Electroanalysis 13 (2001) 397.

[38] K. Endo, T. Miyasaka, S. Mochizuki, S. Aoyagi, N. Himi, H. Asakara, K. Tsujioka, K. Sakai, Sens. Actuators B: Chem. 83 (2002) 30.

[39] B. Ge, F. Lisdat, Anal. Chim. Acta 454 (2002) 53.

[40] S. Ignatov, D. Shishniashvili, B. Ge, F.W. Scheller, F. Lisdat, Biosens. Bioelectron. 17 (2002) 191.

[41] T. Ohsaka, Y. Tian, M. Shioda, S. Kasahara, T. Okajima, Chem. Commun. 9 (2002) 990.

[42] Y. Tian, L. Mao, T. Okajima, T. Ohsaka, Anal. Chem. 74 (2002) 2428.

[43] M.K. Beissenhirtz, F.W. Sheller, F. Lisdat, Anal. Chem. 76 (2004) 4665.

[44] L. Campanella, A. Bonanni, D. Bellantoni, G. Favero, M. Tomassetti, J. Pharm. Biomed. Anal. 36 (2004) 91.

[45] L. Campanella, A. Bonanni, E. Finotti, M. Tomassetti, Biosens. Bioelectron. 19 (2004) 641.

[46] I. Pastor, R. Esquembre, V. Micol, R. Mallavia, C.R. Mateo, Anal. Biochem. 334 (2004) 335.

[47] J. Di, S. Bi, M. Zhang, Biosens. Bioelectron. 19 (2004) 1479.

[48] A.V. Krylov, M. Beissenhirtz, H. Adamzig, F.W. Scheller, F. Lisdat, Anal. Bioanal. Chem. 378 (2004) 1327.

[49] L. Campanella, E. Martini, M. Tomassetti, Talanta 66 (2005) 902.

[50] E. Emregül, Anal. Bioanal. Chem. 383 (2005) 947.

[51] Y. Tian, L. Mao, T. Okajima, T. Ohsaka, Biosens. Bioelectron. 21 (2005) 557.

[52] S. Moncada, J. Physiol. Lond. 523 (2000) 45S.

[53] B. Zhao, Frontiers Biosci. 10 (2005) 454.

[54] S.G. Hummel, A.J. Fischer, S.M. Martin, F.Q. Schafer, G.R. Buettner, Free Radical Biol. Med. 40 (2006) 501.

[55] S. Carlsson, N.P. Wiklund, L. Engstrand, E. Weitzberg, J.O.N. Lundberg, Nitric Oxide 5 (2001) 580.

[56] S. Moncada, Funct. Neurol. 12 (1997) 135.

[57] D. Mancardi, L.A. Ridnour, D.D. Thomas, T. Katori, C.G. Tocchetti, M.G. Espey, K.M. Miranda, N. Paolocci, D.A. Wink, Curr. Mol. Med. 4 (2004) 723.

[58] M. Pallini, A. Curulli, A. Amine, G. Palleschi, Electroanalysis 10 (1998) 1010.

[59] E. Casero, M. Darder, F. Pariente, E. Lorenzo, Anal. Chim. Acta 403 (2000) 1.

[60] C. Fan, G. Li, J. Zhu, D. Zhu, Anal. Chim. Acta 423 (2000) 95.

[61] C. Fan, X. Liu, J. Pang, G. Li, H. Scheer, Anal. Chim. Acta 523 (2004) 225.

[62] A. Meister, Trends Biomed. Sci. 13 (1988) 1885.

[63] A. Meister, M.E. Anderson, Annu. Rev. Biochem. 52 (1983) 711.

[64] O.W. Griffith, Free Radical Biol. Med. 27 (1999) 922.

[65] J. Mandl, G. Banhegyi, Biofactors 17 (2003) 21.

[66] W. Droge, R. Breitkreutz, Proc. Nutr. Soc. 59 (2000) 595.

[67] H.J. Forman, D.A. Dickinson, Biofactors 17 (2003) 1.

[68] J.M. Estrela, A. Ortega, E. Obrador, Crit. Rev. Clin. Labor. Sci. 43 (2006) 143.

[69] I. Rahman, S.R. Yang, S.K. Biswas, Antioxid. Redox Signal. 8 (2006) 681.

[70] G. Filomeni, G. Rotilio, M.R. Cirioli, Biochem. Pharmacol. 64 (2002) 1057.

[71] L. Mao, K. Yamamoto, Electroanalysis 12 (2000) 577.

[72] L. Rover Jr., L.T. Kubota, N.F. Höehr, Clin. Chim. Acta 308 (2001) 55.

[73] M. Carano, S. Cosnier, K. Kordatos, M. Marcaccio, M. Margotti, F. Paolucci, M. Prato, S. Roffia, J. Mater. Chem. 12 (2002) 1996.

[74] T.H. Huang, T. Kuwana, A. Warsinke, Biosens. Bioelectron. 17 (2002) 1107.

[75] M.K. Sezgintürk, E. Dinçkaya, Biosens. Bioelectron. 19 (2004) 835.

[76] J.J.J.R. Diaz, A.A.J. Torriero, E. Salinas, E.J. Marchevsky, M.I. Sanz, J. Raba, Talanta 68 (2006) 1343.

[77] A.A. Alves, L.P. Silva, D.V. Macedo, L.T. Kubota, Anal. Biochem. 323 (2003) 33.

[78] K.R. Maples, R.P. Mason, J. Biol. Chem. 263 (1988) 1709.

[79] J.M. Zen, Y.Y. Lai, H.H. Yang, A.S. Kumar, Sens. Actuators B: Chem. 84 (2002) 237.

[80] G.K. Glantzounis, E.C. Tsimoyiannis, A.M. Kappas, D.A. Galaris, Curr. Pharm. Des. 11 (2005) 4145.

[81] W.L. Nyhan, Mol. Genet. Metab. 86 (2005) 25.

[82] R. Kand'ar, P. Zakova, P. Muzakova, Clin. Chim. Acta 365 (2006) 249.

[83] K.R. Geisinger, J.G. Batsakis, R.C. Bauer, J. Am. Clin. Pathol. 72 (1979) 330.

[84] D.D.M. Wayner, G.W. Burton, K.U. Ingold, L.R.C. Barclay, S.J. Locke, Biochim. Biophys. Acta 924 (1987) 408.

[85] D. Masseoud, K. Rott, R. Liu-Bryan, C. Agudelo, Curr. Pharm. Des. 11 (2005) 4117.

[86] M. Schachter, Curr. Pharm. Des. 11 (2005) 4139.

[87] J.G. Puig, F.A. Mateos, Pharm. Word. Sci. 16 (1994) 40.

[88] M.M.C. Ortega, D.E. Rodriguez, J.C. Encinas, M. Plascencia, F.A.M. Velarde, R. Olayo, Sens. Actuators B: Chem. 85 (2002) 19.

[89] Y.Z. Lv, Z. Zhang, F. Chen, Analyst 127 (2002) 1176.

[90] E. Akyilmaz, M.K. Sezgintürk, E. Dinçkaya, Talanta 61 (2003) 73.

[91] C.A. Marquette, A. Degiuli, L.J. Blum, Biosens. Bioelectron. 19 (2003) 433.

[92] D.M. Pérez, M.L. Ferrer, C.R. Mateo, Anal. Biochem. 322 (2003) 238.

[93] F. Zhang, X. Wang, S. Ai, Z. Sun, Q. Wan, Z. Zhu, Y. Xian, L. Jin, K. Yamamoto, Anal. Chim. Acta 519 (2004) 155.

[94] R.F. Dutra, K.A. Moreira, M.I.P. Oliveira, A.N. Araújo, M.C.B.S. Montenegro, J.L.L. Filho, V.L. Silva, Electroanalysis 17 (2005) 701.

[95] F.F. Zhang, X.L. Wang, C.X. Li, X.H. Li, Q. Wan, Y.Z. Xian, L.T. Jin, K. Yamamoto, Anal. Bioanal. Chem. 382 (2005) 1368.

[96] M.W. Davey, M. Van Montagu, D. Inzé, M. San Martin, A. Kanellis, N. Smirnoff, I.J.J. Benzie, J.J. Strain, D. Favell, J. Fletcher, J. Sci. Food Agric. 80 (2000) 825.

[97] N. Smirnoff, Curr. Opin. Plant Biol. 3 (2000) 229.

[98] W. Lee, K.A. Davis, R.L. Rettmer, R.F. Lable, Am. J. Clin. Nutr. 48 (1988) 289.

[99] G.R. Buettner, Arch. Biochem. Biophys. 300 (1993) 535.

[100] N. Smirnoff, J.E. Pallanca, Biochem. Soc. Trans. 24 (1996) 472.

[101] O. Fatibello, I.C. Vieira, J. Braz. Chem. Soc. 11 (2000) 412.

[102] K. Kriz, M. Anderlund, D. Kriz, Biosens. Bioelectron. 16 (2001) 363.

[103] S. Jawaheer, S.F. White, S.D.D.V. Rughooputh, D.C. Cullen, Biosens. Bioelectron. 18 (2003) 1429.

[104] I.N. Tomita, A. Manzoli, F.L. Fertonani, H. Yamanaka, Eclética Quim. 30 (2005) 37.

[105] B. Zhou, Z.L. Liu, Pure Appl. Chem. 77 (2005) 1887.

[106] H. Hotta, S. Nagano, M. Ueda, Y. Tsujino, J. Koyama, T. Osakai, Biochim. Biophys. Acta 1572 (2002) 123.

[107] N. Balasundram, K. Sundram, S. Samman, Food Chem. 99 (2006) 191.

[108] C.R. Evans, Curr. Med. Chem. 8 (2001) 797.

[109] M.A. Soobrattee, U.S. Neergheen, A.L. Ramma, O.I. Aruoma, T. Bahorun, Mutat. Res. 579 (2005) 200.

[110] V. Thavasi, L.P. Leong, R.P.A. Bettens, J. Phys. Chem. A 110 (2006) 4918.

[111] M.B. Arnao, A. Cano, M. Acosta, Free Radical Res. 31 (1999) S89.

[112] Sites internet http://www.codexalimentarius.net/ (accessed in 07/2006), http://www.eufic.org/en/quickfacts/food_aditives.htm (accessed in 07/2006), http://www.ESFA.eu.int/ (accessed in 07/2006).

[113] P.V. Bernhardt, Austr. J. Chem. 59 (2006) 233.

[114] A.J. Blasco, M.C. Rogerio, M.C. González, A. Escarpa, Anal. Chim. Acta 539 (2005) 237.

[115] C. Capannesi, I. Palchetti, M. Mascini, A. Parenti, Food Chem. 71 (2000) 553.

[116] A. Romani, M. Minunni, N. Mulinacci, P. Pinelli, F.F. Vincieri, M. Del Carlo, M. Mascini, J. Agric. Food Chem. 48 (2000) 1197.

[117] L. Campanella, M.P. Sammartino, M. Tomassetti, S. Zannella, Sens. Actuators B: Chem. 76 (2001) 158.

[118] E.A. Cummings, B.R. Eggins, E.T. McAdams, S. Linquette-Mailley, P. Mailley, D. Madigan, M. Clements, C. Coleman, J. Am. Soc. Brew. Chem. 59 (2001) 84.

[119] S. Imabayashi, Y. Kong, M. Watanabe, Electroanalysis 13 (2001) 408.

[120] W.T. Jewell, S.E. Ebeler, Am. J. Enol. Viticult. 52 (2001) 219.

[121] Y.T. Kong, S. Imabayashi, K. Kano, T. Ikeda, T. Kakiuchi, Am. J. Enol. Viticult. 52 (2001) 381.

[122] S.A.S.S. Gomes, M.J.F. Rebelo, Sensors 3 (2003) 166.

[123] S.A.S.S. Gomes, J.M.F. Nogueira, M.J.F. Rebelo, Biosens. Bioelectron. 20 (2004) 1211.

[124] L.D. Mello, A.A. Alves, D.V. Macedo, L.T. Kubota, Food Chem. 92 (2005) 515.

[125] A.J. Wilkolazka, T. Ruzgas, L. Gorton, Enzyme Microb. Technol. 35 (2004) 238.

[126] V.C. Dall'Orto, J.M. Vago, R.R. Carballo, I. Rezzano, Anal. Lett. 38 (2005) 19.

[127] M.R. Montereali, W. Vastarella, L.D. Seta, R. Pilloton, Intern. J. Environ. Anal. Chem. 85 (2005) 795.

[128] V.C. Sanz, M.L. Mena, A.G. Cortés, P.Y. Sedeño, J.M. Pingarrón, Anal. Chim. Acta 528 (2005) 1.

[129] W.S. Palaroan, J. Bergantin Jr., F. Sevilla III, Anal. Lett. 33 (2000) 1797.

[130] M.D. Morales, M.C. González, A.J. Reviejo, J.M. Pingárron, Microchem. J. 80 (2005) 71.

[131] M.D. Morales, M.C. González, B. Serra, A.J. Reviejo, J.M. Pingárron, Sens. Actuators B: Chem. 106 (2005) 572.

Three-phase solvent bar microextraction and determination of trace amounts of clenbuterol in human urine by liquid chromatography and electrospray tandem mass spectrometry

Mahaveer B. Melwanki [a], Shang-Da Huang [a,*], Ming-Ren Fuh [b]

[a] *Department of Chemistry, National Tsing Hua University, Hsinchu 30013, Taiwan*
[b] *Department of Chemistry, Soochow University, Taipei, Taiwan*

Abstract

Three-phase solvent bar microextraction (TPSBME) technique is described for the quantitative determination of trace amounts of clenbuterol (CB) in urine samples using liquid chromatography (LC) and electrospray tandem mass spectrometry (ES-TMS). CB was extracted from a basified urine sample (donor phase) into the organic solvent residing in the pores of a freely moving hollow fiber and then back extracted into an acidic solution (acceptor phase) inside the lumen of the hollow fiber. The ends of the fiber were pressure-sealed. Here, forward and back extraction took place spontaneously. We studied various parameters affecting the extraction efficiency viz. type of organic solvent (octanol, nonanol and dihexyl ether) used for immobilization in the pores of the hollow fiber, i.e. extraction time (10–40 min), stirring speed (0–1000 rpm), effect of sodium chloride (0–25%, w/v) and concentration of the donor (0.25–3 M NaOH) and the acceptor (0.5–5 M formic acid) phases. After extraction, CB was analyzed by injecting the analyte enriched acceptor phase into LC combined with ES-TMS. Enrichment factor (79), repeatability (R.S.D. = 5.1%), correlation coefficient (0.9972, for the range of 0.1–4 ng mL^{-1}), detection limit (7 pg mL^{-1}) were also investigated. The present technique is compared with the reported solid phase microextraction techniques in terms of selectivity, analysis time per extraction, cost of analysis per extraction, and precision. Among all microextraction techniques reported, this technique is the most economical sample preparation/preconcentration technique to our knowledge. The method was applied for the analysis of CB in human urine.
© 2006 Elsevier B.V. All rights reserved.

Keywords: Solvent bar microextraction; Clenbuterol

1. Introduction

Clenbuterol (CB) {4-amino-α-[(*tert*-butylamino)methyl]-3,5-dichlorbenzyl alcohol}, a representative of the class of sympathomimetic agents, has demonstrated a distinguished medical versatility in the past. It was developed for the treatment of pulmonary diseases such as asthma bronchiale or bronchial hyperreactivity owing to its bronchodilator activity, and its anabolic properties have led to numerous additional therapeutic applications such as prevention of skeletal muscle atrophy caused by injury or denervation. Additionally, due to the similar physiological effects to anabolic steroids (namely promoting the growth of the muscle tissue [1]), the drug has been abused in the cattle industry to improve the lean meat portion of the stock [2] and as a doping agent by athletes to increase strength and performance [3]. Long-term or high dose use, however, has been shown to illicit deleterious physiological side effects [4] and a large enough single dosage may initiate an acute toxic response [5]. Accordingly, its use is banned in athletics and in beef production [3,6]. As low concentrations of CB have been observed in doping control samples in the past with minimum required performance limit established at 2 ng mL^{-1} for urine samples [7], highly sensitive and specific assay procedures are essential.

Various sample preparation techniques are available for the extraction of CB in various matrices. Among these, liquid–liquid extraction (LLE) [8,9] or solid phase extraction (SPE) [10,11] are reported. However, the conventional LLE procedures are time consuming, generally labor intensive and require large

* Corresponding author. Tel.: +886 3 572 1194; fax: +886 3 573 6979.
E-mail address: sdhuang@mx.nthu.edu.tw (S.-D. Huang).

quantities of expensive, toxic and environmentally unfriendly organic solvents. Meanwhile, SPE technique requires less solvent, but needs evaporation of the final organic extract into a small volume to achieve better enrichment. For the past few years, research activities are focused toward the development of efficient, economical and miniaturized sample preparation techniques. Among these, solid phase microextraction (SPME) is most widely developed. CB was extracted by direct immersion of the SPME fiber into the aqueous sample at pH 12 followed by derivatization of the extracted compound by suspending the fiber in the head space of another vial that was saturated with the vapor of the derivatizing agent [12]. Due to the basic nature of CB, sample pH should be sufficiently alkaline to keep the analyte in the molecular form. However, due to the direct immersion of the fiber and due to its restricted working pH range (recommended pH range is 2–11 for polyacryalate SPME fiber), the technique may shorten the life of the SPME fiber depending on the matrix of the sample and additives (like sodium chloride used for salting-out) and pH of the sample to be adjusted for extraction. To address this particular problem associated with direct immersion technique, the method was modified in our laboratory [13] by heating the sample and keeping the SPME fiber in the headspace of the vial followed by derivation of the fiber absorbed analyte in the headspace mode. However, SPME fibers are still comparatively expensive and the coating is fragile and easily broken while handling. To overcome this problem, dynamic liquid–liquid–liquid microextraction with the automated movement of the acceptor phase (LLLME/AMAP) was developed in our laboratory [13] and compared with SPME procedures. Separation and detection was made by liquid chromatography-ultraviolet (LC-UV). However, the technique needed a dedicated syringe pump for every extraction. This limitation was overcome by Jiang and Lee [14] who developed "solvent bar microextraction" (SBME) technique wherein the organic phase was confined within a short length of a hollow fiber (sealed at both ends) that was placed in a stirred aqueous sample solution. Free movement of the extraction device within the sample solution facilitated extraction. Separation was carried out by injecting analyte enriched organic phase into gas chromatography (GC). However, the technique is not suitable for CB unless derivatized prior to injection. To address such related problems, we have demonstrated very recently [15] a three-phase system in SBME technique. Briefly, the technique involves the extraction of the basic compound from a basified (so as to keep the analyte in its molecular form) aqueous sample through a thin film of organic solvent immobilized in the pores of a porous polypropylene hollow fiber and finally into the acidic (to keep the basic analyte charged so as to prevent reverse extraction of the analyte into organic phase residing in the pores of the hollow fiber) acceptor solution inside the lumen of the hollow fiber. The method was applied to the analysis of river water. In the present investigation, the application was extended for the first time to the extraction of CB from urine matrix. Separation and detection were performed using LC combined with electrospray tandem mass spectrometry (ES-TMS). The technique has dual advantage of sample preparation and enrichment of CB in a single step.

2. Experimental

2.1. Reagents and materials

CB was purchased from Sigma (Sigma–Aldrich Co., St. Louis, MO, USA). LC grade acetonitrile (J.T. Baker, NJ, USA) and methanol (Mallinckrodt Baker Inc., NJ, USA) were used for the study. Deionized water was purified in a Milli-Q water purification system (Millipore, Bedford, MA, USA). A stock solution of CB (1 mg mL^{-1}) was prepared in methanol and stored at 4 °C for no longer than 2 months [16]. Standard working solution was prepared in urine everyday using stock solution. All reagents and solvents used were analytical or LC grade unless otherwise mentioned.

The Q 3/2 Accurel Polypropylene hollow fiber membrane (600 μm i.d., 200 μm wall thickness, 0.2 μm pore size) was purchased from Membrana GmbH (Wuppertal, Germany). It was cut into 4.5 cm-segments, cleaned in acetone and dried prior to use.

Urine sample collected from a healthy male adult served as a real sample. This was stored at 4 °C prior to use.

2.2. Instrumentation

The LC system assembled from modular components (Waters, Milford, MA, USA) consisted of a 600E pump and a 486 UV detector. A millennium workstation (Waters) was utilized to control the system and also for data analysis. A Hypersil BDS–C18 (100 mm × 2.1 mm, particle size 3 μm) column was used for the separation of target compound. Mobile phase was a mixture of acetonitrile and 0.2% formic acid. Acetonitrile composition was set at 5% initially and increased linearly up to 95% in 5 min. The same composition was held until 10th min and was brought back to original composition from 10 to 12 min and equilibrated for an additional 5 min (total run time 17 min). The flow rate was kept at 0.25 mL min^{-1}. Detection was made at 240 nm. Two (one for filling-up the acceptor phase into the fiber and one for injection into LC system) 10 μL and one 25 μL (for pushing air to flush out the acceptor phase from the lumen of the fiber after extraction) Hamilton LC syringes (Hamilton, Reno, Nevada, USA) were used in the study.

An HP 1100 LC system (Hewlett-Packard Co., Palo Alto, CA, USA) consisting of a quaternary pump with an online degasser was used. Mass spectrometric detection was performed using an Agilent series LC/MSD trap SL instrument equipped with an electrospray ionization source that was operated in the positive mode with the spray voltage set at −3.5 kV. The capillary exit voltage was 130 V. Agilent 1100 series LC/MSD Trap software (version 4.0) was utilized for system control, data acquisition and data analysis. Heated nitrogen gas (350 °C, 8 L min^{-1}) was used to evaporate solvent from the electrospray chamber, and compressed nitrogen gas (40 psi) was used for nebulization. MS/MS/MS (MS^3) mode and multiple reaction monitoring (MRM) were employed for quantitative measurement. The isolation width for precursor ions was 3. The settings for the MRM were: m/z 277 → 259 → 203. MS/MS/MS data acquisition was performed under the following conditions: normal scan speed,

m/z range 100–350, ion charge control target 30,000 and maximum accumulation time 300 ms.

2.3. TPSBME of CB from urine

A 7.5 mL of basified (overall NaOH concentration adjusted to 1 M) urine sample was taken in 8 mL-sample vial. A 10 μL of 5 M formic acid was drawn into a 10 μL syringe and the needle tip was carefully inserted into one of the open ends of the hollow fiber. The assembly was held upright such that the open end of the fiber faces up and the syringe plunger down. Then the plunger was pushed slowly to dispense formic acid from the syringe into the hollow fiber. The open end was then pressure-sealed using a pair of pliers. The needle was detached from the fiber and this open end was also pressure-sealed. The tip of the end-sealed fiber bar was held using a forceps and was immersed in octanol for impregnation for 20 s. After impregnation, the bar was removed and placed in urine sample kept under stirring (1000 rpm). After 30 min of extraction, the solvent bar was taken out. One end of the hollow fiber was cut with a sharp blade. The open end was kept in a small glass insert. Then the other end was also cut by keeping the open end in the glass insert so as to avoid the loss of acceptor phase from the open end. The acceptor solution was flushed into the glass insert by pushing air using a 25 μL syringe. A 5 μL of the acceptor solution was withdrawn into the 10 μL syringe and injected into the LC for separation and quantification. The used fiber was discarded, and a fresh one was used for the next experiment.

3. Results and discussion

3.1. Influence and choice of the experimental conditions

In the present investigation, various experimental parameters were studied using LC-UV and confirmation was performed using LC-ES-TMS. Although the LC-UV is used for studying the experimental conditions, however, the type of mobile phase and of the acceptor phase to be injected into the LC-ES-TMS was chosen as to be compatible for ES-TMS.

3.1.1. Selection of the hollow fiber

Generally, hollow fiber-based LPME procedures are based on polypropylene fiber, except for a few that use porous polyvinylidene difluoride [17]. Based on our previous experience [13,15] and due to strong immobilization of organic solvents in the pores of polypropylene fiber [18] and to its excellent mechanical stability [19], experiments were performed using polypropylene hollow fiber.

3.1.2. Selection of organic solvent for impregnation

Choice of an organic solvent is an essential consideration in the extraction process. The selection criteria for an organic solvent to be a suitable choice are: it should be easily immobilized in the pores of the polypropylene hollow fiber; secondly it should be of low volatility to prevent solvent loss and must be immiscible with water; the last and the most important requirement is that the solubility of analyte in the solvent should be
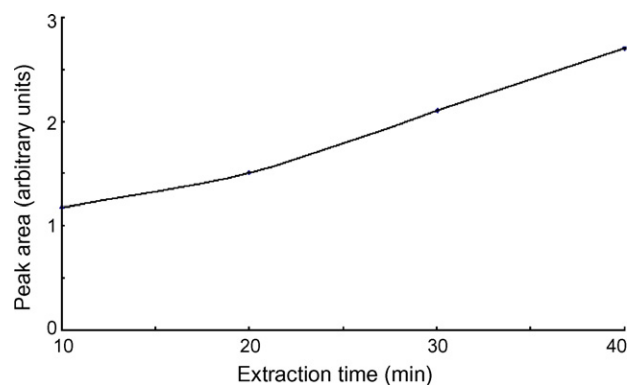

Fig. 1. Influence of extraction time on the extraction efficiency. Experimental conditions: octanol as impregnation solvent, 1 M NaOH as donor phase, 1 M formic acid as acceptor phase, stirring speed 800 rpm, concentration of the sample 1 μg mL^{-1}.

higher than that in the donor phase and be lower than that in the acceptor phase. This is in order to promote the analyte migration from the donor phase through the pores of the hollow fiber and finally into the acceptor phase. Considering these facts into account, octanol, nonanol and dihexyl ether were tested for their suitability. Among these, octanol gave good enrichment. Hence, octanol was used as impregnation solvent for subsequent studies.

3.1.3. Extraction time profile

Extraction efficiency depends on the period of extraction time. Hence, the function of extraction time was studied with respect to extraction efficiency. It was performed by using the hollow fiber impregnated with octanol as impregnation solvent, 1 M NaOH as donor phase and 1 M formic acid as an acceptor phase under a stirring speed of 800 rpm. Fig. 1 describes the influence of extraction time on the extraction efficiency (as a measure of peak area in the chromatogram). Like SPME, TPS-BME is also dependent on equilibrium rather than exhaustive extraction. It requires a period of time for equilibrium to be established. However, it is not normally considered practicable to maintain a long extraction time for equilibrium to be attained. An extraction period of 30 min was chosen for further studies.

3.1.4. Effect of stirring speed on the extraction efficiency

Generally, faster stirring speed increases extraction efficiency. This is because agitation permits a continuous exposure of the extracting surface to a fresh aqueous sample. The free movement of the fiber will also contribute to the mass transfer. The effect of stirring speed was studied up to 1000 rpm. It is evident from Fig. 2 that extraction efficiency increases with stirring speed as compared to the unstirred sample. However, above 1000 rpm the bead started vibrating rather than stirring. Hence, a stirring speed of 1000 rpm was used for subsequent work.

3.1.5. Effect of ionic strength

To evaluate the possibility of salting-out effect, extraction efficiency was studied with increase in sodium chloride
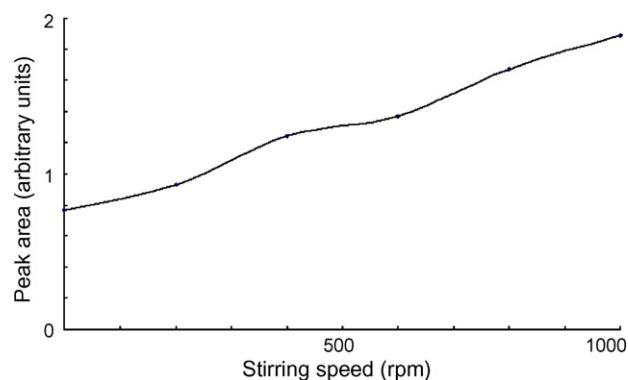
Fig. 2. Influence of stirring speed on the extraction efficiency. Experimental conditions: octanol as impregnation solvent, 1 M NaOH as donor phase, 1 M formic acid as acceptor phase, concentration of the sample 1 μg mL^{-1}, extraction time 30 min.

concentration (%, w/v). It was observed that there was a decrease in extraction efficiency with an increase in salt concentration. This could be due to the fact that ionic strength influenced the physical properties of the Nernst diffusion film, which reduces the rate of diffusion of the analytes into the organic phase [20,21]. Another possible reason is the participation of polar molecule due to an electrostatic interaction with salt ions in solution [22]. Hence, further extractions were made without the addition of sodium chloride.

3.1.6. Effect of donor and acceptor phase composition

Compositions of both the donor and the acceptor phases are very important parameters that affect the extraction efficiency. Basically, the acceptor phase should be sufficiently acidic in order to promote the dissolution of the basic analyte CB, while the donor phase should be strongly basic in order to deionize the analyte and consequently reduce its solubility in the solution. The difference in pH between the donor and acceptor phase is also one of the major parameters that promote the transfer of analytes from the donor phase to the acceptor phase. Hence, a series of experiments were made to find the best compositions of the donor and acceptor phases. For the donor phase, the NaOH concentration was varied from 0.25 to 3 M, and for the acceptor phase the formic acid concentration was varied from 0.5 to 5 M. A concentration of 1 M NaOH in the donor phase and 5 M formic acid in the acceptor phase gave the highest enrichment factors (calculated by dividing the peak area obtained on the chromatogram after injecting the analyte enriched acceptor phase by the peak area obtained on the chromatogram after injecting analyte containing donor phase before enrichment) (Table 1). Hence, for subsequent experiments the compositions of donor and acceptor phases were set at 1 M NaOH and 5 M formic acid, respectively.

3.2. Quantitative aspects

Repeatability, linearity, correlation coefficient, detection limit and enrichment factors were investigated under chosen experimental conditions. R.S.D. was found to be less than 5.1% based on the peak areas for seven replicated runs. Linearity was

Table 1
Effect of composition of donor and acceptor phases on the enrichment factor

Concentration of formic acid (M)	Enrichment factor				
	Concentration of NaOH (M)				
	3	2	1	0.5	0.25
5	55	62	79	54	53
4	50	61	78	48	55
3	48	62	74	52	47
2	44	63	71	47	50
1	49	59	72	55	58
0.5	49	56	70	51	47

tested using LC-ES-TMS. Correlation coefficient (r^2) was found to be 0.9972 for 0.1–4 ng mL^{-1} concentration range. Limit of detection was calculated as three times the standard deviation of seven replicate runs of CB spiked (10 pg mL^{-1}) urine sample and it was found to be 7 pg mL^{-1}.

3.3. Application of the method

The developed technique is applied for the analysis of urine sample. Five urine samples collected from healthy male adults
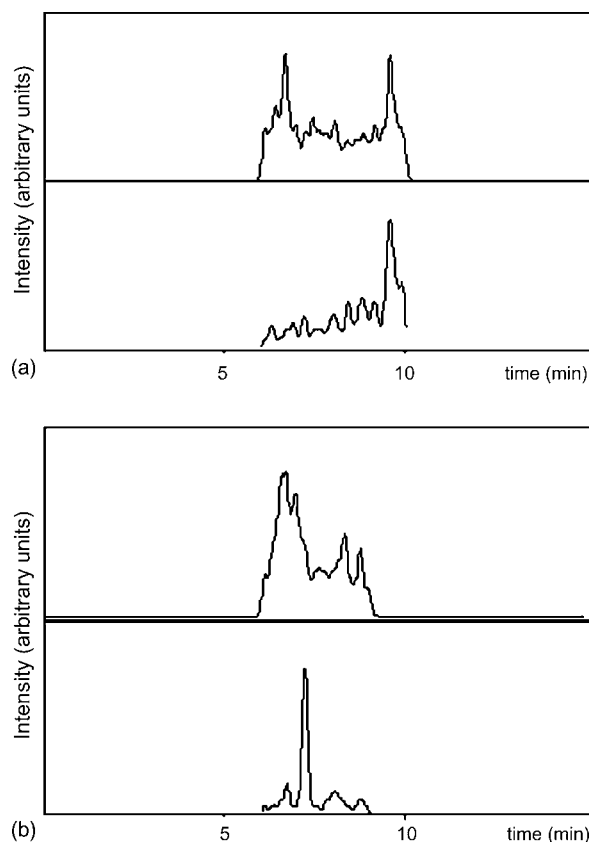

Fig. 3. Total ion chromatogram and the MS/MS/MS ion chromatogram of the extract of the (a) unspiked urine and (b) CB spiked urine sample. Experimental conditions: (a) octanol as impregnation solvent, 1 M NaOH as donor phase, 5 M formic acid as acceptor phase, stirring speed 1000 rpm, extraction time 30 min; (b) CB spiked at a concentration of 10 pg mL^{-1} to urine sample, other conditions are as in (a).

Table 2
Comparison of the technique with the reported SPME techniques [12,13]

Parameter	Reported SPME method		Present method
	Direct immersion SPME [12]	Head space SPME [13]	
Analysis time per sample (min)	90	115	47
Sensitivity (MDL) [ng mL^{-1}]	0.2[a]; 1.1[b]	0.23[a]	0.007
Solvent required per analysis	None	None	Few microliters
Cost of analysis per extraction (in US $)	Not reported	2.68	0.02
R.S.D. (%)	Not reported	3.9	5.1

[a] MDL obtained in GC/MS.
[b] MDL obtained in GC/FID.

(aged 24–30 years) were subjected for extraction and analysis. Urine was basified (1 M NaOH) and extracted in a usual manner. The acceptor phase was injected into LC coupled with ES-TMS. However, it was observed that no target compound was found in any of the urine samples tested. One of the urine samples was spiked with 10 pg mL^{-1} of CB and extracted in a usual manner. A representative chromatogram of the extract of the unspiked and spiked urine samples are shown in Fig. 3a and b, respectively.

3.4. Comparison of the method with the SPME technique

The present technique is compared with the reported SPME techniques [12,13] in terms of selectivity, analysis time per extraction, cost of analysis per extraction, and precision (Table 2). Unlike the reported LLLME/AMAP technique [13], the present technique does not require any syringe pump during extraction.

4. Conclusions

The current design outlines a successful development and application of an extraction method for CB. The experimental setup is extremely simple and highly affordable. Among all microextraction techniques reported, this technique is the most economical sample preparation/preconcentration technique to our knowledge. No syringe is required to hold the fiber in the current technique as the fiber was allowed free in the sample solution kept under stirring. The method does not require any additional specific equipment or training for extraction except a magnetic stirrer, and a separation and detection system. Additionally, single use of the hollow fiber completely eliminates the risk of cross-contamination and carry-over problems. Owing to the offline nature of the concept and extremely low cost of each extraction unit, a large number of samples can be extracted in parallel providing a high number of samples per unit time capac-

ity. Broadly, the technique shares the advantages of both sample preparation and enrichment simultaneously.

References

[1] A. Blass, M. Dave, M.J. Sauer, J. Vet. Pharmacol. Ther. 22 (1999) 234.
[2] G. Brambilla, T. Cenci, F. Franconi, R. Galarini, A. Macri, F. Rodoni, M. Strozzi, A. Loizzo, Toxicol. Lett. 114 (2000) 47.
[3] P.M. Clarkson, H.S. Thompson, Sports Med. 6 (1997) 366.
[4] T.Y.K. Chan, J. Toxicol. Clin. Toxicol. 39 (2001) 345.
[5] T.Y.K. Chan, J. Toxicol. Clin. Toxicol. 37 (1999) 517.
[6] G.A. Mitchell, G. Dunnavan, J. Anim. Sci. 76 (1998) 208.
[7] M. Thevis, T. Schebalkin, A. Thomas, W. Schanzer, Chromatographia 62 (2005) 435.
[8] A. Koole, J. Bosman, J.P. Franke, R.A. de Zeeuw, J. Chromatogr. B 726 (1999) 149.
[9] S. Keskin, D. Ozer, A. Temizer, J. Pharm. Biomed. Anal. 18 (1998) 639.
[10] L.X. Whaites, E.J. Murby, J. Chromatogr. B 728 (1999) 67.
[11] L. Amendola, C. Colamonici, F. Rossi, F. Botre, J. Chromatogr. B 773 (2002) 7.
[12] M.D. Engelmann, D. Hinz, B.W. Wenclawiak, Anal. Bioanal. Chem. 375 (2003) 460.
[13] M.B. Melwanki, W.H. Hsu, S.-D. Huang, Anal. Chim. Acta 552 (2005) 67.
[14] X. Jiang, H.K. Lee, Anal. Chem. 76 (2004) 5591.
[15] M.B. Melwanki, S.-D. Huang, Anal. Chim. Acta 555 (2005) 139.
[16] A. Posyniak, J. Zmudzki, J. Niedzielska, Anal. Chim. Acta 483 (2003) 61.
[17] L.S. de Jager, A.R. Andrews, Analyst 126 (2001) 1298.
[18] K.E. Rasmussen, S. Pedersen-Bjergaard, Trends Anal. Chem. 23 (2004) 1.
[19] K.E. Rasmussen, S. Pedersen-Bjergaard, M. Krogh, H.G. Ugland, T. Gronhaug, J. Chromatogr. A 873 (2000) 3.
[20] M.C. López-Blanco, S. Blanco-Cid, B. Cancho-Grande, J. Simal-Gándara, J. Chromatogr. A 984 (2003) 245.
[21] M. Palit, D. Pardasani, A.K. Gupta, D.K. Dubey, Anal. Chem. 77 (2005) 711.
[22] C. Basheer, H.K. Lee, J.P. Obbard, J. Chromatogr. A 1022 (2004) 161.

Thin layer distillation for matrix isolation in flow analysis

Patrick Mornane [a], Jeroen van den Haak [a], Terence J. Cardwell [b],
Robert W. Cattrall [b], Purnendu K. Dasgupta [c], Spas D. Kolev [a],*

[a] *School of Chemistry, The University of Melbourne, Victoria 3010, Australia*
[b] *Department of Chemistry, La Trobe University, Victoria 3086, Australia*
[c] *Department of Chemistry and Biochemistry, Texas Tech University, Lubbock, TX 79409-1061, USA*

Abstract

Analyte transfer from the matrix in a thin layer distillation (TLD) cell and its subsequent measurement were investigated in a flow injection configuration. We designed the cell such that the donor and acceptor streams flowed in parallel channels separated by a thin dividing wall. The matrix transfer process involved room-temperature distillation of the analyte into the headspace of the TLD cell and its subsequent condensation/uptake by a concurrently flowing acceptor stream. There are no membranes; hence there are no membrane-related problems. The TLD system design was optimized with respect to its dimensions and operational parameters. Throughput and sensitivity were compared with a conventional pervaporation flow injection (PFI) system for ammonia and five different amines. For the higher molecular mass amines, the TLD approach provided comparable or superior performance. The TLD technique should be an attractive approach for online analysis of volatile chemical species in 'dirty' samples, especially for volatile analytes of higher molecular mass.
© 2006 Elsevier B.V. All rights reserved.

Keywords: Thin layer distillation; Membraneless gas-diffusion; Flow injection analysis; Pervaporation flow injection; Amines

1. Introduction

Gas-diffusion flow injection (GD-FI) systems have been used extensively for the determination of analytes which are or can be converted chemically to volatile chemical species [1]. The donor (sample) stream is separated by a membrane from the acceptor stream; the analyte is transferred through the membrane and recaptured by the suitably formulated acceptor solution. However, real samples often contain dissolved or suspended material that adversely affects membrane performance, eventually resulting in membrane failure. The more recently introduced pervaporation flow injection (PFI) technique attempts to solve this problem by avoiding any contact of the sample with the membrane: the analyte evaporates into a headspace above the donor stream and then diffuses across a membrane into the clean acceptor stream [2]. Unfortunately, some performance parameters deteriorate: the throughput rate of a PFI system for cyanide was found to be six times lower than that of a GD-FI system

employing the same chemistry [3,4]. In both techniques, the analyte diffuses across a hydrophobic membrane. In GD-FI the analyte evaporates directly into the pores of the hydrophobic membrane while in PFI it evaporates initially into the headspace of the pervaporation cell, thus resulting in dilution (poorer limits of detection (LODs)) and the *additional* step of gas phase diffusive transfer leading to overall slower mass transfer. To compound matters, whereas in GD-FI systems the acceptor and donor stream pressures can counterbalance each other permitting the use of relatively thin membranes, thicker membranes are needed in PFI cells to support the acceptor stream, further contributing to poorer performance. In both systems, improved sensitivity can generally be obtained by a stopped-flow approach [5], at the further expense of the throughput rate.

Interestingly, prior to the advent of flow analysis, volatile analyte transfer without the use of membranes was well known and well established; improvements were being proposed [6] for the microdiffusion analysis technique, introduced by Conway [7], designed to carry out volatile analyte transfer. Samples that would be considered challenging by present day standards such as heparinized blood, plasma, or serum were analyzed by Christian and Feldman for volatile constituents like ammonia

---

* Corresponding author. Tel.: +61 3 83447931; fax: +61 3 93475180.
 E-mail address: s.kolev@unimelb.edu.au (S.D. Kolev).

[8]. The Conway cell is a circular unit consisting of two concentric chambers sharing a common headspace. The central circle was filled with a sulfuric acid solution to receive the ammonia and the blood sample and a potassium carbonate solution were separately put in the outer ring, the chamber covered and the two outer constituents allowed to mix so that ammonia would evolve. Over 50% of the ammonia was transferred in 10 min, and an aliquot of the inner solution was then titrated with coulometrically generated hypobromite. Despite the fact that there is such extensive information in the extant literature on static volatile analyte transfer, it is interesting that a US patent has been recently granted on this same topic [9]!

To our knowledge, the first flow-based membraneless volatile analyte transfer system was based on macroscale flows. To measure ammonia flux from seawater, Genfa et al. [10] described an approach in which donor and acceptor streams flowed vertically on oppositely placed plates. At the other extreme, in planar devices when the height of a confined channel is small, superlaminar flow occurs and there is very little mixing of two fluid streams even when they flow side by side. This is exploited in the T-sensors of Weigl and Yager [11,12]. In the correspondingly derived H-filter [13], a portion of smaller molecules can be preferentially diffusively removed to an acceptor stream, leaving larger molecules behind, thus functioning as a membraneless dialyzer. However, most GD-FI or PFI applications are not compatible with an H-filter type device, nor is the flux collector device [10] simple to construct and use (designed to use donor flow rates as high as 250 mL/min, far from typical flow analysis arrangements).

Clearly, a need exists to develop a matrix isolation approach applicable to real samples without membranes and applicable to real samples. We describe a more practical approach herein in which the donor and acceptor streams flow concurrently in parallel and share a common shallow headspace. The analyte evaporates from the donor stream and diffuses across the headspace to be captured in the acceptor stream. When we initially explored this approach [14], we called it Membraneless Gas-Diffusion Flow Injection (MGD-FI) and have referred to it the same way elsewhere [15]. We presently believe that the term Thin Layer Distillation Flow Injection (TLD-FI) is more specifically descriptive and thus constitutes more appropriate terminology. The application of such an approach to the determination of ethanol in liquors was independently pursued by Choengchan et al. [16] and reported very recently.

This paper reports on the advantages the TLD approach offers for the determination of large molecular mass analytes in comparison with pervaporation flow injection separation.

2. Experimental

2.1. Reagents

All chemicals were of reagent grade. Deionized water (18 MΩ cm, Millipore) was used for all solutions. The stock indicator solution contained 0.05 and 0.15% (w/v) cresol red and thymol blue, respectively [17]. The acceptor stream solution was made daily by 50× dilution of the stock indicator solution.

The donor solution consisted of 1.0 M NaOH. Both solutions were sonicated before use to remove dissolved gases and CO_2 intrusion was minimized by soda-lime packed vent tubes on each reservoir.

The ammonium stock standard (0.01 M NH_4Cl) was preserved by adding a drop of chloroform and stored refrigerated. Stock solutions (0.1 mol/L) of the following amines were prepared in 0.1 M H_2SO_4 and stored refrigerated: ethylamine, diethylamine, triethylamine, dibutylamine, and *n*-decylamine.

2.2. TLD-FI and PFI systems

For comparability both systems were made from the same equipment components: peristaltic pumps (VS4-10R-Midi, Watson-Marlow) with Tygon® pump tubing, rotary injection valve (model 5020, Rheodyne) with a 500 μL sample loop, spectrophotometric detector (Novaspec II, Amersham) set at 577 nm, equipped with a 80 μL volume and 10 mm path length flow-through cell (Starna, UK) and interfaced by a data acquisition card (DAQ 6062, National Instruments) to a Pentium-IV class personal computer running LabView 7.1.™. Solution reservoirs were thermostated at 20 °C in a water bath (Ratek, Australia). All connecting tubing was 0.5 mm i.d. poly(tetrafluoroethylene) (PTFE). A 100 cm mixing coil with 1 cm diameter followed the injection valve in the 1.0 M NaOH donor stream to ensure mixing (Fig. 1A).

The pervaporation cell (Fig. 1B) was constructed from two 61 mm in diameter Perspex discs, held together by stainless steel ring clamps and four stainless steel bolts. Elliptical shape donor/acceptor chambers were machined in the blocks with major and minor axes of 15.0 and 7.5 mm, respectively. The depths of the donor and acceptor chambers, separated by a 1.5 mm thick PTFE membrane (Trace, Germany), were 5.0 and 0.5 mm, respectively. A single layer of 3 mm glass beads filled the donor chamber to enhance mixing and reduce the sample residence time.

The liquid level in the pervaporation donor chamber affects the attainable sensitivity and reproducibility. The inlet and outlet flow rates of the donor chamber were independently controlled by two peristaltic pumps (Fig. 1A) while the acceptor stream was propelled by a third pump. Glass beads in the donor chamber facilitated both the initial establishment and the maintenance of the liquid level. The liquid level was maintained at the height of the glass beads (3 mm) ensuring a headspace of approximately 2 mm in the pervaporation donor chamber.

The TLD cell (Fig. 2A) required pumped flow inputs to both donor and acceptor channels as well as aspirated outputs to maintain a constant liquid level in each. Several flow configurations from a single four-channel pump to four single channel pumps were tested. All results reported here used the most flexible configuration that involved four independent pumps.

Three TLD cells of different dimensions (Table 1) were tested. A thin layer of Apiezon N siliconefree grease was applied between the two halves of the Perspex TLD cell. Each cell consisted of an identical bottom half incorporating identical donor and acceptor channels divided by a 1 mm thick wall with a height
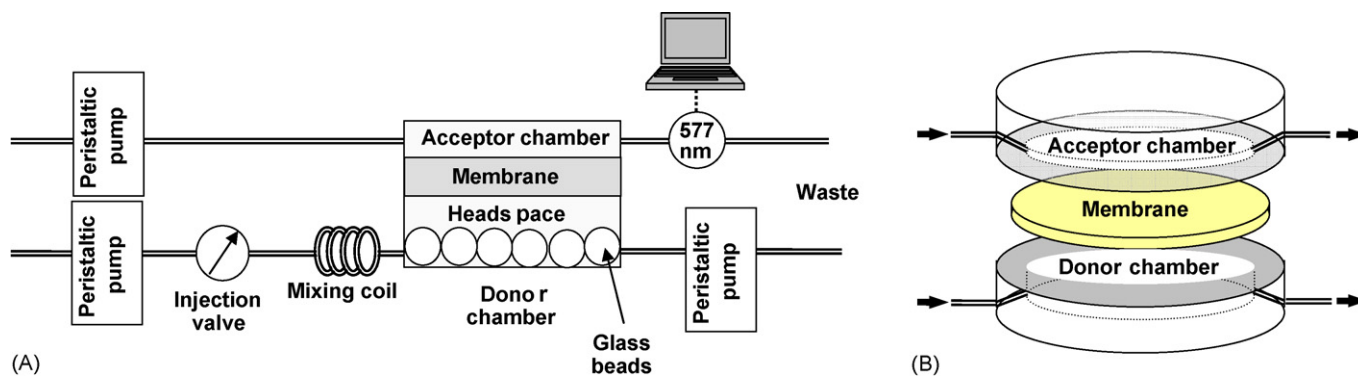
Fig. 1. Schematic of the PFI system (A) and the PFI cell (B).
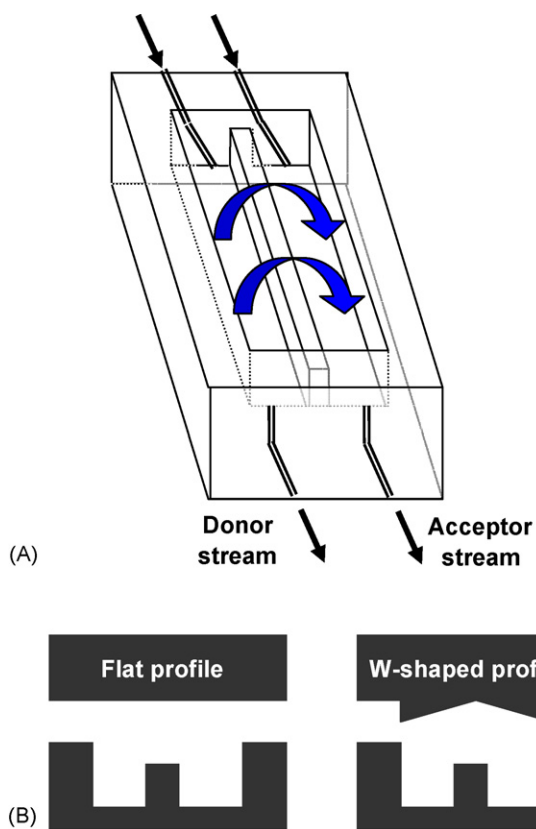

Fig. 2. Schematic of the TLD cell: lower (A) and upper (B) halves.

0.5 or 1 mm lower than the channel depth to form a common headspace (Table 1). The influence of the headspace volume on sensitivity was studied with a flat and a W-shaped cross-section of the top half of the cell (Fig. 2B).

Table 1
Dimensions of the TLD cells (Fig. 2B)

Parameter	TLD cell		
	A	B	C
Channel length (mm)	64.0	64.0	64.0
Channel width (mm)	4.0	3.0	2.0
Channel depth (mm)	4.0	4.0	2.5
Dividing wall width (mm)	1.0	1.0	1.0
Dividing wall height (mm)	3.0	3.0	2.0

The suitability of three different types of packing to improve performance of the TLD cell was investigated; these included glass (1.0, 2.0 and 3.0 mm diameter), and stainless steel (1.7, 2.4 and 3.0 mm diameter) beads, and a helically twisted stainless steel wire (0.70 mm diameter), all occupied the entire channel length.

Pump configuration and optimum TLD cell geometry/packing type were studied with 20 mg/L NH_4Cl with donor/acceptor flow rates of 0.5 mL/min. Donor and acceptor flow rates were optimized for both systems with regard to sensitivity and throughput rate; a flow rate range of 0.2–1.2 mL/min was studied.

3. Results and discussion

3.1. TLD cell geometry

The TLD cell (all tested with the top half flat configuration) with the smallest dimensions (type C, Table 1) exhibited not only the highest throughput rate, expected on the basis of the smallest residence volume, but also the best sensitivity. When TLD cell C was tested with a W-type top half, the sensitivity was approximately 25% lower. This result could be attributed to the fact that the evaporation of ammonia from the donor stream into the TLD cell headspace was faster than its transport and absorption into the acceptor stream. Under these conditions the headspace served as a temporary reservoir for ammonia and the smaller volume of the headspace in the case of a W-shaped upper half produced lower sensitivity compared to the flat profile upper half. Flat-topped cell C was used henceforth.

3.2. TLD cell packing

For both channels of the TLD cell, mixing is crucial for enhancing outward transport of the analyte from the donor stream and its efficient absorption into the surface layer of the acceptor stream. Disruption of laminar flow, e.g., by elements in the flow path, is essential to perturb the stagnation of the surface layer. Packing elements should also reduce the effective volume of the channel and thus increase the throughput rate. As in PFI [3,5,17–22], the presence of packing in the channels should improve the ease of maintaining a lower but constant liquid vol-
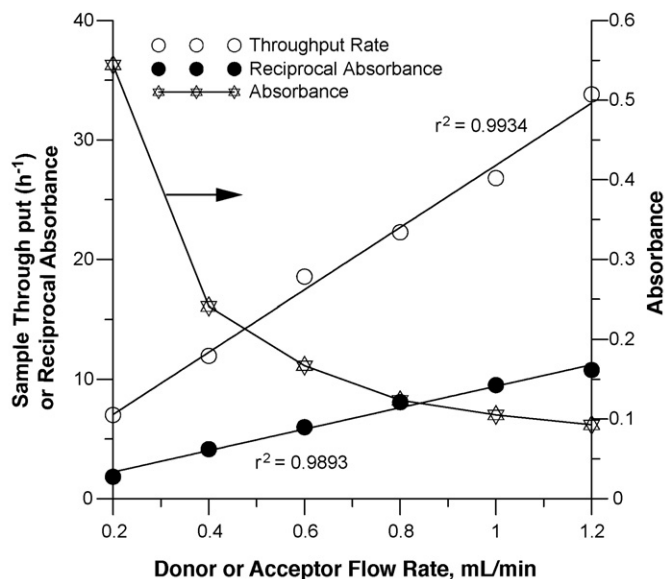
Fig. 3. Effect of the donor and acceptor flow rates on sensitivity and sample throughput of the TLD-FI system (the donor and acceptor flow rates were equal).

ume in a TLD cell as well. Beads, especially the smaller ones, tended to float up in the flowing stream. Larger beads remained but overflow problems were encountered. Most reproducible results were obtained with the twisted stainless steel wire, which also provided a rigid immobile element. This packing was used henceforth.

3.3. Influence of flow rate on sensitivity and sampling rate

With identical flow rates in both the donor and acceptor channels, the flow rate was varied from 0.2–1.2 mL/min. Similar to previous PFI studies [19], a change in flow rate was found to affect the sensitivity (height of absorbance signal) and throughput rate in opposite directions. Both flow systems behaved the same way; illustrative results are given for the TLD system (Fig. 3). Sample throughput rate and reciprocal absorbance show good linear correlation with flow rate ($r^2 = 0.99$). Acceptable sensitivity and sampling rate for both systems were attained at intermediate flow rates (0.5–0.6 mL/min).

Variation of acceptor or donor flow rate (while holding the other constant at 0.6 mL/min) did not suggest that any combination of donor/acceptor flow rates other than 0.6/0.6 mL/min would result in better performance (sensitivity or LOD, sample throughput rate). Donor/acceptor flow rates of 0.6/0.6 mL/min were used henceforth. A representative TLD fiagram is shown for 20 mg/L NH_3 in Fig. 4. The reproducibility in these measurements was 1.5% in R.S.D.

The possibility of improving sensitivity by using a stopped-flow approach was also explored for both flow systems by stopping the acceptor stream for periods up to 5 min. In the present detection system ammonia absorption by the indicator acceptor is a reversible process, unlike e.g., the uptake of AsH_3 by a $KMnO_4$ acceptor [5]. With irreversible chemistries, the sensitivity monotonically increases with the stopped-flow period, however, in the present case, a maximum was observed
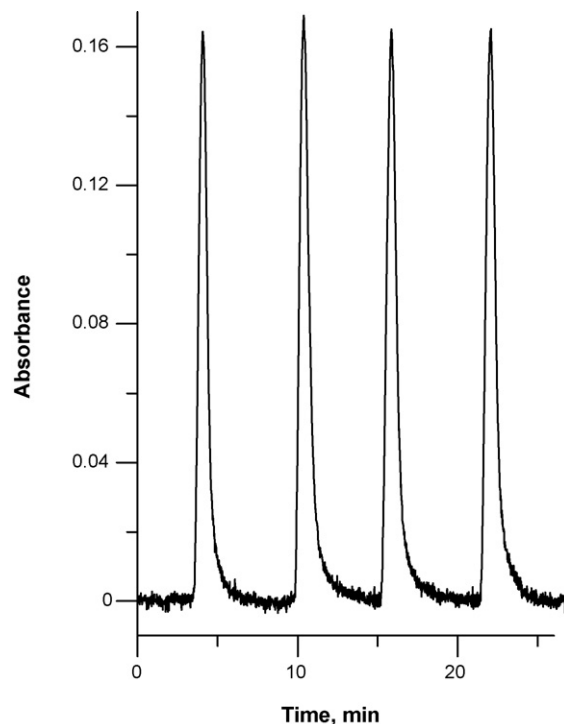

Fig. 4. Typical response of the TLD-FI system, 20 mg/L NH_3.

for both PFI and TLD-FI systems (Fig. 5). Once the ammonia-bearing sample is gone, eventually the ammonia concentration in the acceptor is higher than that in the donor and the direction of transport is reversed. The maximum is more pronounced in the PFI system than in the TLD-FI system, but in neither case a major gain is realized by stopped-flow operation with the reversible detection chemistry. The sample throughput rate predictably decreases in both systems with increasing stopped-flow duration.
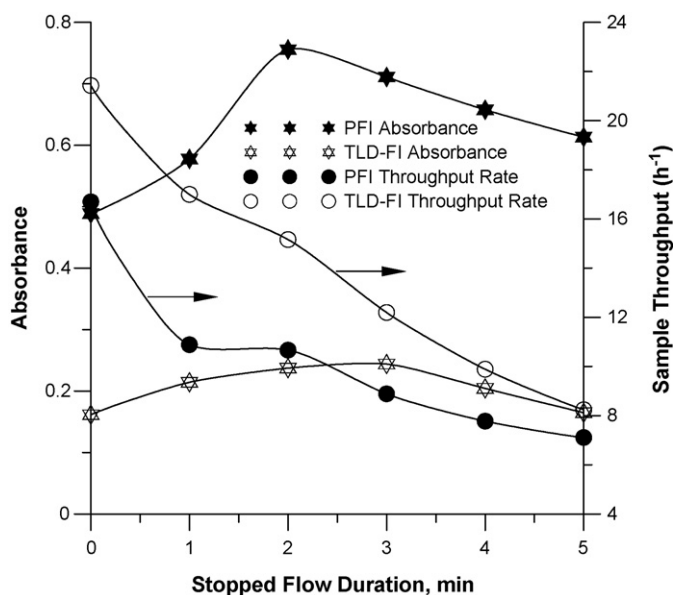

Fig. 5. Effect of the stopped flow time on sensitivity and sample throughput of the TLD-FI and the PFI systems.

3.4. Sensitivity comparison: TLD and PFI systems (ammonia versus amines)

Fig. 4 shows the sensitivity and the throughput rates attainable in the PFI and TLD-FI systems for ammonia. With no stopped-flow the PFI system provided an order of magnitude better LOD (0.50 mg/L versus 5.0 mg/L NH_3, S/N = 3) than the TLD-FI system. The applicable linear range was 0.5–20.0 mg/L and 10.0–100.0 mg/L, respectively. The poorer sensitivity of the TLD system can be attributed at least in part to the threefold lower surface area to volume ratio of the acceptor stream in the TLD cell compared to the pervaporation cell. The rate of ammonia absorption into the acceptor stream is proportional to the interfacial surface area of the acceptor solution. In addition, the TLD cell donor channel had less than half the mean liquid residence time (20.7 s versus 45.2 s) as the pervaporation cell, with a donor flow rate of 0.6 mL/min. The cell washout characteristics would also be expected to be much poorer for the pervaporation cell, further increasing the effective residence time. This is indeed reflected by the more than 2× better sampling rate that is attainable in the TLD-FI versus the PFI system.

Based on the performance parameters for NH_3 as the analyte, the TLD approach may be faster than PFI but is far less sensitive and it would seem that it would be attractive only in specific situations. However, the scenario should be different with larger molecular mass analytes which diffuse only very slowly through membranes. The necessity of using thicker membranes in PFI exacerbates this problem [20]. Because diffusion is slow, throughput rate also decreases. Fig. 6 shows how the relative sensitivity changes as the analyte molecular mass, expressed as the number of carbon atoms in the amine molecule, increases. The relative sensitivity does not change much up to four carbon atoms but begins to increase steeply past that point and for TLD becomes more sensitive than PFI by the time an amine

with 10 carbon atoms is reached. Nonylamine (nine carbon atoms) was not specifically tested but the trend indicates that at this point the sensitivity of the two approaches would be comparable. TLD wins throughout in the throughput rate contest, the advantage increasing exponentially with increasing carbon atoms. Throughput rate for decylamine could not be determined in a reliable fashion because of the very long baseline-to-baseline time (in excess of 30 min) of the PFI peak for this amine due to excessive tailing.

4. Conclusions

Thin layer distillation of the analyte from a donor stream and transfer to an acceptor is a viable approach. This uses no membranes and thus does not suffer from membrane-associated problems. The TLD approach appears to be particularly attractive for higher molecular mass analytes which diffuse only slowly through membranes and can sometimes be strongly adsorbed on hydrophobic membrane matrices. The design of the TLD cell can stand improvement. If the liquid contact part of the channel is machined from stainless steel which can easily be electrooxidized to be hydrophilic [23], and a top PTFE barrier portion is installed thereon, it would be possible to operate the TLD cell better, where the wetted part of the channel is wetted and above that is a barrier to liquid bridging. Thin Peltier devices are easily available and can provide a simple means of simultaneously heating the donor and cooling the acceptor channel, when inserted from the bottom of a hollowed out barrier separating the two channels.

Ultimately and ideally TLD devices may be microfabricated where chemical vapor deposition and plasma etching techniques can be used to tailor surfaces to be hydrophilic or hydrophobic. At the low pressures and superlaminar flows involved in such devices, it should be possible to operate with a "pumping only" protocol, where the force to move forward in a channel bounded by hydrophilic walls (and topped by hydrophobic ledges) will be less than that needed to climb over a hydrophobic barrier into another channel.
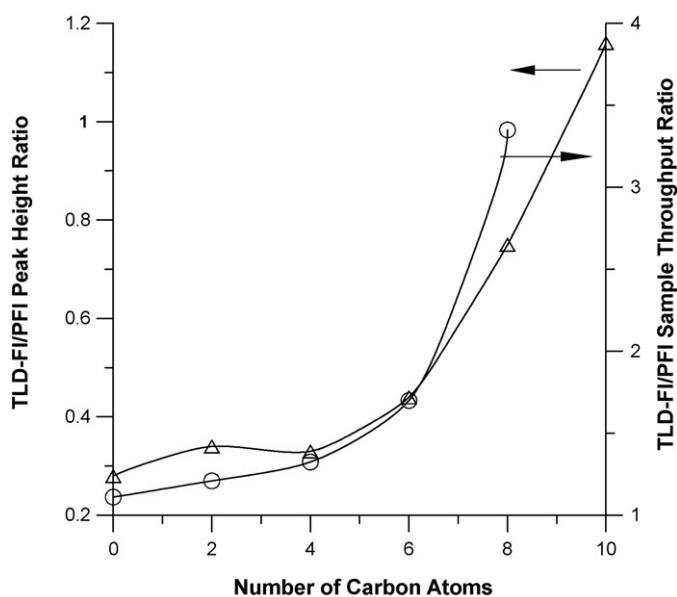

Fig. 6. Relative sensitivity and throughput rates of the TLD-FI vs. the PFI system for different analytes (ammonia and *n*-alkylamines) as a function of the number of carbon atoms in the analyte.

References

[1] Z. Fang, Flow Injection Atomic Absorption Spectrometry, Wiley, New York, 1995.
[2] M.D. Luque de Castro, I. Papaefstathiou, Spectrochim. Acta 53B (1998) 311.
[3] H. Sulistyarti, T.J. Cardwell, S.D. Kolev, Anal. Chim. Acta 390 (1999) 133.
[4] H. Sulistyarti, T.J. Cardwell, S.D. Kolev, Anal. Chim. Acta 357 (1997) 103.
[5] T. Rupasinghe, T.J. Cardwell, R.W. Cattrall, I. Potter, S.D. Kolev, Anal. Chim. Acta 510 (2004) 225.
[6] K.J. Obrink, Biochem J. 59 (1955) 134.
[7] E.J. Conway, Microdiffusion Analysis and Volumetric Error, Macmillan, New York, 1958.
[8] G.D. Christian, F.J. Feldman, Clin. Chim. Acta 17 (1967) 87.
[9] D.L. Harp, Controlled diffusion analysis, US Patent 6,368,870 (April 2002).
[10] Z. Genfa, T. Uehara, P.K. Dasgupta, T. Clarke, W. Winiwater, Anal. Chem. 70 (1998) 3656.
[11] B.H. Weigl, P. Yager, Science 283 (1999) 346.
[12] A.E. Kamholz, E.A. Schilling, P. Yager, Biophys. J. 80 (2001) 1967.
[13] Micronics Inc., The H-filter, http://www.micronics.net/technologies/h_filter.php, 1990.

[14] P. Mornane. An investigation of membraneless gas diffusion as an online separation technique in flow injection analysis, Honours Thesis, The University of Melbourne (Australia), 2003.

[15] J. Van den Haak, P. Mornane, T.J. Cardwell, R.W. Cattrall, S.D. Kolev, Handbook of Interact, 2004, p. 41.

[16] N. Choengchan, P. Wilairat, P.K. Dasgupta, S. Motomizu, D. Nacapricha, Anal. Chim Acta 579 (2006) 33.

[17] L. Wang, T.J. Cardwell, M.D. Luque de Castro, R.W. Cattrall, S.D. Kolev, Anal. Chim. Acta 416 (2000) 177.

[18] S.Y. Sheikheldin, T.J. Cardwell, M.D. Luque de Castro, R.W. Cattrall, S.D. Kolev, Anal. Chim. Acta 419 (2000) 9.

[19] S.Y. Sheikheldin, T.J. Cardwell, M.D. Luque de Castro, R.W. Cattrall, S.D. Kolev, Environ. Sci. Technol. 35 (2001) 178.

[20] T. Rupasinghe, T.J. Cardwell, M.D. Luque de Castro, R.W. Cattrall, S.D. Kolev, Anal. Chim. Acta 445 (2001) 229.

[21] S. Satienperakul, S.Y. Sheikheldin, T.J. Cardwell, M.D. Luque de Castro, I.D. McKelvie, S.D. Kolev, Anal. Chim. Acta 485 (2003) 37.

[22] L. Wang, T.J. Cardwell, M.D. Luque de Castro, R.W. Cattrall, S.D. Kolev, Talanta 60 (2003) 1269.

[23] K. Toda, J. Li, P.K. Dasgupta, Anal. Chem. 78 (2006) 7284.

Pervaporation-flow injection with chemiluminescence detection for determination of iodide in multivitamin tablets

D. Nacapricha [a], P. Sangkarn [a], C. Karuwan [a], T. Mantim [a], W. Waiyawat [a], P. Wilairat [a], T. Cardwell [b], I.D. McKelvie [c], N. Ratanawimarnwong [a,d,*]

[a] *Department of Chemistry, Faculty of Science, Mahidol University, Rama 6 Road, Bangkok 10400, Thailand*
[b] *Analytical Chemistry Laboratories, Department of Chemistry, La Trobe University, Victoria 3086, Australia*
[c] *Water Studies Centre, School of Chemistry, Monash University, Victoria 3800, Australia*
[d] *Department of Chemistry, Faculty of Science, Srinakharinwirot University, Sukhumvit 23, Bangkok 10110, Thailand*

Abstract

This paper describes the use of a pervaporation (PV) technique in a flow injection (FI) system for selective improvement in iodide analysis. Iodide in the sample zone is oxidized to iodine, which permeates through a hydrophobic membrane. Detection of the diffused iodine is achieved using the chemiluminescent (CL) emission at 425 nm that results from the reaction between iodine and luminol. The method was applied for the analysis of some pharmaceutical products, such as nuclear emergency tablets and multivitamin tablets. Ascorbic acid present in multivitamin samples interfered seriously with the analysis, and off-line sample treatment using anion exchange resin was employed to successfully remove ascorbic acid before the analysis. Ascorbic acid was flushed from the column using 0.4 M sodium nitrate followed by elution of iodide with 2 M sodium nitrate. The detection limit (3S.D.) of the system was $0.5 \, mg \, l^{-1}$, with reproducibility of 5.2% R.S.D. at $5 \, mg \, l^{-1}$. Sample throughput was determined as 30 injections h^{-1}. There was good agreement between iodide concentrations from extracted samples determined using four different methods, i.e., PV-FI, gas diffusion-flow injection, potentiometry and ICP-MS. A comparison of the analytical features of the developed pervaporation system with these of the previously reported chemiluminescence gas diffusion-flow injection previously reported is also described.
© 2006 Elsevier B.V. All rights reserved.

Keywords: Pervaporation; Iodide; Chemiluminescence; Multivitamin; Dual detection

1. Introduction

Iodine is an essential micronutrient as a part of thyroid hormone, which is necessary for normal brain development. Inadequate iodine during prenatal and early development periods, can lead to several diseases, including spontaneous abortion, increased infant mortality, hypothyroidism and cretinism [1]. Iodine supplementation in food and the use of multivitamins containing potassium iodide is used to avoid these symptoms. However, excessive iodine intake can reduce thyroid function because large amounts of iodine block the thyroid's ability to produce the hormones thyroxin and triiodothyronine

[2]. Hence, there has been an increase in interest in the analytical control of iodide in food and pharmaceutical products.

In order to determine low level of iodide, many methods based on different principles have been proposed. These include ion [3] and ion-pair reversed-phase [4–6] high performance liquid chromatography with either post column reaction [3] or electrochemical detection [4–6]. Neutron activation analysis [7,8] and inductively coupled plasma-mass spectrometry [9–11] have also been described for determination of iodide. These last two techniques offer high sensitivity and selectivity for iodide measurement but require a high level of specialization and the facilities are expensive to establish and operate. Direct determination of iodide can be performed using ion selective electrode (ISE). Nevertheless, for the complicated sample, such as in urine [12] and milk [13], the matrix interference was suspected to contribute some electrode response.

A number of colorimetric methods for the quantitative determination of iodide in aqueous samples have been proposed

* Corresponding author at: Department of Chemistry, Faculty of Science, Srinakharinwirot University, Sukhumvit 23, Bangkok 10110, Thailand. Fax: +66 2 259 2097.
  E-mail addresses: nuanlaorr@swu.ac.th, nuanlaor@hotmail.com (N. Ratanawimarnwong).

[14–24]. The most frequently used methods are based on the catalytic effect of iodide on a reaction between Ce(IV) and As(III) [14–16] or the decomposition of the Fe(III)–thiocyanate complex in nitric acid solution [17,18]. In these approaches, determinations were very sensitive but selectivity of the methods was not satisfied. Direct colorimetric methods for determination of iodide have also been presented. Agrawa et al. [19] reported that leucocrystal violet was selectively oxidized with iodine (I_2) to form crystal violet dye which was then extracted in chloroform before measuring of absorbance at 588 nm. A procedure for the determination of iodide in charcoal impregnated with potassium iodide was developed by Taylor et al. [20]. An aqueous extract of iodide in the charcoal was converted to iodine with iodate in acidic media followed by spectrophotometric measurement at 460 nm. Similarly, tri-iodide detection by flow injection was reported by Kamson [21] and subsequently by Ensafi and Dehaghi [22]. To improve the sensitivity of the tri-iodide detection, the measurements of tri-iodide starch complex have been proposed [23,24].

Chemiluminescence (CL) detection is attractive in terms of the relatively low cost and the simplicity of the equipment involved. Moreover, the previously reported chemiluminescent iodine–luminol reaction permits detection of iodine to as low as 1×10^{-7} M to be achieved [25]. Iodide does not react with luminol, and it is therefore necessary to first oxidize iodide to elementary iodine, in order to initiate chemiluminescence. A flow injection system with CL detection for the determination of iodide was reported by Burguera et al. [26]. The iodine was generated in a closed headspace device and was carried out in a nitrogen gas flow to a vial, where it was trapped in a KI solution. The trapped iodine was then mixed with Co(II) and luminol solutions in a FI system to produce CL light. This was applied for urinary iodine determination and gave a detection limit of $10 \mu g l^{-1}$. Use of on-line oxidation and solvent extraction coupled with reversed micellar mediated CL detection has also been described for the determination of iodine and iodide in commercial gargle products [27]. A detection limit of 0.02 ng ml^{-1} was achieved.

According to previous reports, detection of iodine by luminol CL may be susceptible to a number of interferences including metal ions, and for this reason, a separation technique is usually carried out in the analysis of real samples [26,27]. Manual separations are always time consuming, laborious and difficult to perform in micro scale, but these can be automated by incorporation of hydrophobic membrane-based gas diffusion (GD) and pervaporation (PV) techniques into a flow injection (FI) system, and used to separate volatile analyte form. Improvement in selectivity is thus achieved because fewer species are converted to the gaseous form at room temperature [28].

To date, only a few methods involving GD-FI have been proposed for determination of iodide [29–31]. All of these detections of iodine were based on a simple photometric measurement of either I_3^- or the I_3^-–starch complex. We have also reported use of the GD-FI method for determination of iodide in some pharmaceutical samples but in this instance, CL detection of diffused iodine was employed for detection.

The method was successfully applied for nuclear emergency tablets (potassium iodide tablet) and Thai liquid medicine formulations, but could not be used for multivitamin sample determination because of interference by ascorbic acid [34].

Pervaporation coupled with FI has been described for the direct measurement of volatile and semi-volatile analytes in samples that may cause deterioration of the gas permeable membrane if used in GD-FI [32,33]. In PV-FI, the presence of an air gap between donor solution (sample) and the membrane ensures that contamination or deterioration of the latter is avoided. This paper presents PV-FI with CL detection for determination of iodide in pharmaceutical products including multivitamin tablets containing ascorbic acid that interfered in the GD-FI method described earlier [34]. Off-line sample treatment with an anion exchange column was used to separate ascorbic acid from iodide before analysis. Using the PV unit brings an advantage that prolongs the life-time of the PTFE membrane by avoiding the direct contact of high salt content solution of sodium nitrate, which was used in the sample treatment.

2. Experimental

2.1. The PV-FI manifold

The FI system with a pervaporation unit is depicted in Fig. 1. An AS-90 series autosampler (Perkin-Elmer, USA) was used for automatically loading of standard or sample solutions into the FI injection valve. A FIAS-300 module (Perkin-Elmer, USA) was employed for pumping the reagents. A home-made pervaporation unit consisted of two circular Perspex blocks (61 mm diameter, 25 mm deep) held together by stainless steel ring clamps and four stainless steel bolts. Both the acceptor chamber (0.3 mm deep) and donor chamber (5.0 mm deep) were hexagonal in shape. PTFE membrane (40 mm diameter, 1.5 mm thickness; Trace Biotech AG, Germany) was used to separate the donor and acceptor chambers of the pervaporation unit. A home-made CL detector, used for monitoring the CL light from iodine–luminol reaction, consisted of a concentric spiral Perfluoroalkoxy (PFA, 0.75 mm i.d., 100 cm length) flow cell fitted in front of the PMT (Oriel 7020 Photomultiplier, USA). PTFE tubing (0.75 mm. i.d.) was used for all manifold connections.

2.2. Dual-detection FI for on-line detection of iodide and ascorbic acid after treated with anion exchange column

In this work, a dual-detection FI system coupled with an anion exchange resin (AER) column (Fig. 2), was used for optimization of the separation step between ascorbic acid and iodide. A mixture of iodide and ascorbic acid solution was loaded onto the AER column, followed by pumping a solution of sodium nitrate, used as the eluent. The stream emerging from the column was split into two lines using a Y-connection tube. This allows for real-time monitoring of the elution of iodide and ascorbic acid. Within this dual-detection FI system, detection of ascorbic acid was based on reduction of potassium permanganate (System I,
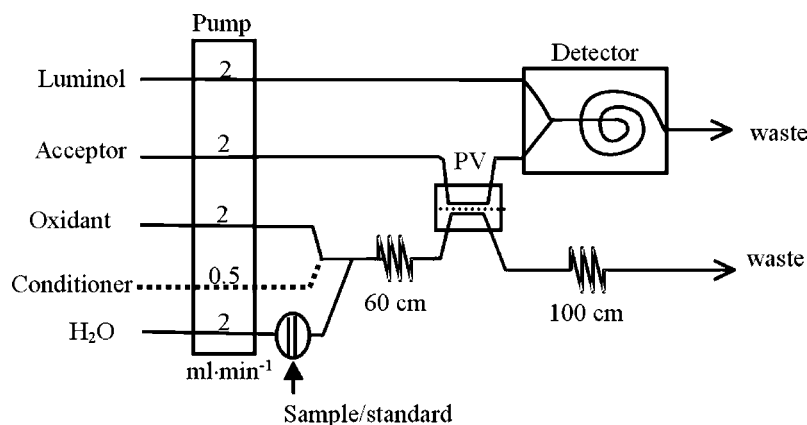
Fig. 1. The employed PV-FI manifold. PV: pervaporation unit. Detector: photomultiplier tube with a home-made flow cell. Luminol: 7.5×10^{-4} M in 0.1 M NaOH. Acceptor: 1% (w/v) KI. Oxidant: 0.01 M $K_2Cr_2O_7$ in 10% (v/v) H_2SO_4. Conditioner: 5 mg l^{-1} KI.

Fig. 2) [36]. Detection of iodide was based on its catalytic effect on the redox reaction of Ce(IV)–As(III) (System II, Fig. 4), with a decrease in Ce(IV) concentration being monitored spectrometrically at 420 nm [15,16]. Note that ascorbic acid was also detected by this redox reaction, since ascorbic acid also causes reduction of Ce(IV).

2.3. Reagents

All chemicals used in this work were AR grade. Ultra-pure water, obtained from a Milli-Q-system, was used for preparation of reagent solutions. A stock solution of standard iodide (1000 mg l^{-1}) was prepared by dissolving 1.307 g of potassium iodide (Merck, Germany) in 1 l of water, and working solutions of iodide were prepared by appropriate dilution with water.

Luminol solution (7.5×10^{-4} M) was prepared in 0.1 M NaOH solution from 3-amino-2,3-dihydro-1,4-phathalazinedione (Sigma, USA). The oxidant was prepared by dissolved 3 g of potassium dichromate (Univar, Australia) in 1 l of 15% (v/v) sulfuric acid (Lab-scan, Ireland).

A rhodium nitrate standard solution of 1000 mg l^{-1} (Accutrace, USA), was used as an internal standard in ICP-MS measurements. The working solution was prepared by dilution of 1.00 ml of the stock solution to 100.0 ml with deionized-distilled water. This solution has Rh at concentration of 10 mg l^{-1}.

2.4. Samples pretreatment

NORAD (Body Gold Inc., USA), RADBLOCK (USDPI, USA), IOSAT (ANBEX Inc., USA) and THYROBLOCK (MedPointe Healthcare Inc., USA) were the KI tablet samples used for this work. These tablets contain iodide 49.7, 50, 99.5 and 99.5 mg I tablet^{-1}, respectively, together with other excipients (fillers, binders and disintegrates). Each tablet was added into approximately 20 ml of deionized-distilled water. Dissolution was made as well as filtering through a Whatman paper no. 1. The final volume of dissolved matters was brought up to 500.0 ml. These were all clear solutions.

Multivitamin tablets that are available in the market from various countries were used in this work. The tablets were fine ground in mortar and a mass containing approximately 300 μg I was dissolved in 50 ml deionized water in a beaker and the mixture was stirred for 30 min. Suspended particulate matter (binder plus oil-soluble vitamins) was separated by centrifugation at 300 rpm for 30 min followed by filtration through 0.45 μm cellulose acetate membrane filter.

A 10 ml aliquot of a multivitamin extract was loaded onto a column (as described in Section 2.2). In the washing step, a solution of NaNO$_3$ (at low concentration) was loaded onto the AER, to remove the Vitamin C followed by the elution step of loading high concentration of NaNO$_3$, for rapid elution of iodide. The collected solution (from elution step), was then injected
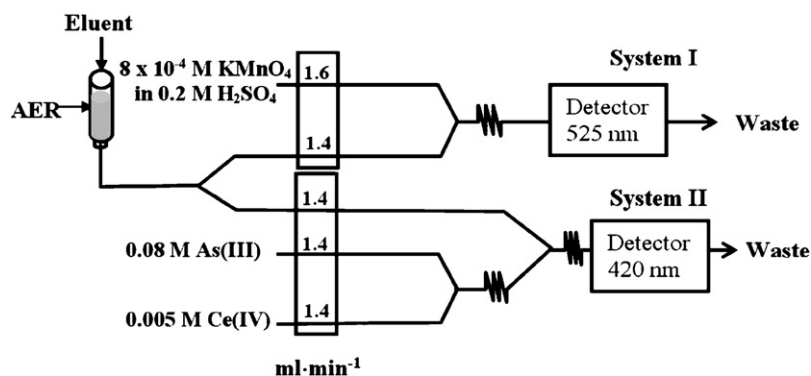

Fig. 2. Dual-detection FI manifold for the optimization of the separation of ascorbic acid from iodide. Eluent: NaNO$_3$ solution. AER: anion exchange resin.

into the developed PV-FI systems in Fig. 1 to measure iodide content.

2.5. Preparation of AER column

The column (22 cm length, i.d. 0.5 cm) contains 3 ml of anion exchange resin (Dowex 1×8 strong basic anion exchange resin, 100–200 mesh, chloride form). The resin was activated before use by soaking in 1 M hydrochloric acid overnight, followed by washing with deionized-distilled water to remove an excess of chloride ion. This column was used in the optimization (Fig. 2) and in the sample clean-up for multivitamin samples.

2.6. Recovery

Standard iodide 200 μl of 1000 mg l^{-1} was pipetted into a 25 ml volumetric flask. Then the mixture was made to the mark using multivitamin extracted solution (obtain 8 mg l^{-1} standard addition). This solution was loaded onto the column. After clean-up step as described in Section 2.4, the eluting solution was injected into the PV-FI system. The same analysis was performed on this sample but with addition of 200 μl deionized-distilled water to the sample instead of standard iodide solution. The recovery was determined for the whole procedural method based on the percentage of the recoverable amount of iodine added to a sample.

2.7. Other methods

2.7.1. Potentiometric method

About 30 ml of the 2.0 M sodium nitrate eluate was transferred into a 50 ml beaker. The potential of this solution was measured using an iodide-ISE (Orion, model 9453, USA) and an Orion saturated calomel electrode, with a digital Ionanalyzer (Orion, model 601A, USA), and the iodide concentration determined by comparison with a 1–10 mg l^{-1} calibration graph.

2.7.2. ICP-MS method

In the ICP-MS method, samples of multivitamin extracts were prepared by diluting 300 μl of sample with 50 μl of rhodium nitrate (10 mg l^{-1}) and 24.65 ml of deionized-distilled water. Rhodium was used as the internal standard to correct for non-spectral interference and signal instability. The calibration curve was obtained by using potassium iodide as the iodine standard. The blank and standard solutions (100–4000 μg l^{-1}), were diluted 10-fold with the same eluent as the samples before introduction into the nebulisation chamber.

3. Results and discussion

3.1. Manifold design and optimization

Our previous work using GD-FI system [34] clearly demonstrated that molecular iodine was readily adsorbed onto the surface of the manifold tubing and the pores of the hydrophobic membrane. Without a conditioning stream of iodide solution (depicted as dashed line in the FI manifold shown in Fig. 1),

signals within this range were not reproducible, and showed a gradual increase to reach a plateau as subsequent injections were made. Moreover, the adsorption of iodine resulted in a non-linear calibration graph even at low iodide concentrations (0.1–1.0 mg l^{-1}). However, these effects were overcome by inclusion of an on-line conditioning stream of iodide [34]. With this background information, we used a similar FI system for PV, the manifold for which is shown in Fig. 1. The necessity for on-line conditioning system with continuous generation of iodine (I$_2$) was investigated by varying the concentration of potassium iodide used in the conditioning stream (dashed line in Fig. 1) from 3 to 8 mg l^{-1}. The results show that the linearity of calibration was not satisfied at 3 mg l^{-1} ($r^2 = 0.983$), whereas higher concentrations of 5 and 8 mg l^{-1} gave satisfactorily linear responses ($r^2 = 0.994$ and 0.999, respectively). This phenomenon agrees with that previously described for GD work [34]. Thus conditioning is also necessary for the pervaporation method, and a concentration of the conditioner at 5 mg l^{-1} was selected as the optimum condition for this purpose.

Some operational parameters, such as the concentration and pH of the luminol stream and the condition of oxidizing agent, were adopted directly from the previously described gas diffusion method [34] whereas other parameters, such as the concentration of iodide in conditioning stream, concentration of iodide in acceptor stream as well as sample volume were optimized for the pervaporation system because they are affected by the different physical characteristics of the gas collection unit (mixing geometry, evaporation rate and diffusion rate of the gas phase).

Potassium iodide was also used as an acceptor reagent since it promotes solubility of iodine across the membrane by forming soluble tri-iodide species, i.e., $I^- + I_2 \rightarrow I_3^-$, for which $K = [I_3^-]/[I_2][I^-] = 10^3$ dm^3 mol^{-1} [20]. The concentration of potassium iodide in the acceptor stream will therefore be a compromise between promoting solubility of I$_2$ after it diffuses through the membrane and avoiding production of an excess of I$^-$, which promotes the formation of I$_3^-$ species that does not react with luminol to produce CL. Our results agree with this prediction. The study was carried out over the concentration range of 0.5–2% (w/v) I$^-$, and it was observed that peak area increased with increasing concentration of potassium iodide up to 1% (w/v) KI. However, increasing potassium iodide concentration above 1% (w/v) gave a decrease in peak area. Thus, 1% (w/v) KI was chosen as the acceptor solution.

The injection volume was varied over the range of 100–1000 μl when other parameters were fixed and replicate injection of 3 and 5 mg l^{-1} solutions were made. An injection volume of 300 μl was chosen as the optimum because it was a compromise between increased sensitivity and sample throughput. The optimal concentrations of chemicals used in the preparation of reagent streams for the PV-FI system are presented in Fig. 1.

3.2. Analytical performance

Under the optimized conditions, the calibration was always linear within the concentration range 1.0–10.0 mg l^{-1}. A typ-

Table 1
Determination of iodide contents in nuclear emergency tablet (KI tablets) by using the present PV-FI method and an ISE method

Trade name	Iodide content (mg tablet^{-1})		
	Nominal	PV-FI method	ISE
1. NORAD[a]	49.7	52.39 ± 0.65	54.50 ± 3.5
2. RADBLOCK KI[b]	49.7	54.79 ± 3.2	58.51 ± 4.4
3. IOSAT[c]	99.5	102.0 ± 7.5	103.81 ± 6.6
4. THYROBLOCK[c]	99.5	99.7 ± 1.2	99.32 ± 3.4

The means and standard errors were from a set of three samples of the same product.

[a] Weight of the tablet: 0.25 g.
[b] Weight of the tablet: 0.30 g.
[c] Weight of the tablet: 0.17 g.

ical calibration equation curve obtained from this work is $y = 2.319x - 1.1318$ ($r^2 = 0.999$), where y is the peak area of CL signal and x is the concentration of iodide injected. A detection limit of $0.5\,\mathrm{mg\,l^{-1}}$ was determined (3S.D. of the blank signal) [35].

3.3. Application to iodide analysis of nuclear emergency tablets

Four samples of potassium iodide tablets, use for protection against thyroid absorption of radioactive iodine, were analyzed for iodide content using the developed PV systems. Table 1 shows the iodide contents obtained from PV-FI system and ISE together with nominal values. The results were compared with the values accordingly to the labels. The contents of iodide, as determined by the PV-FI method, agreed significantly well with the labels. The paired t-test was employed to compare the difference in the results of KI tablets [35]. No significant difference was found between the results from the PV-FI and from the ISE methods ($t_{observed} = 0.120$, $t_{critical} = 3.18$ at $P = 0.05$). This strong agreement demonstrated that the PV-FI method is suitable for analysis of samples of this type. It can be concluded that these pharmaceutical products do not exhibit any interference effects, since only dissolution of the KI tablets was employed before direct sample injection. Therefore, the PV-FI system can be considered a viable alternative method to the GD-FI system [34] and iodide electrode for iodide measurement in this type of sample.

3.4. Application to multivitamin tablets

From previous work performed using the GD-FI system, investigation of possible interfering species that are present in multivitamin extracts (i.e., Vitamin B complex, Vitamin C and some cations such as Mn^{2+}, Zn^{2+} and K^+ and anions such Cl^- and $SO_4{}^{2-}$) was carried out at concentrations that are twice the normal concentration. These substances did not exhibit a marked effect except for Vitamin C which resulted in a negative signal [34]. For that reason, the interference of ascorbic acid was re-investigated in the developed PV-FI system. As expected, the same interfering effect was found. At higher concentrations of ascorbic acid greater negative signals were observed. Increasing the concentration of dichromate oxidant or even premixing sam-

ple with oxidant did not show any improvement in eliminating the interfering effect of ascorbic acid. Pretreatment of sample extracts, by anion exchange separation, was therefore considered the most effective means of removing the ascorbic acid interference before injecting the multivitamin extracted into the FI system.

3.4.1. Development of sample treatment with anion exchange column

By means of this dual-detection FI system (Fig. 2), identification of signals obtained by ascorbic acid and iodide were achieved as well as their elution times. Examples of signal output from the dual-detection FI system are shown in Fig. 3.

To optimize the selective separation of ascorbic acid from iodide, the signal profile from the System II (Fig. 2) was primarily considered. Different concentrations of sodium nitrate were tested for the elution, including 0.1, 0.3 and 0.5 M. It was observed that ascorbic acid was eluted approximately at the same time over the range of 0.1–0.5 M $NaNO_3$, whereas the elution time of iodide decreased significantly with increasing concentration of sodium nitrate. Iodide was eluted at about 27 and 40 min for 0.5 and 0.3 M $NaNO_3$, respectively, whereas elution of iodide was not achieved within 60 min when 0.1 M $NaNO_3$ was used.
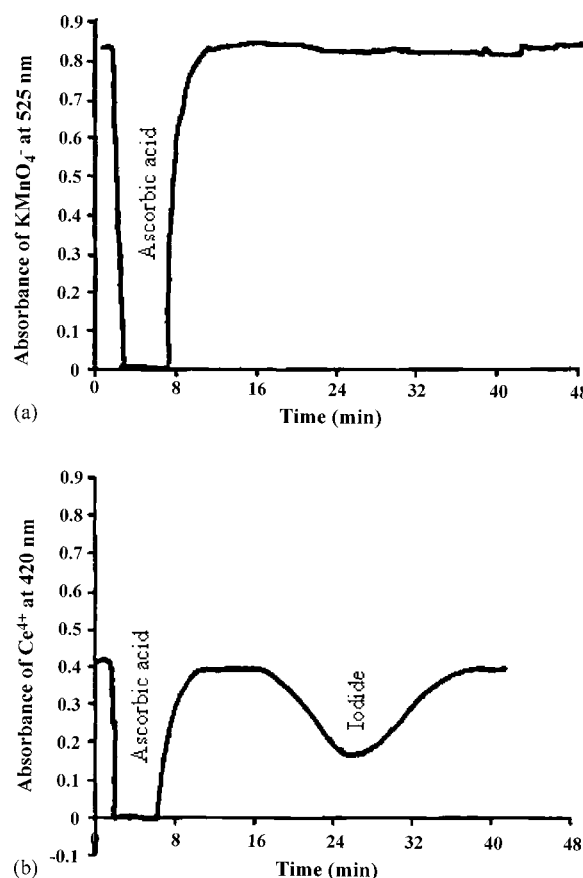

Fig. 3. Example of elution profiles using 0.5 M $NaNO_3$, obtained from the dual-detection FI system at condition of 5.0 ml loading of standard mixture of 50,000 mg ascorbic acid l^{-1} and 4 mg l^{-1}. (a) Profile obtained from System I with reduction of $MnO_4{}^-$ and (b) Profile obtained from System II with reduction of Ce^{4+}.
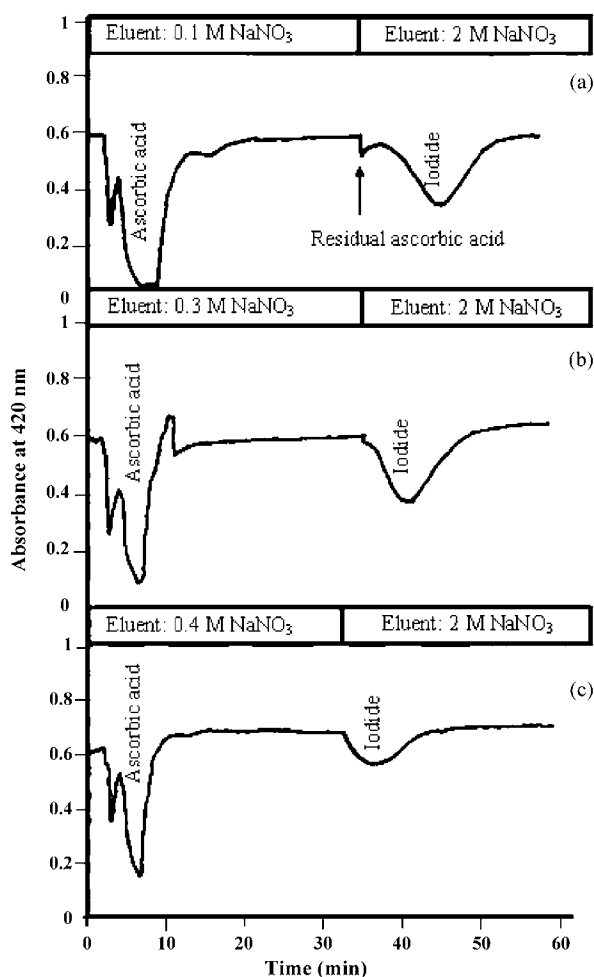
Fig. 4. Elution profiles obtained from the dual-detection FI manifold (System II), at various concentration of NaNO$_3$ used in an elution step: (a) 0.1 M, (b) 0.3 M and (c) 0.4 M, followed by 2 M NaNO$_3$ for elution of iodide. These results also confirmed by the results of the reduction of MnO$_4^-$ (System I).

As described above, a solution of 0.1 M NaNO$_3$ seems to be suitable to use in the first step or so-called the washing step. This step aims to selectively elute ascorbic acid from the column, and was followed by elution with 2 M NaNO$_3$ to elute iodide. However, it was found that ascorbic acid was not completely removed

from the column by elution with 0.1 M NaNO$_3$ since there was always some residue of ascorbic acid (seen as a small peak in front of the iodide peak) that remained in the column, which was eluted immediately after 2 M NaNO$_3$ was loaded (Fig. 4a).

Nevertheless, it was found that complete elution of ascorbic acid was achieved with 0.3 and 0.4 M NaNO$_3$ (Fig. 4b and c) and thus, 0.4 M NaNO$_3$ was selected as the eluent in the washing step for the clean-up of multivitamin extracts. At constant system flow rate, elution times of each species were converted to elution volumes, and the optimum elution volumes for off-line sample preparation. Therefore, 60 ml of 0.4 M NaNO$_3$ was used as the optimal condition for removing of ascorbic acid and 40 ml of 2 M NaNO$_3$, was used in the eluting step.

3.4.2. Method validation

Validation of the proposed method was done by analyzing iodide contents in 18 samples of multivitamin extracts using four different methods (PV-FI, GD-FI, ISE and ICP-MS). We found that sample matrix also interfere the iodide measurements by ISE method, resulting in negative error. Therefore, all the samples were pretreated using the described AER technique prior the analysis using the PV-FI, GD-FI and ISE. It was not necessary to use any type of clean-up for the ICP-MS. Results for the comparison are presented in Fig. 5. The analysis of variance (ANOVA) [35] test was used to compare the iodide content analyzed by the four methods. There was no significant difference between the results from the four methods at 95% confidence limit.

3.5. Recovery

Recoveries of iodide for the whole procedure using the PV-FI system with the AER clean-up were investigated (Table 2), and were found to range from 81.3% to 117% with an average ($n = 8$) of 102%. These results show that the use of AER was generally effective in removing ascorbic acid [37].

3.6. Comparison of the present PV-FI system with the previous GD-FI system

Comparison of the analytical characteristics of the developed PV-FI and GD-FI [34] systems are summarized in Table 3. As
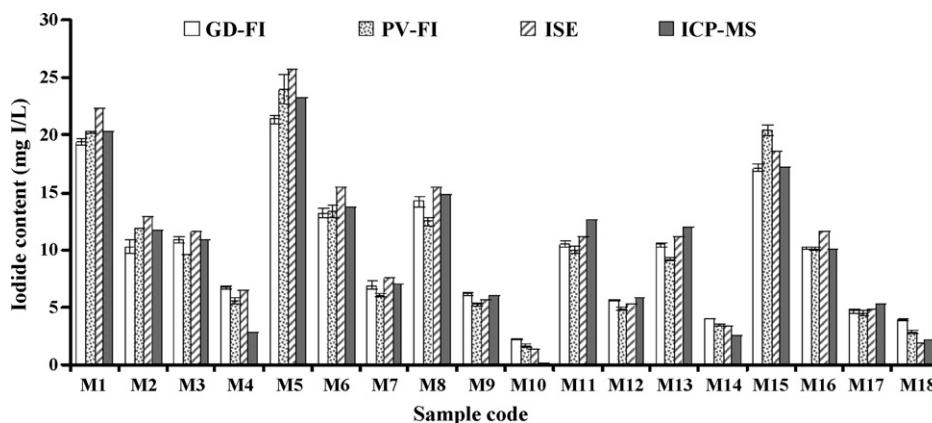

Fig. 5. Comparison of iodide contents in multivitamin extracts determined by using four methods: GD-FI, PV-FI, ISE and ICP-MS.

Table 2
Analytical recovery derived from determination of iodide using PV-FI

Sample	Original content (mean ± S.D.) (mg I)	Standard addition		%Recovery
		Added (mg I)	Found (mean ± S.D.) (mg I)	
1. Synthetic sample	–	0.08	0.0870 ± 0.001	109
2. Centrum	0.075 ± 0.001	0.08	0.161 ± 0.003	108
3. Centrum (+Betacarotine)	0.1185 ± 0.001	0.08	0.203 ± 0.006	105
4. Olay	0.134 ± 0.002	0.08	0.227 ± 0.005	116
5. Aktivpunkt	0.061 ± 0.005	0.08	0.130 ± 0.002	87
6. Biovital	0.080 ± 0.002	0.08	0.153 ± 0.004	90.7
7. Das Gesunde	0.034 ± 0.001	0.08	0.099 ± 0.003	80.9
8. Health Aid	0.091 ± 0.003	0.08	0.185 ± 0.006	117

Table 3
Comparison of analytical characteristics of the developed gas-diffusion and pervaporation FI systems

Feature	Gas diffusion system	Pervaporation system
1. Working range (mg l^{-1})	0.1–1.0	1.0–10
2. Sample throughput	Higher (60 injections h^{-1})	Lower (30 injections h^{-1})
3. Detection limit (mg l^{-1})	0.05	0.50
4. Precision (R.S.D.) ($n = 10$)	4.8% (for 0.5 mg l^{-1})	5.2% (for 5 mg l^{-1})
5. Life of the membrane used	Shorter (approximately 1 day)	Longer (approximately 7 days)
6. Ability to be used with samples containing suspended particles	No	Yes
7. Compatibility with reagents or samples that deteriorate membrane	No	Yes

indicated in Table 3, there are advantages and disadvantages associated with both PV and GD systems. The advantage of the sample–membrane air gap in PV is that potential contamination or deterioration of the membrane is minimized, but the disadvantage of the air gap is that the dilution of the I_2 gas is occurred, resulting in a 10-fold reduction of the sensitivity compared with GD (0.05 and 0.5 mg l^{-1} for GD and PV, respectively). The precision of the GD system developed was 4.8% at 0.5 mg l^{-1}, whereas the precision of the PV system was 5.2% at 5 mg l^{-1}. Note that the iodide concentrations used in these two systems were quite different, as determined by the difference in their working ranges.

However, in this work, the multivitamin extract was pretreated with AER, and the iodide fraction was eluted with 2 M sodium nitrate. At this concentration of sodium nitrate, the GD membrane deteriorated after several injections, causing a negative signal of iodide injection. However, this effect had never been observed when PV was employed. This is due to the presence of air gap in the PV unit that helps avoiding direct contact between the sample and the membrane, overcoming the rapid deterioration of the membrane that occurs in GD. This resulted in an operational life-time for the membrane used in PV of 7 days, whereas for GD the life-time was only 1 day.

4. Conclusions

In this work, a PV-FI method was developed for the determination of iodide based on the chemiluminescent reaction of I_2 with luminol. The method is directly applicable for nuclear emergency tablets, which are basically potassium iodide with pharmaceutical binders. For multivitamins, an off-line clean-up using AER was employed for the separation of ascorbic acid

from iodide. Separate elution between iodide and the Vitamin C interference was optimized using a so-called dual-detection FI manifold.

Determination of iodide in the fraction of high concentration of $NaNO_3$ was observed to cause a short life-time (1 day) of the PTFE membrane, if used with the previous GD-FI system [34]. Thus, employment of the pervaporation technique, with the air-space between the analyte solution and the membrane, has brought in a great benefit to this application.

References

[1] J.T. Dunn, IDD Newsletter, November 1, 1993.
[2] M.G. Wohl, R.S. Goodhart, Modern Nutrition in Health and Desease, 4th ed., Lea & Febiger, Philadelphia, 1983.
[3] W. Hu, P. Yang, K. Hasebe, P.R. Haddad, K. Tanaka, J. Chromatogr. A 956 (2002) 103.
[4] J. Odink, J.J.P. Bogaards, H. Sandman, J. Chromatogr. 431 (1988) 309.
[5] J. Rendl, S. Seybold, W. Borner, Clin. Chem. 40 (1994) 908.
[6] F. Moussa, M.C.R. Demy, F. Veinberg, F. Depasse, R. Gharbi, J.Y. Hautem, P. Aymard, J. Chromatogr. B 667 (1995) 69.
[7] G.T.F. Wong, P.G. Brewer, Anal. Chim. Acta 81 (1976) 81.
[8] X. Hou, H. Dahlgaard, B. Rietz, U. Jacobsen, S.P. Nielsen, A. Arkrog, Anal. Chem. 71 (1999) 2745.
[9] V. Poluzzi, B. Cavalchi, A. Mazzoli, G. Alberini, A. Lutman, P. Coan, I. Ciani, P. Trentini, M. Ascanelli, V. Davoli, J. Anal. Atom. Spectrom. 11 (1996) 731.

[10] P. Allain, Y. Mauras, C. Douge, L. Jaunault, T. Delaporte, C. Beaugrand, Analyst 115 (1990) 813.

[11] M. Haldimann, B. Zimmerli, C. Als, H. Gerber, Clin. Chem. 44 (1998) 817.

[12] Y. Yabu, Endocrinol. Japon. 33 (1986) 905.

[13] J. Melichercik, L. Szijarto, A.R. Hill, J. Dairy Sci. 89 (2006) 934.

[14] E.B. Sandell, I.M. Kolthoff, J. Am. Chem. Soc. 56 (1934) 1426.

[15] W. Chantore, S. Muangkaew, J. Shiowatana, D. Nacapricha, Lab. Rob. Automat. 11 (1999) 37.

[16] D. Nacapricha, S. Muangkaew, N. Ratanawimarnwong, J. Shiowatana, K. Grudpan, Analyst 126 (2001) 121.

[17] R.E.D. Moxon, E.J. Dixon, Analyst 105 (1980) 344.

[18] N. Yonehara, M. Yoshida, I. Iwasaki, Bull. Chem. Soc. Jpn. 43 (1970) 3796.

[19] O. Agrawa, G. Sunita, V.K. Gupta, Talanta 49 (1999) 923.

[20] C.D. Monks, D. Nacapricha, C.G. Taylor, Analyst 118 (1993) 623.

[21] D.F. Kamson, Anal. Chim. Acta 179 (1986) 475.

[22] A.A. Ensafi, G.B. Dehaghi, Anal. Sci. 16 (2000) 61.

[23] M. Amornthammarong, K. Jareonsutasinee, D. Nacapricha, Lab. Rob. Automat. 12 (2000) 138.

[24] N. Choengchan, K. Uraisin, K. Choden, W. Veerasai, K. Grudpan, D. Nacapricha, Talanta 58 (2002) 1195.

[25] W.M. Hardy, W.R. Seitz, D.M. Hercules, Talanta 24 (1977) 297.

[26] J.L. Burguera, M.R. Brunetto, Y. Contreras, M. Burguera, M. Gallignani, P. Carrero, Talanta 43 (1996) 839.

[27] T. Fujiwara, I.U. Mohammadzai, H. Inoue, T. Kumamaru, Analyst 125 (2000) 759.

[28] J. Ruzicka, E.H. Hansen, Flow Injection Analysis, 2nd ed., Wiley, New York, 1998.

[29] S. Motomizu, T. Yoden, Anal. Chim. Acta 261 (1992) 461.

[30] J.T. Hakedal, P.K. Egeberg, Analyst 122 (1997) 1235.

[31] D. Nacapricha, K. Uraisin, N. Ratanawimarnwong, K. Grudpan, Anal. Bioanal. Chem. 378 (2004) 816.

[32] M.D. Luque de Castro, I. Papaefstathiou, Trends Anal. Chem. 17 (1998) 41.

[33] L. Wang, T.J. Cardwell, R.W. Cattrall, M.D. Luque de Castro, S.D. Kolev, Anal. Chim. Acta 416 (2000) 177.

[34] N. Ratanawimarnwong, N. Amornthammarong, N. Choengchan, P. Chaisuwan, M. Amatatongchai, P. Wilairat, I.D. McKelvie, D. Nacapricha, Talanta 65 (2005) 756.

[35] J.C. Miller, J.N. Miller, Statistics for Analytical Chemistry, 3rd ed., Ellis Horwood, New York, 1993.

[36] K. Grudpan, K. Kamfoo, J. Jakmunee, Talanta 49 (1999) 1023.

[37] J.M. Green, Anal. Chem. 68 (1996) 305A.

Application of multi-way data analysis on excitation–emission spectra for plant identification

Safwan M. Obeidat [a], Tzach Glasser [b], Serge Y. Landau [b],
Dean M. Anderson [c], Gary D. Rayson [a,*]

[a] *Department of Chemistry and Biochemistry, New Mexico State University, Las Cruces, Box 30001, NM 88003, USA*
[b] *Jornada Experimental Range, USDA, Las Cruces, Box 30003 MSC JER, NM 88003, USA*
[c] *Department of Natural Resources and Agronomy, Institute of Plant Science, Agriculture Research Organization,
The Volcani Centre, Bet Dagan 50250, Israel*

Abstract

The ability to distinguish among diets fed to Damascus goats using excitation–emission luminescence spectra was investigated. These diets consisted of *Medicago sativa* L. (alfalfa), *Trifolium* spp. (clover), *Pistacia lentiscus*, *Phyllirea latifolia* and *Pinus brutia*. The three-dimensional luminescence response surface from phosphate buffered saline (PBS) extracts of each material was analyzed using muti-way analysis chemometric tools (MPCA) and parallel factor analysis (PARAFAC). Using three principal components, the spectra from each diet material were distinguished. Additionally, fecal samples from goats fed diets of either alfalfa or clover hays were investigated. The application of MPCA and PARAFAC to these samples using models derived from the pre-digested diet materials was strongly suggestive of the utility of similarly derive training samples for the elucidation of botanical diet composition for animals.
© 2007 Elsevier B.V. All rights reserved.

1. Introduction

In the Mediterranean region, goats are very important for brush control and ecological management [1]. The need to differentiate among goat diets is indeed a necessary issue for controlling free-ranging goats [2,3].

Fluorescence spectroscopy shows promise as a rapid and accurate method for identifying plant materials [4–7]. Earlier studies [5,6] used chloroform as the extracting solvent. Unfortunately, this solvent revealed fluorophores throughout the visible region of the spectrum including red chlorophyll fluorescence [8]. However, blue fluorescence from leaf material of higher plants has been suggested to result from a complex mixture of at least three fluorescing components [9]. Lichtenthaler et al. [10] later indicated the phenolic epidermal compounds in leaves (including cafferic, ferulic and sinapic acids as well as chlorogenic acid and quinic acid) may contribute to fluorescence in the blue region of the visible spectrum [10]. Additionally green fluorescence has been attributed to the cell wall components berberine and quercetin [11], epidermal tissue [12] and mesophyll tissue [13]. Although blue and green fluorescence result from multiple components [10], their chemical origins and locations within plants, are yet to be fully understood [14]. It may, however, be possible to differentiate among plant materials without a detailed understanding of the molecular species responsible for the resulting fluorescence signatures [5,6].

Recent research by Danielson et al. [15] suggested phosphate buffered saline (PBS) solutions as suitable solvents for extracting non-chlorophyll fluorophores from plant material. The exclusion of chlorophylls enabled a reduction of the masking of blue and green fluorescence signatures. Other work in our laboratories has also demonstrated the utility of some chemometric tools (e.g., principal component analysis (PCA) and

---

* Corresponding author. Tel.: +1 505 646 5839; fax: +1 505 646 2649.
  E-mail address: garayson@nmsu.edu (G.D. Rayson).

multi-way PCA) for the qualitative processing of luminescence spectra from PBS plant extracts [3].

The aim of the present study was to investigate the ability to differentiate among five different goat diets using fluorescence excitation–emission matrix (EEM) spectra of PBS extract solutions by applying multi-way principal component analysis (MPCA). Additionally, an MPCA calibration model was constructed from diets containing each of two hay species (i.e., alfalfa and clover) in an attempt to identify feces collected from different goats fed each diet. The number of the possible fluorophores in each of the five diets was also investigated using parallel factor analysis (PARAFAC).

2. Experimental

2.1. Samples

Five pre-dried goat diet materials were investigated using spectral fluorescence analysis. These included two *hay* plant species, alfalfa (*Medicago sativa* L.) and clover (*Trifolium* spp.) and gree browse species, *Pistacia lentiscus* (*P. lentiscus*), *Phyllirea latifolia* (*P. latifolia*) and *Pinus brutia* (*P. brutia*). Feces samples of both alfalfa and clover were also investigated using the same technique. These materials were obtained from the Agricultural Research Organization of Israel. The composition of samples used in this study resulted from the actual diets of each of 12 Damascus yearling goats (mean weight of 38.5 ± 0.7 kg) at a feed study facility located south of the Carmel Ridge, Israel. This feed study involved feeding 10 goats alfalfa hay (samples 1–10 in Fig. 3) for 10 days and collecting the corresponding feces. Additionally, clover hay (samples 11–14 in Fig. 3) was fed to four goats for a period of 4 days with similar collection of the corresponding feces. Goat feces from both hay diets were similarly coded with the corresponding goat identification (Table 1). Other pure diet materials were added to this study to check the ability of the current technique to differentiate among different diet materials: and *P. latifolia* and *P. brutia* (15–17 and 18–20 in Fig. 3, respectively) and *P. lentiscus* (21–24 in Fig. 3). The facility consisted of roofed individual dirt-floor pens (1.7 m × 1.7 m) and a roofed collection corral where animals were placed between tests. Each pen was configured with a 15 l water bucket and a trough divided into two compartments for separation of the feed concentrate and the other materials presented to each animal. For more accurate intake measurements collection of residue of each material was facilitated by a shelf located beneath each trough. Diets were weighed and distributed once each morning during 12, 10-day tests. Fecal samples for alfalfa and clover were grab-collected each morning, midday and evening to minimize variance from digestive stages during each of the final five days [16,17].

2.1.1. Sample preparation

Diet and feces materials were initially ground to pass a 2 mm screen, placed in aluminum weighing boats and dried at 60° C for 24 h to constant mass. Three replicates of approximately 0.1500 g of each diet material as well as feces were weighed into separate borosilicate culture tubes (16 mm × 25 mm, Kimble Kontes, Vineland, NJ). The tubes were then sealed using Parafilm and stored at room temperature. All samples within each replicate sample set were randomized prior to analysis to minimize operator bias during data collection.

The phosphate buffered saline solution was autoclaved (35 min at 121 °C, 125 kPa) to minimize any microbial contamination. The solution pH was adjusted to 12.5 using 1.0 M NaOH (Mallinckrodt Chemical Works, Saint Louis, MO). Each 2 l volume of the PBS solution contained 0.263 g, NaN$_3$ (sodium azide, an additional microbial growth inhibitor), 1.422 g NaHPO$_4$, 3.801 Na$_2$HPO$_4$ (Alfa Aesar, Ward Hill, MA), 0.408 g KCl (Sigma, MO) and 13.567 g NaCl (J.T. Baker, Phillipsburg, NJ) dissolved in ultra-pure (18.0 MΩ) water.

Each replicate data set consisted of spectra from each of the five diet materials, fecal materials, three extraction solution blanks and a single solution consisting of a TiO$_2$ suspension. The spectrum of each blank was recorded at three times during the analysis of each replicate: the beginning, middle and end. The spectrum from the TiO$_2$ suspension solution was also collected three times during each replicate to account for any instrument drift. A total of 13 samples including the blanks and the TiO$_2$ solutions were run each day (a single replicate data set).

The incorporation of the light scattering suspension of TiO$_2$(s) provided a signal indicative of the wavelength-dependent intensity of the incident radiation. This enabled compensation for significant drifts in the output of the Xe-arc lamp excitation light source. Immediately following exposure of the TiO$_2$ sample, a blank spectrum was recorded.

A Lab Industries Repipet II (Barnstead/Thermolyne, Dubuque, IA), was calibrated to deliver 10.0 ml of extraction solution to each culture tube containing the diet and the fecal materials. Once filled, all 10 tubes were sealed with Parafilm and manually shaken. The tubes were shaken in an attempt to wet the "plug" of ground plant material that floated in each culture tube. These tubes were then agitated using an orbital shaker (VWR Model 98001;Albuquerque, New Mexico) at 100 RPM for 1 h. The culture tube openings were elevated slightly to minimize contact of the culture tube contents with the Parafilm. The culture tubes were also rotated 180°after 30 min to maximize

Table 1
The identity of samples and goats

Sample number	Diet	Goat ID
1	Alfalfa	G
2	Alfalfa	A
3	Alfalfa	F
4	Alfalfa	I
5	Alfalfa	K (Missing)
6	Alfalfa	E
7	Alfalfa	D (Missing)
8	Alfalfa	H
9	Alfalfa	J
10	Alfalfa	B
11	Clover	C
12	Clover	B
13	Clover	M
14	Clover	F

contact of the ground plant material with the PBS extraction solution.

The culture tubes were then centrifuged at $925 \times$ for 25 min (Beckman Model TJ-6, Labx, Midland, ON, Canada). The liquid from each culture tube was subsequently decanted into a non-sterile 10.0 ml syringe (Allometrics Inc., Franklin Lakes, NJ) and filtered through a 0.2 μm non-sterile nylon filter (Millex, Bedford, MA). Approximately, 3 ml of filtrate was immediately collected in a 3.5 ml disposable acrylate fluorescence cell with a light path of 10 mm (Spectrocell, Oreland, PA). The cell was then capped (Spectrocell Teflon®, LDPE), placed within the fluorometer, and the resulting excitation–emission matrix collected for all samples including both the diet and the fecal materials. These comprised 1024 emission intensity measurements at each of 51 excitation wavelengths (370–580 nm in 4.2 nm increments).

2.2. The fluorometer

The fluorometer used in these studies [18–20], has been previously described by Mukherjee et al. [21]. Briefly, it consists of a 150 watt Xe-arc lamp (Oriel Model 6254, Newport Oriel Instruments, Stratford, CT) as an excitation source. Each wavelength of excitation was selected using an F/4, 1/8 m double monochromator with a bandwidth of 7 nm (CVI Model 120, CVI, Albuquerque, NM). Stray light was reduced using a band pass filter on the monochromator. Scattered light and fluorescence from the PBS filtrate were detected at 90 degrees to the incident radiation. The emitted radiation was imaged into the entrance slit of an F/4, 1/8 m imaging spectrometer (ISA Jobin Yvon, Edison, NJ), with a 200–700 nm range. A 1024-element intensified Reticon array (Model 1420, EG&G Princeton Applied Research, Trenton, NJ) detected the light at the image plane. The detection spectrometer had a 5 nm bandbass.

2.3. Data collection

Instrument control and data acquisition were accomplished using software developed using Lab View software (Version 7.0, National Instruments, Austin, TX) installed in a Gateway desk top PC equipped with a Pentium II processor. The spectral intensities are reported on a relative intensity scale and were blank corrected. Wavelength regions of the spectra were divided in to arbitrary spectral regions and designated as either "blue" (424–491 nm) or "green" (491–575 nm) [22].

3. Statistical analysis

3.1. Multi-way principal component analysis (MPCA)

Chemometric data analysis methods provide powerful tools to analyze multivariate data such as excitation–emission matrices obtained from fluorometry [23]. Principal component analysis and MPCA are multivariate statistical methods for analyzing data measured as a function of two or more parameters (multi-way data) [24].

MPCA is one of the most direct approaches for decomposing the EEM [25]. Statistically and mathematically, MPCA is very similar to PCA and involves the generation of a representation of the eigenvectors for the covariance or correlation matrix of the original measured variable data matrix. There may be as many eigenvectors as there are variables. Each principal component generated describes diminishing contributions of the variance among the measured variables [25].

Consider the measurement of intensity at each jth ($j = 1,\ldots, J$) emission wavelength for every kth excitation wavelength ($k = 1,\ldots, K$) corresponding to the ith sample ($i = 1,\ldots, I$). These data can be then be organized into a three-dimensional matrix X of dimension $I \times J \times K$. In MPCA, the unfolded matrix X is subsequently decomposed into a large two-dimensional matrix X (Fig. 1) followed by conventional PCA. Simply stated, MPCA is the summation of the product of score vectors (t_r) and loading vectors (P_r) plus a residual or error array (E) which is minimized in a least squares sense.

$$X = \sum_{r=1}^{R} t_r \otimes P_r + E \tag{1}$$

Each element of score vectors (t_r) corresponds to a particular data set. The loading vectors (P_r) are then directions of a maximum variability and define the reduced dimension space (R).

In most cases, only few principal components can be used to express the maximum variability especially in data with a high degree of correlation ($R \gg \min (I, JK)$). The choice of R is made for the optimization of the systematic variability of the data and can be described by these few principal components. Additionally, the residual array (E) is minimized according to the least squares sense [26].

3.2. Parallel factor analysis (PARAFAC)

The PARAFAC is another powerful multi-way data analysis tool that assumes a liner relationship between the excitation–emission wavelength pair. It was used to investigate the number of factors (i.e., fluorophores) responsible for features within each spectral signature.

Like MPCA, PARAFAC is an algorithm that decomposes multi-way dimensional arrays into a set of scores and loadings. Because PARAFAC is a constrained version of PCA, any data set that can be modeled by PARAFAC can also be modeled by PCA [27].

Mathematically, the PARAFAC algorithm decomposes the three-dimensions data matrix (X) into a sum of triple product of vectors (components or factors) and an error matrix e (Eq. (2)). While for PCA, each component consists of one score vector and one loading vector, each component (factor) in PARAFAC consists of one score vector and two loading vectors. These components or factors are organized into spectral matrices (i.e., a–c). Each matrix represents a single dimension of the original data cube containing N factors (N is the smallest number of independent factors that can be used to efficiently describe the data
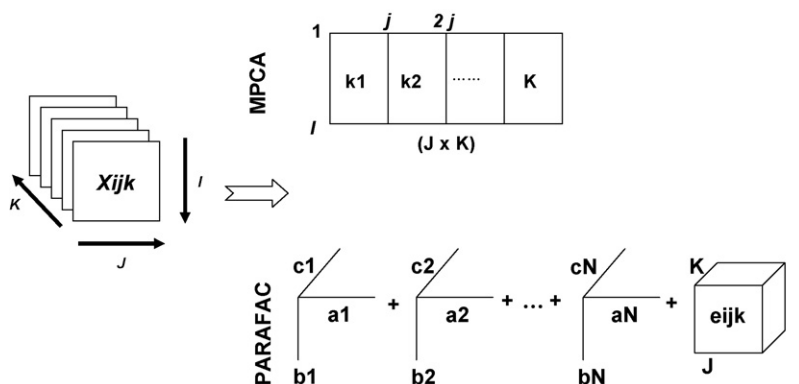
Fig. 1. Unfolding of three-way array **X** (*I, J, K*) into a two-way array in MPCA and its decomposition into a sum of vector or loading products, *J* and *K*. And a sum of triple product of vectors or loadings a–c, and error matrix **E** in PARAFAC.

variances) (Fig. 1) [27–29].

$$X_{ijk} = \sum_{n=1}^{N} a_{in}b_{jn}c_{kn} + e_{ijk} \qquad (2)$$

In Eq. (2), X_{ijk} is a three-dimensional data set (i.e., fluorescence intensity of sample *k* at excitation wavelength *i* and emission wavelength *j*), *N* the unique spectral profiles found in the data cube, the *n* columns of matrix *a* are the predicted pure excitation of the *n* factor, the *n* columns of *b* are the predicted pure emission spectra of the *n* factor and the columns of *c* are the predicted pure spectral intensity profiles of *n* factors and e_{ijk} is the error matrix.

4. Results and discussion

No detectable degradation of the samples was observed over the 3-day data collection period. Additionally, the different PBS solution blanks were found not to differ statistically ($P = 0.912$). Therefore, the mean blank spectrum was subtracted from each sample spectra prior to analysis using MPCA and PARAFAC (PLS-Toolbox, Eigenvector Research, operated under MatLab 7.0.4, MathWorks, Natick, MA). The data were mean centered before applying MPCA. Prior to application of PARAFAC the data were weighted to account for scattering signals and truncated to contain only the regions of the spectra that had significant fluorescence information (i.e., $\lambda_{em} \geq \lambda_{ex}$).

4.1. Diet samples

Fig. 2 shows a typical excitation–emission luminescence spectrum for a PBS extract of an alfalfa hay sample. The broad lines with slopes of approximately 1.0, and 2.0 correspond to the first and second order diffraction of the incident radiation ($\lambda(\text{emission}) = \lambda(\text{excitation})$), respectively, that displays blooming into adjacent pixels. It is, therefore, the region located above this first order Rayleigh scattered radiation that is of primary analytical utility (i.e., $\lambda(\text{emission}) \geq \lambda(\text{excitation})$). Because the Rayleigh scattering features are diagonal lines, studying the region above this scattering results in the loss of that portion of the signal exhibiting an overlap with the Rayleigh scattering [29].

Weighting of the data within each EEM by replacing the values of the Rayleigh scattered signal pixels with zeros has been proposed as an approach to address this problem [30]. This was accomplished by multiplying the data matrix by a weighting matrix that has the same size as the data matrix in which the regions of the matrix corresponding to the Rayleigh scattering are given values of zero and values of one for the rest of the matrix. Weighting the data for PARAFAC application has been proposed as an approach to address the problem associated with the presence of the Rayleigh scattering. For the application of PARAFAC, the data were subjected to both a discrete weighting strategy and truncation of the data sets to include only those spectral regions containing useful signal [29].

The spectral signatures for each material were each recorded several times in accordance to the actual feed study for goats described elsewhere [3]. A three-dimension data matrix containing the EEM for each of the five materials was generated ($\lambda_{ex}, \lambda_{em},$ material). These were subsequently processed using both MPCA and weighted PARAFAC. Two-dimensional MPCA models using either the first and second or the first and third principal components were only able to separate the five diet
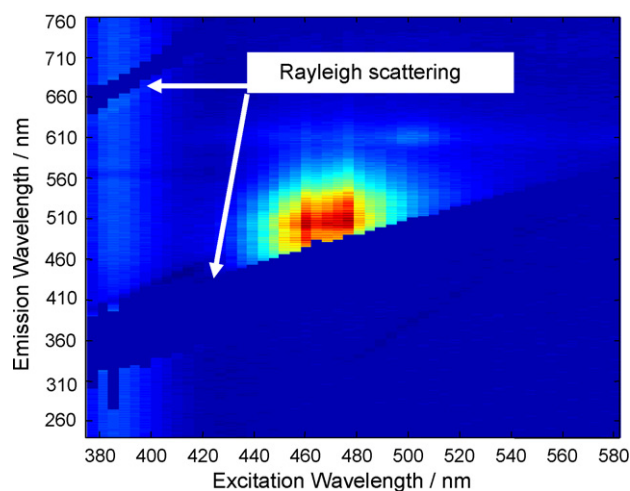

Fig. 2. Contour plot representation of excitation–emission matrix (EEM) recorded from the PBS extract of a sample of *Medicago sativa* L. (alfalfa) showing both first and second order diffraction of the Rayleigh scattered incident radiation.
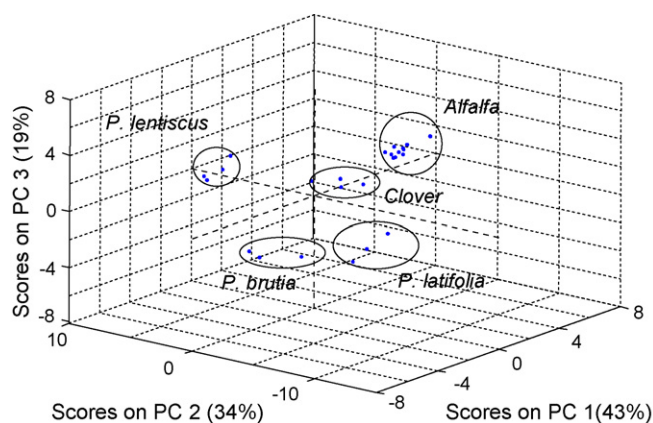
Fig. 3. Three-dimensional MPCA scores plot for each of the materials analyzed. Each point represents a single spectrum acquired for each replicate from each diet material, *Medicago sativa* (alfalfa) hay (samples 1–10), *Trifolium spp.* (clover) hay (samples 11–14), *Phyllirea latifolia* (samples 15–17) *Pinus brutia* (samples 18–20), *Pistacia lentiscus* (samples 21–24). Circles around each cluster are for clarity and do not represent confidence limits.

materials into only four clusters, leaving the *P. brutia* samples distributed among the other clusters. However, application of a three-dimensional MPCA model (Fig. 3) enabled more than 95% of the total variation in the original data matrix to be accounted for using three principal components. Projection of the scores for each sample spectrum yielded five separate, very well resolved clusters (Fig. 3). Each of these five clusters represents one of the diet materials. The centers of each of the five clusters were calculated and the standard deviations of each point in each cluster from its pre-calculated centers were also calculated. The averaged standard deviation for the clusters of alfalfa, clover, *P. lentiscus*, *P. latifolia* and *P. brutia* were 2.7, 1.3, 4.2, 3.0 and 2.9, respectively. Despite the above variations, which might affect the confidence limits of detection for the individual species, discrimination among the plants species used is readily apparent. These results strongly suggest the ability of this technique to discriminate among the five diet materials used in this study.

For the purpose of identifying the possible number of fluorophores in each diet material and their corresponding excitation–emission profiles weighted PARAFAC was also applied on each of these five separate diet materials to investigate the number of fluorophores associated in each of the five plants. The number of factors for each model was determined using both the core consistency test along with visual inspection [28]. PARAFAC application was employed for the truncated data matrices that have significant fluorescence signals. The studied regions of the data matrices for all the samples included excitation and emission boundaries of 415–565 nm and 450–710 nm, respectively.

One or two factors were found among the five diet materials. Both PARAFAC excitation and emission profiles for the five diet materials were investigated. Fig. 4 shows the excitation profiles for each of the five diet materials. For samples such as alfalfa, *P. latifolia* and *P. lentiscus* (Fig. 4a–c, respectively), one factor was identified. This suggests only one fluorophore in these materials is responsible for the measured fluorescence. Fig. 6a–c show the corresponding emission profiles for each factor. In alfalfa,

the excitation–emission profile for the factor lies at an excitation wavelength of 465 nm (Fig. 4a) and an emission wavelength of 520 and 620 nm (Fig. 5a). However, the factor revealed for *P. latifolia* was observed to have different excitation–emission profile with excitation and emission wavelength maxima at 480 (Fig. 4b) and 550 nm (Fig. 5b), respectively. The *P. lentiscus* factor exhibited excitation–emission wavelengths of 480 and 570 nm (Figs. 5c and 6c, respectively). This result is consistent with the MPCA analysis above. Although only one factor was observed in alfalfa, *P. latifolia* and *P. lentiscus*, these factors revealed different excitation–emission profiles, thus enabling them to be distinguished. This was also revealed in separate clusters of alfalfa, *P. latifolia* and *P. lentiscus* in the space of the MPCA model (Fig. 2).

Two factors were found in the remaining materials (Figs. 5 and 6). However, the two factors in each of these samples have unique excitation–emission profiles. Fig. 4d shows the excitation profile of the two factors (blue and green) found in *P. brutia*. The blue factor has an excitation maximum of 420 nm with corresponding emission maxima at 475 and 625 nm (Fig. 5d). Conversely, the green factor displayed an excitation maximum at 480 nm (Fig. 4d) and emission maximum wavelengths at 505 and 625 nm (Fig. 5d). The clover hay sample also revealed two factors. Fig. 4e shows the excitation profile for these factors. The green has an excitation peak at 450 nm and emission maxima at 490 and 610 nm (Fig. 5e). Comparatively, the blue factor showed a peak excitation wavelength of 490 nm (Fig. 4e) and emission wavelength maxima at 530 and 610 nm (Fig. 5e). Again this is consistent with the MPCA analysis. Significant differences in the spectral signatures in these samples (Fig. 3) were indicated through the clustering of each diet material samples in a separated cluster.

Table 2 summarizes the factor number for each of the studied samples a long with the excitation–emission profile for each factor.

4.2. Fecal samples

Fecal samples from animals fed diets consisting of each of the two forvs (alfalfa and clover hay) were similarly analyzed. The

Table 2
PARAFAC factors for each material with the locations of maxima in each resulting excitation and emission profile

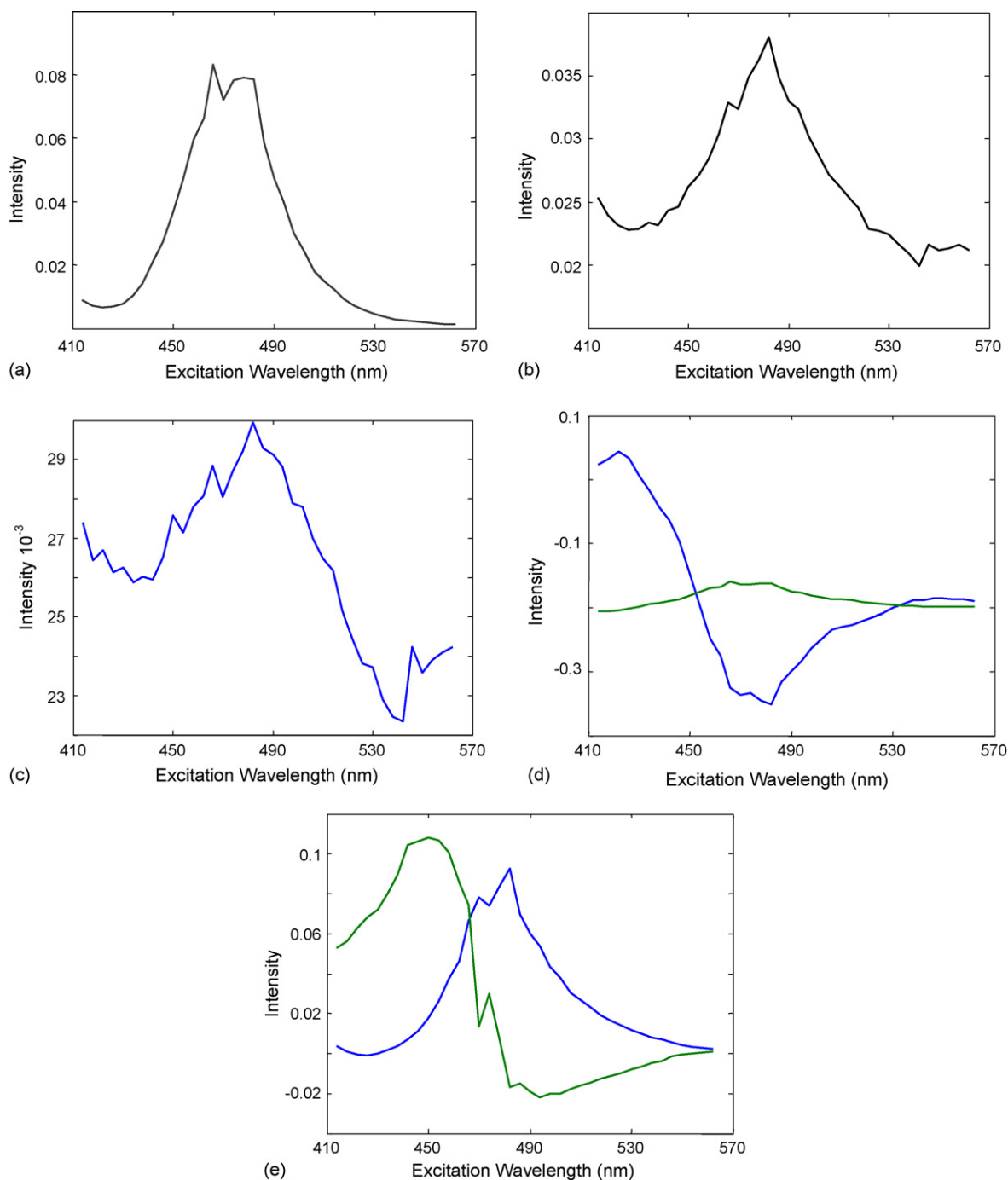| Species	Number of factors	Excitation wavelength (nm)	Emission wavelength (nm)
Alfalfa hay	1	465	520, 620
Phyllirea latifolia	1	480	550
Pistacia lentiscus	1	480	570
Pinus brutia	2	420	475 625
		480	505 625
Clover hay	2	450	490 610
		490	530 610

Fig. 4. Excitation profiles of PARAFAC model for diet samples of (a) *Medicago sativa* (alfalfa), (b) *Phyllicea latifolia*, (c) *Pistacia lentiscus*, (d) *Pinus brutia* and (e) *Trifolium spp.* (cover) hay.

goal of this study was to provide preliminary data regarding the potential application of chemometric models (i.e., MPCA and PARAFAC) derived from diet materials and fecal material samples for the determination of botanical diet materials a MPCA model was therefore constructed using PBS extracts of samples of each of two diet materials species used in Fig. 3, alfalfa and *clover hay* (circles in Fig. 6). (Availability of corresponding fecal samples from animals fed only the single plant species limited these studies to these two-diet materials.) Then extracts from feces collected from each of individual goats were applied to

the above MPCA calibration model (triangles in Fig. 6). Readily apparent are the segregation of spectra based on the plant species for both diet and fecal samples (i.e., alfalfa hay versus clover hay) and the similarities in the projection of spectra from the pre- and post-digested samples of these same plants. Not surprisingly, the greatest distribution of projected points is observed for spectra from fecal samples collected from the different animals fed these diets. The cluster centers for both diet materials, alfalfa and clover in this model were calculated as well as cluster centers for the corresponding fecal samples. Then the maha-
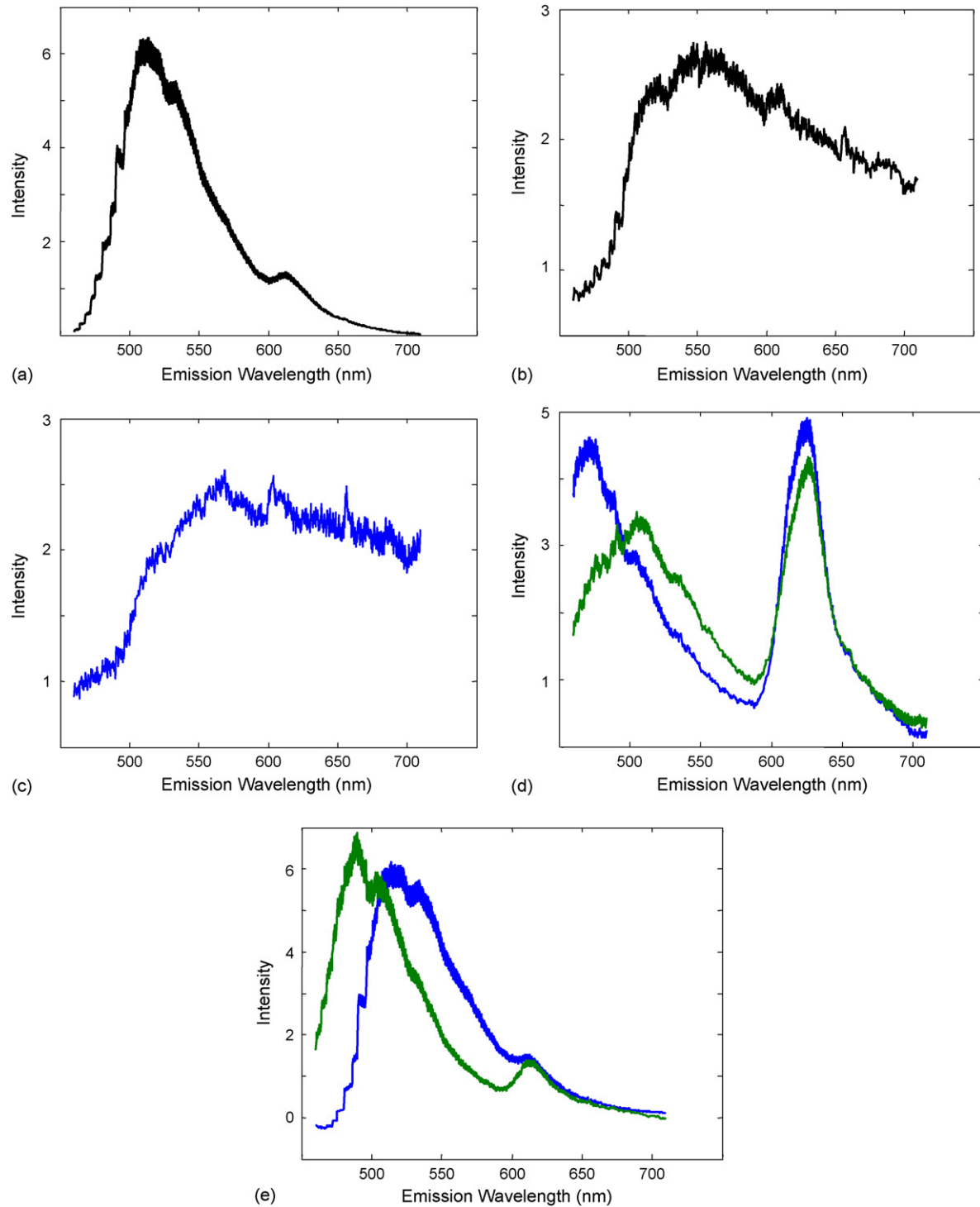
Fig. 5. Emission profiles of PARAFAC model for diet samples of (a) *Medicago sativa* (alfalfa), (b) *Phyllirea latifolia*, (c) *Pistacia lentiscus*, (d) *Pinus brutia* and (e) *Triffolium spp.* (clover) hay.

lanobis distance between the centers of diet materials clusters and the centers of the corresponding fecal samples clusters were calculated. It was determined that the distance between the diet material center of alfalfa and its corresponding fecal center was 13 units. Similarly the distance between the clover diet material center and the corresponding clover fecal samples center was five units. The distance between the centers of alfalfa diet mate-

rials and the fecal samples of clover was similarly calculated and found to equal 23 units. Additionally, the distance between each of the centers of clover diet material and the fecal samples from alfalfa was 18 units. This supports the visual interpretation from Fig. 6 which suggests the clustering of the same species together for both diet and and fecal materials, independent of the animal involved.

To further investigate the source of variance among these samples, and to investigate the possible number of fluorophores responsible for the spectral feature of each species in this research PARAFAC was applied to spectra derived from the feces of only animals fed each of these materials (i.e., alfalfa and clover hay). Comparison of the resulting PARAFAC profiles (excitation, Fig. 7 and emission, Fig. 8) for the pre- (Figs. 4 and 5) and the post-digested (Figs. 7 and 8) forms of alfalfa and clover hay reveal good consistency.

Fig. 7a, shows that only one PARAFAC factor is responsible for the spectrum in the post-digested form of alfalfa. The excitation profile for the alfalfa fecal samples indicated a maximum at 450 nm (Fig. 7a) while that from the pre-digested form displayed a maximum at 465 nm (Fig. 4a). In contrast, the corresponding emission profiles for both forms of alfalfa diet samples were very similar with maxima at 520 and 610 nm (Figs. 6e and 8b).

PARAFAC revealed each of two factors for the clover hay (blue and green curves) in the spectra for both pre- and post-digested samples. The excitation profile for the fecal samples of the clover hay (Fig. 8a) displayed a maximum at 445 nm compared to 450 nm arising from a similar analysis of pre-digested

Fig. 6. Three-dimensional MPCA scores plot for a model generated by spectra from diet samples of *Medicago sativa* (alfalfa) hay (1–10) and *Trifolium spp.* (clover) hay (11–14) (●) and the application of that same model to spectra from fecal samples (▲) collected from individual goats (letter code) fed those same diets.

Fig. 7. Loadings from the PARAFAC model (excitation spectra) applied to fecal samples corresponding to diets consisting of (a) *Medicago sativa* (alfalfa) hay and (b) *Trifolium spp.* (clover) hay.

Fig. 8. Loadings from the PARAFAC model (emission spectra) applied to fecal samples corresponding to diets consisting of (a) *Medicago sativa* (alfalfa) hay and (b) *Trifolium spp.* (clover) hay.

diet samples (Fig. 4e). The emission profile for the same factor (blue) indicated maxima at 480 and 610 nm (Fig. 8b) compared to 490 and 610 nm (Fig. 5e). The second factor (green) revealed a peak at 490 nm in the excitation profile for the fecal extract sample (Fig. 8a) with a maxima in the corresponding emission profiles at 550 and 610 nm (Fig. 8b). This is in comparison with the corresponding excitation (Fig. 4e) and emission (Fig. 5e) profiles for the pre-digested diet samples that exhibited maxima at 490 or 530 and 610 nm, respectively. The similarity and differences in these extracted spectra for the respective diet and fecal samples may contribute to the observed projections of the luminescence spectra using MPCA.

5. Conclusion

Three-dimensional luminescence spectra from PBS extracts of alfalfa and clover hay, and browse samples from the plants *P. lentiscus*, *P. latifolia* and *P. brutia* have been shown to enable material identification. The application of MPCA enables a qualitative identification of animal diet materials. Although the molecular species responsible for the observed spectral signatures is currently unknown, statistical models using PARAFAC suggest the number of a possible fluorophores to vary between (alfalfa hay, *P. lentiscus* and *P. brutia*) and (*P. latifolia*, clover hay). The excitation and emission profiles for the suggested fluorophres detected by PARAFAC are unique. This indicates that the chemical source behind the observed fluorescence is not the same among the current samples. However, in this research suggests that digestion may not affect the fluorescence spectral signatures significantly. This is clear after applying both MPCA and PARAFAC. The fecal samples continued to cluster very close to the diet material samples in the MPCA model that was constructed from the diet materials only. This supports the hypothesis that the spectral signatures for pre- and post-digested samples (used in this study) were similar. The application of these spectroscopic and statistical tools to fecal samples suggests the possible use of model learning sets derived from mixtures of plant or diet materials for the identification of botanical comparition of animal diets. This aspect of the work is the focus of ongoing research.

References

[1] A. Perevolotsky, N.G. Seligman, Biol. Sci. 48 (1998) 1007– 1017.
[2] S. Landau, T. Glasser, H. Muklada, L. Dvash, A. Perevolotsky, E.D. Ungar, J.W. Walker, Small Ruminant Res. 59 (2005) 251–263.
[3] D.M. Anderson, G.D. Rayson, S.M. Obeidat, M. Ralphs, R. Estell, E.L. Fredrickson, E. Parker, P. Gray, Range Ecol. Manag. 59 (2006) 557–563.
[4] G.G. Guilbault, Practical Fluorescence, second ed., Marcel Dekker, Inc., New York, 1990.
[5] D.M. Anderson, P. Nachman, R.E. Estell, T. Ruekgauer, K.M. Havstad, E.L. Fredrickson, L.W. Murray, Small Ruminant Res. 21 (1996) 1–10.
[6] D.M. Anderson, E.L. Fredrickson, P. Nachman, R.E. Estell, K.M. Havstad, L.W. Murray, Anim. Feed Sci. Technol. 70 (1998) 315–337.
[7] E. Parker, M.W. Trahan, J.S. Wagner, S.E. Rosenthal, W.B. Whitten, R.A. Gieray, P.T. Reilly, A. Lazar, J.M. Ramsey, J. Process Anal. Chem. 2 (2000) 50–58.
[8] H.K. Lichtenthaler, F. Stober, Proc. 10th EARSeL Symp., Toulouse, OK, 1990, pp. 234–241.
[9] Y. Goulas, I. Moya, S. Guido, Photosynth. Res. 25 (1990) 299–307.
[10] H.K. Lichtenthaler, M. Lang, F. Stober, Proc. Int. Geosci. Remote Sen. Symp. IGARSS-91, Helsinki, Espoo, Finland, 1991, pp. 2283–2286.
[11] M. Lang, F. Stober, H.K. Lichtenthaler, Radiat. Environ. Biophys. 30 (1991) 333–347.
[12] M. Broglia, Appl. Optics 32 (1993) 334–338.
[13] M. Lang, P. Siffel, Z. Braunova, H.K. Lichtenthaler, Botanical Acta 105 (1992) 435–440.
[14] F. Stober, H.K. Lichtenthaler, Physiol. Plant. 88 (1993) 696–703.
[15] T.L. Danielson, S.M. Obeidat, G.D. Rayson, D.M. Anderson, E.L. Fredreckson, R. Estell, Appl. Spec. 60 (2006) 800–807.
[16] S. Landau, T. Glasser, L. Dvassh, A. Perevolotsky, S. African, J. Anim. Sci. 34 (2004) 76–80.
[17] S. Landau, T. Glasser, H. Muklada, L. Dvash, A. Perevolotsky, E.e. Ungar, J.W. Walker, Small Ruminant Res. 59 (2005) 251–263.
[18] J.S. Wagner, M.W. Tarahan, W.E. Nelson, G.C. Tisone, B.L. Preppernau, Comput. Phys. 10 (2) (1996) 114–118.
[19] E. Parker, M.W. Tarahan, J.S. Wagner, S.E. Rosenthal, W.B. Whitten, R.A. Gieray, P.T. Reilly, A. Lazer, J.M. Ramsey, Field Anal. Chem. Technol. 49 (1) (2000) 31–42.
[20] E. Parker, M.W. Tarahan, J.S. Wagner, S.E. Rosenthal, W.B. Whitten, R.A. Gieray, P.T. Reilly, A. Lazer, J.M. Ramsey, J. Process Anal. Chem. 5 (1, 2) (2000) 50–58.
[21] A. Mukherjee, D.M. Anderson, D.L. Daniel, L.W. Murray, G. Tisone, E.L. Fredrickson, R.E. Estell, G.D. Rayson, K.M. Havstad, J. Range Manag. 54 (2001) 370–377.
[22] R.C. West, Handbook of Chemistry and Physics, 48th ed., CRC Press, Cleveland, OH, 1967, p. 133.
[23] K.A. Karlene, D.S. Kenneth, P.J. Micheal, Ind. Eng. Chem. Res. 35 (1996) 138–146.
[24] R.G. Brereton, Chemometrics: Data Analysis for the Laboratory and Chemical Plant, 2003.
[25] B.M. Wise, N.B. Gallagher, S.W. Butler, D.D. White, G.G. Barna, J. Chemometrics 13 (1999) 379–396.
[26] D.S. Lee, P.A. Vanrolleghem, Biotechnol. Bioeng. 82 (2003) 489–497.
[27] C.M. Anderson, R. Bro, J. Chemometrics 17 (2003) 200–215.
[28] G.J. Hall, K.E. Clow, J.E. Kenny, Environ. Sci. Technol. 39 (2005), pp. 7569–7567.
[29] M.L. Nahorniak, K.S. Booksh, J. Chemometrics 17 (2003) 608–617.
[30] R.D. Jiji, K.S. Booksh, Anal. Chem. 72 (2000) 718–725.

A study of the Pb(II) binding to recombinant mouse Zn$_7$-metallothionein 1 and its domains by ESI TOF MS

Òscar Palacios [a], Àngels Leiva-Presa [b], Sílvia Atrian [c], Ryszard Lobinski [a],*

[a] *Equipe de Chimie Analytique, CNRS UMR 5034, Hélioparc, 2, av. Pr. Angot, F-64053 Pau, France*
[b] *Departament de Química, Universitat Autònoma de Barcelona, 08193 Cerdanyola del Vallés, Barcelona, Spain*
[c] *Departament de Genètica, Facultat de Biologia, Universitat de Barcelona, 08028 Barcelona, Spain*

Abstract

This work reports, for the first time, a complete analysis of the binding of Pb(II) ions to mammalian Zn-metallothionein (MT) and its individual domains (α and β) by means of ESI TOF MS. The use of highly pure recombinant Zn-MT and high resolution MS allowed the identification of the different heteronuclear Pb,Zn-MT and homonuclear Pb-MT complexes formed by Zn/Pb replacement in the initial Zn-MT complexes at pH 7. The results obtained showed, both for the whole Zn$_7$-MT and for its individual Zn$_4$-α and Zn$_3$-β fragments, a partial substitution of the Zn initially bound to give rise to the formation of both Pb,Zn-MT and Pb-MT species. In the case of the whole Zn$_7$-MT, the addition of seven equivalents of Pb(II) give rise to the formation of several Pb$_x$Zn$_y$-MT species ($x + y = 7$ or 8) as well as Pb$_8$-MT and Pb$_9$-MT coexisting with the initial Zn$_7$-MT species. The addition of a five-fold excess of Pb(II) showed the formation of species containing a higher amount of lead(II), Pb$_x$Zn$_y$-MT species ($x = 8$–12, $y = 0$–1). In both cases, the evolution with time showed the disappearance of the species containing lead and concomitantly only detection of the initial Zn-MT clusters within 48 h. This behaviour was also observed for the Zn$_4$-α and Zn$_3$-β aggregates, confirming the reversibility of the Pb^{2+} displacement of Zn^{2+} ions in the three forms of MT. A similar result was obtained at acidic pH, when the apo-form was the major species in solution, this therefore confirming the low affinity of MT for Pb(II), even in the absence of zinc. The results obtained were consistent with the increase of MT synthesis in response to Pb^{2+} administered to rats reported in the literature, since the initial release of Zn(II) would promote the biosynthesis of MT, in agreement with the function of this ion as primary activator of the MTF-1 transcription factor; and could explain the difficulty of recovering homonuclear Pb-MT species from lead-treated organisms.
© 2006 Published by Elsevier B.V.

Keywords: Recombinant mouse Zn$_7$-metallothionein 1; Lead(II); ESI TOF MS; α and β Zn complexes

1. Introduction

Lead has been widely used for the production of ammunition, printing, batteries, glasses, pigments and fuel, and thus, its concentration in the environment has lately increased dramatically. Lead is a toxic element. It interferes with several natural processes, provokes inhibition of protein synthesis and hinders the formation of essential complexes, such as hemoglobin, and additionally damages the central nervous system [1]. Living organisms have developed various mechanisms to reduce the toxicity of heavy metals which are also effective against lead intoxication. In the case of eukaryotes, metal detoxification is mainly carried out by glutathione, phytochelatins and metallothioneins [2].

Metallothioneins (MT) are low-molecular-weight proteins (6000–7000 Da), rich in cysteine (*ca.* 30% of all the amino acids) which confers them with a high capacity to bind heavy metal ions (Zn, Cd, Cu, Ag, Hg, etc.) in biological systems [3,4]. The role of MT in the detoxification of lead has been demonstrated [5,6] but the bibliographic data concerning the interaction of Pb^{2+} with MT are confusing and difficult to systematise. Most of the papers published are based on spectroscopic data [7–15] and many authors point to the formation of Pb$_7$-MT by mammalian MT. However, the use of low-purity protein preparations in these studies and the heterogeneity of results obtained by different authors require a deeper consideration of this subject.

Electrospray mass spectrometry offers the possibility to determine the molecular distribution of various metal–MT

---

species in the same sample. This technique was first used for rabbit liver MT [16] and since then applied to the analysis of the metal binding properties of mammalian MT [17]. We reported the binding of silver(I) to mammalian MT1 [18] where the use of ESI MS was the key to the understanding of the Ag–MT interaction beyond the level possible with other spectroscopic data. Recently two Pb-containing (in addition to Cd, Zn and Cu) MT species have been detected by ESI MS, both in carp liver MT after exposure to cadmium [19].

The aim of this work is to study the Pb^{2+} binding to recombinant mouse Zn_7-MT1 and its Zn_4-α and Zn_3-β domains by the titration of these aggregates with lead salts, and to identify the complexes formed by electrospray-ionisation time-of-flight mass spectrometry (ESI TOF MS). The use of a TOF analyzer provides a higher resolution than the quadrupole analyzers, thus, allowing a higher accuracy in assignment of the metal composition to the mixed–metal complexes formed, even at low protein concentrations.

2. Materials and methods

2.1. Protein preparation and characterization

Expression assays, fermentator-scale cultures, purification of the fusion protein and recovery and analysis of the recombinant mouse Zn_7-MT, Zn_4-αMT and Zn_3-βMT fragments were performed as previously described [20,21]. Polypeptide solutions were obtained in the Tris–$HClO_4$ buffer at pH 7 [22] and had a final concentration of 31.1 μM Zn_7-MT, 106 μM Zn_4-αMT and 387 μM Zn_3-βMT.

2.2. Buffer exchange

Buffer exchange (the initial 50 mM Tris buffer against a 15 mM ammonium acetate, both at pH 7) was performed using a 5 mL "HiTrap Desalting" column (Amersham Pharmacia Biotech) connected to an AKTA Prime LC system (Amersham Biosciences, Uppsala, Sweden) equipped with UV and conductivity detectors. An aliquot of 200 μL of protein solution was injected and eluted at 1 mL min^{-1}. The peptide containing fraction eluted between 2 and 5.4 min. The final polypeptide concentration was measured by ICP MS. ^{34}S and ^{66}Zn isotopes were determined and quantification was carried out by the method of standard additions. The recovery of the procedure was *ca.* 85% of the total polypeptide loaded.

2.3. Lead-binding reactions

Metal-binding experiments were carried out by adding molar ratio aliquots of a 5.46 mM $Pb(ClO_4)_2$ aqueous solution to 200 μL of the protein solutions. For each addition, the protein was allowed to react, under argon at room temperature, with the metal ion, and an aliquot of each sample was analyzed at certain times. The addition of "*x* molar equivalents of lead" is denoted below as "*x* Pb(II) eq".

2.4. ESI TOF experiments

An 20-μL aliquot of each sample was analyzed by infusion using a QStar XL spectrometer (Applied Biosystems) equipped with an ESI source. Spectra were recorded at 5 μL min^{-1} flow rate, between 850 and 2500 *m/z* units, at 4500 V of ionspray voltage and 60 V of declustering potential.

When Pb(II) was added to a protein solution, a 20-μL aliquot of each sample was analyzed under the same conditions at different times: immediately after the addition (T0), and after 2, 6, 24 and 48 h.

3. Results

3.1. MS spectra of the initial species

The spectra recorded for the original MT samples showed clearly peaks corresponding to the Zn_7-MT, Zn_4-αMT and Zn_3-βMT species (Fig. 1). These results confirmed the integrity of the Zn-MT clusters as indicated elsewhere [20,21]. The insets in Fig. 1 demonstrate the isotopic resolution at low protein concentration (down to 1 μM) possible owing to the use of TOF MS.

3.2. Addition of the stoichiometric amounts of lead to the full-length MT and its α and β fragments

An amount of lead corresponding stoichiometrically to that of Zn present was added to each Zn-MT solution: 7 Pb(II) eq to Zn_7-MT; 4 Pb(II) eq to Zn_4-αMT; and 3 Pb(II) eq to Zn_3-βMT. The mass spectra recorded immediately after the addition of lead (time 0) (Fig. 2) already show the formation of several Pb-containing species, but different behaviour was observed depending on the MT peptide. In the case of the full-length MT (Fig. 2A), the addition of lead promoted the formation of several heteronuclear Pb_xZn_y-MT species ($x + y = 7$, 8) where Pb_4Zn_4-MT was the main species. Two homonuclear species, Pb_8-MT and Pb_9-MT, were also formed. A considerable amount of the initial Zn_7-MT remained unaffected. Note that peaks of MT adducts with ammonium cations and/or perchlorate anions were present in many spectra, due to the high concentration of these ions in the solution. Consequently, in the samples with highest concentration of the protein, the high resolution of the spectra recorded allowed us to observe several peaks due to adducts with ammonium cations (+18 and +36 Da) as well as with perchlorate anions (+100 Da).

In the case of the individual MT domains, the behaviour was quite different. In both cases the addition of Pb^{2+} promoted the formation of small amounts of several species containing lead while the initial Zn complexes remained the major species in solution. Most of the species observed after the addition of lead to the Zn_4-αMT solution were matching the Pb_xZn_y-αMT formula where $x + y = 4$. Pb_4Zn_1-αMT and Pb_5-αMT were also observed. The titration of the Zn_3-βMT solution produced both heteronuclear (Pb_1Zn_1-βMT, Pb_1Zn_2-βMT, Pb_2Zn_1-βMT and Pb_3Zn_1-βMT) and homonuclear species (Pb_2-βMT, Pb_3-βMT and Pb_4-βMT).
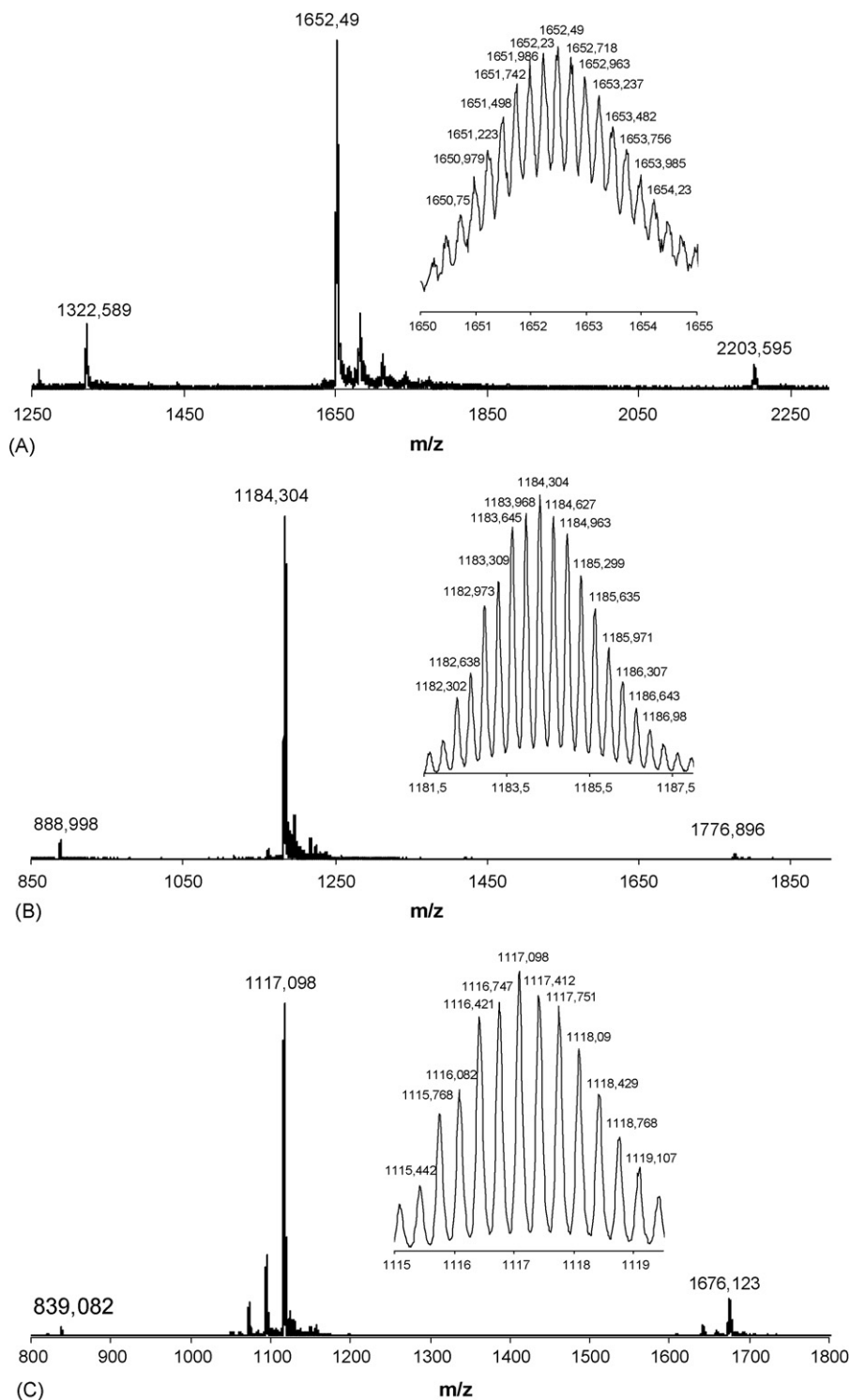
Fig. 1. ESI TOF spectra of (A) Zn_7-MT (1.5 μM), (B) Zn_4-αMT (4.8 μM) and (C) Zn_3-βMT (19.4 μM). The insets show the isotopic peaks of the highest intensity obtained for each species.

In order to study the evolution of the species formed as a function of time, several aliquots from each sample were analyzed by ESI TOF at 2, 6, 24 and 48 h after the addition of lead. Surprisingly, the spectra recorded after the addition of lead to the full-length MT (Fig. 3) showed the disappearance of the initial Pb-containing species formed, with concomitant detection of mainly Zn_7-MT. After 2 h, all the species with lead content

higher than Pb_4Zn_4-MT virtually disappeared. After 24 and 48 h, the main Zn_7-MT species coexisted only with a small amount of Pb_1Zn_6-MT.

The data recorded after addition of 4 Pb(II) eq to a Zn_4-αMT solution (Fig. 4) showed a behaviour similar to that of the entire MT: Zn_4-αMT remained the major species and the lead-containing species observed at time
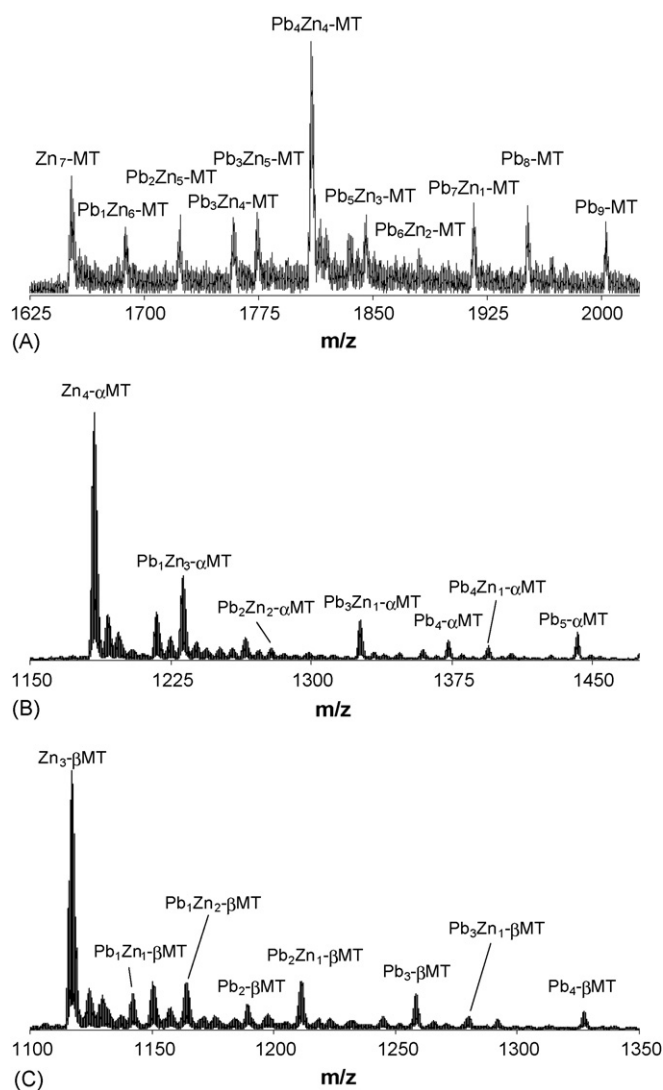
Fig. 2. ESI TOF spectra at "time 0" after addition of stoichiometric amounts of lead(II): (A) Zn_7-MT + 7 Pb^{2+}, (B) Zn_4-αMT + 4 Pb^{2+} and (C) Zn_3-βMT + 3 Pb^{2+}.
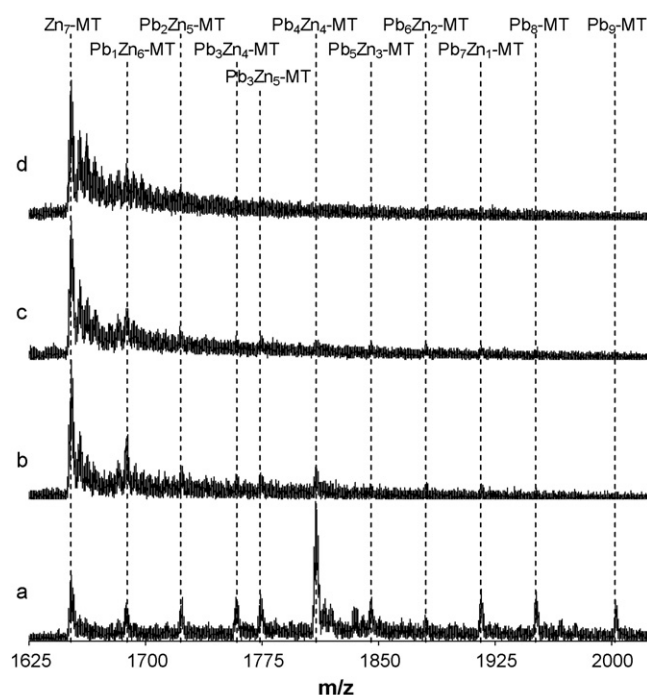

Fig. 3. Effect of the addition of 7 Pb^{2+} eq to a 1.5 μM Zn_7-MT solution. Evolution with time: (a) time 0, (b) 2 h, (c) 6 h and (d) 24 h after lead(II) addition. The spectrum recorded at 48 h after the injection was identical to the one recorded at 24 h.

metric amount) was added to the different MT solutions and the evolution with time was monitored as above.

The addition of *ca.* 35 Pb(II) eq to the Zn_7-MT solution revealed (Fig. 6) the initial formation of mainly homometallic
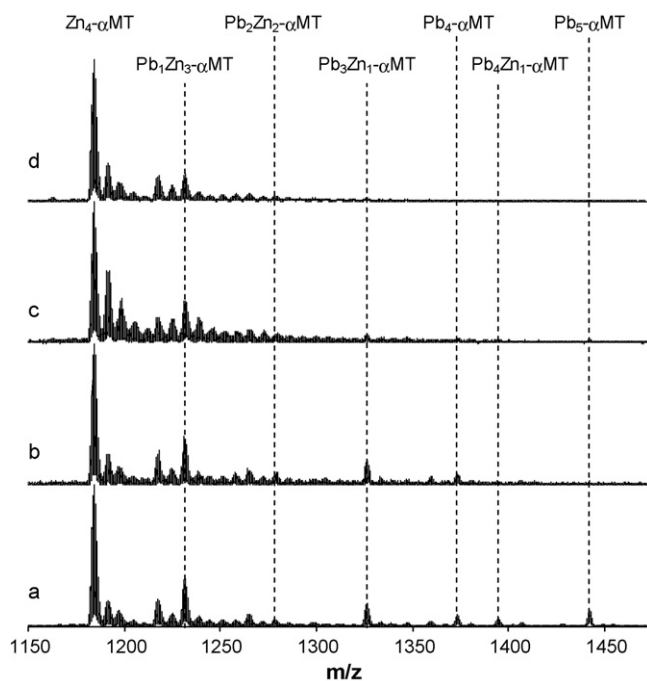
0 gradually disappeared. At the end of the experiment, at 24 and 48 h, the only Pb-containing species detected was Pb_1Zn_3-αMT.

The evolution of the spectra recorded after addition of 3 Pb^{2+} eq to the Zn_3-βMT solution (Fig. 5) as a function of time was slightly different from that of the α fragment or of the full-length MT. The species observed at time 0 were also observed unaltered after 2 h. After 24 h the number of the remaining Pb-containing species was higher than that observed for the other peptides under study (Pb_1Zn_1-βMT, Pb_1Zn_2-βMT, Pb_2Zn_1-βMT and Pb_2-βMT). This indicates not only a higher capacity of lead to exchange the initial zinc, but also a higher stability of the Pb-MT species formed.

3.3. Addition of lead in molar excess to the whole MT and its α and β fragments

In order to promote an increased replacement of the zinc ions initially present, an excess of lead (in relation to the stoichio-

Fig. 4. Effect of the addition of 4 Pb^{2+} eq to a 4.8 μM Zn_4-αMT solution. Evolution with time: (a) time 0, (b) 2 h, (c) 6 h and (d) 24 h after lead(II) addition. The spectrum recorded at 48 h after the injection was identical to the one recorded at 24 h.
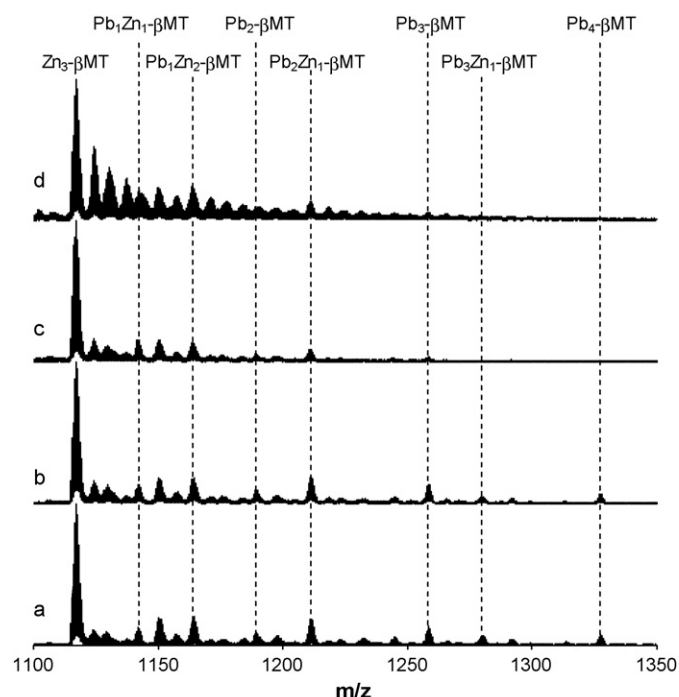
Fig. 5. Effect of the addition of 3 Pb^{2+} eq to a 19.4 μM Zn_3-βMT solution. Evolution with time: (a) time 0, (b) 2 h, (c) 6 h and (d) 24 h after lead(II) addition. The spectrum recorded at 48 h after the injection was identical to the one recorded at 24 h.
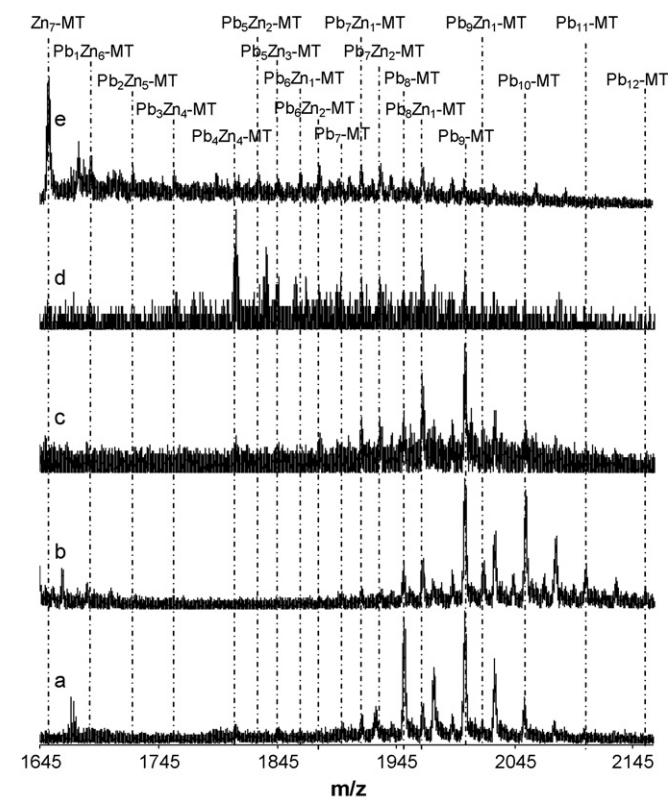
Fig. 6. Effect of the addition of 35 Pb^{2+} eq to a 1.5 μM Zn_7-MT solution. Evolution with time: (a) time 0, (b) 2 h, (c) 6 h, (d) 24 h and (e) 48 h after lead(II) addition.

Fig. 7. Effect of the addition of 20 Pb^{2+} eq to a 4.8 μM Zn_4-αMT solution. Evolution with time: (a) time 0, (b) 2 h, (c) 6 h, (d) 24 h and (e) 48 h after lead(II) addition.

species (Pb_8-MT, Pb_9-MT and Pb_{10}-MT) which after 2 h evolved towards new species with higher amounts of lead (Pb_{11}-MT and Pb_{12}-MT). Some heterometallic species (Pb_8Zn_1-MT and Pb_9Zn_1-MT) were also observed. Six hours after the addition of lead, the situation was quite similar to that at time 0, but higher amounts of the previously detected heterometallic species were observed. After 24 h, the number of heterometallic species increased, Pb_4Zn_4-MT being the most abundant species in solution. Finally, after 48 h, the spectra showed only the presence of the initial Zn_7-MT while very small amounts of several Pb(II)-containing species were detected.

When Pb(II) was added in excess to the αMT solution (Fig. 7), several species containing only Pb(II) (Pb_4-αMT, Pb_5-αMT, Pb_6-αMT and Pb_7-αMT), small amounts of some heterometallic species (Pb_1Zn_3-αMT, Pb_3Zn_1-αMT, Pb_3Zn_2-αMT and Pb_4Zn_1-αMT) and a significant amount of the initial zinc species were observed. After 2 and 6 h the amount of homometallic Pb^{2+} species increased, species with higher nuclearity were detected (Pb_8-αMT), and the Zn-containing heterometallic species almost disappeared. But 24 h after the addition of lead, the homometallic Pb species became the minority and the major species was again Zn_4-αMT, together with small amounts of several heterometallic species. After 48 h, only Zn_4-αMT and Pb_1Zn_3-αMT were present in solution.

The addition of excess Pb^{2+} (9 eq) to the Zn_3-βMT solution (Fig. 8) showed initially only the formation of homometallic Pb_x-βMT complexes for $x = 2$–7, Pb_5-βMT being the major species. After 2 h, the species distribution changed, Pb_4-βMT
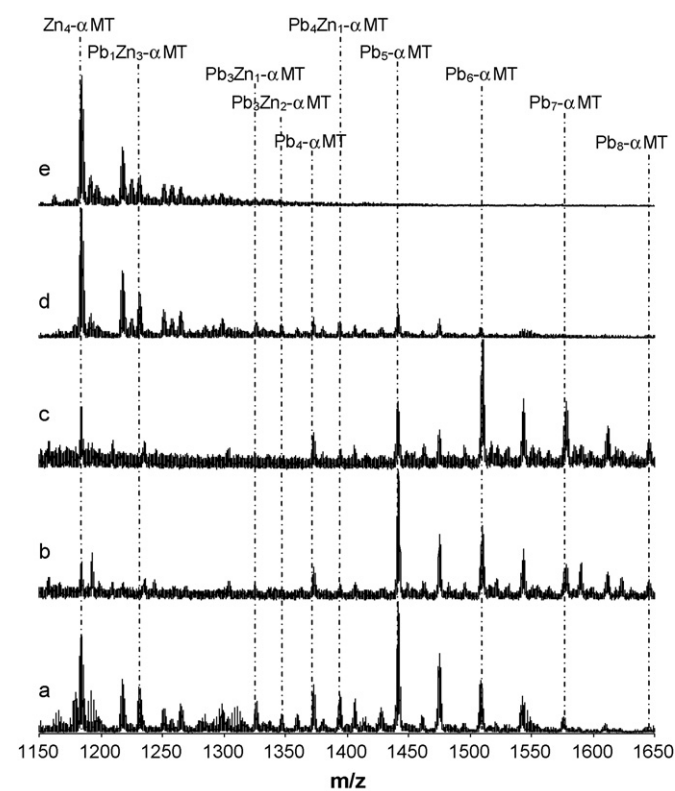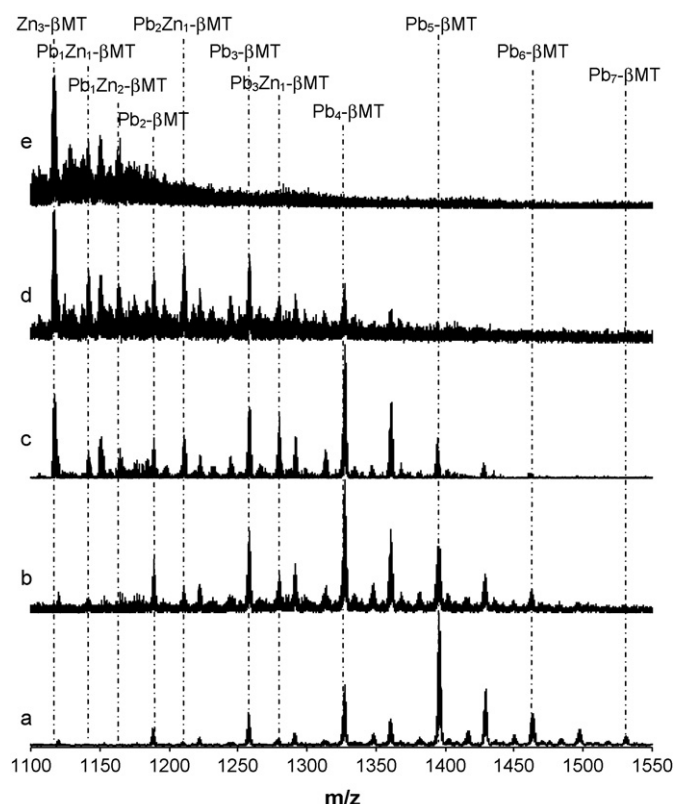
Fig. 8. Effect of the addition of 9 Pb^{2+} eq to a 19.4 μM Zn_3-βMT solution. Evolution with time: (a) time 0, (b) 2 h, (c) 6 h, (d) 24 h and (e) 48 h after lead(II) addition.

Fig. 9. Effect of the addition of 3 Pb^{2+} eq to a 15.8 μM Zn_3-βMT solution at pH 4.5. Evolution with time: (a) before the addition of Pb(II), (b) time 0, (c) 2 h, (d) 6 h and (e) 24 h after lead(II) addition.

Fig. 10. Effect of the addition of 10 Pb^{2+} eq to a 15.8 μM Zn_3-βMT solution at pH 4.5. Evolution with time: (a) time 0 and (b) 24 h after lead(II) addition.

appearing as the major species, while small amounts of some heterometallic species were observed. Spectra recorded after 6 h showed an increase in the intensity of the peaks related to Zn(II)-containing species and the appearance of a peak corresponding to the initial Zn_3-βMT species. After 24 and 48 h, the amount of Pb(II) complexes was decreasing while that of Zn(II) complexes was increasing. The last spectrum recorded showed the presence of mainly Zn_3-βMT with small peaks corresponding to Pb_1Zn_1-βMT and Pb_1Zn_2-βMT.

3.4. Addition of lead to the β fragment at acidic pH

Because the protonation of the cysteine residue (pK_a 8.33) at acidic pH may cause partial release of the Zn(II) ions, the titration of the βMT domain with lead was repeated at pH 4.5. This peptide was chosen because its higher concentration allowed intense signals to be obtained. The spectrum revealed the apoform as the major species in solution while less than 50% of the initial amount of zinc remained bound to the protein (Fig. 9) under the forms of Zn_1-βMT, Zn_2-βMT and Zn_3-βMT. When an equimolar amount of lead (3 Pb(II) eq) was added, the spectra at time 0 showed several species (Pb_1-βMT, Pb_2-βMT, Pb_3-βMT, Pb_4-βMT, Pb_1Zn_1-βMT and Pb_2Zn_1-βMT) coexisting with apo-βMT (Fig. 9). But again, evolution with time showed the consecutive loss of lead from the complexes, to return, after 24 h, to the initial situation: the apo-form present with small amounts of Zn species.
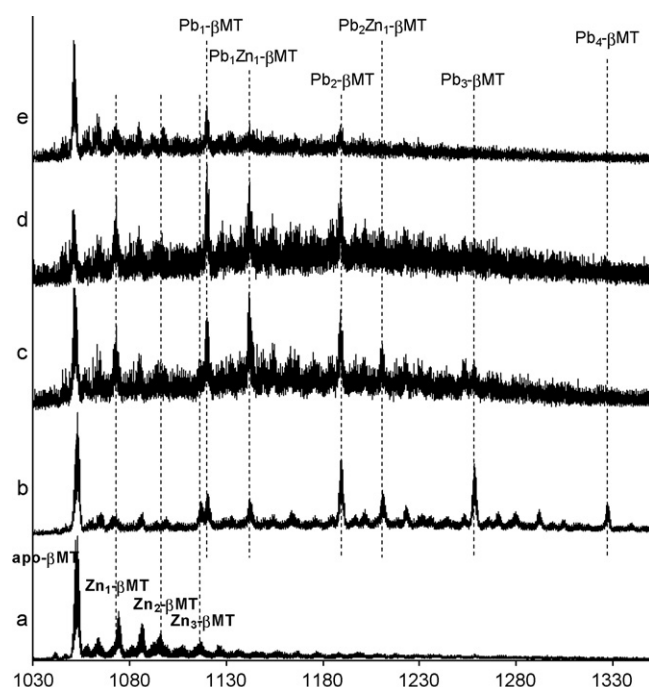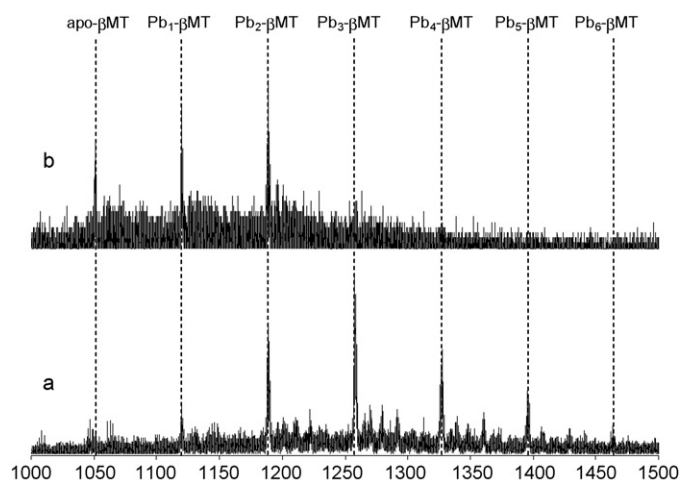
The experiment was repeated by adding an excess of lead to the βMT peptide at pH 4.5. When 10 and 20 Pb(II) eq were added (Fig. 10, only the addition of 10 Pb^{2+} eq is shown), the formation of mainly Pb_3-βMT was observed in both cases at $t = 0$. It coexisted with minor amounts of other homometallic Pb_x-βMT species ($x = 1–6$). After 24 h only Pb_2-βMT, Pb_1-βMT and apo-βMT (in decreasing intensity order) were observed.

4. Discussion

The data recorded by titration of the recombinant mouse Zn_7-MT1 and its Zn_4-α and Zn_3-β fragments with Pb(II) allowed common trends for the results of all the experiments performed

Table 1
Identification of the metal aggregates formed during the addition of Pb^{2+} to the whole Zn_7-MT

Metal complex	m/z (for +4 charged ion)	MW calculated	MW theoretical	Detection[a]	
				Stoichiometric	Excess
Zn_7-MT	1652.54	6606.2 ± 0.4	6605.86	✓	✓
Pb_1Zn_6-MT	1688.07	6748.3 ± 3.6	6747.67	✓	✓
Pb_2Zn_5-MT	1723.62	6890.5 ± 0.5	6889.48	✓	✓
Pb_3Zn_4-MT	1759.01	7032.0 ± 1.6	7031.29	✓	✓
Pb_3Zn_5-MT	1774.64	7094.5 ± 3.4	7094.68		✓
Pb_4Zn_4-MT	1809.22	7233.9 ± 3.1	7236.49	✓	✓
Pb_5Zn_2-MT	1829.46	7313.8 ± 1.2	7314.91		✓
Pb_5Zn_3-MT	1845.83	7379.3 ± 0.5	7378.30	✓	✓
Pb_6Zn_1-MT	1864.73	7454.9 ± 1.5	7456.72		✓
Pb_6Zn_2-MT	1880.82	7519.3 ± 4.2	7520.11	✓	✓
Pb_7-MT	1900.95	7599.8 ± 3.7	7598,53		✓
Pb_7Zn_1-MT	1916.35	7661.4 ± 0.0	7661.92	✓	✓
Pb_7Zn_2-MT	1931.98	7723.9 ± 1.1	7725.31		✓
Pb_8-MT	1952.09	7804.4 ± 0.2	7803.73	✓	✓
Pb_8Zn_1-MT	1968.11	7868.4 ± 2.1	7867.12		✓
Pb_9-MT	2003.31	8009.2 ± 0.3	8008.93	✓	✓
Pb_9Zn_1-MT	2019.57	8074.3 ± 2.1	8072.32		✓
Pb_{10}-MT	2054.40	8213.6 ± 0.6	8214.13		✓
Pb_{11}-MT	2105.36	8417.4 ± 2.5	8419.33		✓
Pb_{12}-MT	2156.41	8621.6 ± 3.9	8624.53		✓

[a] Detection of the complex for the stoichiometric addition of lead and for the molar excess of lead. See text for additional information.

to be observed: (a) a low efficiency of lead to replace the initial zinc, it was at least lower than other metal ions as Cd^{2+} or Cu^+ [22,23], although it depended on the peptide considered; (b) the formation and coexistence of several homometallic Pb-MT, as well as heterometallic Pb,Zn-MT species, the lead content of these species being proportional to the amount of added lead; (c) disappearance with time of the Pb(II) species formed to return mainly to the initial Zn-MT species, with small amounts of some heterometallic species with low Pb^{2+} content remaining in solution.

All the mass spectrometric data obtained for the addition of lead(II) are summarized in Table 1 for the whole MT, in Table 2 for the αMT fragment and in Table 3 for the βMT fragment.

As it happened in the case of Cd [24] and Ag [18], where the first publications proposed the formation of single metal-MT species, but further and more accurate experiments demonstrated the formation of several homo- and heterometallic species, the formation of a single metal-MT species for the addition of Pb(II) to the whole MT, proposed in the bibliography [7–11], has to be questioned. The relationship observed *in vivo* between lead(II) administration to rats and MT production [25,26] is consistent with our data: the initial release of Zn(II), which depends on the initial concentration of Pb(II) present in solution, promotes the biosynthesis of MT, in agreement with the function of Zn(II) as primary activator of the MTF-1 transcription factor, which induces the synthesis of MT [27]. Thus, when the concentration

Table 2
Identification of the metal aggregates formed during the addition of Pb^{2+} to the Zn_4-αMT aggregate

Metal complex	m/z (for +3 charged ion)	MW calculated	MW theoretical	Detection[a]	
				Stoichiometric	Excess
Zn_4-MT	1184.30	3551.2 ± 1.1	3550.49	✓	✓
Pb_1Zn_3-αMT	1231.70	3692.1 ± 0.4	3692.30	✓	✓
Pb_2Zn_2-αMT	1279.38	3835.1 ± 1.2	3834.11	✓	
Pb_3Zn_1-αMT	1326.41	3976.2 ± 0.3	3975.92	✓	✓
Pb_3Zn_2-αMT	1348.05	4041.2 ± 2.3	4039.01		✓
Pb_4-αMT	1373.42	4117.3 ± 1.0	4117.73	✓	✓
Pb_4Zn_1-αMT	1394.72	4181.2	4181.12	✓	✓
Pb_5-αMT	1442.09	4323.3 ± 0.6	4322.93	✓	✓
Pb_6-αMT	1510.78	4529.3 ± 0.8	4528.13		✓
Pb_7-αMT	1578.78	4733.3 ± 0.2	4733.33		✓
Pb_8-αMT	1646.77	4937.3 ± 3.1	4938.53		✓

[a] Detection of the complex for the stoichiometric addition of lead and for the molar excess of lead. See text for additional information.

Table 3
Identification of the metal aggregates formed during the addition of Pb^{2+} to the Zn_3-βMT aggregate

Metal complex	m/z (for +3 charged ion)	MW calculated	MW theoretical	Distrib. pH 7[a]		Distrib. pH 4.5[b]	
				Stoichiometric	Excess	Stoichiometric	Excess
Apo-βMT	1053.09	3156.3 ± 2.1	3158.54			√	√
Zn_1-βMT	1074.36	3220.1 ± 1.7	3221.93			√	
Zn_2-βMT	1096.37	3286.1 ± 1.1	3285.32			√	
Zn_3-βMT	1117.10	3350.3 ± 2.0	3348.71	√	√	√	
Pb_1-βMT	1122.00	3363.1 ± 1.3	3363.74			√	√
Pb_1Zn_1-βMT	1142.48	3424.4 ± 3.2	3427.13	√	√	√	
Pb_1Zn_2-βMT	1164.78	3491.3 ± 1.1	3490.52	√	√		
Pb_2-βMT	1189.81	3566.4 ± 3.0	3568.94	√	√	√	√
Pb_2Zn_1-βMT	1211.47	3631.4 ± 0.9	3632.33	√	√	√	
Pb_3-βMT	1258.48	3772.4 ± 1.9	3774.14	√	√	√	√
Pb_3Zn_1-βMT	1280.12	3837.4 ± 0.5	3837.53	√	√		
Pb_4-βMT	1327.84	3980.5 ± 0.7	3979.34	√	√	√	√
Pb_5-βMT	1395.64	4183.9 ± 1.4	4184.54		√		√
Pb_6-βMT	1463.96	4388.9 ± 2.2	4389.74		√		√
Pb_7-βMT	1531.62	4591.9 ± 3.1	4594.94		√		

[a] Detection of the complex for the stoichiometric addition of lead and for the molar excess of lead at neutral pH. See text for additional information.

[b] Detection of the complex for the stoichiometric addition of lead and for the molar excess of lead at acidic pH. See text for additional information.

of Pb(II) is high, the release of Zn(II) and the subsequent synthesis of MT will be also high and *vice versa*. The results presented here can also explain why it was not possible [26] to isolate any homometallic Pb-MT species 1 day after the injection of this metal to animals.

When comparing the individual behaviour of the entire MT and of its α and β fragments some differences are observed. First, the capacity to substitute the zinc is higher for Zn-MT than for the individual fragments when the stoichiometric amounts of Pb are added. In this case, for both individual domains, the main complex observed in solution was the initial Zn(II) species coexisting with some hetero- and homometallic species.

However, when an excess of Pb(II) was added to the MT solutions, an opposite behaviour was observed. Whereas several heterometallic species were observed for MT at time 0 coexisting with homometallic Pb_x-MT species (x = 7–12), mainly homometallic species were observed at the initial stages after the addition of lead to the α and β fragments. Thus, the release of zinc in the presence of excess Pb(II) seems easier for the fragments than for the whole MT. The binding of Pb(II) and the release of Zn(II) for the individual αMT and βMT fragments is different than for the whole MT, suggesting possibly a cooperation effect or some folding restrictions.

The results at neutral pH suggested the existence of a secondary reaction which could be responsible for the release of the lead after a certain time. Taking into account the low solubility of lead hydroxides (pKs = 4.92), this behaviour can be explained by a slow precipitation of $Pb(OH)_2$ at pH 7 [28] or the formation of another complex, e.g. $[Pb_4(OH)_4]^{4+}$ which is known to form in aqueous solutions containing Pb(II) [29,30]. When lead was added at pH 4.5 to the β fragment, the behaviour observed was similar to that observed at neutral pH. So, the initial formation of Pb(II) species coexisting with the initial apo-form and the subsequent release of it were observed. Even after an addition of a considerable excess of lead at acidic pH, the species formed did not reach a high content of Pb(II), Pb_6-βMT being the species with the highest lead content detected. A loss of lead with time was observed.

A second hypothesis to explain the constant disappearance of the lead bound to the protein was a possible precipitation of the Pb-MT species over time. Hence, only the Zn-MT species remaining in the solution could be observed. However, some facts contradict this hypothesis: (1) the near disappearance of the initial Zn-MT species and its restitution at the end of the experiment and (2) the maintenance of the intensity of the MS peaks for all the titrations as a function of time, suggesting a constant concentration of all the species.

5. Conclusions

The use of ESI TOF MS to monitor the reaction between $Pb(ClO_4)_2$ and the recombinant mouse Zn_7-MT1 (and its Zn_4-α and Zn_3-β fragments) allowed to obtain for the first time in mammalian MT an accurate and precise determination of the Pb-MT species formed, even at low protein concentration (1.5 μM).

The data obtained lead to the conclusion that the substitution of Zn^{2+} by Pb^{2+} in MT is not favoured, due to the difficulty of releasing Zn^{2+}, despite the theoretically higher affinity of Pb^{2+} for the cysteine residues than that of Zn^{2+}. As a result, the formation of several heterometallic Pb,Zn-MT species and the preservation of the initial Zn-MT species were observed under all conditions studied. The addition of a high excess of Pb(II) was necessary to achieve the formation of species with a high content of Pb^{2+}, but even then, the mixed Pb,Zn-MT species were omnipresent. Also, with a lower presence of zinc bound to the protein (acidic pH), the behaviour was similar to that shown at neutral pH, confirming thus the low ability of MT to bind Pb(II).

The Pb(II) species formed in solution tend to dissociate as a function of time until they were nearly absent within 48 h of forming. This is the first metal for which such a MT binding behaviour is described.

Acknowledgements

References

[1] (a) M.E. Hilburn, Chem. Soc. Rev. 8 (1979) 63;
(b) N.N. Greenwood, A. Earnshaw, Chemistry of the Elements, Butterworth Einemann, 1997;
(c) J.J. Chisholm, Sci. Am. 224 (1971) 15;
(d) R.M. Harrison, D.P.H. Laxen, Lead Pollution, Chapman and Hall, London, 1981.

[2] (a) S. Silver, Plasmid 27 (1992) 1;
(b) R.K. Singhal, M.E. Anderson, A. Meister, FASEB J. 1 (1987) 220;
(c) W.E. Rauser, Annu. Rev. Biochem. 59 (1990) 61;
(d) R.K. Mehra, D.R. Winge, J. Cell Biochem. 45 (1991) 30;
(e) R.K. Mehra, J. Miclat, V.R. Kodati, R. Abdullah, T.C. Hunter, P. Mulchandani, Biochem. J. 314 (1996) 73;
(f) M.J. Stillman, C.F. Shaw III, K.T. Suzuki (Eds.), Metallothioneins, VCH, New York, 1992.

[3] K.T. Suzuki, N. Imura, M. Kimura (Eds.), Metallothionein III, Birkhäuser Verlag, Basel, 1993.

[4] C.D. Klaassen (Ed.), Metallothionein IV, Birkhäuser Verlag, Basel, 1999.

[5] H.J. Church, J.P. Day, R.A. Braithwaite, S.S. Brown, J. Inorg. Biochem. 49 (1993) 55.

[6] W. Qu, B.A. Diwan, J. Liu, R.A. Goyer, T. Dawson, J.L. Horton, M.G. Cherian, M.P. Waalkes, Am. J. Pathol. 160 (2002) 1047.

[7] W. Bernhard, M. Good, M. Vasák, J.H.R. Kägi, Inorg. Chim. Acta 79 (1983) 154.

[8] K.B. Nielson, C.L. Atkin, D.R. Winge, J. Biol. Chem. 260 (1985) 5342.

[9] S.S. Hasnain, G.P. Diakun, I. Abrahams, I. Ross, C.D. Garner, I. Bremner, M. Vasák, Experientia Supp., Metallothionein II 52 (1987) 227.

[10] M.J. Stillman, Coord. Chem. Rev. 144 (1995) 461.

[11] (a) W.G. He, D.Y. Chu, J.Y. Yang, D.F. Yao, M.C. Shao, Chem. J. Chin. Univ. 20 (1999) 248;
(b) W.G. He, D.Y. Chu, J.Y. Yang, D.F. Yao, M.C. Shao, Chin. Chem. Lett. 10 (1999) 87.

[12] X. Wei, B. Ru, Chin. J. Biochem. Mol. Biol. 15 (1999) 289–295.

[13] Q. Ji, L. Wang, B. Ru, Chin. J. Biochem. Mol. Biol. 15 (1999) 928.

[14] Q. Ji, L. Wang, Y. Zhou, B. Ru, Beijing Daxue Xuebao, Ziran Kexueban 36 (2000) 503.

[15] X. Li, S. Hao, Y. Liu, B. Ru, Weisheng Yanjiu 30 (2001) 198.

[16] X. Yu, M. Wojciechowski, C. Fenselau, Anal. Chem. 65 (1993) 1355.

[17] (a) L.T. Jensen, J.M. Peltier, D.T. Winge, J. Bioinorg. Chem. 3 (1998) 627;
(b) P.M. Gehrig, C. You, R. Dallinger, C. Gruber, M. Brouwer, J.H.R. Kagi, P.E. Hunziker, Protein Sci. 9 (2000) 395;
(c) M.J. Stillman, D. Thomas, C. Trevithick, X. Guo, J. Siu, J. Inorg. Biochem. 79 (2000) 11.

[18] O. Palacios, K. Polec-Pawlak, R. Lobinski, M. Capdevila, P. González-Duarte, J. Biol. Inorg. Chem. 8 (2003) 831.

[19] H.G. Infante, F. Cuyckens, K.V. Campenhout, R. Blust, M. Claeys, L.V. Vaeck, F.C. Adams, J. Anal. At. Spectrom. 19 (2004) 159.

[20] M. Capdevila, N. Cols, N. Romero-Isart, R. González-Duarte, S. Atrian, P. González-Duarte, CMLS Cell. Mol. Life Sci. 53 (1997) 681.

[21] N. Cols, N. Romero-Isart, M. Capdevila, B. Oliva, P. González-Duarte, R. González-Duarte, S. Atrian, J. Inorg. Biochem. 68 (1997) 157.

[22] R. Bofill, O. Palacios, M. Capdevila, N. Cols, R. González-Duarte, S. Atrian, P. González-Duarte, J. Inorg. Biochem. 73 (1999) 57.

[23] M. Capdevila, N. Cols, N. Romero-Isart, R. Gonzalez-Duarte, S. Atrian, P. Gonzalez-Duarte, Cell Mol. Life Sci. 53 (1997) 681.

[24] K. Polec, O. Palacios, M. Capdevila, P. González-Duarte, R. Lobinski, Talanta 57 (2002) 1011.

[25] H. Ikebuchi, R. Teshima, K. Suzuki, T. Terao, Y. Yamane, Biochem. J. 233 (1986) 541.

[26] T. Maitani, A. Watahiki, K.T. Suzuki, Toxicol. Appl. Pharmacol. 83 (1986) 211.

[27] (a) G.K. Andrews, Biometals 14 (2001) 223;
(b) B. Zhang, O. Georgiev, M. Hagmann, C. Gunes, M. Cramer, P. Faller, M. Vasak, W. Schaffner, Mol. Cell Biol. 23 (2003) 8471.

[28] W. Cai, M.J. Stillman, Inorg. Chim. Acta 152 (1988) 111.

[29] F.A. Cotton, G. Wilkinson (Eds.), Advanced Inorganic Chemistry, John Wiley & Sons, New York, 1999.

[30] P. Tsai, R.P. Cooney, J. Chem. Soc., Dalton Trans. (1976) 1631.

Short communication

A surface plasmon resonance biosensor for detecting *Pseudomonas aeruginosa* cells with self-assembled chitosan-alginate multilayers

Jung-Soon Park [a,1], Chang-Moon Lee [b,1], Ki-Young Lee [c,*]

[a] *Department of Material and Biochemical Engineering, Chonnam National University, Gwangju 500-757, South Korea*
[b] *Department of Nuclear Medicine & Research Institute of Clinical Medicine, Chonbuk National University School of Medicine, Jeonju, Jeonbuk 561-712, South Korea*
[c] *Department of Applied Chemical Engineering & The Research Institute for Catalysis, Chonnam National University, Gwangju 500-757, South Korea*

Abstract

A self-assembled multilayer (SAMu) including the alginate layer was prepared for detecting *Pseudomonas aeruginosa* cells in a solution and its potential was evaluated with a BIAcore system. After layer-by-layer formation, the refractive units (RU) values monitored with the biosensor increased by the interaction between the layers. The responses by the binding of *P. aeruginosa* cells to the alginate-immobilized SAMu were visualized immediately upon injection of the cell suspension. The RU values after injection of the cells were measured with approximately 1152, 656 and 173 for 1×10^9, 1×10^8 and 1×10^7 CFU/ml. This result suggests that the alginate-immobilized SAMu will have useful application for detecting *P. aeruginosa* cells in a biosensor analysis.
© 2006 Elsevier B.V. All rights reserved.

Keywords: Biosensor; Chitosan; Alginate; *Pseudomonas aeruginosa*; Self-assembled multilayers; Pathogen detection

1. Introduction

Rapid detection of *Pseudomonas aeruginosa* emerged as one of the most problematic Gram-negative pathogenic bacteria is an essential mission due to their clinical importance [1,2]. *P. aeruginosa* is the major causative bacteria in food putrefaction and leads cause of pseudomonal infections to burn patients, mechanically ventilated patients, cystic fibrosis patients, etc.

Recently, to analyze the pathogen several detectable methods including polymerase chain reaction (PCR), enzyme linked immunosorbent assay (ELISA), bioluminescence and florescent labeling analytic techniques have been employed [3]. However, the detection techniques may require relatively long time and many process including isolation, biochemical testing and morphological examination. In some other way, a technology based

on surface plasmon resonance (SPR) offers rapid and real-time measurement for monitoring antigen–antibody interactions. Its good points is also label-free and a specific analysis.

In the present study, the potential of a self-assembled multilayer (SAMu) applied to a SPR sensor for detecting *P. aeruginosa* was investigated. The SAMu was constructed using polyelectrolytes formed between positively-charged chitosan and alginate bearing negatively-charged sites. Alginate immobilized on the end of the SAMu is an exopolysaccharide produced by *P. aeruginosa* that has repeating units of mannuronic acid and glucuronic acid. Alginate acts as an adhesion molecule to anchor *P. aeruginosa* to the surface of the colonized respiratory epithelium [4,5] and *P. aeruginosa* increases alginate synthesis to protect oneself from phagocytosis, antibiotics and even attenuates the host response [6,7]. Alginate layer attached on the surface of a sensor chip may show strong interaction with *P. aeruginosa* and the SAMu bearing alginate layer can used as the sensor chip to detect *P. aeruginosa*.

The aim of this study was to prepare the SAMu immobilizing alginate on the end of the sensor chip, which is applied as

---

* Corresponding author. Fax: +82 62 530 1849.
E-mail address: kilee@chonnam.ac.kr (K.-Y. Lee).
[1] These authors contributed equally to this work.

biosensor for detecting *P. aeruginosa*. The interactions between the SAMu bearing alginate and *P. aeruginosa* were monitored by SPR based estimation using a BIAcore instrument.

2. Materials and methods

2.1. Microorganism

P. aeruginosa (KCTC No. 1928) obtained from Korean Collection for Type Cultures (KCTC) was used in this study. *P. aeruginosa* was grown for 18 h at 37 °C in Luria-Bertani (LB) broth.

2.2. Reagents

Alginate (Medium viscosity, 3500 cps at 2% concentration), glutaraldehyde and cysteamine were purchased from Sigma–Aldrich (St. Louis, MO, USA). Chitosan (Mw 50–80 K) with degree of 85% deacetylation was obtained from Chitoful Co. (Yeosu, Republic of Korea). All other chemicals were of regent grade and used without further purification.

2.3. Preparation of self-assembled chitosan-alginate multilayer

Alginate-attached SAMu was prepared with the method described by Deng et al. [8]. In brief, the gold surface of the sensor chip was treated with 'piranha' solution, which is consisted of sulfuric acid and NaOH solution and then immersed in 0.2% (w/v) aqueous solution of cysteamine for 2 h. The resultant gold surface was rinsed with distilled water and dried with nitrogen. After immersing the gold surface in 2.5% of glutaraldehyde solution for 1 h, the modified surface was then treated with 0.4% (w/v) of chitosan dissolved in 2% acetic acid for 1 h, washed with distilled water to remove the adhesive chitosan on the surface of chip, and then dried with nitrogen at the room temperature. Alginate solution (1% (w/v) in distilled water) was dropped on the chitosan layer to form the alginate-chitosan multilayer by ionic interaction, rinsed with distilled water and then dried at room temperature.

The SAMu formed on the gold surface was characterized through measurement of SPR responses at interval of each preparation steps. After each procedure, the changed refractive units (RU) values were investigated with BIAcore®J system (BIAcore® AB, Uppsala, Sweden).

2.4. Evaluation of P. aeruginosa binding to the SAMu of the sensor chip surface

P. aeruginosa cells were harvested by centrifugation after incubation in LB medium for 18 h. The cells were washed once and re-suspended to ~1 × 10^9 CFU/ml with 0.5 M sodium acetate buffer. The prepared whole cells suspension was injected in the BIAcore system fitted with the SAMu chip at a flow rate of 17 μl/min for 7 min. The specific interaction between *P. aeruginosa* cell and the SAMu of the sensor chip surface was determined by monitoring changes of RU values using. To inves-

Table 1
The changes of RU and mass value after the ligand immobilization

Type	ΔRU
Cysteamine	1367
Glutaraldehyde	245
Chitosan	307
Alginate	280

ΔRU is individual differences of RU values between the former step and the latter step.

tigate specific interaction of *P. aeruginosa* cell on the SAMu of the sensor chip, *P. fluorescens* cell and *Seratia marcenscens* cell were employed as contrast groups. The signal changes produced by the interaction of the cells on the SAMu of the sensor chip were monitored by measuring the shift of resonance angle in SPREETA™ system (Texas Instruments Inc., USA).

3. Results and discussion

The SAMu on the surface of sensor chip for detecting *P. aeruginosa* was prepared by modifying a gold chip and the interaction between the SAMu and *P. aeruginosa* was monitored with a BIAcore system. The modification of a chip surface by ligand immobilization was characterized by measuring the changed RU values after the immobilization steps [9,10]. Table 1 shows the RU and mass values measured by a BIAcore system after layer-by-layer formation. After cysteamine binding to the chip surface, the RU value increased about 1367 and then individual differences of RU values between the former step and the latter step was about 250–300 after subsequent events. The increment of RU and mass values in the steps means that the SAMu by the layer-by-layer formation was prepared on the chip surface. It is concluded that alginate as a ligand to detect *P. aeruginosa* could be immobilized on the chip surface by ionic interaction with chitosan layer. Liu et al. [11] proposed the self-assembly chitosan/glutaraldehyde/cysteamine (CGC) on the gold surface for an assay using a piezoelectric quartz crystal (PQC) sensor. From their results, it is confirmed that chitosan layer can be formed by interaction with glutaraldehyde/cysteamine layers (Fig. 1).
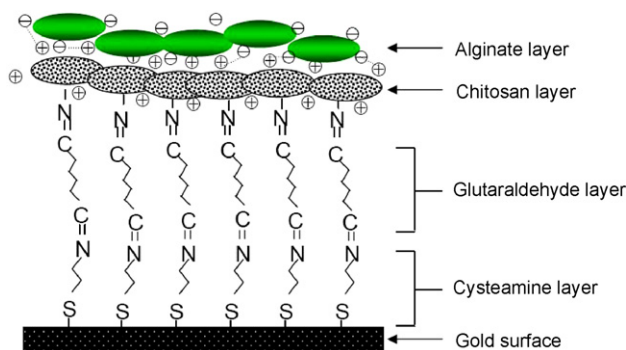

Fig. 1. Illustration of the self-assembled chitosan-alginate multilayers. Cysteamine molecules were conjugated by multipoint electrostatic bonding between their sulfur groups and gold surface. To cross-link chitosan layer glutaraldehyde was bonded to the cysteamine layer. Alginate layer formed with ionic interaction between chitosan layer can interact with *P. aeruginosa* cells.
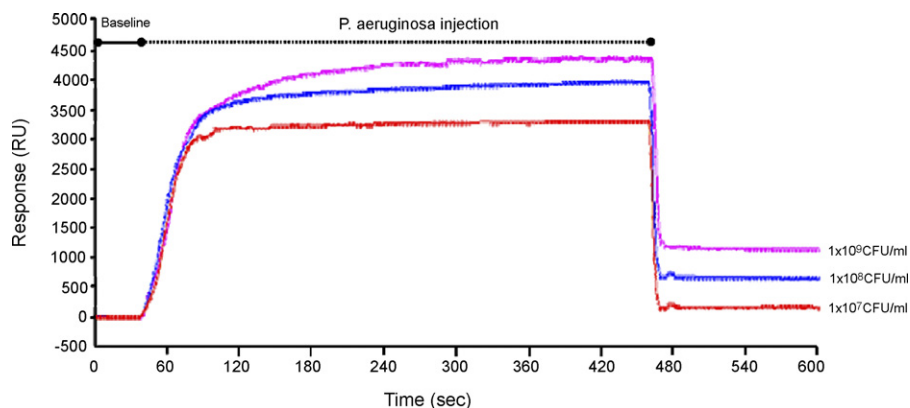
Fig. 2. Binding sensorgram of *P. aeruginosa* to the alginate-immobilized SAMu. After injection of a suspension of *P. aeruginosa* cells ($\sim 1 \times 10^9$ CFU/ml), the responses were typically showed by the interaction of the SAMu and the cells.
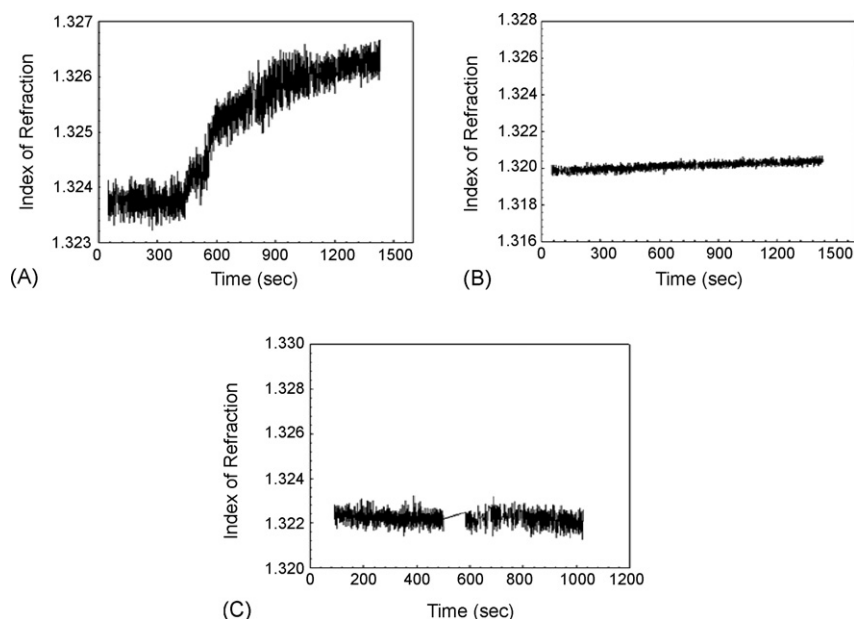

Fig. 3. Refractive index change by the interaction of (A) *P. aeruginosa*, (B) *P. fluorescens* and (C) *S. marcenscens* to the SAMu on the sensor chip. The number of the cells was 1×10^8 CFU/ml for all the groups.

The binding of *P. aeruginosa* cells using the SAMu based on alginate was evaluated with a BIAcore system. The sensogram showing the binding of *P. aeruginosa* on the SAMu of the chip surface was presented in Fig. 2. The responses by the binding of the cells were rapid and visualized immediately upon injection of the *P. aeruginosa* suspension. In the binding analyzes of the cells, the RU values reached approximately 1152, 656 and 173 for 1×10^9, 1×10^8 and 1×10^7 CFU/ml. The responses were dependent on the concentration of the cells administered for detecting. *P. aeruginosa* produces a polysaccharide, alginate, to anchor on the surface of the colonized respiratory epithelium. It may be concluded that an interaction between *P. aeruginosa* and alginate exists and the SAMu including alginate can be used to detect *P. aeruginosa* cells. As shown in Fig. 3, it was confirmed that *P. aeruginosa* could be specifically interacted with the SAMu on the sensor chip compared with *P. fluorescens* and *S. marcenscens*. In the interaction test between *P. aeruginosa* and the SAMu, the index of refraction was clearly changed by the specific binding to the surface of the sensor chip. On the other hand, the change of the index of refraction weakly happened in the interaction test with *P. fluorescens* and the refractive index change did not happen in the test with *S. marcenscens*.

In summary, the SAMu immobilizing alginate to analyze *P. aeruginosa* cells in a solution showed the useful results in this study. The formation of the alginate-immobilized SAMu was confirmed by measuring the changed RU in the BIAcore system. In the study for the detecting *P. aeruginosa* cells, the RU values by the specific interaction with the SAMu increased, depending on the concentration of *P. aeruginosa* cells. Therefore, it is concluded that the alginate-immobilized SAMu may has potential applications for detecting *P. aeruginosa* cells in a solution.

Acknowledgement

References

[1] K.C. Keum, S.M. Yoo, S.Y. Lee, K.H. Chang, N.C. Yoo, W.M. Yoo, J.M. Kim, J.Y. Choi, J.S. Kim, G. Lee, Mol. Cell. Probes 20 (2006) 42–50.

[2] P. Kurupati, G. Kumarasinghe, C.L. Poh, Mol. Cell. Probes 19 (2005), 417-412.

[3] C. Subramanian, J. Woo, X. Cai, X. Xu, S. Servick, C.H. Johnson, A. Nebenfuhr, A.G. von Arnim, Plant J. 48 (2006) 138–152.

[4] J.C. Davies, Paediatr. Respir. Rev. 3 (2002) 128–134.

[5] K. Mathee, O. Ciofu, C. Sternberg, P.W. Lindum, J.I. Campbell, P. Jensen, A.H. Johnsen, M. Givskov, D.E. Ohman, S. Molin, N. Hoiby, A. Kharazmi, Microbiology 145 (1999) 1349–1357.

[6] M. Hentzer, G.M. Teitzel, G.J. Balzer, A. Heydorn, S. Molin, M. Givskov, M.R. Parsek, J. Bacteriol. 183 (2001) 5395–5401.

[7] L.M. Cobb, J.C. Mychaleckyj, D.J. Wozniak, Y.S. Lopez-Boado, J. Immunol. 173 (2004) 5659–5670.

[8] T. Deng, H. Wang, J.S. Li, S.Q. Hu, G.L. Shen, R.Q. Yu, Sens. Actuators B Chem. 99 (2004) 123–129.

[9] B.A. Snopok, Yu. G. Goltsov, E.V. Kostyukevich, L.A. Matkovskaja, Yu. M. Shirshov, E.F. Venger, Sens. Actuators B Chem. 95 (2003) 336–343.

[10] M.W. Oli, W.P. McArthur, L.J. Brady, J. Microbiol. Methods 65 (2006) 503–511.

[11] Y. Liu, Y. Li, S. Liu, J. Li, S. Yao, Biomaterials 25 (2004) 5725–5733.

Preventing biofilm development on DGT devices using metals and antibiotics

Catherine Pichette [a], Hao Zhang [b], William Davison [b], Sébastien Sauvé [a],*

[a] *Department of Chemistry, Université de Montréal, 2900 Edouard-Montpetit, Montréal, Que., Canada H3C 3J7*
[b] *Department of Environmental Science, LEC, Lancaster University, Lancaster LA1 4YQ, UK*

Abstract

The DGT technique has potential as a tool for monitoring reactive phosphorus in freshwater aquaculture effluents. Because those waters have high concentrations of suspended matter and nutrients, biofilms may form on the surface of the DGT devices. Those biofilms may hinder the movement of reactive phosphorus and hence interfere with the DGT measurements. We tested two antibiotics, glutaraldehyde and chloramphenicol, two metal-iodides, copper and silver and also two alternative filter types, nucleopore membrane and silver-based filters, to evaluate their respective potential to prevent the formation of algae. The treatment with silver iodide seems to affect the properties of the diffusive gel and changes the flux measurements of the DGT device. The DGT response observed using the copper iodide and chloramphenicol treatments was not significantly different from the control. Glutaraldehyde changed the macroproperties of the diffusive gel and interfered with the phosphorus detection using spectrophotometric determinations. The effect of the anti-biofilm treatments on the DGT measurements was independent of pH and ionic strength of the water. For the field deployment in fish farms, copper and silver were the best anti-biofilm agents. Copper prevented algal colonisation for 14-days post-deployment and the response was unaffected by the anti-biofilm agent throughout this period. Silver was even better and prevented biofilm formation up to a 21-days post-deployment. Conversely, chloramphenicol did not prevent algal colonisation for the 14- and 21-days deployments. However, for deployments longer than 14 days, it was difficult to obtain consistently good results for all of anti-biofilm agents tested, due to the high concentration of suspended matter in the freshwater effluents of the fish farms tested. This approach suggests a metal pre-treatment of the membrane filters is useful to prevent biofilm formation for DGT deployments aimed at P measurements. DGT deployments for metal measurements would likely require a different approach.
© 2006 Elsevier B.V. All rights reserved.

Keywords: Phosphorus; Phosphate; Aquaculture; DGT; In situ measurement; Biofilm; Anti-biofilm agent; Filters

1. Introduction

The DGT technique is an in situ method for measuring labile species in water, soils and sediments [1–5]. It directly integrates actual concentrations in the field, and with built-in preconcentration there is a reduced risk of contaminating the samples before their analysis in the laboratory. The DGT device consists of two gel layers, the diffusive polyacrylamide gel and the binding layer, which is made using a gel impregnated with Chelex for metals or with Fe-oxide for phosphorus [5]. On the top of those two gel layers, there is a polysulfone membrane to minimize particles sticking to the surface. The labile species, reactive

phosphate in this case, passes through the filter and the diffusive gel and is then bound by the binding layer (Fe-oxide). The mass of the phosphorus collected by the Fe-oxide-gel can be related to the solution concentration of phosphorus according to Eq. (1).

$$C = \frac{M \, \Delta g}{D t A} \tag{1}$$

All symbols are described in Table 1. The mass of phosphorus is calculated after elution of the Fe-oxide-gel according to Eq. (2).

$$M = \frac{C_e(V_g + V_e)}{f_e} \tag{2}$$

It is important that the diffusion of reactive phosphorus is not impeded by fouling films. For long deployment periods in

---

Table 1
Parameters for the equations of the DGT techniques [3]

Parameters	Units	Description
C	$\mu g\,P\,L^{-1}$	Concentration of the reactive phosphorus species in the bulk solution
M	ng	Mass of P in the resin
Δg	cm	Diffusion layer thickness
D	$cm^2\,s^{-1}$	Diffusion coefficient in diffusion gel
T	s	Deployment time
A	cm^2	Surface area of binding layer
C_e	$\mu g\,P\,L^{-1}$	Concentration of P in the elution solution
V_g	mL	Volume of the binding gel
V_e	mL	Volume of H_2SO_4 added to the binding gel for the extraction
f_e	Dimensionless	Elution factor

waters containing high concentrations of phosphorus and suspended matter, a surface film is likely to appear on the DGT filter and potentially affect the diffusion pathway. This surface film can be formed by algae growing on the filter, thus generating a biofilm, or it can result from the adhesion of suspended sediment particles onto the filter. As the sediment particles contain micro-organisms, they can encourage the growth of algae on the surface of the filter. The aim of this study was to reduce the growth of algae to enable deployment of DGT devices for longer periods.

Most exposed surfaces in natural water are colonized by micro-organisms in biofilms, including DGT device surfaces. The characteristics of biofilms vary widely and depend on their environment. Several studies have shown that biofilm growth does not afford any additional bacterial resistance against metal toxicity [6–8]. Biofilm formation can be a nuisance in many diverse applications and several approaches have been investigated to eliminate them. Trace metals have also been shown to be useful as antimicrobials and disinfectants in recent medical and industrial anti-biofilm applications [8]. Harrison et al. [6] compared the effects of pharmaceutical antibiotics and various metals on biofilm formation. According to these studies, the trace metals most effective at preventing biofilm formation are silver, mercury and copper. The effectiveness of the metal depends on the tolerance of the bacterial community in the biofilm. Biofilm bacteria have also be shown to have a 10- to 100-fold increased tolerance to antibiotics relative to their tolerance to trace metals [7,9]. Several antibiotics have been tried for various types of microbial communities that form biofilms; their effectiveness varies according to the tolerance of the biofilm to the antibiotic. Microbial populations in drinking water are commonly controlled by chlorination, using free chlorine or monochloramines [10,11]. Alternatively, bismuth thiols have been suggested for the elimination of biofilms in drinking water [12,13]. Similarly to copper and silver ions, the bismuth thiols show more persistent residual effects on biofilm control than chlorine and hyper heating. Many of those approaches introduce compounds into the water that would potentially be toxic and difficult to apply within the context of freshwater aquaculture.

In this work, concerned with the prevention of algal growth on DGT devices, the algaecide potential of silver and copper and two antibiotics, chloramphenicol and glutaraldehyde was investigated. Two alternative types of filter, a nucleopore membrane and a silver membrane (SKC, Eighty Four, PA, USA), were also tested for their potential to prevent the formation of biofilms. The potential interference of these reagents on the phosphorus determinations was investigated, and DGT performance was tested in natural water, i.e., directly in fish farms ponds. The addition of high concentrations of metals on the filter surfaces has a significant potential to interact with P, which could lead to sorption or precipitation of metal-phosphate mineral phases. Our objectives are to evaluate the efficiency of the various agents tested to prevent biofilm development and to determine whether the anti-biofilm agents interfere with the diffusion properties of the gels.

2. Experimental

2.1. Antibiotic solutions

Chloramphenicol (Sigma) solutions were prepared in double-distilled water at concentrations of 10, 5, 2 and 0.5 mM and glutaraldehyde (Sigma) solutions were prepared at concentrations of 5, 3, 1 and 0.5 M. They were stored in polyethylene (PE) bottles at 4 °C. The filters and diffusive gel discs were soaked in the solutions for a minimum of 24 h.

2.2. Metal solutions

Silver nitrate ($AgNO_3$), copper nitrate ($CuNO_3$) and potassium iodide (KI) were obtained from Fisher Scientific (UK and Canada). All metal solutions were made up in double-distilled water and stored in PE bottles at 20 °C. Filters were immersed in 0.01 M solutions of silver nitrate and copper nitrate for a minimum of 24 h, with shaking throughout this period. Filters were then transferred into a 0.1 M potassium iodide solution and shaken for a minimum of 24 h. Cu^{2+} and Ag^+ ions react with iodide to form solid phase AgI and CuI_2 in the filter.

2.3. Preparation of DGT devices

The diffusive gel and oxide-gel were made identically to the DGT Research Ltd. method (Zhang et al. [1]). Briefly, the diffusive gel was made with a polyacrylamide gel solution comprising 15% (v/v) acrylamide and 0.3% (v/v) cross-linker. To initiate polymerisation, 10% (w/v) ammonium persulfate (70 μL) and 20 μL of TEMED catalyst were added to 10 mL of the polyacrylamide gel solution. The solution was immediately pipetted between two glass plates separated by plastic spacers and then incubated at 42 ± 2 °C for 45 min. After hydration and copious washing, the thickness of the diffusive gel discs was 0.80 mm.

The oxide-gel is a binding layer of gel impregnated with iron oxide. It was formed with 3 g of ferrihydrite slurried into 10 mL of gel solution. Then the same casting procedure as for the diffusive gel was used. The thickness of the hydrated oxide-gel was 0.60 mm.

The standard piston-type DGT devices were used. The flat face of the piston receives in sequence, a disc of oxide-gel, a
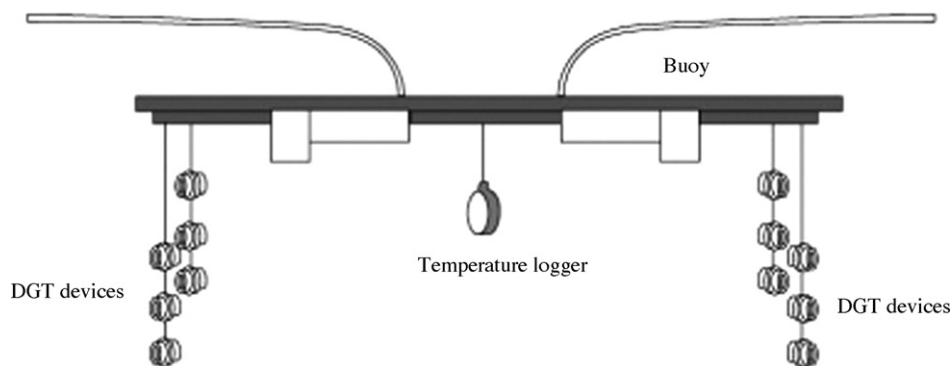
Fig. 1. DGT station set-up.

disc of diffusive gel and a polysulfone filter membrane (0.45 μm pore size). The tightly fitting plastic cap had an exposure window of 3.14 cm^2 that allowed contact of the membrane with the solution. The filter membranes, treated with the various anti-biofilm agents, and the antibiotics in the diffusive gel, were tested alongside normal filters (controls with no agent).

2.4. Tests on the DGT response

DGT measurements in the laboratory were made in well-stirred KH$_2$PO$_4$ (200 μg P L^{-1}) solutions (2 L) at constant temperature (20 ± 1 °C). For all tests, each type of DGT device was deployed in triplicate and a minimum of two DGT control devices without any anti-biofilm agent were deployed in the same solution as the other DGT devices.

The reactive phosphorus collected by the oxide-gel resin was eluted with 0.25 M H$_2$SO$_4$ acid and measured spectrophotometrically (Cecil CE 1011) using the phosphomolybdenum blue method. The detection limit is around 0.002 mg P L^{-1} and we used a 100% elution efficiency [1].

In the initial tests, the DGT devices were deployed for 4 h in KH$_2$PO$_4$ solution (200 μg P L^{-1}) at pH 6. To study the effect of pH variations, the immersion solution was adjusted with dilute (∼0.01 M) NaOH or HCl in the pH range 3–7.5. The effect of ionic strength was investigated by adjusting the KH$_2$PO$_4$ (200 μg P L^{-1}) solutions with either NaNO$_3$ or NaCl, with final Na concentrations ranging from 1×10^{-4} to 0.5 M. All deployments for a given solution were analysed within a single batch.

2.5. Deployment in spiked water

We obtained a nutrient-rich water by increasing P to about 100 μg L^{-1} in an aquarium by adding KH$_2$PO$_4$ to 10 L of natural water collected from Lake Carter (Lancaster University, Lancaster, UK). Triplicate DGT devices with different types of anti-biofilm agents were deployed in the aquarium for 20 days; (1) CuI$_2$, (2) AgI, (3) nucleopore membranes and (4) controls with normal polysulfone filter membranes.

2.6. Deployment in fish farm waters

Deployments lasting up to 21 days were made in ponds operated as freshwater fish farms in Lancashire, UK. Triplicate DGT

devices, comprising controls and devices treated with silver, copper and chloramphenicol were used. The DGT station set-up is illustrated in Fig. 1. DGT devices were attached with a fishing line to a buoy that maintained them all at a depth of 0.1–0.2 m. To record the temperature, a data logger (StowAway Tidbit) was attached to the buoy for the duration of the deployment. During the 21-days assay, the four types of DGT devices were also deployed in triplicate for 4, 7 and 14 days. At each deployment and retrieval of the DGT devices, water samples were collected into 100-mL PE bottles and the temperature was recorded. The mass of biofilm material that collected on the membranes was estimated by weighing unused membranes and those from the deployments (all dried at 85 °C).

3. Results and discussion

3.1. Test in synthetic solutions

To maintain the measurement capabilities of DGT, the anti-biofilm agent must not modify the properties of the binding gel or affect the transport of phosphate across the cellulose nitrate membrane and the diffusive gel. DGT measurements in a solution of 200 μg P L^{-1} showed that one of the two antibiotics, glutaraldehyde, changed the properties of the diffusive gel by reducing its thickness by 14 ± 2%. Furthermore, glutaraldehyde interferes with the colorimetric determination of phosphorus by introducing an absorbance at a wavelength of 882 nm, preventing us from quantifying the response. As it was not possible to measure phosphorus correctly with the phosphomolybdene blue method in the presence of this antibiotic, it was not used in further trials.

The response of DGT devices impregnated with the anti-biofilm agents were tested for a range of pH and ionic strengths (Fig. 2). Statistical treatment of the results was undertaken using the software SPSS 11.5. for Windows. The variance analysis used the Hukey post hoc test. Only devices containing the silver salt showed any effects associated with the concentration of ions in solution. All other measurements were unaffected by pH and ionic strength. For the control devices this agrees with the previous findings of Zhang et al. [1]. For devices with the silver treatment, we measured a smaller concentration than in the control DGT device at pH 3, 6 and 7.5 and for all the solutions where NaCl was added. In all these solutions, the DGT measurement
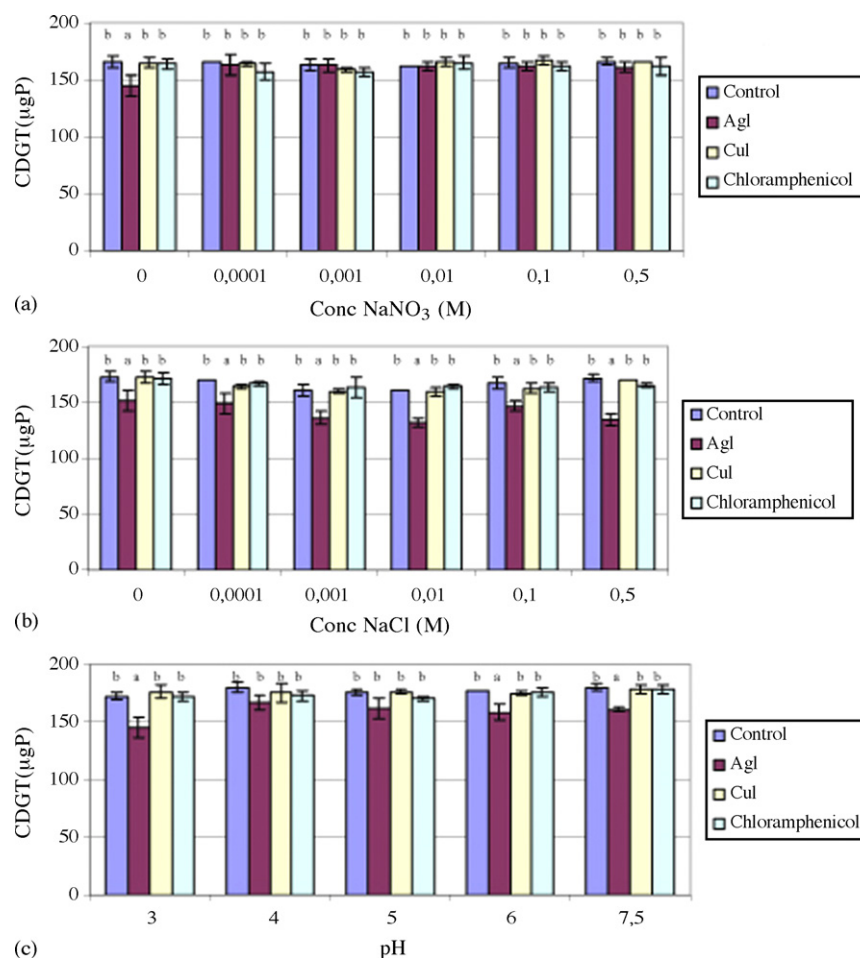
Fig. 2. The mass of P accumulated by the DGT devices when exposed to phosphate solutions containing different concentrations of NaNO$_3$ (a) and NaCl (b) and solutions at different pH (c). Bars represent the mean and standard deviation of three replicates; means followed by the same letter are not statistically different (Tukey's B post hoc test $p > 0.05$).

was suppressed to a similar extent ($14 \pm 3\%$). For the pH 4 and 5 solutions, the measurements were not significantly different from the response of the control DGT devices. Moreover, when NaNO$_3$ was added, there was no apparent effect attributable to the presence of the silver salt. These results suggest that the interaction of Ag and chloride ions may affect the DGT response. We could speculate that a mineral form or ternary precipitate combines Ag, Cl and P thus retaining P and hindering its diffusion but, there is no mechanistic evidence for this. As the introduction of copper and chloramphenicol did not adversely affect the DGT performance, it is reasonable to deploy DGT devices with these anti-biofilm agents in both acid and circumneutral natural waters. Moreover, even the devices containing silver would not be expected to have large errors.

3.2. Tests in natural water spiked with phosphate

An algal layer developed on the control polysulfone membranes as well as on the nucleopore membranes of the DGT devices deployed in the aquarium for 20 days (Fig. 3). The nucleopore membrane is a smooth sheet of polycarbonate with regular holes while the polysulfone membrane consists of a mat of fibres. This textural difference between the membranes does

not prevent the formation of algae on their surfaces. No algal growth was observed on the polysulfone membranes containing copper or silver iodide. The toxicity of these two metals seems to prevent the growth of the algae on the surface of the filters.

3.3. In situ DGT measurements in fish farms

To evaluate the performance of the anti-biofilm agents in the field, DGT devices were deployed in situ in the ponds of two fish farms in Lancashire (UK): Bentham Trout Farm and Bank House. They contained high concentrations of suspended matter and between 10 and 40 $\mu g\,P\,L^{-1}$ of reactive phosphorus. The suspended matter, which was higher in Bentham Trout Farm, was composed of excess fish food, feces and other particles coming from resuspended sediments.

Two distinct types of deposits developed, representing algal growth and adhesion of suspended material. The algal biofilms were visible on devices deployed for 14 and 21 days and were more pronounced on the DGT devices deployed in the Bentham Trout farm (Fig. 4). Table 2 shows the mass of algal growth on the surface of cellulose nitrate membranes illustrated in Fig. 4. Silver iodide appeared to be most effective at preventing biofilm formation, as the mass that accumulated is least in this case. It
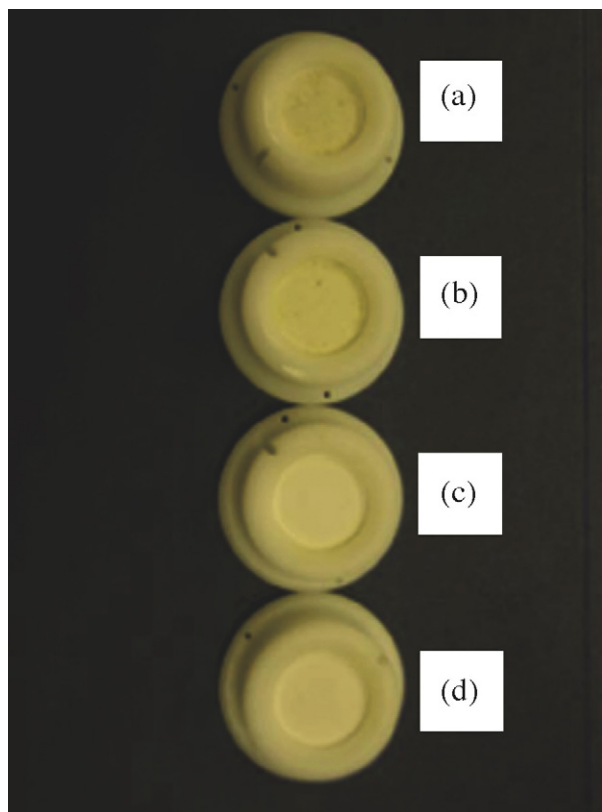
Fig. 3. DGT devices deployed for 20 days in the aquarium with $100\,\mu g\,P\,L^{-1}$. DGT devices with (a) normal cellulose nitrate membranes, (b) nucleopore membranes, (c) cellulose nitrate membranes containing silver iodide and (d) cellulose nitrate membranes containing copper iodide.

Table 2
Mass (mg) of algae accumulated on the filter membranes after deployment in the two fish farms tested.

Deployment time (days)	DGT control	DGT AgI	DGT CuI$_2$	DGT chloramphenicol
Bentham Trout Farm				
4	0.0	0.6	0.3	1.2
7	0.9	0.1	1.4	0.0
14	28.8	1.1	8.8	15.8
21	39.1	8.2	29.6	30.4
Bank House				
4	1.6	1.8	0.6	1.4
7	1.8	1.6	0.3	1.5
14	24.5	1.4	15.9	8.6
21	28.3	8.5	27.9	26.5

for the Bentham Trout Farm where these deposits were much more pronounced after 21 days of deployment.

The concentrations of phosphorus measured by the four different types of DGT devices, C_{DGT}, were compared for each fish farm and are shown in Fig. 6. For the two fisheries, we obtain a generally higher concentrations measured by DGT for the first 4 days, because we directly measured concentrations in water change with the time. Indeed, the concentrations of phosphorus in water were higher at the beginning of the deployment and they decreased after 4 days of the deployment. Deployments of 7 and 14 days in both fish farms showed similar C_{DGT} for all the DGT devices. After 21 days C_{DGT} was higher for devices treated with AgI than the other devices. Thus the incorporation of a biocide does not appear to have affected the results until 14 days, but for 21 days the silver iodide biocide increased the response. It appears that the biofilm that grows on the surface of the filter membrane in both fish farms prevents the reactive phosphorus from passing through the filter at 21 days.

A silver membrane filter was investigated to prevent biofilm formation. This filter is made of pure metallic silver (99.97%) with 0.45-μm pore size and used to replace the usual membrane filter of the DGT device. Three DGT devices with the silver membrane were deployed in Chartierville and Artabaska fishfarms (Québec, Canada) along with three DGT devices con-

clearly suppressed the growth of algae for up to 21 days. While there was some evidence that both copper iodide and chloramphenicol limited the growth of algae on the surface of filters up to 14 days, there were minimal effects after 21 days. For deployment times less than 7 days in these fish farm waters there appears to be no problem due to algal growth, even for DGT devices without biocides. The deposits on the filter membranes due to the adhesion of suspended material are illustrated in Fig. 5 for devices retrieved after 14 and 21 days, particularly
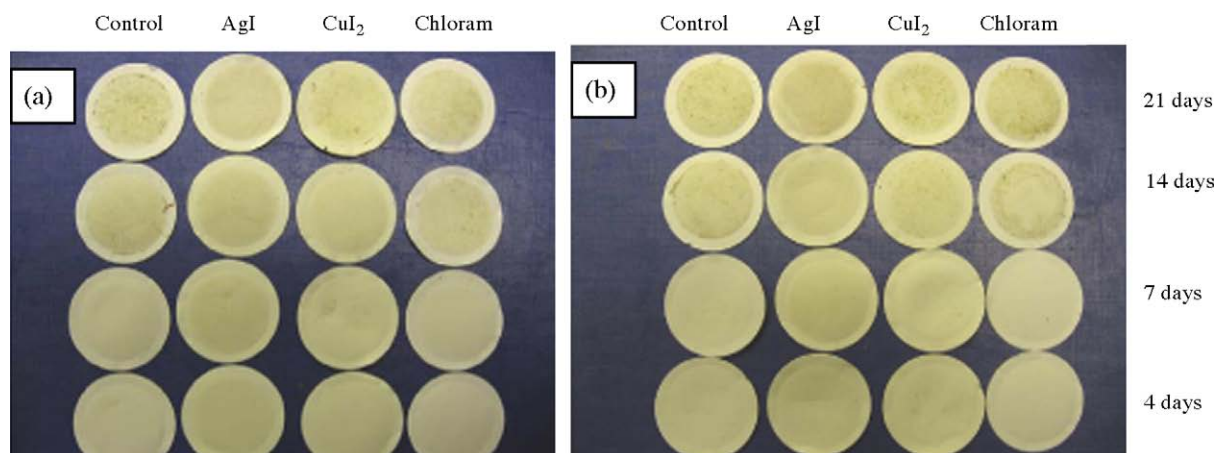

Fig. 4. Growth of algae on filter membrane after deployment in fish farms. (a) Deployment in Bentham Trout Farm. (b) Deployment in Bank House.
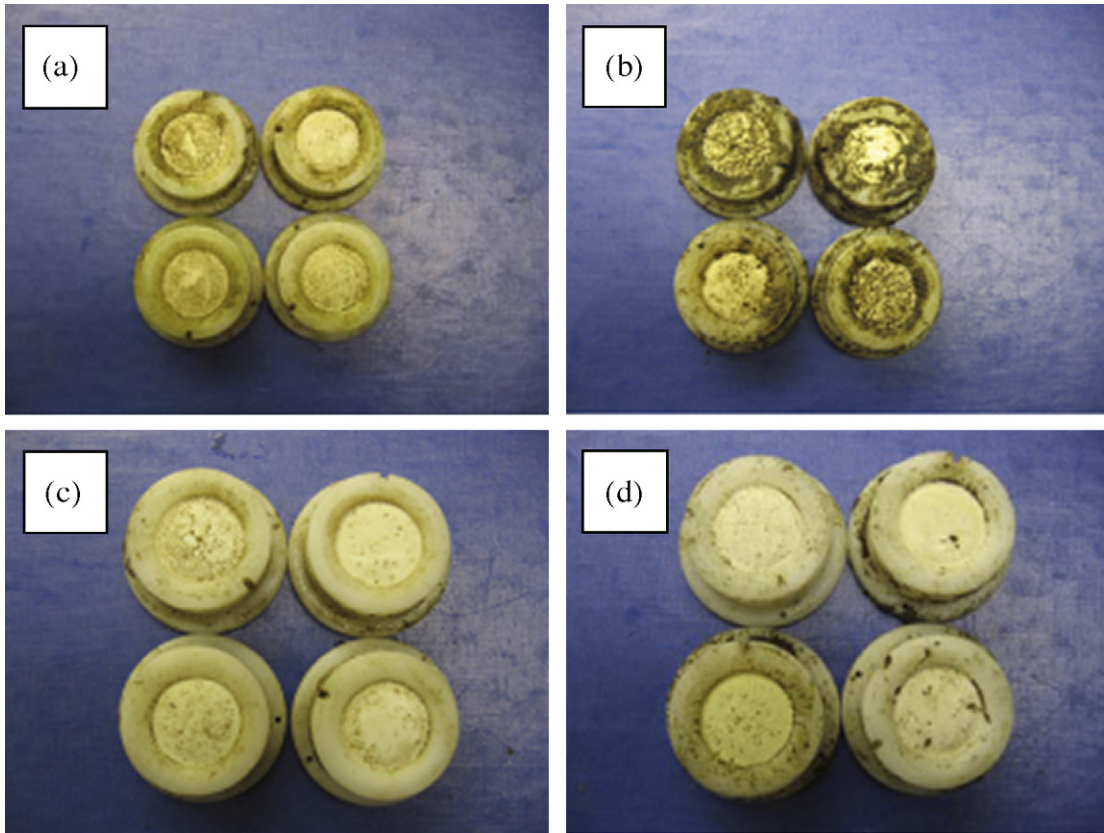
Fig. 5. Adhesion of suspended materials on DGT devices after deployment in fish farms. Deployments were: (a) 14 days in Bentham Trout Farm, (b) 21 days in Bentham Trout Farm, (c) 14 days in Bank House and (d) 21 days in Bank House. For all pictures, the top left device of the picture is the DGT control, the right top device is the DGT with copper iodide, the bottom left device is the DGT with silver iodide and the bottom right device is the DGT with chloramphenicol.
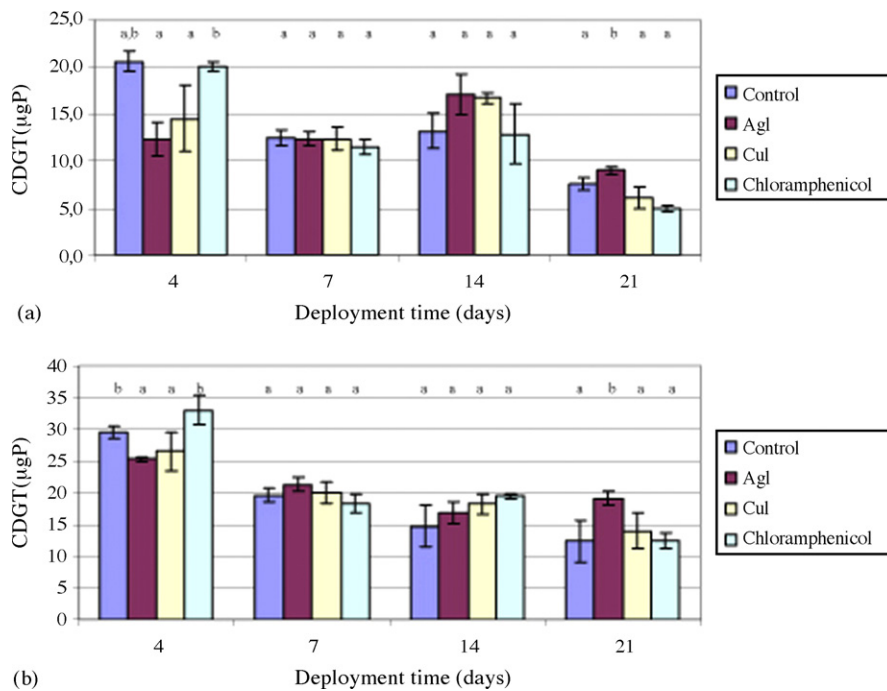

Fig. 6. Concentration of phosphorus measured by DGT devices, C_{DGT}, for each deployment (a) Bentham Trout farm and (b) Bank House farm. Bars represent the mean response of three replicates; means followed by the same letter are not statistically different (Tukey's B post hoc test $p > 0.05$).

Table 3
Concentration of reactive phosphorus (μg P L^{-1}) measured with three different types of DGT devices in two fisheries at Québec, Canada

Deployment time (h)	C_{DGT} control	C_{DGT} Ag	C_{DGT} CuI$_2$
Chartierville			
12	40 ± 3	88 ± 1	41 ± 1
24	38 ± 3	58 ± 10	36 ± 2
48	38 ± 1	36 ± 4	42 ± 8
Artabaska			
12	116 ± 2	175 ± 74	115 ± 1
24	108 ± 1	98 ± 8	102 ± 9
48	94 ± 2	79 ± 8	91 ± 1

taining a control treatment (standard DGT) and a CuI$_2$-treated polysulfone membrane. Table 3 shows the result obtained during a 48-h deployment in the two fisheries. We observed that the responses of the devices treated with CuI$_2$ were close to the control devices. However, the responses obtained by the DGT with the silver membrane were variable. Indeed, it seems that there is a phosphorus contamination originating from the silver membrane filter and for short deployment times (less than 24 h), the values were higher than the control. This problem does not appear for 48 h deployments, but this is probably due to a conteracting artefact reducing diffusion across the gel, i.e., following the deployment of the DGT devices, the silver membrane filter tarnished and the diffusive and binding gels became red and more elastic. Given those difficulties, no further tests were made using the silver membrane filters.

4. Conclusion

This study has demonstrated that it is possible to prevent algal biofilm formation on the surfaces of DGT devices using different anti-biofilm agents. Laboratory tests on solutions spanning a range of pH and ionic strengths showed that the mass of P accumulated by DGT devices containing copper iodide and chloramphenicol was similar to that accumulated by control DGT devices in all solutions. It might still be pertinent to test for pH effects for applications in alkaline waters above pH 7.5. The presence of silver iodide in the diffusive gel and filter membrane reduced the amount of phosphorus accumulated by up to 14% in some solutions, particularly those containing chloride ions. Variations in pH (3–7.5) and ionic strength did not affect the response of the DGT devices with the different anti-biofilm agents.

Deployments in the laboratory in a natural water spiked with phosphate and in situ in fish farms showed that silver iodide was most effective at preventing algal growth. Both copper iodide and chloramphenicol were partially effective in preventing the formation of algae. For deployments longer than 14 days in the fish farm waters, the major problem was the adherence of suspended material to the membrane surface.

For the long deployment periods of DGT devices in freshwater containing a high concentration of nutrients that promote algal growth, the addition of copper or silver iodide to the membrane filters will help to prevent the formation of algae on the surface of polysulfone membrane. These two metals appear to be more effective than antibiotics in limiting algal growth in this environment. While silver iodide seems to be more effective than copper iodide, there is some evidence that it may affect the DGT measurement, whereas copper iodide does not appear to interfere with the DGT measurements. Unfortunately, a copper treatment is very likely to interfere with metal measurements and deployments of DGT units for metal measurements would require a different approach.

Acknowledgements

References

[1] H. Zhang, W. Davison, R. Gadi, T. Kobayashi, Anal. Chim. Acta 370 (1998) 29–38.
[2] N. Odzak, D. Kistler, H. Xue, L. Sigg, Aquat. Sci. 64 (2002) 292–299.
[3] S. Alcock, D. Barcelo, P.-D. Hansen, Biosens. Bioelectron. 18 (2003) 1077–1083.
[4] J. Rachou, W. Hendershot, S. Sauvé, Commun. Soil Sci. Plant Anal. 35 (2004) 2655–2673.
[5] H. Zhang, W. Davison, Anal. Chem. 67 (1995) 3391–3400.
[6] J.J. Harrison, J.T. Raymond, C. Howard, BMC Microbiol. 5 (2005) 53.
[7] J.J. Harrison, C. Howard, C.A. Stremick, R. Turner, J. Environ. Microbiol. 6 (2004) 1220–1227.
[8] C. Geslin, J. Llanos, D. Prieur, C. Jeanthon, Res. Microbiol. 152 (2001) 901–905.
[9] M.E. Olson, C. Howard, D.W. Morck, A.G. Buret, R.R. Read, Can. J. Vet. Res. 66 (2002) 86–92.
[10] P.S. Stewart, J. Rayner, F. Roe, W.M. Rees, J. Appl. Microbiol. 91 (2001) 525–532.
[11] A.K. Camper, Int. J. Food Microbiol. 92 (2004) 355–364.
[12] F. Codony, J. Morato, F. Ribas, J. Mas, J. Basic Microbiol. 42 (2002) 311–319.
[13] F. Codony, P. Domenico, J. Mas, J. Appl. Microbiol. 95 (2003) 288–293.

Determination of trace arsenic on hanging copper amalgam drop electrode

Robert Piech [*], Bogusław Baś, Ewa Niewiara, Władysław W. Kubiak [*]

Faculty of Materials Science and Ceramics, AGH University of Science and Technology, 30-059 Krakow, Poland

Abstract

Hanging copper amalgam drop electrode has been applied for trace determination of arsenic by cathodic stripping analysis. Detection limit for As(III) as low as 0.33 nM (0.02 µg/L) at deposition time (240 s) could be obtained. For seven successive determinations of As(III) at concentration of 5 nM relative standard deviation was 2.5% ($n = 7$). Interferences from selected metals and surfactant substances were examined. Absence of copper ions in sample solution causes easier optimization and makes method less vulnerable on contamination. The developed method was validated by analysis of certified reference materials (CRMs) and applied to arsenic determinations in natural water samples.
© 2006 Elsevier B.V. All rights reserved.

Keywords: Trace analysis; Arsenic determination; Hanging copper amalgam drop electrode; Differential pulse cathodic stripping voltammetry
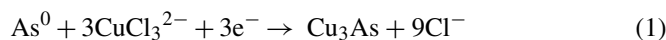
1. Introduction

The most of arsenic forms and compounds are very toxic and cancerogenic. Arsenic toxicity depends on its speciation, i.e. compounds of As(III) are much more toxic than compounds of As(V). Inorganic compounds of arsenic are more toxic than organic. Considering the very low concentration limits of arsenic acceptable in the environment, drinking water, food and similar products. The ultra trace analytical methods which allow speciation are required. Unfortunately, most of analytical methods for determination of arsenic are troublesome, unsensitive and their detection limits are not satisfactory. Methods such as inductively coupled plasma-mass spectrometry (ICP-MS) and graphite furnace atomic absorption spectrometry (GFAAS) give favorable detection limits for elemental analysis but fail in speciation. Cathodic stripping voltammetric method of arsenic(III) determination in presence of copper which has been introduced by Henze et al. [1] seems to be suitable for this task. Other voltammetric methods for arsenic determination and speciation have been also applied [2–7]. Recently Piech and Kubiak [8] described variation of H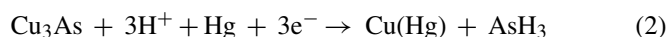enze method in which ligand sodium diethyldithiocarbamate is added to supporting electrolyte. It allows to lower detection limit approximately one order of magnitude.

Determination of arsenic(III) by cathodic stripping voltammetry (CSV) in presence of copper allows reaching level of concentration even below 1 nM. Arsenic determination in these conditions depends on the several factors such as: copper concentration, time, deposition potential, concentration of supporting electrolyte and its pH. They were studied by Kowalska and Golimowski [9,10]. The transport conditions during the deposition step on determination of trace arsenic by CSV have also very strong influence. This aspect had been studied by Piech et al. [11]. Electrochemistry of the system has been studied by Li and Smart [12]. They showed mechanism of reaction taking place at the mercury electrode in 2 M hydrochloric acid containing copper(II) ions:

Deposition:

$$As^0 + 3CuCl_3{}^{2-} + 3e^- \rightarrow Cu_3As + 9Cl^- \tag{1}$$

Stripping:

$$Cu_3As + 3H^+ + Hg + 3e^- \rightarrow Cu(Hg) + AsH_3 \tag{2}$$

The use of voltammetry for arsenic determination seems to be very promising because of its ability to perform speciation

* Corresponding authors. Tel.: +48 12 6172473; fax: +48 12 6341201.
E-mail addresses: rpiech@agh.edu.pl (R. Piech), kubiak@agh.edu.pl (W.W. Kubiak).

analysis. Arsenic(V) is considered to be electrochemically inactive. In order to determine arsenic(V) the chemical reduction to As(III) must be performed. Several substances may be used as arsenic(V) reducing agents. Among them are ascorbic acid and potassium iodide [13], sodium thiosulfate [14], sodium sulfite [15,16], hydrazine [12], aqueous sulfur dioxide [17], sodium bisulfite [18] and sodium *meta*-bisulfite/sodium thiosulfate stabilized with ascorbic acid [19]. Other voltammetric methods of arsenic(V) determination utilize D-mannitol [20,21].

In CSV arsenic determination the most promising supporting electrolyte is HCl in the concentration range from 0.1 to 7 M. Good results were obtained using H_2SO_4 alone [13,22] or in the presence of D-mannitol [21]. Other possibility includes mixture of $NaClO_4$–NaCl and D-mannitol for the determination of As(V) [20]. Profumo et al. [23] applied HBr as an alternative to HCl as a supporting electrolyte. Determination of arsenic is usually preformed at hanging mercury drop electrodes and their variations such as static mercury drop electrode (SMDE) [24], controlled growth mercury drop electrode (CGMDE) [25]. Generally in stripping voltammetry besides mercury drop electrodes are applied film electrodes and sometimes amalgam electrodes. As yet such electrodes were not applied for arsenic determination. General characteristics of the copper-based mercury film electrode were described by Donten and Kublik [26]. They showed optimal conditions for preparation, storage, conditioning and renewal of copper-based mercury film electrode (CBMFEs). In next work [27], they described application of such mercury film electrode in cathodic stripping voltammetry for the determination of thiocyanate, tryptophane, cysteine and benzotriazole. Glodowski et al. [28] described the determination of traces of purine by cathodic stripping voltammetry at the hanging copper amalgam drop electrode.

In this work, the determination of trace arsenic(III) was carried out using differential pulse cathodic stripping voltammetry (DPCSV) at the hanging copper amalgam electrode. The proposed method is easily optimized due to the absence of copper ions in the supporting electrolyte. This method may be used for determination of As(V) after chemical reduction to As(III). Thus, speciation of arsenic may be performed. Method was tested with CRM's obtaining good agreement with the certified values.

2. Experimental

2.1. Apparatus

Multipurpose Electrochemical Analyzer EA9 (model M161) with the electrode stand M164 (both MTM-ANKO, Poland) were used for all voltammetric measurements. The standard three-electrode cell consisted of a hanging copper amalgam drop electrode (HCADE) as working, Ag/AgCl in 3 M KCl with additional electrolytic key filled with 3 M KCl (Mineral, Poland) as reference and platinum wire as an auxiliary electrodes.

Voltammograms were recorded, interpreted and stored by EAGRAPH (MTM-ANKO, Poland) software.

2.2. Reagents

Sodium arsenide (Merck CAS: 7784-46-5) was of analytical grade, HCl used was selected from several high purity products and production series to have extremely low arsenic and selenium contents (below 0.15 and 0.1 nM, respectively). The best selected for this was HCl produced by Cheman, Poland (serial number 18/05/05 CAS: 7647-01-0). Certified Reference Materials (tobacco leaves (CTA-OTL-1) from Institute of Nuclear Chemistry and Technology, Poland; and river sediment (CRM 320) from Commission of the European Communities, Community Bureau of References) were used as delivered.

Copper of high purity was obtained from faculty of Non-Ferrous Metals, AGH. Content of selenium, arsenic, lead and cadmium was checked by stripping voltammetry method to be below detection limit.

All solutions were prepared with double-distilled water.

2.3. Copper amalgam preparation

The copper amalgam was prepared by sinking three copper wires (size: 1 mm diameter, 10 mm long) in 1 mL of mercury (for analysis, Merck CAS: 7-45-60-61) for at least 1 month. In that time amalgam was often mixed (several times each day). Before preparation copper wires were carefully cleaned and activated with HNO_3 1:1 and next rinsed with double-distilled water and dried. The wires were transferred into eppendorf vessel. Next 1 mL of mercury was added and vessel was hermetically closed. The wires were immerse completely in mercury for whole time necessary to obtain the copper amalgam. The process was carried out at room temperature. Next the copper amalgam was filtered, transferred to glass vessel, hermetically closed and stored at room temperature for further work.

2.4. Sample preparation

For determination of arsenic in references materials the microwave digestion was carried out. About 250 mg of samples (river sediment, CRM 320; Tobacco leaves, CTA-OTL-1) was weighted into Teflon vessel and 4 mL of HNO_3 was added. Next vessel was placed in microwave oven. Digestion of the samples was carried out under following program: 15 min 90% microwave power, 10 min cooling time, 5 waiting time (repeated twice). After digestion samples were heated to evaporate and to remove nitrate. Next samples were quantitatively transferred into volumetric flask (10 mL) and diluted to the mark with double-distilled water.

For determination of arsenic in water from Dunajec River a 100 mL of the sample was taken directly into especially prepared polyethylene bottle (volume 100 mL). Before sampling polyethylene bottle was cleaned with concentrated hydrochloric acid, next conditioned during 1 week with 1:100 hydrochloric acid and finally rinsed with double-distilled water. To the 8 mL of the sample taken from the bottle was added 2 mL of concentrated hydrochloric acid to obtain final concentration of 2 M and volume 10 mL. Next measurements were performed according procedure described in next section.

2.5. Procedure

The day before measurements the electrodes and voltammetric cell were conditioned in double-distilled water. Immediately before measurements electrodes and voltammetric cell were rinsed with distilled water. The voltammetric cell was filled with 10 mL of 2 M hydrochloric acid. The solution was stirred for 30 min. Next solution was removed from the cell and new solution of the same composition was introduced and purged with argon gas for at least 15 min. Finally 5 μL of 10 μM As(III) was added (final concentration 5 nM) for optimization study.

All measurements were made using cathodic stripping voltammetry in differential pulse mode during the stripping step. The following parameters were adjusted: pulse amplitude −50 mV; step height 4 mV; probing and waiting time 20 ms; resting time 5 s; drop size 0.7 mm^2; stirring rate 640 rpm; stirring bar, fleamicro (Aldrich). The deposition potential and deposition time have been varied depending on the experiment. The voltammograms were recorded in the potential range of −0.500 to −0.860 V.

3. Results and discussion

3.1. Hanging copper amalgam drop electrode

The determination of arsenic(III) by CSV method usually involves presence of copper ions in supporting electrolyte which in deposition step are reduced on working electrode. Copper is necessary to form copper arsenide which is the base of arsenic determination. Presence of copper ions in supporting electrolyte causes troublesome optimization of the method. Thus, elimination of copper from the supporting electrolyte should be attractive variation of this method. The alternative source of copper may be electrode itself. However, usage of copper wire or copper deposited at solid electrodes in anodic stripping voltammetry (ASV) gives no satisfactory signal from arsenic. The best possibility is application of copper amalgam which may be used in hanging mercury drop electrode assembly. Such hanging copper amalgam drop electrode may be used to obtain signal from copper arsenide reduction (Fig. 1). The obtained arsenic(III) peaks are shift to the more positive potential about 0.04 V (peak potential −0.69 V) in comparison with Henze method as recently described [11]. Very good reproducibility for this electrode (each measurement performed at fresh copper amalgam drop) R.S.D. = 2.5% (for $n = 7$) were obtained. Other parameters of method such as sensitivity, detection limit are very similar as in Henze method [11,12]. Influence of hydrodynamics conditions on determination at HCADE is similar to other stripping systems, i.e. peak current is linearly dependent on square root of stirring rate. There is no such maximum as observed in Henze method [11].

3.2. Influence of the deposition potential on arsenic(III) peak

Optimal potential for arsenic(III) determination is in range from −0.375 to −0.425 V (Fig. 2A). Outside that range peak
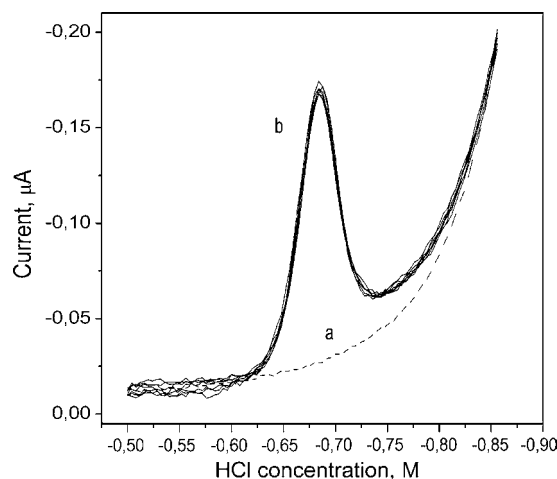

Fig. 1. Background current (a) and DPCSV voltammograms of 5 nM arsenic(III) (b) in 2 M HCl in the potential range from −0.5 to −0.86 V. Stirring rate 640 rpm, deposition potential −0.4 V and deposition time 60 s. Flea micro stirring bar.

drops almost completely. In the same time arsenic peak potential is strongly dependent on deposition potential. It changes monotonically from −0.645 V (at deposition potential −0.3 V) to −0.724 V (at deposition potential −0.5 V) (Fig. 2B). If deposition potential is low (from −0.3 to −0.375 V) and As(III) concentration higher than 3 nM smaller peak at lower potential appears. Probably due to underpotential deposition phenomena or different stoichiometry of electrode reaction [12]. That smaller peak is not utilized analytically in this work. To avoid its presence deposition should be held at potential lower than −0.38 V.

3.3. Influence of HCl concentration on DPCSV arsenic(III) signal

Determination of arsenic in the presence of copper ions by CSV method requires acidic medium. As has been shown previously [8] the best results are obtained using hydrochloric acid.
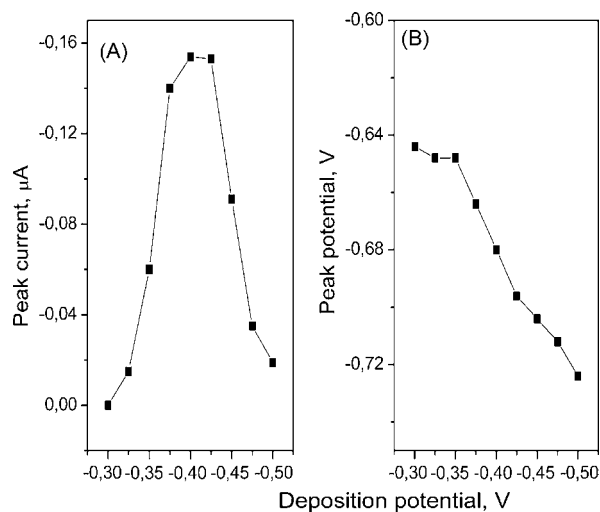

Fig. 2. Dependence of 5 nM arsenic(III) peak current (A) and its potential (B) on deposition potential in the range from −0.3 to −0.5 V in 2 M HCl, deposition time 60 s.
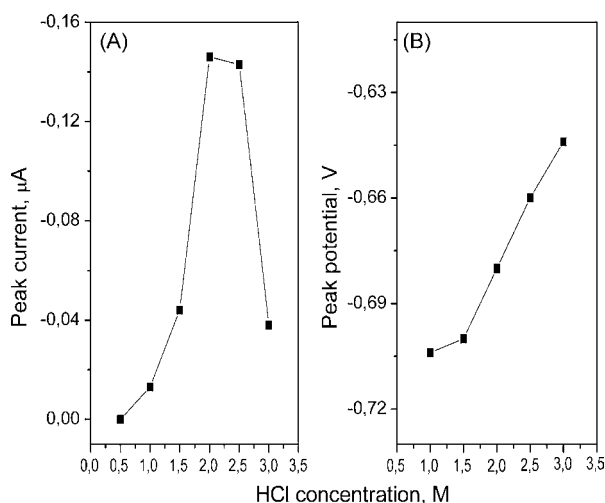
Fig. 3. Dependence of 5 nM arsenic(III) peak current (A) and its potential (B) on concentration of HCl in the range from 0.5 to 3 M. Deposition potential −0.4 V, deposition time 60 s.
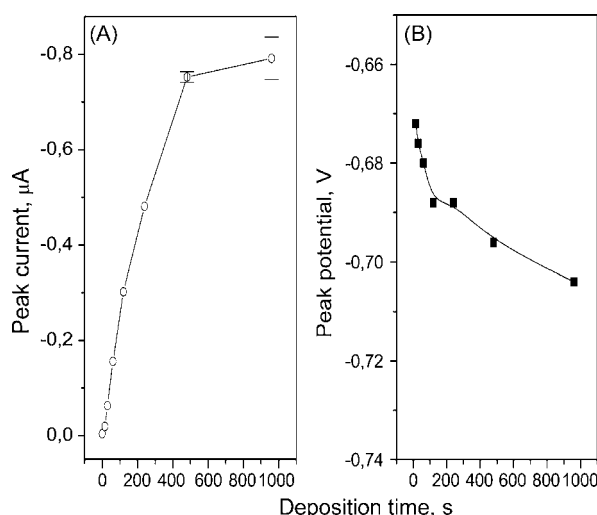

Fig. 4. Dependence of 5 nM arsenic(III) peak current (A) and its potential (B) on deposition time in the range from 0 to 1000 s in 2 M HCl. Deposition potential −0.4 V.

The arsenic peak current and potential depend strongly on HCl concentrations. Fig. 3A presented dependence of peak current on HCl concentration. For 0.5 M HCl practically no arsenic peak was observed. For higher hydrochloric acid concentrations signal growths reaching maximal value for 2–2.5 M HCl. Further increase of acid concentration cause decrease of arsenic peak and formation of second peak at more negative potential. The second peak current increase with increasing of the HCl concentration. Concentrations of HCl also influence the peak potential which changed monotonically to the more positive values (Fig. 3B). The best results are obtained for 2 M HCl. The peak potential is then −0.680 V (versus Ag/AgCl/3 M KCl reference).

3.4. Influence of deposition time

The deposition time is always important factor in stripping voltammetric analysis because of its prevailing influence on sensitivity and detection limit of the method. In case of cathodic stripping voltammetry of arsenic in the presence of copper ions the deposition time is even more important because of decrease the arsenic peak for long deposition time [8,12]. The changes of magnitude of arsenic peak current and peak potential versus deposition time are presented in Fig. 4A and B, respectively. Peak current increase with growth deposition time from 0 μA (deposition time 0 s) to −0.8 μA (for deposition time 16 min). For long deposition time (i.e. above 6 min) growth of the peak current is insignificant. Thus, application of deposition time longer than 5 min is purposeless. Increase of deposition time shifts peak potential to the more negative values. For deposition time of 15 s peak potential was −0.672 V and for 16 min peak potential was −0.704 V. Dependence of peak current on deposition time on amalgam electrode is more similar to other stripping method, not like determination of As(III) on mercury electrode in presence of copper ions in solution [11,12]. In the latter case observed is maximum which cause necessity of optimization of the deposition time. Unfortunately, even in this case described

in this paper usage of long deposition time is restricted because of increase of background current and distortion of arsenic(III) peak.

3.5. Interferences

As was shown elsewhere [8] strong interferences for arsenic determination originates from selenium(IV), tellurium(IV) and surface-active substances. Selenium(IV) is known [11,12] as a strong interferent in arsenic determinations by CSV method in the presence of copper ions. Selenium(IV) may be determined in similar conditions using CSV method in presence of copper. The dependence of selenium ions concentration on arsenic stripping signal is showed in Fig. 5A. It was observed that for concentration of selenium ions below 0.5 nM the peak current for arsenic(III) increase. Larger concentrations of selenium ions
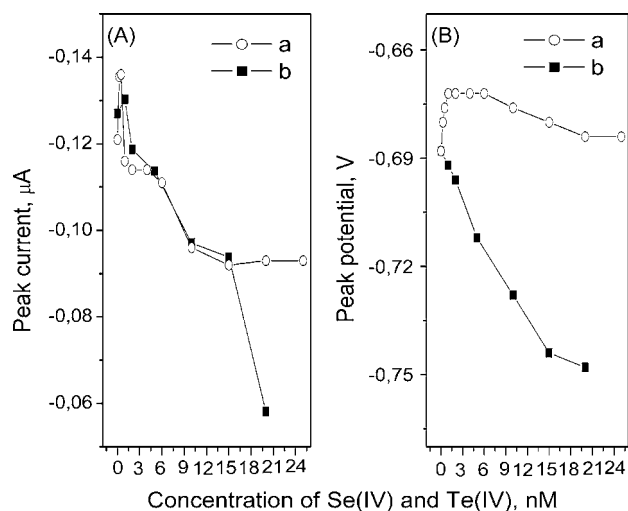

Fig. 5. Dependence of 5 nM arsenic(III) peak current (A) and its potential (B) on Se(IV) (a) and Te(IV) (b) concentration in the range from 0 to 25 nM in 2 M HCl. Deposition potential −0.4 V, deposition time 60 s.
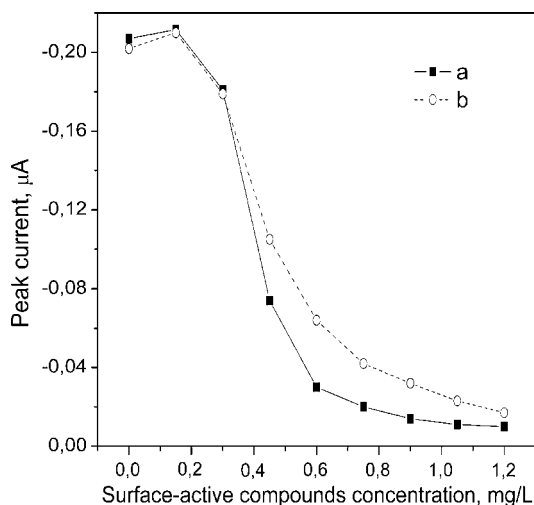
Fig. 6. Dependence of 5 nM arsenic(III) peak current in 2 M HCl for Triton X-100 (a) and SDS (b) concentrations respectively, equal: 0; 0.15; 0.30; 0.45; 0.60; 0.75; 0.90; 1.05; 1.20 mg/L. Deposition potential −0.4 V, deposition time 60 s.
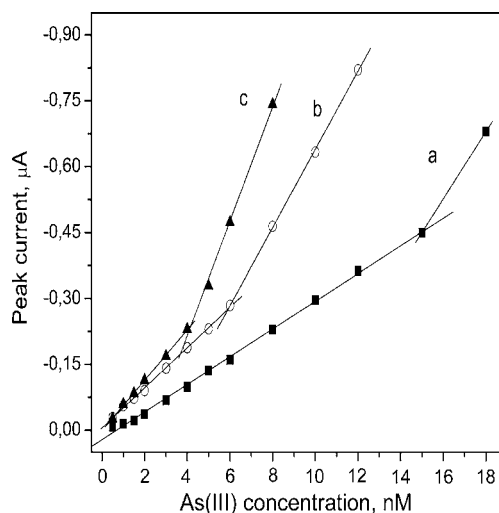

Fig. 7. The changes of DPCSV arsenic(III) peak current in concentration range 0.5–20 nM in 2 M HCl for deposition time: (a) 60 s (deposition potential −0.4 V), (b) 120 s (deposition potential −0.4 V) and (c) 240 s (deposition potential −0.425 V).

cause decrease of arsenic(III) signal. For three-fold excess of selenium arsenic signal decrease 30%. Higher concentration of selenium ions have no further influence on As(III) peak current. Selenium ions also influenced arsenic peak potential. When the concentration of selenium(IV) is below 6 nM arsenic peak shifts to the positive values from −0.688 V (for Se(IV) = 0 nM) to −0.672 V (for Se(IV) = 6 nM). For higher selenium concentrations arsenic peak shifts to the more negative potentials (for Se(IV) = 25 nM observed arsenic peak potential was −0.684 V). Influence of selenium(IV) in case of copper amalgam electrode is much smaller than in case of mercury electrode with copper in solution [11].

Presence of tellurium(IV) ions cause decrease of arsenic peak current and shift of peak potential to the more negative values. For 20 nM Te(IV) a 2.3-fold decrease peak current was observed. Peak potential changed from −0.688 V (for Te(IV) = 0 nM) to −0.748 V (for Te(IV) = 20 nM). Additionally, the presence of tellurium ions causes a significant background current increase. The changes of arsenic signal versus concentrations of Te(IV) ions are showed in Fig. 5.

The surface-active compounds usually give interferences in cathodic stripping voltammetric methods. In the work non-ionic surface-active compound (Triton X-100) and anionic surface-active compound (sodium dodecyl sulfate (SDS)) were checked. The results show that the stripping peaks of arsenic would significantly decrease in the addition of both Triton X-100 and SDS into the supporting electrolytes (Fig. 6). For concentration Triton

X-100 and SDS on the level 1.2 mg/L observed arsenic signals are almost completely suppressed.

3.6. Analytical performance

Dependences of the peak current as a function arsenic(III) concentration at different deposition potentials are shown in Fig. 7. Obtained calibration curves consist of two parts with different slopes. Concentration at which slope changes depends on deposition time. At short deposition time (60 s) obtained detection limit is 0.45 nM and linearity is up to 15 nM. Longer deposition time causes shorter linearity range but better detection limit. For example, for deposition time 120 s linearity was up to 6 nM and detection limit 0.4 nM. Increasing deposition time above 120 s cause distortion of arsenic signal. However, distortions may be reduced by usage of lower deposition potential, i.e. −0.4 V. In each case correlation coefficients are very good, i.e. 0.999. Slope for low concentrations are −0.0315 ± 0.0004 [μA/nM]; −0.0458 ± 0.0008 [μA/nM]; −0.0575 ± 0.0007 [μA/nM] for deposition time 60 s; 120 and 240 s, respectively.

Analysis of Certified Reference Materials river sediment, CRM 320 and tobacco leaves CTA-OTL-1 were performed. Obtained results are in very good agreement with certified values [Table 1]. Very low detection limit makes possible the arsenic determination in natural water. Arsenic(V) was determined after reduction to arsenic(III) using sodium thiosulfate [14].

Table 1
Determination of arsenic in several samples (procedure described in Section 2)

Sample	As(III)	As(V)	As$_{tot}$	Remarks
River sediment: CRM 320 (n = 6)	<0.04 μg/L	76 ± 3 mg/L	76 ± 3 mg/L	Certified value: 77 ± 3 mg/L
Tobacco leaves: CTA-OTL-1 (n = 6)	<0.04 μg/L	0.6 ± 0.1 mg/L	0.6 ± 0.1 mg/L	Certified value: 0.5 ± 0.1 mg/L
Dunajec River Added As(III): 0.37 μg/L	0.63 ± 0.03 μg/L	0.10 ± 0.04 μg/L	0.73 ± 0.02 μg/L 1.07 ± 0.06 μg/L (Found)	– Recovery: 97 ± 6%

4. Conclusion

Described method allows to determine arsenic at trace level as low as 0.33 nM (0.02 μg/L) for deposition time 240 s. Reproducibility of the method is very good, i.e. measured as relative standard deviation is 2.5% (each measurement performed at fresh copper amalgam drop). In comparison to Henze method determination of As(III) by the proposed method is easier to optimize due to absence of copper ions in supporting electrolyte. Method was validated with certified reference materials and may be used for determination and speciation of arsenic in natural waters.

Acknowledgement

References

[1] G. Henze, A.P. Joshi, R. Neeb, Fresenius J. Anal. Chem. 300 (1980) 267.
[2] G. Forsberg, J.W. O'Laughlin, R.G. Megargle, Anal. Chem. 47 (1975) 1586.
[3] P.H. Davis, G.R. Dulude, R.M. Griffin, W.R. Matson, E.W. Zink, Anal. Chem. 50 (1978) 137.
[4] S. Jaya, T. Prasada Rao, G. Prabhakara Rao, Talanta 34 (1987) 574.
[5] D.G. Williams, D.C. Johnson, Anal. Chem. 64 (1992) 1785.
[6] L. Chiang, B.D. James, R.J. Magee, Mikrochim. Acta, II (1989) 149.
[7] J. Zima, C.M.G. Van Den Berg, Anal. Chim. Acta 289 (1994) 291.
[8] R. Piech, W.W. Kubiak, J. Electroanal. Chem. 599 (2007) 59.
[9] J. Kowalska, J. Golimowski, Electroanalysis 10 (1998) 857.
[10] J. Kowalska, J. Golimowski, E. Kazimierska, Electroanalysis 13 (2001) 872.
[11] R. Piech, W.W. Kubiak, J. Golas, Pol. J. Chem. 78 (2004) 1667.
[12] H. Li, R.B. Smart, Anal. Chim. Acta 325 (1996) 25.
[13] J. Kowalska, E. Stryjewska, P. Szymański, J. Golimowski, Electroanalysis 11 (1999) 1301.
[14] M.A. Ferreira, A.A. Barros, Anal. Chim. Acta 495 (2002) 151.
[15] R. Feeney, S.P. Kounaves, Talanta 58 (2002) 23.
[16] S.B. Rasul, A.K.M. Munir, Z.A. Hossain, A.H. Khan, M. Alauddin, A. Hussam, Talanta 58 (2002) 33.
[17] F.T. Henry, T.M. Thorpe, Anal. Chem. 52 (1980) 80.
[18] F.T. Henry, T.O. Kirch, T.M. Thorpe, Anal. Chem. 51 (1979) 215.
[19] Y. He, Y. Zheng, M. Ramnaraine, D.C. Locke, Anal. Chim. Acta 511 (2004) 55.
[20] U. Greulach, G. Henze, Anal. Chim. Acta 306 (1995) 217.
[21] G. Henze, W. Wagner, S. Sander, Fresenius J. Anal. Chem. 358 (1997) 741.
[22] W. Holak, Anal. Chem. 52 (1980) 2189.
[23] A. Profumo, D. Merli, M. Pasavento, Anal. Chim. Acta 539 (2005) 245.
[24] J.J. Vogel, J. Electroanal. Chem. 8 (1964) 82.
[25] Z. Kowalski, J. Osteryoung, US Patent 4,846,955 (1989).
[26] M. Donten, Z. Kublik, J. Electroanal. Chem. 196 (1985) 275.
[27] M. Donten, Z. Kublik, Anal. Chim. Acta 185 (1986) 209.
[28] S. Glodowski, R. Bilewicz, Z. Kublik, Anal. Chim. Acta 186 (1986) 39.

ELSEVIER

Organically modified sols as pseudostationary phases for microchip electrophoresis

Martin Pumera [a],[*], Joseph Wang [b],[**], Eli Grushka [c],[**], Ovadia Lev [d],[**]

[a] *ICYS, National Institute for Materials Science, 1-1 Namiki, Tsukuba 305-0044, Japan*
[b] *Departments of Chemical and Materials Engineering and Chemistry and Biochemistry, Arizona State University, Tempe, AZ 85287, USA*
[c] *Department of Inorganic and Analytical Chemistry, The Hebrew University, Jerusalem 91904, Israel*
[d] *Graduate School of Applied Sciences, The Hebrew University, Jerusalem 91904, Israel*

Abstract

We demonstrate that the selectivity of microchip electrophoresis separations is greatly improved by the presence of organically modified silica (Ormosil) sols in the run buffer. A negatively-charged *N*-(trimethoxysilylpropyl)ethylenediamine triacetic-acid (TETT)-based sol is used for improving the selectivity between nitroaromatic explosives and a methyltrimethoxysilane (MTMOS)-based sol is employed for enhancing the microchip separation of environmental pollutants, aminophenols. These sols are added to the run buffer and act as pseudostationary phases. Their presence in the run buffer changes the apparent mobility of studied solutes, and leads to a higher resolution. The observed mobilities changes reflect the interactions between the Ormosil sols and the solutes. Relevant experimental variables have been characterized and optimized. The diverse chemistry of Ormosil sols should be extremely useful for tailoring the selectivity of a wide range of electrophoresis microchip separations.
© 2006 Elsevier B.V. All rights reserved.

Keywords: Microchip capillary electrokinetic chromatography; Ormosil; Explosives; Environmental pollutants

1. Introduction

Lab-on-a-chip devices have experienced an explosive growth since their introduction [1–3]. Such microscale devices represent the ability to shrink the conventional analytical systems with major advantages of high-throughput, portability, automation, solvent/reagent economy, integration and cost. Particular attention has been given to microchip-based capillary electrophoresis [4]. While offering remarkable separation efficiency (with up to a million theoretical plates) [5], there are major needs for controlling and manipulating the separation selectivity of electrophoresis microchips. Such tailoring of the separation selectivity has been accomplished through control of the microchannel surface chemistry or by the presence of additives in the run buffer [6]. The affinity of sample solutes to a micellar pseudostationary phase [7], to gold nanoparticle additives [8] or

to *n*-octyl [9] or octadecyl [10] surface coatings has thus been exploited for tuning the separation selectivity.

This paper reports on the use of organically modified (Ormosil) sols for manipulating the separation selectivity in electrophoresis microchips. The use of silica sol as run buffer additives is analogous to the use of sol–gel derived materials in conventional packed-capillary electrokinetic chromatography (PCEC) [11–13] and of micelles in micellar electrokinetic chromatography (MEKC) [14]. Fujimoto and Muranaka employed commercially available silica gel nanoparticles as run buffer additives in conventional CE systems [15]. Silica-based polymer particles [16] and polymeric surfactants based on linear-chain silicone (polydimethylsiloxane) backbones [17,18] were used as pseudostationary phases in conventional electrokinetic chromatography. Collins and co-workers recently prepared CEC column using sol–gels prepared from methyltrimethoxysilane for separation of explosives [19]. Neiman et al. [20] reported on the use of several Ormosil sols for enhancing the separation of aromatic acids and nitrobenzenes in conventional CE systems.

To the best of our knowledge, sols have not been used as run buffer additives in microchip electrophoresis systems. The rich and diverse chemistry of Ormosil sols opens the door for a wide

---

* Corresponding author. Tel.: +81 29 851 3354/8816; fax: +81 29 860 4706.
** Corresponding authors.
E-mail addresses: pumera.martin@nims.go.jp (M. Pumera),
joseph.wang@asu.edu (J. Wang), eliga@chem.ch.huji.ac.il (E. Grushka).

range of sol–solute interactions and hence selectivity manipulations in electrophoresis microchips. Such tailoring is illustrated in following sections in connection to TETT and MTMOS-based separations of neutral nitroaromatic explosives [21] and positively charged aminophenols [22], respectively.

2. Experimental

2.1. Reagents

Stock solutions (1000 ppm) of 2,4,6-trinitrotoluene (TNT) and 1,3-dinitrobenzene (DNB) were received from Cerilliant (Austin, TX). Sodium phosphate monobasic, sodium phosphate dibasic and phosphoric acid and *o*- and *p*-aminophenols were purchased from Aldrich. The sol precursors, methyltrimethoxysilane (MTMOS) and *N*-(trimethoxysilylpropyl)ethylenediamine triacetic-acid, trisodium salt (TETT) were obtained from Gelest (Tullytown, PA). Sodium hydroxide was obtained from Sigma. The gold atomic absorption standard solution (1000 mg/L Au(III)/0.1 M HCl) was received from Aldrich. All chemicals were used without any further purification. The phosphate run buffer was prepared by adjusting the pH of the 40 mM sodium phosphate monobasic solution to 3.5 with concentrated (15 M) phosphoric acid. The phosphate run buffer (pH 10.1) solution was prepared by titrating 40 mM sodium phosphate dibasic with 1 M sodium hydroxide. Both phosphate buffers contained 13% (v/v) of methanol.

2.2. Apparatus

Details of the integrated electrophoresis glass chip/detection microsystem were described previously [23]. A Plexiglas holder was fabricated for holding the separation chip and housing the detector and reservoirs. The microchip received from Micralyne (model MC-BF4-SC, Edmonton, Canada), consisted of two crossed channels with a half-circle cross section and three reservoirs, including four-way injection cross. The separation channel was 80 mm long, 20 μm deep and 50 μm wide. The thick-film working electrode [23] was placed opposite to the channel outlet, at 60 μm distance (controlled by a plastic screw and a thin-layer spacer). The thick-film carbon electrodes were printed with a semi-automatic printer (model TF 100, MPM, Franklin, MA) using the Acheson ink (Electrodag 440B; Acheson Colloids, Ontario, CA). Gold plated thick-film electrodes were prepared according to previously described procedure [24,25].

2.3. Preparation of organically modified sols

Silica sols were prepared by mixing different concentrations of silane precursors with 40 mM phosphate buffer (initial pH of 3.5), containing 13% (v/v) methanol. (The latter served as homogenization agent; it should be noted that the actual percentage of methanol in the run buffer containing silanes exceeded 13% (v/v) since methanol was generated during sol formation). The solutions were sonicated for 5 min and refrigerated for 1 week, during which the polymerization process proceeded. At the end of this period the solutions were ready for use as run buffers. The concentrations of silane precursors were relatively low (up to about 1.4 M), hence the polymerization process was completed at the stage of the sol formation [20]. After mixing with the silane precursor the pH of TETT solutions increased to 8.0 or 10.1 (in connection with TETT concentrations of 35 or 175–350 mM) due to the presence of sodium salt of weak carboxyl functionality. The pH of the MTMOS solution did not change and remained at 3.5.

The different sol solutions used in this study were obtained by appropriate dilutions of the sol reaction solutions. Due to the polydispersity of the sols, their actual solution concentrations cannot be determined accurately. The concentration values given throughout this paper are thus based on the original monomeric concentrations. The buffers used for sample preparation did not contain the sols, and their pH was identical to that of the run buffer.
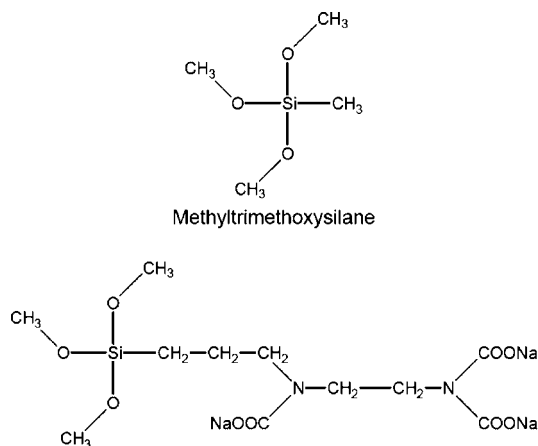
2.4. Electrophoresis procedure

The channels of the glass chip were treated before use by rinsing with 0.1 M NaOH and deionized water for 10 and 5 min, respectively. The run buffer and unused reservoirs were filled with the electrophoresis run buffer solution, while the sample reservoir was filled with a mixture of nitroaromatic explosives or aminophenols (in the 40 mM phosphate buffer, pH 10.1 or 3.5, respectively). After an initial loading of the sample in the injection channel, the sample was injected by applying a potential +1500 V between the sample reservoir and the grounded detection reservoir. This drove the sample "plug" into the separation channel through the intersection. By switching the high-voltage contacts, the separation potential was subsequently applied to the run buffer reservoir with the detection reservoir grounded and all other reservoirs floating for the separation of the analytes. Catechol was used as an electroosmotic flow marker in the MTMOS sol modified run buffer.

2.5. Amperometric detection

The electropherograms were recorded with a time resolution of 0.1 s while the detection potential (usually +0.8 and –0.5 V versus Ag/AgCl wire for the aminophenols and nitroaromatic explosives, respectively) was applied. Sample injections were performed after stabilization of the baseline. All experiments were performed at room temperature.
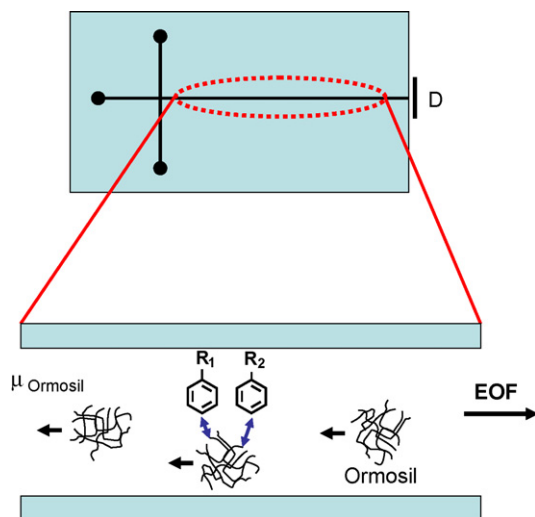
3. Results and discussion

The addition of organically modified silica (Ormosil) sols to the CE run buffer provides interaction sites for solutes and hence adds another separation vector to the orthogonal electrophoretic vector. The coexistence of these two vectors results in selectivity changes that are highly beneficial to the separation process. Changes in the sol chemistry can have a profound effect upon the sol–solute interactions and hence on the resulting selectivity. Such selectivity improvements are illustrated here using sols based on the negatively-charged *N*-

Scheme 1. Structural formulas of Ormosil sol precursors used in present study.

Fig. 1. Electrophoregrams showing the separation of 15 ppm TNT (a) and DNB (b) in the presence of different concentrations of the TETT sol in the phosphate run buffer (40 mM, pH 10.1): 0 (A), 35 (B), 175 (C) and 350 (D) mM TETT. The inset shows the influence of TETT sol concentration upon the resolution of TNT and DNB. Conditions: sample injection at +1500 V for 3 s; separation voltage, +1500 V; detection at −0.5 V using a screen-printed bare carbon electrode.

(trimethoxysilylpropyl)ethylenediamine triacetic-acid (TETT) or neutral methyltrimethoxysilane (Scheme 1) in connection to microchip separations of nitroaromatic explosives and aminophenols, respectively. Proposed separation mechanism is described in Scheme 2.

For example, Fig. 1 shows electrophoregrams for a mixture of the nitroaromatic explosives TNT (a) and DNB (b) in the absence (trace A) and presence (traces B–D) of a negatively-charged TETT sol. As expected, no resolution of the neutral explosives is observed in the untreated buffer (40 mM phosphate buffer, 13% (v/v) methanol, pH 10.1). In contrast, well-defined, baseline-resolved peaks are observed with the sol-containing run buffers. Increasing the TETT concentration in the run buffer results in increased observed selectivity (α_{obs}) between DNB and TNT (from 1.08 to 1.38 between 35 and 350 mM TETT). The resolution between the two explosives changes from 0 to 3.01 upon raising the TETT concentration from 0 to 175 mM, and decreased slightly at higher TETT levels (Fig. 1, inset).

A similar control of the migration properties is illustrated in Fig. 2 in connection to the presence of MTMOS and the separation of aminophenols. This figure displays electropherograms for a mixture of aminophenols obtained with an unmodified run

Scheme 2. Schematics of Ormosil sol–solute interactions in microfluidic channel. The neutral explosives interact with negatively-charged TETT sol and are they are separated based on their different partitioning between the TETT sol and running buffer. The positively charged aminophenols interact with neutral MTMOS sol and they are separated based on their different partitioning between the MTMOS sol and running buffer. Unlike micellar additives that require a minimum surfactant concentration, such concentration limitation does not exist for Ormosil sol running buffer additives. The diverse chemistry of Ormosil sols is extremely useful for tailoring the selectivity of a range of electrophoresis microchip separations.
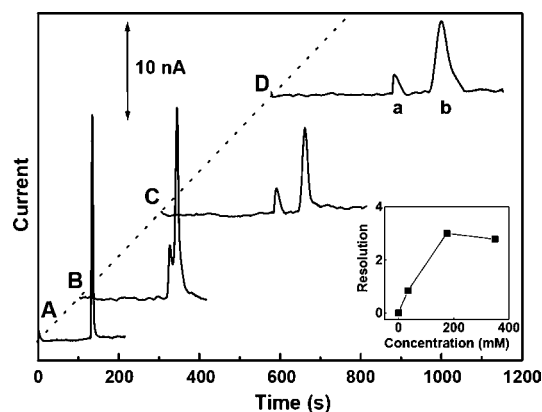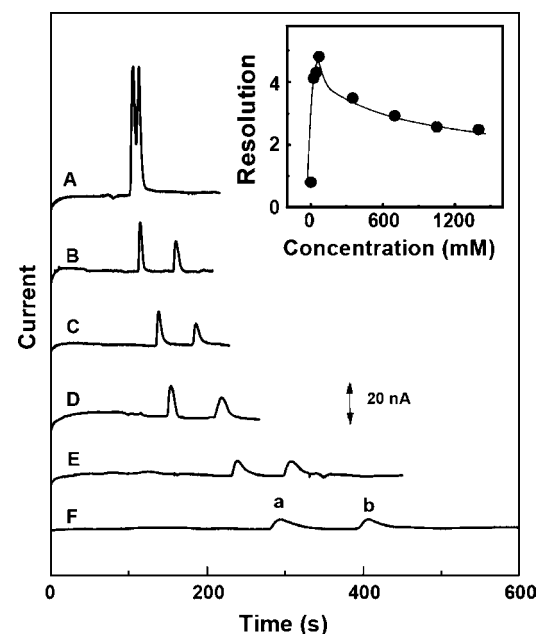

Fig. 2. Electrophoregrams showing the separations of 1 mM *p*-aminophenol (a) and *o*-aminophenol (b) in the presence of different concentrations of MTMOS in the phosphate (40 mM, pH 3.5) run buffer: 0 (A), 70 (B), 350 (C), 700 (D), 1050 (E) and 1400 (F) mM MTMOS. The inset shows the influence of the MTMOS sol concentration upon the resolution of *p*- and *o*-aminophenol. Conditions: sample injection at +1500 V for 3 s; separation voltage, +1500 V; detection at +0.8 V using a gold-coated screen-printed carbon electrode.

buffer (trace A) and using the MTMOS sol-modified run buffer (traces B–F), in connection to a separation voltage +1500 V. A dramatic increase in the selectivity, and therefore in the resolution, is observed in the presence of the sol additive. The resolution between *p*- and *o*-aminophenols in the untreated run buffer is 0.8. The resolution increases to a maximum value 4.81 upon raising the MTMOS concentration to 70 mM and decreases gradually (to 2.48) between 70 and 1400 mM MTMOS (see inset). However, the higher resolution is achieved at the cost of a longer (3.5 min) analysis time, as compared to 2.5 min with the untreated run buffer.

The data of Fig. 2 indicate that the combination of changes in the electroosmotic mobility and the apparent mobilities of the solutes results in a greatly improved resolution. Such changes in the mobilities in the presence of the Ormosil reflect the effective interaction of the solutes with the surface of the sol additive. Fig. 3 shows the effect of the concentration of the MTMOS sol additive upon the apparent mobilities of *p*- and *o*-aminophenol. The μ_{app} of *p*-aminophenol (trace a) decreases gradually (from 2.38×10^{-4} to 0.40×10^{-4} cm^2/V s) upon raising the MTMOS concentration from 0 to 1400 mM; the μ_{app} of *o*-aminophenol (trace b) decreases initially rapidly (from 2.13×10^{-4} to 1.28×10^{-4} cm^2/V s) upon increasing the MTMOS concentration from 0 to 23 mM and more slowly (from 1.28×10^{-4} to 0.07×10^{-4} cm^2/V s) at higher MTMOS concentrations. These data indicate that the *ortho* isomer has a larger partition coefficient and 'spend' more time in the neutral MTMOS sol than the *para* isomer. Apparently, aromatic solutes with two functional groups, in *ortho* position, form hydrogen bonds with the MTMOS sol and interact stronger with the sol then *para* isomer. A similar effect was observed by Neiman et
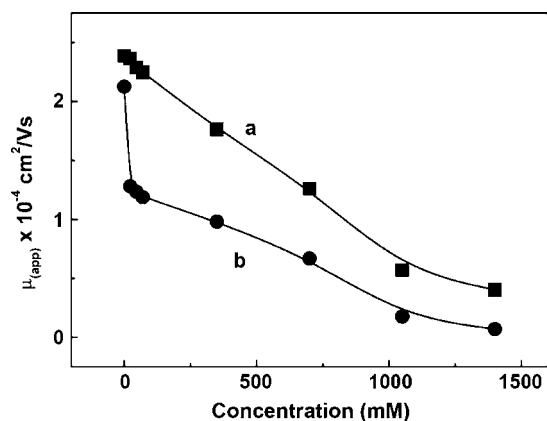

Fig. 3. Influence of the MTMOS sol concentration upon the apparent mobilities of *p*-aminophenol (a) and *o*-aminophenol (b). Other conditions, as in Fig. 2.

al. [20] and Wang et al. [12]. The formation of hydrogen bonds was suggested as a partial explanation of the observed migration pattern. Overall, the different profiles (of Fig. 3) allow the selection of the optimal sol concentration for a given pair of solutes. Their different solute interactions with the sol additive thus form the basis for the enhanced selectivity reported in this study.

The voltage applied to the separation channels affects the performance of the Ormosil sol-enhanced electrophoresis microchip. Fig. 4 shows the influence of the separation voltage on the resolution between *para* and *ortho* aminophenols (panel A), and on the separation efficiency (panel B) in the absence (a) and presence (b) of MTMOS sol. Both profiles clearly indicate that the MTMOS-based buffer leads to improved performance compared to the unmodified phosphate buffer (a versus b). The
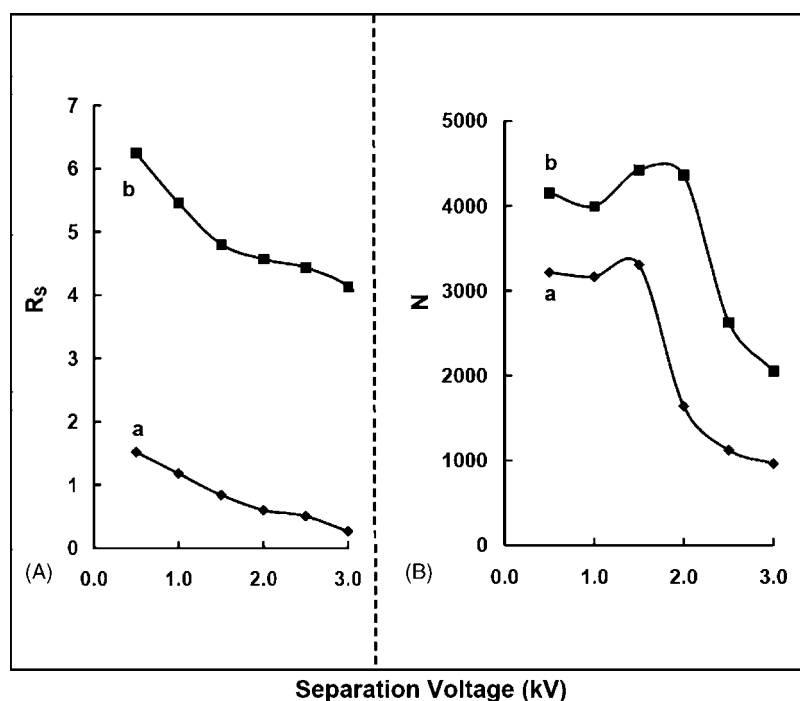

Fig. 4. Influence of the separation voltage on the resolution of *p*- and *o*-aminophenol (A) and upon the number of theoretical plates for *o*-aminophenol (B), using phosphate run buffer (40 mM; pH 3.5) without (a) and with (b) MTMOS sol (70 mM). Other conditions, as in Fig. 2.

resolution and the plate number in the sol-treated run buffer are higher than those observed with the untreated buffer. For example, R_s values ranging from 4.3 to 6.3 are observed with the sol-containing buffer, as compared to 0.2–1.6 in the absence of the sol. In both media, the plate number varies slightly with the applied potential until +1500 V and decreases thereafter. While one would expect increased number of plates at higher voltages, other factors (such as end-column broadening and incomplete isolation of detection system and Joule heating) apparently dominate the efficiency at voltages higher than +1500 V.

The influence of the sol additive upon the detection process should be also considered. We compared hydrodynamic voltammograms (HDV) at the carbon thick-film detector for the reduction of TNT using unmodified and TETT-modified (175 mM) phosphate run buffers (pH 10.1). The curves were recorded pointwise by making 100 mV changes in the applied potential over the 0.0 to −0.8 V range using the separation voltage +1500 V. Both buffers display similar sigmoidal profiles, with the TNT wave starting at −0.1 V and leveling off at −0.4 V. The half-wave potentials are −0.12 and −0.08 V. It is important to note that there is 60% decrease of the maximum current in the presence of TETT sol. Such decrease indicates a slower rate of mass transport associated with a smaller diffusion coefficient in the sol-modified buffer and can poses drawback in applications where the low detection limits are crucial; however, it is also important to underline that separation selectivity strongly improves in presence of Ormosil sol. Subsequent amperometric detection work on explosives employed a detection potential of −0.5 V that offered the most favorable signal-to-noise characteristics. Limit of detection (LOD) of TNT was found to be about 50 ppb in Ormosil sol-free buffer, which is coherent with previously published study [26] and LOD of TNT was found to be about 120 ppb in TETT sol-modified running buffer. Microchip assays based on sol-containing run buffers are characterized with linear calibration curves. For example, using the MTMOS system, *p*- and *o*-aminophenol yielded linear calibration plots over the 50–300 μM concentration range with sensitivities of 35.9 and 30.3 nA/mM, respectively (correlation coefficients, 0.9993 and 0.9995). This demonstrates that even thought our microfluidic device uses electrochemical detector, which is in contact with the solution, the addition of Ormosil sols does not have negative effect on linearity of response of the detector. Furthermore, such good linearity is coupled to good reproducibility. A series of six repetitive injections of a mixture containing 200 μM *p*- and *o*-aminophenol resulted in reproducible peak currents, with relative standard deviations of 2.72 and 3.16%, respectively. Good day-to-day reproducibility was also obtained (e.g., R.S.D. of 3.51 and 6.00% for *p*- and *o*-aminophenol; *n* = 3). Moreover, the sols were found to be quite stable upon storage at +4 °C with run buffer lifetimes of more than 6 months. In contrast, the stability of micellar phases is limited.

4. Conclusions

In conclusion, we have demonstrated that the selectivity of electrophoresis microchips can be enhanced by the presence of Ormosil sols in the run buffer. Such selectivity improvements reflect changes in the observed mobility due to interactions of solutes with the Ormosil sol surface. While the concept of Ormosil sol-enhanced electrophoresis microchips has been illustrated in connection to electrochemical detection of nitroaromatic explosives and aminophenols, it could be readily extended to other classes of analytes and detection modes. The rich Ormosil sol chemistry allows tailoring the selectivities of different solutes for specific separations. Unlike micellar additives that require a minimum surfactant concentration ($\geq$CMC) such concentration limitation does not exist for sol additives. Other additives (separation vectors) that may manipulate the selectivity of electrophoresis microchips are currently under investigation.

Acknowledgements

References

[1] D.R. Reyes, D. Iossifidis, P.A. Auroux, A. Manz, Anal. Chem. 74 (2002) 2623.
[2] P.S. Dittrich, K. Tachikawa, A. Manz, Anal. Chem. 78 (2006) 3887.
[3] M. Pumera, A. Merkoci, S. Alegret, Trends Anal. Chem. 25 (2006) 219.
[4] V. Dolnik, S. Liu, S. Jovanovich, Electrophoresis 21 (2000) 41.
[5] C.T. Culbertson, S.C. Jacobson, J.M. Ramsey, Anal. Chem. 72 (2000) 5814.
[6] M. Pumera, Talanta 66 (2005) 1048.
[7] A.W. Moore, S.C. Jacobson, J.M. Ramsey, Anal. Chem. 67 (1995) 4184.
[8] M. Pumera, J. Wang, E. Grushka, R. Polsky, Anal. Chem. 73 (2001) 5625.
[9] S. Constantin, R. Freitag, D. Solignac, A. Sayah, M.A.M. Gijs, Sens. Actuators B 78 (2001) 267.
[10] J.P. Kutter, S.C. Jacobson, N. Matsubara, J.M. Ramsey, Anal. Chem. 70 (1998) 3291.
[11] M.T. Dulay, J.P. Quirino, B.D. Benett, M. Kato, R.N. Zare, Anal. Chem. 73 (2001) 3921.
[12] Y. Wang, Z. Zeng, C.H. Xie, N. Guan, E.Q. Fu, J.K. Cheng, Chromatographia 54 (2001) 475.
[13] N. Ishizuka, H. Minakuchi, K. Nakanishi, N. Soga, H. Nagayama, K. Hosoya, N. Tanaka, Anal. Chem. 72 (2000) 1275.
[14] S. Terabe, K. Otsuka, K. Ichikawa, A. Tsuchiya, T. Ando, Anal. Chem. 56 (1984) 111.
[15] C. Fujimoto, Y. Muranaka, J. High Resol. Chromatogr. 20 (1997) 400.
[16] B. Gottlicher, K. Bachmann, J. Chromatogr. A 780 (1997) 63.
[17] D.S. Peterson, C.P. Palmer, Electrophoresis 21 (2000) 3174.
[18] S. Schulte, A.K. Singh, E. Rauk, C.P. Palmer, Anal. Bioanal. Chem. 382 (2005) 777.
[19] B.C. Giordano, C.L. Copper, G.E. Collins, Electrophoresis 27 (2006) 778.
[20] B. Neiman, E. Grushka, J. Gun, O. Lev, Anal. Chem. 74 (2002) 3484.
[21] M. Pumera, Electrophoresis 27 (2006) 244.
[22] G. Chen, Y.H. Lin, J. Wang, Talanta 68 (2006) 497.
[23] J. Wang, B. Tian, E. Sahlin, Anal. Chem. 71 (1999) 5436.
[24] J. Wang, M.P. Chatrathi, B. Tian, Anal. Chim. Acta 416 (2000) 9.
[25] J. Wang, M. Pumera, M.P. Chatrathi, A. Escarpa, R. Konrad, A. Griebel, W. Dorner, H. Lowe, Electrophoresis 23 (2002) 596.
[26] J. Wang, M. Pumera, M.P. Chatrathi, A. Escarpa, M. Musameh, G. Collins, A. Mulchandani, Y. Lin, K. Olsen, Anal. Chem. 74 (2002) 1187.

Multielement determination of trace metals in seawater by ICP-MS with aid of down-sized chelating resin-packed minicolumn for preconcentration

Dwinna Rahmi, Yanbei Zhu, Eiji Fujimori, Tomonari Umemura, Hiroki Haraguchi *

Department of Applied Chemistry, Graduate School of Engineering, Nagoya University, Furo-cho, Chikusa-ku, Nagoya 464-8603, Japan

Abstract

The multielement determination of trace metals in seawater was carried out by inductively coupled plasma mass spectrometry (ICP-MS) with aid of a down-sized chelating resin-packed minicolumn for preconcentration. The down-sized chelating resin-packed minicolumn was constructed with two syringe filters (DISMIC 13HP and Millex-LH) and an iminodiacetate chelating resin (Chelex 100, 200–400 mesh), with which trace metals in 50 mL of original seawater sample were concentrated into 0.50 mL of 2 M nitric acid, and then 100-fold preconcentration of trace metals was achieved. Then, 0.50 mL analysis solution was subjected to the multielement determination by ICP-MS equipped with a MicroMist nebulizer for micro-sampling introduction. The preconcentration and elution parameters such as the sample-loading flow rate, the amount of 1 M ammonium acetate for elimination of matrix elements, and the amount of 2 M nitric acid for eluting trace metals were optimized to obtain good recoveries and analytical detection limits for trace metals. The analytical results for V, Mn, Co, Ni, Cu, Zn, Mo, Cd, Pb, and U in three kinds of seawater certified reference materials (CRMs; CASS-3, NASS-4, and NASS-5) agreed well with their certified values. The observed values of rare earth elements (REEs) in the above seawater CRMs were also consistent with the reference values. Therefore, the compiled reference values for the concentrations of REEs in CASS-3, NASS-4, and NASS-5 were proposed based on the observed values and reference data for REEs in these CRMs.
© 2006 Elsevier B.V. All rights reserved.

Keywords: Chelating resin-packed minicolumn; Trace metals; Seawater certified reference material; ICP-MS; Micro-sampling introduction

1. Introduction

Nowadays, inductively coupled plasma mass spectrometry (ICP-MS) has become one of the most powerful analytical techniques for trace element analysis with high sensitivity as well as with wide linear dynamic range and simultaneous multielement detection capability [1,2]. However, weak tolerance to dissolved salts and polyatomic interferences is the principal disadvantage of ICP-MS, and makes it difficult to perform direct injection analysis of seawater containing ca. 3% of dissolved salts. Furthermore, the concentrations of most trace metals in seawater are extremely low at pg mL^{-1} levels [1]. In order to overcome these difficulties, various methods such as solvent extraction [3,4], coprecipitation [5–8], and chelating resin adsorption [9–21] have been developed for preconcentration of trace metals in seawa-

ter. Among them, the chelating resin adsorption technique is the most promising approach because of no use of harmful organic solvent and low risk of contamination.

Recently, the present authors have reported a chelating resin-packed minicolumn for preconcentration of trace metals in seawater [22], where trace metals in 50 mL of original seawater sample were concentrated into 2.5 mL of 2 M nitric acid (final solution). It has been proved that the minicolumn is a convenient preconcentration device for trace metals in seawater as well as in mineral waters prior to the determination by the ICP-MS instrument equipped with a conventional concentric nebulizer [22,23].

A MicroMist nebulizer is now commercially available as a micro-sampling device, which can be operated efficiently at very low solution uptake rates (down to sub-mL min^{-1}) [24]. Then, the simultaneous multielement determination may be performed using only 0.1–0.2 mL of sample solution with the MicroMist nebulizer. Thus, the combined system of ICP-MS with a MicroMist nebulizer is expected to be a next generation

* Corresponding author. Tel.: +81 52 789 4603; fax: +81 52 789 5290.
E-mail address: haraguch@apchem.nagoya-u.ac.jp (H. Haraguchi).

Table 1
Operating conditions with micro-sampling and concentric nebulization for ICP-MS instrument

Operating parameters	Operating conditions	
	Micro-sample nebulization	Conventional concentric nebulization
Plasma conditions		
Incident power (kW)	1.3	1.3
Coolant gas flow rate (L min^{-1})	Ar 15.0	Ar 15.0
Auxiliary gas flow rate (L min^{-1})	Ar 1.0	Ar 1.0
Carrier gas flow rate (L min^{-1})	Ar 1.0	Ar 1.0
Sampling depth (mm from load coil)	5.5	9
Nebulizer	MicroMist	Conikal
Sample uptake rate (mL min^{-1})	0.1	1
Data acquisition		
Measurement mode	Peak hopping	Peak hopping
Dwell time (ms/point)	50	50
Data point (points/peak)	3	3
Number of scans	100	100

analytical method for the multielement determination of trace metals in seawater, if a proper preconcentration technique is established.

In the present paper, hence, a downsized syringe-driven chelating resin-packed minicolumn was developed to obtain the large preconcentration factors for trace metals in seawater, i.e., from 50 mL of original seawater to 0.5 mL of analysis solution. Then, the experimental parameters were optimized for the multielement determination by micro-sampling ICP-MS. The present analytical method was validated by analyzing seawater certified reference materials (CRMs; CASS-3, NASS-4, and NASS-5) issued by the National Research Council of Canada (NRCC).

2. Experimental

2.1. Instrumentation

An ICP-MS instrument (Agilent HP 4500, Yokogawa, Tokyo, Japan) was used for the multielement determination of trace metals in seawater, which was equipped with a MicroMist nebulizer (AR35-1-FM01E, Glass Expansion Pty Ltd., West Melbourne, Australia). This micro-sampling ICP-MS system allowed us to determine 40 trace metals with less than 0.5 mL of analysis solution. The operating conditions for micro-sampling ICP-MS are summarized in Table 1, all of which were optimized for each instrumental parameter. For comparison, the operating conditions for conventional ICP-MS with a concentric nebulizer (Conikal, AR35-1-FC1E, Glass Expansion Pty Ltd.) are also given in Table 1. A syringe pump (KDS200, KD Scientific, MA, USA), which could flow the solution at the adjustable flow rate automatically, was used for *on-line* monitoring of the signal profiles for trace metals and matrix elements with ICP-MS as well as for passing the rinsing solutions through the column.

2.2. Chemicals and samples

Nitric acid, acetic acid and aqueous ammonia solutions of electronics industry grade were purchased from Kanto Chem-

icals (Tokyo, Japan). The multielement standard solutions for making the working calibration curves were prepared by diluting the single-element standard stock solutions (1000 μg mL^{-1}) for atomic absorption spectrometry (Wako Pure Chemicals, Osaka, Japan). The multielement standard solutions were prepared in three groups, as is shown in Table 2, in which Ge, In, Re, and Tl were added as the internal standard elements to be 10 ng mL^{-1} each. The Chelex 100 resin in 200–400 mesh was purchased from Bio-Rad Laboratories (Richmond, CA, USA). Before packing the chelating resin into the minicolumn, the resin was cleaned by soaking in fresh 5 M HCl, which was changed daily for 5 days. The resin was collected on a G4 glass filter, and after rinsing with 2 M nitric acid and pure water, it was kept in a 0.1 M of ammonium acetate at pH 6.0. Pure water used throughout the present experiment was prepared by a Milli-Q purification system (Element A-10, Nihon Millipore Kogyo, Tokyo, Japan).

Three kinds of seawater CRMs (CASS-3, NASS-4, and NASS-5) were purchased from NRCC. Coastal seawater sample collected from the shore near the Take Island (Gamagori, Aichi Prefecture, Japan) was used for optimizing the experimental conditions of the present preconcentration method. It was filtered with a membrane filter (pore size 0.45 μm) and acidified to pH 1 with concentrated nitric acid.

Table 2
Multielement standard solutions for calibration[a]

Group	Element	Concentration (ng mL^{-1})
Group I	V, Co, Pb	50
	Dy, Ho, Er, Tm, Lu	5
Group II	Cu, Zn, Cd	50
	La, Ce, Pr, Nd, Yb	5
Group III	Mn, Ni, Mo	50
	Y, Sm, Eu, Gd, Tb, U	5

[a] Each of the multielement standard solutions contains Ge, In, Re, and Tl (10 ng mL^{-1} each) as internal standard elements.
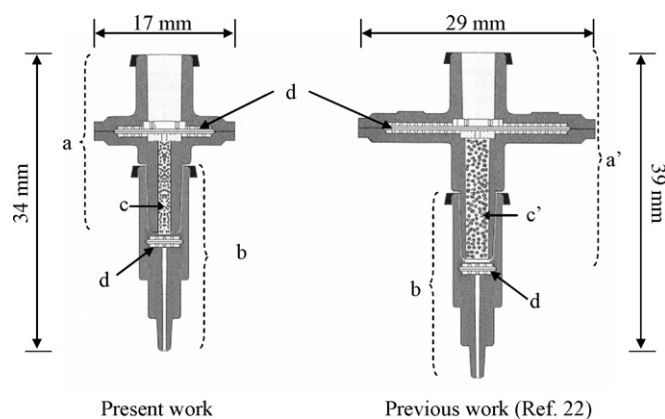
Fig. 1. A schematic structure of the chelating resin-packed minicolumn (a) prefilter tube (DISMIC-13HP, ADVANTEC); (a') prefilter tube (DISMIC-25HP, ADVANTEC); (b) prefilter tube (Millex-LH, Nihon Millipore Kogyo); (c) Chelex 100 resin, 200–400 mesh, 0.088 g; (c') Chelex 100 resin, 100–200 mesh, 0.40 g; (d) built-in membrane filter (pore size 0.45 μm).

2.3. Design of a down-sized chelating resin-packed minicolumn

The structure of the down-sized chelating resin-packed mini-column is shown in Fig. 1, where the previous minicolumn [22] is also shown for comparison of size. The minicolumn was constructed with three components, i.e., two syringe filters (a: DISMIC-13HP, ADVANTEC, Tokyo, Japan and b: Millex-LH; Nihon Millipore Kogyo, Tokyo, Japan) and a Chelex 100 resin (c: 200–400 mesh, Bio-Rad Laboratories, Richmond, CA, USA). As is shown in Fig. 1, the size of the minicolumn was 34 mm × 17 mm, while that of the old one was 39 mm × 29 mm, as a result, the bed volume (c) for packing the chelating resin could be reduced from 0.08 mL in the previous minicolumn to 0.01 mL in the present one. The pore sizes of built-in membrane filters (d) in both syringe filters were 0.45 μm. After the Chelex 100 resin was soaked in 0.1 M of ammonium acetate buffer (pH 6.0) overnight, the slurry of Chelex 100 resin was packed into the space from the outlet of the syringe filter (a), and then a smaller syringe filter (b) was capped to construct the minicolumn. The amount of Chelex 100 resin in the column was (0.088 ± 0.004) g $(n = 10)$ in wet weight. All the sample, rinsing, and eluent solutions were loaded automatically, using the KDS200 syringe pump, into the minicolumn with different single-use plastic syringes of Terumo series (Terumo Corporation, Tokyo, Japan).

2.4. Preconcentration procedure for trace metals in seawater

The procedure for preconcentration of trace metals in seawater was almost similar to that in previous work [22]. First, the seawater sample was adjusted to pH 6.0 with ammonia solution and acetic acid, and 50 mL of pH-adjusted seawater sample was loaded into the minicolumn at the flow rate of 1.0 mL min^{-1} with a 50 mL volume syringe. Second, 3 mL of 1 M ammonium acetate buffer (pH 6.0) was passed into the minicolumn at the flow rate of 1 mL min^{-1} to rinse matrix elements, such as Mg and

Ca, which were partly adsorbed on the resin. Then, trace metals adsorbed on the chelating resin were eluted with 0.45 mL of 2 M HNO$_3$ into a test tube, in which 0.05 mL of internal standard solution (Ge, In, Re, and Tl; 100 ng mL^{-1} each) was added for correction of matrix effects. The final analysis solution was subjected to the determination of trace metals by ICP-MS equipped with the MicroMist nebulizer.

In the recovery test, trace metals were spiked in the coastal seawater sample, taking into consideration their concentrations in seawater. The same preconcentration procedure as described above was carried out to estimate the concentration recoveries for trace metals by the calibration method.

3. Results and discussion

3.1. Optimization of sample-loading flow rate

Since the present down-sized chelating resin-packed minicolumn was packed with less amount of chelating resins, compared to the previous one [22], the operating parameters such as sample-loading flow rate, matrix element elimination, and trace metal elution were carefully optimized for the present minicolumn. The pH dependence of the recoveries for trace metals in seawater obtained with the Chelex 100 resin was almost the same as that reported in detail in the previous paper [22], in which pH 6.0 was recommended as the compromised pH condition to obtain the better recoveries for most elements. In the present experiment, thus, the preconcentration was carried out at pH 6.0.

Using the coastal seawater sample adjusted to pH 6.0, the sample-loading flow rate was optimized in the range from 0.2 to 1.4 mL min^{-1} at the interval of 0.2 mL min^{-1}, where the syringe pump (KDS200) was used for loading the seawater samples into the column. When the flow rate was larger than 1.0 mL min^{-1}, the recoveries for analyte elements decreased significantly, where the recoveries were estimated in a similar manner to the procedure described in Section 2. Then, the sample-loading flow rate of 1.0 mL min^{-1} was chosen as the optimum condition to obtain the better recovery.

3.2. Elution profile of matrix elements from the minicolumn

Matrix elements such as Na, K, Mg, and Ca in seawater often cause instrumental drift, isobaric polyatomic interferences, and signal suppression in the determination of trace metals by ICP-MS. In order to reduce such interferences, matrix elements adsorbed on the resin are usually eliminated by rinsing the chelating resin with ammonium acetate buffer solution [9–11,15,22]. However, the use of excessive amount of rinsing solution often results in losses of analyte metals. Therefore, the optimization for the amount of ammonium acetate buffer solution (1 M, pH 6.0) should be carefully performed in the sample pretreatment. In the present experiment, thus, the elution signal profiles for matrix elements after the sample loading were *on-line* monitored by ICP-MS with passing ammonium acetate buffer solution through the minicolumn at the flow rate of 0.9 mL min^{-1} with the KDS200 syringe pump. The elution
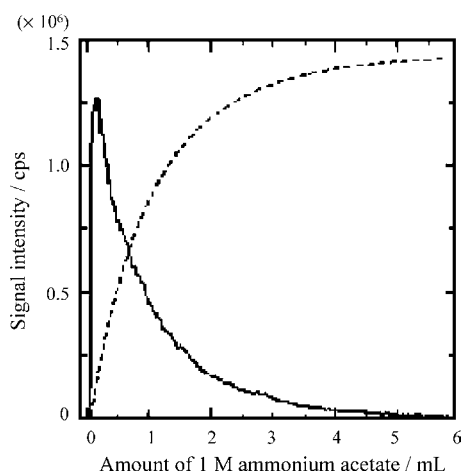
Fig. 2. Elution signal profile of Ca^{2+} from the minicolumn with 1 M ammonium acetate (pH 6.0).

signal profile of Ca is shown in Fig. 2, as a typical example. It is seen from Fig. 2 that more than 95% of Ca was eluted from the minicolumn when 3 mL of ammonium acetate was passed. After this rinsing process, the concentrations of Na, K, Mg, and Ca in the residual solution were 20, 3, 39, and 37 $\mu g\,mL^{-1}$, respectively. As a result, the total concentration of Na, K, Mg, and Ca in the analysis solution was less than 100 $\mu g\,mL^{-1}$, which was low enough to correct matrix effects by the internal standard correction method [11]. Consequently, 3 mL of ammonium acetate

buffer solution was chosen as the optimum volume for rinsing the chelating resin-packed minicolumn.

3.3. Elution profiles of trace metals from the minicolumn

In the present experiment, trace metals adsorbed on the chelating resin were eluted with 2 M nitric acid. It is apparent that the larger concentration factor can be obtained when the eluent of 2 M nitric acid is used as less as possible. Then, after loading the sample, the elution signal profiles of trace metals were *online* monitored by ICP-MS, with flowing 2 M nitric acid solution into the minicolumn at the flow rate of 0.9 mL min^{-1} with the KDS200 syringe pump. The signal profiles for Zn, Cu, and Y are shown in Fig. 3, as the representatives. When 0.45 mL of 2 M nitric acid was passed through the minicolumn, all of these trace metals were eluted almost completely. Therefore, 0.45 mL of nitric acid was found to be enough to elute trace metals from the minicolumn. It was also enough for the determination of more than 40 trace metals by the ICP-MS equipped with a MicroMist nebulizer.

3.4. Analytical figures of merit

First, the recoveries for trace metals in the present preconcentration procedure were evaluated by spiking certain amounts of trace metals in the seawater samples. The results for the recoveries of 24 trace metals are summarized in Table 3, although

Table 3
Recoveries and analytical detection limits for trace metals

Element	m/z	Spike (ng mL^{-1})	Recovery (%)[a]	ADL (ng mL^{-1})	
				Present work[b]	Previous work[c]
Co	59	1.00	96.3 ± 0.4	0.00003	0.0004
Ni	60	1.00	95.2 ± 0.2	0.001	0.002
Cu	65	1.00	95.4 ± 0.9	0.0003	0.001
Zn	68	1.00	89.9 ± 0.8	0.0007	0.009
Y	89	0.100	85 ± 1	0.000008	0.0001
Cd	111	1.00	89 ± 1	0.0006	0.003
La	139	0.100	85.9 ± 0.5	0.00001	0.0001
Ce	140	0.100	86.8 ± 0.7	0.00001	0.0001
Pr	141	0.100	86.7 ± 0.6	0.000006	0.00007
Nd	143	0.100	92 ± 2	0.00006	0.0003
Sm	147	0.100	85.3 ± 0.9	0.00003	0.0005
Eu	153	0.100	85.3 ± 0.2	0.00001	0.0001
Gd	157	0.100	86.4 ± 0.4	0.00005	0.0004
Tb	159	0.100	85.9 ± 0.7	0.000006	0.00008
Dy	163	0.100	87.2 ± 0.3	0.00002	0.0003
Ho	165	0.100	85.6 ± 0.1	0.00001	0.00007
Er	166	0.100	87 ± 1	0.00003	0.0002
Tm	169	0.100	87.1 ± 0.5	0.000008	0.00008
Yb	172	0.100	86 ± 1	0.00003	0.0003
Lu	175	0.100	87.5 ± 0.4	0.000006	0.00006
Pb	207	1.00	89.3 ± 0.4	0.0001	0.001
U	238	10.0	97.6 ± 0.5	0.00002	0.00008
V	51	10.0	39.5 ± 0.4	0.0001	0.0007
Mn	55	10.0	40.3 ± 0.5	0.0006	0.02
Mo	98	10.0	28 ± 1	0.0005	0.001

[a] Mean ± standard deviation, $n = 3$.
[b] Analytical detection limit, calculated from instrumental detection limits, taking into account the concentration factor (1 0 0) and recovery values.
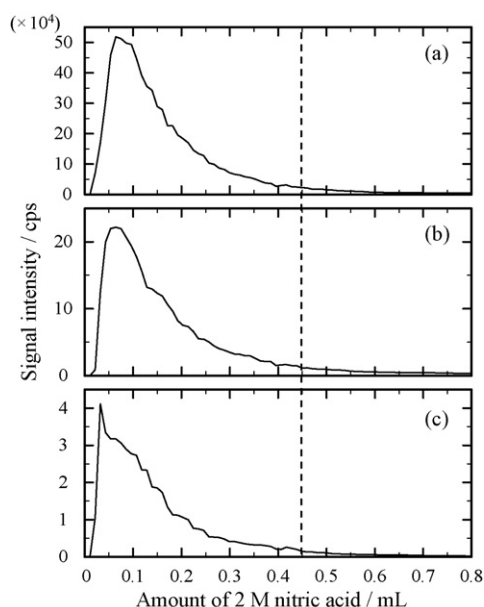[c] Cited from Ref. [22].

Fig. 3. Elution signal profiles of trace metals from the minicolumn with 2 M nitric acid (a) Zn; (b) Cu; (c) Y.

35 elements were examined in total. They were selected as the elements whose certified, information or reference values were available. The recoveries for Co, Ni, Cu, Zn, Y, Cd, rare earth elements (REEs), Pb, and U were better than 85% with good reproducibility less than 2% (R.S.D.). The recoveries for V, Mn, and Mo were smaller than 50% with their R.S.D.s less than 2%, which indicate that the analytical results for these elements should be treated carefully because of their poor recoveries.

The analytical detection limits obtained by the present method are summarized in Table 3, along with those obtained using the old-type chelating resin-packed minicolumn. They were calculated from the instrumental detection limits, taking into account the concentration factor (1 0 0) and the recovery values for trace metals. The instrumental detection limits were defined as the concentrations corresponding to three-fold the standard deviation of the background signal intensities, which were estimated from the 10-times duplicated measurements of the blank solution (2 M nitric acid solution) containing internal standard elements (Ge, In, Re, and Tl; 10 ng mL^{-1} each). The analytical detection limits for 24 elements were in the range from 0.001 ng mL^{-1} of Ni to 0.000006 ng mL^{-1} of Pr, Tb, and Lu. The present analytical detection limits were significantly better than the previous ones, because the concentration factors for trace metals in the present method was five-fold larger than those obtained in the previous work [22].

The blank values were also estimated using 50 mL of 0.1 M nitric acid as a test solution, for which the same preconcentration and measurement procedures as those for seawater samples were performed. The blank values for Pb and Zn were observed to be 0.0080 and 0.06 ng mL^{-1}, respectively, which might be originated from the impurities in the reagents. They were not negligible compared to the concentrations in seawater samples, and then the analytical results for Pb and Zn were obtained by

subtracting the blank values. The blank values for V, Co, Ni, Cu, La, and Ce were observed, but they were negligibly small compared to the concentrations of these elements in seawater.

In the ICP-MS measurements, major and trace elements in the sample solution often cause polyatomic interferences [24]. In the present experiment, the polyatomic interferences due to $^{43}Ca^{16}O$, $^{43}Ca^{16}O^{1}H^{+}$, $^{48}Ca^{16}O^{1}H^{+}$, and $^{141}Pr^{16}O$ with ^{59}Co, ^{60}Ni, ^{65}Cu, and ^{157}Gd, respectively, were observed and corrected by the interference correction coefficient method reported by Yabutani et al. [11]. In the present experiment, however, the polyatomic interferences were less than 5% of the observed values.

3.5. Analytical results for trace metals in seawater CRMs (CASS-3, NASS-4, and NASS-5)

Trace metals in one coastal seawater CRM (CASS-3) and two open seawater CRMs (NASS-4 and NASS-5) were determined by the analytical method proposed in the present experiment. The analytical results for V, Mn, Co, Ni, Cu, Zn, Mo, Cd, Pb, and U, whose certified or information values have been issued by NRCC, are summarized in Table 4. It is seen in Table 3 that all the observed values for trace metals examined agreed quite well with the certified values. This agreement indicates that the present method is accurate enough for the determination of trace metals in seawater. It should be noted here that large relative standard deviations (R.S.D. > 25%) were found for the observed values of Pb in all the three seawater CRMs and those of Zn in NASS-4 and NASS-5. Such large R.S.D.s for Pb and Zn may be attributed to their low concentrations close to the blank values.

The analytical results for REEs are summarized in Table 5. Although all of REEs in seawater CRMs examined were extremely low, they were determined with fairly good reproducibility in the present experiment. However, the certified or information values for REEs have not been issued by NRCC yet.

As stated above, the certified or information values for REEs in seawater CRMs are not available even now. However, REEs in seawater have been widely investigated as the tracers of water masses and ocean circulation as well as a valuable probe for investigating the scavenging processes of particulate matter in the ocean [25–30]. Therefore, the reliable reference values for REE concentrations in seawater CRMs are necessary to promote further development of marine chemistry. Then, the compiled data for REEs in seawater CRMs were proposed in the present paper. Such compiled data were estimated as the mean values of their reference values [11,16,21,31,32] including the data obtained in the present work. The results are shown in Table 6. As is seen in Table 6, the compiled data for all seawater CRMs were within fairly small standard deviations. Thus, the compiled data summarized in Table 6 may be available as the tentatively certified reference values for REEs in seawater CRMs.

In addition, the shale-normalized REE distribution patterns plotted against atomic number, which are usually shown as the relative concentrations of REEs normalized to their concentra-

Table 4
Analytical results for trace metals in seawater CRMs

Element	m/z	Observed value (ng mL^{-1})[a]	Certified value (ng mL^{-1})
CASS-3			
(V)[b]	51	(1.4 ± 0.2)	1.43 ± 0.04[c]
(Mn)[b]	55	(2.8 ± 0.3)	2.51 ± 0.36
Co	59	0.038 ± 0.002	0.041 ± 0.009
Ni	60	0.38 ± 0.03	0.39 ± 0.06
Cu	65	0.48 ± 0.03	0.52 ± 0.06
Zn	68	1.4 ± 0.2	1.24 ± 0.25
(Mo)[b]	98	(9.0 ± 0.5)	8.95 ± 0.26
Cd	111	0.031 ± 0.003	0.030 ± 0.005
Pb	207	0.010 ± 0.005	0.012 ± 0.004
U	238	3.0 ± 0.2	2.84[d]
NASS-4			
(V)[b]	51	(1.3 ± 0.3)	1.18 ± 0.16
(Mn)[b]	55	(3.0 ± 0.3)	2.78 ± 0.19
Co	59	0.010 ± 0.002	0.009 ± 0.001
Ni	60	0.22 ± 0.02	0.228 ± 0.009
Cu	65	0.21 ± 0.01	0.228 ± 0.011
Zn	68	0.12 ± 0.03	0.12 ± 0.02
(Mo)[b]	98	(8.5 ± 0.6)	8.78 ± 0.86
Cd	111	0.018 ± 0.001	0.016 ± 0.003
Pb	207	0.012 ± 0.004	0.013 ± 0.005
U	238	3.0 ± 0.2	2.68 ± 0.12
NASS-5			
(V)[b]	51	(1.0 ± 0.3)	1.2[d]
(Mn)[b]	55	(0.88 ± 0.6)	0.919 ± 0.057
Co	59	0.011 ± 0.001	0.011 ± 0.003
Ni	60	0.24 ± 0.00	0.25 ± 0.03
Cu	65	0.27 ± 0.01	0.30 ± 0.05
Zn	68	0.07 ± 0.04	0.10 ± 0.04
(Mo)[b]	98	(9.3 ± 0.7)	9.6 ± 1.0
Cd	111	0.024 ± 0.001	0.023 ± 0.003
Pb	207	0.006 ± 0.003	0.008 ± 0.005
U	238	2.8 ± 0.1	2.60[d]

[a] Mean ± standard deviation, n = 5.
[b] Recovery values were less than 85%.
[c] Reference value, cited from Ref. [11].
[d] Information value issued by NRCC.

Table 5
Analytical results for REEs in seawater CRMs

Element	m/z	Concentration (pg mL^{-1})[a]		
		CASS-3	NASS-4	NASS-5
Y	89	23.3 ± 0.9	18 ± 1	20.7 ± 0.7
La	139	13.9 ± 0.6	9.9 ± 0.6	11.8 ± 0.4
Ce	140	5.6 ± 0.2	3.9 ± 0.2	5.23 ± 0.05
Pr	141	1.9 ± 0.1	1.5 ± 0.1	1.84 ± 0.06
Nd	143	7.8 ± 0.4	7.2 ± 0.3	7.5 ± 0.1
Sm	147	6.6 ± 0.4	3.0 ± 0.1	4.5 ± 0.3
Eu	153	0.33 ± 0.03	0.24 ± 0.02	0.29 ± 0.02
Gd	157	1.7 ± 0.1	1.4 ± 0.1	1.59 ± 0.08
Tb	159	0.27 ± 0.03	0.21 ± 0.03	0.24 ± 0.02
Dy	163	1.8 ± 0.1	1.6 ± 0.1	1.8 ± 0.2
Ho	165	0.48 ± 0.04	0.39 ± 0.02	0.43 ± 0.08
Er	166	1.4 ± 0.1	1.2 ± 0.2	1.36 ± 0.08
Tm	169	0.22 ± 0.02	0.18 ± 0.02	0.18 ± 0.01
Yb	172	1.3 ± 0.1	1.1 ± 0.1	1.13 ± 0.07
Lu	175	0.23 ± 0.02	0.17 ± 0.01	0.20 ± 0.02

[a] Mean ± standard deviation, n = 5.

Table 6
Compiled data for the concentrations of REEs in seawater CRMs

Element	m/z	Concentration (pg mL^{-1})		
		CASS-3[a]	NASS-4[b]	NASS-5[c]
Y	89	23.6[d]	18.7[e]	20.7[f]
La	139	13 ± 2	9 ± 1	12.2 ± 0.5
Ce	140	5.4 ± 0.9	3.9 ± 0.4	4.6 ± 0.6
Pr	141	1.9 ± 0.2	1.54 ± 0.07	1.8 ± 0.3
Nd	143	8.3 ± 0.5	7.4 ± 0.2	9 ± 1
Sm	147	6.7 ± 0.1	3.2 ± 0.3	4.3 ± 0.3
Eu	153	0.36 ± 0.03	0.26 ± 0.03	0.27 ± 0.02
Gd	157	2.3 ± 0.7	1.7 ± 0.7	1.57 ± 0.04
Tb	159	0.32 ± 0.06	0.24 ± 0.05	0.25 ± 0.04
Dy	163	2.0 ± 0.1	1.63 ± 0.06	1.71 ± 0.09
Ho	165	0.50 ± 0.02	0.40 ± 0.03	0.39 ± 0.04
Er	166	1.6 ± 0.2	1.4 ± 0.1	1.35 ± 0.03
Tm	169	0.23 ± 0.02	0.18 ± 0.01	0.16 ± 0.02
Yb	172	1.5 ± 0.2	1.2 ± 0.1	1.14 ± 0.05
Lu	175	0.25 ± 0.02	0.18 ± 0.02	0.19 ± 0.01

[a] Mean ± standard deviation, n = 3, calculated from the data in the present work, Refs. [11] and [21].
[b] Mean ± standard deviation, n = 4, calculated from the data in the present work, Refs. [21,31] and [32].
[c] Mean ± standard deviation, n = 3, calculated from the data in the present work, Refs. [16] and [32].
[d] Mean, n = 2, calculated from the data in the present work and Ref. [11].
[e] Mean, n = 2, calculated from the data in the present work and Ref. [31].
[f] Single data, cited from the present work.

tions in shale, were examined in order to evaluate the reliability of the compiled data for REEs in seawater CRMs. The REE distribution patterns for seawater CRMs are shown in Fig. 4, in which the compiled data for the concentrations of REEs were normalized to those in post-Archean average Australian shale (PAAS) [33]. It is seen in Fig. 4 that the REE distribution patterns show the typical characteristic pattern for seawater [10], i.e., smooth curves as well as slight enrichment of heavy REEs and clear negative anomalies of Ce in all seawater CRMs. However, it should be noted here that the significantly higher concentrations of Sm were observed for all seawater CRMs, which were seemingly due to the possible contamination caused during preparation process of these CRMs.
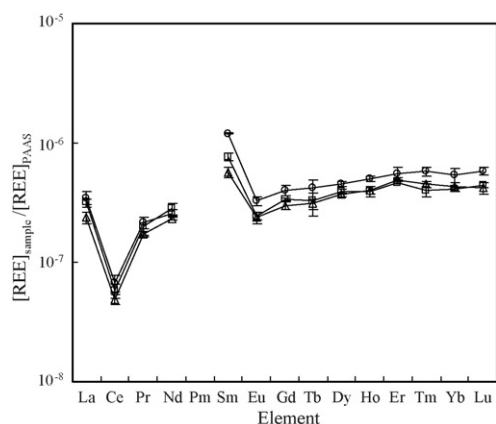

Fig. 4. Shale-normalized REE distribution patterns for seawater CRMs, based on their compiled data (○) CASS-3; (△), NASS-4; (□) NASS-5.

4. Conclusion

A down-sized chelating resin-packed minicolumn was developed as the efficient preconcentration tool for trace metals in seawater. The optimized preconcentration procedure was proposed for 100-fold preconcentration of trace metals using only 50 mL of seawater. The recoveries for most trace metals were larger than 85% with good reproducibility (standard deviation ≤2%). The analytical results for V, Mn, Co, Ni, Cu, Zn, Mo, Cd, Pb, and U in seawater CRMs were consistent with their certified or information values from NRCC. In addition, based on the observed and reference values for REEs in these CRMs, the compiled data for the concentrations of REEs in CASS-3, NASS-4, and NASS-5 were estimated which may be available as the information values of REEs in seawater CRMs.

References

[1] H. Haraguchi, J. Anal. At. Spectrom. 19 (2004) 5.
[2] H. Haraguchi, Bull. Chem. Soc. Jpn. 72 (1999) 1163.
[3] M.B. Shabani, T. Akagi, H. Shimizu, A. Masuda, Anal. Chem. 62 (1990) 2709.
[4] G.J. Batterham, N.C. Munksgaard, D.L. Parry, J. Anal. At. Spectrom. 12 (1997) 1277.
[5] H. Sawatari, T. Hayashi, E. Fujimori, A. Hirose, H. Haraguchi, Bull. Chem. Soc. Jpn. 69 (1996) 1925.
[6] T. Yabutani, S. Ji, F. Mouri, A. Itoh, K. Chiba, H. Haraguchi, Bull. Chem. Soc. Jpn. 73 (2000) 895.
[7] C.L. Chou, J.D. Moffatt, Fresen. J Anal. Chem. 368 (2000) 59.
[8] D. Weiss, E.A. Boyle, V. Chavagnac, M. Herwegh, J.-F. Wu, Spectrochim. Acta 55B (2000) 363.
[9] C.J. Cheng, T. Akagi, H. Haraguchi, Anal. Chim. Acta 198 (1987) 173.
[10] H. Sawatari, T. Toda, T. Saizuka, C. Kimata, A. Itoh, H. Haraguchi, Bull. Chem. Soc. Jpn. 68 (1995) 3065.
[11] T. Yabutani, S. Ji, F. Mouri, H. Sawatari, A. Itoh, K. Chiba, H. Haraguchi, Bull. Chem. Soc. Jpn. 72 (1999) 2253.
[12] Y. Sohrin, S. Iwamoto, S. Akiyama, T. Fujita, T. Kugii, H. Obata, E. Nakayama, S. Goda, Y. Fujishima, H. Hasegawa, K. Ueda, M. Matsui, Anal. Chim. Acta 363 (1998) 11.
[13] S. Mito, M. Ohata, N. Furuta, Bunseki Kagaku 52 (2003) 575.
[14] T. Sumida, T. Nakazato, H. Tao, Bunseki Kagaku 52 (2003) 619.
[15] M.S. Jimenez, R. Velarte, J.R. Castillo, Spectrochim. Acta 57B (2002) 391.
[16] S.N. Willie, R.E. Sturgeon, Spectrochim. Acta 56B (2001) 1707.
[17] K.W. Warnken, G.A. Gill, L.-S. Wen, L.L. Griffin, P.H. Santschi, J. Anal. At. Spectrom. 14 (1999) 247.
[18] S. Hirata, Y. Ishida, M. Aihara, K. Honda, O. Shikino, Anal. Chim. Acta 438 (2001) 205.
[19] K.-H. Lee, M. Oshima, S. Motomizu, Analyst 127 (2002) 769.
[20] T. Miura, T. Morimoto, K. Hayano, T. Kishimoto, Bunseki Kagaku 49 (2000) 245.
[21] Y. Takaku, Y. Kudo, J. Kimura, T. Hayashi, I. Ota, H. Hasegawa, S. Ueda, Bunseki Kagaku 51 (2002) 539.
[22] Y. Zhu, A. Itoh, H. Haraguchi, Bull. Chem. Soc. Jpn. 78 (2005) 107.
[23] H. Haraguchi, Y. Zhu, R. Hattori, A. Itoh, T. Umemura, Biomed. Res. Trace Elem. 15 (2004) 355.
[24] A. Montaser, Inductively Coupled Plasma Mass Spectrometry, Wiley–VCH Inc., 1998, pp. 543–548.
[25] G.J. Piepgras, G.J. Wasserburg, Science 217 (1982) 207.
[26] C.R. German, T. Masuzawa, M.J. Greaves, H. Elderfield, J.M. Edmond, Geochim. Cosmochim. Acta 59 (1995) 1551.
[27] J. Zhang, Y. Nozaki, Geochim. Cosmochim. Acta 60 (1996) 4631.
[28] H. Elderfield, M.J. Greaves, Nature 296 (1982) 214.
[29] E.R. Sholkovitz, D.L. Schneider, Geochim. Cosmochim. Acta 55 (1991) 2737.
[30] R.H. Byrne, K.-H. Kim, Geochim. Cosmochim. Acta 54 (1990) 2645.
[31] T. Yabutani, K. Chiba, H. Haraguchi, Bull. Chem. Soc. Jpn. 74 (2001) 31.
[32] T.J. Shaw, T. Duncan, B. Schnetger, Anal. Chem. 75 (2003) 3396.
[33] S.R. Taylor, S.M. McLennan, The Continental Crust: Its Composition and Evolution. An examination of the Geochemical Record Preserved in Sedimentary Rocks, Blackwell, 1985, p. 30.

Theoretical prediction of the photoinduced chemiluminescence of pesticides

I. Sahuquillo Ricart [a], G.M. Antón-Fos [a,*], M.J. Duart [b], J.V. García Mateo [a,*],
L. Lahuerta Zamora [a], J. Martínez Calatayud [c]

[a] *Departamento de Química, Bioquímica y Biología Molecular,*
Universidad Cardenal Herrera-CEU, Moncada, Valencia, Spain
[b] *Departamento de Ingeniería, División de Farmacia y Tecnología Farmacéutica,*
Facultad de Farmacia, Universidad Miguel Hernández, Alicante, Spain
[c] *Departamento de Química Analítica, Universidad de Valencia, Valencia, Spain*

Abstract

Although it is relatively easy to find chemiluminescent (CL) molecules working on the field of direct liquid phase (especially employing strong oxidants), the molecules found as chemiluminescent are normally very weak CL compounds for developing suitable analytical CL-procedures. Therefore, it is mandatory to develop new strategies to enhance in a simple way the native chemiluminescence of such a compounds, and even to increase the number of compounds to be determined by direct chemiluminescence. Photoinduced chemiluminescence (Ph-CL) results in a simple and easily on-line accessible strategy to solve these disadvantages. In the present paper, molecular connectivity, a topological method which allows an unique mathematical characterization of molecular structures by the so-named topological descriptors and their correlation with physical, chemical and biological properties of molecules was applied to predict the Ph-CL in liquid phase. Molecular connectivity calculations and discriminant analysis was applied to 72 pesticides for which either a Ph-CL or non Ph-CL behaviour was observed in an experimental screening. The screening test is based on the on-line photodegradation of pesticides by using an automated multicommutation based flow asssembly provided with a photoreactor consisting of 150 cm × 0.8 mm PTFE tubing helically coiled around a 20 W low-pressure mercury lamp. Photodegraded pesticides are detected by direct chemiluminescence of the resulting photo-fragments and their subsequent reaction with potassium permanganate in sulfuric acid medium as oxidant. The screening comprised pesticides with different molecular structures and relevant members of the most important families of pesticides were tested (oxime carbamates, sulfonylcarbamates, thiocarbamates, 1,3,5-triazines, organophosphorous, hydroxybenzonitrile, sulfonylureas, phosphonic acid derivatives, imidazolinones, carboxamides, aryloxyalkanoic acids, 1,2,4-triazinones, etc.). The theoretical predictions agree with the empirical results obtained by means of the screening test performed in the multicommutation flow-assembly.
© 2006 Elsevier B.V. All rights reserved.

Keywords: Pesticides; Multicommutation; Molecular connectivity; Chemiluminescence; Photodegradation

1. Introduction

Chemiluminescence research is in continuous expansion by virtue of the search on new processes allowing the direct chemiluminescence-based determination of substances of pharmaceutical, clinical or environmental interest [1,2]. In this sense, direct chemiluminescence methods based on strong oxidant such as potassium permanganate have found a wide range of analytical applications [3,4].

Luminescence techniques for organic pesticides residue analysis have been limited by the fact that, relatively few of these compounds are strongly luminescent. This can be overcome converting the weakly luminescent pesticide into a luminescent compound by means of a chemical derivatization using fluorogenic labeling [5–7]. A more recent and relatively widely employed approach based on UV irradiation of non-fluorescent analytes into strongly fluorescent photoproducts has demonstrated the viability of photochemically induced fluorimetry in pesticide quantitative analysis [8]. On the other hand, it

has been established that the irradiation of photoreactive analytes leads to the formation of species that can be detected by CL providing very sensitive procedures [9–11]. Between the luminescent techniques it is remarkable the scarcely use of the chemiluminescent (CL) detection in the determination of pesticides. It is also to emphasize that in spite of the well demonstrated approach UV irradiation-photochemical reaction of pesticides [12], only a few works dealing with photodegradation and chemiluminescent detection have been published [13–16].

On the other hand, molecular topology and particularly molecular connectivity has widely demonstrated its ability for an easy and efficient characterization of molecular structure through the so-called topological indices. In this mathematical formalism a molecule is assimilated to a graph, where each vertex represents one atom and each axis one bond. Starting from the interconnections among the different vertexes, an adjacency topological matrix can be built whose elements *ij* take the values 1 or 0, depending whether the vertex *i* is connected to the vertex *j* or not, respectively. The manipulation of this matrix gives origin to a set of topological indices or topological descriptors. When these indices are selected adequately, it is possible to have a very specific characterization of each chemical compound [17–21]. Molecular connectivity has been tested on several properties of different classes of organic, bioorganic and inorganic compounds. This topological method has been applied to the determination of biological activities [22] and physical [23] and chemical properties [24].

Molecular connectivity has been successfully employed in the design of drugs, bronchodilator [25] and antimalarial compounds [26], hypoglycaemic agents [27], anti-neoplastics [28], cytostatic agents [29], antibacterial agents [30] and new antihistaminic compounds [31,32] have been found by means of molecular connectivity. Physico-chemical properties such as soil adsorption coefficients [33], water solubility and boiling points [34] have been tested by molecular connectivity. Also, molecular connectivity has been applied to the prediction of analytical properties, basically to chromatographic processes [35–38] and recently to liquid-phase chemiluminescence [39–41].

The work presented in this paper was mainly focused to put into the analytical chemistry fields the molecular connectivity as a new and useful tool to enhance the yield of the analytical research. The immediate purpose of the present work was to develop a simpler assay for determination of pesticides using a multicommutation flow system coupled to photochemically induced CL. The method allows on the basis of the UV irradiation and chemiluminometric detection of photoproducts the determination of pesticides which present very weak or null native chemiluminescence. The viability of this purpose was supported by molecular connectivity calculations. The appropriated selection of topological descriptors allows the prediction of pesticides properties, namely, tendency to photodegradation and chemiluminescent behaviour of photofragments. A theoretical discrimination of the Ph-CL activity of a pesticide is possible, and consequently, to develop new and suitable Ph-CL analytical procedures.

2. Experimental

2.1. Reagents

All reagents were analytically pure unless stated otherwise and prepared in deionized water (18 MΩ cm) using a Sybron/Barnstead Nanopure II water purification system. Pesticides were obtained from Dr. Ehrenstorfer (Augsburg, Germany). Mineral acids and alkalis, $KMnO_4$, H_2O_2, tested in preliminary assays (all from Panreac, Barcelona, Spain), $Fe(NO_3)_3 \cdot 9H_2O$ (Probus, Barcelona, Spain), $FeSO_4 \cdot 7H_2O$ (Fluka, Buchs, Switzerland).

2.2. Apparatus

The flow manifold used (see Fig. 1) comprised a PTFE coil of 0.8 mm i.d. and a Gilson Minipuls 2 (Worthington, OH, USA) peristaltic pump. For the fully automated manifolds three Model 161T031 solenoid valves (NResearch, Northboro, MA, USA) were used. The solenoid valves were connected to a laboratory-made interface type KSP. Its actuation was programmed using a home made Solenoid Valves software running on a Pentium-type computer in Microsoft Windows 98. The programme and interface allow an independent control of the solenoid valve, the sequence of insertions and the number of cycles according to the number of samples, reagent solutions or standards to be inserted. The photoreactor consisted of a 150 cm length and 0.8 mm i.d. PTFE tubing helically coiled around a 20 W low-pressure mercury lamp (Zalux) for germicidal use. The flow cell was a flat-spiral quartz tube of 1 mm inner diameter and 3 cm total diameter backed by a mirror for maximum light collection. The photodetector package was a P30CWAD5F-29 Type 9125 photomultiplier tube (PMT) supplied by Electron Tubes operating at 1280 V and was located in a laboratory-made light-
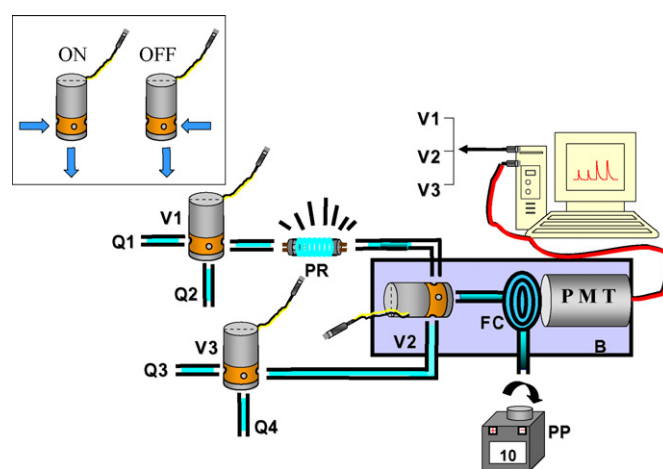

Fig. 1. Solenoid valve flow-assembly. Q_1: pesticide aqueous solution; Q_2: medium of photodegradation; Q_3: oxidant ($KMnO_4$ 7×10^{-4} M in H_2SO_4 2 M); Q_4: H_2O. V_1, V_2 and V_3: solenoid valves; PR: photoreactor; PP: peristaltic pump (flow-rate 10 mL min^{-1}); PR: photoreactor (150 cm length and 0.8 mm i.d. PTFE tubing helically coiled around a 20 W low-pressure mercury lamp (Zalux) for germicidal use); PMT: photomultiplier tube (1280 V); FC: spiral flow-cell (flat-spiral quartz tube of 1 mm inner diameter and 3 cm total diameter backed by a mirror for maximum light collection); B: light-tight box.

tight box. The output was fed to a computer equipped with a counter-timer, also supplied by Electron Tubes.

2.3. Procedures

2.3.1. Stock solution preparation

Stock standard solutions of pesticide ($50\,\mu g\,mL^{-1}$) were prepared by exactly weighing and dissolving the pesticide in deionized water. The working standard solutions were freshly prepared by diluting the stock standard solution in the appropriate volume of deionized water. All solutions of pesticides were protected against light.

2.3.2. Analytical measurements and solenoid valve flow-assembly

The peristaltic pump was placed after the detector and the sample and reagent streams were driven to the detector flow-cell by aspiration at a flow-rate of $10\,mL\,min^{-1}$. The manifold is constituted of a set of three solenoid valves, each one acting as an independent commutator (see Fig. 1). The way of work of a valve can be described as follows: $N(t_1, t_2)$, where t_1 is the time of valve in ON, t_2 the time of valve in OFF, and N is the number of cycles ON/OFF. Changes in the manifold configuration affected only the number and length of pulses (time ON/time OFF) applied to each solenid valve. The reconfiguration of the flow system was thus a logical reconfiguration via software. The insertion profile for obtaining a typical transient analytical signal in the screening procedure is depicted in Fig. 2. First, 50 alternated microinsertions of pesticide and medium of photodegradation were performed. During each microinsertion V_1 remains activated during 0.4 s (valve ON, the pesticide Q_1 is aspirated), and deactivated during 0.2 s (valve OFF, medium of photodegradation Q_2 is aspirated). During the 30 s that the sample insertion takes place, V_2 remains in ON, allowing that the photoreactor fills of the mixture pesticide-medium of photodegradation. This loading time also is used for washing the inner walls of the pho-

toreactor avoiding contamination between samples. Then V_1 and V_2 are switched simultaneously and remained OFF during 150 s of stopped-flow (time of UV photoirradiation). Previously to the chemiluminescent reaction ($t = 165$ s, see Fig. 2), chemiluminescent reagent ($KMnO_4$ (Q_3)) is flowing by switching ON valve V_3. After the stopped flow, V_2 is activated and 30 alternated microsegments of photodegradated pesticide and chemiluminescent reagent are inserted. A chemiliminometric response is obtained and the transient analytical signal returns to the base line ready for a new cycle.

2.3.3. Molecular connectivity and topological descriptors

Molecular connectivity has demonstrated to be an excellent tool for a quick and accurate prediction of many analytical, physicochemical and biological properties. One of the most interesting advantages of molecular connectivity is the straight-forward calculation of molecular descriptors to work with.

In this mathematical formalism a molecule is assimilated to a graph, where each vertex represents one atom and each axis one bond. Starting from the interconnections among the different vertexes, an adjacency topological matrix can be built up, which elements ij, take the values either 1 or 0, depending upon the vertex i is connected to the vertex j or not, respectively. The manipulation of this matrix gives origin to a set of topological indices or topological descriptors, which characterize each graph and they can be used to perform QSAR studies as well.

In this work we use several graph-theoretical descriptors like the connectivity indices χ up to the order 10—including descriptors type path, cluster, path-cluster and chain [42], topological charge indices G_i, J_i until order 5 [43] tom type electrotopological state indices 49 [44,45] other simple descriptors such as the number of atoms and ramifications, the Wiener index, etc. All these descriptors, more than 140, were obtained for each compound, using the programs Molconn [46] and Desmol11 [47].

Table 1 depicts the indices used in this work, definition and the references describing their calculation in detail. All descriptors were computed from the adjacency topological matrix obtained from the hydrogen depleted graph.

2.3.4. Linear discriminant analysis

Stepwise linear discriminant analysis, SLDA, is a useful technique for finding discriminant functions. It is a pattern-recognition method, which permits (facilitates), by combining variables, the evaluation of the ability to distinguish among two or more groups of populations. In our work the independent variables were the topological indices and the discrimination property was the chemiluminescent activity. The SLDA study is performed with two groups of compounds, the training group, which includes compounds with photoinduced chemiluminescence (active), and not chemiluminescent compounds even by on-line UV-photoirradiation (inactive), facilitating the discovery of the discriminant function, and the test group (also with active and inactive structures, randomly chosen from the training group), which facilitates the evaluation of the quality of the discriminant function obtained. Election of connectivity functions was performed with the BMDP Biomedical package [50]. The method used for selection of the descriptors was the F-Snedecor
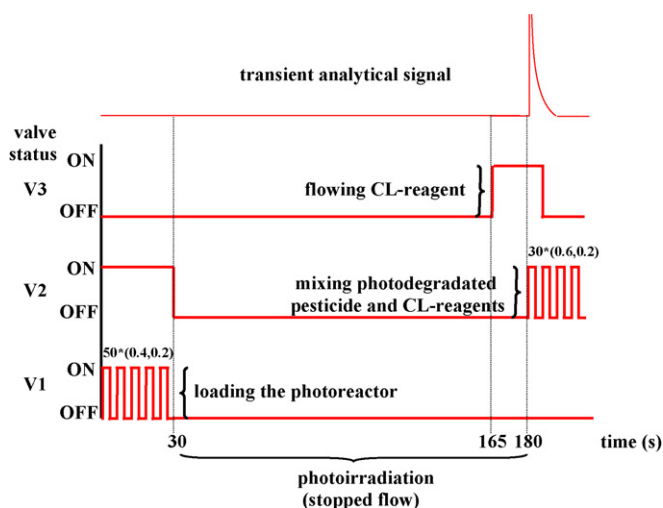

Fig. 2. Schematic profile of a multi-insertion cycle. $N(t_1,t_2)$. N: number of insertions. In each insertion the solenoid valve is t_1 seconds ON and t_2 seconds OFF. [$V_1 = 50(0.4,0.2)$; $V_2 = 30$(ON), 165(OFF), 30(0.6,0.2); $V_3 = 165$(OFF), 39(ON)].

Table 1
Symbols and definitions of topological indices used in this work

Symbol	Name	Definition	References
$^{\kappa}\chi_{\tau}$ ($k = 0\text{--}4$; $t = $ p, c, pc)	Randić-like indices of order k and type path (p), cluster (c) and path-cluster (pc)	$^{k}\chi_{t} = \sum_{j=1}^{k_{n_t}} \left(\prod_{i \in S_j} \delta_i \right)^{-1/2}$ δ_I, number of bonds, σ or π of the atom i to non-hydrogen atoms. S_j, jth sub-structure of order k and type t	[42]
$^{k}\chi_{t}^{v}$ ($k = 0\text{--}4$; $t = $ p, c, pc)	Kier–Hall indices of order k and type path (p), cluster (c) and path-cluster (pc)	$^{k}\chi_{t}^{v} = \sum_{j=1}^{k_{n_t}} \left(\prod_{i \in S_j} \delta_i^{v} \right)^{-1/2}$ δ_i^{v}, Kier–Hall valence of the atom i. S_j, jth sub-structure of order k and type t	[42]
$^{k}D_{t}$ ($k = 0\text{--}4$; $t = $ p, c, pc)	Connectivity differences of order k and type path (p), cluster (c) and path-cluster (pc)	$^{k}D_{t} = {}^{k}\chi_{t} - {}^{k}\chi_{t}^{v}$	[42]
G_k ($k = 1\text{--}5$)	Topological charge indices of order k	$G_k = \sum_{i=1}^{N-1} \sum_{j=i+1}^{N} |\mathbf{M}_{ij} - \mathbf{M}_{ji}| \delta(k, \mathbf{D}_{ij})$ $\mathbf{M} = \mathbf{AQ}$, product of the adjacency and inverse squared distance matrices for the hydrogen-depleted molecular graph. $\mathbf{D}$, distance matrix; δ, Kronecker delta	[43]
G_k^{v} ($k = 1\text{--}5$)	Valence topological charge indices of order k	$G_k^{v} = \sum_{i=1}^{N-1} \sum_{j=i+1}^{N} |\mathbf{M}_{ij}^{v} \mathbf{M}_{ji}^{v}| \delta(k, \mathbf{D}_{ij})$ $\mathbf{M}^{v} = \mathbf{A}^{v}\mathbf{Q}$, product of the electronegativity-modified adjacency and inverse squared distance matrices for the hydrogen-depleted molecular graph. $\mathbf{D}$, distance matrix; δ, Kronecker delta	[43]
J_k, J_k^{v} ($k = 1\text{--}5$)	Pondered topological charge indices of order k	$J_k = \dfrac{G_k}{N-1}$, $\quad J_k^{v} = \dfrac{G_k^{v}}{N-1}$	[43]
$^{m}\kappa$	Kappa index	$^{m}\kappa = m \dfrac{^{m}P_{\max}{}^{m}P_{\min}}{(^{m}P)^2}$, defined in terms of the number of graph vertices A and the number of paths ^{m}P with length $m = 1, 2$ and 3	[48]
S_i	Sum-electrotopological indexes type	$S_i = I_i + \Delta I_i$	[44,45]
V_i	V_3 and V_4	Number of graph vertices with topological valence 3 or 4	[49]

Topological descriptors were calculated for each compound by using Molconn-Z [46] and DESMOL11 [47] programs.

parameter, and the classification criterion used was the minimum value of the Mahalanobis distance. The quality of the discriminant function is evaluated through Wilk's *U*-statistical parameter.

By applying the topological pattern to the whole group, a distribution pattern [51] can be constructed to represent the expectancy for each classification group in each function interval. In general, the expectancy for a group A over an interval x is defined mathematically as:

$$E_a = \frac{\text{percentage of A in } x}{\text{percentage if non-A in } x + 100}$$

E_a and E_i denoting activity expectancy and inactivity expectancy, respectively, in our case.

3. Results and discussion

3.1. Experimental screening in a multicommutation flow-assembly

Aldicarb[13] was employed as a test substance and prior to a new screening session the system was checked with the aid of a $50\,\mu\text{g}\,\text{mL}^{-1}$ aqueous solution of aldicarb and NaOH as medium of photodegradation. First, the homogeneous-phase photodegradation of pesticides in different media and combined with chemiluminescence detection of the photoirradiated analyte was studied. The study of media was focused on chemical species forming after UV irradiation hydroxyl radicals, which react with organic pollutants in a non selective manner and lead to an efficient photocatalyst for pesticide degradation [52]. NaOH, Fe(II) and H_2O_2 employed in the photo-Fenton reaction, and Fe(III) aquacomplexes described as an efficient photocatalytic system for the mineralisation of pesticides by sunlight irradiation [12,53] were tested.

The tandem-flow assembly used is depicted in Fig. 2. The sample solution Q_1 (blank or pesticide aqueous solution, $50\,\mu\text{g}\,\text{mL}^{-1}$) was mixed with the photodegradation medium solution Q_2 (H_2O, 10^{-3} NaOH, 0.05% H_2O_2, Fe(III) 6×10^{-5} M or Fe(II) 6×10^{-5} M). The mixture was obtained by means of V_1 (50(0.4, 0.2)). After the alternated microinsertions of pesticide and medium, V_1 switched OFF and the flow was stopped 150 s. Then, V_2 was activated (30(0.6, 0.2)) and 30 alternated insertions of photoirradiated pesticide (V_2 ON, 0.6 s) and oxidant solution Q_4 (KMnO$_4$ 5×10^{-4} M + H_2SO_4 2 M, V_2 OFF, 0.2 s) were performed. V_3 worked as follows: (165,39). Water (Q3) was aspirated the first 165 s of the cycle, then V_3 switched ON and the last 39 s of the cycle (Q4) was aspirated according to V_2 configuration. All pesticides were tested with the lamp OFF and ON. All solution were aspirated at a flow rate of $10\,\text{mL}\,\text{min}^{-1}$.

The criteria for selecting the suitable chemical and physico-chemical variables for the screening were established employing aldicarb[13] as test substance.

The effect of the time of exposure to UV light was studied by changing the time of stopped-flow (time of V_2 in OFF). The analytical signal was found to increase with increasing irradiation time as a result of an increased photodegradation yield. The increase in irradiation time resulted in an increase in the output up to around 120 s; then, the increase was small tending to a plateau. The signal was found to level off after 180 s. A irradiation time of 150 s was chosen for the screening.

The selected insertion profile was: $V_1 = 50(0.4, 0.2)$; $V_2 = 30(ON), 165(OFF), 30(0.6, 0.2)$; $V_3 = 165(OFF), 39(ON)$ (see symbols in Section 2.3.2). The insertion of a large sequence of sample–medium segments (N) was essential due to the large length of the photo-reactor (150 cm) and to ensure an effective mixture of the photo-reactor effluent with the mixture of the oxidant for the chemiluminometric process. Values of $t_1/t_2 > 1$ in V_1 and V_2 avoided the excessive dilution of the pesticide in the flow system. Excellent reproducibility was obtained for times of insertion as short as 0.2 s, equivalent to the insertion of 32 μL of solution.

Flow rates lower than 6 mL min^{-1} were discarded due to the fast kinetic of the chemiluminescent reaction. The increase in flow rate resulted in an increase in the output up to around 9.5 mL min^{-1}; then, a plateau was obtained. The selected flow rate for aspirating sample and reagent solutions was 10 mL min^{-1}.

Acidic permanganate system gives rise to light emission for many compounds and was selected for the present screening. In fact, it is presented as the most efficient oxidant for direct liquid phase chemiluminescent processes. A search employing the analytical abstract data base (1980–2005) and the key words chemiluminescence and the oxidants KMnO$_4$, Ce(IV), Fe(CN)$_6$[3], N-bromosuccinimide yielded as conclusions that 42% of the published papers used potassium permanganate as strong oxidant. The reason of this behaviour is associated to the mechanism of chemiluminescence generation by potassium permanganate. Several authors [4] have contributed to explain it. According to Barnett, it seems the emitter responsible for acidic potassium permanganate chemiluminescence is an excited manganese (II) species of unknown constitution. This hypothesis seems to be verified by enhancing effect of polyphosphates on the chemiluminescent emission using KMO$_4$ as oxidant. The excellent behaviour of potassium permanganate associated to direct chemiluminescence procedures should be due to an unusual case of phosphorescence at room temperature.

On the other hand, the behaviour of permanganate requires special care in selecting its concentration. The signal shows a parabolic profile increasing sharply with concentration up to a maximum value beyond which it decreases abruptly. Attending to the robustness of the procedure, 7×10^{-4} mol L^{-1} KMnO$_4$ in 2 M H$_2$SO$_4$ was selected for the screening.

Attending to the observed Ph-CL response, pesticides can be divided into two groups: (a) compounds which do not present chemiluminescence with lamp OFF and ON; (b) CL-pesticides which either increased dramatically the CL-response with lamp ON, or turns into chemiluminescent ones after irradiation.

From an analytical point of view the most interesting Ph-CL effects are included in group (b) (see Tables 1 and 2) and they are suitable for developing new and sensitive chemiluminescent analytical procedures. Following comments are focused on this group.

In general, a significant increase in the chemiluminescent emission intensity was observed with lamp ON [I(ON)/I(OFF) ratios] for reference compounds in different media were: asulam (46.7), ethoprophos (43.4), imazamethabenz-methyl (45), all in 10^{-3} M NaOH medium; aldicarb (87.5), ethoprophos (500), MCPA (125) and propoxur (150), all in 6×10^{-5} M Fe(III); azamathiphos (50), bromoxymil (300), monolinuron (117), imazamethabenz-methyl and imazapyr (60), in 0.05% H$_2$O$_2$; aldicarb (58), ethoprophos (300) and ametryn (36) in aqueous solution; aldicarb (70), EPTC (57), ethoprophos (40), MCPA (125) and oxadixyl (45), all 6×10^{-5} M in Fe(II). Only aldicarb in H$_2$O$_2$, methomyl in NaOH and H$_2$O$_2$ media, and chlorpropham in H$_2$O$_2$ and aqueous media yielded negative results with lamp ON and OFF. The only pesticide for which a diminution of the chemiluminescence behaviour was observed after irradiation was azamethiphos in NaOH medium. Ametryn, aminocarb, carbetamide, chlorfenac, dichloprop, endothal, hymexazole, imazapyr, isocarbamide, metalaxyl, metazachlor, monolinuron, nicotine, phosphamidon, 2,4,5-T, thiofanox and tribenuron did not presented native chemiluminescence in at least four of the tested media, but turned into strong chemiluminescent compounds in all media after irradiation (Table 3).

Attending the media of photodegradation, H$_2$O$_2$ provided the best analytical signals (number of counts) after irradiation with the low-pressure mercury lamp. Nevertheless, the effectiveness of this medium on the chemiluminescent response was also confirmed with lamp OFF; only 25% of the pesticides tested with H$_2$O$_2$ did not present chemiluminescence with lamp OFF and they did with lamp ON. This percentage increased remarkably in the rest of media. About 65, 68, 75 and 57% of pesticides which did not present chemiluminescence or very weak chemiluminescence behaviour (close to zero) with lamp OFF, were clearly chemiluminescent after UV-irradiation in NaOH, Fe(III), aqueous solution and Fe(II) medium, respectively. The best results (compromise between chemiluminescence intensity and effective conversion of non-chemiluminescent pesticides into chemiluminescent ones) were obtained employing Fe(III) as photocatalyst.

Although the Ph-CL study was applied to a hetereogeneous group of pesticides, some families of pesticides are widely represented, so that the influence of the chemical structure on the Ph-CL behaviour of pesticides can be studied by comparing the analytical signal for structurally related compounds (e.g. carbamates, ureas, organophosphorus, 1,3,5-triazines and imidazolinones). Imidazolinone pesticides imazapyr, imazaquin and imazamethabenz presented good Ph-CL behaviour; nevertheless imazethapyr, differing from imazapyr in a ethyl radical bonded to the N-heterocyclic ring, yielded a negative response against UV-irradiation. Opposite to this behaviour are the 1,3,5-triazines. The non-chemiluminescent character of atraton, prometon

Table 2
Results obtained in the LDA study and classification of the compounds from pattern of induced chemiluminescence activity proposed

Compound	DF[a]	Probability[b]	Class[c]
Training group—active			
Aminocarb	5.77	0.997	+
Benzatone	7.35	0.999	+
Carbetamide	8.03	1.000	+
Cinosulfuron	3.26	0.963	+
Dichlorprop	4.71	0.991	+
Endothall	2.00	0.881	+
2,5,4-T	3.18	0.962	+
Hymexazol	−0.40	0.400	−
Imazapyr	2.10	0.891	+
Isocarbamide	−4.15	0.016	−
MCPB	3.33	0.965	+
Metalaxyl	6.72	0.999	+
Metsulfuron methyl	3.45	0.969	+
Nicotine	4.67	0.991	+
Phosphamidon	−0.82	0.306	−
Azamethiphos	2.72	0.938	+
Bromoxynil	4.01	0.982	+
Chlorpropham	5.20	0.995	+
Cloprop	6.26	0.998	+
Dioxacarb	4.60	0.990	+
Ethoprophos	9.28	1.000	+
Fenuron	8.21	1.000	+
Imazamethabenz A	4.24	0.986	+
Imazaquin	2.66	0.934	+
MCPA	4.49	0.989	+
Mecoprop	5.09	0.994	+
Metamitron	9.75	1.000	+
Monolinuron	6.15	0.998	+
Oxadixyl	5.00	0.993	+
Thiofanox	1.85	0.864	+
Training group—inactive			
Aldisuf	−5.37	0.995	−
Amitrole	−1.60	0.831	−
Chloralose alphe	−7.59	0.999	−
Cyromazine	−3.53	0.972	−
DNOC	−0.01	0.503	−
Ethylene thiourea	−8.92	1.000	−
Glufosinate ammoniun	−6.25	0.988	−
Monocrotophos	−3.61	0.974	−
Propanocarb	−5.52	0.996	−
Secbumeton	−2.81	0.943	−
Trichlorfon	−7.61	1.000	−
Allidochlor	−4.15	0.984	−
Butoxycarboxim	−3.45	0.969	−
Crimidine	−1.02	0.736	−
Dichlorvos	−4.66	0.991	−
Ethephon	−9.88	1.000	−
Fosetyl Al	−8.42	1.000	−
Imazethapyr	−0.17	0.543	−
Prometon	−3.09	0.957	−
Propiconazole	0.79	0.312	+
Terbacil	−2.44	0.920	−
Triflumizole	−2.72	0.938	−
Test group—active			
Aldicarb	0.36	0.589	+
Ametryn	3.66	0.975	+
Asulam	4.00	0.982	+
Chlorfenac	4.07	0.983	+
EPTC	1.77	0.854	+
Imazamethabenz B	3.79	0.978	+
Metazachlor	6.65	0.999	+

Table 2 (Continued)

Compound	DF[a]	Probability[b]	Class[c]
Methomyl	2.46	0.921	+
Propoxur	6.01	0.998	+
Tribenuron	4.63	0.990	+
Test group—inactive			
Bronopol	−8.24	1.000	−
Daminozide	−4.84	0.922	−
Dikegulac	−13.20	1.000	−
Ethidimuron	−0.40	0.598	−
2,4-D	4.10	0.016	+
Flupropanate	−8.12	1.000	−
Methyl isothiocyanate	−8.10	1.000	−
Pirimicarb	−1.28	0.783	−
TCA	−8.38	1.000	−
Thiazafluron	−4.07	0.983	−

Training active and inactive group and test active and inactive group.

[a] Value of the DF (discriminant function) for each compound.
[b] Probability of activity.
[c] The compounds are classified either as active (+) or inactive (−) according to the value of column DF.

and cyromazine was not affected by UV-irradiation; however, ametryn, containing a sulfur group (easily oxidisable under experimental conditions) bonded to the monocyclic heterocycle, is a Ph-CL active compound. In general, carbamate pesticides can be included in the active group presenting Ph-CL. This was the case for aldicarb, asulam, carbetamide, chlorpropham, dioxicarb, methomyl, propoxur and thiofanox. Butoxycarboxim and propanocarb were exceptions to the observed tendency. Organophosphorus and urea pesticides are not clearly classified. Ureas are not significantly represented in the screening test and organophosphorus were found to be non-chemiluminescent and Ph-CL compounds in similar proportion.

The Ph-CL of pesticides is strongly dependent on the chemical structure. Structurally related compounds presenting scarcely differences in their structure show very often different chemiluminometric behaviour.

In order to check the present strategy as an effective way for increasing and improving the number of substances and suitable analytical procedures based on direct chemiluminescence detection, a search employing the analytical abstract data base (1980–2005) and the key words chemiluminescence and the name of pesticide included in group (b) was performed. The search yielded negative results (no previous reported works related to the direct chemiluminescence behaviour of these compounds were published) for aminocarb, azamethiphos, bentazone, carbetamide, chlorfenac, cloprop, dichlorprop, dioxicarb, endothall, EPTC, ethoprophos, fenuron, hymexazol, imazamethabenz-methyl, imazapyr, imazaquin, isocarbamid, MCPA, metalaxyl, metazachlor, metsulfuron-methyl, monolinuron, oxadixyl, phosphamidon, 2,4,5-T, thiofanox and tribenuron. Nevertheless, the positive response with lamp ON was confirmed by the screening test.

3.2. Molecular connectivity calculations

In this work, a set of 72 structurally heterogeneous pesticides was analyzed. These comprise an inactive group (pesticides,

Table 3
Theoretical classification and experimental results for tested compounds

Compound	DF[a]	Probability[b]	Theoretical class[c]	Experimental result	Medium[d]
Clopyralid	1.48	0.805	+	+	All tested media
Cycluron	−5.43	0.995	−	+	Fe(III)/Fe(II)/H_2O_2
Cymoxanil	−2.47	0.920	−	−	H_2O_2[e]
Dimethenamid	3.40	0.968	+	+	All media
Fosamine	−6.12	0.986	−	−	Fe(II)
Glyphosate	−8.07	1.000	−	+	All media
Mecoprop	5.09	0.993	+	+	Fe(III)/Fe(II)/H_2O/H_2O_2
Mepiquat	−1.28	0.783	−	+	NaOH/Fe(III)/Fe(II)/H_2O_2
Metolcarb	6.25	0.998	+	+	All media
Picloram	0.21	0.541	+	+	Fe(III)/Fe(II)/H_2O/H_2O_2
Trinexapac-ethyl	2.77	0.940	+	+	All media

[a] Value of the DF (discriminant function) for each compound.
[b] Probability of activity.
[c] The compounds are classified either as active (+) or inactive (−) according to the value of column DF.
[d] Media with chemiluminescent response after UV-irradiation.
[e] Very weak chemiluminescent behaviour.

which do not present chemiluminescence with lamp OFF and ON, and an active group (CL-pesticides, which either increased dramatically the CL-response with lamp ON, or turns into chemiluminescent ones after irradiation). From an analytical point of view the most interesting Ph-CL effects are included in group (b) and these pesticides are suitable for developing new and sensitive chemiluminescent analytical procedures. Each group was separated in two groups, the training and the test group. Based on this, the obtained discriminant functions were validated. The discriminant function (DF) chosen was:

$$DF = 1.061\, S^T(aCHa) + 3.374\, SS + 7.867\, J^2 - 15.014\,^{10}\chi_P$$
$$+ 1.346\,^1\chi^v - 9.604\,^4\chi_C + 102.62\,^6\chi^v_{CH} - 12.740$$

$$N = 72, \qquad F = 18.37, \qquad U\text{-statistics (Wilks' } \lambda) = 0.238$$

Charge indices J_i, $^m\chi_t$ connectivity indices and electrotopological indices used as topological descriptors in the discriminant function are related to the distribution of intramolecular charge and pure structural features, respectively.

Table 2 shows the classification of the results obtained with the DF for each group. A pesticide will be considered active if $DF_i > 0$, or inactive if $DF_i < 0$. In the training group (active and inactive group) an accuracy of 90 and 95.5%, respectively was observed. Moreover, a success of probability of 100% and 90% was obtained respectively with the test groups (active and inactive).

Distribution diagrams can be constructed representing the expectancy for each classification group in any range of DF. The overlapping region of the graphs is related to the discriminant power of the DF function. The discriminant ability of the DF function is associated to a small or nonexistent (in the limit) overlapping region. Distribution diagrams for training and test groups are depicted in Fig. 3.

The discriminant power of the proposed DF was confirmed by the correct classification of closed structurally related compounds. Imidazolinone pesticides imazapyr, imazaquin (training active group) $DF_i > 0$ and a probability higher than

0.89. Imazamethabenz (actually a mixture of imazamethabenz A (2-(4-isopropyl-4-methyl-5-oxo-4,5-dihydro-1*H*-imidazol-2-yl)-5-methyl-benzoic acid methyl ester) and imazamethabenz B (2-(4-isopropyl-4-methyl-5-oxo-4,5-dihydro-1*H*-imidazol-2-yl)-4-methyl-benzoic acid methyl ester) could be emphasized. Both of them (imazamethabenz A and B) were classified as active compounds, the first one in the training group and the other one in the test group, with a probability higher than 0.97. In the 1,3,5-triazine family cyromazine and prometon were inactive but ametryn was correctly included in the
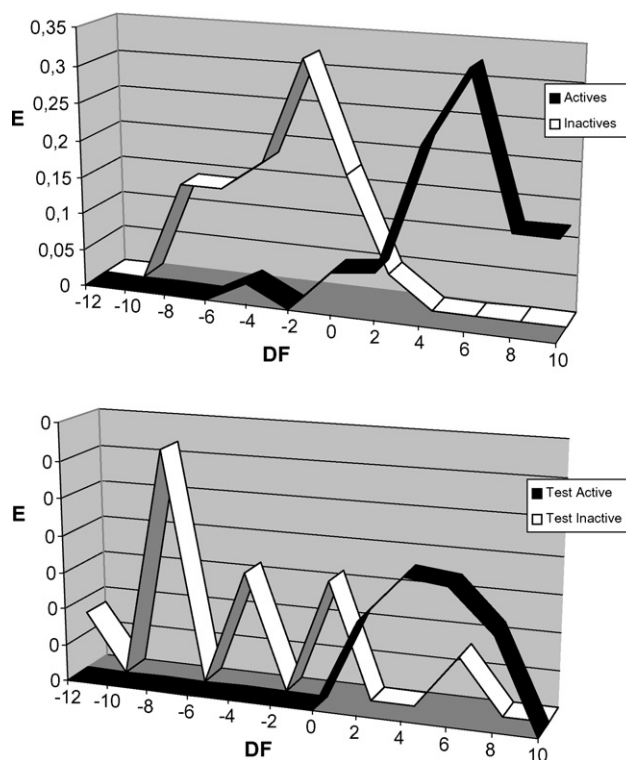

Fig. 3. Distribution diagrams for photoinduced chemiluminescence activity. White line: non-photoinduced chemiluminescence pesticides. Black line: photoinduced chemiluminescence pesticides. Upper: training group. Lower: testing group.

active group. In general, carbamate pesticides presented $DF_i > 0$. This was the case of aldicarb, aminocarb, asulam, carbetamide, chlorpropham, EPTC, methomyl, propoxur and thiofanox. Nevertheless, propamocarb, pirimicarb and butoxycarboxim were classified as inactive compounds.

Finally, the discriminant function was applied to structures not employed in the development and validation of the DF function. The criterion $DF > 0$ was chosen for selecting new pesticides as potential Ph-CL compounds. The viability of the theoretical prediction of the Ph-CL of pesticides was experimentally confirmed by testing the theoretically active pesticides in the multicommutation flow assembly. Good correlation was found for the tested compounds (see Table 3).

4. Conclusions

An automated procedure based on the multicommutation approach for the on-line photodegradation-direct chemiluminescent determination of pesticides is presented.

The photolysis provided by low-pressure mercury lamps of germicidal use permits to increase the number of compounds of environmental interest to be determined by direct chemiluminescence (even compounds without or very weak chemiluminescent behaviour) thanks to the chemiluminescence properties of the resulting photofragments. Although the short time of photoirradiation (150 s), dramatic differences were observed for many pesticides.

The use of low pressure mercury lamps in photodegradation processes allows the determination of compounds which do not present "native" chemiluminescence by using the appropriated medium of photodegradation (e.g. chlorpropham, dichloprop, endothall, hymexazol, methomyl, nicotine, phosphamidon, etc.).

The proposed systems led to strong chemiluminescence for aldicarb, aminocarb, bromoxymil, ethoprophos, imazapyr, imazaquin, imazamethabenz methyl, monolinuron, propoxur, etc. In general, a great improvement of the sensitivity was obtained.

Molecular connectivity is a effective molecular topological tool for the prediction of photoinduced chemiluminescence. It is possible to predict the Ph-CL tendency for a pesticide and, therefore, to develop suitable direct chemiluminescent analytical methods. From six compounds whose Ph-CL behaviour was predicted, six were found experimentally as chemiluminescent after UV-irradiation with a low-pressure mercury lamp. The obtained results corroborate the goodness of the selected descriptors for a topological characterization of pesticides.

LDA provides a pattern for the classification of pesticides (active and inactive against Ph-CL) attending their topological similarity.

Moreover, Ph-CL behaviour was found for pesticides (e.g. aminocarb, bentazone, carbetamide, chlorfenac, dichloprop, EPTC, hymexazol, imazamethabenz-methyl, imazaquin, isocarbamid, MCPA, metazachlor, metsulfuron-methyl, oxadixyl, 2,4,5-T, etc.) for which no previous reported works related to the direct chemiluminescence behaviour of these compounds were published.

References

[1] P.J. Worsfold, A.R. Bowie, M.G. Sanders, J. Bioluminesc. Chemiluminesc. 11 (1996) 61.
[2] A.M. García Campaña, W.R.G. Baeyens, Chemiluminescence in Analytical Chemistry, Marcel Dekker, New York, 2001.
[3] B.J. Hindson, N.W. Barnett, Anal. Chim. Acta 445 (2001) 1.
[4] N.W. Barnett, B.J. Hindson, P. Jones, T.A. Smith, Anal. Chim. Acta 451 (2002) 181.
[5] D. Chaput, J. Assoc. Off. Anal. Chem. 69 (1986) 985.
[6] K.M. Hill, R.H. Hollowell, L.A. Dal Cortivo, Anal. Chem. 56 (1984) 2465.
[7] F. Rouberty, J. Fournier, J. Liq. Chromatogr. Relat. Tech. 19 (1996) 37.
[8] J.J. Aaron, A. Coly, Analusis 28 (2000) 699.
[9] V. David, J.V. García Mateo, J. Martínez Calatayud, Analyst 125 (2000) 1313.
[10] M. Catalá Icardo, J.V. García Mateo, M. Fernández Lozano, J. Martínez Calatayud, Anal. Chim. Acta 499 (2003) 57.
[11] M. Ciborowski, M. Catalá Icardo, J.V. García Mateo, J. Martínez Calatayud, J. Pharm. Biomed. Anal. 36 (2004) 693.
[12] M.M. Halmann, Photodegradation of Water Pollutants, CRC Press, Inc., New York, 1996, p. 195.
[13] M. Palomeque, J.A. García Bautista, M. Catalá Icardo, J.V. García Mateo, J. Martínez Calatayud, Anal. Chim. Acta 512 (2004) 149.
[14] A. Chivulescu, M. Catalá Icardo, J.V. García Mateo, J. Martínez Calatayud, Anal. Chim. Acta 519 (2004) 113.
[15] T. Pérez Ruiz, C.M. Lozano, V. Tomás, J. Martín, Anal. Chim. Acta 476 (2003) 141.
[16] T. Pérez Ruiz, C.M. Lozano, V. Tomás, J. Martín, The Analyst 127 (2002) 1526.
[17] M. Karelson, in: R. Todeschini, V. Consonni (Eds.), Molecular Descriptors in QSAR/QSPR, John Wiley & Sons, New York, 2000.
[18] R. Mannhold, H. Kubinyi, H. Timmerman (Eds.), Handbook of Molecular Descriptors, Methods and Principles in Medicinal Chemistry, vol. 11, Wiley VCH Verlag GmbH, Weinheim, Germany, 2000.
[19] J. Devillers, A.T. Balaban, Topological Indices and Related Descriptors in QSAR and QSPAR, Overseas Publishers Association, Amsterdam, 1999.
[20] H. Hosoya, M. Gotoh, M. Murakami, S. Ikeda, J. Chem. Inf. Comput. Sci. 39 (39) (1999) 192.
[21] L.B. Kier, L.H. Hall, J. Chem. Inf. Compt. Sci. 40 (2000) 792.
[22] L.B. Kier, W.J. Murray, L.H. Hall, J. Med. Chem. 18 (1975) 1272.
[23] R. García Domenech, A. Villanueva, J. Gálvez, R. Gozalbes, J. Chim. Phys. 96 (1999) 1172.
[24] M.C. Icardo, L.L. Zamora, G.M. Antón Fos, J.M. Martínez Calatayd, M.J. Duart, TrAC Trends Anal. Chem. 24 (2005) 782.
[25] I. Ríos Santamaría, R. García Doménech, J. Gálvez Álvarez, J.M. Esteban, P. Santamaría, J. Cortijo, Eu. J. Pharm. Sci. 22 (2004) 271.
[26] R. Gozalbes, J. Gálvez, A. Moreno, R. García Doménech, J. Pharm. Pharmacol. 51 (1999) 111.
[27] C. Calabuig, G.M. Antón Fos, J. Gálvez Álvarez, R. García Domenech, Int. J. Pharm. 278 (2004) 111.
[28] S. Villagra, E. Jauregui, J. Gálvez Álvarez, Molecules 5 (2000) 330.
[29] J. Gálvez Álvarez, M.J. Gómez Lechón, R. García Domenech, J.V. Castell, Biorg. Med. Chem. Lett. 6 (1996) 2301.
[30] S. Mut Ronda, M.T. Salabert Salvador, M.J. Duart, G.M. Antón Fos, Bioorg. Med. Chem. Lett. 13 (2003) 2699.
[31] E. Casaban Ros, G.M. Antón Fos, M.J. Duart, R. García Domenech, Quant. Struct.-Act. Relat. 18 (1999) 35.

[32] M. Duart, G.M. Antón-Fos, P.A. Alemán, J.B. Gay-Roig, M.E. González-Rosende, J. Gálvez, R. García-Domenech, J. Med. Chem. 48 (2005) 1260.

[33] B.M. Gawlik, N. Sotiriou, E.A. Feicht, S. Schulte Hostede, A. Ketttrup, Chemosphere 34 (1997) 2525.

[34] L.H. Hall, L.B. Kier, W.J. Murray, J. Pharm. Sci. 64 (1975) 1974.

[35] L.B. Kier, L.H. Hall, J. Pharm. Sci. 68 (1979) 120.

[36] Q.S. Wang, L. Zhang, J. Liq. Chromatogr. R.T. 22 (1999) 1.

[37] R. Gozalbes, J.V. Julián Ortiz, G.M. Antón Fos, J. Gálvez Álvarez, R. García Domenech, Chromatographia 51 (2000) 331.

[38] R.J. Hurtubise, T.W. Allen, H.F. Silver, J. Chromatogr. 235 (1982) 517.

[39] L. Lahuerta Zamora, Y. Fuster Mestre, M.J. Duart Duart, G.M. Antón Fos, R. García Domenech, J. Gálvez Álvarez, J. Martínez Calatayud, Anal. Chem. 73 (2001) 4301.

[40] B. Gómez-Taylor Corominas, G.M. Antón Fos, J.V. García Mateo, L. Lahuerta Zamora, J. Martínez Calatayud, Talanta 60 (2003) 623.

[41] E.P. Martí, M.C. Icardo, L.L. Zamora, G.M. Antón Fos, J.M. Calatayud, Anal. Chim. Acta 527 (2004) 177.

[42] L.B. Kier, L.H. Hall, Molecular Connectivity in Chemistry and Drug Research, Academic Press, London, 1976.

[43] J. Gálvez, R. García Doménech, M.T. Salabert, R. Soler, J. Chem. Inf. Comput. Sci. 34 (1994) 520.

[44] L.B. Kier, L.H. Hall, J. Chem. Inf. Comput. Sci. 37 (1997) 548.

[45] L.B. Kier, L.H. Hall, Molecular Structure Description. The Electrotopological State, Academic Press, San Diego, 1999.

[46] L.H. Hall, MOLCONN–Z software, Eastern Nazarene College, Quincy, MA, 1995.

[47] Desmol13 Software, 2000. Unidad de Investigación de Diseño de Fármacos y Conectividad Molecular, Facultad de Farmacia, Universitat de València, Spain.

[48] L.B. Kier, Quant. Struct.–Act. Relat. 4 (1985) 109.

[49] J. Gálvez, R. García, J.V. Julian-Ortiz, R. Soler, J. Chem. Inf. Comput. Sci. 35 (1995) 272.

[50] W.J. Dixon, BMDP Statistical Software, University of California, Berkeley, 1990.

[51] J. Gálvez, R. García–Domenech, J.V. de Julián–Ortiz, L. Popa, J. Mol. Graph. 14 (1996) 272.

[52] C. Baird, Environmental Chemistry, 2nd ed., Ed. W.H. Freeman and Company, New York, 1995, pp. 509–510.

[53] C. Catastini, G. Mailhot, S. Malato, M. Sarakha, Proceedings of the Paper presented at the IHP-Users Workshop on Iron Aquacomplexes for Pesticides Mineralisation by Sunlight Irradiation, 2002.

Study of the nonenzymatic glucose sensor based on highly dispersed Pt nanoparticles supported on carbon nanotubes

Lian-Qing Rong [a,b], Chen Yang [a], Qing-Yun Qian [a], Xing-Hua Xia [a,*]

[a] *Key Laboratory of Analytical Chemistry for Life Science, School of Chemistry and Chemical Engineering, Nanjing University, Nanjing 210093, China*
[b] *Department of Chemical Engineering, Pingxiang College, Pingxiang 337055, China*

Abstract

An amperometric biosensor for sensitive and selective detection of glucose has been constructed by using highly dispersed Pt nanoparticles supported on carbon nanotubes (Pt-MWCNTs) as sensing interface. The Pt-MWCNTs were synthesized by using the two-step pyrolysis method. This composite shows good electrocatalytic activity towards the oxidation of glucose in alkaline and thus can be used to selectively detect glucose. We found that detection potential and Nafion amount covered on the Pt-MWCNTs modified glassy carbon electrode had considerable influence on the selectivity for amperometric detection of glucose. Under optimal detection conditions (detection potential of 0.0 V versus SCE and 10 μL 1.5% Nafion), selective detection of glucose in the glucose concentration range of 1.0–26.5 mM (correlation coefficient, >0.999) can be performed. The results demonstrate that the Pt-MWCNTs composite is promising for the fabrication of nonenzymatic glucose sensors.
© 2007 Elsevier B.V. All rights reserved.

Keywords: Carbon nanotubes; Platinum; Nonenzymatic biosensor; Glucose; Electroanalysis

1. Introduction

Determination of dissolved glucose is of great importance in various areas [1–4]. Many previous studies on glucose detection included the use of enzyme glucose oxidase [2,5], which catalyzes the oxidation of glucose in the presence of oxygen to hydrogen peroxide that can be amperometric detected. However, due to the intrinsic nature of enzymes, such enzyme-based sensors suffer from the instability problem [6–8]. Studies have been attempted to detect glucose based on its direct electrochemical oxidation. However, conventional platinum or gold electrodes have the shortcoming of low electrocatalytic activity towards the oxidation of glucose due to the poisoning effect of reaction intermediates (e.g., adsorbed CO) [6,9], resulting in low sensibility, poor selectivity. On the other hand, the electrochemical detection of glucose with conventional electrodes was influenced heavily by the interfering electroactive species such as ascorbic acid (AA), uric acid (UA), and *p*-acetamidophenol (PP) under physiological conditions [10,11]. Since the electrocatalytic oxidation of glucose on platinum electrodes is a kinetic controlled reaction, its oxidation rate can be enhanced by increasing the real surface area. While the electrochemical responses of the common interfering species of ascorbic acid, uric acid and *p*-acetamedophenol will not be changed significantly since their electrochemical oxidation are diffusion controlled. Therefore, porous platinum electrodes with high roughness factors can be used to sensitively and selectively detect glucose without interference from the common interfering electroactive species. We and others reported that mesoporous platinum [12], three-dimensionally ordered macroporous platinum [9], and highly ordered platinum-nanotubes arrays [11,13,14] could be the potential catalytic interfaces for construction of nonenzymatic glucose sensors with high selectivity and sensitivity.

Carbon nanotube (CNT) has been proven to be one of the most functional nanomaterials because of its remarkable electronic and mechanical properties [15]. Explorations of the CNTs in biological and medical applications have become a rapidly expanding research field [16,17], especially in electrochemistry.

* Corresponding author. Tel.: +86 25 83597436; fax: +86 25 83597436.
E-mail address: xhxia@nju.edu.cn (X.-H. Xia).

Ye et al. [2] for the first time reported the nonenzymatic detection of glucose using a CNTs modified Glass Carbon (GC) electrode. Electrochemical detection of carbohydrates at carbon nanotube modified glassy carbon electrodes was also reported [3]. However, Compton and his coworkers recently reported that the previously reported electrocatalytic activity of carbon nanotubes came from the metal impurities [18]. They also demonstrated that the electrocatalytic reduction of hydrogen peroxide at a multi-walled carbon nanotube modified electrode is due to the iron oxide particles arising from the chemical vapor deposition process rather than due to the intrinsic catalytic activity of the carbon nanotubes [19].

We recently reported a method for the fabrication of noble metallic nanoparticles supported on carbon nanotubes by using a two-step approach including adsorption and pyrolysis [20,21]. In this method, the functional groups of the carbon nanotubes act as nucleation sites for the growth of platinum particles, thus, the platinum nanoparticles are highly dispersed on the side wall of the carbon nanotubes (Pt-MWCNTs) and have good stability. As mentioned above, glucose can be electrochemically oxidized to gluconic acid at a platinum electrode. Parallel to this reaction, poisoning intermediate (adsorbed CO) is formed, which poisons the electrode surface. The total oxidation mechanism of glucose at platinum electrode is similar to that of ethanol. The generally accepted dual-pathway mechanism of the electrooxidation of ethanol has been demonstrated [22–25]. The ethanol molecules adsorb on a site which is initially covered by a water molecule. Adsorbed ethanol can dissociate to produce adsorbed CO and some other H-containing adsorbed residues. Platinum electrode surface will be rapidly poisoned by the strongly adsorbed CO and ethanol electrooxidation is thus prevented before CO being oxidized at much higher overpotentials. In another oxidation way, ethanol is directly oxidized to form solvable intermediates of acetaldehyde or acetic acid. We believe that the Pt-MWCNTs composite could be an active electrocatalyst towards the oxidation of glucose and is promising for the fabrication of a nonenzymatic glucose sensor.

In this communication, we report the fabrication of a nonenzymatic biosensor for selective detection of glucose by using platinum nanoparticles supported on multi-walled carbon nanotubes as the catalyst. The Pt-MWCNTs composite was prepared as we reported previously [20,26] and characterized by Transmission Electron Microscope (TEM). Electrochemical methods were used to characterize the electrocatalytic activity of the Pt-MWCNTs towards the oxidation of glucose. Selective detection of glucose using the present catalyst was optimized by choosing proper experimental conditions.

2. Materials and methods

2.1. Functionalization of multi-walled carbon nanotubes

Carbon nanotube is very hydrophobic and cannot be wetted by aqueous solution for its high surface tension [27]. Surface modification is of importance to improve metal ions adhesion to the carbon nanotube. According to our previous report [20,21], the multi-walled carbon nanotube (Shenzhen Nanotech Co. Ltd.)

was purified by refluxing in a 5 M HNO_3 aqueous solution for 5 h to remove the metallic nickel particles that served as a catalyst for the growth of MWCNTs, and then washed with deionized water for several times. The purified MWCNTs were refluxed in a mixture of HNO_3 and H_2SO_4 (1:1) for 2 h and then filtrated and washed with deionized water until the solution pH approached 7.0. FTIR analysis of the resulting MWCNTs shows that the MWCNTs surface has functional groups such as phenol, carbonyl and carboxyl groups located at ca. 1720 and 3440 cm^{-1}, respectively [20].

2.2. Deposition of Pt nanoparticles on the multi-walled carbon nanotubes

The functional MWCNTs were stirred in 0.04 M $PtCl_4$–C_2H_5OH solution for ca. 2 h. Then, they were filtrated and dried at room temperature. Pyrolysis of the pretreated MWCNTs adsorbed with platinum salts was carried out in a self-made furnace at 500 °C for 1 h to form black powder of Pt-MWCNTs composite. The whole process was carried out under N_2 atmosphere for avoiding the incursion of oxygen and at the meantime removing the gaseous byproducts formed during the pyrolysis process.

Infrared spectroscopic analysis of the functional carbon nanotube was carried out on a Tensor-27 Fourier IR spectrometer (Bruker, USA) equipped with a MCT detector. Transmission electron microscopic (TEM) images and X-ray diffraction patterns were measured on JEM 200CX (JEOL, Japan), ESCALAB MKII (VG company, United Kingdom) using an Mg Kα X-ray source, X'Pert X-ray diffraction spectrometer (Philips, USA), respectively.

2.3. Preparation of Pt-MWCNTs electrode

1.2 mg Pt-MWCNTs powder was dispersed in 300 μL dimethylformamide (DMF). Nafion solution (1.5%) was prepared by diluting 5% Nafion solution (Aldrich) with ethanol. 2.5 μL Pt-MWCNTs composite in DMF was cast on a well-polished glassy carbon electrode ($\phi = 3$ mm) twice under atmosphere. After the film was dried, Nafion solution (1.5% in ethanol) was pipetted on the catalyst surface for protection.

Electrochemical characterization of the Pt-MWCNTs-Nafion modified GC electrode was performed on a CHI 800 Electrochemical Station (CH Instrument, USA) with a modified electrode as the working electrode, a platinum sheet as the counter electrode and a Saturated Calomel Electrode (SCE) as the reference, respectively. All potentials in this work refer to the SCE. Amperometric measurements were carried out under stirred condition, and the response currents were marked with the change value between the steady-state current and background current.

All chemicals were of analytical grade and solutions were prepared with deionized water from a pure system (>18 MΩ, Purelab Classic Corp., USA). All the electrochemical experiments were carried out in nitrogen saturated solutions and at room temperature.
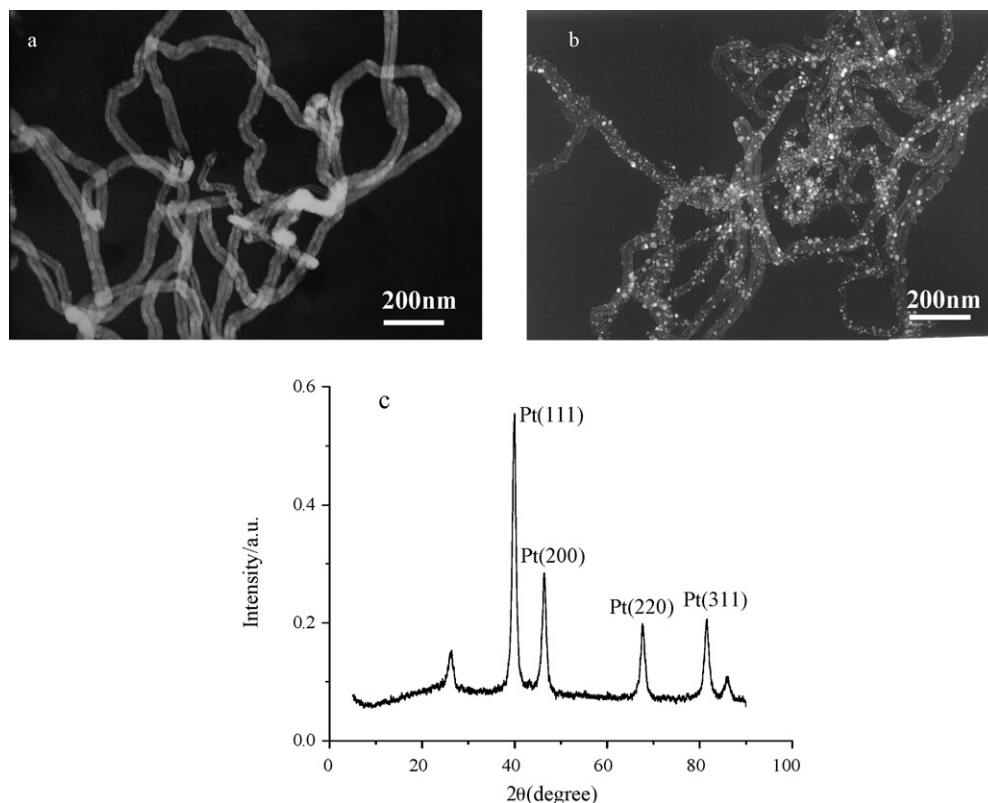
Fig. 1. (a) TEM image of the functional MWCNTs; (b) TEM image of the Pt-MWCNTs; (c) XRD pattern of the Pt-MWCNTs.

3. Results and discussion

3.1. Characterization of the Pt-MWCNTs composite

Fig. 1 shows the TEM images of the functional multi-walled carbon nanotube (a) and the Pt nanoparticles supported on the MWCNTs (b), respectively. As shown in Fig. 1a, the functional MWCNTs has an outer diameter of ca. 40 nm and inner diameter of ca. 5 nm. After deposition of Pt, the TEM image shows that highly dispersed Pt nanoparticles evenly distributed on the sidewall of the MWCNTs. The highly dispersed Pt nanoparticles on the sidewall of the MWCNTs may provide large available surface and enhance the electrocatalytic activity towards the oxidation of glucose.

Fig. 1c shows the X-ray diffraction pattern of the Pt nanoparticles supported on carbon nanotubes. The diffraction peaks at around 2θ of 39.7° (1 1 1), 46.2° (2 0 0), 67.4° (2 2 0), and 81.2° (3 1 1) can be assigned to the Pt face-centered cubic (fcc) structure. The diffraction peak at 26.5° can be attributed to the hexagonal graphite structures (0 0 2). The average particle size of the deposited Pt-catalysts was calculated to be ca. 9 nm from the (1 1 1), (2 0 0) and (2 2 0) X-ray diffraction peaks of the Pt cubic (fcc) lattice in terms of the Scherrer's equation [28].

3.2. Electrocatalysis of glucose at a Pt-MWCNTs composite modified electrode

The electrocatalytic activity of the Pt-MWCNTs composite towards the oxidation of glucose in an alkaline solution was first demonstrated. Fig. 2 shows the cyclic voltammograms of the Pt-MWCNTs-Nafion modified GC electrode in a 0.1 M NaOH solution with (solid curve) and without (dashed curve) 5 mM glucose at a scan rate of 100 mV s^{-1}. In the alkaline solution, the CV shows the characteristics of a platinum electrode including the hydrogen region (−1.0 to −0.6 V), double layer region (−0.6 to −0.3 V) and the oxide formation region (−0.4 to +0.6 V). With glucose in solution, the CV shows a very complicated electrochemical behavior. In the positive potential scan, three anodic current peaks appear at −0.73, −0.25 and +0.11 V, respectively.
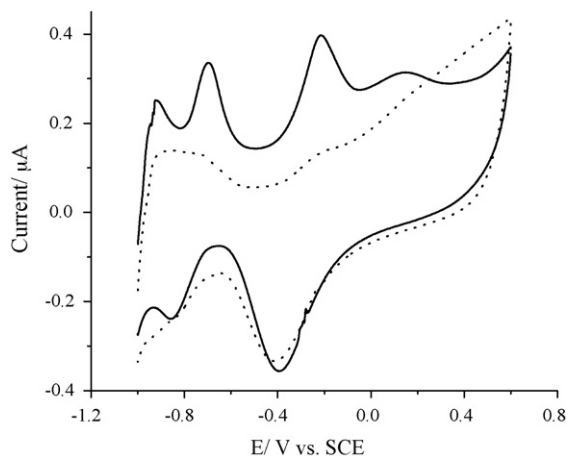
Fig. 2. Cyclic voltammograms (CVs) of a Pt-MWCNTs-Nafion modified GC electrode in a 0.1 M NaOH solution in the presence (solid curve) and absence (dotted curve) of 5 mM glucose at a scan rate of 100 mV s^{-1}.
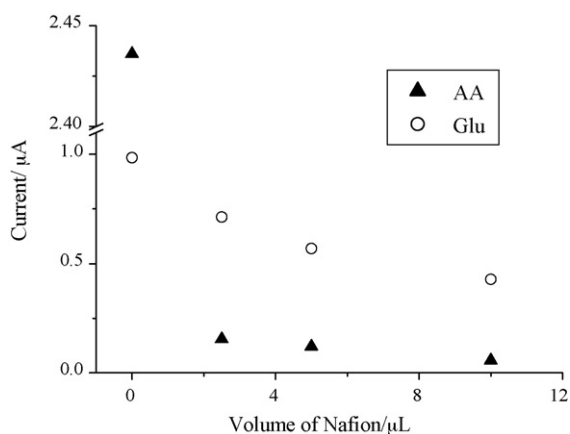
Fig. 3. Effect of the volume of 1.5 wt% Nafion solution on the amperometric response of the Pt-MWCNTs modified GC electrode at 0.0 V in a solution of 0.1 M NaOH containing 0.1 mM ascorbic acid (solid triangles) or 1 mM glucose (empty circle).

The first current peak should be due to the electrochemical adsorption of glucose to form an adsorbed intermediate. At potentials positive with respect to this peak, accumulation of the intermediates (e.g., adsorbed CO) on the electrode surface inhibits the further adsorption of glucose, resulting in a decrease in current. At a potential of about −0.53 V, Pt–OH surface species start to form in the NaOH solution (compare with the CV in alkaline solution without glucose). The Pt–OH species can then oxidize the poisoning intermediates derived from the electrochemical adsorption of glucose to form the anodic current peak at −0.25 V. This process releases free platinum active sites for the direct oxidation of glucose, resulting in the third anodic current peak at +0.11 V. The decrease in current after the third current peak could be due to the formation of thick platinum oxide which in turn inhibits the oxidation of glucose as well. In the negative potential scan, two cathodic current peaks

appear. The cathodic current peak at −0.40 V should be due to the reduction of platinum oxide that is formed in the positive potential scan. The peak at −0.82 V could be due to the reduction of the oxidized products of glucose or desorption of the oxidation products (gluconic acid and any derivatives), since this peak is only apparent in the presence of glucose.

In order to understand the observed electrochemical behavior of the Pt-MWCNTs-Nafion modified GC electrode for glucose oxidation, CVs of glucose on MWCNTs that experienced the same pyrolysis conditions as the Pt-MWCNTs was also carried out. In this experiment, cyclic voltammograms (CVs) of

Fig. 4. Amperometric responses of the Pt-MWCNTs-Nafion modified GC electrode at different detection potential upon successive additions of 80 μL solution containing 0.5 M glucose into 40 mL 0.1 M NaOH. The detection solution was continuously stirred. Detection potential: −0.2 V (a), −0.1 V (b), 0.0 V (c), +0.1 V (d) and +0.2 V (e).
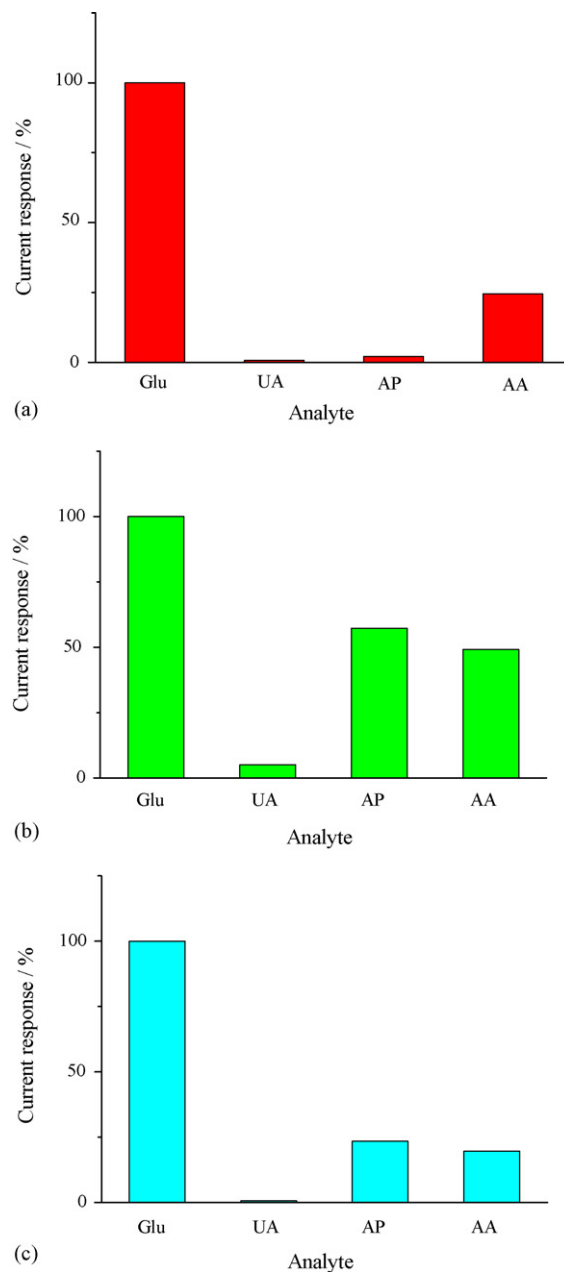
Fig. 5. Selectivity of the modified electrode at 0.0 V (a), 0.1 V (b) and 0.2 V (c) in a solution of 0.1 M NaOH + 1.0 mM glucose upon continuous addition of 0.02 mM UA, 0.10 mM AP, and 0.10 mM AA in 0.1 M NaOH. The current for glucose on the modified electrode was taken as 100%, and the currents for the interfering electroactive species were normalized to the current for glucose.

the MWCNTs-Nafion modified GC electrode in a 0.1 M NaOH solution with and without glucose are almost the same, only showing a peak pair located at around −0.4 V which is due to the redox behavior of the carboxylic acid groups on the functional MWCNTs surface [29]. Obviously, the functional MWCNTs do not show obvious electrocatalytic activity towards the oxidation of glucose in alkaline solution. Therefore, the observed electro-catalytic oxidation of glucose on the Pt-MWCNTs composite modified electrode is due to the presence of platinum nanoparticles, but not the MWCNTs itself or impurities such as iron oxide, which is in good agreement with that reported recently [18,19].

3.3. Effect of Nafion on the electrochemical response of the modified electrode

Curulli et al. [30] reported a glucose biosensor based on PB supported on non-conventional conducting polymer nanotubes. It had high selectivity for H_2O_2 and high rejection towards the common interferences. Alternatively, we used Prussian blue as electrocatalyst for the reduction of hydrogen peroxide generated from an enzymatic reaction [31]. In addition, we suggested a dual-electrode pair system with diffusion layer distance gap to completely deplete interfering species, thus, selective and sensitive detection of glucose can be realized [32,33]. In addition, Tang et al. [14] reported that Nafion film has good anti-interferent ability to ascorbic acid during glucose detection.

Fig. 3 indicates that the anodic response of the Pt-MWCNTs modified GC electrode at 0.0 V in a solution of 0.1 M NaOH containing 0.1 mM ascorbic acid or 1 mM glucose decreases with the increase of Nafion amount covered on the electrode surface. As the Nafion volume increased from 0 to 10 μL, the amperometric response of AA significantly decreased from 2.44 to 0.06 μA; while for glucose, it decreases slightly from 0.99 to 0.43 μA. It is clear that the decrease in amperometric response for ascorbic acid upon increase of Nafion is much faster than for glucose. Therefore, we can selectively detect glucose simply by increasing the Nafion amount. In the following experiments, 10 μL 1.5% Nafion solution was cast on the modified electrodes.

3.4. Amperometric response to glucose and interfering electroactive species

In this section, the effect of detection potential on the amperometric detection of glucose was investigated. In the measurements, the amperometric responses of the Pt-MWCNTs-Nafion modified GC electrode at different detection potential in a solution of 0.1 M NaOH upon addition of glucose were recorded. The results are shown in Fig. 4. Addition of glucose was marked with arrows to the concentrations mentioned. It is clear that the response current of the modified electrode abruptly increases to steady-state values upon addition of glucose. The response time is only about 10 s. In addition, the response sensitivity of glucose increases significantly with the potential increasing from −0.1 to 0.0 V. At more positive detection potentials (0.0 to +0.2 V), it changes slightly.

The normal physiological level of glucose is 3–8 mM, which is much higher than that of the interfering species, AA, UA and PP, ∼0.1 mM. Since the interfering species have higher electron transfer rates than glucose, their oxidation currents are comparable to that from highly concentrated glucose. Therefore, the amperometric responses of the modified electrode at 0.0, 0.1 and 0.2 V in solutions of 0.1 M NaOH + 1 mM glucose and 0.1 M NaOH with continuous addition of 0.02 mM UA, 0.10 mM AP, and 0.10 mM AA were evaluated, respectively. For a better comparison, the response current of 1 mM glucose is set as 100%, and the responses of the interfering species are normalized by this value. The results are shown in Fig. 5. For all these three detection potentials, the interference from UA is neglectable; while interferences from the AP and AA are significant and they increase with the increase of the detection potential. At the detection potential of 0.0 V (Fig. 5a), the interferences from UA, AP and AA are only 0.72%, and 2.14% and 24.5%, respectively. This indicates that at the detection potential of 0.0 V, the present sensor has good anti-interfere ability towards the three interferents and the selective and sensitive detection of glucose on the modified electrode can be achieved.

Based on the above measurements, the optimal detection conditions of the modified electrode towards glucose can be summarized as: the volume of 1.5% Nafion is 10 μL and the
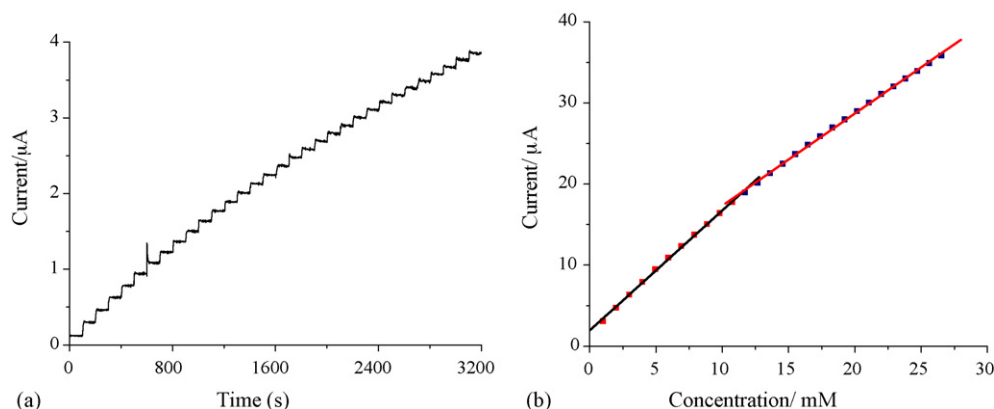

Fig. 6. Hydrodynamic response (a) of the Pt-MWCNTs-Nafion modified gold electrode at 0.0 V upon addition of 80 μL solution containing 0.5 M glucose into 40 mL 0.1 M NaOH (volume correction considered) for each current step and the corresponding calibration curve (b).

detection potential is 0.0 V. Under these optimal conditions, amperometric determination of glucose was carried out. As shown in Fig. 6a, the amperometric response of glucose on this modified electrode shows good stability over long term performance. The corresponding calibration curve (Fig. 6b) shows two linear regions of glucose concentration, respectively, in 1.0–11.7 mM (correlation coefficient, 0.9993) and 11.7–26.5 mM (correlation coefficient, 0.9995).

4. Conclusions

We have synthesized Pt-catalysts supported on carbon nanotubes by using the two-step process including adsorption and pyrolysis. The Pt nanoparticles disperse uniformly on the sidewalls of the carbon nanotubes. The resulting Pt-MWCNTs catalyst shows high electrocatalytic activity towards the oxidation of glucose in alkaline solution, and thus can be successfully used to selectively detect glucose. Results showed that the Pt-MWCNTs catalyst modified electrode covered with 10 μL 1.5% Nafion at a detection potential of 0.0 V versus SCE had good anti-interfere ability towards UA, AP and AA. Good linear dependence of the amperometric response of the modified electrode on the glucose concentration range from 1 to 26.5 mM was achieved. The present communication shows that the Pt-MWCNTs composite is promising for the fabrication of nonenzymatic glucose sensors.

References

[1] X. Zhang, K.Y. Chan, A. Tseung, J. Electrochem. Chem. 386 (1995) 241.
[2] J. Ye, Y. Wen, W.D. Zhang, L.M. Gan, G.Q. Xu, F.S. Sheu, Electrochem. Commun. 6 (2004) 66.
[3] R.P. Deo, J. Wang, Electrochem. Commun. 6 (2004) 284.
[4] J. Zhao, F. Wang, J.J. Yu, S.S. Hu, Talanta 70 (2006) 449.
[5] G.L. Luque, M.C. Rodriguez, G.A. Rivas, Talanta 66 (2005) 467.
[6] I.T. Bae, E. Yeager, X. Xing, C.C. Liu, J. Electroanal. Chem. 309 (1991) 131.
[7] Y.P. Sun, H. Buck, T.E. Mallouk, Anal. Chem. 73 (2001) 1599.
[8] E. Shoji, M.S. Freund, J. Am. Chem. Soc. 123 (2001) 3383.
[9] X.L. Wei, P.K. Shen, Chin. J. Chem. Phys. 16 (2003) 395.
[10] Y.Y. Song, D. Zhang, W. Gao, X.H. Xia, Chem. Eur. J. 11 (2005) 2177.
[11] J.H. Yuan, K. Wang, X.H. Xia, Adv. Funct. Mater. 15 (2005) 803.
[12] S. Park, T.D. Chung, H.C. Kim, Anal. Chem. 75 (2003) 3046.
[13] S. Hrapovic, Y. Liu, K.B. Male, J. Luong, Anal. Chem. 76 (2004) 1083.
[14] H. Tang, J. Chen, S. Yao, L. Nie, G. Deng, Y. Kuang, Anal. Biochem. 331 (2004) 89.
[15] H.J. Dai, Surf. Sci. 500 (2002) 218.
[16] A. Bianco, M. Prato, Adv. Mater. 15 (2003) 1765.
[17] E. Katz, I. Willner, Chem Phys Chem 5 (2004) 1085.
[18] C.E. Banks, A. Crossley, C. Salter, S.J. Wilkins, R.G. Compton, Angew. Chem. Int. Ed. 45 (2006) 2533.
[19] B. Šljukić, C.E. Banks, R.G. Compton, Nano Lett. 6 (2006) 1556.
[20] Y.L. Yao, D. Zhang, X.H. Xia, Chin. J. Inorg. Chem. 20 (2004) 531.
[21] Y.L. Yao, Y. Ding, L.S. Ye, X.H. Xia, Carbon 44 (2006) 61.
[22] J. Willsau, J. Heitbaum, J. Electroanal. Chem. 194 (1985) 27.
[23] T. Iwasita, B. Rasch, E. Cattaneo, W. Vielstich, Electrochim. Acta 34 (1989) 1073.
[24] S.C. Chang, L.W.H. Leung, M.J. Weaver, J. Phys. Chem. 94 (1990) 6013.
[25] J. Shin, W.J. Tornquist, C. Korzeniewski, C.S. Hoaglund, Surf. Sci. 364 (1996) 122.
[26] J. Li, Y.B. Wang, J.D. Qiu, D.C. Sun, X.H. Xia, Anal. Bioanal. Chem. 383 (2005) 918.
[27] E. Dujardin, T.W. Ebbesen, H. Hiura, K. Tanigaki, Science 265 (1994) 1850.
[28] J.Z. Wang, H.Z. Huang, X.A. Mao, in: L. Fei, J.M. Hu, G.S. Pan (Eds.), Nanoparticle Analyse, vol. 1, Chemical Engineering Press, Beijing, 2003 (Chapter 9).
[29] H.X. Luo, Z.J. Shi, N.Q. Li, Z.N. Gu, Q.K. Zhuang, Anal. Chem. 73 (2001) 915.
[30] A. Curulli, F. Valentini, S. Orlanduci, M.L. Terranova, G. Palleschi, Biosens. Bioelectron. 20 (2004) 1223.
[31] D. Zhang, K. Zhang, Y.L. Yao, X.H. Xia, H.Y. Chen, Langmuir 20 (2004) 7303.
[32] K. Wang, D. Zhang, T. Zhou, X.H. Xia, Chem. Eur. J. 11 (2005) 1341.
[33] K. Wang, J.J. Xu, D.C. Sun, H. Wei, X.H. Xia, Biosens. Bioelectron. 20 (2005) 1366.

Multisensor system for determination of polyoxometalates containing vanadium at its different oxidation states

Alisa Rudnitskaya [a],*, Dmitry V. Evtuguin [b], Jose A.F. Gamelas [b], Andrey Legin [a]

[a] *Department of Chemistry, St. Petersburg University, Russia*
[b] *Department of Chemistry, University of Aveiro, 3810-193 Aveiro, Portugal*

Abstract

The electronic tongue (ET) multisensor system has been employed for the detection of metal-oxygen cluster anions (polyoxometalates) containing vanadium (IV/V) atoms. Sensitivity of a variety of potentiometric chemical sensors with plasticized polyvinyl chloride and chalcogenide glass membranes was evaluated with respect to vanadyl/vanadate ions, decavanadate and a series of Keggin-type polyoxometalates (POM) such as α-$[SiW_{11}V^{IV}O_{40}]^{6-}$, α-$[SiW_{11}V^{V}O_{40}]^{5-}$, α-$[BW_{11}V^{IV}O_{40}]^{7-}$, α-$[BW_{11}V^{V}O_{40}]^{6-}$, α-$[PW_{11}V^{IV}O_{40}]^{5-}$ and α-$[PW_{12-n}V_nO_{40}]^{(3+n)-}$ ($n = 1, 2, 3$). Sensor's responses to vanadium complexes were evaluated in the pH range of 2.4–6.5 and a set of sensors appropriate for detecting a variety of vanadium species was selected. Such sensor array was able to distinguish different vanadium complexes allowing their simultaneous quantification in binary (V(IV)/V(V)) mixtures. The vanillyl alcohol oxidation with α-$[SiW_{11}V^{V}O_{40}]^{5-}$ was monitored using ET to evaluate the capacity of proposed analytic system to detect simultaneously V(IV)/V(V) in POM under dynamic equilibrium. ET was demonstrated to be a promising tool for the discrimination and quantification of vanadium-containing POMs at different oxidation states. In particular, such a system could represent a significant interest for the mechanistic studies of redox reactions with POMs.
© 2006 Elsevier B.V. All rights reserved.

Keywords: Electronic tongue multisensor system; Keggin-type polyoxometalates; Potentiometric chemical sensors; Vanadium detection

1. Introduction

Polyoxometalates (abbreviated as POM) [1,2] have been a topic of interest among researchers due to their high potential in several fields that range from classical coordination chemistry to homogeneous and heterogeneous catalysis [3,4], material science [5], medicine [6], etc. One topic of special interest from the point of view of polyoxometalate science and catalysis is the speciation of polyoxometalates in aqueous or organic solutions. In homogeneous catalytic systems, where POMs are used as catalysts, several species of a POM may co-exist simultaneously in solution during catalysis experiments that depends on the POM origin and its stability under particular experimental conditions.

Phosphovanadomolybdates of the Keggin-type and formulae $[PMo_xV_{12-x}O_{40}]^{(3+x)-}$, such as $[PMo_{10}V_2O_{40}]^{5-}$ among others, have been extensively studied as catalysts for the oxidation of several types of organic substrates with oxygen in liquid phase systems [7–9], including delignification of lignocellulosic materials [10–12]. In the catalytic process it is assumed that the substrate is oxidized while the vanadium (V) atoms of polyoxometalates are reduced to V(IV). The cycle is completed by re-oxidation of vanadium centres in polyoxometalate by O_2. It is of some controversy if vanadium redox processes occur inside the Keggin-type structure of POM or outside. Whether or not vanadium leaves the POM in the form of "VO_2^+" (or perhaps more probable in the form of the more labile "VO^{2+}" after reduction step) remains to be solved. In such case, a mixture of POM in oxidized and reduced forms and of vanadium outside POM, as VO_2^+ and VO^{2+}, respectively, or other species is possible. Therefore, a rapid analytical technique capable of distinguishing all these forms of vanadium species in solution is of significant interest.

Several analytical methods can be used for measuring and speciating vanadium and vanadium-containing POM in solutions. ^{17}O, ^{183}W (1D and 2D), ^{51}V and ^{31}P NMR have been used for the characterization of POM (mostly diamagnetic species) in both aqueous and non-aqueous systems. ^{183}W NMR, in particular, was used to determine the structures of POM in solution

e.g. [13–16]. This is, however, a difficult nucleus due to its comparatively low natural abundance and low inherent sensitivity [13,17], and satisfactory NMR spectra require the use of concentrated solutions and long accumulation times: typically, good 2D ^{183}W NMR requires the use of concentrations higher than 0.1 M and total time of acquisition of several days (about 3 days).

In contrast, ^{51}V and ^{31}P NMR provide relatively rapid identification because of their inherently higher sensitivity and abundance [17]. Solutions with concentrations of POM in the millimole range may be enough for a relatively fast acquisition of spectrum. Several works concerning the speciation of vanadium by using ^{51}V NMR in aqueous solutions at different pH and in the presence of several types of ligands such as amino acids, and hydrogen peroxide were reported [18,19]. The major limitation of ^{51}V and ^{31}P NMR is the analyses of solutions of POM that have paramagnetic ions such as vanadium (IV), manganese (II, III) or iron (III) in their (primary) structure. Most of the signals are broad or even unobservable by NMR.

EPR spectroscopy was used for characterization of vanadium (IV)-containing POM. Information regarding the g and A parameters and delocalization of electrons among the vanadium centres in vanadium-substituted Keggin-type anions has been provided [20,21]. Due to the hyperfine coupling with the vanadium nucleus and the usual delocalization of the unpaired electron in more than one vanadium centre for those multisubstituted vanadium anions the spectra are usually complex. In the case of solutions, where more than one species including different isomers are present, the spectra of the several paramagnetic components will overlap, which will make difficult or even impossible the quantification of the different vanadium (IV) species by EPR. It is worth noting that in the case of vanadium (V) species, EPR cannot be applied due to the d^0 electronic configuration of vanadium (V). Simultaneous and instantaneous detection of V(IV) and V(V) containing species in solution using NMR and EPR techniques is impossible.

One of the emerging analytical techniques promising for speciation of vanadium-containing species is the application of multisensor systems or electronic tongues (ET). ET comprises an array of cross-sensitive (partially selective) chemical sensors and pattern recognition and multivariate calibration methods for the processing of their complex output [22,23]. The concept of the electronic tongue is based on organisation principles of human sensory systems such as taste and olfaction, hence the name of the device. However, actual design and sensing materials of the electronic tongues have nothing in common with biological counterparts, thus, the performance also differs drastically. In particular, the electronic tongues can be used for analysis of poisonous and inedible media and also for multicomponent quantitative analysis. This approach became popular during the last decade and several applications of multisensor systems for quantitative and qualitative analysis of various liquids were reported. These included analysis of foodstuffs (both recognition and detection of nutrients' content), analysis of wastewaters, natural waters, biotechnological growth media, etc. [20,21 and references therein].

Electronic tongue based on potentiometric chemical sensors has been developed in the ET group of St. Petersburg University. Chemical sensors with chalcogenide glass, crystalline and plasticized polyvinyl chloride based membranes are employed. A wide range of sensor compositions is necessary to achieve sensitivity to a big number of inorganic and organic ions as well as to certain red-ox substances. Applications of the ET to the quantitative analysis and recognition or classification of a number of various media including foodstuffs and industrial solutions were reported [22]. Simultaneous determination of concentrations of transition metals in industrial streams [24], natural waters [25] and at low ppb levels in artificial seawater [26] using the ET system was performed. The results particularly relevant to the present study include simultaneous determination of metals in different oxidation states, namely Fe(III), Fe(II), U(IV) and U(VI) in mixed solutions [27]. This became possible largely due to the use of the sensors displaying redox cross-sensitivity in the array of ET. Thus, potentiometric electronic tongue appears to be a promising tool for solving such problem as detection and speciation of vanadium-containing species at the different oxidation states.

The main goal of the present study was the development of a potentiometric multisensor system (ET) for fast measuring of concentrations and discrimination of vanadium at different oxidation states in polyoxometalates.

2. Experimental

2.1. Preparation of polyoxometalate compounds

All studied compounds are listed in Table 1. Vanadyl sulphate (**1**) and sodium or potassium metavanadates (**2**) were from Merck Chem. Co. (Madrid). All POMs were synthesized in laboratory at the Department of Chemistry of the University of Aveiro.

Sodium decavanadate $Na_6[V_{10}O_{28}]\cdot18H_2O$ (**3**) was prepared following known procedure [28]. Compounds α-K$_6$[α-SiW$_{11}$V^{IV}O$_{40}$]·7H$_2$O (**4**), α-K$_5$[α-SiW$_{11}$V^{V}O$_{40}$]·10H$_2$O (**5**), α-K$_7$[BW$_{11}$V^{IV}O$_{40}$]·7H$_2$O (**6**) and α-K$_6$[BW$_{11}$V^{V}O$_{40}$]·8H$_2$O (**7**) were prepared according to the previously described procedures [14,17]. The purity of these compounds was confirmed using UV–vis spectroscopy for vanadium (IV) compounds

Table 1
The studied vanadium-containing compounds

	Compound	pH stability range	Concentration range (mM)
1	V^{IV}OSO$_4$		0.001–10
2	KV^{V}O$_3$, NaV^{V}O$_3$		0.001–10
3	Na$_6$[V$_{10}$^{V}O$_{28}$]		0.001–10
4	α-K$_6$[SiW$_{11}$V^{IV}O$_{40}$]	2–8	0.001–1
5	α-K$_5$[SiW$_{11}$V^{V}O$_{40}$]	2–8	0.001–1
6	α-K$_7$[BW$_{11}$V^{IV}O$_{40}$]	2–8	0.001–1
7	α-K$_6$[BW$_{11}$V^{V}O$_{40}$]	2–8	0.001–1
8	α-K$_5$[PW$_{11}$V^{IV}O$_{40}$]	Up to 5	0.001–1
9	α-K$_4$[PW$_{11}$V^{V}O$_{40}$]	Up to 3	0.001–0.5
10	$\alpha_{1,2}$-K$_5$[PW$_{10}$V$_2$^{V}O$_{40}$]	Up to 3	0.001–0.5
11	$\alpha_{1,2,3}$-K$_6$[PW$_9$V$_3$^{V}O$_{40}$]	Up to 5	0.001–0.5

(**4** and **6**) and ^{51}V NMR for vanadium (V) compounds (**5** and **7**). Compound α-K$_5$[PW$_{11}$V^{IV}O$_{40}$]·10H$_2$O (**8**) was prepared according to the procedure described in [14]. The purity of this compound was confirmed by UV–vis spectroscopy.

Compound α-K$_4$[PW$_{11}$V^{V}O$_{40}$]·4H$_2$O (**9**) was prepared according to the procedure described in [14,29]. Elemental analyses, infrared spectroscopy data and ^{51}V NMR confirmed the isolation of the vanadium mono-substituted α anion. Analyses (%), found (calcd.): P, 0.94 (1.04); W, 69.2 (68.0); V, 1.58 (1.71); K, 5.06 (5.26). FTIR (cm^{-1})—ν_{as}(P–O): 1999, 1077; 1065 (sh); ν_{as}(W–O$_d$): 982; ν_{as}(W–O$_b$–W): 884; ν_{as}(W–O$_c$–W): 788.

Compound α-1,2-K$_5$[PW$_{10}$V$_2^V$O$_{40}$]·11H$_2$O (**10**) was prepared by reaction of α-A-[PW$_9$O$_{34}$]$^{9-}$ with VOSO$_4$ followed by oxidation with Br$_2$ and re-crystallization in acidified water at pH 2 [14]. Elemental analyses, infrared spectroscopy data and ^{51}V NMR confirmed the isolation of the pure isomeric form of the vanadium di-substituted anion. Analysis: P, 0.91 (1.03); W, 61.7 (61.2); V, 3.41 (3.39); K, 6.95 (6.50); W/V = 5.0. FTIR (cm^{-1})—ν_{as}(P–O): 1095, 1077, 1059; ν_{as}(W–O$_d$): 963; ν_{as}(W–O$_b$–W): 893; ν_{as}(W–O$_c$–W): 788. ^{51}V: −546.0 ppm (*versus* VOCl$_3$), $\Delta\nu_{1/2}$ = 150 Hz.

Compound α-1,2,3-K$_6$[PW$_9$V$_3^V$O$_{40}$]·13H$_2$O (**11**) was prepared by reaction of α-A-[PW$_9$O$_{34}$]$^{9-}$ with NaVO$_3$ in sodium acetate buffered solution at pH of 4.8 [14]. Chemical analysis, infrared data and ^{51}V NMR confirmed the isolation of the pure isomeric form of the vanadium tri-substituted anion. Analysis: P, 1.00 (1.05); W, 55.6 (56.1); V, 5.08 (5.19); K, 7.66 (7.96); W/V = 3.0. FTIR (cm^{-1}): ν_{as}(P–O): 1086, 1055; ν_{as}(W–O$_d$): 961; ν_{as}(W–O$_b$–W): 875; ν_{as}(W–O$_c$–W): 797. ^{51}V: −558.8 ppm (*versus* VOCl$_3$, pH 2.5), $\Delta\nu_{1/2}$ = 332 Hz.

2.2. Measurement procedures

Individual solutions of vanadyl sulphate, sodium and potassium metavanadates and decavanadate and potassium salts of the various heteropolyanions were measured using the sensor array. In particular, sensors' sensitivity to POMs, containing silicon, boron or phosphorus and vanadium at oxidation states IV and V as well as to vanadium salts was evaluated. The list of the studied substances together with ranges of their pH stability and concentrations are shown in Table 1. Stock solutions were prepared by dissolving weighed amount of corresponding dry salt in the distilled water acidified to pH 2 by sulphuric acid.

Calibration solutions were prepared by diluting the stock solutions with buffers. The following buffers were used as background solutions for calibration measurements: sulphate with pH 2.4 and 3.2; acetate with pH 4.2 and 5.1 and phosphate with pH 6.5. All buffers were prepared from corresponding acids, pH being adjusted by addition of NaOH solutions. Concentration of all buffers was 0.1 mol L^{-1}. At least three replicated calibration measurements in solutions of each substance were run.

Measurements with the sensor system were carried out in mixed solutions containing two substances simultaneously. Compositions of these solutions are shown in Table 2. Mixed solutions were prepared on the acetate buffer with pH 4.2, which was found to be an optimal pH for measuring different species of interest. Solutions were run in random order. At least three replicated measurements were made.

The oxidation of 4-hydroxy-3-methoxybenzyl (vanillyl) alcohol with K$_5$[SiW$_{11}$V^{V}O$_{40}$] was monitored using the sensor array. Sensors were chosen based on the results of the previous experiments. This reaction was carried out at room temperature in the acetate buffer at pH 4.2, where 1 mM of POM reacted with 1 mM of alcohol. The reaction was monitored employing ET and UV–vis spectroscopy. Concentrations of oxidized and reduced forms of vanadium were calculated using molar absorptivities at 490 nm of 641 mol^{-1} 1 cm^{-1} for [SiW$_{11}$V^{IV}O$_{40}$]$^{6-}$ and 35 mol^{-1} 1 cm^{-1} for [SiW$_{11}$V^{V}O$_{40}$]$^{5-}$. Sample for spectroscopic measurements were taken 5 min, 10 min, 15 min, 20 min, 30 min, 61 min, 93 min, 120 min, 180 min, 241 min, 24 h 53 min and 52 h 13 min after the start of the reaction. It was found that full reduction of K$_5$[SiW$_{11}$V^{V}O$_{40}$] takes about 24 h. Measurements with ET were carried out during only first 2 h after the reaction start due to the limited time. Sensors' potentials were registered every 20 s during this period, thus producing 316 points.

2.3. Sensor array

The sensor array comprised 23 potentiometric cross-sensitive chemical sensors, of which 6 were with chalcogenide glass membranes (G series), 16 with polymer membranes based on plasticized polyvinyl chloride (C series) and glass pH electrode.

Table 2
Compositions of mixed solutions

	Compounds	Concentration (mM)								
		1	2	3	4	5	6	7	8	9
1	V^{IV}OSO$_4$	0.02	0.2	2	0.02	0.2	2	0.02	0.06	0.2
	Na$_6$V$_{10}^V$O$_{28}$	0.02	0.02	0.02	0.2	0.2	0.2	2	2	2
2	K$_6$[SiW$_{11}$V^{IV}O$_{40}$]	0.1	0.4	1.3	0.1	0.4	1.3	0.1	0.4	1
	K$_5$[SiW$_{11}$V^{V}O$_{40}$]	0.1	0.1	0.1	0.3	0.3	0.3	1	1	1
3	K$_5$[SiW$_{11}$V^{V}O$_{40}$]	0.1	0.1	0.1	0.3	0.3	0.3	1	1	1
	Na$_6$V$_{10}^V$O$_{28}$	0.01	0.1	1	0.01	0.1	1	0.01	0.1	1
4	K$_5$[SiW$_{11}$V^{V}O$_{40}$]	0.01	0.1	1	0.01	0.1	1	0.01	0.1	1
	V^{IV}OSO$_4$	0.1	0.1	0.1	0.3	0.3	0.3	1	1	1

The sensors for the present study were chosen according to the following considerations: (i) sensors with chalcogenide glass membranes, usually displaying red-ox sensitivity, were supposed to be sensitive to vanadium at different oxidation states, namely in POMs; (ii) sensors with plasticized polyvinyl chloride membranes were expected to display sensitivity to vanadyl ions (this was confirmed in preliminary experiments) and, possibly, to vanadates and decavanadates. All sensors were developed and produced in the Laboratory of Chemical Sensors of St. Petersburg University. Compositions of sensor membranes and preparation details were published elsewhere [30,31].

Potentiometric measurements were carried out using a custom-made multichannel voltmeter with high input impedance. Sensors' potentials were measured *versus* conventional Ag/AgCl reference electrode. The sensors were washed with distilled water till they reached stable potential before and between measurements.

2.4. Data processing

Parameters of sensor response in individual solutions of measured substances such as the slope of the electrode function (sensitivity) and the standard potential were calculated according to the Nernst equation. The detection limit was estimated as an interception of two linear parts of the sensor response curve corresponding to presence and absence of response to the primary ion.

Processing of the data from the sensor array was done using principal component analysis (PCA) and partial least square regression (PLS). Both PCA and PLS are so-called projection methods that efficiently reduce number of original variables and reject noise at the same [32]. Recognition of samples that is solutions of different POMs was performed using principal component analysis (PCA). PCA is unsupervised method where only matrix of independent X-variables is employed and no additional information is necessary to perform analysis (data decomposition). This is a powerful tool for the data exploration since it allows to represent output of in 2D form and give an impression about similarity and difference between samples, clustering, etc. In the present work results of measurements using ET in the solutions of different POMs were shown as plots of PCA scores (values of new, calculated variables).

Multivariate calibration models for concentration prediction in mixed solutions were made using PLS. Separate calibration models were made for each compound. Test set validation was used in all cases. Test set comprised one-third of all data. Commercial software the Unscrambler v. 7.8 by CAMO, Norway was used for running PCA and PLS [32].

3. Results and discussion

3.1. Evaluation of sensor's sensitivity in individual solutions of vanadium-containing compounds

Sensitivity of potentiometric chemical sensors to vanadium at different oxidation states (Table 1) was evaluated in the individual solutions. The measurements were carried out at different
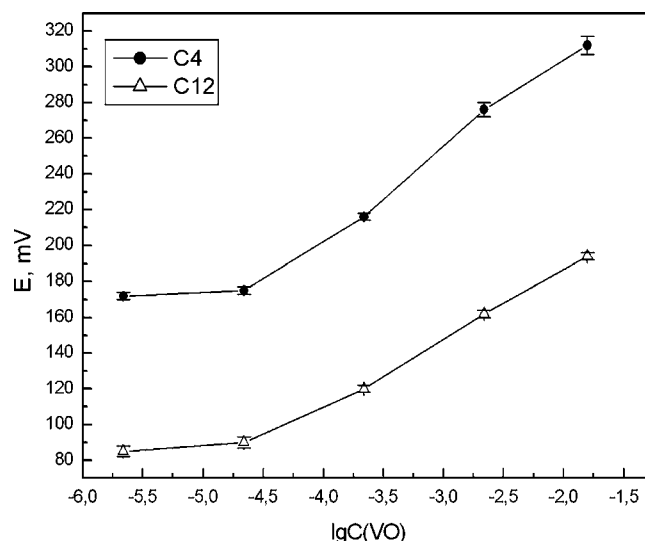

Fig. 1. Typical responses of two chemical sensors in the individual solutions of vanadyl sulphate at pH 4.2. Mean of three replicated measurements together with standard deviations of sensor potential are shown.

pH in the range from 2.4 to 6. As an example, typical responses of potentiometric chemical sensors in the individual solutions of vanadyl sulphate at the pH 4.2 are shown in Fig. 1.

Slopes of electrode functions of the sensors in solutions of vanadyl and vanadates at different pH are shown in Fig. 2. The sensors with plasticized polymer membranes (series C) displayed sensitivity to vanadyl ions, whereas the sensors with chalcogenide glass membranes (series G) displayed sensitivity to "vanadate" ion. Solutions of three vanadium (V) salts were measured: potassium and sodium metavanadate, and sodium decavanadate. The aim of this experiment was to evaluate influence of different cations (sodium or potassium) and different anion forms in salts (metavanadate or decavanadate) on the sensor's responses. Though metavanadate is supposed to form
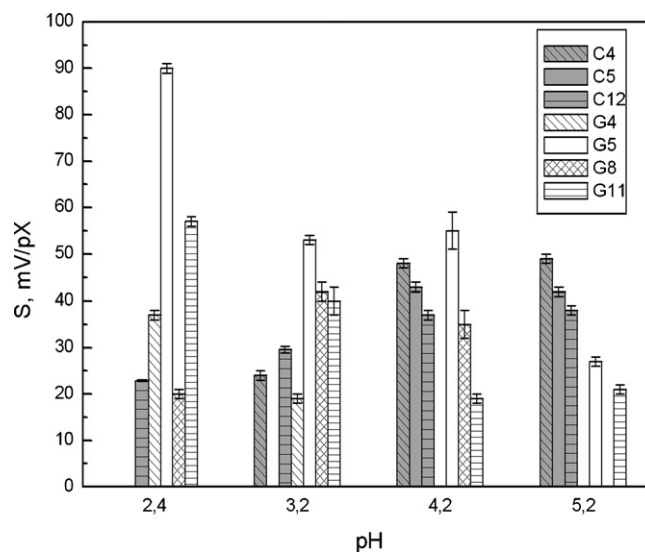

Fig. 2. Slopes of sensor's responses in the solutions of vanadyl sulphate (grey bars with patterns) and sodium decavanadate (white bars with patterns) at different pH.
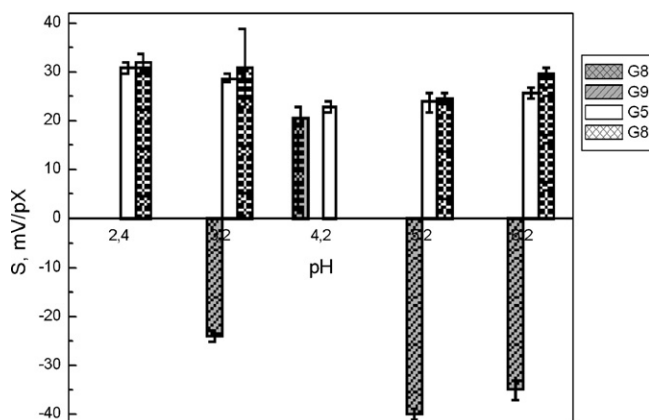
Fig. 3. Slopes of sensor's response in the solutions of α-K$_7$[BW$_{11}$V^{IV}O$_{40}$] (grey bars with patterns) and α-K$_6$[BW$_{11}$V^{V}O$_{40}$] (white bars with patterns) at different pH.

decavanadate anion in solutions at the studied pH range, it was not known if this equilibrium had been rapidly established. No difference between sensors' responses in solutions of these three compounds was observed. Thus, sodium decavanadate was used for all further experiments.

Responses of the sensors with chalcogenide glass membranes to all studied heteropolyanions at different pH are shown in Figs. 3–5a and b. The sensors displayed sensitivity toward all studied substances. Only three chalcogenide glass sensors responded in the solutions of the boron-containing POMs (Fig. 3), while all six glass sensors responded in the solutions of the phosphorus or silicon-containing POM (e.g. Figs. 4 and 5). All studied compounds of POMs dissociate in aqueous solutions giving rise to a polyanion, containing vanadium, and a countercation (sodium or potassium). Though the observed responses of chalcogenide sensors were cationic i.e. potential of the sensor increases with the increase of the analyte concentrations, we assume that they are related to the change of polyanion's concentrations. This statement may be supported by the following
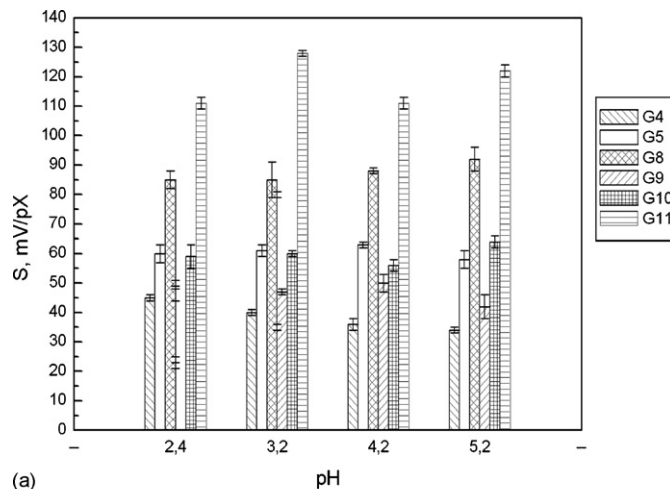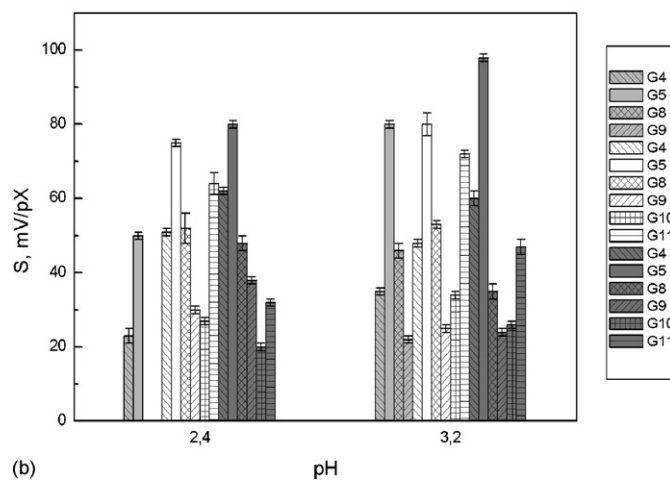

(a)

(b)

Fig. 5. Slopes of sensor's response in the solutions of: (a) α-K$_5$[PW$_{11}$V^{IV}O$_{40}$] at different pH and (b) α-K$_4$[PW$_{11}$V^{V}O$_{40}$] (grey bars), $\alpha_{1,2}$-K$_5$[PW$_{10}$V$_2$^{V}O$_{40}$] (white bars) and $\alpha_{1,2,3}$-K$_6$[PW$_9$V$_3$^{V}O$_{40}$] (dark grey bars) at different pH.

considerations. It is well known [33] that chalcogenide glass sensors are not sensitive at all to alkali cations, such as sodium or potassium. Moreover, all measurements were made on the background of 0.1 mol L^{-1} buffer, containing 0.2–0.3 mol L^{-1} of sodium, while maximum concentration of cation coming from POM dissociation was about 0.06 mol L^{-1}. Thus, the response to sodium or potassium cations as potential generating process can be excluded. Cationic response of some chalcogenide glass sensors to anions was observed in the solutions of chromium (VI) or, in fact, of chromate at pH 2 [33]. It is assumed that a mechanism of sensor response in this case is redox based and the same consideration may be likely assigned to the sensor's response regarding vanadium-containing polyanions. It is also interesting to note that there is a correlation between redox potential of the compound and the sensor sensitivity. Thus, the higher was the redox potential the higher sensors' responses with lower detection limits were observed. However, further investigations are necessary for the elucidation of precise mechanism of chalcogenide glass sensors' response in solutions of redox substances.

The response of sensors depended on pH of solutions in the studied pH range. There are several reasons for this including

Fig. 4. Slopes of sensor's response in the solutions of α-K$_6$[SiW$_{11}$V^{IV}O$_{40}$] (grey bars with patterns) and α-K$_5$[SiW$_{11}$V^{V}O$_{40}$] (white bars with patterns) at different pH.

the presence of different ionic forms of measured compounds at different pH and the influence of protons on the potential generation process of sensors. Polymeric sensors displayed high sensitivity to vanadyl ions only at pH 4.2 or higher (Fig. 2), probably due to the interference from protons at lower pH. Some phosphorus-containing POMs (α-PW$_{11}$V^{V}O$_{40}$ and α-1,2-PW$_{10}$V$_2{}^V$O$_{40}$) are not stable at pH higher than 3 [17,29]. After analysing sensors' responses to other compounds (Figs. 2–5), it was concluded that pH 4.2 is an optimal one for the determination of most of them. Good sensitivity to all compounds and high potential reproducibility of the sensors was observed at this pH. Thus, the acetate buffer with pH 4.2 was chosen for further experiments involving all studied substances but phosphorus-containing POMs.

It also follows from the experimental data that it is possible to manipulate the sensitivity of the sensor array by changing pH of solutions. For example, it is possible to measure both reduced and oxidized forms of silicon-containing POMs (K$_6$[SiW$_{11}$V^{IV}O$_{40}$] and K$_5$[SiW$_{11}$V^{V}O$_{40}$], respectively) at pH 4.2, while only oxidized form can be detected at pH 3.2 (Fig. 3). This feature might be used in the measurements of mixed solutions for improving response of the sensor array to a particular substance.

It was found that 13 sensors of initially chosen 23 displayed sensitivity to at least one of the studied substances. Importantly, not all sensors were sensitive to all compounds and also sensitivity of the same sensor to different compounds was different. Thus, it was expected that combination of these sensors, i.e. the sensor array, should allow discrimination and quantitative determination of substances of interest. Therefore, those 13 sensors were used for sample recognition and quantitative analysis reported below.

3.2. Discrimination of individual solutions of vanadium-containing compounds

Recognition of individual solutions of all studied substances was performed. PCA score plot of individual solutions of compounds at pH 3.2 is shown in Fig. 6a and b. This pH (3.2) was chosen to make comparison of compounds, including those of phosphorus-containing POMs that are not stable at higher pH. The most significant separation was observed between vanadyl ions and all other compounds (Fig. 6a). Distances between sample points on the score plot roughly correspond to the differences between the samples. The bigger distance between the samples corresponds to the bigger difference in the sensor array response to the compound(s) in question. In the same way the bigger is the distance between points corresponding to different concentration levels for the same compounds, the higher is sensor array sensitivity to this compound. Thus, PCA was run on the data excluding measurements in solutions of vanadyl ions, which allowed improving visual separation between other compounds (Fig. 6b). It became clear after making a PCA model without vanadyls that all compounds could be discriminated using the ET. It is important noting that though different concentration levels for each compound were plotted, it was still possible to discriminate among all substances.
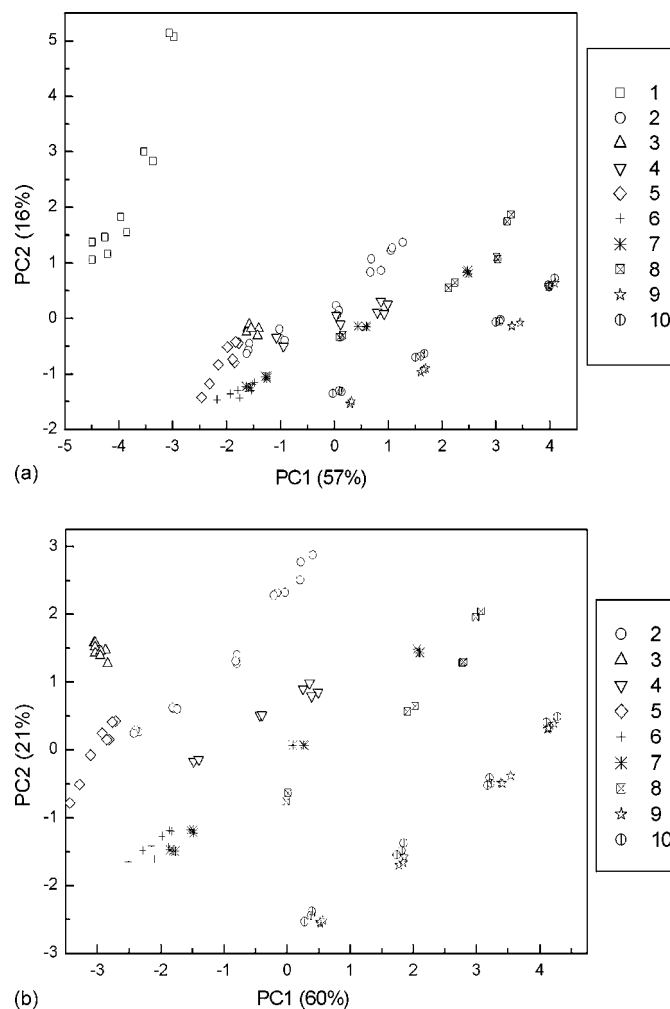

Fig. 6. PCA score plot of measurements using sensor array in the individual solutions at pH 3.2 of (a) all studied compounds and (b) all studied compounds except vanadyl sulphate. (1) VOSO$_4$, (2) Na$_6$V$_{10}$O$_{28}$, (3) α-K$_6$[SiW$_{11}$V^{IV}O$_{40}$], (4) α-K$_5$[SiW$_{11}$V^{V}O$_{40}$], (5) α-K$_7$[BW$_{11}$V^{IV}O$_{40}$], (6) α-K$_6$[BW$_{11}$V^{V}O$_{40}$], (7) α-K$_5$[PW$_{11}$V^{IV}O$_{40}$], (8) α-K$_4$[PW$_{11}$V^{V}O$_{40}$], (9) α-1,2-K$_5$[PW$_{10}$V$_2{}^V$O$_{40}$], and (10) α-1,2,3-K$_6$[PW$_9$V$_3{}^V$O$_{40}$].

3.3. Recognition and quantitative determination of vanadium-containing compounds in mixed solutions

The sensor system was demonstrated to be capable of measuring quantitatively different vanadium-containing compounds and of discriminating them in individual solutions. This is a promising result, which should be confirmed, however, in the mixed solutions, containing simultaneously both compounds of interest. The measurements with sensor array were made in binary mixed solutions containing two compounds simultaneously. Compositions of these solutions are shown in Table 2.

Results of prediction on the concentration of components for the test set are shown in Table 3. Calibration models were calculated using PLS regression for each compound separately. It was possible to quantify all compounds with good precision. The highest error was obtained for determination of decavanadate in the presence of K$_5$[SiW$_{11}$V^{V}O$_{40}$]. Though individual solutions of these compounds were easily distinguished by the sensor

Table 3
Root mean square error of prediction (RMSEP) and parameters of predicted *vs.* measured curves for the prediction of the concentrations of vanadium-containing compounds in the binary mixed solutions using ET

	Compound	RMSEP	Bias	SEP	Slope	Offset	Correlation
1	$V^{IV}OSO_4$	0.06	0.003	0.06	1	0.01	0.99
	$Na_6V_{10}{}^V O_{28}$	0.1	−0.05	0.09	0.96	−0.2	0.99
2	$\alpha\text{-}K_6[SiW_{11}V^{IV}O_{40}]$	0.1	−0.02	0.1	0.95	−0.2	0.97
	$\alpha\text{-}K_5[SiW_{11}V^V O_{40}]$	0.07	−0.01	0.07	0.91	−0.3	0.99
3	$\alpha\text{-}K_5[SiW_{11}V^V O_{40}]$	0.06	0.001	0.06	0.98	−0.08	0.99
	$Na_6V_{10}{}^V O_{28}$	0.18	−0.02	0.18	0.96	−0.18	0.97
4	$\alpha\text{-}K_5[SiW_{11}V^V O_{40}]$	0.07	0.001	0.07	0.90	−0.35	0.98
	$V^{IV}OSO_4$	0.05	−0.006	0.05	1	0.07	0.99

Note: Results are shown only for the test samples.

array (Fig. 6b), when present simultaneously $K_5[SiW_{11}V^V O_{40}]$ interferes with determination of decavanadate. PCA score plot of the measurements in these solutions is shown in Fig. 7. The samples form three well-separated groups on the score plot corresponding to three concentration levels of $K_5[SiW_{11}V^V O_{40}]$. The separation between samples within each group, i.e. the separation between different concentration levels of decavanadate is much smaller. As a consequence, decavanadate concentration was determined with higher error.

In contrast, vanadyl and decavanadate species were easily distinguished by the sensor array both in the individual and mixed solutions. A PCA score plot of the measurements in solutions containing simultaneously vanadyl and decavanadate species is shown in Fig. 8. All nine solutions of different compositions form well-separated clusters on this plot. Direction of PC1 roughly corresponds to the change of vanadyl ions concentration, while direction of PC2—to the change of decavanadate concentration. Both compounds could be determined by the sensor array with a good precision.
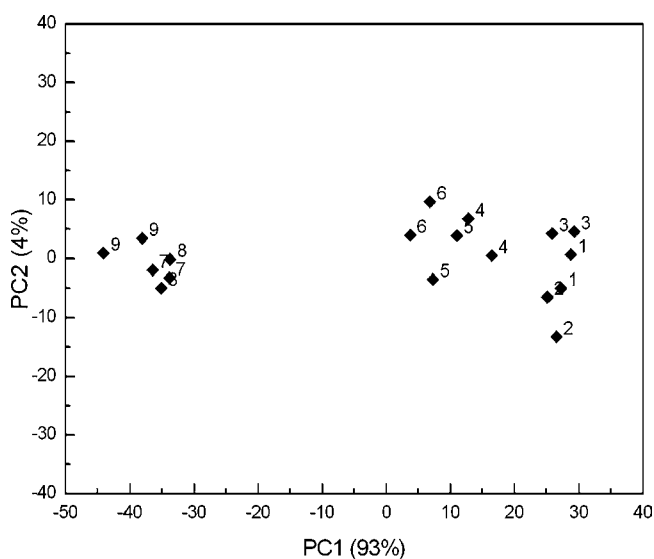
Thus, sensor array demonstrated the capability to quantify vanadium-containing compounds in the mixed solutions. However, further development of the sensor array to improve its selectivity towards some compounds e.g. to decavanadate in the presence of $K_5[SiW_{11}V^V O_{40}]$, is highly desirable.

3.4. Monitoring of $K_5[SiW_{11}V^V O_{40}]$ reduction with organic substrate using the sensor array

An attempt to monitor the reaction of $K_5[SiW_{11}V^V O_{40}]$ reduction with vanillyl alcohol using the sensor array was performed. Vanillyl alcohol was supposed to reduce $[SiW_{11}V^V O_{40}]^{5-}$ to $[SiW_{11}V^{IV}O_{40}]^{6-}$, i.e. to reduce V(V) to V(IV) in the polyanion. Unfortunately, this reaction appeared being slow and it was not accomplished even after more than two hours. According to visible spectroscopy data, concentrations of oxidized form of POM decreased from 1 to 0.23 mM, while concentration of reduced form changed from 0 to 0.69 mM. Thus, about 75% of the POM got reduced during the first 2 h of the reaction.

Fig. 7. PCA score plot of measurements using sensor array in the solutions containing simultaneously $\alpha\text{-}K_5[SiW_{11}V^V O_{40}]$ and decavanadate. Compositions of the solutions are shown in Table 2 (mixture 3). Measurements were made on the acetate buffer with pH 4.2.
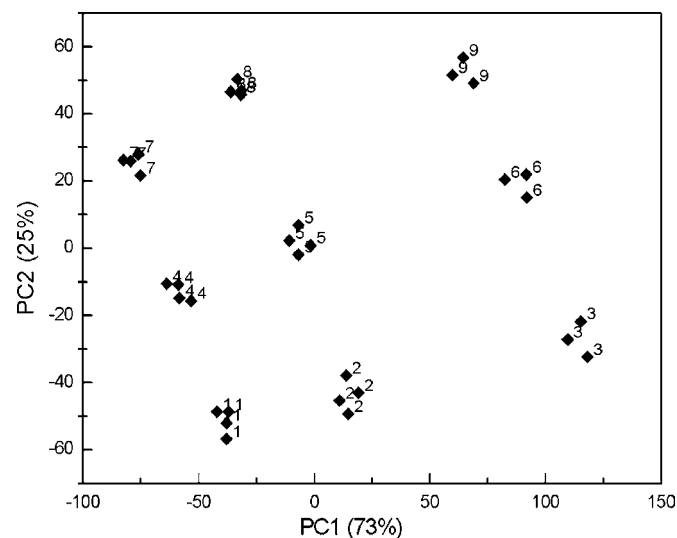

Fig. 8. PCA score plot of measurements using sensor array in the solutions containing simultaneously vanadyl and decavanadate. Compositions of the solutions are shown in Table 2 (mixture 1). Measurements were made in the acetate buffer with pH 4.2.
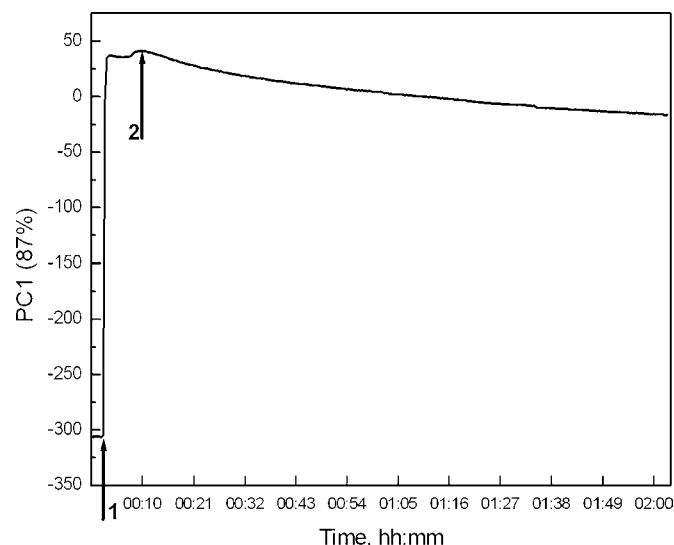
Fig. 9. PC1 score *vs.* time dependence for the sensor array measurements during reaction of $K_5[SiW_{11}V^VO_{40}]$ with vanillyl alcohol: (1) addition of 1 mM POM to the buffer; (2) addition of 1 mM vanillyl alcohol.

Several sensors of the array responded during this reaction. PCA was run based on these experimental data for the visual representation. The first PC plotted *versus* time is shown in Fig. 9. Additions of POM and of vanillyl alcohol are shown with the arrows. It was possible to follow the course of this reaction using the sensor array. Furthermore, an attempt to quantify both reduced and oxidized forms of POM was entertained. Firstly, a calibration model was made using the measurements in binary solutions of silicon-containing POM (Table 2, mixture 2). Cross-validation was used in this case (model I). Further on, calibration models were made using the measurements with ET in solutions during reduction and the values of component concentrations from the reference analysis, i.e. UV–vis spectroscopy (model II). In this case the test set validation was used, the first run being used for calibration and the second one solely as tests. In both cases models were made separately for each compound. Afterwards, these two types of the calibration mod-

els were used for predicting the concentration of two compounds during the reaction with vanillyl alcohol. Predicted concentrations in the test data set together with reference data are shown in Table 4. It was found that employing the reference data for the calibration results gives higher accuracy of the prediction when compared to the use of mixed binary solutions. It is important to note that in the latter case calibration measurements were made some time earlier due to the experimental circumstances and the compositions of calibration solutions (mixed model) and analysed solutions (during the reaction) were slightly different. Despite this, the prediction results obtained using calibration model I were reasonably good. Therefore, it is advisable to use solutions with very close or, ideally, the same compositions as the solutions to be analysed for the calibration of ET.

4. Conclusions

An electronic tongue (ET) multisensor system based on potentiometric chemical sensors for the determination of vanadium-containing polyoxometalates (POMs) at different oxidation states was developed. Sensitivity of sensors to vanadyl/vanadate ions, decavanadate and to Keggin-type POMs containing silicon, boron or phosphorus and vanadium at the oxidation state IV or V was evaluated at different pH. Sensitivity to all studied compounds was observed for the studied sensors. The measurements with the ET were made in the mixed solutions containing two compounds at different oxidation state (V(IV)/V(V)) simultaneously. It was found that the ET allows the determination of concentrations of both compounds in mixtures with reasonable precision. Furthermore, an attempt was made to monitor the reduction of α-$[SiW_{11}V^VO_{40}]^{5-}$ by phenolic substrate using the ET. Good agreement between the concentrations of components predicted by ET and by reference method (spectrophotometry) was obtained. Thus, the ET was demonstrated to be a promising tool for the discrimination and quantification of vanadium-containing POMs at different oxidation state.

Table 4
Concentrations of α-$K_6[SiW_{11}V^{IV}O_{40}]$ and α-$K_5[SiW_{11}V^VO_{40}]$ during reduction of the latter by vanillic alcohol as predicted using ET

α-$K_6[SiW_{11}V^{IV}O_{40}]$			α-$K_5[SiW_{11}V^VO_{40}]$		
Reference (mM)	Predicted (mM)		Reference (mM)	Predicted (mM)	
	I	II		I	II
0.22	0.39	0.20	0.94	0.55	0.95
0.28	0.35	0.27	0.72	0.68	0.73
0.34	0.34	0.32	0.65	0.64	0.66
0.38	0.34	0.42	0.60	0.59	0.61
0.44	0.32		0.56	0.54	0.51
0.56	0.47		0.49	0.47	
0.64	0.64		0.38	0.26	
0.69	0.86		0.30	0.15	

Note: (I) Calibration models were made using ET measurements in binary mixed solutions of these compounds; (II) calibration models were made using ET measurements during reaction and concentration data from the reference analysis (spectroscopy).

References

[1] M.T. Pope, Heteropoly and Isopoly Oxometalates, Springer-Verlag, Berlin, 1983.
[2] M.T. Pope, A. Muller (Eds.), Polyoxometalate Chemistry: From Topology via Self-assembly to Applications, Kluwer, Dordrecht, 2001.
[3] R. Neumann, in: J.E. Bäckvall (Ed.), Modern Oxidative Methods, Wiley–VCH, Weinheim, 2004 [Chapter 8].
[4] N. Mizuno, M. Misono, Chem. Rev. 98 (1998) 199.
[5] E. Coronado, P. Day, Chem. Rev. 104 (2004) 5419.
[6] J.T. Rhule, C.L. Hill, D.A. Judd, Chem. Rev. 98 (1998) 327.
[7] J.H. Grate, D.R. Hamm, S. Mahajan, Catal. Org. React. 52 (1994) 213.
[8] R. Neumann, M. Levin, J. Am. Chem. Soc. 114 (1992) 7278.
[9] D.C. Duncan, C.L. Hill, J. Am. Chem. Soc. 119 (1997) 243.

[10] I.A. Weinstock, R.H. Atalla, R.S. Reiner, M.A. Moen, K.E. Hammel, C.J. Houtman, C.L. Hill, M.K. Harrup, J. Mol. Catal. 116 (1997) 59.

[11] D.V. Evtuguin, C. Pascoal Neto, Holzforchung 51 (1997) 338.

[12] D.V. Evtuguin, C. Pascoal Neto, J. Rocha, J.D. Pedrosa de Jesus, Appl. Catal. A: Gen. 167 (1998) 123.

[13] P.J. Domaille, G. Watunyia, Inorg. Chem. 25 (1986) 1239.

[14] P.J. Domaille, J. Am. Chem. Soc. 106 (1984) 7677.

[15] R. Acerete, C.F. Hammer, L.C.W. Baker, J. Am. Chem. Soc. 101 (1979) 267.

[16] C. Brévard, R. Schimpf, G. Tourné, C.M. Tourné, J. Am. Chem. Soc. 105 (1983) 7059.

[17] M. Leparulo-Loftus, M.T. Pope, Inorg. Chem. 26 (1987) 2112.

[18] I. Andersson, A. Gorzsás, L. Pettersson, Dalton Trans. (2004) 421.

[19] A. Gorzsás, I. Andersson, H. Schimtt, D. Rehder, L. Pettersson, Dalton Trans. (2003) 1161.

[20] J. Altenau, M.T. Pope, R. Prados, H. So, Inorg. Chem. 14 (1975) 417.

[21] M. Mossoba, C. O'Connor, M.T. Pope, E. Sinn, G. Hervé, A. Tézé, J. Am. Chem. Soc. 102 (1980) 6864.

[22] A. Legin, A. Rudnitskaya, Yu. Vlasov, in: S. Alegret (Ed.), Integrated Analytical Systems, Comprehensive Analytical Chemistry, vol. XXXIX, Elsevier, Amsterdam, 2003, pp. 437–486.

[23] F. Winquist, C. Krantz-Rülcker, I. Lundström, in: T.C. Pearce, J.W. Gardner, S.S. Schiffman, H.T. Nagle (Eds.), Handbook of Machine Olfaction, Wiley–VCH Verlag, GmbH, 2003, pp. 267–291.

[24] J. Mortensen, A. Legin, A. Ipatov, A. Rudnitskaya, Yu. Vlasov, K. Hjuler, Anal. Chim. Acta 403 (2000) 273.

[25] A. Rudnitskaya, A. Ehlert, A. Legin, Yu. Vlasov, S. Buttgenbach, Talanta 55 (2001) 425.

[26] A. Legin, A. Rudnitskaya, B. Seleznev, D. Kirsanov, Yu. Vlasov, Proceedings of the Eurosensors XVIII, Rome, Italy, September 12–15, 2004, p. A.34.

[27] A.V. Legin, B.L. Seleznev, A.M. Rudnitskaya, Yu.G. Vlasov, S.V. Tverdokhlebov, B. Mack, A. Abraham, T. Arnold, L. Baraniak, H. Nitsche, Czech. J. Phys. 49 (1999) 679.

[28] G.K. Johnson, R.K. Murmann, Inorg. Synth. 19 (1979) 140.

[29] P.J. Domaille, Inorg. Synth. 27 (1990) 96.

[30] Yu. Vlasov, A. Legin, A. Rudnitskaya, Sens. Actuators B 44 (1997) 532.

[31] A. Legin, A. Rudnitskaya, B. Seleznev, Yu. Vlasov, in: J.W. Gardner, K.C. Persaud F K.C. (Eds.), Electronic Noses and Olfaction 2000, in: B.E. Jones (Series Ed.), Series in Sensors, IOP Publishing Ltd., Bristol, 2000, p. 13.

[32] K. Esbensen, Multivariate Data Analysis in Practice, 5th ed., CAMO AS, Norway, 2001.

[33] Yu.G. Vlasov, E.A. Bychkov, A.V. Legin, Talanta 41 (1994) 1059.

Short communication

Fourier transform Raman spectral measurements of powdered quaternary mixtures of organic compounds Exceptional pure component spectral reconstruction using band-target entropy minimization (BTEM)

Chilukoti Srilakshmi [a,b], Effendi Widjaja [a], Bruce G. Anderson [b,*], Marc Garland [a,c,**]

[a] *Institute of Chemical and Engineering Sciences, 1 Pesek Road, Jurong Island, Singapore 627833, Singapore*
[b] *Schuit Institute of Catalysis, Eindhoven University of Technology, P.O. Box 513, 5600 MB Eindhoven, The Netherlands*
[c] *Department of Chemical and Biomolecular Engineering, National University of Singapore, Singapore 117576, Singapore*

Abstract

Fourier transform Raman spectra of eight mixtures of four organic solids, namely dicyandiamide, melamine, acetamide and urea were measured. Matrices formed from these spectra were first subjected to singular value decomposition to obtain the right singular vectors. The right singular vectors were then subjected to blind source separation using band-target entropy minimization (BTEM), thus no a priori information (i.e. involving the nature of the components present, their spectra, nor their concentrations) was included in the analysis. The recovered pure component spectra are of exceptionally high quality and are consistent with pure reference spectra. Various empirical and statistical tests, such as the Euclidean norm and target transform factor analysis, were employed to assess the quality of the recovered spectra. The present results indicate the applicability of combined Raman and BTEM analysis for solid mixtures.
© 2006 Elsevier B.V. All rights reserved.

Keywords: Spectral reconstruction; Band-target entropy minimization (BTEM); Acetamide; Dicyandiamide; Melamine; Urea; Quaternary mixtures; FT-Raman

1. Introduction

Various techniques have been proposed in the past few decades for resolving spectral data into pure component spectra and their concentration profiles. In general they can be divided into two categories: one is based on the use of principle component analysis or singular value decomposition in order to reduce the dimensionality of the observations, and another one directly utilizes the measured spectra without factor analysis. Self-modeling curve resolution (SMCR) was first proposed for estimating the pure component spectra using principle com-

ponent analysis for a two component system by Lawton and Sylvestre [1]. Since the 1980s, various SMCR techniques have been developed and most of these methods are based on the identification of pure variables, local rank map, and iterative least-squares. Pure variable approaches can be found in key set factor analysis (KSFA) [2], simple-to-use interactive self modeling mixture analysis (SIMPLISMA) [3], and interactive principal component analysis (IPCA) [4] methods, whereas local rank map approaches can be found in evolving factor analysis (EFA) [5], window factor analysis (WFA) [6], heuristics evolving latent projections (HELP) [7], orthogonal projection resolution (OPR) [8], etc. Iterative least-squares methods are used in iterative target-testing factor analysis (ITFFA) [9], multivariate curve resolution-alternating least squares (MCR-ALS) [10], and positive matrix factorization (PMF) [11] techniques.

Recently, a different kind of algorithm based on information entropy minimization was introduced [12,13]. The program, band-target entropy minimization, does not require any a priori chemical or spectral information what-so-ever. Furthermore,

---

* Corresponding author at: Sasol Technologies R & D (Pty) Ltd, Postbox 1, 1 Klasie Havenga Road, Sasolburg, 1947, South Africa. Tel.: +27 16 960 4629; fax: +27 11 219 2442.

** Corresponding author at: Institute of Chemical and Engineering Sciences, 1 Pesek Road, Jurong Island, Singapore 627833, Singapore. Tel.: +656 796 3947; fax: +656 316 6185.

E-mail addresses: Bruce.Anderson@sasol.com (B.G. Anderson), marc_garland@ices.a-star.edu.sg (M. Garland).
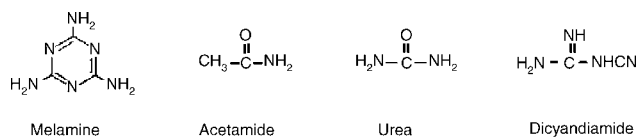
Fig. 1. Structures of the organic compounds used in this study.

it does not rely on any tests for statistical significance, which is difficult to address in the context of non-linear and non-stationary chemical spectra. This easy to use algorithm has now been used on a large variety liquid phase multi-component problems, particular in the areas of chemical synthesis and catalysis [12,14–19]. Some of BTEM's most advantageous properties include its one-at-a-time spectral recovery procedure and its ability to deconvolute signals from trace components, whose signal contribution may be 10^{-4} or less [15]. Quite favourable one-to-one comparisons between BTEM and more conventional SMCR techniques have appeared [18].

Recently, BTEM has begun to be applied to solid state chemical problems, notably mixtures of inorganics using Raman [20], mixtures of polyaromatic hydrocarbons using Raman [21], and mixtures of crystalline inorganics using XRD [22]. The present study extends these solid state studies by demonstrating the utility of BTEM to mixtures of highly-functionalized organics.

Melamine ($C_3H_6N_6$) is an industrially important monomer for polymerization. It is the trimer of cyanamide (CH_2N_2); the dimer of which is dicyandiamide ($C_2H_4N_4$). Urea (CH_4N_2O) is used as an initial starting material for the synthesis of these compounds and is also formed during their hydrolysis. Acetamide (C_2H_5NO) is also formed during hydrolysis. All of these compounds form (stable) solids. As they are related chemically they often occur together as mixtures. Further, there are many structural similarities within this group (Fig. 1). They are all either amides or amines. Two contain a carbonyl moiety. Two contain either C=N and/or cyano groups. All of these substituents give rise to characteristic features in vibrational spectra. Hence mixtures of these chemicals were chosen as an appropriate system for this study. As cyanamide melts at only 4 °C it was excluded.

2. Experimental

2.1. Apparatus

Fourier transform laser Raman spectroscopic measurements were carried out using a Bruker RFS 100/S spectrometer equipped with a near infrared Nd:YAG laser (1.064 μm) and an InGaAs detector. A laser power of 100 mW was employed. The aperture was 10 mm and the scanner velocity was maintained at 5.0 kHz. Spectra were measured by analyzing the 180° backscattered light between 0 and 4000 cm^{-1} at 4 cm^{-1} resolution. A 256 scans were coadded in order to obtain good S/N ratios for each experimental spectrum.

2.2. Reagents

Dicyandiamide, melamine, acetamide and urea were purchased from Aldrich (99.9%) and used without further purification.

Table 1
Compositions of urea, dicyandiamide, acetamide and melamine mixtures (wt.%)

Mixture no.	Urea	Dicyandiamide	Acetamide	Melamine
1	10	20	30	40
2	20	30	40	10
3	30	40	10	20
4	40	10	20	30
5	12	22	30	36
6	34	16	22	28
7	22	28	26	24
8	25	25	25	25

2.3. Procedure

A set of eight quaternary mixtures of dicyandiamide, melamine, acetamide and urea were prepared according to the proportions given in Table 1. The compounds were mixed and ground to a finer powder to ensure greater homogeneity. Each finely powdered mixture was compressed into a stainless steel sample holder. All spectra were measured at room temperature and atmospheric pressure. Replicate measurements were made; the experimental Raman spectra were measured eight times for each quaternary mixture resulting in a total of 64 spectra.

In addition, the spectra of the four pure compounds were measured for reference purposes and the entire spectra (from 0 to 4000 cm^{-1}) are displayed in Fig. 2. The spectra were consistent with those previously reported in the literature [23–29].

As shown in Fig. 2 most of the bands below 2500 cm^{-1} are relatively sharp and symmetrical. However, there is considerable overlap between the bands of different compounds, i.e. several compounds have bands at or very close to the same frequency. BTEM analyses were performed on spectral data in the full region (0–4000 cm^{-1}). The region 0–1100 cm^{-1} has most of the characteristic vibrations in these compounds The region 2800–3500 cm^{-1} is specific for the stretching modes of NH_2 and CH_3 moieties and shows overlap of all components. Of course this is not surprising as each of the four compounds contains either an amine or an amide functionality. In addition many of the bands in this region are broad and asymmetrical due to hydrogen bonding. Extraction of pure component spectra of these amines and amides from their mixtures is potentially difficult. The spectrum of dicyandiamide contains a very distinct peak at 2157 cm^{-1}. This band is due to the stretching mode of the cyano moiety. Actually, dicyandiamide has two tautomeric forms (imino and amino); the former, theoretically more stable form, being much more abundant in the solid state at room temperature. The stretching vibration of the cyano moiety of the amino tautomer occurs at 2186 cm^{-1} [23]. A very weak, band at 2186 cm^{-1} was observed in this study. Therefore, the dicyandiamide is predominantly the imino form with trace amounts of the amino form.

3. Computational aspects

3.1. Band-target entropy minimization (BTEM)

As mentioned, the primary use of BTEM is to extract the pure component spectra from a set of multi-component mixture
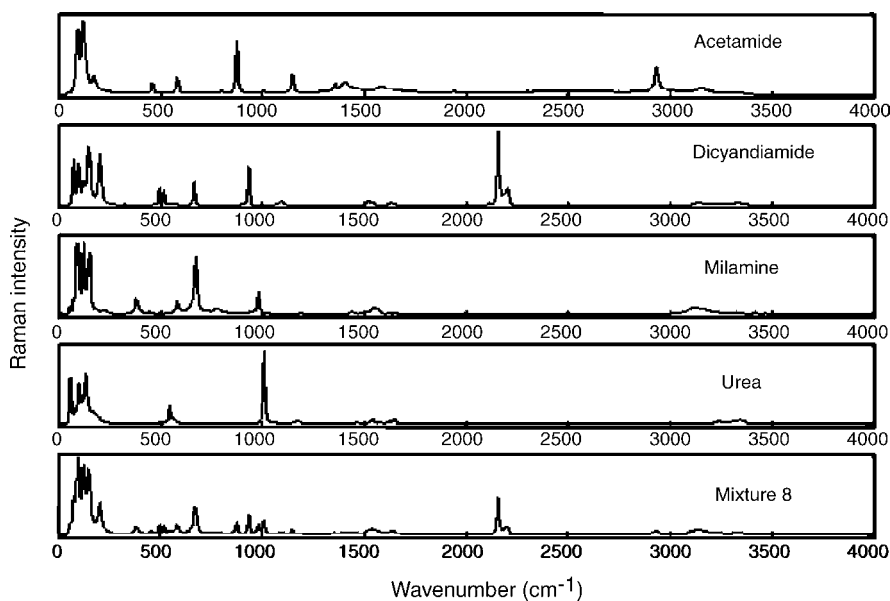
Fig. 2. FT-Raman spectra of pure compounds.

spectra. Afterwards, the contributions of each individual pure component spectrum to the sum-total measured experimental spectrum can be back-calculated.

Let $I_{k \times v}$ represent the Raman intensity in the consolidated spectroscopic data matrix where k denotes the number of spectra taken, and v denotes the number of data channels associated with the spectroscopic range. The experimental intensities $I_{k \times v}$ has a bilinear data structure and can be described as a product of two submatrices, namely, the concentration matrix $C_{k \times s}$ and the Raman pure component scattering coefficient matrix $J_{s \times v}$ (where s denotes number of observable species in the chemical mixture). Accordingly, the associated error matrix $\varepsilon_{k \times v}$ contains both experimental error and model error (non-linearities) [30].

$$I_{k \times v} = C_{k \times s} J_{s \times v} + \varepsilon_{k \times v} \tag{1}$$

The BTEM algorithm proceeds by first decomposing $I_{k \times v}$ into its singular vectors using singular value decomposition (SVD) as shown in Eq. (2) [31]. This is then followed by the appropriate transformation of right singular vectors, $V_{z \times v}^{T}$, into physically meaningful pure component spectra.

$$I_{k \times v} = U_{k \times k} \Sigma_{k \times v} V_{v \times v}^{T} \tag{2}$$

In contrast to other SMCR methods, BTEM was uniquely developed to resolve one pure spectrum at a time. The number of eigenvectors, z, taken for inclusion in the transformation, is

usually much larger than s due to the non-linearities present (non-stationary spectral characteristics). The number z is usually determined by identifying the vectors which possess localized signals of clear physical significance and retaining these, while discarding the vectors that are more-or-less randomly distributed noise. The principle equation representing the transformation of the right singular vectors into each spectral estimate is given by Eq. (3).

$$\widehat{J}_{1 \times v} = T_{1 \times z} V_{z \times v}^{T} \tag{3}$$

To extract a pure scattering coefficient, $\widehat{J}_{1 \times v}$, a selected band in the first few V^{T} vectors is targeted. The BTEM algorithm then retains this feature, and at the same time, returns an entire spectrum which has minimum entropy. This routine is repeated for all important observable physical features in the selected V^{T} vectors. A superset of reconstructed pure component scattering coefficients are obtained and this set is reduced to eliminate redundancies. This results in an enumeration of all observable pure component spectra. For a detailed description of the associated scaling procedure, and estimates of the signal contribution of each component, readers are referred to Refs. [12,14,18,19]. Fig. 3 indicates the number of steps involved in the BTEM algorithm.
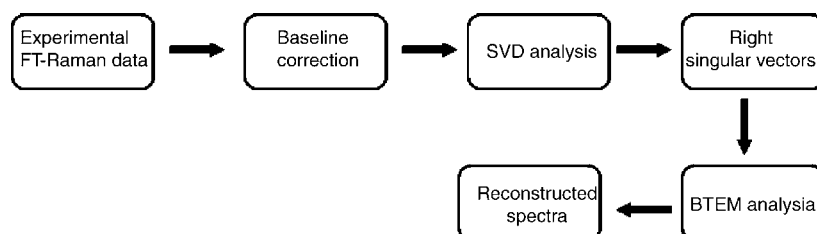

Fig. 3. Flow diagram of the BTEM analysis of the Raman data set.

4. Results and discussion

The analyses are structured into the full-spectral regions and partial-spectral regions. These different analyses permit an overview of the characteristics of BTEM deconvolution in the presence of a very large number of spectral channels versus a more limited number of spectral channels. The raw spectral data was not pre-processed in any manner what-so-ever, e.g. base line corrected, smoothed, etc.

4.1. BTEM analysis

4.1.1. Singular value decomposition

The 64 raw FT-Raman mixture spectra $I_{64 \times 2075}$ were subjected to a vector-space decomposition using singular value decomposition, yielding two orthonormal matrices $U_{64 \times 64}$ and $V^{T}_{2075 \times 2075}$ and the diagonal singular value matrix $\Sigma_{64 \times 2075}$. The row vectors of the V^{T} matrix (normally called the right singular vectors) represent a set of basis vectors which contain abstract information on the pure component spectra of the observable components present in the system. These basis vectors are ordered according to their contribution to the total variance in the observations. Hence, the first few vectors are associated with the chemically significant information in the system, and the remaining vectors are primarily associated with the random instrumental and experimental error. In addition, it should be noted that although after decomposition, there are a total of 2075 basis vectors in V^{T}, only 64 vectors are physically meaningful (either chemical signals or random error signals). This is due to the fact that there are only 64 spectra in the original data set.

Since not all 64 right singular vectors are needed in further analysis, the set of vectors can be truncated, and only a sub-set used in the BTEM spectral reconstructions. Fig. 4, presents the first 16 right singular vectors. The first eight have clear local-ized signals and little noise. The next four vectors still possess localized signals but considerably more noise. Vectors 13–16 are primarily noise, but it is structured (there is a wavy baseline) and heteroscedasticly distributed. The remaining vectors were essentially white noise. Accordingly, 16 right singular vectors were used in the subsequent BTEM spectral reconstructions.

4.1.2. Full-scale spectral reconstruction

It is known that if one targets all the extrema (minima and maxima) in the primary right singular vectors, then a super-set of observable pure component spectra are obtained, where many replicates appear [12]. This is the approach that has been taken with FTIR for new chemically reactive liquid phase systems with an unknown number of new and previously un-observed species [15]. In the present test case for Raman analysis of organic solids, the situation is more straight forward. Accordingly, from the first eight V^{T} vectors four significant spectral features were selected as band-targets in the spectral reconstructions. These four band regions were selected: 98–102 (melamine), 117–122 (acetamide), 1008–1012 (Urea) and 2154–2160 cm−1 (dicyandiamide). These bands correspond to the following vibrational modes: external modes of (melamine); τ_{s} (C–N) (acetamide); υ_{s} (C–N) (urea) and υ (C≡N) (dicyandiamide).

The resulting BTEM results for the pure component spectra over the full-spectral range are shown in Fig. 5. It is clear, from visual inspection, that there is considerable correspondence between the reconstructed spectra and the measured pure spectra. The relative intensities of the bands and their positions are quite similar in all cases. Moreover, the difference spectra confirm that the discrepancies for individual bands are small. In addition, it can be seen in the difference spectra that there are few signals (artifacts) remaining from other components. The Euclidean inner products between the reference experimental spectra and BTEM estimates were (a) dicyandiamide (0.9917),
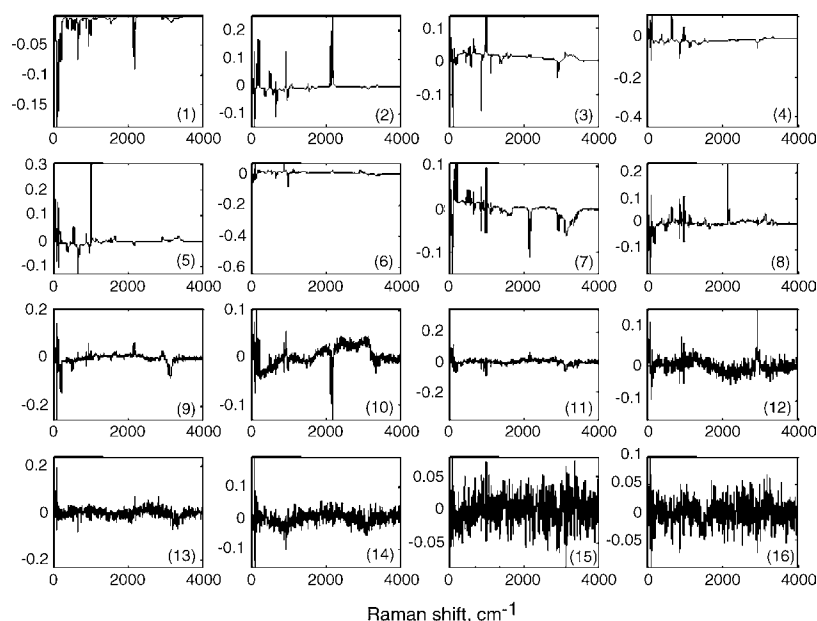

Fig. 4. The first 16 of 64 right singular vectors from the matrix V^{T}. The first eight right singular vectors have significant signal to noise ratios. The remaining vectors have a clear and visually apparent decrease in signal to noise.
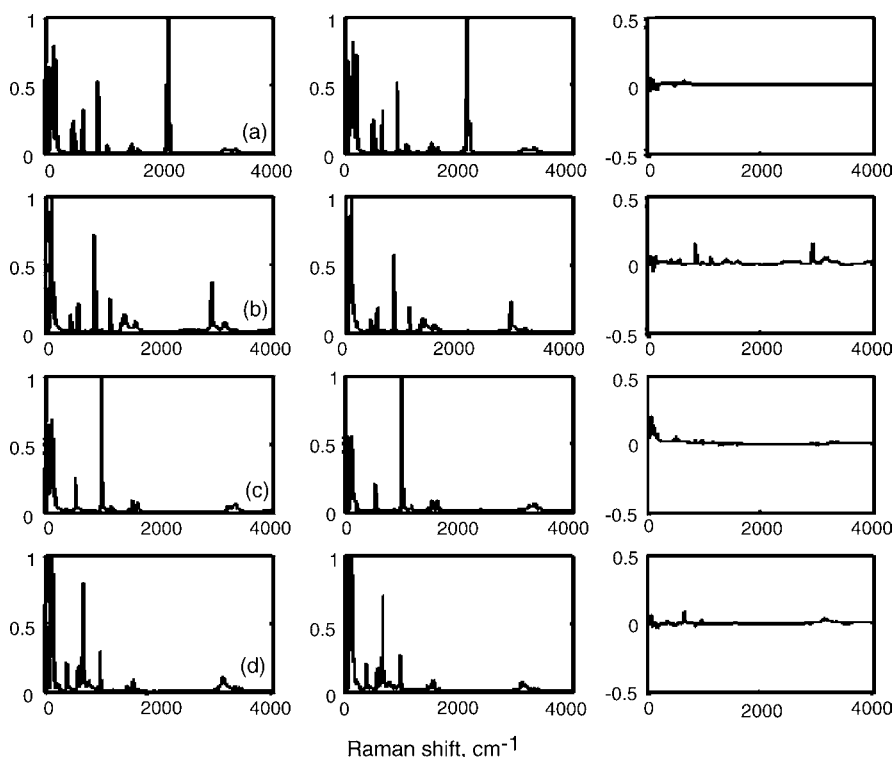
Fig. 5. Raman spectra of each pure component. Left-hand figures are measured spectra and centre figures are spectra reconstructed using BTEM algorithm. Right-hand figures are the difference spectra (measured − reconstructed): (a) dicyandiamide, (b) acetamide, (c) urea and (d) melamine using the same scale.

(b) acetamide (0.9447), (c) urea (0.9696), and (d) melamine (0.9876). The fact that the inner products are close to unity confirms that there is very high statistical correspondence between experimental and estimated spectra.

4.2. Target transformation factor analysis

Target transformation factor analysis (TTFA) can be used to confirm the presence of a particular component in a set of mixture spectra. This approach works by checking if a suspected/target pure component spectrum, i.e. a pure experimental reference spectrum, is present in an experimental data set. The projection of a target pure spectrum, $a_{1 \times v}^{tar}$, onto the right singular vectors, $V_{z \times v}^{T}$, is performed according to Eq. (4). If the target and the projected pure component spectrum are similar (identical), then this implies that the component is present in the mixture [32].

$$a_{1 \times v}^{proj} = a_{1 \times v}^{tar}[V_{z \times v}^{T}]^{+}V_{z \times v}^{T} \qquad (4)$$

Since four components (acetamide, urea, dicyandiamide, and melamine) are present in the mixture data, we can use TTFA method as a tool to check the quality (linearity) of FT-Raman data. Twelve right singular vectors were used for TTFA, and the resulting projected spectra are compared to the reference spectra in Fig. 6. There is a very high degree of similarity. The sum of square errors (SSE) between target and projected pure component spectra for dicyandiamide, acetamide, urea, and melamine were calculated. The results were 4.0773E-003, 2.8383E-001, 4.1403E-002, and 3.0538E-002 respectively. As can be seen,

all SSEs are quite small and hence it can be concluded that the multi-component FT-Raman data exhibits a high degree of additivity. As an extra comparison, the Euclidean inner products between the reference experimental spectra and TTFA estimates
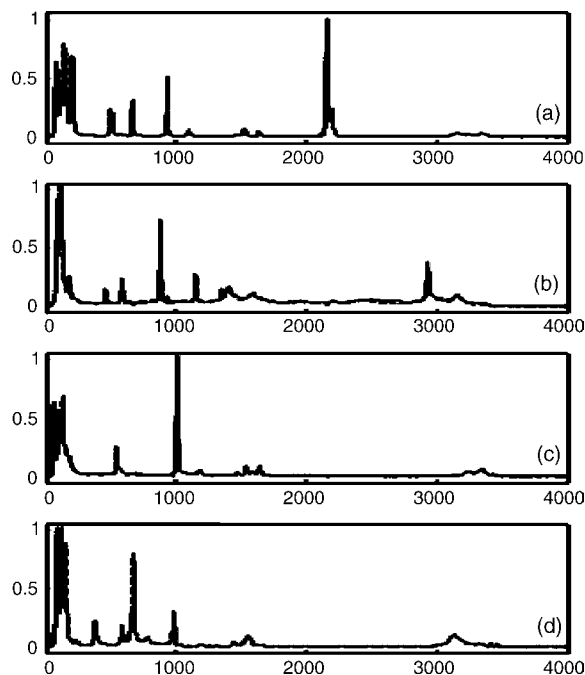

Fig. 6. Target and projected pure component spectra via TTFA; solid lines are target pure component spectra, and dashed line are projected pure component spectra: (a) dicyandiamide, (b) acetamide, (c) urea and (d) melamine. Note that the two curves in each figure are almost identical.
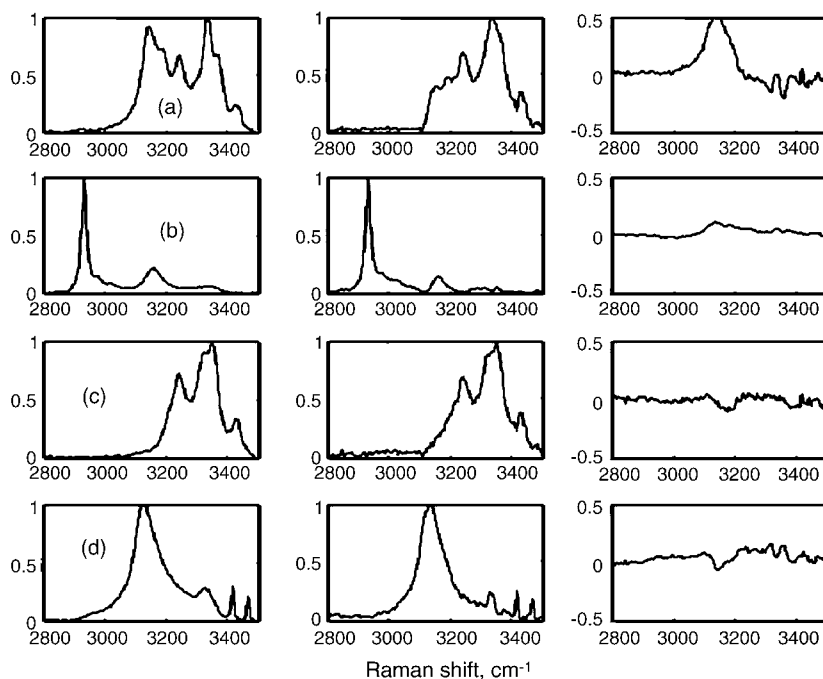
Fig. 7. Raman spectra of each pure component in the sub-region 2800–3500 cm^{-1}. Lefthand figures are measured spectra, centre figures are spectra reconstructed using BTEM algorithm. Right-hand figures are the difference spectra (measured − reconstructed): (a) dicyandiamide, (b) acetamide, (c) urea, (d) melamine using the same scale.

were calculated as (a) dicyandiamide (0.9999), (b) acetamide (0.9943), (c) urea (0.9986) and (d) melamine (0.9994). A figure of the almost-identical target and projected spectra is provided in Fig. 6.

4.3. Partial-scale spectral reconstruction

SVD was performed on a sub-region of spectra. Results of the BTEM analysis in the sub-region 2800 and 3500 cm^{-1} are shown in Fig. 7; pure component spectra on the left, BTEM reconstructed spectra in the centre and their difference spectra are shown on the right. The deviations between reference spectra and BTEM estimated spectra are quite large for some of the component. The Euclidean inner products between the reference experimental spectra and BTEM estimates were calculated as (a) dicyandiamide (0.9144), (b) acetamide (0.9709) (c) urea (0.9957), (d) melamine (0.9851). In general, more information available leads to better spectral reconstruction. Indeed, BTEM is a blind source separation technique [33] and as such it is totally dependent on the quality and quantity of information provided as input.

5. Conclusions

Multi-component solid state FT-Raman intensity data, obtained from a four component system of similar organic components, has been successfully deconvoluted using the blind source separation algorithm BTEM. Comparison of pure references with the spectral reconstructions shows that very accurate estimates were obtained when the full-spectral region was used.

Analyses of sub-regions confirmed that the quality of spectral reconstructions decreases when more limited data sets are used. The present results hold promise for the analysis of more complex multi-component organic powders.

References

[1] L.H. Lawton, E.A. Sylvestre, Technometrics 13 (1971) 617.
[2] E.R. Malinowski, Anal. Chim. Acta 134 (1982) 129.
[3] W. Windig, J. Guilment, Anal. Chem. 63 (1991) 1425.
[4] D.S. Bu, C.W. Brown, Appl. Spectrosc. 5 (2000) 1214.
[5] M. Maeder, Anal. Chem. 59 (1987) 527.
[6] Y.Z. Liang, O.M. Kvalheim, Anal. Chim. Acta 292 (1994) 5.
[7] O.M. Kvalheim, Y.Z. Liang, Anal. Chem. 64 (1992) 936.
[8] H.L. Shen, R. Manne, Q.S. Xu, D.Z. Chen, Y.Z. Liang, Chemom. Intell. Lab. Syst. 45 (1999) 171.
[9] P.J. Gemperline, J. Chem. Inf. Comput. Sci. 24 (1984) 206.
[10] R. Tauler, B.R. Kowalski, S. Flemming, Anal. Chem. 65 (1993) 2040.
[11] Y.L. Xie, P.K. Hopke, P. Paatero, J. Chemom. 12 (1998) 357.
[12] W. Chew, E. Widjaja, M. Garland, Organometallics 21 (2002) 1982.
[13] E. Widjaja, M. Garland, in: H.P. Lee, K. Kumar (Eds.), Proceeding of the International Conference on Scientific & Engineering Computation (IC-SEC), Recent Advances in Computational Sciences and Engineering, Imperial College Press, London, 2002, p. 62.
[14] E. Widjaja, C. Li, M. Garland, Organometallics 21 (2002) 1991.
[15] C.Z. Li, E. Widjaja, W. Chew, M. Garland, Angew. Chem. Int. (2002) 413785.
[16] C.Z. Li, E. Widjaja, M. Garland, J. Am. Chem. Soc. 125 (2003) 5540.
[17] C.Z. Li, E. Widjaja, M. Garland, J. Catal. 213 (2003) 126.
[18] E. Widjaja, C.Z. Li, W. Chew, M. Garland, Anal. Chem. 75 (2003) 4499.
[19] E. Widjaja, C.Z. Li, M. Garland, J. Catal. 223 (2004) 278.
[20] L.R. Ong, E. Widjaja, R. Stanforth, M. Garland, J. Raman Spectrosc. 34 (2003) 282.
[21] S.Y. Sin, E. Widjaja, L.E. Yu, M. Garland, J. Raman Spectrosc. 34 (10) (2003) 795.

[22] L.F. Guo, F. Kooli, M. Garland, Anal. Chim. Acta 517 (2004) 229.

[23] J.M. Alia, H.G.M. Edwards, F.J. Garcia Navarro, J. Mol. Struct. 597 (2001) 49.

[24] A.J. Belsky, T.B. Brill, J. Phys. Chem. A 102 (1998) 4509.

[25] A. Vijay, D.N. Sathyanarayana, J. Mol. Struct. 295 (1993) 245.

[26] G. Nandini, D.N. Sathyanarayana, Spectrochim. Acta 60 (2004) 1115.

[27] Y. Hu, Z. Wang, H. Li, X. Huang, L. Chen, Vib. Spectrosc. 37 (2005) 1.

[28] J.R. Schneider, B. Schrader, J. Mol. Struct. 29 (1975) 1.

[29] C.Y. Panicker, H.T. Varghese, A. John, D. Philip, H.I.S. Nogueira, Spectrochim. Acta 58 (2002) 1545.

[30] M. Garland, E. Visser, P. Terwiesch, D.W.T. Rippin, Anal. Chim. Acta 35 (1997) 1337.

[31] G.H. Golub, C.F. Van Loan, Matrix Computations, Johns Hopkins University Press, Baltimore, 1996.

[32] E.R. Malinowski, Factor Analysis in Chemistry, third ed., John Wiley Sons Inc., New York, 2002.

[33] M. Garland, in: B. Heaton (Ed.), Mechanistic Studies in Homogeneous Catalysis: A Spectroscopic Approach, Wiley, 2005.

ELSEVIER

Stripping voltammetric determination of platinum metals at a carbon paste electrode modified with cationic surfactants

Ivan Švancara [*], Michal Galík, Karel Vytřas

Department of Analytical Chemistry, Faculty of Chemical Technology, University of Pardubice,
Namesti Cs. legii 565, CZ-532 10 Pardubice, Czech Republic

Abstract

In this contribution, a novel method is described for the determination of platinum metals. The procedure developed employs a carbon paste electrode modified *in situ* with cationic surfactants of the quaternary ammonium salt type. The pre-concentration step is based on a specific accumulation mechanism involving ion-pair formation; the detection being performed by cathodic scanning in the differential pulse voltammetric mode. Regarding the individual forms of platinum metals, the method has been found convenient for the determination of three heavy platinum metals in the form of Pt(IV), Ir(III) and Os(IV), whereas for the remaining elements (Ru, Rh, and Pd) was almost inapplicable. Platinum metals of the former group can be pre-concentrated in chloride-containing supporting media *via* $PtCl_6^{2-}$, $IrCl_6^{3-}$ and $OsCl_6^{2-}$ complex anions, the central atom of each species being fairly reducible during the voltammetric scan. Stripping signals for both platinum and iridium were proportional to the concentration in a range of $1–10 \times 10^{-6}$ M Pt(IV) and Ir(III); the response for osmium being linear within $0.1–6 \times 10^{-7}$ M Os(IV) with a detection limit of about 5×10^{-9} mol l^{-1}. During optimisation, special attention was paid to the accumulation mechanism, choice of key experimental conditions, and to interference effects from foreign ions with potentially ion-pairing capabilities ($AuCl_4^-$, $TlCl_4^-$, CrO_4^{2-}, MnO_4^-, SCN^-, and I^-). The method elaborated has been tested on both model solutions and real samples of industrial waste water, showing in both cases satisfactory analytical performance.
© 2006 Elsevier B.V. All rights reserved.

Keywords: Stripping voltammetry; Carbon paste electrode; *In situ* modification; Cationic surfactants; Heavy platinum metals (Pt, Ir, Os)

1. Introduction

Platinum metals represent a sextet of the elements with related properties occasionally divided into two sub-classes [1] as light platinum metals (Ru, Rh, Pd) and heavy platinum metals (Os, Ir, Pt). Among their specific characteristics, one should not omit a high chemical stability in the elemental state, distinct catalytic properties, and capabilities to form stable complex structures.

Such features are more or less reflected in analytical procedures employing modern instrumental techniques: for example, atomic absorption spectrometry (AAS), ion-coupled plasma mass spectrometry (ICP-MS) or neutron activation analysis (NAA)—see *e.g.* [2] and references therein. Platinum metals are also determinable *via* electrochemical principles. In

this respect, electrochemical stripping analysis (ESA [3]) is especially suitable, offering a high analytical performance at relatively low expenses. The respective procedures usually involve the above-mentioned catalytic effect making such measurements extremely sensitive [4]. This is also the case of classical formazone method, being able of achieving down to 1×10^{-13} M Pt(IV), thus allowing one to determine platinum in sea water at the base level [5,6]. Similar extraordinary detection capabilities have been reported again for determinations in the presence of thiosemicarbazon [7] or formaldoxim [8]; both methods quoted having also profited from unique properties of mercury drop electrodes.

Determination of platinum metals can, however, be accomplished with the aid of carbon paste electrodes (CPEs) and their chemically modified variants (CMCPEs) [9,10], offering an interesting alternative of how to omit the use of momentarily controversial mercury-based electrodes [11,12]. Most methods developed for the determination of platinum metals have dealt with palladium as documented in a freshly compiled

* Corresponding author. Tel.: +420 466 037 031; fax: +420 466 037 068.
E-mail address: Ivan.Svancara@upce.cz (I. Švancara).

comprehensive survey [13]. Hitherto the only report has concerned the platinum itself and its adsorptive pre-concentration *via* the $[(Pt–Sn)Cl_5]^{2-}$ adduct [14]. Finally, iridium has been of interest in a couple of studies that utilised either accumulation of Ir(III)–[4-phenyl-8-thioquinolinate] complex onto a carbon paste containing 1,4-dichlorobenzene [15] or the ion-pair formation at CPEs bulk modified with Amberlite LA-2 or tricaprylmethylammonium chloride [16]. As shown recently, highly effective and selective ion-pairing mechanism can be utilised in a simple arrangement of *in situ* modification when a cationic surfactant of the quaternary ammonium salt type is added into the sample. Such an approach has successfully been used to accumulate and determine iodide, I^- [17], or hydrogenchromate, $HCrO_4^-$ [18], in selected food samples.

In this paper, another possible application of a CPE modified *in situ* with cationic surfactants is reported as a novel method for the determination of platinum metals *via* suitable complex ions. Initial investigations on this topic have already been presented in two conference contributions [19,20] and the text given below is the resultant publication form, summarising all the important results and observations.

2. Experimental

2.1. Chemicals, reagents, stock and standard solutions

All chemicals used to prepare stock and standard solutions were of analytical reagent grade and purchased from Lachema, Aldrich, Fluka or Merck unless stated otherwise. Stock solutions of the supporting electrolytes were made 1 M in concentration. The Pt(IV), Ir(III), and Os(IV) standards were prepared as 0.01 M solutions when using solid compounds $(Na_2PtCl_6 \cdot 6H_2O, IrCl_3 \cdot 3H_2O, and (NH_4)_2OsCl_6)$ dissolved in in 100 ml redistilled water, always in the presence of 5 ml 30% HCl. In the same way, standards of Ru(III), Rh(III), and Pd(II) were also made (from $RuCl_3$, $RhCl_3$, and $PdCl_2$ salts) and used for some comparative studies. Hydrochloric acid was also used to stabilise the individual standard solutions with concentrations lower than 1×10^{-3} mol l^{-1}. Ion-pairing agents prepared as 0.001 M stock solutions contained 1-(ethoxycarbonyl)pentadecyltrimethylammonium bromide (Septonex®), cetyltrimethylammonium bromide (CTAB), or cetylpyridinium bromide (CPB).

Water used throughout the experimental work was obtained by passing deionised water through a laboratory-made distillation unit. All solutions analysed were deoxygenated by bubbling with argon (purity: 99.99%; Linde Technoplyn, Prague).

2.2. Instrumentation

A portable electrochemical analyser PalmSens (Palm Instruments BV, The Netherlands) incorporated the three-electrode system (see below) and the stirring was devised with a magnetic bar agitated by electromotor at *ca.* 300 rpm.

The pH values were measured on a portable pH-meter (model CPH 52; Elteca, Turnov, Czech Republic) equipped with a combined glass sensor (OP-0808P; Radelkis, Budapest, Hungary) and calibrated using commercially marketed standard buffers.

2.3. Electrodes

2.3.1. Carbon paste electrode

The paste mixture was prepared by intimately homogenising 0.50 g spectroscopic graphite powder (RW-B type; Ringsdorff Werke, Germany) with 0.20 ml silicone oil (LUKOIL MV 15500; Lucebni zavody Kolin, Czech Republic) using a recommended procedure [21]. The ready-made paste was packed into a piston-driven carbon paste holder of own construction with the surface diameter of 3 mm [22]. The electrode surface was renewed by extrusion of *ca.* 0.5 mm carbon paste from the holder and smoothing with a wet filter paper. Typically, this mechanical renewal of the carbon paste surface was made when starting a new series of measurements (*e.g.* prior to analysis of each sample).

2.3.2. Other electrodes

A self-made Ag/AgCl/3 M KCl reference electrode was used, together with the glassy carbon electrode (GCE, Ø = 3 mm; Metrohm) employed either as the counter or the working electrode for some comparative voltammetric studies.

2.4. Procedures and methods

2.4.1. Stripping voltammetry

After preparing the solution to be analysed and its purging with inert gas for *ca.* 5 min, the measurements were carried out in the differential pulse cathodic stripping voltammetric mode (DPCSV). A typical experiment consisted of three consecutive steps with the following experimental conditions: the pre-concentration at +0.8 V *versus* Ag/AgCl for 30 s, the rest period for 15 s, and a polarisation (stripping step) run from +0.8 to −0.4 V by applying a scan rate, $v = 10$ mV s^{-1}, and the pulse height, $\Delta E = -25$ mV.

2.4.2. Analysis of model solutions and real sample

Typical model solution contained a mixture of 0.10 M acetate buffer + 0.15 M NaCl + 1×10^{-5} M Septonex® spiked with the respective platinum metal standard at two different concentrations. Real samples represented a set of heavily polluted waters collected inside the area of a factory refining some heavy and noble metals from the industrial waste material. Specification of the individual samples was provided, declaring the approximate content of numerous metal ions, including three platinum metals ([23], see also discussion in Section 3.4). The specimens selected had contained a considerable amount of the CN^- ions in highly alkaline matrix (pH ≈ 13), thus requiring pre-treatment and additional buffering before analysis. This was accomplished with a few drops of 30% HCl at carefully adjusted pH, followed by short heating for 5 min. It should be emphasised that the whole procedure must be performed under well aerated conditions in order to avoid a possible intoxication by HCN vapours.

The proper solutions to be analysed were prepared by pipetting the chosen volume of pre-treated waste water together with

a mixture of stock solutions of both main constituents of the supporting electrolyte and the modifying agent. When making the final volume up to 20 ml, sample solutions obtained were then subjected to voltammetric analysis as described above.
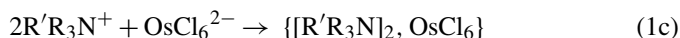
2.5. Evaluation and calculation of the results

Model solutions or real samples spiked with Os(IV) were analysed by the standard addition method with two or three aliquots when each DPCSV measurement had always been repeated in order to check the reproducibility; in the case of one analysis using the same carbon paste surface (see Section 2.3). The individual voltammetric signals were evaluated as the peak areas by manual base-line setting enabled by the software.

3. Results and discussion

3.1. Principles of the pre-concentration and detection step

Analogously to the previous methods [17,18], the determination of platinum metals benefits from a "double" effect of the modifiers chosen. First, cationic surfactants of the $R'R_3N^+$ type (*i.e.* CTAB and Septonex®) or related compounds (CPB) exhibit a strong ion-pairing affinity and secondly, they are highly lipophilic in nature, thus enabling to be anchored firmly onto the hydrophobic carbon paste surface. Both phenomena result in a very efficient pre-concentration of the respective anion with either tetravalent or trivalent platinum metal complexes. Then, for a counterpart of the quaternary ammonium cation, one has:

$$2R'R_3N^+ + PtCl_6{}^{2-} \rightarrow \{[R'R_3N]_2, PtCl_6\} \qquad (1a)$$

$$3R'R_3N^+ + IrCl_6{}^{3-} \rightarrow \{[R'R_3N]_3, IrCl_6\} \qquad (1b)$$

$$2R'R_3N^+ + OsCl_6{}^{2-} \rightarrow \{[R'R_3N]_2, OsCl_6\} \qquad (1c)$$

As can be seen, both schemes also reflect the different stoichiometry between the surfactant moiety and the corresponding complex anion.

Whereas the already published results from potentiometric ion-pair formation-based titrations could be used to postulate the structure of ion-associates for both $PtCl_6{}^{2-}$ and $IrCl_6{}^{3-}$ anions [24–26], the relevant data for Os(IV) species were not available and the reaction ratio had to be defined newly [20]; again, using potentiometric titration combined with a special carbon paste-based indicator electrode [27]. In connection with the above-given pre-concentration schemes, it should be noted that both (1a) and (1b) can be written in an alternate way since both Pt^{IV}- and Ir^{III}-anions tend to form mixed hydroxo/chloro complexes of the $Pt(OH)_mCl_n{}^{2-}$ or $Ir(OH)_mCl_n{}^{3-}$ general structure [28] (where the sum $m + n = 6$).

In the detection step, all three ion-associates formed ((1a)–(1c)) are reduced during cathodic voltammetric scan in consequence of electrochemical transformation of the central atom down to the elemental state:

$$\{[R'R_3N]_2, PtCl_6\} + 4e^- \rightarrow 2R'R_3N^+ + Pt + 6Cl^- \qquad (2a)$$

$$\{[R'R_3N]_3, IrCl_6\} + 3e^- \rightarrow 3R'R_3N^+ + Ir + 6Cl^- \qquad (2b)$$

$$\{[R'R_3N]_2, OsCl_6\} + 4e^- \rightarrow 2R'R_3N^+ + Os + 6Cl^- \qquad (2c)$$
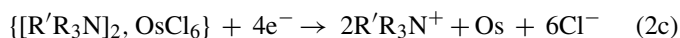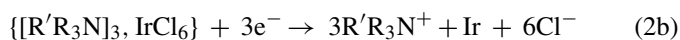
Regarding tetravalent central atoms in both $PtCl_6{}^{2-}$ and $OsCl_6{}^{2-}$ anions and trivalent iridium in the $IrCl_6{}^{3-}$ complex, the different number of electrons involved in the reduction pathway could be observed *via* the overall character and shape of the respective peaks. Namely, voltammetric reduction according to schemes (2a) and (2c) had resulted in higher and sharper signals compared to that in (2b), which was attributed to a lesser number of electrons for the $Ir^{III} \rightarrow Ir^0$ reduction.

In order to further explore the faradaic process taking place at the CPE in the presence/absence of ion-pairing agent of the $R'R_3N^+$ type, the behaviour of platinum metal complexes was additionally studied by cyclic voltammetry (CV). In case of the $OsCl_6{}^{2-}$ anion, these experiments can be surveyed as follows: (i) electrochemical transformation of Os(IV) in both regimes tested (with or without modifying agent) has been found practically reversible in acidic media tested. (ii) In solutions with pH > 7, CV-studies revealed a decrease of the peaks of interest and a quasi-reversible behaviour, typical for moderated reaction kinetics at carbon paste-based electrodes [13,29]. (iii) Repetitive cycling gave stable and reproducible peaks, implying almost no contribution of adsorption into the accumulation process. Also these results have suggested us that the ion-pairing with $R'R_3N^+$ cations would be dominating in the pre-concentration mechanism of a procedure adapted for the determination of heavy platinum metals in the form of $PtCl_6{}^{2-}$, $IrCl_6{}^{3-}$ and $OsCl_6{}^{2-}$ anions.

In another study, it was examined how the type of working electrode and the character of its surface contribute to the efficiency of the accumulation mechanism and, eventually, the following electrochemical detection. A typical result of such studies is depicted in Fig. 1, making comparison of the reduction responses for iridium obtained at either CPE or GCE; both having been modified *in situ* with Septonex®. The corresponding voltammograms document clearly that the accumulation of hexachloroiridate(III) and its subsequent reduction at the GCE gave rise to a very poor analytical signal compared to that obtained with CPE under otherwise identical conditions. Yet more pronounced differences in both peaks at the two electrodes confronted were noticed for responses of Pt and Os (not shown). These observations seem to indicate a significant benefit of the hydrophobic carbon paste surface facilitating a very intimate anchoring of the ion-pairing agent through its lipophilic chain.

Finally, in some measurements, especially those performed with analytes at lower concentrations, voltammograms obtained at *in situ* modified CPE had exhibited notably increased background currents in the potential range of interest. This could be due to mutual interaction between the lipophilic chain of the surfactant used and the carbon paste itself. For electroanalysis with CPEs, this phenomenon has already been postulated as the so-called "erosion effect" [30,31] and – when considering the method discussed herein – studied in detail during our previous investigations [18]. Similarly with experiments reported, both CPE and GCE (as *in situ* modified) were able
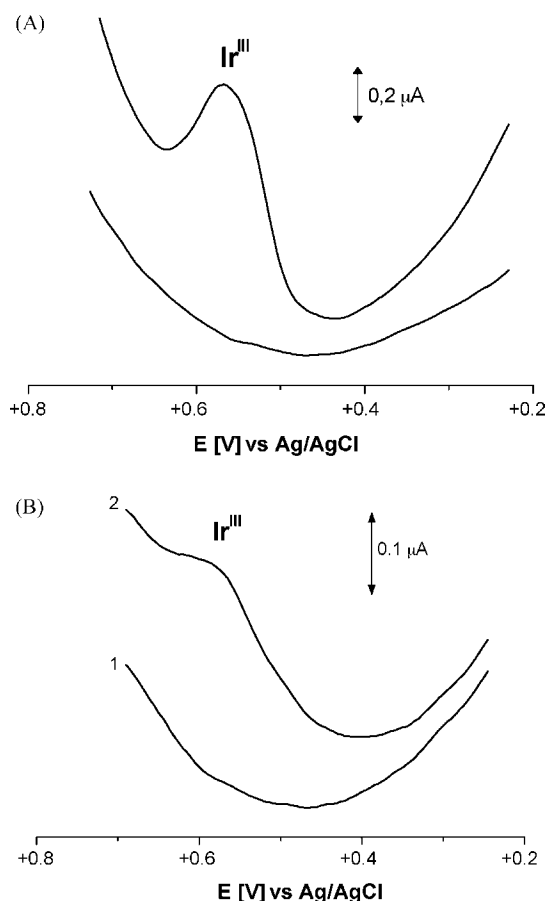
Fig. 1. Comparison of the reduction response for iridium at two different working electrodes. (A) Carbon paste electrode of the C/SO type; (B) glassy carbon electrode; (1) base-line, (2) $c(Ir^{III}) = 9 \times 10^{-6}$ mol l^{-1}. Experimental conditions: DPCSV; 0.10 M acetate buffer + 0.15 M KCl + 1 × 10^{-5} M CTAB (pH 4.4); E_{ACC} = +0.8 V. For other conditions and parameters, see the figure.

of accumulating the individual platinum metals in the form of MeCl$_6^{2/3-}$ anions under open-circuit conditions; nevertheless, with markedly lower intensity compared to analogous tests carried out with HCrO$_4^-$.

The whole study on the accumulation mechanism of a method based on *in situ* modification with cationic surfactants of the quaternary ammonium salt type was completed by experiments involving all three light platinum metals and their Ru(III), Rh(III) and Pd(II) compounds. Regarding the latter, modification with both CTAB and Septonex® has been shown completely ineffective with no evidence to accumulate palladium(II) in a form of its anionic complexes such as PdCl$_4^{2-}$ and related structures of the PdX$_4^{2-}$ or Pd$_2$X$_6^{2-}$ type [24,34]. This rather surprising finding could perhaps be due to complicated interactions between these complex halide anions and quaternary ammonium or arsonium salts [32–34] and the determination of Pd(II) at cationic surfactant modified CPE would require further investigations, including tests with some alternate supporting media. When analysing model solutions containing Ru(III) and Rh(III), the resultant responses were small, badly developed, and practically irreproducible.

In both cases, however, it was expected because these metals occurring usually as complex cations would require an inverse approach—an ion-pairing with suitable anionic moieties such as water-soluble alkyl sulphonates, R–SO$_3^-$, that have already been shown highly effective in binding and accumulating the Ag$^+$ ions (down to the picomolar concentration level [35]). Or, better, both Ru(III) and Rh(III) could be converted into voluminous complex cations with some neutral ligands (*e.g.* 1,10-phenanthroline or its derivatives [36]) that form structures with a lipophilic skeleton, thus offering particularly high ion-pairing affinity towards a suitable counter ion.

3.2. Method development and optimisation of key experimental parameters

3.2.1. Choice of ion-pairing agents and of modification regime

By following the original procedures [17,18], three related quaternary ammonium salts were selected, cetyltrimethylammonium bromide (CTAB), cetylpyridium bromide (CPB), and 1-(ethoxycarbonyl)pentadecyltrimethylammonium bromide (Septonex®). All of them exhibited the best performance at concentrations of about 1 × 10^{-5} mol l^{-1}. With respect to their selectivity towards the individual anions, Septonex® and CTAB were effective for PtCl$_6^{2-}$ as well as for IrCl$_6^{3-}$, whereas OsCl$_6^{2-}$ interacted predominantly with Septonex®. The third agent examined, CPB, had showed rather unsatisfactory performance in a majority of measurements; apparently, due to some steric effect of the pyridinium structure.

3.2.2. Supporting electrolyte composition

Already initial studies established the suitability of mixed media of the acetate buffer/chloride type. Concerning Cl$^-$ ions, their increasing content was found to affect mainly the overall signal-to-noise characteristics and, in a series of supporting electrolytes tested, a mixture of 0.1 M CH$_3$COONa + 0.1 M CH$_3$COOH + 0.15 M KCl was found optimal for all Pt(IV), Ir(III) and Os(IV).

3.2.3. Effect of pH

Stripping voltammetric behaviour of heavy platinum metal anions was investigated in mixed media containing Britton–Robinson buffers. For PtCl$_6^{2-}$, such a study is depicted in Fig. 2, showing a set of the corresponding voltammograms with responses for Pt varying widely in dependence of pH. As can be seen, the highest signals at a potential of *ca.* +0.30 V *versus* Ag/AgCl were obtained in mild acidic media (pH 3.0–5.5), whereas the decreasing acidity had led to a diminishing or even disappearance of the response of interest.

At pH < 3, a plateau-like peak at +0.45 V was also observed; being attributed – according to previous reports [17,18] – to an electroactivity or interaction of Septonex® under strongly acidic conditions. Similarly, weekly acidic solutions were found suitable also for IrCl$_6^{3-}$ and OsCl$_6^{2-}$; the corresponding maximum being at a pH of 4.0–5.5 for Ir and 4.2–6.0 for Os (not shown). In case of iridium, however, small reduction responses could also be registered in neutral, basic or even slightly alkaline media.
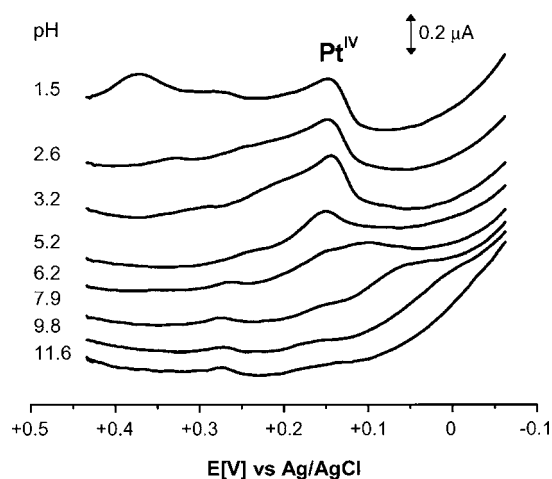
Fig. 2. Voltammetric stripping response for platinum at a carbon paste electrode modified *in situ* with cationic surfactant in dependence of pH. Experimental conditions: differential pulse cathodic stripping voltammetry; Britton–Robinson buffer (with actual pH) + 0.15 M KCl + 1 × 10^{-5} M Septonex$^{®}$ + 1 × 10^{-6} M Pt(IV); accumulation potential, E_{ACC} = +0.9 V vs. Ag/AgCl; potential range, E_R = +0.9 to −0.3 V; accumulation time, t_{ACC} = 30 s; the rest period, t_R = 15 s; scan rate, v = 10 mV s^{-1}; pulse height, ΔE = −25 mV.

3.2.4. Accumulation potential (E_{ACC}) and accumulation time (t_{ACC})

Anions of PtCl$_6{}^{2-}$, IrCl$_6{}^{3-}$ and OsCl$_6{}^{2-}$ were subjected to a series of measurements to set up optimum conditions for each one. After varying the E_{ACC} potential from +0.3 to +1.3 V, PtCl$_6{}^{2-}$ and IrCl$_6{}^{3-}$ anions exhibited a very similar behaviour towards the modified CPE. In both cases, the I_P(Me) *versus* E_{ACC} plots resulted in a parabolic curve with a sharp maximum at about +0.8 V. The I_P(Me) *versus* t_{ACC} dependence was examined next. Lengthy accumulation periods had often been accompanied by saturation effects, which was characteristic for a mechanism involving the ion-pair formation and subsequent accumulation onto the carbon paste [9,10,13,21]. Thus, optimal approach required shorter pre-concentrations, typically from 30 to 60 s. The values of E_{ACC} = +0.8 V and t_{ACC} = 30 s were found to be convenient also for OsCl$_6{}^{2-}$.

3.3. Analytical performance of the method for Pt(IV), Ir(II), and Os(IV)

3.3.1. Calibration plots

The I_P(Me) *versus* c(Me) dependence was investigated for all three heavy platinum metals. Calibration for Pt(IV) is shown in Fig. 3, depicting typical voltammograms over the linear range (A) and the corresponding plots obtained in the presence of all ion-pairing agents tested (B); the latter demonstrating clearly that the method performance significantly depends upon the surfactant used (see a decrease in sensitivity for the sequence Septonex$^{®}$ → CTAB → CPB). As can be seen, the responses of interest proportional to the Pt(IV) concentration could be plotted up to 1.5 × 10^{-5} mol l^{-1}, but calibration at higher concentrations had already exhibited slight deviations from linearity; again, due to saturation of the CPE surface. Similar observations were made with Ir(III), only the effective-
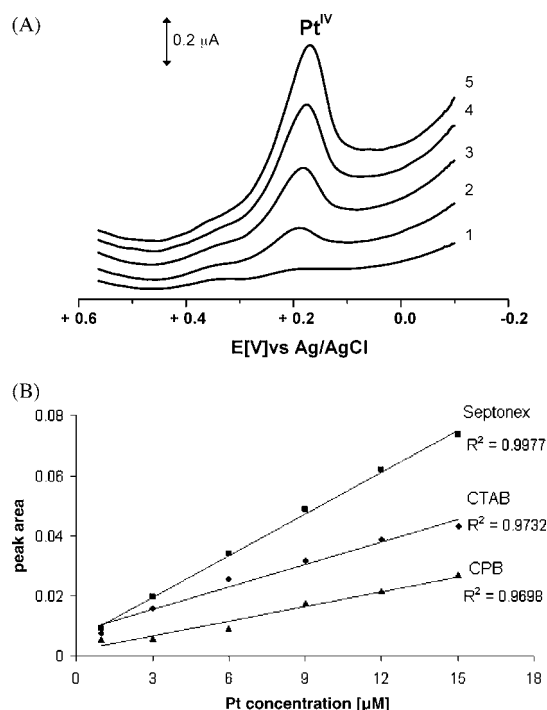

Fig. 3. Calibration of Pt(IV) at the micromolar concentration level at a CPE modified *in situ* with quarternary ammonium salts. (A) Voltammograms for concentration range of 1–10 × 10^{-6} mol l^{-1}: (1) base-line, (2–5) addition of 1, 3, 6, and 9 μM Pt(IV), four aliquots; (B) calibration plots for measurements with the individual modifiers (see inscriptions) for the whole linear range. Experimental conditions: DPCSV; 0.10 M acetate buffer + 0.15 M KCl; c(Septonex$^{®}$, CTAB, CPB) = 1 × 10^{-5} mol l^{-1}. For other conditions, see Fig. 1.

ness of the individual ion-pairing agents decreased in the order CTAB → Septonex$^{®}$ → CPB. Quite attractive analytical performance of the method was achieved when calibrating the response for osmium since the concentration of OsCl$_6{}^{2-}$ complex could be detected down to the nanomolar level; *i.e.* at considerably lower concentrations compared to those sufficient for the determination of PtCl$_6{}^{2-}$ or IrCl$_6{}^{3-}$.

Such remarkable detection characteristics for Os could perhaps be due to a higher lipophilicity of the hexachloroosmiate(IV) compared to related Pt(IV) and Ir(III) complex anions or, eventually, because of abnormal stability of the respective ion-associate. But, in order to support such hypotheses, there are no relevant data available [28].

3.3.2. Limits of detection (LODs)

These parameters were evaluated for all three metals when using model solutions containing the single element at a concentration of 2.5 × 10^{-6} mol l^{-1} for both Pt^{IV} and Ir^{III}, and 5 × 10^{-9} mol l^{-1} for Os^{IV} (all with t_{ACC} for 60 s). By means of the 3:1 signal-to-noise ratio criterion, the corresponding LODs were estimated to be 9 × 10^{-7} M Ir(III) (with CTAB), 7 × 10^{-7} M Pt(IV) and 5 × 10^{-9} M Os(IV) (both with Septonex$^{®}$).

3.3.3. Reproducibility

Also this parameter was examined for all three PtCl$_6{}^{2-}$, IrCl$_6{}^{3-}$, and OsCl$_6{}^{2-}$ complexes with the ion-pairing agent

selected using a series of voltammograms recorded in 10 replicates in samples with 2.0×10^{-6} M Pt(IV), 7.5×10^{-6} M Ir(III) or 2.5×10^{-7} M Os(IV). The resultant reproducibility was calculated to be within ± 8–15% for responses of Pt or Ir, and about $\pm 5\%$ for signal of Os, respectively. Even such values could be regarded as satisfactory for a method combining the ion-pair formation with subsequent accumulation.

3.3.4. Interference studies

Attention was paid to such anionic species that might affect the determination of platinum metals as possible competitors in the ion-pairing processes. Important results of this study comprising a sextet of analytes (AuCl$_4$$^-$, TlCl$_4$$^-$, MnO$_4$$^-$, CrO$_4$$^{2-}$, SCN$^-$, and I$^-$) can be summarised in this way: as anticipated, seriously interfering were chloroaurate [27] and chlorothallates [37]; both being able to form stable ion-pairs with R$'$R$_3$N$^+$ cations over a wide pH-interval. On the contrary, only minor interference was from chromate and iodide, exhibiting strong ion-pairing affinity in highly acidic solutions [17,18], which is not the case of acetate buffer-based media used in this method variant.

Definitely the most valuable finding to be emphasised within interference studies is the fact that the method has been able to discriminate between all three heavy platinum metals, which is illustrated in Fig. 4. To the authors' knowledge, there is no comparable experiment ever reported in an electrochemical or electroanalytical journal, featuring simultaneous determination of platinum, iridium, and osmium with such successful separation of all the corresponding peaks in the single voltammetric scan.

3.4. Analysis of model solutions and real samples

First, the method is characterised with the aid of recovery rates by analysing model solutions containing 0.10 M acetate buffer + 0.15 M KCl + 1×10^{-5} M modifier (see below) plus a spike of either 1×10^{-6} or 5×10^{-6} M Pt(IV), the same concentrations of Ir(III), and 1×10^{-7} or 5×10^{-7} M Os(IV), respectively. The individual analyses, performed always in replicate measurements for the respective model solution as well as each standard addition, yielded the recovery rates within an interval of 90–115% for Pt(IV) or Ir(III) and of 97–99% for Os(IV); especially the latter being surprisingly good results for a method based on non-faradaic accumulation. All these results were obtained with either CTAB or Septonex® as modifiers of choice, analyses with CPB had not been successful (when the recovery reached up to 150% because of poorly reproducible signals).

As stated in Section 2, real samples selected to test practical applicability of the method were three specimens of heavily polluted water collected at various sampling sites inside a factory processing and separating some precious and heavy metals from industrial waste waters. According to the specification given [23], the individual samples contained a number of heavy or noble metals; namely: Zn, Cd, Pb, Cu, and Ag (at concentrations of 1–20 mg l^{-1}), traces of Cr, Fe, Ni, Hg, and Au (<1 mg l^{-1}) plus three platinum metals: Rh, Pd, and Pt; the content of the latter being declared to be 2.7–3.0 mg l^{-1} in specimens supplied.

Platinum was also the element of interest in order to test the method. Typical voltammograms obtained by analysing sample no. 1 are shown in Fig. 5, with peaks for Pt at a peak potential of *ca.* +0.2 V *versus* ref. The concentration found in this sample was 1.56×10^{-5} mol l^{-1} ($\approx$3.04 mg l^{-1}); the remaining two samples containing 1.25×10^{-5} and 1.34×10^{-5} mol l^{-1} (2.44 and 2.61 mg l^{-1}), respectively. All these results agreed well to the contents declared, showing a satisfactory performance of the method for the determination of Pt(IV).

In case of industrial waste water, the integral part of the procedure was also a pre-treatment, comprising the acidification of originally highly alkaline matrices and the removal of cyanides. Whereas the first operation was necessary in order to ensure the optimal pH, the presence of CN$^-$ ions was evaluated as undesirable due to their capabilities to form highly stable complexes with metallic elements, including platinum metals [28,38] that
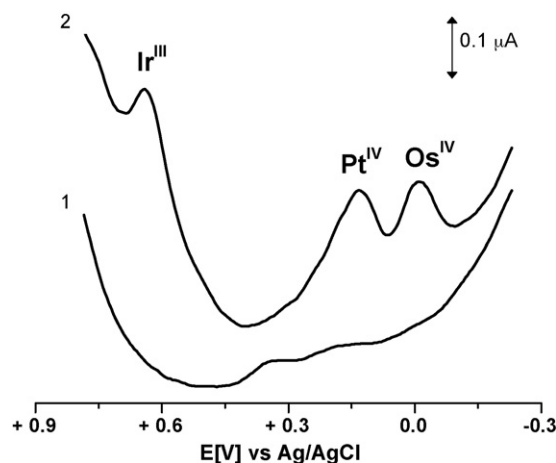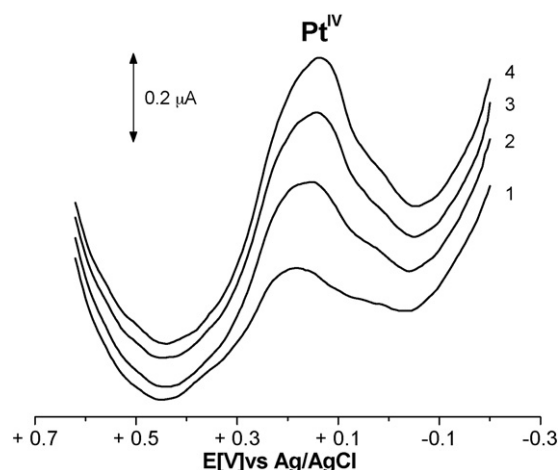

Fig. 4. Voltammetric analysis of a mixture of Pt(IV), Ir(III), and Os(IV) at a carbon paste electrode modified with Septonex®. (1) Base-line (supporting electrolyte, see below), (2) addition of 5×10^{-7} M Pt(IV) + 3.5×10^{-6} M Ir(III) + 5×10^{-8} M Os(IV). Experimental conditions: DPCSV; 0.10 M acetate buffer + 0.15 M KCl + 1×10^{-5} M Septonex® (pH 4.5); accumulation potential, E_{ACC} = +0.8 V. For other conditions and parameters, see Fig. 1.

Fig. 5. Determination of Pt(IV) in real sample of industrial waste water. (1) Sample solution [2 ml 1 M CH$_3$COOH/CH$_3$COONa + 3 ml 1 M KCl + 200 μl 0.001 M Septonex® + 9.8 ml distilled water + 5 ml pre-treated waste water]; (2–4) +2, 4, 6 μM Pt(IV). For experimental conditions, see Fig. 1.

might affect the complexing function of chlorides—one of the two main constituents in the supporting electrolyte. The results of analyses suggest one that the whole pre-treatment has been chosen properly and did not lead to any losses of the analyte.

4. Conclusions

Results and observations summarised above have shown that a simple method based on *in situ* modification of CPE with cationic surfactants of the $R'R_3N^+$ type, originally invented for the determination of iodide, I^- [17], later adapted for hydrogenchromate, $HCrO_4^-$ [18], can also be maintained for the determination of all three heavy platinum metals—platinum, iridium, and osmium. This documents clearly a flexibility of the respective procedure, having offered attractive analytical performance in each hitherto tested application. In case of platinum metals, such a characterisation can also be made if one takes into account, for instance, remarkable feature to determine simultaneously Pt, Ir, and Os. Although the method developed does not offer detection capabilities comparable to those reported for classical procedures utilising electrocatalytic principles (see *e.g.* [39] and references therein), it can be recommended – thanks to a sufficient selectivity – for the determination of platinum or iridium in heavily polluted water and similar samples.

Regarding osmium, the approach presented here is so far the only attempt to determine this platinum metal using carbon paste-based electrode or related sensors [9,10,13]. This priority in the determination of Os at a CPE and, in particular, rather astonishing finding that there is a nearly 30 years gap in database with contributions falling into the electrochemistry of osmium [40] have motivated our research group to continue in investigations with this interesting chemical element. In this respect, some new studies have already been started and other valuable results obtained.

Acknowledgements

References

[1] A. Earnshaw, N. Greenwood, Chemistry of the Elements, 2nd ed., Elsevier Science, Oxford, UK, 1997, pp. 1070–1171.
[2] Y.-B. Qu, Analyst 121 (1996) 139.
[3] J. Wang, Stripping Analysis: Principles, Instrumentation and Applications, Deerfield Beach, Florida, USA, 1985.
[4] A. Bobrowski, J. Zarebski, Electroanalysis 12 (2000) 1177.
[5] C.M.G. van den Berg, G.S. Jacinto, Anal. Chim. Acta 211 (1988) 129.
[6] J. Kowalska, S. Huszal, M.G. Sawicki, M. Asztemborska, E. Stryjewska, E. Szalacha, S.W. Golimowski, Electroanalysis 16 (2004) 1266.
[7] S. Huszal, J. Kowalska, M. Krzeminska, J. Golimowski, Electroanalysis 17 (2005) 299.
[8] J. Wang, M. Czae, J. Lu, M. Vuki, Microchem. J. 62 (1999) 121.
[9] K. Kalcher, J. Wang, J.-M. Kauffmann, I. Švancara, K. Vytras, C. Neuhold, Z. Yang, Electroanalysis 7 (1995) 5.
[10] I. Svancara, K. Vytras, J. Zima, J. Barek, Crit. Rev. Anal. Chem. 31 (2001) 311.
[11] A. Economou, Trends Anal. Chem. 24 (2005) 334.
[12] J. Wang, Electroanalysis 17 (2005) 1341.
[13] K. Kalcher, I. Svancara, R. Metelka, K. Vytras, A. Walcarius, in: C.A. Grimes, E.C. Dickey, M.V. Pishko (Eds.), Encyclopedia of Sensors, vol. 4, American Scientific Publishers, Stevenson Ranch, FL, USA, 2006, pp. 283–430.
[14] V.A. Zarinskii, L.S. Chulkina, Zavod. Lab. 43 (5) (1977) 148.
[15] N.A. Ulakhovich, E.P. Medyantseva, S.V. Mashkina, J. Anal. Chem. 52 (1997) 331.
[16] K. Kalcher, Fresen. Z. Anal. Chem. 324 (1986) 47.
[17] I. Svancara, I. Cermakova, K. Vytras, W. Goessler, K. Kalcher, Sci. Pap. Univ. Pardubice, Ser. A 5 (1999) 95.
[18] I. Svancara, P. Foret, K. Vytras, Talanta 64 (2004) 844.
[19] M. Galik, I. Svancara, K. Vytras, ESEAC 2006, 11th International Conference on Electroanalysis, Book of Abstracts, European Society for Electroanalytical Chemistry, Bordeaux, France, 2006, p. P2-074.
[20] M. Galik, M. Cholota, I. Svancara, K. Vytras, YISAC '06, 13th Youth Investigators' Seminar on Analytical Chemistry, Book of Abstracts, University of Zagreb, Zagreb, Croatia, 2006, p. P3.
[21] I. Svancara, K. Schachl, Chem. Listy 93 (1999) 490.
[22] I. Svancara, R. Metelka, K. Vytras, in: K. Vytras, K. Kalcher (Eds.), Sensing in Electroanalysis, University of Pardubice, Pardubice, 2005, pp. 7–18.
[23] Firm Inner Documentation, Safina Vestec, Czech Republic, 2006.
[24] W. Selig, Fresen. Z. Anal. Chem. 312 (1982) 419.
[25] K. Vytras, Ion Sel. Electrode Rev. 7 (1985) 77.
[26] B. Simickova, K. Vytras, Chem. Listy 82 (1988) 1093.
[27] I. Svancara, K. Vytras, Anal. Chim. Acta 273 (1993) 195.
[28] S. Kotrly, L. Sucha, Handbook of Chemical Equilibria in Analytical Chemistry, Ellis Horwood, Chichester, UK, 1985.
[29] R.N. Adams, Electrochemistry at Solid Electrodes, M. Dekker, New York, 1969.
[30] K. Digua, J.-M. Kauffmann, J.-L. Delplancke, Electroanalysis 6 (1994) 451.
[31] C. Petit, A.G. Cortes, J.-M. Kauffmann, Bioelectrochem. Bioenerg. 41 (1996) 101.
[32] C.M. Harris, S.E. Livingstone, N.C. Stephenson, J. Chem. Soc. (1958) 3697.
[33] S.E. Livingstone, in: J.C. Bailar, H.J. Emeleus, R. Nyholm, A.F. Trotman-Dickenson (Eds.), Comprehensive Inorganic Chemistry, vol. III, Pergamon Press, Oxford, UK, 1973, p. 1284.
[34] K. Vytras, J. Kalous, B. Simickova, J. Cerna, I. Silena, Anal. Chim. Acta 209 (1988) 357.
[35] I. Svancara, K. Kalcher, W. Diewald, K. Vytras, Electroanalysis 8 (1996) 336.
[36] K. Vytras, I. Varmuzova, Electroanalysis 6 (1994) 151.
[37] K. Vytras, E. Khaled, J. Jezkova, H.N.A. Hassan, B.N. Barsoum, Fresen. J. Anal. Chem. 367 (2000) 203.
[38] (a) F. Opekar, P. Beran, Z. Samec, Electrochim. Acta 22 (1977) 243;
(b) F. Opekar, P. Beran, Electrochim. Acta 22 (1977) 249.
[39] A. Bobrowski, J. Zarebski, Electroanalysis 12 (2000) 1177.
[40] http://portal.isiknowledge.com/portal.cgi?DestApp=WOS&Func=Frame, 2006.

Application of 1-alkyl-3-methylimidazolium-based ionic liquids as background electrolyte in capillary zone electrophoresis for the simultaneous determination of five anthraquinones in Rhubarb

Kan Tian [a,b], Yushang Wang [c], Yonglei Chen [a,b], Xingguo Chen [a,b,*], Zhide Hu [a,b]

[a] *Department of Chemistry, Lanzhou University, Lanzhou, China*
[b] *State Key Laboratory of Applied Organic Chemistry, Lanzhou University, Lanzhou 730000, China*
[c] *College of Earth and Environmental Science, Lanzhou University, Lanzhou 730000, China*

Abstract

A capillary zone electrophoresis method using only 1-alkyl-3-methylimidazolium-based ionic liquids as background electrolyte for the simultaneous determination of five anthraquinone derivatives including aloe-emodin, emodin, chrysophanol, physcion and rhein in Rhubarb species was described. Ion association constants, K_{ass}, between anthraquinone anions and imidazolium cations were determined by analyzing the electrophoretic mobility change of anthraquinone anions using a non-linear least-squares method and factors contributing to ion associability were systematically clarified. For method optimization, several parameters such as ionic liquids concentration, background electrolyte pH and applied voltage, on the separation were evaluated and the optimum conditions were obtained as follows: 90 mM 1-butyl-3-methylimidazolium tetrafluoroborate (pH 11.0) with an applied voltage of 20 kV. Under these conditions, the method has been successfully applied to the determination of anthraquinones in extracts of two kinds of Rhubarb plants (*R. palmatum* and *R. hotaoense*) within 12 min. The method proposed herein was shown to be much simpler than the previously reported methods.
© 2006 Elsevier B.V. All rights reserved.

Keywords: Capillary zone electrophoresis; Ionic liquids; Ion association constants; Anthraquinones; Rhubarb

1. Introduction

Rhubarb, one of the oldest and best-known herbal medicines, has been used for thousands of years. It is officially listed in the pharmacopoeias of many countries [1,2]. Rhubarb has the effect of purgation, antibacterial, curing mental and renal disorders, antitumor and antimutagenicity [3,4]. Some related investigations show that the pharmaceutically relevant biologically active components in Rhubarb are hydroxyanthraquinoids including chrysophanol, emodin, physcion, aloe-emodin and rhein [5]. Structures of these five anthraquinons are presented in Fig. 1.

The methods commonly used for the determination of anthraquinone derivatives in Rhubarb are thin layer chromatography (TLC) [6] and high performance liquid chromatography (HPLC) [7]. Recently, various capillary electrophoresis (CE)

methods have also been proposed for the determination of these anthraquinones, such as micellar electrokinetic chromatography (MEKC) [8,9], microemulsion electrokinetic chromatography (MEEKC) [10,11], capillary electrochromatography (CEC) [12], and capillary zone electrophoresis (CZE) [13–17]. In all of these studies on CZE mode, the analysis time was too long in some literature [15]. Moreover, such approaches were particularly through the addition of modifiers to the background electrolyte (BGE) [13-17]. In contrast, the present study demonstrated that such modifiers were unnecessary, requiring only a selective interaction of anthraquinones anions with the counterion provided by the BGE, and thereby the method proposed herein was shown to be much simpler than the previously reported methods [15,16].

Room temperature ionic liquids (RTILs) are those compounds which are liquids at room temperature or whose melting points are slightly higher than ambient temperature. Generally, the ILs present a variety of desirable properties, such as conductivity, nonflammability, air and water stable, thermal stability,

* Corresponding author. Tel.: +86 931 8912763; fax: +86 931 8912582.
E-mail address: chenxg@lzu.edu.cn (X. Chen).
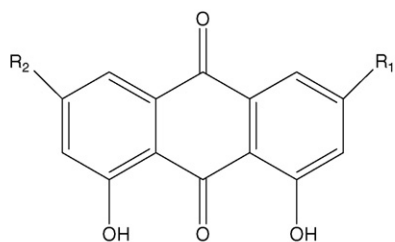
No.	Compound	R_1	R_2
1	Physcion	CH_3	OCH_3
2	Chrysophanol	CH_3	H
3	Aloe-emodin	CH_2OH	H
4	Emodin	CH_3	OH
5	Rhein	COOH	H

Fig. 1. Structures of the five anthraquinones.

and can be easily and economically prepared. Moreover, ILs are less volatile and are referred to as "green solvents". In the past several years, many scientific investigations have focused on ILs for their potential in different chemical processes [18–20], the application of ILs for the separation of various classes of compounds in CE has also been recognized [21–23]. However, to the best of our knowledge, no study on the using of ILs as BGE in CZE for the separation of these five anthraquinone derivatives has been reported until now. Apart from its high resolving power, CE has also proved to be most suitable for the study of molecular association [24–26], which is usually weak (particularly in water) and therefore difficult to study by other analytical techniques. Although several studies have reported the use of ILs as BGE in CZE, very little attention has been paid to the use of CE as a tool for studying ion association involving ILs cations and organic anions and was now a goal of the present study.

The aims of the present study were: (i) to investigate the potential of ILs as BGE in CZE for the simultaneous determination of the five anthraquinones in non-pretreated rhubarb extracts; (ii) to explore the possibility of CE for studying ion association between imidazolium cations and anthraquinone anions. It was hoped that the phenomena implied in the selectivity modification and factors contributing to ion associability could be clarified.

2. Experimental

2.1. Apparatus and procedures

A Waters Quanta 4000 capillary electrophoresis system (Milford, MA, USA), equipped with a UV detector, was used. Data were processed by a Maxima 820 chromatography workstation. The temperature was maintained at $25.0 \pm 0.5\,^\circ$C with a forced-air cooling system. A fused-silica capillary of 60.0 cm (52.5 cm effective length, 50 μm i.d. and 365 μm o.d.) was purchased from Yongnian Photoconductive Fiber Factory (Hebei, China). A hydrodynamic injection was made with a 5 s injection time

at 10 cm height difference (anodic injection) and the detection wavelength was operated at 254 nm. A PHS-10A acidity meter (Xiaoshan Science Instrumentation Factory, Zhejiang, China) was used for the pH measurement. The pH was adjusted with 0.5 M NaOH or HCl. The viscosity of the different composition of buffers was determinated by an Ostwald viscosity meter. Acetonitrile (ACN) was the marker of electroosmotic flow (EOF). The measurements were run at least in triplicate for each different composition of the running buffer to ensure repeatability. Before its first use, the capillary was washed successively with 1 M NaOH for 5 min, water for 3 min, 0.1 M NaOH for 5 min and water for 3 min. The capillary rinsed between the runs as follows: 2 min with water, 3 min with 0.1 M NaOH, 2 min with water and 5 min with BGE.

2.2. Materials

Rhubarb plants (*R. palmatum* and *R. hotaoense*) were purchased from Tongji drugstore (Lanzhou, China). Standards of anthraquinone derivatives aloe-emodin, emodin, chrysophanol, physcion and rhein were purchased from the National Institute for the Control of Pharmaceutical and Biological Products (Beijing, China). Phosphate, borate, sodium chloride, sodium hydroxide and hydrochloric acid were purchased from Tianjin Chemical Reagent Factory (Tianjin, China). The ILs 1-butyl-3-methylimidazolium tetrafluoroborate (BMIM-BF$_4$) and 1-ethyl-3-methylimidazolium tetrafluoroborate (EMIM-BF$_4$) were synthesized according to literatures [21,27]. All chemicals and solvents were of analytical regent grade and were used without further purification. Distilled water was used throughout.

2.3. Solutions and sample preparation

All analytes were dissolved separately in ACN for identification purposes and as a mixture for selectivity studies. The running buffers were prepared daily by direct addition of ILs in water to give a concentration of 200 mM and further diluted to the desired concentration with water.

A 0.04 g sample of *R. palmatum* powder (100 mesh) was immersed in 10.0 mL ethanol at room temperature for 12 h, after that, it was extracted for 20 min in an ultrasonic bath and followed by centrifugation at $1500 \times g$ for 5 min. This procedure was repeated three times, then the extracts were combined, evaporated to near-dryness on a water bath and the residue was dissolved in 1.0 mL ACN as the stock solution. A 0.04 g powder of *R. hotaoense* was extracted, respectively, using the same procedure as mentioned above. Before injection into the CE system, the solutions were appropriately diluted. All solutions were filtered through a 0.45 μm membrane filter (Shanghai Xinya Purification Apparatus Factory, Shanghai, China) prior to use.

2.4. Calculations

The resolution R_s was calculated by

$$R_s = \frac{2(t_2 - t_1)}{W_1 + W_2} \tag{1}$$

where t_1 and t_2 are the respective migration times of each analyte; W_1 and W_2 are the peak widths at the baseline. The mobility of the analyte was calculated from the observed migration times with the equation:

$$\mu_{\text{eff}} = \frac{Ll}{V}\left(\frac{1}{t_{\text{m}}} - \frac{1}{t_{\text{eo}}}\right) \qquad (2)$$

where μ_{eff} is the electrophoretic mobility of the analyte tested, t_{m} and t_{eo} are the measured migration times of the analyte and EOF marker (ACN) measured directly from the electropherogram, respectively. L is the total length of capillary, l is the length of capillary between injection and detection, and V is the applied voltage.

3. Results and discussion

3.1. Separation of anthraquinones derivatives using BMIM-BF₄ or EMIM-BF₄ as BGE

In previous studies, it has proved that complete separation of the studied anthraquinones could not be achieved by ordinary CZE without modifiers addition due to the little differences in pK_a values between chrysophanol and aloe-emodin [15,16]. In the work of Wilkes and Zaworotko, they concluded that 1-ethyl-3-methylimidazolium was a general useful cation [28]. In our laboratory, Qi et al. reported the determination of four anthraquinones in Chinese herb *Paedicalyx attopevensis Pierre ex Pitard* by CZE using BMIM-BF₄ with β-cyclodextrin as modifier [29]. On the basis of these preliminary results, our attention was focused on the use of 1-alkyl-3-methylimidazolium-based ILs as BGE in CZE for the separation of anthraquinones in Rhubarb. It was expected that hydrophobic imidazolium cations could interact with hydrophobic anthraquinone anions to improve the separation. The miscibility of 1-alkyl-3-methylimidazolium-based ILs in water, to a great extent, was dictated by the inorganic anion and alkyl chain lengths, the tetrafluoroborate anion and the salt with short alkyl chain lengths ($n < 6$) were shown to provide high miscibility of ILs in water [30,31]. Therefore, the ILs BMIM-BF₄ and EMIM-BF₄ were chosen in this experiment.

With the aim of evaluating the effect of ILs concentration on the separation, a series of buffers (pH 11.0) containing only ILs, ranging from 30 to 105 mM, were investigated. It was found that the proposed method provided a different separation profile compared to that obtained by ordinary CZE using borate or phosphate buffers. The two analytes chrysophanol and aloe-emodin, which were difficult to separate by ordinary CZE, could be well separated by using ILs as BGE. Fig. 2 shows the effect of ILs concentration on the resolution of chrysophanol and aloe-emodin. It clearly illustrated that the resolution increased dramatically with increasing ILs concentration, especially in the range 30–60 mM for BMIM-BF₄ and 45–75 mM for EMIM-BF₄. Complete separation of these two analytes was achieved with the addition of 60 mM BMIM-BF₄. It also can be seen that the resolution observed using BMIM-BF₄ was higher than that obtained using equal concentration of EMIM-BF₄. In terms of the separation, it
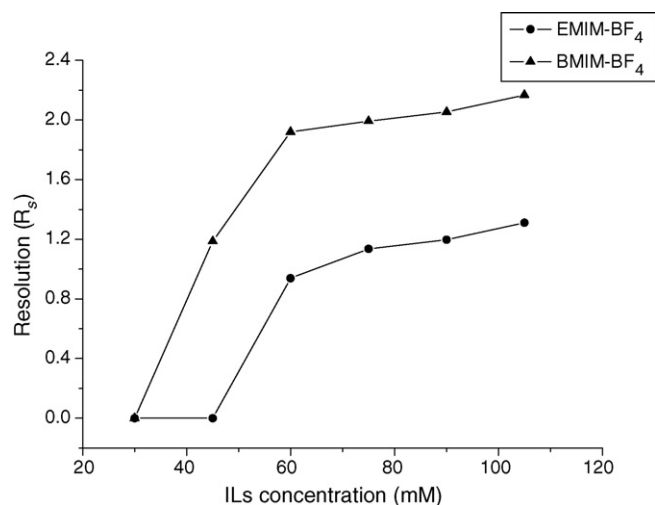

Fig. 2. Effect of ILs concentration on the resolution of chrysophanol and aloe-emodin. Conditions: 30–105 mM EMIM-BF₄ or BMIM-BF₄ at pH 11.0; uncoated fused-silica capillary, total length 60.0 cm (52.5 cm effective length) × 50 μm i.d.; applied voltage, 20 kV; temperature, 25.0 ± 0.5 °C; detection, 254 nm.

was apparent that BMIM-BF₄ provided better resolution. Therefore, 90 mM BMIM-BF₄ was selected in the subsequent work.

The mobilities of five anthraquinones were found to increase with increasing amounts of ILs added to the separation buffers. This was explained by ion association between imidazolium cations and anthraquinone anions. In this experiment, all separations were performed under conditions in which only the negatively charged forms of the analytes were present and migrated opposite to the direction of EOF. The pK_a values of these anthraquinones are shown in Table 1 [32]. After formation of the associated complexes with imidazolium cations, the charges on these negatively charged anthraquinones were decreased. This effect was expected to accelerate the migration of negatively charged anthraquinones to the detector, resulting in increased mobilities.

3.2. Selection of other conditions for optimization

The pH of the BGE plays an important role in the separation of ionizable analytes because it determines the ionization extent of each analyte. In this study, alkaline conditions were found to favor the separation due to the phenolic (and acidic) nature of these anthraquinones. Therefore, separations were performed with pH ranging from 9.5 to 11.5 and 90 mM BMIM-BF₄. Other

Table 1
The values of pK_a and hydrophobic parameter ($\log P_{\text{ow}}$) of the studied anthraquinones

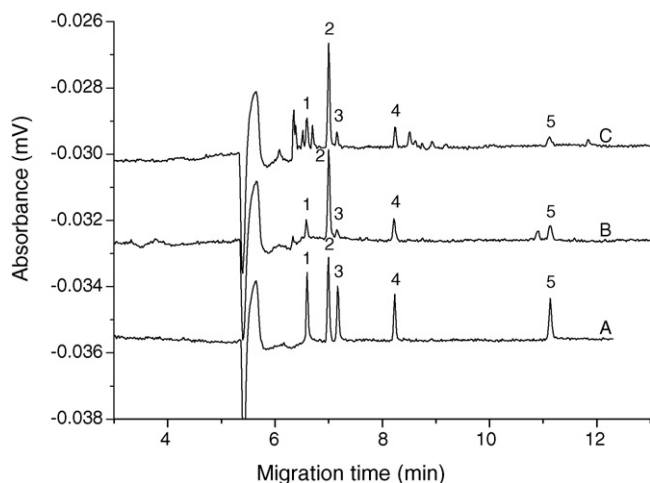|	Compound				
	1	2	3	4	5
pK_a[a]	8.49	8.51	8.49	5.70, 7.94	4.51, 8.41
Log P_{ow}[b]	3.85	3.63	2.68	2.91	2.42

[a] Ref. [32].
[b] Ref. [8].

Fig. 3. The typical electropherograms of the standard mixture and the real samples under the optimum conditions. (A) The standard mixture; (B) *R. hotaoense*; (C) *R. palmatum*; the concentrations of the standards were $50\,\mu g\,mL^{-1}$ for chrysophanol, physcion, emodin and aloe-emodin, $40\,\mu g\,mL^{-1}$ for rhein, respectively. Conditions: 90 mM BMIM-BF$_4$ at pH 11.0. The peaks were numbered according to the analytes number in Fig. 1. Other conditions are as in Fig. 2.

conditions were the same as in Fig. 2. It was found that the analytes chrysophanol and aloe-emodin were comigrated or poorly separated when the pH was lower than 10.0. With the increase of pH above 10.0, the resolution between chrysophanol and aloe-emodin increased for pH up to 11.0, and then decreased. At pH 11.0, the five anthraquinones could be well separated within a relatively short time and thus it was chosen as the optimum.

The high voltage was necessary for rapid CE analysis. Within the applied voltage ranging from 15 to 30 kV, it was found that higher separation voltages were not beneficial to the resolution of the real samples. However, lower separation voltages would increase the analysis time considerably. Based on experiments, 20 kV was selected to accomplish a good compromise.

From the above results, the optimum conditions were obtained as follows: 90 mM BMIM-BF$_4$ (pH 11.0) with an applied voltage of 20 kV. Under these conditions, all the five anthraquinones were well separated in less than 12 min with symmetrical peaks. Fig. 3A demonstrates the typical electropherogram for a standard mixture of the five anthraquinones.

3.3. Determination of ion association constants

To clarify the mobility change in the presence of imidazolium cations, ion association constants between imidazolium cations and anthraquinone anions were examined. Since the ion asso-

ciate was not so stable, only 1:1 ion association was assumed to take place. An imidazolium cation, C^+ and an anthraquinone anion, A^{m-} can form an ion associate according to the following equilibrium [24]:

$$C^+ + A^{m-} \; K_{ass} \; CA^{(m-1)-} \tag{3}$$

The corresponding ion association constant, K_{ass}, was obtained by:

$$K_{ass} = \frac{[CA^{(m-1)-}]}{[C^+][A^{m-}]} \tag{4}$$

where $[CA^{(m-1)-}]$ represented the concentration of the association complex between anthraquinone anions and imidazolium cations. $[C^+]$ and $[A^{m-}]$ were the equilibrium concentration of imidazolium cations and anthraquinone anions, respectively. Because in this case the imidazolium cations were present in excess over the anthraquinone anions, the equilibrium concentration $[C^+]$ can be considered as equal to the total concentration of the ILs. Under fast exchange conditions, the electrophoretic mobility of a certain anthraquinone anion, μ_{eff} was a weighted average of the mobilities of its free and complexed forms (μ_A and μ_{CA}, respectively) [24–27], which can be represented as follows:

$$\mu_{eff} = \frac{[A^{m-}]\mu_A + [CA^{(m-1)-}]\mu_{CA}}{[A^{m-}] + [CA^{(m-1)-}]} \tag{5}$$

where μ_A and μ_{CA} were the mobility of the analyte anions and that of the 1:1 ion associate, respectively. Combining Eqs. (4) and (5) show that mobility was related to the association constants through the general binding isotherm relationship [24–27], which can be expressed as

$$\mu_{eff} = \frac{\mu_A + K_{ass}[C^+]\mu_{CA}}{1 + K_{ass}[C^+]} \tag{6}$$

In this study, the ion association constants of K_{ass} was determined by using buffers containing 10 mM disodium hydrogen phosphate (pH 11.0) and 0–90 mM BMIM-BF$_4$ or EMIM-BF$_4$. Other conditions were the same as in Fig. 2. In previous studies, it has been reported that the mobility of species was affected by buffer concentration (ionic strength) and viscosity when high concentration of additives were added during the association process [33,34]. In order to eliminate these influences, sodium chloride was used as electrolyte for adjusting the ionic strength (at a constant of 0.12 M) of the BGE on account of sodium ions reported low ability to associate with most of the anions [35,36]. In this experiment, it was found that the viscosity changes due to the addition of ILs were small and could be neglected. The

Table 2
Ion association constants (M^{-1}) obtained by the non-linear least-squares method (at 25.0 °C)

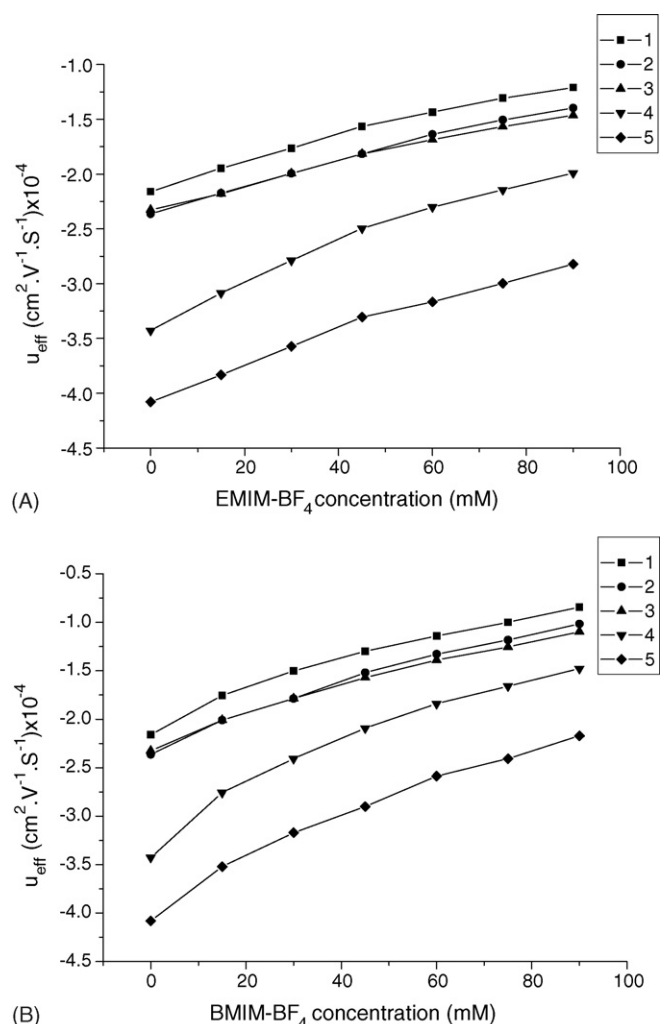|	Compounds				
	1	2	3	4	5
EMIM-BF$_4$	5.7 ± 0.8 (0.9990)[a]	3.1 ± 0.7 (0.9990)	2.6 ± 0.8 (0.9987)	7.5 ± 0.9 (0.9990)	4.5 ± 1.1 (0.9980)
BMIM-BF$_4$	11.9 ± 1.4 (0.9982)	7.2 ± 0.9 (0.9987)	6.2 ± 0.5 (0.9959)	15.2 ± 1.4 (0.9985)	9.5 ± 1.3 (0.9979)

[a] Error 1.96σ.

Fig. 4. Effect of ILs concentration on the effective mobility of anthraquinone derivatives with the ionic strength correction. (A) EMIM-BF$_4$; (B) BMIM-BF$_4$. The number of each curve was corresponding to the analytes number in Fig. 1. Other conditions are as in Fig. 2.

ion association constants were next determined from the anion mobility μ_{eff} as a function of $[C^+]$ by a non-linear least-squares method. The mobility of anthraquinone anions with increasing concentration of ILs in the BGE is shown in Fig. 4A and B. The K_{ass} values obtained are summarized in Table 2.

The association constants (K_{ass}) derived from this method provided fundamental information on the interaction between

the anthraquinone anions and the imidazolium cations. In this study, all the experiments were performed at pH 11.0. Under such high alkaline condition, the anthraquinones were completely ionized, which eliminated alternative explanations for our results due to variability in dissociation constants of anthraquinones. In previous papers, ion associability was discussed from the viewpoint of the hydrophobicity of pairing ions [26,37]. In the ion associability examined in this work, the ion associability also appeared to be correlated to the hydrophobicity and/or polarizability of the pairing cations and anions. As can be seen from Table 2, the ion associability order was found to be physcion > chrysophanol > aloe-emodin, emodin > rhein for both kinds of ILs. Accordingly, it was the order of the decreasing hydrophobicity of analytes introduced by different substituent group(s) in the R position(s) of aromatic ring. The values of hydrophobic parameter, log P_{ow} are shown in Table 1. Moreover, the results in Table 2 showed that the K_{ass} values were higher for the butylimidazolium cations than for the ethyl analogue, such observations further supported the view that a hydrophobicity mechanism located in the BGE was operating in both cases. Interestingly, K_{ass} values consistently showed that emodin and rhein interacted extensively with the imidazolium cations, despite these two compounds were relatively less hydrophobic compared to other three analytes. Hence the hydrophobicity concept could not be applied simply to the ion associability. In view of the structures of the anthraquinones, it was found that these two analytes possessed higher charges (trivalence) than the other three analytes (bivalence) and therefore possessed higher charge density. Certainly, the negatively charged anions were able to interact electrostatically with the positively charged cations, which meant that the high ion associability was considered by means of increased electrostatic interactions. From the above discussion, we may conclude that the separation of anthraquinones was achieved by differing affinities or association interactions of anthraquinones for the imidazolium cations. In Fig. 2, the higher R_s observed with BMIM-BF$_4$ compared to that obtained with equal concentrations of EMIM-BF$_4$ may be attributable to the fact the interactions of anthraquinones with BMIM-BF$_4$ were stronger than those with EMIM-BF$_4$.

3.4. Method validation

Under the optimum conditions, a series of standard mixture solutions of these five analytes were tested to determine the lin-

Table 3
The results of regression analysis on calibration curves and the detection limits

Compound	Calibration curve $(y = a + bx)^{a,b}$		Correlation coefficient	Linear range (µg mL^{-1})	Detection limit (µg mL^{-1})^c
	a	b			
1	242.1 ± 161.5	89.4 ± 1.7	0.9993	2.8–90	0.46
2	368.7 ± 154.4	123.5 ± 1.6	0.9997	1.4–90	0.33
3	409.8 ± 143.3	78.5 ± 1.5	0.9993	1.9–120	0.53
4	157.2 ± 108.7	66.6 ± 1.2	0.9994	4.2–135	0.62
5	287.4 ± 221.8	118.7 ± 2.4	0.9992	1.9–120	0.35

[a] y and x stand for the peak area and the concentration (µg mL^{-1}) of the analytes, respectively.

[b] Error 1.96σ.

[c] The detection limits (LOD) corresponding to concentrations giving signal-to-noise ratio of 3.

Table 4
Recoveries of five anthraquinones in sample analysis ($n = 4$)

Sample	Component	Amount ($\mu g\,mL^{-1}$)			Recovery (%)	R.S.D. (%)
		Original	Added	Found		
R. hotaoens	1	12.84	9.00	22.16	104	3.4
	2	58.20	9.00	67.46	103	2.7
	3	2.72	12.00	14.78	101	1.2
	4	25.31	13.50	38.59	98.4	2.9
	5	8.96	12.00	20.79	98.6	3.3
R. palmatum	1	24.46	9.00	33.96	106	5.2
	2	64.47	9.00	73.87	104	3.7
	3	5.66	12.00	17.91	102	2.6
	4	22.80	13.50	37.02	105	4.7
	5	5.24	12.00	17.89	105	4.9

The conditions are the same as in Fig. 3.

Table 5
Contents of the five anthraquinones in real samples and R.S.D.s ($n = 5$)

	Samples				
	1	2	3	4	5
R. hotaoens[a]	0.16 (1.04)[b]	0.73 (1.52)	0.034 (1.25)	0.32 (1.43)	0.11 (1.58)
R. palmatum	0.31 (1.19)	0.81 (1.21)	0.071 (1.47)	0.29 (2.27)	0.066 (1.71)

[a] % of dry mass.
[b] The data in parentheses refer to the R.S.D.

earity between the analyte concentration and the corresponding peak areas [38]. The results of regression analysis on calibration curves and the detection limits are summarized in Table 3. The correlation coefficients calculated were between 0.9992 and 0.9997 over the concentration range (2.8–90 $\mu g\,mL^{-1}$ for 1, 1.4–90 $\mu g\,mL^{-1}$ for 2, 1.9–120 $\mu g\,mL^{-1}$ for 3, 4.2–135 $\mu g\,mL^{-1}$ for 4, 1.9–120 $\mu g\,mL^{-1}$ for 5). The limits of detection (S/N = 3) were below 0.7 $\mu g\,mL^{-1}$. These results were similar to those obtained in previous studies [15,16] and were lower than those obtained in Ref. [17].

The precision of CE depends on the repeatability of migration times and peak areas. The repeatability of the method was determined by repeated ($n = 6$) injection of the standard mixture solutions at the concentration levels of 25, 50, 75 $\mu g\,mL^{-1}$ for all analytes. The R.S.D.s of the migration times and peak areas were 0.43–0.79, 0.98–1.87% (intra-day, $n = 6$), and 0.74–1.53, 1.18–2.39% (inter-day, $n = 5$), respectively.

Ensure accuracy of the method, the recoveries of the method were determined by standard addition method, and the results are listed in Table 4. It was shown that the recoveries of the five anthraquinones were ranged from 98.4 to 106%.

3.5. Application

Two kinds of Rhubarb plants, R. palmatum and R. hotaoen were assayed by the proposed method. The typical electropherograms are shown in Fig. 3B and C. Peaks were identified by spiking five anthraquinones individually into the sample solutions. The contents of the five anthraquinones together with R.S.D.s ($n = 5$) are listed in Table 5. Just as our previ-

ous study [16], the contents of anthraquinones were different in two kinds of Rhubarb plants, which proved that the contents of anthraquinone derivatives were related to the species to a great extent. It was instructive for the selection of medicinal plants in clinic treatment. The contents of anthraquinones in the extracts determined by this method were in good agreement with those obtained by our previous study except the content of emodin in R. palmatum [16]. The reason for this was most probably the different collection time and cultivation region.

4. Conclusions

The effective separation of five anthraquinone derivatives in Rhubarb species was achieved by CZE using only ILs as BGE. The ion association reaction between anthraquinone anions and imidazolium cations were studied. From the ion association constants obtained, factors contributing to ion associability were systematically clarified. The technique proposed in this paper offered merits of simplicity, rapidity and high selectivity. It provided a complementary method to CZE for the quality control of Rhubarb. This study also highlighted that ion association reaction was one of the most promising methods for improving the separability of various analyte ions that have very similar or identical migration behavior in CZE.

Acknowledgement

References

[1] Stationary Office, Department of Health, 17th ed., British Pharmacopoeia, London, 1999, p. 1251.

[2] European Department for the Quality of Medicines, Council of Europe, 3rd ed., European Pharmacopoeia, Strasbourg, 1997, p. 1441.

[3] W. Tang, G. Eisenbrand, Chinese Drugs of Plant Origin, Springer, Berlin, Heidelberg, 1992, p. 855.

[4] C.A. Newall, L.A. Anderson, J.D. Phillipson, Herbal Medicines, The Pharmaceutical Press, London, 1996, p. 228.

[5] P.G. Xiao, L.Y. He, L.W. Wang, J. Ethnopharmacol. 10 (1984) 275.

[6] S. Nyiredy, T. Dallenbach, G.C. Zogg, O. Sticher, J. Chromatogr. 499 (1990) 453.

[7] D. Djozan, Y. Assadi, Talanta 42 (1995) 861.

[8] X.Y. Shang, Z.B. Yuan, Bioorg. Med. Chem. Lett. 13 (2003) 617.

[9] C.H. Kuo, S.W. Sun, Anal. Chim. Acta 482 (2003) 47.

[10] S.W. Sun, P.C. Yeh, J. Pharm. Biomed. Anal. 36 (2005) 995.

[11] G.B. Li, X.G. Chen, M.C. Liu, Z.D. Hu, Analyst 123 (1998) 1501.

[12] Y. Li, H. Liu, X. Ji, J. Li, Electrophoresis 21 (2000) 3109.

[13] W.C. Weng, S.J. Sheu, J. High Resolut. Chromatogr. 23 (2000) 143.

[14] Y.F. Chai, S.G. Ji, Y.T. Wu, D.S. Liang, Z.M. Xu, Biomed. Chromatogr. 12 (1998) 193.

[15] Y.X. Gong, S.P. Li, Y.T. Wang, P. Li, F.Q. Yang, Electrophoresis 26 (2005) 1778.

[16] K. Tian, H.G. Zhang, X.G. Chen, Z.D. Hu, J. Chromatogr. A 1123 (2006) 134.

[17] L.H. Liu, L.Y. Fan, H.L. Chen, X.G. Chen, Z.D. Hu, Electrophoresis 26 (2005) 2999.

[18] H. Heitzman, B.A. Young, D.J. Rausch, P. Rickert, D.C. Stepinski, M.L. Dietz, Talanta 69 (2006) 527.

[19] J.-F. Liu, J.-F. Peng, Y.-G. Ch, G.-B. Jiang, Talanta 65 (2005) 705.

[20] N. Hirayama, M. Deguchi, H. Kawasumi, T. Honjo, Talanta 65 (2005) 255.

[21] E.G. Yanes, S.R. Gratz, M.J. Baldwin, S.E. Robison, A.M. Stalcup, Anal. Chem. 73 (2001) 3838.

[22] W.D. Qin, H.P. Wei, S.F.Y. Li, J. Chromatogr. A 985 (2003) 447.

[23] M. Vaher, M. Koel, M. Kaljurand, Electrophoresis 23 (2002) 426.

[24] T. Takayanagi, E. Wada, S. Motomizu, Analyst 122 (1997) 1387.

[25] B.W. Rasmussen, M.J. Bjerrum, J. Chromatogr. A 836 (1999) 93.

[26] E. Wada, T. Takayanagi, S. Motomizu, Analyst 123 (1998) 493.

[27] P. Bonhǒte, A.-P. Dias, N. Papageorgiou, K. Kalyanasundaram, M. Grätzel, Inorg. Chem. 35 (1996) 1168.

[28] J.S. Wilkes, M.J. Zaworotko, J. Chem. Soc., Chem. Commun. (1992) 965.

[29] S.D. Qi, S.Y. Cui, X.G. Chen, Z.D. Hu, J. Chromatogr. A 1059 (2004) 191.

[30] J.G. Huddleston, A.E. Visser, W.M. Reichert, H.D. Willauer, G.A. Broker, R.D. Rogers, Green Chem. 3 (2001) 156.

[31] J.D. Holbrey, K.R. Seddon, J. Chem. Soc., Dalton Trans. (1999) 2133.

[32] D.X. Wang, G.L. Yang, X.R. Song, Electrophoresis 22 (2001) 464.

[33] B. Henry, J. High Resolut. Chromatogr. 22 (1999) 595.

[34] M.T. Bowser, D.D.Y. Chen, Anal. Chem. 70 (1998) 3261.

[35] S. Motomizu, T. Takayanagi, J. Chromatogr. A 853 (1999) 63.

[36] E. Hogfeldt, Stability Constants of Metal–Ion Complexes (Part A), Pergamon Press, Oxford, 1982, p. 187.

[37] T. Takayanagi, E. Wada, S. Motomizu, Analyst 122 (1997) 57.

[38] L.A. Currie, Talanta 391 (1999) 105.

Axial temperature gradient and mobile phase gradient in microcolumn high-performance liquid chromatography

Hongzhe Tian, Jing Xu, Yafeng Guan *

Department of Instrumentation & Analytical Chemistry, Dalian Institute of Chemical Physics, Chinese Academy of Sciences, 457 Zhongshan Road, Dalian 116023, China

Abstract

The effect of axial temperature gradient (ATG) along a microcolumn on the separation performance at both isocratic and gradient elution mode was investigated. A thermostat system was designed to form an ATG along the packed column. Polycyclic aromatic hydrocarbons (PAHs) were separated on a 0.53 mm × 150 mm i.d. 5 μm C_{18} microcolumn, with water and acetonitrile as mobile phase. The separation results obtained at mobile phase gradient (MPG) and ATG in microcolumn HPLC were compared with the results performed at ambient conditions. Extrapolated curves of peak width at half height (w_h) *versus* ln$k$ showed that w_h is narrower at the same retention time when ATG was applied in addition to MPG. The column efficiency was enhanced 20–30% and the resolution was slightly reduced because of reduction of selectivity at elevated temperature at ATG condition. The RSD of retention time in ATG mode was less than 2.5%.
© 2006 Elsevier B.V. All rights reserved.

Keywords: Axial temperature gradient; High temperature liquid chromatography; Micro-HPLC; Polycyclic aromatic hydrocarbons

1. Introduction

Historically, the effect of temperature on retention was first reported half a century ago [1]. From then on, more researchers investigated the effect of temperature on retention factors, peaks symmetry, and separation efficiency in liquid chromatography [2,3].

Recently, more attention was focused on the high-speed chromatographic separation at elevated temperature [4]. Carr and coworkers [5] studied the theoretical benefits of temperature on speed in liquid chromatography. Their work showed that the elution speed of LC could be improved at elevated temperature.

In reversed phase HPLC, an increase of column temperature leads to either a decrease in retention (negative temperature dependence) [6] or an increase in solute-stationary phase interaction with temperature (positive temperature dependence) [7–9] according to the difference of analytes and stationary phase.

Nearly all of the physical parameters that play a role in LC separation are a function of temperature. It is, therefore, very complicated to optimize the operational temperature.

Optimization of mobile phase composition [10,11] is a common approach for optimization of separation in HPLC. Temperature plays a relatively minor role on retention and selectivity in LC than in GC. Furthermore, it is easier to manipulate the mobile phase composition (solvent strength programming) than to adjust oven temperature with conventional size LC columns.

For capillary column HPLC, solvent gradient suffers from great technical difficulties such as precise low flow rate control (microlitre or nanolitre per minute), stability of micropump, and slow column equilibration. In microcolumn and capillary column liquid chromatography, it is not essential to preheat the mobile phase since the radial temperature gradient inside the packed bed is very small because of their low heat capacities and small radius of the columns compared to conventional columns. The small volumes of both mobile and stationary phases in these columns facilitate rapid heating and cooling across the narrow column bed without creating large radial temperature profiles [12]. Therefore, it is more convenient to manipulate the column temperature in capillary column LC than in conventional column LC.

* Corresponding author. Tel.: +86 411 84379590; fax: +86 411 84379570.
E-mail addresses: kfguan@mail.dlptt.ln.cn,
guan_yafeng@yahoo.com.cn (Y. Guan).

The first attempt to study the effects of temperature on narrow-bore columns was performed in 1981 by Ishii and co-workers [13]. Later, McNair and Bowermaster [14] evaluated the potential of temperature programming in conjunction with microbore column LC and concluded that it produced faster analysis and increased efficiency. Sheng et al. [15] also investigated the separation efficiency of capillary column LC at different column temperatures and found that temperature could have a better or worse effect on selectivity, depending on the retention factors, enthalpies, and entropies of the compounds analyzed. Houdiere et al. [16] assessed the combination of temperature and flow gradient in microcolumn and capillary column liquid chromatography separation. They found that simultaneous temperature and flow rate programming is a promising means of reducing the total analysis time.

The application of an axial temperature gradient, which combined flow and temperature programming, has been previously reported [17]. In their work the axial temperature gradient was generated by pre-heating the mobile phase higher than the average column temperature, and the report claimed good separation efficiency with reduced analysis time.

Instead of temperature programming [14], this paper reports a study on ATG along the column in RPLC. The effect on chromatographic bandwidth, column efficiency and resolution by the ATG were investigated. The instrumentation set-up and the results of comparative study are also described.

2. Experimental

2.1. Instrumentation

An Ultra-Plus II model liquid chromatograph, consisting of quaternary pumps, a pump controller, two mixers, a 10-port valve and a six-port valve, was from Micro-Tech Scientific (Vista, CA, USA). The chromatograph is equipped with a UVIS 200 detector (Linear, CA, USA).

A homemade column thermostat is illustrated in Fig. 1. A stainless steel union (Valco) on head of the column is placed inside a hole in the center of the heating block (made from aluminum). The inner diameter of the hole is identical as the outside diameter of the union to have a good thermal conductance. A copper tube of 3 mm o.d. and 2 mm i.d. is fixed between the heating block and another aluminum block, which is kept at room

temperature by a fan. The separation column is placed inside the copper tube. The outside wall of the copper tube is covered with a thermal insulating material to maintain the temperature gradient along the copper tube. A negative temperature gradient was generated along the copper tube. Thin film miniature Pt resistors (Juchheim, GmbH, Germany) were used to measure the temperatures of the heating block, copper tube at different locations and cooling block. Fused-silica capillary tubing of 50 μm i.d. is used as connection tubing of the packed column to injection valve and detector, respectively.

Chrom Perfect for Windows software, from Justice Innovations (Mountain View, CA, USA), was used for data acquisition and processing. Temperature was controlled and monitored by a Model REX-C100 controller (RKC Instrument Inc., Japan).

2.2. Reagents

All solvents are of HPLC grade from Fluka (Buchs, Switzerland). The test compounds are analytical grade and obtained from the domestic company. The primary standards are dissolved in acetonitrile. Working standards are diluted with the mobile phase from the primary standard solutions and are filtered with a syringe filter before analysis.

2.3. Column condition

A microcolumn of 150 mm × 0.53 mm i.d. packed with 5 μm, 100 Å C_{18} (Varian, USA) was prepared in the laboratory according to a procedure described by Guan et al. [18]. The inlet of column was connected to a stainless steel union (Valco) using polyetheretherketone (PEEK) sleeve and a stainless steel ferrule. The inner diameter of the PEEK sleeve was drilled to match closely the outer diameter of the column i.e., 700 μm. A (1/16) in. porous TFL filter was placed in the connecting union for holding the stationary phase in the column. A 150 mm × 25 μm i.d. bare fused-silica capillary was attached to the end of the detector cell to generate backpressure to prevent bubble formation.

All experiments were carried out at injection volume of 0.24 μL, column flow rate of 6 μL/min and detection wavelength of 254 nm. Mobile phase was 30/70 (v/v) water/acetonitrile for isocratic experiments, and was water and acetonitrile for gradient elution. The composition of mobile phase was changed from 70% to 80% (v/v) within 20 min. Uracil was used as dead time marker. The resolution (R_S) is estimated on the basis of the equation for R_S in a literature [19].

3. Results and discussion

Previous report [20] on ATG was concerned with the temperature difference between the entrance of the column and the column outlet originating from cold mobile phase entering the heated column. The ATG along the column was increasing (positive temperature gradient) towards the outlet of the column in their experiment.

In our study, the radial temperature gradient inside the separation column was negligible due to the fast heat equilibrium
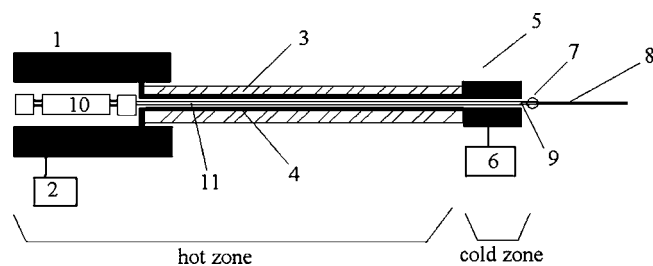

Fig. 1. Schematic illustration of the concept and device for ATG along a column. (1) heating block; (2) temperature controller; (3) heat insulating material; (4) copper tube; (5) aluminum block; (6) fan; (7) epoxy adhesive; (8) fused silica capillary for connecting; (9) frit; (10) stainless steel union; (11) packed microcolumn.
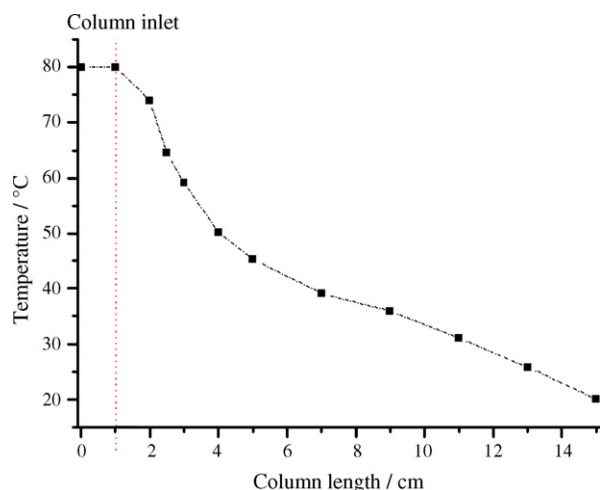
Fig. 2. The temperature gradient profile as a function of column length using the ATG device.

Table 1
The comparison of the peak symmetry under different separation conditions

Peak no.	Peak symmetry (at 10%)			
	A-I	A-G	H-I	H-G
1	1.06	1.10	1.14	1.17
2	1.13	1.12	1.16	1.12
3	1.56	1.74	1.70	1.70
4	1.10	1.12	1.07	1.12
5	1.12	1.03	1.11	1.07

and low heat capacity of microcolumn. The study focused on the ATG along the packed column that was generated deliberately by using the device shown in Fig. 1. The temperature of the column inlet was the same as the set temperature of the heating block (T_i), while the temperature of the column outlet was the same as room temperature ($T_0 = 20\,°C$). The system was stabilized to reach thermal equilibrium within 15 min. At equilibrium, the temperature at certain point of the column is constant with time ($dT/dt = 0$, $dT/dL < 0$).

In our experiment, the temperature of the heating block was set at $T_i = 80\,°C$ considering the temperature limit of the column. Fig. 2 showed the temperature profile along the copper tube that surrounded the separation column. Although only the head of the column was heated, the heat transfer along the copper tube is sufficient to form a temperature gradient that is not too sharp since the heat loss due to the convective heat transfer from the tube to ambient air is reduced by using thermal insulating material outside the copper tube. The negative ATG along the column can reduce the chromatographic band broadening (see Fig. 3).

The mass transfer rates of compounds and the viscosity of mobile phase along the column are different at given location. While the temperature and mass transfer rates in isothermal column are constant along the axial direction of a column ($dT/dt = 0$,

$dT/dL = 0$). Therefore, the column efficiency and selectivity at ATG condition should be different from that at isothermal condition.

The effects of negative ATG along the column on retention factor, column efficiency, resolution and peak symmetry were investigated. The results were described and discussed below.

3.1. The effect of ATG on peak symmetry and column efficiency

Previous study showed that the positive ATG along column at elevated temperature had detrimental effect on the peak shape [20]. Table 1 illustrated the separation results about peak symmetry at different separation condition, including ambient–isocratic elution (A-I), ambient–MPG elution (A-G), ATG–isocratic elution (H-I), ATG–MPG elution (H-G). The peak symmetry under different separation conditions was between 1.0 and 1.5 except peak 3. The results indicated that the ATG along the column had little adverse effect on the peak shape.

Figs. 4a–c showed the separation of PAHs mixture utilizing a microcolumn under A-I, H-I and A-G, respectively. Complete separation of the test mixtures was achieved at isocratic (ACN/H$_2$O, 70:30, v/v) and isothermal (20 °C) condition. When the column inlet temperature was increased to 80 °C to form a negative ATG on the column while keeping other operation parameters constant (Fig. 4b), the analysis time was reduced from 22 min down to less than 19 min with a little decrease in resolution. The MPG elution reduced the analysis time but sacrificed resolution (Fig. 4c), between anthracene and phenanthrene peaks, in particular. The increase of the organic content in mobile phase will reduce the selectivity for structural isomers that have the same molecular volume and similar hydrophobicity. Gradient elution will reduce the resolution of homologue as compared with isocratic elution when higher content of organic solvent is used in mobile phase. For ATG and isocratic elution, there was only slightly decrease on resolution (refer to Table 2). The results showed that the loss of resolution at ATG was less than that of gradient elution.

3.2. The effect of ATG on retention factors

Retention time was responsive to temperature change in chromatographic separation. Since the chromatographic process was under ATG rather than isothermal condition, we used apparent retention factor to evaluate the effect of ATG
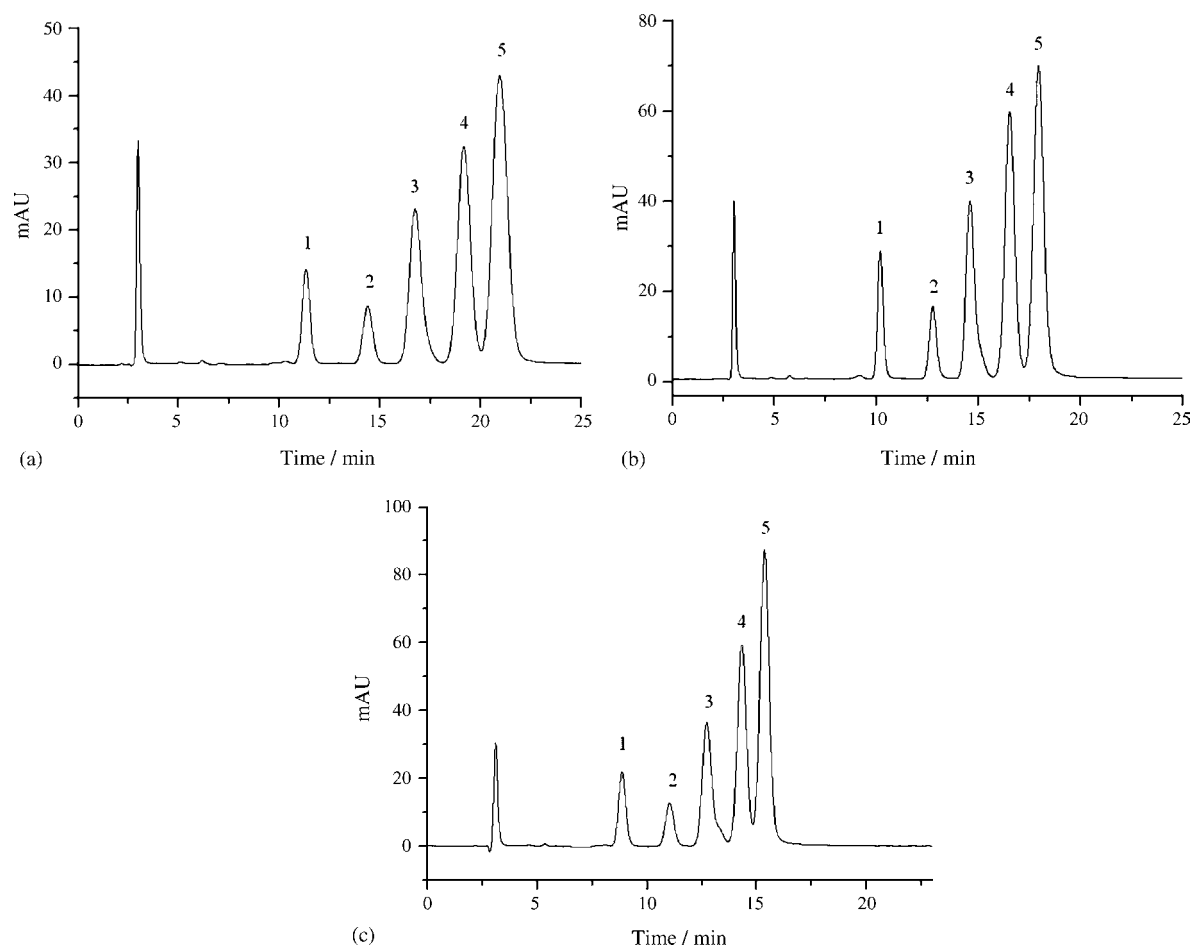

Fig. 3. Schematic description of the distribution of axial temperature and mass transfer rates along the separation column at ATG condition.

Fig. 4. The chromatograms of five PAHs at different separation conditions. 1-Naphthalene, 20.5 µg/mL; 2-biphenyl, 15.1 µg/mL; 3-fluorene, 22.3 µg/mL; 4-phenanthrene, 4.8 µg/mL; 5-anthracene, 4.5 µg/mL. (a) Isocratic elution at ambient; (b) isocratic elution at ATG; (c) gradient elution at ambient.

on chromatographic retention. Fig. 5 depicted retention factors of five PAHs at different separation conditions. The results illustrated that the retention factors of the compounds decreased as the temperature of column raised or under gradient elution.

The integrated effect of both MPG and negative ATG at inlet temperature of 80 °C (H-G) on retention factors was also studied, and demonstrated in Fig. 5. Inspection of the results indicated that there was a relative large change in k of the all solutes between A-I and H-G (the difference is 1.03–2.43) while a relative small change in k of the all solutes was observed between A-G and H-G (the difference is 0.25–0.5). Gradient elution had a more pronounced effect on retention factors of PAHs than temperature.

3.3. The effect of ATG on peak width

ATG plays a role in tuning selectivity by changing the separation temperature of the solutes on the eluting direction along the whole column length. High temperature operation increases the diffusion rate of both solutes and mobile phase, and improves

Table 2
The comparison of the peak resolution under different separation conditions

Separation mode	Peak resolution			
	1–2	2–3	3–4	4–5
A-I	4.65	2.61	2.33	1.56
A-G	3.53	2.29	2.02	1.32
H-I	4.40	2.47	2.28	1.50
H-G	3.50	2.33	2.12	1.34
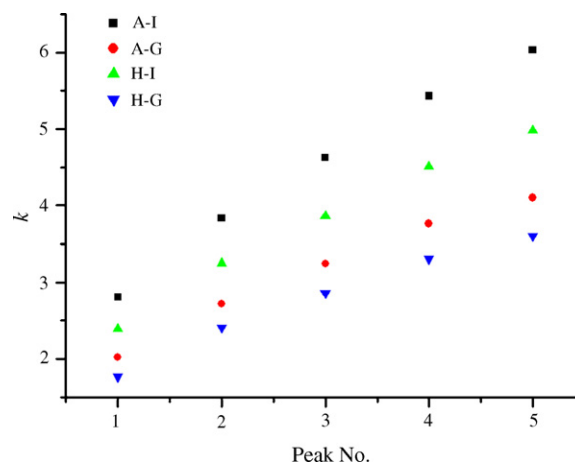
Fig. 5. The comparison of retention factors under different temperature and eluting conditions.
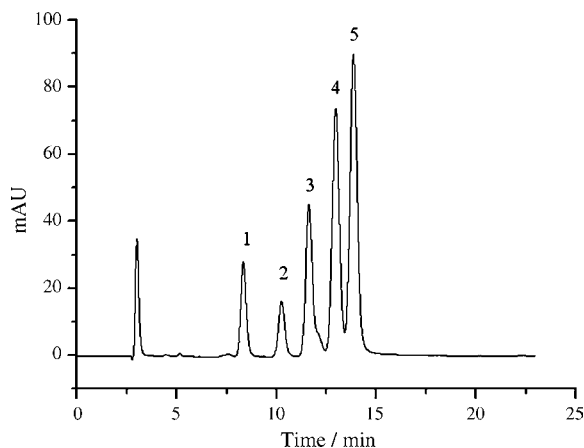
Fig. 6. The chromatogram of separation of five PAHs at ATG mode and MPG elution. The peaks were the same as in Fig. 4.

column efficiency to certain extent. Fig. 6 showed the separation of a mixture of PAHs using simultaneous ATG and MPG. The integrated effect produced more than a 30–45% reduction in w_h as compared with that of isocratic run at room temperature. w_h *versus* $\ln k$ at different separation conditions was shown in Fig. 7. The slope of each plot was given by the Eq (1):

$$\text{slope} = \frac{\partial w_h}{\partial \ln k} \tag{1}$$

The slope was applied to evaluate the effect of ATG and MPG on the relation between w_h and retention factor. It can be concluded that the smaller the slope, the better the column efficiency, and the narrower w_h at the same retention factor. Therefore, the peak bandwidth is narrower in ATG or MPG mode than in isothermal and isocratic elution. Recently Neue et al. [21] reaffirmed peak compression effects in RPLC gradient elution. The results from Fig. 7 showed also that a trap effect originating from a steep ATG might compress the sample bandwidth and improve the sensitivity of detection. The negative ATG can generate peak focusing effect (refer to Table 3), which could partly counteract the normal band broadening and negative impacts on efficiency in isocratic elution.
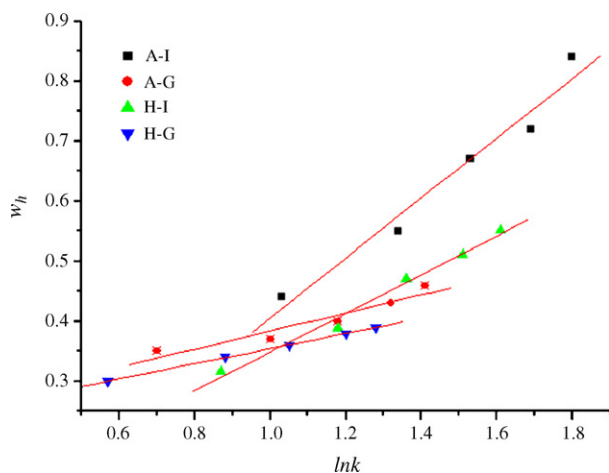
Table 3
The linearity studies of the dependence of w_h on $\ln k$

Separation mode	Calibration curve	Slope	Intercept
A-I	$y = -0.09 + 0.50x$	0.50	−0.09
A-G	$y = 0.23 + 0.15x$	0.15	0.23
H-I	$y = 0.03 + 0.32x$	0.32	0.03
H-G	$y = 0.23 + 0.13x$	0.13	0.23

3.4. The reproducibility of ATG operation

The temperature along the column operated at ATG mode decreased from 80 °C at inlet down to room temperature at the outlet. The average temperature of the column was only about 35–38 °C. The viscosity of the mobile phase on average is almost equivalent to the value at 35–38 °C of isothermal condition. The pressure drop across the column was only slightly lower than that at room temperature, but higher than that at isothermal condition of 80 °C. The insulating material covered on the copper tube reduced the temperature fluctuation in ATG mode in a degree that is less than ±0.3 °C.

The reproducibility of retention times under ATG mode plus MPG condition was evaluated using PAHs as test sample, and was found that the relative standard deviation (RSD) was less than 2.5% for the solute in five consecutive runs. The RSD value is comparable to conventional HPLC operated at MPG condition. It clearly indicated that the reproducibility of the ATG mode is sufficient for routine analysis.

4. Conclusions

The study showed that the ATG in microcolumn LC could improve column efficiency and compress peak bandwidth. Stationary phases of HPLC that can withstand high temperature shall benefit from the ATG mode operation since the absolute value of ATG can be increased further. The instrumentation and operation of the ATG system is relatively simple, and can be used in routine analysis. Additional applications include the separation of ionic compounds or macromolecules in complex biological samples since these compounds are more sensitive to the change of column temperature.

References

[1] H.H. Strain, Ind. Eng. Chem. Anal. Ed. 18 (1946) 605.
[2] E. Gruska, H. Colin, G. Guiochon, J. Chromatogr. 248 (1982) 325.
[3] G. Liu, N.M. Djordjevic, F. Erni, J. Chromatogr. 592 (1992) 239.
[4] L. Nováková, L. Matysová, P. Solich, Talanta 68 (2006) 908.
[5] J.D. Thompson, P.W. Carr, Anal. Chem. 74 (2002) 4150.
[6] J. Chmielowiec, H. Sawatzky, J. Chromatogr. Sci. 17 (1979) 245.
[7] Cs. Horváth, W. Melander, J. Chromatogr. Sci. 15 (1977) 393.
[8] L.A. Cole, J.G. Dorsey, K.A. Dill, Anal. Chem. 64 (1992) 1324.
[9] C.H. Lohmüler, M.A. Moebus, Q. Liu, C. Jiang, J. Chromatogr. Sci. 34 (1996) 69.
[10] S. Mas, G. Fonrodona, R. Tauler, J. Barbosa, Talanta 71 (2007) 1455.
[11] A.T.K. Tran, R.V. Hyne, F. Pablo, W.R. Day, P. Doble, Talanta 71 (2007) 1268.
[12] H. Poppe, J.C. Kraak, J.F.K. Huber, J.H.M. van den Berg, Chromatographia 14 (1981) 515.

Fig. 7. w_h as a function of retention factor under different separation conditions.

[13] T. Takeuchi, Y. Watanabe, D. Ishii, J. High Resol. Chromatogr. 4 (1981) 300.

[14] H.M. McNair, J. Bowermaster, J. High Resolut. Chromatogr. Chromatogr. Commun. 10 (1987) 27.

[15] G.C. Sheng, Y.F. Shen, M.L. Lee, J. Microcol. Sep. 9 (1997) 63.

[16] F. Houdiere, P.W.J. Fowler, N.M. Djordjevic, Anal. Chem. 69 (1997) 2589.

[17] L.K. Moore, R.E. Synovec, Anal. Chem. 65 (1993) 2663.

[18] Y.F. Guan, L.M. Zhou, Z.H. Shang, J. High. Resolut. Chromatogr. 15 (1992) 434.

[19] A. Brandt, G. Mann, W. Arlt, J. Chromatogr. A 769 (1997) 109.

[20] N.M. Djordjevic, P.W.J. Fowler, F. Houdiere, J. Microcol. Sep. 11 (1999) 403.

[21] U.D. Neue, D.H. Marchand, L.R. Snyder, J. Chromatogr. A 1111 (2006) 32.

ELSEVIER

Optimization of the separation of malachite green in water by capillary electrophoresis Raman spectroscopy (CE-RS) based on the stacking and sweeping modes

Chih-Hsin Tsai, Jia-Der Lin, Cheng-Huang Lin *

Department of Chemistry, National Taiwan Normal University, 88 Sec. 4, Tingchow Road, Taipei, Taiwan

Abstract

A capillary electrophoresis Raman spectroscopy (CE-RS) method based on the stacking and sweeping modes are described. A non-fluorescent compound (malachite green, MG; crystal violet, CV) and a doubled Nd:YAG laser (532 nm, 300 mW) were selected as the model compound and light source, respectively. In order to carry out a quantitative and analysis of MG, a monochromator was used to collect the specific Raman line at $1616\,cm^{-1}$ (the N-φ and C–C stretching, corresponding to 582 nm when the wavelength of the exciting source is 532 nm). The limit of detection (LOD) for MG was 1.6×10^{-5} and 1.1×10^{-5} M, respectively, based on the CZE and MEKC modes. This could be improved to 3.4×10^{-7} and 5.3×10^{-9} M, respectively, when the stacking and sweeping modes were applied. The method was also extended to the determination of MG in an actual sample.
© 2006 Elsevier B.V. All rights reserved.

Keywords: Capillary electrophoresis; Raman spectroscopy; Malachite green; Crystal violet; Stacking; Sweeping

1. Introduction

Laser induced fluorescence and optical UV absorbance are the most common detection methods used in CE. However, if the analyte does not emit or absorb UV/visible radiation, alternate types of detection, such as indirect fluorescence/absorbance detection, refractive index, light scattering, chemiluminescence, electrochemistry, even mass spectrometric detection, etc. can be used. Although each method has unique advantages and disadvantages with respect to selectivity, sensitivity, precision and simplicity of use, the typical optical detections used in CE show less of selectivity, since the spectra obtained at ambient temperature are broad, and this limits the spectral characteristics needed for analyte identification. In contrast to this, Raman spectroscopy (RS) provides a unique spectrum of an analyte with a very high spectral resolution. Thus far, it is a very useful method, but is seldom used for detection in CE [1–7], although the first demonstration of Raman spectroscopic detector for CE has been reported by Morris and co-workers [8,9].

This is because Raman emission is a very inefficient process, resulting in poor sensitivity in detection, compared to fluorescence/absorbance methods. In this study, we selected malachite green (MG) oxalate and crystal violet (CV), two compounds with similar chemical structures, as model samples to determine the extent to which the selectivity can be improved when the capillary electrophoresis Raman spectroscopy (CE-RS) method is used. In order to improve the sensitivity when RS is used, we introduced on-line sample concentration techniques to the CE-RS detection method, including the stacking and sweeping modes [10–18]. The method was also extended to the determination of MG in an actual sample. Several experimental parameters were optimized and the data for these are reported herein.

2. Materials and methods

2.1. Chemicals

Malachite green oxalate and crystal violet ([4-[4,4′-bis(di-methylamino)benzhydrylidene]cyclohexa-2,5-dien-1-ylidene]-dimethylammonium chloride) were obtained from Acros (NJ,

* Corresponding author. Tel.: +886 2 8931 6955; fax: +886 2 2932 4249.
E-mail address: chenglin@ntnu.edu.tw (C.-H. Lin).

USA). Sodium dodecyl sulfate (SDS) was obtained from Sigma (St. Louis, MO, USA). Citric acid was purchased from Yakuri Pure Chemical Co., Ltd. (Osaka, Japan), respectively. All other chemicals were of analytical grade and were commercially available.

2.2. CE apparatus

The CE set-up and data acquisition system used were similar to a previously described set-up [19], but the light source was changed to a doubled Nd:YAG laser (532 nm, 300 mW). The laser beam was focused on the CE capillary (fused silica capillary, i.d., 75 μm; J&W Scientific, CA, USA) by means of a lens (focus length, 3 cm). The Raman emission was collected at a right angle to the light source by means of a microscope eyepiece (10×), passed through a long-pass filter, dispersed by a monochromator (Acton Research Corporation, Model SP-300i; detection window was set at 582 ± 0.2 nm), followed by detection using a photomultiplier tube. A commercial Raman instrument (Dilor XY800 Triple-grating spectrometer; resolution, 0.1 cm^{-1}) equipped with a charge coupled detector was also used to assist in the identification of Raman shifts.

3. Results and discussion

3.1. Improvement in selectivity between malachite green and crystal violet

Conventional Raman spectra of malachite green and crystal violet are shown in Fig. 1A and B, respectively; the numbers above the peaks indicate the Raman shifts, in wavenumbers (cm^{-1}) and are in reasonable agreement with published literature values; the strongest Raman bands at 1616 cm^{-1} of MG and 1620 cm^{-1} of CV were assigned to the ring breathing and N-φ stretching modes [20]. A further detailed discussion of these assignments can be found in the literature [20]. Fig. 2A shows a typical electropherogram of a mixture of MG and CV; the detection window was set at 582 ± 0.2 nm, corresponding to the strongest Raman line (1616 ± 7 cm^{-1}; indicated as arrow-marks in Fig. 1A and B). A doubled Nd:YAG laser (532 nm, 300 mW) was used for excitation. The separation mode used was the CZE mode. Two peaks were observed, corresponding to MG and CV,
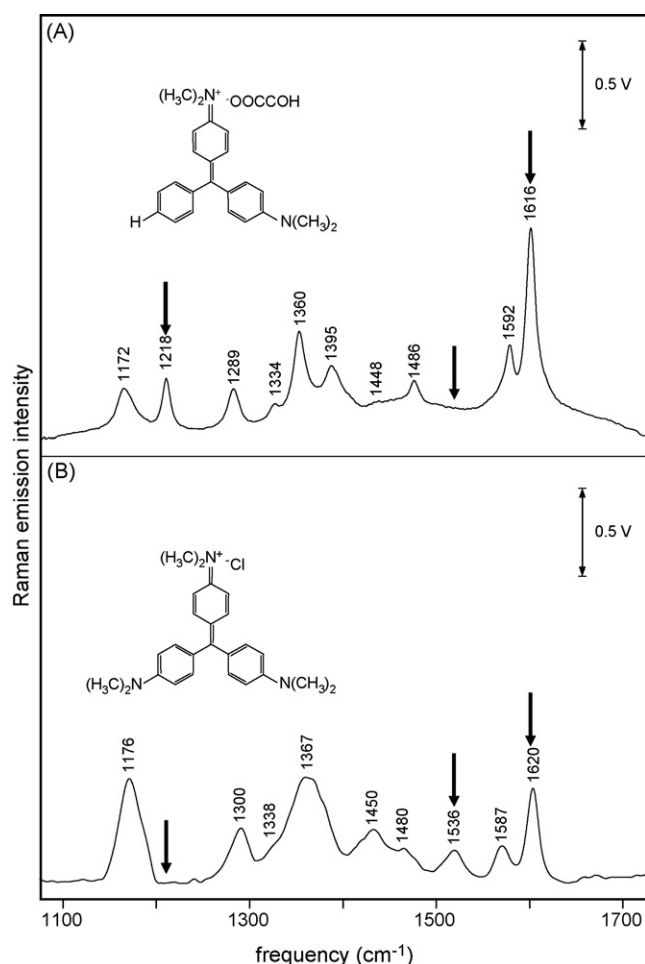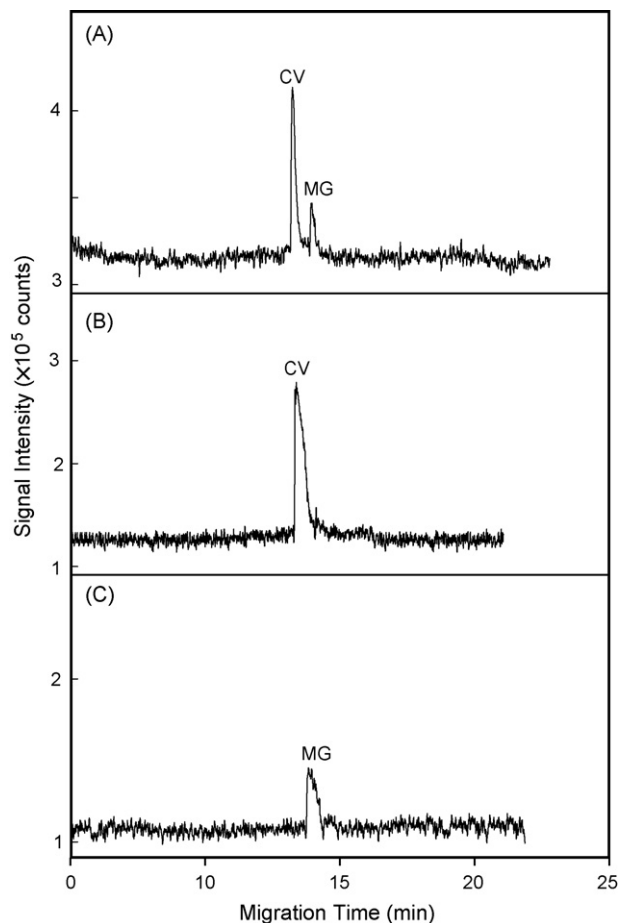

Fig. 2. Typical electropherogram of a mixture of CV and MG; the detection window was set at specific frequencies: (A) 1616 cm^{-1}; (B) 1535 cm^{-1}; (C) 1218 cm^{-1} (indicated as arrow-marks in Fig. 1). CE conditions used are the same as described in Fig. 3A. Sample concentrations of CV and MG used in frames (A–C): (A) 1.6×10^{-3} and 2.7×10^{-4} M; (B) 6.1×10^{-3} and 2.4×10^{-4} M; (C) 2.5×10^{-3} and 1.1×10^{-3} M, respectively. CE conditions: CZE, an aqueous citric acid (50 mM) buffer (pH 2.2; 512 μS/cm) and the applied voltage was +20 kV.

Fig. 1. Raman spectra of: (A) malachite green (1.6×10^{-4} M) and (B) crystal violet (1.2×10^{-4} M); the insets show their chemical structures.

respectively. However, when the detection frequency was set at $1536\,cm^{-1}$, only CV was observed (as shown in Fig. 2B). In contrast to this, when the detection frequency was set at $1218\,cm^{-1}$, only MG was observed (as shown in Fig. 2C). The concentrations of MG used in Figs. 1A and 2A were different, resulting in an inconsistent peak height. In principle, the separation efficiency is not dependent on the detection frequency. However, when the detection frequency is set to a specific Raman line, it can be used to select a specific analyte from a mixture, and this is achieved only with difficulty when regular optical methods are used if the analytes provide similar fluorescence/absorbance spectra.

3.2. Improvement on sensitivity of malachite green

Malachite green, a synthetic dye that is potentially dangerous to human health, is used to color fabrics and paper, and has been used illegally in the treatment of certain fish diseases, mainly, against parasites in freshwater and marine fishes. Thus far, the current detection methods for MG include HPLC [21–23], LC–MS [24–26], UV/CE-stacking [27] methods, etc. In this study, we selected MG as model compound, and investigated its separation and on-line sample concentration condi-

tions under the CZE, stacking, MEKC and sweeping-MEKC modes, respectively. The detection window was also set and matched with the strongest Raman line $(1616 \pm 7\,cm^{-1})$. In the case of the CZE and stacking modes, optimal conditions involved the use of an aqueous citric acid (50 mM) buffer (pH 2.2; conductivity = 512 μS/cm). When the stacking technique was introduced, the running buffer was the same as that used in the CZE mode. The sample was prepared in a matrix solution, obtained by diluting the aqueous citric acid (50 mM) buffer to 1/100, which lowered the conductivity of the solution (pH 2.6; conductivity = 4.16 μS/cm), for use in the stacking mode. Fig. 3A and B show typical electropherograms of MG (sample concentrations used in the CZE mode, 2.2×10^{-4} M; in the stacking mode, 1.1×10^{-6} M). The buffer conditions were as described in Fig. 2A. Since the detection window was extremely narrow, the limit of detection (LOD) for MG was 1.6×10^{-5} and 3.4×10^{-7} M, respectively, based on the CZE and stacking (sample injection length, 16 cm; effective/total length, 61/70 cm) modes. The linearity of these methods for MG was also fairly good and these data (including the calibration curve, coefficient of correlation, limit of detection values and theoretical plate numbers) are summarized in Table 1. Fig. 3C shows a typical electropherogram of MG $(5.4 \times 10^{-5}$ M) based on the
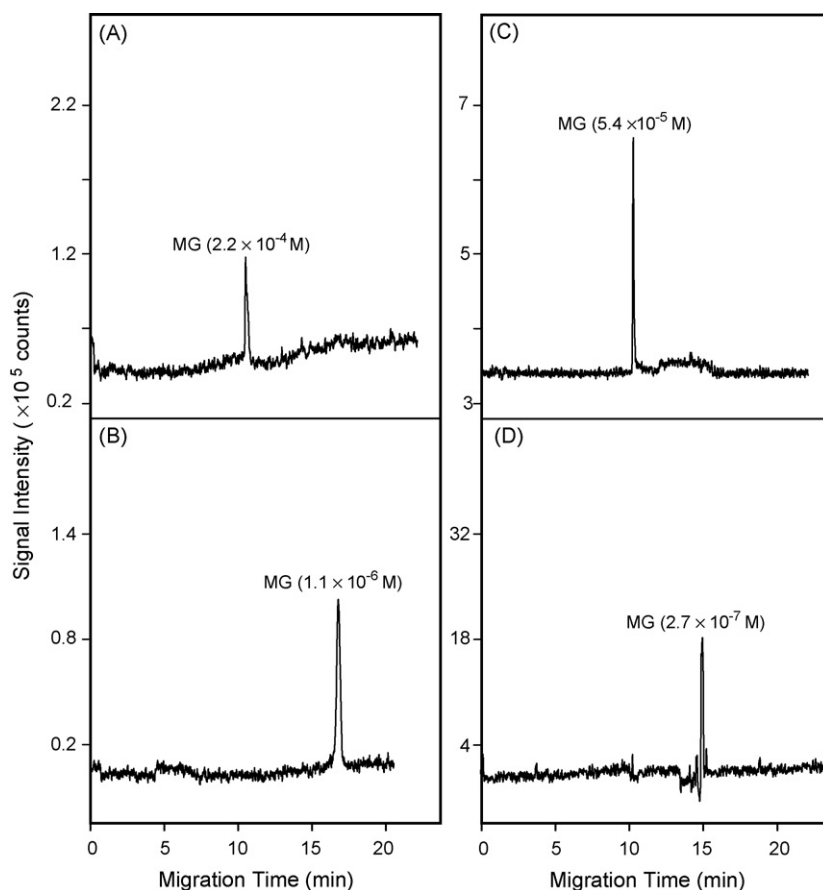

Fig. 3. Typical electropherograms of MG obtained by the CZE (A), stacking (B), MEKC (C) and sweeping-MEKC (D) modes, respectively. CE conditions are described as in Fig. 2A; stacking, buffer was the same as that used in the CZE mode but the samples were prepared in the matrix solution (diluted aqueous citric acid buffer, with pH and conductivity values of 2.56 and 4.16 μS/cm, respectively). MEKC, an aqueous citric acid (50 mM) containing SDS (50 mM) buffer (pH, 2.1); sweeping-MEKC, the same running buffer system as described for the MEKC mode, but the sample was dissolved in the matrix (50 mM citric acid aqueous buffer without SDS). The applied voltages used were +20 kV in the CZE and stacking modes; −16 and −8 kV in the MEKC and sweeping-MEKC modes, respectively.

MEKC mode. The detection limit for MG was determined to be 1.1×10^{-5} M (S/N = 3). Fig. 3D shows a typical electropherogram of MG (2.7×10^{-7} M) obtained by the sweeping-MEKC mode. The CE buffer system was basically identical to that used for the MEKC mode. The sample was dissolved in the matrix (50 mM citric acid aqueous buffer without SDS) and an injection length of 22 cm was used (effective/total length, 61/70 cm). When the sweeping-MEKC mode was applied, a dramatic improvement in detection sensitivity was obtained, and the limit of detection was improved to 5.3×10^{-9} M (at S/N = 3). Basically the signal intensity increased with increasing injection length. However, an optimal sample injection length should be determined because if a longer capillary column is used for sample concentration strategies, the subsequent CE separation becomes insufficient. The linearity of these methods for MG was also fairly good and these data are also summarized in Table 1.

3.3. Application to a real-life sample

The sample, water in which marketed fish are kept, was obtained from a supermarket near the campus in Taipei. The sample was filtered, and a 20 μL aliquot was placed in a vacuum chamber for drying. The residue was acidified by the addition of 20 μL of citric acid (50 mM) and was used in the subsequent CE

Table 1
Calibration curve, coefficient of correlation, limit of detection values (S/N = 3) and theoretical plate numbers (N) for malachite green by CZE/Raman, stacking-CZE/Raman, MEKC/Raman, sweeping-MEKC/Raman methods, respectively, by using a green diode laser

(A) CZE/Raman	
Equation of the line	$y = 5.27 \times 10^7 x + 9.08 \times 10^2$
Coefficient of correlation	$R^2 = 0.9978$
Detection range (M)	5.4×10^{-4} to 5.4×10^{-5}
Sample injection length (cm)	0.4
LOD (M)	1.6×10^{-5}
Theoretical plate number	8.4×10^3 to 3.5×10^4
(B) Stacking-CZE/Raman	
Equation of the line	$y = 1.08 \times 10^4 x + 1.53 \times 10^4$
Coefficient of correlation	$R^2 = 0.9917$
Detection range (M)	2.2×10^{-6} to 5.4×10^{-7}
Sample injection length (cm)	16
LOD (M)	3.4×10^{-7}
Theoretical plate number	6.6×10^3 to 1.8×10^4
(C) MEKC/Raman	
Equation of the line	$y = 3.6 \times 10^5 + 1.8 \times 10^6$
Coefficient of correlation	$R^2 = 0.9911$
Detection range (M)	1.1×10^{-4} to 1.3×10^{-5}
Sample injection length (cm)	0.4
LOD (M)	1.1×10^{-5}
Theoretical plate number	2.2×10^4 to 4.2×10^4
(D) Sweeping-MEKC/Raman	
Equation of the line	$y = 1.5 \times 10^7 + 1.9 \times 10^5$
Coefficient of correlation	$R^2 = 0.9905$
Detection range (M)	5.4×10^{-6} to 5.4×10^{-9}
Sample injection length (cm)	22
LOD (M)	5.3×10^{-9}
Theoretical plate number	2.3×10^5 to 3.0×10^5

Light source: doubled Nd:YAG laser (532 nm, 300 mW); detection frequency was set at 1616 ± 7 cm^{-1}.
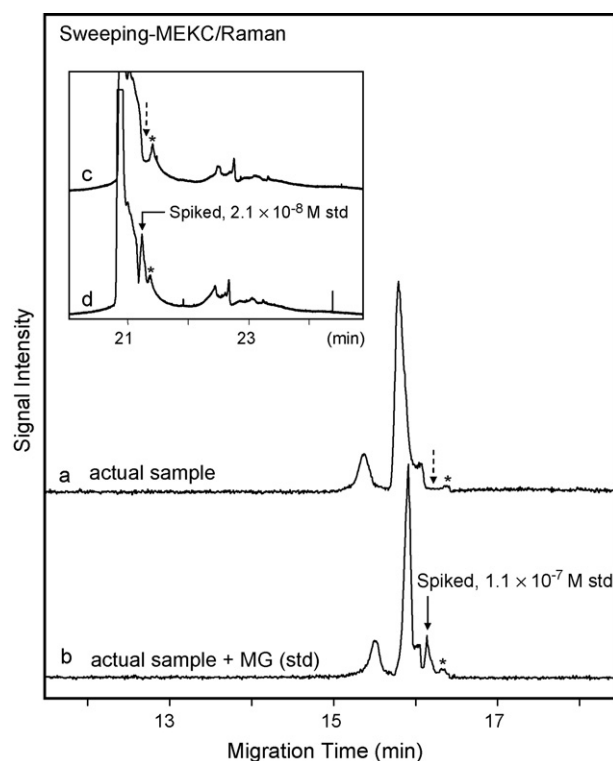

Fig. 4. Typical CE electropherograms obtained from an actual water sample, in which fish were kept in a commercial supermarket, by applying the sweeping-MEKC mode (conditions, as described in Fig. 3D). Electropherograms a and b show the results obtained before and after spiking with an MG standard (1.1×10^{-7} M), respectively. Electropherograms c and d in the inset show results obtained before and after spiking with an MG standard (2.1×10^{-8} M) by recording all emissions.

separation. Fig. 4 shows typical CE electropherograms obtained for an actual sample, obtained from a fish market, by applying the sweeping-MEKC/Raman mode. The CE conditions are as described above in Fig. 3D. Electropherograms a and b show the results obtained before and after spiking with an MG standard (1.1×10^{-7} M), respectively. Herein, the sample was directly used without any pretreatment procedures. All of these peaks were detected at an emission of 1616 ± 7 cm^{-1}, either native fluorescence or Raman lines. When a single-wavelength set-up was performed upon Raman emission, it can exclude specific emissions from a number of unknown compounds. Electropherograms a and b in the inset also show the results obtained before and after spiking with an MG standard (1.1×10^{-7} M). The entire range of emissions was detected, and, as a result, a broad background was detected in electropherograms c and d. For a comparison of the separation efficiency, an indicated peak (marked as "*" in electropherograms a–d) was selected for evaluation. In electropherograms a and c, the broken arrow indicates the expected migration time for MG, but it did not show up in the sample. This indicates that, if it exists, its concentration is below a certain LOD. Using the standard addition method, the results were compared and the findings show that the peaks (marked spiking peaks in electropherograms b and d) clearly appeared. If it were possible to arrange a CCD detector to record the entire range of emission, further accuracy in identification could be achieved, since characteristic Raman shifts (spectral

fingerprinting) can be used for the unambiguous identification of a compound.

4. Conclusions

This work successfully demonstrates a new approach for detecting a non-fluorescent compound by a capillary electrophoresis Raman spectroscopy method combined with an on-line sample concentration technique. This proposed method may solve problems that are frequently encountered for non-fluorescent analytes, even when they are present at low levels. Thus, a combination of a compact high power laser, interference filters, a PMT detector based on either a CE or microchip system, would be useful as a rapid-screening tool, in which only a miniaturized system would be needed. Further applications of this technique are currently under investigation.

Acknowledgment

References

[1] G.L. DeVault, M.J. Sepaniak, Electrophoresis 22 (2001) 2303.
[2] L. He, M.J. Natan, C.D. Keating, Anal. Chem. 72 (2000) 5348.
[3] R.J. Dijkstra, E.V. Efremov, F. Ariese, U.A.Th. Brinkman, C. Gooijer, Anal. Chem. 75 (2003) 5697.
[4] R.J. Dijkstra, A.N. Bader, G.Ph. Hoornweg, U.A.Th. Brinkman, C. Gooijer, Anal. Chem. 71 (1999) 4575.
[5] R.J. Dijkstra, C.T. Martha, F. Ariese, U.A.Th. Brinkman, C. Gooijer, Anal. Chem. 73 (2001) 4977.
[6] L. He, M.J. Natan, C.D. Keating, Anal. Chem. 72 (2000) 5348.
[7] W.F. Nirode, G.L. Devault, M.J. Sepaniak, Anal. Chem. 72 (2000) 1866.
[8] C.-Y. Chen, M.D. Morris, Appl. Spectrosc. 42 (1988) 515.
[9] W.K. Kowalchyk, P.A. Walker III, M.D. Morris, Appl. Spectrosc. 49 (1995) 1183.
[10] J.P. Quirino, S. Terabe, Science 282 (1998) 465.
[11] D.S. Burgi, R.L. Chien, Anal. Chem. 63 (1991) 2042.
[12] J. Palmer, N.J. Munro, J.P. Landers, Anal. Chem. 71 (1999) 1679.
[13] G. Hempel, Electrophoresis 21 (2000) 691.
[14] R.L. Chien, D.S. Burgi, Anal. Chem. 64 (1992) 489A.
[15] A. Vinther, H. Soeeberg, J. Chromatogr. 559 (1991) 3.
[16] L. Farry, D.A. Oxspring, W. Franklin Smyth, R. Marchant, Anal. Chim. Acta 349 (1997) 221.
[17] P. Britz-McKibbin, D.D.Y. Chen, Anal. Chem. 72 (2000) 1242.
[18] P. Britz-McKibbin, K. Otsuka, S. Terabe, Anal. Chem. 74 (2002) 3736.
[19] T.Y. Kuo, S.P. Wang, C.H. Lin, Electrophoresis 26 (2005) 4355.
[20] H.B. Lueck, D.C. Daniel, J.L. McHale, J. Raman Spectrosc. 24 (1993) 363.
[21] L.G. Rushing, H.C. Thompson Jr., J. Chromatogr. B 688 (1997) 325.
[22] K. Mitrowska, A. Posyniak, J. Zmudzki, J. Chromatogr. A 1089 (2005) 187.
[23] N. Haagsma, C.A.J. Hajee, J. Chromatogr. B 669 (1995) 219.
[24] P. Scherpenisse, A.A. Bergwerff, Anal. Chim. Acta 529 (2005) 173.
[25] L. Valle, C. Dĭiaz, A.L. Zanocco, P. Richter, J. Chromatogr. A 1067 (2005) 101.
[26] M. Mazereeuw, V. Spikmans, U.R. Tjaden, J. van der Greef, J. Chromatogr. A 1067 (2005) 101.
[27] L. Farry, D.A. Oxspring, W. Franklin Smyth, R. Marchant, Anal. Chim. Acta 349 (1997) 221.

Characterization of chemiluminescence from singlet oxygen under laminar flow conditions in a micro-channel and its quenching with beverages

Kazuhiko Tsukagoshi [a,*], Kazuaki Fukumoto [a], Riichiro Nakajima [a],
Kenichi Yamashita [b], Hideaki Maeda [b,c]

[a] *Department of Chemical Engineering and Materials Science, Faculty of Engineering, Doshisha University, Kyotanabe 610-0321, Japan*
[b] *Micro- & Nano-space Chemistry Group, Nanotechnology Research Institute, National Institute of Advanced Industrial Science and Technology (AIST) 807-1, Shuku-machi, Tosu, Saga 841-0052, Japan*
[c] *JST, CREST, 807-1, Shuku-machi, Tosu, Saga 841-0052, Japan*

Abstract

Singlet oxygen was generated by reaction of sodium hypochlorite and hydrogen peroxide in a micro-channel. The two reagent solutions were delivered into the micro-channel by a syringe pump, providing a laminar flow liquid–liquid interface. The chemiluminescence from the singlet oxygen was emitted in the collapse of the interface due to molecular diffusion under laminar flow conditions. The chemiluminescence intensity was observed continuously and stably for each combination of reagents fed into the micro-channel; while, in the normal batch-type reactor the chemiluminescence peaks from singlet oxygen were observed within *ca.* 5 s. The features of the chemiluminescence emitted under laminar flow conditions were examined by changing the concentrations of sodium hypochlorite and hydrogen peroxide; the concentrations of 2.5 mM sodium hypochlorite and 7.5 mM hydrogen peroxide provided highest chemiluminescence intensities without bubble formation. Also, the effects of beverages, such as green tea, coffee, white wine, red wine, and *sake* (rice wine), on the chemiluminescence intensity as well as the concentrations of sodium hypochlorite and hydrogen peroxide were examined. The chemiluminescence intensities observed with addition of the beverages to the reagents decreased in the following orders; green tea > coffee > red wine > rice wine > white wine (being added to sodium hypochlorite); coffee > white wine > green tea > red wine > rice wine (being added to hydrogen peroxide). It was found that coffee decreased the chemiluminescence intensity (*ca.* 33% chemiluminescence decrease) without altering the concentrations of sodium hypochlorite or hydrogen peroxide. The cause of the decrease in chemiluminescence with coffee is discussed.
© 2006 Elsevier B.V. All rights reserved.

Keywords: Chemiluminescence; Singlet oxygen; Laminar flow conditions; Micro-channel; Quenching with beverages

1. Introduction

Active oxygen has attracted a great deal of attention from the viewpoint of not only specific chemical species in chemical reactions but also medical science with regard to disease factors, health maintenance, and aging [1–3]. Active oxygen species generally include singlet oxygen ($^1O_2$), hydroxyl radicals ($^\bullet OH$), and superoxide radical anions ($O_2{}^{-\bullet}$), sometimes adding hydrogen peroxide (H_2O_2) and hypochlorite ion (OCl^-). Singlet oxygen is generated by the reaction of sodium hypochlorite and hydrogen peroxide,

and emits chemiluminescence (CL) (630–650 nm) [4] as follows: $H_2O_2 + NaClO \rightarrow {}^1O_2 + H_2O + NaCl$; $2\,{}^1O_2 \rightarrow 2\,{}^3O_2 + h\nu$ (630–650 nm). The half-life of singlet oxygen is short and is dependent on the solvent [5,6], e.g., 3.3 μs in water and 68.0 μs in heavy water. In a normal batch-type CL detector, with mixing of reagent solutions in volumes of the order of several milliliters, CL from singlet oxygen is observed with a very sharp CL peak and poor reproducibility (data shown in Fig. 2 and explained in the text).

Over the past decade, miniaturized chemical analysis systems, commonly referred to as micro-total analysis systems (μ-TAS) [7,8], have been reported in various fields. A micro-reactor consisting of a micro-channel [9,10] has several features useful for chemical reactions, including: rapid heat exchange and mass transfer that cannot be achieved using a conventional

---

* Corresponding author. Tel.: +81 774 65 6595; fax: +81 774 65 6803.
E-mail address: ktsukago@mail.doshisha.ac.jp (K. Tsukagoshi).

batch-wise system; laminar flow, which can be obtained in a micro-fluidic system; and large specific surface area to volume ratio. In our previous work, a CL detection system in a micro-reactor was developed, taking advantage of the laminar flow liquid-liquid interface in a micro-channel [11,12]. The two reagent solutions were delivered into the micro-channel, providing a laminar flow liquid–liquid interface. The previous work, mainly summarizing initial data, is regarded as the first report describing the CL from singlet oxygen under laminar flow in a micro-channel and the effect of antioxidants on the CL.

In the present study, in order to provide more detail information concerning the CL from singlet oxygen and the effects of antioxidants, first, we compared the CL profiles between the normal batch-type reactor and the present micro-reactor. Also, the effects of reagent concentrations, sodium hypochlorite and hydrogen peroxide, on the CL intensities were examined to decide their optimum analytical conditions. After the optimization, the calibration curves of sodium hypochlorite and hydrogen peroxide were constructed. On the basis of the above results, the influences of the beverages on not only CL intensity but also hydrogen peroxide and sodium hypochlorite concentrations were examined. The data obtained in the present study provide unique information for analyzing the effects of beverages containing antioxidants against active oxygen, such as single oxygen, hydrogen peroxide, and hypochlorite ions, taking advantage of the specific "micro-environment area" for reaction/detection in a micro-channel.

2. Experimental

2.1. Reagents and beverages

All reagents used were commercially available and of analytical grade. Ion-exchanged water was distilled for use. Sodium hypochlorite, hydrogen peroxide solution (30 wt%), and heavy water were purchased from Nacalai Tesque (Kyoto, Japan). The following beverages were used: green tea (Iemon, Suntory), coffee (no sugar, UCC), white wine and red wine (Cuvee Select 500 Series, Lawson), and rice wine (sake) (Gekkeikan).

2.2. Analysis of sodium hypochlorite and hydrogen peroxide

We used an SBT Kit (ZK01-50; Dojindo), which uses a colorimetric method developed to determine chloride radical concentration, to examine the concentration of sodium hypochlorite in Reagent 1 in accordance with the manufacturer's instructions. The concentration of hydrogen peroxide in Reagent 2 was determined by a normal titration method using potassium permanganate.

2.3. Batch-type reactor and analytical procedure

The CL profile in a batch-type reactor was obtained using a CL detector (Chemiluminescence Analyzer System; Model CLD-100FC; Tohoku Electronic Industrial Co., Ltd.) under the following analytical conditions. Sodium hypochlorite solution
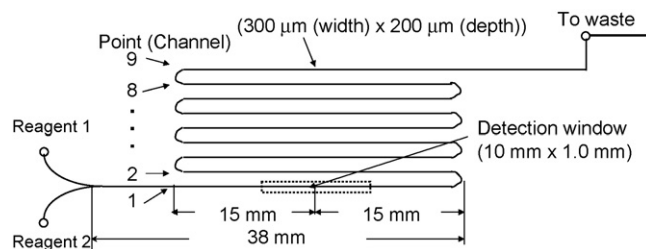

Fig. 1. An illustration of the micro-reactor consisting of a micro-channel. Top view.

(5 ml, 1 mM; pH 6.8 and pH 8.5 (100 mM phosphate buffer), pH 10.8 (100 mM carbonate buffer)) was put in a laboratory dish. Then, 1 ml of hydrogen peroxide solution (1 mM; pH corresponding to that of the sodium hypochlorite solution) was added to the dish with a micro-syringe, and the solution was stirred.

2.4. Micro-reactor and analytical procedure

Fig. 1 shows an illustration of the micro-reactor used in the present study, incorporating a micro-channel (300 μm in width × 200 μm in depth) made of polymethylmethacrylate [13,14]. The CL was detected at the detection window (10 mm length along each channel). The detection windows were named Points 1–9 along the channel from the junction point on the micro-reactor. In this study, we used Points 1 and 2.

Although experiments were carried out using various reagent concentrations, the following analytical conditions were mainly used through optimization. Reagent 1 was 2.5 mM sodium hypochlorite in 100 mM carbonate buffer (pH 10.8, $H_2O/D_2O = 1/1$ (v/v)). Reagent 2 was 7.5 mM hydrogen peroxide in 100 mM carbonate buffer (pH 10.8, $H_2O/D_2O = 1/1$ (v/v)). When examining the effects of beverages on the CL intensity, Reagent 1 or 2 included a given amount of beverage.

The two reagent solutions were delivered with a syringe pump (MF-9090; Bioanalytical Systems Inc.). They were joined at the junction point and subsequently fed to the micro-channel. The resulting CL in the micro-channel was detected at the detection window with a photomultiplier tube (H5783; Hamamatsu Photonics Co. Ltd.) located under the micro-reactor, measured with a CL detector (Model EN-21; Kimoto Electric Inc.), and treated with an integrator (Chromatopac C-R6A; Shimadzu Co.).

3. Results and discussion

3.1. CL from singlet oxygen in a batch reactor

The CL profile obtained with the batch-type reactor under alkaline conditions (pH 10.8) is shown in Fig. 2. As described in the Introduction, singlet oxygen is generated by the reaction of sodium hypochlorite and hydrogen peroxide and emits CL [4]. The half-life of singlet oxygen is very short [5,6], e.g., 3.3 μs in water. As shown in Fig. 2, the CL from singlet oxygen appeared quickly and decreased within several seconds, making a very sharp CL profile. Similar CL profiles were observed under conditions of pH 6.5 and 8.5, although the CL heights
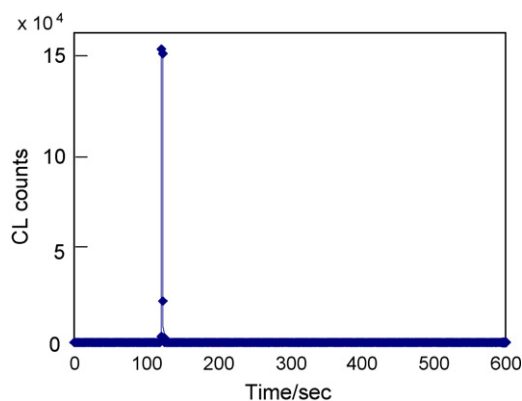
Fig. 2. CL response from singlet oxygen in a batch-reactor. Conditions: 1 mM hydrogen peroxide (1 ml; pH 10.8 (100 mM carbonate buffer)) was added to 1 mM sodium hypochlorite (5 ml; pH 10.8 (100 mM carbonate buffer)) in a laboratory dish. The CL detector measured CL counts every one seconds and indicated the values with the closed diamond plots in the figure.
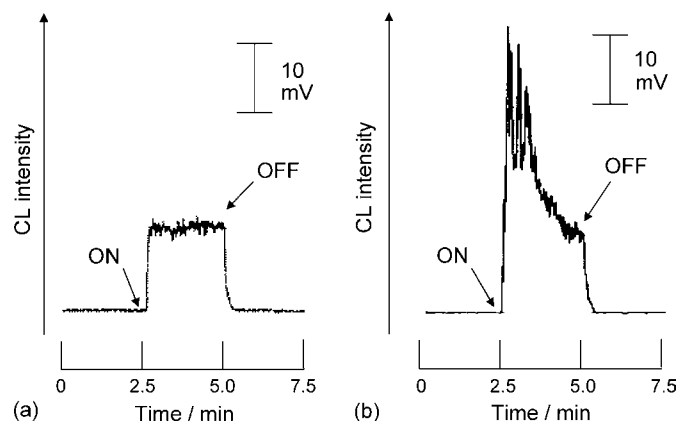

Fig. 3. CL response from singlet oxygen in a micro-channel. Conditions: (a) Reagent 1, 2.5 mM sodium hypochlorite in 100 mM carbonate buffer (pH 10.8, $H_2O/D_2O = 1/1$ (v/v)); Reagent 2, 7.5 mM hydrogen peroxide in 100 mM carbonate buffer (pH 10.8, $H_2O/D_2O = 1/1$ (v/v)). (b) Reagent 1, 10 mM sodium hypochlorite in 100 mM carbonate buffer (pH 10.8, $H_2O/D_2O = 1/1$ (v/v)); Reagent 2, 10 mM hydrogen peroxide in 100 mM carbonate buffer (pH 10.8, $H_2O/D_2O = 1/1$ (v/v)). Flow rate, 100 μl min⁻¹; detection point, Point 1 (Channel 1). "ON" and "OFF" indicate the times when the syringe pump was turned on and off, respectively.

were different. The CL heights at pH 6.5, 8.5, and 10.8 were *ca.* 1900, 100,000, and 160,000 counts, respectively. The relative standard deviations of CL heights increased with increases in pH value; generally, batch-reactors lack reproducibility in their data. Although the analytical conditions in the batch-type reactor have not been examined in detail, even at the low pH of 6.5 the relative standard deviations were > *ca.* 20% (*n* = 10).

3.2. CL from singlet oxygen in a micro-reactor

The two reagents, sodium hypochlorite and hydrogen peroxide, were delivered into the micro-channel to form a laminar flow liquid–liquid interface; the Reynolds number was calculated as *ca.* 18 at 100 μl min⁻¹. Such a laminar flow forms a liquid–liquid interface instantly in the micro-channel, and then the interface collapses gradually through molecular diffusion with the residence times [1,14]. The CL from the singlet oxygen was emitted in the course of the collapse of the interface under laminar flow conditions. The CL intensity was observed continuously and stably in the micro-channel as long as the reagents were fed into the channel. Good reproducibility and stabilization of the CL was caused by the formation of liquid–liquid interface under a laminar flow condition in a micro-channel. The normal FIA systems comprise mostly *ca.* 1 mm inner diameter tube and *ca.* 1 ml min⁻¹ flow rate, leading to a turbulent flow condition. We do not have any data about any FIA systems, but the FIA systems, not including micro-channels, would never provide the same performance concerning reproducibility and stabilization for CL of singlet oxygen as the micro-channel in a micro-reactor, although comparatively constant CL may be observed just only at the junction point in the flow lines by any chance.

When the reagent flow into the micro-channel was turned "on" and "off" by operating the syringe pump controller [11,12], CL from singlet oxygen in the micro-channel responded rapidly to the changes. The CL profile obtained with reagent concentrations of 2.5 mM sodium hypochlorite and 7.5 mM hydrogen peroxide is shown in Fig. 3(a). The time of 2.5 min between "ON" and "OFF" in Fig. 3 means the pump-operating time, not

the reaction time. The rapid response suggested that CL from singlet oxygen was generated through the rapid reaction rate and the short lifetime in the course of collapse of the liquid–liquid interface formed under the conditions of laminar flow. The collapse of the interface is caused mainly by molecular diffusion. Tentatively, the diffusion length of the molecules was estimated using the following equation: $T = L^2/D$ (T = residence time, L = diffusion length, and D = diffusion coefficient; *ca.* 1×10^{-5} cm² s⁻¹). The diffusion length of the molecules was estimated to be *ca.* 20 μm at a residence time of 0.4 s under the analytical conditions shown in Fig. 3(a).

On the other hand, at higher reagent concentrations of 10 mM hydrogen peroxide and 10 mM sodium hypochlorite, the CL profile had a sawtooth shape (Fig. 3(b)). Some bubbles in the micro-channel were observed, which were probably responsible for the turbulence of CL. In addition, the solubility of oxygen in water is known to be *ca.* 10^{-4} M. The solubility value does not seem to contradict the reagent concentrations and bubble formation in the micro-channel.

3.3. Effects of reagent concentrations on the CL intensities in the micro-channel

CL intensities in the micro-channel were examined by changing the reagent concentrations; sodium hypochlorite, and hydrogen peroxide concentrations were changed 1.0–10 mM. The obtained CL intensities are summarized in Table 1. At high reagent concentrations, bubble formation disturbed the constant CL, as shown in Fig. 3(b). The highest CL intensity was observed at 2.5 mM sodium hypochlorite and 7.5 mM hydrogen peroxide without bubble formation. The following experiments were mainly carried out under these reagent concentrations. Point 2 (Channel 2) was used in the following experiments, as our previous study indicated the benefits of Point 2 with regard to sensitivity for CL measurement [12].

Table 1
Effects of reagent concentrations on the CL intensities

NaClO/mM	CL intensity (mV)				
	$1.0\,mM\text{-}H_2O_2$	$2.5\,mM\text{-}H_2O_2$	$5.0\,mM\text{-}H_2O_2$	$7.5\,mM\text{-}H_2O_2$	$10.0\,mM\text{-}H_2O_2$
1.0	2.2	3.8	5.8	6.7	7.0
2.5	2.4	5.9	6.9	9.5	(Bubbles)
5.0	3.1	7.5	(Bubbles)	(Bubbles)	(Bubbles)
7.5	3.6	8.2	(Bubbles)	(Bubbles)	(Bubbles)
10.0	5.1	(Bubbles)	(Bubbles)	(Bubbles)	(Bubbles)

(Bubbles): bubble formation in the micro-channel leading to unstable CL, as shown in Fig. 3(b). Conditions: Reagent 1, 1–10 mM sodium hypochlorite in 100 mM carbonate buffer (pH 10.8, $H_2O/D_2O = 1/1$ (v/v)); Reagent 2, 1–10 mM hydrogen peroxide in 100 mM carbonate buffer (pH 10.8, $H_2O/D_2O = 1/1$ (v/v)); flow rate, $100\,\mu l\,min^{-1}$; and detection point, Point 1 (Channel 1).

Next, the relationships between reagent concentrations and CL intensities were examined, changing the concentration of one reagent and keeping that of the other constant. Sodium hypochlorite was determined linearly over the range of 0.25–2.5 mM at 7.5 mM hydrogen peroxide. Hydrogen peroxide was also determined linearly over the range of 0.1–7.5 mM at 2.5 mM sodium hypochlorite. The relationships are represented with coefficient values of 0.999 and relative standard deviations of <5% ($n = 8$).

3.4. Effects of beverages on the CL intensities in the micro-channel and reagent concentrations

The effects of beverages, such as green tea, coffee, white wine, red wine, and *sake* (rice wine), on the CL intensities in the micro-channel, as well as the reagent concentrations in Reagents 1 and 2 were examined. Each beverage diluted 50-fold was added to Reagent 1 or Reagent 2. After 1 h, the CL intensities in the micro-channel were determined, and also sodium hypochlorite concentration in Reagent 1 was determined with an SBT Kit and the hydrogen peroxide concentration in Reagent 2 was determined by the standard titration method using potassium permanganate. Table 2 shows the obtained CL intensities and the reagent concentrations of sodium hypochlorite and hydrogen peroxide.

All CL intensities observed with addition of the beverages to Reagents 1 and 2 decreased in the following orders: Reagent 1, green tea > coffee > red wine > rice wine > white wine; Reagent 2, coffee > white wine > green tea > red wine > rice wine. Sodium hypochlorite concentration in Reagent 1 decreased in the presence of white wine, red wine, and rice wine, while there

were no changes in the presence of green tea or coffee. Hydrogen peroxide concentration in Reagent 2 decreased in the presence of green tea, red wine, and rice wine, while there were no changes in the presence of coffee or white wine.

The above results indicated that red wine and rice wine interacted with both sodium hypochlorite and hydrogen peroxide; green tea reacted only with hydrogen peroxide; white wine reacted only with sodium hypochlorite. These interactions decreased the CL intensities, although the reactions of the beverages with singlet oxygen in the micro-channel cannot be excluded. On the other hand, coffee did not interact with either hydrogen peroxide or sodium hypochlorite under the present conditions, but the CL intensity in the channel decreased; *ca*. 33 % CL decrease was observed. That is, coffee decreased the CL intensity in the micro-channel without decreasing the reagent concentrations in Reagents 1 and 2.

These observations raise questions regarding the nature of the contents in coffee that decreased the CL intensity in the micro-channel. Tentatively, we considered chlorogenic acid ($C_{16}H_{18}O_9$; MW, 354.3) as the cause of the decrease in CL, because chlorogenic acid is included in coffee at concentrations higher than caffeine. Coffee beans contain *ca*. 5–8 wt% chlorogenic acid. Although chlorogenic acid decomposes during roasting, commercial coffee is usually thought to include chlorogenic acid at 10^{-4}–10^{-3} M. Chlorogenic acid has attracted interest as an antioxidant. Generally, chlorogenic acid, which has a polyphenol structure, is thought to act as an antioxidant against hydroxyl radicals. However, as the structure of chlorogenic acid also has an ethylenic linkage, it may react with singlet oxygen.

Table 2
Effects of beverages on the CL intensities and reagent concentrations

Beverages	NaClO + beverage (Reagent 1)		H_2O_2 + beverage (Reagent 2)	
	CL intensity (mV)	NaOCl concentration (mM)	CL intensity (mV)	H_2O_2 concentration (mM)
Blank	18.0	2.5	18.0	7.5
Green tea	13.3	2.5	5.0	1.7
Coffee	12.4	2.5	11.8	7.5
White wine	4.5	1.6	5.9	7.5
Red wine	8.3	2.3	4.0	1.3
Rice wine	5.1	1.9	2.0	2.3

Conditions: Reagent 1, 2.5 mM sodium hypochlorite (+ 50-fold diluted beverage) in 100 mM carbonate buffer (pH 10.8, $H_2O/D_2O = 1/1$ (v/v)); Reagent 2, 7.5 mM hydrogen peroxide (+ 50-fold diluted beverage) in 100 mM carbonate buffer (pH 10.8, $H_2O/D_2O = 1/1$ (v/v)); flow rate, $100\,\mu l\,min^{-1}$; and detection point, Point 2 (Channel 2).
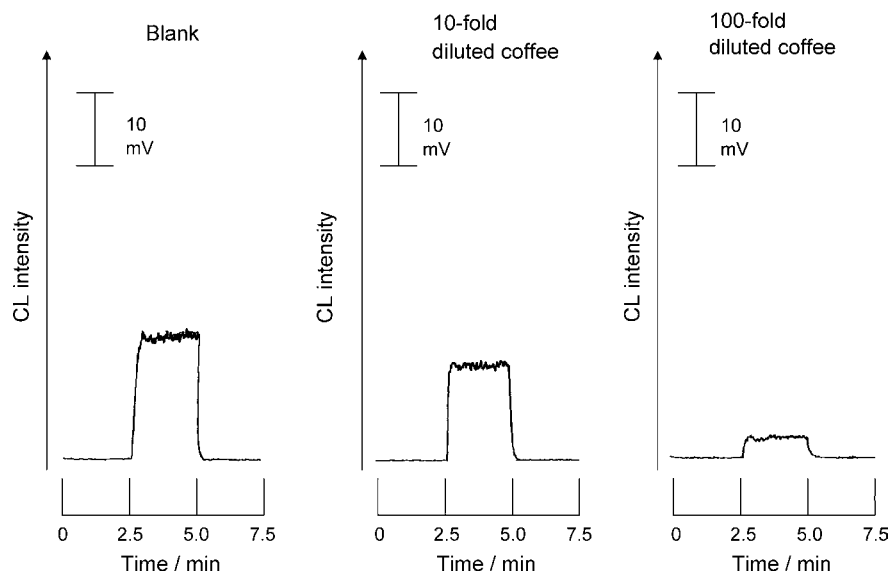
Fig. 4. Effects of coffee on the CL profiles obtained in the micro-channel. Conditions: Reagent 1, 2.5 mM sodium hypochlorite + 10 or 100-fold diluted coffee in 100 mM carbonate buffer (pH 10.8, $H_2O/D_2O = 1/1$ (v/v)); Reagent 2, 7.5 mM hydrogen peroxide in 100 mM carbonate buffer (pH 10.8, $H_2O/D_2O = 1/1$ (v/v)); flow rate, 100 μl min^{-1}; and detection point, Point 2 (Channel 2).

When we diluted coffee 10- and 100-fold, the CL in the micro-channel decreased gradually, as shown in Fig. 4. It is well known that the reactions concerning superoxide radical anions and hydroxyl radicals are radical reactions and proceed *via* chain reactions in a non-quantitative manner, while reactions concerning singlet oxygen are quantitative with no chain reaction. As little information is available concerning the manner of mixing among sodium hypochlorite, hydrogen peroxide, and chlorogenic acid in micro-channels, as well as the reaction rates regarding the generation of singlet oxygen and the extinction of singlet oxygen with antioxidant, such as chlorogenic acid, detailed discussion of the data is very difficult. However, chlorogenic acid and singlet oxygen concentrations may be of similar orders, $10^{-4}–10^{-3}$ M, as described above. Therefore, the data shown in Fig. 5 support the quantitative reaction between singlet oxygen and antioxidant species, such as chlorogenic acid, in coffee.

4. Conclusions

After optimizing the reagent concentrations, the CL from the singlet oxygen could be observed constantly and stably for each combination of reagents fed into the system with high CL intensity and no bubble formation. Such CL observation was brought about by the formation of liquid–liquid interface under a laminar flow condition in a micro-channel. Although the diffusion length of the molecules was briefly discussed with the residence time (reaction time) in this study, the CL observed through the collapse of the liquid–liquid interface in a micro-channel is interesting for not only analytical chemistry but also chemical engineering, including diffusion engineering and transport phenomena. We also examined the effects of several beverages on the CL intensity, as well as the changes in the reagent concentrations with beverages. Our results indicated that coffee decreased the CL intensity without affecting the concentrations of sodium hypochlorite or hydrogen peroxide. That supported the singlet oxygen reacted antioxidant species, such as chlorogenic acid, in coffee. The data obtained here provided unique information for analyzing beverages containing antioxidants using a micro-reactor comprising a micro-channel.

References

[1] G.R.A. Johnson, N.B. Nazhat, R.A. Saadalla-Nazhat, J. Chem. Soc. Chem. Commun. (1985) 407.
[2] G.R.A. Johnson, N.B. Nazhat, J. Am. Chem. Soc. 109 (1987) 1990.
[3] A. Takahashi, H. Totsune-Nakano, M. Nakano, S. Mashiko, N. Suzuki, C. Ohma, H. Inaba, FEBS Lett. 246 (1989) 117.
[4] Kikan Kagaku Sosetsu, Chemistry of Active Oxygen Species, ed. Nippon Kagaku-kai, Gakkai-Shuppan Center, 1990.
[5] D. Bellus, Adv. Photochem. 11 (1979) 105.
[6] M.A.J. Rodjers, J. Am. Chem. Soc. 105 (1983) 6021.
[7] T.B. Stachowiak, F. Svec, J.M.J. Frechet, J. Chromatogr. A 1044 (2004) 97.
[8] K. Tsukagoshi, N. Jinno, R. Nakajima, Anal. Chem. 77 (2005) 1684.
[9] P.D.I. Fletcher, S.J. Haswell, P. Watts, S.Y.F. Wong, Lab Chip 309 (2003) 309.
[10] H. Nakamura, Y. Yamaguchi, M. Miyazaki, H. Maeda, M. Uehara, P. Mulvaney, Chem. Commun. 23 (2002) 2844.
[11] K. Tsukagoshi, K. Ikegami, R. Nakajima, K. Yamashita, H. Maeda, Chem. Lett. 33 (2004) 1178.
[12] K. Tsukagoshi, K. Fukumoto, K. Noda, R. Nakajima, K. Yamashita, H. Maeda, Anal. Chim. Acta 570 (2006) 202.
[13] M. Miyazaki, H. Nakamura, H. Maeda, Chem. Lett. (2001) 442.
[14] H. Kawazumi, A. Tashiro, K. Ogino, H. Maeda, Lab Chip 2 (2002) 8.

Liquid chromatography on an amide stationary phase with post-column derivatization and fluorimetric detection for the determination of streptomycin and dihydrostreptomycin in foods

Pilar Viñas, Nuria Balsalobre, Manuel Hernández-Córdoba [*]

Department of Analytical Chemistry, Faculty of Chemistry, University of Murcia, E-30071 Murcia, Spain

Received 19 September 2006; received in revised form 29 November 2006; accepted 4 December 2006
Available online 4 January 2007

Abstract

The separation of streptomycin and its derivative dihydrostreptomycin using ion-pair liquid chromatography is proposed. The method is based on the use of a new stationary phase based on a ligand with amide groups and the endcapping of trimethylsilyl which avoids the appearance of tailed peaks. The isocratic mobile phase consisted of a 6:94 (v/v) acetonitrile/10 mM pentanesulfonic acid (pH 3.3) mixture at a flow-rate of 1 mL min^{-1} and fluorescence detection involved a post-column derivatization reaction using β-naphthoquinone-4-sulfonate. Linearity, precision, recovery and sensitivity were satisfactory. The procedure was applied to the analysis of the aminoglycoside antibiotics in different types of foods, as honey, milk, egg and liver. Extraction was carried out by acidic hydrolysis to release protein-bound antibiotics. Detection limits in the food samples are 7.5 and 15 µg kg^{-1} for streptomycin and dihydrostreptomycin, respectively.
© 2006 Elsevier B.V. All rights reserved.

Keywords: Streptomycin; Dihydrostreptomycin; Honey; Milk; Egg; Liver; Liquid chromatography

1. Introduction

Streptomycin (STR) and dihydrostreptomycin (DHSTR) are aminoglycoside antibiotics which show activity against aerobic gram-negative bacteria. STR is produced by *Streptomyces griseus*. All aminoglycoside contained aminosugars bonded to an aminocyclitol ring by glycoside links [1]. Both drugs have been widely used for the treatment of infectious diseases in food-producing animals. However, they are potentially toxic by causing damage in vestibular and auditory functions.

The European Union (EU) has limited residues of veterinary drugs in foodstuffs of animal origin because the use of antibiotics may increase the resistance of target pathogens and must therefore be subject to strict control. Thus, the EU Maximum Residue Limits (MRLs) for STR and DHSTR established in Regulation 2377/90/EEC (1990) for food-producing animals were 500 µg kg^{-1} in muscle, skin, fat and liver, 1000 µg kg^{-1} in kidney and 200 µg kg^{-1} in milk [2]. In other type of food as

honey, contamination by STR was also found after the direct treatment of infectious problems with this antibiotic. However, no MRLs have been fixed for use with bee products in the EU. On the other hand, the antibiotic was also used for the control of bacterial infections caused by *Erwina amylovora* which affected to fruit trees during flowering. Treatment of the trees with high concentrations of STR could produce a contamination chain from pollen to nectar, bees and honey.

Different chemical and physical methods for the determination of STR and DHSTR have been developed. Official methods of analysis are turbidimetric microbiological procedures USP and Eur. Ph. and the photometric method Eur. Ph. [3,4]. The fluorescence derivatization of STR could be performed using different reagents [5]. Thus, STR and DHSTR have a guanidino group which reacts with 1,2-naphthoquinone-4-sulfonic acid (NQS) under alkaline conditions to give highly fluorescent derivatives. However, the methods which provided higher speed, specificity and precision are chromatographic procedures. Liquid chromatography (LC) is the most useful technique and different procedures have been proposed for the determination of residues of STR and DHSTR in foods [6–22] using LC with ion-pairing and spectrophotometric detection [6–8],

---

* Corresponding author. Fax: +34 96 836 4148.
  E-mail address: hcordoba@um.es (M. Hernández-Córdoba).

evaporative light scattering detection [9], fluorescent derivatization [10–19] or mass spectrometry (MS) [20–24]. Sample preparation procedures involve different extraction processes with solvent mixtures including tedious solid phase extraction steps. Reversed phase chromatography using a common C_{18} column provided non-reproducible results due to the interaction of the basic nature streptomycins with the silanol groups of the silica-based columns. The RP-AmideC_{16} column is an ideal choice for basic compounds because avoids the interaction of these compounds with the silanol groups due to the endcapping of trimethylsilyl which permitted the residual silanol groups to react more strongly.

As the instrumentation required for the LC–MS coupling has a high cost and it is not accessible for laboratory control, in the present study the determination of STR and DHSTR was optimized using LC with the ion-pairing technique and fluorescence detection using a post-column derivatization reaction with β-naphthoquinone-4-sulfonate. Isocratic elution and a stationary phase involving a ligand with amide groups (RP-AmideC_{16}) and the endcapping of trimethylsilyl were used. The extraction procedure included a simple acid hydrolysis to release antibiotics from the proteins, avoiding the need of solid-phase extraction steps. As the sample treatment is very simple, the procedure was applied to the analysis of residues of these aminoglycosides in different types of foods, including beef liver, egg, milk and honey.

2. Experimental

2.1. Apparatus

The LC system consisted of a Shimadzu FCV-10ALvp (Shimadzu, Kyoto, Japan) liquid chromatograph operating at room temperature with a flow-rate of $1 \, \text{mL min}^{-1}$. The solvents were degassed using a membrane system Shimadzu DGU-14A. The fluorescence detector was an Agilent FLD 1100 (Agilent Technologies, Waldbronn, Germany) operating at wavelengths of 356/439 nm (excitation and emission). Aliquots of $100 \, \mu\text{L}$ were injected manually using a Model 7125-075 Rheodyne injection valve (Rheodyne, Berkeley, CA, USA). The analytical column ($150 \, \text{mm} \times 4.6 \, \text{mm}$) used for the reversed-phase technique was packed with Discovery RP-AmideC_{16} with a particle size of $5 \, \mu\text{m}$ (Supelco, Bellefonte, PA, USA). A guard column packed with the same stationary phase was also used. The post-column flow injection system consisted of a Gilson Minipuls HP4 peristaltic pump (Gilson, Villiers-Bel, France), 0.3 mm i.d. PTFE tubing and various end fittings and connectors (Omnifit, Cambridge, UK). An IKA KS 130 basic vibratory stirrer (IKA, Germany), a centrifuge EBA 20 (Hettich, Germany) and a P-Selecta ultrasonic bath of variable power were used for extracting the analytes from samples.

2.2. Reagents

Acetonitrile (ACN, Romil, Loughborough, UK) was of liquid chromatographic grade. Doubly distilled water was purified using a Milli-Q system (Millipore, Bedford, MA, USA). Stock solutions ($1000 \, \mu\text{g mL}^{-1}$) of STR and DHSTR were prepared by dissolving 10 mg of the commercial products (Sigma, St. Louis, MO, U.S.A.), without previous purification, in 10 mL of water. They were kept in dark bottles at $4 \, °\text{C}$. Working standard solutions were prepared by dilution with the mobile phase on the same day of use. The derivatization solution was 0.4 mM 1,2-naphthoquinone-4-sulfonic acid (NQS, Sigma) dissolved in water. Other reagents used were sodium pentanesulfonate (Sigma), perchloric acid and sodium hydroxide (Panreac, Barcelona, Spain).

2.3. Samples

The samples of different type of honey (eucalyptus, acacia, citrus and rosemary) were obtained commercially and from several beekeepers. Other food samples were beef liver, egg and milk obtained commercially. Recovery experiments were carried out using food samples which were finely ground and spiked with a standard mixture of STR and DHSTR. Next, the samples were left to equilibrate at room temperature for at least half an hour before proceeding with the extraction procedure.

2.4. Analytical procedure

To carry out the acid hydrolysis, amounts of 2 g of the samples were weighed into polypropylene tubes and 2 mL of 0.5 M perchloric acid was added. The sample was homogenized by using a magnetic stirrer for 10 min at 800 rpm and after centrifuged at 6000 rpm for 10 min. The supernatant was recovered and adjusted to pH 7 with saturated sodium hydroxide, $500 \, \mu\text{L}$ of 0.1 M sodium pentanesulfonate solution were added and the extract was diluted to 5 mL in a calibrated flask. Aliquots were filtered through $0.45 \, \mu\text{m}$ nylon Millipore chromatographic filters and injected into the chromatograph. Separation was carried out with an isocratic mobile phase of 94:6 (v/v) 10 mM sodium pentanesulfonate (pH 3.3):acetonitrile. The flow-rate was $1 \, \text{mL min}^{-1}$. The post-column flow manifold consisted of a T-piece in which the separated drugs are mixed with the derivatization reagent, 0.4 mM NQS, and a second T-piece in which merged with a 0.3 M sodium hydroxide solution. The resulting solution was then passed through a reaction coil ($5 \, \text{m} \times 0.3 \, \text{mm}$ i.d.) at a temperature of $70 \, °\text{C}$, into the flow cell for fluorescence recording at wavelengths of 356/439 nm (excitation and emission). The NQS and sodium hydroxide solutions were pumped at $0.2 \, \text{mL min}^{-1}$ with a peristaltic pump.

3. Results and discussion

3.1. Optimization of the chromatographic conditions

The aminoglycoside are strongly polar cations and, for this reason, STR and DHSTR were separated using ion-pair reversed phase chromatography (IPC), which is adequate for analytes having high ionic character in aqueous solution. A Discovery RP-AmideC_{16} endcapped with trimethylsilyl stationary phase was appropriate for the separation of these basic compounds

because the endcapping process permits the residual silanol groups to react more strongly and prevents the interaction of analytes with the silanol groups. Most organic solvents used for reversed phase could also be used in IPC. For this separation, acetonitrile (ACN) was selected due to its adequate transmittance in the UV and its low viscosity. Consequently, mobile phase optimization was carried out using mixtures of ACN and an aqueous solution containing an ion-pair reagent at a flow-rate of 1 mL min^{-1}. A detailed study on the influence of the ACN percentage, pH and the ion-pair reagent concentration was performed.

The influence of the organic solvent was studied using mixtures of 10 mM pentanesulfonic acid (pH 3) with ACN at percentages between 5 and 20% (v/v). As expected, both retention and peak widths decreased when the proportion of organic solvent was increased, while a 20% (v/v) mixture produced elution of the two compounds at the dead time. With the aim of separating the peaks from the void time, thus avoiding matrix interferences, a mobile phase having 6% (v/v) ACN was selected. For basic samples, most ion-pairing reagents are alkylsulfonates which increased retention for cations. Similar separations could be achieved with reagents differing in their chain length, by varying the reagent concentration to provide the same charge of the stationary phase. The selection of the reagent is also conditioned by the proportion of the organic solvent in the mobile phase. Thus, a study was carried out using different ion-pairing reagents such as pentanesulfonate, heptanesulfonate and octanesulfonate, and best separation was obtained using pentanesulfonate. The retention process can be modified by varying the concentration of the ion-pairing reagent. The increase of the concentration in the mobile phase led to a higher charge in the column, up to reach saturation. Thus, the influence of the pentanesulfonate concentration in the mobile phase was studied between 2 and 30 mM at pH 3, in the presence of 6% (v/v) ACN. For basic analytes as STR and DHSTR, retention increases with the column charge up to a 30 mM concentration and, once the column was saturated with the reagent, retention of the sample decreases because the sodium ions compete with the ion analytes by retention on the column. Consequently, a 10 mM pentanesulfonate concentration was selected as optimal to obtain good separation of the antibiotic peaks. Higher concentrations led to very large analysis times. The variation of the mobile phase pH produces an important effect on retention and peaks overlapping. This influence was studied using several pentanesulfonate solutions at different pH values in the 3–5 range. For low pH values the basic analytes are completely ionized and best separation between STR and DHSTR was achieved at pH 3.3, which was selected. Higher values of pH led to increased retention of the analytes.

The chromatographic profile obtained by isocratic elution with the Discovery RP-AmideC$_{16}$ column and a mobile phase of 6:94 (v/v) acetonitrile:10 mM pentanesulfonate (pH 3.3) at a flow-rate of 1 mL min^{-1} shows that the elution order and the retention characteristics for the antibiotics, expressed as retention time (t_R) and retention factor (k), were: 1, STR ($t_R = 16.4$; $k = 5.6$) and 2, DHSTR ($t_R = 18.2$; $k = 6.4$). Values for the separa-

tion factor (α) and resolution (R_S) were 1.1 and 1.5, respectively. The peaks are sharp and non-tailed when using the AmideC$_{16}$ column endcapped with trimethylsilyl.

3.2. Optimization of the post-column fluorescence derivatization

Derivatization of streptomycins was carried out by a post-column reaction using NQS in alkaline conditions to give derivatives, which have high fluorescent yields. The experimental parameters were optimized to obtain maximum fluorescence intensity when injecting 100 ng mL^{-1} of STR and DHSTR, ensuring at the same time that the separation of the compounds was not modified. Fig. 1 shows the results obtained. When varying the flow-rate of the peristaltic pump between 0.1 and 0.5 mL min^{-1}, fluorescence increased up to 0.2 mL min^{-1} and then remained constant, this value being chosen as optimal. The length of the reactor was varied in the 0.5–10 m range (Fig. 1A) and the fluorescence strongly increased up to 4.5 m. Reactor lengths between 4.5 and 6 m slightly increased the signal, which was maintained constant for higher lengths. Thus,
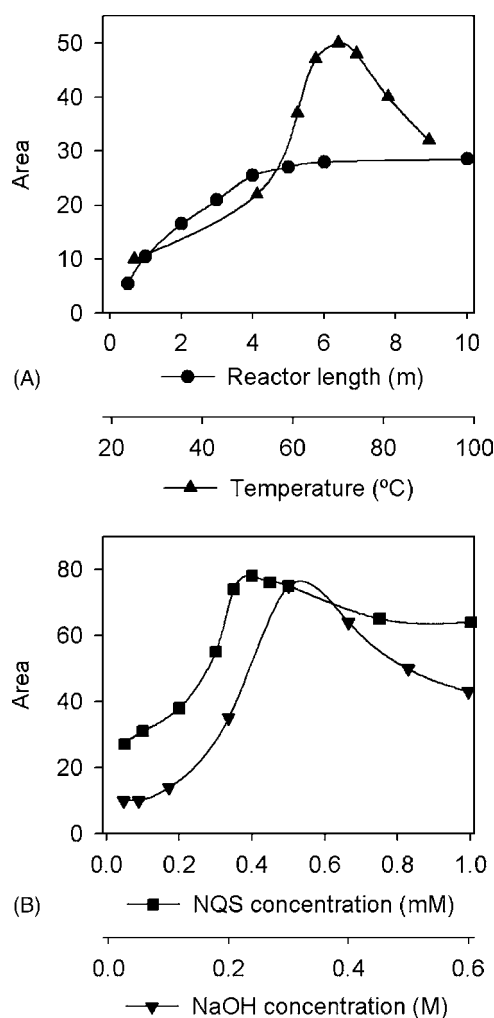

Fig. 1. Influence of the post-column derivatization conditions (reactor length and temperature (A), derivatizing reagent concentration and sodium hydroxide concentration (B)) on the fluorescence signal. STR injected, 100 ng mL^{-1}.

a 5 m reactor length was selected as a compromise between sensitivity and good resolution of the chromatographic peaks. Similar results were obtained for DHSTR. The influence of the reactor temperature was studied in the 25–90 °C range, using a thermostated water bath, and Fig. 1A shows as fluorescence increased for higher temperatures up to 70 °C and then slowly decreased, because of the fluorescent derivative decomposition. Consequently, an optimal temperature of 70 °C was selected. Fig. 1B shows the influence of the derivatizing reagent (NQS) concentration between 0.05 and 1 mM. Maximum sensitivity was obtained at a 0.4 mM concentration, which was therefore selected. The influence of the sodium hydroxide concentration in the 0.025–0.6 M range is shown in Fig. 1B and demonstrated that maximum fluorescence was obtained for a 0.3 M concentration. Again, similar results were obtained for DHSTR.

3.3. Calibration, detection limits and repeatability

Calibration graphs were performed by the external standard technique following linear regression analysis by plotting concentration (ng mL^{-1}) against peak area. Table 1 shows the equations obtained for the calibration graphs and the regression coefficients. The repeatability of the method was calculated using the average relative standard deviation (R.S.D.) for 10 replicate injections of the same sample at 100 ng mL^{-1} level. The detection limits were calculated on the basis of 3σ (σ being the residual standard deviation of the intercept) and the quantitation limits on the basis of 10σ, using the regression lines for the standards. Values are also given in Table 1.

3.4. Analysis of food samples: recovery studies

The extraction of STR and DHSTR from foods involved acid hydrolysis to release the protein-bound antibiotics. To precipitate proteins, perchloric acid and trichloroacetic acid are usually used, and when we tested different concentrations of both acids, the best results were obtained using 0.5 M perchloric acid. The optimal sample homogenization procedure was then checked using an ultrasonic bath, an ultrasonic processor, an automatic vibratory stirrer and manual stirring. The results obtained show that recovery percentages were similar for the different homogenization techniques tested. Consequently, the automatic stirring method was chosen as it was easy to use. The efficiency of the extraction method was confirmed by performing recovery studies. First, the stability of the drugs was studied under these

Table 2
Recovery of streptomycins from food samples

Food sample	STR		DHSTR	
	Recovery (%)	R.S.D. (%)	Recovery (%)	R.S.D. (%)
Milk	97.1	1.8	92.5	2.1
Egg	101.4	2.9	99.4	3.2
Beef liver	95.7	4.4	90.1	5.7
Eucalyptus honey	98.2	0.9	98.3	2.0
Acacia honey	97.8	1.1	95.7	1.6
Citrus honey	96.9	2.5	100.2	4.8
Rosemary honey	98.8	1.3	95.1	4.1

conditions and no degradation occurred during the extraction process. The samples were spiked with the two streptomycins at the beginning of the extraction procedure at 100 μg kg^{-1} for the food samples (these values being below the maximum limits, in each type of sample). Then, spiked samples were treated as described in the experimental procedure and analyzed. Recovery data and repeatability results are shown in Table 2. The average values (mean ± S.D.) for the recovery percentages in the food samples analyzed ($n = 7$) were: STR, 98 ± 1.8 and DHSTR, 96 ± 3.7. These results demonstrate that recovery values were satisfactory.
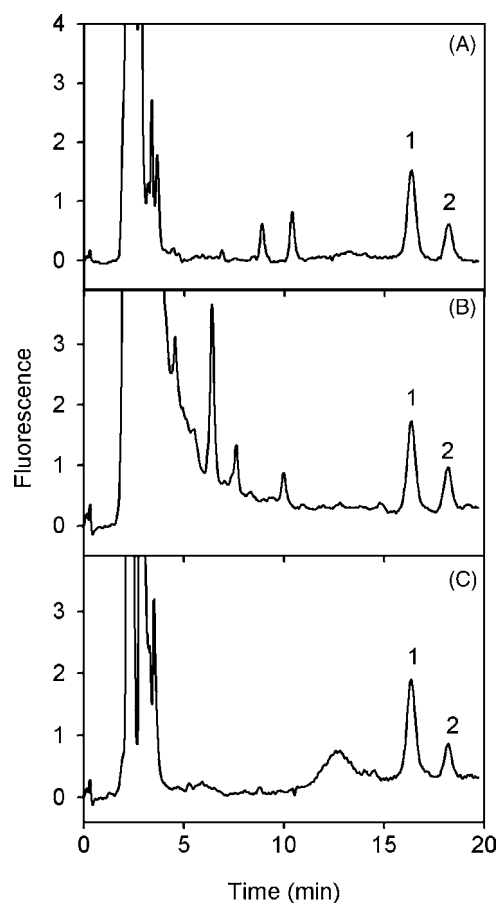

Fig. 2. Elution profiles obtained for milk (A), beef liver (B) and honey (C) samples spiked with 100 ng g^{-1} of both STR and DHSTR. Flow-rate, 1 mL min^{-1}; injected sample, 100 μL. Peaks correspond to: (1) STR and (2) DHSTR.

Table 1
Calibration characteristics of streptomycins

Parameter	STR	DHSTR
Intercept	2.7 ± 0.7	1.5 ± 0.3
Slope (mL ng^{-1})	0.73 ± 0.01	0.19 ± 0.02
Correlation coefficient	0.9997	0.9993
Linearity (ng mL^{-1})	10–200	25–275
Detection limit (ng mL^{-1})	3	6
Quantitation limit (ng mL^{-1})	9	19
Repeatability, R.S.D. (%)	2.8	3.7

Fig. 2 shows typical chromatographic profiles obtained by spiking milk (A), beef liver (B) and honey (C) samples. Similar chromatograms were obtained for the other samples. The profiles demonstrated the absence of interfering peaks for streptomycin quantitation. The standard additions method was used to investigate the possibility of matrix interference. Slopes of the standard additions calibration graphs for the food samples were similar to those of aqueous standards, confirming that the matrix did not interfere and that calibration can be carried out using aqueous standards. The antibiotics STR and DHSTR were not present above their respective detection limits in any milk, egg, beef liver or honey analyzed sample. Detection limits in the food samples were 7.5 and 15 ng g^{-1} for STR and DHSTR, respectively.

The chromatographic peaks were first identified by comparing the retention data obtained for the STR and DHSTR standards and the different food samples spiked with the standards under identical conditions. The average values (mean $\pm$ S.D.) for the retention times in the different samples ($n = 8$) were: STR, 16.4 $\pm$ 0.23 and DHSTR, 18.2 $\pm$ 0.19. These values indicate very good agreement between the retention data of streptomycins in the different samples. The peaks were identified again using the fluorescence detector to continuously measure the spectrum while the solute passed through the flow-cell, thus confirming the identity and the purity of the peaks. Good agreement was found between the fluorescence spectra of the different peaks obtained for the standards and the spiked samples.

4. Conclusion

A rapid method for the analysis of residual streptomycin and dihydrostreptomycin is proposed. The use of a fluorescence detector avoids the need for a mass spectrometer which is expensive and beyond the means of many laboratories. The procedure used ion-pairing reversed phase liquid chromatography with isocratic elution and a Discovery Amide-C$_{16}$ column with the endcapping of trimethylsilyl to prevent the appearance of tailing peaks. Sample preparation involved acid hydrolysis and was very simple, satisfactory recovery results being achieved with no need for solid-phase extraction steps. Detection limits were in the low ng g^{-1} range. The method could be applied to residue controls and screening tests as it satisfies the maximum limits for the concentration of streptomycin drugs in foods.

References

[1] G.A. Goodman, L.S. Goodman, T.W. Rall, F. Murad (Eds.), The Pharmacological Basis of Therapeutics, seventh ed., Mac-Millan, New York, 1985.
[2] Regulation 2377/90/EC, 1990.
[3] Code of Federal Regulations, Title 21, Parts 1416.108, 141.102, 441.70a (b)(2), 444.270a, Food and Drugs, Food and Drug Administration, Washington, DC, 1974.
[4] European Pharmacopoeia, vol. II, Maisonneuve S.A., Francia, p. 366, 1971.
[5] T. Toyo'oka (Ed.), Modern Derivatization Method for Separation Sciences, Wiley, New York, 1999.
[6] T.J. Whall, J. Chromatogr. 219 (1981) 89.
[7] E. Adams, E. Roets, J. Hoogmartens, J. Pharm. Biomed. Anal. 21 (1999) 715.
[8] E. Adams, M. Rafiee, E. Roets, J. Hoogmartens, J. Pharm. Biomed. Anal. 24 (2000) 219.
[9] A.K. Sarri, N.C. Megoulas, M.A. Koupparis, J. Chromatogr. A 1122 (2006) 275.
[10] G.C. Gerhardt, C.D.C. Salisbury, J.D. McNeil, J. Assoc. Off. Anal. Chem. Int. 77 (1994) 334.
[11] G.C. Gerhardt, C.D.C. Salisbury, J.D. McNeil, J. Assoc. Off. Anal. Chem. Int. 77 (1994) 765.
[12] V. Hormazabal, M. Yndestad, J. Liq. Chromatogr. Relat. Technol. 18 (1995) 2695.
[13] V. Hormazabal, M. Yndestad, J. Liq. Chromatogr. Relat. Technol. 20 (1997) 2259.
[14] H. Abbasi, K.E. Hellenäs, Analyst 123 (1998) 2725.
[15] G. Suhren, K. Knappstein, Analyst 123 (1998) 2797.
[16] P. Edder, A. Cominoli, C. Corvi, Mitt. Geb. Lebens. Hyg. 89 (1998) 369.
[17] P. Edder, A. Cominoli, C. Corvi, J. Chromatogr. A 830 (1999) 345.
[18] D. Guggisberg, C. Aeppli, H. Koch, Mitt. Geb. Lebens. Hyg. 91 (2000) 539.
[19] G.F. Pang, J.J. Zhang, Y.Z. Cao, C.L. Fan, X.M. Lin, Z.Y. Li, G.Q. Jia, J. Assoc. Off. Anal. Chem. Int. 87 (2004) 39.
[20] M. Horie, T. Yoshida, Y. Kikuchi, H. Nakazawa, Shok. Eisei. Zass. 42 (2001) 374.
[21] A. Kaufmann, P. Butcher, P. Koelbener, Rapid Comm. Mass Spectrom. 22 (2003) 2575.
[22] M. Horie, H. Saito, T. Natori, J. Nagata, H. Nakazawa, J. Liq. Chromatogr. Relat. Technol. 27 (2004) 863.
[23] M. van Bruijnsvoort, S.J.M. Ottink, K.M. Jonker, E. de Boer, J. Chromatogr. A 1058 (2004) 137.
[24] S. Bogialli, R. Curini, A. di Corcia, A. Lagana, M. Mele, M. Nazzari, J. Chromatogr. A 1067 (2005) 93.

Synthesis and LPG sensing properties of nano-sized cadmium oxide

R.B. Waghulade [a], P.P. Patil [a,*], Renu Pasricha [b]

[a] *Department of Physics, North Maharashtra University, Jalgaon 425 001, Maharashtra, India*
[b] *Center for Materials Characterization, National Chemical Laboratory, Pashan, Pune 411 008, Maharashtra, India*

Abstract

This paper reports the synthesis and liquid petroleum gas (LPG) sensing properties of nano-sized cadmium oxide (CdO). The nano-sized CdO powder was successfully synthesized by using a chemical co-precipitation method using cadmium acetate and the ammonium hydroxide, as starting materials and water as a carrier. The resulting nano-sized powder was characterized by X-ray diffraction (XRD) measurements and the transmission electron microscopy (TEM). The LPG sensing properties of the synthesized nano-sized CdO were investigated at different operating temperatures and LPG concentrations. It was found that the calcination temperature and the operating temperature significantly affect the sensitivity of the nano-sized CdO powder to the LPG. The sensitivity is found to be maximum when the calcination temperature was 400 °C. The sensitivity to 75 ppm of LPG is maximum at an operating temperature 450 °C and it was found to be ~341%. The response and recovery times were found to be nearly 3–5 s and 8–10 s, respectively. The synthesized nano-sized CdO powder is able to detect up to 25 ppm for LPG with reasonable sensitivity at an operating temperature 450 °C and it can be reliably used to monitor the concentration of LPG over the range (25–75 ppm). The experimental results of the LPG sensing studies reveal that the nano-sized CdO powder synthesized by a simple co-precipitation method is a suitable material for the fabrication of the LPG sensor.
© 2006 Elsevier B.V. All rights reserved.

Keywords: Nano-sized CdO; Chemical co-precipitation; LPG; Gas sensor

1. Introduction

In recent years, the synthesis of nano-crystalline oxide materials has been a focal point of research and developmental activities in the area of nano-materials owing to the quest for their various technological applications [1–10]. Semiconducting metal oxides such as SnO_2 [11], ZnO [12], WO_3 [13] and Fe_2O_3 [14] have been widely used as gas sensing materials for the detection of inflammable and toxic gases. The sensor performance is strongly dependent on the microstructural features such as crystallite size, grain boundary characteristics and thermal stability [15]. Several approaches have been explored to fabricate the sensors with an improved performance, which include nano-sized crystallites [16,17], solid solution [18,19] and additives or surface functionalization [20,21].

Out of these approaches, the successful synthesis of nano-crystalline semiconducting oxides with high surface area for gas adsorption opens up a new paradigm for sensor materials. Several research groups have systematically studied the synthesis of nano-crystalline metal oxides and their nanocomposites and investigated their gas sensing properties [1–10]. For example, more recently, Aifan et al. [4] prepared the nano-crystalline SnO_2–In_2O_3 composites using a chemically controlled co-precipitation method and studied their sensing properties for the detection of CO and NO_2. They observed that the preparation parameters are crucial in controlling the grain size and crystallinity of the nano-crystalline SnO_2–In_2O_3 composites. These nanocomposites exhibit high sensitivity and selectivity for the detection of CO and NO_2. Further, it was found that the nanocomposite composition, calcination temperature and operating temperature significantly affects the sensitivity and selectivity.

LPG is a combustible gas and it is widely used as a fuel for domestic heating and industrial use. Although it is one of the extensively used gases, it is hazardous. Hence, it is crucial to detect it in its early stages of the leakage and to perform the active suppression [22]. In order to accomplish this, more attention has been paid to develop the gas sensors for the detection

---

* Corresponding author. Tel.: +91 257 2258411; fax: +91 257 2258403.
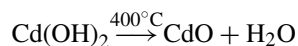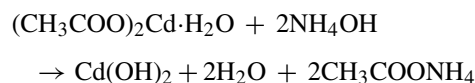*E-mail address:* pnmu@yahoo.co.in (P.P. Patil).

of LPG, using several sensing materials such as Ag_2O doped γ-Fe_2O_3, Pt modified Al_2O_3 [23], $ZnGa_2O_4$ [24], Sb doped SnO_2 [25], $MgFe_2O_4$, $CdFe_2O_4$ [26] etc. Recently, the thick films of the mixed oxide of WO_3, TiO_2, In_2O_3 and SnO_2 and doped with nobel metals Au, Pd and Pt were investigated as sensing materials by Chaudhari et al. [3] for the detection of LPG. Srivastava et al. [2] studied the influence of microwave irradiation on SnO_2 powder prepared by precipitation method using water as a medium. They observed that the microwave irradiation results into the increase in LPG sensitivity.

CdO is degenerate, n-type semiconductor and it has interesting properties like large band gap, low electrical resistivity, high transmission in the visible region etc; which make it useful for a wide range of applications such as photodiodes [27], phototransistors [28], photovoltaic cell [29], transparent electrodes [30], liquid crystal displays, IR reflectors and anti-reflection coatings [31]. To the best of our knowledge, there are no reports in the literature dealing with the use of CdO as sensing material for the fabrication of the gas sensors. However, it was reported that the CdO can be used as the dopant to improve the sensor performance. Xiangfeng et al. [32] studied the influence of CdO dopant on the gas sensing properties of zinc ferrite ($ZnFe_2O_4$) to C_2H_2OH. It was shown that the CdO improves the sensitivity, selectivity, response and recovery times of $ZnFe_2O_4$.

With the objective to search for new sensing materials for the detection of LPG, we have made an attempt to synthesize nano-sized CdO by a simple chemical co-precipitation method and to investigate the LPG response of the resultant nano-sized CdO.

2. Experimental

The nano-sized powder of CdO was prepared by a simple co-precipitation method. In this method, a diluted ammonium hydroxide solution was used to hydrolyze the metal salt precursors at a certain solution pH value. Fig. 1 is a schematic representation of the synthesis procedure. In this work, the aqueous solution of 0.5 M cadmium acetate was prepared in double distilled water. To this solution the ammonium hydroxide was added drop-wise under stirring until the final solution pH value of about 8 was achieved. The resulting precipitate was filtered and washed three to four times using double distilled water to remove impurities. The hydroxide, thus formed was dried at $100\,^\circ$C and grinded into a powder, which is the precursor. The precursor was calcined in air at different temperatures of $300\,^\circ$C, $400\,^\circ$C, $500\,^\circ$C and $600\,^\circ$C for 2 h to produce nanocrystalline powders with different grain size. During the calcinations, the as-prepared powder was decomposed as follows:

$$(CH_3COO)_2Cd{\cdot}H_2O + 2NH_4OH$$

$$\rightarrow Cd(OH)_2 + 2H_2O + 2CH_3COONH_4$$

$$Cd(OH)_2 \xrightarrow{400\,^\circ C} CdO + H_2O$$

The structure of the calcined powder was investigated by using X-ray diffraction (XRD) technique. The X-ray diffraction patterns were recorded with a Rigaku diffractometer (Miniflex Model, Rigaku, Japan) having Cu K_α ($\lambda = 0.1542$ nm). The crys-
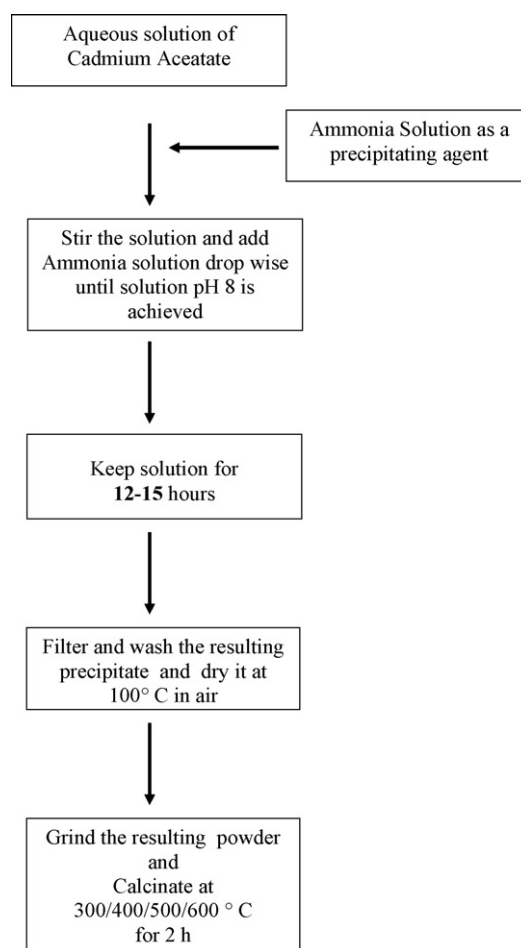

Fig. 1. Schematic diagram of the synthesis procedure for nano-sized CdO.

talline size was estimated from the broadening of CdO (111) diffraction peak ($2\theta = 32.2^\circ$) using Debye-Scherrer's formula. The transmission electron microscopy (TEM) was used to determine the particle size and the morphology of the nano-sized powder with JEOL 1200 EX.

The nanocrystalline CdO powder was pressed into pellets under a pressure of 15 MPa and the ohmic contacts were made with the help of silver paste to form the sensing element. The gas sensing studies were carried out on these sensing elements in a static gas chamber to sense LPG in air ambient. The sensing element was kept directly on a heater in the gas chamber and the temperature was varied from 150 to $500\,^\circ$C. The temperature of the sensing element was monitored by chromel-alumel thermocouple placed in contact with the sensor. The known volume of the LPG was introduced into the gas chamber pre-filled with air and it was maintained at atmospheric pressure. The electrical resistance of the sensing element was measured before and after exposure to LPG using a sensitive digital multi meter (METRAVI 603). The sensitivity (S) of the sensing element is defined as:

$$S(\%) = \frac{R_g - R_a}{R_a} \times 100$$

where R_a and R_g are the resistance values of the sensor element in air and in the presence of LPG.

3. Results and discussion

3.1. Synthesis of nano-sized CdO

The XRD pattern of the calcinied powder at 400 °C for 2 h is shown in Fig. 2. It indicates the diffraction peaks at 2θ values of 32.2°, 37.4° and 54.2°, which are attributed to the formation of CdO. The crystal structure is cubic face centered cubic and all the d-line patterns match with reported values. The crystallite size was calculated by using the Scherrer formula:

$$t = \frac{k\lambda}{B\cos\theta}$$

where t is the average size of the crystallite, assuming that the grains are spherical, k is 0.9, λ is the wavelength of X-ray radiation, B is the peak full width at half maximum (FWHM) and θ is the angle of diffraction. The crystalline size of the powder calcinied at 400 °C is found to be ~11.20 nm.

The TEM micrograph of the powder calcinied at 400 °C along with the electron diffraction pattern is shown in Fig. 3. The TEM micrograph shows clearly that the particle size of powder calcinied at 400 °C is ~12 nm. This result is in well agreement with the crystallite size calculated using the XRD data. The ED pattern gives the d spacing consistent with those obtained from XRD data.

In order to study the effect of the calcination temperature on the crystallite size, the as-prepared powder was calcinied at 300, 400, 500 and 600 °C for 2 h in air. The variation of the crystallite size on the calcinations temperature is shown in Fig. 4. The crystallite size is found to be smallest when the as-prepared powder was calcinied at 400 °C for 2 h. However, the crystallite size increases with the increase in the calcinations temperature after 400 °C. This observation is consistent with crystallite sizes obtained from XRD patterns (not shown here). This observation may be attributed to the particles growth and a lot small particles aggregation after being calcinied at higher temperatures. Indeed, the TEM micrograph of the powder calcinied at 600 °C [Fig. 5] clearly shows the aggregation of small particles.

3.2. LPG sensing properties of synthesized nano-sized CdO

In this study, the LPG sensing properties of the nano-sized CdO synthesized by chemical co-precipitation method were investigated. For comparison, the LPG sensing properties of the commercially available CdO were also studied under identical experimental conditions. The appropriate calcination temperature is an important parameter for gas sensing materials and in

Fig. 3. TEM micrograph with electron diffraction pattern of nano-sized CdO calcined at 400 °C for 2 h.

Fig. 2. XRD pattern of nano-sized CdO calcined at 400 °C for 2 h.
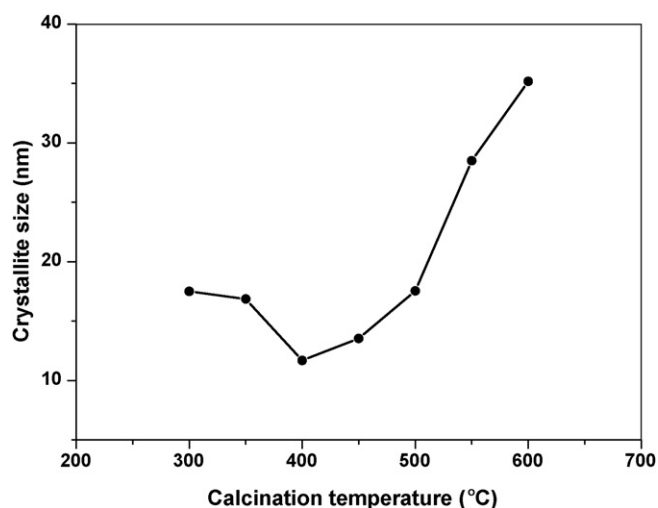

Fig. 4. Variation of the crystallite size of nano-sized CdO on calcination temperature.

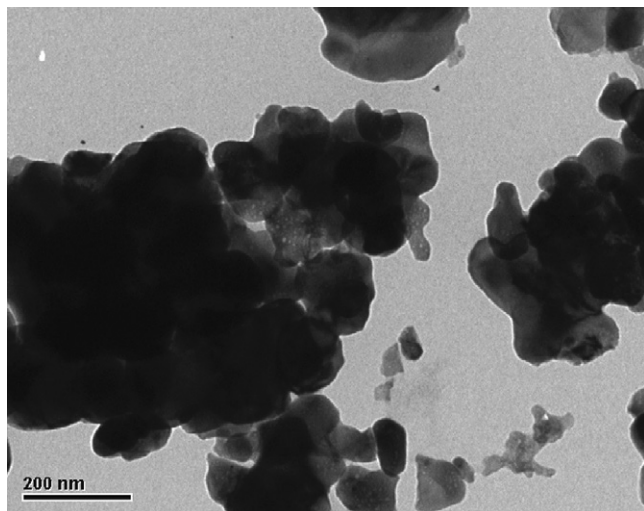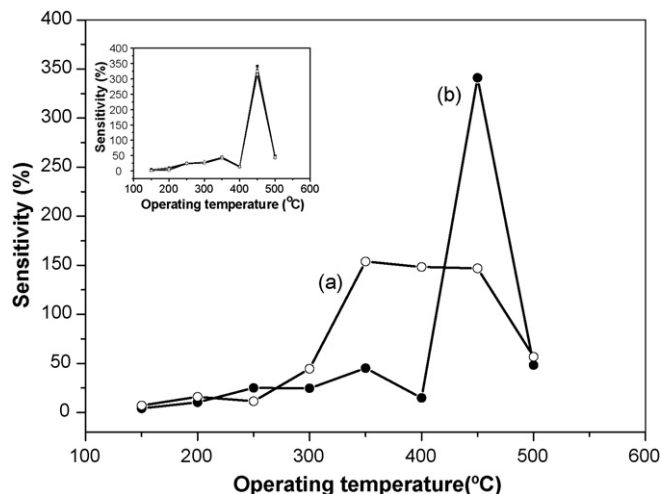Fig. 5. TEM micrograph of nano-sized CdO calcined at 600 °C for 2 h.

Fig. 7. Effect of operating temperature on the sensitivity of (a) commercially available CdO and (b) nano-sized CdO to 75 ppm of LPG. Inset presents the replicates of the measurements for the sensitivity as a function of operating temperature.

designing of sensors. The sensing materials have to be calcined at appropriate temperatures to achieve crystallization and structural evolution. A sufficient degree of crystallinity is required to attain the desired electronic properties necessary for gas sensor application. The dependence of the sensitivity of the synthesized nano-sized CdO to 75 ppm of LPG at operating temperature of 450 °C on the calcination temperature is shown in Fig. 6. It is observed that first the sensitivity increases from 164.58% to 341% as the calcination temperature is raised from 300 to 400 °C and then decreases with the further increase in the calcination temperature. The sensitivity is found to be maximum when the calcination temperature was 400 °C, which is the optimal calcination temperature. The calcination in air renders more oxygen vacancy generation, which enhances the gas sensitivity. However, after the calcination temperature of 400 °C, the crystallite size of the calcinied powders becomes larger due to agglomeration and therefore the specific surface area decreased. This leads to the decrease of gas sensitivity and as a result 400 °C is found to be the optimal calcination temperature.

It is quite apparent that the operating temperature plays a vital role in determining the sensitivity of the CdO. Fig. 7 shows the effect of the operating temperature on the sensitivity of nano-sized CdO powder and the commercially available CdO towards LPG. It is obvious from Fig. 7 that the nano-sized CdO powder exhibits an excellent sensitivity to LPG than a commercially available CdO. When the commercially available CdO powder was used, the maximum sensitivity to 75 ppm of LPG occurs at 350 °C and it remains fairly constant at ~154% between the operating temperatures 350 to 450 °C.

It is clearly observed that the sensitivity of the synthesized nano-sized CdO powder to 75 ppm of LPG is considerably lower for the operating temperature less than 400 °C. The sensitivity increases from 14.8% to 341% as the operating temperature is raised from 400 to 450 °C and then decreases to 48.29% when the temperature is further raised to 500 °C. Thus, the sensitivity to 75 ppm of LPG is maximum at an operating temperature of 450 °C and it is found to be ~341%. The response time of the nano-sized CdO powder to LPG was nearly 3–5 s and the recovery time was found to be 8–10 s. These results indicate that the nano-sized CdO powder synthesized by a simple co-precipitation method is a suitable material for the fabrication of the LPG sensor. A number of experiments have been carried out to measure the sensitivity as a function of the operating temperature. All the time the sensitivity of the sensor element has approximately constant (standard deviation ~0.022) values, indicating the repeatability of the sensor.

The LPG sensing mechanism is a complex process and it is believed that it proceeds through several intermediate steps which are not yet understood. It is based on the changes in the resistance of the CdO which is controlled by the LPG species and the amount of the chemisorbed oxygen on the surface [33–40]. It is known that a certain amount of oxygen from air is adsorbed on the surface of the CdO. The CdO interacts with the oxygen, by transferring the electrons from the conduction band to adsorbed oxygen atoms, resulting into the formation of ionic species such

Fig. 6. Dependence of sensitivity on the calcination temperature of the nano-sized CdO to 75 ppm of LPG at operating temperature of 450 °C.

as O_2^- or O^-. The reaction kinematics may be explained by the following reactions [33–40]:

$$O_2(gas) \Leftrightarrow O_2(absorbed)$$

$$O_2(absorbed) + e^- \Leftrightarrow O_2^-$$

$$O_2^- + e^- \Leftrightarrow 2O^-$$
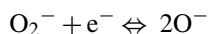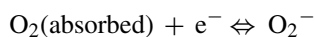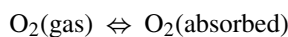
The electron transfer from the conduction band to the chemisorbed oxygen results into the decrease in the electron concentration. As a consequence, an increase in the resistance of the CdO is observed.

It is well known that the LPG consists of CH_4, C_3H_8 and C_4H_{10} etc. In these molecules the reducing hydrogen species are bound to carbon therefore the LPG dissociates less easily into the reactive reducing components on the CdO surface. When the nano-sized CdO is exposed to reducing gas like LPG, the LPG reacts with the chemisorbed oxygen thereby releasing an electron back to the conduction band which decreases the resistance of the CdO [33–40]. The overall reaction of the LPG with the chemisorbed oxygen can be explained as follows:

$$C_nH_{2n+2} + 2O^- \rightarrow H_2O + C_nH_{2n}O^- + e^-$$
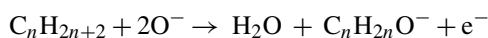
When the nano-sized CdO is heated at a temperature of 150–400 °C, the reaction products do not desorb from the film surface. Nevertheless, they cover the sensing sites on the surface of the film which prevents the further reaction of the LPG with chemisorbed oxygen. Subsequently, no appreciable change in the resistance of the film is observed.

At temperature 450 °C, the reaction products may get desorbed immediately after their formation providing the opportunity for new gas species to react with the sensing sites on the film surface. Thus, the LPG reacts most effectively with chemisorbed oxygen at such particular temperature, which results in the significant decrease in the resistance of the film. Therefore, the maximum sensitivity of the nano-sized CdO towards LPG is expected at such particular temperature.

At higher temperatures (>450 °C), the amount of the adsorbed oxygen is less and therefore, a lesser amount of ionic species is formed. Therefore, in presence of the LPG, the probability of the reduction reaction of the gas with chemisorbed oxygen is less, which results into a very small change in resistance of the film at higher temperatures. Therefore, the nano-sized CdO operates as a sensing element to the LPG only within a specific temperature window. In the present case, the optimum operating temperature for the nano-sized CdO is 450 °C at which the sensor sensitivity attains its maximum value.

The dependence of the sensitivity of the synthesized nano-sized CdO powder on the LPG concentration at an operating temperature 450 °C is shown in Fig. 8. It is observed that the sensitivity increases linearly as the LPG concentration increases from 25 to 75 ppm and then decreases with further increase in the LPG concentration. The linear relationship between the sensitivity and the LPG concentration at low concentrations may be attributed to the availability of sufficient number of sensing sites on the film to act upon the LPG. The low gas concentra-
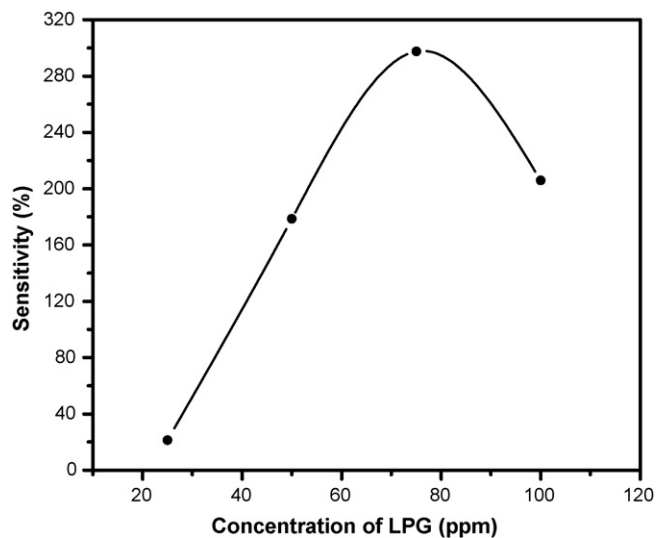

Fig. 8. Dependence of sensitivity of nano-sized CdO on the LPG concentration at operating temperature of 450 °C.

tion implies a lower surface coverage of gas molecules, resulting into lower surface reaction between the surface adsorbed oxygen species and the gas molecules. The increase in the gas concentration increases the surface reaction due to a large surface coverage. Further increase in the surface reaction will be gradual when saturation of the surface coverage of gas molecules is reached. Thus, the maximum sensitivity was obtained at an operating temperature of 450 °C for the exposure of 75 ppm of LPG. The nanosized CdO is able to detect up to 25 ppm for LPG with reasonable sensitivity at an operating temperature 450 °C. The linearity of the sensitivity in the low LPG concentration range (25–75 ppm) suggests that the nano-sized CdO can be reliably used to monitor the concentration of LPG over this range.

4. Conclusions

The nano-sized CdO powder was synthesized by a simple chemical co-precipitation method and the LPG sensing properties of the synthesized nano-sized CdO were investigated. The following main findings resulted from the present investigation:

- We have successfully synthesized the nano-sized CdO powder at low cost by using a chemical co-precipitation method using cadmium acetate and the ammonium hydroxide, as starting materials and water as a carrier. The resulting powder was characterized by XRD measurements and TEM.
- The crystallite size is found to be smallest when the as-prepared powder was calcinied at 400 °C for 2 h. However, the crystallite size increases with the increase in the calcination temperatures above 400 °C.
- The calcination temperature and the operating temperature significantly affect the sensitivity of the synthesized nano-sized CdO powder to the LPG.
- The sensitivity is found to be maximum when the calcination temperature was 400 °C, which is the optimal calcination temperature.

- The synthesized nano-sized CdO powder is able to detect up to 25 ppm for LPG with reasonable sensitivity at an operating temperature 450 °C. Further, it was shown that the nano-sized CdO can be reliably used to monitor the concentration of LPG over the range (25–75 ppm).
- The sensitivity to 75 ppm of LPG is maximum at an operating temperature 450 °C and it is found to be ~341%. The response time was nearly 3–5 s and the recovery time was found to be 8–10 s.
- The results of the LPG sensing studies reveal that the nano-sized CdO powder synthesized by a simple co-precipitation method is a suitable material for the fabrication of the LPG sensor.

Acknowledgement

References

[1] G.N. Chaudhari, A.M. Bende, A.B. Bodade, S.S. Patil, V.S. Sapkal, Sens. Actuators B 115 (2006) 297.
[2] A. Srivastava, K. Jain, A.K. Rashmi, S.T. Srivastava, Lakshmikumar, Mater. Chem. Phys. 97 (2006) 85.
[3] G.N. Chaudhari, A.M. Bende, A.B. Bodade, S.S. Patil, S.V. Manorama, Talanta 69 (2006) 187.
[4] C. Aifan, H. Xiaodong, T. Zhangfa, B. Shouli, L. Ruixian, L.C. Chiun, Sens. Actuators B 115 (2006) 316.
[5] J. Gong, Q. Chen, M.R. Lian, N.C. Liu, R.G. Stevenson, F. Adami, Sens. Actuators B 114 (2006) 32.
[6] H. Tang, M. Yan, H. Zhang, S. Li, X. Ma, M. Wang, D. Yang, Sens. Actuators B 114 (2006) 910.
[7] T. Gao, T.H. Wang, Appl. Phys. A 80 (2005) 1451.
[8] V. Khatko, E. Llobet, X. Vilanova, J. Brezmes, J. Hubalek, K. Malysz, S. Correig, Sens. Actuators B 111 (2005) 45.
[9] D.S. Torkhov, A.A. Burukhin, B.R. Churagulov, M.N. Rumyantseva, V.D. Maksimov, Inorg. Mater. 39 (11) (2003) 1158.
[10] A. Chiorino, G. Ghiotti, F. Prinetto, M.C. Carotta, C. Malagu, G. Martinelli, Sens. Actuators B 78 (2001) 89.
[11] Y. Sun, X. Huang, J. Liu, Sensors 4 (2004) 95.
[12] A.P. Chartterjee, P. Mitra, A.K. Mukhopadhyay, J. Mater. Sci. 34 (1999) 4225.
[13] M. Stankova, X. Vilanova, E. Llobet, J. Calderer, M. Vinaixa, I. Gracia, C. Cane, X. Correig, Thin Solid Films 500 (2006) 302.
[14] E.T. Lee, G.E. Jang, C.K. Kim, D.H. Yoon, Sens. Actuators B 77 (2001) 221.
[15] M. Egashira, Y. Shimizu, in: N. Yamazoe (Ed.), Chemical Sensors Technology, 3, Kodansha, Tokyo, 1991, pp. 1–17.
[16] N.S. Baik, G. Sakai, N. Miura, N. Yamazoe, Sens. Actuators B 63 (2000) 74.
[17] S. Shukla, S. Patil, S.C. Kuiry, Z. Rahman, T. Du, L. Ludwig, C. Parish, S. Seal, Sens. Actuators B 96 (2003) 343.
[18] U.S. Choi, K.G. Sakai, N. Shimanoe, Yamazoe, Sens. Actuators B 98 (2004) 166.
[19] K. Zakrzewska, Thin Solid Films 391 (2001) 229.
[20] V.A. Chaudhary, I.S. Mulla, K. Vijayamohanan, Sens. Actuators B 55 (1999) 154.
[21] O.V. Safonova, G. Delabouglise, B. Chenevier, A.M. Gaskov, M. Labeau, Mater. Sci. Eng. C 21 (2002) 105.
[22] L.D. Feng, X.J. Huang, Y.K. Choi, Microchim. Acta (2006).
[23] J.Z. Wang, M.S. Tong, X.Q. Wang, X.Q. Ma, Y. Liu, D.L. Wu, J.K. Gao, D.S. Du, Sens. Actuators B 84 (2002) 95.
[24] L. Satyanarayana, C.V. Gopal Reddy, S.V. Manorama, V.J. Rao, Sens. Actuators B 46 (1998) 1.
[25] N.S. Subramanian, B. Santhi, T. Sornakurnar, G.K. Subbaraj, C. Vinoth, G. Murugan, Ionics 10 (2004) 273.
[26] N.S. Chen, X.J. Yang, X.J. Liu, E.S. Huang, Sens. Actuators B 66 (2000) 178.
[27] R. Kondo, H. Okhimura, Y. Sakai, Jpn. J. Appl. Phys. 10 (1971) 176.
[28] L.M. Su, N. Grote, F. Schmitt, Electron Lett. 20 (1984) 717.
[29] C.H. Champness, K. Ghoneim, J.K. Chen, Can. J. Phys. 63 (1985) 767.
[30] F.A. Benko, F.P. Koffyberg, Solid State Commun. 57 (1986) 901.
[31] I.M. Ocampo, A.M. Ferandez, P.J. Sabastian, Semicond. Sci. Technol. 8 (1993) 750.
[32] C. Xiangfeng, L. Xingqin, M. Guangyao, Sens. Actuators B 65 (2000) 64.
[33] A.R. Phani, S. Manorma, V.J. Rao, Mat. Chem. Phy. 58 (1999) 101.
[34] J. Wang, M. Tong, X. Wang, Y. Ma, D. Liu, J. Wu, D. Gao, G. Du, Sens. Actuators B 4201 (2002) 1.
[35] M. Regragui, M. Addou, B.El. Idrissi, J.C. Bernede, A. Outzourhit, E. Ec-Chamikh, Mat. Chem. Phy. 70 (2001) 84.
[36] D.E. Dyshel', Powder Metall. Met. Ceram. 40 (2001) 5.
[37] T.G. Nenov, S.P. Yordanov, Ceramic Sensors, Technology and Applications, Technomic Publisher, Lancaster, 1996, p. 138.
[38] H. Mbarek, M. Saadoun, B. Bessis, Mat. Sci. Eng. C 26 (2006) 500.
[39] K. Arshak, I. Gaidan, Sens. Actuators B 111–112 (2005) 58.
[40] P. Mitra, A.P. Chatterjee, H.S. Maiti, Mat. Letters 35 (1998) 254.

ELSEVIER

Fingerprint quality control of *Angelica sinensis* (*Oliv*.) *Diels* by high-performance liquid chromatography coupled with discriminant analysis

Shuai Wang [a,b], Hua-Qiao Ma [a,b], Ya-Jie Sun [c], Cheng-Dong Qiao [a,b],
Shi-Jun Shao [a], Sheng-Xiang Jiang [a,*]

[a] *Key Laboratory for Natural Medicine of Gansu Province, Lanzhou Institute of Chemical Physics,*
Chinese Academy of Sciences, Lanzhou 730000, PR China
[b] *Graduate School of the Chinese Academy of Sciences, Beijing 100039, PR China*
[c] *Shenzhen Drug & Medical Apparatus Evaluation Center, Shenzhen 518034, PR China*

Abstract

High-performance liquid chromatography (HPLC) was employed in the fingerprint analysis of *Angelica sinensis* (*Oliv*.) *Diels*. A chromatographic profile of *A. sinensis* (*Oliv*.) *Diels* from the Dingxi District of Gansu province, China, was established as the characteristic fingerprint. The feasibility and advantages of employing chromatographic fingerprint combined with discriminant analysis were investigated and demonstrated for the evaluation of *A. sinensis* (*Oliv*.) *Diels* for the first time. Our results showed that the chromatographic fingerprint combining with discriminant analysis can efficiently distinguish *A. sinensis* (*Oliv*.) *Diels* from various areas.
© 2006 Elsevier B.V. All rights reserved.

Keywords: *Angelica sinensis* (*Oliv*.) *Diels*; HPLC; Fingerprint; Discriminant

1. Introduction

Angelica sinensis (*Oliv*.) *Diels* is one of the main traditional Chinese medicines (TCM), which has been used for more than 2000 years. It has been used generally as one of the herbal ingredients in prescriptions of TCM to treat gynecological diseases. Traditionally, only a few markers or pharmacologically active constituents are employed to assess the authenticity and quality of the herb [1]. But because herbal medicines are of natural products with complex matrixes, which are different from western synthetic medicines, the curative effects of herbal medicines principally are based on the synergic effect of their mass constituents [2–4]. So the traditional quality control of herbal medicines encounters severe challenges and to find a more efficient and accurate method is desirable.

Fingerprint analysis has been introduced and accepted by many countries and organizations [5–11]. Among the quality control systems, fingerprint has gained much attention [12–17] because by using the fingerprint analysis, a particular herb can be identified and, moreover, this herb can be distinguished from some closely related species. Since HPLC is a widely used methodology and can easily be adapted to the quantification of individual compounds, it has the advantage of generating a chemical fingerprint, which is useful in defining the identity and the quality of a given species.

Although some studies on the fingerprints of *A. sinensis* (*Oliv*.) *Diels* using HPLC have been published [18–19], none of them involved in the comparison among the *A. sinensis* (*Oliv*.) *Diels* from the main planting areas in China. More than 70.0% of *A. sinensis* (*Oliv*.) *Diels* are planted in the Dingxi District of Gansu province, so it is urgent for us to set up a reliable and accurate methodology based on the samples collected from these areas to substitute the traditional ones and to differentiate them. In the present study, with reference to the method of [18], which was the earlier work in our laboratory, we used high-performance liquid chromatography-diode array detection (HPLC-DAD) to establish a valid chromatographic fingerprint method. Combining with discriminant analysis, we efficiently differentiated the

---

* Corresponding author. Tel.: +86 931 4968266; fax: +86 931 8277088.
  E-mail address: ws777879@163.com (S.-X. Jiang).

A. sinensis (*Oliv*.) *Diels* from three main planting areas of the Dingxi District of Gansu province, China.

Usually some other statistic analyses such as principal component analysis, etc. were also used to deal with the data [20–22]. However, they were not appropriate to distinguish the three *A. sinensis* (*Oliv*.) *Diels* from different main planting areas because the chromatograms of these samples were generally identical.

2. Experimental

2.1. Instrumentation and reagents

An Agilent 1100 series HPLC system (USA) including a quaternary pump, a diode array detector, a vacuum degasser, a manual injector, a column oven, and a data system (Agilent Chem Station) was used. Methanol and acetonitrile was of chromatographic grade and acetic acid was of analytical grade. They were all purchased from the Tianjing Chemical Reagent Co. (China). Distilled and deionized water was used for the preparation of all the samples and solutions.

2.2. Reference compound

Biphenyl was purchased from Aldrich.

2.3. Materials

Thirty raw herbs of *A. sinensis* (*Oliv*.) *Diels* were investigated and collected from three main planting areas of the Dingxi District of Gansu province, China. Ten of them were from the Min County, another 10 of them were from the Wei-Yuan County and the remains were from the Zhang County. Voucher specimens are stored in the Research Center of Natural Products of our institute.

2.4. Sample preparation

An accurately weighed dried sample powder (2.00 g) was ultrasonically extracted with 40 mL of methanol–water (1/1, v/v) solution for 45 min, and then centrifuged for 15 min under 600 rpm. The supernatant was filtered through a 0.46 μm membrane filter before injection. Before the extraction, 3.6 μg of biphenyl was added the solution as an internal standard.

2.5. HPLC procedure

The chromatographic separation was performed on an ODS column (5 μm, 250 mm × 4.6 mm i.d.) (Lanzhou Institute of Chemical Physics, Chinese Academy of Sciences; Lanzhou, China) using a gradient of water/acetic acid (200/1, v/v; A) and methanol (B). The gradient condition was as follows: 0 min, 30% B; 20 min, 70% B; 70 min, 100% B. The detection wavelength, reference wavelength and column temperature were set at 275 nm, 400 nm and 25 °C, respectively. The flow rate was 0.6 mL/min and the loading volume was 20 μL.

2.6. Data analysis

The discriminant analysis was calculated using the *SPSS* 11.5 software.

3. Results and discussion

3.1. Optimization of extraction conditions

To obtain a stable and reproducible fingerprint, a sufficient extraction of the main components should be guaranteed. One sample was subjected to a set of nine extraction conditions, using different extraction times, volumes of solvent and extraction methods. The results (data and chromatograms not shown) revealed that the ultrasonic extraction of the samples in methanol/water (1:1, v/v) gave the best stable and reproducible results.

3.2. Optimization of HPLC conditions

To develop an accurate and reproducible fingerprint of *A. sinensis* (*Oliv*.) *Diels*, the optimization of the conditions of separation is a must. We tried different elution conditions with methanol–water, acetonitrile–water and different concentrations of acid in water. Through trial and error, the methanol–water/acetic acid (200/1, v/v) system was chosen for the separation. The selection of the detection wavelength was one of the key factors contributing to a reliable and reproducible HPLC fingerprint of *A. sinensis* (*Oliv*.) *Diels*. In the present study, analyzing the 3D-plots of chromatograms acquired from the HPLC-DAD system showed that the maximal absorbances of the main peaks were not at the same wavelength. The spectra of all the main peaks were investigated and 275 nm was chosen as the detection wavelength.

3.3. Standardization of fingerprint

In order to develop characteristic fingerprints, the experimental process must be standardized. Under the optimized conditions of extraction and chromatographic separation, a well-separated and reproducible chromatogram was achieved. Eighteen peaks were marked as the common peaks in the chromatograms of total the 30 raw herbs. The established chromatogram of *A. sinensis* (*Oliv*.) *Diels* is as follows (Fig. 1), where S denotes the internal substance (biphenyl).
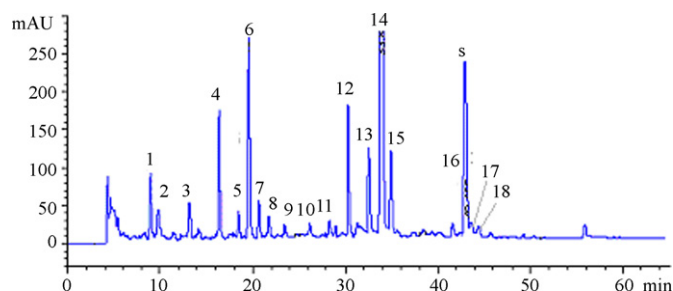

Fig. 1. Chromatogram of *A. sinensis* (*Oliv*.) *Diels*.

Table 1
The results of discriminant analysis

Discriminant grouping		Original grouping			Accuracy (%)
		A	B	C	
A	9	10	0	0	90.0
B	9	0	10	0	90.0
C	9	0	0	10	90.0

3.4. Discriminant analysis

Discriminant analysis can be used to build a predictive model of the group membership based on observed characteristics of each case. This procedure generates a discriminant function (or, for more than two groups, a set of discriminant functions) based on linear combinations of the predictor variables that provide the best discrimination among the groups. The functions are generated from the samples with known membership; the functions can then be applied to new cases with measurements for the predictor variables but with unknown group membership.

Here, we collected 30 samples from three different areas, so they could be classified into three groups. When we established the fingerprint, we selected 18 peaks as their common peaks, so each case would have 18 variables. However, not all the variables are of value to the establishment of discriminant function. The procedure will generate discriminant functions only by use of valuable predictor variables. The three discriminant functions of *A. sinensis* (*Oliv*.) *Diels* generated from three different areas were as follows:

$$A = 165.546 \times Var006 - 4.940 \times Var009 - 35.146$$
$$\times Var012 + 88.586 \times Var013 - 9.794 \tag{1}$$

$$B = 81.015 \times Var006 - 0.842 \times Var009 - 32.969$$
$$\times Var012 + 92.302 \times Var013 - 6.283 \tag{2}$$

$$C = 150.459 \times Var006 + 19.250 \times Var009 + 1.127$$
$$\times Var012 - 64.155 \times Var013 - 10.816 \tag{3}$$

where *A* denotes samples from the Min County, *B* denotes samples from the Wei-Yuan County, *C* denotes samples from the Zhang County, and Var denotes the variables.

From the discriminant functions, we can see that only four variables were used to generate the functions. These four variables denoted the areas of the peaks of No. 6, No. 9, No. 12 and No. 13, respectively. When we want to know which group an unknown sample is classified into, we put the values of the four variables into the three functions, respectively. The sample belongs to the group where the calculated value of the function is the highest. The result of discriminant analysis is shown in Table 1.

4. Conclusion

The studies on the fingerprints of the herbs and the data analysis have largely been published. However, none of them have involved in the analysis of the herbs using discriminant analysis. In the present study, we selected the samples of *A. sinensis* (*Oliv*.) *Diels* from three main planting areas as the study objects. By introducing a novel method "discriminant analysis", we have established a criterion for distinguishing *A. sinensis* (*Oliv*.) *Diels* from the three areas. Because the chromatograms of these samples were generally identical, some other analytical methods are of no effect to deal with the data obtained from these chromatograms. But our results showed that the model we established can efficiently distinguish *A. sinensis* (*Oliv*.) *Diels* from the three areas and the accuracy of the model is as high as 90.0%, which is much better than guessing or traditional methods.

Acknowledgements

References

[1] Chinese Pharmacopoeia, National Pharmacopoeia Committee, Chemical Industry Press, 2005, p. 89.
[2] W.J. Welsh, W. Lin, Anal. Chem. 68 (1996) 3473.
[3] P. Valentao, P.B. Andrade, J. Agric. Food. Chem. 47 (1999) 4579.
[4] P.S. Xie, Trad. Chin. Drug Res. Clin. Pharm. 12 (2001) 141.
[5] General Guidelines for Methodologies on Research and Evaluation of Traditional Medicine, World Health Organization, Geneva, 2000.
[6] FDA Guidance for Industry-Botanical Drug Products (Draft Guidance), US Food and Drug Administration, 2000.
[7] Final Proposals for Revision of the Note for Guidance on Quality of Herbal Remedies, EMEA, 1999.
[8] J.B. Calixto, Braz. J. Med. Biol. Res. 33 (2000) 179.
[9] J.D. Philipsom, British Herbal Medicine Association, Forword, 1996.
[10] Indian Drug Manufacturers' Association, Vedams Books International, 1998.
[11] State Food Drug Administration of China, Drug Stand. Chin. 1 (2000) 3.
[12] P.S. Xie, Proceedings of the International Symposium on Quality of TCM with Chromatographic Fingerprint, Guangzhou, 2001, p. 18.
[13] M. Gu, F. Ouyang, J. Chromatogr. A 1022 (2003) 139.
[14] A.J. Lau, M.J. Holmes, J. Pharmaceut. Biomed. Anal. 31 (2003) 401.
[15] W.W. Su, Z. Wu, Proceedings of the International Symposium on Quality of TCM with Chromatographic Fingerprint, Guangzhou, 2001, p. 164.
[16] R. Upton, Proceedings of the International Symposium on Quality of TCM with Chromatographic Fingerprint, Guangzhou, 2001, p. 6.
[17] M. Hajimahmoodi, Y. Vander Heyden, N. Sadeghi, B. Jannat, M.R. Oveisi, S. Shahbazian, Talanta 66 (2005) 1108.
[18] H.Q. Ma, D.L. Di, Chin. Trad. Herb. Drugs 35 (2004) 930.
[19] G.H. Lu, K. Chan, J. Chromatogr. A 1073 (2005) 383.
[20] C. Sârbua, H.F. Pop, Talanta 65 (2005) 1215.
[21] J.S. Cámara, M. Arminda Alves, J.C. Marques, Talanta 68 (2006) 1512.
[22] A.M. van Nederkassel, C.J. Xu, P. Lancelin, M. Sarraf, D.A. MacKenzie, N.J. Walton, F. Bensaid, M. Lees, G.J. Martin, J.R. Desmurs, D.L. Massart, J. Smeyers-Verbeke, Y. Vander Heyden, J. Chromatogr. A 1120 (2006) 291.

Layer-by-layer thin film-coated electrodes for electrocatalytic determination of ascorbic acid

Baozhen Wang, Takio Noguchi, Jun-ichi Anzai *

Graduate School of Pharmaceutical Sciences, Tohoku University, Aramaki, Aoba-ku, Sendai 980-8578, Japan

Abstract

Multilayer thin films composed of poly(allylamine hydrochloride) (PAH) and carboxymethyl cellulose (CMC) have been prepared on the surface of a gold (Au) disk electrode by a layer-by-layer deposition of PAH and CMC and ferricyanide ions ($[Fe(CN)_6]^{3-}$) were confined in the film. $[Fe(CN)_6]^{3-}$ ions can be successfully confined in the films from weakly acidic or neutral $[Fe(CN)_6]^{3-}$ solutions, while, in basic solution, $[Fe(CN)_6]^{3-}$ ion was not confined. The $[Fe(CN)_6]^{3-}$ ion-confined Au electrode showed clear redox peaks in the cyclic voltammogram around 0.35 V versus Ag/AgCl. The amounts of $[Fe(CN)_6]^{3-}$ ions confined in the films depended on the thickness of the films or the number of layers in the LbL films. The $[Fe(CN)_6]^{3-}$ ion-confined Au electrode was used for electrocatalytic determination of ascorbic acid in the concentration range of 1–50 mM.
© 2006 Elsevier B.V. All rights reserved.

Keywords: LbL film; Ascorbic acid; Ferricyanide ion; Electrocatalysis

1. Introduction

The development of electrochemical biosensors has been a focal subject in biosciences and biotechnologies [1,2]. For example, biosensors for determining ascorbic acid have been studied for its usefulness in the process control in food and pharmaceutical industries [3–8]. The ascorbic acid sensors can be divided into two classes depending on the catalytic elements employed for constructing sensors. The first type of ascorbic acid sensors uses enzyme (i.e., ascorbate oxidase) to effect the selective determination of ascorbic acid while the second type of sensors employ synthetic catalysts such as metal complexes [3–7]. A drawback of former sensors is a short life and high cost, which stems from the use of enzyme though a high selectivity to ascorbic acid is a merit [3,4]. On the other hand, use of synthetic catalysts may enable us to develop durable and low-cost sensors at the expense of high selectivity toward ascorbic acid [5,6]. In this context, we have recently reported a preliminary result that ferricyanide ion, $[Fe(CN)_6]^{3-}$, can be confined to the surface of thin film-modified electrodes and the modified electrodes are used as sensor for the catalytic determination of ascorbic acid in solution [7]. In fact, we prepared a thin

film on the surface of a gold (Au) electrode by a layer-by-layer (LbL) deposition of poly(allylamine hydrochloride) (PAH) and polysaccharides and $[Fe(CN)_6]^{3-}$ ions were successfully confined in the PAH/polysaccharide films by immersing the film-coated electrode in a solution of $[Fe(CN)_6]^{3-}$ ion for a short time (15 min) [9]. Thus, we have succeeded in the preparation of $[Fe(CN)_6]^{3-}$ ion-confined electrodes which can be used for the electrochemical determination of ascorbic acid in solution. During the course of the study, we have found that LbL thin films composed of polysaccharides are effective to confine higher amounts of $[Fe(CN)_6]^{3-}$ ion as compared to LbL films prepared using conventional synthetic polymers such as poly(vinyl sulfate) and poly(styrene sulfonate) probably due to a high swelling ability of polysaccharide films [10]. This is the reason why we use polysaccharide LbL films in this study. The present paper reports preparation of the $[Fe(CN)_6]^{3-}$-confined electrodes and electrocatalytic properties of the sensors in the determination of ascorbic acid in detail.

2. Experimental

2.1. Materials

An aqueous solution (20%) of poly(allylamine) hydrochloride [PAH; average molecular weight (MW), ~10,000] was

---

* Corresponding author. Tel: +81 22 795 6841; fax: +81 22 795 6840.
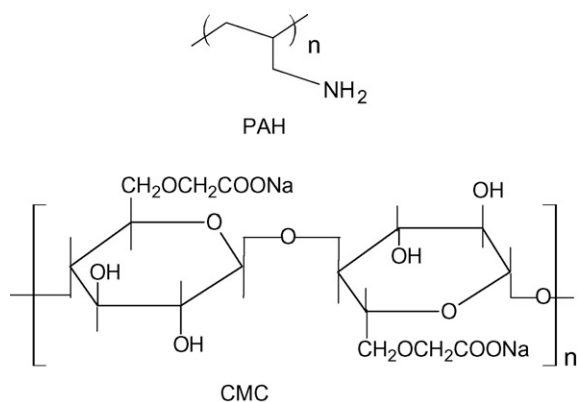*E-mail address:* junanzai@mail.pharm.tohoku.ac.jp (J.-i. Anzai).

Fig. 1. The chemical structures of polymers used.

purchased from Nittobo Co. (Tokyo, Japan). Sodium carboxymethylcellulose (CMC; MW, ~245,000) was obtained from Tokyo Kasei Co. (Tokyo, Japan). The chemical structures of the polymeric materials are shown in Fig. 1. Sodium 3-mercapto-1-propanesulfonate (MPS) was purchased from Tokyo Kasei Co. All other reagents were of the highest grade available and were used without further purification. All solutions were prepared in Milli-Q water.

2.2. Apparatus

All electrochemical measurements were carried out using an electrochemical analyzer (ALS, model 660B).

2.3. Preparation of LbL film-coated electrodes

The layer-by-layer (LbL) films were prepared on the surface of a gold (Au) disk electrode (3-mm diameter), according to the reported procedure [7]. The surface of the Au electrode was polished thoroughly using an aqueous alumina slurry and rinsed in distilled water before use. The polished Au electrode was further treated electrochemically in a 0.5 M H_2SO_4 solution by scanning the potential from −0.2 to 1.5 V versus Ag/AgCl at scan rate of 0.1 V s^{-1} for 15 min. The Au electrode thus cleaned was first treated in a freshly prepared MPS solution in water (5 mM) overnight to form a self-assembled monolayer of MPS on the Au surface through thiol-Au bonding. After this treatment, the surface of the Au electrode should be negatively charged due to $-SO_3^-$ residues on the MPS monolayer. The negatively charged surface of the electrode was further modified with LbL film by dipping it alternately in a 0.5 mg ml^{-1} PAH and a 0.5 mg ml^{-1} CMC solution (10 mM Tris–HCl buffer containing 150 mM NaCl, pH 7.4) for 30 min with an intermediate 5 min-rinse in the buffer. The multilayer films were prepared by repeating above procedure.

2.4. Electrochemical measurements

$[Fe(CN)_6]^{3-}$ ion-confined electrodes were prepared by immersing the LbL film-coated electrodes in 1 mM $[Fe(CN)_6]^{3-}$ solution for 15 min. The electrochemical response of the elec-

trodes was measured in a glass cell using the LbL film-modified electrode as working electrode, a platinum wire as a counter electrode, and a Ag/AgCl electrode (3.3 M KCl) as a reference electrode. All measurements were performed under air at room temperature (~20 °C).

3. Results and discussion

We have recently reported that nano-meter-sized thin films composed of PAH and CMC can be prepared on the surface of a gold (Au) disk electrode by a layer-by-layer (LbL) deposition of PAH and CMC from the aqueous solutions [9]. The formation of the PAH/CMC LbL film was characterized using a quartz crystal microbalance (QCM) and an electrochemistry. The QCM study revealed that the thickness of the films thus prepared is typically 150 ± 20 nm for the five-bilayer $(PAH/CMC)_5$ film [9]. Another characteristic feature was that $[Fe(CN)_6]^{3-}$ ion can be confined in the LbL films prepared on the surface of Au electrode by immersing the LbL film-coated electrode in an aqueous solution of $[Fe(CN)_6]^{3-}$ for a short time (~15 min) [9].

In the present study, we have used aqueous $[Fe(CN)_6]^{3-}$ solutions with different pH and ionic strength to evaluate the effects of these variables on the amounts of $[Fe(CN)_6]^{3-}$ ions confined on the $(PAH/CMC)_5PAH$ film-coated electrode. Fig. 2 shows cyclic voltammograms (CV) of the Au electrodes coated with the $(PAH/CMC)_5PAH$ film in which $[Fe(CN)_6]^{3-}$ ions were confined from the 1 mM $[Fe(CN)_6]^{3-}$ solutions at pH 7.4 and 9.2. The $[Fe(CN)_6]^{3-}$ ion-confined electrodes were rinsed in the working buffer overnight to eliminate weakly bound $[Fe(CN)_6]^{3-}$ ions from the film, and then CV was recorded in the fresh buffer solution containing no $[Fe(CN)_6]^{3-}$ ion. The electrode exhibited redox peaks around 0.35 V originating from $[Fe(CN)_6]^{3-}$ ion when the ion was confined at pH 7.4, while the redox peaks were very small when the $[Fe(CN)_6]^{3-}$ ions were confined from pH 9.2 solution. Fig. 3 plots the anodic peak current (i_p) of the $[Fe(CN)_6]^{3-}$ ion-confined electrode recorded in the buffer solutions, as a function of pH of the $[Fe(CN)_6]^{3-}$ solution from
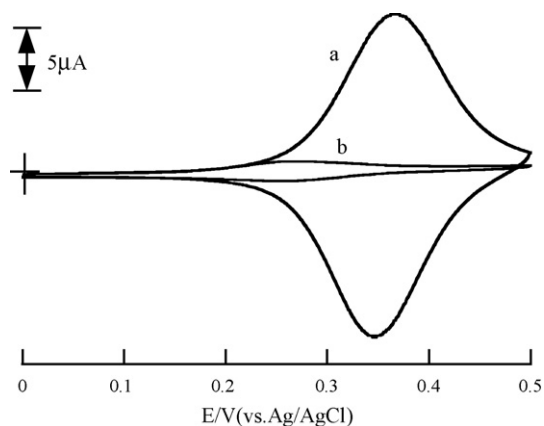

Fig. 2. Cyclic voltammograms of the Au electrode coated with the $Fe(CN)_6^{3-}$ ion-confined $(PAH–CMC)_5PAH$ film. The $Fe(CN)_6^{3-}$ ion was confined in Tris–HCl buffer containing 150 mM NaCl at pH 7.4 (a) and at pH 9.2 (b). The CVs were recorded in the buffers of pH 7.4 (a) and pH 9.2 (b). Scan rate was 0.05 V s^{-1}.
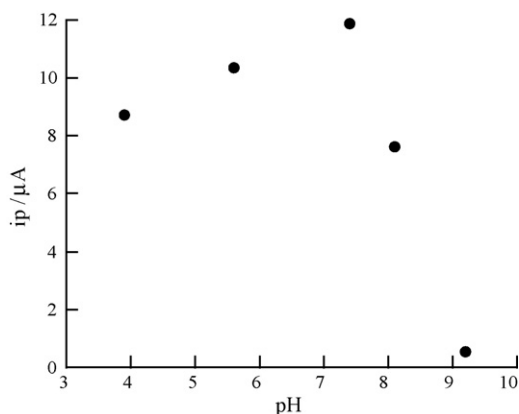
Fig. 3. The effects of pH on the peak currents of the Fe(CN)$_6$$^{3-}$ ion-confined (PAH–CMC)$_5$PAH film-coated electrodes. A 10 mM acetate buffer containing 150 mM NaCl was used for pH 3.9 and 5.6 solutions, while the solutions of pH 7.4, 8.1, and 9.2 were prepared by 10 mM Tris–HCl buffer containing 150 mM NaCl. Scan rate was 0.05 V s^{-1}.

Fig. 4. Cyclic voltammograms of ascorbic acid on the Fe(CN)$_6$$^{3-}$ ion-confined (PAH–CMC)$_5$PAH film-coated electrode. The sample solutions were 0 mM (a), 5 mM (b), 10 mM (c), and 15 mM ascorbic acid (d) in 10 mM Tris–HCl buffer containing 150 mM NaCl. Scan rate was 0.05 V s^{-1}.

which $[Fe(CN)_6]^{3-}$ ions were immobilized. The i_p values are higher when $[Fe(CN)_6]^{3-}$ ions were confined at pH 3.9, 5.6, and 7.4 than those for pH 8.1 and 9.2. These results suggest that $[Fe(CN)_6]^{3-}$ ions are electrostatically bound to the positively charged binding sites in the (PAH/CMC)$_5$PAH film originating from protonated amino groups in PAH. It has been reported that the fraction of protonated amino groups in PAH is pH-dependent and ~20% of amino groups are protonated at pH 6 while only ~3% are charged at pH 10 [11,12]. It is thus clear that a neutral or weakly acidic solution of $[Fe(CN)_6]^{3-}$ ion should be used to confine $[Fe(CN)_6]^{3-}$ ions in the (PAH/CMC)$_5$PAH film.

The effects of ionic strength of the $[Fe(CN)_6]^{3-}$ solutions were evaluated by using the $[Fe(CN)_6]^{3-}$ solutions containing varying amounts of NaCl. The $[Fe(CN)_6]^{3-}$ ions were confined to the (PAH/CMC)$_5$PAH film-coated electrode from the solutions of $[Fe(CN)_6]^{3-}$ ion containing 10, 50, 100, and 150 mM NaCl (pH 7.4) and CV of the electrode was recorded in the buffer solution at pH 7.4. The effects of the ionic strength were found to be unexpectedly small; the i_p values in CV were $(1.6 \pm 0.2) \times 10^{-5}$ A, regardless of the ionic strength. This is probably due to the fact that binding of monovalent anion such as Cl$^-$ to the film is very weak as compared to the multivalent $[Fe(CN)_6]^{3-}$ ion.

The catalytic oxidation of ascorbic acid by the $[Fe(CN)_6]^{3-}$ ion-confined electrodes was electrochemically evaluated. The CV of the $[Fe(CN)_6]^{3-}$ ion-confined electrode was recorded in the absence and presence of ascorbic acid. Fig. 4 depicts typical CVs of the $[Fe(CN)_6]^{3-}$ ion-confined (PAH/CMC)$_5$PAH film-coated electrode. The oxidation peak was highly enhanced and the reduction peak disappeared in the presence of ascorbic acid in solution, suggesting ascorbic acid was electrocatalytically oxidized by the $[Fe(CN)_6]^{3-}$ ion-confined electrode. In other words, ascorbic acid was chemically oxidized by $[Fe(CN)_6]^{3-}$ ion in the (PAH/CMC)$_5$PAH film into dehydroascorbic acid (Eq. (1)) and the resulting $[Fe(CN)_6]^{4-}$ ion was electrochemically reoxidized to $[Fe(CN)_6]^{3-}$ ion (Eq. (2)). Thus, in the CV in Fig. 4, the anodic current of the $[Fe(CN)_6]^{3-}/[Fe(CN)_6]^{4-}$

couple was enhanced in the presence of ascorbic acid:
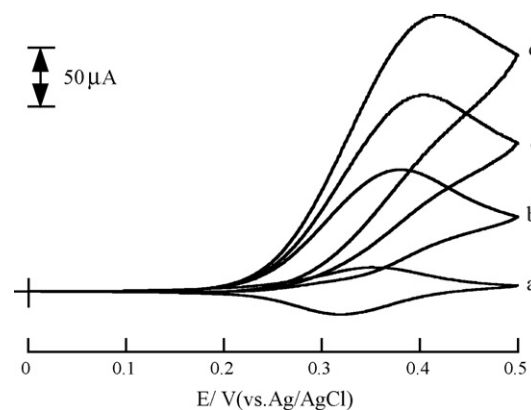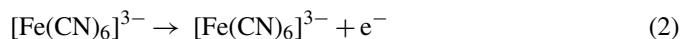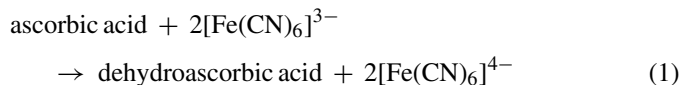
$$\text{ascorbic acid} + 2[Fe(CN)_6]^{3-}$$
$$\rightarrow \text{dehydroascorbic acid} + 2[Fe(CN)_6]^{4-} \tag{1}$$

$$[Fe(CN)_6]^{3-} \rightarrow [Fe(CN)_6]^{3-} + e^- \tag{2}$$

A merit of the electrocatalytic system for the oxidation of ascorbic acid is that the detection potential is sufficiently lower as compared to the direct electrochemical oxidation. In fact, without using $[Fe(CN)_6]^{3-}$ ion or other catalysts, ascorbic acid can be oxidized electrochemically at higher electrode potential (typically at 0.5 V or higher). At the higher electrode potential, side-reactions originating from other oxidizable contaminants may be accompanied. Thus, the use of $[Fe(CN)_6]^{3-}$ ion-confined electrodes may enable us to circumvent interferences from oxidizable contaminants to some extent. In this context, it should be noted that some oxidizable compounds such as dopamine, uric acid, and hydrogen peroxide are still oxidized by $[Fe(CN)_6]^{3-}$ ion-mediated electrodes [3,13,14].

Fig. 5 plots i_p values in CV recorded in the presence of 5 mM ascorbic acid as a function of the number of layers in
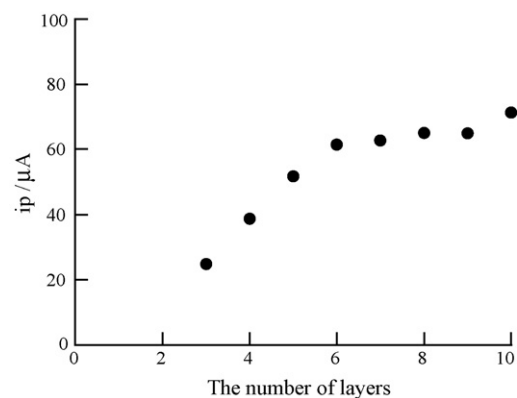

Fig. 5. Anodic peak current of the (PAH–CMC)$_n$PAH film-coated electrodes in the presence of 5 mM ascorbic acid in 10 mM Tris–HCl buffer containing 150 mM NaCl, as a function of the number of layers (n). Scan rate was 0.05 V s^{-1}.
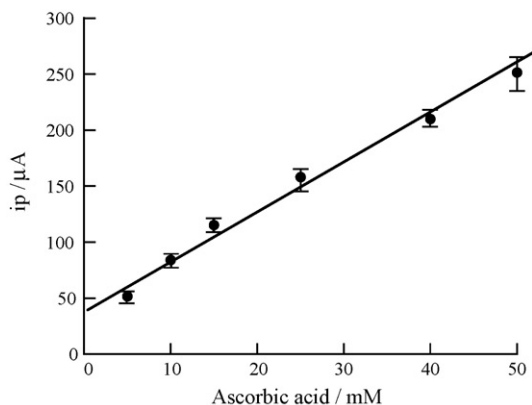
Fig. 6. A calibration graph of the $Fe(CN)_6{}^{3-}$ ion-confined (PAH–CMC)$_5$PAH film-coated electrodes to ascorbic acid at pH 7.4. Scan rate was 0.05 V s^{-1}. The average values of peak current for three independent measurements are plotted.

the (PAH/CMC)$_n$PAH films ($n = 3$–10). The data for the thinner films ($n = 1$ and 2) are omitted because the response was somewhat unstable probably due to a rapid leaching of $[Fe(CN)_6]^{3-}$ ions out of the films. The catalytic current to 5 mM ascorbic acid increased up to 6 layers and leveled off for thicker films ($n = 7$–10). This is probably because the diffusion of ascorbic acid through the thicker films determines the rate of the whole reaction process. Thus, the thicker films ($n = 7$ or higher) as well as thinner films ($n = 1$ and 2) are not suitable for effecting maximum performance of the (PAH/CMC)$_n$PAH film-coated electrode in the determination of ascorbic acid.
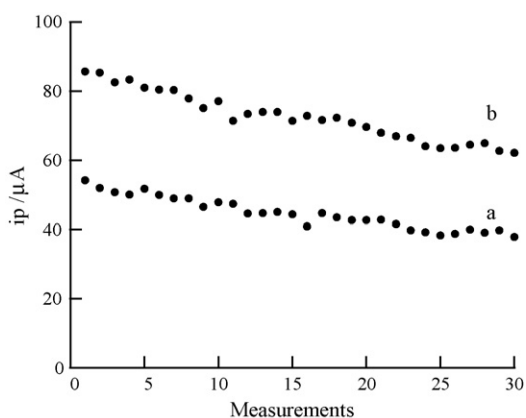

Fig. 7. The anodic peak currents of the $Fe(CN)_6{}^{3-}$ ion-confined (PAH–CMC)$_5$PAH film-coated electrode to 5 mM (a) and 10 mM ascorbic acid (b) during 30 successive measurements in 10 mM Tris–HCl buffer containing 150 mM NaCl. Scan rate was 0.05 V s^{-1}.

Fig. 6 shows a typical calibration graph of the $[Fe(CN)_6]^{3-}$ ion-confined (PAH/CMC)$_5$PAH film-coated electrode to ascorbic acid. The i_p linearly increased with increasing the concentration of ascorbic acid up to 50 mM. The lower detection limit was ca. 1 mM.

Fig. 7 illustrates i_p values of the $[Fe(CN)_6]^{3-}$ ion-confined (PAH/CMC)$_5$PAH film-coated electrode to 5 and 10 mM ascorbic acid for successive 30 measurements. The i_p values slightly decreased after 30 measurements because $[Fe(CN)_6]^{3-}$ ions gradually leached out of the film. However, it is possible to recover the original value in i_p by treating the electrode in the $[Fe(CN)_6]^{3-}$ solution again. It might be possible to improve the stability by changing the nano-structure of the LbL film or using other polymeric materials for constructing the film.

4. Conclusions

We have demonstrated that the $[Fe(CN)_6]^{3-}$ ion-confined (PAH/CMC)$_5$PAH film-coated electrode can be successfully used for electrocatalytic determination of ascorbic acid. The $[Fe(CN)_6]^{3-}$ ions are confined effectively from aqueous solutions of $[Fe(CN)_6]^{3-}$ ion at a neutral or weakly acidic solution. The effects of ionic strength of the solution of $[Fe(CN)_6]^{3-}$ ion are small. The maximum performance of the $[Fe(CN)_6]^{3-}$ ion-confined electrode can be obtained for six-bilayer film rather than the thinner or thicker films. Thus, ascorbic acid over the concentration range of 1–50 mM can be successfully determined.

References

[1] S.E. Moulton, A.I. Minett, G.G. Wallace, Sensor Lett. 3 (2005) 183.
[2] I.J. Allan, B. Vrana, R. Greenwood, G.A. Mills, B. Roig, C. Gonzalez, Talanta 69 (2006) 302.
[3] P.C. Pandey, B.C. Upadhyay, A.K. Upadhyay, Anal. Chim. Acta 523 (2004) 219.
[4] P.J.O. Connell, C. Gonnally, M. Pravda, G.G. Guilbault, Anal. Chim. Acta 431 (2001) 239.
[5] S. Ivanov, V. Tsakova, V.M. Mirsky, Electrochem. Commun. 8 (2006) 643.
[6] T. Noguchi, T. Hoshi, J. Anzai, Sensor Lett. 3 (2005) 164.
[7] A. Liu, J. Anzai, Anal. Bioanal. Chem. 380 (2004) 98.
[8] K. Wang, J.J. Xu, K.S. Tang, H.Y. Chen, Talanta 67 (2005) 798.
[9] T. Noguchi, J. Anzai, Langmuir 22 (2006) 2870.
[10] R. Takita, Y. Okamura, Y. Endo, J. Anzai, Electroanalysis 18 (2006) 1627.
[11] Y. Yoshikawa, H. Matsuoka, N. Ise, Br. Polym. J. 18 (1986) 242.
[12] J. Hodak, R. Etchenique, E.J. Calvo, K. Singhal, P.N. Bartlett, Langmuir 13 (1997) 2708.
[13] P.C. Pandy, B.C. Upadhyay, Talanta 67 (2005) 997.
[14] V.S. Vasantha, S.-M. Chen, Electrochim. Acta 51 (2005) 347.

Method development for the analysis of polybrominated dibenzo-*p*-dioxins, dibenzofurans and diphenyl ethers in sediment samples

Dongli Wang [a], Guibin Jiang [c], Zongwei Cai [a,b,*]

[a] *Department of Chemistry, Hong Kong Baptist University, Kowloon, Hong Kong SAR, China*
[b] *Dioxin Analysis Laboratory, Hong Kong Baptist University, Kowloon, Hong Kong SAR, China*
[c] *Research Center for Eco-environmental Sciences, The Chinese Academy of Sciences, Beijing, China*

Abstract

A column chromatography procedure was developed for the clean-up of solvent-extracted sediment samples for the fractionation of polybrominated diphenyl ethers (PBDEs) and polybrominated dibenzo-*p*-dioxins and dibenzofurans (PBDD/Fs). The procedure included multiple column chromatography steps for clean-up for the separation of PBDEs from PBDD/Fs. The separation of the two chemical groups overcame the mutual interfering problem during the GC–ion trap MS analysis. The method was validated with the analysis of quality control samples. The method accuracy represented with relative error was less than 16% for all targeted PBDEs and PBDD/Fs congeners. Recoveries of the ^{13}C-labeled standards ranged from 64% to 117% with relative standard deviation from 7.3% to 15%. Results from the analysis of environmental sediment samples collected in the vicinity of a recycling site for electronic wastes showed high levels of PBDEs (1.5–12 ng/g, dry weight), trace levels of PBDFs (0.025–0.92 ng/g, dry weight) and non-detectable PBDDs.

1. Introduction

Polybrominated diphenyl ethers (PBDEs) are extensively used as flame-retardants in many electronic products. In the process of manufacturing PBDEs, polybrominated dibenzo-*p*-dioxins and dibenzofurans (PBDD/Fs) (Fig. 1) are often formed [1–10]. Furthermore, the combustion of polyvinyl chloride and brominated flame retardants may generate PBDD/Fs and mixed brominated/chlorinated dibenzo-*p*-dioxns and dibenzofurans, in addition to polychlorinated biphenyls (PCBs), polychlorinated dibenzo-*p*-dioxins and dibenzofurans (PCDD/Fs) [10–13].

PBDEs are released into the environment from the products because they are not chemically bound to materials. PBDEs have been detected in environmental matrices at high levels such as air, sediment and sewage sludge as well as biologi-

cal samples such as biota, human blood, adipose tissues and breast milk [14–17]. Recent studies showed higher concentration of PBDEs were found in sediments around an electronic waste processing site in Gui Yu, Guangdong Province, China [18]. PBDD/Fs are often formed in the process of manufacturing brominated flame retardants and from the combustion of e-waste products containing flame retardants BFR [5]. Congeners of PBDD/F have been found in ambient air, flue gas, fly ash from municipal solid waste incinerators and in vehicle exhaust [5,19–21]. However, there is only limited information on the environmental concentrations and human exposure of PBDD/Fs. TeBDD/Fs–HxBDD/Fs were below the detection limits in carp (*Cyprinus carpio*) collected from the Buffalo River in New York [22]. Three PBDD/F congeners, namely 2,3,7,8-TeBDD, 2,3,7,8-TeBDF and 2,3,4,7,8-PeBDF were found in Japanese human adipose tissue and sediments samples taken from industrialized areas [23–25]. Ambient concentrations of PBDD/Fs in New York Harbor are similar to those of PCDD/Fs, suggesting that it is important to investigate PBDD/Fs with respect to toxicity, sources, and fate in the environment [26]. However, currently there are no standard analytical methodologies for

* Corresponding author at: Department of Chemistry, Hong Kong Baptist University, Kowloon, Hong Kong SAR, China. Tel.: +852 34117070; fax: +852 34117348.
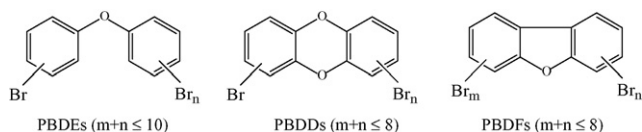*E-mail address:* zwcai@hkbu.edu.hk (Z. Cai).

Fig. 1. Chemical structures of PBDEs, PBDDs and PBDFs.

PBDD/Fs. Moreover, most of the methods reported in literature involve two individual sample preparation procedures followed by instrument analysis, which is time, solvent and labor consuming. Thus, a rapid and reliable procedure for simultaneous sample preparation for PBDEs and PBD/Fs is needed.

Separation of PBDEs and PBDD/Fs during simultaneous sample preparation procedure is vital in trace analysis because the two groups of compounds often interfere with each other during the instrumental analysis due to the co-elution problem on GC-column with the same fragment ions [27,28]. Although column chromatographic separation of PBDEs and PBDD/Fs is feasible due to the polarity difference, the method development with good performance is a challenge because data on the physical and chemical properties of PBDD/Fs are sparse and PBDD/F congeners have not been completely identified in environmental matrices. Choi et al. reported a procedure using active carbon column for the separation of PBDEs and PBDD/Fs [25]. While active carbon column chromatography has been employed for the clean-up purpose for dioxins and PCBs analysis, the reproducibility and recovery are sometimes variable. Moreover, the preparation of carbon column and its solvent elution procedure are not as simple as those of Florisil column. This paper describes method development for the separation of PBDD/Fs and PBDEs from one single sample extraction by using Florisil column chromatography. The method was validated and applied for the analysis of sediment samples collected from a river near an electronic waste recycling site.

2. Experimental

2.1. Chemical reagents and standard solutions

Dichloromethane, hexane and toluene of Absolve grade were purchased from Tedia Company Inc. (Fairfield, OH, USA). Granular anhydrous sodium sulfate (Tedia, Fairfield, USA), silica gel 60 (0.063–0.200 mm, Merck, Whitehouse Station, USA) and neutral alumina (Brockmann I, Standard Grade, ~150 mesh, Aldrich Chemical Co., Milwaukee, USA) were heated at 170 °C for more than 24 h. Copper powder was supplied from UniChem (Surrey, UK). Concentrated sulfuric acid was purchased from BDH Laboratory Supplies (Dorset, UK). Silica gel with 30% sulfuric acid-impregnated (w/w) was prepared by combining concentrated sulfuric acid with activated neutral silica gel. Florisil (60–100 mesh, Supelco, US) was heated at 170 °C for 13 h and deactivated with 1% water.

Native PBDD/F standard solution was purchased from Cambridge Isotope Laboratory (Andover, MA, USA) with individual concentration of 1000 pg/μL containing 2,3,7,8-tetrabrominated dibenzo-*p*-dioxins (2,3,7,8-TeBDD), 1,2,3,7,8-pentabrominated dibenzo-*p*-dioxins (1,2,3,7,8-PeBDD), 1,2,3,4,-

7,8-hexabrominated dibenzo-*p*-dioxins (1,2,3,4,7,8-HxBDD), 1,2,3,6,7,8-hexabrominated dibenzo-*p*-dioxins (1,2,3,6,7,8-HxBDD), 1,2,3,7,8,9-hexabrominated dibenzo-*p*-dioxins (1,2,3,7,-8,9-HxBDD), 2,3,7,8-tetrabrominated dibenzofuran (2,3,7,-8-TeBDF), 1,2,3,7,8-pentabrominated dibenzofuran (1,2,-3,7,8-PeBDF), 2,3,4,7,8-pentabrominated dibenzofuran (2,3,4,-7,8-PeBDF), and 1,2,3,4,7,8-hexabrominated dibenzofuran (1,2,3,4,7,8-HxBDF). A mixed native standard solution of PBDEs containing 2,2′,4,4′-tetrabromodiphenyl ether (BDE-47), 2,3′,4,4′-tetrabromodiphenyl ether (BDE-99), 2,2′,4,4′,6-pentabromodiphenyl ether (BDE-100), 2,2′,4,-4′,5,5′-hexabromodiphenyl ether (BDE-153), 2,2′,3,4,4′,5′,6-heptabromodiphenyl ether (BDE-183) at 5 μg/mL and deca-bromodiphenyl ether (BDE-209) at 10 μg/mL was purchased from Wellington Laboratories (Ontario, Canada). $^{13}C_{12}$-labelled PBDEs (BDE-3, BDE-15, BDE-28 BDE-27, BDE-99, BDE-139, BDE-153, BDE-154 and BDE-183), $^{13}C_{12}$-1,2,3,4-tetrachlorodibenzo-*p*-dioxin (TeCDD) and $^{13}C_{12}$-1,2,3,7,-8,9-hexachlorodibenzo-*p*-dioxin (HxCDD) (Wellington Laboratories) were used as internal standards for the analyses of PBDEs and PBDD/Fs, respectively. $^{13}C_{12}$-BDE-139 (Wellington Laboratories) was used as recovery standard. The response factors for PBDD/F congeners (based on native PBDD/F standards) determined by injecting same amounts of selected PBDD/F and PCDD/F congeners ranged from 0.55 to 1.2.

2.2. Sample collection and preparation

Eight field sediment samples were collected from an area of about 6 m² along the Lianjiang River that flows through the town of Guiyu (Guangdong Province, China) where an open e-waste recycling site is located. The samples were placed in glass bottles and frozen at −20 °C until the analysis. Blank sediment samples were obtained from the Environmental Protection Department of Hong Kong SAR. The sample preparation procedure is presented in Fig. 2. After being air-dried at ambient temperature, samples were thoroughly mixed and ground with a mortar and pestle before being passed through a 250 μm sieve to obtain a homogeneous matrix. Ten grams of each sample were precisely weighed, mixed with approximately 20 g anhydrous sodium sulphate and 15 g of acid activated copper powder for removing sulfur in the samples, and spiked with 10 ng of $^{13}C_{12}$-labelled PBDEs, 2 ng of $^{13}C_{12}$-1,2,3,4-TeCDD and $^{13}C_{12}$-1,2,3,7,8,9-HxCDD. The prepared samples were extracted for 18 h in Soxhlet extractor with 300 mL of toluene. The extract was concentrated to near dryness by rotary evaporation and a gentle stream of nitrogen, and diluted to 1 mL in hexane. One mililiter of sample extract was transferred to a glass column packed with 6 g of acidic silica gel (30%, w/w). PBDEs and PBDD/Fs were directly eluted with 20 mL of hexane to another glass column packed with 6 g of neutral alumina. Then acid silica column was removed, and neutral alumina column was eluted with 10 mL of hexane and 20 mL of a mixed solvent of hexane and dichloromethane (60/40, v/v). The mixed solvent fraction containing PBDE and PBDD/Fs congeners was concentrated to 1 mL under a gentle stream of nitrogen and transferred to a glass column packed with 5 g of deactivated Florisil. This column was eluted with 100 mL of hex-
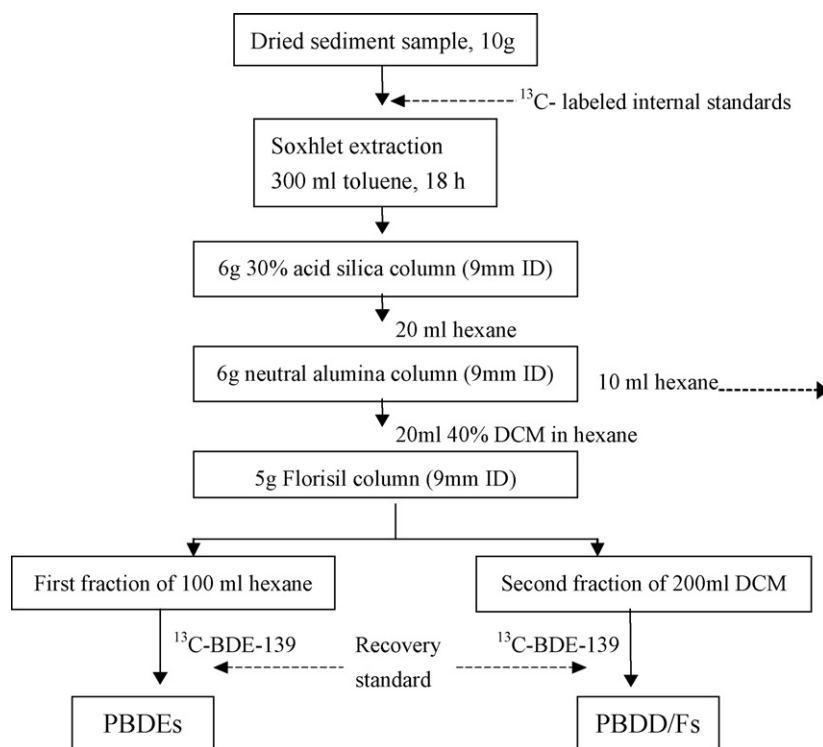
Fig. 2. Scheme of sample preparation procedure including column chromatography clean-up and separation of PBDD/Fs and PBDEs.

ane and 200 mL of dichloromethane. The former fraction was concentrated to 100 μL for analyzing PBDEs, and 10 ng $^{13}C_{12}$-BDE-139 was added before the GC–MS/MS analysis. The latter fraction was concentrated to 20 μL for analyzing PBDD/Fs, and 2 ng of $^{13}C_{12}$-BDE-139 were added to determine recoveries of $^{13}C_{12}$-1,2,3,4-TeCDD and $^{13}C_{12}$-1,2,3,6,7,8-HxCDD.

2.3. GC–MS/MS analysis

The sample extracts were analyzed by GC–MS/MS using a ThermoQuest Trace GC-PolarisQ ion trap mass spectrometer (Austin, TX, USA). The GC system was operated in splitless injection mode, and the purge valve was activated for 2 min after sample injection. A DB-5 column (30 m × 0.25 mm i.d., 0.25 μm film thickness) was used with the following temperature program for the analysis of PBDD/Fs: 150 °C for 2 min, 20 °C/min to 250 °C and hold for 5 min, 2 °C/min to 290 °C and held for 15 min. Helium was used as the carrier gas at a constant flow rate of 1.2 mL/min with vacuum compensation. The injector port, the MS ion source and transfer line were kept at 290 °C, 250 °C and 300 °C, respectively. A different temperature program was applied for PBDEs analysis: 110 °C for 2 min, 8 °C/min to 180 °C and hold for 1 min, 4 °C/min to 240 °C and hold for 5 min, 4 °C/min to 280 °C and hold for 6 min. One microliter of the sample extract or standard solution was injected with a solvent delay set for 8 min for the analysis of PBDD/Fs and 6 min for PBDEs. The mass spectrometer was operated with electron impact ionization (EI) mode with the electron energy of 70 eV. Details of the ion trap MS method development for the detection of PBDEs and PCDD/Fs will be reported elsewhere. Under the EI-MS conditions, the molecular ions were observed

as the most intensive peaks for PBDD/Fs and thus selected as the precursor ions for the subsequent tandem mass spectrometric analysis, while for PBDEs, molecular ions or $[M - Br_2]^+$ ion (for all *ortho*-substituted tetra- through hepta-PBDEs) were selected as the precursor ions. The selected precursor ions were fragmented by using collision-induced dissociation (CID) mass spectrometry with argon as the CID gas. The main fragments are $[M - COBr]^+$, $[M - 2(COBr)]^+$, $[M - Br]^+$ and $[M - Br_2]^+$ for PBDEs and PBDD/Fs, depending on the congeners. The quantitative ions were selected based on the criteria including peak intensity and ion specificity as well as potential interference from other compounds.

Base-line separation was achieved for the PBDE congeners except BDE-209 that was not measured under the present gas chromatography conditions. The analysis of BDE-209 usually involves a special GC approach such as pressure programming or a short chromatography column due to its higher boiling point. Identification of the analytes in the sediment samples was performed with the following criteria: retention time matching with the corresponding authentic standards, signal-to-noise of greater than 3 for the selected ions, bromine isotope ratio of at least two characteristic ions matching the theoretical values within 20% deviation. Quantification of the PBDD/Fs and PBDEs was performed by using internal standard method. $^{13}C_{12}$-labelled PBDEs were used for the determination of PBDEs by using isotope dilution technique. Due to lack of $^{13}C_{12}$-labellled PBDD/Fs, $^{13}C_{12}$-1,2,3,4-TeCDD was used as the internal standard for the quantification of TeBDD/F and PeBDD/F, and $^{13}C_{12}$-1,2,3,6,7,8-HxCDD for HxBDD/F. The $^{13}C_{12}$-labelled internal standards were spiked into the environmental samples prior to the sample preparation and GC–MS/MS

analysis. $^{13}C_{12}$-BDE-139 was used to determine the recoveries of the internal standards. Linear calibration with r^2 better than 0.985 for PBDD/Fs was performed from analysis of the mixtures of 11 native PBDD/Fs with concentrations ranged from 25 pg/μL to 1000 pg/μL, together with $^{13}C_{12}$-1,2,3,4-TeCDD and $^{13}C_{12}$-1,2,3,7,8,9-HxCDD with a constant concentration of 100 pg/μL. Calibration for PBDEs with r^2 better than 0.996 was performed from the analysis of the mixtures of 19 native PBDEs with the concentration ranged from 1 pg/μL to 400 pg/μL, together with 10 $^{13}C_{12}$-labeled PBDEs with a concentration of 100 pg/μL. Relative response factors (RRFs) of the native analytes to the corresponding $^{13}C_{12}$-labeled internal standards were determined.

2.4. Quality assurance and quality control

The quality assurance and quality control (QA/QC) samples included solvent blank, matrix blank and spiked matrix, all of which were analyzed together with the real sediment samples. Matrix-spiked samples at two concentrations were also analyzed in triplicate during the method development. The blank sediment sample that was tested and demonstrated to be free of the PBDD/Fs and PBDEs was used for the matrix blank and matrix-spiked samples. Exact amounts of 4 ng and 20 ng of the 11 individual native PBDD/Fs standards, 10 ng and 40 ng of the nine individual native PBDE standards were spiked into 10 g of the blank sediment to prepare the matrix-spiked samples to evaluate the method performance, respectively. Relative error and relative standard deviation obtained from triplicate analysis of matrix-spiked samples were used to evaluate the accuracy and precision of the analytical method.

3. Results and discussion

3.1. Separation of PBDD/Fs and PBDEs in sediment sample extract

Sample preparation procedure for PBDD/Fs and PBDEs in sediment samples was performed by using Soxhlet extraction followed by column chromatographic clean-up. Soxhlet extraction provided good efficiency for extracting brominated flame-retardants from environmental sediment and biota samples [24]. Elimination of interferences was achieved by applying the chromatographic clean-up steps with acid silica gel, alumina and Florisil. The separation of PBDEs and PBDFs is particularly important because the two groups of chemical may interfere during the instrument analysis. The fragment ions of PBDE resulted from losing HBr or Br_2, for example, cannot be distinguished from those fragment ions formed by the corresponding PBDF. Ebert et al. [28] also reported that fragment ions of PBDF cannot be separated from those of PBDE during the GC–MS analysis.

Because PBDEs have different chemical structures from PBDD/Fs and thus different polarities, it is possible to separate the two groups of chemicals by using column chromatography. Separation of PBDEs from PBDD/Fs was investigated by using different chromatography columns with various sol-

Table 1
QA/QC data from three replicate analyses of 10 g spiked sediment samples

Native standards	Added (ng)	Found (ng)	R.S.D.[a] (%)
BDE-17	10	8.4	6.9
	40	49	4.0
BDE-47	10	11	15
	40	43	6.6
BDE-99	10	12	22
	40	50	5.5
BDE-100	10	14	17
	40	50	21
BDE-153	10	14	20
	40	41	10
BDE-183	10	11	14
	40	37	1.9
2,3,78-TeBDD	4.0	5.0	5.0
	20	25	18
1,2,3,7,8-PtBDD	4.0	3.8	14
	20	19	21
1,2,3,4,7,8-/1,2,3,6,7,8-HxBDD	4.0	3.3	5.6
	20	15	20
1,2,3,7,8,9-HxBDD	4.0	3.0	40
	20	17	24
2,3,7,8-TeBDF	4.0	3.5	8.6
	20	17	8.2
1,2,3,7,8-PtBDF	4.0	5.1	15
	20	27	28
2,3,4,7,8-PtBDF	4.0	3.9	11
	20	26	21
1,2,3,4,7,8-HxBDF	4.0	5.2	32
	20	17	17

Labeled standards	Added (ng)	Recovery (%)	R.S.D. (%)
^{13}C-BDE28	10	66	7.8
^{13}C-BDE47	10	98	7.3
^{13}C-BDE99	10	91	13
^{13}C-BDE154	10	101	14
^{13}C-BDE153	10	101	9.9
^{13}C-BDE183	10	117	14
^{13}C-1234-TeCDD	2.0	110	17
^{13}C-123678-HxBDD	2.0	112	10
^{13}C-1234-TeCDD	2.0	64	15
^{13}C-123678-HxBDD	2.0	109	13

[a] R.S.D. = relative standard deviation ($n = 3$).

vent mixtures. It was found that Florisil column suited the best for the separation purpose with good recovery and reproducibility (Table 1). With the optimized column and elution solvent conditions, PBDEs could be separated completely from PBDD/Fs. The PBDEs fraction was eluted and colleted from the Florisil column with 100 mL of hexane, followed by the elution of PBDD/F congeners by using 200 mL of dichloromethane. Compared to the use of a solvent mixture of dichloromethane and hexane [24,25], dichloromethane elution consistently provided better recovery of PBDD/Fs. GC–MS analysis of the hexane fraction showed that PBDEs were recovered more than 85%, while no PBDD/Fs were detected. The analysis of the dichloromethane fraction gave the result of recovery better than 90% for PBDD/Fs. The obtained data indicated that PBDEs and PBDD/Fs could be quantitatively separated from each other by using the Florisil column chromatography procedure. No other

significant interferences were observed when the procedure was applied for the field sediment sample analysis.

3.2. Method validation

Method performance was evaluated not only with the analysis of standard compounds, but also with quality insurance and quality control (QA/QC) samples. The above procedure was applied in the analysis of blank and spiked sediment samples. The results showed no severe matrix effect on the separation efficiency. It should be noted, however, that the clean-up using acidic silica gel and neutral alumina prior to the Florisil step was crucial for removing interference in order to ensure the good separation efficiency on the Florisil column. This is especially true when analyzing the real sediment samples.

The QA/QC sample analysis showed no detectable levels of PBDD/Fs and PBDEs in matrix and method blanks. The accuracy and precision of the method were evaluated by analyzing the spiked sediment samples with PBDEs at levels of 1 ng/g and 4 ng/g and PBDD/Fs at levels of 0.4 ng/g and 2 ng/g. $^{13}C_{12}$-PBDEs was spiked at the level of 1 ng/g, and $^{13}C_{12}$-1,2,3,4-TeCDD and $^{13}C_{12}$-1,2,3,6,7,8-HxCDD were spiked at 0.2 ng/g. The prepared standard sediment samples were analyzed with the sample preparation procedure and GC–MS/MS determination. Data of accuracy, recovery and precision were presented in Table 1. The analysis of the spiked matrix samples with 1 ng/g of PBDEs gave results of concentration ranges from 0.84 ng/g to 1.4 ng/g, with relative standard deviation varying from 5.5 to 22% ($n = 3$). Levels of the PBDEs in the spiked matrix samples with 4 ng/g of PBDEs were 3.7 ng/g to 5.0 ng/g, with relative standard deviation varying from 1.9 to 21% ($n = 3$). Quantitative recoveries of 81–121% were achieved for the extraction and clean-up procedures for the $^{13}C_{12}$-labeled internal standards. The PBDD/Fs levels were found in the range of 3.0–5.2 ng/g in the spiked samples at 4 ng/g, with relative

standard deviation from 5.0% to 40%. When the PBDE/Fs spiked level was 20 ng/g, the detected concentrations were in the range of 15–27 ng/g, with relative standard deviation from 8.2% to 32%. Generally, higher analytical error and relative standard deviation were obtained for the determination of PBDD/Fs because $^{13}C_{12}$-1,2,3,4-TeCDD and $^{13}C_{12}$-1,2,3,6,7,8-HxCDD were used as the internal standards that were not the corresponding isotope-labeled compounds of the analytes. The use of labeled chlorinated dioxin congeners as internal standards for PBD/Fs determination led to high R.S.D. For the determination of PBDEs, a true isotope dilution technique was applied because the $^{13}C_{12}$-labelled PBDEs were used as the internal standards. The isotopic dilution MS method provides better accuracy and precision for the quantification of the analytes at ultra-trace levels in complex matrices. Method detection limits (define as when achieving signal-to-noise better than 3) for the developed sample preparation procedure and with the GC–ion trap MS analysis were obtained from the analysis of spiked matrix samples. The method detection limits ranged from 0.013 ng/g to 0.25 ng/g for the PBDEs and from 0.02 ng/g to 0.4 ng/g for analysis of PBDD/Fs.

3.3. Analysis of PBDD/F and PBDEs in environmental sediment samples

The developed sample preparation procedure including the multiple steps of column chromatography was applied for analyzing PBDD/Fs and PBDEs in the sediment samples collected from a river located in the vicinity of an open e-waste treatment sites in Guiyu, Guangdong, China. Several congeners of PBDF and PBDE were detected in the sediment. Identification was performed based on the following criteria: retention time of the analytes were less than 2 s compared with that of the standard; selected product ions are detected and their isotopic ratios must be within the range of 20% of the theoretical values;

Table 2

Average levels of PBDD/Fs and PBDEs from eight sediment samples and the data from duplicated analysis of the sediment sample #3 (ng/g, dried weight)

Compounds	DL[a] (ng/g)	Ave ± S.D.[b] (ng/g)	Duplicated[c] (ng/g)	
2,3,7,8-TeBDD	0.02	nd[d]	nd	nd
1,2,3,7,8-PtBDD	0.02	nd	nd	nd
1,2,3,4,7,8-/1,2,3,6,7,8-HxBDD	0.40	nd	nd	nd
1,2,3,7,8,9-HxBDD	0.40	nd	nd	nd
2,3,7,8-TeBDF	0.02	0.025 ± 0.004	0.020	0.022
1,2,3,7,8-PtBDF	0.02	0.037 ± 0.006	0.035	0.039
2,3,4,7,8-PtBDF	0.02	0.15 ± 0.012	0.14	0.15
1,2,3,4,7,8-HxBDF	0.40	0.92 ± 0.13	0.89	0.99
1,2,3,4,6,7,8-HpBDF	0.40	nd	nd	nd
BDE-17	0.013	1.5 ± 0.20	1.6	1.8
BDE-47	0.013	11 ± 0.8	9.5	10.2
BDE-99	0.013	12 ± 0.6	9.9	10.1
BDE-100	0.050	2.0 ± 0.2	2.1	2.0
BDE-153	0.25	7.4 ± 0.7	7.0	7.8
BDE-183	0.25	9.5 ± 0.6	9.3	9.6

[a] DL = detection limit.

[b] Ave ± S.D. = averaged ± standard deviation (from eight sediment samples).

[c] Duplicated data from the sediment sample #3.
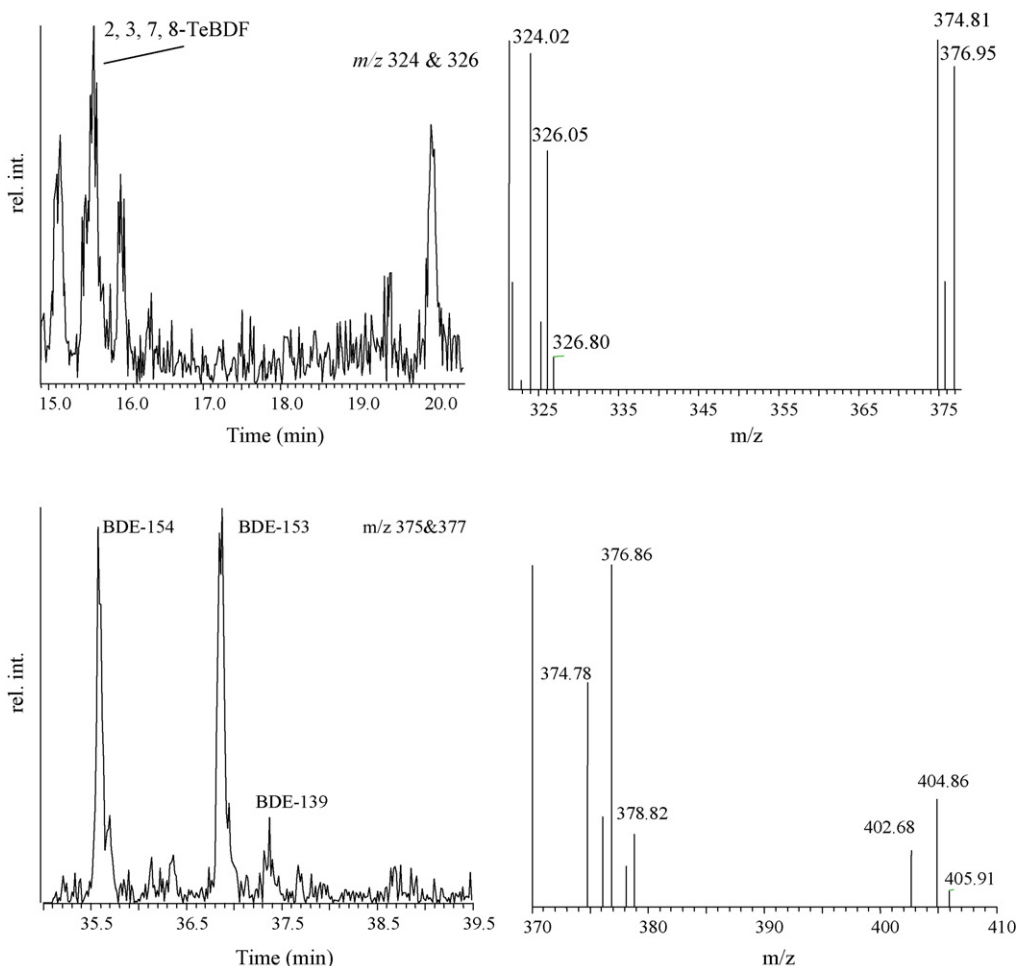
[d] nd = not detected.

Fig. 3. Typical mass chromatograms and mass spectra of 2,3,7,8-TeBDF and BDE-153 obtained from the analysis of one sediment sample (#3). The signal to noise of the 2,3,7,8-TeBDF peak was not good due to the low levels (0.021 ng/g) detected in the sediment sample.

and signal-to noise ratio of the all detected peaks must be more than 3. PBDDs were not detected in all eight sediment samples, but several peaks of PBDFs were observed in the extracted MS/MS chromatograms of PBDFs. The toxic 2,3,7,8-TeBDF, 1,2,3,7,8-PeBDF, 2,3,4,7,8–2,3,4,7,8-PeBDF, and 1,2,3,4,7,8-HxBDF were identified, while other peaks cannot be assigned due to the lack of authentic standards. Table 2 lists the PBDE congeners with the mono- to hepta-brominated substitutions that were detected in the chromatographic windows. Typical mass chromatograms and mass spectra of 2,3,7,8-TeBDF and BDE-153 obtained from the analysis of one sediment sample are shown in Fig. 3. No cross interference was observed during the analyses of PBDEs and PBDD/Fs, indicating the separation based on the Florisil column chromatography was efficient.

Table 2 also presents the quantitative results of those identified PBDF and PBDE congeners whose standards were available. The recoveries of $^{13}C_{12}$-1,2,3,4-TeCDD and $^{13}C_{12}$-1,2,3,6,7,8-HxCDD were 64–112%. 2,3,7,8-TeBDD was not detected, while 2,3,7,8-TeBDF was identified in the sediment samples with averaged concentration of 0.025 ng/g. The concentration of 2,3,7,8-substituted PtBDF ranged from 0.037 ng/g to 0.15 ng/g. Higher level was found for 2,3,7,8-substituted HxBDF congeners. PBDEs existed in the sediment samples

at relatively high levels. The recoveries of the $^{13}C_{12}$-labeled PBDE internal standards averaged from 66% to 117%. The major PBDE congeners detected were BDE-17, BDE-47, BDE-99, BDE-100, BDE-153, BDE-154 and BDE-183, which were comparable to those reported in Swedish river sediments [29] in the upper layer of a sediment core collected in the Baltic Sea [30] and in Portugal river and coastal sediments [31].

4. Conclusion

Column chromatography with Florisil was successfully used for the separation of PBDEs and PBDD/Fs, which enabled the determination of the two groups of chemicals from one single sample extraction procedure. Florisil column chromatography, followed after the clean-up with individual acidic silica and neutral alumina columns, was successfully used to separate PBDEs from PBDD/Fs. The developed sample preparation procedure, along with gas chromatography–ion trap mass spectrometry analysis, was applied to the analysis of PBDD/Fs and PBDEs in sediment samples collected from a river in the vicinity of e-waste recycling sites. The data indicated that uncontrolled e-waste recycling may have caused the environmental contamination

by PBDFs, along with PBDEs. The application of GC–ion trap MS/MS enhanced detection specificity and sensitivity compared to low resolution GC–MS method. The specificity of ion trap MS/MS has permitted the determination of PBDEs and PBDFs in environmental sediment samples.

Acknowledgements

References

[1] H. Thoma, S. Rist, G. Hauschulz, O. Hutzinger, Chemosphere 15 (1986) 649.
[2] H. Thomas, S. Rist, G. Hauschulz, O. Hutzinger, Chemosphere 15 (1986) 2111.
[3] R.L. Harless, R.G. Lewis, D.D. McDaniel, A.E. Dupuy Jr., Chemosphere 18 (1989) 201.
[4] K. Wiberg, C. Rappe, P. Haglund, Chemosphere 24 (1992) 1431.
[5] S. Sakai, J. Watanabe, Y. Honda, H. Takatsuki, I. Aoki, M. Furamatsu, K. Shiozaki, Chemosphere 42 (2001) 519.
[6] H.R. Buser, Environ. Sci. Technol. 20 (1986) 404.125.
[7] P.W. O'Keefe, Environ. Health Perspect. 23 (1978) 347.
[8] J. Kanters, R. Louw, Chemosphere 32 (1996) 89.
[9] P.M. Lemieux, J.V. Ryan, Waste Manage. 18 (1998) 361.
[10] G. Söderström, S. Marklund, Environ. Sci. Technol. 36 (2002) 1959.
[11] J. Ebert, M. Bahadir, Environ. Int. 29 (2003) 711.
[12] R. Weber, B. Kuch, Environ. Int. 29 (2003) 699.
[13] D. Schuler, J. Jager, Chemosphere 54 (2004) 49.
[14] C. de Wit, Chemosphere 46 (2002) 583.
[15] S. Ohta, D. Ishizuka, H. Nishimura, T. Nakao, O. Aozasa, Y. Shimidzu, F. Ochiai, T. Kida, M. Nishi, H. Miyata, Chemosphere 46 (2002) 689.
[16] A. Sjödin, L. Hagmar, E. Klasson-Wehler, J. Björk, Å. Bergman, Environ. Health Perspect. 108 (2000) 1035.
[17] P.O. Darnerud, G.S. Eriksen, T. Johannesson, P.B. Larsen, M. Viluksela, Environ. Health Perspect. 109 (2001) 49.
[18] D.L. Wang, Z.W. Cai, G.B. Jiang, M.H. Wong, W.K. Wong, Rapid Commun. Mass Spec. 19 (2005) 83.
[19] K. Hayakawa, H. Takatsuki, I. Watanabe, S. Sakai, Chemosphere 57 (2004) 343.
[20] P. Haglund, K.-E. Egebäck, B. Jansson, Chemosphere 17 (1988) 2129.
[21] R. Luijk, H. Wever, K. Olie, H.A.J. Govers, J.J. Boon, Chemosphere 23 (1991) 957.
[22] B.G. Loganathan, K. Kannan, I. Watanabe, M. Kawano, K. Irvine, S. Kumar, H.C. Sikka, Environ. Sci. Technol. 29 (1995) 1832.
[23] K. Kannan, S. Watanabe, J.P. Giesy, Toxicol. Environ. Chem. 67 (1998) 135.
[24] J.W. Choi, S. Fujimaki, K. Kitamura, S. Hashamoto, H. Ito, N. Suzuki, S. Sakai, M. Morita, Environ. Sci. Technol. 37 (2003) 817.
[25] J.W. Choi, J. Onodera, K. Kitamura, S. Hashimoto, H. Ito, S. Suzuki, M. Morita, Chemosphere 53 (2003) 637.
[26] S. Litten, D.J. McChesney, M.C. Hamilton, B. Fowler, Environ. Sci. Technol. 37 (2003) 5502.
[27] J.R. Donnelly, W.D. Munslow, T.L. Vonnahme, N.J. Nunn, C.M. Hedin, C.W. Sovocool, R.K. Mitchum, Biomed. Environ. Mass Spec. 14 (1987) 465.
[28] J. Ebert, W. Lorenz, M. Bahadir, Chemosphere 39 (1999) 977.
[29] U. Sellstrom, A. Kierkegaard, C. de Wit, B. Jansson, Environ. Toxicol. Chem. 17 (1998) 1065.
[30] K. Nylund, L. Asplund, B. Jansson, P. Jonsson, K. Litzén, U. Sellström, Chemosphere 24 (1992) 1721.
[31] S. Lacorte, M. Guillamon, E. Martinez, P. Viana, D. Barcelo, Environ. Sci. Technol. 37 (2003) 892.

Synthesis and characterization of *p*-toluenesulfonate incorporated poly(3,4-ethylenedioxythiophene)

Yinghong Xiao [a,b,c], Chang Ming Li [a,b,*], Shucong Yu [a],
Qin Zhou [a,b], Vee. S. Lee [d], Shabbir. M. Moochhala [d]

[a] *School of Chemical and Biomedical Engineering, Nanyang Technological University, Singapore 637457, Singapore*
[b] *Center for Advanced Bionanosystems, Nanyang Technological University, Singapore 637457, Singapore*
[c] *School of Chemical Engineering, Nanjing University of Science and Technology, Nanjing 210014, China*
[d] *Defence Medical & Environmental Research Institute, DSO National Laboratories, Singapore 117510, Singapore*

Abstract

Poly(3,4-ethylenedioxythiophene) (PEDOT), a conducting polymer, was electrochemically synthesized with *p*-toluenesulfonate (TSNa) as a dopant on gold surface. The electrochemical properties of the polymer were studied by impedance spectroscopy and cyclic voltammetry (CV). It was found that the impedance magnitude of the electrode significantly decreased over a wide range of frequency from 10^0 to 10^4 Hz after the polymer deposition. The CV demonstrated enhanced reversibility of the PEDOT film. The surface morphology was investigated by scanning electronic microscope (SEM) and atomic force microscope (AFM). Due to the effect of TSNa structure, nano-fungus was observed. Polymerization time was optimized and 30 min deposition resulted in the highest charge capacity, showing the highest electroactive surface area, possibly due to its porous structured polymer. Moreover, the high specific surface area could be favorable for cell attachment. The stability of PEDOT in glutathione (GSH), a common biologically relevant reducing agent, was studied with polypyrrole (PPy) as a baseline. It showed that the former had much better stability than the latter and it could be an excellent candidate for potential applications of in vivo neural devices.
© 2006 Elsevier B.V. All rights reserved.

Keywords: PEDOT; Electrochemical properties; Surface morphology; Stability against reducing agents

1. Introduction

Since the highly conductive polyacetylene was discovered in the late 1970s [1], conducting polymers have been intensively studied and successfully used in various areas such as sensors and actuators [2–4], batteries [5], antistatic coatings for photographic films [6], processing of electronic circuit boards [7]. Conducting polymers show interesting chemical and physical properties derived from their unique conjugated π-electron system [8]. Amongst these polymers, polypyrrole (PPy) is often chosen for biological applications due to its ease of preparation, good conductivity and biocompatibility [9–11]. PPy was applied to modify implantable devices for neural recording and drug delivery [12,13]. However, applications of

PPy suffer from its instability in biological environment due to its structural disorder. Oxidized PPy is particularly unstable in biologically relevant reducing agents such as dithiothreitol (DTT) and glutathione (GSH). It is apparently disadvantageous to PPy modified electrodes which are implanted in brain tissues for long term use. Thiophene is difficult to polymerize electrochemically due to its high oxidation potential in aqueous media [14]. Recently a derivative of polythiophene, poly(3,4-ethylenedioxythiophene) (PEDOT), which could be easily electrochemically synthesized has aroused great interest of material scientists. PEDOT has been classified as a low band gap conducting polymer. The 3,4-dioxy substitution pattern blocks the possibility of α-β(β′) coupling normally presented in PPy (Scheme 1, left), which can result in a more regiochemically defined material (Scheme 1, right), adds electron density to the aromatic heterocycle, and reduces the monomer oxidation potential. Its high thermal stability has been reported [15]. Additionally, the decrease of the polymer reduction potential would

* Corresponding author. Tel.: +65 67904485; fax: +65 67911761.
E-mail address: ecmli@ntu.edu.sg (C.M. Li).
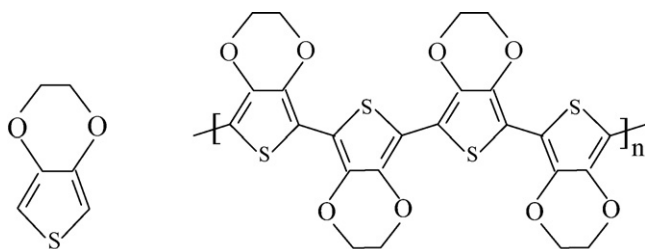
Scheme 1. Chemical structures of EDOT monomer (left) and PEDOT polymer (right).

yield an increased stability in the oxidized conducting form [16]. The superior properties of PEDOT discussed above render it favorable as an electrode material in implantable devices.

Implantable electronic systems in the brain tissues particularly require low impedance of the electrode, high charge capacity, high surface area and stability to the reducing agents in the brain tissue environment. There is a great need to provide a stable electrode material that can not only facilitate electron transfer between the neurons and electrode, but can also attach neural cells onto the electrode sites.

In our study, PEDOT was electrosynthesized with *p*-toluenesulfonate (TSNa) as the dopant onto the gold electrode. TSNa was selected since its molecules are large enough to occupy free spaces in the polymer while small enough to dedope from the polymer matrix. The feature provides the possibility to incorporate bulky negatively charged biomolecules by subsequent ion exchange [17] for implantable devices. TSNa could be replaced by the biomolecules in the ion exchange process to eliminate the cytotoxicity of the devices. Thus, the synthesized PEDOT/TSNa films in this work were optimized and characterized for such a potential application. Thomas et al. reported that 3,4-dioxy substituted PPy showed better stability against reducing agents than PPy in DTT solution [16]. For the first time we studied the stability of PEDOT against a typical biological reducing species, GSH, and proposed its stability enhancement mechanisms.

2. Experimental

2.1. Instrumentation

All controlled-potential electrochemical syntheses were performed with CHI 760B Electrochemical Station (USA). A three-electrode cell was set up for all electrochemical experiments, in which a gold disk electrode, a platinum wire, Ag/AgCl (saturated KCl) were used as working, counter and reference electrode, respectively. Electrochemical impedance spectroscopy and cyclic voltammetry (CV) were performed using the same instrument as for the electrosynthesis and the same cell set-up was employed. 0.01 M PBS (pH 7.4) was used as the electrolyte. During impedance measurements, 5.0 mV ac sinusoid signal was applied as the input perturbation and dc bias potential was set at 0.0 V. The impedance measurements were carried out over 10^0–10^4 Hz. The CV was conducted with a scan rate of 100 mV/s and scan potential range over −0.8 to 0.4 V.

SEM (JEOL JSM-6700F FEG, USA) was used to study the surface morphology of the resultant PEDOT/TSNa film with a voltage of 5.0 kV and spot size of 4 (arbitrary units).

Surface topography of the PEDOT/TSNa film was investigated with AFM (Dimension 3100 SPM, Veeco, USA) and high resolution surface images were produced. In AFM characterization, the tapping mode with a silicon probe (RTESP, Veeco, USA) over scan sizes of 15 μm and the scan rate of 0.20 Hz was used.

2.2. Materials

EDOT monomer was purchased from Aldrich, purified via vacuum distillation and kept refrigerated at 4 °C under nitrogen before use. TSNa (95%) from Sigma–Aldrich was of analytical grade and was used as received. L-Glutathione (reduced, 98%) was purchased from Aldrich. Deionized Milli-Q water (18.2 MΩ cm, Millipore Inc.) was used in all experiments. The gold electrodes (2 mm in diameter) were sequentially polished with 1.0, 0.3 and 0.05 μm Al_2O_3 slurry, then washed with acetone and isopropyl alcohol followed by thorough rinsing with deionized water. All experiments were performed at room temperature, unless otherwise stated.

2.3. Electrosynthesis and stability test

Different electrosynthesis methods were discussed in [18]. Preparation of PEDOT in this report was carried out by the potentiostatic method in 0.01 M EDOT + 0.1 M TSNa solution. Before polymerization, the electrochemical cell was ultrasonically cleaned in water and the monomer solution was purged with N_2 for 20 min. All electrochemical polymerizations were performed with CHI 760B potentiostat (USA).

The polymer stability against the reducing agent was studied by immersing the PEDOT coated electrode in 10 mM GSH aqueous solution. The samples were removed from the solution followed by CV measurements at 1-day intervals.

3. Results and discussion

3.1. Electrodeposition of PEDOT

EDOT monomer has poor solubility (0.01 M at room temperature) in water. The solubility can be increased by mixtures of water and some organic solvents [19]. However, water is preferred in our study due to the potential bio-applications of the polymer film. We found that TSNa, as a surfactant, could not cause significant increase of EDOT solubility in water as sodium dodecylsulfate (SDS) or sodium dodecylbenzenesulfonate (SDBS) did [20].

A suitable potential for the potentiostatic synthesis of PEDOT is critical, since the conducting polymers can be over-oxidized at higher potentials, leading to its deterioration and even destruction. The linear sweep voltammetry (LSV) was conducted to determine the suitable polymerization potential.

Results in Fig. 1 show two oxidation peaks of PEDOT in a potential range from 0.2 to 1.6 V. As discussed in [21], the
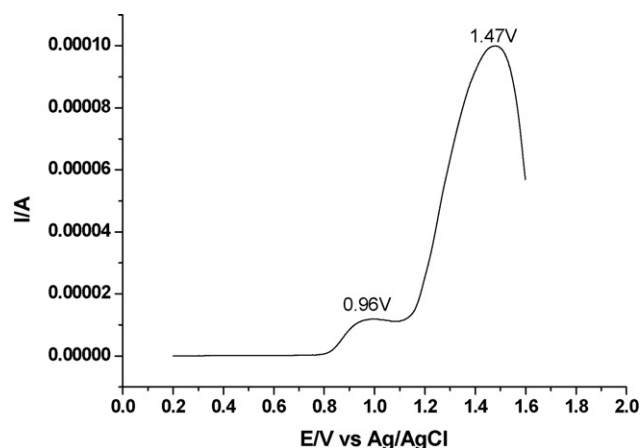
Fig. 1. LSV of 0.01 M EDOT in 0.1 M TSNa aqueous solution.

first poorly defined peak at about 0.96 V corresponded to the oxidation of the monomer whereas the second one at 1.47 V was attributed to the over-oxidation of the deposited polymer. Apparently, the suitable potential for PEDOT synthesis should be higher than 0.96 V and lower than 1.47 V. In our work, 1.0 V was chosen as the deposition potential.

3.2. Electrochemical behavior of PEDOT/TSNa

PEDOT was potentiostatically synthesized with different polymerization times. It was clearly observed that a sky-blue thin film formed on the gold electrode surface within several seconds. Impedance magnitude was measured on both bare and PEDOT coated electrodes. As shown in Fig. 2, the impedance magnitude of all PEDOT-coated electrodes was significantly reduced over 10^0–10^4 Hz in comparison to that of the bare gold. At lower frequency range (1–10 Hz) capacitance was the prime component for the impedance while at frequencies above 30 Hz, including the frequencies of most neural activity (300–1000 Hz), the dominant impedance changed from capacitive to resistive. Since the resistance reduction of the electrode is essential to produce high-quality signals including high S/N and superior sensitivity
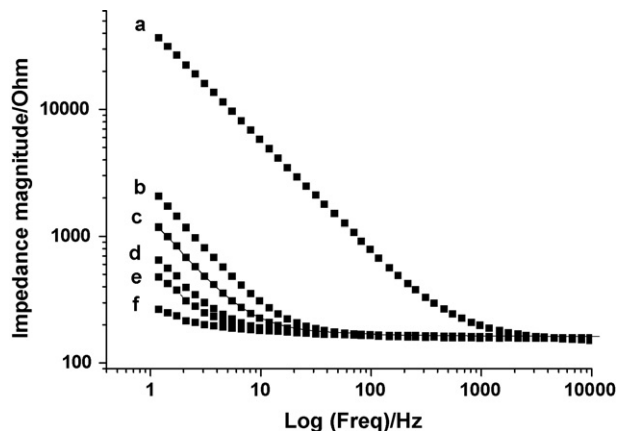

Fig. 2. Impedance spectroscopy of bare gold (a) and PEDOT coated electrodes (b–f). Deposition time was 5 min (b), 10 min (c), 20 min (d), 30 min (e) and 60 min (f).
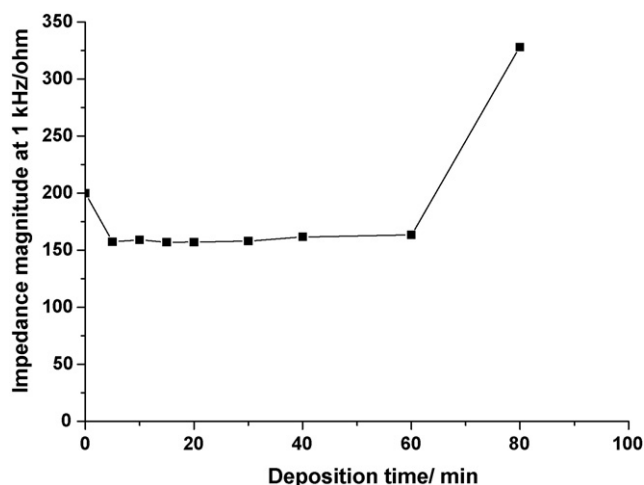

Fig. 3. Relationship between magnitude at 1 kHz and deposition time.

[22] for in vivo measurements of neuron activity, apparently, the PEDOT electrode could be potentially used in miniaturized implantable devices.

Since 1 kHz is the frequency often used for measurements of the biologically relevant activity, relationship of the impedance magnitude at 1 kHz versus PEDOT deposited time was studied. The results are shown in Fig. 3. It was observed that the impedance magnitude had a relatively sharp decrease initially with the deposition time, indicating a thin layer formation on the gold surface increased greatly the true electrode surface area due to the porous and very conductive polymer. However, with the further increment of deposition time, the film impedance magnitude became relatively stable even with slight increase. When the deposition time was increased to more than 60 min, the impedance sharply increased even worse than that of the bare gold.

CV characteristics of a conducting polymer could show its reversibility, which directly affect its switching ability in electronic measurements. CVs of PEDOT films prepared by using different deposition times were measured in PBS (Fig. 4). Up to 30 min of deposition time, the enclosed area of CV curves increased with the deposition time, and the CV curves showed better reversible, symmetric redox waves (Fig. 4A). The shape of the curve became more symmetric and the redox waves were getting better defined, indicating the doping redox reaction was more reversible for electron or charge transfer in the film. However, when the time was more than 30 min, the area sharply became smaller (Fig. 4B) and the redox waves became less prominent. In order to show the reversibility and stability of the film, multiple CV measurements were conducted on the 30 min deposited film. The results are shown in Fig. 4C. It was observed that the enclosed area was reduced for the first three cycles and then became stabilized up to 200th cycles. The reduction of the enclosed area during the first few cycles of reversible reactions is common for electrodes even inert ones such as Au and Pt due to surface stabilization. However, all CV curves for the PEDOT showed well defined, reversible redox waves, demonstrating good reversibility. The enclosed area of CV is proportional to the charge capacity of
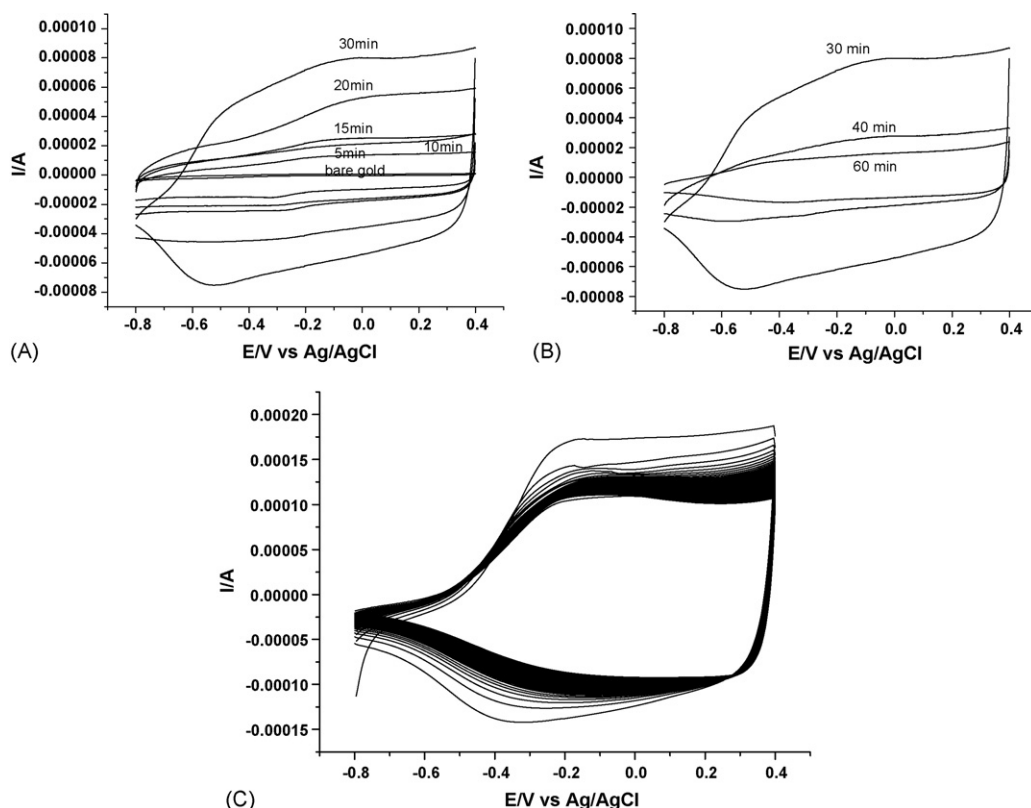
Fig. 4. Cyclic voltammograms of PEDOT films, which were prepared with different synthesis times as indicated in the figure (A and B). CV of bare gold was plotted in the figure as a negative control. Electrochemical reversibility of the 30 min deposited film was demonstrated by multiple CV sweeping (C).

the electrode, which was determined by electrochemical doping/dedoping process + double layer capacitance of the PEDOT film. Fig. 5 shows the change of charge capacity versus the deposition time. Clearly, within 30 min, the charge capacity increased because both electrochemically active doping sites and true surface area increased with the film growth. Fig. 3 shows that the resistance did not increase significantly for the 40 and 60 min deposited PEDOT, but their charge capacity sharply dropped and no doping/dedoping redox waves were observed. The results might indicate that further deposited polymer changed the film morphology and porous structure, leading to decrease of real surface area and deactivation of doping sites. The explanation is discussed in more detail later by the SEM and AFM results.
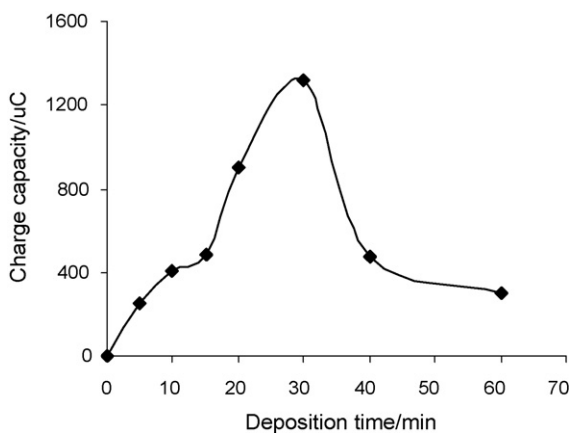
3.3. Morphologies of PEDOT/TSNa films

SEM characterization was conducted on different time-deposited PEDOT films. As shown in Fig. 6, the morphology of the films exhibited a nano-fungus-like structure, which has not been reported up to date. A possible mechanism for the formation of such morphology is that the dopant of TSNa is a surfactant and existed in the form of lamella at the concentration of 0.1 M applied in our experiments [23]. The polymer could grow with the pseudo-molecular template and thus to form the fungus-like shapes. The rough surface shown in Fig. 6 will evidently provide more sites for attachment of neural cells and enhance adhesion between PEDOT and neurons. From image (a) to (f) we clearly observed that the density of the nano-fungus was getting higher and higher and finally the adjacent fungi merged together. The surface roughness, i.e. the specific surface area increased until the maximum (d) followed by a decrease with deposition time (from (e) to (f)). The large fungus in (e) and (f) looked like a sintered, melted material and lost its porous structure shown in (d). This might indicate that the deposition for more than 30 min not only grew the film thickness, but also filled the pores. A typical nano-fungus structure can be clearly observed from the lower high magnification SEM image. It is known that the high specific area is mainly contributed by the micropore but not macropore structure. Obviously, the

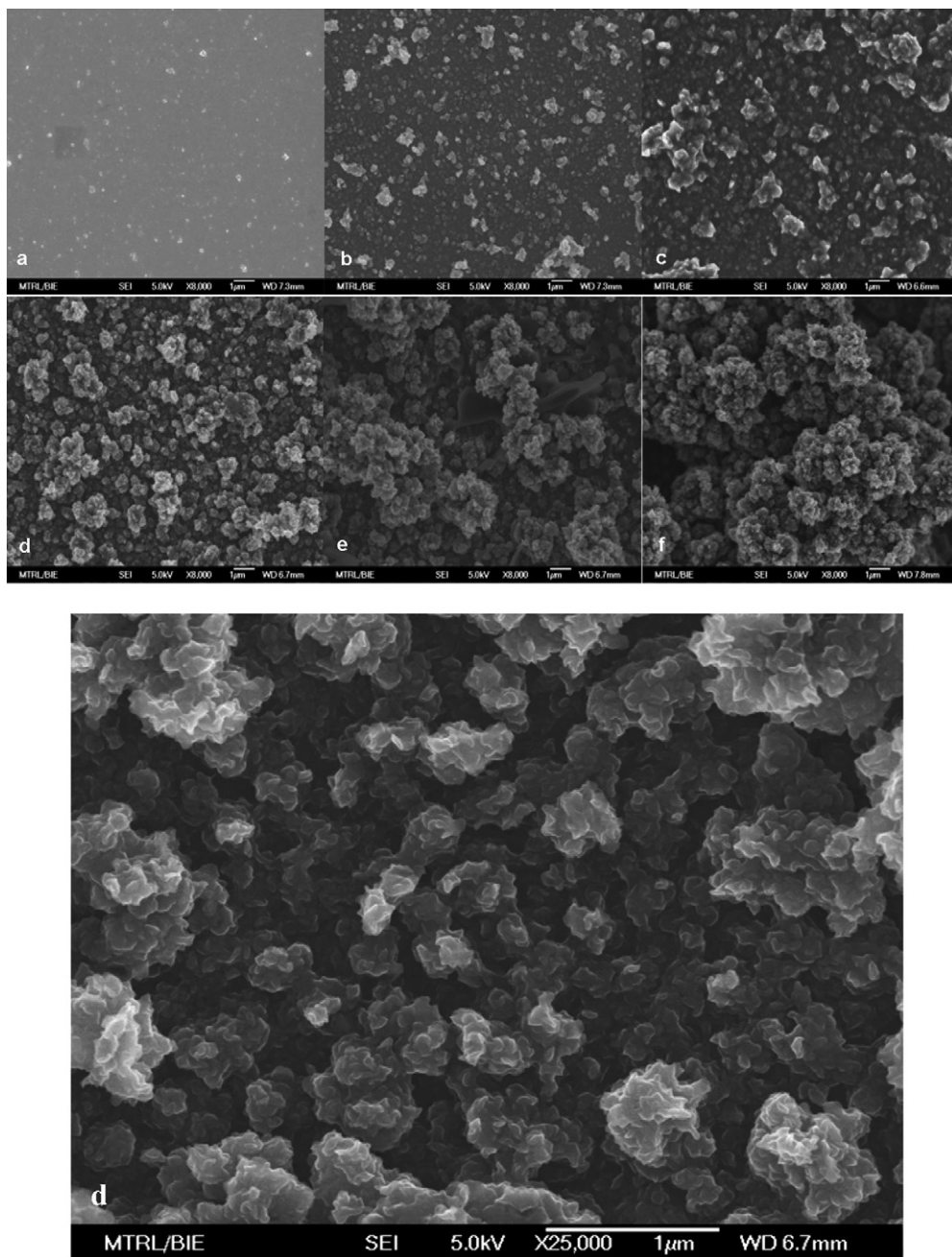Fig. 5. Relationship between the film charge capacity and deposition time.

Fig. 6. SEM images of PEDOT film with different deposition time. (a) 5 min, (b) 10 min, (c) 20 min, (d) 30 min, (e) 60 min and (f) 120 min. Lower: high magnification image of (d).

structure in (e) and (f) significantly reduced the specific surface area. This is one of the main reasons to cause the dramatic decrease of the charge capacity in Fig. 5. It demonstrates that the deposition time is very critical to obtain a superior PEDOT film.

Three PEDOT samples with different deposition times which showed typical different morphology were characterized by AFM. The results are shown in Fig. 7. It could be seen that the topographies in (b)–(d) had very notable variations from that of the smooth bare gold (a). From (b) to (c), the surface became rougher and size of the clusters was getting more uniform as the film grew thicker. The clusters coalesced as the film continued to grow (d). The lower 3D images clearly show that the roughness increased with deposition time until its maximum (c) followed by a decrease when some micropores were filled with the material. This might not only decrease the specific surface area, but also could block the doping site. The results are in agreement with the SEM images.

3.4. Stability of PEDOT compared with PPy against biological reducing agent

It is well known that lower reduction potential of a conducting oxidized polymer (p-type polymer) can give higher
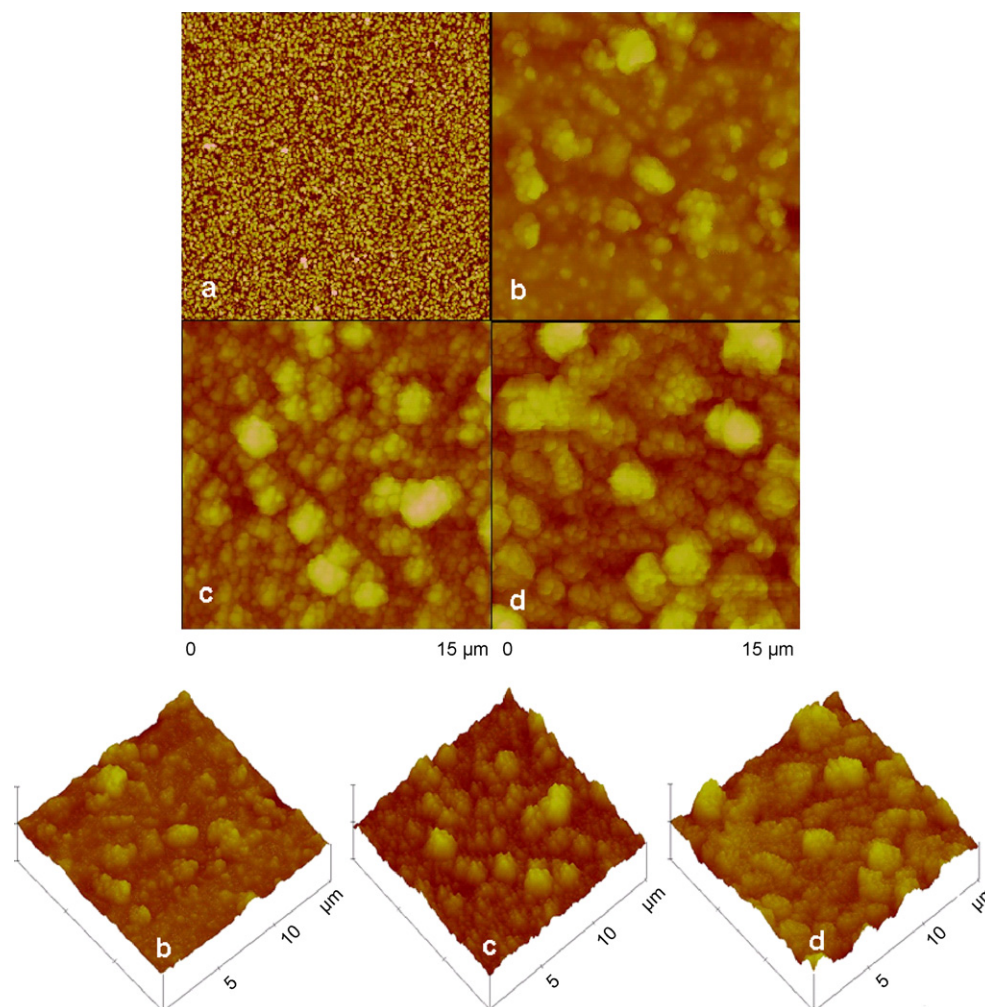
Fig. 7. AFM images of PEDOT coated electrode with deposition time of (a) 0 min, (b) 15 min, (c) 30 min and (d) 60 min. Lower: three-dimension images.

stability against biological reducing agents. Lower reduction potential of the p-type polymer can eliminate reactions of the reducing agents and oxidized form which would result in loss of conductivity of the polymer. The result of PEDOT stability in reducing agent solutions is shown in Fig. 8. As
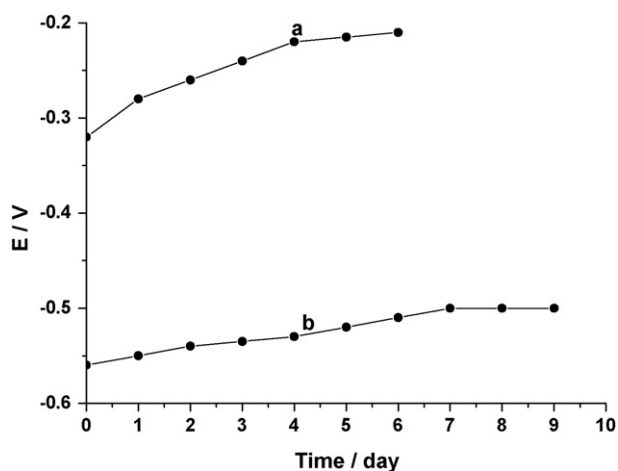

Fig. 8. Comparison of the stability of PPy (a) and PEDOT (b) against GSH.

control, a film of PPy/TSNa was potentiostatically electrosynthesized at 0.8 V and exposed to the same reducing agent. In comparison of the reduction potential for PPy (reduction potential = -0.32 V), PEDOT had a much lower reduction potential (-0.56 V), indicating that the latter had better stability against the reducing agents than the former. The reduction potentials of both PPy (a) and PEDOT (b) positively shifted with immersing in GSH, a common reducing agent in biological system. However, the deteriorate rate of the reduction potential for PEDOT was only about 5 mV/day (about 50 mV shift for 10 days), whereas the deteriorate rate of reduction potential for PPy was about 20 mV/day. This showed that the positive shift rate of the reduction potential for PEDOT was much lower than that for PPy. The results indicate that PEDOT coated electrode is favorable for long-term applications as an implantable device.

4. Conclusion

Electrosynthesis and characterization of PEDOT on gold was conducted. The suitable potential for the polymerization was experimentally determined to be 1.0 V to prevent

the polymer from over-oxidation. The PEDOT film greatly decreased the impedance of the electrode, which is favorable for obtaining high-quality signals in an electronic device in a biological system. At the characteristic frequencies of neural biological activity (300–1000 Hz), the dominant factor of the PEDOT impedance changed from capacitive to more resistive. The PEDOT electrode was most reversible and had highest charge capacity when it was formed with 30 min deposition time. The electrochemical properties correlated well with the surface morphology variation during the polymerization process observed by SEM and AFM. The change of the surface area and morphology plays a critical role in the electrochemical and electronic properties of the film. The results demonstrated that there was an optimized deposition time to prepare the superior PEDOT electrode. With the potentiostatic deposition method, our experimental results demonstrated that the 30 min deposited polymer had the best electrochemical reversibility, highest charge capacity and lowest resistance. This work also demonstrated that the PEDOT stability against reducing agents was significantly better than that of PPy. Thus, PEDOT could be a good candidate to apply in the implantable neural devices for long-term operation. The cell attachment and the biocompatibility of PEDOT/TSNa electrode are under investigation in our lab for potential applications.

Acknowledgments

References

[1] H. Shirakawa, E.J. Lewis, A.G. MacDiarmid, C.K. Chiang, A.J. Heeger, J. Chem. Soc. Chem. Commun. (1977) 578.
[2] C.M. Li, W. Chen, X. Yang, C.Q. Sun, C. Gao, Z.X. Zheng, J. Sawyer, Front. Biosci. 10 (2005) 2518.
[3] J. Jang, M. Chang, H. Yoon, Adv. Mater. 17 (2005) 1616.
[4] Y. Berdichevsky, Y.-H. Lo, Adv. Mater. 18 (2006) 122.
[5] J.H. Burroughs, D.D.C. Bradley, A.R. Brown, R.N. Marks, K. Mackay, R.H. Friend, P.L. Burns, A.B. Holmes, Nature 347 (1990) 539.
[6] L. Groenendaal, F. Jonas, D. Freitag, H. Pielartzik, J.R. Reynolds, Adv. Mater. 12 (2000) 481.
[7] Z.N. Bao, Adv. Mater. 12 (2000) 227.
[8] A.J. Heeger, Angew. Chem. Int. Ed. 40 (2001) 2591.
[9] G. Shi, M. Rouabhia, Z. Wang, L.H. Dao, Z. Zhang, Biomaterials 25 (2004) 2477.
[10] C.E. Schimidt, V.R. Shastri, J.P. Vacanti, R. Langer, Proc. Natl. Acad. Sci. U.S.A. 94 (1997) 8948.
[11] N.A. Peppas, R. Langer, Science 263 (1994) 1715.
[12] P.M. George, D.A. LaVan, J.A. Burdick, C.-Y. Chen, E. Liang, R. Langer, Adv. Mater. 18 (2006) 577.
[13] D.-H. Kim, M. Abidian, D.C. Martin, J. Biomed. Mater. Res. 71A (2004) 577.
[14] L.B. Groenendaal, G. Zotti, P.-H. Aubert, S.M. Waybright, J.R. Reynolds, Adv. Mater. 15 (2003) 855.
[15] H. Yamato, M. Ohwa, W. Wernet, J. Electroanal. Chem. 397 (1995) 163.
[16] C.A. Thomas, K. Zong, P. Schottland, J.R. Reynolds, Adv. Mater. 12 (2000) 222.
[17] Y.H. Xiao, J.F. Che, C.M. Li, C.Q. Sun, Y.T. Chua, V.S. Lee, J.H.T. Luong, J. Biomed. Mater. Res. A 80A (2006) 925.
[18] C.M. Li, C.Q. Sun, W. Chen, L. Pan, Surf. Coat. Tech. 198 (2005) 474.
[19] M. Ilic, F.-H. Haegel, S. Zlatanovic, N. Potkonjak, B. Simonovic, Environ. Chem. Lett. 3 (2005) 82.
[20] A. Lima, P. Schottland, S. Sadki, C. Chevrot, Synthetic Met. 93 (1998) 33.
[21] X. Du, Z. Wang, Electrochim. Acta 48 (2003) 1713.
[22] D.R. Kipke, R.J. Vetter, J.C. Willianms, J.F. Hetke, IEEE T Neur. Sys. Reh. 11 (2003) 151.
[23] M.J. Rosen, Micelle Formation by Surfactants, third ed., John Wiley & Sons, Inc., New York, 2004 (Chapter 3).

Determination of phosphate in water by means of a new electrochemiluminescence technique based on the combination of liquid–liquid extraction with benzene-modified carbon paste electrode

Yan Xue, Xingwang Zheng [*], Guixin Li

School of Chemistry and Material Science, Shaanxi Normal University, Xi'an 710062, PR China

Received 24 July 2006; received in revised form 1 November 2006; accepted 1 November 2006
Available online 4 December 2006

Abstract

In this paper, it was found that the hydrophobic ion-associated complex of the molybdophosphoric heteropoly acid with protonated butyl-rhodamine B (BRhB) could be formed and was further selectively extracted into the bulk of the paraffin oil-based carbon paste electrode (CPE). At the same time, compared with other modifiers, the benzene-modified CPE created a suitable electrochemiluminescence (ECL) reaction microenvironment for electro-oxidation BRhB to produce the stronger ECL signal when a 1.30 V electrolytic potential was applied to the CPE in the alkaline medium. Based on these findings, a selective and sensitive ECL method for indirectly detecting phosphate was developed. Under the optimum experimental conditions, the ECL intensity was linear with the concentration of phosphate in the range of 2.0×10^{-10} to 1.0×10^{-8} g mL^{-1}. The detection limit was 8.0×10^{-11} g mL^{-1}. The proposed method has been applied successfully to the analysis of phosphate in the water samples.
© 2006 Elsevier B.V. All rights reserved.

Keywords: Electrochemiluminescence; Phosphate; Butyl-rhodamine B; Benzene-modified carbon paste electrode; Liquid–liquid extraction; Water

1. Introduction

Phosphorus plays an important role in biochemical processes [1]. Phosphate concentration in a body of water is commonly used as an index for the estimation of its degree of eutrophication. Therefore, sensitive analytical techniques are needed to determine phosphate. For this purpose, the spectrophotometric methods, based on the formation of the phosphomolybdate blue, are the most frequently used for inorganic phosphorus determinations [2,3]. However, this kind of method suffered from time consuming and poor sensitivity. Several alternative methods have also been developed for measuring low concentrations of phosphate, including ion exchange chromatography [4], gas chromatography [5], fluorometry [6] and chemiluminescence [7,8]. But, due to requirement well-controlled experimental conditions, the requirement of the tedious sample pretreatment procedures and the poor selectivity, a simple, sensitive and selective method for phosphate is still desirable.

In recent years, as a powerful luminescence technique, electrochemiluminescence (ECL) analysis has been received much attention in analytical science since this analytical technique not only offers the advantages of the conventional chemiluminescence (CL) (such as the higher sensitivity and rapid response time), but also offers some additional advantages [9]. For example, in ECL analysis, the ECL reaction can be controlled and manipulated by the applied potential, and the ECL emission is concentrated close to the electrode surface, which can be chemical modified and accurately positioned in relation to both the modification of the special ECL reaction step and the optical measurement system for excellent sensitivity. Based on these advantages mentioned above, many applications with ECL technique, such as chemical sensor [10], imaging [11], optical studies [12] and the detector for chromatography [13], etc., have been widely reported.

However, as reviewing the analytical applications of the ECL methods for the real samples, it is easily found that the selectivity of ECL methods is poor due to the use of high electrolytic potential. In addition, compared with other analytical methods such as electroanalytical methods or the CL methods, the analytical application fields of the ECL analysis are narrow since the

* Corresponding author. Tel.: +86 29 85308184.
  E-mail address: zhengxw@snnu.edu.cn (X. Zheng).

useful ECL reagents are limited. To overcome these drawbacks, the combination of the ECL analysis with different separation techniques, such as capillary electrophoresis (CE) [14] and high performance liquid chromatogram (HPLC) [15], the introduction of the chemically modified electrode (CME) technique [16] in the ECL analysis, synthesis of new ECL reagents [17], etc., were developed to improve performances of the ECL analysis. Unfortunately, these analytical schemes suffered from complicated operation, the use of expensive apparatus and requirement of complicated samples pretreatment procedure. Thus, developing the simple, cheap and highly selective ECL detecting scheme was more desirable.

On the one hand, as another powerful separation technique, liquid–liquid extraction (LLE) can be used to move species dissolved in an aqueous phase into an organic phase. In analytical applications, LLE may serve the following three purposes: to preconcentrate the analyte, to eliminate interferences and to increase the selectivity. LLE has still been paid much attention by the analyst due to cheap experimental set-up and simple operation in contrast with that of the CE or HPLC. Thus, the combination of LLE with ECL analysis offers more potential. For example, based on extraction pretreatment of ion-associated complex and ECL analysis, Xu and co-workers [18] proposed a new investigative idea to determine non-electroactive species (perchlorate). And it was also a new idea to broaden the analytical application fields of the ECL analysis and improve the ECL analytical selectivity. However, analytical performance was influenced since the whole analytical process relating to multi-steps, such as extracting preconcentration, back-extraction, ECL analysis and so on. Furthermore, because the introduction of back-extraction induced dilution effect of sample solution, sensitivity of that method was seriously influenced. Thus, the new scheme to achieve the effective combination of the ECL analysis with LLE was still more desirable.

In this paper, it was found that, while the paraffin oil-based carbon paste electrode (CPE) was modified with benzene, this chemically modified carbon paste electrode (CMCPE) could not only effectively extract a hydrophobic ion-associated complex, formed by the electrostatic interaction of the molybdophosphoric heteropoly acid with protonated BRhB, but also create a suitable ECL reaction microenvironment for electro-oxidation BRhB to produce a strong ECL emission signal for indirectly detecting phosphate. Based on these findings, a novel and sensitive ECL technique for the determination of phosphate in water was developed. At the same time, a new idea, the in situ combination of the LLE (decreasing sample and reagent consumption, and reducing analysis time) with the CME technique to improve the ECL analytical performances by modifying the ECL reaction microenvironment and to broaden the analytical application fields of the ECL analysis, was also proposed.

2. Experimental

2.1. Reagents

All chemicals were of analytical reagent grade and deionized water was used for the preparation of solutions. Phosphate stock solution (1.0×10^{-3} g P mL^{-1}) was prepared by dissolving 0.4395 g of potassium dihydrogenphosphate (dried at 110 °C for 1 h) in 100 mL of deionized water; working solutions of different concentrations were obtained by step-wise dilution of the stock solution. Ammonium molybdate stock solution (1.0×10^{-2} mol L^{-1}) was prepared by dissolving 1.24 g of ammonium molybdate(VI) tetrahydrate in 100 mL of deionized water. A working solution (1.0×10^{-3} mol L^{-1}) was prepared by diluting 10.0 mL of the stock solution in 100 mL of water. BRhB stock solution (3.0×10^{-4} mol L^{-1}) was prepared by dissolving 0.1606 g BRhB in deionized water and further diluted to 1 L.

2.2. Apparatus

The electrolytic cell utilizes a conventional three-electrode set-up. The ECL cell was made of a micro weighing bottle (height: 3.5 cm, diameter: 2.5 cm). A benzene-modified CPE, coiled platinum wire and Ag wire were used as working electrode, counter electrode and pseudo-reference electrode, respectively. All potentials were measured and reported with respect to the silver pseudo-reference electrode.

The applied potential for single-step potential electrolysis was achieved by the combination of the DJS-292 potentiostat with the XFD-8B ultra-low frequency signal generator. The ECL intensity was transformed into an electrical signal by a R456 photomultiplier (PMT) (Hamamatsu), which was biased at 800 V, and the ECL cell was placed in front of the PMT. The signal was recorded with a MCDR-A ECL analytical system (Xi'an Remax Electronic Science Tech. Co. Ltd., Xi'an, China). Cyclic voltammetric measurements were achieved by a CHI660 electrochemistry working station (CH Instruments Inc.). Preconcentration procedure of the sample or standard phosphate solutions was carried out in 50 mL solution stirred by a magnetic stirrer.

2.3. Preparation of benzene-modified CPE

The modified electrode was fabricated as the following steps: first, the paraffin oil and benzene were mixed to form a uniform mixture; second, the graphite powder was then added into the paraffin oil–benzene mixture in 2:1 proportion (weight to bulk ratio). The constituents were thoroughly hand-mixed to produce a homogeneous paste in a mortar and pestle for 30 min, followed by packing the resulting paste firmly into the cavity (5-mm diameter, 3-mm depth) of graphite electrode tip and a copper wire was inserted through the opposite end to produce the electrical contact. The surface of the CPE was smoothed on a weighing paper and rinsed with deionized water prior to each experiment.

2.4. Procedure

For the preconcentration step, 2.5 mL 1.0×10^{-3} mol L^{-1} (NH$_4$)$_2$MoO$_4$, 4.8 mL 0.06 mol L^{-1} HCl and 5.0 mL 3.0×10^{-5} mol L^{-1} BRhB were added into a 50 mL calibrated flask

and the solution was diluted to volume with water, and mixed well. The freshly polished CPE was immersed into this stirred blank solution and an appropriate interfacial potential was applied to the electrode for a given time period. Afterward, the electrode was removed, rinsed with deionized water, and placed in the ECL cell containing $0.06 \, \text{mol} \, \text{L}^{-1}$ NaOH. A stable blank ECL signal was recorded when 1.30 V electrolytic potential was applied to the working electrode. The sample or standard phosphate solution, which contained not only reagents of the blank solution but also appropriate concentration of phosphate, was also measured in similar way using the same electrode. The concentration of phosphate was quantified via the peak height of the relative ECL emission intensity that was obtained by subtracting the blank ECL emission intensity from that of the sample or standard phosphate solution. Finally, the CPE was held at +1.40 V for 100 s to clean the remaining accumulated species.

3. Results and discussions

3.1. The choice of the ECL indicator

Based on the ion association reaction of phosphomolybdate with a cationic dye, spectrophotometry and spectrofluorimetry for measuring phosphate have been proposed [6,19]. In this study, we tried to develop an ECL method for measuring phosphate in the same way. Thus, suitable cationic dyes should be chosen for their ability to form a hydrophobic ion-associated complex with the molybdophosphoric heteropoly acid as well as excellent stability and ability to offer the better ECL performance for indirect determination phosphate in the alkaline medium.

Based on this consideration, a series of cationic dyes, including malachite green, rhodamine B, butyl-rhodamine B, methylene blue and crystal violet, were investigated. The experimental results showed that by employing a fixed concentration of dyes, ECL reaction medium of $0.1 \, \text{mol} \, \text{L}^{-1}$ NaOH and final potential of 1.2 V, BRhB presented the strongest ECL signal compared with that of other cationic dyes and was most suitable for this purpose. Therefore, BRhB was selected for the subsequent experiments.

3.2. The fabrication of the CMCPE

The properties of the binder used to fabricate the CPE strongly affected extraction performances of the resulting CPE for the target analyte [20,21]. Based on this consideration, some binders, such as nujol oil, mineral oil, paraffin oil and silicone oil, were investigated for effective extracting the ion-associated complex into the bulk of the resulting CPE. The experimental results showed that the obvious ECL signal could be observed at the CPE with the paraffin oil as the binder. At the same time, to demonstrate the extracting behavior of the paraffin oil for this hydrophobic ion-associated complex, the extraction experiment was done in test tube. About $100 \, \mu\text{L}$ $1.0 \times 10^{-3} \, \text{mol} \, \text{L}^{-1}$ $(\text{NH}_4)_2\text{MoO}_4$, $200 \, \mu\text{L}$ $0.06 \, \text{mol} \, \text{L}^{-1}$ HCl and $200 \, \mu\text{L}$ $3.0 \times 10^{-5} \, \text{mol} \, \text{L}^{-1}$ BRhB solutions were mixed and

diluted to 2 mL with water, then 2 mL paraffin oil was added and it was shaken slightly for 5 min. After the solution was allowed to stand for 20 min, the color of the paraffin oil layer almost did not change. But while the standard phosphate solution was added into the tube, the red color of BRhB in the paraffin oil phase was presented. These results indicated that the hydrophobic ion-associated complex of the BRhB with molybdophosphoric heteropoly acid was effectively extracted into the paraffin oil phase. So the paraffin oil was selected as the binder for CPE.

On the other hand, it was also found that although the ECL signal of electro-oxidation BRhB extracted into the proposed CPE was obvious, this ECL signal cannot be used to develop a sensitive ECL method for indirectly detecting phosphate. Considering that the microenvironment or the structure of the electrode surface often strongly affected the properties of the ECL reaction, the relating research work was focused on modifying a suitable modifier in the CPE to create a suitable ECL reaction microenvironment for improving the analytical performances. To the best of our knowledge, the hydrophobic organic solvents had been used as the hydrophobic medium in the ECL reactions and presented the better ECL performances [22,23]. Based on these considerations, some hydrophobic organic solvents such as benzene, toluene, dimethylbenzene, nitrobenzene, etc., were investigated as the modifiers, respectively. The experimental results showed that the strongest ECL signal was obtained by using the benzene-modified CPE.

At the same time, the cyclic voltammetric experiment of electro-oxidation BRhB preconcentrated into the benzene-modified CPE and bare CPE were investigated, respectively. As shown in Fig. 1, these results showed that, compared with the bare CPE, although the ECL performances of electro-oxidation BRhB were obviously different (S/N in bare CPE is 2.1, S/N in
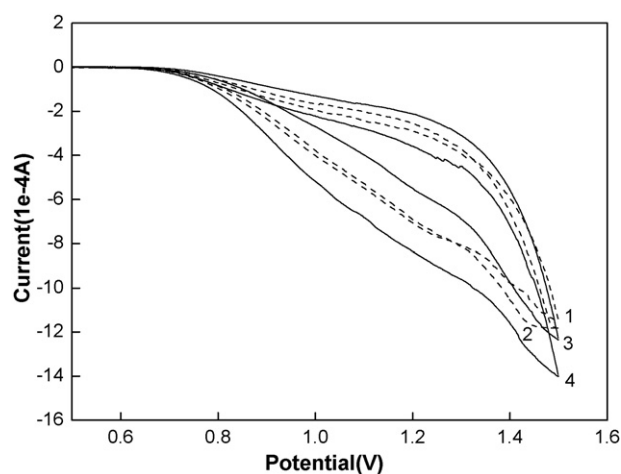

Fig. 1. The cyclic voltammograms of the bare and the benzene-modified CPE in $0.1 \, \text{mol} \, \text{L}^{-1}$ NaOH solution. Curve 1 represents the voltammogram of the bare CPE preconcentrated in blank solution; curve 2 represents the voltammogram of the bare CPE preconcentrated in sample solution; curve 3 represents the voltammogram of the benzene-modified CPE preconcentrated in blank solution; curve 4 represents the voltammogram of the benzene-modified CPE preconcentrated in sample solution; scan rate: $0.1 \, \text{V} \, \text{s}^{-1}$; initiative *E*: 0 V; high *E*: 1.50 V.
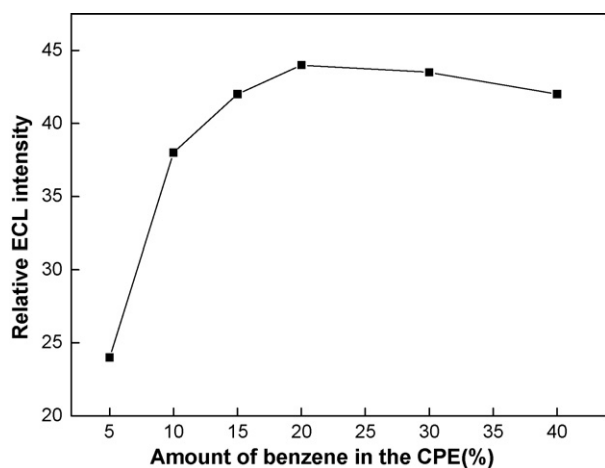
Fig. 2. Effect of amount of benzene in CPE on the relative ECL intensity. Ammonium molybdate: 5.0×10^{-4} mol L^{-1}; hydrochloric acid: 0.1 mol L^{-1}; phosphate: 1.0×10^{-9} g mL^{-1}; BRhB: 1.0×10^{-5} mol L^{-1}; preconcentration time: 1 min; ECL reaction medium: 0.1 mol L^{-1} NaOH; electrolytic potential: 1.0 V.

benzene-modified CPE is 4.5), the peak potential and the peak current of electro-oxidation BRhB at these two electrodes did not presented the obvious changes. Thus, these results strongly indicated that the role of the benzene in the CPE did not present co-extracting ability for that ion-associated complex, but mainly created a suitable ECL reaction microenvironment for the electro-oxidation of BRhB. So the benzene was selected to modify CPE.

For obtaining the optimum ECL reaction conditions, the amount of the benzene in the CPE was also investigated. As shown in Fig. 2, while the volume ratio (benzene/paraffin oil, v/v) of the benzene in the CPE was increased to 20%, the maximum ECL signal was obtained. But the continuous increase of the volume ratio of the benzene caused a decrease of the ECL signal. Thus, 20% was selected as the volume ratio of benzene in the CPE.

3.3. Choice of experimental conditions for the preconcentration stage

3.3.1. Effect of preconcentration potential

Considering that the blank ECL signal mainly resulted from the unselective adsorption of the BRhB on the benzene modifying CPE, we found that while an appropriate positive potential was applied to the CPE in the preconcentration step, the blank ECL signal was greatly decreased due to the electrostatic interaction between the protonated BRhB and working electrode. The experimental results showed that while potential was increased from 0 to 0.20 V, the ECL signal-to-noise ratio was obviously increased, above 0.20 V the ratio was decreased. Thus, 0.2 V was selected as preconcentration potential for further investigations.

3.3.2. Effect of ammonium molybdate concentrations and pH on preconcentration

The influence of ammonium molybdate concentration on the formation of the molybdophosphoric heteropoly acid was

studied over the range of 2.5×10^{-4} to 5.0×10^{-3} mol L^{-1}. The ECL response reached a maximum at 1.0×10^{-3} mol L^{-1} and showed a slight decline with further increase of the concentration, probably due to a low acid/molybdate ratio. Therefore, ammonium molybdate concentration of 1.0×10^{-3} mol L^{-1} was used for all subsequent experiments.

The pH of the solution in the preconcentration step has a very significant effect on the ion-associated complex formation. The experimental results showed that maximum relative ECL intensity could be obtained by using 6.0×10^{-2} mol L^{-1} of hydrochloric acid, but a sharp decrease of the relative ECL intensity was observed with further increase this concentration. Therefore, hydrochloric acid concentration of 6.0×10^{-2} mol L^{-1} was used in further experiments.

3.3.3. Effect of preconcentration time on the relative ECL intensity

The time required for the preconcentration process was an important parameter to be investigated. The amount of extractable ion-associated complex into the benzene-modified CPE increased by increasing the preconcentration period as shown in Fig. 3. The results showed that a 3 min or longer was best to get the strongest ECL signal. Taking account of the efficiency of the analytical process, we selected 3 min as a period of optimal preconcentration time for this experiment.

3.4. The other experiment conditions

3.4.1. Effect of ECL reaction medium

The medium usually has significant effect on the ECL reaction. This is also hold true for the present case. Therefore, the ECL signal of BRhB in different mediums, such as borax buffer, NaHCO$_3$, Na$_2$CO$_3$ and NaOH, was investigated in a suitable concentration range. The results showed that the strongest ECL signal could be detected in NaOH solution. Considering the ECL signal-to-noise ratio and the stability of the ECL signal in
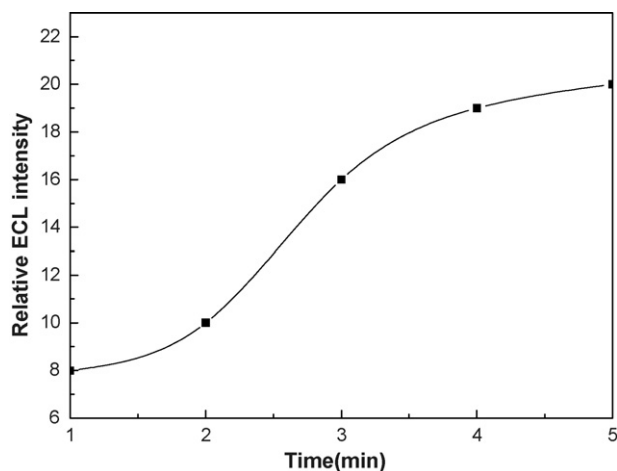

Fig. 3. Effect of preconcentration time on the relative ECL intensity. Ammonium molybdate: 5.0×10^{-4} mol L^{-1}; hydrochloric acid: 0.1 mol L^{-1}; phosphate: 1.0×10^{-9} g mL^{-1}; BRhB: 1.0×10^{-5} mol L^{-1}; amount of benzene: 20%; preconcentration potential: 0.20 V; ECL reaction medium: 0.1 mol L^{-1} NaOH; electrolytic potential: 1.0 V.
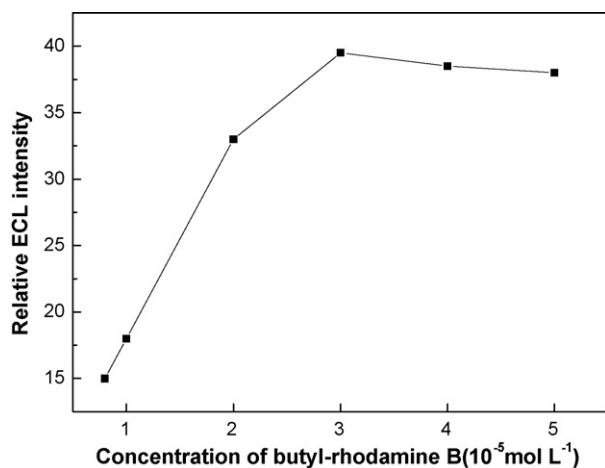
Fig. 4. Effect of BRhB concentration on the relative ECL intensity. Ammonium molybdate: 1.0×10^{-3} mol L^{-1}; hydrochloric acid: 6.0×10^{-2} mol L^{-1}; phosphate: 1.0×10^{-9} g mL^{-1}; amount of benzene: 20%; preconcentration potential: 0.20 V; preconcentration time: 3 min; ECL reaction medium: 0.06 mol L^{-1} NaOH; electrolytic potential: 1.0 V.

different concentration of NaOH solution, 0.06 mol L^{-1} NaOH solution was chosen for detecting phosphate in this ECL system.

3.4.2. Effect of BRhB concentration

The concentration of BRhB has significant effect on the relative ECL intensity for indirectly detecting phosphate in the proposed method. Therefore, the concentration of BRhB was investigated from 8.0×10^{-6} to 5.0×10^{-5} mol L^{-1}, as illustrated in Fig. 4. When the concentration of BRhB was 3.0×10^{-5} mol L^{-1}, the relative ECL intensity was strongest. Hence, 3.0×10^{-5} mol L^{-1} BRhB was selected as optimum for the following experiments.

3.4.3. Effect of electrochemical parameters

The electrochemical parameter plays an important role on the properties of the relating ECL reactions. For obtaining the higher ECL signal of electro-oxidation BRhB, different electrolytic ways, such as linear sweep, square-wave, single-potential-steps and cyclic sweep, were investigated, respectively. The results showed that the single-potential-steps offered best ECL performances for BRhB. Therefore, the single-potential-steps electrolytic method was chosen.

The effect of the final potential on the enhancing ECL signal was also investigated over the range 0.90–1.40 V. The investigations showed that an increase of the ECL signal of was recorded

with increase of final potential up to 1.30 V, while afterwards a remarkable decline of the signal was observed when exceeding this potential. For the ensuing studies, a final potential of 1.30 V was selected.

3.5. Analytical performance for phosphor measurements

Under the aforementioned optimal conditions, relative ECL intensity (ΔI_{ECL}) was proportional to the concentration of phosphor (c) in the range of 2.0×10^{-10} to 1.0×10^{-8} g mL^{-1}. The regression equation was $\Delta I_{ECL} = -19.6 + 14.3c$ ($r = 0.9954$, $n = 10$), where c was measured in 10^{-10} g mL^{-1}. According to suggestion of IUPAC, the detection limit of the system for phosphate was 8.0×10^{-11} g mL^{-1} (equal to 0.8 nM). The relative standard deviation for 2.0×10^{-9} g mL^{-1} of phosphate solution was 2.4% ($n = 11$). A satisfactory precision of the proposed method was observed.

3.6. Interference study

According to the property and pretreatment of samples, the effect of foreign substances was tested by analyzing a standard solution of phosphate (1.0×10^{-9} g mL^{-1}) to which increasing amounts of interfering substances was added, and the relative error was not larger than 5%. With regard to anions, sulfate, bicarbonate, nitrate and fluoride had no significant effect. No interferences could be observed when including the up to 1000-fold weight of concentration of Cu^{2+}, Mg^{2+}, Zn^{2+}, Ca^{2+}, 100-fold weight of concentration of Fe^{3+}, Al^{3+}, BO_3^{3-}, As(III), 80-fold weight of concentration of Si(IV), 0.5-fold weight of concentration of As(V). It is obvious that As(V) is potentially interferent for the determination of phosphate, and its removal from the sample solution is highly required. The elimination of As(V) was demonstrated in Section 3.7.

3.7. Applications

In order to demonstrate potential analytical application ability, the proposed method was applied to the analysis of three different water samples including tap water, river water and commercialized mineral water. Considering that arsenate can positively interfere the measurement of phosphate, the reducing As(V) to As(III) prior to measurement was employed to eliminate the interfere [24]. As a pretreatment, 0.5 mL of sodium thiosulfate (0.1 mol L^{-1}) was employed as reducing agent to mask the interfering effect from As(V) in 25 mL of water sample.

Table 1
Analysis of water samples with the proposed method

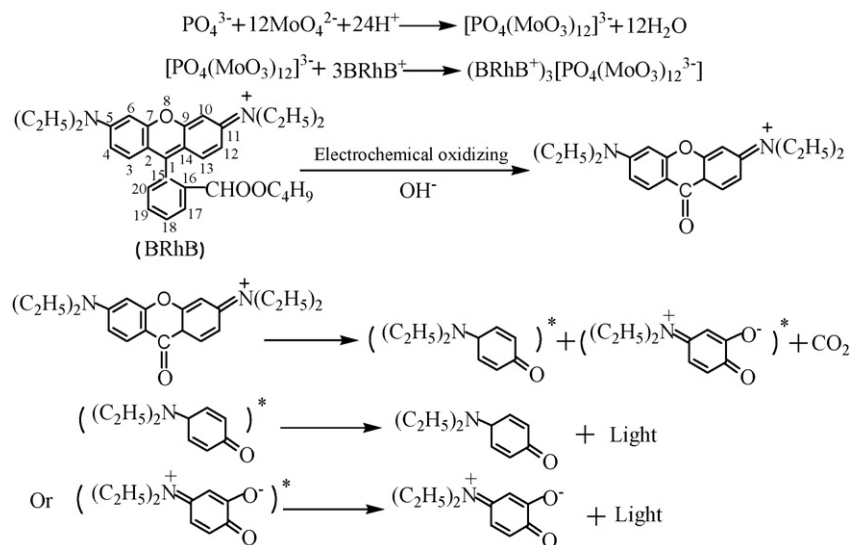| Samples	Detected (μg L^{-1})[a]	Recovery results		
		Added (μg L^{-1})	Found (μg L^{-1})[a]	Recovery (%)
Tap water	0.78	2.0	2.83	102.5
River water	1.85	2.0	3.82	98.5
Commercialized mineral water	0.53	2.0	2.55	101

[a] Average of three determinations.

Fig. 5. Possible ECL reaction scheme for the CPE in phosphate detection.

Each sample was treated according to the procedure described above, and the analyte concentration was calculated by interpolating on the calibration curve. The obtained results were listed in Table 1. As shown in Table 1, the proposed method presented better accurate ability and was suitable for practical applications.

3.8. Possible ECL reaction mechanism

The molecular construction of BRhB shows a compound of multiple aromatic rings in which there are a rigid plane structure and a rotatable benzene ring directly linking to the bridge carbon atom (C1). The spectral characteristics of BRhB dye depend to great extent on the molecular state of a portion of the rigid plane structure. The CL characteristics based on oxidation of some xanthene dyes have been studied by Chen and co-workers [25–27]. Several works consider that the introduction of a carboxy group at C16 atom could decrease the π-electron density at C1 atom and increase greatly the chemiluminescent intensity. This conclusion indicates that there is a reaction route by means of breaking the chemical bond of xanthene molecule between the C1 and C15 atoms.

The ECL behaviors of some dyes, which owned the similar structure to that of BRhB, such as methyl violet, crystal violet, light green, basic fuchsin, fluorescein, etc., have been investigated. The results showed that: fluorescein could be electrochemically oxidized accompanying by the weak ECL signals at the nearly the same electrode potential (1.30 V) to that of the BRhB; methyl violet produced the weak ECL signal above the 1.50 V electrolytic potential; light green, basic fuchsin and crystal violet did not offer any ECL signal in a widely potential range at the same experimental conditions with that of BRhB.

Therefore, in the proposed ECL reaction system, BRhB as the analogue of xanthene molecule, the reactive site of BRhB molecule would be on C1. We presumed while appropriate electrolytic potential was applied to the benzene-modified CPE, the extracted-state BRhB itself could be electro-oxidized to emit light in the alkaline medium. The possible ECL reaction scheme might be the following chemical reaction steps (as shown in Fig. 5).

4. Conclusions

In this work, a new ECL technique was established to determine phosphate in water samples. By means of the CME technique, the ECL reaction microenvironment was improved greatly and the in situ combination of the LLE technique with the ECL analysis was achieved successfully. This proposed method offered excellent sensitivity and it had been used to determine phosphate in water successfully. The further research works on this aspect are still under study in our lab.

Acknowledgement

References

[1] V.H. Smith, G.D. Tilman, J.C. Nekola, Environ. Pollut. 100 (1999) 179.
[2] J.Z. Zhang, C.J. Fischer, P.B. Ortner, Talanta 49 (1999) 293.
[3] J.F. Liu, G.B. Jiang, Talanta 52 (2000) 211.
[4] V. Ruiz-Calero, M.T. Galceran, Talanta 66 (2005) 376.
[5] S. Hashimoto, K. Fujiwara, K. Fuwa, Anal. Chem. 57 (1985) 1305.
[6] T. Taniai, M. Sukegawa, A. Sakuragawa, A. Uzawa, Talanta 61 (2003) 905.
[7] O.V. Zui, J.W. Birks, Anal. Chem. 72 (2000) 1699.
[8] I.P.A. Morais, I.V. Tóth, A.O.S.S. Rangel, Talanta 66 (2005) 341.
[9] A.W. Knight, Trends Anal. Chem. 18 (1999) 47.
[10] W. Zhan, J. Alvarez, R.M. Crooks, Anal. Chem. 75 (2003) 313.
[11] R.G. Maus, R.M. Wightman, Anal. Chem. 73 (2001) 3993.
[12] S. Szunerits, J.M. Tam, L. Thouin, C. Amatore, D.R. Walt, Anal. Chem. 75 (2003) 4382.
[13] O.M. Steijger, D.A. Kamminga, A. Brummelhuis, H. Lingeman, J. Chromatogr. A 799 (1998) 57.
[14] S.C. Liu, Y.J. Liu, J. Li, M.L. Guo, W. Pan, S.Z. Yao, Talanta 69 (2006) 154.

[15] T. Ikehara, N. Habu, I. Nishino, H. Kamimori, Anal. Chim. Acta 536 (2005) 129.

[16] G.B. Xu, S.J. Dong, Anal. Chem. 72 (2000) 5308.

[17] B.H. Kim, D.N. Lee, H.J. Park, J.H. Min, Y.M. Jun, S.J. Park, W.Y. Lee, Talanta 62 (2004) 595.

[18] G.B. Xu, S.J. Dong, Electrochem. Commun. 1 (1999) 463.

[19] S.J. Motomizu, Z.H. Li, Talanta 66 (2005) 332.

[20] J. Wang, B.A. Freiha, Anal. Chem. 56 (1984) 849.

[21] T.B. Jarbawi, W.R. Heineman, Anal. Chim. Acta 135 (1982) 359.

[22] R.E. Visco, E.A. Chandross, J. Am. Chem. Soc. 86 (23) (1964) 5350.

[23] S. Kulmala, J. Suomi, Anal. Chim. Acta 500 (2003) 21.

[24] K.L. Linge, C.E. Oldham, Anal. Chim. Acta 450 (2001) 247.

[25] R.W. Ramette, E.B. Sandell, J. Am. Chem. Soc. 78 (1956) 4872.

[26] G.N. Chen, C.S. Huang, Talanta 35 (1988) 625.

[27] Y.J. Ma, X.Y. Jin, M. Zhou, Z.Y. Zhang, X.L. Teng, H. Chen, Anal. Chim. Acta 489 (2003) 173.

ELSEVIER

Direct LD-FTMS detection of mineral-associated PAHs and their influence on the detection of co-existing amino acids

Beizhan Yan [a,1], Daphne L. Stoner [a], Jill R. Scott [b,*]

[a] *Department of Chemistry, University of Idaho, Idaho Falls, ID 83402, United States*
[b] *Chemical Sciences, Idaho National Laboratory, Idaho Falls, ID 83415, United States*

Abstract

Polycyclic aromatic hydrocarbon (PAH) compounds and amino acids (AAs) are both ubiquitous throughout the universe and can be co-located in mineral matrices (e.g., meteorites); therefore, co-detection of PAHs and AAs associated with terrestrial and extra-terrestrial minerals is of interest. Nine PAH compounds representing four chemical classes of PAH (unsubstituted, acetyl-, amino-, and nitro-substituted) were applied onto the surface of quartz, plagioclase, olivine, and ilmenite mineral standards and analyzed using laser desorption/ionization Fourier transform mass spectrometry (LD-FTMS). Mass-to-charge peaks derived from PAH compounds were detected from the surfaces of all minerals evaluated. All PAH compounds were detected in the positive ion mode, whereas only nitro-substituted PAH compounds were detected in negative ion mode. In this and earlier studies, the ability to directly detect mineral-associated AAs by LD-FTMS was dependent on the mineral geomatrix. On iron-bearing minerals AAs appeared as highly fragmented ions in the spectra or were not detectable; however, the addition of the PAH chrysene enabled the ionization and detection of AAs threonine and histidine by LD-FTMS. Thus, for mineral systems such as meteorites, interstellar dust particles, soils, and sediments, the co-detection of AAs associated with PAHs by LD-FTMS is feasible.
© 2006 Elsevier B.V. All rights reserved.

Keywords: PAH; Minerals; Amino acids; Laser desorption; FTMS; LDMS

1. Introduction

Polycyclic aromatic hydrocarbon (PAH) compounds and amino acids (AAs) are ubiquitous in both extraterrestrial [1] and terrestrial [2] environments and both have been detected in a variety of meteorites [3]. Additionally, the co-existance of PAHs and AAs are of interest because AAs can be synthesized by aqueous alteration of PAHs in carbonaceous meteorites [4]. PAHs have been detected in dense interstellar clouds [5], cometary ices [6], interplanetary dust particles [7], carbonaceous chondrites (meteorites) [8,9], and are abundant in natural sources of terrestrial fossil fuels [2]. PAHs are also common environmental pollutants on earth and have two major anthropogenic sources: petrogenic (oil or coal dust releases) and pyrogenic

(incomplete combustion of fossil fuels) [10]. PAHs, especially high molecular weight (HMW) compounds, are carcinogens and mutagens [2]. In natural environments, PAHs tend to adsorb onto fine particles, mainly minerals, making them difficult to detect [2]; therefore, direct identification of PAHs associated with particles is vital for their detection in natural environments [2] and extra-terrestrial materials [8,11].

Amino acids (AAs) are widespread in terrestrial and extraterrestrial systems and have been detected in terrestrial soils and sediments [12–15], lunar soils [16], meteorites [3,17], and interplanetary dust particles [18]. AAs are one of the building blocks for life and their distribution in the environmental and geological record is being studied to examine biogeochemical cycling, re-mineralization of carbon and nitrogen in the environment, [13,15,19] and the impact of hydrothermal conditions on the transformation of amino acids [14]. Amino acids may be formed by abiotic as well as biotic processes. Unknown and rare amino acids, along with those that are commonly found on Earth, have been detected in meteorites [17].

In the past two decades, laser desorption/ionization mass spectrometry (LDMS), which circumvents time- and solvent-

* Corresponding author at: Chemical Sciences, Idaho National Laboratory, P.O. Box 1625, Idaho Falls, ID 83415-2208, United States.
Tel.: +1 208 526 0429; fax: +1 208 526 8541.
E-mail address: jill.scott@inl.gov (J.R. Scott).
[1] Current address: Department of Energy, Environmental, Chemical Engineering, Washington University, St. Louis, MO 63130, United States.

consuming sample preparation procedures, has developed into a powerful method for direct analysis of PAHs [20–22] and biologically-derived molecules associated with solid mineral phases [23–25]. LDMS and microprobe laser desorption/laser ionization mass spectrometry ($\mu L^2 MS$) have been utilized to analyze PAHs in various geomatrix samples, such as dust, soil, sediments, and air filter samples [20,22,26–28]. In LDMS, the ionization process occurs at the same time as the desorption event. In contrast, $\mu L^2 MS$ uses a two-step process; desorption of the constituent molecules as intact neutral species using a pulsed infra-red laser beam followed by photo-ionization of the desorbed neutral molecules with a pulsed ultraviolet laser [22].

In this study, the impact of mineral type on the detection of PAHs and AAs was examined and the effect that the presence of PAH on the co-detection of AAs was explored using an imaging LD-FTMS [24,29]. PAHs and AAs are often studied as individual classes (e.g., PAH versus AA) or subclasses (e.g., unsubstituted versus alkylated PAH) of compounds. In terrestrial environments and extraterrestrial materials, PAHs and AAs may co-exist and should be analyzed as such to discern any possible relationships or interactions among these compounds [6,30]. Furthermore, in natural environments, PAHs and AA may be preferentially associated with specific mineral phases within geomatrices (e.g., the clay in soils and sediments) and chemical imaging over the surface of the mineral substrate would be needed to identify these associations.

2. Experimental

2.1. Materials

PAH compounds (2,7-dinitrofluorene, pyrene, chrysene, 6-aminochrysene, coronene, 9-nitroanthracene, 2-nitrofluorene, 1-aminoanthracene, 2,3-benzanthracene, and 9-acetylanthracene) were purchased from Sigma–Aldrich (St. Louis, MO). L-Threonine and L-histidine were purchased from Kodak (Rochester, NY) and Sigma–Aldrich (St. Louis, MO), respectively. All chemicals were used as received. Quartz (SiO_2) and plagioclase ($(Na, K, Ca)Al(Al, Si)Si_2O_8$) were acquired from the mineral inventory at Rensselaer Polytechnic Institute (Troy, NY), while ilmenite ($FeTiO_3$) and olivine ($(Fe, Mg, Ni, Mn)_2SiO_4$) were purchased from Ward's Natural Science Establishment, Inc. (St. Urbain, Quebec, Canada).

2.2. Sample preparation

Relatively flat areas of the mineral samples were selected and cut into ∼0.3-in × 0.3-in pieces using a slow-rate saw (Lu6x-130, Lonnie Inc., Phoenix, AZ) using deionized water as lubricant. The average sample roughness of cut pieces was 4 μm as characterized using a profilometer (Wyko NT1100, Veeco, Woodbury, NY). Cut pieces were washed with deionized water and methanol to eliminate inorganic and organic contamination introduced during sample preparation. A lab-built aerospray apparatus [31] was used to spray approximately 2–7 nmol of analyte dissolved in a solvent mixture consisting of methanol:acetonitrile:acetone (2:1:1) onto the surface

(∼0.2-in^2) of minerals or standard stainless steel disc (SSD) using a nitrogen pressure of 80 psi for 1 min. Concentrations of PAH compounds, alone or mixed, ranged from 0.3 to 1.5 mM. For studying PAH assisted amino acid identification, chrysene (0.5 mM) was mixed with either threonine (0.5 mM) or histidine (0.5 mM). Approximately 20% of the sprayed volume is lost to overspray that missed the rotating target. After air-drying, prepared analyte-mineral samples were mounted on a 19 mm diameter stainless steel probe tip using double-sided sticky tape (3 M, St. Paul, MN).

2.3. FTMS instrumentation and parameters

Mass spectra were obtained using a custom-built imaging Fourier transform mass spectrometer [29] equipped with a 7 T Oxford (Oxford, England) superconducting magnet, 2-in cubic cell, and Odyssey control and data acquisition system (Finnigan FT/MS, Bremen, Germany). The imaging LD-FTMS has high mass accuracy (error ±0.003 amu), high resolution (typically >10,000), high sensitivity (∼200 ions for peaks with S/N ∼3), and high spatial resolution (∼6 μm) [32]. A Nd:YAG laser (Continuum, Santa Clara, CA) operating at 355 nm with a 6 ns pulse width was used for desorption/ionization using a laser fluence of 1×10^8 W/cm^2 for ∼6 μm diameter. The sample was located ∼0.5 cm from the front trap plate. During the ionization event, the potential on the front and rear trap plates was maintained at 0 V. After ionization, a trapping potential of 2 V was applied to both trap plates and maintained until the quench event at the end of the sequence. A delay of 0.5 s was imposed prior to application of a chirp excitation over the range of 50 Hz to 4 MHz with a sweep rate of 3600 Hz/μs. The ions were detected in direct mode using 64 K data points. Raw data were baseline corrected, Hamming apodized, zero filled, and Fourier transformed to produce the mass spectra. Pressure during analysis was ∼2×10^{-9} Torr.

Each spectrum was collected from a single laser shot. The amount of analyte present in the area illuminated by one laser shot was approximately 10^{-16} mol based on the laser desorption spot size (6 μm) and the amount of analyte applied to the surface. Single shot detection was employed rather than averaging over 50–100 shots as reported by others for using time-of-flight MS [33,34] or FTMS [27] as our ultimate goal is to chemical image natural samples where organics are expected to be distributed unevenly upon or within a rock matrix [24]. Chemical imaging requires many analyses of spatially discrete areas; thus, making acquisition of multiple pulses at all sampled areas excessively time consuming. Additionally, signal averaging, while improving the S/N of spectra of prepared samples, may obscure or decrease signals of organics present at extremely low concentrations or occurring at only a few locations in a natural sample.

3. Results and discussion

3.1. Impact of volatility on analysis

The volatility of analytes under the evacuated conditions of the LD-FTMS must be considered when interpreting data.
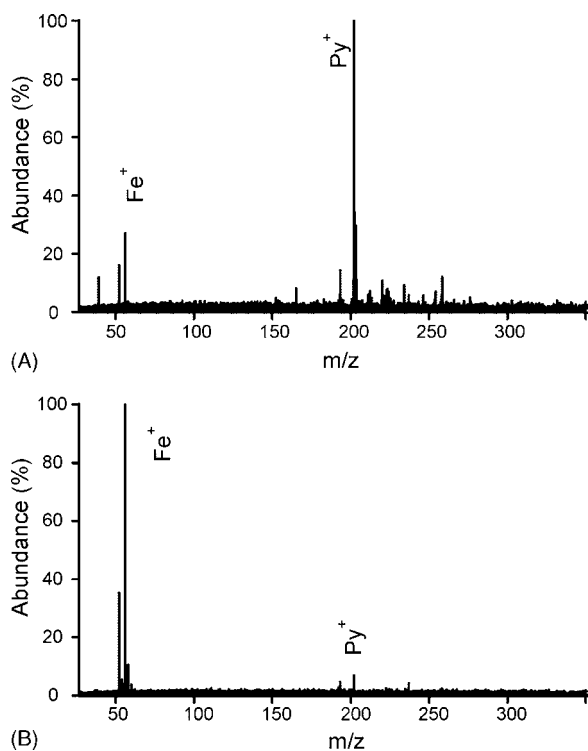
Fig. 1. Comparison of mass spectra of PAH mixture applied to stainless steel surface (A) 10 min and (B) 2 h after the sample was loaded into LD-FTMS. See Table 1 for PAH abbreviations.

Generally, water soluble analytes, such as amino acids, are non-volatile and will remain in vacuum for hours or even days. However, compounds such as PAHs have higher vapor pressures than do the AAs; therefore, their relative abundances can change within the vacuum environment. Fig. 1A and B show the mass spectra of positive ions 10 min and 2 h, respectively, after a PAH mixture sample was introduced into the sample chamber (see Table 1 for PAH abbreviations). Most of the parent- and amino-PAHs, which produced only positive ion species, virtually disappeared within 2 h as shown by comparing the peak abundance for pyrene (Py^+) to iron (Fe^+) in Fig. 1. Further investigation found that nitro-PAHs were detectable in the negative ion mode with a S/N >5 after remaining in the sample chamber overnight (data not shown). The lower vapor pressure of nitro-

PAHs relative to other PAH compounds may account for the differences in evaporation rates.

3.2. Detection of PAH compounds on SSD standard

LD-FTMS spectra for a PAH mixture were obtained by single laser-shots in both positive (Fig. 2A) and negative (Fig. 2B) ion detection modes. The relative intensities of mass ions generated by PAH compounds in positive and negative ion detection modes are tabulated in Tables 1 and 2, respectively. Spectra for the individual PAH compounds generated peaks for the molecular ions as the most abundant with the expected isotopic peaks in lower abundance. In positive mode analysis of the mixture, spectra were also dominated by odd-electron molecular ion M^+ species.
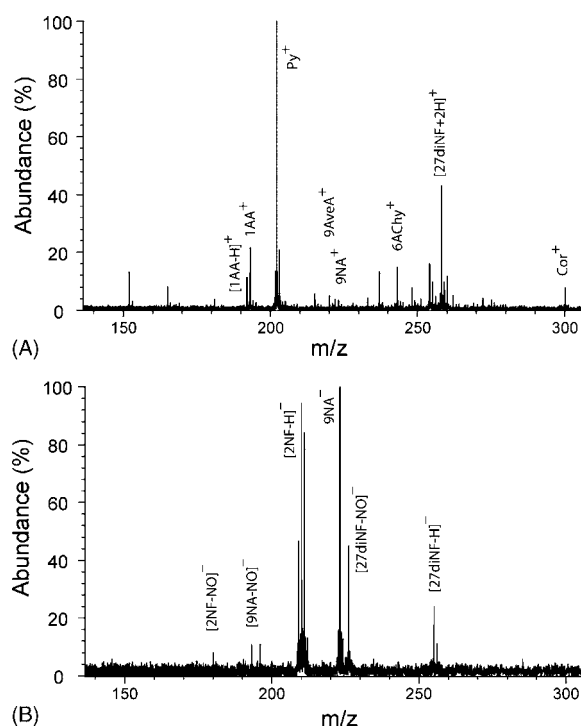

Fig. 2. LD-FTMS mass spectra of PAH mixture in (A) positive ion detection mode and (B) negative ion detection mode. See Table 1 for abbreviations of PAH compounds and relative PAH amounts.

Table 1
Relative peak intensities of PAHs in positive ion detection mode

PAH compounds	Abbreviations	Monoisotopic molecular weight	Amount sprayed (μg)	Relative intensities of positive ions[a]				
				$[M-2H]^+$	$[M-H]^+$	M^+	$[M+1]^+$	$[M+2H]^+$
2,7-Dinitrofluorene	27diNF	256.048	0.725	16.2	2.6	4.8	9.8	43.2
Pyrene	Py	202.078	1.175	~	~	100.0	20.5	2.7
6-Aminochrysene	6AChy	243.105	0.725	~	~	15.0	2.9	~
Coronene	Cor	300.094	0.7	~	~	7.5	~	~
9-Nitroanthracene	9NA	223.063	0.65	~	~	3.5	~	~
2-Nitrofluorene	2NF	211.063	1.525	~	~	2.2	~	~
1-Aminoanthracene	1AA	193.089	0.775	~	11.5	22.0	3.5	~
2,3-Benzanthracene	23BenzA	228.094	0.75	~	~	2.4	~	~
9-Acetylanthracene	9AceA	220.089	0.4	~	~	4.9	2.4	~

[a] Relative intensities of various ion species are compared to the peak abundance of molecular ion (M^+) of pyrene. Signal abundances below S/N 3 are designated with ~.

Table 2
Relative peak intensity of PAHs in negative ion detection mode

PAH compounds	Relative intensities of negative ions[a]				
	[M − NO]	[M − 2H]	[M − H]$^-$	M$^-$	[M + 1]$^-$
2,7-Dinitrofluorene	44.58	∼	23.763	10.756	∼
9-Nitroanthracene	10.653	∼	∼	100	12.738
2-Nitrofluorene	8	46.198	94.528	84.72	12.73

[a] Relative intensities of various negative ion species are compared to the peak abundance of molecular ion of 9-nitroanthracene (M$^-$). Signal abundances below S/N 3 are designated with ∼.

In most cases, the [M + 1]$^+$ peak, which is one mass unit higher than M$^+$, was approximately 20% of the major peak M$^+$, consistent with the ^{13}C isotopic contribution to monoisotopic M$^+$. This indicated that the protonated ion species [M + H]$^+$, which has the same mass-to-charge (*m/z*) ratio as [M + 1]$^+$, was negligible. The oxygen-containing PAH acetylanthracene was also observed in positive ion mode, but with lower abundance than the un-substituted PAHs having similar applied concentrations. In addition to the molecular ion M$^+$, 1-aminoanthracene produced the [M − H]$^+$ ion. The types of positive ion species generated by the three nitro-PAHs were different from each other. The two nitro-PAH compounds, 9-nitroanthracene and 2-nitrofluorene, generated signals from positive molecular ions (M$^+$) at *m/z* 223 and 211, respectively. The nitro-PAH 2,7-dinitrofluorene generated abundant positive signals not only from M$^+$, but also from [M − H]$^+$, [M − 2H]$^+$, [M + 1]$^+$, and [M + 2H]$^+$ observed at *m/z* 255, 254, 257, and 258, respectively (Fig. 2A and Table 1). For 2,7-dinitrofluorene, the ratio of [M + 1]$^+$ to M$^+$ was about 200%, much higher than the expected ∼20% for ^{13}C carbon isotope distribution of M$^+$. Abundance of the ^{13}C species at *m/z* 257 ([M + 1]$^+$) should be 20% of the peak at *m/z* 256 (M$^+$), which translates into 10% of the total peak at *m/z* 257. Therefore ∼90% of the peak was thought to be derived from [M + H]$^+$ ion, the protonated ion species of M$^+$. Because plagioclase contains alkali metals (e.g., Na and/or K), which are easily ionized at 355 nm [35], abundant alkali ions are generated [24,36]. Therefore, cationization, such as [M + Na]$^+$, may be expected due to the aromaticity of PAHs (i.e., π-cation interactions) [37], but was not observed.

Negative ion species were generated only by nitro-PAHs (Fig. 2B and Table 2). All three nitro-PAH compounds produced M$^-$, [M − H]$^-$, and [M + 1]$^-$ ions. Similar to the positive ion mode, the ratio of [M + 1]$^-$ to M$^-$ produced from the three compounds is ∼20%, indicating that the [M + 1]$^-$ species was mainly the ^{13}C isotopic distribution from M$^-$. [M − NO]$^-$ ions were produced by all of three nitro-PAH compounds with much more abundant signal from 2,7-dinitrofluorene being observed relative to those from 9-nitroanthracene and 2-nitrofluorene.

The PAH detection results were different than those reported by others [38]. Variations in PAH constituents, ionization method, and/or laser wavelength may account for the differences. For example, Balasanmugam et al. [39] observed both positive and negative ion species from unsubstituted-PAH compounds. However, only positive ions from parent-PAH compounds were observed in LD-FTMS spectra in this study. While

Balasanmugam et al. used a zinc foil substrate as opposed the surfaces used in this study, it is unlikely that the dissimilarity of the substrates can account for the observed differences because no significant variation in PAH distribution was observed in the current study for any of the surfaces used (i.e., SSD standard or minerals). The differences are probably caused by variations in PAH constituents used in the two studies. In the study of Balasanmugam et al. [39], parental and alkylated PAHs, which have similar electron affinities, were used, but in the current investigation a mixture of four PAH groups with large difference in electron affinities was chosen. Nitro-PAHs have higher electron affinities than other PAHs; therefore, in the gas phase they can easily "steal" electrons from themselves (i.e., self-ionization) or other PAH compounds to produce negative molecular ion species. Another example also demonstrates the importance of PAH components for ion production. While Dotter et al. [40] observed abundant positive nitro-PAH ion species using LDMS, in this study, nitro-PAHs were mainly observed in negative ion detection mode of the LD-FTMS analyses. Again, because of the larger difference in electron affinities between nitro-PAH compounds and parent-PAH compounds, nitro-PAHs are prone to be electron acceptors and generate negative ion species. The composition of the PAH mixture for this study appears closer to the real condition in outer space, because parent- and nitro-PAHs have both been identified in interplanetary dust particles [7,30].

The difference in laser wavelength is also thought to be another reason leading to the observed variations. Muller et al. [41] observed ion species of [M + O − H]$^-$ from 9-nitroanthracene in addition to the other peaks ([M − H]$^-$, [M − 2H]$^-$, and [M − NO]$^-$) observed in this study. Their research also found that the distribution of negative ion species were largely affected by the laser wavelengths (225.7 and 286.5 nm) used [41]. A laser radiation at 355 nm was used for the LD-FTMS analyses in this work; hence, it is not surprising that the ion production was different than that observed by Muller et al. [41].

The ionization method may also influence the type of ion species being produced. The µL^{2}MS technique can result in fragmentation, such as [M − C$_2$H$_2$]$^+$, [M − C$_2$H$_3$]$^+$, and [M − C$_2$H$_5$]$^+$ [26]. However, in this study the fragmentation of positive ions was rarely observed using a single laser shot at 355 nm. Fragmentation may interfere with the analysis of other PAH compounds. For instance, a peak in *m/z* 152 was observed and assigned to [M$_{178}$ − C$_2$H$_2$]$^+$ by Hankins and John [26]; however, in natural samples acenaphthene, a major PAH constituent in the crude oil and combustion particles, has the identical monoisotopic weight of 152.078 amu. Therefore, for detecting organics in natural samples that generally contain complicated organic compositions [2], fragmentation should be avoided.

3.3. LD-FTMS detection of polycyclic aromatic hydrocarbons on mineral surfaces

PAH were detected on the surface of ilmenite (Fig. 3A), plagioclase (Fig. 3B), quartz, and olivine (data not shown).
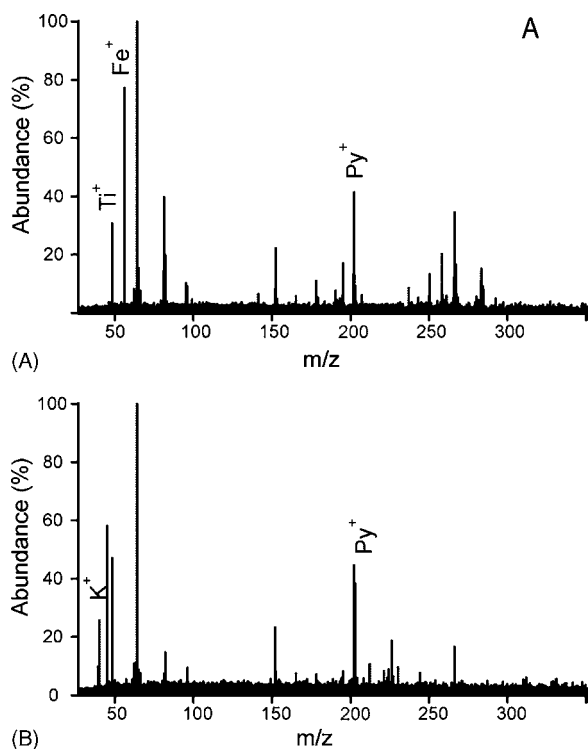
Fig. 3. LD-FTMS mass spectra of PAH mixture applied to the surface of (A) ilmenite and (B) plagioclase. See Table 1 for PAH abbreviations.

Table 3
Mineral-surface dependence of LD-FTMS detection of amino acids and protein

	Threonine	Histidine	Cysteine	Gramicidin-S
Halite (NaCl)	+	+	+	+
Hematite (Fe$_2$O$_3$)	–	–	–	–
Ilmenite (FeTiO$_3$)	–	–	–	–

Positive detection of molecular related species is designated as "+", while unsuccessful detection is designated as "–".

3.4. LD-FTMS detection of amino acids on mineral surfaces

The LD-FTMS detection of amino acids and a small protein (i.e., gramicidin S) varied depending on the nature of the underlying mineral surface. The amino acids histidine, threonine, and cysteine and gramicidin S were detected on the surface of halite (NaCl) (Table 3). A common peak in these spectra was related to a positive ion species, [NaClNa]$^+$, which corresponded to a mass-to-charge ratio (m/z) of 81. Two sodium-adducted ions, [M + Na]$^+$ and [M − H + 2Na]$^+$, where M represents the analyte (in this case, histidine) were observed at m/z 178 and 200, respectively (Fig. 4A). However, on the surface of the iron-bearing SSD, hematite (Fe$_2$O$_3$), or ilmenite (FeTiO$_3$) samples the amino acids and gramicidin S were not detected or were present as highly fragmented ions instead of the parent ions (Table 3). For example, the spectra for histidine on Fe$_2$O$_3$ (Fig. 4B) were dominated by iron-derived signals.

The absence of biomolecular ion species from samples prepared with hematite, ilmenite, or SSD (Table 3) suggests that iron-bearing minerals may not be appropriate materials for the laser desorption and/or ionization of biomolecules. Fragmentation of the organic molecules may be one possible explanation that contributed to the inability to detect molecular ions of amino

LD-FTMS spectral results of the minerals have been previously reported [24,36,42]. Quantitative variations among the spectra were observed for each of the samples that were analyzed. This slight variation may be attributed to the differences in vacuum pressures when samples were analyzed and/or the variations of interactions between analyte species with the different minerals. PAH evaporation in a vacuum chamber of an instrument may be decreased when PAHs are associated with minerals. Rodgers et al. [28] detected soil surface-bound PAHs in petroleum-contaminated soils, which included naphthalene that has the lowest molecular weight and lowest vapor pressure of the PAHs. Abundant low molecular weight (LMW) PAH compounds, including naphthalene, were also identified in interplanetary dust particles by μL^{2}MS [7] that were subject to low pressure conditions in space. Nevertheless, when analyzing PAHs adsorbed to mineral samples using the FTMS, some evaporation is inevitable, which limits PAH quantification.

Signals from underlying minerals were observed in the mass spectra along with those derived from the PAH. For example, peaks for the ion species Ti$^+$ and Fe$^+$ from ilmenite were detected in spectra (Fig. 3A). The co-detection of PAH and the underlying minerals by LDMS has application to the study of organic-mineral and contaminant-mineral associations in terrestrial and extra-terrestrial materials [21,22,43]. For instance, the detection of PAH on the surface of quartz has positive implications for PAH detection in cometary materials where chemically-similar amorphous silica is a major solid phase [6].
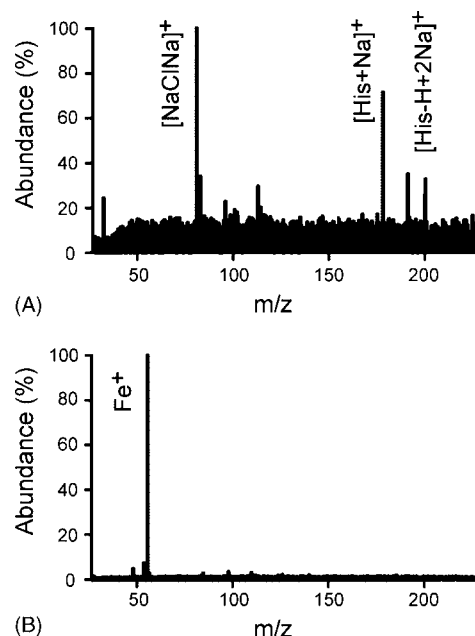

Fig. 4. LD-FTMS mass spectra of histidine applied to the pellet surface of (A) halite (NaCl) and (B) hematite (Fe$_2$O$_3$).
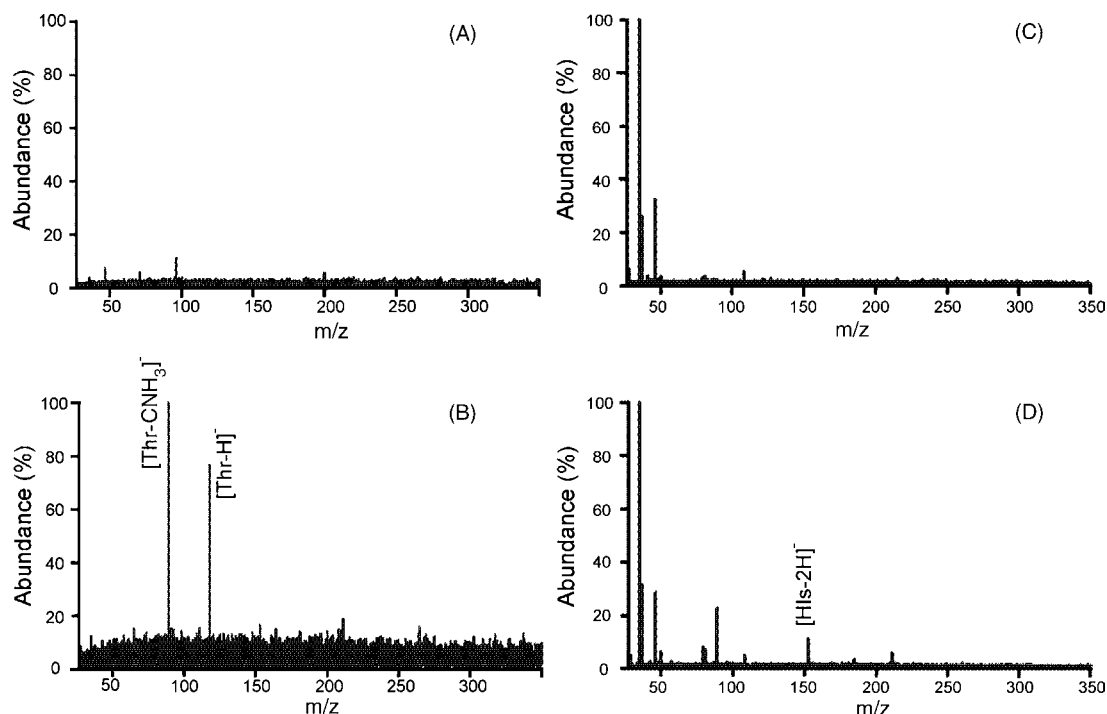
Fig. 5. Mass spectra of negative ion species of (A) threonine (Thr) alone on SSD surface, (B) 1:1 mixture of chrysene and threonine on SSD surface, (C) histidine (His) alone on ilmenite surface, and (D) 1:1 mixture of chrysene and histidine on ilmenite surface.

acids in the gas phase. Transition metals are known to insert between C–C bonds, leading to fragmentation of biomolecules, [44] which suggests that Fe from the mineral matrix may be causing fragmentation of the amino acids.

The sharp detection contrast of PAHs and AAs on the Fe-bearing surfaces is presumably due to the difference in their molecular structure. The stability of the π-ring [45] of the PAHs may render the PAHs less prone to Fe^+ insertion and fragmentation. In addition, PAHs are more easily ionized by electron capture or loss as opposed to AAs that are ionized predominantly by protonation, cationization, or proton abstraction [39,40,46].

Currently, detection of AAs in mineral samples is usually accomplished by time-consuming extraction methods followed by derivitization for analysis via gas chromatography [3]. A somewhat less complicated method might be to overspray the sample with a thin layer of matrix (i.e., aromatic carboxylic acid) to perform a type of matrix-assisted laser desorption/ionization (MALDI) experiment similar to the preparation used for imaging biological tissues [47]. However, such an approach would still require sample preparation and would not be useful if depth profiling of a sample were necessary or desired [24]. For detection of amino acids *in situ* within a mineral sample, it may be possible for other organics naturally present, such as PAHs, to assist the ionization/desorption process.

3.5. PAH assistance for LD-FTMS detection amino acids

PAH compounds have the ability to undergo self-ionization reactions, so they do not need assistance from other organic compounds (i.e., matrices) [27]. However, most biomolecules (e.g., amino acids, proteins, and DNA) do not self-ionize

[33]. The well-developed technique MALDI enables detection of biomolecules, typically using aromatic carboxylic acids as matrices [48]. In traditional MALDI sample preparation, the analyte and an excess amount of matrix (molar ratios of 1000:1 or higher of matrix-to-analyte) are dissolved in an organic solvent and then deposited and dried onto a sample holder [49]. The excess amount of matrix molecules is thought to isolate analyte molecules from each other, protect the analyte molecules from the damaging laser radiation, assist desorption, and ionize the analyte, usually by acting as a protonation or deprotonation agent [48]. Some PAH compounds (e.g., pyrene) have been successfully utilized as matrices for the analysis of polybutadiene and polystyrene samples [50]. A compound with three aromatic rings, 9-aminoacridine, was also successfully introduced by Vermillion-Salsbury and Hercules [51] to desorb and ionize LMW compounds, such as amines and phenols, HMW proteins, and small peptides.

Because PAHs and AAs are both commonly found in natural samples, the possibility exists that PAHs could act as matrices to assist the detection of the AAs. Although relative concentration of PAHs and AAs in natural samples is variable, in meteorites the concentration of PAHs has been reported to be much greater than that for AAs [3]. Therefore, a less than optimal scenario was chosen for testing, where the PAH and AA exist in equal amounts. Chrysene, a principal PAH compound in terrestrial and extraterrestrial environments [7,10], was chosen to mix in a simple 1:1 molar ratio with either threonine or histidine prior to sample application on a iron-bearing surface. Without chrysene, threonine was not detected on the surface of the SSD (Fig. 5A). However, in the presence of chrysene the $[M - H]^-$ and $[M - N_2H]^-$ ions of threonine were detected on the sur-

face of the SSD (Fig. 5B). This suggested that chrysene assisted in the ionization of threonine or protected threonine from iron-induced fragmentation in the gas phase. Similar results were obtained for the detection of histidine on the surface of ilmenite, an iron-bearing mineral. Small fragment ions for histidine were observed in the absence of chrysene (Fig. 5C), while the molecular ion of histidine minus two hydrogens (m/z 153) was detected in the presence of chrysene (Fig. 5D). LDMS detection of AAs is highly mineral-dependent (Table 3), which complicates the application of this approach to explore biosignatures in outer space [25]. The successful assistance of the ionization of AAs by a small amount of chrysene is encouraging for applying LD-FTMS to detect amino acids in extraterrestrial materials because both AAs and PAHs are common and abundant compounds in outer space [6,8,30]. PAH and amino acids also co-exist in natural sediment samples; therefore, PAHs may be helpful for assisting detection of AAs in mineral samples.

4. Conclusion

PAH compounds were successfully detected on the surface of all tested minerals, demonstrating the high probability of the direct detection of PAHs associated with terrestrial and extraterrestrial minerals with direct LDMS. In a mixture where nitro-PAHs and nonpolar PAH compounds (i.e., parent- and amino-PAHs) co-exist, nitro-PAHs can be easily detected in negative ion mode, but the rest of the PAHs were mainly detected as positive ions. Unlike the PAH compounds, amino acid detection using LDMS is mineral dependent, with detection on Fe-bearing minerals being the most difficult. However, the presence of a co-existing PAH assisted the ionization of amino acids on Fe-bearing surfaces, which demonstrated LDMS as a promising method for the co-detection of PAHs and amino acids or other biomolecules in extraterrestrial and terrestrial materials.

Acknowledgements

References

[1] D.M. Hudgins, C.W. Bauschlicher, L.J. Allamandola, Astrophys. J. 632 (2005) 316–332.

[2] T.A. Abrajano, B. Yan, V.P. O'Malley, High-molecular weight petrogenic and pyrogenic hydrocarbons in aquatic environments, in: H.D. Holland, K.K. Turekian (Eds.), Treatise on Geochemistry, Elsevier-Pergamon, Oxford, 2003, pp. 475–510.

[3] O. Botta, J.L. Bada, Surv. Geophys. 23 (2002) 411–467.

[4] E.L. Shock, M.D. Schulte, Nature 343 (1990) 728–731.

[5] J.E. Chiar, A. Tielens, D.C.B. Whittet, W.A. Schutte, A.C.A. Boogert, D. Lutz, E.F. van Dishoeck, M.P. Bernstein, Astrophys. J. 537 (2000) 749–762.

[6] G. Moreels, J. Clairemidi, P. Hermine, P. Brechignac, P. Rousselot, Astron. Astrophys. 282 (1994) 643–656.

[7] S.J. Clemett, C.R. Maechling, R.N. Zare, P.D. Swan, R.M. Walker, Science 262 (1993) 721–725.

[8] D.S. McKay, E.K. Gibson, K.L. ThomasKeprta, H. Vali, C.S. Romanek, S.J. Clemett, X.D.F. Chillier, C.R. Maechling, R.N. Zare, Science 273 (1996) 924–930.

[9] L. Becker, B. Popp, T. Rust, J.L. Bada, The Origin of Organic Matter in the Martian Meteorite alh84001, Life Sciences: New Insights into Complex Organics in Space, Pergamon Press Ltd., Oxford, 1999, pp. 477–488.

[10] B. Yan, T.A. Abrajano, R.F. Bopp, D.A. Chaky, L. Benedict, S.N. Chillrud, Env. Sci. Technol. 39 (2005) 7012–7019.

[11] D.P. Glavin, J.L. Bada, K.L.F. Brinton, G.D. McDonald, Proc. Natl. Acad. Sci. U.S.A. 96 (1999) 8835–8838.

[12] G. Belluomini, M. Branca, G. Calderoni, M. Scnitzer, Org. Geochem. 9 (1986) 127–133.

[13] M.J. Collins, D. Walton, A. King, Nitrogen-containing Macromolecules in the Bio- and Geo-sphere, ACS Symposium Series, vol. 707, 1998, pp. 74–87.

[14] E. Andersson, B.R.T. Simoneit, N.G. Holma, Appl. Geochem. 15 (2000) 1169–1190.

[15] J.-E. Haugen, R. Lichtentaler, Geochim. Cosmochim. Acta 55 (1991) 1649–1661.

[16] K.L.F. Brinton, J.L. Bada, Geochim. Cosmochim. Acta 60 (1996) 349–354.

[17] S. Pizzarello, J.R. Cronin, Geochim. et Cosmochim. Acta 64 (2000) 329–338.

[18] M. Maurette, J. Duprat, C. Engrand, M. Gounelle, G. Kurat, G. Matrajt, A. Toppani, Planet. Space Sci. 48 (2000) 1117–1137.

[19] D.J. Burdige, C.S. Martens, Geochim. Cosmochim. Acta 52 (1988) 1571–1584.

[20] D.Z. Bezabeh, A.D. Jones, L.L. Ashbaugh, P.B. Kelly, Aerosol Sci. Technol. 30 (1999) 288–299.

[21] V. Carre, F. Aubriet, P.T. Scheepers, G. Krier, J.F. Muller, Rapid Commun. Mass Spectrom. 19 (2005) 871–880.

[22] M.J. Dale, A.C. Jones, S.J.T. Pollard, P.R.R. Langridgesmith, Analyst 119 (1994) 571–578.

[23] S.K. Lower, M.F. Hochella, T.J. Beveridge, Science 292 (2001) 1360–1363.

[24] J.R. Scott, B. Yan, D.L. Stoner, J. Microbiol. Methods 67 (2006) 381–384.

[25] B. Yan, D.L. Stoner, J.M. Kotler, N.W. Hinman, J.R. Scott, Geomicrobiol. J. 24 (2007), in press.

[26] S.M. Hankin, P. John, Anal. Chem. 71 (1999) 1100–1104.

[27] R. Zimmermann, L. Van Vaeck, M. Davidovic, M. Beckmann, F. Adams, Environ. Sci. Technol. 34 (2000) 4780–4788.

[28] R.P. Rodgers, A.C. Lazar, P.T.A. Reilly, W.B. Whitten, J.M. Ramsey, Anal. Chem. 72 (2000) 5040–5046.

[29] J.R. Scott, P.L. Tremblay, Rev. Sci. Instrum. 73 (2002) 1108–1116.

[30] M. Maurette, Origins Life Evol. Biosphere 28 (1998) 385–412.

[31] J.E. Ham, B. Durham, J.R. Scott, J. Am. Soc. Mass Spectrom. 14 (2003) 393–400.

[32] J.R. Scott, J.E. Ham, B. Durham, P.L. Tremblay, Spectr. Int. J. 18 (2004) 387–396.

[33] M. Karas, F. Hillenkamp, Anal. Chem. 60 (1988) 2299–2301.

[34] S.D. Hanton, D.M. Parees, J. Am. Soc. Mass Spectrom. 16 (2005) 90–93.

[35] B. Yan, D.L. Stoner, J.R. Scott, Appl. Surf. Sci. 253 (2006) 2011–2017.

[36] J.R. Scott, T.R. McJunkin, P.L. Tremblay, JALA 8 (2003) 61–63.

[37] A.S. Reddy, G.N. Sastry, J. Phys. Chem. A 109 (2005) 8893–8903.

[38] L. Van Vaeck, J. Claereboudt, J. De Waele, E. Esmans, R. Gijbels, Anal. Chem. 57 (1985) 2944–2951.

[39] K. Balasanmugam, S.K. Viswanadham, D.M. Hercules, Anal. Chem. 58 (1986) 1102–1108.

[40] R.N. Dotter, C.H. Smith, M.K. Young, P.B. Kelly, A.D. Jones, E.M. McCauley, D.P.Y. Chang, Anal. Chem. 68 (1996) 2319–2324.

[41] J.F. Muller, G. Krier, F. Verdun, M. Lamboule, D. Muller, Int. J. Mass Spectrom. Ion Process. 64 (1985) 127–138.

[42] T.R. McJunkin, J.R. Scott (2006) arXiv:cs.AI/0611085.

[43] F.L. Plows, J.E. Elsilai, R.N. Zare, P.R. Buseck, Geochim. Cosmochim. Acta 67 (2003) 1429–1436.

[44] K. Eller, H. Schwarz, Chem. Rev. 91 (1991) 1121–1177.

[45] J. March, Advanced Organic Chemistry, forth ed., John Wiley and Sons, New York, 1992, p. 1495.

[46] M.M. Stone, A.H. Franz, C.B. Lebrilla, J. Am. Soc. Mass Spectrom. 13 (2002) 964–974.

[47] H.R. Aerni, D.S. Cornett, R.M. Caprioli, Anal. Chem. 78 (2006) 827–834.

[48] J.T. Stults, Curr. Opin. Struct. Biol. 5 (1995) 691–698.

[49] J. Yao, J.R. Scott, M.K. Young, C.L. Wilkins, J. Am. Soc. Mass Spectrom. 9 (1998) 805–813.

[50] S.F. Macha, P.A. Limbach, P.J. Savickas, J. Am. Soc. Mass Spectrom. 11 (2000) 731–737.

[51] R.L. Vermillion-Salsbury, D.M. Hercules, Rapid Commun. Mass Spectrom. 16 (2002) 1575–1581.

Talanta

Short communication

Direct atomic absorption spectrometry determination of tin, lead, cadmium and zinc in high-purity graphite with flame furnace atomizer[☆]

A. Zacharia [a,∗], S. Gucer [b], B. Izgi [b], A. Chebotarev [a], H. Karaaslan [b]

[a] *I.I.Mechnikov Odessa National University, Department of Analytical Chemistry, str.Marazlievskaya, 1A/8, 65014 Odessa, Ukraine*
[b] *Uludag University, Science and Art Faculty, Department of Chemistry, 16059 Bursa, Turkey*

Abstract

This work described methodology of Sn, Pb, Cd and Zn impurities determination in high-purity graphite at direct atomic absorption spectrometry (AAS) with flame furnace (FF) atomizer. It was evidence that quality of AAS measurements are depended from sample amount, its homogeneity, particle size, as well as calibration procedure and operation parameters of FF atomizer. Prior to analysis the method has been developed and optimized with respect to the furnace heating temperature and flame composition of FF atomizer. Conditions of absorption peak areas (Q_A) formation to each element were studied on the basis of contribution into its value some of individual parameters of analytes, including mass-transporting process from increasing mass of graphite samples into gas phase. Because particle size and homogeneous distribution of analyte in powdered materials has an enormous influence on accuracy and precision of measurement results, graphite as well as appropriate series of powdered reference standards was previously ground and investigated. Graphite samples to be analyzed and standard reference materials with mass from 0.025 to 0.200 g was previously briquetted as pellet and insert on corresponding hole in furnace. The characteristic mass (g_0) of Sn, Pb, Cd and Zn were 0.35, 0.1, 0.008 and 0.025 ng, respectively, and relative standard deviation (S_r) not more than 20%.
© 2006 Elsevier B.V. All rights reserved.

Keywords: FF AAS; Solid samples; Graphite analysis; Atomic absorption spectrometry

1. Introduction

Graphite, carbon and some of their compounds are one of the important materials for modern technology. Their application in various fields of high-technology and industry required powerful, rapid and reliable methods for determination of trace components. The direct analysis of solid and powdered materials including graphite and corresponding materials (various carbides, natural coals, etc.) by so-called solid sampling technique (SoS) atomic absorption spectrometry is now one of the most promising analytical methods. The advantages of the SoS technique have been reviewed and compared to conventional procedures with regard to aspects of risk of contamination, minimization of losses in the pre-treatment operation steps and incomplete atomization of elements to be determined from solid matrix [1–4]. But the main drawbacks of SoS can be given as follows: (i) unrepresentative mass (<10 mg) of solids to be analyzed, (ii) non-homogenous distribution of analytes in the whole sample, (iii) high background level and (iv) calibration problems. Slurry sampling (SlS) was considered by some to have certain advantages over SoS that are summarized in review [4], where has been noted that slurry analysis of solids samples does not have advantages over direct solid sampling and the that most probable critical factor is the need for maintaining the stability of the slurry until sample injection. Only few authors report about direct SoS AAS for graphite, coal and similar materials analysis [5–12]. It has been noted [9] that determination of Cd in coal

---

using SoS graphite furnace AAS with conventional equipment turned out to be difficult, particularly as calibration against aqueous standards was not possible, necessitating the use of certified reference materials (CRM) for that purpose.

So, to find the simplest and most reliable calibration technique for coal analysis by SlS-ET-AAS the authors [10] proposed to use as chemical modifier Ru or Pd/Mg to Cd and Pb determination. In this work they noted that when coal samples were analyzed the excessively high background absorption at low pyrolysis temperature only allowed reliable measurements Pb analyte signal above 650 °C, where the background signal was low. When Pb is determined in solid coal samples without a modifier, losses start to become significant at pyrolysis temperature >750 °C. In this procedure aqueous and solid coal standards were used and in the case of Cd and Pb determination solid standards were chosen.

In [11], at the SoS AAS determination of 14 common impurities, including Pb and Zn, in graphite and silicon carbide, the authors used platform-technique and a sample portion between 0.1 and 8.0 mg. No-significant gas-phase matrix interferences, background signals for any elements or memory effects were observed. When silicon carbide was analyzed by heating about 5 mg of this material at 2400, 2500, 2600 and 2700 °C for 20 s and weighing the residue, mass losses of 13, 26, 60 and 68%, respectively, were found. When applying a temperature of 2600 °C the matrix remains quantitatively on the platform were physically and chemically unchanged. For elements atomized at temperature lower than 2400 °C no significant background signals were observed. Authors of this work point out that with graphite analysis small differences between the transient behaviors in atomization from the graphite sample and compared to aqueous solutions were not significant and no background signals or memory effects were observed. For calibration 10 μl aliquots of aqueous standard solution were used.

Baxter and Frech [11] examined different SlS AAS calibration techniques with respect to accuracy and found that a necessary condition for the calibration is that the matrix be identical as far as possible in both the solid samples and the calibration standard.

To improve SlS AAS analysis construction of several corresponding laboratory manufacturing devices were proposed and successfully used at the analytical practice [13–15] and only one type of special commercial instrument for solid—SM 30 Zeeman GF AAS (Grün Analysengerate, Wetzlar, FRG). As was noted [10], one of the major reasons why direct SoS has been abandoned in favor of SlS was the availability of commercial accessories for the latter technique, whereas the former technique was not support by any major instrument manufacturer.

Several authors [16–19] pointed out some of advantages of the flame furnace (FF) atomizer over conventional atomizers such as: (i) simplicity of construction and exploitation; (ii) satisfactory sensitivity determination of high and medium volatility elements; (iii) not so significant differences in comparison with commercial variants of HGA-type atomizers exposed to different sorts of interferences; (iv) possibility of AAS analysis of a representative mass of solid and powdered materials; (v) simplicity of reproduction (without losses) when inserting solid or powdered samples into the furnace and removing them from the furnace (without remains).

Unfortunately, till now FF atomizer is not widely used in direct AAS analysis because it is not constructed commercially.

The aim of this work was to investigate analytical possibility and peculiarity of the FF AAS technique for direct solid sampling technique at determination of Sn, Pb, Cd and Zn impurities (≥0.005 ppm) in representative mass (≥0.100 g) of high-purity graphite.

The investigation takes into account questions of sample mass, its homogeneity, particle size, and the character of calibration procedure.

2. Experimental

2.1. Instruments, FF AAS system and sample preparation

An ATI-Unicam 929 Model AAS equipped with deuterium background correction was used in the absorption mode with the parameters of air-acetylene flame and graphite furnace mentioned below. Hollow cathode lamps were used as radiation sources for Sn, Pb, Cd and Zn determinations. The general scheme of the FF atomizer was adapted from L'vov design [16].

Graphite furnaces were prepared from high-purity carbon rod and before analysis was heated up to 600 °C for 1.0–1.5 h, impregnated for 3 h by 30% (v/v) zirconium oxychloride solution and then dried and purified by electrically heating at 2500 °C for 20–25 s in an argon atmosphere with the FF atomizer.

2.2. Analytical procedure

Graphite samples to be analyzed as well as standard reference materials with mass from 0.025 to 0.200 g were previously briquetted as pellet (diameter 6.0 mm) and inserted into the corresponding hole in graphite furnace. This technique allows with very simple tools the sampling of solid and powdered materials without losses and removing their remains from furnace after the operation cycle. Emission spectral analysis (ESA) was additionally used at pre-investigations at condition that have been detailed before [19].

All graphite samples were previously ground and powdered for 60–90 min with agate mortar and particle size distribution was obtained by photo sedimentation analysis.

The appropriate aqueous calibration standards were prepared by dilutions of stock solution in 0.01 mol l^{-1} nitric acid and series of calibration graphite standards samples – by mechanical dilutions (at 5–10 times) from sample to sample with high-purity graphite its general certificate reference material (CRM) with content of Sn, Pb, Cd, Zn – 250 ppm. High-purity grade materials were used for this investigation.

Peak areas of absorption values (Q_A) were used throughout.

In order to optimize and develop the FF AAS method, the general operation parameters of graphite temperature, its timing and air-acetylene flame composition (last characterized by relative contents of oxidizer) were investigated.

The conditions of Q_A formation of each element were studied on the basis of contribution to its value some of individual param-
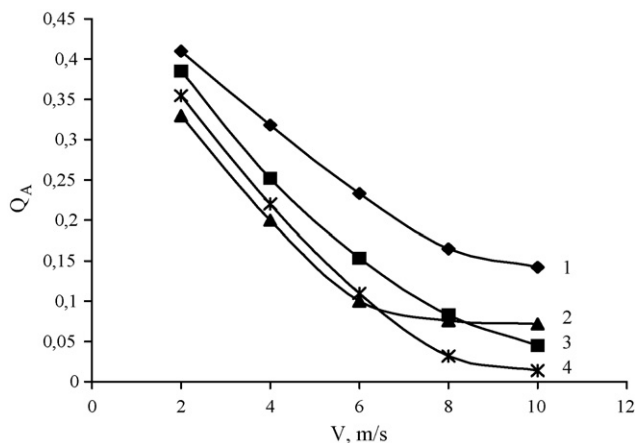
Fig. 1. Effect of linear speed flame gas particles (*V*) on peak area absorbance values (Q_A) of Cd (1), Pb (2), Zn (3) and Sn (4) at FF AAS analysis of graphite.

eters of mass-transporting process from the increasing mass of graphite into the gas phase (flame). It must be noted that in the FF atomizer the areas of elements evaporation and formation of analytical signal are separated. That is why some sorts of interference in AAS with the FF atomizer are less compared to with the HGA-type furnace. We think that distribution of atoms and their number density (n_h) in any points of flame on its height (*h*) above the furnace surface can be approximated by the equation [17]:

$$n_h = 0.280 n_0 (DVh)^{-1/2} \qquad (1)$$

where n_0 is the total number of atoms of the element that enters from graphite furnace surface or solid sample into flame at the unit of time, *D* the coefficient of atoms diffusion, *V* the linear speed of flame gas particles (calculated by formula: $V = v/S$, where *v* is the total flow rate of gases components at the unit of time and *S* is the total area of holes on head of the Mekker burner (at this work, -0.251 sm^2).

Operation parameters of the FF atomizer: flame composition, furnace temperature, as well as mass of graphite to be analyzed, were investigated and it was decided that the following criteria must be provided:

(a) the stability of evaporation process of analytes, that ensured preservation of the solids in an uncaked state (at this position it seems that graphite is an ideal material to direct AAS analysis);

(b) the high value of coefficient extraction (*q*) of elements (mass transporting parameters from solids to flame); $q = Q/100$, where *Q* is the yield of element from analyte (mass%) into gaseous phase;

(c) the minimum time of elements evaporation (*t*), the value of which is conditioned by corresponding its high-temperature chemical transformations in the ondensing phase with matrix components of solids;

(d) impossibility to form elements into new stable chemical compounds with air-acetylene flame components (high probability of these processes are well known [18]).

3. Results and discussion

Peak area values of elements absorption (Q_A) were considered when choosing proper furnace and operation flame parameters. It can be easily noted (Figs. 1 and 2) that the variation of *V* parameter means in Eq. (1) lead to increasing the range of elements concentration can be determined with the FF.

At operation parameters of FF AAS determination of Sn, Pb, Cd and Zn (Table 1) in graphite samples (mass 0.100 g) the relative standard deviation values (S_r) does not exceed 25%. Life time of one furnace under these parameters was 35–40 measurements.

It has been established that evaporation and atomization of elements microquantities from increasing mass of graphite (0.020–0.200 g) produced essential differences compared to those of dry residues of solutions not only on peak (*A*) but area (Q_A) atomic absorption values as well as on corresponding calibration curves positions (Figs. 3 and 4).

In this connection quantification was performed using calibration curves measured with powdered graphite standard samples.

The results of EAS of graphite residues in the furnace, which were collected after 25–30 replicates in operation conditions (Table 1) at investigation from 0.025 to 0.200 g of CRM (concentration of Sn, Pb, Cd and Zn—250 ppm) are clearly show that at an increasing mass of graphite the rates of elements evaporation and mass-transporting (*q*) change significantly only for Sn (Table 2).

Because the particle size and homogeneous distribution of the analyte in powdered samples have an enormous influence on the accuracy and precision of analytical results especially with
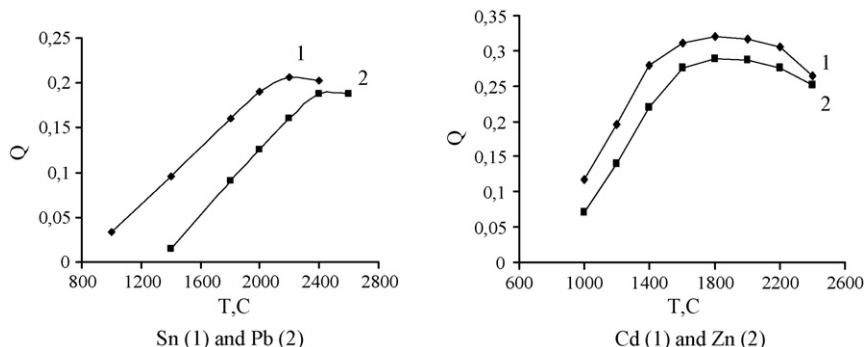

Fig. 2. Effect of furnace temperature (*T*, °C) on peak area absorbance values (Q_A) of Sn, Pb, Cd and Zn at FF AAS analysis of graphite.

Table 1
Operation parameters for FF AAS determination of Sn, Pb, Cd and Zn in high-purity graphite

Element	h (mm)	Analytical line (nm)	Gas flow rate (l min^{-1})		Furnace temperature on atomization step	g_0 (ng)
			C_2H_2	Oxidizer[a]		
Sn	1.0–1.5	286.3	2.0	3.5	2400	0.35
Pb	2.0	283.3	0.7	2.3	2200	0.10
Cd	2.0	228.8	0.7	2.3	2000	0.008
Zn	2.0	213.9	0.7	2.3	2100	0.025

h: high of zone photometry above furnace surface; g_0: characteristic mass of elements.

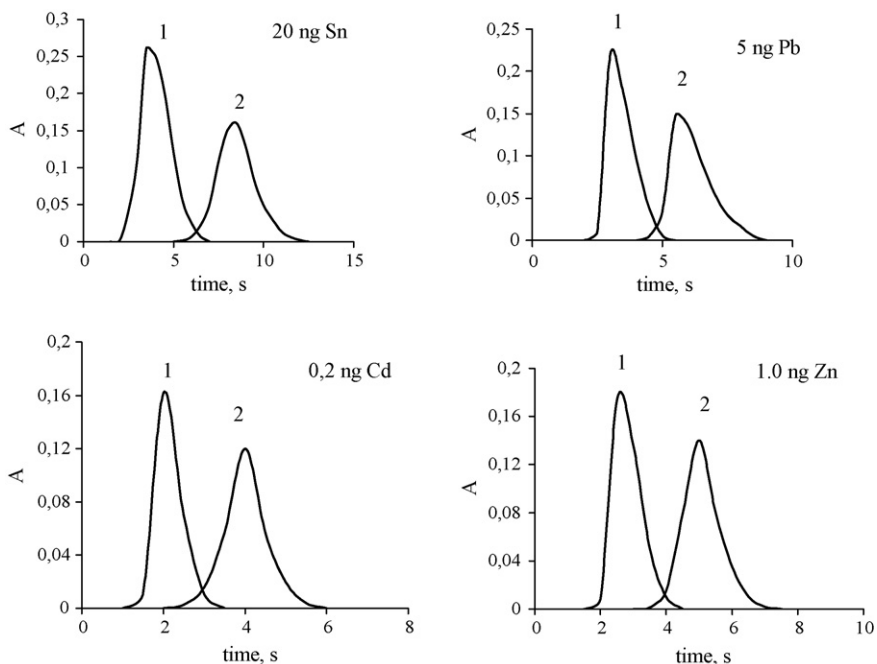[a] For Sn: N_2O; for Pb, Cd and Zd: air.

Fig. 3. Absorption signals of Sn, Pb, Cd and Zn at evaporation from aqueous standard solutions (1) and graphite standard samples (2) (mass 0.100 g).
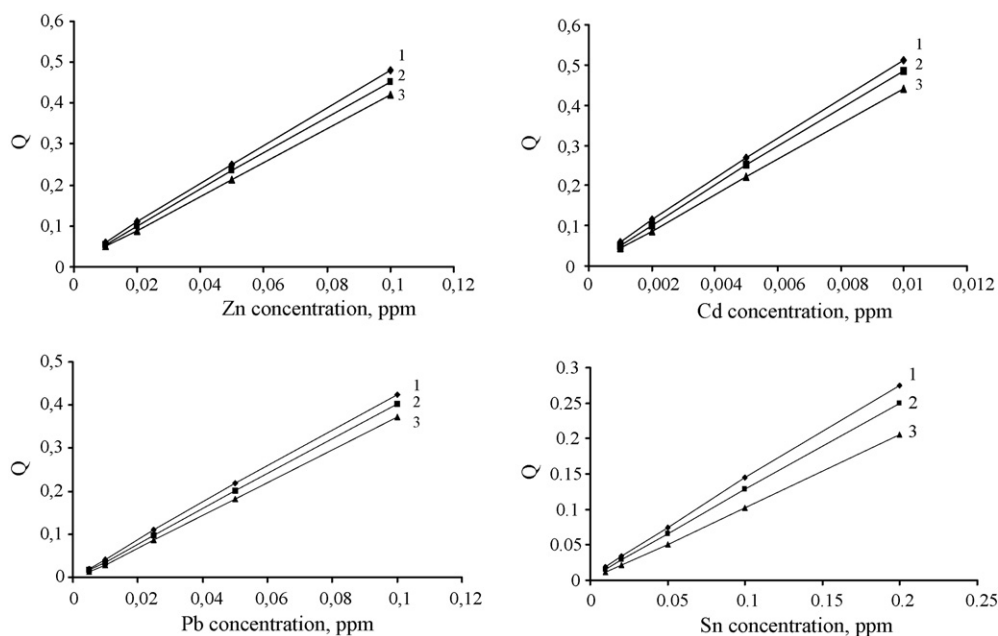

Fig. 4. Calibration curves of FF AAS Zn, Cd, Pb and Sn determination at evaporation from aqueous calibration standard solutions (1) and calibration graphite standard samples with mass: 0.050 (2) and 0.200 g (3).

Table 2
Values of q and t (s) at Sn, Pb, Cd and Zn evaporation creasing mass of graphite at its direct AAS determination with FF atomizer

Graphite mass (g)	Parameters of Sn, Pb, Cd and Zn evaporation from graphite at its FF AAS determination							
	Sn		Pb		Cd		Zn	
	q	t	q	t	q	t	q	t
0.025	0.96	6.7	0.98	3.9	1.0	3.3	1.0	3.6
0.050	0.91	7.0	0.98	4.4	1.0	3.5	1.0	3.9
0.100	0.84	7.3	0.92	5.1	0.93	4.0	0.94	4.2
0.200	0.76	7.9	0.90	5.5	0.92	4.4	0.90	4.7

q: coefficient extraction of elements transporting from mass of analyte into flame; t: time (s) of full evaporation of elements.

the SlS AAS [12], when graphite samples to be analyzed as well as appropriate series of calibration standards were previously ground for 60 min.

The particle size distribution of samples obtained by this procedure by photosedimentation analysis is illustrated in Table 3. After grinding approximately 90% of graphite samples consisted of particle size <12 μm compared before grinding—40%. These samples ($m = 0.100$ g) were analyzed and the results obtained permit us to state that using SoS technique with FF AAS analysis and increasing mass of graphite, the influences of particle size on accuracy and reproducibility of measurements are negligible.

Simultaneously it was assumed that not only the mass of the sample introduced into FF atomizer but also graphite homogeneity could be a reason for some of the interference effects. For the calculation of homogeneity of a small sample mass Kurfürst et al. [20] proposed the H_E factor because its quadratic relation, rather than the linear sampling constant of Ingmells, is more suitable. To quantify the homogeneity of an element when increasing the mass (0.025–0.200 g) of graphite samples, we used a dispersion analysis [21,22]. At the total mass of 20–30 g after grinding and mixing (60 min) the graphite samples were separate approximately into seven equal parts. Each of them was additionally mixed for 20 min and analyzed with five replicates. On all results the mean of standard deviations (S_r), average S_i mean of S_I and S_{II}, that characterized dispersion of all average results of analysis (x_i) concerning their total average mean ($\bar{X}$), and F^I-factor, were calculate:

$$F^I = \frac{S_{II}^2}{S_I^2} \quad (2)$$

Table 3
The results of Sn, Pb, Cd and Zn determination in graphite samples with FF AAS and emission spectral analysis (ESA), $n = 5$; $p = 0.95$

Sample no.	Element	Mean value of element ($C \pm \Delta c$) (ppm)			
		FF AAS	S_{r1}	ESA	S_{r2}
G-02	Sn	0.17 ± 0.02	0.12	0.21 ± 0.05	0.19
	Pb	0.028 ± 0.004	0.12	0.023 ± 0.007	0.25
	Cd	0.011 ± 0.002	0.14	0.014 ± 0.004	0.21
	Zn	0.25 ± 0.05	0.16	0.30 ± 0.09	0.23
PG-4	Pb	0.016 ± 0.003	0.17	0.013 ± 0.004	0.24
	Cd	0.0055 ± 0.0010	0.15	0.0045 ± 0.0015	0.25
PG-5	Sn	0.037 ± 0.006	0.14	0.042 ± 0.011	0.21
	Pb	0.054 ± 0.008	0.12	0.050 ± 0.014	0.22
	Cd	0.014 ± 0.002	0.13	0.011 ± 0.003	0.24
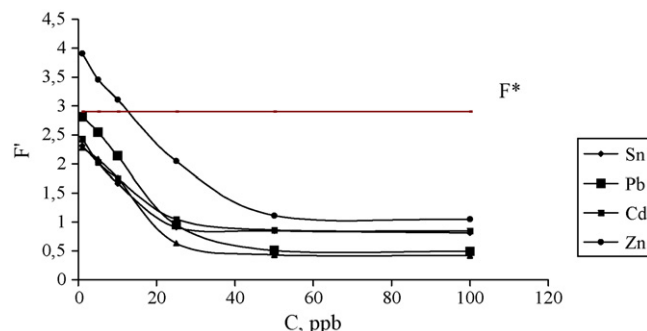
Fig. 5. Relations of F'-values for Sn, Pb, Cd, Zn and its concentrations at the delution-technique of graphite CRM preparation.

F^I was compared with F^* (at $f_1 = m - 1$ and $f_2 = mn - m$ $F^* = 2.9$). Accordingly this solid powdered materials can be considered homogenous when $F^1 \leq F^*$ and no-homogenous at $F^1 > F^*$.

Unfortunately, the conditions of operations in our laboratory did not permit us to prepare a series graphite standard to Zn, Fe, Cu, Si, Mg, Al, Ca, Na and K on ppb level because of the absence of appropriate high-purity graphite matrix, and the very high probability of contamination during this procedure. The results obtained (Fig. 5) very clearly illustrated this for Zn and for other elements at high rates of dilutions the initial CRM of graphite when F^I means are drawn near to F^*.

On this evidence, for the direct FF AAS analysis representative analytes (≥ 0.100 g) of powdered graphite and similar materials, it is necessary to use as calibration samples the composition on the corresponding matrix as well as integral absorption profile (Q_A) registration.

The results obtained were used at direct FF AAS determination 0.005–0.25 ppm Sn, Pb, Cd and Zn in some of graphite samples and compared with ESA data (Table 3). Statistically significant differences between the values received have not been established.

4. Conclusion

SoS AAS using a FF atomizer was applied to direct analysis of graphite for Sn, Pb, Cd and Zn impurities. The major advantage of this proposed technique, which includes pressing material for analysis into pellets, is that it is possible with simple means to analyze the representative mass (≥ 0.100 g) of solids. However, quantification performed using calibration curves measurements

required use of powdered graphite standard samples. The accuracy of this method was checked by comparison of its results with those obtained by ESA. The characteristic mass (g_0) of Sn, Pb, Cd and Zn were 0.35, 0.1, 0.008 and 0.025 ng, respectively, and relative standard deviation (S_r) not more then 20%.

Acknowledgements

References

[1] B.V. L'vov, Talanta 23 (1976) 109.

[2] F.J. Langmyhr, Analyst 104 (1979) 993.

[3] U. Kurfürst, in: U. Kurfürst (Ed.), Solid Sample Analysis, Springer-Verlag, Berlin, 1998.

[4] D.L.G. Borges, A.F. da Silva, A.J. Curtius, B. Welz, U. Heitmann, Microchim. Acta 154 (2006) 101.

[5] A.F. da Silva, D.L.G. Borges, Far bio Grandis Lepri, B. Welz, A.J. Curtius, U. Heitmann, Anal. Bioanal. Chem. 382 (2005) 1835.

[6] É.M.M. Flores, J.N.G. Paniz, A.P.F. Saidelles, J.S. Barin, V.L. Dressler, E.I. Müller, A.B. Costa, J. Br. Chem. Soc. 15 (2) (2004), São Paulo, March/April.

[7] M.G.R. Vale, M.M Silva, B. Welz, E.C. Lima, Spectrochim. Acta Part B 56 (2001) 1859.

[8] M.J. Cal-Prieto, M. Felipe-Sotelo, A. Carlosena, J.M. Andrade, P. Lopez-Mahina, S. Muniategui, D. Prada, Talanta 56 (2002) 1.

[9] M.G.R. Vale, M.M. Silva, B. Welz, E.C. Lima, Spectrochim. Acta Part B 56 (2001) 1859.

[10] U. Schaffer, V. Krivan, Fresenius J. Anal. Chem. 371 (2001) 859.

[11] D. Baxter, W. Frech, Fresenius J. Anal. Chem. 327 (1990) 253.

[12] R. Nowka, H. Müller, Fresenius J. Anal. Chem. 359 (1997) 132.

[13] B. Docekal, Spectrochim. Acta Part B 53 (1987) 427.

[14] R. Nowka, I.L. Marr, T.M. Ansari, H. Muller, Fresenius J. Anal. Chem. 364 (1999) 533.

[15] V.P. Borzov, B.V. L'vov, G.V. Plushch, Zh. Prikl. Spectrosc. 11 (1969) 271.

[16] B.V. L'vov, L.P. Kruglikova, D.A. Katzkov, A.I. Manchikov, Zh. Prikl. Spectrosc. 24 (1976) 372.

[17] B.V. L'vov, L.P. Kruglikova, G.V. Plushch, Zh. Prikl. Spectrosc. 15 (1971) 975.

[18] B.V. L'vov, L.A. Pelieva, Zh. Anal. Chem. (Russ.) 33 (1978) 1695.

[19] N.F. Zacharia, L.A. Karpenko, T.F. Nazarova, L.A. Fadeeva, A.I. Staikov, Investigations on Theory and Analytical Practice of Spectral Analysis of Rare Elements. Techn. Reglam. Analysis of High-Purity Graphite, Ukrainian National Academy of Sciences, Institute of General and Inorganic Chemistry, Odessa, 1967.

[20] U. Kurfürst, J. Pauwels, K.H. Grobecker, M. Stoeppler, H. Muntau, Fresenius J. Anal. Chem. 345 (1993) 112.

[21] R.I. Alekseev, Yu.I. Korovin, Guidance to calculations and processing of quantitative analysis results, Moscow, Atomizdat, 1972.

[22] K. Doerffel, Statistik in der analytishen Chemie, Deutscher Verlag Fur Grundstoffindustrie GmbH, Leipzig, 1990.

Extraction and determination of trace amounts of energetic compounds in blood by gas chromatography with electron capture detection (GC/ECD)

Baohong Zhang [*,1], Xiaoping Pan [1], Jordan N. Smith, Todd A. Anderson, George P. Cobb

The Institute of Environmental and Human Health, and Department of Environmental Toxicology, Texas Tech University, Lubbock, TX 79409, USA

Abstract

This paper describes an efficient and sensitive method for determining five energetic compounds at trace levels (ng/mL) in blood by gas chromatography with electron capture detection (GC/ECD). For seven test concentrations (1–1250 ng/mL), the average recoveries (%) were 104 ± 16, 108 ± 22, 105 ± 14, 100 ± 22 and 108 ± 16 for hexahydro-1,3,5-trinitroso-1,3,5-triazine (TNX), hexahydro-1,3-dinitroso-5-nitro-1,3,5-triazine (DNX), hexahydro-1-nitroso-3,5-dinitro-1,3,5-triazine (MNX), hexahydro-1,3,5-trinitro-1,3,5-triazacyclohexane (RDX) and 2,4,6-trinitrotoluene (TNT) ($n = 84$), respectively. Analysis of DNX and RDX produced lower precision than other energetic compounds. Acetonitrile extracts of blood samples should be analyzed immediately as the test compounds can transform into unknown compounds, which lowered the recovery by 0–45% within 10 days at room temperature ($\sim$20 °C). Maintaining sample extracts at 4 °C decreased loss of test compounds. The method described herein was validated by different analysis teams on different days. Two-way ANOVA indicated that there was no significant difference between analysis teams or days of analysis. The method was successfully employed in the analysis of blood samples from a mouse dosing study involving TNX and RDX.
© 2006 Elsevier B.V. All rights reserved.

Keywords: Energetic compound; Explosive; Blood; Gas chromatography; Electron capture detection

1. Introduction

In the past century, energetic compounds, such as 2,4,6-trinitrotoluene (TNT), hexahydro-1,3,5-trinitro-1,3,5-triazacyclohexane (RDX), and octahydro-1,3,5,7-tetranitro-1,3,5,7-tetraazacyclooctane (HMX), were produced as explosives and widely used for military and civil purposes around the world [1,2]. In some instances, these activities released energetic compounds into the environment, contaminating water and soil [1,3]. An estimated 12,000 sites across the U.S. are contaminated by energetic compounds; TNT, RDX and HMX are the most prevalent of these contaminants [2,4,5]. Laboratory and field studies indicate that these energetic compounds are toxic at relatively low concentrations to microorganisms [6–8], plants [9,10], invertebrates [4,5,11–14], birds [15], rats [16], and humans [17,18]. Energetic compounds inhibit growth and development of organisms [19], cause seizures in humans [20–23] and rats [24], and may cause genotoxicity, cancer, or death [17,25].

To better understand the environmental and biological fate of energetic compounds and to better understand the potential health risks, sensitive analytical methods must be available to measure these compounds and their biotransformation products [1,3,26]. Although some methods have been developed for the determination of energetic compounds using HPLC [27] and GC, the majority of these methods were developed for analyzing explosive residues in water [28–36], soil [1,31,36–41] and plant samples [1]. Little information exists in the literature describing methods that can be used on animal tissues and biological fluids. This could hamper investigations on the effect of energetic compounds on animals [42,43].

Biological tissues and fluids are complex mixtures that contain many endogenous compounds (such as proteins, lipids) that can interfere with analyte determination and obstruct the separation and analysis of energetic compounds. Animals are usually indirectly exposed by drinking contaminated water or by eating contaminated food, so provided the contaminants

---

* Corresponding author. Tel.: +1 806 885 4567; fax: +1 806 885 4577.
  E-mail address: baohong.zhang@tiehh.ttu.edu (B. Zhang).
[1] Co-first authors.

are usually not biomagnified, concentrations of energetic compounds and their biotransformation products should be lower than in the primary contamination source. Thus, more efficient methods are needed to detect energetic compounds and their biotransformation products in animal tissues and fluids for risk assessment. Unfortunately, analytical methods specifically developed for detecting energetic compounds and their biotransformation products in animal tissues are limited [44].

In this study, we describe a rapid and sensitive method to determine RDX, TNT, and three transformation products of RDX [45–47] in blood samples using gas chromatography with electron capture detection (GC/ECD). This method should facilitate risk assessments of explosives by allowing for the determination of exposure and distribution of explosive residues in humans and wildlife.

2. Experimental

2.1. Chemicals and reagents

TNT (CAS: 118-96-7), RDX (CAS: 121-82-4), MNX (CAS: 5755-27-1), DNX (CAS: 80251-29-2), and TNX (CAS: 13980-04-6) (Fig. 1) were analyzed in this study. RDX (purity > 99%) was purchased from Supelco (Bellafonte, PA). TNT (purity > 99.9%), MNX (purity = 98.4%), DNX (purity = 67%), and TNX (purity > 99.9%) were obtained from SRI International (Menlo Park, CA). HPLC-grade acetone and acetonitrile were purchased from Fisher Scientific (Pittsburg, PA). Ultra-pure water (>18 MΩ) was prepared by a Barnstead NANOpure infinity ultrapure water system (Dubuque, IA). Glassware was washed with phosphate-free detergent and rinsed with deionized water, acetone, and acetonitrile.

2.2. Standard solution, calibration curve, and method detection limits

A stock standard solution for each of the test compounds was prepared in acetonitrile at a concentration of 1000 mg/L. Working standard solutions of each energetic compound (0, 1, 2, 5, 10, 20, 50, 100, 200, 500, 1000 and 1250 ng/mL) were made
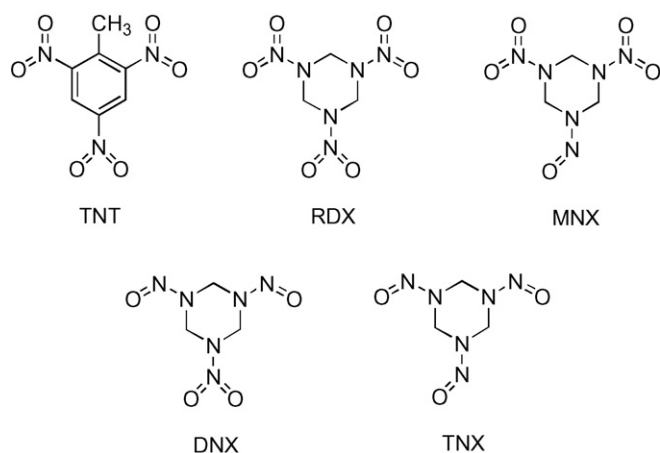

Fig. 1. Structures of energetic compounds and their biotransformation products.

by dilution of the stock standard solution with acetonitrile. All stock and working standard solutions were stored at 4 °C prior to analysis.

Working standard solutions were individually analyzed (described below) from low concentration to high. Each standard was analyzed three times and the average peak area was computed. A graph of analyte concentration versus GC–ECD response was constructed.

The method detection limits (MDLs) of the analytes were determined in the test blood matrix described below, and calculated according to EPA guidelines using a 2 ng/mL standard of each analyte [48] and the following equation:

$$MDL = \text{standard deviation of seven replicates}$$
$$\times \text{Student's } t\text{-value at 99\% confidence level}$$
$$(t = 3.14 \text{ for } n = 7).$$

2.3. Blood sample treatment and extraction procedure

The blood used for method development and validation was porcine blood, which was collected during ongoing slaughter operations that were unrelated to our study. Collected pig blood samples were placed into 50 mL centrifuge tubes containing heparin and stored at 4 °C prior to treatment and analysis.

A 1 mL aliquot of blood was placed into a 15 mL glass centrifuge tube and spiked with a standard solution of the test compound to final concentrations of 1, 5, 10, 20, 50, 250, and 1250 ng/mL. Spiked samples were mixed with a vortex-mixer for 1 min. Blank (untreated) blood samples were similarly prepared by amendment with the same volume of acetonitrile. Blank and spiked blood samples were stored overnight at 4 °C before extraction and GC–ECD analysis.

Liquid extraction coupled with sonication was employed for extracting explosives from blood samples. Briefly, 7 mL of acetonitrile was added to the 1 mL blood sample, followed by mixing with a vortex-mixer for 1 min. Samples were sonicated using an ultrasonic water bath (Branson, Danbury, CT) at 50 °C. During sonication, the samples were mixed periodically with a vortex-mixer for 1 min. After liquid extraction for 2–3 h, the blood samples were centrifuged (3500 rpm) using a Beckman Allegra 6R centrifuge (Palo Alto, CA) for 10 min. The supernatants were collected and cleaned using Florisil solid-phase extraction (SPE) cartridges according to the following procedure: Florisil SPE cartridges were first placed on a 24-port manifold (Supelco, Bellafonte, PA) and were conditioned with acetonitrile (3 × 10 mL). Samples were then loaded, and eluates were collected. The Florisil cartridges were rinsed three times with acetonitrile (3 × 1 mL). The collected samples from SPE cartridges were concentrated to 1 mL under nitrogen using N-EVAP™ 111 nitrogen evaporator (Organomation Associates Inc., Berlin, MA), and filtered (0.2 μm) prior to GC analysis.

2.4. Sample analysis by GC–ECD

Analyses were performed using an HP 6890 gas chromatograph equipped with an HP 6890 autosampler and an electron

capture detector (Agilent, Palo Alto, CA). Separation was performed with a 30 m × 0.25 mm i.d. × 0.25 μm film thickness HP-5 column from Hewlett-Packard (Wilmington, DE). Helium (99.999% purity) served as carrier gas at a constant linear velocity of 80 cm/s. Argon:methane served as make-up gas for the detector.

The oven temperature program began at 90 °C, held for 2 min, increased to 130 °C at a rate of 25 °C/min, then made a 10 °C/min ramp to 200 °C, finally increased to 250 °C at a rate of 25 °C/min. The injection port temperature was 170 °C, while the detector was 270 °C. A 2 μL standard or sample was injected in splitless EPC mode. A splitless inlet liner (4.0 mm i.d.) with glass wool was used in this analysis. The septum and inlet liner were replaced after every 60 injections. The ECD was operated in constant current mode.

A set of working standards was used to construct a calibration curve based on average peak area. One calibration standard (100 ng/mL) was also injected after every 10 samples to insure that the calibration was maintained; the response of that check standard was incorporated into the existing calibration curve. If the calibration check failed, a new calibration curve was constructed prior to any further analyses. Typically, more than 100 samples could be run (for all analytes except RDX) before a calibration failure occurred. This frequency of standard analysis ensured that analyte and detector stability were maintained during instrumental analysis. In each sample batch ($n = 60$), three blank (untreated blood) samples were also analyzed.

The measurement of intra- and inter-day variability was used to determine the precision of the developed method. Precision estimates were based on relative standard deviation (R.S.D.) of the analyses.

2.5. Method validation, reproducibility, and stability test

Two research teams were employed to validate and test the stability and reproducibility of the method during seven consecutive days. These tests were performed with pig blood samples spiked with RDX, MNX, TNX, DNX, or TNT (12 replicate samples at 50, 250, and 1250 ng/mL.

2.6. Application of the developed method

The developed method was used to analyze blood samples from deer mice (*Peromyscus maniculatus*) obtained from an ongoing toxicity study with TNX and RDX. In the toxicity study, deer mice were dosed daily with 10 or 100 ng/mL TNX- or RDX-containing water for more than 1 month. Deer mice blood sample extraction and analysis followed the protocol described above.

2.7. Statistical analysis

Recovery data were processed using standard statistical software (SigmaPlot, Version 8.0, SPSS, Chicago, Illinois, USA). Two-way ANOVA was employed to compare potential differences among days and teams. A significance level of $\alpha = 0.05$ was used in all comparative statistics.

2.8. Safety consideration

RDX and TNT are explosives and can only be received in milligram quantities without permit. Thus, RDX, TNT, and their biotransformation products must be carefully handled. RDX, TNT, and RDX biotransformation products are also potentially toxic and carcinogenic compounds [42,43]. Personnel involved in work with explosives residues should wear protective gloves and goggles (ANSI Z 87.1-2003), especially when handling neat explosives. All waste solutions containing these energetic materials and their biotransformation products should be collected and discarded appropriately.

3. Results

3.1. Method development

Each test compound was efficiently separated (baseline resolution) from endogenous compounds in hog blood and from each other (Fig. 2). The GC–ECD response versus concentration was best fitted to a quadratic model ($y = ax^2 + bx + c$) with excellent correlation coefficients (>0.99) for each of the energetic compounds over the tested concentration range (1–1250 ng/mL) (Table 1). We also attempted to analyze HMX (another important explosive) using this method, however, the detector response was low. In addition, the low volatility of HMX precluded elution in a reasonable time without thermal degradation. Although several modifications to the method were attempted (inlet temperature, shorter column), significant progress was not made in HMX analysis by GC/ECD.

The GC/ECD method was sensitive to TNX, DNX, TNT, MNX, and RDX; method detection limits (MDLs) in pig blood samples were 0.05, 0.10, 0.20, 0.25, and 0.50 ng/mL for TNX, DNX, TNT, MNX, and RDX, respectively. In addition, high recoveries of the analytes of interest were achieved at all of the concentrations tested (Table 2). However, different energetic compounds gave slightly different recoveries; the recovery range for DNX and RDX was wider than the other test compounds. At all tested concentrations, the recovery for MNX was 99–111%, while it was 97–114%, 97–125%, 98–130%, and 84–129% for TNX, TNT, DNX, and RDX, respectively. However, statistical analyses indicated that there was no significant difference among recoveries. This suggests that the method for extracting and analyzing explosive residues from blood was not analyte- or concentration-dependent.

Table 1
Parameters of the standard calibration curves for five analytes

Analytes	a	b	c	r^2	Concentration range (ng/mL)
TNX	0.2134	33.3	−2.78	0.9987	1–1250
DNX	0.0064	17.5	−16.56	0.9989	1–1250
TNT	0.1081	12.8	−11.25	0.9921	1–1250
MNX	0.0056	8.41	−8.79	0.9985	1–1250
RDX	0.0062	2.72	−1.67	0.9998	1–1250

The GC–ECD response versus concentration was best fit to a quadratic model ($y = ax^2 + bx + c$) with excellent correlation coefficients.
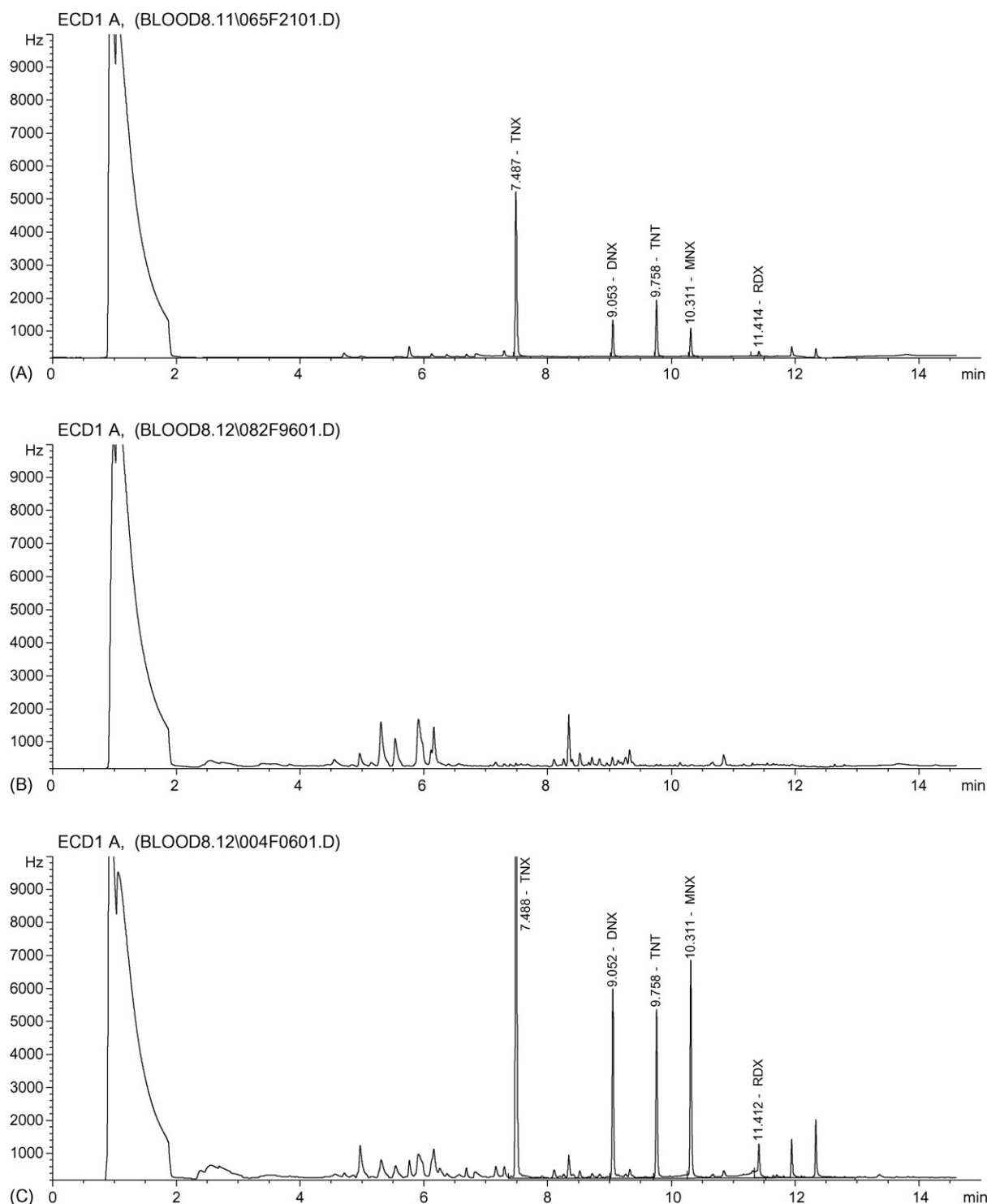
Fig. 2. Representative GC/ECD chromatograms. (A) Standard solution (10 ng/mL) of a mixture of explosives; (B) blank blood sample; (C) pig blood sample spiked with a mixture (30 ng/mL) of explosives.

The precision ranged from 2.5 to 27% for all the analytes at all tested concentrations (1–1250 ng/mL). At relatively high concentrations (1250, 250, and 50 ng/mL), the precision ranged from 2.5 to 5.1, 3.8 to 7.7, 6.2 to 11.7, and 4.0 to 13.0 for TNX,

DNX, TNT, and MNX, respectively; the accuracy [accuracy (%) = (observed concentration−spiked concentration)/(spiked concentration) × 100] ranged from −2.7 to 2.2, −1.7 to 1.5, −2.9 to 6.4, −0.1 to 6.0, and −4.4 to 0.1 for TNX, DNX,

Table 2
Recovery and precision for energetic compounds in pig blood by GC–ECD (%)

Compound	n	Recovery	Precision
Level: 1250 ng/mL			
TNX	12	99 ± 2.5	2.48
DNX	12	102 ± 4.4	4.31
TNT	12	106 ± 8.7	8.15
MNX	12	100 ± 4.0	4.04
RDX	12	100 ± 3.0	3.30
Level: 250 ng/mL			
TNX	12	102 ± 3.3	3.26
DNX	12	100 ± 3.8	3.82
TNT	12	97 ± 11	11.75
MNX	12	106 ± 6.6	6.25
RDX	12	97 ± 7.8	8.05
Level: 50 ng/mL			
TNX	12	97 ± 5.0	5.14
DNX	12	98 ± 7.6	7.69
TNT	12	98 ± 6.1	6.16
MNX	12	105 ± 14	13.02
RDX	12	96 ± 23	23.98
Level: 20 ng/mL			
TNX	12	114 ± 19	16.45
DNX	12	118 ± 27	22.99
TNT	12	125 ± 8.1	6.49
MNX	12	99 ± 15	14.69
RDX	12	84 ± 14	17.28
Level: 10 ng/mL			
TNX	12	110 ± 19	17.20
DNX	12	115 ± 34	29.34
TNT	12	113 ± 14	12.03
MNX	12	102 ± 14	13.22
RDX	12	96 ± 19	19.89
Level: 5 ng/mL			
TNX	12	108 ± 29	26.68
DNX	12	113 ± 30	26.99
TNT	12	116 ± 7.6	6.54
MNX	12	111 ± 22	19.47
RDX	12	123 ± 33	26.68
Level: 1 ng/mL			
TNX	12	106 ± 26	24.88
DNX	12	130 ± 29	22.17
TNT	12	114 ± 31	26.69
MNX	12	107 ± 17	15.93
RDX	12	129 ± 35	27.02
Average			
TNX	84	104 ± 16	15.14
DNX	84	108 ± 22	20.07
TNT	84	108 ± 16	14.87
MNX	84	105 ± 14	13.10
RDX	84	100 ± 22	21.69

Precision was expressed by relative standard deviation (R.S.D.) (%). R.S.D. (%) = (S.D./mean) × 100%.

TNT, MNX, and RDX, respectively. Precision and accuracy increased slightly as concentration increased for most energetic compounds. Precision and accuracy for DNX and RDX were the lowest of the tested compounds possibly due to the instability of DNX and the relatively high detection limit for RDX. However, we considered both the precision and accuracy for this type of analysis in a blood matrix to be acceptable.

Table 3
Method validation by different research teams on different days using pig blood samples spiked with 50, 250, and 1250 ng/mL of each test compound (recovery %)

Compound	Day I		Day II	
	Team I	Team II	Team I	Team II
Level: 1250 ng/mL				
TNX	102 ± 4.9	105 ± 6.4	98 ± 4.1	96 ± 0.9
DNX	104 ± 9.2	98 ± 19	105 ± 0.7	101 ± 3.2
TNT	104 ± 9.3	112 ± 14	114 ± 2.0	106 ± 5.0
MNX	103 ± 9.8	108 ± 13	105 ± 3.7	103 ± 4.5
RDX	98 ± 3.7	105 ± 8.4	97 ± 12	96 ± 7.0
Level: 250 ng/mL				
TNX	100 ± 2.6	104 ± 15	106 ± 0.8	107 ± 9.5
DNX	100 ± 19	101 ± 4.4	102 ± 4.2	101 ± 2.6
TNT	95 ± 23	93 ± 9.7	100 ± 13	96 ± 13
MNX	110 ± 13	106 ± 19	109 ± 5.8	110 ± 3.9
RDX	101 ± 22	90 ± 15	106 ± 13	94 ± 8.0
Level: 50 ng/mL				
TNX	95 ± 5.7	94 ± 9.1	99 ± 2.4	101 ± 15
DNX	96 ± 12	105 ± 16	95 ± 14	99 ± 16
TNT	96 ± 3.5	100 ± 14	97 ± 2.8	99 ± 6.6
MNX	106 ± 21	101 ± 24	100 ± 17	108 ± 9.6
RDX	96 ± 19	91 ± 32	97 ± 29	96 ± 16

Six replicates for each data group.

3.2. Method validation

An interlaboratory study was employed to determine the stability and reproducibility of the developed extraction and analysis method using pig blood samples spiked with RDX, TNX, DNX, MNX, and TNT at three concentrations (50, 250, and 1250 ng/mL). Each treatment had high recovery (91–114%) (Table 3). Two way ANOVA indicated no significant difference between analysis teams or days of analysis ($p < 0.001$).

3.3. Application of the developed extraction and analysis method

The developed method was employed to analyze blood samples obtained from TNX or RDX-exposed deer mice. We did not detect TNX in blood samples from the control group ($n = 4$) (Fig. 3A). Trace amounts of TNX (0.14–0.53 ng/mL) were detected in the low dose group ($n = 9$). Relatively high concentrations of TNX (0.63–43 ng/mL) were detected in the high dose group ($n = 5$) (Table 4). Similar results were obtained from blood samples collected in the RDX-dosing study (Fig. 3C). These

Table 4
Measured TNX concentrations in blood samples obtained from deer mice exposed to 0, 10, and 100 ng/mL TNX for 30 days

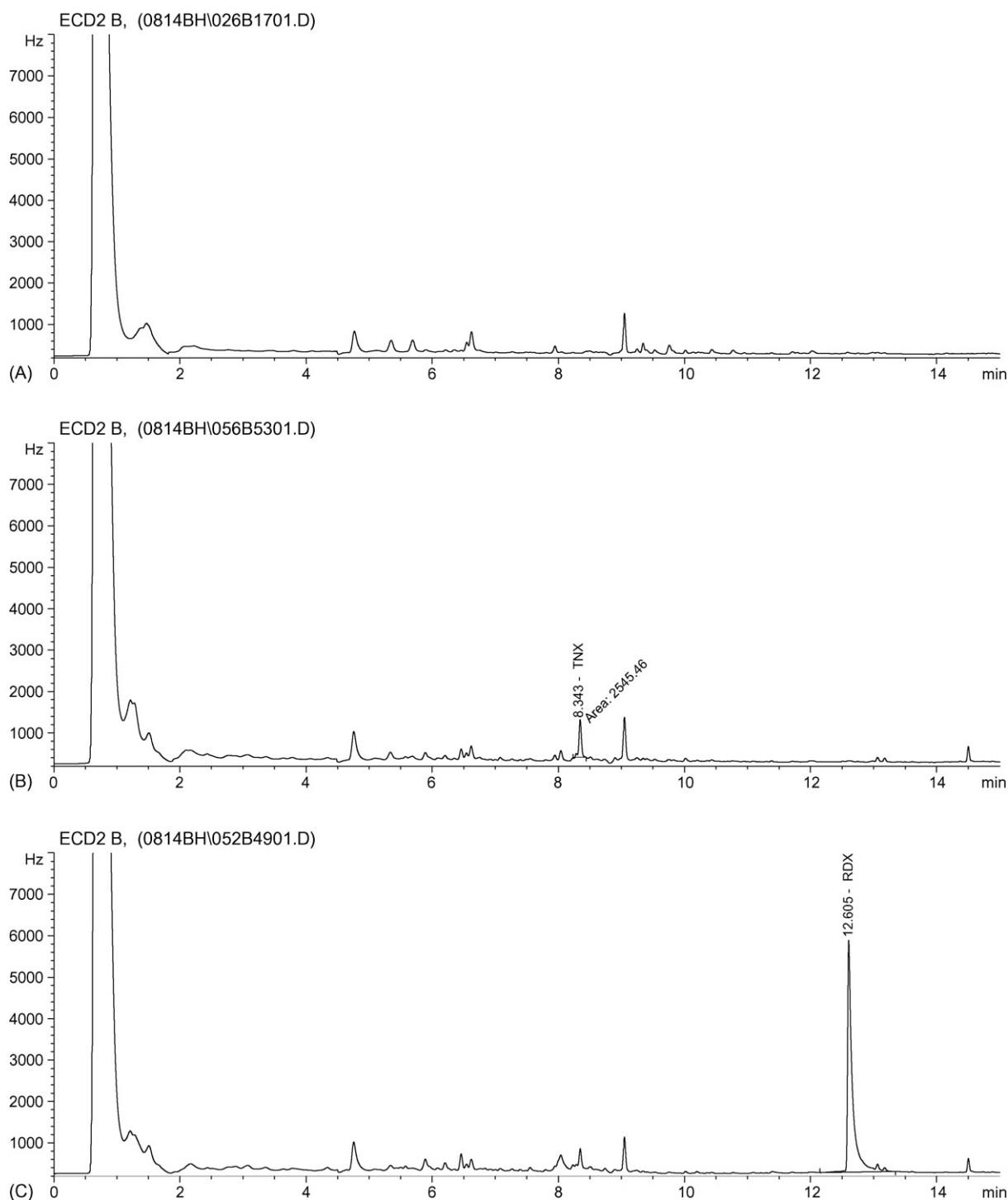| Dose (ng/mL)	Number of deer mice	TNX concentration in blood (mean) (ng/mL)
0	4	N.D.
10	9	0.14–0.53 (0.29)
100	5	0.63–42.99 (13.35)

N.D.: not detected.

Fig. 3. Representative chromatograms of blood samples obtained from TNX or RDX-dosed deer mice. (A) Control; (B) TNX-treated; (C) RDX-treated. The slight retention time shift compared to the previous figure was due to the use of a different analytical column. The peak tailing was caused by the overused column.

data indicate that this method can be used in basic toxicology and toxiokinetic studies.

3.4. Stability of energetic compounds in extracted solution

The stability of each energetic compound (RDX and TNT) and RDX biotransformation products (MNX, DNX, and TNX) in acetonitrile extracts ($n = 3$) was monitored for 10 days using GC/ECD analysis. All energetic compounds and RDX biotransformation products were unstable in the acetonitrile extracts at room temperature. After 10 days, 15–40% of the extracted compounds were lost (transformed into other unknown compounds) (Fig. 4). RDX and MNX easily degraded into other compounds. After 10 days in the extract, 64 and 60% of RDX and MNX were still present. TNT and TNX were more stable than other energetic compounds tested; only 16 and 22% of parent compound
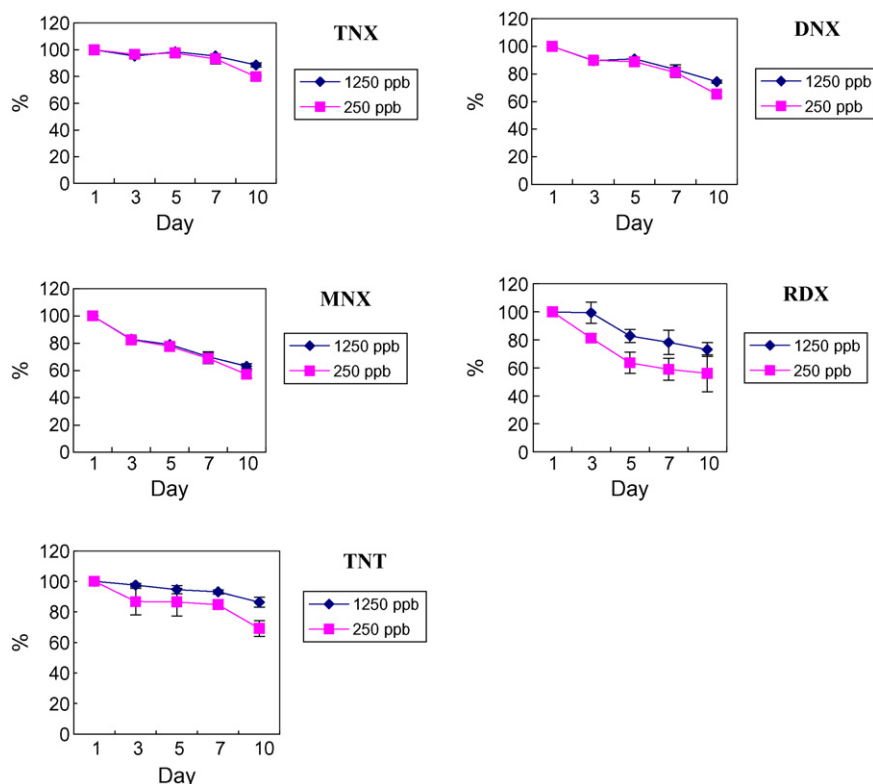
B. Zhang et al. / Talanta 72 (2007) 612–619

Fig. 4. Stability of energetic compounds and their transformation products in acetonitrile extracts of blood. The *Y*-axis was calculated as the ratio of the concentration of energetic compounds to the concentration at time 0. Error bars indicate the standard deviation for triplicate samples.

was lost in extracts after 10 days. Analyte concentrations only slightly affected the degradation rate of energetic compounds in acetonitrile extracts. Low temperature, such as maintaining extracts in a refrigerator (4 °C), slowed the transformations (data not shown).

RDX can be biotransformed to MNX, DNX, and TNX by some bacteria under anaerobic conditions [45–47]. However, no studies have found that RDX can be transformed to TNX under aerobic conditions. TNX, DNX, MNX or any other identifiable compound was not observed in extracts of RDX-spiked blood samples stored at room temperature for 10 days, although 45% of RDX was lost (degraded) during that time; the transformation pathway(s) remains unclear.

4. Discussion

Several laboratory and field studies have indicated that RDX can be biotransformed into a series of *N*-nitroso metabolites (MNX, DNX, and TNX), which have also been detected in groundwater [28]. To better understand the potential health effects and environmental fate of these energetic compounds, sensitive analytical methods must be available to measure these compounds and their biotransformation products [1,3,26]. Based on our best knowledge, there has been only one report on analytical methods for detecting explosive residues in blood samples. Ozhan et al. (2004) developed an HPLC–UV method for detecting RDX in human blood. However, the method was only capable of detecting 5 ng/mL RDX in human plasma based on 3:1 signal-to-noise ratio [44]. GC–ECD is a common instru-

ment in environmental laboratories. Determination of explosive residues using GC–ECD is advantageous due to the lower detection limits and improved chromatographic resolution. Because of its low vapor pressure and thermal lability, RDX is difficult to quantify by gas chromatography. Thus, HPLC is used in the majority of methods for detecting RDX. Our study showed that injection port temperature is important for determining RDX and its biotransformation products using GC–ECD. The optimal injection port temperature was 160–170 °C. Higher or lower inlet temperatures significantly reduced GC–ECD response to RDX and its *N*-nitroso-metabolites [49].

5. Conclusions

A simple, efficient, and sensitive GC–ECD method for determination of explosives or their biotransformation products in blood samples was developed with detection limits <0.5 ng/mL. This method gave high recovery, precision, and accuracy within a concentration range of 1–1250 ng/mL. This method was validated by different analysis teams on different days and successfully employed to monitor explosive residues in blood samples from TNX- and RDX-exposed deer mice.

References

[1] A. Halasz, C. Groom, E. Zhou, L. Paquet, C. Beaulieu, S. Deschamps, A. Corriveau, S. Thiboutot, G. Ampleman, A. Dubois, et al., J. Chromatogr. A 963 (2002) 411.

[2] S.S. Talmage, D.M. Opresko, C.J. Maxwell, C.J. Welsh, F.M. Cretella, P.H. Reno, F.B. Daniel, Rev. Environ. Contam. Toxicol. 161 (1999) 1.

[3] J.I. Steinfield, J. Wormhoudt, Annu. Rev. Phys. Chem. 49 (1988) 203.

[4] P.Y. Robidoux, C. Dubois, J. Hawari, G.I. Sunahara, Ecotoxicology 13 (2004) 603.

[5] P.Y. Robidoux, G.I. Sunahara, K. Savard, Y. Berthelot, S. Dodard, M. Martel, P. Gong, J. Hawari, Environ. Toxicol. Chem. 23 (2004) 1026.

[6] D. Juck, B.T. Driscoll, T.C. Charles, C.W. Greer, FEMS Microbiol. Ecol. 43 (2003) 255.

[7] R.J. Spanggord, K.R. Stewart, E.S. Riccio, Mutat. Res. 335 (1995) 207.

[8] G.I. Sunahara, S. Dodard, M. Sarrazin, L. Paquet, G. Ampleman, S. Thiboutot, J. Hawari, A.Y. Renoux, Ecotoxicol. Environ. Saf. 39 (1998) 185.

[9] A.J. Palazzo, D.C. Leggett, J. Environ. Qual. 15 (1986) 49.

[10] L.E. Winfield, J.H. Rodgers Jr., S.J. D'Surney, Ecotoxicology 13 (2004) 335.

[11] R.G. Kuperman, R.T. Checkai, M. Simini, C.T. Phillips, J.E. Kolakowski, C.W. Kurnas, G.I. Sunahara, Pedobiologia 47 (2003) 651.

[12] P.Y. Robidoux, J. Hawari, G. Bardai, L. Paquet, G. Ampleman, S. Thiboutot, G.I. Sunahara, Arch. Environ. Contam. Toxicol. 43 (2002) 379.

[13] B.H. Zhang, C.M. Freitag, J.E. Canas, Q.Q. Cheng, T.A. Anderson, Environ. Pollut. 144 (2006) 540.

[14] P.Y. Robidoux, C. Svendsen, J. Caumartin, J. Hawari, G. Ampleman, S. Thiboutot, J.M. Weeks, G.I. Sunahara, Environ. Toxicol. Chem. 19 (2000) 1764.

[15] R.M. Gogal, M.S. Johnson, C.T. Larsen, M.R. Prater, R.B. Duncan, D.L. Ward, R.B. Lee, C.J. Salice, B. Jortner, S.D. Holladay, Environ. Toxicol. Chem. 22 (2003) 381.

[16] S. Homma-Takeda, Y. Hiraku, Y. Ohkuma, S. Oikawa, M. Murata, K. Ogawa, T. Iwamuro, S. Li, G.F. Sun, A. Kumagai, et al., Free Radic. Res. 36 (2002) 555.

[17] B. Lachance, P.Y. Robidoux, J. Hawari, G. Ampleman, S. Thiboutot, G.I. Sunahara, Mutat. Res. 444 (1999) 25.

[18] D. Bruns-Nagel, S. Scheffer, B. Casper, H. Garn, O. Drzyzga, E.V. Low, D. Gemsa, Environ. Sci. Technol. 33 (1999) 2566.

[19] J.A. Steevens, B.M. Duke, G.R. Lotufo, T.S. Bridges, Environ. Toxicol. Chem. 21 (2002) 1475.

[20] Y. Kucukardali, H.V. Acar, S. Ozkan, S. Nalbant, Y. Yazgan, E.M. Atasoyu, O. Keskin, A. Naz, N. Akyatan, A. Gokben, et al., J. Intensive Care Med. 18 (2003) 42.

[21] L.J. Burdette, L.L. Cook, R.S. Dyer, Toxicol. Appl. Pharmacol. 92 (1988) 436.

[22] D.J. Goldberg, S.T. Green, D. Nathwani, J. McMenamin, N. Hamlet, D.H. Kennedy, J. R. Soc. Med. 85 (1992) 181.

[23] B. Harrell-Bruder, K.L. Hutchins, Ann. Emerg. Med. 26 (1995) 746.

[24] S.A. Meyer, A.J. Marchand, J.L. Hight, G.H. Roberts, L.B. Escalon, L.S. Inouye, D.K. MacMillan, J. Appl. Toxicol. 25 (2005) 427.

[25] M.E. Honeycutt, A.S. Jarvis, V.A. McFarland, Ecotoxicol. Environ. Saf. 35 (1996) 282.

[26] D.S. Moore, Rev. Sci. Instruments 75 (2004) 2499.

[27] USEPA, SW846 Method 8330, Nitroaromatics and Nitramines by High Performance Liquid Chromatography [HPLC], US EPA, Washington, DC, 1994.

[28] H.R. Beller, K. Tiemeier, Environ. Sci. Technol. 36 (2002) 2060.

[29] T.L. Buxton, P.D. Harrington, Appl. Spectrosc. 57 (2003) 223.

[30] T.M. Chow, M.R. Wilcoxon, M.D. Piwoni, N.R. Adrian, J. Chromatogr. Sci. 42 (2004) 470.

[31] A. Hilmi, J.H. Luong, A.L. Nguyen, J. Chromatogr. 844 (1999) 97.

[32] F. Monteil-Rivera, C. Beaulieu, S. Deschamps, L. Paquet, J. Hawari, J. Chromatogr. A 1048 (2004) 213.

[33] F. Monteil-Rivera, C. Beaulieu, J. Hawari, J. Chromatogr. 1066 (2005) 177.

[34] M.E. Walsh, T.F. Jenkins, Anal. Chim. Acta 231 (1990) 313.

[35] J. Yinon, J. Chromatogr. A 742 (1996) 205.

[36] R.W. Bishop, M.A. Hable, C.G. Oliver, R.J. Valis, USACHPPM, J. Chromatogr. Sci. 41 (2003) 73.

[37] M.E. Walsh, Talanta 54 (2001) 427.

[38] S. Campbell, R. Ogoshi, G. Uehara, Q.X. Li, J. Chromatogr. Sci. 41 (2003) 284.

[39] C.A. Groom, S. Beaudet, A. Halasz, L. Paquet, J. Hawari, J. Chromatogr. 909 (2001) 53.

[40] B.H. Zhang, X.P. Pan, G.P. Cobb, T.A. Anderson, J. Chromatogr. B 824 (2005) 277.

[41] X.P. Pan, B.H. Zhang, S.B. Cox, T.A. Anderson, G.P. Cobb, J. Chromatogr. A 1107 (2006) 2.

[42] ATSDR, Toxicological Profile for RDX, US Department of Health and Services. http://www.atsdr.cdc/gov/toxprofiles/tp78.pdf, 1995.

[43] ATSDR, Toxicological Profile for HMX, Agency for Toxic Substances and Disease Registry, US Department of Health and Human Services. Atlanta, GA, 1997.

[44] G. Ozhan, S. Topuz, B. Alpertunga, Farmaco (Societa Chimica Italiana: 1989) 58 (2003) 445.

[45] N.R. Adrian, C.M. Arnett, Curr. Microbiol. 48 (2004) 332.

[46] J. Hawari, A. Halasz, T. Sheremata, S. Beaudet, C. Groom, L. Paquet, C. Rhofir, G. Ampleman, S. Thiboutot, Appl. Environ. Microbiol. 66 (2000) 2652.

[47] J. Hawari, S. Beaudet, A. Halasz, S. Thiboutot, G. Ampleman, Appl. Microbiol. Biotechnol. 54 (2000) 605.

[48] EPA, SW846 Test Methods, US EPA, Washington, DC, 2000.

[49] X.P. Pan, B.H. Zhang, G.P. Cobb, Talanta 67 (2005) 816.

Inorganic speciation of As(III, V), Se(IV, VI) and Sb(III, V) in natural water with GF-AAS using solid phase extraction technology

Liang Zhang [a,b,*], Yukitoki Morita [a], Akio Sakuragawa [a], Akinori Isozaki [a]

[a] *Department of Materials and Applied Chemistry, College of Science and Technology,*
Nihon University, 1-8 Kanda-Surugadai, Chiyoda-ku, Tokyo 101-8308, Japan
[b] *Department of Applied Chemistry, College of Science, Xi'an University of Architecture*
and Technology, Yanta Road 13, Xi'an, Shannxi, China

Abstract

The paper presents a procedure for the multi-element inorganic speciation of As(III, V), Se(IV, VI) and Sb(III, V) in natural water with GF-AAS using solid phase extraction technology. Total As(III, V), Se(IV, VI) and Sb(III, V) were determined according to the following procedure: titanium dioxide (TiO_2) was used to adsorb inorganic species of As, Se and Sb in sample solution; after filtration, the solid phase was prepared to be slurry for determination. For As(III), Se(IV) and Sb(III), their inorganic species were coprecipitated with Pb-PDC, dissolved in dilute nitric acid, and then determined. The concentrations of As(V), Se(VI) and Sb(V) can be calculated by the difference of the concentrations obtained by the above determinations. For the determination of As(III), Se(IV) and Sb(III), palladium was chosen as a modifier and pyrolysis temperature was 800 °C. Optimum conditions for the coprecipitation were listed for 100 ml of sample solution: pH 3.0, 15 min of stirring time, $40.0\,\mu g\,l^{-1}$ $Pb(NO_3)_2$ and $150.0\,\mu g\,l^{-1}$ APDC. The proposed method was applied to the determination of trace amounts of As(III, V), Se(IV, VI) and Sb(III, V) in river water and seawater.
© 2006 Elsevier B.V. All rights reserved.

Keywords: Multi-element determination; GF-AAS; Speciation analysis; Arsenic; Selenium; Antimony

1. Introduction

In recent years, speciation analysis of As, Se and Sb is very attractive due to the toxicity of their combinations. The toxicity of the different species for the same element is different, in which the inorganic compounds are more toxic than the organic compounds and the toxicity of As(III), Se(IV) and Sb(III) is stronger than that of As(V), Se(VI) and Sb(V) [1–3]. In addition, selenium has been also reported as an essential element for human body at low concentration [2]. Therefore, a high sensitive and simple method is necessary for determining the concentration of the different oxidation state of the inorganic compounds for these elements present in environment. With volatilization for their hydrides, hydride generation (HG) as a sampling tech-

nology, which is coupled with the detected systems, such as atomic absorption spectrometry (AAS) [4], inductively coupled plasma atomic emission spectrometry (ICP-AES) [5] and inductively coupled plasma mass spectrometry (ICP-MS) [6,7], has been applied in analytical field. Though requirement for the determination of trace level elements is met for HG, speciation analysis for these elements is difficult because the sampling technology has trouble separating the different oxidation state for a single element in complicated matrix. With introduction of separation technique, chromatography coupled with the above instruments, the hyphenated systems, has been utilized to perform speciation analysis. Because of high performance liquid chromatograph (HPLC) with excellent separation for species in aqueous samples, there are a great many reports [1,8–14] on these elements with HPLC-AAS, HPLC-ICP-AES and HPLC-ICP-MS. However, HPLC are suitable for separating species in aqueous sample, but it cannot perform enrichment for the detected element. Therefore, for ultratrace As, Se and Sb in natural waters, the coupled detectors except for ICP-MS, are poor in sensitivity; ICP-MS with high sensitivity is too expensive for the

---

* Corresponding author at: Department of Materials and Applied Chemistry, College of Science and Technology, Nihon University, 1-8 Kanda-Surugadai, Chiyoda-ku, Tokyo 101-8308, Japan. Tel.: +81 3 3259 0820; fax: +81 3 3293 7572.

E-mail address: zl98zl@hotmail.com (L. Zhang).

most researchers to be equipped. Furthermore, the combination of instruments makes the determined procedure more complex and the continuous determining mode is also not suitable for GF-AAS.

With development of filtration technology, some macro-molecule compounds can be collected on filtration membrane with the precipitation of the similar structure compound [15–17]. Owing to the selectivity of macromolecule for the specific oxidation state of some elements, the species of the different oxidation state can be separated during the stage of pretreatment. APDC as a typical macromolecule has been utilized to selectively collect these inorganic ions of As(III), Se(IV) and Sb(III). In the method, As(III), Se(IV) and Sb(III) are determined by using APDC; total concentration for each element is determined according to the same method after As(V), Se(VI) and Sb(V) are reduced to As(III), Se(IV) and Sb(III) [15,16,18]. The speciation procedure for multi-element is mainly used for neutron activation analysis, but for GF-AAS, there are only a few available for single element [15]. Different from the detector and determination of total concentration in the above multi-element analysis, a method has been proposed on simultaneous determination of total As, Se and Sb with GF-AAS by TiO_2-slurry sampling in previous paper [19]. In the study, speciation of these elements in aqueous samples was performed by simultaneously determining total concentration for each element [19] and the concentration of As(III), Se(IV) and Sb(III) according to the subsequent analytical procedure.

The aim of the study is to perform the determination of As (III, V), Se(IV, VI) and Sb(III, V) in the environmental water samples. The optimal conditions for coprecipitation including furnace condition, effect of modifier, pH of preconcentration, and coexisting ions were investigated in detail. The proposed method was applied to river water and seawater.

2. Experimental

2.1. Instrumentation

A simultaneous multi-element graphite furnace atomic absorption spectrometer, SIMAA 6000, from Perkin-Elmer was used with a transversely heated graphite atomizer (THGA), longitudinal Zeeman-effect background correction and an AS-72 autosampler. Standard THGA graphite tubes (Part no. B0504033) and Perkin-Elmer 'EDL system 2' electrodeless discharge lamps (As: 193.7 nm, 380 mA; Se: 196.0 nm, 290 mA; Sb: 223.1 nm, 380 mA) were applied. The measurements were in peak area mode (integrated absorbance). A pH meter (HM-26S) manufactured by DKK-TOA Corporation and an analytical balance (Sartorius model BP301S-EA BR-1010, 300 g × 0.0001 g) were employed. Ultrasonic (Bransonic 12, branson) was used to dispend the slurry to improve adsorption and homogeneity of slurry. A magnetic stirrer (ADVANTEC SR 506) was used to stir. A Milli-Q Water System, Millipore, was employed to produce ultrapure water. In addition, before being used, all glassware, pipette tips and storage bottles were soaked in dilute HNO_3 for 24 h and rinsed at least three times according to the order of water, purity water and ultrapure water.

2.2. Reagents and materials

All the reagents were of analytical grade. The standard solutions of As(III), Sb(III) and Sb(V) ($100 \mu g l^{-1}$) were prepared on a daily basis by diluting appropriate aliquots of a $1000 mg l^{-1}$ stock metal solution, respectively. The stock solutions ($1000 mg l^{-1}$) of As(V) and Se(VI) were separately prepared by dissolving the corresponding salts ($Na_2HAsO_4·7H_2O$ and Na_2SeO_4) and adding 0.75 ml of 60% nitric acid and 1.0 ml of 30% hydrogen peroxide. The stock solution ($1000 mg l^{-1}$) of Se(IV) was obtained by dissolving Na_2SeO_3. These solutions were properly diluted to use. The two stock solutions of Sb(V) and Sb(III) with 20% HCl was from SPEX CERTIPREP LTD. Ammonium pyrrolidinedithio-carbamate (APDC, $10,000 mg l^{-1}$) solution was prepared by weighing 1.0 g of APDC powder and dissolving in 100 ml of ultrapure water. $Pb(NO_3)_2$ ($4000 mg l^{-1}$) solution was obtained by dissolving 0.4 g of $Pb(NO_3)_2$ in 100 ml of ultrapure water. Hydrochloric acid (35%), nitric acid (60%) for poisonous metal analysis and sulfuric acid were from KANTO CHEMICAL CO. ING. Titanium(IV) dioxide (anatase form, 99%, $-0.5 \mu m$) was utilized as a sorbent. $ZrO(NO_3)_2·2H_2O$ was employed to coat the graphite tube. A river water sample was collected in the Edokawa river in Tokyo and a seawater sample was obtained from Inage coast in Chiba in Japan. The samples were filtrated with a 0.45 μm pore size cellulose acetate membrane filter (Advantec, Tokyo) and treated for determination in 24 h. The above reagents without the source and the other reagents used in this work were from Wako Co. in Japan.

2.3. Analytical procedure

2.3.1. Determination of total As, Se and Sb [19]

The enrichment ratio of 20 was used in the study. Hundred-milliliter of sample solution with less than $5.0 \mu g l^{-1}$ of As, Se and Sb was placed in a beaker; pH was adjusted to 2.0 with 2.0 M HNO_3. The sample solution added 20.0 mg of TiO_2 was stirred by a magnetic stirrer about 10 min, and immerged in a sonication bath about 10 min. After the solution was filtrated with a 0.45 μm membrane filter, the remained solid phase was transferred to a 15.0 ml centrifugal tube, and then 5.0 ml ultrapure water was added to form 5.0 ml of the slurry sample. Then, 20 μl of the slurry was injected into a graphite tube by an autosampler for each cycle.

2.3.2. Determination of As(III), Se(IV) and Sb(III)

The enrichment ratio of 20 was used for investigating the influential factors for coprecipitation. Hundred-milliliter of sample solution with less than $5.0 \mu g l^{-1}$ of As(III), Se(IV) and Sb(III) was placed in a beaker; pH was adjusted to 3.0 with 1.0 M HCl. 1.5 ml of $10,000 mg l^{-1}$ APDC and 1.0 ml of $4000 mg l^{-1}$ $Pb(NO_3)_2$ solution was added and stirred for 15 min. After filtration with a 0.45 μm membrane filter, the remained solid phase was transferred to a 15.0 ml centrifugal tube and dissolved in 1.0 ml HNO_3 (1:1) solution; the solution was diluted to 5.0 ml. Then 20 μl of sample solution was injected into a graphite tube,

Table 1
Furnace conditions

	Steps	Temp. (°C)	Time (s)		Ar gas (ml/min)
			Ramp	Hold	
1	Dry1	130	1	30	250
2	Dry2	150	15	30	250
3[a]	Pyrolysis	800	10	20	250
4	Atomization	2300	0	5	0
5	Clean up	2450	1	3	250

[a] Step 3 is only used for determination of As(III), Se(IV) and Sb(III) on coprecipitation.

and accompanied with 10 μl of 1000 mg l^{-1} Pd^{2+} (Pd(NO$_3$)$_2$) for each cycle.

2.3.3. Estimation of As(V), Se(VI) and Sb(V)

As(V), Se(VI) and Sb(V) could not be determined directly according to the above analytical procedure, but their concentrations were given by the difference between the two determinations.

2.3.4. Analysis of real samples

The water samples were filtrated with a 0.45 μm membrane filter and then the suitable amount of APDC was added for 100 ml sample before adjusting pH. Subsequently, according to the above analytical procedure, these elements were determined at a 20 of enrichment rate. In the determination of total As, Se and Sb, the samples were firstly diluted two-fold to minimize the interferences from SO$_4{}^{2-}$ and PO$_4{}^{3-}$.

2.4. Furnace condition for determination of As, Se and Sb

Graphite tube for determination of total arsenic, selenium and antimony was coated with zirconium nitrate [19]. The conditions of temperature in pyrolysis stage and atomization stage for the determination of total concentration of these elements had been optimized with the standard solution in previous paper [19]. The optimal operating conditions for SIMAA6000 are listed in Table 1. Compared with furnace conditions for the determination of total concentration, except for an optimal pyrolysis temperature, others were same for the determination of As(III), Se(IV) and Sb(III). In addition, a THGA tube was utilized for the determination of As(III), Se(IV) and Sb(III) rather than a Zr-coating THGA tube.

3. Results and discussion

3.1. Optimization of coprecipitation system for As(III), Se(IV) and Sb(III)

3.1.1. Selection of solvents for coprecipitate

In order to select a suitable solvent for coprecipitate, nitric acid, sulfuric acid and *N,N*-Dimethylformamide (DMF) were investigated in this work. As described in the analytical procedure, the obtained coprecipitate was separately dissolved in nitric acid, sulfuric acid and DMF. The availability of the three

solvents was evaluated by their solubility for the coprecipitate and influence on the detected elements in pyrolysis and atomization stage. We observed that membrane was dissolved completely in DMF, but coprecipitate was dissolved partly to form slurry. In addition, background absorbance was very high in the determination of these elements so that the reliable and stable results could not be obtained. When sulfuric acid was chosen, homogeneous solution was formed, but the similar high background absorbance was found. As dilute sulfuric acid (2.0 M) was in place of sulfuric acid, the same phenomenon of high background absorbance was found. While nitric acid (1.0, 2.0 and 3.0 M) was used, precipitate was dissolved, but membrane could not dissolve to avoid the influence resulted by it. Furthermore, low background absorption was suitable for the determination of these elements. We also observed that with increasing the concentration of nitric acid, the time of dissolution became fast. In order to fast dissolve coprecipitate and avoid the interference resulted nitric acid, 1.0 ml nitric acid solution (1:1) was added, and then diluted to 5.0 ml for determination.

3.1.2. Optimization of furnace conditions

An important parameter of GF-AAS is the optimization of pyrolysis temperature. Generally, without the use of modifiers, pyrolysis temperature are in the range from 200 (Se) to 500 °C (As) [20]. Because APDC as a coprecipant was much used, the two elements could not be detected without modifier. Hence, the investigations with the use of a modifier were presented in this work. According to the above analytical procedure, the influence of pyrolysis temperature was studied in the range 400–1200 °C, with atomization temperature for 2300 °C. In order to find out a suitable pyrolysis temperature, in the presence of 10 μg of the Pd^{2+}, the behavior of these elements was considered. Fig. 1 indicates that with increasing pyrolysis temperature, integrated absorbance of As(III) and Sb(III) kept basically the constant from 400 to 1200 °C, but that of Se decreased over 900 °C. In addition, the background absorbance of three elements kept at a stable and low constant when temperature was over 800 °C. For the matrices containing lot of organic compounds could not be eliminated at low temperature (<650 °C), the interference
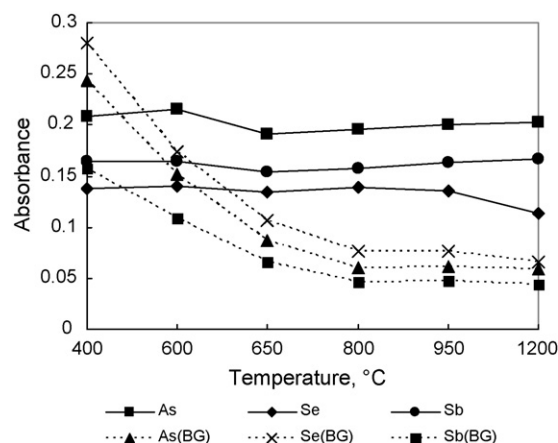

Fig. 1. Pyrolysis curves for 5.0 μg l^{-1} of As(III), Se(IV) and Sb(III). Atomization temperature: 2300 °C; enrichment rate: 20; injected volume: 20 μl.
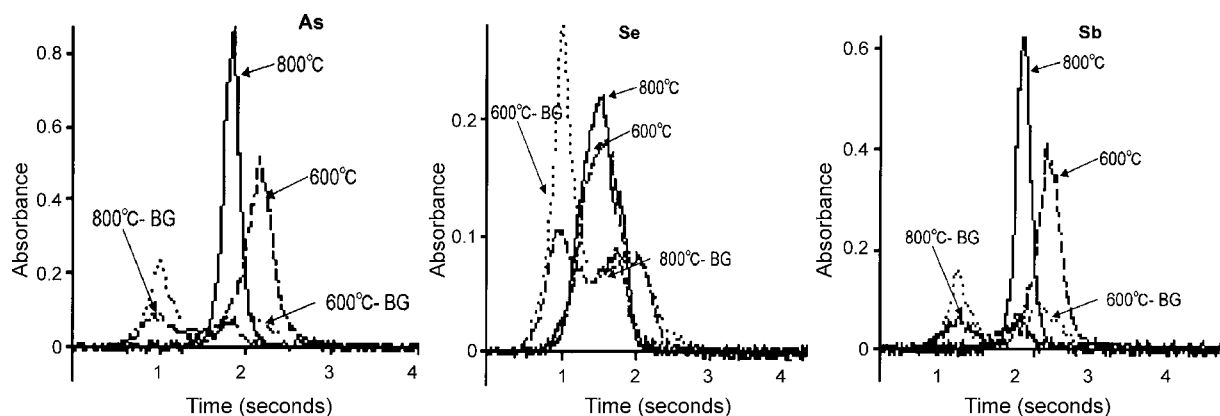
Fig. 2. Atomic profiles for 5.0 μg l^{-1} of As(III), Se(IV) and Sb(III) in pyrolysis stage. Atomization temperature: 2300 °C; enrichment rate: 20; injected volume: 20 μl.

of background absorbance from them made the results unstable. However, when temperature was up to 800 °C, organic compounds were removed in pyrolysis stage to minimize the interference. The phenomenon can also be found from the atomic profiles for these elements in Fig. 2. Background absorbance at 600 °C is obviously higher than that of these elements at 800 °C. As a result, pyrolysis temperature was chosen at 800 °C in the subsequent studies for As(III), Se(IV) and Sb(III). Atomization temperature had a little effect on integrated absorbance and the shape of atomic profiles for these elements when exceeding 2100 °C. The compromise temperature of 2300 °C, hence, were chosen in the following experiments.

3.1.3. Effect of modifier

As the amount of the modifier introduced on the surface of graphite tube had an effect on the determination of these elements, the dependence of integrated absorbance on the amount of modifier was also investigated. In order to correlate the data, in all cases pyrolysis temperature as well as atomization temperatures in Table 1 were used. The sample solutions obtained according to the analytical procedure were used to perform the study. The amount of Pd^{2+} was added in the range 0–15 μg/cycle. Fig. 3 shows that for multi-element determination, Pd^{2+} in the amount of 10 μg was sufficient to get a good sensitivity. When the amount of Pd^{2+} was over 10 μg, the sensitivity of these elements did not have the correspondent increasing.

3.1.4. Effect of pH

The effect of pH was investigated by the experiments carried out using 100 ml ultrapure water spiked with 4.0 μg l^{-1} levels of As(III), Se(IV) and Sb(III), respectively. The similar experiments spiked with As(V), Se(VI) and Sb(V) were also performed in the same way. As descried in the analytical procedure, the investigation for the spiked solutions was performed at the different pH. The results are presented in Fig. 4. The curves display that in the pH range 2–4, the separation of the inorganic species between the low and high oxidation state was very complete with Pb-PDC coprecipitant. The inorganic species of As(III), Se(IV) and Sb(III) reacted with APDC to form stable complexes in the aqueous solution, and were quantitatively coprecipitated with

Pb-PDC in the pH range 2–4. At pH <2, some coprecipitate were dissolved, so the recoveries were lower than those in pH 2–4. The general trend observed on As(V) indicates when pH was changed from 6 to 11, the recoveries increased slightly. As discussed by Sun and Yang [16], it is attributed to the precipitate of Pb$_3$(AsO$_4$)$_2$. However, the inorganic species of As(V), Se(VI) and Sb(V) cannot react with APDC to form any complexes with APDC under the investigated conditions. Therefore, the selective separation of As(III), Se(IV) and Sb(III) in the presence of As(V), Se(VI) and Sb(V) is possible at pH 2–4. The results are similar to those in Sun and Yang [16]. The rest of investigations were at pH 3.0.

3.1.5. Effect of coprecipitants

APDC system can perform a selective extraction of As(III), Se(IV) and Sb(III) in presence of As(V), Se(VI) and Sb(V), which has been reported by Y.C. Sun et al., and the separation of single element with the system was also reported [15,18]. In our research, APDC did not only impact on background absorbance and sensitivity for these elements but on dispersing of Pd^{2+} in sample solution owing to the form of the indissoluble Pd(PDC)$_2$ as well. The optimization of the amount of APDC is

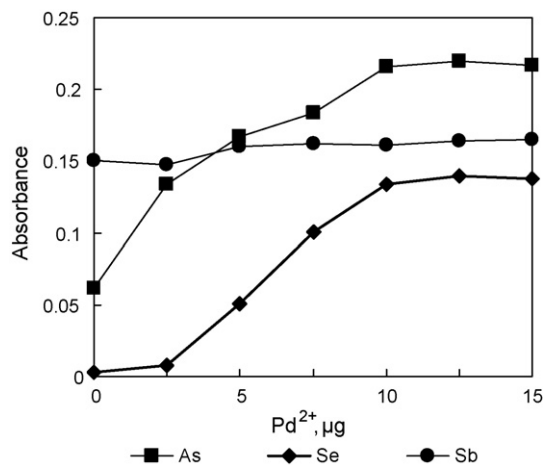Fig. 3. Effect of amount of paladium on determination for 5.0 μg l^{-1} of As(III), Se(IV) and Sb(III). Atomization temperature: 2300 °C; pyrolysis temperature: 800 °C; enrichment rate: 20; injected volume: 20 μl.
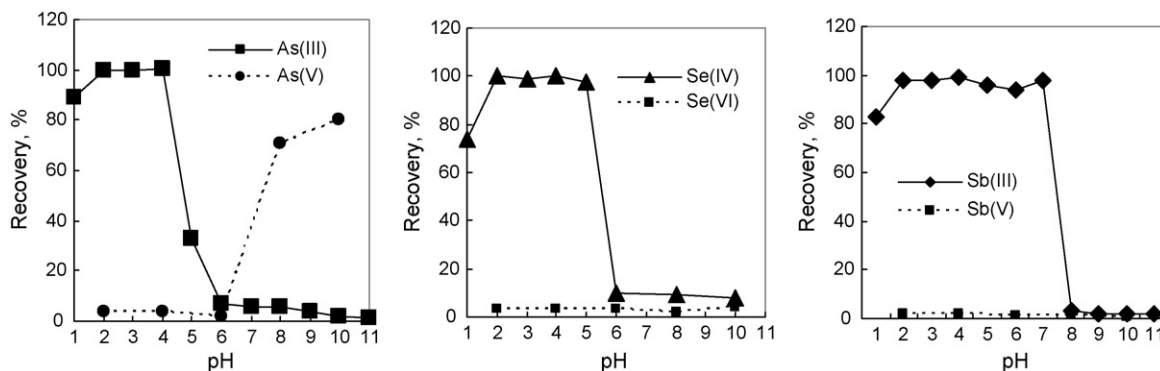
Fig. 4. Effect of pH on the recoveries of $4.0\,\mu g\,l^{-1}$ of As(III), Se(IV) and Sb(III) coprecipitated with Pb-APDC; enrichment rate: 20.

necessary for the experiments carried out according to the recommended analytical procedure. The curves in Fig. 5 indicate when APDC concentration was raised up to $150\,l^{-1}$ in the solution, the recoveries kept 95% stably; after that no obvious change on recoveries was observed. However, as discussed in Section 3.1.2, the concentration of APDC had directly effect on the reproducibility of results. In addition, with increasing concentration, the dispersing of Pd^{2+} in sample became more difficult so that the function of modifier was minimized. Considering the factors, a suited concentration was $150.0\,mg\,l^{-1}$ for APDC.

The optimization of the amount of $Pb(NO_3)_2$ was similar to the above investigation for APDC. The results in Fig. 6 display that without $Pb(NO_3)_2$, there was some detected compounds formed by APDC and these detected elements. The general trends for these element show that the recoveries of As and Sb were independent on the amount of $Pb(NO_3)_2$ when up to $37.5\,mg\,l^{-1}$; while the concentration of $Pb(NO_3)_2$ was more than $50.0\,mg\,l^{-1}$, the recoveries of Se were found to decrease with increasing concentration of $Pb(NO_3)_2$. The phenomenon for minimizing of Se is possible in the case that with increasing concentration of $Pb(NO_3)_2$, APDC was much precipitated, and the remained APDC was provided to As and Sb prior to Se. Finally, a $40.0\,mg\,l^{-1}$ concentration of $Pb(NO_3)_2$ was applied.

3.1.6. Effect of stirring time

To understand the effect of stirring time on the recoveries, $4.0\,\mu g\,l^{-1}$ of sample solutions (As(III), Se(IV) and Sb(III)) were investigated under the above optimal coprecipitation conditions. Stirring time of 0–30 min was performed. The recoveries for these elements exceeded 95% up to 10 min; with increasing stirring time, the recoveries for these elements were kept. Therefore, 10 min of stirring time was chosen for the subsequent experiment.

3.1.7. Effect of sample volumes

In order to explore the possibility of enriching trace amounts of elements from large volumes, the maximum applicable sample volumes must be determined. For this purpose 50, 100, 200, 300, 400 and 500 ml of sample solutions (containing 400 ng of As(III), Se(IV) and Sb(III), respectively) were used under the optimal coprecipitation conditions. As shown in Fig. 7, the recoveries of As, Se and Sb are quantitative (>95%) up to 300 ml of sample volume. It makes rate of enrichment be increased from 20 to 60, enlarges the detecting range for these trace elements.

3.1.8. Effect of coexisting ions

The effect of the coexisting ions on the recovery of As(III), Se(IV) and Sb(III) was investigated under the optimal conditions. The coexisting ions and their concentrations in this study are listed in Table 2. The sample solutions of $4.0\,\mu g\,l^{-1}$ (As(III), Se(IV) and Sb(III)) containing a different foreign ion were sep-
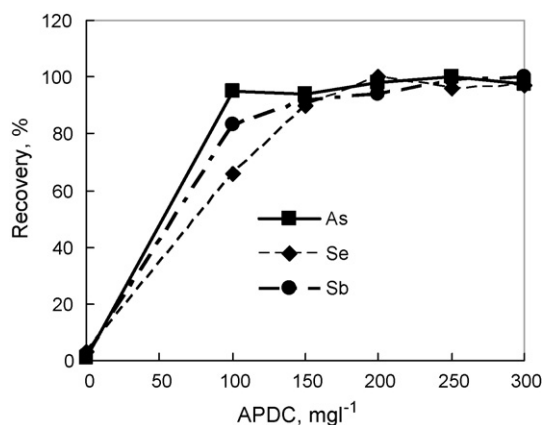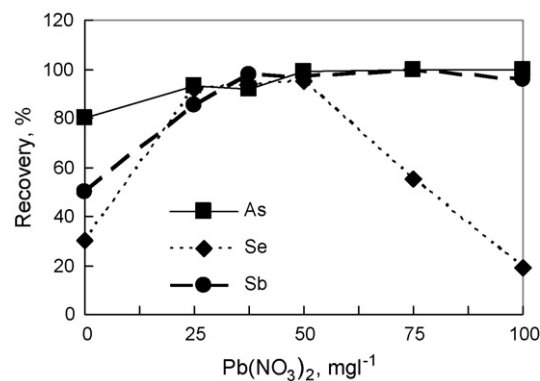

Fig. 5. Effect of concentration of APDC on the recoveries of $4.0\,\mu g\,l^{-1}$ of As(III), Se(IV) and Sb(III) coprecipitated with Pb-APDC; enrichment rate: 20.

Fig. 6. Effect of concentration of $Pb(NO_3)_2$ on the recoveries of $4.0\,\mu g\,l^{-1}$ of As(III), Se(IV) and Sb(III) coprecipitated with Pb-APDC; enrichment rate: 20.
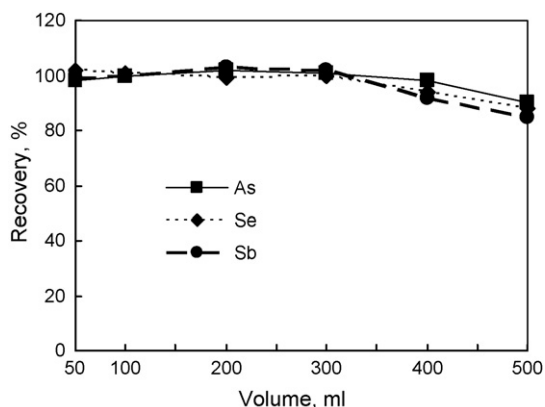
Fig. 7. Effect of sample volume. The amount of As(III), Se(IV) and Sb(III) is 400 ng, respectively; enrichment rate: 20.

arately pretreated according to the analytical procedure. The results obtained in Table 2 suggest that the presence of the anions had no obvious influence on the determination under the selected conditions; Co^{2+}, Ni^{2+} and Cu^{2+} had the positive effect on determination owing to acting as modifiers on the atomization of analyte ions. However, the positive effect can be neglected because the several ions in actual samples are in low content. The other cations did not obviously impact on determination.

3.2. Calibration and precision

For the determination of total As, Se and Sb in solution samples, as described in previous paper [19], a linear relationship between the intensity of the integrated absorbance (measured as peak area) and the concentration for each element was obtained by using a $5.0\,\mu g\,l^{-1}$ of mixed standard solution according to the recommended analytical procedure. The precision of this method was studied for reproducibility and expressed as the relative standard deviation for a mixed solution of standards of As, Se and Sb. R.S.D. (%) ($n = 5$) values for peak area were 2.4, 3.3 and 6.8%, respectively.

Table 2
Effect of foreign ions on the recoveries of $4.0\,\mu g\,l^{-1}$ of As(III), Se(IV) and Sb(III) coprecipitated with Pb-PDC

Ion	Concentration	Recovery (%)		
	Added (mg l^{-1})	As(III)	Se(IV)	Sb(III)
Na$^+$	10,000	97	104	94
K$^+$	100	100	95	97
Ca^{2+}	100	98	97	96
Mg^{2+}	100	91	97	101
Cu^{2+}	1.0	109	110	109
Co^{2+}	1.0	113	95	107
Ni^{2+}	1.0	123	101	107
Fe^{3+}	1.0	98	96	99
Al^{3+}	1.0	96	98	101
SO$_4^{2-}$	100	100	95	97
PO$_4^{3-}$	100	103	91	101
Cl$^-$	15,000	97	104	94

A $5.0\,\mu g\,l^{-1}$ of mixed standard solution was used to obtain the calibration curves of As(III), Se(IV) and Sb(III) by using the optimum conditions described above. The calibration curves were linear in concentration range from determination limit (ten times the signal-to-noise ratio (S/N)) to $5.0\,\mu g\,l^{-1}$ for each element ($R = 0.9997$ for As(III), 0.9999 for Se(IV), and 0.9978 for Sb(III)). Detection limits, defined as three times the signal-to-noise ratio, were found to 0.10, 0.06, and $0.14\,\mu g\,l^{-1}$, respectively ($C = 2.5\,\mu g\,l^{-1}$, $n = 5$).

3.3. Applications of analysis

The evaluation of the validation of analytical method for simultaneous speciation of As, Se and Sb is difficult owing to the absence of certified reference material for these species of the three elements. In addition, the lack of the stability of compounds of these elements through analytical process results in the difficulty of speciation of these elements. To date, no reliable studies on the stability of these elements species in river water and seawater have been published. Therefore, a study on the coexistence of As(III)/As(V), Se(IV)/Se(VI) and Sb(III)/Sb(V) was achieved for ultrapure water and tap water for the analytical process. The ultrapure water spiked with As(III)/As(V), Se(IV)/Se(VI), Sb(III)/Sb(V) separately were used to carry out the investigation as described in the analytical procedure. The results obtained in Table 3 indicate that the spiked As(III) and Se(IV) were almost completely recovered, but recoveries of Sb(III) were up to 120%. For these species of Sb spiked in ultrapure water, the conversion of the different oxidation states of the same element occurred due to the difference of preserved condition for the low/high oxidation states; consequently, some of species of Sb(V) was converted to those of Sb(III). The similar investigations were carried out with tap water instead of ultrapure water. The results show that As(III), Se(IV) and Sb(III) were not found in tap water without addition for these elements, but 10% As(III), 20% Se(IV) and 100% Sb(III) were found for the tap water spiked with these elements. Obviously, the matrices in tap water are more complex than that in ultrapure water. Therefore, the species of As(III) and Se(IV) are unstable, compared with those of Sb(III) in tap water. Furthermore, it also indicates that matrices in samples have impact on the species of these elements. In order to gain more accurate results for speciation, the stable species of As(III) and Se(IV) are necessary for speciation analysis. Therefore, for the above investigations on tap water spiked with these elements, APDC was added prior to the adjustment of pH. The subsequent procedure was same as listed in the analytical procedure. The results (in Table 3) obtained according to the adjusted analytical procedure indicate that the spiked As(III), Se(IV) and Sb(III) in tap water were almost recovered up to 95%. Clearly, APDC acts as a stable reagent for As(III), Se(IV) and Sb(III) in tap water.

The research [1,11] shows that As(III) and Sb(III) are easily converted to As(V) and Sb(V) in river water or seawater without interference; As(V) and Sb(V) become main species in the two samples after sampling. Therefore, these elements in the samples should be determined as soon as possible to

Table 3
Recovery test for inorganic As(III, V), Se(IV, IV) and Sb(III, V) in a mixed solution for pure water and tap water

Samples	Added ($\mu g \, l^{-1}$)						Found $\pm \sigma$ ($\mu g \, l^{-1}$)					
	As(III)	As(V)	Se(IV)	Se(VI)	Sb(III)	Sb(V)	As(III)	As(V)[a]	Se(IV)	Se(VI)[a]	Sb(III)	Sb(V)[a]
Pure water	2.0	3.0	2.0	3.0	2.0	3.0	1.9 ± 0.2	2.8	1.8 ± 0.2	3.0	2.4 ± 0.2	2.6
	–	–	–	–	–	–	N.D.	N.D.	N.D.	N.D.	N.D.	N.D.
Tap water[b]	3.0	3.0	3.0	3.0	3.0	3.0	3.1 ± 0.2	2.9	2.9 ± 0.1	3.0	3.1 ± 0.2	2.8

N.D.: not detected; mean $\pm$ range, $n = 3$.
[a] The calculated value for As(V), Se(VI) and Sb(V).
[b] In Tokyo (07.15, 2006); enrichment rate: 20.

Table 4
Analytical results for water samples and several literature values

Samples	Concentration ($\mu g \, l^{-1}$)								
	As(III)	As(V)[a]	Total As	Se(IV)	Se(VI)[a]	Total Se	Sb(III)	Sb(V)[a]	Total Sb
River water[b]	0.54 ± 0.03	1.02	1.56 ± 0.05	N.D.	N.D.	N.D.	0.42 ± 0.03	0.44	0.86 ± 0.05
Sea water[c]	0.40 ± 0.01	0.66	1.06 ± 0.06	N.D.	N.D.	N.D.	0.60 ± 0.04	0.37	0.97 ± 0.06
[16]	0.027	1.061	–	0.053	0.062	–	0.025	0.126	–
[7]			1.209						0.265
[14]							0.20	0. 23	

N.D.: not detected; mean $\pm$ range, $n = 3$.
[a] The calculated value for As(V), Se(VI) and Sb(V).
[b] Edogawa, Tokyo (07. 28, 2006).
[c] Pacific in Inage coast in Chibaken (08.04, 2006); enrichment rate: 20.

get a good data after sampling. According to analytical procedure for real sample, the obtained results for determination of As, Se, and Sb in surface seawater and river water samples are shown in Table 4. These values for total As are comparable to those reported in the literature for seawater and river water.

4. Conclusions

A simple and rapid analytical method for the determination of inorganic As(III)/As(V), Se(IV)/Se(VI) and Sb(III)/Sb(V) in environmental water samples with GF-AAS was described. Speciation analysis was carried out by the two analytical procedures. The determination of total As, Se and Sb was studied in our previous work; the determination of As(III), Se(IV) and Sb(III) was investigated in detail. The concentrations of As(V), Se(VI) and Sb(V) in sample solution could be calculated by the difference between the two determinations. The proposed method has been applied to the determination of trace amounts of As(III)/As(V), Se(IV)/Se(VI) and Sb(III)/Sb(V) in river water and seawater.

Acknowledgements

References

[1] K.A. Francesconi, D. Kuehnelt, Analyst 129 (2004) 373.
[2] K. Pyrzyńska, Talanta 55 (2001) 657.
[3] M. Krachler, H. Emons, Trends Anal. Chem. 20 (2001) 79.
[4] R.M. Camero, R.E. Sturgeon, Spectrochim. Acta B 54 (1999) 753.
[5] M. Thompson, B. Pahlavanpour, S.J. Walton, G.F. Kirkbright, Analyst 103 (1978) 568.
[6] A.S. Ribeiro, M.A. Vieira, A.J. Curtius, Spectrochim. Acta B 59 (2004) 243.
[7] S.J. Santosa, H. Mokudai, S. Tanaka, J. Anal. At. Spectrom. 12 (1997) 409.
[8] P. Niedzielski, Anal. Chim. Acta 551 (2005) 199.
[9] B. Do, S. Robinet, D. Pradeau, F. Guyon, J. Chromatogr. A 918 (2001) 87.
[10] A. Sayago, R. Beltrán, M.A.F. Recamales, J.L. Gómez-Ariza, J. Anal. At. Spectrom. 17 (2002) 1400.
[11] J. Zheng, A. Iijima, N. Furuta, J. Anal. At. Spectrom. 16 (2001) 812.
[12] Y. Martínez-Bravo, A.F. Roig-Navarro, F.J. López, F. Hernández, J. Chromatogr. A 926 (2001) 265.
[13] N.M.M. Coelho, L.M. Coelho, E.S. de Lima, A. Pastor, M. de la Guardia, Talanta 66 (2005) 818.
[14] I.D. Gregori, W. Quiroz, H. Pinochet, F. Pannier, M. Potin-Gautier, J. Chromatogr. A 1091 (2005) 94.
[15] Q. Zhang, H. Minami, S. Inoue, I. Atsuya, Anal. Chim. Acta 508 (2004) 99.
[16] Y.C. Sun, J.Y. Yang, Anal. Chim. Acta 395 (1999) 293.
[17] Y. Morita, M. Yashikawa, A. Isozaki, BUNSEKI KAGAKU 45 (1996) 909 (in Japanese).
[18] V.M. Mok, C.M. Wai, Anal. Chem. 59 (1987) 233.
[19] L. Zhang, D. Ishi, K. Shitou, Y. Morita, A. Isozaki, Talanta 68 (2005) 336.
[20] E. Kopyść, E. Bulska, R. Wennrich, Spectrochim. Acta B 58 (2003) 1515.

ELSEVIER

Study of interactions between actinomycin D and oligonucleotides by microchip electrophoresis and ESI-MS

Xiaomian Zhou [a,b,*], Zheng Shen [b], Dazhi Li [b], Xinya He [b,1], Bingcheng Lin [b,**]

[a] *Department of Laboratory Medicine, Guangzhou First Municipal People's Hospital, Affiliated of Guangzhou Medical College,
510180 Guangzhou, PR China*
[b] *Institute of Chemical Physics, Chinese Academy of Sciences, Dalian 116023, PR China*

Abstract

In the present study, the interactions between actinomycin D (ActD) and single stranded DNA (ssDNA) 5′-CGTAACCAACTGCAACGT-3′ and a duplex stranded DNA (dsDNA) with this sequence were investigated by microchip-based non-gel sieving electrophoresis and electrospray ionization mass spectrometry (ESI-MS). The ssDNA was designed according to the conserved regions of open reading frame 1b (replicase 1B) following the Tor 2 SARS genome sequence of 15611-15593. The binding constants of the interactions between ActD and ssDNA/dsDNA were $(8.3 \pm 0.32) \times 10^6 \, \text{M}^{-1}$ (ssDNA) and $(2.8 \pm 0.02) \times 10^5 \, \text{M}^{-1}$ (dsDNA), respectively, calculated from microchip electrophoresis *via* Scatchard plot. The binding stoichiometries were 1:1 (single/1ActD molecule) and 1:2 (duplex/2ActD molecules) calculated from microchip electrophoresis, and the results were further verified by ESI-MS. The results obtained by these two methods indicated that ActD bound much more tightly to ssDNA used in this work than dsDNA. Furthermore, this is shown that the microchip-based non-gel sieving electrophoresis method is a rapid, highly sensitive and convenient method for the studies of interactions between DNA and small molecule drugs.
© 2006 Published by Elsevier B.V.

Keywords: Microchip non-gel sieving electrophoresis; Actinomycin D; DNA; Interaction; Electrospray ionization mass spectrometry

1. Introduction

A wide variety of physical and chemical techniques have been used to study ligand–DNA binding, from the simple measurement of UV absorption and melting temperature to highly informative methods including nuclear magnetic resonance spectrometry (NMR) [1–3], X-ray [4,5], mass spectrometry

Abbreviations: ActD, actinomycin D; CD, circular dichroism; dsDNA, double-stranded DNA; ESI-MS, electrospray ionization mass spectrometry; HIV, human immunodeficiency virus; HPMC, hydroxyprolymethyl cellulose; NMR, nuclear magnetic resonance spectrometry; PMMA, poly(methyl methacrylate); ssDNA, single-stranded DNA

* Corresponding author at: Department of Laboratory Medicine, Guangzhou First Municipal People's Hospital, Affiliated of Guangzhou Medical College, 510180 Guangzhou, PR China. Tel.: +86 2 81048082; fax: +86 20 81045258.
** Corresponding author. Fax: +86 411 84379059.
E-mail addresses: zhouximi@yahoo.com (X. Zhou), bclin@dicp.ac.cn (B. Lin).
[1] Now is working at the Department of Chemistry, Colorado State University, Fort Collins, CO 80523, USA.

(MS) [6], circular dichroism (CD) [7], gel footprinting [8,9], fluorescence [3], equilibrium dialysis [10], and capillary electrophoresis (CE) [11–13]. However, NMR, X-ray, MS, CD and fluorescence not only require expensive equipments and elaborate procedures for sample purification prior to analysis, but also are tedious, time-consuming, and requiring a large sample size. Among the above-mentioned methods, CE is a powerful method with low sample consumption and short analysis time for studying the interactions of DNA-drugs [11]. Many biomolecule interacting systems such as protein–DNA, DNA–peptide, protein–protein, protein–drug, antibody–antigen, peptide–drug, peptide–carbohydrate, peptide–dye and carbohydrate–drug have been studied using CE techniques [14]. As a new method combining the CE technology and the microfluidic platform, microchip electrophoresis has the potential to study molecular interactions [15]. There are few reports on characterization or quantification determination of the binding constants by microchip-based electrophoresis [16,17], and there is no report for the study of the interactions between DNA and small molecules by microchip electrophoresis.

Microchip electrophoresis has being studied as a highly promising method for rapid and sensitive analysis, and is widely applied to genetic analysis [18,19], drug discovery [20], clinical diagnostic [21–23], proteomics [24,25] and so on [26–28]. The manipulation and transportation of analytes in microchip devices is based on electrokinetic phenomena, e.g., electrophoretic and electroosmotic effects. Buffer and sample flow within the channel network can be precisely controlled through high voltages applied on the buffer/sample reservoirs. The technique allows the manipulation of picoliter volumes with high precision that ultimately leads to performance equivalent to or exceeding current techniques. In contrast to conventional CE, the higher surface-to-volume ratio in microchip devices results in better heat dissipation, therefore, allows separations at higher field strengths. In a word, compared with conventional bench-scale systems, the advantages of microchip electrophoresis are numerous, such as less reagent consumption, low manufacturing costs, increased performance, faster analysis, high sample throughput, integration and automation possibility, and disposability [29,30].

ActD's biological activity has been attributed to binding ability with the double-stranded DNA (dsDNA) through the intercalation onto the planar phenoxazone ring into the double helix and then forming a stable complex with DNA and blocking the movement of RNA polymerase that interferes with DNA-dependent RNA synthesis [31,32]. However, recent discovery showed that the sequence-specific ActD binding to single strand DNA (ssDNA) could inhibit human immunodeficiency virus (HIV) reverse transcriptase and other polymerase [33]. Drugs with high selection for single-stranded forms of the HIV genome should cause minimal damage to the host genome DNA. ActD could inhibit HIV reverse transcriptase and other polymerase. This result provides useful information for the treatment of new disease caused by some new viruses. The severe respiratory syndrome-associated coronavirus (SARS-CoV) is a new viral RNA coronavirus with single-stranded forms of SARS genome that causes an acute respiratory illness in this century [21]. It is worth studying whether or not ActD also play a role in inhibiting SARS-CoV.

To our knowledge, no article concerning the research of ActD–oligonucleotides interactions and even quantitative determination of the binding constants and stoichiometries was reported using microchip electrophoresis. In the present work, we explored the interactions between 18-mer ssDNA with a sequence of 5′-CGTAACCAACTGCAACGT-3′, or the 18-mer dsDNA and ActD by microchip electrophoresis. The peak height of DNA was monitored to get practical data. The binding constants and stoichiometries were obtained using Scatchard analysis. To validate the results provided by microchip electrophoresis, the stoichiometries of ActD and oligonucleotides were compared with ESI-MS data.

2. Materials and methods

2.1. Materials

ActD was purchased from AMRESCO Inc. (30175 Solon Industrial, Parkway, Solon, OH, USA). The single-stranded DNAs of 3′-GCATTGGTTGACGTTGCA-5′ and 5′-CGTAACCAACTGCAACGT-3′, whose sequence were designed according to the conserved regions of open reading frame 1b (replicase 1B) following the Tor 2 severe acute respiratory syndrome (SARS) genome sequence of 15611-15593 [23], were purchased from the TaKaRa Biotechnology Co., Ltd. (Dalian, China). A 100 mM Tris (tris(hydroxymethyl)-methylamine, Sigma)/100 mM boric acid/2 mM EDTA buffer (TBE)/2.0% hydroxyprolymethyl cellulose (HPMC) (HPMC, 50 cps. Sigma Chemical Co., St. Louis, MO)/with a pH 8.5 was used as running buffer in the experiment. A 1 μmol/L SYTOX orange nucleic acid stain (Molecular Probes, Eugene, OR) solution was prepared in 2.0% HPMC TBE buffer in order to label DNA on-line. All buffer solutions were prepared in doubly distilled water.

2.2. Sample preparation

For microchip electrophoresis analysis, each of the ssDNAs was dissolved in 10 mM Tris/50 mM NaCl/1 mM EDTA buffer (pH 8.5) to prepare the 18-mer dsDNA by the annealing test. Equal aliquots of the equimolar ssDNAs (50 μL) were mixed, and then was annealed by heating to 96 °C for 6 min to obtain the dsDNA and cooled to room temperature slowly (about 2–3 h). The 20 μL of the solution containing the annealed dsDNA (0.1 μM) or the ssDNA was incubated with a 20 μL of ActD with different concentration (in water) in a 37 °C water bath for 2 h prior to analysis. For ESI-MS analysis, sample preparation was performed as follows: the 16.7 ng non-self-complementary 18 bases single strands were separately diluted into 100 μM stock solutions with 1 M ammonium acetate. After a 50 μL of each non-self-complementary stock solution was mixed, the solution of 100 μL was annealed by heating to 85 °C for 10 min and cooling to room temperature slowly (over 3 h). Then 20 μL of the solution containing the annealed duplex DNA was interacted with 30 μL of the different μM ActD (in water) to make the complex in a 37 °C water bath for 2 h. Each 50-μL solution containing the complex was diluted with spray solvent (50/50, v/v, MeOH/100 mM aqueous ammonium acetate) to 100 μL for mass spectrometry analysis.

2.3. Microchip electrophoresis analyzer

The homemade microchip analytical apparatus with a 532 nm wavelength laser used in this study was illustrated in our literatures [21,34]. In brief, the output radiation (532 nm) from an air-cooled LD-pumped solid-state laser (20 mW) (Mektec Seiwa Corporation, Beijing, China) passes through a 532 nm filter (Omega Optical, Brattleboro, VT). The beam is reflected by a dichroic beamsplitter tube (Omega Optical) and focused into the channel through a 20× microscope objective (0.4 N.A). The emission signal is collected by the same objective and transmitted back through the dichroic beamsplitter. The emission beam passes through a 570 nm bandpass filter (Omega Optical), which may be alternated easily to fit a wide selection of dyes, and is focused by a focusing lens through a 400 μm pinhole. The photomultiplier tuber (R212, Japan) is mounted in

an integrated detection module including high voltage power supply, voltage divider, and amplifier. The focus was finished by a charge coupled device (CCD) camera. The whole optical system was installed on the *X–Y–Z* translational stage (3D micro-manipulator, which adjusting precision is 1 μm) and the focus can be controlled via picture displayed on the screen.

2.4. Microchip

The homemade poly(methyl methacrylate) (PMMA) microchips used in this study were depicted in our former publications [35,36]. In brief, there are three suits of capillary channels on one microchip chip. Each reservoir volume is 13 μL.

2.5. Microchip electrophoresis

Separations were carried out using a homemade microchip electrophoresis analyzer described above. A PMMA microchip was used with an effective length of 4 cm and a total length of 5.5 cm. Buffer and separation media were pipetted into reservoirs, and the microchannels were filled by applying vacuum on one of the reservoirs. Sample was pipetted into the sample reservoir, and, the platinum electrodes were dipped into all reservoirs. After the run was finished, the microchannels were rinsed with distilled water. The pretreatment of the channel walls did not need before separation. The conditions for each run were as follows: the injection voltage and time were 400 V/cm and 30 s, respectively. The separation voltage and time were 130 V/cm and 220 s, respectively.

2.6. Quantitative model of the binding assay

Regarding molecular interactions, the binding constant is an important parameter. Scatchard analysis is a common way to linearize the binding data, and the model can be expressed as equation:

$$\frac{r}{C_f} = -Kr + nK$$

where *r* is the ratio of concentrations of the bound ligand (or receptor) to total receptor (or ligand) and C_f is the unbound ligand (or receptor) concentration. *K* is the apparent binding constant and *n* is the number of binding sites [37]. In the microchip electrophoresis section of this work, *r* is the ratio of concentration of the bound DNA to total ActD in the reacting solution.

2.7. ESI-MS with an ion-trap mass spectrometer

Mass spectrometric measurements were carried out with a Finnigan LCQ ion trap instrument (Thermo Finnigan, San Jose, CA) equipped with a standard heated capillary electrospray source. Since DNA is a kind of negatively charged polyelectrolyte at neutral pH, the electrospray source was operated in the negative mode, with a needle voltage of −4 kV. To obtain a good spray, it was necessary to add 25% methanol to the injected solution. Methanol was added just before injection, after

the complexation equilibrium in NH₄OAc was established. The solutions containing noncovalent complexes, single-stranded DNA or double-stranded DNA were infused at 3 μL/min directly into the mass spectrometer. The spray voltage was 4.0 kV. The capillary temperature was 175 °C. Sheath gas flow rate was 70 arb. Auxiliary gas flow rate was 5 arb. Tube lens offset voltage was 55 V. Lens voltage was 50 V. Multipole 1 offset voltage was 7 V. Multipole 2 offset voltage was 10.5 V. Entrance lens was 90 V. The N_2 bath gas flow was increased by approximately 1.5 times volume more than that normally used for electrospray at 200 °C to ensure efficient desolvation. The analyzer was operated at a background pressure of 1.79×10^{-5} Torr, as measured by a remote ion gauge. In all experiments, helium was introduced to an estimated pressure of 1 mTorr for improving the trapping efficiency. Data were collected for approximately 10 scans and analyzed with both the instrument software and the ICIS software developed by the manufacturer.

3. Results and discussion

The experimental results showed that the relative standard deviations (R.S.D.) of the migration time and peak height for 18-mer ssDNA peak and dsDNA are 1.29% and 4.22%, 1.31% and 4.75%, respectively. They show that the run-to-run reproducibility is good.

In general, the LIF method may cause disturbances at the binding sites of the biomolecules because it is necessary to use a fluorigenic labeling or to need a derivatization reaction. If the interactions of ligand–DNA were completed before DNA was labeled by the fluorescence dye, disturbance at the binding sites of the biomolecules might be avoided. Therefore, separation and analysis with on-line labeling DNA on microchips were carried out after the interactions of ActD and 18-mer dsDNA happened. Meanwhile, many marcobiomolecules are prone to be adsorbed electrostatically on the surface of plastic channel and, in general, this phenomenon is unfavorable, or even fatal for the analysis of macrobiomolecules. In our experiments, the use of hydroxypro-lymethyl cellulose as an additive that gave a dynamical coating in the running buffer could suppress the electroosmotic flow (EOF) as well as the adsorption of DNA to the PMMA channel wall, the channel was dynamically coated with hydroxyprolymethyl cellulose; on the other hand, hydroxyprolymethyl cellulose worked as a sieving matrix of DNA fragments separation.

3.1. The interaction between ActD and ssDNA or dsDNA

Standard samples containing 0.0127–1.27 μM of the 18-mer ssDNA or 0.005–0.3 μM of the 18-mer dsDNA were analyzed by microchip electrophoresis. The peak height of each sample was proportional to the concentration of ssDNA or dsDNA. The relationships between peak height and ssDNA or dsDNA concentration could be expressed as $y = 252.59x - 1.73$ ($r = 0.998$) and $y = 1151.7x + 0.55$ ($r = 0.997$), respectively. Then the corresponding concentrations of ssDNA in the binding assay were calculated from this calibration curve. Fig. 1 shows electrophoergraphs of interaction between 0.127 μM 18-mer ssDNA (5′–3′) and various concentrations of ActD. Fig. 2 shows electro-
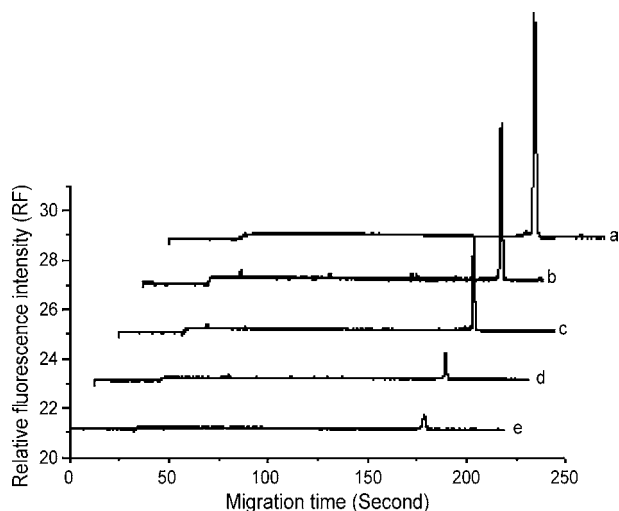
Fig. 1. Electrophoergraphs of interaction between 0.127 µM 18-mer ssDNA (5′–3′) and various concentrations of ActD. (a) 0 µM ActD; (b) 0.1 µM ActD; (c) 0.3 µM ActD; (d) 0.8 µM ActD; (e) 1.25 µM ActD.

pherograms of 0.05 µM 18-mer dsDNA mixed with various concentrations of ActD. When a mixture of ssDNA or dsDNA and ActD was injected into the channel of microchip, SYTOX orange dye in the buffer intercalated the 18-mer ssDNA or dsDNA, and thus the ssDNA or dsDNA could be detected. Then the dye could not intercalate ActD, which could not be detected in the assay. With increasing the concentrations of ActD, the peak heights of ssDNA or dsDNA fall as shown in Figs. 1 and 2. Since the fluorescent dye reacted with free DNA, the observed signals represent the fraction which did not bind to ActD. When the concentration of ActD was excessive, the peaks of ssDNA and dsDNA could be not detected. This is a basic for the quantitative determination. The ActD contributed positive charges to DNA, therefore, the complex became neutral or near-neutral. As a result, through an electro-migration injection mode, the complex might not be loaded into separation channel or, although there were a few complexes injected, separation time was too short to detect them in the separation conditions using the dynamoelectric injection mode.
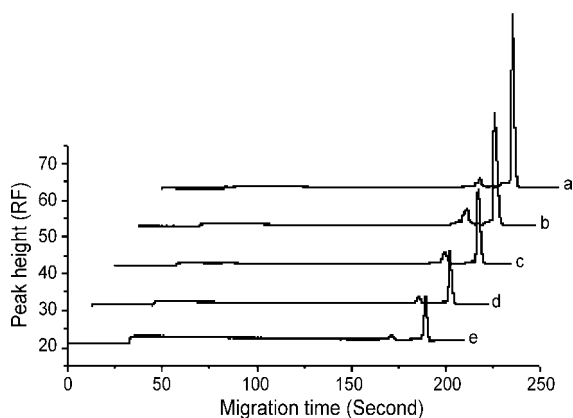

Fig. 2. Electropherograms of 0.05 µM 18-mer dsDNA mixed with various concentrations of ActD. (a) 0 µM ActD; (b) 0.25 µM ActD; (c) 0.5 µM ActD; (d) 0.75 µM ActD; (e) 1.0 µM ActD.

To quantitatively characterize the interaction between ActD and the 18-mer ssDNA or dsDNA, the concentrations of free ssDNA and free dsDNA were calculated from the calibration curves, and thus the r-values were obtained. Two K were calculated to be $(8.3 \pm 0.32) \times 10^6 \, \mathrm{M^{-1}}$, $(2.8 \pm 0.02) \times 10^5 \, \mathrm{M^{-1}}$ from the slope, respectively. When the intercept was divided by the slope, a value of 1.22 ± 0.11 or 1.96 ± 0.1 for n was obtained. These results indicated the binding stoichiometries for ssDNA and dsDNA were 1:1 and 1:2, respectively. The results were in good agreement with the data obtained using the spectrophotometer by Wadkins and Jovin [38] and Sha [11]. Compared with the above two binding constants, the results indicated that ActD bound much more tightly to the single strand than DNA helix with a specific sequence in SARS genome sequence.

3.2. Electrospray of single and duplex oligodeoxynucleotides

To easily understand the ESI spectra of oligonucleotides and their complex (oligonucleotide–ActD), ssDNA and dsDNA were analyzed by ESI-MS. The oligonucleotides concentration was optimized as 10 µM. Fig. 3 shows the ESI/spectra of 10 µM solutions of 18-mer single-stranded oligonucleotides (A and B) and annealed 18-mer dsDNA (C). Figs. 3A or 4B shows that the single-stranded DNA with four negatively charged is dominating, and then the duplex DNA with six negatively charged is in the majority, a small quantity of single-stranded DNAs with four negatively charged, which are 3′-GCATTGGTTGACGTTGCA-5′ and 5′-CGTAACCAACTGCAACGT-3′, appeared in Fig. 3C. These results are in favor of estimating the noncovalent complex of ActD and 18-mer dsDNA.

To detect the noncovalent duplex in the gas phase using ESI-MS, we referenced the reported method [40]. In brief, the non-self-complementary strands in 1 M ammonium acetate were annealed and the annealed sample in 100 mM ammonium acetate was sprayed. The molar numbers of the ssDNAs added were equal, and the duplex DNA was inspected by microchip electrophoresis. Distinctly, the annealing process insures duplex formation for non-self-complementary oligodeoxynucleotides. ESI/MS spectra of two complementary ssDNA and dsDNA in Fig. 3 show that the single or duplex stranded oligonucleotides do not form any nonspecific aggregation of duplex. These results favor the subsequently observation of dsDNA and its noncovalent complexes between drug and duplex oligonucleotides. ESI-MS can reveal binding stoichiometry for relatively small amounts of material and study the noncovalent complexes of small organic molecules to single-[6] and double-stranded [39–41] oligonucleotides.

3.3. Observation of noncovalent complexes between ActD and 18-mer ssDNA or 18-mer dsDNA

The solution was injected to ESI-MS and the binding stoichiometry was measured by mixing ssDNA or dsDNA with ActD in a 1:1 molar ratio. Fig. 4A shows a 1:1 ssDNA/ActD complex is mostly product. Therefore, ActD has 1:1 binding stoichiometry. Because the ion-trap instrument here we used
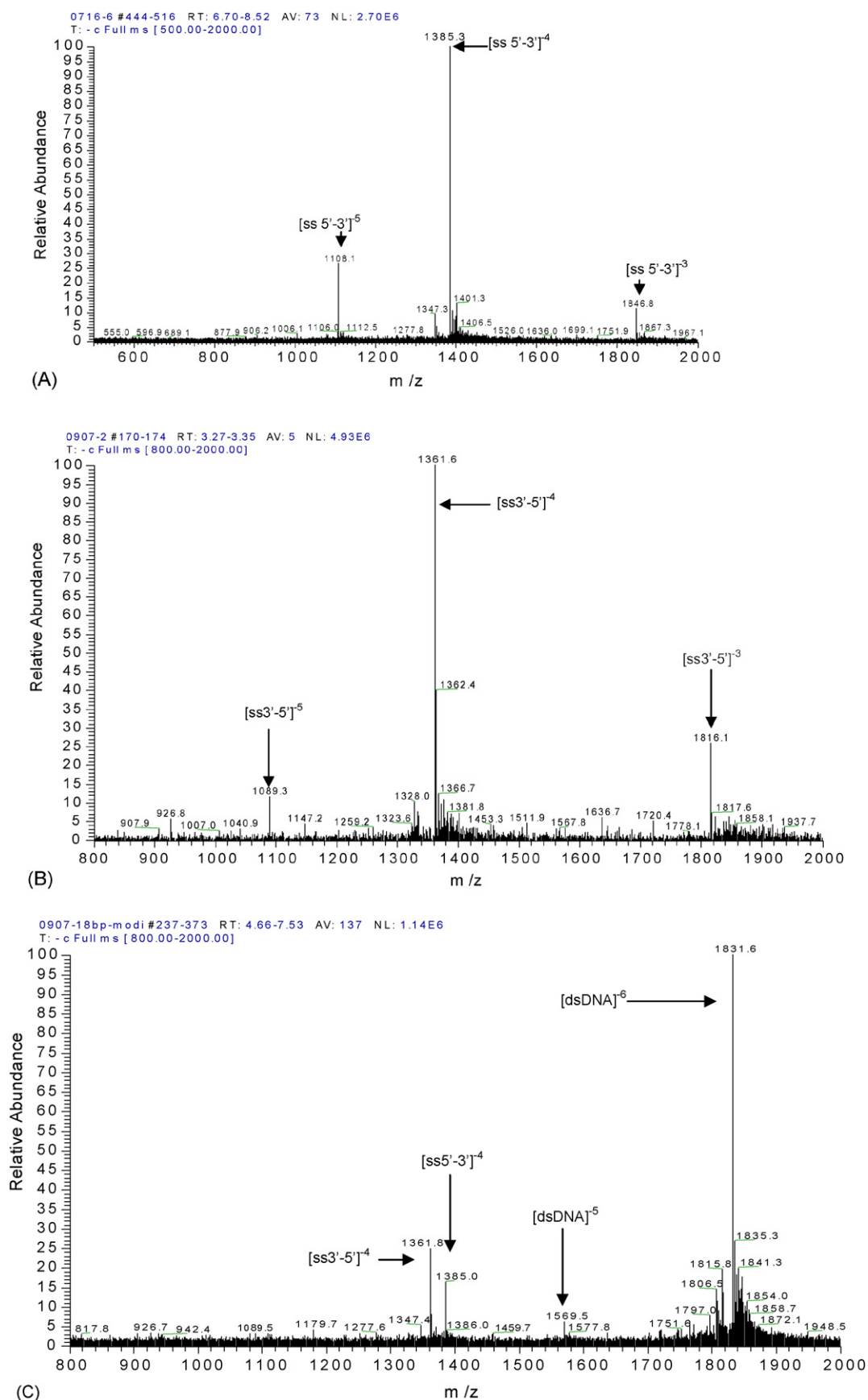
Fig. 3. ESI/MS spectra of single and duplex oligodeoxynucleotides: (A) 5′-CGTAACCAACTGCAACGT-3′; (B) 3′-GCATTGGTTGACGTTGCA-5′; (C) *d*(CGTAACCAACTGCAACGT)$_2$. The designation ss and ds are single-stranded and double-stranded.

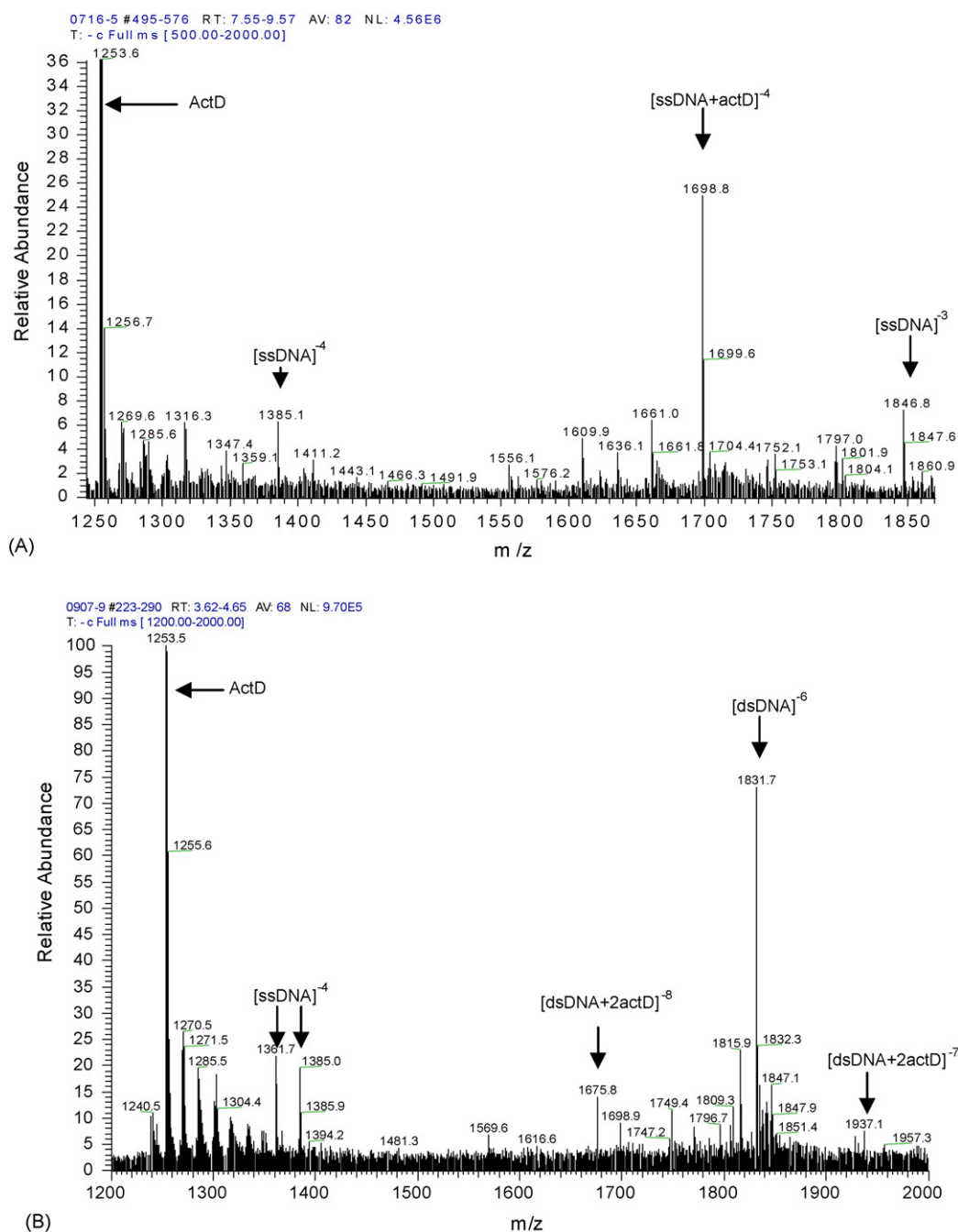Fig. 4. Product-ion mass spectra (MS/MS) of 5′-CGTAACCAACTGCAACGT-3′ (A) and d(CGTAACCAACTGCAACGT)$_2$ (B) with ActD.

has an upper mass limit of m/z 2000, we could not get the whole charge distribution for each species. So, the ration of the abundance of the even-charge complex to that of the even-charge free single or duplex was used to evaluate the binding affinity. The result in Fig. 4A shows that the ration of the even-charge ssDNA–ActD complex/the even-charge free ssDNA is approximately 3, which indicates that there is stronger binding affinity between ActD and 18-mer single-stranded DNA (5′–3′). Then, the results in Fig. 4B show that the ration of the even-charge dsDNA–ActD complex/the even-charge free dsDNA is only nearly one fourth, which is significantly less than the former, and there are formation of 1:2 oligonucleotide duplex/ActD

complexes and 1:1 oligonucleotide single/ActD complexes. The above demonstrated results showed that ActD bound much more tightly to the single strand used here than double-stranded DNA, and ActD has 1:2 binding stoichiometry (18-mer dsDNA/ActD). This result is in good agreement with that obtained by microchip electrophoresis.

4. Conclusion

The microchip electrophoresis has been proved to be a successful method for studying ligand–DNA interactions. The results from both microchip electrophoresis and ESI-MS showed

that ActD bound much more tightly to the ssDNA related SARS-CoV than its complementary dsDNA.

Acknowledgements

References

[1] X. Liu, H. Chen, D.J. Patel, J. Biomol. NMR 1 (1991) 323–347.
[2] R.M. Wadkins, E.A. Jares-Erijman, R. Klement, A. Rudiger, T.M. Jovin, J. Mol. Biol. 262 (1996) 53–68.
[3] K.H. Chin, F.M. Chen, S.H. Chou, Nucleic Acids Res. 31 (2003) 2622–2629.
[4] H. Chen, X. Liu, D.J. Patel, J. Mol. Biol. 258 (1996) 457–479.
[5] S. Kamitori, F. Takusagawa, J. Am. Chem. Soc. 116 (1994) 4154–4165.
[6] Y.L. Hsieh, Y.T. Li, J.D. Henion, Biol. Mass Spectrom. 116 (1994) 272–276.
[7] R.B. Hommer, Arch. Biochem. Biophys. 129 (1969) 405–407.
[8] J. Goodisman, R. Rehfuss, B. Ward, J.C. Dabrowiak, Biochemistry 31 (1992) 1046–1058.
[9] A.V. Scramrov, R.S. Beabealashivilli, FEBS Lett. 164 (1983) 97–101.
[10] G. Kollmann, D. Martin, B. Shapiro, Int. J. Radiat. Biol. 16 (1969) 121–128.
[11] F. Sha, F.M. Chen, Biophys. J. 79 (2000) 2095–2104.
[12] X.Y. He, D.Z. Li, A.Y. Liang, B.C. Lin, J. Chromatogr. A 982 (2002) 285–291.
[13] X.Y. He, D.Z. Li, A.Y. Liang, B.C. Lin, Chin. Chem. Lett. 14 (2003) 304–307.
[14] F.A. Gomez, J.N. Mirkovich, V.M. Dominguez, K.W. Liu, D.M. Macias, J. Chromatogr. A 727 (1996) 291–299.
[15] A.R. Stettler, M.A. Schwarz, J. Chromatogr. A 1063 (2005) 217–225.
[16] N.H. Chiem, D.J. Harrison, Electrophoresis 19 (1998) 3040–3044.
[17] X.J. Liu, X. Liu, A.Y. Liang, Z. Shen, Y. Zhang, Z.P. Dai, B.H. Xiong, B.C. Lin, Electrophoresis 27 (2006) 3125–3218.
[18] X.M. Zhou, S.J. Shao, G.D. Xu, G. Liu, R.T. Zhong, D.Y. Liu, J.W. Tang, Y.N. Gao, L. Sun, S.J. Cheng, B.C. Lin, J. Chromatogr. B 816 (2005) 145–151.
[19] D.Y. Liu, X.M. Zhou, R.T. Zhong, N.N. Ye, G.H. Chang, W. Xiong, X.D. Mei, B.C. Lin, Talanta 68 (2006) 616–622.
[20] J. Houston, M. Banks, Curr. Opin. Biotechnol. 9 (1998) 643–649.
[21] X.M. Zhou, D.Y. Liu, R.T. Zhong, D.P. Dai, D.P. Wu, H. Wang, Y.G. Du, Z.N. Xia, L.P. Zhang, X.D. Mei, B.C. Lin, Electrophoresis 25 (2004) 3032–3039.
[22] E. Verpoorte, Electrophoresis 23 (2002) 677–712.
[23] H. Nakajima, M. Yagi, Y. Kudo, T. Nakagama, T. Shimosaka, K. Uchiyama, Talanta 70 (2006) 122–127.
[24] A. Lueking, M. Horn, H. Eickhoff, K. Bussow, H. Lehrach, G. Walter, Anal. Biochem. 270 (1999) 103–111.
[25] G. Sanders, A. Manz, Trends Anal. Chem. 19 (2000) 364–378.
[26] G. Chen, Y.H. Lin, J. Wang, Talanta 68 (2006) 497–503.
[27] P. Martin, Talanta 66 (2005) 1048–1062.
[28] W. Chang, Y. Ono, M. Kumemura, T. Korenaga, Talanta 67 (2005) 646–650.
[29] C.S. Effenhauser, G.J. Bruin, A. Paulus, Electrophoresis 18 (1997) 2203–22013.
[30] S. DeWitt, Curr. Opin. Chem. Biol. 3 (1999) 350–356.
[31] M.J. Waring, Annu. Rev. Biochem. 50 (1981) 159–192.
[32] F.M. Chen, Biochemistry 31 (1992) 6223–6228.
[33] R.E. Jeeninga, H.T. Huthoff, A.P. Gultyaev, B. Berkhout, Nucleic Acids Res. 26 (1998) 5472–5479.
[34] X.M. Zhou, Z.P. Dai, B.C. Lin, Chem. J. Chin. Univ. 3 (2004) 336–340.
[35] X.M. Zhou, Z.P. Dai, X. Liu, Y. Luo, H. Wang, B.C. Lin, JSS 26 (2005) 219–224.
[36] X.M. Zhou, Z.P. Dai, X. Liu, Y. Luo, H. Wang, X.L. Mao, D.P. Wu, B.C. Lin, Chem. J. Chin. Univ. 26 (2005) 52–54.
[37] G. Scatchard, NY Ann. Acad. Sci. 51 (1949) 660–672.
[38] R.M. Wadkins, T.M. Jovin, Biochemsitry 30 (1991) 9469–9478.
[39] Q. Gao, X. Cheng, R.D. Smith, C.F. Yang, I.H. Goldberg, J. Mass Spectrom. 31 (1996) 31–36.
[40] A. Triolo, F.M. Arcamone, A. Raffaelli, P.J. Alvadori, Mass Spectrom. 32 (1997) 1186–1194.
[41] K.X. Wan, T. Shibue, M.L. Gross, J. Am. Chem. Soc. 122 (2000) 300–307.

Prussian Blue electrodeposited on MWNTs–PANI hybrid composites for H_2O_2 detection

Yongjin Zou [a,b], Lixian Sun [a,*], Fen Xu [a]

[a] *Dalian Institute of Chemical Physics, Chinese Academy of Sciences, Dalian 116023, China*
[b] *Graduate School of the Chinese Academy of Sciences, Beijing 100049, China*

Abstract

A Prussian Blue (PB)/polyaniline (PANI)/multi-walled carbon nanotubes (MWNTs) composite film was fabricated by step-by-step electrodeposition on glassy carbon electrode (GCE). The electrode prepared exhibits enhanced electrocatalytic behavior and good stability for detection of H_2O_2 at an applied potential of 0.0 V. The effects of MWNTs thickness, electrodeposition time of PANI and rotating rate on the current response of the composite modified electrode toward H_2O_2 were optimized to obtain the maximal sensitivity. A linear range from 8×10^{-9} to 5×10^{-6} M for H_2O_2 detection has been observed at the PB/PANI/MWNTs modified GCE with a correlation coefficient of 0.997. The detection limit is 5×10^{-9} M on signal-to-noise ratio of 3. To the best of our knowledge, this is the lowest detection limit for H_2O_2 detection. The electrode also shows high sensitivity (526.43 $\mu A\,\mu M^{-1}\,cm^{-2}$) for H_2O_2 detection which is more than three orders of magnitude higher than the reported.
© 2006 Elsevier B.V. All rights reserved.

Keywords: Prussian Blue; Multi-walled carbon nanotubes; Polyaniline; Hybrid composite; H_2O_2

1. Introduction

With their unique electronic and mechanical properties, carbon nanotubes (either multi-walled or single-walled carbon nanotubes) are of great interest for the fabrication of new classes of advanced materials [1]. In addition, the ability of carbon nanotubes (CNTs) to promote the electron-transfer reactions of important molecules, such as cytochrome *c* [2], ascorbic acid [3], neurotransmitters [4], NADH [5] and H_2O_2 [6,7], have made them attractive for the construction of various electrochemical sensors. Recently, conducting polymer/CNTs composites have received significant interest because the incorporation of CNTs in conducting polymers can lead to new composite materials possessing the properties of each component with a synergistic effect that would be useful in particular applications [8]. Among the various conducting polymers, polyaniline, a particular conducting polymer with a high application potential, has become the most attractive one because of its facile preparation,

high conductivity and good environmental stability. PANI/CNTs composites have been prepared by electropolymerization of aniline [9] or in situation chemical polymerization [10] which have improved the electrical conductivity, electrochemical capacitance and electrocatalytic properties of the polymers [11].

On the other hand, Prussian Blue, known as an "artificial peroxidase" [12], has high electrocatalytic activity, stability and selectivity for H_2O_2 electroreduction. It has been extensively studied and used for H_2O_2 detection [13,14]. It is superior to noble metal such as platinum or platinised electrodes which detect H_2O_2 through its oxidation at anodic potential (>+0.6 V, Ag/AgCl) [15]. Many substances, such as uric acid and ascorbic acid, normally present in biologic samples, can also be electrochemically oxidized at such a potential, which may cause an interfering response in the quantization of substrate concentration. Low-potential detection of H_2O_2 is also possible with peroxidase modified electrodes [16–19]. Despite the low detection limits achieved, peroxidase electrodes demonstrate saturation with the H_2O_2, which affects linear calibration range. In addition, peroxidase electrodes are usually less selective relative to oxygen. Moreover, the use of the enzyme obviously deteriorates transducer properties because of its instability and high cost.

* Corresponding author at: Materials & Thermochemistry Laboratory, Dalian Institute of Chemical Physics, Chinese Academy of Sciences, Dalian 116023, China. Tel.: +86 411 84379213; fax: +86 411 84379213.
E-mail address: lxsun@dicp.ac.cn (L. Sun).

Monitoring of low levels of H_2O_2 is of great importance for modern medicine, environmental control, and various branches of industry [20,21]. Many of the sensors so far developed show a satisfactory sensitivity for the detection relatively lower concentration of H_2O_2 and the possibility to detect H_2O_2 down to 10^{-8} M is achieved. But monitoring of lower H_2O_2 levels is significance both in clinical diagnostics and environmental control [13].

Prussian Blue films have been deposited on a variety of surfaces, the most common being glassy carbon [12–14], graphite [22], Pt [23] and carbon fiber [24]. To our knowledge, there is no literature which electrodeposits PB on MWNTs substrate for H_2O_2 detection. The authors of the present paper have studied glucose biosensor based on platinum catalyst and porphine [25]. In this work, a PB/PANI/MWNTs composites modified electrode has been fabricated by step-by-step electrodeposition on GCE. Cyclic voltammetry (CV) was used to investigate the electrochemical behavior to the reduction of H_2O_2 of the modified electrode. Effects of electrodeposition time of PANI, MWNTs thickness and rotating rate on amperometric response of the PB/PANI/MWNTs composite modified electrode to H_2O_2 have been investigated and discussed.

2. Experimental

2.1. Reagents

All chemicals from commercial source were of analytical grade. Aniline ($\geq$99.5%, Shenyang Lianbang Reagent Factory, Shengyang, China) was distilled before experiments. Multiwalled carbon nanotubes (95% 20–60 nm) purchased from Shenzhen Nanotech. Port. Co., Ltd. (Shenzhen, China) were treated with nitric acid during purification process and then filtered, rinsed with double-distilled water and dried. Double-distilled water was used throughout the experiments. A fresh H_2O_2 aqueous solution was prepared prior to use. 0.1 M phosphate buffer solution (PBS, pH 6.5), which was made from Na_2HPO_4 and NaH_2PO_4, was always employed as supporting electrolyte.

2.2. Instruments

Scanning electron microscopy (SEM) images were obtained by using JSM-6360LV SEM (JEOL, Japan). Electrodeposition and electrochemical characterization experiments were performed with an IM6e electrochemical workstation (Zahner-Elektrik, Kronach, Germany). All electrochemical experiments were carried out with a conventional three-electrode system. The working electrode was the Bioanalytical Systems (BAS) cavity glassy carbon electrode (3-mm diameter). The rotating disk electrode experiments were performed by BAS rotator system in conjunction with an IM6e. The rotating rate is 3000 rpm when detect H_2O_2 unless stated otherwise. An Ag/AgCl (saturated with NaCl) reference electrode was used for all measurements, and all the potentials were reported in this paper versus this reference electrode. A platinum wire was used as a counter electrode. Before all batch amperometric experiments, the potential of each

electrode was held at the operating value, allowing the background current to decay to a steady state value. All experiments were performed at room temperature.

2.3. Fabrication of the modified electrode

The fabrication of the PB/PANI/MWNTs glassy carbon electrode was summarized as follows. One milligram of purified MWNTs was dispersed in 5 ml dimethylformamide (DMF) with the aid of ultrasonic agitation to give a 0.2 mg ml^{-1} black suspension. The GCE was carefully polished with 1.0 and 0.3 μm a-Al_2O_3 powders successively according to the literature [18], and then cleaned ultrasonically in the double distill water and ethanol for a few minutes, respectively. The well-polished GCE with a fresh surface was preheated at about 80 °C for 30 min. The GCE was treated by dropping a suspension (15 μl) of the MWNTs in DMF and then dried under an infrared lamp. The MWNT/GCE obtained was thoroughly rinsed with water.

PANI was electrochemically prepared via cyclic voltammetry in a three-electrode cell containing an aqueous solution of 0.1 M HCl and 0.1 M aniline. The working electrode was the MWNTs/GCE. The PANI film was obtained on the working electrode by cycling between -0.2 and 0.7 V versus Ag/AgCl at a sweep rate 0.1 V s^{-1} for 10 cycles. After electrodeposition, the electrode was rinsed with pure water, and the next electrochemical experiment was performed.

PB film was potentiostatically deposited at a potential value of 0.40 V for 40 s from aqueous solutions of 2×10^{-3} M $K_3[Fe(CN)_6] + 2 \times 10^{-3}$ M $FeCl_3$ in the supporting electrolyte 0.1 M KCl + 0.01 M HCl [26]. After deposition, the modified electrode was rinsed with water (pH 5.3) and immersed into a solution containing 0.1 M KCl + 0.01 M HCl, where the electrode potential was cycled between -0.05 and 0.35 V at a scan rate of 0.05 V s^{-1}, until a stable voltammetric response was obtained.

3. Results and discussion

3.1. Effect of the MWNTs thickness

The amount of MWNTs modified on the glassy carbon electrode was one of the important factors to be considered. The calibration plots for H_2O_2 obtained at electrode by adjusting thickness of the MWNTs were compared. The sensitivity increased with the MWNTs loading from 5 to 20 μl. When the magnitude of MWNTs increased, the sensitivity increased, but when the amount of MWNTs beyond 15 μl, the sensitivity decreased. This may be attributed to too much MWNTs loading on the GCE so as to make the mechanical stability of the MWNTs film rather poor. As a compromise, the amount of MWNTs magnitude of 15 μl was selected in the experiments.

3.2. Electropolymerization of aniline

The composites of MWNTs/PANI can be obtained from chemical polymerization in a solution containing MWNTs and aniline. In the present paper, PANI was deposited on the surface
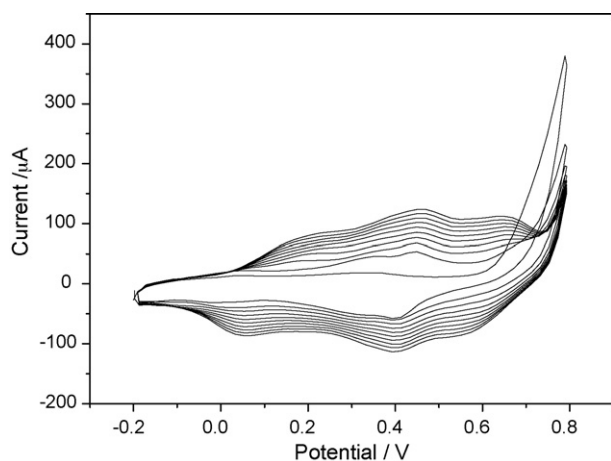
Fig. 1. Cyclic voltammograms recorded during electrochemical deposition of polyaniline at a MWNTs/GCE in solutions containing 0.1 M aniline and 0.1 M HCl. Potentials were swept between −0.2 and 0.7 V (vs. Ag/AgCl) with a sweep rate of 0.1 V s^{-1}.

of MWNTs by an electrochemical potential cycling process. It was reported that the morphology of the polymer films depended on the electropolymerization process [27]. To obtain a compact and relatively thin film, the electropolymerization of PANI was performed in the solution of aniline scanning from −0.2 to 0.7 V (versus Ag/AgCl) with a sweep rate of 0.1 V s^{-1} for 10 full voltammetric cycles. From Fig. 1, it can be seen that there are three pairs of redox peaks indicating the presence of discrete electroactive regions in the film. Three reversible pairs of peaks can be distinguished at potentials around +0.15, +0.47 and +0.65 V. The first and the third pairs have been ascribed to the polaron and bipolaron forms of the PANI [28]. The origin of the second peak is much more complex and it has been attributed to many different intermediates and degradation products (cross-linked polymer, benzoquinone, etc.) [29]. It is similar to the reported in the literature [30].

3.3. Optimization of electropolymerization condition

The scan cycles in PANI electropolymerization was also important factors to be considered. When the polymer film is thin, the response time will be increased, whereas the modified electrode is unstable and the sensitivity is low when the film is thick. The sensitivity increases with the increasing of the scan cycles. When the scan cycles are up to 10 cycles, the best sensitivity is obtained. The aniline solution was chosen to be electropolymerized on MWNTs/GCE with a sweep rate of 0.1 V s^{-1} for 10 cycles when the PB/PANI/MWNTs modified GCE was prepared.

3.4. Effect of rotating rate

The effect of rotating rate for H$_2$O$_2$ detection was also investigated. Microelectrode can decrease the diffusion polarization effectively, but it generates low currents, which is hardly detectable with the conventional electrochemical technique. In the present work, the rotating disk electrode was used for H$_2$O$_2$

detection. When the rotating rate is increased, the response current is also increased. The Levich plot (i_L^{-1} versus $\omega^{-1/2}$) is linear up to 3000 rpm, and after that it reaches the kinetic limitation. The response current does not increase and keep steady which is in agreement to the literature [31]. Therefore, the rotating rate 3000 rpm was chose for H$_2$O$_2$ detection.

3.5. Characterization of the PB/PANI/MWNTs modified GCE

Fig. 2 shows the SEM images of the modified glassy carbon electrodes at the optimized condition: (a) MWNTs, (b) PANI/MWNTs and (c) PB/PANI/MWNTs. As shown in Fig. 2a, the porous MWNTs film has large surface area which provides an ideal matrix for the distribution of PB. The SEM images also reveal that the MWNTs, with a diameter ranging from 30 to 60 nm, are well distributed on the surface and that most of the MWNTs are in the form of small bundles or single tubes. Such small bundles and single tubes assembled homogeneously on the substrate are believed to be very beneficial for the modified electrode performance because most of the well-dispersed MWNTs are electrochemically accessible. After electropolymerization of PANI film on MWNTs modified electrode, the majority of MWNTs has been entrapped in the PANI film (Fig. 2b). From Fig. 2c, it can be seen that Prussian Blue particles are dispersed on the surface of PANI/MWNTs.

Fig. 3 shows cyclic voltammograms of PB/PANI/MWNTs modified GCE at various scan rates. The ratio of cathodic to anodic peak currents is nearly unity. Peak currents vary linearly with the scan rates, as shown in the inset of Fig. 3. When the scan rate is increased the E_{pc} shifts negatively and the E_{pa} shifts positively. When the scan rate is higher than 200 mV s^{-1}, the wave shape is distorted severely ($\Delta E_p > 200$ mV). This indicates that the electrode reaction becomes electrochemically irreversible at higher scan rates. Though PB films for H$_2$O$_2$ detection is very well established, the operational stability of the PB is not solved completely because the PB film is unstable in neutral and alkaline solution. The hydroxyl ions are known to be able to break the Fe–CN–Fe bond and solve the PB [32]. Moreover, Prussian-White (PW, the reduced redox state of PB at 0.0 V) is thermodynamically unstable on electrode surfaces, and hydroxyl ions (produced in the hydrogen peroxide reduction in neutral media) may solubilize the inorganic polycrystal. Polypyrrole have been used to protect the PB film, but the electropolymerization of Polypyrrole is difficult to control. The polymer film is usually thick and the response time will be increased [33].

In this work, the PB/PANI/MWNTs modified GCE also shows good stability after scanned in 0.1 M PBS + 0.1 M KCl (pH 6.5) for 50 cycles with no peak current decrease. It is still electroactive and sufficient to catalyze the H$_2$O$_2$ after 300 cycles in the PBS solution and the decrease of the signal was only 8% of the initial value. The peak currents decrease slightly after 300 cycles in PBS solution. In our opinion, the good results in the present paper achieved, similar to these observed in a previous paper, are due to the proposed method of deposition, which involves the chemical synthesis of PB in the presence of graphite. The treated MWNTs have carboxylic groups similar
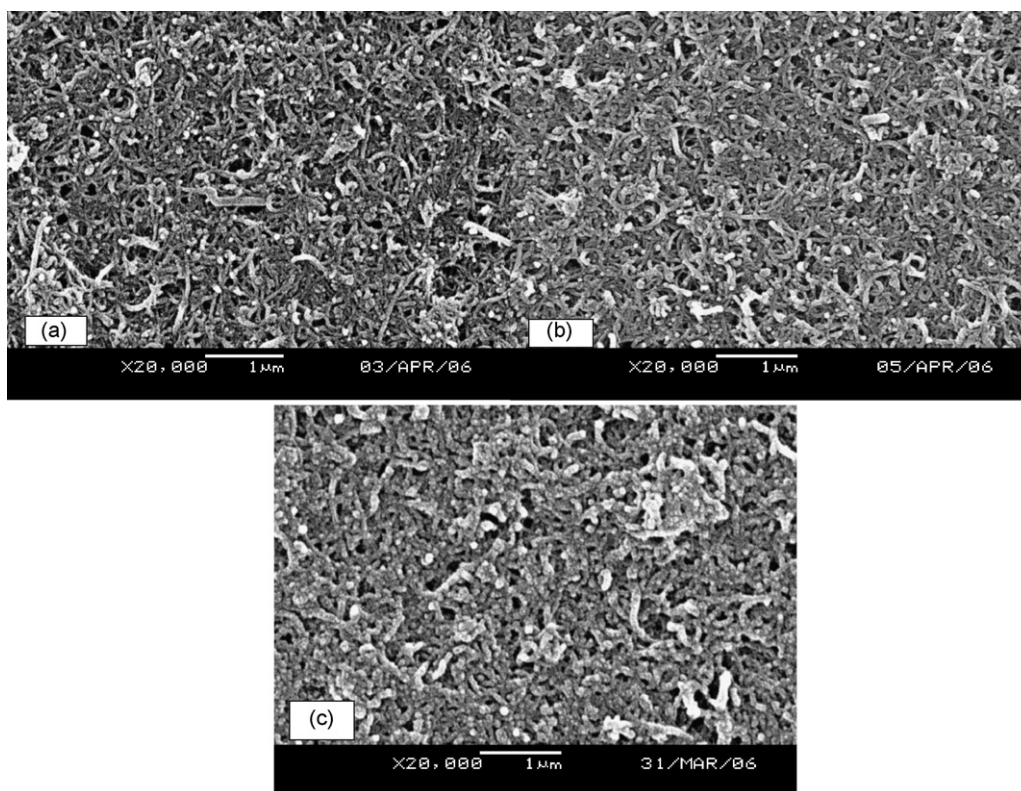
Fig. 2. SEM images of the modified GCEs: (a) MWNTs, (b) PANI/MWNTs and (c) PB/PANI/MWNTs.

to those produced with aqua regia on graphite power and the presence of these groups seems to be good to PB films [34]. On the other hand, MWNTs increase the surface dimension. The porous high surface area MWNTs matrix provides a high loading capacity for the deposition of PB particles while the PANI thin film further stabilizes the PB film.

Fig. 4 shows the cyclic voltammograms obtained with the PB/PANI/MWNTs modified GCE in 0.1 M PBS + 0.1 M KCl (pH 6.5) without H_2O_2 and with 5×10^{-7} M H_2O_2, respectively. In the absence of H_2O_2, the modified electrode gives no response

and only the electrochemical behavior of PB was observed. The redox behavior of PB at the modified GCE shows a reversible electrochemical response. When added 5×10^{-7} M H_2O_2 in the solution, the cyclic voltammogram changed, with a decrease in the reduction current. It indicates that electrocatalytic reduction of H_2O_2 produced is preferable for H_2O_2 detection.

3.6. Electrochemical performance of the modified GCE

Analytical performances of the modified electrode for H_2O_2 detection were investigated. Fig. 5 shows amperometric
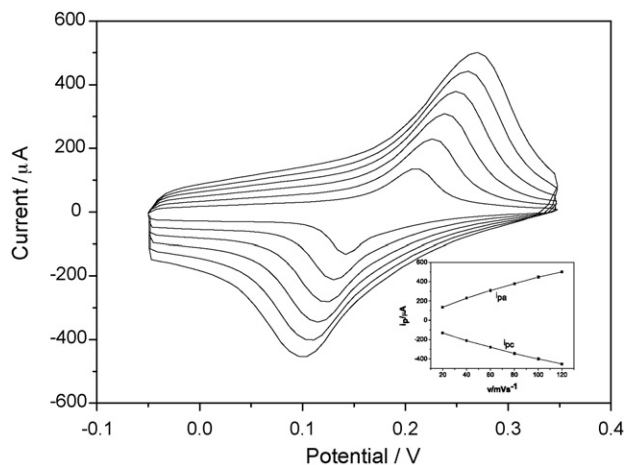

Fig. 3. Cyclic voltammograms at the PB/PANI/MWNTs/GC electrodes in 0.1 M PBS + 0.1 M KCl (pH 6.5) at different scan rates, from inside to outside: 20, 40, 60, 80, 100 and 120 mV s^{-1}. Insert is the plot cathodic and anodic peak current vs. scan rate.
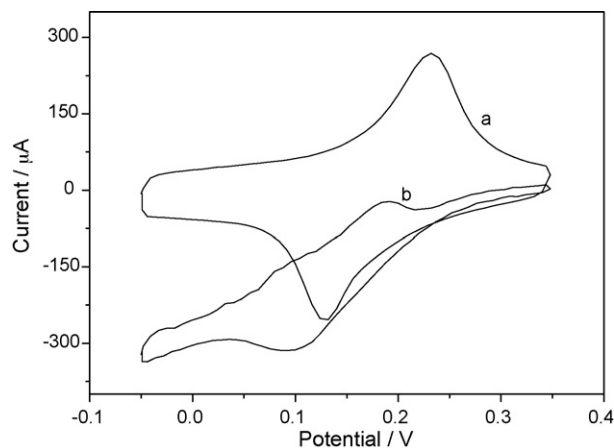

Fig. 4. Cyclic voltammograms of the PB/PANI/MWNTs modified GCE at the scan rate of 0.05 V s^{-1} in 0.1 M PBS + 0.1 M KCl (pH 6.5): (a) in the absence of H_2O_2 and (b) in the presence of 5×10^{-7} M H_2O_2.

Table 1
Prussian Blue-based modified electrodes for H_2O_2 detection in comparison with literature

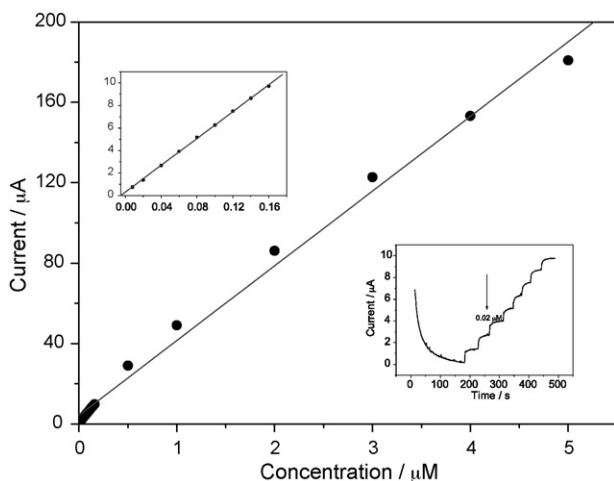| Electrode	Range of linearity (M)	Detection limit (M)	Sensitivity ($\mu A\,\mu M^{-1}\,cm^{-2}$)	Reference
PB/PANI/MWNTs	8×10^{-9} to 2×10^{-6}	5×10^{-9}	526.43	This paper
PB/SPEs	10^{-7} to 5×10^{-5}	10^{-7}	0.324	[32]
PB nanoelectrode arrays	1×10^{-8} to 10^{-2}	10^{-8}	0.06	[13]

Fig. 5. Calibration curve for H_2O_2 detection in pH 6.5 0.1 M PBS + 0.1 M KCl at 0.0 V, rotating rate 3000 rpm. In the lower insert, the actual response curve for some H_2O_2 additions is also shown. The addition successive is $0.02\,\mu M\,l^{-1}$.

responses of the PB/PANI/MWNTs modified GCE for H_2O_2 detection. The modified GCE displays rapid response and an expanded linear response range. The linear response range of 8×10^{-9} to 5×10^{-6} M with a correlation coefficient of 0.997 is achieved. The response time is 5 s when the current reach 90% of the steady state. The detection limit is 5×10^{-9} M on signal-to-noise ratio of 3. To our knowledge, this is the lowest detection limit as compared with the known H_2O_2 sensors [13,16–19,30]. The sensitivity is 526.43 $\mu A\,\mu M^{-1}\,cm^{-2}$ which is more than three orders of magnitude higher than the reported (shown in Table 1). The high sensitivity and low detection limit may attribute the superior transducing ability of PANI [35] and the excellent performance of the composites of PANI/MWNTs. The synergistic effect among MWNTs, PANI and PB is preferable for the H_2O_2 detection and improves the performances of the modified electrode.

The fabrication reproducibility, investigated at 5×10^{-7} M H_2O_2, was the relative standard deviation (R.S.D.) of 5.1% for five different modified electrodes. For five replicate measurements at 5×10^{-7} M H_2O_2 using a typical modified electrode, the R.S.D. was 2.5%. The typical interfering specie–ascorbic acid was investigated through adding 0.2 mM ascorbic acid to 5×10^{-7} M H_2O_2 and do not produce any observable interference in the modified electrode response. It may be attributed to the low potential (0.0 V) employed for the electrocatalysis of H_2O_2 reduction promoted by the PB layer [36].

The analytical applicability of the modified electrode was evaluated by determining the recoveries of 0.050, 0.250, 0.500 and 1.20 μM H_2O_2 by standard addition method [37]. The recov-

ery rate of the modified electrode is 98% ($0.049 \pm 0.016\,\mu M$), 99.2% ($0.248 \pm 0.062\,\mu M$), 102% ($0.511 \pm 0.014\,\mu M$) and 103% ($1.23 \pm 0.035\,\mu M$), respectively. The average recovery is 101%.

4. Conclusions

An organic/inorganic hybrid material composed of a conducting polyaniline thin film and Prussian Blue in a porous MWNTs matrix was synthesized. The composite film shows enhanced electrocatalytic activity to H_2O_2. The performances of PB/PANI/MWNTs modified electrode were characterized with cyclic voltammetry and scanning electron microscopy. Compared with the known amperometric detection of H_2O_2, the PB/PANI/MWNTs modified GCE shows better stability and lower detection limit. The modified GCE can also be used to develop into biosensor for detection of glucose and further work is in progress.

References

[1] W.K. Maser, A.M. Benito, M.A. Callejas, T. Seeger, M.T. Martínez, J. Schreiber, J. Muszynski, O. Chauvet, Z. Osváth, A.A. Koós, L.P. Biro, Mater. Sci. Eng. C 23 (2003) 97.
[2] J. Wang, M. Li, Z. Shi, N. Li, Z. Gu, Anal. Chem. 74 (2002) 1993.
[3] Z. Wang, J. Liu, Q. Liang, Y. Wang, G. Luo, Analyst 127 (2002) 653.
[4] R.S. Chen, W.H. Huang, H. Tong, Z.L. Wang, J.K. Cheng, Anal. Chem. 75 (2003) 6341.
[5] J. Wang, M. Musameh, Anal. Chem. 75 (2003) 2075.
[6] S. Sotiropoulou, N.A. Chaniotakis, Anal. Bioanal. Chem. 375 (2003) 103.
[7] S.G. Wang, Q. Zhang, R. Wang, S.F. Yoon, J. Ahn, D.J. Yang, J.Z. Tian, J.Q. Li, Q. Zhou, Electrochem. Commun. 5 (2003) 800.
[8] G.Z. Chen, M.S.P. Shaffer, D. Coleby, G. Dixon, W. Zhou, D.J. Fray, A.H. Windle, Adv. Mater. 12 (2000) 522.
[9] J.E. Huang, X.H. Li, J.C. Xu, H.L. Li, Carbon 41 (2003) 2731.
[10] Y. Zhou, B. He, W. Zhou, J. Huang, X. Li, B. Wu, H. Li, Electrochim. Acta 49 (2004) 257.
[11] M. Guo, J. Chen, J. Li, Bo Tao, S. Yao, Anal. Chim. Acta 532 (2005) 71.
[12] A.A. Karyakin, E.E. Karyakina, Russ. Chem. Bull. Int. Ed. 55 (2001) 1811.
[13] A.A. Karyakin, E.A. Puganova, I.A. Budashov, I.N. Kurochkin, E.E. Karyakina, V.A. Levchenko, V.N. Matveyenko, S.D. Varfolomeyev, Anal. Chem. 76 (2004) 474.
[14] M.P. O'Halloran, M. Pravda, G.G. Guilbault, Talanta 55 (2001) 605.
[15] Z.L. Liu, B.H. Liu, M. Zhang, Anal. Chim. Acta 392 (1999) 135.
[16] E.E. Ferapontova, V.G. Grigorenko, A.M. Egorov, T. Borchers, T. Ruzgas, L. Gorton, Biosens. Bioelectron. 16 (2001) 147.
[17] G. Kenausis, Q. Chen, A. Heller, Anal. Chem. 69 (1997) 1054.

[18] M. Wang, Y. Shen, Y. Liu, T. Wang, F. Zhao, B. Liu, S. Dong, J. Electroanal. Chem. 578 (2005) 121.

[19] Y. Liu, M. Wang, F. Zhao, Z. Guo, H. Chen, S. Dong, J. Electroanal. Chem. 581 (2005) 1.

[20] W.B. Nowalled, W.G. Kuhr, Electroanalysis 9 (1997) 102.

[21] A.A. Karyakin, O.V. Gitelmacher, E.E. Karyakina, Anal. Chem. 67 (1995) 2419.

[22] S.S. Narayanan, F. Sholz, Electroanalysis 11 (1999) 465.

[23] R. Garjonyte, A. Malinauskas, Sens. Actuators B 56 (1999) 93.

[24] X. Zhang, J. Wang, B. Ogorevc, U.S. Spichiger, Electroanalysis 11 (1999) 945.

[25] L.X. Sun, F. Xu, T. Okada, Talanta 47 (1998) 1165.

[26] J.G. Guan, Y.Q. Miao, J.R. Chen, Biosens. Bioelectron. 19 (2004) 789.

[27] H.S. Shim, I.H. Yeo, S.M. Park, Anal. Chem. 74 (2002) 3540.

[28] F. Qu, M. Yang, J. Jiang, G. Shen, R. Yu, Anal. Biochem. 344 (2005) 108.

[29] S.Y. Hong, Y.M. Jung, S. Bin Kim, S.M. Park, J. Phys. Chem. B 109 (2005) 3844.

[30] W.J. Cho, H.J. Huang, Anal. Chem. 70 (1998) 3946.

[31] J.-M. Zen, A.S. Kumar, C.-R. Chung, Anal. Chem. 75 (2003) 2703.

[32] F. Ricci, A. Amine, G. Palleschi, D. Moscone, Biosens. Bioelectron. 18 (2003) 165.

[33] J.-C. Vidal, J. Espuelas, E. Garcia-Ruiz, J.-R. Castillo, Talanta 64 (2004) 655.

[34] D. Moscone, D. D'Ottavi, D. Compagnone, G. Palleschi, A. Amine, Anal. Chem. 73 (2001) 2529.

[35] J. Liu, Y. Lin, L. Liang, J.A. Voigt, D.L. Huber, Z. Tian, E. Coker, B. Mckenzie, M.J. Mcdermott, Chem. Eur. J. 9 (2003) 604.

[36] M. Ferrerra, P.A. Fiorito, O.N. Oliveira, S.C. Torresi, Biosens. Bioelectron. 19 (2004) 1611.

[37] S. Chen, R. Yuan, Y. Chai, L. Zhang, N. Wang, X. Li, Biosens. Bioelectron. 22 (2007) 1268.